

GEOLOGICAL SURVEY OF FINLAND

Special Paper 55

2014



**Geology and Geodynamic Development of Uganda with
Explanation of the 1:1,000,000 Scale Geological Map**

A.B. Phil Westerhof, Paavo Härmä, Edward Isabirye, Edwards Katto, Tapio Koistinen,
Eira Kuosmanen, Tapio Lehto, Matti I. Lehtonen, Hannu Mäkitie, Tuomo Manninen,
Irmeli Mänttari, Yrjö Pekkala, Jussi Pokki, Kerstin Saalman and Petri Virransalo



Geology and Geodynamic Development of Uganda with Explanation of the 1:1,000,000 -Scale Geological Map

A.B. Phil Westerhof, Paavo Härmä, Edward Isabirye, Edwards Katto, Tapio Koistinen,
Eira Kuosmanen, Tapio Lehto, Matti I. Lehtonen, Hannu Mäkitie, Tuomo Manninen,
Irmeli Mänttari, Yrjö Pekkala, Jussi Pokki, Kerstin Saalman and Petri Virransalo

Unless otherwise indicated, the figures have been prepared and photos taken by
GTK Consortium personnel.

Front cover: Rocky landscape composed of charnockite and granulite hills, 10 km SE of
Koboko town in NW Uganda. Photo: Hannu Mäkitie, GTK.

ISBN 978-952-217-294-5 (paperback)

ISBN 978-952-217-295-2 (PDF)

ISSN 0782-8535

Layout: Elvi Turtiainen Oy
Printing house: Tammerprint Oy

Westerhof¹, A. B., Härmä², P., Isabirye⁴, E., Katto⁴, E., Koistinen⁵, T., Kuosmanen², E., Lehto², T., Lehtonen⁵, M. I., Mäkitie², H., Manninen³, T., Mänttari², I., Pekkala⁵, Y., Pokki², J., Saalman⁶, K. & Virransalo², P. 2014. Geology and Geodynamic Development of Uganda with Explanation of the 1:1,000,000 -Scale Geological Map. *Geological Survey of Finland, Special Paper 55*, 387 pages, 329 figures, 29 tables and 2 appendices.

By integrating regional tectonics, geochronology and geophysical data, Africa's major tectono-thermal terranes or 'building blocks', each characterised by a specific geodynamic development, can be identified. Their evolution is viewed in terms of Supercontinent or Wilson Cycles. Although some overlap may exist, it is justifiable to translate the above cycles into alternating periods of bulk crustal extension and compression on global and continental scales. Each cycle produces a variable amount of juvenile crust and partial reworking of older crust. Hence, these cycles are associated with alternating periods of enhanced and reduced continental crust formation.

The geology of Uganda spans more than three billion years. It comprises Archaean lithospheric fragments, welded together, intersected or surrounded by Proterozoic fold belts. These fold belts can be related to the Eburnian (2.20–1.85 Ga), Grenvillian (1.10–0.95 Ga) and Pan-African (0.75–0.50 Ga) Orogenic Cycles. In places, molasse-type platform deposits, post-orogenic to each of the above cycles, have been preserved. These include post-Pan-African deposits in Karoo basins and the two branches of the Neogene East Africa Rift System.

Structurally, Uganda is part of the proto-Congo Craton, composed of several Archaean nuclei and Palaeoproterozoic mobile belts. Uganda constitutes the northeastern corner of this proto-Congo Craton with two major Archaean 'building blocks' – the Tanzania Craton and Bomu-Kibalian or NE Congo-Uganda Shield. The Tanzania Craton in southern-central Uganda has been divided into two smaller tectono-thermal terranes, called the Lake Victoria and West Tanzania Terranes, respectively. The first is a classic granite-greenstone terrain, the second a granito-gneissic-migmatitic cratonic fragment. Both are Neoproterozoic in age (~2.63–2.59 Ga and 2.65–2.64 Ga, respectively) although dark enclaves in TTG gneisses of the second contain Meso- and possibly even Eoarchaean zircons.

The West Nile Block of NW Uganda constitutes the easternmost segment of the Bomu-Kibalian Shield of NE DRC. It is composed of a Mesoproterozoic (> 3.08 Ga) nucleus, called the Uleppi Complex, unconformably overlain by infolded mafic volcanic dominated lithologies of the ~2.64 Ga War Group and accreted with Neoproterozoic (> 2.63–2.59 Ga) rocks of the Arua-Lobule Supergroup. The North Uganda Terrane is separated from the West Tanzania Terrane in the south by the Nakasongola Discontinuity and from the West Nile Block in the west by the newly defined ~1.0 Ga Madi-Igisi Belt. To the north and east it is surrounded by Pan-African fold belts. It is also composed of a Mesoproterozoic nucleus (the 2.99 Ga Karuma Complex) with the bulk of this terrane having Neoproterozoic ages.

The Palaeoproterozoic Eburnian Orogenic Cycle in Uganda is represented by the Rwenzori Belt, comprising an older (2.21–2.15 Ga) gneissose/granitoid basement (Eburnian I) that can be correlated with Rusizian and Ubendian rocks further south. This is covered by metasediments and mafic volcanics of the Buganda Group (~2.00 Ga to 1.95 Ga) into which syn-

tectonic granitoids (1.99–1.96 Ga) and post-tectonic granitoids (1.85 Ga) have been emplaced (Eburnian II). The North Kibaran Belt in southwestern Uganda can be correlated with the Grenvillean Orogenic Cycle. It is mainly composed of granitoids of the bimodal North Kibaran Igneous Province (NKIP, 1.40–1.33 Ga) and a broadly coeval thick pile of terrigenous metasediments of the Akanyaru-Ankole Supergroup. The NKIP comprises an alignment of mafic and ultramafic layered complexes (1.40–1.38 Ga) and mafic dykes and sills, including the huge Lake Victoria Arcuate Dyke Swarm (1.37 Ga).

Amalgamation of East and West Gondwana gave rise to development of the East African Orogen, in eastern Uganda represented by the Karamoja Belt with the Karasuk Supergroup and the newly identified West Karamoja Group. The latter is characterised by widespread UHT granulites and 0.74–0.68 Ga charnockites. Ensuing collision with the Sahara meta-Craton resulted in emplacement of 0.66 Ga granitoids in northernmost Uganda. Pan-African secondary zircon rim growths and monazite blastesis in pre-Pan-African rocks is widespread in Uganda, in particular in older intracratonic weakness zones such as the North Kibaran and Igisi-Madi Belts.

The present volume is an explanation to the recently published new 1:1 million scale geological map of Uganda. Together these two form the first modern account of the bedrock geology of Uganda.

Keywords (GeoRef Thesaurus, AGI): areal geology, granites, metasedimentary rocks, metavolcanic rocks, cratons, terranes, orogenic belts, East African Rift, geodynamics, geochemistry, petrography, lithostratigraphy, explanatory text, geologic maps, data bases, Phanerozoic, Proterozoic, Archean, Uganda.

¹ *Westcourt GeoConsult, the Hague Area, the Netherlands;*
e-mail: westcourtgeo@hotmail.es

² *Geological Survey of Finland (GTK), P.O. Box 96, FI-02151 Espoo,*
Finland; e-mail: info@gtk.fi

³ *Geological Survey of Finland (GTK), P.O. Box 77, FI-96101 Rovaniemi,*
Finland; e-mail: info@gtk.fi

⁴ *Department of Geological Survey and Mines, Entebbe, Uganda*

⁵ *Retired from GTK*

⁶ *Norges Geologiske Undersøkelse, Trondheim, Norway*

CONTENTS

| | |
|---|----|
| FOREWORD | 9 |
| SUMMARY | 10 |
| | |
| 1 AFRICA'S MAJOR CHRONO-TECTONO-THERMAL DOMAINS | |
| – THE 'BUILDING BLOCKS' | 15 |
| 1.1 Introduction | 15 |
| 1.2 Archaean Cratons and Mobile Belts | 18 |
| 1.3 Palaeoproterozoic Fold Belts of the Eburnian Orogenic Cycle | 20 |
| 1.4 Palaeoproterozoic post-Eburnian Platform Deposits | 23 |
| 1.5 Mesoproterozoic Grenvillean/ Kibaran Fold Belts | 25 |
| 1.6 Post-Rodinia Neoproterozoic Platform Rocks of the Malagarasi Supergroup | 28 |
| 1.7 Neoproterozoic-Cambrian Pan-African Fold Belts | 32 |
| 1.8 Phanerozoic post-Pan-African Extensional Basins | 38 |
| | |
| 2 LAKE VICTORIA TERRANE OF THE ARCHAEAN TANZANIA CRATON | 44 |
| 2.1 Tanzania Craton | 44 |
| 2.2 Major Lithostratigraphic Units of the Lake Victoria Terrane | 47 |
| 2.2.1 Pre-Nyanzian Basement | 47 |
| 2.2.2 Nyanzian Supergroup | 48 |
| 2.2.3 Syn- to post-Nyanzian granitoids | 48 |
| 2.2.4 Kavirondian Supergroup | 48 |
| 2.2.5 Younger granitoids | 49 |
| 2.3 Lithostratigraphy of the Lake Victoria Terrane in SE Uganda | 49 |
| 2.3.1 Nyanzian Supergroup | 50 |
| 2.3.2 Kavirondian Supergroup | 51 |
| 2.3.3 Synkinematic granitoids of the Lake Victoria Terrane | 52 |
| 2.3.4 Postkinematic intrusives of the Lake Victoria Terrane | 53 |
| 2.3.5 Iganga Suite | 55 |
| 2.3.6 Nabukalu gabbro intrusions | 59 |
| 2.3.7 Geochemistry | 63 |
| 2.4 Geochronology | 64 |
| 2.5 Geodynamic Development | 64 |
| | |
| 3 WEST TANZANIA TERRANE OF THE ARCHAEAN TANZANIA CRATON | 69 |
| 3.1 Introduction – Archaean 'Building Blocks' of Uganda | 69 |
| 3.2 Airborne Geophysical Data | 69 |
| 3.3 Litho-Stratigraphy of the West Tanzania Terrane | 74 |
| 3.3.1 TTG Gneisses | 75 |
| 3.3.2 Tororo Suite | 77 |
| 3.3.3 Kampala Suite | 80 |
| 3.3.4 Kiboga Suite | 81 |
| 3.3.5 Bubulo Formation | 82 |
| 3.4 Geochronology | 83 |
| 3.5 Geodynamic Development of the West Tanzania Terrane | 84 |
| | |
| 4 WEST NILE BLOCK OF THE BOMU-KIBALIAN SHIELD (CONGO CRATON) | 86 |
| 4.1 Introduction | 86 |
| 4.2 Bomu-Kibalian Shield (Congo Craton) | 86 |
| 4.3 Tectono-Thermal Domains of the West Nile Block | 88 |
| 4.3.1 Introduction | 88 |

| | | |
|--------------------------------|--|-----|
| 4.3.2 | Redefinition of tectono-thermal units in the West Nile Block | 90 |
| 4.4 | Lithostratigraphy of the Uleppi Complex | 91 |
| 4.4.1 | Uleppi Group | 92 |
| 4.4.2 | Plutonic Units of the Uleppi Complex | 96 |
| 4.5 | Lithostratigraphy of the War Group (Arua-Kibale Supergroup) | 98 |
| 4.6 | Lithostratigraphy of the Lobule Group and Abiba Formation (Arua-Kibale Supergroup) | 101 |
| 4.6.1 | Lobule Group..... | 102 |
| 4.6.2 | Abiba Formation | 106 |
| 4.6.3 | Plutonic Rocks..... | 106 |
| 4.7 | Lithostratigraphy of the Yumbe Complex | 110 |
| 4.7.1 | Introduction..... | 110 |
| 4.7.2 | Supracrustal rocks of the Yumbe Complex..... | 111 |
| 4.7.3 | Plutonic rocks of the Yumbe Complex..... | 112 |
| 4.8 | Geochemistry..... | 113 |
| Mafic metavolcanic rocks | | 113 |
| 4.9 | Geochronology..... | 117 |
| 4.10 | Tectono-Thermal Evolution of the West Nile Block..... | 118 |
| 5 | ROCKS OF THE NORTH UGANDA TERRANE..... | 121 |
| 5.1 | Introduction | 121 |
| 5.2 | Tectono-Thermal Domains of the North Uganda Terrane | 121 |
| 5.3 | Geology of the Mesoarchaeon Karuma Group of the North Uganda Terrane | 121 |
| 5.4 | Geology of the Neoproterozoic Amuru Group of the North Uganda Terrane | 125 |
| 5.5 | Geology of Neoproterozoic Granitoids and Gneisses of the North Uganda Terrane | 131 |
| 5.6 | Nakasongola-Bukungu Suite..... | 147 |
| 5.7 | Geochronology..... | 148 |
| 5.8 | Tectono-Thermal Evolution of the North Uganda Terrane | 148 |
| 5.8.1 | Archaean development of the NUT | 148 |
| 5.8.2 | Late Mesoproterozoic development of the NUT | 150 |
| 5.8.3 | Neoproterozoic development of the NUT during the Pan-African | 151 |
| 6 | PALAEOPROTEROZOIC ROCKS OF THE RWENZORI FOLD BELT..... | 152 |
| 6.1 | Introduction | 152 |
| 6.2 | Lithostratigraphy of the Palaeoproterozoic Rwenzori Basement | 155 |
| Rukungiri Suite | | 155 |
| 6.3 | Lithostratigraphy of the Palaeoproterozoic Buganda Group | 157 |
| 6.3.1 | Introduction | 157 |
| 6.3.2 | Victoria Formation | 157 |
| 6.3.3 | Nile Formation (incl. Bujagali Member) | 159 |
| 6.4 | Synkinematic Granitoids of the Rwenzori Belt | 165 |
| Sembabule Suite | | 165 |
| 6.5 | Postkinematic Granitoids of the Rwenzori Belt..... | 167 |
| Mubende-Singo Suite | | 167 |
| 6.6 | Lithostratigraphy and Structure of the Rwenzori Block | 170 |
| 6.7 | Geochronology | 174 |
| 6.8 | Tectono-Thermal Evolution of the Rwenzori Belt | 175 |
| 7 | PALAEOPROTEROZOIC POST-RWENZORI PLATFORM SEDIMENTS..... | 180 |
| 7.1 | Introduction | 180 |
| 7.2 | Geology of the Namuwasa Group | 182 |
| 7.2.1 | Introduction..... | 182 |
| 7.2.2 | Lithostratigraphic units..... | 182 |

| | | |
|--------|--|-----|
| 7.3 | Geology of the Bwezigoro Group | 185 |
| 7.3.1 | Introduction | 185 |
| 7.3.2 | Lithostratigraphic units | 185 |
| 7.4 | Geology of the Kagera-Buhjewe supergroup | 187 |
| 7.4.1 | Introduction | 187 |
| 7.4.2 | Lithostratigraphic units | 188 |
| | Muyaga Group | 188 |
| | Ruvubu Group | 191 |
| 7.5 | Geochronology | 193 |
| 7.6 | Geodynamic Development | 194 |
| 8 | ROCKS OF THE MESOPROTEROZOIC NORTH KIBARAN BELT | 199 |
| 8.1 | Introduction | 199 |
| 8.1.1 | Kibaran Belt | 199 |
| 8.1.2 | Short Outline of the South Kibaran Belt | 200 |
| 8.1.3 | Structural Zones of the North Kibaran Belt | 201 |
| 8.2 | Lithostratigraphy of the pre-Kibaran Basement | 202 |
| 8.3 | Lithostratigraphy of the Akanyaru-Ankole Supergroup | 204 |
| 8.3.1 | Introduction | 204 |
| 8.3.2 | Gikoro Group | 208 |
| 8.3.3 | Pindura Group | 211 |
| 8.3.4 | Cyohoha Group | 213 |
| 8.3.5 | Rugezi Group | 216 |
| 8.4 | Plutonic Rocks of the North Kibaran Belt | 218 |
| 8.4.1 | Introduction | 218 |
| 8.4.2 | 'Older' Kibaran granitoids (1.57–1.45 Ga) | 219 |
| 8.4.3 | Plutonic Rocks of the bimodal North Kibaran Igneous Province (1.38–1.33 Ga) | 221 |
| 8.4.4 | A-type granites of the Transition Zone (1.25 Ga) | 226 |
| 8.4.5 | 'Tin granites' and other 'younger granites' (1.10–1.00 Ga) and related pegmatite bodies (0.97 Ga) and quartz veins (0.95 Ga) | 226 |
| 8.5 | Geochronology | 227 |
| 8.6 | Geodynamic Evolution of the North Kibaran Belt | 230 |
| 9 | ROCKS OF THE LATE MESOPROTEROZOIC MADI-IGISI BELT | 236 |
| 9.1 | Introduction | 236 |
| 9.2 | Lithostratigraphy of the Madi Group | 236 |
| 9.3 | Lithostratigraphy of the Igisi Group | 244 |
| 9.4 | Geochronology | 253 |
| 9.5 | Geodynamic Evolution of the Madi-Igisi Belt | 254 |
| 10 | POST-RODINIAN NEOPROTEROZOIC PLATFORM ROCKS OF THE MALAGARASI SUPERGROUP | 263 |
| 10.1 | Malagarasi Supergroup | 263 |
| 10.2 | Geology of the Mityana Group | 264 |
| 10.2.1 | Introduction | 264 |
| 10.2.2 | Lithostratigraphy of the Mityana Group | 265 |
| 10.3 | Geology the Bunyoro Group | 267 |
| 10.3.1 | Introduction | 267 |
| 10.3.2 | Lithostratigraphy of the Bunyoro Group | 268 |
| 10.4 | Geochronology | 275 |
| 10.5 | Geodynamic Evolution of the Bunyoro Group | 275 |

| | |
|--|-----|
| 11 ROCKS OF THE KARAMOJA BELT AND OTHER ROCKS OF THE NEOPROTEROZOIC | |
| PAN-AFRICAN CYCLE | 279 |
| 11.1 Introduction | 279 |
| 11.2 Karamoja Belt (East Africa Orogen) | 279 |
| 11.3 Lithostratigraphy of the Karasuk Supergroup | 282 |
| 11.3.1 Ophiolites from the Neoproterozoic Mozambique Ocean | 284 |
| 11.3.2 Metasediments from the post-Rodinia passive margin | 284 |
| 11.3.3 Rocks of the syn-collisional magmatic arc | 286 |
| 11.3.4 Rocks of uncertain derivation | 286 |
| 11.4 Geology of the West Karamoja Group | 288 |
| 11.4.1 Introduction | 288 |
| 11.4.2 Structural subdivision of the West Karamoja Complex | 288 |
| 11.4.3 Lithostratigraphy of the West Karamoja Group | 289 |
| 11.4.4 Intrusive rocks of the West Karamoja Complex | 297 |
| 11.5 In-situ Intrusive Rocks in the Karamoja Belt | 302 |
| 11.6 Other Pan-African Granitoids in North Uganda | 305 |
| 11.7 Lithogeochemistry | 309 |
| 11.8 Aswa Shear Zone | 310 |
| 11.8.1 Introduction | 310 |
| 11.8.2 Textures and Structures within the ASZ | 310 |
| 11.9 Geochronology | 314 |
| 11.10 Geodynamic Development during the Pan-African Orogenic Cycle | 315 |
| 11.10.1 Introduction | 315 |
| 11.10.2 Karamoja Belt | 316 |
| 11.10.3 Geodynamic development of the Aswa Shear Zone | 320 |
| 12 POST-PAN-AFRICAN PHANEROZOIC DEPOSITS: KAROO, EAST AFRICAN RIFT | |
| SYSTEM AND QUATERNARY DEPOSITS | 323 |
| 12.1 Introduction | 323 |
| 12.2 Palaeozoic–Mesozoic Karoo Supergroup | 323 |
| 12.2.1 Introduction | 323 |
| 12.2.2 Lithology of Karoo Supergroup in Uganda | 324 |
| 12.2.3 Geodynamic development | 325 |
| 12.3 Cenozoic Lithologies of the East African Rift System | 326 |
| 12.3.1 Introduction | 326 |
| 12.3.2 Neogene Elgon Complex (Eastern branch of EARS) | 327 |
| 12.3.3 Albertine Supergroup (Western branch of EARS) | 337 |
| 12.3.4 Geodynamic setting of the EARS volcanics in Uganda | 357 |
| 12.4 Quaternary deposits outside the EARS | 360 |
| 12.4.1 Introduction | 360 |
| 12.4.2 Stratigraphy of Pleistocene and Holocene Deposits | 361 |
| Acknowledgement | 364 |
| References | 365 |

Appendices

- App. 1: Tectono-Thermal Units of Uganda 1:2 500 000
- App. 2: Representative chemical whole-rock analyses

Back cover envelope

Geological Map of Uganda 1:1 000 000

FOREWORD

During the period 2008–2012 Uganda has been remapped in the framework of two projects both named “*Geological mapping, geochemical surveys and mineral resources assessment in selected areas of Uganda*”, a component of the World Bank Group funded “*Sustainable Management of Mineral Resources Project (SMMRP)*”, of which the mapping component in the southern part of the country (south of 1° N) was funded by the World Bank/ International Development Agency and in the northern part (north of 1° N) by the World Bank/ Nordic Development Fund. Both projects were executed by a consortium¹ headed by the Geological Survey of Finland (GTK) in close cooperation with the Department of Geological Survey and Mines (DGSM) in Entebbe.

Implementation of the mapping projects was facilitated by extensive usage of up-to-date information technology, satellite imagery and recently gathered aerogeophysical data (magnetic and radiometric), which covers 80% of the country, save the Karamoja area along the border with Kenya. This, together with field observations, limited thin section and geochemistry studies, and re-evaluation of the existing knowledge base (publications, unpublished reports, maps) produced by geologists in the past who have spent decades mapping the territory of Uganda, has resulted in digital seamless radiometric, magnetometric, geologic and metallogenetic maps, 11 map explanations (GTK Consortium 2012a–k), a huge data base with some 13 500 GPS-controlled observation stations (with digital photographs of rock exposures) and some 50 U-Pb zircon ages. Hard copies of maps at scales 1:250 000, 1:100 000 and for some areas with mineral potential at scale 1:50 000 as well as all the related data can be obtained from DGSM in Entebbe.

This publication is based on the accrued new data from the above projects. It is the first modern account of the bedrock geology of Uganda and its geodynamic development in one volume by one coherent team of experts. This volume includes a new geological map (Lehto et al. 2014), scale 1:1,000,000, more than 50 years after the first 1:1.5 M map by Robert Macdonald, published by the DGSM in 1966.

Mapping projects, like all other projects, have a start and a closing date. Remapping Uganda has resulted in a major leap forward in understanding its geology and geodynamic development. But due to limitations in time and funding many knowledge gaps remain to be filled. Much more geochronological, structural, petrologic and geochemical data is needed to complete the picture. The present publication must therefore be considered as an interim report of ‘work in progress’, covering the northeastern corner of the Congo proto-Craton, presumably one of the least known segments of the Earth crust.

The geology of Uganda is very varied and spans more than three billion years. It comprises Mesozoic and Neoproterozoic lithospheric fragments, welded together by Palaeo-, Meso- and Neoproterozoic fold belts. Neogene extension gave rise the development of the East African Rift System with emplacement of some of the world’s most potassium-rich rocks in its Eastern Branch. The latter, of which the northern segment is called the Albertine Rift, is also the locus of the Rwenzori Mountains, a promontory of up to 5109 m in altitude and most extreme expression of rift-flank uplift on earth.

In order to sketch the geodynamic development of Uganda and to properly describe the multitude of lithostratigraphic units, their hierarchy and mutual relationships, the territory has been divided into a limited number of building blocks or tectono-thermal terranes (see below and App. 1). These terranes have been identified by integrating regional tectonics, metamorphism, magmatism and geochronology with geophysical data (magnetic, gravity and seismic). Each terrane is characterised by a specific geodynamic evolution. Terranes and terrane boundaries – the lithospheric architecture – are fundamental in understanding the geology and the constructional history of Uganda (or any other part of the Earth crust). In addition, terrane boundaries – in particular between tectono-thermal domains with different types of Subcontinental Lithospheric Mantle (SCLM) – have a strong influence on crustal tectonics and are important from an economic point of view: they constitute first order fault/ shear zones that can tap lithospheric-scale hydrother-

¹ Other members of the consortium were CGS (Pretoria, RSA), GAF (Munich, Germany), ITC (Enschede, the Netherlands) and FCL (Entebbe, Uganda).

mal fluids from deep crustal sources into favourable metallogenetic traps through interconnections of first- and second-order fault/ shear zones. As such they may have important implications for

the distribution of major ore bodies. An understanding of crust-mantle linkages and lithospheric architecture is therefore of direct economic relevance.

SUMMARY

In Chapter 1 Africa's major tectono-thermal terranes or 'building blocks' are outlined. Their evolution is viewed in terms of Supercontinent or Wilson Cycles. Although some overlap may exist it is justifiable to translate the above cycles into alternating periods of bulk crustal extension and compression on global and continental scales. Each cycle produces a variable amount of juvenile crust and partial reworking of older crust. Hence, these cycles are associated with alternating periods of enhanced and reduced continental crust formation.

Unknown continental assemblies formed during the Archaean, mainly at 2.7 to 2.6 Ga. Stable Archaean cratonic nuclei were progressively sutured into successively larger cratons during the Proterozoic and, ultimately, assembled in supercontinents together with the formation of elongated mobile belts. These cycles include the Palaeoproterozoic Eburnian with two major compressional phases at 2.10–2.03 Ga (Eburnian I) and ~1.95 Ga (Eburnian II), culminating in the Columbia (or Nuna) Supercontinent. This was followed by the mainly Mesoproterozoic Grenvillian Cycle, resulting in the Rodinia Supercontinent at 1.2–1.0 Ga and finally the mainly Neoproterozoic Pan-African Cycle, culminating in Gondwana at 650–550 Ma and subsequently Pangea (450–250 Ma). Undeformed basin successions have been preserved in between the anastomosing network of Proterozoic fold belts.

Phanerozoic compression in Africa was strictly local, confined to the southern and northwestern margins of the continent, with most of Africa being affected by extensional forces, giving rise to Gondwanide (542–318 Ma), Karoo (318–180 Ma) and post-Karoo basins. The latter can be divided into three sub-phases: (1) Early Cretaceous break-up, (2) stabilisation between ~100 Ma and ~35 Ma and ultimately (3) Late Eocene-Neogene rifting and development of the East African Rift System.

The Archaean basement of Uganda was created during prolonged and multiple phases of crust

formation, mainly between >3.08 Ga and 2.55 Ga, a period of over 500 million years. This basement can be attributed to the Tanzania Craton and the Bomu-Kibalian Shield, two major 'building stones' belonging to the Congo proto-Craton. We have divided the Archaean basement of Uganda into:

- (1) *Lake Victoria Terrane* (LVT, Chapter 2 and App. 1) of the Tanzania Craton: a classical Neoproterozoic granite-greenstone terrane. Greenstones of the Ugandan segment of this terrane include the volcanic-dominated Nyanzian Supergroup and the sediment-dominated Kavi-rondian Supergroup. Granitoids are mainly syn-kinematic (~2.63 Ga) and 'Younger Granites' (2.59 Ga). This terrane also comprises a nepheline syenite body (2.63 Ga) and several, newly discovered oval-shaped gabbro intrusions (2.61 Ga).
- (2) *West Tanzania Terrane* (WTT, Chapter 3) of the Tanzania Craton: This is a vast and slightly older but also Neoproterozoic (2.65–2.64 Ga) granito-gneissic-migmatitic terrane in central-southern Uganda. The WTT and the overlying rocks of the Palaeoproterozoic Rwenzori Belt correspond with an anomalous magnetic zone, separating it from the LVT (south) and North Uganda Terrane, NUT (north). The WTT has been divided into three major map units: (1) TTG gneisses, (2) Tororo Suite and (3) Kampala Suite. Particularly the TTG gneisses contain locally abundant enclaves showing older, pre-migmatite deformation, confirmed by zircons yielding ages of 3.2 Ga or possibly even 3.6 Ga. Small granitoid and feldspar porphyry bodies of the 2.49 Ga Kiboga Suite have been emplaced into the northern suture – the Nakasongola Discontinuity – with the NUT, supposedly reflecting transtensional rejuvenation of this contact zone.
- (3) *West Nile Block* (WNB, Chapter 4) constitutes the eastern, Ugandan segment of the

Bomu-Kibalian Shield (or NE Congo-Uganda Block) of northeastern Congo. The Archaean rocks of the WNB have been traditionally divided between 2.9 Ga 'Watian' granulites and 2.59–2.55 Ga 'Aruan' gneisses (all Rb-Sr ages). New U-Pb zircon data has evidenced that the WNB comprises a Mesoarchaeoan core, assembled in the Uleppi Complex, composed of granulites (> 3.08 Ga) and associated charnockites. This Mesoarchaeoan core has accreted with Neoproterozoic rocks of the Arua Complex, comprising mainly amphibolite-grade supracrustals of the Lobule Group, variable gneissose granitoids (2.65 Ga), charnockites (e.g. 'Tara brown granite' > 2.63–2.62 Ga) and extensive 'younger gneissose granitoids' (2.59 Ga). Mafic volcanic and subvolcanic rocks and subordinate associated sediments of the Neoproterozoic (~2.64 Ga) War Group, have intruded or deposited unconformably on top of the Uleppi Group. Some Archaean rock bodies (e.g., Yumbe Complex) occur as allochthonous slabs that have been tectonically emplaced during the much younger 'Mirian' (~1.0 Ga) tectonic phase. Based on U-Pb zircon data we postulate accretion of the Uleppi and Arua Complexes at 2.7–2.6 Ga, followed by a younger event at 2.58 Ga.

- (4) *North Uganda Terrane* (NUT, Chapter 5). This tectono-thermal unit is separated from the WNB in the west by the ~1.0 Ga Madi-Igisi Belt, from the WTT in the south by a complex Archaean suture – the Nakasongola Discontinuity – and bounded in the north and east by Pan-African fold belts. The terrane comprises a small segment of Mesoarchaeoan (2.99 Ga) crust composed of granulites of the Karuma Complex in the Masindi area. The bulk of the NUT is composed of Neoproterozoic rocks that have been divided into supracrustals of the Amaru Group and some 20 units of igneous or uncertain derivation with ages ranging from 2.73 (Kaseeta granite) to 2.61 Ga. Summarising the geochronological data from this terrane, we conclude that most gneissose-migmatitic rocks have U-Pb zircon ages between 2.6 and 2.5 Ga but frequently older inherited zircons with 'Kaseeta' ages have been encountered. Examples are Gulu banded gneiss (2.7 Ga), Awela granite (> 2.83 Ga and > 2.73 Ga) and TTG granites (~2.79 Ga). The Katakwi granite contains a zircon with a 2.74 Ga core, surrounded by a 2.62–2.63

Ga rim. Less deformed, non-migmatitic granitoids such as the Katakwi granite, are believed to have formed from partial melting of 2.6–2.5 Ga orthogneissose-migmatitic rocks. Metamorphic U-Pb zircon ages of 2.58 Ga have been encountered in several samples.

Based on the scarce geochronological data at hand we postulate the formation of Mesoarchaeoan crust (Uleppi and Karuma Complexes) prior to 3.07 Ga. Maximum zircon ages of ~3.00 Ga and 2.87 Ga possibly represent the timing of peak granulite-grade metamorphism. This was followed by a thermal event at 2.73 Ga (emplacement of the Kaseeta granite), accretion with Neoproterozoic crust in the area around 2.64–2.61 Ga, together with emplacement of mafic volcanics of the War and Amaru Groups and, finally, accretion with the LVT at 2.59 Ga to 2.55 Ga. Late Archaean (2.49 Ga) lithologies of the Kiboga Suite are most likely related to a post-kinematic transtensional event, effecting the suture between the WTT and NUT.

Archaean crust formation in Uganda was followed by a long period of quiescence. The post-Archaean geological evolution of Uganda can best be viewed in the context of the evolution of the entire proto-Congo Craton, composed of several Archaean terranes and Palaeoproterozoic mobile belts. Unlike the Palaeoproterozoic fold belts covered by Phanerozoic sediments of the Congo River Basin, the Usagaran-Ubendian-Rusizian-Rwenzori system of fold belts (2.1 to 1.85 Ga), wrapping around the Tanzania Craton, is widely exposed. Eclogite-facies metamorphism and the formation of an Andean-type calc-alkaline magmatic arc in the Usagaran-Ubendian segment of this fold belt manifest oceanic crust subduction, collision and amalgamation of the Tanzania and Congo Cratons. In Uganda the Palaeoproterozoic Eburnian Cycle is expressed by:

- (5) *Rwenzori Fold Belt* (Chapter 6) comprising an older (2.21–2.15 Ga) gneissose/ granitoid basement assembled in the Rukungiri Suite (Eburnian I) that can be correlated with Rusizian and Ubendian rocks further south. This is covered by metasediments and mafic, partly pillow-textured volcanics of the Buganda Group (~2.00 Ga to 1.95 Ga) into which syn-tectonic granitoids of the Sembabule Suite (1.99–1.96 Ga) and post-tectonic granitoids of

the Mubende-Singo Suite (1.85 Ga) have been emplaced (Eburnian II).

The Eburnian Orogenic Cycle in Uganda and neighbouring areas was followed almost immediately by deposition of:

- (6) *Platform rocks of the Namuwasa and Bwezigoro Groups and Kagera-Buhweju Supergroup* (Chapter 7): Field evidence and U-Pb data from detrital zircons of the post-tectonic molasse-type sediments of the Namuwaza Group indicate deposition, burial and deformation between < 2.05 Ga and >1.85 Ga. The Bwezigoro Group was deposited after 1.97 Ga and may be 50 million or 200 years younger than the rocks of the Namuwasa Group. Deposition of similar molasse-type deposits of the Kagera-Buhweju Supergroup started at 1.79 Ga. Field verification has further indicated that the rocks of the above units have been subjected to complex tectonic processes.

After a lull of 200 million years, the mainly Mesoproterozoic Grenvillean Cycle is expressed by continued rifting and basin formation. The centre of deposition, compared to the sediments of the Namuwasa and Bwezigoro Groups and the Kagera-Buhweju Supergroup, shifted south- and westwards, spatially coinciding with the Palaeoproterozoic suture between the Tanzania and Congo Cratons. Extension started around 1.55 Ga but deposition rates in the North Kibaran trough accelerated during a relatively short interval around 1.38 Ga with the emplacement of the North Kibaran Igneous Province (NKIP), allegedly related to a thermal (mantle) anomaly and giving rise to a coeval phase of bimodal magmatism. Inversion of this trough gave rise to formation of the:

- (7) *North Kibaran Belt* (~1.55–0.95 Ga; Chapter 8), comprising abundant S-type, peraluminous granitoids that can be divided into scarce 'older' Kibaran granitoids (1.57–1.45 Ga) and abundant granitoids of the bimodal North Kibaran Igneous Province (1.40–1.33 Ga). The latter comprises the Kabanga-Musongati alignment of mafic and ultramafic layered complexes (1.40–1.38 Ga) and mafic dykes and sills, including the huge Lake Victoria Arcuate Dyke Swarm (LVADS; 1.37 Ga). These igneous rocks are more or less coeval with a thick pile of

metasediments of the Akanyaru-Ankole Supergroup with a total thickness estimated to range from 9 to 14.5 km in the centre of the North Kibaran trough (e.g., in central Rwanda) to a few kilometres in the east (e.g., NW Tanzania). Subordinate felsic volcanics yield a poorly constrained Whole Rock (WR) Rb-Sr age of 1353 ± 46 Ma. The Akanyaru-Ankole metasediments have been invaded by minor A-type granites (1.25 Ga) and largely sub-outcropping so-called 'tin granites' (1.10–1.00 Ga) and related pegmatite bodies (0.97 Ga) and quartz veins (0.95 Ga).

- (8) *Madi-Igisi Belt* (Chapter 9) in NW Uganda. This is a newly identified, rather narrow, intracratonic, N-S-trending, double-verging thrust and shear belt, separating the WNB from the NUT. It comprises a thin- or thick-skinned stack of undated, but presumably reworked Archaean rocks of the WNB and/or NUT – e.g., the Yumbe duplex structure – and juvenile lithologies. The latter are assembled in Mirian Supergroup, comprising variably metamorphic volcanics (0.98 Ga), metasediments (< 1.0 Ga) and rare ultramafics of the Madi and Igisi Groups. Monazite blastesis with ages between 0.66 Ga to 0.62 Ga point to widespread Pan-African reworking, most likely a far-field effect of E-W compression in the Karamoja Belt, followed by N-S compression due to collision with the Sahara meta-Craton (see below). Intriguing is the occurrence of lenses of metamorphosed and metasomatised ultramafic rock in a strike-slip fault zone east of the Madi-Igisi Belt, between the town of Moyo and Lake Albert.

Post-Rodinia, early Neoproterozoic extension affected the proto-Congo Craton, giving rise to the development of intracratonic troughs with deposition of clastic sequences and local (alkaline or CFB) volcanism. The rift to drift phase during early divergence along the southern margin of the proto-Congo Craton took place between 880 and 820 Ma, followed by a second depositional cycle starting at ~765 Ma. Along the western margin of the Tanzania Craton this gave rise to deposition of:

- (9) *Platform Rocks of the Malagarasi Supergroup* (Chapter 10) of western Tanzania and eastern Burundi. Deposition started prior to 0.89 Ga and was concluded with deposition of glaciogene diamictites, resting on dated continental

flood volcanics with an age of 0.82–0.79 Ga. Molasse-type deposits of the Mityana Group and younger glacial to periglacial rocks of the Bunyoro Group in Uganda have been correlated with the Malagarasi Supergroup, with the first having an age between 0.89 and 0.79 Ga and rocks of the Bunyoro Group supposedly coeval with the global Sturtian glaciation dated between 765 and 735 Ma.

Orogenic processes pertaining to the Neoproterozoic Pan-African Orogenic Cycle (~0.90–0.55 Ga), culminating in the creation of the Gondwana Supercontinent, took place along the proto-Congo Craton margins, although weakness zones (e.g., former sutures) within the craton have been extensively rejuvenated. Pan-African collisional belts affecting Uganda include the East African Orogen (EAO) in the east and the Oubangides or Central African Fold Belt (CAFB) in the north.

- (10) *Karamoja Belt and other rocks of the Pan-African Orogenic Cycle* (Chapter 11): Collision between and amalgamation of East and West Gondwana gave rise to development of the East African Orogen, in eastern Uganda represented by the Karamoja Belt. Traditionally, juvenile allochthonous rocks of the Karamoja Belt have been attributed to the Karasuk Series, renamed Karasuk Supergroup, composed of a W- to NW-verging, stacked pile of thrust amphibolite-grade supracrustals (0.58 Ga), granitoids and ophiolites and interleaved slices of older crust. The supracrustal rocks include calc-alkaline metavolcanics with island-arc affinity (0.66 Ga) that have been intruded by granitoids (0.59 Ga, all WR Rb/Sr ages).

The Karamoja Belt also comprises the allochthonous rocks of the newly identified West Karamoja Group, characterised by the presence of ultra high temperature (UHT) granulites and 0.74–0.68 Ga charnockites.

The brittle-ductile Aswa Shear Zone (ASZ) is a prominent NW-trending, mega strike-slip shear zone, composed of a complex, anastomosing set of fault planes with maximum strain (blastomylonites and pseudotachylites) and non- or weakly deformed lozenge-shaped blocks in between. The ASZ mimics the Pan-African geodynamic processes that took place in the area, comprising (1) oblique collision (~0.69 Ga) with escape of the northeastern segment of the NUT, followed by transtension

(0.66 Ga), possibly related to N-S compression (see below) and late Pan-African final docking events (till 0.49 Ga).

Finally, a number of *in situ* Pan-African granitoid bodies of the Midigo-Adjumani Suite (0.66 Ga) have been identified in the northernmost part of Uganda (in the WNB and NUT). We tentatively relate these intrusives to the southward subduction of the Sahara meta-Craton below the already united East + West Gondwana lithospheric plates with development of the E-W-trending Central African Fold Belt or Oubangides.

As mentioned, Pan-African deformation was restricted to the margins of the proto-Congo Craton. Notwithstanding the above, reworking of pre-Pan-African lithologies, including rocks belonging to the various Archaean terranes in Uganda, is manifested by secondary zircon rim growths with (poorly constrained) ages between 0.8 and 0.4 Ga. Pan-African reworking was particularly strong in older intracratonic weakness zones such as the North Kibaran and Igisi-Madi Belts, even to the extent that metallogenesis of structurally-hosted gold deposits in the Mesoproterozoic North Kibaran Belt is considered either a two-stage, late Kibaran/Pan-African, process or mainly Pan-African, dated at 0.64 Ga (WR Rb/Sr isochrone age). Monazite from Burundi yielded a U-Pb age of 0.54 Ga, comparable with monazite from the Madi-Igisi Belt with ages of 0.66–0.62 Ga.

The Phanerozoic evolution (Chapter 12) of the African plate, including the proto-Congo Craton, can be viewed in terms of the polyphase break-up of the Gondwana Supercontinent, which preferentially took place through reactivation of Pan-African and older sutures. Three major phases of Phanerozoic crustal extension and basin development can be distinguished: (1) Gondwanide, (2) Karoo and (3) post-Karoo, eventually giving rise to development of the East Africa Rift System (EARS).

- (11a) *Gondwanide extension* between 570 Ma and 290 Ma is expressed within the proto-Congo Craton by deposition of pre-Karoo Red Beds, approximately 1000 m in thickness, in the Congo River Basin and by emplacement of a number of post-Pan-African (~0.55 to ~0.44 Ga) alkaline complexes along a weakness zone

that developed later into the Western Branch of the East African Rift System.

- (11b) *Karoo basins* (290–180 Ma) in southern Uganda are restricted to a few small occurrences, but may have covered much more extensive areas prior to EARS uplift and erosion.

Post-Karoo extension can be divided into three phases: (1) Early Cretaceous break-up, (2) stabilisation between ~100 Ma and ~35 Ma and (3) Late Eocene-Neogene neo-rifting. Early Cretaceous break-up gave rise to opening of the South Atlantic and separation of the São Francisco Shield (Brazil) from the proto-Congo Craton. This extensional phase is further manifested by emplacement of a clan of carbonatites and associated peralkaline rocks, called the Chilwa Alkaline Province (~133 Ma to ~110 Ma) and a family of ~140 Ma kimberlites in East Africa, but outside Uganda. Late Eocene-Neogene rifting and development of

the East African Rift System (EARS) in Uganda is expressed by:

- (11c) *Elgon Complex* deposited in the linear Elgon Depression of eastern Uganda, comprising a subordinate sequence of basal sediments, covered by a huge pile of predominantly pyroclastic and lahar-type alkaline/ sodic volcanic rocks and associated carbonatite plugs and fenites of Neogene (20–18 Ma) age.
- (11d) *Albertine Group* laid down in the Albertine Rift, i.e., the northern segment of the Western Rift of the EARS. It is filled by a relatively thick (4 km), hydrocarbon-bearing sequence of terrigenous sediments of Miocene-Recent age (< ~16 Ma), alkaline/ sodic volcanics of Oligo-Miocene age (~28–9 Ma) and ultrapotassic and carbonatitic volcanic rocks of Pleistocene-Holocene age. Rift tectonics also gave birth to the mighty Rwenzori Mountains.

1 AFRICA'S MAJOR CHRONO-TECTONO-THERMAL DOMAINS – THE 'BUILDING BLOCKS'

1.1 Introduction

The lithosphere is the relatively rigid outer shell of the Earth separated by the asthenosphere from its lower mantle and core. Continental lithosphere is composed of sialic crust and subcontinental lithospheric mantle (SCLM). The SCLM is composed of peridotite (mainly olivine + orthopyroxene \pm clinopyroxene) and varies widely in thickness, from a few tens of kilometres beneath rift zones to > 250 km below some Archaean cratons. Unlike peridotite of the relatively young ocean floors, Re-Os isotopes show that SCLM of Archaean cratons is as old as the oldest crustal rocks (Carlson et al. 1999, Griffin et al. 2004). By integrating African regional tectonics, geochronology and geophysical data (magnetic, gravity and seismic), major lithospheric domains or tectono-thermal terranes¹ (Fig. 1.1; Begg et al. 2009) or 'building blocks' (Westerhof 2006) can be identified, each characterised by a specific geodynamic evolution.

The evolution of these major 'building blocks' can be viewed in terms of Wilson Cycles (Wilson 1966, Hartz & Torsvik 2002, Stern 2004) or Supercontinent Cycles (Rogers & Santosh 2003, Condie 2007, 2008). In its simplest form a Wilson or Supercontinent Cycle involves the break-up of a supercontinent into smaller continental blocks, followed by re-assembly of these fragments into a new supercontinent. Each cycle produces a variable amount of juvenile crust. Hence, these cycles are associated with alternating periods of enhanced and reduced continental crust formation. Supercontinents last approximately 150 million years after complete assembly and both assembly and break-up occur diachronously (Li et al. 2008). Most models of the Wilson Cycle suggest that continental break-up and fragmentation is caused by shielding of the mantle by a large plate that carries the supercontinent which, in turn, results in mantle upwelling beneath the plate during a period of 200–500 million years (Gurnis 1988, Lowman & Jarvis 1999, Condie 2002). Mantle plumes, developing in a mantle upwelling (Courtillot et al. 1999, Golonka & Bocharova 2000), in combination with pre-existing weakness zones of

crustal or lithospheric dimension define the actual sites of fragmentation.

Unknown crustal assemblies formed during the Archaean, mainly from 2.7 to 2.5 Ga. Stable Archaean cratonic nuclei were progressively sutured into successively larger cratons during the Proterozoic and, ultimately, assembled in supercontinents together with the formation of elongated mobile belts. Supercontinent cycles include the Palaeoproterozoic Eburnian with two major compressional phases at 2.10–2.03 Ga (Eburnian I) and ~1.95 Ga (Eburnian II), culmination in the Columbia (or Nuna) Supercontinent. This was followed by the mainly Mesoproterozoic Grenvillian Cycle (1.3–0.9 Ga), resulting in the Rodinia Supercontinent at ~1.0 Ga and finally the mainly Neoproterozoic Pan-African Cycle (750–530 Ma), culminating in Gondwana and subsequently Pangea (450–250 Ma) (Condie 1998, 2000, 2001). The youngest orogenic peak at 100–50 Ma, as expressed by the Alpine-Himalayan-Cordilleran fold belts, can be considered as the first step in the formation of a future supercontinent. As mentioned, periods of fragmentation (at one location) and collision (at another location) may overlap. The coeval development of the East African Rift System (EARS) and the continuous movement of the Indian Craton below Asia may serve as a modern analogue. Nevertheless it is justifiable to translate the above cycles into alternating periods of bulk crustal extension and compression on global and continental scales, each characterised by specific geodynamic processes.

Mantle-derived xenoliths and the distribution of diamonds (Janse 1994) manifest that the nature of the SCLM is related to the tectono-thermal age of the overlying continental crust, i.e., the timing of the last major tectono-thermal event (Griffin et al. 1998, 1999, O'Reilly et al. 2001). Archaean SCLM is strongly depleted in basaltic components, with Mg-rich olivine and pyroxenes. SCLM with an age roughly between 2.5 and 1.0 Ga is only mildly depleted relative to primitive mantle compositions. SCLM younger than 1.0 Ga tends to be intermediate between these two extremes. The

¹ In this Special Paper 'terrain' refers to a geographical area, whereas 'terrane' is used to indicate a distinct geodynamic element.

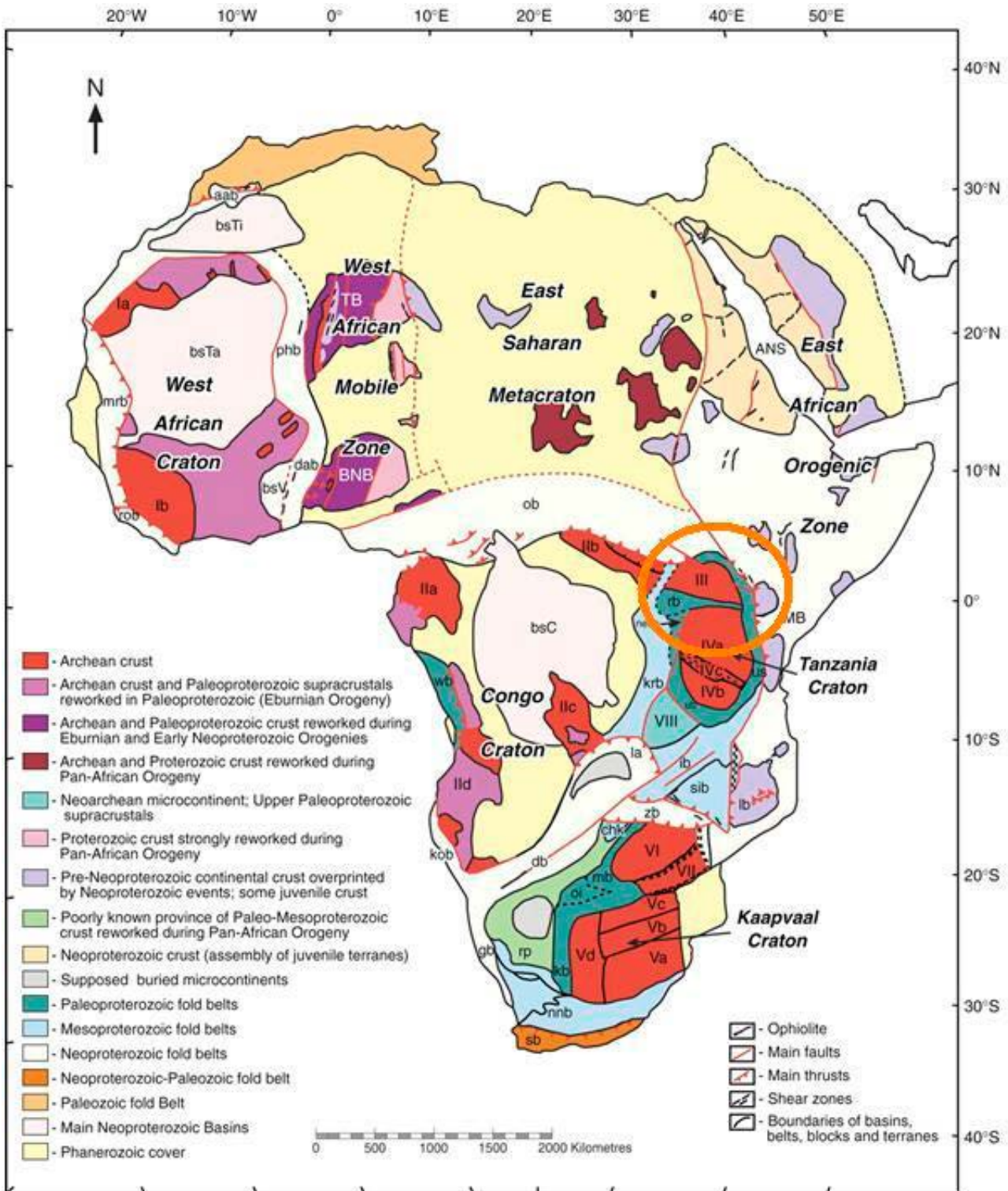


Fig. 1.1. Map of the tectono-thermal domains of Africa (after Begg et al. 2009). Orange circle indicates approximate position of Uganda. **Cratons and Micro-continents:** West African Craton (Ia-Reguibat Shield; Ib—Man-Lèò Shield); Congo Craton (IIa-Gabon-Kameroun Shield; IIb-Bomu-Kibalian Shield; IIc-Kasai Shield; IId-Angolan Shield); Ugandan Craton-III; Tanzanian Craton (IVa-Northern Terrane; IVb-Southern Terrane; IVc-Dodoma Zone); Kaapvaal Craton (Va-Southern Terrane; Vb-Central Terrane; Vc-Pietersburg Terrane; Vd-Western Terrane); Zimbabwe Craton-VI; Limpopo Block-VII; Bangwuelu Block-VIII. **West African Mobile Zone:** TB-Tuareg Block; BNB-Benin-Nigerian Block. **East African Orogenic Zone:** ANS-Arabian-Nubian Shield; MB-Mozambique Orogenic Belt. **Fold Belts: Palaeoproterozoic Belts:** ub-Ubendian; us-USagaran; rb-Rwenzori; kb-Kheis; oi-Okwa inlier; mb-Magondi; wb-West Central African; nekb-North-Eastern Kibaran. **Palaeo-Mesoproterozoic Province:** rp-Rehoboth. **Mesoproterozoic Belts:** krb-Kibaran; ib-Irumide; sib-Southern Irumide; chk-Chomo-Kolomo; nnb-Namaqua-Natal. **Neoproterozoic Belts:** zb-Zambezi; la-Lufilian arc; db-Damara; kob-Kaoko; gb-Gariep; ob-Oubanguides; aab-Anti-Atlas; phb-Pharusian; dab-Dahomeyan; rob-Rockellides; mrb-Mauritanides; lb-Lúrio; sb-Saldania. **Neoproterozoic Basins:** bsC-Congo; bsTa-Taoudeni; bsTi-Tindouf; bsV-Volta.

secular evolution of the SCLM may reflect changes in the processes that produce juvenile SCLM, or the progressive refertilisation of old SCLM, or both (Griffin et al. 2003, Beyer et al. 2006). Regardless of the interpretation, this broad correlation between crustal history and SCLM composition implies a strong linkage between crust and mantle and the processes affecting both, over time spans measured in eons.

The secular evolution of SCLM composition has major consequences for the nature of crustal tectonics through time. Archaean SCLM is buoyant relative to the underlying asthenosphere, and this buoyancy may have played an important role in the stabilisation of cratons (Poudjom Djomani et al. 2001). Being less depleted, SCLM with an age between 2.5 and 1.0 Ga is buoyant relative to the asthenosphere as long as its geotherm remains elevated, but on cooling it is likely to become unstable and may delaminate and sink.

At some convergent margins, crustal thickening and the transformation of mafic lower crust to eclogite may result in a more continuous drip-style of lithosphere removal (e.g., Sobolev & Babeyko 2005). In either case, the ensuing upwelling of asthenospheric material can lead to widespread crustal melting. Refertilisation of older SCLM by asthenosphere-derived melts leads to an increase in SCLM density, enhancing the probability of de-

lamination. The nature and history of the SCLM therefore will affect the response of the overlying crust to tectonic stresses.

Lithospheric architecture and in particular the presence of boundaries between tectono-thermal domains with different types of SCLM, will be important in controlling crustal tectonics and, especially, the transport of fluids and magmas from depth. This control may have important implications for the distribution of major ore deposits. An understanding of crust-mantle linkages and lithospheric architecture is therefore of direct economic relevance.

Following the above ideas, one can view Africa as being largely composed of a mosaic of Archaean cratons and mobile belts (3.8–2.5 Ga), amalgamated by elongated, continental-scale, mainly Proterozoic fold belts (2.5 Ga – 542 Ma). Phanerozoic deformation (< 542 Ma) is restricted to the north-eastern (the Hercynian Mauritides and Alpine Betic-Rif-Kabylian orocline) and southern extremes (the Hercynian Cape Fold Belt) of the African plate. Undeformed basin successions are found in between this anastomosing network of folds belts. These include Archaean (e.g., the Witwatersrand Basin, the world's largest gold depository), Palaeoproterozoic (e.g., the Kagera-Buhweju Supergroup, Muva Group), Mesoproterozoic and Neoproterozoic intracratonic basins (e.g., the Malagarasian)

Table 1.1. Africa's major chrono-tectono-thermal cycles (adapted from Westerhof 2006).

| | Event/Cycle | | Era | Age (Ma) |
|---|-----------------------------------|--------------------------|-------------------------------------|------------|
| E | Late post-Karoo rifts | EARS | Latest Eocene - Present | ~35–0 |
| E | Early post-Karoo rifts | Initial Phase | Late Jurassic – Early Cretaceous | ~165--~100 |
| E | Gondwanide Basins | Karoo Basins/ Rifts | Late Carboniferous – Early Jurassic | 318–180 |
| E | | Post-Pan-African Basins | Cambrian – Late Carboniferous | 542–318 |
| C | Pan-African | Pan-African Orogeny | Neoproterozoic- Cambrian | 750–490 |
| E | | Post-Rodinia Basins | Neoproterozoic | 900–700 |
| C | Grenvillean | Kibaran Belt | Mesoproterozoic | 1450–950 |
| E | | Post-Eburnian Basins | Palaeoproterozoic | <2050–1795 |
| E | Eburnian | Post-tectonic granitoids | Palaeoproterozoic | ~1860 |
| C | | Late Tectonic Phase | | ~1950 |
| E | | Buganda Basin | | >1950 |
| C | | Early Tectonic Phase | | 2100–2025 |
| E | | Post-Archaean Basins | | < 2500 |
| C | Archaean Cratons and Mobile Belts | | Neoarchaeon | 2900–2500 |
| C | | | Mesoarchaeon | 3200–2900 |

Key: C = compression; E = extension; EARS = East African Rift System.

and Phanerozoic basin and rift structures (Karoo and East Africa Rift System). The 'building blocks' are presented in Table 1.1 (mainly after Gabert

1984, Dirks & Ashwal 2002) and Fig. 1.1 (Begg et al. 2009) and will be briefly reviewed below.

1.2 Archaean Cratons and Mobile Belts

Africa's major Archaean cratonic blocks include the West Africa Craton, the Southern Africa or Kalahari Craton, the Nile or East Sahara (meta-)Craton and the Central Africa or Congo Craton (Fig. 1.2). The latter corresponds with the former proto-Congo Craton, which includes the Tanzania Craton and till the Cretaceous also the São Francisco Block of Brazil (Fig. 1.6). The Nile or East Sahara Craton or rather (meta-)Craton is an enigmatic ghost craton, largely overprinted by Neoproterozoic events (Schandelmeier et al. 1994, Abdelsalam et al. 2002, 2011). The oldest cratonic rocks in Africa include the 3.55–3.23 Ga Barberton Greenstone Belt of the Kaapvaal Craton (part of the Kalahari Craton) in South Africa. The bulk of Africa's cratons, however, is composed of Neoarchaeal (2.9–2.5 Ga, clustering around 2.7–2.5 Ga) tectono-thermal terranes, stitched together by interlocking Archaean or Palaeoproterozoic fold belts.

Archaean cratons represent stable remnants of the Earth's earliest continental lithosphere. Their high-velocity, strongly depleted mantle roots extend to depths of at least 200 km, locally reaching up to 250–300 km. This thick SCLM is most likely the single most important reason for their survival. Mantle xenoliths indicate a dynamic and protracted history of tectono-thermal activity and cratonisation did not occur as a discrete event, but took place in stages, with final stabilisation post-dating crustal formation.

The crustal parts of Archaean cratons are generally composed of (from old to young) (1) granulite-gneiss belts and (2) granite-greenstone associations with 'younger granites' and late-Archaean basins, mobile belts and dykes and layered intrusions. Irrespective of their thick upper mantle root zone, large parts of Archaean cratons have been reworked during younger orogenic cycles (e.g., the Sahara meta-Craton). Archaean rocks occur, in addition, outside cratonic blocks in younger fold belts.

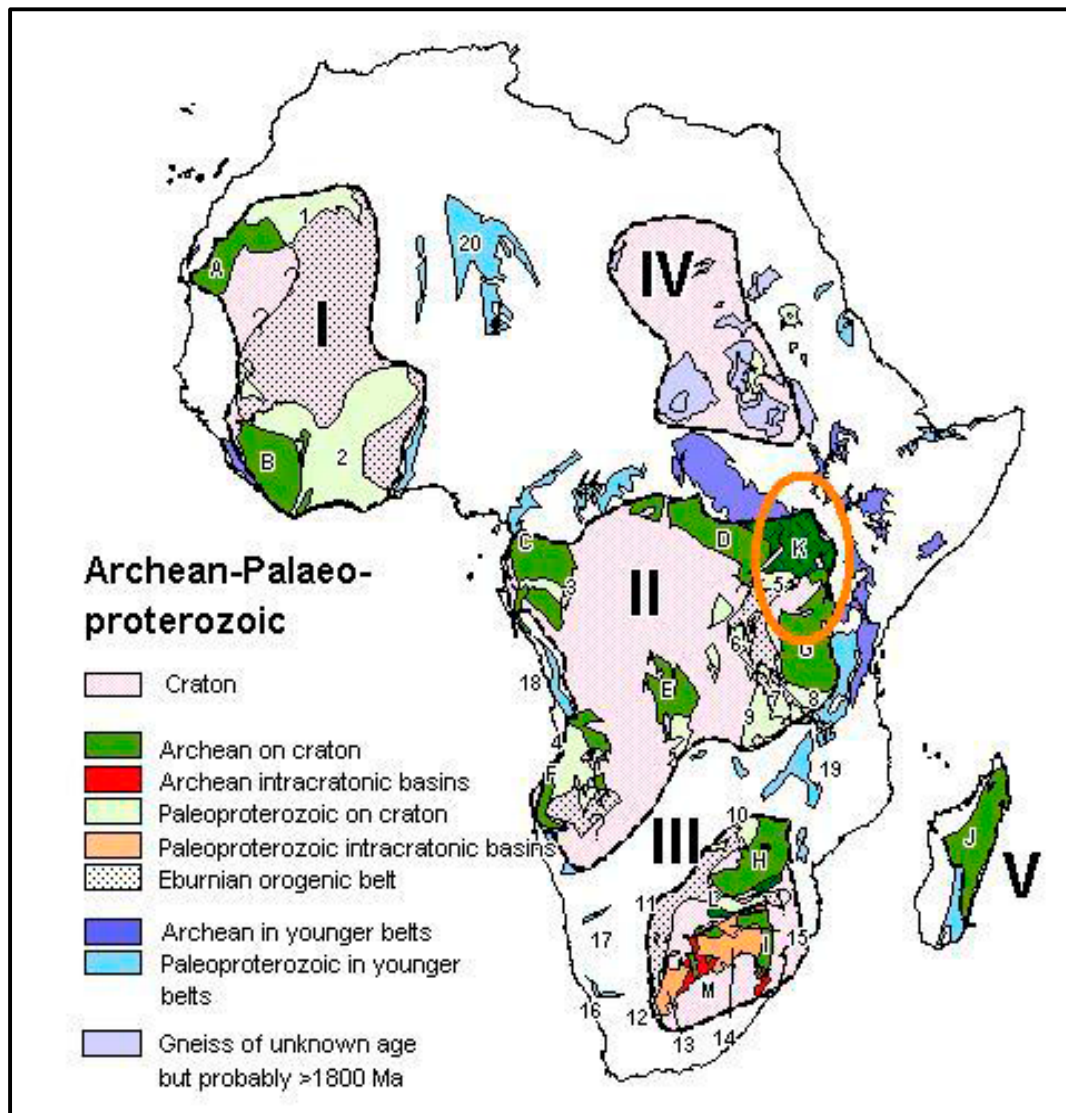
Granulite-Gneiss Belts – Granulite-gneiss belts represent exhumed, high-grade, mid- to lower crustal rocks with a complex tectono-thermal evo-

lution. Some retain a history that goes back to 4.0 Ga and beyond. Predominant lithologies include granulite- to upper amphibolite-facies quartzo-feldspathic gneisses, containing the remnants of some of the world's earliest known sedimentary and volcanic rocks, as well as of layered igneous complexes (anorthosites).

Two major types of high-grade gneiss assemblages can be distinguished (e.g., Passchier et al. 1990). A first one is derived mostly from mafic to felsic volcanics, with only little metasediments, intruded by granitoid gneisses of the TTG association². A second type, largely composed of metamorphosed clastic and carbonate sediments, often of fluvial or shelf-type, is intruded by dominantly S-type granitoids. Field observations suggest that the above two types merely represent the end-members of a continuous spectrum. Rock types of the granulite-gneiss belts include quartzo-feldspathic gneisses, mostly belonging to the TTG suite (with a volumetrically small component of paragneiss), amphibolite (derived from mafic volcanic rocks), mica schist (assumedly derived from pelitic protoliths), marble, Ca-silicate and quartzite (stable shelf settings?), banded iron formation (BIF) and layered igneous complexes. These units are commonly conformable, probably as a result of intense deformation under ductile conditions.

Granite-greenstone terrains – These comprise the oldest belts of well-preserved volcano-sedimentary successions, composed of felsic to ultramafic igneous rocks and subordinate volcanoclastic, siliciclastic and chemical sediments, intruded by voluminous granitoid bodies. Since the late 1980's, general consensus has developed on the applicability of accretionary plate tectonics to the Archaean in general (albeit with adapted geodynamic parameters) and on the equivalence, in principle, between greenstone belts and island arc/ophiolite complexes in particular (e.g., Windley 1993, de Wit 1998). Nevertheless, opponents argue either that unequivocal proof of Archaean ophiolites is still

² TTG: Tonalite-trondhjemite-granodiorite, geochemically similar to modern, mantle-derived I-type granitoids.



Courtesy Paul Dirks 2003

| Cratonic blocks | Archean terrains in cratons | |
|---|---|---|
| I = West African Craton II = Central African Craton III = Southern African Craton IV = Nile or East Sahara Craton V = Malagasy Shield | A = Reguibat Shield B = Man Shield C = Chaillu – Gabon Block D = Zaire Block E = Kasai Block F = Angola Block | G = Tanzania Craton H = Zimbabwe Craton I = Kaapvaal Craton J = Malagasy Shield K = Uganda & West Nile Complex L = Limpopo Belt (also 2000 Ma) |
| Palaeoproterozoic terrains outside cratons | Palaeoproterozoic terrains in cratons | |
| 16 = Richtersveld terrane 17 = Rehoboth Arc 18 = Kimezian 19 = Nyasa province 20 = Hoggar-Air massifs | 1 = Birimian: Reguibat Shield 2 = Birimian: Leo Shield 3 = Gabon belt: Francevillian 4 = Angolan Birimian 5 = Ruwenzori belt 6 = Rusizian gneiss | 7 = Ubendian belt 8 = Usagaran belt 9 = Bangweulu Block 10 = Magondi belt 11 = Okwa gneiss 12 = Kheiss belt |
| Archean intracratonic basins | Palaeoproterozoic intracratonic basins | |
| M = Witwatersrand & Ventersdorp basins | 13 = Griqualand basin 14 = Transvaal basin 15 = Waterberg-Soutpansberg basins | |

Fig. 1.2. Archean and Palaeoproterozoic (Eburnian) terranes (3800–1750 Ma). The Central African Craton (II) is most relevant for understanding the geology of Uganda (orange oval=approximate location of Uganda) (Dirks & Ashwal 2002, with kind permission of the University of the Witwatersrand, Scholarly Communications & Copyright Service Office). Together with the Tanzania and São Francisco Cratons and Palaeoproterozoic mobile belts it constituted the erstwhile proto-Congo Craton (Fig. 1.6).

lacking (Bickle et al. 1994) or that plate tectonic processes were inoperative during the Archaean (Hamilton 1998).

Many greenstone belts display a common subdivision into a lower, dominantly volcanic sequence and an upper predominantly sedimentary succession. The lower sequence can be further subdivided into a basal section of primarily ultramafic komatiites and an upper volcanic section with a predominance of calc-alkaline or tholeiitic, mafic to felsic volcanics. The upper volcanic section con-

sists of basalts, andesites and rhyolites. Sediments in the volcanic group comprise chemically precipitated chert, jasper and BIF, whereas the upper sedimentary succession consists of terrigenous clastic deposits of shale, pelitic sandstone, greywacke, conglomerate and quartzite.

These piles are generally invaded by so-called 'Younger Granites'. It is generally believed that the volcano-sedimentary rocks represent deeply eroded root zones equivalent to modern magmatic arcs.

1.3 Palaeoproterozoic Fold Belts of the Eburnian Orogenic Cycle

Post-Archaean rift, drift and dispersal and reassembly and partial reworking of Archaean tectonic fragments, together with formation of ju-

venile crust resulted in the Columbia (or Nuna) Supercontinent (Rogers & Santosh 2002, Li et al. 2008), making it the oldest hypothetical supercontinent (Fig. 1.3), whose existence is mainly based on palaeo-magnetic data. Columbia was assembled along global-scale 2.1–1.8 Ga collisional orogens and contained most of the Earth's continental masses (Zhao et al. 2002, 2004). This includes the 2.1–2.0 Ga Trans-Amazonian Belt (Fig. 1.3) between cratonic blocks in South America and West Africa, welded by Eburnian Orogens and the term 'Eburnian Orogenic Cycle' (Fig. 1.2; see West African Craton, no. 1) is now generally used to describe Palaeoproterozoic orogenesis in Africa.

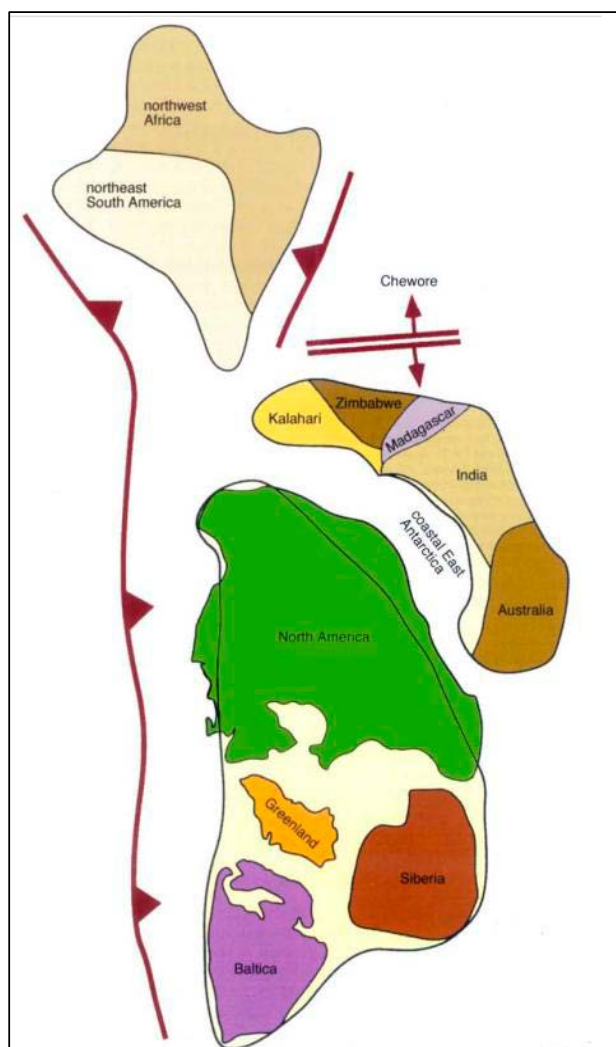


Fig. 1.3. Columbia Supercontinent at the beginning of the Mesoproterozoic, according to the configuration of Rogers & Santosh (2002, with kind permission of Elsevier Ltd.). Modified from Schobbenhaus & Brito Neves (2003). The proto-Congo Craton is part of the Northwest Africa/ Northeast South America plate.

Usagaran-Ubendian Fold Belt – This belt is one of the mobile belts that formed during the Eburnian Orogenic Cycle. Traditionally, it is related to collision and amalgamation between the Congo and Tanzania Cratons and Bengweulu Block with the Usagaran-Ubendian Fold Belt in between. It is the product of two successive tectonic events: the Early and Late Eburnian orogenic phases (Fig. 1.4). The early phase (Eburnian I) resulted in the formation of the Usagaran Fold Belt during north-directed collision and accretion around ~2100–2025 Ma (Daly et al. 1985, Daly 1988) along the southern margin of the Tanzania Craton under granulite-facies metamorphic conditions. Zircon U-Pb data, corresponding with a phase of granitic magmatism, yielded ages of 2084 ± 8 Ma (Lenoir et al. 1994, Boven et al. 1999). In the Ubendian Belt this early phase of tectogenesis was followed by a Late Palaeoproterozoic phase of exhumation and extensive dextral shearing along major, steep NW-SE directed shear zones: Eburnian II (Fig. 1.4). This resulted in widespread penetrative deformation and development of a NW-SE fabric, transposition

of the older E-W fabric and retrogradation under amphibolite-facies P,T-conditions. Timing of this event is constrained by the emplacement age of late-kinematic granitoids dated at 1847 ± 37 Ma and 1864 ± 32 Ma (both whole rock Rb-Sr and zircon U-Pb ages; Lenoir et al. 1994, Boven et al. 1999). An upper limit for the Ubendian shear event can be inferred from the age of the shallow-level Kate granite, emplaced at ~ 1825 Ma (Schandelmeier

1983). The latter is associated with volcanics that unconformably overly Ubendian gneisses. Rb-Sr data from the Kate granite further suggest that the main boundary fault between the Bengweulu Block (northern Zambia) and the Ubendian shear belt was reactivated 100 Ma after its emplacement (at 1724 ± 31 Ma; Lenoir et al. 1993). Whether this age has regional significance is, however, uncertain. Ar-Ar stepwise heating analyses of several

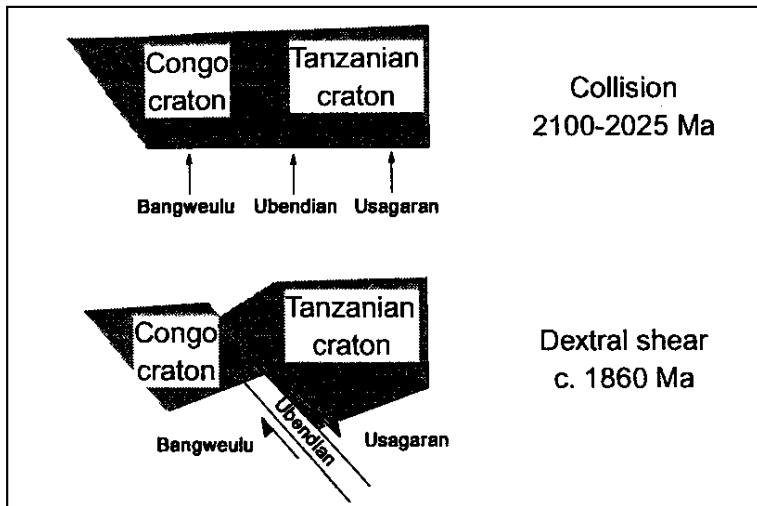


Fig. 1.4. Schematic plan of the Palaeoproterozoic evolution of the Ubendian Belt according to Lenoir et al. (1994, with kind permission from Elsevier Ltd.). The first phase (2100–2025 Ma) concerns the formation of an E-W directed orogen resulting from collision between a southern craton (that included the Bengweulu Block) and a northern craton (Tanzania + Congo Cratons). The second phase (~ 1860 Ma) in this segment of the belt is interpreted as a shear event affecting only the orogenic domain close to the western border of the Tanzanian Craton.

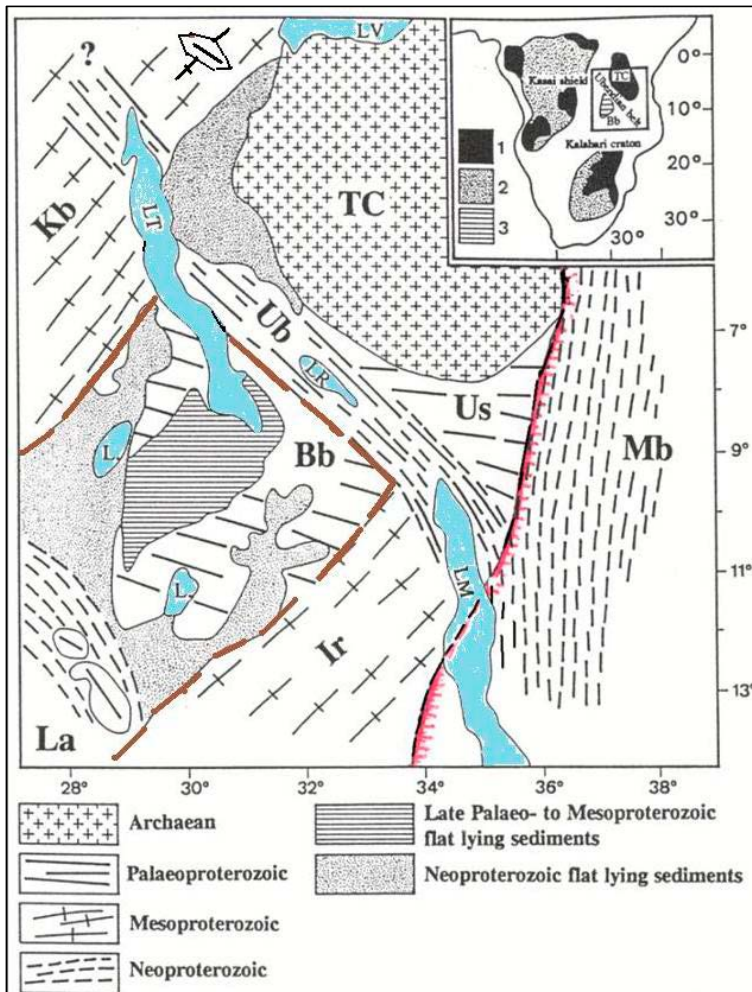


Fig. 1.5. Geological outline of the Ubendian and Usagaran Belts and surrounding areas (modified after Cahen & Snelling 1966, Andersen & Unrug 1984, with kind permission from the Elsevier Ltd.) showing the major geotectonic units and structural trends. Key: TC = Archaean Tanzanian Craton; Palaeoproterozoic domains: Ub = Ubendian Belt; Us = Usagaran Belt; Bb = Bengweulu Block (sub-outcropping Archaean craton is indicated by brown line); Mesoproterozoic belts: Kb = Kibaran Belt (with Ubendian windows); Ir = Irumide Belt; Neoproterozoic belts: Mb = Mozambique Belt; La = Lufilian Arc. LT = Lake Tanganyika; LV = Lake Victoria; LR = Lake Rukwa; LM = Lake Malawi; L = other lakes. Inset: 1 = Archaean; 2 = stable cratons since 1750, including hidden Archaean; 3 = Bengweulu Block, stable since 1750 Ma but post-Archaean.

blue-green amphibole separates from mafic tectonite has yielded a weighted average cooling age of 1848 ± 6 Ma for the argon fractions released at intermediate temperatures. This corroborates the above data and confirms the age of 1950–1850 Ma for the Late Palaeoproterozoic Ubendian tectogenesis (Boven et al. 1999).

Petrologic and litho-geochemical data from volcanic and plutonic rocks of the Marungu plateau (NE Shaba/ Katanga, DRC) confirm the above (Kabengele et al. 1991). The plutonic and volcanic rocks are characterised as “Andino-type” igneous rocks with an emplacement age of 1861 ± 28 Ma (WR Rb-Sr isochron). In a regional context it is concluded that this magmatic event is part of an extensive pluto-volcanic complex of Ubendian age in western Tanzania, NE Zambia and the eastern part of the DRC. Two magmatic cycles define a spatial and temporal zonation manifesting a geodynamic evolution model for the Ubendian Fold Belt comprising subduction-obduction-collision processes. A relaxation phase (orogenic collapse?) is manifest posterior to the collision episode. It is marked by emplacement of a third tholeiitic cycle, represented by major intrusions of olivine- or quartz-bearing gabbros and dolerite dyke swarms with an age of ~ 1750 Ma (K/Ar method; Kabengele et al. 1989).

The Bengweulu Block and Irumide Belt in northern Zambia (Bb and Ir in Fig. 1.5) largely escaped Pan-African overprinting and Palaeoproterozoic (Usagaran-Ubendian) events are expressed by juvenile (~ 1.8 Ga) greenschist-facies metamorphic rocks, amphibolites, eclogite lenses and some granulites. Usagaran and older rocks east of the Tanzania Craton are largely overprinted during the Pan-African Orogeny.

Palaeoproterozoic Rwenzori Fold Belt in Uganda

– The Usagaran-Ubendian Fold Belt can be traced northwards into Burundi, Rwanda and Kivu Province (DRC), exposed in Rusizian windows, below folded Mesoproterozoic metasediments of the North Kibaran Belt (see below, Section 1.5). Further northwards, in Uganda, it comprises the rocks of the Rwenzori Fold Belt (Chapter 6), which includes variable granite gneisses of the Rukungiri Suite and granitoids of the Sembabule Suite

yielding zircon U-Pb ages of 2.21–2.15 Ga and 1.99–1.96 Ga, respectively, covered by metasediments and mafic volcanics of the Buganda Group and intruded by post-kinematic granitoids of the Mubende-Singo Suite (1.85 Ga) (Mänttari 2014).

Proto-Congo Craton – The loosely defined Congo Craton (Lepersonne 1974, Cahen et al. 1984 and references therein) corresponds to the circular Congo River Basin (CRB) with a surrounding rim of spatially discontinuous Palaeoproterozoic and Archaean terranes of central Africa. The present-day, continent-scale CRB coincides with a gravity low and is filled with a pile of sedimentary rocks of Palaeozoic to Holocene age (Tack 2006b, 2008a, Delpomdor et al. 2008, Kanda-Nkula et al. 2011). Geophysical data show that there is no unexposed Archaean nucleus in the basement below the CRB but that it is supposedly entirely composed of rocks belonging to Palaeoproterozoic fold belts (Crosby et al. 2010). Fernandez-Alonso et al. (2011) postulated the proto-Congo Craton, which apart from the former Congo Craton, also comprises the Tanzania and São Francisco Cratons (Fig. 1.6). This proto-Congo Craton should be understood as an assemblage of 6 Archaean terranes welded together around 2.1 Ga and later exhumed around 1.8 Ga as a result of the Eburnian Orogenic Cycle (Pinna et al. 1996, de Waele et al. 2006, 2008, Noce et al. 2007, Delor et al. 2008). The location of the suture between two of these tectono-thermal units of the proto-Congo Craton – between the Tanzania Craton and the Bomu-Kibalian Shield (the red line in Fig. 1.6) – is fundamental in understanding the geology of Uganda (Chapters 3, 4 and 5).

The Usagaran-Ubendian-Rusizian-Rwenzori system of fold belts, separating the Central Africa Craton from the Tanzania Craton, is the only Palaeoproterozoic mobile belt of the proto-Congo Craton not covered by sediments of the CRB. As described above, subduction, collision and amalgamation of the Tanzania and Central Africa Cratons – and formation of the proto-Congo Craton – was associated with eclogite-facies metamorphism (Klerkx et al. 1997, Collins et al. 2004a, 2004b, Boniface 2009, Boniface et al. 2011) and the formation of an Andean-type calc-alkaline magmatic arc (Kabengele et al. 1991, Boven et al. 1999).

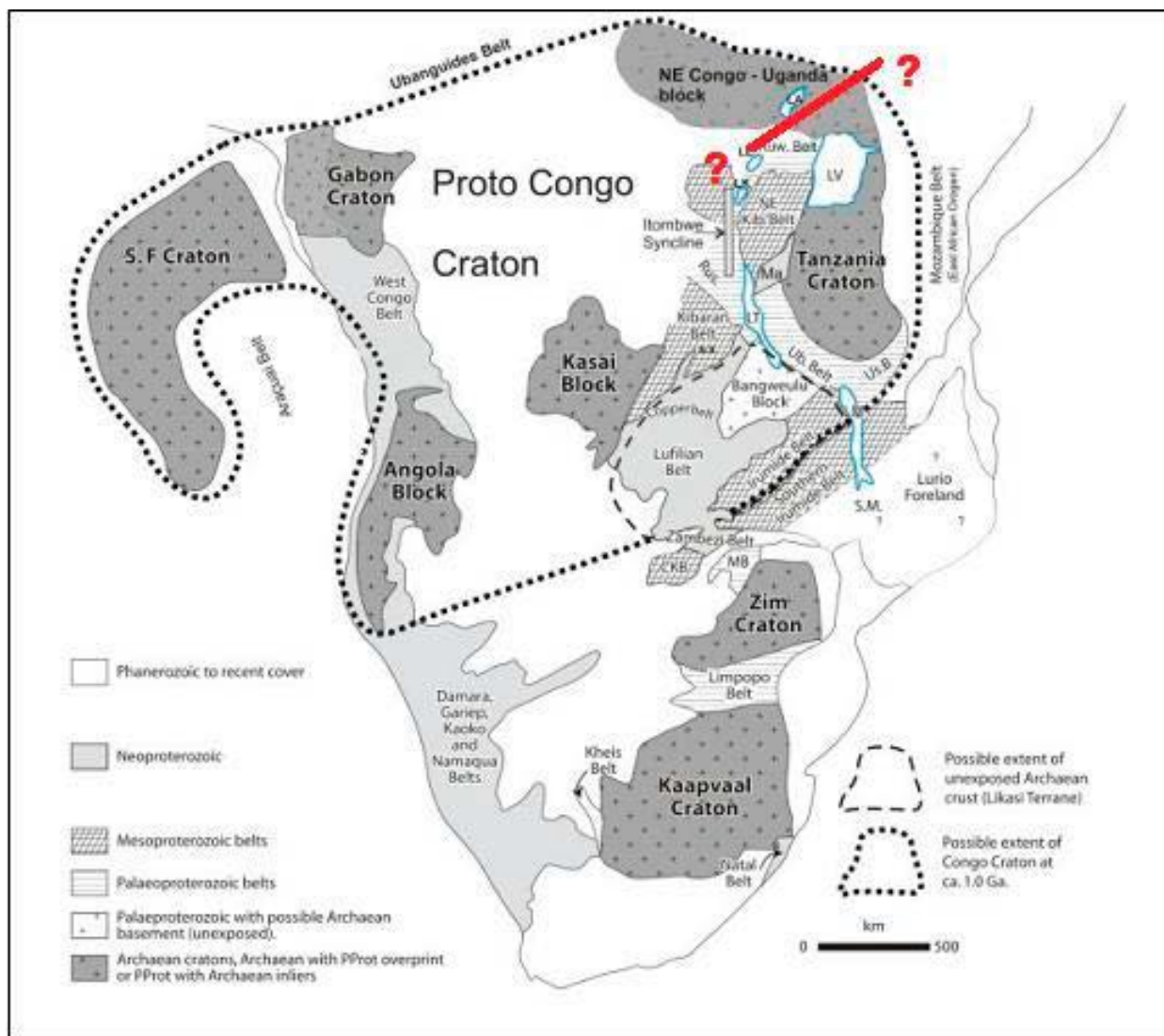


Fig. 1.6. Geological outline of the proto-Congo Craton showing the central Congo River Basin, surrounded by Archaean terranes. Note that in the Bengweulu Block Archaean rocks are sub-outcropping. Archaean basement in Uganda belongs partly to the Tanzania Craton and NE Congo-Uganda Block, renamed Bomu-Kibalian Shield in this report (from Fernandez-Alonso et al. 2011, with kind permission of the University of the Witwatersrand, Scholarly Communications & Copyright Service Office). Red line=a proposed suture.

1.4 Palaeoproterozoic post-Eburnian Platform Deposits

Introduction – Deposition of Palaeo- to Mesoproterozoic sedimentary rocks on the proto-Congo Craton (Fig. 1.7) started during post-Eburnian taphrogenesis (1.8–1.75 Ga), as verified by ages of ~1.7 Ga for volcanic rocks of the lower part of the Espinhaço Supergroup in the São Francisco Craton, the Brazilian segment of the proto-Congo Craton. These basins contain volcanic rocks and conglomerates alternating with sandstones, argillites and dolomites, deposited in continental, transitional and marine environments (Pedreira & de Waele 2008).

Similar sandstone – argillite – dolomite successions compose the Chela Group ('cg' in Fig. 1.7) in

the westernmost segment of the proto-Congo Craton. The Kibaran, Akanyaru-Ankole, Kagera-Buhweju and Muva Supergroups ('ki', 'ak', 'ka' and 'ib' in Fig. 1.7) have been deposited in the easternmost segment of the proto-Congo Craton, the first two in the Kibaran Belt and the last one in the Irumide Belt and on the Bengweulu Block. Their deposition ages are constrained through ages from felsic tuff interlayers and include the 1790 ± 17 Ma Chela Group and 1879 ± 13 Ma Muva Supergroup. These data show the development of broadly coeval and similar epi-continental sedimentary basins over the entire proto-Congo Craton, suggesting the existence of a long-lived wide epi-continental sea

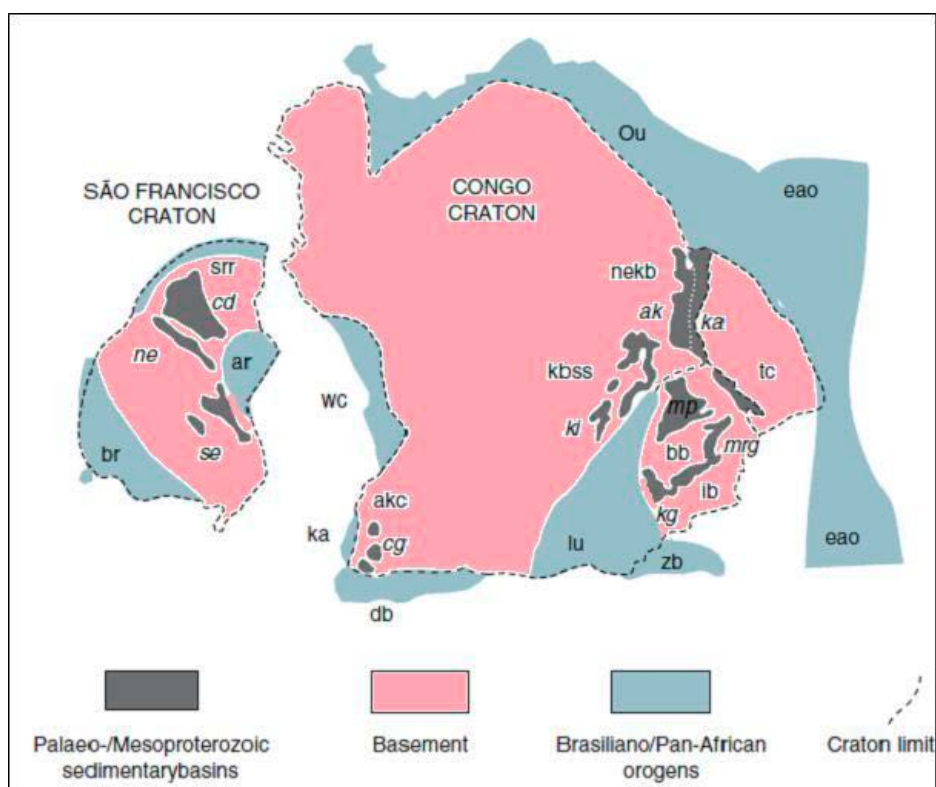


Fig. 1.7. Approximate Palaeo–Mesoproterozoic positions of the present São Francisco and Congo Cratons (formerly forming the proto-Congo Craton) and Palaeo-Mesoproterozoic volcano-sedimentary basins and Neoproterozoic fold belts. Key: br = Brasília Belt; srr = Sergipano/ Riacho do Pontal/Rio Preto Belts; ar = Araçuaí Belt; ka = Kaoko Belt; wc = West Congo Belt; akc = Angola-Kasai Block; db = Damara Belt; lu = Lufilian Belt; kbss = Kibaran Belt sensu stricto; ou = Oubanguides; nek = North-eastern Kibaran Belt; bb = Bengweulu Block; ib = Irumide Belt; zb = Zambezi Belt; tc = Tanzania Craton; eao = East African Orogen. Sedimentary successions discussed in the text are indicated in italics as follows: ne = northern Espinhaço Supergroup; se = southern Espinhaço Supergroup; cd = Chapada Diamantina; cg = Chela Group; ki = Kibaran Supergroup; ak = Akanyaru Supergroup; ka = Kagera Supergroup (here: Akanyaru-Kagera Supergroup); mp = Mporokoso Group; mrg = Manshya River Group (including the Kasama Formation); and kg = Kanona Group. Modified from Brito Neves (2004) and Pedreira & de Waele (2008).



Fig. 1.8. Typical landscape formed by rocks of the Bukoba Group (Kagera-Buhjewu Supergroup) south of Biharamulo, NW Tanzania. Steep cliffs are composed of thick-bedded quartzitic sandstones. Smoother slopes comprise mudstone and dolerite sills. Chocolate-brown clayey soil on right photograph is a typical weathering product of underlying dolerite (from Westerhof & Koistinen 2005).

covering large areas of this proto-Congo Craton during post-Eburnian times, manifesting break-up of the Columbia Supercontinent (Pedreira & de Waele 2008). Post-Eburnian platform deposits

in Uganda are attributed to the Namuwasa Group (< 2.05–1.86 Ga), the Bwezigoro Group (< 1.97 Ga, most likely < 1.86 Ga) and the 1.79 Ga Kagera-Buhjewu Supergroup (Chapter 7).

1.5 Mesoproterozoic Grenvillean/ Kibaran Fold Belts

Introduction – Since the late Palaeoproterozoic the proto-Congo Craton has remained stable and united (Tack et al. 2006a, 2008b, 2009, 2010). It experienced only intra-cratonic tectonic events, including rifting, rift inversion and magmatism. A most notably geodynamic event, spatially partly coinciding with the Palaeoproterozoic suture formed by the Ubendian-Rusizian-Rwenzori system of fold belts, was the creation of the Mesoproterozoic Kibaran trough (1.55–1.20 Ga), which, upon inversion, evolved into the Kibaran Fold Belt (~1.20–0.95 Ga) in the eastern segment of the proto-Congo Craton. This mobile belt has always remained intracratonic and never evolved into continental break-up and the formation of a juvenile oceanic basin (Tack et al. 2010, Delvaux et al. 2011).

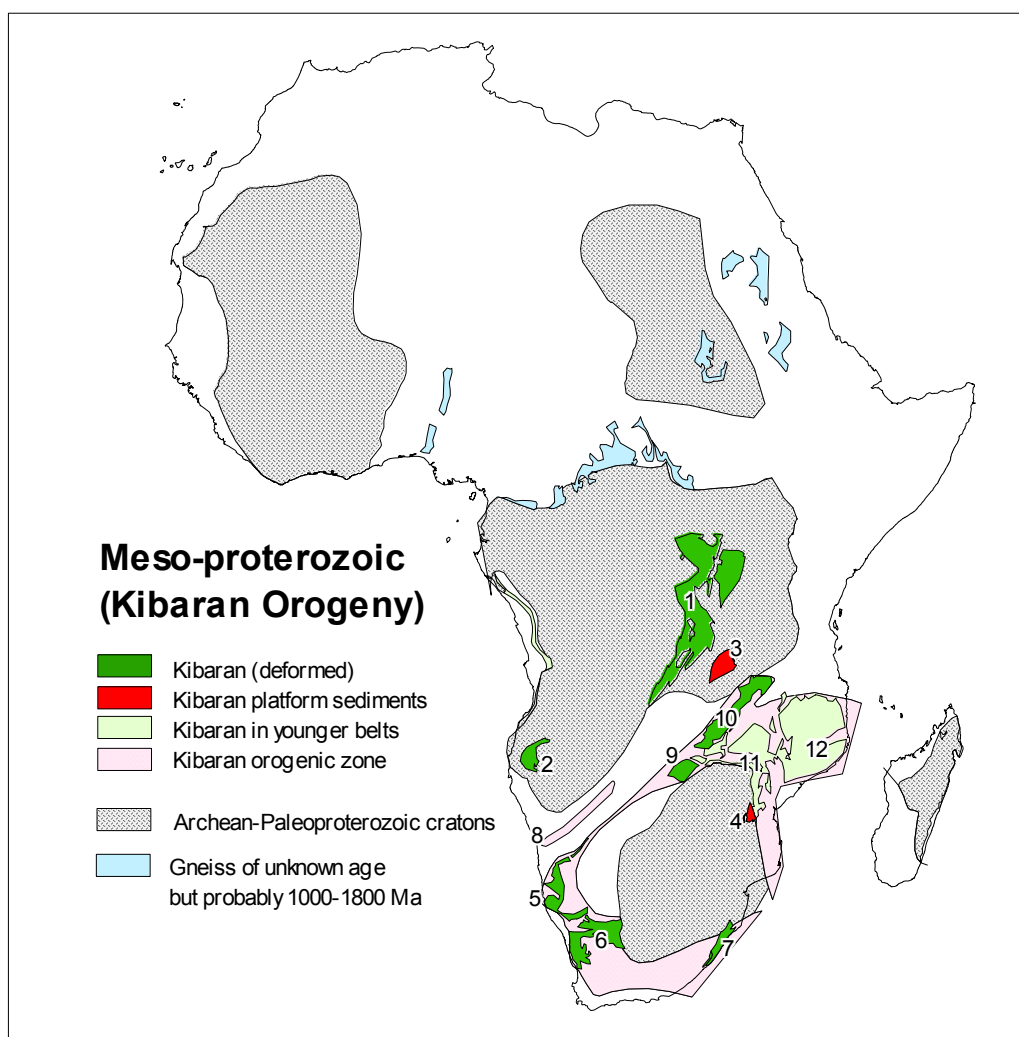
Fragmentation of the Columbia Supercontinent, which commenced during 1.85–1.75 Ga taphrogenesis (Fig. 1.7; Pedreira & de Waele 2008), accelerated in the eastern segment of the proto-Congo Craton around 1.4–1.38 Ga, coeval with emplacement of the bimodal North Kibaran Magmatic Province (i.e., the bimodal Large Igneous Province of Tack et al. 2009, 2010, 2011a) giving rise to em-

placement of pre-kinematic per-aluminous S-type granitoids in the Kibaran trough and mafic rocks mainly in the Kibaran foreland. Formation and inversion of the Kibaran trough and tectogenesis of the Kibaran Fold Belts can be correlated with the global *Grenville* or *Grenvillean Orogenic Cycle* (GOC, > 1.55 to ~0.9 Ga), culminating around 1.1–1.0 Ga with the formation of the Rodinia Supercontinent (Fig. 1.9). Rift/drift/dispersal of this supercontinent started as early as 850 to 800 million years ago, with evidence for large scale rifting at about 750 million years ago.

In Africa, the term ‘Kibaran’ was traditionally used as a synonym for the global term ‘Grenvillean’ to designate Mesoproterozoic fold belts in eastern and southern Africa. This used to comprise a curvi-linear alignment of fold belts striking from Namibia and Namaqualand (RSA) (Fig. 1.10, nos. 5 and 6) to southern Uganda (Fig. 1.10, northern segment of no. 1) over a distance of 3500 km. The juxtaposition of the Sinclair Province and Namaqua Belt *vis-à-vis* the northern Kibaran Belt is, however, coincidental as demonstrated by the palaeo-geographic position of the Kalahari Craton within Rodinia (Fig. 1.9). Their alignment resulted



Fig. 1.9. Reconstruction of Rodinia after Li et al. (1995), Dalziel (1997), Hoffman (1991) showing mountain belts formed during the Grenville Orogenic Cycle and the formation of juvenile crust (1.35–0.9 Ga). Key: M = Madagascar, S = Sri Lanka, KAL = Kalahari Craton, N = Natal, A = Areachap and associated terrains, Fk = Falkland Islands, H = Haag Nunatacks. L = Lúrio Thrust Belt, K = Kibaran Belt and NET = NE Tanzania. Note the position of the Kalahari proto-Craton, amalgamated with Antarctica, and located far away from the other African ‘building blocks’ (in brown-reddish).



Courtesy Paul Dirks 2003

| Mesoproterozoic terrains on cratons | Mesoproterozoic active continental margins | Mesoproterozoic collisional orogens |
|-------------------------------------|--|-------------------------------------|
| 1 = Kibaran belt (failed rift) | 5 = Sinclair Province | 9 = Choma-Kaloma block |
| 2 = Kunene Anorthosite Cplx | 6 = Namaqua belt | 10 = Irumide Belt |
| 3 = Muva Group (platform) | 7 = Natal belt | 11 = Zambezi belt |
| 4 = Umkondo Group (platform) | 8 = Abbabis Gneiss | 12 = Lurio belt |

Fig. 1.10. Mesoproterozoic (Grenvillean) terrains (> 1.55 to ~0.9 Ga) (after Dirks & Ashwal 2002, with kind permission of the University of the Witwatersrand, Scholarly Communications & Copyright Service Office).

from formation of the Damara-Lufilian-Zambezi Belt, a major Neoproterozoic suture between the Kalahari and proto-Congo Cratons formed during assembly of Gondwana (Burke et al. 1977, Oliver et al. 1998, Porada & Berhorst 2000, John et al. 2003, Johnson & Oliver 2000, 2004, Johnson et al. 2005, Westerhof et al. 2008). Centred on the proto-Congo Craton, three Mesoproterozoic Grenvillean structural domains, each with a specific geodynamic development, can now be identified: (1) Irumide Fold Belt, (2) Tete-Chipata Belt (or Southern Irumide Belt) and (3) Kibaran Belt.

Irumide Fold Belt – The development of the North Kibaran Belt of Burundi, Rwanda, Kivu (DRC), NW Tanzania and southern Uganda can be viewed as a far field effect of tectono-genesis in the Irumide Belt of Zambia. This fold belt (Fig. 1.10, no. 10) resulted from post-Eburnian extension and basin development followed by Grenvillean convergent tectonism along the southeastern margin of the proto-Congo Craton (de Waele et al. 2006). Granites, metavolcanics and undeformed quartzite-pelite units in the Bengweulu Block represent the northwestern foreland to the Irumide Belt.

The Irumide Fold Belt is composed of Palaeoproterozoic metamorphosed platform sediments of the ~1.88 Ga Muva Supergroup (de Waele & Fitzsimons 2004). The latter is divided into the Manshya River Group (de Waele & Mapani 2002, de Waele et al. 2006) and the Mporokoso Group (Andersen & Unrug 1984). The folded and metamorphosed succession of the Manshya River Group, most prominently exposed along the NW-verging Irumide front in the northwestern part of the belt, consists of metasiltstones, phyllites, slates and quartzites, with sporadic calc-silicate rocks and marbles at the top (Daly & Unrug 1982, de Waele & Mapani 2002, de Waele et al. 2006). Its depositional environment is interpreted as shallow-marine (Daly & Unrug 1982, de Waele & Mapani 2002) with fluvial units in the northeastern Irumide Belt (Daly & Unrug 1982).

The Mporokoso Group (Andersen & Unrug 1984) in the Bengweulu Block consists of sandstones, conglomerates, chert layers and volcanic rocks deposited in fluvial and shallow-marine environments (Andrews-Speed 1989). Mporokoso rocks unconformably cover a plutonic-volcanic basement dated, using zircon U–Pb data, at 1.87–1.86 Ga and TDM crustal residence ages of 2.3–2.2 Ga (de Waele et al. 2004a, 2004b, de Waele 2005). Tuff layers, associated with this basement occur within the basal parts of the Mporokoso Group, strongly suggesting also a depositional age of ~1.86 Ga. Similar tuffs and lavas occur within the Manshya River succession of the Irumide Belt and yielded zircon U–Pb SHRIMP ages of 1.88–1.86 Ga, manifesting that rocks of the Manshya River Group are broadly coeval with deposition of the Mporokoso Group (de Waele 2005).

Two generations of granitoids invaded the Muva metasediments in the Irumide Belt. These comprise a minor suite of anorogenic plutons dated between 1.66 and 1.55 Ga (de Waele et al. 2003a, 2003b) and voluminous K-feldspar porphyritic granitoids dated between 1.05 and 0.95 Ga (de Waele et al. 2006). Both generations of granitoids have bulk-rock geochemical signatures and highly negative $\epsilon_{Nd}(t)$ values manifesting their formation by the recycling of older continental crust (de Waele et al. 2003a). SHRIMP analysis of deformed granitic basement within the Irumide Belt has identified the widespread presence of 2.0 Ga protoliths with TDM ages of 2.5 Ga. These data confirm that basement in the Irumide Belt and adjacent Bengweulu Block are dominated by ~2000

and 1850 Ma protoliths that also characterise the Usagaran-Ubendian-Rusizian-Rwenzori system of fold belts fringing the Tanzania Craton.

Using metamorphic monazite and zircon overgrowths, polyphase MP-HT metamorphism in the Irumide Belt has been dated at 1046 ± 3 Ma (Schenk & Appel 2001, 2002) and between 1020 ± 7 Ma and 1004 ± 20 Ma (de Waele et al. 2003b), ages that may also apply to convergence in the North Kibaran Belt (Chapter 8).

Tete-Chipata Belt – This structural domain (Westerhof et al. 2008) is synonymous with the *Southern Irumide Belt* of Johnson et al. (2005) and extends into southern Zambia and western Mozambique, including the Choma-Kalomo Block (Figs 1.10, no. 9 and Fig. 1.11). This recently identified structural domain is mainly composed of Mesoproterozoic supracrustal and plutonic rocks, including ~1.3 Ga metamorphosed volcano-sedimentary successions (Fingoè Supergroup), ~1.3 Ga metamorphosed ocean floor rocks (Chewore ophiolite; see Fig. 1.3), ~1.2–1.3 Ga metasediments (Zámbeú Supergroup), undated (>1.08 Ga) granulites and gneisses (Chidzolomondo, Cazula and Mualadzi Groups) and metavolcanics of the ~1.0 Ga Kaouera Arc. Plutonic rocks comprise a large number of granitoid clans and a bimodal suite with ages ranging from > 1.2 to ~1.05 Ga with ‘volcanic-arc’ to ‘within-plate’ affinities. Neoproterozoic Pan-African fault or thrust zones border the Tete-Chipata Belt. These are two steep strike-slip faults zones in the north and south (the Mwembeshi Dislocation and Sanangoè Shear Zone, respectively) and a sub-horizontal thrust zone in the east (Fig. 1.11).

In view of the fact that the above tectono-stratigraphic units show little cohesion, as manifested by differences in metamorphic grade, structural development, geodynamic setting and age, it is concluded that the Tete-Chipata Belt forms a collage of stacked ‘suspect terranes’ that assembled, collided and amalgamated with the coeval Irumide Belt and southern margin of the proto-Congo Craton during the Grenvillian Orogenic Cycle (Johnson et al. 2006).

The Choma-Kalomo Block was previously considered to represent the southwestern extension of the Irumide Belt. Being one of the terranes in the Tete-Chipata Belt (Fig. 1.11), it is characterised by a specific geodynamic development with major plutonic events dated at ~1.37 Ga and ~1.18 Ga, respectively (Bulambo et al. 2006).

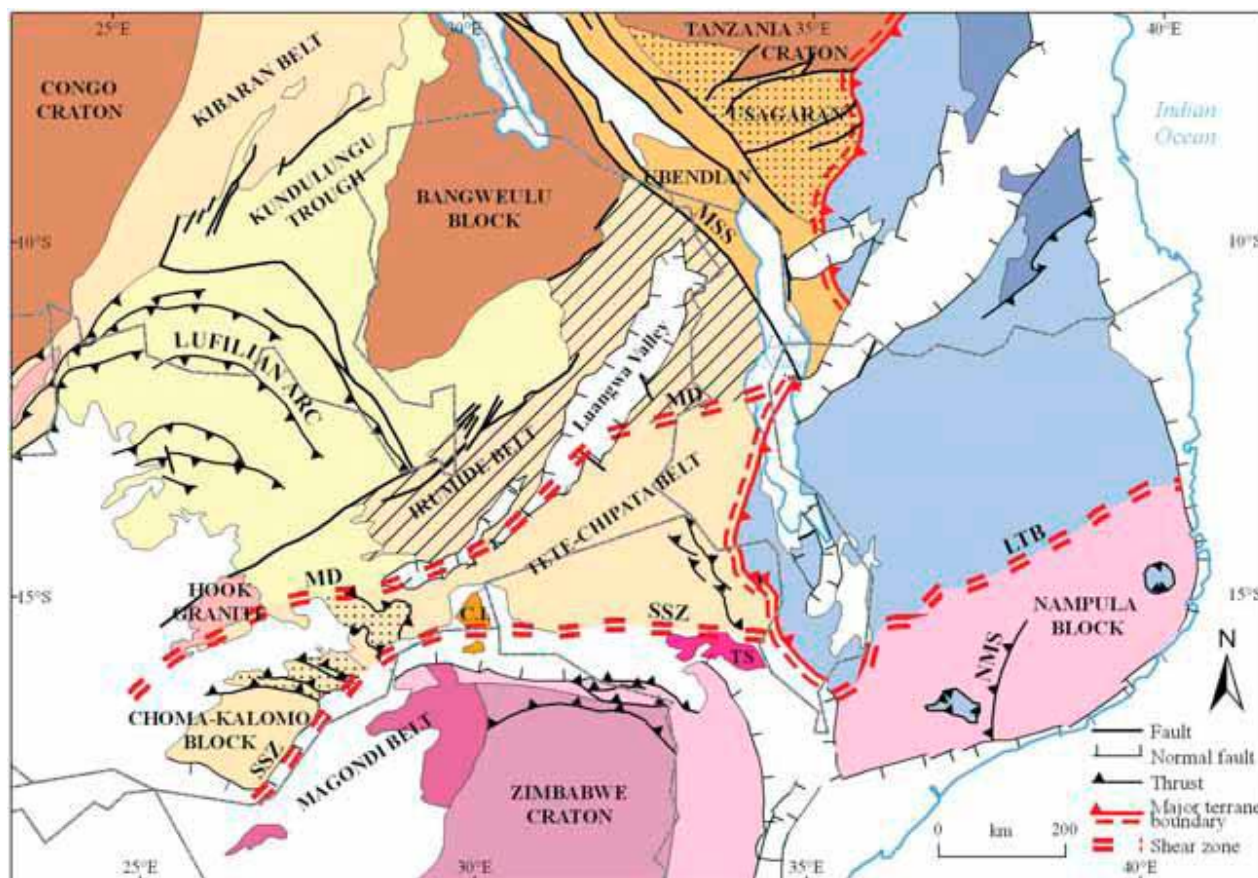


Fig. 1.11. Simplified geological map of the Tete-Chipata Belt and the Zambezi-Lufilian segment of the Damara-Lufilian-Zambezi Belt (adapted from Vrána et al. 2004). Key: MSS = Mugesse Shear Zone, MD = Mwembeshi Dislocation, SSZ = Sanangò Shear Zone, C.I. = Chewore Inliers, TS = Tête Suite, NMS = Namama Megashear, LTB = Lúrio Thrust Belt. The dotted section in the southwestern part of the TCB corresponds to Neoproterozoic (post-Rodinia, early Pan-African) metasediments (mainly pelites and carbonates) with minor metavolcanics (from Westerhof et al. 2008).

Kibaran Belt –This belt (Fig. 1.10, no. 1) was traditionally described as a continuous, NNE- to NE-trending orogenic belt, from Katanga in the south to SW Uganda in the north over a distance of ~1500 km. The belt is composed of two segments, separated by a NW-trending Karoo rift, superposed on a Palaeoproterozoic Rusizian basement high (Fig. 9.1). For the sake of clarity, the two segments of the Kibaran Belt *s.l.* will be referred to as

(1) the Kibaran Belt *s.s.* (a name coined by de Margn e 1935, after the Kibara Mountains type-locality) or South Kibaran Belt (Katanga Province and western Tanzania) and (2) the North Kibaran Belt (NKB) exposed in Kivu (DRC), Burundi, Rwanda, NW Tanzania and SW Uganda (Tack et al. 1994, Fernandez-Alonso et al. 2006). The Kibaran Belt will be further discussed in Chapter 8.

1.6 Post-Rodinia Neoproterozoic Platform Rocks of the Malagarasi Supergroup

Introduction – Several post-Rodinia extensional basins in central Africa have remained intracratonic and undeformed during the ensuing Neoproterozoic-Cambrian Pan-African Orogenic Cycle. They comprise the Kundulungu of Katanga (DRC), the Plateau Series of the Bengweulu Block of northern Zambia (Figs 1.7 and 1.11), the Buschimag, Bilatian and Lindian in the eastern

DRC and the Malagarasi in Burundi and western Tanzania.

The ‘Malagarasian’, named after the Malagarasi River in NW Tanzania, was originally defined in Burundi (Waleffe 1965) and considered to be equivalent to the previously defined ‘Bukoban System’, a term coined by Stockley (1943) in northwestern Tanzania (Henderson 1961). The

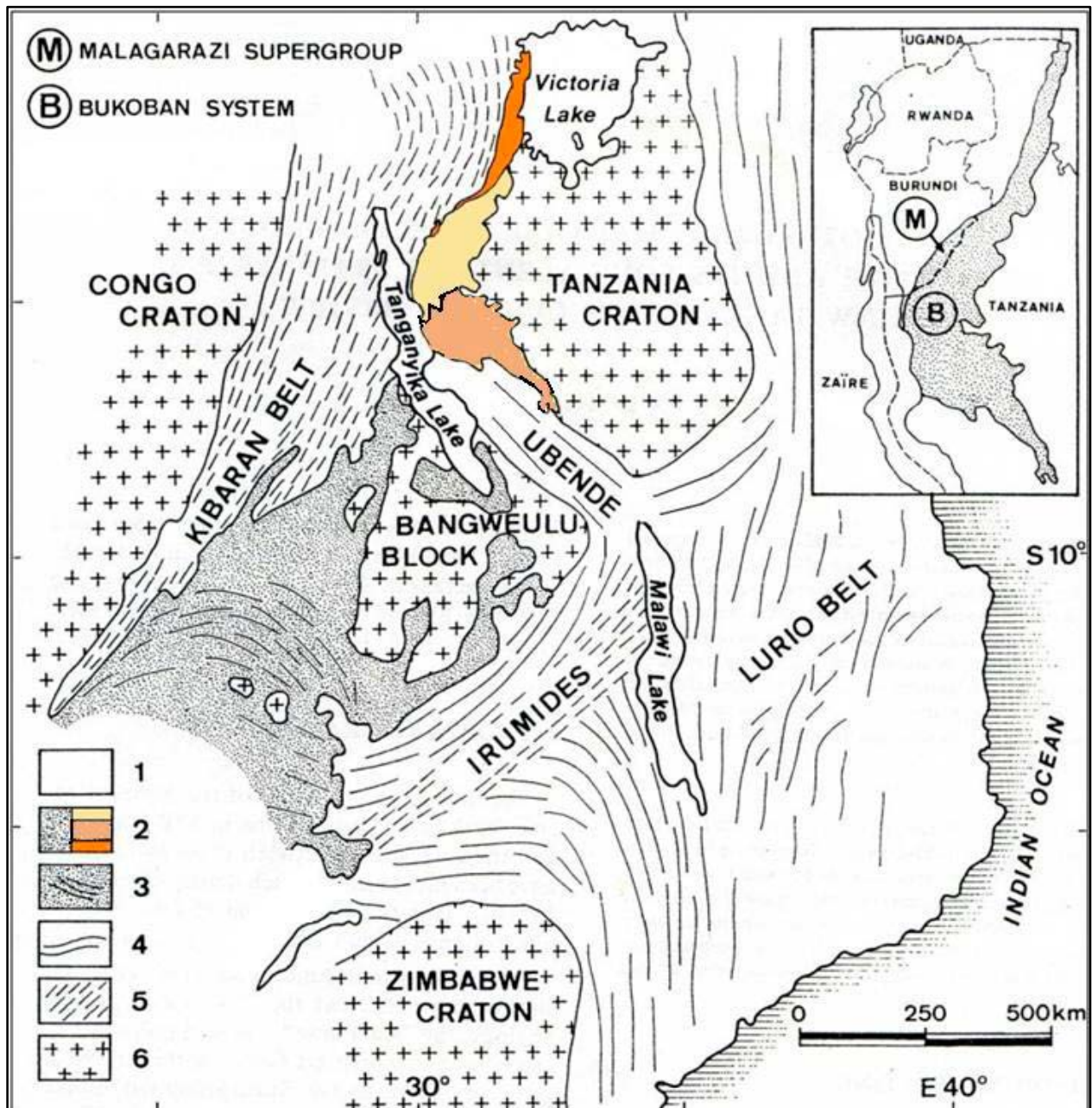


Fig. 1.12. Geological outline of Eastern Africa, showing distribution of Proterozoic intra-cratonic basins in the eastern segment of the proto-Congo Craton. Rocks in box (M and B) were previously all attributed to 'Malagarasian'. Key: 1 = Lakes and recent sediments; 2 = Proterozoic platform rocks, yellow = Malagarazi Supergroup; brown = Busondo-Masontwa and Itiaso Group of supposedly Mesoproterozoic age; orange = Kavumwe-Nkoma (Burundi) and Bukoba (Tanzania) Groups, previously considered part of the Malagarazi Supergroup, now part of the Palaeoproterozoic Kagera-Buhweju Supergroup (Chapter 8); 3 = folded Proterozoic rocks; 4 = Fold belts; 5 = Mesoproterozoic Kibaran Belt (Rusizian windows not shown); 6 = Cratonised areas (> 1.8 Ga). Adapted from Tack (1995, with kind permission of the Royal Museum of Central Africa), after Cahen et al. (1984).

unit was attributed the rank of supergroup by Tack et al. (1992). Rocks of the Malagarazi Supergroup are deposited in a conjugate strike-slip basin (Tack 1995), located between the Mesoproterozoic Kibaran Belt (west), the Archaean Tanzanian Craton (east) and Palaeoproterozoic Ubendian (south) (Fig. 1.12). The succession, with an overall maximum thickness of ~2000 m,

is composed of shales, siltstones, sandstones, arkoses and frequently dolomitic and partially chertified limestones, including stromatolite- and occasional oolite-bearing members. The sequence indicates shallow water conditions, either in oxygenated open marine or restricted, oxygen-starved basins. Intraformational para- and unconformities are common.

The rocks of the Malagarasi Supergroup have been sub-divided (from old to young) into Musindozi, Mosso and Kibago in eastern Burundi and Kigonera Flags and Uha Groups in NW Tanzania (Tack 1995, Deblond et al. 2001) (Fig. 1.13). In Tanzania they overlie older platform rocks of the Busondo-Masontwa and Itiaso Groups (Halligan 1963). The latter has been intruded by a mafic body with a poorly constrained K-Ar age of 1239 ± 50 Ma (Cahen et al. 1984). Recent U-Pb zircon has indicated that also the Bukoba Sandstone (Tanzania) and equivalent Nkoma-Kavumwe (Burundi) Groups are far older: They are now attributed to the Palaeoproterozoic Kagera-Buhweju Supergroup (Chapter 7).

Mainly mafic amygdaloidal lavas, up to several hundreds of metres thick, known as *Gagwe Volcanics* or *Gagwe Amygdaloidal Lavas*, are covered by dolomitic limestones and red beds and constitute most of the Mosso Group or the lower part of the Uha Group (Table 10.1; Fig. 1.12) (de Paepe et al. 1991). These basalts of tholeiitic composition are exposed in individual massive, fine-grained flows, 80 to 100 m in thickness, that may become amygdaloidal near the top of individual flows with pillow textures in places. Geochemical and field data point to continental flood basalt (CFB)-type volcanics derived from the mantle, fitting a scenario of crustal extension that, in turn, resulted in crustal thinning and basaltic underplating.

Rocks of the basal Musindozi Group (Fig. 1.13) yielded an age of 888 ± 16 Ma (Tack & Thorez 1990, de Paepe et al. 1991), indicating that deposition commenced prior to 0.89 Ga. The Gagwe volcanics yielded rather consistent K-Ar ages of 822 ± 30 Ma (whole rock; Briden et al. 1971) recalculated by de Paepe et al. (1991), 815 ± 14 Ma (Cahen et al. 1984) and 813 ± 21 Ma (whole rock) and 810 ± 25 Ma (clinopyroxene-plagioclase separates) (de Paepe et al. 1991; recalculated after Piper 1972 and Cahen & Snelling 1974). Supposedly due to Ar excess, the above ages were considered too old apparent ages and superseded by a more precise age of 795 ± 7 Ma from ^{40}Ar - ^{39}Ar step-wise heating results (Meert et al. 1994; recalculated by Deblond et al. 2001).

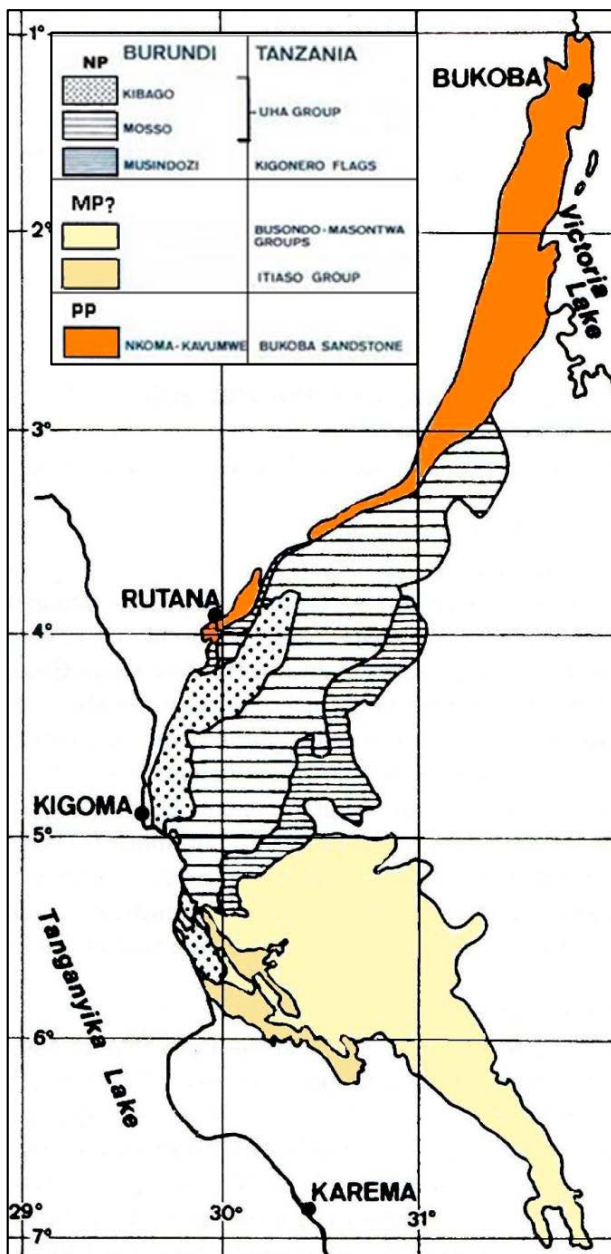


Fig. 1.13. Geological outline and litho-stratigraphy of platform successions in eastern Burundi and NW Tanzania (adapted after Theunissen 1988a, Tack 1995, Deblond et al. 2001, with kind permission of the Museum of Central Africa). The Busondo-Masontwa and Itiaso Groups are supposedly deposited in local basins related to (Meso- or Palaeoproterozoic; > 1.24 Ga) reactivation of the Ubendian shear belt. Subsequently, the Bukoba Sandstone/ Nkoma-Kavumwe unit has been attributed to the Palaeoproterozoic Kagera-Buhweju Supergroup (< 2.05–1.78 Ga; see Chapter 7).

Platform rocks of the former ‘Mityana Series’ in the Lake Wamala area and similar deposits of the Ssesse islands in Uganda are attributed to the Mityana Group, which is presumably equivalent to part of the Uha Group of the Malagarasi Supergroup.

The Kibago and equivalent superior part of the Uha Groups are covered by Nyakanazi diamictites in NW Tanzania (Westerhof & Koistinen 2005) and similar rocks in eastern Burundi (Tack et al. 1992). These are correlated with glacial to periglacial rocks of the Bunyoro Group (Chapter 10) of central Uganda. Obviously, they overlie the Gagwe volcanics and, hence, have a maximum age of $< 795 \pm 7$ Ma.

Post-Rodinia and post-Gondwana Alkaline Complexes – Apart from basin development and the emplacement of flood basalts, post-Rodinia crustal extension in the eastern segment of the proto-Congo Craton is also manifested by the emplacement of alkaline complexes in a curvi-linear belt stretching over more than 1200 km from NE DRC to NE Zambia (Tack et al. 1984). The belt coincides with the – much younger – Neogene Western Rift (Fig. 1.14).

Carbonatites and associated alkaline complexes (and kimberlites) are emplaced during incipient continental rifting, marking the initial phase of a Wilson Cycle and are as such potential indicators

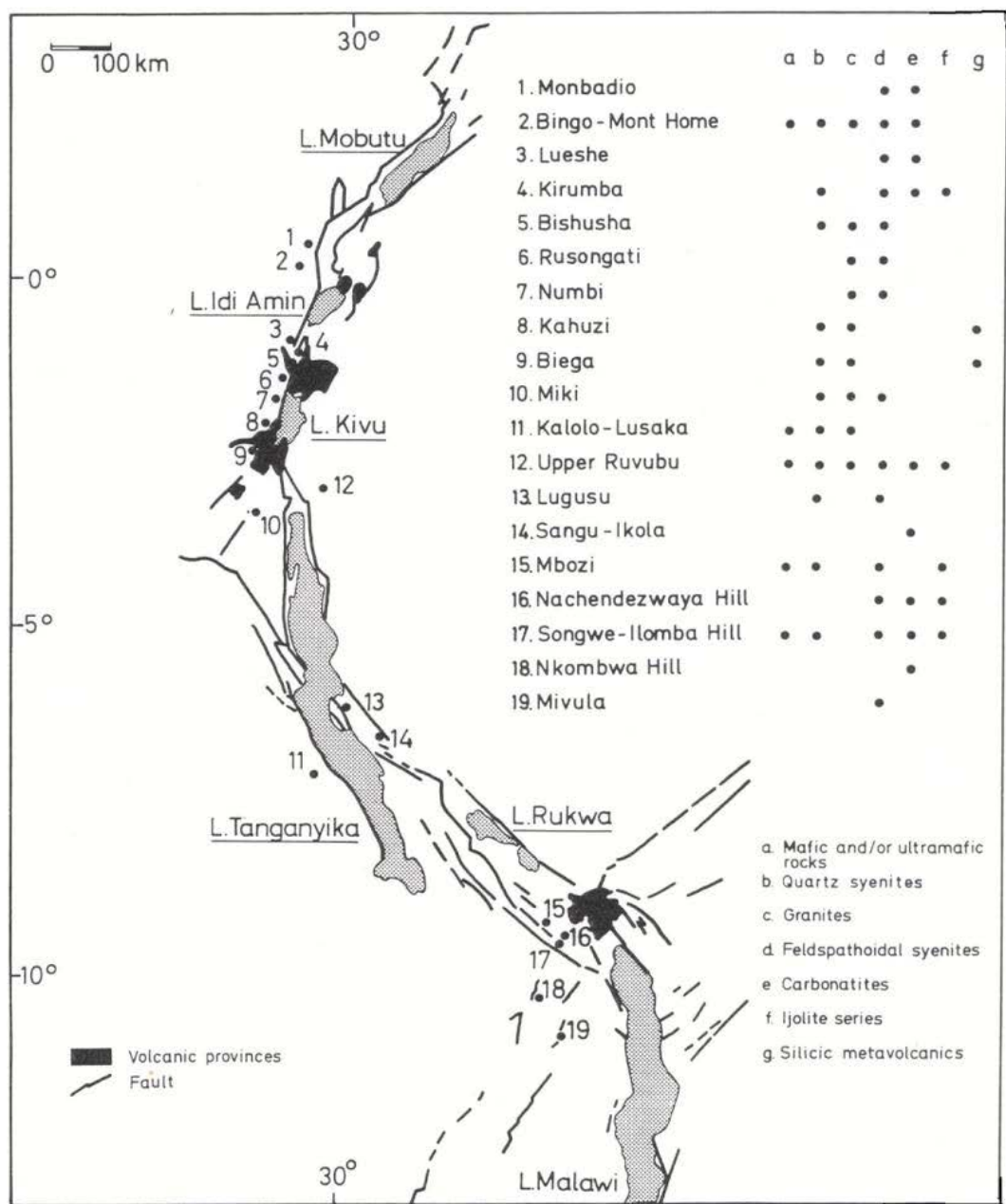


Fig. 1.14. Spatial distribution and rock types of 19 alkaline complexes of post-Rodinia or post-Gondwana age, located along the Neogene Western Rift (from Tack et al. 1984, with kind permission of the Museum of Central Africa).

of cratonic margins (Burke et al. 2003). Deformation during subsequent re-assembly of lithospheric plates will focus along these cratonic margins, including the contained alkaline complexes. A compilation of African alkaline igneous rocks and carbonatites shows that nearly 90% of nepheline syenite gneisses and deformed carbonatites are concentrated within known or inferred Proterozoic suture zones (Burke et al. 2003).

Radiometric dating (Rb/Sr and K/Ar whole rock as well as biotite ages) of these 19 alkaline complexes (Fig. 1.14) yielded a wide variety of ages ranging from 713 ± 26 Ma (Ledent & Cahen 1965) to 442 ± 11 Ma (Vellutini et al. 1981) and fits well with emplacement ages of other alkaline complexes in eastern Africa such as Mbozi (Tanzania) 745 ± 25 Ma to 743 ± 30 Ma (K/Ar, biotite), Nkombwa Hill (NE Zambia) 680 ± 25 Ma (K/Ar, phlogopite) and others. An overview is contained in Tack et al. (1984), Rumvegeri et al. (1985), Kampunzu et al. (1985) and Maravic et al. (1989). Two separate age clusters can be observed, one corresponding with post-Rodinia (~ 0.81 to ~ 0.65 Ga) and a second one manifesting post-Pan-African (~ 0.55 to ~ 0.44 Ga) extension. Although not known from Uganda, they are relevant to understanding its geology since the distribution of these alkaline massifs corresponds with deep-rooted fractures and manifest crustal weakness zones within the proto-Congo Craton, corresponding with the Ubendian/Rusizian/Rwenzori and Kibaran orogenic belts. The obvious conclusion is that the Neogene Western Rift, is superposed on a much older crustal weakness zone or suture.

1.7 Neoproterozoic-Cambrian Pan-African Fold Belts

Introduction – Recognising a structural discontinuity between the Archaean Tanzanian Craton and younger gneisses to the east, Holmes (1951) introduced the term ‘*Mozambique Belt*’. Kennedy (1964) coined the term ‘*Pan-African Orogeny*’ but he preferred the term ‘*Pan-African thermo-tectonic event*’ stressing that evidence for this orogeny was initially mainly based on conventional whole-rock Rb-Sr and K-Ar geochronology, yielding remobilisation ages of ~ 650 to 490 Ma of presumably older rocks (Cahen & Snelling 1966).

The Pan-African Orogenic Cycle is a worldwide orogenic system culminating in the for-

Upper Ruvubu Alkaline Plutonic Complex – This better studied post-Rodinia alkaline complex is emplaced into metasediments of the Mesoproterozoic Akanyaru-Ankole Supergroup (Tack & de Paepe 1981, 1983, Tack et al. 1983, 1984) in the North Kibaran Belt of Burundi (Fig. 1.14, no. 12). It is discussed here in some more detail because it shows evidence of significant Pan-African tectonism within the North Kibaran Belt.

Dating of foidal syenite (U-Pb, single zircon) yielded an emplacement age of 739 ± 7 Ma. Rb/Sr dating of the same syenite produced an age of 699 ± 13 Ma. Quartz syenite and granite of the outer zone yielded a Rb/Sr age of 707 ± 17 Ma (Tack et al. 1996). The carbonatite intrusion was dated at 690 ± 32 Ma (Pb-Pb isochron; Demaiffe 2008). Nd, Sr and Pb isotope data indicate a cogenetic relationship between feldspathoidal syenites and carbonatite (Demaiffe et al. 1986). Based on an integrated interpretation of structural and geochronological data Tack et al. (1984) developed the following scenario:

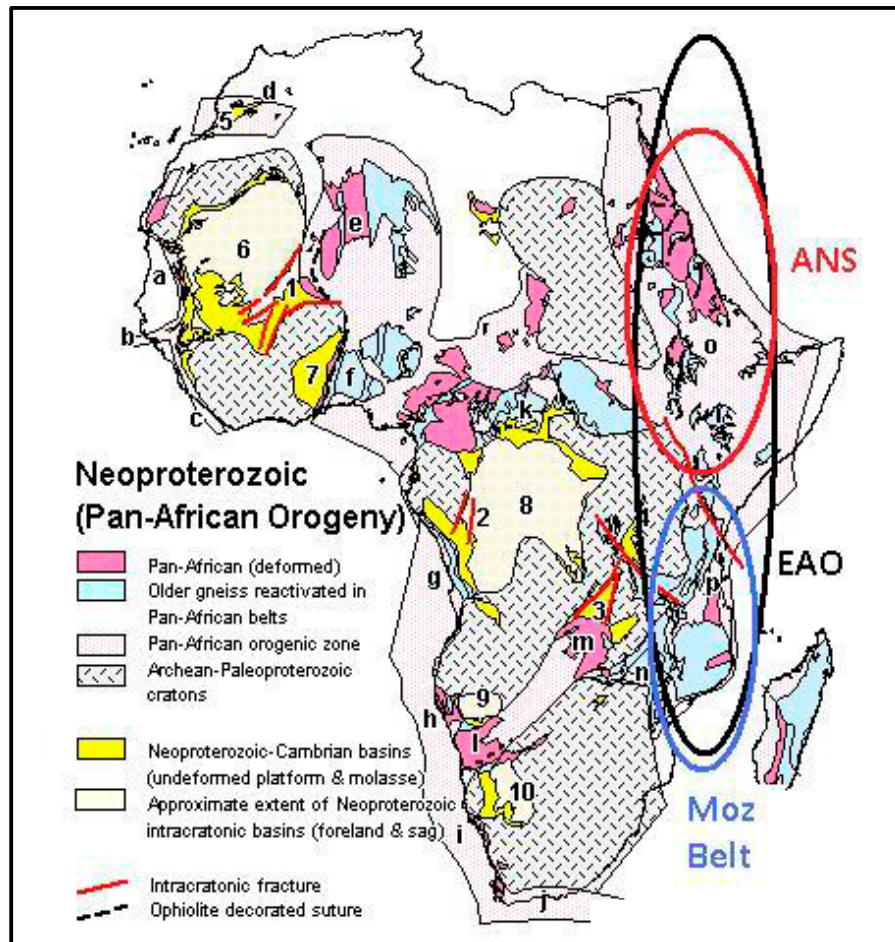
- Anorogenic high-level emplacement of the outer unit between 773 and 739 Ma.
- N-S faulting with development of local shear zones and non-penetrative S₂ foliation and cataclastic deformation of outer unit and Kibaran country rocks; incomplete isotopic re-homogenisation of Sr.
- N-S structurally controlled diapiric emplacement of foidal syenite, followed by carbonatite emplacement around 739 Ma.
- N-S faulting with incomplete Sr isotope re-homogenisation and thermal peak related to N-S phase and reactivation of older N-S faults.

mation of the Gondwana Supercontinent. Over the years there have been discussions about the duration of the Pan-African Cycle. Based on evidence in Saharan Africa – where there is little evidence for Mesoproterozoic tectonism – Liégeois et al. (2013) proposed to divide the Pan-African Orogenic Cycle into an early phase of accretion of oceanic terranes, roughly between ~ 900 Ma and ~ 630 Ma and a phase of amalgamation of the Gondwana Supercontinent through collision of cratons and smaller lithospheric fragments between ~ 630 Ma and ~ 540 Ma. We apply the term Pan-African Orogenic Cycle to all events starting

with the break-up of Rodinia till the formation of Gondwana, including the ‘final docking’ effects, which lasted well into the Palaeozoic.

Pan-African Fold Belts and the proto-Congo Craton – Orogenic processes pertaining to the Pan-African Orogenic Cycle (~0.90 Ga to ~0.54 Ga), took place along the craton mar-

gins, although weakness zones (e.g., former sutures) within the proto-Congo Craton have been extensively rejuvenated. During Pan-African tectogenesis the proto-Congo Craton occupied a more or less central position in the assembly of Gondwana. Consequently, the proto-Congo Craton is bordered entirely by Pan-African collisional belts, comprising the West



Courtesy Paul Dirks 2003

| Neoproterozoic collisional orogens | | |
|---|---|--|
| a = Mauritides b = Bessarides c = Rokolites d = Anti Atlas e = Trans-Saharan: Pharusian Belt f = Trans-Saharan: Dahomeyan Belt | g = West Congo Belt h = Kaoko Belt i = Gariep Belt j = Saldahnia Belt k = Oubangide Belt l = Damara Belt | m = Lufillian Arc n = Zambezi Belt o = East African: Nubian Shield p = East African: Mozambique Belt q = Ubendian Belt |
| Neoproterozoic failed rifts | Neoproterozoic platforms-foreland-molasse basins | |
| 1 = Gourma Trough 2 = Sangha Rift 3 = Kundelungu Basin 4 = Malagarasian Basin | 5 = Anti-Atlas 6 = Taoudeni Basin 7 = Volta Basin 8 = Congo River Basin* | 9 = Owambo Basin 10 = Nama Basin |

Sub-basins in the Congo basin include: NW: Sembe Ouessou basin; NNE: Bangui-Lindian basins; SE: Bushimay basin; SW: West Congo basin

Fig. 1.15. Neoproterozoic-Early Palaeozoic (Pan-African) terranes (900–450 Ma) (after Dirks & Ashwal 2002, with kind permission of the University of the Witwatersrand, Scholarly Communications & Copyright Service Office). Approximate locations of East African Orogen (EAO) in black, Arabian-Nubian Shield (ANS) in red and Mozambique Belt in blue ellipses.

African or Brazilian Belt to the west, the Damara-Lufilian-Zambezi Belt in the south, the East African Orogen (EAO) in the east and the Oubanguides or Central African Fold Belt (CAFB) in the north (Fig. 1.15). Being located in the northeastern corner of the proto-Congo Craton, especially the latter two fold belts are of particular relevance to the geology and geodynamic development of Uganda.

East African Orogen (EAO) – The term ‘East African Orogen’ (EAO, Fig. 1.15) has been introduced to describe the Pan-African orogenic belt of eastern Africa (Stern 1994). It is one of the Earth’s greatest collision belts that can be followed over a distance of several thousands of kilometres and has developed over ~350 million years of evolution (e.g., Stern 1994, 2002, Jacobs et al. 1998, Kröner et al. 2000a, 2000b). The EAO now comprises the Mozambique Belt in the south (northern Mozambique, western Tanzania and Kenya and eastern Uganda) and the Arabian-Nubian Shield in the north (Fig. 1.15, ANS). The latter is mainly composed of a collage of juvenile Neoproterozoic island-arc and back-arc terranes, with remnants of 900 Ma and younger oceanic crust. The Mozambique Belt, on the other hand, is interpreted as a Himalayan-style continent-continent collisional orogen between West and East Gondwana (Burke & Sengör 1986, Shackleton 1986, Key et al. 1989, Behre 1990; Section 11.10). It comprises of early Neoproterozoic passive margin metasediments, tectonically intercalated with Archaean gneisses (Kenya and northern Tanzania) or Palaeoproterozoic to Mesoproterozoic gneisses and granulites, reworked in Pan-African time (southern Tanzania, most of Malawi and northern Mozambique). Ophiolites are relatively rare.

There are essentially two geodynamic scenarios to explain the assembly of the Gondwana Supercontinent in southern and eastern Africa during the Pan-African Orogenic Cycle. The first scenario involved consumption of the Mozambique Ocean between 841 and 632 Ma (Cutten & Johnson 2006) and collision and amalgamation (~640 to ~530 Ma) of two crustal plates, provisionally named West Gondwana and East Gondwana (Shackleton 1994, Wilson et al. 1997, Kröner et al. 2001, Jacobs et al. 2006). In this scenario West Gondwana comprised most of Africa and South America. East Gondwana was composed of juvenile crust, now attributed to the Arabian-Nubian Shield,

and older crystalline basement in present-day Madagascar, India, Antarctica and Australia. Collision and amalgamation of these two lithospheric plates created the N-S directed East Africa Orogen (EAO) (Stern 1994) or, stressing its southernmost continuity in between Antarctica and the Kalahari Cratons, the East Africa-Antarctica Orogen (EAAO) (Jacobs et al. 2006).

The second scenario (Fig. 1.16) assumes collision and amalgamation of not two but three lithospheric plates during the Pan-African Orogeny in southern and eastern Africa (Grantham et al. 2003), provisionally named East, West and South Gondwana. East Gondwana is centered on the Arabian-Nubian Shield and older crystalline basement of the Dharwar Craton of southern India, Madagascar and the eastern granulites of Kenya and Tanzania (Fig. 1.16). West Gondwana comprises most of the proto-Congo Craton. South Gondwana is mainly composed of Antarctica and the Kalahari Craton, amalgamated since the ~1.0 Ga Grenvillean Orogenic Cycle. In this scenario East and West Gondwana first collided and amalgamated, followed by collision and amalgamation with South Gondwana. In this scenario the N-S directed OAE suture does not continue southwards between Antarctica and the Kalahari Craton (as in the previous scenario, e.g., Jacobs et al. 2006) but impinges on the E-W directed suture of the Kunga Orogen, comprising (from west to east) the Damara-Lufilian-Zambezi (DLZ) Belt, the Lúrio Thrust Belt (LTB; see also Fig. 1.11) and, further eastwards, thrust belts of Sri Lanka.

We prefer the second scenario because in Uganda we have indications of N-vergent thrusting (North Kibaran rocks over Kagera-Buhweju and Buganda rocks over Archaean basement), which can be viewed as a far-field effects of N-S compression in the Damara-Lufilian-Zambezi (DLZ) Belt or, alternatively, due to collision between the proto-Congo Craton and Sahara meta-Craton. The second scenario is essentially based on four lines of evidence:

- (1) *Structural position of the Choma-Kalomo Block* – The SW-NE structural grain of the Choma-Kalomo Block (Fig. 1.12) is in line with the dominant structural trends of the Irumide Belt. As a consequence the Choma-Kalomo Block was previously considered to represent the southwestern extension of the Irumide Belt, south of the Neoproterozoic Damara-Lufilian-Zambezi

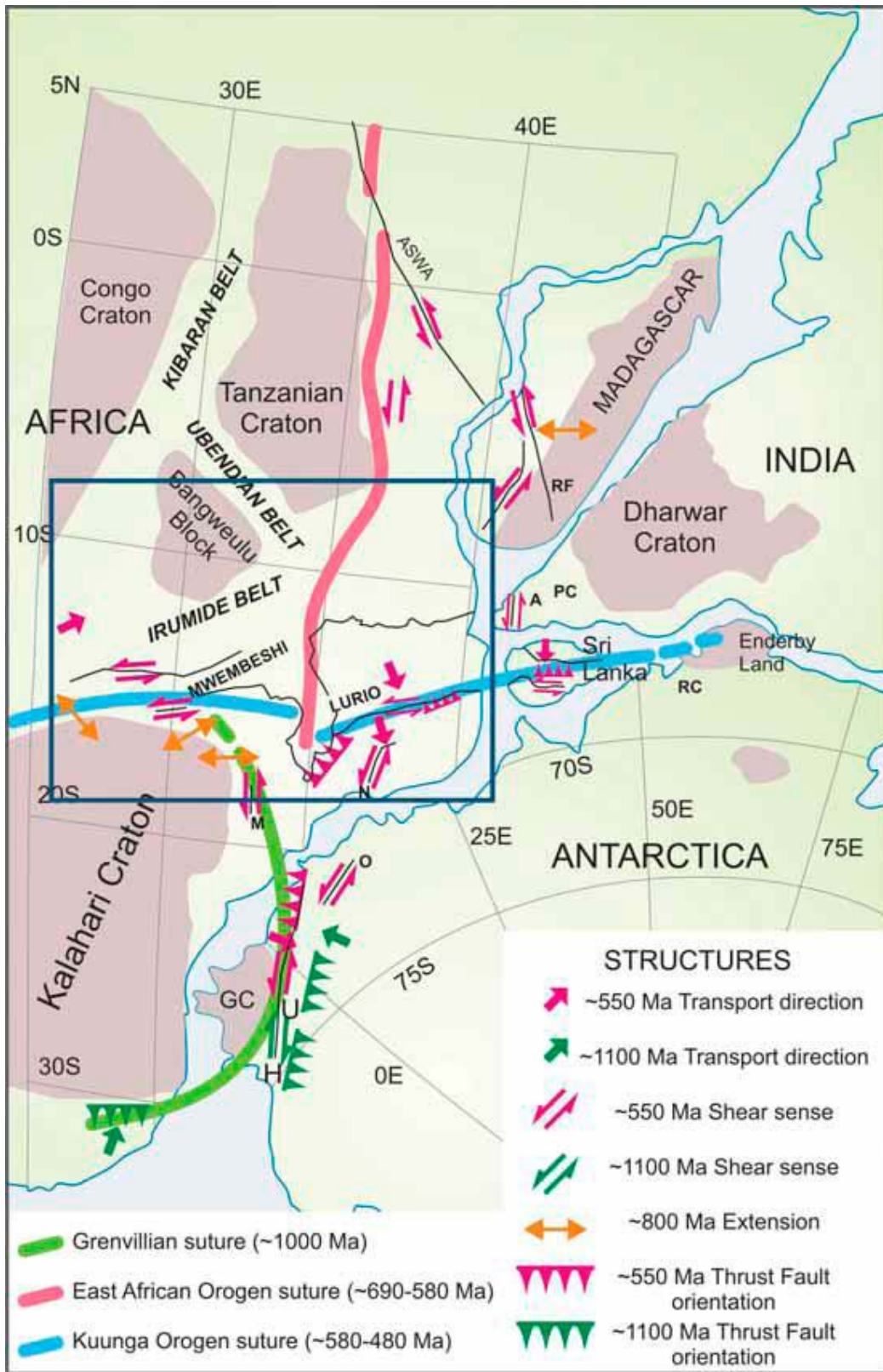


Fig. 1.16. Gondwana reconstruction after Lawver et al. (1998). Ages and locations of various major structural/ tectonic features (e.g., major thrust belts, shear zones) showing direction of tectonic transport and shear sense. Key: PC = Palgat-Cauvery Shear Zone; RC = Rayner Complex; A = Achankovil Shearzone; GC = Grunehogna cratonic fragment; H = Heimfrontfjella; RF = Ranotsara Shear Zone; U = Urjell; N = Namama Shear Belt; O = Orvinfjella Shear Zone; M = Manica Shear Zone (adapted from Grantham et al. 2003). Blue square corresponds to area of Fig. 1.11.

suture. Recent data show, however, that the Irumide Belt and the Choma-Kalomo Block followed different geodynamic evolutionary paths (de Waele et al. 2003a, 2003b, 2006, Bulambo et al. 2006). The Choma-Kalomo Block is now considered to represent a major terrane, attributed to the multi-terrane Tete-Chipata Belt (Fig. 1.11).

- (2) *Evidence for Pan-African subduction-related HP-LT metamorphism in the Zambezi segment of the DLZ Belt and N-S convergence in the Lúrio Thrust Belt* – Closure of the Zambezi-Adamastor oceanic basin (Johnson et al. 2005) and collision and amalgamation of the Kalahari Craton (part of South Gondwana) and Central Africa Craton (part of West Gondwana) resulted in the Damara-Lufilian-Zambezi Belt, a major Neoproterozoic suture (Burke et al. 1977, Oliver et al. 1998, Porada & Berhorst 2000, John et al. 2003, Johnson & Oliver 2000, 2004). Mafic and ultramafic rock fragments in Neoproterozoic metasediments (Roan Group, Katanga Supergroup) of the Lufilian and Zambezi segments of the DLZ Belt supposedly represent relics of obducted ocean floor rocks, forming a tectonic mélangé. The Chewore Ophiolite in the Chewore Inliers (Fig. 1.11) represents a larger fragment of oceanic crust. Amphibolites in the Damara segment of the DLZ Belt show MORB tholeiitic affinities (Breitkopf & Maiden 1988) and are also believed to have been derived from ocean floor protoliths.
- Pan-African, subduction-related HP-LT metamorphism is reflected by eclogites and white-schists (kyanite + talc + yoderite) in ophiolite and by kyanite in metapelite (Vrána & Barr 1972, Vrána et al. 1975) and manifest peak metamorphic conditions with T estimated at 630–690°C and P ranging from > 13 to 26–28 kb (John & Schenk 2003, John et al. 2004). Sm-Nd whole rock-garnet and Lu-Hf whole rock garnet dating yielded ages ranging from 659 ± 14 Ma to 595 ± 10 Ma, interpreted as indicating the age of Pan-African eclogite-facies metamorphism (John & Schenk 2003, John et al. 2004). The Lufilian and Zambezi segments of the DLZ Belt can be described as a thin- and thick-skinned, double-verging orogen with thrust transport to the NNE-NE (Wilson et al. 1993, Hanson et al. 1994, Johnson & Oliver 2004) and SSE (Barton et al. 1991, Dirks et al. 1999, Vinyu et al. 1999, Müller et al. 2001).

Transport directions and sinistral shear along the Mwembeshi Dislocation (Fig. 1.11) suggest oblique convergence between West and South Gondwana. The spatial arrangement of metamorphic ages and range in timing of peak metamorphic conditions indicate that the closure of the Zambezi-Adamastor Ocean and amalgamation of South and West Gondwana was not a simple collision between two large lithospheric plates, but rather a series of collisional events among several cratonic fragments, taking place between ~615 Ma and 520 Ma, a period of almost 100 million years. This was followed by a period of uplift, denudation and cooling passing the ~350°C isotherm in the DLZ Belt at ~480 Ma (Goscombe et al. 2000).

The rigid Choma-Kalomo Block (Fig. 1.11) supposedly acted as an indenter when it became caught between West and South Gondwana. Its presence within the collision zone changed the geometry of compression and thrusting, resulting in the arcuate shape of the Lufilian segment – the Lufilian Arc (Fig. 1.11) – of the DLZ Belt (Bulambo et al. 2006), comprising Neoproterozoic folded and north-thrusted metasediments of the Katanga Supergroup.

Although the DLZ collisional event is well documented by Neoproterozoic metamorphic U-Pb data of older rocks, the scarcity of juvenile TTG suites having ages between ~616 and 520 Ma is notable. In Zambia, the few known examples of syn-kinematic felsic igneous rocks include the Hook Granite (~533 to ~566 Ma; Fig. 1.11) and nearby Mwembeshi Rhyolite (~551 Ma). They precede the clearly late to post-kinematic 0.47–0.50 Ga ages of the Sinda Suite granites (502 ± 8 Ma) and Macanga granite (470 ± 14 Ma) in the Tête area of western Mozambique (Mänttári 2008).

In this scenario the Lúrio Thrust Belt (LTB) is considered to represent the eastward continuation of the DLZ suture. In northern Mozambique, north of the LTB, the age of Pan-African metamorphic overprinting of Mesoproterozoic rocks, associated with amphibolite- to granulite-facies metamorphism, is estimated at about 560 to 520 Ma (Bingen et al. 2006, Viola et al. 2006). Macey et al. (2006) attribute the younger ages of ~550 Ma in the Nampula sub-Province, south of the LTB (Figs 1.11 and 1.16), to the maximum age of the termination of the principal Pan-African D₂/M₂ collisional tectono-

metamorphic event (NB: D_1/M_1 is attributed to the older Mesoproterozoic, ~1.0 Ga, Grenville Orogenic Cycle) as manifested by five granitoid orthogneiss samples that provided zircon metamorphic rim ages of 513 ± 10 Ma, 525 ± 20 Ma, 538 ± 8 Ma and 505 ± 10 Ma (Macey & Armstrong 2005). Supracrustal rocks equally located in the Nampula sub-Province south of the LTB yielded zircon metamorphic rim ages of 555 ± 12 , 502 ± 80 and 527 ± 18 Ma, and a weakly deformed porphyritic quartz monzonite yielded a precise U-Pb concordia crystallisation age of 532 ± 5 Ma (Macey & Armstrong 2005), which provides another constraint on a waning Pan-African D_2 deformation phase.

Macey et al. (2006) refer to the LTB as a linear tectonic *mélange* consisting of strongly flattened granulitic gneisses with a variety of protolith rock types and ages that probably represents a major tectonic boundary between several tectono-stratigraphic blocks of northern Mozambique (Pinna et al. 1993, Kröner et al. 2001, Macey & Armstrong 2005, Macey et al. 2006, Grantham et al. 2003, 2006). A well-defined NNW to NW plunging stretching lineation indicates a SE transport direction. Amphibolite to granulite-facies metamorphism and deformation in the LTB is dated at between 578 ± 10 Ma and 545 ± 6 Ma (Bingen et al. 2006).

Steep sinistral and dextral shear zones frequently cut through and deform the older blastomylonitic fabric in the LTB and contribute to a new transposing blastomylonitic foliation. In response to even further flattening, this blastomylonitic foliation was then itself extended and flattened, leading to a second generation of extensional shear bands and asymmetric drag folds, indicating the 'stretching fault' characteristics of these shear zones. Bingen et al. (2006) stress that it are these structures, resulting from late Pan-African SE-NW directed compression, that define the currently attenuated geometry of the LTB. Monazite in extensional shear bands has been dated at 531 ± 6 Ma.

- (3) **Absence of Pan-African magmatism in Mozambique south of 17° S** – In the ~1100 Ma Mesoproterozoic fold belts along the eastern margin of the Zimbabwe Craton (northern segment of the Kalahari Craton), the Pan-African Orogenic Cycle is expressed by thermal reactivation and metamorphic overprinting followed by cooling through the ~350°C iso-

therm at ~553 Ma (west) and ~468 Ma (east) (Manhiça et al. 2001). The Pan-African ages are confined to a narrow N-S directed zone of ductile shear that coincides with the eastern border of exposed Archaean rocks of the Zimbabwe Craton. In the model by Jacobs et al. (2006) this zone of maximum shear can be viewed as a suture between East and West Gondwana (Fig. 1.16). Recent field observations (Manhiça et al. 2001, GTK Consortium 2006, Koistinen et al. 2008) demonstrate, however, the absence of Pan-African ophiolites and, in particular, calc-alkaline TTG suites that can be related to a magmatic arc above a subduction zone having an age between 841 and 632 Ma (Cutten & Johnson 2006). Consequently, these authors conclude that accretion of the Mozambique Belt to the Kalahari Craton and amalgamation with Antarctica during the Grenville Orogenic Cycle (GOC) was maintained after the break-up of Rodinia but suffered repeated deformation and reactivation during the Pan-African at ~550 Ma and 470 Ma. The latter event involved the formation of N-S foliation with neosomes, rehydration, retromorphism and migmatisation of the older rocks.

- (4) **Reconstruction of the ~1.0 Ga Rodinia Supercontinent** – Reconstruction of Rodinia, mainly based on palaeo-magnetic data (Li et al. 1995, 2008, Dalziel 1997, Hoffman 1999), shows a close spatial relationship between the Kalahari and Antarctica proto-Cratons, amalgamated since the Grenville Orogenic Cycle, on the one hand and the remaining African 'building blocks' on the other hand (Fig. 1.9). Post-Rodinia rift/drift/dispersal and Pan-African reassembly requires the proto-Kalahari-Antarctica craton to spin and travel over a huge distance.

Oubanguides – Being located in the northeastern corner of the proto-Congo Craton, not only Neoproterozoic tectogenesis related to the EAO but also orogenic effects connected to formation of the Oubanguides or Central African Fold Belt (CAFB) can be observed in Uganda (Fig. 1.1; k in Fig. 1.16). The Oubanguides constitute an E-W belt that straddles the northern margin of the proto-Congo Craton and we relate some dated Pan-African granitoids in the northernmost part of Uganda – the 659 ± 15 Ma granitoids of the Adjumani-Midigo Suite (Section 11.6) – to subduction,

collision and amalgamation of the proto-Congo Craton and the Nile or East Sahara Craton (IV in Fig. 1.2) or meta-Craton³ (Fig. 1.1).

This belt is mainly known from Cameroon, but the history of the CAFB goes back to the 1980s when southward nappe tectonics in the Central African Republic was first described by Pin & Poidevin (1987), associated with poorly constrained (833 ± 66 Ma, 652 ± 19 Ma and 639 ± 3 Ma) Pan-African granulite-facies metamorphism. This solitary study further described a major low- to medium-grade sedimentary sequence of Palaeoproterozoic age (the Yangana schists), separating the Pan-African nappe units from the Congo Craton. Further eastwards – NE Congo, Central African Republic, South Sudan, northern Uganda – virtually no data was available.

Preliminary geochronological investigations from the Central African Republic (Toteu et al. 2008) manifest that: (1) two granodiorites involved in the Pan-African nappe tectonics yield a zircon U-Pb age of ~ 700 Ma; (2) a mafic amphibolite intrusive into gneiss involved in the nappe tectonics was dated at 562 Ma; (3) U-Pb (laser-ICPMS-

MC) data on well-rounded detrital zircons from a quartzite interlayered within the Palaeoproterozoic Yangana schists gave a majority of concordant plots defining an age of 2007 ± 12 Ma corresponding to the age of the dominant detrital source for quartzite; (4) 20 whole rock samples from granitoids and Yangana schists gave $e(Nd)$ at 0.6 Ga from -30 to -1 with TDM range from 2.7 to 1.5 Ga indicating a dominant old crustal component. The assumed Mesoproterozoic Sangha granitoids gave consistent Mesoarchean U-Pb zircon and Sm TDM ages, which definitely link these granitoids to the Congo Craton.

Zircon U-Pb data and Sm-Nd analyses of minerals and whole rock samples from north-central Cameroon show a long and complex crustal evolution beginning in the late Archaean and extending to the late Neoproterozoic. The northern margin of the Congo Craton shows again two successive orogenic cycles, the Eburnian at 2.1 Ga and the Pan-African at 0.6 Ga with a less prominent role for Mesoproterozoic (1.1–0.95 Ga) magmatic activity (Toteu et al. 1987, 1995, 2001, 2003, 2004a, 2004b, 2005, 2008).

1.8 Phanerozoic post-Pan-African Extensional Basins

Introduction – As a result of the generally extensive tectonic regime affecting Gondwana, in combination with the relatively central position of the present African plate, post-Pan-African convergent plate margin activity affecting the African plate was restricted to its northwestern (Moroccan Meseta, Mauritanides) and southern (Cape Fold Belt) margins (present-day orientation). Phanerozoic, compressive tectonism was associated with the closure of the Palaeo-Tethys (Palaeozoic Hercynian Rif-Tell) and subduction of the Palaeo-Pacific plate (Palaeozoic Hercynian Cape Fold Belt), as well as the closure of the Neo-Tethys Ocean during the Cretaceous-Tertiary, resulting in the formation of the Kabylia-Rif-Betic orocline – Arc of Gibraltar – that encloses the Alborán Sea, the westernmost part of the Mediterranean.

The development of African basins during the Phanerozoic can thus be related to the polyphase break-up of Gondwana, which was accomplished,

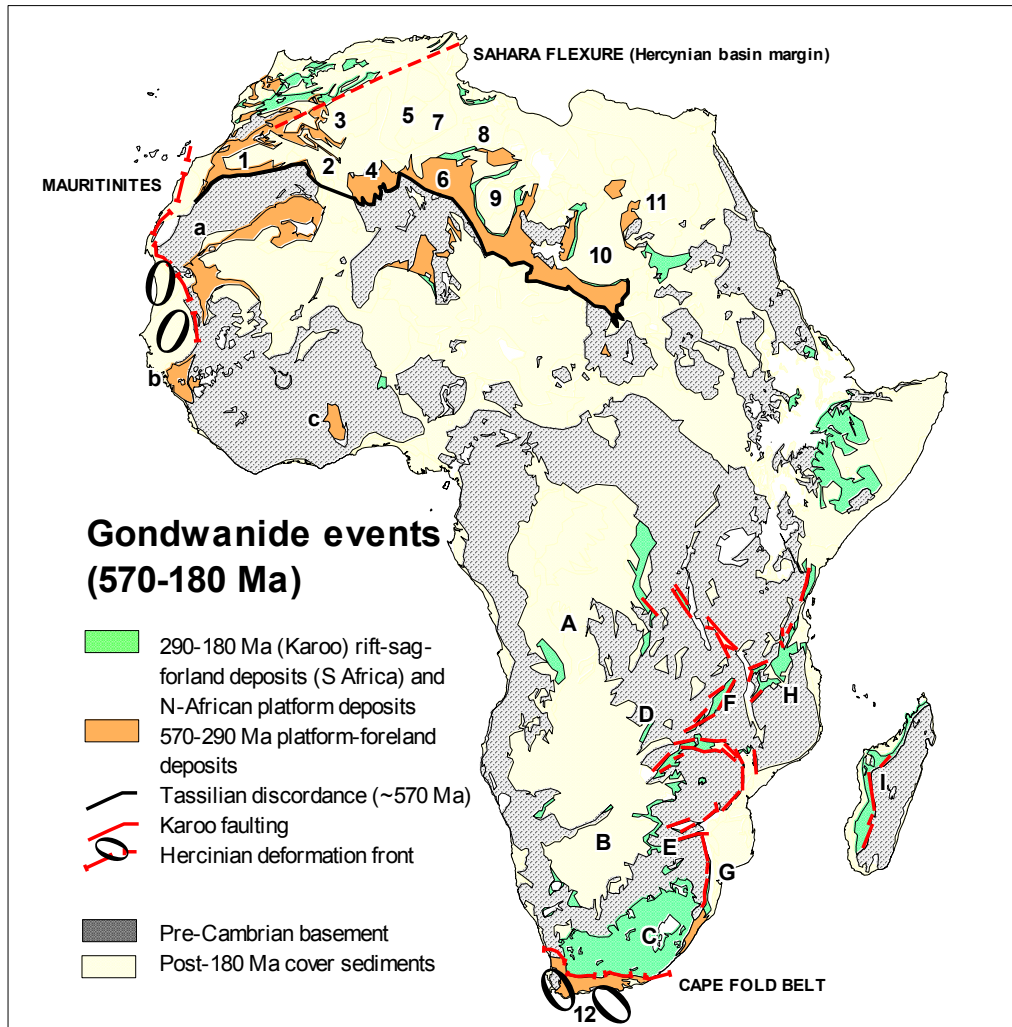
in general, by reactivation along Pan-African or older sutures or zones of crustal weakness. Four major phases of crustal extension and basin development can be distinguished: (1) Gondwanide (570–290 Ma), (2) Karoo (290–180 Ma), (3) Late Jurassic to Early Cretaceous Rifting (~ 160 Ma to ~ 100 Ma) and (4) the East African Rift System (EARS), which was initiated between the Late Eocene (~ 35 Ma) and Early Miocene (~ 20 Ma) and continues till today.

Gondwanide Basins – Gondwanide extensional basins of Cambrian-Carboniferous age (570–290 Ma) developed along the North and South African Gondwana margin in northern and western Africa (Morocco, Mauritania, Algeria and Libya) and the Cape Fold Belt (South Africa) and in foreland basins such as the Taoudeni, Bove and Volta basins (Fig. 1.17). Gondwanide basins are not exposed in Uganda but post-Pan-African, pre-Karoo Red

3 Meta-Craton refers to a craton that has been mobilised during subsequent orogenic event(s) but that is still recognisable through its rheological, geochronological and isotopic characteristics as Archaean–Paleoproterozoic cratonic lithosphere (Abdelsalam et al. 2003, 2011).

Beds, approximately 1000 m in thickness, underlie nearby Karoo to Holocene sediments in the present-day Congo River Basin (Tack et al. 2009, Kanda-Nkula et al. 2011). Post-Pan-African extension also gave rise to the emplacement of a number of

alkaline complexes and associated carbonatites in a crustal weakness zone corresponding with the present Western Branch of the East Africa Rift System (Fig. 1.14) with ages between ~550 and ~470 Ma (Tack et al. 1984).



Courtesy Paul Dirks 2003

| Cambrian-Carboniferous basins of the North & South African Gondwana margin (570–290 Ma) | | |
|--|---------------------------------|----------------------|
| 1 = Tindouf basin | 5 = Oed Mya basin | 9 = Murzuq basin |
| 2 = Reggane basin | 6 = Illizi basin | 10 = Kufrah basin |
| 3 = Bechar basin | 7 = Ghadames basin | 11 = Western Desert |
| 4 = Ahnet basin | 8 = Hamra basin | 12 = Cape Sequence |
| Base of sequence is formed by the Tassilian discordance (~570 Ma) Top of sequence is formed by the Hercynian unconformity (~290 Ma) | | |
| Cambrian-Carboniferous foreland basins (570–290 Ma) | | |
| a = Taoudeni | b = Bove | c = Volta basin |
| Permian-Triassic rift-sag basins (Karoo: 290–180 Ma) | | |
| A = Congo basin | D = Mid & Lower Zambezi rift | G = Lebombo rift |
| B = Kalahari basin | E = Luangwa rift | H = East Africa rift |
| C = Karoo basin | F = Tuli-Sabi-Soutpansberg rift | I = Malagasy basin |

Fig. 1.17. Gondwanide, post-Pan-African terrains (~570–180 Ma) (after Dirks & Ashwal 2002, with kind permission of the University of the Witwatersrand, Scholarly Communications & Copyright Service Office).

Karoo Basins – The term “Karoo” was first used to describe a 12 km thick depositional sequence from the Main Karoo Basin in South Africa, a retro-arc foreland basin associated with a magmatic arc and fold-thrust belt (Cape Fold Belt) system (e.g., Cole 1992). Karoo basins in sub-Saharan Africa manifest the break-up of Gondwana, which was initiated as early as the Late Carboniferous, though crustal break-up only began in earnest in the Jurassic and culminated with the emplacement of flood basalts and pyroclastics, starting in the Lower Jurassic around 183 ± 1 Ma (Johnson et al. 1996, Duncan et al. 1997), when Gondwana separated and the central Atlantic Ocean began to open (since ~ 200 Ma). In the Main Karoo Basin of South Africa the 183 ± 1 Ma (Duncan et al. 1997) continental flood basalts of the Drakensberg Group are considered to represent the integral top part of the Karoo Supergroup. It should be noted, however, that the distribution of Jurassic volcanics, supposedly related to pre-rift hot spot activity in Africa, is quite independent from the presence of Karoo sediments (compare Figs 1.17 and 1.19).

From a geodynamic point of view three types of Karoo basins can be distinguished: (1) large fore-deep/ sag basins, (2) passive margin basins and (3) intracratonic rifts. Foredeep/ sag basins include, apart from the Great Karoo Basin, the Kalahari, Barotse and Congo River basins. Intracratonic rift basins appear controlled by crustal weakness zones that were rejuvenated during the Late Palaeozoic Hercynian Orogeny (e.g., Cape Fold Belt) and ensuing continental break-up. Some of them evolved into passive margin basins, which are particularly developed along the Indian Ocean coast.

Karoo sediments were originally deposited in broad down-warps. As the deposition continued, rifting of such down-warps produced Graben-type structures, in which deposition of a great thickness of Karoo sediments took place. When comparing Karoo sedimentary successions, similar underlying processes and sequence of events are reflected in individual basin fills. Each lithological sequence normally commences with fluvioglacigenic rock types. This is followed by an interval in which red colours are absent and coal seams are commonly

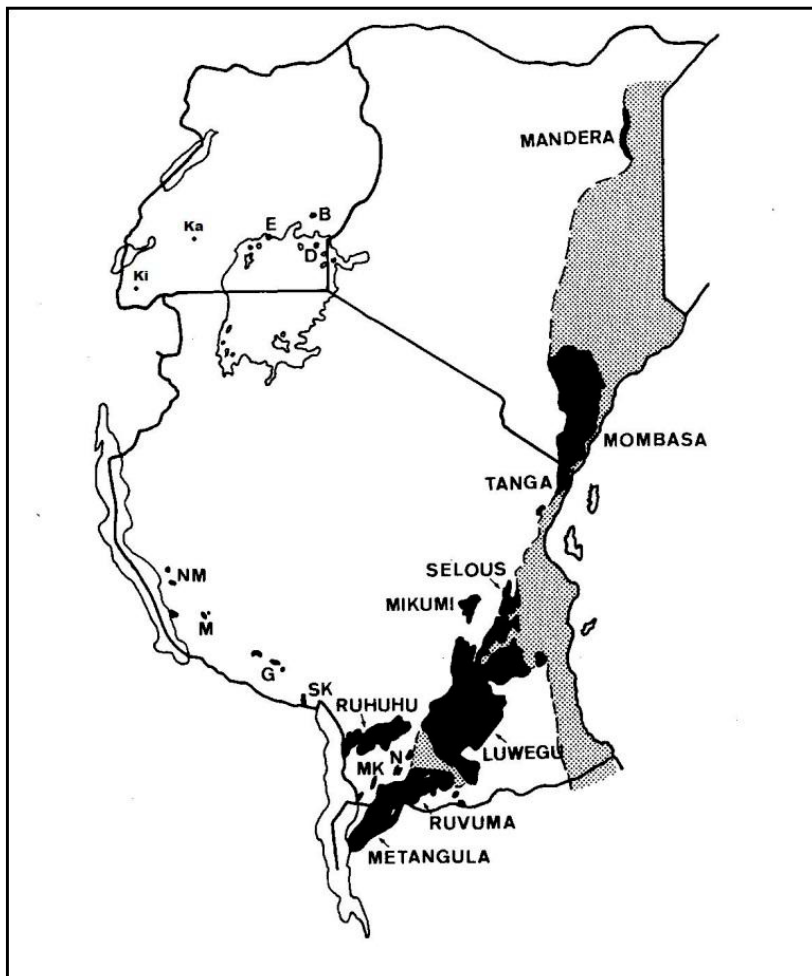
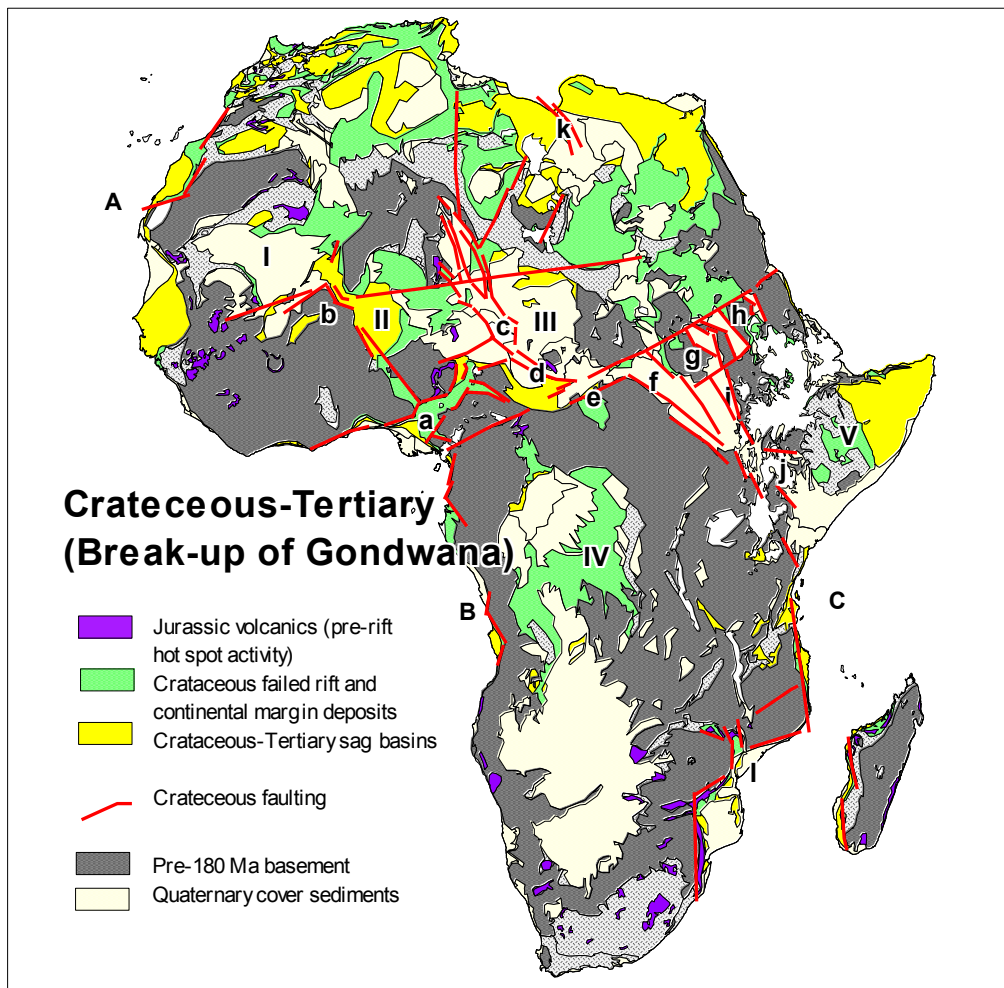


Fig. 1.18. Schematic distribution of Karoo rocks in East Africa. Key: black = outcropping; grey = sub-outcropping. SK = Songwe-Kiwira, G = Galula, M = Muze and NM = Namwele-Mkomolo. Small Karoo deposits in Uganda include: E = Entebbe, B = Bugiri, D = Dagusi Island, Ka = Katonga River and Ki = Kiruruma River Formation (Schlüter 1997, Westerhof et al. 2014).

present. The higher strata exhibit reddish and greenish mud rocks manifesting a change to oxidising sub-aerial conditions. Next, aeolian sandstones often cap the older succession and reflect increasing aridity. Finally, at ~180 Ma ago, basaltic lavas completed the succession in places. Although the above general trends can be observed in most Karoo sequences in southern and eastern Africa, rift development appears largely controlled by lo-

cal basin tectonics and, consequently, Karoo sequences may differ along strike in individual rift basins and between different rift basins (Schlüter 1997).

Thick deposits of the Karoo Supergroup are well preserved throughout southern and eastern Africa with deposits having been found as far north as the Mandera-Lugh basin extending within Kenya, Somalia and Ethiopia (Fig. 1.18). Major Karoo rift-



Courtesy Paul Dirks 2003

| Cretaceous failed rifts | | |
|---|---|---------------------------------------|
| a = Benue trough | e = Doba-Doseo basin | i = Melut basin |
| b = Gao basin | f = Muglad basin | j = Anza basin |
| c = Tenere basin | g = White Nile rift | k = Sirt basin |
| d = Bongor basin | h = Blue Nile rift | l = Lower Zambezi basin |
| Cretaceous Rifts developed into passive margins of the African Craton | | |
| A = North Atlantic Margin (~200 Ma) | B = South Atlantic Margin (~135 & 115 Ma) | C = Indian Transform Margin (~165 Ma) |
| Cretaceous-Tertiary sag basins | | |
| I = Taoudeni basin | III = Chad basin | V = Ogaden basin |
| II = Iullemeden basin | IV = Congo basin | |

Fig. 1.19. Post-Karoo break-up of Gondwana (180-40 Ma) (after Dirks & Ashwal 2002, with kind permission of the University of the Witwatersrand, Scholarly Communications & Copyright Service Office).

type basins occur in East Africa and include the SW-NE trending Metangula-Ruvumu-Luwegu-Selous Graben (e.g. Kreuser 1983, 1984, Wopfner & Kaaya 1991) and its northward extension along the Tanzanian-Kenyan coast (Fig. 1.18). Elsewhere, Karoo rift successions occur as windows below Cenozoic (and Mesozoic?) sediments in rather small and isolated polygons – e.g., Songwe-Kiwira, Galula, Muze and Namwele-Mkomolo units in the Rukwa Rift in southern Tanzania (Fig. 1.18) and the Congo River basin.

Karoo deposits are restricted to a few small polygons in southern Uganda (Fig. 1.18), particularly near the northern shores of Lake Victoria, but may have covered more extensive areas prior to EARS uplift and erosion. We report here for the first time a supposedly Karoo-age glaciogene deposit, comprising diamictites and drop stones in the North Kibaran Belt of SW Uganda (Ki in Fig. 1.18; West-erhof et al. 2014).

Late Jurassic – Early Cretaceous rifting – Salman & Abdula (1995) divided post-Karoo rift/drift/dispersal of Gondwana into three phases: (1) Early Cretaceous break-up, (2) Stabilisation between ~100 Ma and ~35 Ma and (3) Late Eocene-Neogene neo-rifting.

In our scheme crustal extension in Africa was rejuvenated already in the Late Jurassic (~165 Ma), lasted till the Early Cretaceous (~100 Ma) and was most notably heralded in eastern Africa by the emplacement of a clan of carbonatites and associated peralkaline rocks, called the Chilwa Alkaline Province (~133 Ma to ~110 Ma; Eby 2006) of southeastern Malawi and by a family of ~140 Ma kimberlites. The latter include an isochron age of 138 ± 9 Ma from a nearby kimberlite, structurally hosted by a margin fault of the Karoo Metangula Graben in northern Mozambique (Fig. 1.18) (Rb-Sr analyses of phlogopite; Key et al. 2007). Extensional structures developed as passive margin basins during continued opening of the North Atlantic, the Indian Transform Margin (~165 Ma) and the progressively northward opening of the South Atlantic (135–115 Ma). During the latter event the São Francisco Shield separated from the proto-Congo Craton (Fig. 1.6). Intraplate extension further led to the development of (failed) rift basins above triple junctions such as, e.g., the Benue Trough in west Africa ('a' in Fig. 1.22) and others developed into Cretaceous-Tertiary sag basins. Many of these basinal structures hold signifi-

cant hydrocarbon potential (e.g., Muglad Basin in the Sudan; Sirte Basin in Lybia; 'f' and 'k' in Fig. 1.22).

East Africa Rift System (EARS) – In eastern Africa rifting accelerated between the Late Eocene (~35 Ma) and Early Miocene (~20 Ma) and continues to the present day (Bumby & Guiraud 2005). The EARS (Fig.1.20) comprises an eastern branch that can be followed from south of Lake Nyasa (Lake Malawi) into the Afar Triangle (Ethiopia) and further northwards into the Red Sea, a young ocean, Gulf of Aden and Dead Sea pull apart basins. The Western Rift of the EARS branches off the Eastern Rift north of Lake Nyasa (Lake Malawi) and describes an arc-like structure of 1500 km in length till north of Lake Albert in northwestern Uganda. The northern segment of the Western Rift, between DRC and Uganda, called Albertine Rift, is characterised by ultrapotassic volcanics and the Rwenzori Mountains (up to 5109 m), the highest example of rift shoulder uplift of a block of crystalline basement in an extensional setting in the world.

A most characteristic feature of the EARS is the presence of narrow elongate zones of thinned continental lithosphere related to asthenospheric intrusions in the upper mantle (Chorowicz 2005). This hidden part of the rift structure is expressed on the surface by thermal uplift of the rift shoulders. Hence, the rift valleys and basins are organised over a major failure in the lithospheric mantle and in the crust they comprise a major border fault, linked in depth to a low angle detachment fault, inducing a symmetric roll-over pattern, eventually accompanied by smaller normal faulting and tilted blocks. Along strike, the EARS is composed of a unique succession of rift basins linked and segmented by intracontinental transform, transfer and accommodation zones (Chorowicz 2005).

In an attempt to sketch the EARS evolution through time and space, the role of plume impacts is considered primordial (Chorowicz 2005). The main phenomenon is formation of plume-related domes, weakening of lithosphere and, long after, failure inducing focused upper mantle thinning, asthenospheric intrusion and related thermal uplift of shoulders.

Considering the kinematics, divergent movements caused the continent to split along lines of pre-existing lithospheric weaknesses marked by ancient tectonic patterns that focus the exten-

sional strain (Chorowicz 1992). The plume-head, being 1000+ km in diameter, weakened the lithosphere and prepared the later first rifting episode along a pre-existing weak zone, a Pan-African suture zone bordering the future Afar region. The

Western Branch of the EARS also developed in a lithospheric weakness zone of anastomosing Ubendian, Kibaran and Pan-African fold belts in between the Tanzania and Congo Cratons.

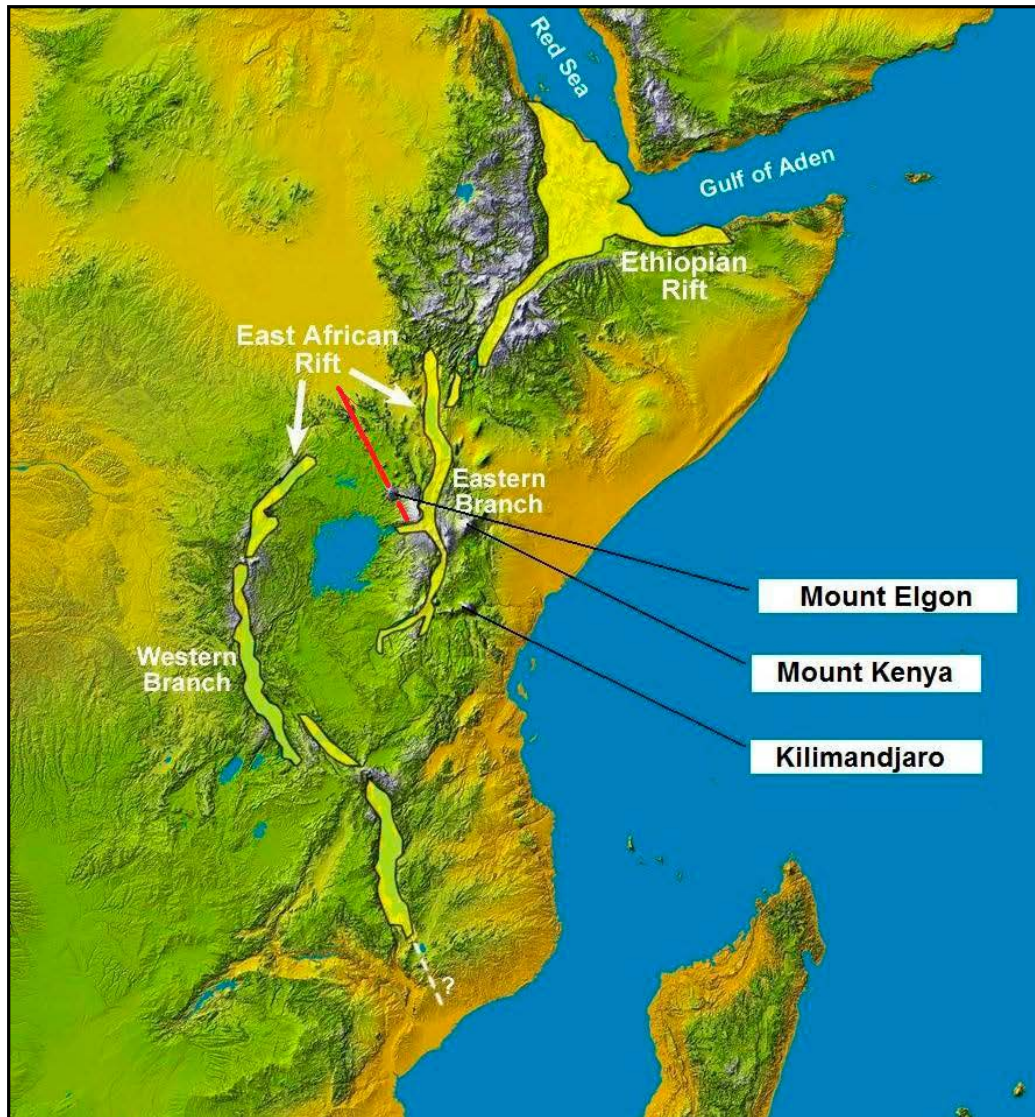


Fig. 1.20. Crustal extension in eastern Africa resulting in formation of the East Africa Rift System (EARS), comprising the Western Rift and Eastern or Main Rift. The latter progrades northward into the Red Sea, a young ocean, and pull-apart basins corresponding with the Gulf of Aqaba and Dead Sea. The Afar triangle is underlain by ocean floor rocks. Red line shows Elgon trend. Digital Elevation Model by SRTM.

2 LAKE VICTORIA TERRANE OF THE ARCHAEOAN TANZANIA CRATON

2.1 Tanzania Craton

In this publication the term ‘Tanzania Craton’ supersedes older names such as ‘Tanganyika Shield’, ‘Central Shield’ or ‘Central Plateau’. It is an Archaean oval-shaped lithospheric fragment, measuring 950 km from N to S and 500 km from W to E, covering an area of ~500,000 km² (Pinna et al. 1996).

The Tanzania Craton was amalgamated with the Congo Craton during the Palaeoproterozoic Eburnian Orogenic Cycle, forming the proto-Congo Craton (Fig. 1.6). As a consequence the Usagaran-Ubendian-Rusizian-Rwenzori system of fold belts was formed, one of various Palaeoproterozoic fold belts stitching the proto-Congo Craton together. There are differences of opinion whether the Tanzania Craton accreted to the Congo Craton as a new cratonic element (forming the proto-Congo Craton), or whether the Tanzania Craton was already part of the proto-Congo Craton prior to the Palaeoproterozoic, to be only temporarily separated from it, followed by re-unification.

The first map of the Tanzania Craton (scale 1:2,000,000) was prepared by Quennell (1956a) and shows an older, Early Archaean ‘Dodoman System’ overlain by the ‘Nyanzian and Kavirondian Systems’, surrounded by Usagaran and Ubendian Belts. Barth (1990) produced a more detailed map (scale 1:500 000), based on compilation of existing QDS maps. More recently, an updated map was prepared by BRGM et al. (2004), which was mainly based on the works of Pinna et al. (1996, 2000, 2004a, 2004b). This map portrays the Tanzania Craton not as a homogeneous

lithospheric block but composed of different tectono-thermal terranes. These are (from old to young): (1) the ~3.0–2.85 Ga Isanga-Mtera Terrane, (2) the ~2.90–2.50 Ga Dodoman Terrane, (3) undifferentiated Neoproterozoic migmatite–granitoids, mafic–ultramafic rocks overlain by the Kavirondian sedimentary rocks in the Basement Complex of Barth et al. (1996), later called Western Granitic Complex (Pinna et al. 1976) or Western Gneissic Terrane (Pinna et al. 2004b) and (4) the ~2.9–2.7 Ga Nyanzian Supergroup and ~2.75–2.50 Ga Kavirondian Supergroup of clastic-sedimentary rocks (late basins) in the Lake Victoria Goldfields of Barth (1990). These terranes amalgamated during the Archaean Era, roughly between >3.2 Ga and ~2.5 Ga, over a period of more than 700 Ma. Tectonic events include the ~2.93–2.85 Ga Dodoman and ~2.73–2.53 Ga Victorian orogenies, the latter marked by an early and late phase as shown by the unconformity between the Nyanzian and Kavirondian (see legend Fig. 2.1). Most recently, Kabete et al. (2012) divided the Tanzania Craton into several tectonic-metallogenic superterranes. We will follow the subdivision of Pinna et al. (1996, 2000; with additions of Schlüter 1997), as shown in Table 2.1, which is partly based on earlier work, including available K–Ar and Rb/Sr geochronological data, from Cahen & Snelling (1966), Wendt et al. (1972), Dodson et al. (1975), Ueda et al. (1975), Harris (1981), Bell & Dodson (1981), Cahen et al. (1984), Priem et al. (1979), SADC (1998), Gabert (1990) and Rammlmair et al. (1990). A subdivision by BRGM et al. (2004) is shown for comparison.

Table 2.1. Subdivision of the Tanzania Craton.

| Pinna et al. (1996, 2000, 2004a, 2004b; Schlüter (1997)) | | BRGM et al. (2004) |
|--|--|--|
| Kisii System (2.53 Ga) | | |
| Western Granitic Complex (2.56–2.58 Ga) | | Basement Complex, Western Gneissic Terrane |
| Lake Victoria Terrane | ‘Younger Granites’ (~2.5 Ga) | |
| (~2.9–2.5 Ga) | Kavirondian System (2.68 Ga) | Kavirondian Supergroup (~2.75–2.50 Ga) |
| | syn-to post-Nyanzian granitoids | |
| | Nyanzian System (~2.75 Ga) | Nyanzian Supergroup (~2.9–2.7 Ga) |
| | pre-Nyanzian basement (e.g. ‘Older granitoids’, ~3.1 Ga) | |
| Mtera Terrane (>2.7 Ga) | | Isanga-Mtera Terrane (~3.0–2.85 Ga) |
| Dodoma Terrane (2.9 Ga) | | Dodoman Terrane (~2.93–2.50 Ga) |
| Southern Basement Terrane (>3.2 Ga) | | |

Southern Basement Terrane – Mesoarchaean granitic gneisses and migmatites with ages of ~3.1 Ga (Schlüter 1997) or > 3.2 Ga (Pinna et al. 1996).

Dodoma Terrane – According to Pinna et al. (1996), this comprises an Archaean crustal nu-

cleus composed of gneissic or migmatitic tonalite, trondhjemite and granodiorite (TTG suite) with anatectic granite and cross-cutting mafic dykes (Fig. 2.1 with A¹D/ 24). This TTG suite has a typical Archaean geochemical signature, being highly depleted in HREE and less incompatible elements.

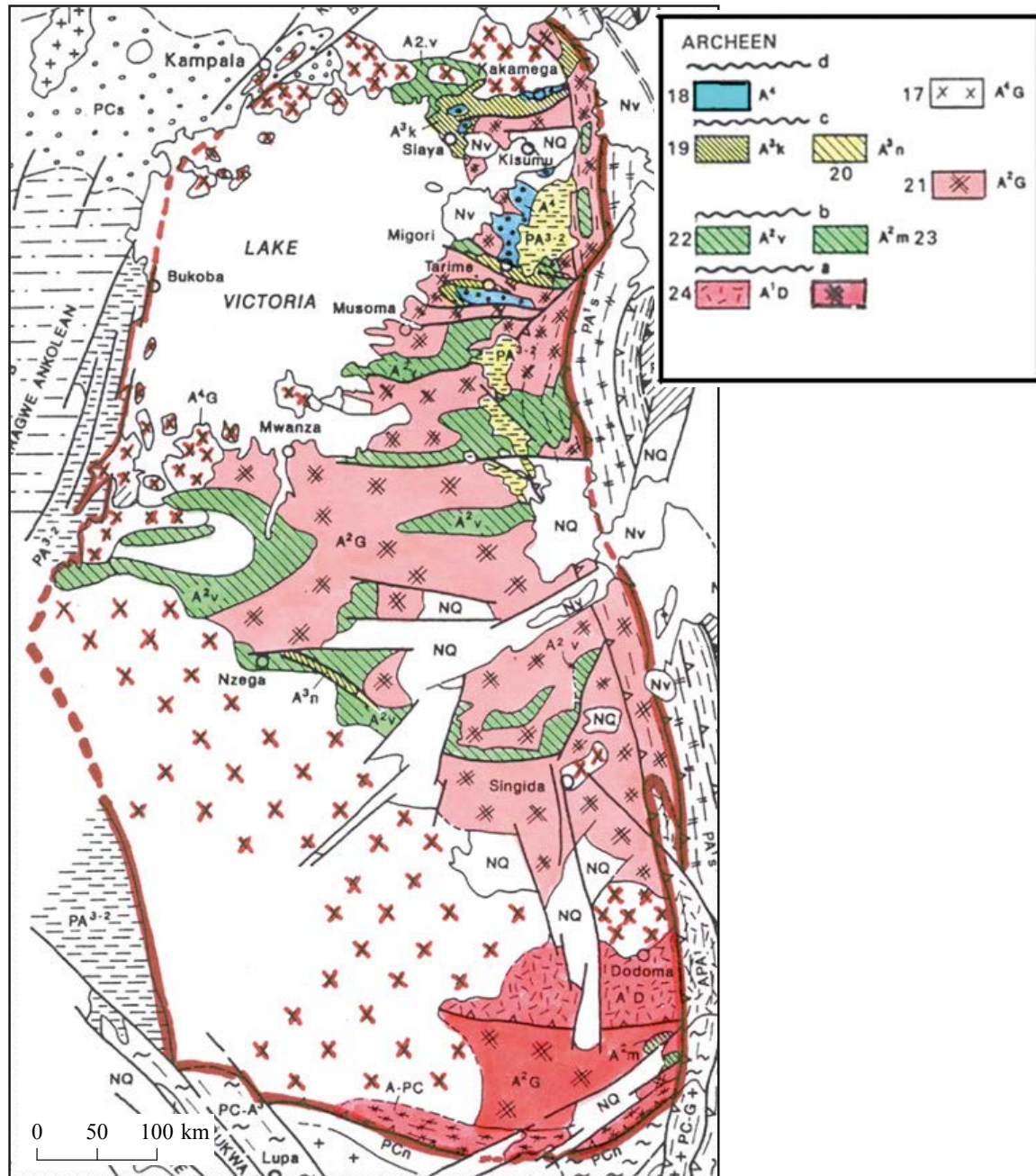


Fig. 2.1. Tanzanian Craton (adapted sketch map of the Tanzania Craton according to Pinna et al. (1966, with kind permission of BRGM) with colours added). Explanation of codes used: PA³⁻² = Kisii Group (yellow; 2.53 Ga); 17/A⁴G = post-orogenic granites (2.58–2.56 Ga) of Western Granite Complex; 18/A⁴, 19/A³k and 20/A³n = Kavirondian Supergroup (2.68–2.63 Ga), comprising 18 = Ronga Group, 19 = Kakamega Group and 20 = Nzega Group; 21/A²G = post-Nyanzian TTG suite (2.73–2.64 Ga) and 22/A²v = Nyanzian Supergroup (2.80–2.70 Ga); 23/A²m = Mtera Terrane (> 2.7 Ga; southeastern corner of Tanzania Craton); 24/A¹D = Dodoma Terrane (2.9 Ga). 15/A-PC = now incorporated in the Southern Basement terrain (> 3.2 Ga). Tectonic phases (in legend) include: a: Dodoman (~2.9 Ga), b: first Victorian phase (unconformity between Nyanzian and Kavirondian); c: second Victorian phase (unconformity between Kavirondian and Kisii Group); d: Palaeoproterozoic Eburnian Cycle (amongst others formation of the Usagaran-Ubendian-Rusizian-Rwenzori system of fold belts and proto-Congo Craton).

The Dodoma Terrane was affected by a major phase of NNW-directed deformation, restricted to the Dodoma Terrane (D_d), with widespread formation of blastomylonite and migmatite at ~2.9 Ga. Emplacement of the TTG parent rock thus took place prior to ~2.9 Ga as confirmed by ages up to 3.0 Ga (SADC 1998). Pb/Pb zircon geochronological results yielded ages between 2.93 and 2.87 Ga. The margins of the Dodoma Terrane have been thoroughly affected by intrusive granitoids and pegmatite dykes between 2.73 and 2.59 Ga (Hepworth 1972). Subsequently, the terrane was affected by a second E-W directed phase of deformation (D_2) that can be correlated with the Nyanzian Orogenic Cycle and recognisable in the entire Tanzanian Craton.

According to Schlüter (1997), the rocks of the equivalent Dodoman System represent an Archaean mobile belt that amalgamated the northern and southern parts of the Tanzanian Craton. The 'Dodoman Series' comprise high-grade metamorphic rocks such as granulite and charnockite with a steeply dipping E-W trending foliation (Coolen 1980), but also supracrustal rocks such as quartzites, sericite schists, talc-chlorite schists, amphibolites and hornblende gneisses. These metamorphosed sediments and other supracrustal rocks have been intruded by granite and pegmatite (Hepworth 1972).

Mtera Terrane – The Mtera Terrane is a small area (Fig. 2.1, code 23/A²m) located south of and formerly incorporated into the Dodoma Terrane (Gabert 1973). It is composed of thrust-transported, amphibolite-granulite facies supracrustal relics of mafic lava, ultramafic rock, quartzite and Mg-rich phyllite that have been intruded by a post-kinematic 2.71 Ga TTG suite. Hence, these supracrustal rocks have an age > 2.71 Ga.

Western Granitic Complex – This tectono-thermal domain forms a complex assemblage of gneisses, migmatites and weakly deformed granitoids in the western part of the Tanzania Craton (Fig. 2.1, code A⁴G/17). The terrane comprises alkali granites that are only slightly affected by Archaean deformation and are remarkably homogeneous, having a syn- to post-collisional crustal signature, very different from the TTG of older granites. The alkali granites are considered to be coeval with the "Younger Granites" of the Lake Victoria Granite-Greenstone

Terrane (Section 3.3) and an emplacement age of ~2.6 Ga is generally accepted (Pinna et al. 1996, 1997).

This terrane continues into southern Uganda (Chapter 3). Since 'Western Granitic Complex' is a very generic term we have renamed this tectono-thermal unit as 'West Tanzania Terrane'.

Lake Victoria Terrane – This Neo-Archaean granite-greenstone terrane will be discussed in further detail in Section 2.3.

Kisii Group (Fig. 2.1, code A₄/PA³⁻²) – The 'Kisii System', termed here the Kisii Group, located in the northeastern part of the Tanzania Craton, comprises an undeformed volcano-sedimentary sequence deposited on top of the rock units of the Lake Victoria Terrane. The sequence is composed of (Pinna et al. 2000) (from top to bottom):

- (5) *Upper Volcanoclastic Formation* – Lapilli tuffs of rhyolitic composition and a thick lahar agglomerate.
- (4) *Ikonge Ignimbrite Formation* – Coarse pyroclastic rocks passing upward into welded rhyolite tuff and massive rhyolite capped by volcanoclastic conglomerate and lapilli tuff.
- (3) *Arenite Formation* – Fine sandstones, sandy siltite and medium- to coarse-grained pure sandstones, 20 to 100 m in thickness.
- (2) *Kisii Basalt Formation* – Basalts and andesitic basalts (100–400 m in thickness).
- (1) *Lower Detrital Formation* – Local basal conglomerate, overlain by polymict conglomerate, silt-arenite and silt-pelite. The conglomeratic layers contain a complete lithological sampling of the underlying Lake Victoria Granite-Greenstone Terrane, including BIF, chert, rhyolite, basalt and schist fragments of the Nyanzian Supergroup.

K-Ar data have yielded an age of ~930 Ma for the Kisii Group (Cahen et al. 1984), which suggests post-Rodinia deposition and a relation with the Neoproterozoic Malagarasi Supergroup. New geochronological data (Pb evaporation on zircon) yields, however, an Archaean age of c. 2531 Ma (average of four measurements, Pinna et al. 2000). The Kisii Group was thus deposited after the last 'Victorian' deformation phase (~2.63 Ga), shortly after the emplacement of the "Younger Granites" (Borg & Shackleton 1997).

2.2 Major Lithostratigraphic Units of the Lake Victoria Terrane

Lake Victoria Terrane underlies the northern and eastern part of the Tanzania Craton (mostly north of 5° S). It is a typical Neoarchean granite-greenstone assemblage consisting of large amounts of intrusive granitoids and variably tectonised, epito non-metamorphic supracrustal rocks. The latter are not randomly distributed but occur in a number of greenstone clusters (Fig. 2.2). In general and in simple terms the Lake Victoria Terrane can be divided into (from old to young):

- (1) gneisses of the pre-Nyanzian Basement
- (2) metavolcanic-dominated supracrustals of the Nyanzian Supergroup
- (3) syn- to post-Nyanzian Granitoids;
- (4) metasedimentary-dominated supracrustals of the Kavirondian Supergroup
- (5) 'Younger Granites'

2.2.1 Pre-Nyanzian Basement

Large volumes of syn- to post-Nyanzian (2.72 Ga) and post-Kavirondian (2.58–2.55 Ga) "Younger Granites" have largely obliterated possible remains of older 'Dodoman' basement in the Lake Victoria Terrane. The present state of mapping does not allow distinguishing between pre-, syn- and post-Nyanzian granites/gneisses and younger felsic to intermediate plutonic rocks. Stockley (1935) attributed foliated "G₁" granite in the Musoma District (MM in Fig. 2.2) to an undifferentiated Basement Complex of the craton. In a later publication (Stockley 1947), he reported a few patches of granite gneisses in the Mwanza area as pre-Nyanzian basement that he could distinguish from extensive zones of syn- and post-Nyanzian granites comprising leucogranite, porphyritic granite, biotite

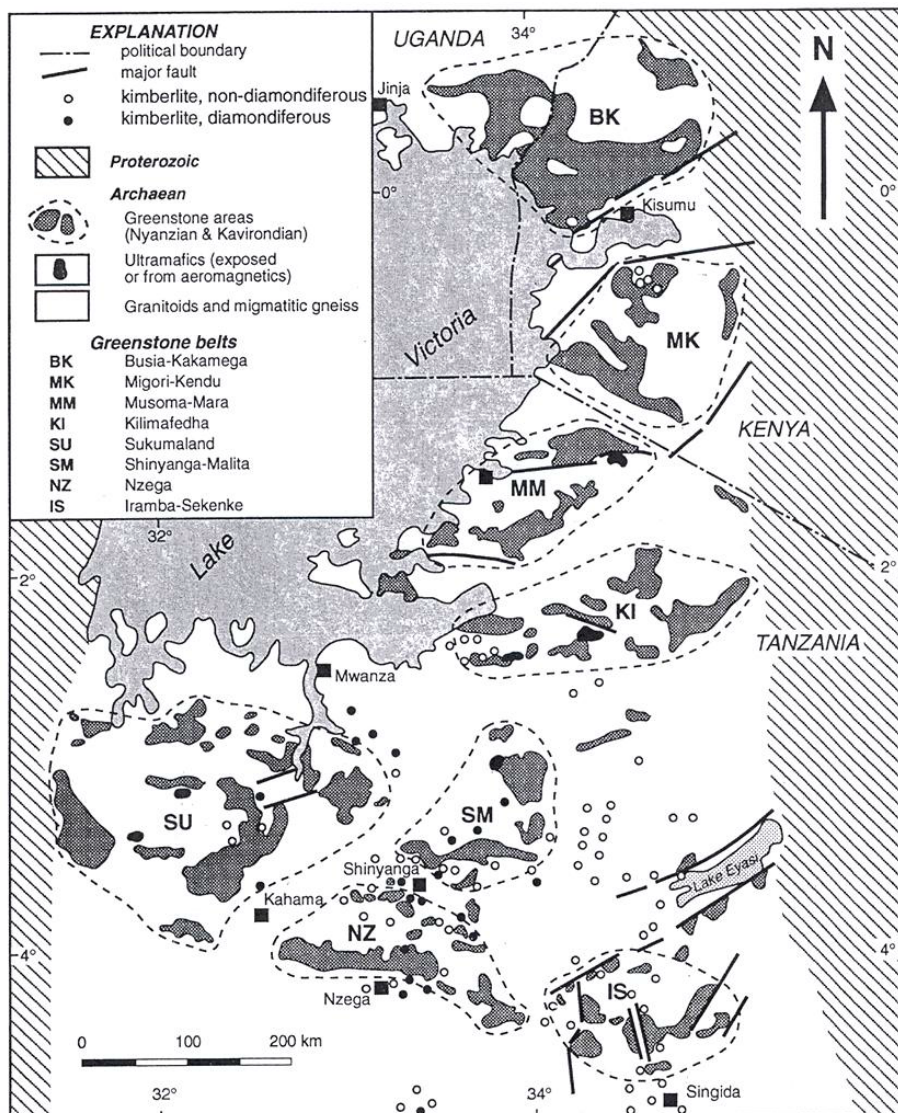


Fig. 2.2. Lake Victoria Terrane is a typical Neoarchean granite-greenstone assemblage showing clustering of greenstone belts and kimberlite pipes. These clusters are: SU = Sukumaland; NZ = Nzega; SM = Shinyanga-Malita; IS = Iramba-Sekenke; KI = Kilimafedha; MM = Musoma-Mara; MK = Migori-Kendu and BK = Busia-Kakamega (which continues into SE Uganda). Few greenstone belts occur south of Singida. From Borg & Shackleton (1997 with kind permission of the Oxford University Press).

granite, hornblende granite, tonalite and undifferentiated and inferred granitoids.

Borg & Shackleton (1997) also searched, in vain, for older, pre-Nyanzian granitoids. Paragneisses attributed to the so-called 'Dodoman G_3 -basement' (*sensu* Grantham et al. 1945) north of Kahama, show indications of former sedimentary layering and graded bedding. A first single zircon age from a melanosome of these paragneisses (2680 ± 3 Ma, see Borg & Krogh 1999) shows that at least a part of the alleged 'basement gneisses' is of syn-Nyanzian origin. Nearby orthogneisses yielded a whole-rock Rb/Sr age of 2570 ± 50 Ma (Rammlmair et al. 1990), an age that is attributed to a regional phase of migmatitisation.

2.2.2 Nyanzian Supergroup

Initially, Pinna et al. (1996) divided these supracrustal rocks (Fig. 2.1, code 22/A²v) into four lithostratigraphic units, i.e., the Nyanzian, Kakamega, Nzega and Rongo Groups. In a later publication (Pinna et al. 2000), the predominantly metavolcanic supracrustals of the Nyanzian Group have been regrouped into the Nyanzian Supergroup. This term was introduced by the SADC Mining Sector Co-ordinating Unit (Härtzer et al., in SADC 1998) and named after the type-area at the SE edge of Lake Victoria, also called Victoria Nyanza. The Nyanzian Supergroup correspond with the greenstone belts of the Lake Victoria Terrane established by Stockley (1943) and supersedes the generic name 'Upper Division Basement Complex'. Predominantly sedimentary rocks of the Kakamega, Nzega and Rongo belts are attributed to the Kavirondian Supergroup.

Compared to other Neoproterozoic cratons, the greenstone belts of the Lake Victoria Terrane are characterised by notably less tholeiites and komatiites and more andesites and pyroclastic rocks. The greenstones have been strongly deformed and affected by greenschist-facies metamorphism. A geodynamic setting, analogous to that of a back-arc or continental magmatic arc, is generally envisaged in SW Kenya (Ichang'i & MacLean 1991, Opiyo-Akech 1991, Opiyo-Akech et al. 2006).

The base of the Nyanzian Supergroup is nowhere exposed. A typical metavolcanic sequence comprises (from bottom to top) basalts, covered

by andesitic to dacitic lavas and tuffs, overlain by rhyolitic lavas and tuffs, commonly with relatively thick interbedded metasediments throughout the succession. Pinna et al. (1996) reported an imprecise Sm/Nd isochrone age of 2743 ± 87 Ma for chondritic basalts (of the Ngasamo Formation) with minor ultrabasic metavolcanics. Metabasalts are commonly intermediate K-basalts with tholeiitic affinity, close to compositions of Phanerozoic MORB, but the REE, incompatible elements and Nd isotopes are typically Archean and suggest slightly depleted sources still close to the primordial mantle. Felsic metavolcanics comprise calc-alkaline and high-K rhyolites. The latter yield a zircon age of 2.71 Ga (Pinna et al. 1996). The lower part of the metavolcanic succession is emplaced sub-aqueously, the upper part sub-aerially. The interbedded sedimentary rocks are composed of probably volcanogenic greywacke turbidites and horizons of banded iron formation (BIF).

2.2.3 Syn- to post-Nyanzian granitoids

Syn- to post-Nyanzian granitoids are feldspar-porphyrific, hornblende-bearing granitoids (Fig. 2.1, code 21/A²G) with plagioclase dominating K-feldspar and dated at ~ 2.72 Ga (Pinna et al. 1996). When plotted on An-Ab-Or diagrams they straddle the field between tonalite-trondhjemite and granodiorite-adamellite. According to Opiyo-Akech et al. (1999, 2006) they are primitive I-type granitoids of calc-alkaline affinity. Most of them have high Ba and Sr contents and low Y and HREE, typical of many TTG plutonic suites (Opiyo-Akech et al. 2006), as in modern adakites¹. They concluded that the geochemistry of these granitoids is most compatible with subduction-related melting of a mafic source under eclogite-facies conditions. Crustal assimilation and fractional crystallisation are suggested to have played only minor roles.

2.2.4 Kavirondian Supergroup

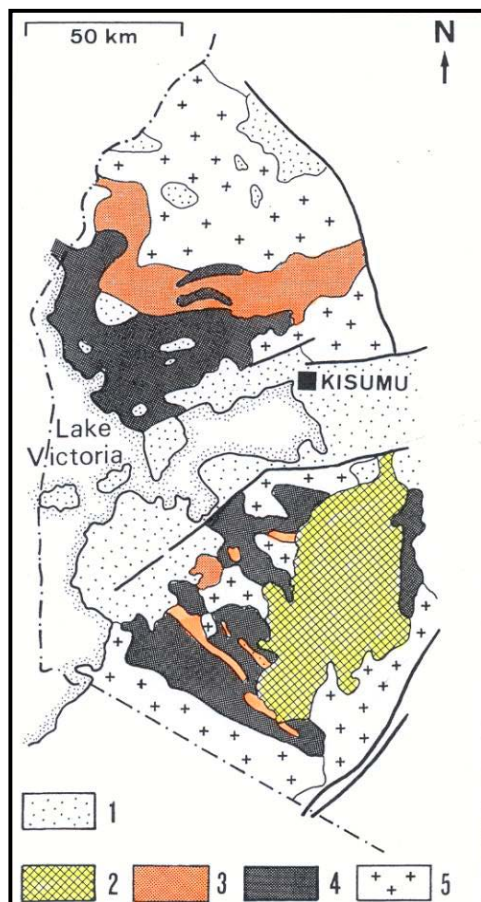
The Kavirondian was originally described as the 'North Mara Series' (Stockley 1935) in the Musoma-Mara cluster (Fig. 2.2) as an intensely folded assemblage of clastic rocks, overlying unconformably the volcanics of the Nyanzian (Harpum 1956).

¹ **Adakite** is a petrologic term for a volcanic or intrusive igneous rock that forms by melting of a subducting slab of oceanic crust basalt.

Lithologies of the Kavirondian are predominantly deposited in the NE part of the Tanzanian Craton (Fig. 2.1, code 19/A³k), particularly in the central Nzego Basin (Fig. 2.2), where they are less intensively deformed as manifested by relatively wide to open folds and a single cleavage, instead of two as in Nyanzian rocks. Major rock types comprise basal conglomerates, fining-upwards into grits, quartzites and minor pelites. The basal conglomerate contains boulders, up to one metre in size, that include most Nyanzian lithologies such as banded chert, Fe-rich BIF, vein quartz, felsic volcanics and granitoid. Clasts of Lower Nyanzian mafic metavolcanics are generally absent. In some greenstone belts – e.g., the Busia-Kakamega (Section 2.3), Rongo and Nzego greenstone belt (Fig. 2.2) – the supracrustal successions are mainly composed of lithologies tentatively attributed to the Kavirondian Supergroup.

2.3 Lithostratigraphy of the Lake Victoria Terrane in SE Uganda

In the geological map of Uganda compiled by Trendall (1961a) and Macdonald (DGSM 1966), the Lake Victoria Terrane of the Tanzania Craton extends into the southeastern corner of Uganda,



2.2.5 Younger granitoids

Post-Kavirondian granitoids (Fig. 2.1, code 17/A⁴G) are concordantly emplaced into lithologies of the Nyanzian and Kavirondian Supergroups and older units of the Lake Victoria Terrane. They are dated at ~2.58 to 2.55 Ga throughout the Tanzania Craton (Pinna et al. 1997, Borg & Shackleton 1997). Ages between 2644 and 2490 Ma have been reported by Härtzer et al. (in SADC 1998), but could actually represent a mixture of syn-Nyanzian and younger granitoids. Opiyo-Akech (1992) even attributes a post-Archaean age of ~2.4 Ga to these rocks. So far these granitoids have not been mapped as separate plutons in the Lake Victoria Terrane.

where it occupies an area of some 5000 km². It is mainly composed of supracrustal rocks attributed to the Nyanzian and/or Kavirondian Supergroups and ‘Younger Granites’ and constitutes the northward extension of the Busia-Kakamega greenstone belt of western Kenya (Fig. 2.3).

Mapping by the GTK Consortium has enlarged considerably the extent of the Lake Victoria Terrane to the west, where it is mainly covered by folded and epimetamorphic rocks of the Palaeoproterozoic Buganda Group (Fig. 2.4). It comprises predominantly mafic metavolcanic rocks of the Nyanzian Supergroup, overlain by a unit composed of felsic metavolcanics and metasediments of the Kavirondian Supergroup and several granitoids attributed mainly to the ‘syn- to post-Nyanzian Granitoids’ and ‘Younger Granites’. The Lake Victoria Terrane further comprises a number of Archaean pipe-like gabbroic bodies along

Fig. 2.3. Geological sketch map of southwestern Kenya. The northernmost greenstone belt is the Busia-Kakamega belt, which continues into SE Uganda. It is separated by Neogene rift from the southern Migori-Kendu greenstone belt, which is partly covered by rocks of the Kisii Group (slightly modified after Schlüter 1997, with kind permission of Springer Verlag). Key: 1 = Cenozoic cover (sediments and volcanics); 2 = Kisii Group; 3 = Kavirondian Supergroup; 4 = Nyanzian Supergroup; 5 = Granites. Black lines = Major faults.

its northern contact with the West Tanzania Terrane, supposedly representing 'stitching plutons'. Of interest in the Lake Victoria Terrane is also, the presence of the Archaean Maluba nepheline syenite.

2.3.1 Nyanzian Supergroup

Nyanzian rocks in SE Uganda are composed of predominantly mafic metavolcanics with subordinate intermediate and felsic metavolcanic rocks and metasediments. Detailed mapping of the Nyanzian rocks is, however, difficult. Exposures are scarce, in particular of the mafic metavolcanic rocks. Felsic metavolcanic rocks and more resistant metasediments form local ridges, while mafic metavolcanics occupy the flat lower ground, as

indicated by a chocolate brown soil cover. Fortunately, airborne geophysics allows an accurate delineation of this unit.

The Nyanzian Supergroup in SE Uganda is divided here into the Bulamba (A3VB; bottom) and Sitambogo (A3VL; top) Groups. The lower group is dominated by mafic metavolcanics, with the amount of intermediate and felsic metavolcanic (and associated chert) increasing upward. Pillow-textured metabasalt is exposed in the lowermost sub-facies with pillows typically ca. 30 cm in size and younging upwards. Acidic to intermediate metavolcanic layers have been outlined as topographic ridges and include metarhyolite and layered metatuff. Metarhyolite typically exhibits a porphyritic texture, with an aphanitic to fine-grained matrix containing

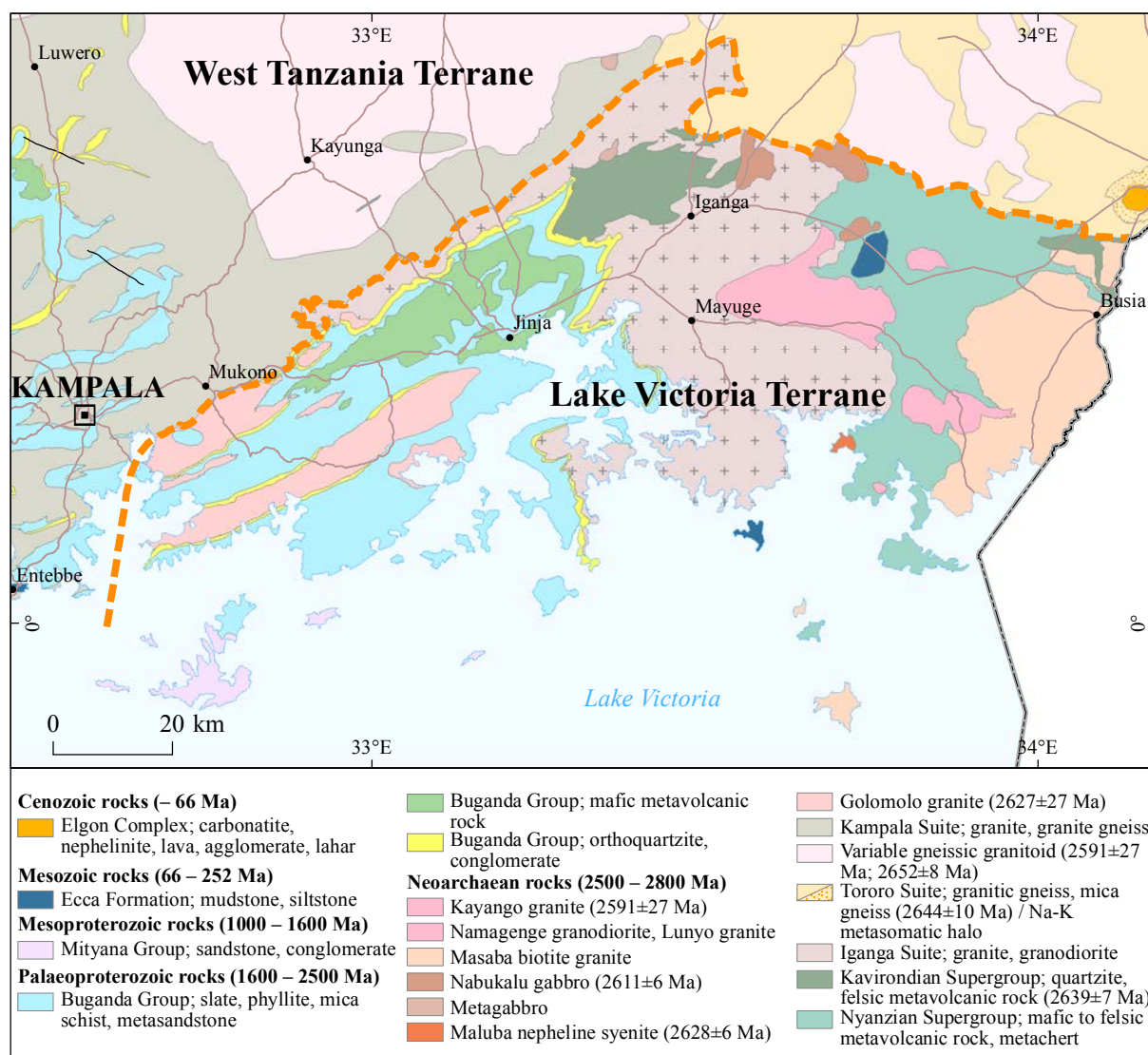


Fig. 2.4. Contact between the Lake Victoria and West Tanzania Terranes (orange line) of the Tanzania Craton. Between Jinja and Kampala, the Lake Victoria Terrane is overlain by metasediments of the Palaeoproterozoic Buganda Group and emerges only as elongated domes in the cores of anticlines.



Fig. 2.5. Distinctly bedded chert horizon with solid chert layers, 1–10 cm wide, separated by thinner (1–2 cm) ferruginous chert layers (608768E / 58061N).

quartz phenocrysts. Chemical analyses by the GTK Consortium show basaltic and andesitic to rhyolitic compositions and affinities ranging from calc-alkalic and tholeiitic to komatiitic. Representative chemical analyses are shown in Appendix 2 (anal. 1–6).

The rocks of the Sitambogo Group are mainly cherty quartzite, shale, black shale and BIF. Owing to their hardness and resistance to weathering, cherty quartzites constitute some conspicuous ridges. The pure, cherty quartzites are mainly cryptocrystalline to very fine-grained rocks with, in some places, a visible layering (Fig. 2.5). Their iron content is generally low, and elevated iron content is observed only in places (see App. 2, anal. 7).

2.3.2 Kavirondian Supergroup

Davies (1956) attributed sediments of the overlying Kavirondian Supergroup along Malaba River at the Kenyan border to the erstwhile ‘Samia Series’. They contain fragments of the Nyanzian ‘Bulugwe Series’. In southeastern Uganda Kavirondian rocks are divided into the Malaba River and Busiro Formations.

The Malaba River Formation (A3VKss) comprises a heterogeneous succession of psammitic metasediments, including polymict conglomerates, grey-

wackes, sandstones, shales and mudstones that cover metavolcanic rocks of the Nyanzian in western Kenya (e.g. Mathu & Davies 1996). Davies (1956) also described metagreywackes and conglomerates, the latter with clasts of lava, porphyries and metasediments. Locally, veins and dykes of light brown, leucocratic granite intrude bluish grey, buff-weathering quartzite exposed in the river, south of the Malaba railway bridge.

The Busiro Formation (A3S) is mainly composed of felsic metavolcanic rocks, randomly exposed NW and N of Iganga town (Fig. 2.4), in an area extending over 30 km NE of the quartzite hills of the Lake Victoria Formation (Fig. 2.11), a landmark formed by the base of the Palaeoproterozoic Buganda Group. These felsic metavolcanics, interpreted to mostly represent pyroclastic deposits, are light coloured, fine- to medium-grained, weakly foliated and rather massive rocks, the primary bedding being only seldom visible as a vague banding (Fig. 2.6A). Some outcrops near the contact with the overlying quartzites of the Victoria Formation exhibit a volcanic breccia structure with angular to sub-rounded fragments, ranging in size from a few centimetres (Fig. 2.6B) to roundish blocks up to 15 x 40 cm (Fig. 2.6C). Frequently, these felsic metavolcanic rocks have been intruded by leucogranitic dykes, and isolated



Fig. 2.6. Pyroclastic structures in felsic metavolcanics of the Busiro Formation. (A) Vague banding in felsic metatuff, intruded by granitic dykes. Note a thin, diagonal shear zones (546731E / 84059N). (B) Angular to rounded lava and ignimbrite fragments in a tuffitic matrix. (C) Large lava fragments (bombs?) in a tuff matrix (536837E / 64263N). Length of hammer 60 cm, number tag 10 cm.

fragments of pyroclastic rock, enclosed in granite, are rather common.

The average modal composition of fine-grained matrix of the breccia, dominated by subhedral crystals with an average size of 1–2 mm, is quartz (~35 vol%), K-feldspar (~35 vol%), hornblende (5–15 vol%), biotite (5–20 vol%) and plagioclase (~5 vol%); apatite, zircon, sericite, chlorite and opaque minerals occur in accessory amounts. Chemical composition of felsic metavolcanites of the Busiro Formation correspond to dacite and rhyolite (see App. 2, anal. 8–10).

U-Pb isotope dating (MC-LA-ICP-MS method) of 20 zircon grains extracted from a felsic metatuff sample yields an age of 2639 ± 7 Ma (sample UG-22_4258 in Mänttari 2014).

2.3.3 Synkinematic granitoids of the Lake Victoria Terrane

Pre-Nyanzian felsic or intermediate plutonic rocks have not been observed in the Ugandan segment of the Lake Victoria Terrane. Only the Golomolo granite with a 'Kavirondian' age qualifies as synkinematic granite.

Golomolo granite (A3Gpgr) – The Golomolo granite occurs east of Kampala city in three 'pseudodomes' in the core of anticlines below folded metasediments of the Proterozoic Buganda Group. Two of the domes are elongated, 25 x 6 km and 50 x 6 km in size, and the third one has an oval shape with a diameter about 6 km.

Both coarse porphyritic and medium-grained subfacies are observed in the Golomolo granite (Fig. 2.7). The mostly pinkish and greyish granites are generally mildly deformed and show a tectonic fabric due to a preferred orientation of the minerals that formed after emplacement of pegmatite dykes. Main minerals are K-feldspar, plagioclase, quartz and biotite, euhedral to subhedral K-feldspar (microcline) phenocrysts having diameters between 1 and 4 cm. The amount of biotite varies between 5 and 10 vol%, while epidote and magnetite are common accessory minerals. Locally, the granite grades into leucocratic granodioritic types, with K_2O contents less than 4 wt% (see App. 2, anal. 11–13).

U-Pb zircon dating (MC-LA-ICP-MS method) of the porphyritic Golomolo granite shown in Fig. 2.8. yields a crystallization age of ca. 2.63 Ga (UG-



Fig. 2.7. Porphyritic Golomolo granite with pegmatite dykes. Note the post-pegmatite ENE-trending tectonic foliation (503611E / 26731N). Number plate 10 cm.

1_1015; Mänttari 2014), synkinematically with metatuffites of the Busiro Formation (Kavirondian Supergroup).

2.3.4 Postkinematic intrusives of the Lake Victoria Terrane

Most granitoids of the Lake Victoria Terrane can be regarded as post-Nyanzian/post-Kavirondian ‘Younger Granites’ of the Busia-Kakamega granite-greenstone belt. This includes the large Masaba biotite granite, the variegated granitoids of

the Iganga Suite and three smaller granite plutons, namely the Lunyo granite, the Namagenge granodiorite and the Kayango granite. A small alkaline pluton, supposedly bound to the Nyanzian volcanic rocks is called Maluba nepheline syenite.

Masaba biotite granite (A3VMgr) – The 1:50 000 Busia Map Sheet of Davies (1934b) portrays the Masaba pluton as being composed of three granite bodies: (1) biotite granite, (2) granite porphyry and (3) muscovite granite (Fig. 2.8). Biotite granite is allegedly the most prominent rock and is sur-

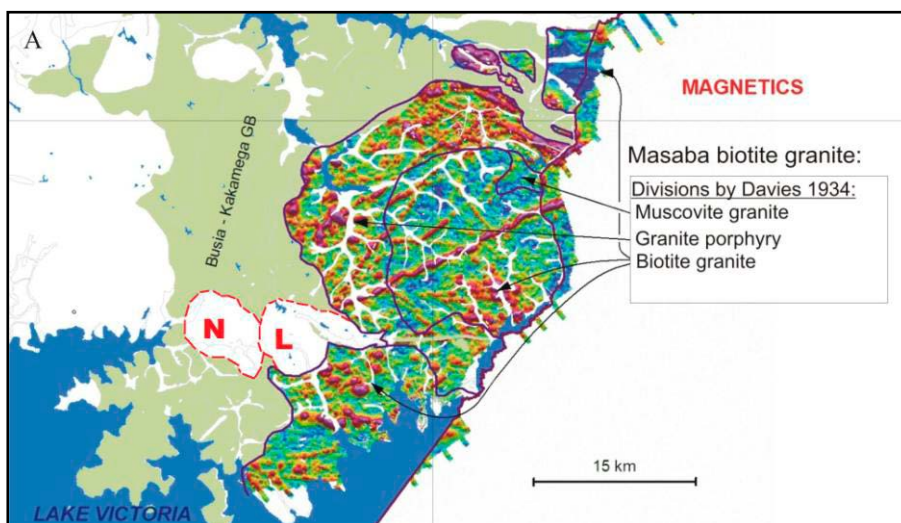


Fig. 2.8. Distribution of the Masaba biotite granite. Image shows subdivision into various granitic members according to map prepared by Davies (1934b). Linear magnetic features portray mafic dykes. Key: N = Namagenge granodiorite; L = Lunyo granite.

rounded in the west by an arcuate, ca. 5 km wide body of granite porphyry. Finally, a minor body of muscovite granite occurs within the biotite granite. This subdivision has not been confirmed by recent field verification by the GTK Consortium.

The Masaba biotite granite underlies a fairly flat to moderately undulating surface, being of ca. 15 x 50 km in size, with occasional inselbergs (Fig. 2.9). The results of analysed samples from the Masaba biotite granite are shown in Appendix 2 (anal. 14–17). They plot within the granite field of the TAS diagram (Fig. 2.22A). The total alkali content is low in comparison to nearby granitoids, which is due to low potassium contents (Fig. 2.21G). Also the CaO content does separate the Masaba biotite granite from other granites. The CaO/SiO₂ ratios of the Masaba granite are noticeably high and the samples form a distinct trend from other granitoids (Fig. 2.21E). The chemistry of the Masaba biotite granite – like lower K-content but higher Ca-content with same SiO₂ concentrations compared with other nearby granitoids – points towards tonalitic compositions. Five samples of the Masaba granite show peraluminous affinities while one sample is clearly metaluminous (Fig. 2.22B). On tectonomagmatic discrimination diagrams, all samples plot in either the ‘volcanic arc’ or ‘syn-orogenic granite’ fields (Figs 2.22D-E).

Namagenge granodiorite (A3Ngrdr) – West of the Masaba pluton two smaller intrusives that show strongly different radiometric signatures have been emplaced into the Nyanzian metavolcanics. These are the Namagenge and Lunyo granites, respectively (Figs 2.8 and 2.10). The Namagenge granodiorite is an oval shaped body of nearly 40 km² in size. In airborne geophysical maps, the Namagenge granodiorite shows a high potassium signature, similar to the Lunyo granite to the east. However, thorium and uranium contents are significantly lower when compared to the Lunyo granite (Fig. 2.10). Magnetic intensities of the Namagenge granodiorite are low and do not differ from the surrounding Nyanzian country rocks.

From scarce geological observations it is concluded that this medium- to coarse-grained, partly porphyritic igneous rock is monzodioritic to granodioritic (possibly with amphibole) in composition. Enclaves of (quartz)-dioritic and mafic compositions occur in places.

Lunyo granite (A3Lgr) –The Lunyo granite pluton is also about 40 km² in surface exposure and it is characterised by high U and Th (Fig. 2.10). The typically red brown coloured, medium- to coarse-grained Lunyo granite is a porphyritic rock with K-feldspar phenocrysts up to ~15 mm in length. The rock has a pronounced E-W directed fabric, which



Fig. 2.9. Masaba biotite granite at Buteba Hill near the Kenyan border (624805E / 59710N).

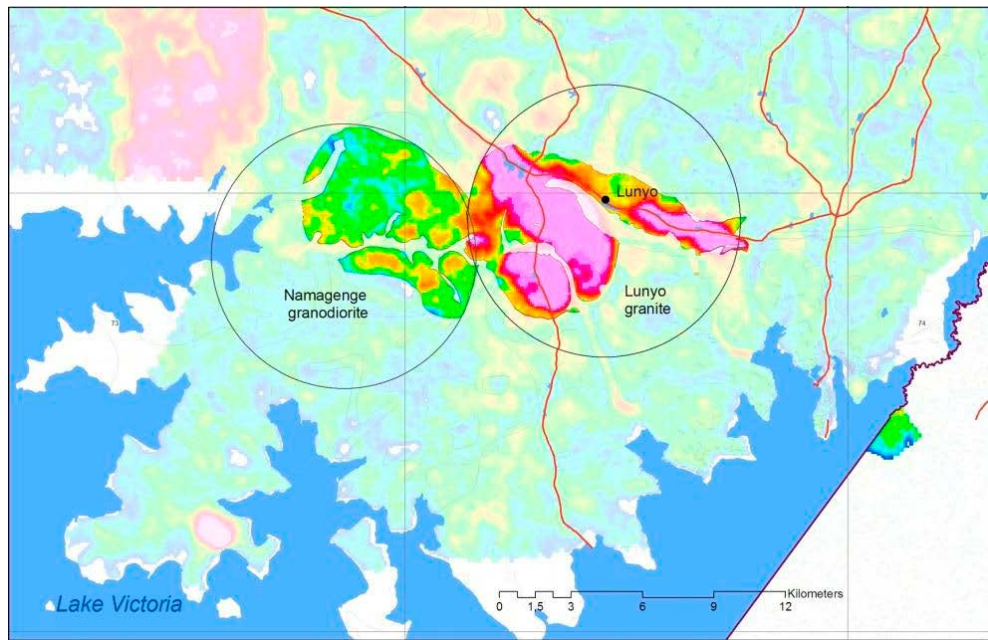


Fig. 2.10. Contrasting thorium signatures of the Lunyo granite and the Namagenge granodiorite, showing Th and U values that strongly differ from each other and the surrounding Nyanzian country rock. Potassium values of both intrusions are approximately equal.

is particularly shown on weathered surfaces. Numerous quartz veins, typically 10–20 cm wide and locally folded, intersect the Lunyo granite.

2.3.5 Iganga Suite

The Iganga Suite covers an area of over 2000 km² from north of Iganga town to Lake Victoria (Fig. 2.11) and is unconformably overlain by quartzites and shales of the Palaeoproterozoic Buganda Group in the west. The Iganga Suite has been divided into seven related calc-alkaline granitic to granodioritic members (Fig. 2.11) of which (1) the locally porphyritic *Mayuge granite* is the most extensive. Five less extensive members include (2) *Gogero porphyritic granite*, (3) *Kibuye porphyritic granite*, (4) *Butte granite*, (5) *Porphyritic granodiorite* and (6) *Medium-grained granite*.

Mayuge granite, locally porphyritic – The Mayuge granite, which covers an extensive area of ca. 1400 km² (Fig. 2.11, A3Igrp), is typically a red to pink, medium- to coarse-grained, generally equigranular but, locally, also porphyritic rock, exhibiting occasionally a weak E-W oriented planar fabric (Fig. 2.12A). It is a genuine alkali granite composed of quartz (30–50 vol%) and feldspar (40–60 vol%), whereby K-feldspar is dominant with white plagioclase only occurring in subordinate amounts.

Mafic constituents include biotite (5–20 vol%) with or without hornblende. Locally, plagioclase is (almost) absent and the rock attains a quartz syenitic composition, being composed almost exclusively of quartz and K-feldspar.

Locally, small, round enclaves of microgranodioritic to dioritic composition and finer-grained granite porphyry are observed (Fig. 2.12B). Aplite and quartz veins, as well as dykes of fine- to medium-grained leucogranite to granodiorite or dolerite occur in places.

Gogero porphyritic granite – The Gogero granite member occurs in the NE corner of the Iganga Suite, where it occupies an oval-shaped area ~200 km² in size (Fig. 2.11, A3Igrp). The contours of the Gogero granite member can be readily delineated from the surrounding rock units by its high potassium signature. The granite shows usually a variety of textures, being megacrystic with K-feldspar phenocrysts up to 2–5 cm in size in one place (Fig. 2.13) and with medium-grained, equigranular textures elsewhere. The rock is rather homogeneous, often mildly deformed with narrow shear zones and banding. Thin granitic veins and small mafic inclusions occur in places. Main minerals of the Gogero porphyritic granite are K-feldspar, plagioclase, quartz and biotite, while hornblende is only locally present in subordinate amounts.

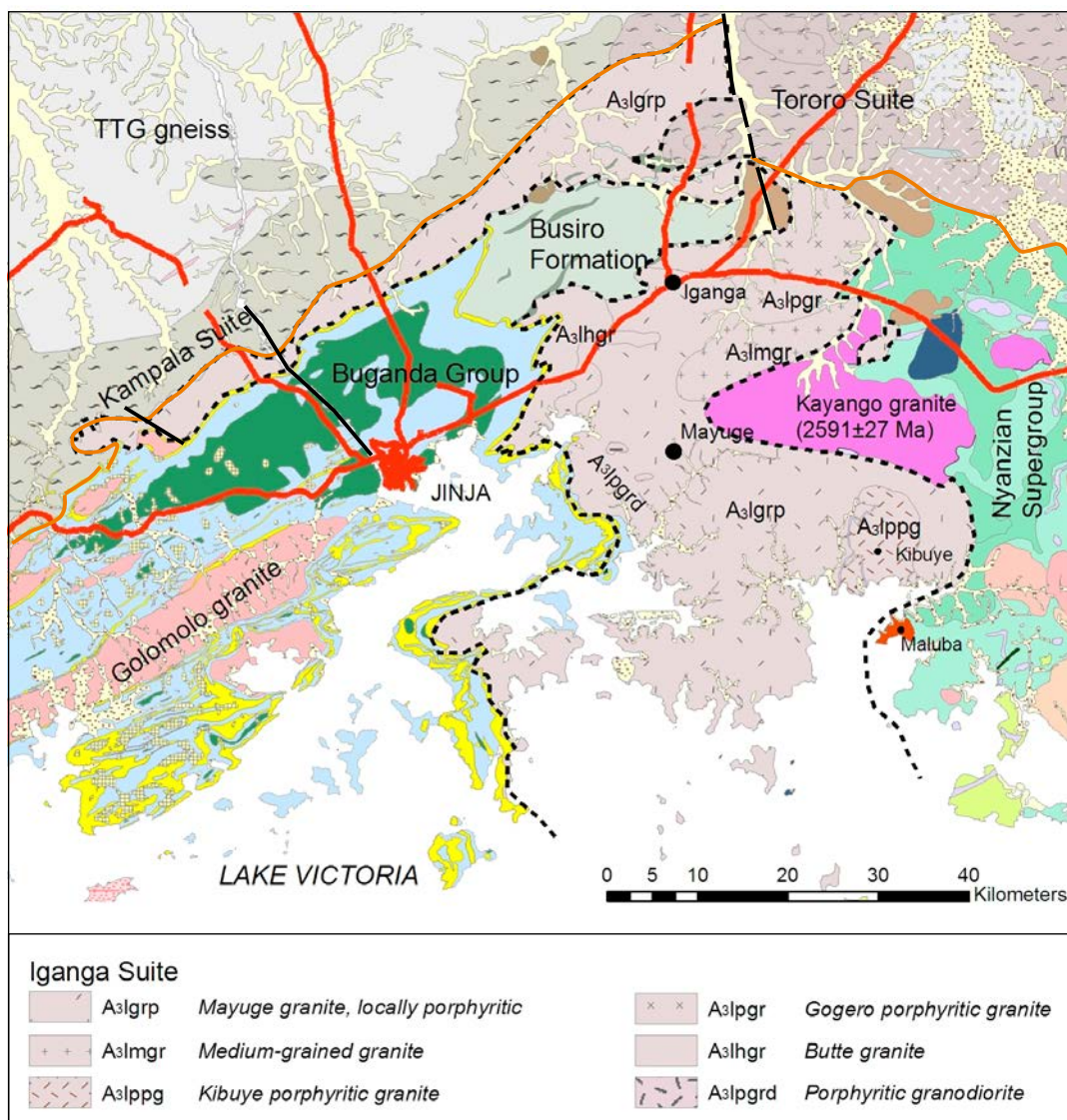


Fig. 2.11. Distribution of Iganga Suite granitoid members (dashed line on map).

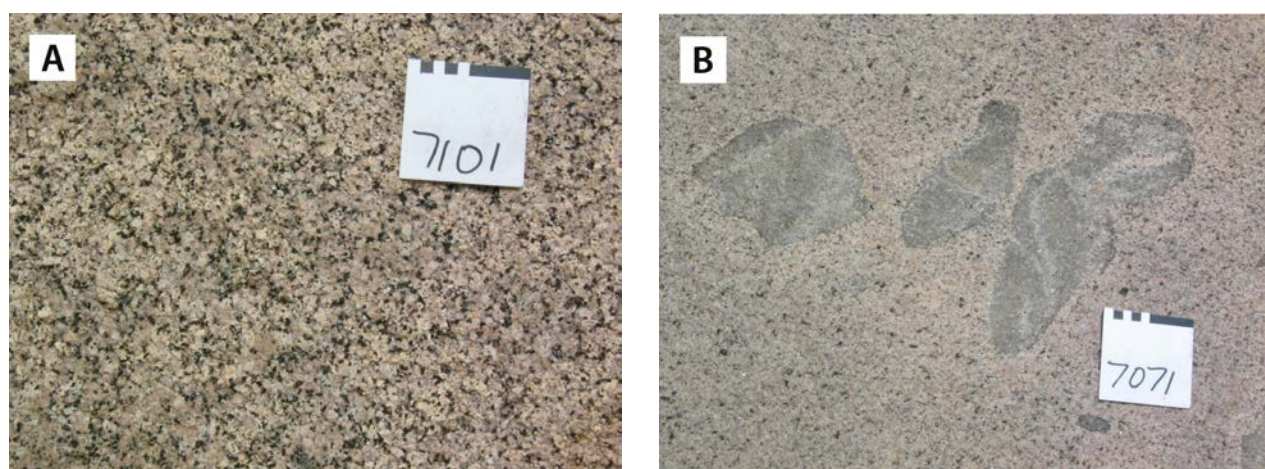


Fig. 2.12. The equigranular Mayuge granite showing field characteristics such as (A) equigranular appearance (558849E / 29634N), and (B) enclaves (581798E / 37623N). Number plate 10 cm.



Fig. 2.13. Mildly deformed, megacrystic Gogero granite of the Iganga Suite (572883E / 72407N). Number tag 8 cm.

Kibuye porphyritic granite – Centred on the village of Kibuye, this granite member forms a near elliptical pluton, 7 x 10 km in size, on the northern shore of Lake Victoria (Fig. 2.11, *A3Ippg*). The Kibuye porphyritic granite stands out in the airborne magnetic map due to its low magnetic signature when compared to the Mayuge granite. Texturally, the Kibuye porphyritic granite is a strongly variable rock, locally having a distinctly porphyritic fabric with coarse euhedral (>2 cm) K-feldspar phenocrysts in a relatively fine-grained

matrix (Fig. 2.14A). Elsewhere, concentrations of euhedral K-feldspar phenocrysts form localised patches in otherwise fine- to medium-grained, equigranular granite (Fig. 2.14B). The origin of these variable textures is uncertain, but it is possible that the concentration of K-feldspar phenocrysts may represent some form of disrupted flow cumulate. Mineral proportions are typically granitic with almost equal quantities of quartz, K-feldspar and plagioclase with biotite as the dominant ferromagnesian mineral.



Fig. 2.14. (A) Pink, porphyritic variety of the Kibuye granite (576231E / 43607N). (B) Concentration of euhedral K-feldspar phenocrysts in the medium-grained, equigranular Kibuye granite (576644E / 41491N). Number plate 10 cm.

Butte granite – The Butte granite forms a reasonably well-exposed, roundish body of about 8 x 12 km in size west of Iganga town (Fig. 2.11, A3Ihgr). This granite member differs from the other members of the Iganga Suite by its stronger magnetic intensities and a weaker radiometric signature, i.e., lower Th and U values. The pale brownish to pinkish grey, medium- to coarse-grained, equigranular granite is only incipiently foliated and, except for narrow quartz veins, no dykes or xenoliths have been observed.

Porphyritic granodiorite – This areally limited granitoid variety has only been observed at two localities within the Mayuge granite (Fig. 2.11, A3Ipgrd), about 5 km W and SW from Mayuge town. The greyish, whitish spotted, generally medium-grained rock contains 20–25 vol% of K-feldspar phenocrysts, which are 1–2 cm in size (Fig. 2.15). There is also some 10 vol% of biotite in this massive, homogeneous rock. In terms of modal composition, the rock is intermediate between granite and granodiorite.

Medium-grained granite – Medium- and even-grained aplitic granite occurs south of the Gogero porphyritic granite member, and forms a 5 x 20

km, E-W trending body (Fig. 2.11, A3Imgr). This aplitic granite has a slightly weaker potassium signature on radiometric maps in comparison with the Gogero granite. This rather homogeneous and weakly deformed granite member is more fine-grained when compared to other granitic members of the Iganga Suite. The medium-grained aplitic granite is composed of quartz, plagioclase, K-feldspar and biotite; muscovite is present in subordinate amounts and garnet is sporadically present as rather euhedral and isolated crystals, up to 10 mm in size. The rock resembles aplite in crosscutting dykes found in coarse-grained granite nearby and supposedly represents a late magmatic phase.

Kayango Granite – The Kayango granite forms an isolated elliptical E-W trending intrusion, about 400 km² in surface extent, between the granites of the Iganga Suite and the volcano-sedimentary sequence of the Nyanzian Supergroup (Fig. 2.11, A3Agr). Radiometric data, particularly its potassium signature, allows easy delineation of this granite body from neighbouring rocks. The Kayango granite is a relatively homogeneous, slightly porphyritic, coarse-grained and only weakly deformed rock. Mafic inclusions are rare. Main minerals of this granite are K-feldspar, quartz,



Fig. 2.15. Fresh surface of homogeneous porphyritic granodiorite member of the Iganga Suite with subhedral K-feldspar phenocrysts (551450E / 46916N). Number tag 8 cm.

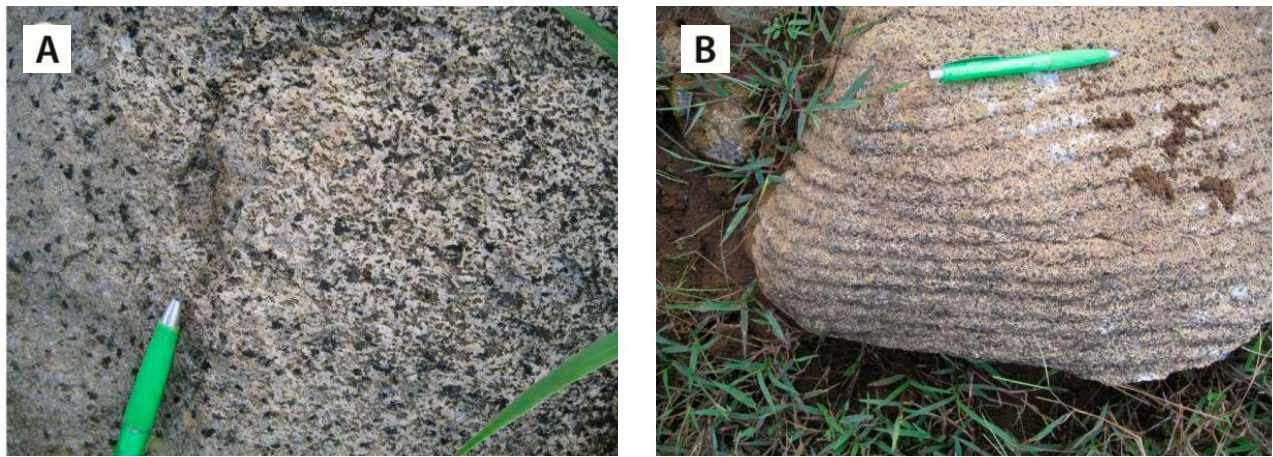


Fig. 2.16. (A) Coarse-grained Malube nepheline syenite. (B) Regular magmatic layering in the same Maluba nepheline syenite (578963E / 30439N). Pen is 13 cm long.

plagioclase and biotite. The amount of biotite – the only mafic mineral in the rock – is small, generally ≤ 10 vol%. The low Fe_2O_3 content of only ~ 2 wt% confirms the leucocratic character of the rock.

Since the Kayango granite intrudes rocks of the Nyanzian Supergroup, it is classified as a “Younger Granite” of the Lake Victoria Terrane. U-Pb zircon data (MC-LA-ICP-MS method) yields an age of 2591 ± 27 Ma (UG-4_3002 in Mänttari 2014).

Maluba nepheline syenite (A3Mns) – Rare stocks of alkali syenite are known from the Lake Victoria Terrane in Tanzania (Stockley 1947; Barth 1990). Nepheline syenite rocks are exposed on a peninsula at McDonald Bay (Fig. 2.11) and differ considerably from all other felsic and intermediate plutonic rocks of the Lake Victoria Terrane. The rocks form one single igneous intrusive, comprising of plutonic and sub-volcanic varieties of the same magmatic source. They appear as partly foliated, greyish, usually medium- to coarse-grained rocks (Fig. 2.16A) with biotite (\pm amphibole), feldspars and foids and little if any quartz. Its alkalic nature is supported by chemical analysis, showing high Na_2O (9.8 wt%) and K_2O (5.35 wt%) (see App. 2, anal. 26). Al_2O_3 content is 23.28 wt%. In the TAS diagram the Maluba nepheline syenite plots in the field of foid syenite (Fig. 2.22A). Magmatic layering is observed in the rock near contact to the east with Nyanzian country rocks (Fig. 2.16B).

U-Pb zircon dating (MC-LA-ICP-MS method) of the Maluba nepheline syenite (UG-24_12040; 580298E / 30441N) yields an age of 2628 ± 6 Ma (Mänttari 2014).

2.3.6 Nabukalu gabbro intrusions

Three previously unknown, roundish to oval-shaped Neoproterozoic gabbro intrusions, each 10–25 km² in size and named after Nabukalu village, are located east of Iganga town (Figs 2.11 and 2.17). In magnetic maps these gabbro intrusions stand out from the surroundings as pronounced circular to oval-shaped anomalies (Fig. 2.18). They are recently studied by Kärkkäinen et al. (2014), who called them Iganga gabbros.

Recent field verification by GTK Consortium, supported by ground geophysical studies, indicates that the aforementioned airborne magnetic anomalies are far wider than the real dimension of the intrusive, supposedly pipe-shaped gabbro bodies. Field measurements confirm the high magnetic susceptibility of the rocks; ranging from 15 to 200 SI units, with the highest values observed particularly in some of the doleritic subtypes. Topographically, these magnetic anomalies correspond to shallow depressions in the landscape, which are generally covered by marsh land and small lakes, surrounded by slightly higher ground. In places, isolated gabbro boulders or *in-situ* boulder fields can be encountered in the low ground (Fig. 2.19A).

The Nabukalu gabbros are dark grey to greenish, isotropic rocks, the most common type being a massive, coarse-grained hornblende gabbro (Fig. 2.19B). In some outcrops, hornblende gabbro shows network textures, where domains of fine-grained gabbro are surrounded by a network of coarser-grained, plagioclase-rich material (Fig. 2.20A). Magmatic layering can be found in

some gabbro outcrops, appearing there as thin but regular plagioclase-rich bands (Fig. 2.20B). Locally, variation in grain size can be found in the Nabukalu gabbro with patches and bands with a pegmatitic texture (Fig. 2.20C). Other modal and structural rock types include some medium-

grained varieties, mottled gabbros, anorthositic gabbros, coarse grained, vari-textured or breccia-structured gabbros, and gabbro-pegmatoids (Kärkkäinen et al. 2014).

Minerals of the Nabukalu gabbros mainly comprise labradoritic plagioclase (45–55 vol%) and

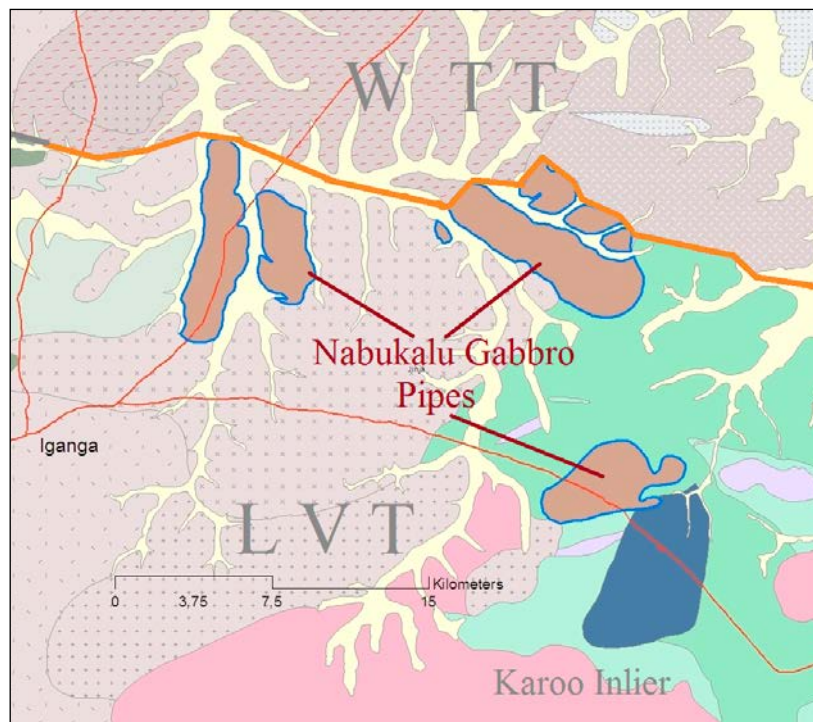


Fig. 2.17. Geological sketch map showing distribution of Nabukalu gabbros (brown with blue borders) in main cluster (no. 3 in Fig. 2.18). For the other lithological units in the map, see Fig. 2.11.

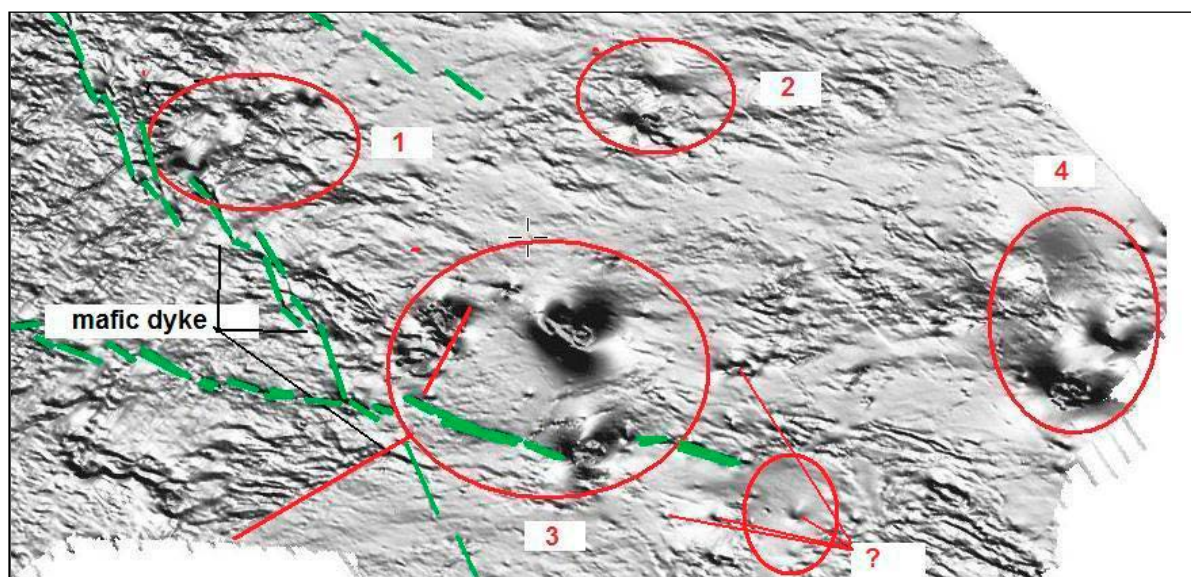


Fig. 2.18. Magnetic image (grey tones) of the Neoproterozoic Nabukalu gabbro region. Key: 3 = main cluster with three major bodies, shown in Figs 2.19–20; 1 = secondary cluster but with gabbro exposures; 2 = similar magnetic feature but no gabbro exposures; 4 = carbonatite bodies of the Neogene alkaline Elgon Complex in the Tororo-Sukulu area. Green = mafic dyke. ? = Other, smaller scale point anomalies.

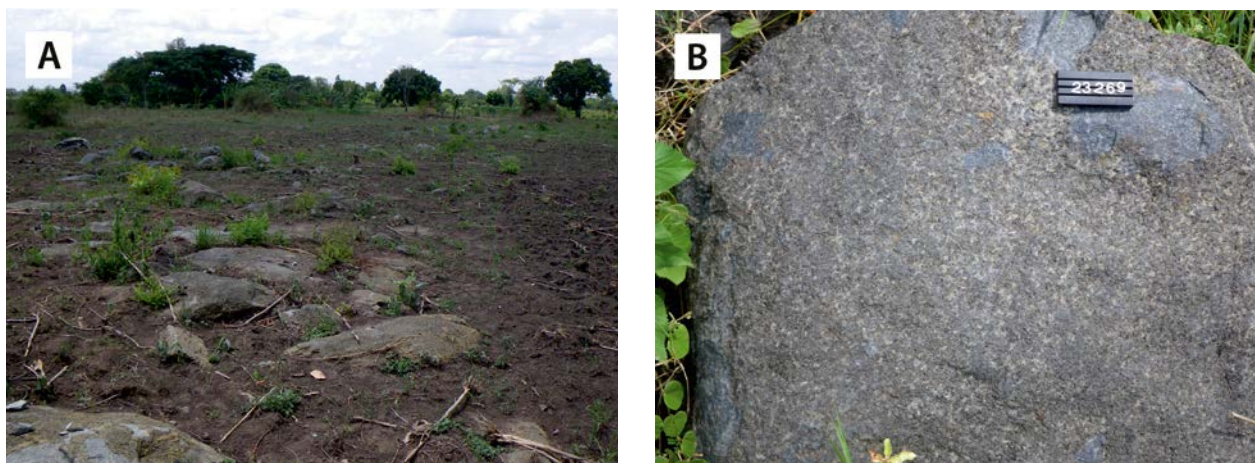


Fig. 2.19. (A) Boulder field of the Nabukalu gabbro in the low ground (579987E / 76595N). (B) Massive, coarse-grained Nabukalu gabbro (576415E / 77510N). Number tag 10 cm.



Fig. 2.20. Nabukalu hornblende gabbro showing network texture (575534E / 77356N). (B) Magmatic layering in the Nabukalu gabbro (575565E / 77342N). (C) Same hornblende gabbro outcrop showing bands with pegmatitic texture. Number tag is 10 cm.

hornblende (40–50 vol%), but not pyroxene or olivine. Reaction rims have been observed with the naked eye, and weathering has locally produced a pinkish colour in the feldspar crystals. Typical accessory and retrograde minerals are quartz, chlorite, biotite, apatite and opaque minerals. Pyrite is often present in modes varying from 0.1 to 4 vol%. U-Pb isotope dating (MC-LA-ICP-MS method)

of the Nabukalu gabbro (UG-21_3189; 580002E / 76578N) yields an emplacement age of 2611 ± 6 Ma, based on analyses of unaltered low-U zircon domains that plot in a tight cluster (Mänttari 2014). The U-Pb data from altered zircon grains define a fairly well determined lower intercept age of 602 ± 49 Ma for the timing of Pan-African alteration.

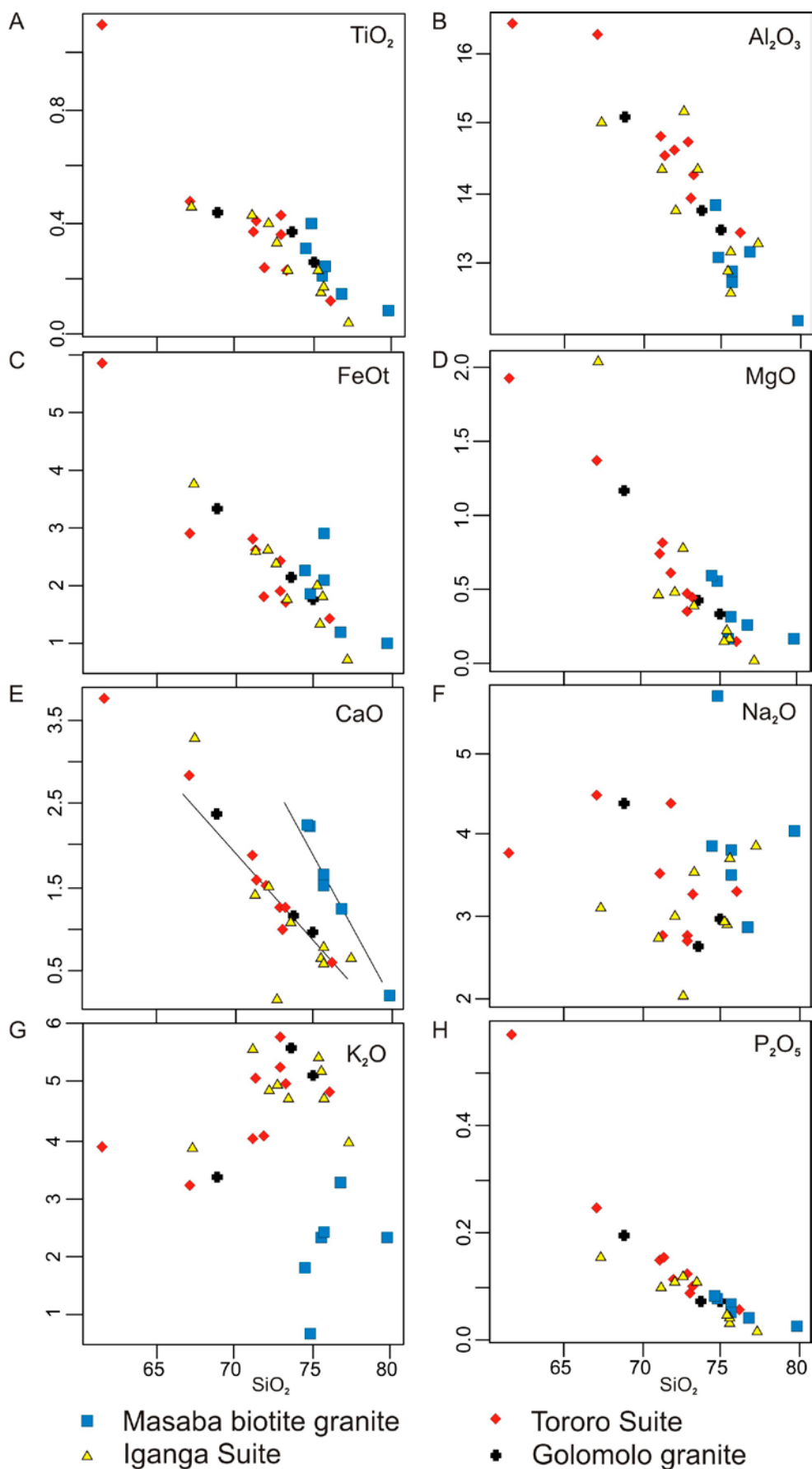


Fig. 2.21. Harker variation diagrams for the Masaba biotite granite, Golomolo granite and for the granitoids of the Iganga Suite of the Lake Victoria Terrane and the Tororo Suite of the West Tanzania Terrane (Chapter 3). The chemical data are presented in Appendix 2 (e.g. Iganga Suite in anal. 18–25).

2.3.7 Geochemistry

The chemical composition of the granitoids in the Lake Victoria Terrane is studied with several whole rock chemical analyses (see Appendix 2). These data have been plotted on Harker variation

diagrams (Fig. 2.21). They show generally clear differentiation trends or dispersed data (e.g., K_2O/SiO_2 and Na_2O/SiO_2 ratios).

The geochemical data has also been plotted in various discrimination diagrams (Fig. 2.22). According to the classification diagram of Middle-

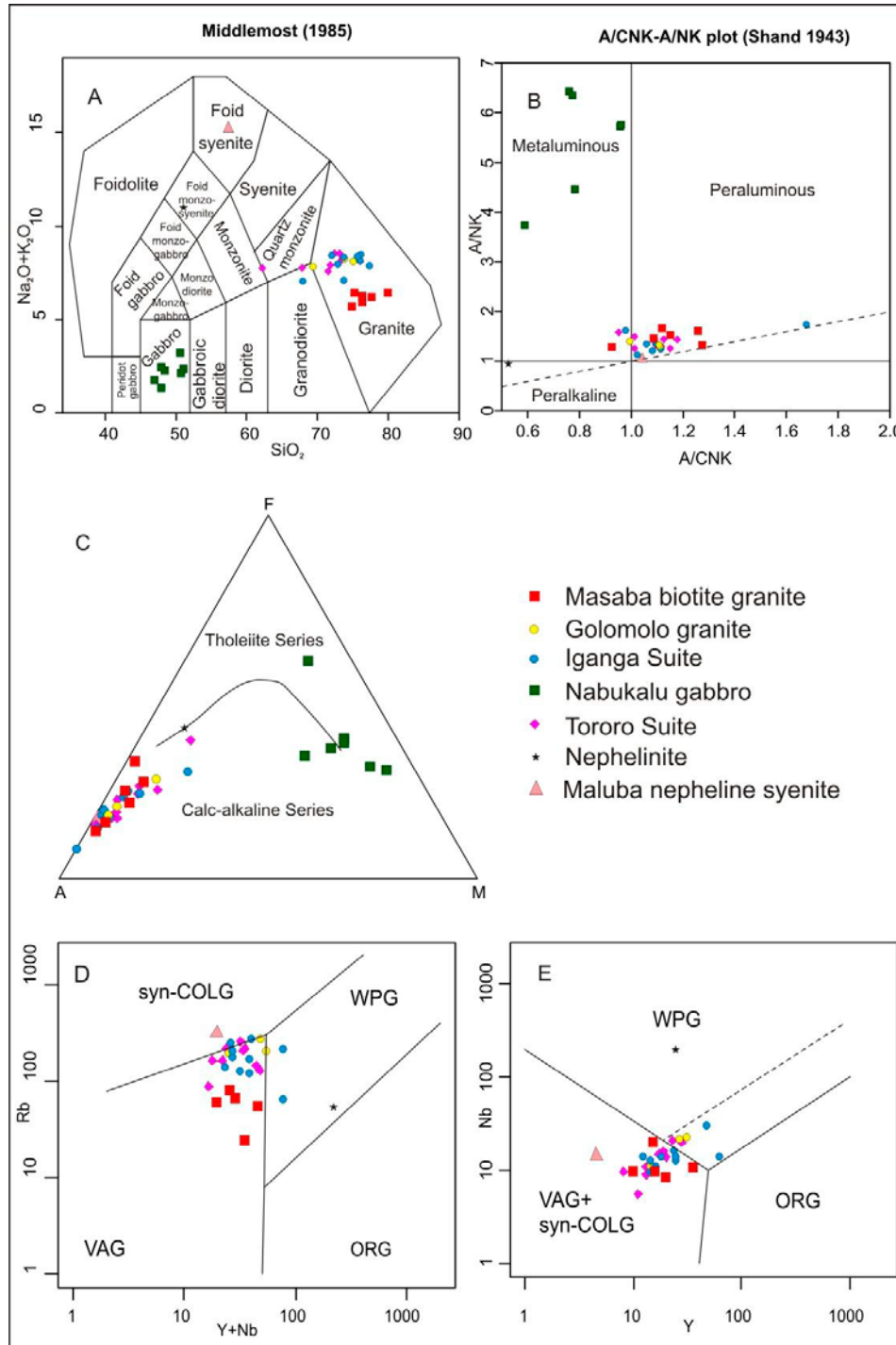


Fig. 2.22. Geochemical discrimination diagrams for granitoids of the Masaba biotite granite, Golomolo granite and Iganga Suite of the Lake Victoria Terrane and the Tororo Suite of the West Tanzania Terrane (see Chapter 3). Also plotted are analyses of the Nabukalu gabbro, the Maluba nepheline syenite and a nephelinite of the Elgon complex (see Chapter 12). (A) SiO₂-Alk plot (Middlemost 1985), (B) A/CNK vs. A/NK diagram (Maniar & Picoli 1989), (C) AFM diagram (Irvine & Baragar 1971) and (D-E) diagrams indicating geotectonic settings after Pearce et al. (1984). Chemical data of Nabukalu gabbros are after Kärkkäinen et al. (2014).

most (1985), the rocks of the Masaba biotite granite, Golomolo granite and Iganga Suite are true granites with the latter having a few granodioritic outliers (see App. 2, e.g. anal. 19–25). They are peraluminous with some members being metaluminous (Fig. 2.22B). The Maluba nepheline syenite and the Nabukalu gabbro plot in the foid syenite and gabbro fields, respectively (Fig. 2.22A). In the

AFM diagram gabbro scattered data points plot in the tholeiite and calc-alkaline series (Fig. 2.22C).

In diagrams indicating geo-tectonic settings after Pearce et al. (1984) most granitoids plot in the 'volcanic arc' field and/or 'syn-collision granite' field, with a few data points plotting in the 'within plate' field (see Figs 2.22D-E).

2.4 Geochronology

Poorly constrained whole rock Rb-Sr age determinations on granitic bodies in SE Uganda gave ages of 2.93 Ga for the Masaba granite and 2.43 Ga for the Buteba granite and granitic gneisses (Old & Rex 1971). The former age was considered to represent the upper age limit of the post-Nyanzian Orogeny, and 2.43 Ga the upper age limit of the post-Kavirondian Orogeny. A second isochron age of 2.10 Ga for the Masaba Granite was believed to reflect a second intrusion, or remobilisation of part of the original granite related to the Rwenzori Belt (Old & Rex 1971). A list of obsolete and poorly constrained K-Ar and Rb-Sr age determinations of the Lake Victoria region shows a range from 2.6 Ga to 2.4 Ga (Bell & Dodson 1981). Although at least two events can be delineated, one at 2740 Ma, the other at 2540 Ma, the younger is more widespread and reflects extensive granitoid magmatism throughout large areas of Tanzania, southeastern Uganda and western Kenya. Lacking ages greater than 2800 Ma, the granite-greenstone segment of the Tanzanian Craton is unique among the Archaean cratons of Africa.

Modern single zircon U-Pb data portray a more diversified picture with respect to the geodynamic processes in the granite-greenstone assemblages of the Lake Victoria Terrane. These data suggest significant age differences between volcanic rocks in different greenstone clusters. The oldest volcanics comprise rhyolite and tuffs from Siga Hills yielding an age of 2808 ± 3 Ma, overlain by slightly younger crystal tuffs with an age of 2780 ± 3 Ma (Borg & Shackleton 1997). Volcanics from the Kilimafedha cluster (Fig. 2.2, KI) have been dated at

~ 2720 Ma, while a thick package of mafic volcanics from Musoma-Mara (Fig. 2.2, MM) yield ages from ~ 2676 Ma to ~ 2667 Ma, with a felsic interlayer dated at ~ 2668 Ma (Manya et al. 2006). These geochronological data suggest that the entire volcano-sedimentary sequence in the Musoma-Mara Greenstone Belt probably was emplaced in a short time interval. On the other hand trachy-andesite and rhyolite from Sukumaland (Fig. 2.2, SU) yield ages of 2699 ± 9 Ma (Borg 1992) and 2654 ± 15 Ma (Borg 1994), respectively, suggesting long-lived volcanic activity spread over some 50 million years.

Granitoids from three belts have produced ages ranging between ~ 2.69 Ga and 2.55 Ga (Manya et al. 2006) and comprise most likely both 'syn-kinematic' granitoids and post-kinematic 'Younger Granites'. An allegedly younger phase of post-orogenic granites of the Musoma-Mara Greenstone Belt dated at ~ 2649 Ma (Manya et al. 2006) equals the age of a lamprophyric dyke from Sukumaland, dated at 2644 Ma (Borg & Krogh 1999).

Scarce single zircon geochronological data (Mänttari 2014) from the Ugandan segment of the Lake Victoria Terrane comprise metamorphosed Kavirondian tuffites dated at 2639 ± 7 Ma and coeval syntectonic Golomolo granites, yielding an age of 2.63 Ga. The Maluba nepheline syenite and Nabukalu gabbros are slightly younger, yielding ages of 2628 ± 6 Ma and 2611 ± 6 Ma, respectively. The apparently younger Kayango granite, with a less well constrained age of 2591 ± 27 Ma, falls also in the 2.64–2.61 Ga bracket.

2.5 Geodynamic Development

A simple geodynamic model of the Lake Victoria Terrane is based on work by Ichang'i & Maclean (1991) in the Migori-Kendu greenstone belt (MK

in Fig. 2.2), portrayed in Fig. 2.23 (Borg & Shackleton 1997). It consists of two volcanic centres, each with central, proximal and distal volcanic facies

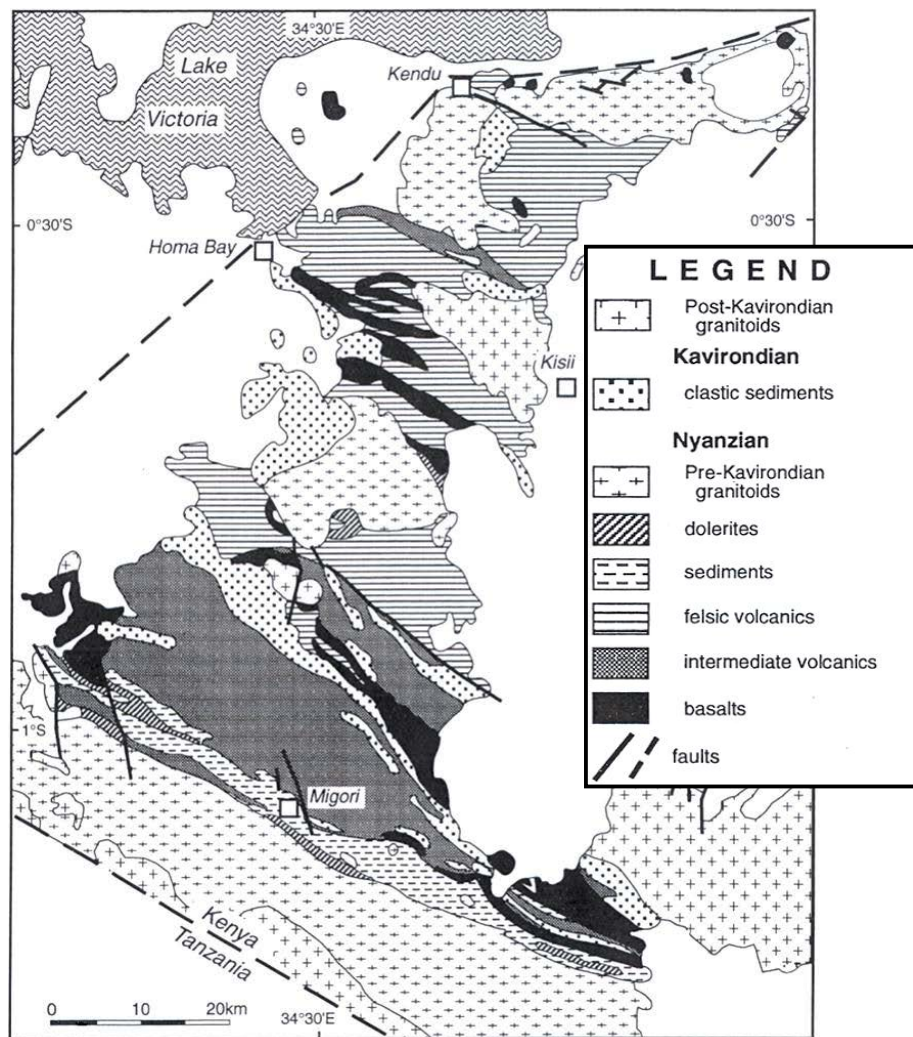


Fig. 2.23. Generalised geological map of the Migori Greenstone Belt of SW Kenya (from Borg & Shackleton 1997, with kind permission of Oxford University Press).

and volcano-sedimentary formations. The centres are separated by a basin of tuffs and greywacke turbidites. The volcanics are bimodal mafic basalt and dolerite and felsic calc-alkaline dacite-rhyolite and high-K dacite. Felsic units form approximately three-fourths of the volcanic stratigraphy. Basalts, calc-alkaline dacites and rhyolites were deposited in a submarine environment, but the voluminous high-K dacites were erupted sub-aerially. The turbidites contain units of banded iron formations. Granitic intrusions are chemically continuous with the high-K dacites. The felsic volcanics are analogous to those found at modern volcanic arc subduction settings involving continental crust.

Granitic magmatism coeval with 'Younger Granites' has been reported in different parts of the Tanzania Craton suggesting that it was responsible for the late Archaean crustal growth and marks the beginning of a period of crustal stability (or cratonisation). A model for the formation of the Lake

Victoria Terrane according to Opiyo-Akech (1991) is presented in Fig. 2.24. The model is oversimplified and suggests a uniform sequence of events in time, which is not supported by the differences in ages of the various greenstone clusters.

According to Pinna et al. (1997, 2004a) crustal growth of the Tanzania Craton is related to two major orogenic cycles, the Dodoman (phase 'a' in Fig. 2.1) and Victorian (phases 'b' and 'c' in Fig. 2.1) orogenies, respectively, followed by merging of the Tanzania Craton into the proto-Congo Craton (phase 'd' in Fig. 2.1). The first phase resulted in TTG accumulation resulting from HP melting of mafic slabs (2.93–2.85 Ga) in the southwest, probably coeval with oceanic/back-arc crust formation ("chondritic" basalts, minor ultramafics, BIF) in the south. The Victorian Orogeny is manifested by a succession of three magmatic/tectonic pulses in the north:

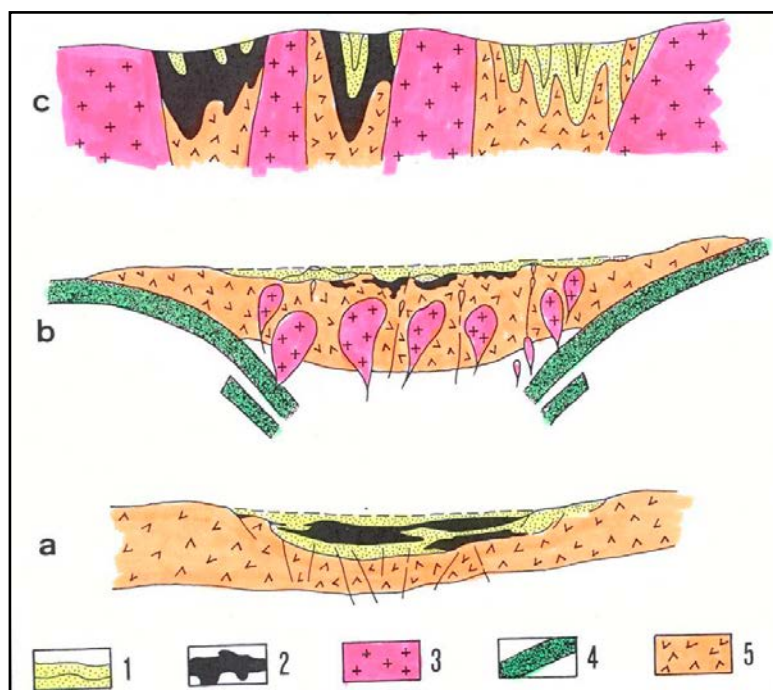


Fig. 2.24. Model for a granite-greenstone terrain of the Tanzania Craton. a: Phase of crustal extension and initial rifting; b: Emplacement of volcanics of the Nyanzian coeval with subduction; c: Erosion of supracrustal material and deposition of Kavirondian sediments. Key: 1 = Sediments of the Nyanzian (greywackes, shales, BIFs) and Kavirondian (banded quartzites, mudstones and greywackes); 2 = tholeiitic and komatiitic basalts, subordinate dacite and rhyolite; 3 = 'Younger Granites'; 4 = subducting oceanic crust; 5 = Pre-Nyanzian crust (after Opiyo-Akech 1991).

- (a) post-kinematic TTG emplacement (2.73–2.69 Ga), followed by extension-related rhyolite (2.70 ± 0.01 Ga);
- (b) bimodal calcalkaline volcanism (2.66 ± 0.01 Ga) with torrential to turbidite sediments and emplacement of syn-kinematic calc-alkaline granitoids (2.64 ± 0.01 Ga);
- (c) outer-zone sedimentary basins, deformed with emplacement of shallow, syn-kinematic, syn- to post-collisional granite (2.60 ± 0.01 Ga) in the northwest, and coeval(?) with undeformed Andean-type tholeiite and deltaic sediments in the northeast. The latter are postdated by post-orogenic, extension-linked rhyolite (2.53 Ga). Active subduction involving “archaic” mantle and hydrated basic crust was responsible for crustal growth, resulting in late-orogenic juvenile continental crust with P-T regime (LP-HT) close to modern equivalents.

Based on more recent data, the above general geodynamic development is challenged. Greenstone belts in the Lake Victoria Terrane can be grouped into eight different E-W trending clusters, separated by areas underlain by granitoids (Fig. 2.2). There is little evidence as to whether these greenstone clusters represent separate depositional ba-

sins that developed according to a uniform scenario in space and time. On the contrary, several of the belts within a specific cluster manifest distinctly different lithostratigraphic developments, with rapid lateral facies changes at different times. It thus appears that the generally accepted geodynamic sequence of Neo-Archaean crustal development in the Lake Victoria Terrane – deposition of volcanic-dominated Nyanzian, followed by deposition of sediment-dominated Kavirondian, followed by emplacement of “Younger Granites” – is an over-simplification. The trend from mafic to felsic and from volcanic-dominated to sediment-dominated, followed by post-tectonic granite magmatism may be correct; the time path of this evolution differs, however, significantly from place to place. As a consequence, correlation of litho-stratigraphic units within greenstone clusters may be difficult, let alone between different clusters.

Sukumaland greenstone belt – The above point is well illustrated by mapping in the Sukumaland greenstone belt (Fig. 2.2) by Barth (1990), Borg et al. (1990), Borg (1992), Borg & Shackleton (1997) and Borg & Krogh (1999). The Sukumaland greenstone belt comprises two concentric, oval-shaped

greenstone belt segments. The inner ring, allegedly of Lower Nyanzian age, is composed predominantly of Fe-rich tholeiitic, locally pillowed basalts, andesite and minor mafic tuffs (> 1000 m thick) and horizons of graphitic schists (< 30 m in thickness). Subordinate to minor lithologies include feldspar porphyry and quartz-feldspar porphyritic rhyolite, grading into pyroclastic rock (possibly < 300 m). Ultramafic rocks are only exposed in well material. The allegedly Upper Nyanzian lithostratigraphic units in the outer ring comprises felsic volcanic flows, pyroclastic rocks, minor intermediate volcanics (< 800 m) and a laterally consistent BIF horizon, measuring in average 500 m in thickness. The BIF horizon is covered by graphitic or pelitic schists or tuffs. Single zircon U-Pb dating showed, however, that rhyolite from the mafic-dominated inner ring yielded an age of 2654 ± 15 Ma (Borg 1992), while trachy-andesite from the felsic-dominated outer ring yielded an older age of 2699 ± 9 Ma (Borg 1994). This inverse succession can be explained by tectonic stacking of felsic metavolcanics on top of mafic rocks, on idea in line with Kabete et al. (2012), who advocate the allochthonous nature of the Sukumaland greenstones.

Musoma-Mara greenstone belt – While in some clusters deposition of the greenstones took several tens of millions of years, emplacement of mafic and felsic volcanics and granitoids in the Musoma-Mara greenstone belt (Fig. 2.2) occurred in a short span of time that differed considerably from other clusters in the Lake Victoria Terrane (Manya et al. 2006). Ion microprobe zircon U-Pb ages from metavolcanic and associated granitic rocks of the Musoma-Mara greenstone belt reveal that the oldest mafic volcanism in the belt occurred at 2676–2669 Ma, followed shortly by felsic volcanism at ~2668 Ma. Felsic volcanism was coeval with the emplacement of the oldest pulse of massive “Younger Granites”, dated at 2668 Ma. The youngest volcanic episode, represented by a volcanic horizon in the largely sedimentary Kavirondian Supergroup occurred at ~2667 Ma. A younger phase of post-orogenic granites concluded the magmatic evolution of the Musoma-Mara greenstone belt at ~2649 Ma.

When compared to other Neoproterozoic greenstone belts, volcanism in the Lake Victoria Terrane is further characterised by a deficiency in mafic and ultramafic and komatiitic products and a surplus in intermediate and felsic products. Manya et

al. (2007a) have drawn attention to two unusual magmatic suites from the Musoma-Mara greenstone belt composed of high magnesium andesites and an adakitic suite. The geochemical features of the first are analogous to those shown by modern High Magnesium Andesites (HMA).

The geochemical characteristics of the HMA are consistent with derivation of their parent magma by partial melting of mantle peridotite that has been fluxed by slab-derived aqueous fluids in a continental arc setting. As the slab further descended into the mantle, partial melting of the subducted oceanic crust occurred in the garnet stability field producing a melt that was depleted in HREE. The slab-derived melts percolated into the mantle wedge and reacted with mantle peridotite resulting in parental magmas of rocks of the adakitic suite. Subsequently, the parental magmas of both rock suites ascended through and were contaminated by older felsic crust forming the continental arc basement. Subsequent fractional crystallisation of pyroxene and hornblende led to the range in Mg numbers, CaO, Cr and Ni contents observed in the rocks. The association of some members of the adakitic suite with locally derived clastic sedimentary rocks suggests that the latest volcanic episode in the Musoma-Mara greenstone belt occurred in a continental back arc basin (Manya et al. 2007a). They further claim that the rapid emplacement of volcanic and plutonic rocks in a relatively short time interval is best explained in terms of the ridge-subduction model of Iwamori (2000) whereby subduction of the ridge crest results in anomalously high thermal input into the subduction zone leading to rapid arc magmatism within a few tens of kilometres from the slab-crust interface and within a time interval of 30 Ma after ridge subduction.

The geochemical characteristics of abundant, ~2649 Ma post-orogenic potassic-rich granites in the Musoma-Mara greenstone belt are similar to those of experimental melts derived from partial melting of tonalite (Manya et al. 2007b). These K-rich granites have ϵNd_0 (at 2649 Ma) values of +0.55 to +1.70 that compare well with those of associated volcanic rocks and TTG ($\epsilon\text{Nd} = +0.44$ to +2.66), which predate the emplacement of the K-rich granitoids. Their mean crustal residence ages are 170 to 450 Ma older than their emplacement ages (Manya et al. 2007b).

The overall geochemical features of this suite of rocks, together with evidence from experimental

results, are consistent with their generation by partial melting of relatively juvenile igneous rocks within the continental crust at pressures corresponding to depths <15 km where plagioclase was a stable phase. The transition from earlier TTG magmatism to potassic magmatism in the Musoma-Mara greenstone belt is interpreted as marking a transition from growth of the Neoproterozoic continental crust through the addition of juvenile mantle-derived material to intra-crustal recycling of pre-existing material (Manya et al. 2007b).

Zircon U–Pb and whole rock Sm–Nd dating of the Suguti volcanics, a bimodal suite of tholeiitic basalts/ basaltic andesites and calc-alkaline rhyolites with subordinate intermediate rocks in the southern Musoma-Mara greenstone belt, yield an age of 2755 ± 1 Ma (Mtoro et al. 2009). Geochemi-

cal characteristics suggest that the basalts were formed by low pressure melting of a mantle wedge in an active continental margin setting. The rhyolites are interpreted to have formed from the parental magma of the basalts by fractional crystallisation and/or partial melting of a relatively young basaltic crust. This confirms data from trace element and Nd-isotope compositions from Manya & Maboko (2008) that are consistent with the generation of mafic volcanics from a depleted MORB mantle source, which had been metasomatised by a subduction component in a late Proterozoic back arc setting.

Finally, it should be remarked that the Lake Victoria Terrane is host to a number of world-class gold deposits.

3 WEST TANZANIA TERRANE OF THE ARCHAEOAN TANZANIA CRATON

3.1 Introduction – Archaean ‘Building Blocks’ of Uganda

Traditionally, the Archaean crystalline basement of Uganda has been divided in two parts:

- (1) *Nyanzian System* (i.e., a granite-greenstone assemblage), mainly consisting of metavolcanics and metasediments in SE Uganda (Fig. 3.1. No. 1 on map) and
- (2) *Basement Complex*, i.e., *Crystalline basement* mainly composed of *Gneissic Granulite Complex* (Fig. 3.1. No. 4) with small enclaves of *Watian* (No. 3) and *Aruan* (No. 2) rocks (e.g., Hepworth 1961a, 1964, Macdonald 1963b, 1964a, 1966, Hepworth & Macdonald 1966), see also Table 4.1.

In this Chapter a vast area in central-southern Uganda is described, underlain by weakly deformed gneissose granitoids and migmatites that we correlate with the Western Granitic Complex (Pinna et al. 1996) of the western segment of the Tanzania Craton (Fig. 2.1). Because the term ‘Western Granitic Complex’ is too generic, we introduce the name ‘West Tanzania Terrane’ for this tectono-thermal domain. The West Tanzania Terrane (WTT) forms an E-W- to WSW-ENE-trending domain bounded in the south by the Lake Victoria Terrane (Chapter 2) and in the north by the North Uganda Terrane (NUT, Chapter 5) and in the west covered by rocks of the Palaeoproterozoic Rwenzori Fold Belt (Chapter 6).

3.2 Airborne Geophysical Data

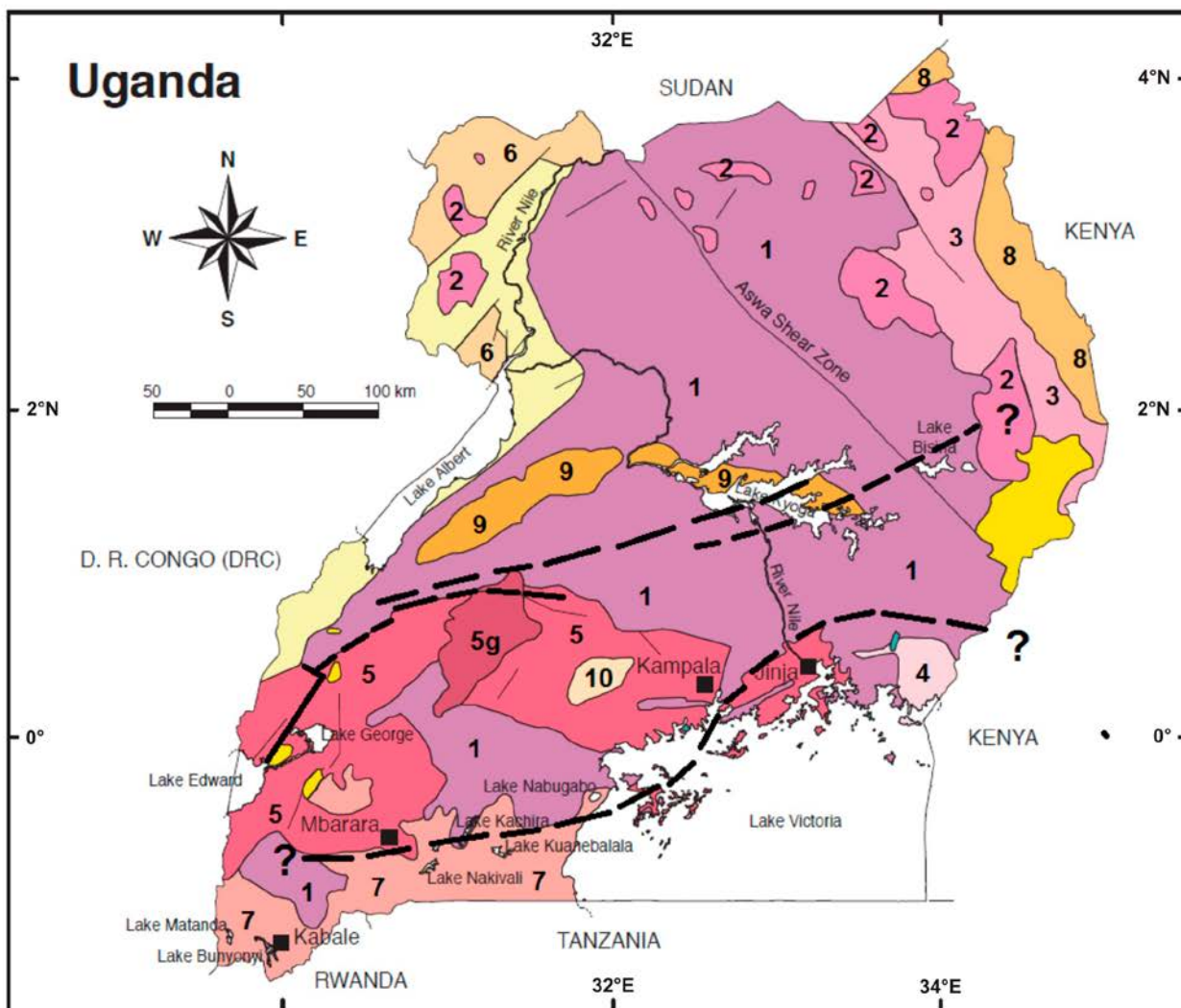
The West Tanzania Terrane, especially its northern contact with the North Uganda Terrane, is highlighted by recently acquired aero-magnetic data (FUGRO 2009). These data indicate that the WTT and its western continuation below rocks of the Rwenzori Fold Belt correspond to a well-constrained belt of low magnetic intensities on magnetic field reduced to equator (Fig. 3.3) and, as such, this ‘low-magnetic belt’ can represent a specific geophysical domain. Broadly, three magnetic zones can be distinguished: a zone with a high magnetic signature in the north (1 in Fig. 3.3), separated by a central, WSW-ENE trending low-magnetic belt (2 in Fig. 3.3) from a domain of high magnetic intensity in the southeastern part of the country (3 in Fig. 3.3). In view of its large

The Lake Victoria and West Tanzania Terranes are generally attributed to the Tanzania Craton. However, for the NUT there are three possibilities or scenarios: (1) the ‘Basement Complex’ of northern Uganda is part of the Congo Craton or, more precisely, part of the Bomu-Kibalian Shield (Fig. 1.6), a major tectono-thermal domain in the northeastern corner of the Congo Craton (Schlüter 1997, Schenk et al. 2004), (2) the NUT is part of the Tanzania Craton and (3) the NUT is a separate lithospheric fragment.

Obvious questions arise: (1) Where is the suture between the Tanzania Craton and Bomu-Kibalian Shield? and (2) When did these two tectono-thermal domains collide and merge? Scenario (1) above implies a suture between the WTT and NUT (blue line in Fig. 3.2), a zone characterised by structural complexity and a conspicuous geophysical break. Scenario (2) implies a suture between the West Nile Block (WNB) and NUT (red line in Fig. 3.2). This suture would largely coincide with and being superposed on an intracratonic thrust/ shear belt – the Madi-Igisi Belt (Chapter 9) – between the NUT and WNB of the Bomu-Kibalian Shield that developed during the late Mesoproterozoic (ca. 1.0 Ga). Finally, scenario (3) implies the presence of two sutures (blue and red lines in Fig. 3.2).

wavelength, the above magnetic feature reflects a deep crustal geological feature (oral comm. Colin Reeves 2012). The threefold subdivision shown by the magnetic intensity map was so far not reflected in the geological map by DGSM (1966) (Fig. 3.1).

The southeastern geophysical break (between areas 2 and 3 in Fig. 3.3) coincides broadly with the suture between the Lake Victoria and West Tanzania Terranes. The middle segment of this break is obscured by Lake Victoria but the southwestern contact coincides again with a structural feature: the faulted (and thrust?) contact between the Mesoproterozoic Akanyaru-Ankole Supergroup of the North Kibaran Belt and the Palaeoproterozoic mildly deformed open folded platform rocks of the Palaeoproterozoic Kagera-Buhweju Supergroup.



| | | | |
|---|--|---|--|
| PHANEROZOIC | | PROTEROZOIC | |
|  | Alluvials, rift sediments | Recent - Neogene | |
|  | Volcanics | Neogene (-Paleogene) | |
|  | Terrestrial sediments of the Karoo Supergroup | Permian - Upper Carboniferous | |
| PROTEROZOIC | | PROTEROZOIC | |
|  | 10 Mostly sediments of the Bukoban System |  | 5 Low to high grade metamorphic rocks of the Buganda-Toro System (Ruwenzori Fold Belt) |
|  | 9 Mostly sediments of the Bunyoro-Kyoga Series |  | 5g Granites |
|  | 8 Gneisses, amphibolites, marbles, quartzites, ultramafic rocks of the Karasuk Group (Mozambique Belt) | | |
|  | 7 Low grade metasediments of the Karagwe-Ankolean System (Kibaran Fold Belt) | | |
|  | 6 Gneisses of the Mirian Group | | |
| | | | |
| | | ARCHEAN | |
| | |  | 4 Metavolcanics, metasediments of the Nyanzian System |
| | |  | 3 Gneisses of the Aruan Event |
| | |  | 2 Gneisses of the Watian Event |
| | |  | 1 Gneissic-Granulitic Complex |
| | | | |
| | | STRUCTURES | |
| | |  | Fault, shear zone (cataclasites) |

Fig. 3.1. Geological outline of Uganda showing the location of two magnetic block borders (black lines), map modified from Fig. 3.3 (Muwanga et al. 2001, after Macdonald/ DGSM 1966, with kind permission of the Nature Publishing Group).

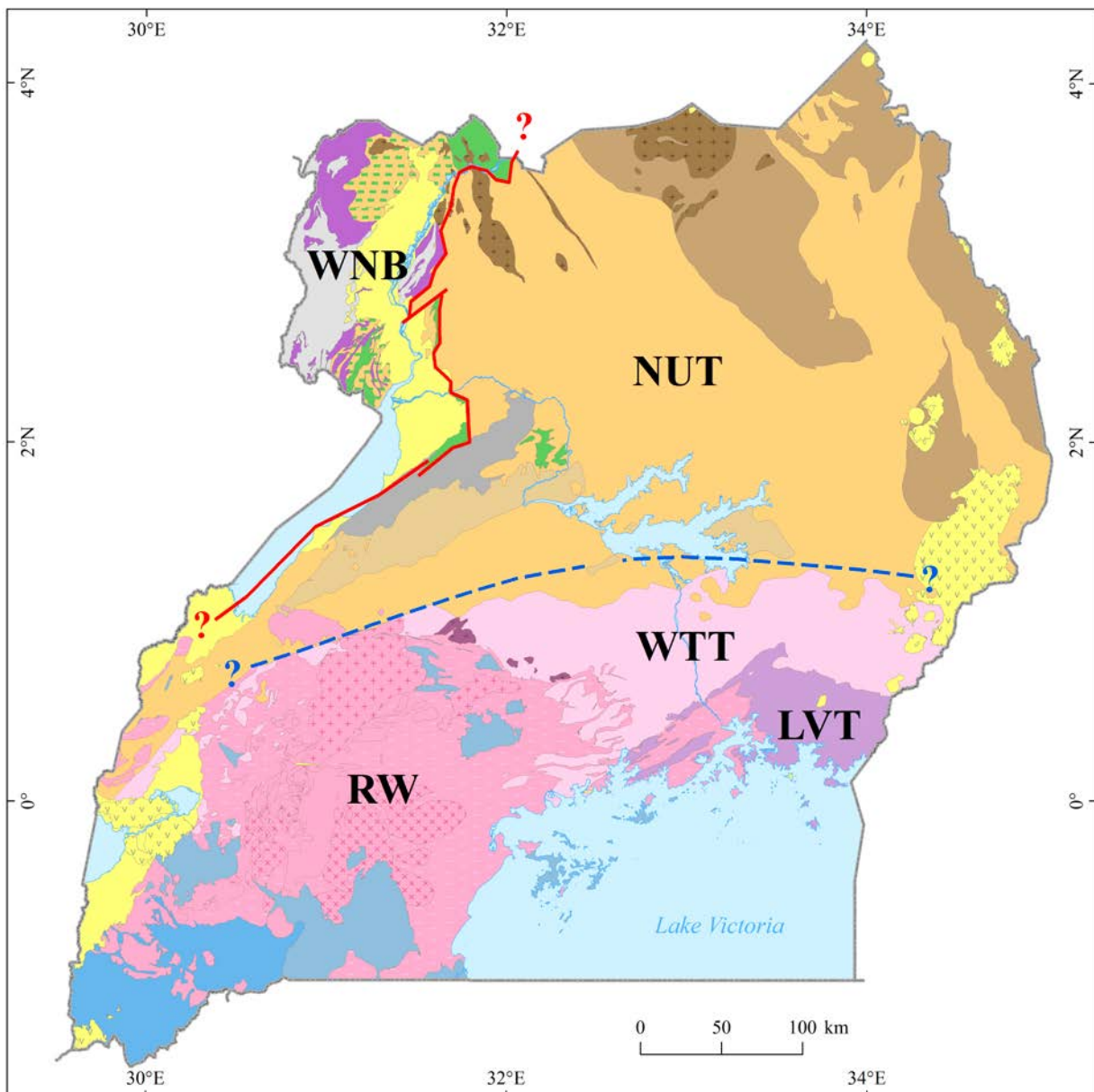


Fig. 3.2. Simplified geological map of Uganda showing different tectono-thermal terranes. We distinguish four Archaean domains: WNB = West Nile Block, NUT = North Uganda Terrane, WTT = West Tanzania Terrane and LVT = Lake Victoria Terrane. RW = Rwenzori Terrane (Palaeoproterozoic). Red line is eastern thrust front of Madi-Igisi Belt; blue line approximate boundary – the Nakasonbola discontinuity – between NUT and WTT. Rocks of the NUT south of the blue line are interpreted as thrust masses underlain by rocks of the WTT.

The northern geophysical lineament (between areas 1 and 2 in Figs 3.3 and 3.4) in eastern Uganda is particularly sharp. It intersects the Pan-African Aswa Shear Zone (ASZ) without notable off-set. From this we conclude that the geophysical break corresponds with a major ‘dislocation’ that was re-activated and invaded by mafic dyke posterior to sinistral strike-slip of the ASZ, meaning later than 400 Ma before present (Section 11.10.3). The geophysical lineament can be traced further to the WSW, where it intersects the 1.85 Ga Mubende

granite (Mänttäre 2014), before reaching the Albertine Rift near the Rwenzori horst.

Field verification by the GTK Consortium of the sharp magnetic change between blocks 1 and 2 in southeastern Uganda (Fig. 3.4) failed to observe any dramatic change in surface geology of the area. Dark grey to creamy coloured, medium- to coarse-grained, equigranular to porphyroblastic gneisses, probably metamorphosed tonalites or andesites, with numerous quartz veins and pegmatite streaks (in places up to 40% of the rock volume) alternate

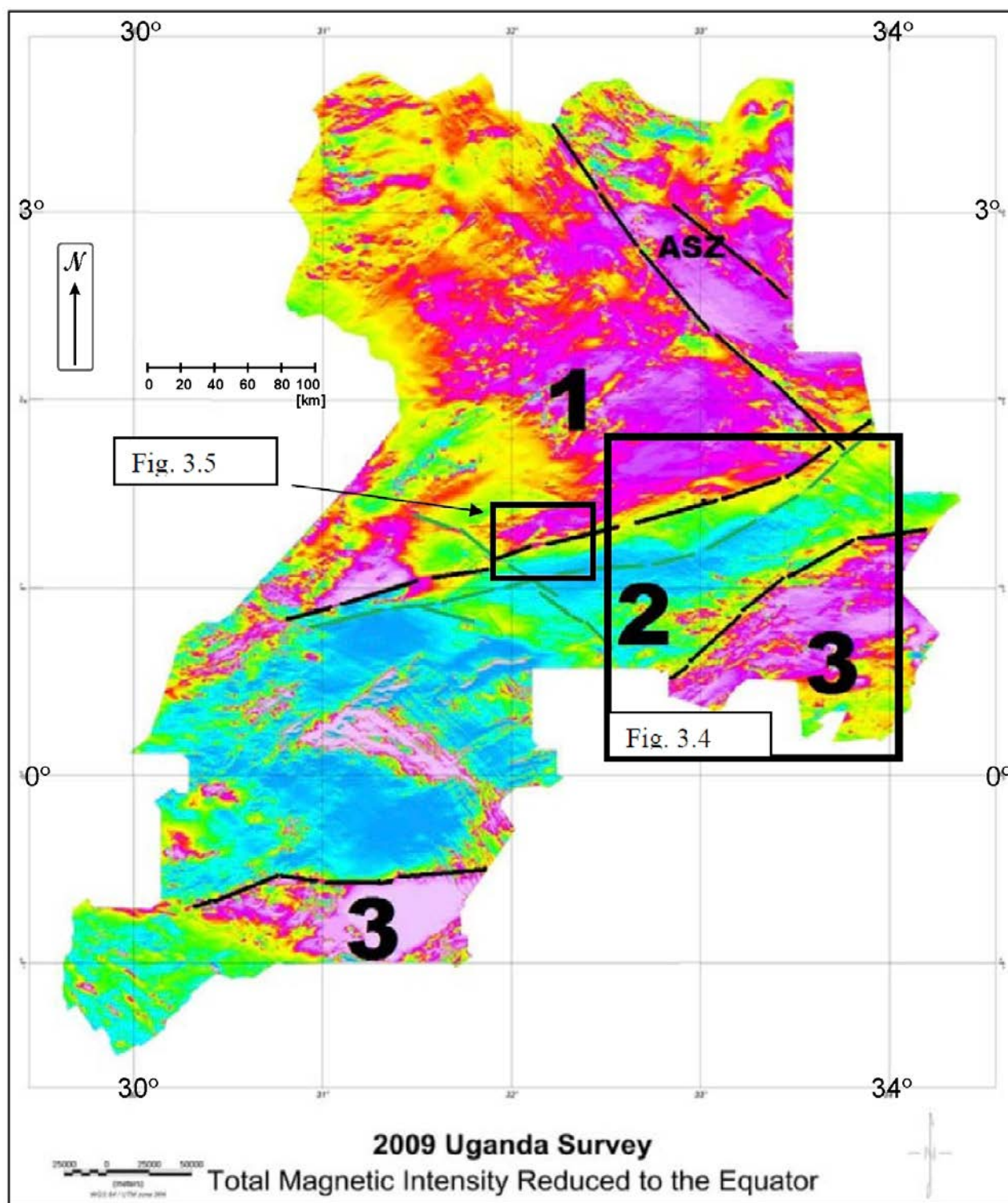


Fig. 3.3. Map of total magnetic intensity reduced to the equator of Uganda showing three-fold division with high-magnetic zones in north (1) and SE and SW of the country (3) and a low-magnetic belt in between (2). Some major and fundamental linear features are also shown. Note E-W magnetic trends in West Nile Block, which continue beneath the sedimentary cover of Albertine Rift. Key: ASZ = Aswa Shear Zone. Green line portrays some major dolerite dykes. Geophysical base map by FUGRO, original scale 1:1 000 000.

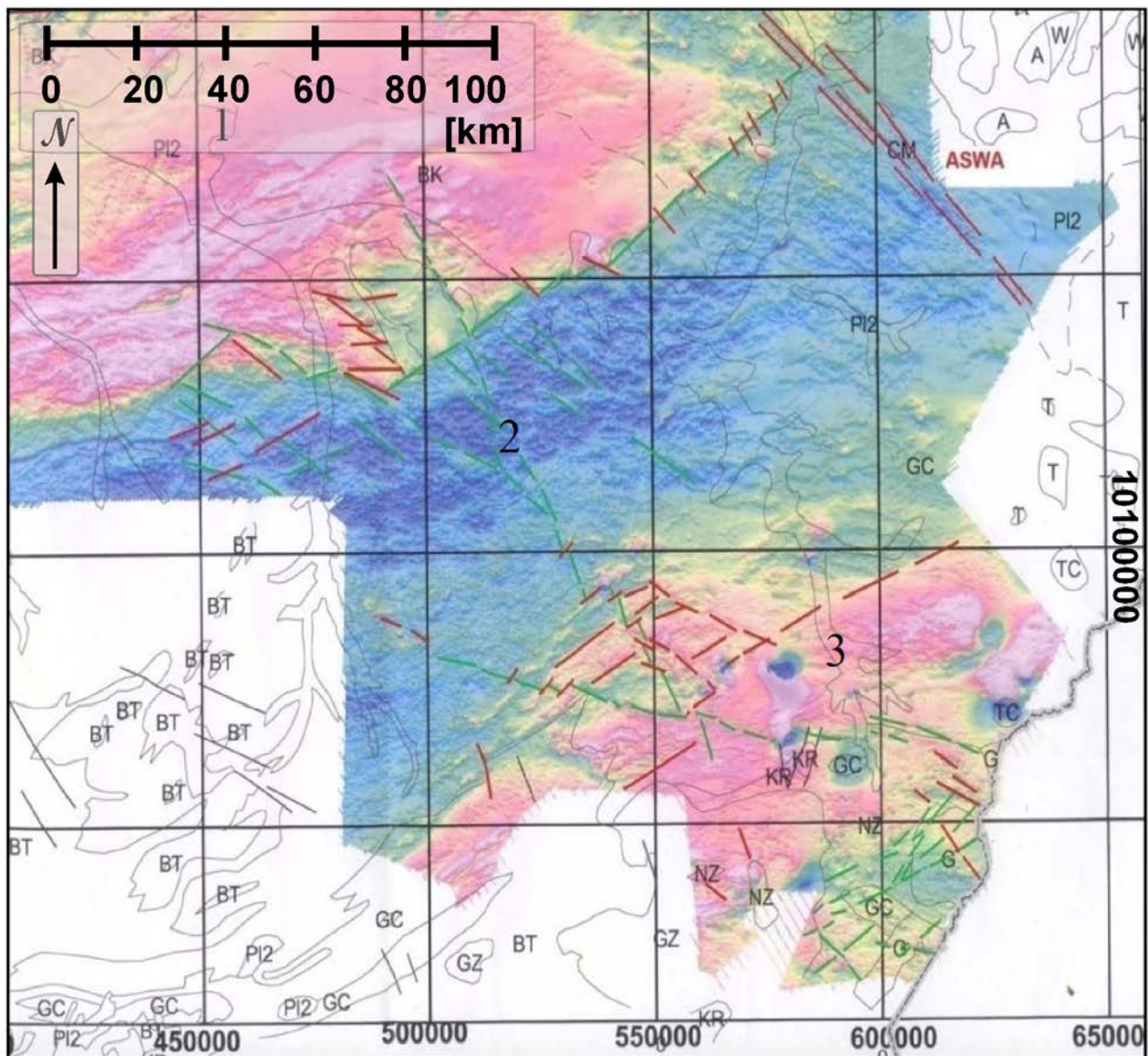


Fig. 3.4. High- and low-magnetic intensity zones in southeastern Uganda on airborne magnetic map reduced to equator, blue low magnetic. Green lines possible dolerite dykes, red-brown lines lineaments. Note in particular the sharp contact in the north between areas 1 and 2 where a mafic dyke appears emplaced along the contact. An interim working map with preliminary geology imposed on geophysics.

with migmatitic granitoids and occur on both sides of the linear feature.

The above field observations are confirmed by Figure 3.5. WTT lithologies apparently extend at depth north of the magnetic lineament and the zone of intense foliation may represent a palaeo-suture for which Ruotoistenmäki (2014) coined the term Nakasongola discontinuity (Figs 3.3 and 3.4; see also pink line in Fig. 3.5.), a distinct magnetic, gravimetric and radiometric discontinuity, interpreted to represent a collision (suture) zone, where the northern block has been thrust over the southern denser block

It is furthermore assumed that the presence of rocks of the Kiboga Suite (Section 3.3.4) and the Bukungu granite within the fracture zone between domains (1) and (2) (Fig. 3.3) is not fortuitous. Kiboga Suite rocks are small, massive, undeformed, but locally intensively sheared, intrusive, columnar-jointed granitic bodies with a unique age of 2.49 Ga (Mänttari 2014).

From the above we conclude that the geophysical break shown in Fig. 3.3 represents a mid-crustal dislocation, a suture between the West Tanzania and North Uganda Terranes and, possibly, between the Tanzania Craton and Bomu-Kibalian

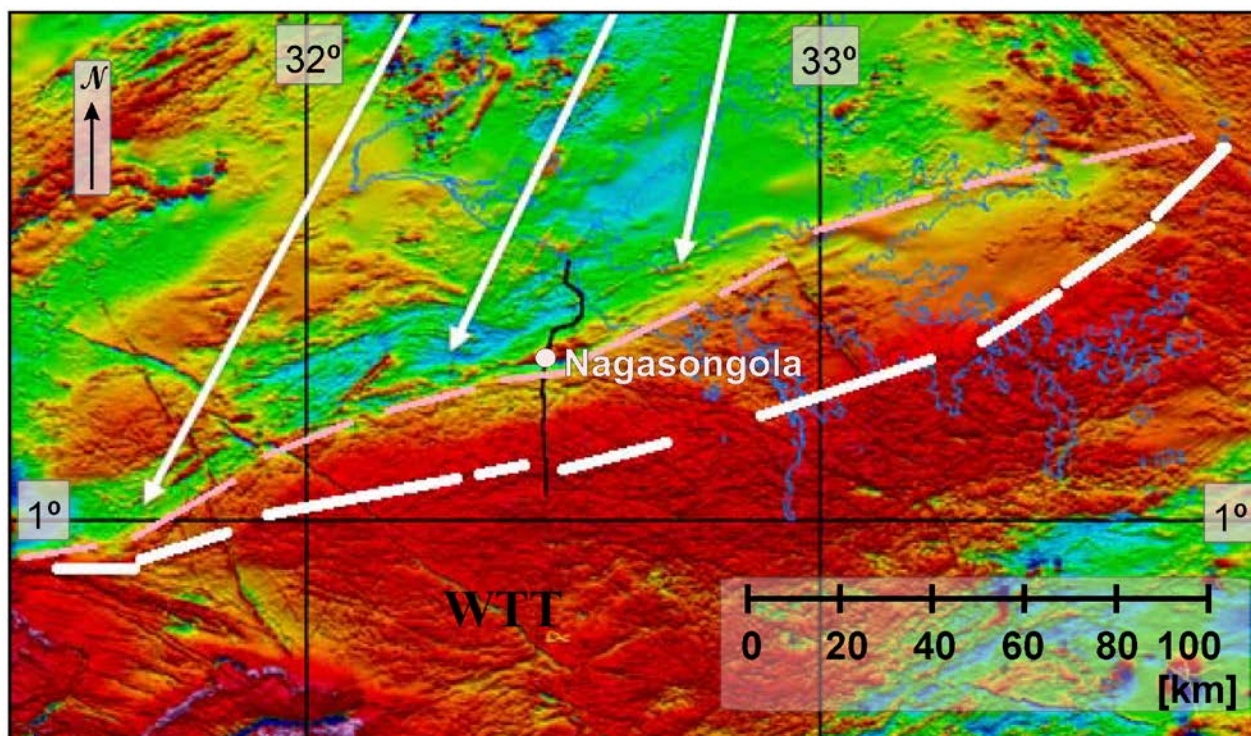


Fig. 3.5. Airborne magnetic map reduced to pole. The low-magnetic belt in Figs. 3.3 now show up as magnetic 'high' (red colour). The magnetic lineament in Fig 3.3 is indicated here as white line. Lithologies of the WTT (Fig. 3.2) may extend further northwards as indicated by the pink line highlighted by white arrows. Thin blue lines indicate water bodies. Geophysical ground survey in Nagasongola that was carried out by the GTK Consortium is marked as black curved line in the middle of the map (courtesy Dr. Tapio Ruotoistenmäki).

Shield of the proto-Congo Craton (Fig. 1.6). In view of the intrusive contact between lithologies of both terranes, the age of this suture is Archaean, supposedly older than 2.62 Ga. Assuming that this conclusion is correct, the WTT and NUT were already united before being jointly incorporated into the proto-Congo Craton during the Palaeoproterozoic.

Subsequently, this weakness zone was reactivated repeatedly, first around 2.49 Ga, giving rise to emplacement of the rocks of the Kiboga Suite and the Bukungu alkali biotite granite. Later, during

the Palaeoproterozoic, it gave rise to development of a WSW-ENE-trending aulacogen (or aborted rift) with deposition of the Buganda Group (ca. 2.0 Ga) (Table 6.1). This WSW-ENE-trending aulacogen is part of the 2.1 to 1.85 Ga Rwenzori-Rusizi-an-Ubendian-Usagaran system of fold belts, wrapping around the Tanzania Craton. The fact that the northern boundary line portrayed in Figure 3.3 is hardly off-set by the Aswa Shear Zone manifests reactivation posterior to this Pan-African sinistral strike-slip fault zone, later than 400 Ma (Section 11.10.3).

3.3 Litho-Stratigraphy of the West Tanzania Terrane

The complex assemblage of Neoproterozoic para- and orthogneisses, migmatites and weakly deformed granitoids of the WTT has been divided into the following major map units: (1) TTG gneisses, (2) Tororo Suite and (3) Kampala Suite. Rocks of the Kiboga Suite also belong to the West Tanzania Terrane (Fig. 3.6). Although they have ages that are slightly younger than the arbitrary

boundary between the Archaean and the Palaeoproterozoic (Gradstein et al. 2004a, 2004b) at 2.5 Ga ago, these units are without doubt part of the prolonged 'Neoproterozoic consolidation event' of the northern Tanzania Craton. Less than 1% of the WTT is underlain by rocks previously attributed to the variegated and enigmatic Bubulo Formation (Section 3.3.5).

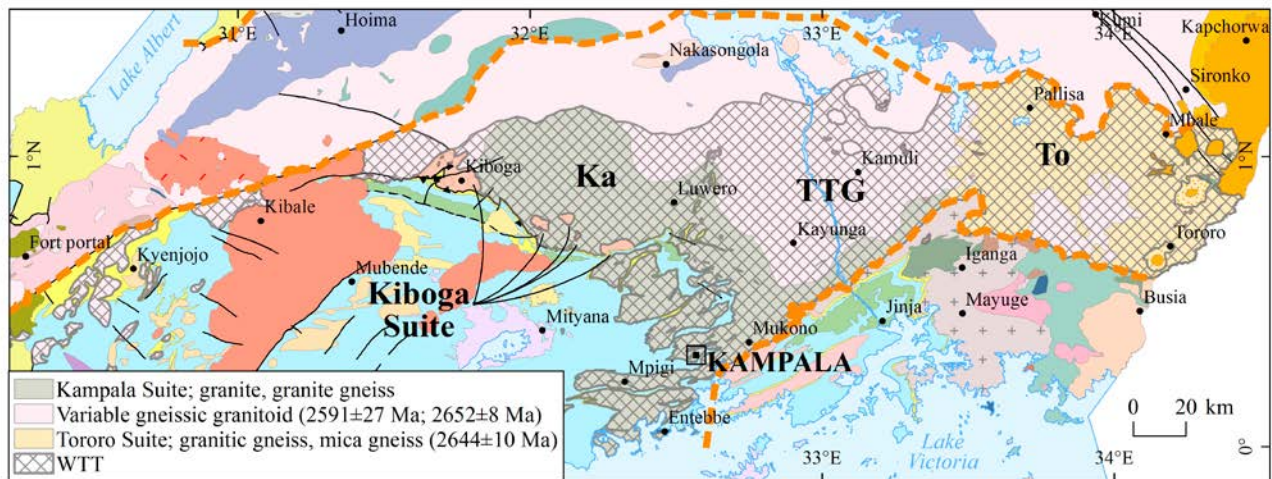


Fig. 3.6. Geological map of the West Tanzania Terrane with TTG gneisses, Tororo Suite and Kampala Suite.

3.3.1 TTG Gneisses

Migmatitic TTG gneisses occupy a relatively flat area with local isolated hills and are generally of granodioritic composition. They can be distinguished from non-migmatitic biotite-bearing Kampala Suite granitoids by the latter having higher total intensity and potassium aero-radiometric signatures. Major silicate minerals are K-feldspar, plagioclase, quartz, hornblende and biotite. Hornblende generally predominates over biotite and its mode varies between 5 and 15% by volume. The rocks have undergone partial melting resulting in variable amounts of anatectic felsic veins with K-feldspar porphyroblasts.

In places, solitary mafic enclaves and inclusions may have sharp boundaries, manifesting little or no resorption. More commonly, however, large, angular and abundant mafic inclusions form significant proportions of these rocks (Fig. 3.7). In places, the abundance of these angular fragments is so great that the rock grades into a 'pseudo-breccia'. Locally, mafic enclaves may form fragments that still fit as pieces in a jig saw puzzle, but generally they are aligned parallel to a nebulitic compositional banding consisting of pinkish, more or less leucocratic bands alternating with more greyish bands that contain up to 20–25 vol% mafic minerals. Occasionally, these mafic fragments show a folded planar fabric that is older than the preferred orientation in the granitic gneisses (Fig. 3.8A). We suggest that these enclaves are derived from an older unexposed or poorly outcropping mafic country rock.

Widespread resorption is demonstrated by nebulitic patches around the enclaves with neoblastesis of large plagioclase and hornblende crystals up to 10 mm in size (Fig. 3.8B). Resorption affected the felsic bands in the enclaves preferentially. In some places the above process is in an advanced stage and only a few dark patches have been preserved. Resorption is manifested by the presence of two granitoid phases, comprising (1) an older medium-grained, equigranular phase and (2) a younger coarser grained phase, which occurs in anastomosing stringers with hornblende blasts.

In some places, where TTG gneisses are rather homogeneous and free from mafic enclaves, biotite may dominate over hornblende. They can be called TTG biotite gneisses that also occur as isolated and relative small polygons within granitoids of the Kampala and Tororo Suites. They are locally granitic in appearance or are composed of a mixture of deformed biotite granite and biotite granite gneiss. Both are peraluminous in composition and have a supracrustal origin as shown by relicts of sedimentary bedding. Where partial melting of this supracrustal gneiss was particularly intensive, diatexite has formed.

Biotite in TTG biotite gneisses occurs in amounts up to 15–25 vol%. Hornblende is absent or locally observed as an accessory mineral. In places, relatively angular K-feldspar porphyroblasts have crystallised in anatectic accumulations. As in hornblende-bearing TTG gneisses, common cracks, joints or narrow fractures are filled by secondary epidote. A couple chemical whole rock analyses are shown in Appendix 2 (anal. 28–29).



Fig. 3.7. Example of migmatitic TTG gneiss (533941E / 144907N) with a great abundance of mafic enclaves showing compositional banding, resorption and formation of nebulitic patches with coarse feldspar and hornblende.

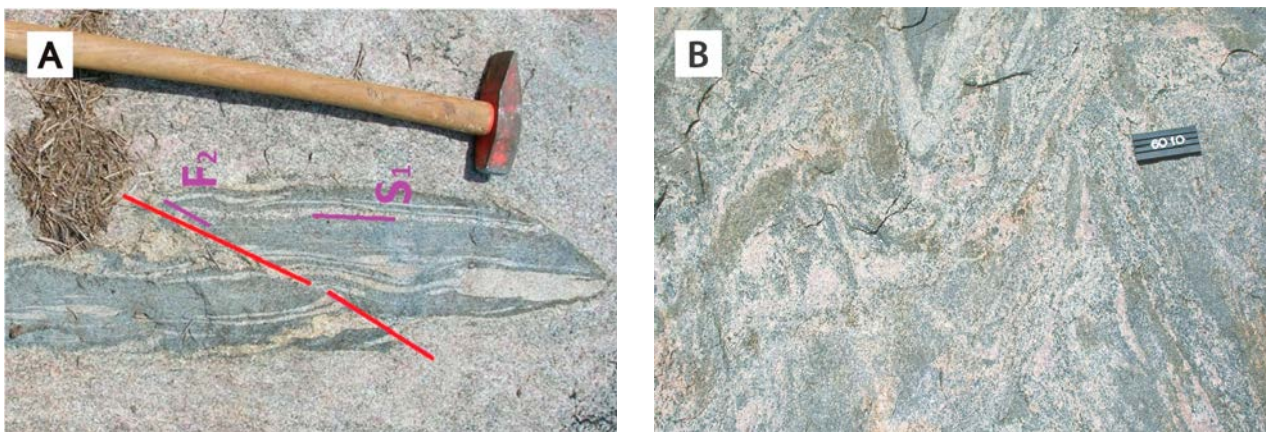


Fig. 3.8. (A) Enclave showing refolded isoclinal small folds with shearing along the F2 fold plane. (B) Migmatitic gneiss showing an advanced stage of resorption (533941E / 144907N). Number tag 10 cm.

3.3.2 Tororo Suite

Rocks of the Tororo Suite occupy the eastern segment of the WTT (Fig. 3.6), underlying a surface of ca. 3,000 km². Tororo Suite granitoids are typically biotite-bearing and composed of several sub-facies including: (1) gneissic granite and granodiorite, (2) hornblende-bearing granodiorite, granite and diorite, (3) porphyritic granite, (4) biotite granite, (5) medium-grained granite with pegmatite and (6) the dated Kisoko granite (~2.664 Ga). Typical chemical compositions of these granitoids are presented in Appendix 2 (anal. 30–38). A special facies of Tororo Suite rocks is formed by (7) Na-K metasomatic halos surrounding the Neogene carbonatite plugs of the alkaline Elgon Complex. Regionally, the contours of the Tororo Suite can be distinguished from the surrounding rock units by their high potassium signature in aero-radiometric maps.

Gneissic granite and granodiorite (Fig. 3.9, A3Tgrs) – These are grey to pinkish grey, medium- to coarse-grained, more or less heterogeneous and

moderately foliated gneissic rocks. Minor parts are tonalitic in composition (Fig. 3.11A). Major minerals are quartz, K-feldspar, plagioclase and biotite in varying proportions depending on the composition of the rock. Biotite is the main mafic mineral and mostly ranges between 15 and 20 vol%. Elongated inclusions of mafic and supracrustal rocks, measuring up to 1.5 m in length, occur sporadically and are generally arranged parallel to the foliated fabric of the rock.

Aplitic veins and dykes with thicknesses up to 0.5 m occur randomly or show a preference for NE-SW and NW-SE directions. Judging from their mutual relationships, they have been emplaced at different, successive occasions. Metamorphosed, deformed, and even boudinaged mafic dykes, up to one metre in thickness, occur sporadically.

Hornblende-bearing granodiorite, granite and diorite (Fig. 3.9, A3Thg) – Hornblende-bearing granite is a light brownish grey, coarse-grained, massive to weakly foliated and porphyritic rock with plenty of euhedral, randomly oriented K-feldspar phenocrysts, measuring up to 30 mm in size

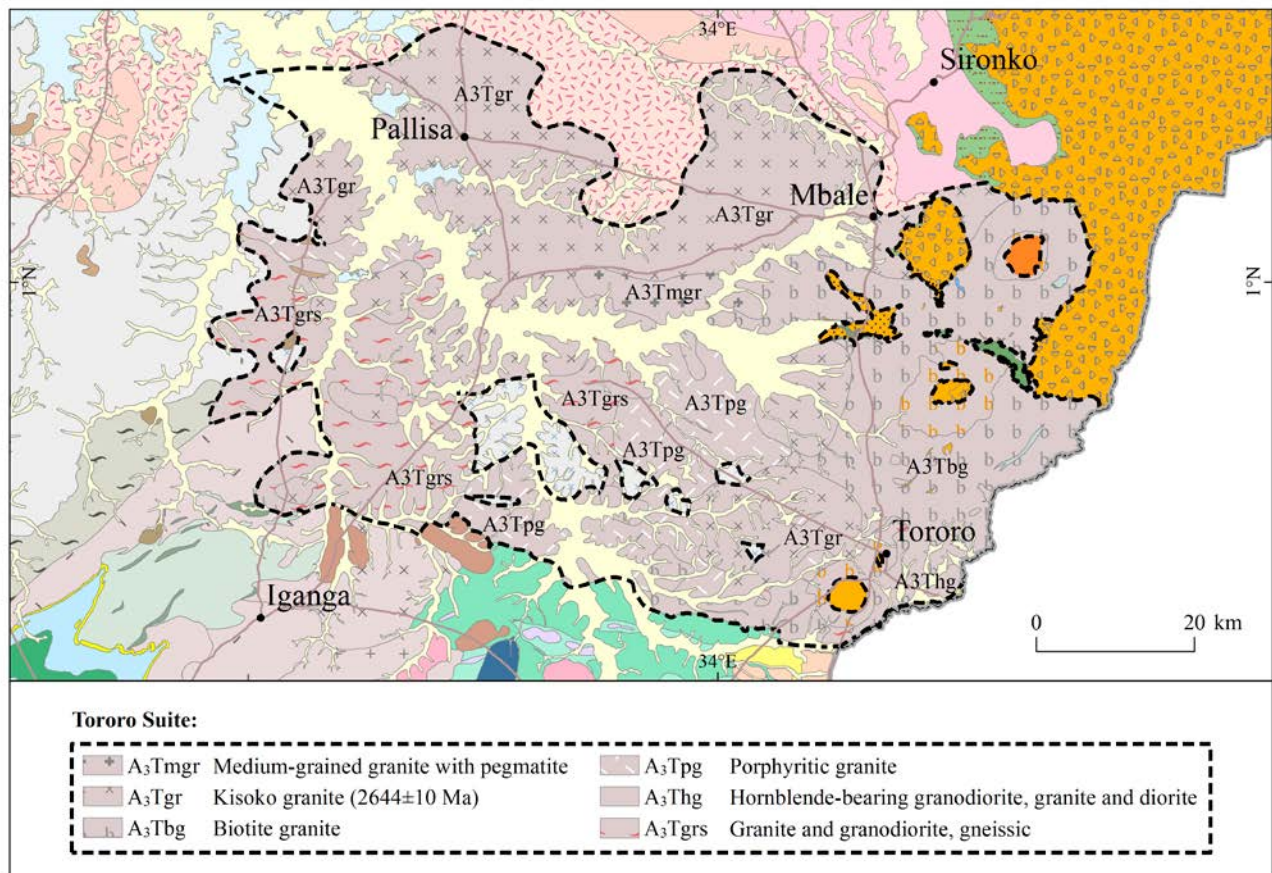


Fig. 3.9. Distribution of Tororo Suite granitoids (code A3T- within black dashed line on map).

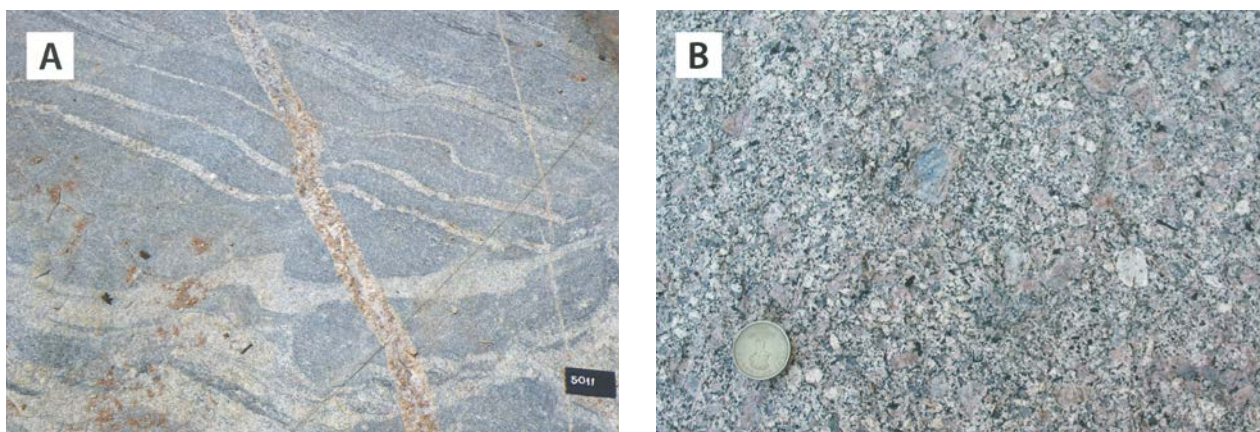


Fig. 3.10. (A) Gneissic granodiorite with granitic bands cut by pegmatite vein (594820E / 97767N). Number tag 8 cm. (B) Heterogeneous hornblende-bearing granitoid (641762E / 73407N). Diameter of the coin is 2 cm.

(Fig. 3.11B). The rock is locally heterogeneous and contains many sub-rounded, mafic enclaves and grey, rather fine-grained felsic xenoliths, measuring up to 1.0 to 1.5 m in size. Major minerals are K-feldspar, quartz, plagioclase, hornblende and biotite. The mafic minerals constitute ca. 15–20 vol% of the rock, with their proportions varying in function of the rock chemistry. Dark coloured roundish grains of hornblende, up to 8 mm in size, apparently formed by neoblastesis, have been found in places. Narrow aplitic granite veins and dykes, up to 5 cm in thickness, occur randomly.

Porphyritic granite (Fig. 3.9, A3Tpg) – These are exposed in rocky hills (kopjes as in Fig. 3.11A) as grey or pinkish grey, mainly coarse-grained, generally rather homogeneous and weakly foliated rocks (Fig. 3.11B). They are composed of rather

euohedral K-feldspar phenocrysts (\varnothing 3 cm), quartz, plagioclase and biotite (15 to 20 vol%). Amphibole is locally present in minute amounts. Elongate, amphibole-rich enclaves, up to 50 cm in size, occur in places and are mostly aligned parallel to the weakly developed planar fabric. Narrow granitic and aplitic veins occur randomly.

Biotite granite (Fig. 3.10, A3Tbg) – Extensive biotite granites are inconspicuous in aero-geophysical data and usually exposed in small hills. The northern part of the unit is a light grey, medium-grained, equigranular, almost massive and leucocratic rock with small amounts (ca. 10 vol%) of biotite. The southern part of the biotite granite is a dark grey, medium- to coarse-grained, slightly porphyritic, foliated and heterogeneous rock. It contains a variety of elongated, heterogeneous enclaves of

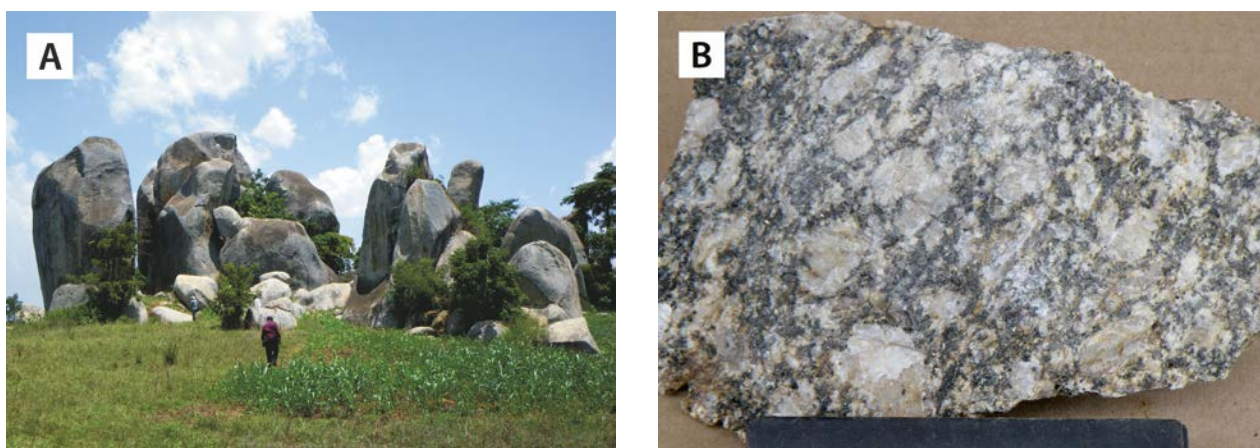


Fig. 3.11. (A) Porphyritic granite hill or (kopje) (615483E / 87010N), (B) porphyritic granite (599780E / 94568N). Tag 10 cm.

amphibolite or mica gneiss with diameters up to 1.5 m. Major minerals are K-feldspar, locally in phenocrysts up to 1.5 cm in size, quartz, plagioclase and biotite (10–15 vol%), with only minute amounts of hornblende. Narrow pegmatite granite veins and dykes occur randomly.

Medium-grained granite with pegmatite (Fig. 3.9, A3Tmgr) – Members of this biotite-bearing granitic sub-facies are pinkish grey or grey, weakly foliated, medium-grained granites with common cross cutting pegmatite veins and dykes with thicknesses ranging from a few centimetres to up to one metre (Fig. 3.12). Most pegmatite veins trend parallel to the weak foliation of the host granite. Scattered enclaves of mafic minerals, up to 2 cm in size, are common.

Kisoko granite (2644 ± 10 Ma) (Fig. 3.9, A3Tgr) – Inconspicuous rocks in aero-geophysical maps, the Kisoko granite is a grey or pinkish grey, medium-grained, mainly equigranular, rather homogeneous, massive to weakly foliated rock. In places, fine- or coarse-grained varieties can be encountered. Major minerals are quartz, K-feldspar, plagioclase and mafic minerals amounting to 15–20% by volume with biotite being dominant over hornblende.

gioclase and mafic minerals amounting to 15–20% by volume with biotite being dominant over hornblende.

Veins of aplitic granite and quartz are common. Scarce pegmatite veins, generally up to 5 cm, but occasionally up to 50 cm in width, occur often in parallel arrangement with the weakly developed foliation in the granite. Epidote is found in some narrow sub-vertical, brittle, NW-SE directed fractures.

Field observations suggest that these granites, which underlie large areas in eastern Uganda, have intruded older porphyritic granite, biotite granite and gneissic granitoids. U-Pb zircon dating (MC-LA-ICP-MS method) yields an emplacement age of 2644 ± 10 Ma (Mänttari 2014).

Na-K metasomatic halo (Fig. 3.10, A3Tbgh) – Fe-nitisation and related Na-K metasomatism around carbonatite plugs of the Neogene alkaline Mount Elgon Complex of SE Uganda has been known for a long time (Davies 1956). These halos are 2–3 km wide and can be well distinguished in the field by their positive relief and by their aero-radiometric signature, showing elevated K values.



Fig. 3.12. Medium-grained granite with pegmatite dykes (616270E / 107727N). Number tag 8 cm.

The metasomatic ‘halo’ occurring in the rocks of the Tororo Suite around the Neogene Tororo carbonatite complex (see Williams 1952) is well described by Davies (1956): “surrounding the Tororo carbonatite one observes roughly progression from (1) an outer fenitised granitoid zone through (2) mixed syenites with feldspar and nepheline into (3) types with mainly nepheline and pyroxene, and (4) finally to the carbonatite rock”. The outermost zone of fenitised granitoids comprises locally Na-amphibole, which penetrates along cracks and crystal boundaries. The syenites can be classified as leucocratic fenites. Feldspar in these syenites is commonly crystallised as interpenetrating tablets while the interspaces are filled with calcite and ferromagnesian minerals. Calcite and aegirine augitic pyroxene are common minerals and the pyroxene often occurs as ‘graphic’ intergrowths with feldspar. Calcite may replace pyroxene. Moreover, apatite and magnetite are very common in the interstices between the feldspars. In the nepheline-syenites, the amount of feldspar is high (60–70 vol%) and nepheline has often broken down to a fine mass of flaky mica (Davies 1956).

Just around Tororo carbonatite hill, there occur some greyish rocks, which can be classified as ijolites. They contain little or no feldspar but anhedral nepheline and variable amounts of ferromagnesian minerals, including pyroxene, generally aegirine or diopside. Perovskite, sphene, calcite and wollastonite are also observed in many samples.

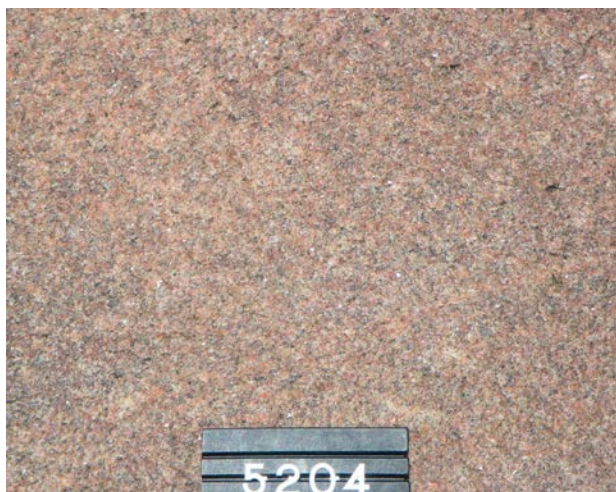


Fig. 3.13. Medium-grained granite (456798E / 102304N). Number tag 8 cm.

3.3.3 Kampala Suite

The Kampala Suite, composed of variably deformed granitoids and orthogneisses, covers an extensive area between the Palaeoproterozoic Buganda metasediments in the south and various TTG gneisses in the north (Fig. 3.9). On airborne geophysical maps, Kampala Suite granitoids can be distinguished from surrounding granitic rocks by a slightly stronger radiometric signature, in particular higher K values. They are particularly common in and north of the city of Kampala from which this unit derives its name. Most commonly this is a medium-grained, equigranular and weakly deformed biotite granite or gneiss and SiO₂ concentration may vary from 65 to 72 wt% (App. 2, anal. 39–40). Two sub-facies have been identified: (1) *Medium-grained granite* and (2) *Kampala granitoids, orthogneiss*.

Medium-grained granite (Fig. 3.9, A3KA_{mg}) – This member of the Kampala Suite shows slightly higher radiometric values compared to the surrounding rocks. Being a compact and weathering resistant rock, it constitutes usually high hills, particularly NW of Mukono.

This granite member is a dark grey or pinkish grey, mostly medium-grained to occasionally fine-grained, equigranular, rather homogeneous and undeformed to weakly foliated rock (Fig. 3.13). Major minerals are quartz, K-feldspar, plagioclase and biotite, the latter in quantities of usually 5 vol% or less. No enclaves or nests of mafic minerals have been observed. Scattered narrow veins of pegmatite, up to 5 cm in width, occur mainly parallel to the weak foliation.

Kampala granitoids and orthogneisses (Fig. 3.9, A3KA_{gr}) – Kampala granitoids and orthogneisses are mainly composed of heterogeneous, generally equigranular, more or less deformed granitoids (Fig. 3.14A) and banded gneisses (Fig. 3.14B), showing distinctive variations in grain size and mineral composition. Granitic and pegmatitic veins and stripes and elongated darker granitic patches occur commonly. Although locally intensively deformed, a plutonic origin is postulated for most of the rocks. Large hill top outcrops in an area about 10 km SSE of Bombo town comprise, however, granitic rocks with a distinct, regular banding, suggesting a possible volcanic protolith for this orthogneiss.

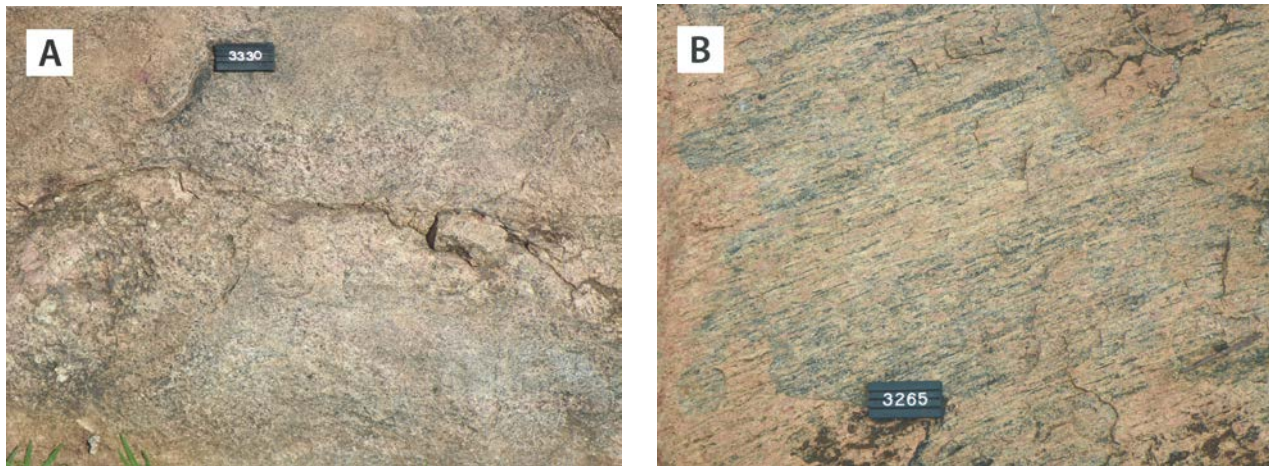


Fig. 3.14. (A) Typical heterogeneities in the Kampala Suite granite (442002E / 88071N). (B) Intensively deformed Kampala Suite granite, orthogneissic in appearance (484638E / 57158N). Number tag 8 cm.

3.3.4 Kiboga Suite

The Kiboga Suite (Fig. 3.7) comprises three sub-facies or members: (1) *Granite, porphyritic in places*, (2) *Naluvule feldspar porphyry* and (3) *Lutukuma granite*. Members (2) and (3) have been dated and yield ages of 2.49 Ga (Mänttäre 2014).

Granite, porphyritic in places (PIKgp) –The largest Kiboga intrusion, measuring about 13x17 km in size, comprises the hilly terrain around the town of Kiboga. Like other Kiboga granite bodies, further to the east, they differ with their elevated relief and distinctly positive signatures in ternary radiometric maps from the generally flat granito-gneissose basement areas.

This is a light brown to brownish grey, massive biotite granite with textures varying from equigranular to slightly porphyritic. Porphyritic members contain subhedral K-feldspar phenocrysts, on average ca. 2–15 mm, but locally reaching around 20–30 mm in size. These phenocrysts are set in a grey, fine- to medium-grained quartz-feldspar-biotite groundmass with apatite and ilmenite as accessory minerals. Epidote occurs as a retrogressive mineral.

Generally, granites of the Kiboga Suite are massive, not foliated or show only a weak deformation. NW-trending quartz-filled joints are locally common, however, and in the northern part of the largest granite body progressive deformation has turned the prevailing porphyritic variety into Augen gneiss-like granite, which is often cut by coarse pegmatite dykes. This deformed granite yielded a

U-Pb zircon age of 2.49 Ga (Mänttäre 2014). Mafic enclaves or xenoliths are rare in these rather homogeneous granites. Three km west of Kiboga town, however, a large amphibolite xenolith or country rock roof pendant has been found in this granite body, dated at 2.65 Ga (Mänttäre 2014).

Naluvule feldspar porphyry (PIKfp) (2.49 Ga) – Outcrops of feldspar porphyry are locally found in the hills around Kiboga town. Textural and mineralogical similarities with porphyritic varieties of the above biotite granite suggest that the Naluvule feldspar porphyry represents a co-magmatic, but shallower intrusive phase. On Naluvule hill, located about 3 km east of Kiboga town, this massive, homogeneous rock is quarried for aggregate. Sub-vertical columnar jointing (Fig. 3.15A) is predominant in the rock aggregate quarry.

Dark grey to pinkish grey Naluvule porphyry is composed of randomly oriented, euhedral feldspar phenocrysts, averaging ca. 2–15 mm in size, set in a fine-grained feldspar-quartz-biotite groundmass (Fig. 3.15B). U-Pb zircon dating yields an age of 2.49 Ga (Mänttäre 2014).

Lutukuma granite (PIKag) (2.49 Ga) – A deformed granite variety of Kiboga Suite, named Lutukuma granite after the nearby village, is exposed NW of the largest Kiboga granite body. In some large outcrops, brittle deformation has converted medium- to coarse-grained, massive and porphyritic biotite granite into dark brownish grey, foliated gneissic granite, giving the rock an Augen-like appearance due to the presence of K-feldspar

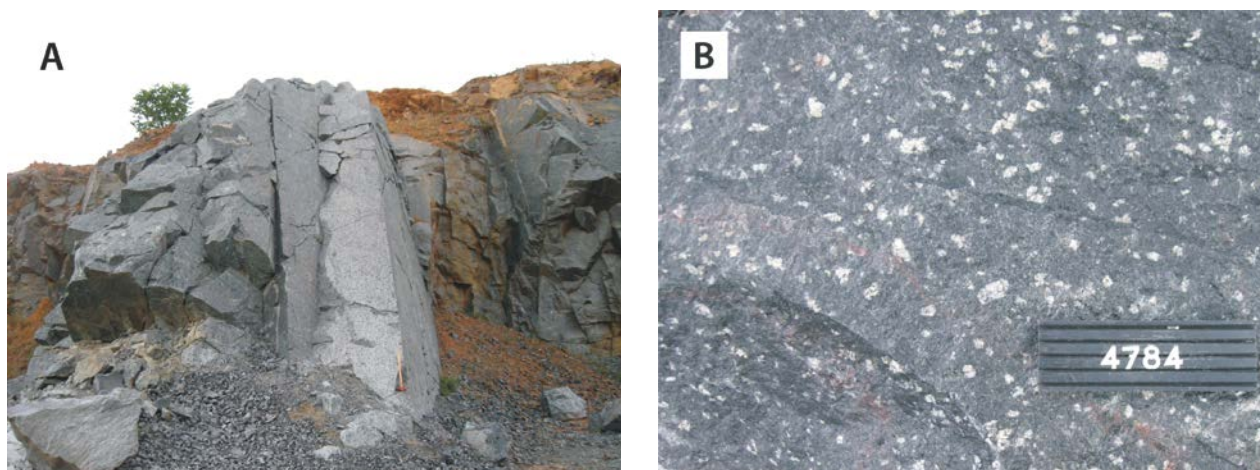


Fig. 3.15. (A) Sub-vertical columnar jointing showing smooth facets in feldspar porphyry. (B) Detailed photograph of Naluvule feldspar porphyry. Quarry ca. 3 km E of the town of Kiboga (367147E / 99837N). Number tag 12 cm.

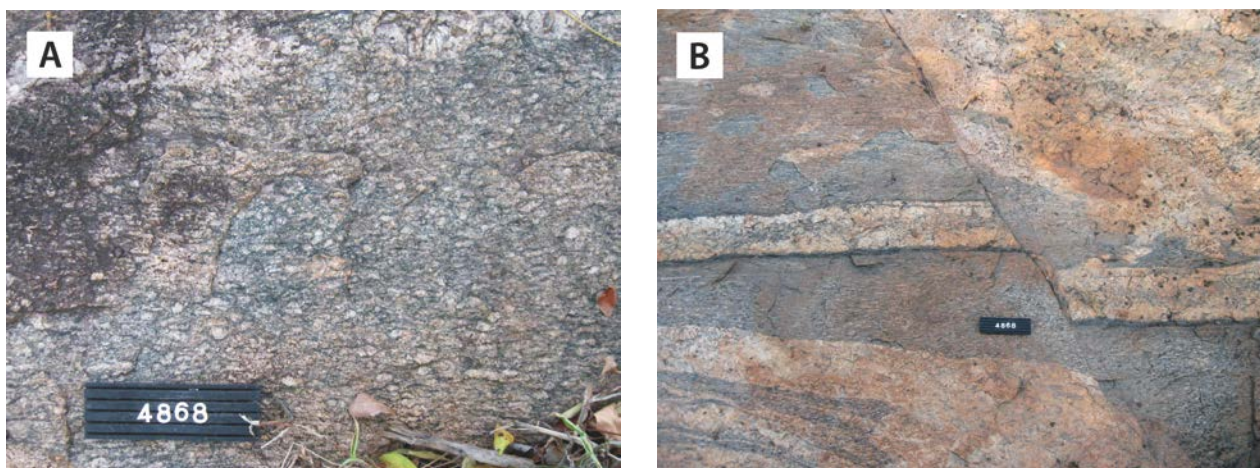


Fig. 3.16. (A) Deformed, augen-like K-feldspar phenocrysts in the Lutukuma granite. (B) Dextral strike-slip fault of a pegmatite dyke in migmatized granite (357303E / 100510N). Number tag is 10 cm.

phenocrysts turned into porphyroclasts (Fig. 3.16A). The progressive transformation from originally porphyritic granite into an Augen gneiss-like, migmatitic rock has been accompanied by multiple injections of large pegmatite bodies and sub-parallel pegmatite dykes, locally off-set by small strike-slip faults (Fig. 3.16B). U-Pb zircon dating of the Lutukuma granite yields an age 2.49 Ga (Mänttari 2014).

3.3.5 Bubulo Formation

Rocks of the Bubulo Formation constitute an insignificant proportion (< 1%) of the lithologies in the WTT. According to Davies (1956) they comprise of a great variety of supracrustal rock types including (1) *epidote-garnet gneiss* (A3WBegn), (2) *mafic*

and intermediate metavolcanic rock (A3WBhgs) and (3) *quartz-mica schist* (A3WBqs).

Light brownish to pinkish grey, epidote- and garnet-bearing paragneisses (A3WBegn) are exposed along the banks of the Nile River, about 25 km northwest of the Bujagali Falls, on a hill top ~10 km further southwest and as large xenoliths in some granite outcrops of the Kampala Suite.

Irregular patches of mafic and intermediate metavolcanic rocks (A3WBhgs), formerly named '*Precambrian hornblende gneiss and -schist*' by Davies (1956), occur widely in an area west of Mount Elgon. These are dark greenish, mafic, fine- to medium-grained, heterogeneous and weakly foliated metavolcanic rocks (Figs 3.17A, B). A thin section study (632486E / 102772N) confirms the presence of quartz, plagioclase, amphibole (horn-

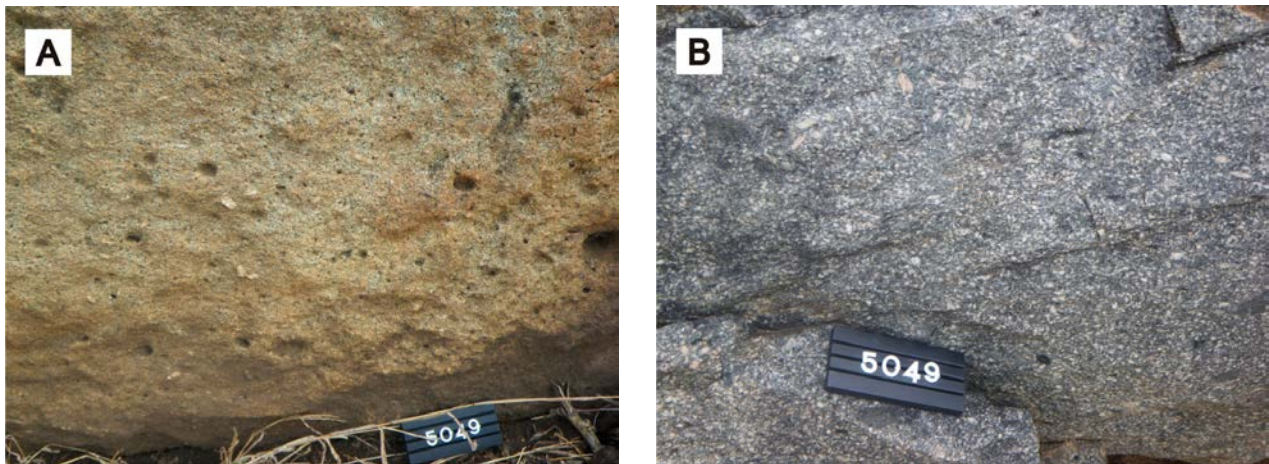


Fig. 3.17. (A) Weathered surface of mafic and intermediate metavolcanic rock (632486E / 102772N), (B) unweathered surface of the same rock type. Number tag 10/12 cm.

blende) and biotite as major minerals; titanite and chlorite are common accessories. A light green, fine-grained, strongly foliated, banded and folded, intermediate variety of amphibole-bearing metavolcanic rock occurs in places, closely associated with the above rock and may resemble hornblende schist described by Davies (1956). The chemical composition of this metavolcanic rock is shown in Appendix 2 (anal. 27).

Small, scattered outcrops of quartz-rich meta-sediments (A3WBqs) range from purple, banded quartzite to mica schist containing up to 50 vol% of white mica (Davies 1956). Elsewhere, they comprise yellowish brown quartz-sericite schist with dark grey, fine-grained mica schist or metagreywacke interlayers.

In places, some varieties of these rocks resemble supracrustal inclusions occurring in the TTG gneisses in the northwestern part of the WTT. As a consequence, these undated and enigmatic Bubulo lithologies have been provisionally attributed an Archaean age. Alternatively, they may represent erosional relics of the Palaeoproterozoic Rwenzori Belt (Chapter 6). According to Davies (1956) the Bubulo Formation also comprises metagreywacke (A3WBgw), which occurs as randomly distributed, small outcrops in the extensive Iganga Granite Suite of the LVT (Section 2.3.4). The presence of Bubulo lithologies in both the WTT and LVT favours the idea that these rocks are Rwenzori erosional relics. But again, as an alternative, the metagreywackes may not be part of the Bubulo Formation and belong to the Kavirondian Super-group (Section 2.2.4).

3.4 Geochronology

The first, now obsolete, whole-rock Rb-Sr ages from the western Tanzania Craton, falling in the range 2.7 to 2.4 Ga, have been reported by Bell & Dodson (1981). At least two events were delineated, one at 2.74 Ga and the other at 2.54 Ga. The younger one was reported to be more widespread and believed to reflect extensive granitoid magmatism throughout large areas of Tanzania, south-eastern Uganda and western Kenya. Bell & Dodson (1981) argued that there was little evidence to support the origin of the 2.5 Ga Tanzanian crustal segment by simple reworking of ancient continen-

tal crust. Pinna et al. (1996) reported ages between 2.56 and 2.58 Ga (Table 2.1) for rocks belonging to the Western Granitic Complex, the presumed Tanzanian equivalent of the West Tanzania Terrane in Uganda.

Initial U-Th-total Pb age determinations of granitoids of the Kampala Suite by Schumann & Kulyanyingi (2001), using microprobe techniques on zoned zircons, gave an age of 2.59 ± 0.07 Ga for the core and 2.22 ± 0.08 Ga and 0.74 ± 0.22 Ga for zircon rims. Subsequent U-Pb zircon ages (MC-LA-ICP-MS method) from a quartz-monzodiorite

member of the Kampala Suite yielded an age of 2.62 ± 0.21 Ga (Schumann et al. 1999, 2004). A well-banded gneiss xenolith in one of the studied granitoid samples contains high U zircons that appear to record normally discordant minimum $^{207}\text{Pb}/^{206}\text{Pb}$ ages of about 3.2 Ga and perhaps as old as 3.6 Ga (Schumann et al. 2004).

U-Pb zircon dating (laser-ICP-MS method) of

Archaean units belonging to the West Tanzania Terrane of the Rwenzori horst yielded ages of 2637 to 2584 Ma (Link et al. 2010, 2011a). The above ages have been confirmed by geochronological studies (all U-Pb zircon ages using the LA-MC-ICP-MS method) carried out by the GTK Mapping Project. The results are presented and discussed by Mänttari (2014).

3.5 Geodynamic Development of the West Tanzania Terrane

The Tanzania Craton, one of the major 'building blocks' of the proto-Congo Craton (Fig. 1.6), is itself composed of several smaller tectono-thermal terranes that amalgamated during the Archaean. Pinna et al. (2004a) attributed crustal growth of the Tanzania Craton to two Archaean orogenic cycles:

- (1) The *Dodoman Orogeny*, with TTG accumulation resulting from high-pressure (HP) melting of mafic slabs (2.93–2.85 Ga) in the southwest of the craton, probably coeval with oceanic/back-arc crust formation in the north.
- (2) The *Victorian Orogeny*, with a succession of three magmatic/tectonic events in the northern part of the Lake Victoria Terrane, broadly between 2.8 Ga and 2.6 Ga (Table 2.1), related to deposition of the Nyanzian and Kavirondian Supergroups in the Lake Victoria Terrane, followed by emplacement of 'Younger Granites', prior to deposition of the 2.53 Ga Kisii Group (Chapter 2).

How relevant is the above geodynamic events to the West Tanzania Terrane and equivalent rocks in Tanzania? According to Schumann et al. (1999, 2004) granitoids of the Kampala Suite display a complex history of Archaean crust formation, either by partial melting or anatexis of pre-existing sedimentary, volcanic or plutonic protoliths (Schumann & Kulyanyingi 2001), culminating around 2.6 Ga and accompanied by extensive emplacement of granitic melts. Almost all analysed granitoids show polyphase tectono-thermal overprinting, as documented from their textures and age dating results.

Well-banded mafic gneiss xenoliths in granitoids yield zircon ages of about 3.2 Ga and perhaps as old as 3.6 Ga (Schumann et al. 2004). The mafic enclaves described in Section 3.3.1 could be identical (Fig. 3.8). The 2.93–2.85 Ga Dodoman

Orogeny recognised by Pinna et al. (2004a) in the Tanzanian Craton is obviously too old for the main phase of granite emplacement and migmatisation but it may be responsible for the formation of pre-granitoid and pre-migmatization planar fabrics and small folds (at least two deformation phases) in some mafic enclaves (Fig. 3.8A). They possibly constitute the badly exposed or sub-outcropping country rocks – an older part of the West Tanzania Terrane, into which the younger (ca. 2.64 Ga) Neoproterozoic granites have been emplaced, coeval with high-grade metamorphism and migmatization. Resorption of these enclaves explains the presence of inherited zircon grains with ages ranging between 2.92 Ga and 2.73 Ga (Mänttari 2014).

We stress that the Lake Victoria and West Tanzania Terranes represent two different geodynamic environments with some major differences:

Low-grade supracrustal rocks in the LVT *versus* high-grade metamorphic rocks, migmatites and granitoids in the WTT.

Low-grade greenstones from the LVT show a variety of ages (2.81–2.65 Ga); granitoids from the same block have ages from around 2.69 Ga to 2.55 Ga; available ages in the Uganda segment of the LVT fall in the 2.64–2.61 Ga bracket. Granitoids from the WTT yield little variation with an age between 2.65 Ga and 2.64 Ga.

Summarising the above, we conclude that the complex assemblage of mildly deformed granitoids, migmatites and gneisses of the West Tanzania Terrane, previously mapped as 'undifferentiated basement' (DGSM 1966) are characterised by a protracted geological history:

- (1) Palaeo- to Mesoarchaean deposition (3.6–3.2 Ga?) of a magmatic belt, followed by subduction during Dodoman Orogeny at 2.93–2.85 Ga with melting of a supra-subductional mantle wedge, triggered by slab dehydration.

- (2) A Neoarchaean phase of crustal extension that resulted in flooding of the western and northwestern parts of the Tanzania Craton with 2.64–2.61 Ga granitoids of both mantle (I-type) and crustal (S-type) derivation. In southern Uganda these granitoids invaded older Archaean basement of about 3.2 Ga and perhaps as old as 3.6 Ga (oldest zircons have ages between 2.92 and 2.73 Ga).
- (3) Merging of the LVT and WTT Terranes must have taken place posterior to emplacement of the 2.59 Ga ‘Younger Granites’ in the LVT and prior to deposition of the 2.53 Ga Kisii Group. This event is possibly manifested by the presence of zircons that have ages ranging from 2.58 to 2.56 Ga in TTG gneisses of the WTT.
- (4) A minor and local phase of late Archaean (2.49 Ga) crustal extension or transtension in a curvi-linear, E-W to WSW-ESE directed palaeo-suture – the Nakasongola discontinuity – between the WTT and NUT, with localised emplacement of granites and feldspar porphyries of the Kiboga Suite. The preservation of coarse columnar jointing (Fig. 3.16A) might manifest a relatively shallow emplacement and rapid cooling and hence significant erosion and uplift between 2.64 Ga and 2.49 Ga, a period of 150 million years. The discontinuity is currently visible as a mid-crustal accident in the magnetic, radiometric and gravimetric data (Ruotoistenmäki 2014).
- (5) Subsequently, during the Palaeoproterozoic (at ~2.1 Ga) this palaeo-suture developed into a similarly trending aulacogen (or aborted rift) in southern Uganda, now showing as a low-magnetic belt (Fig. 3.1). Upon inversion at ~2.0 Ga this aulacogen evolved into the E-W to WSW-ENE-trending segment of the otherwise N-S-directed Rwenzori-Rusizian-Ubendian system of fold belts. The magnetic lineaments that form the northern and southern boundary faults of the low-magnetic belt are considered to represent the marginal faults of this aborted and subsequently inverted rift. Most granitic gneisses and gneissose granitoids have a well-developed, roughly E-W to WSW-ENE trending tectonic planar fabric (e.g., Fig. 2.7), which is related to subsequent mild N-S compression. This mild N-S compression gave no rise to overprinting of the WTT lithologies or formation of zircon rims with ~2.0 Ga ages, possibly with exception of rare 2.22 ± 0.08 Ga zircon rims reported by Schumann & Kulyanyingi (2001).
- (6) Widespread Pan-African overprinting of the WTT is manifested by zircon rims with imprecise ages ranging between 0.74 Ga and 0.40 Ga.

4 WEST NILE BLOCK OF THE BOMU-KIBALIAN SHIELD (CONGO CRATON)

4.1 Introduction

Traditionally, the loosely defined Congo Craton (Lepersonne 1974, Cahen et al. 1984 and references therein) corresponded geographically to the circular Congo River Basin (CRB), largely filled by Cretaceous-Tertiary sediments and a peripheral zone of spatially discontinuous Archaean terranes that are separated from the other Archaean cratons by Proterozoic fold belts.

The present-day CRB coincides with a gravity low and is filled with a pile of sedimentary rocks nowhere thicker than 2000 m, composed of Palaeozoic, post-Pan-African, pre-Karoo Gondwanide Red Beds, covered by a pile of non- or poorly consolidated rocks of Karoo (~320 Ma) to Holocene age. Geophysical data has been interpreted to show that there is no pristine Archaean nucleus in the basement below the CRB but that it is probably entirely composed of Palaeoproterozoic fold-deformed rocks (Crosby et al. 2010). This view finds strong support in seismic tomography undertaken for central Africa (Pasyanos & Nyblade 2007), also indicating the absence of any Archaean central nucleus and associated thick keel of sub-crustal, harzburgitic-dunitic upper mantle rocks beneath the CRB. Fernandez-Alonso et al. (2011) postulated that the proto-Congo Craton should be understood as an assemblage of six Archaean terranes welded together around 2.1 Ga and later exhumed around 1.8 Ga as a result of the Eburnean Orogenic Cycle, culminating in amalgamation of the Columbia Supercontinent (Pinna et al. 1996, de Waele et al. 2006, 2008, Noce et al. 2007, Deltor et al. 2008). One such Palaeoproterozoic fold belt, not covered by sediments of the CRB, is the Usagaran-Ubendian-Rusizian-Rwenzori system of fold belts, separating the Central Africa Craton (or Congo Craton) from the Tanzania Craton.

A variety of local names has been given to the distinct Archaean-Palaeoproterozoic terranes believed to be included in the proto-Congo Craton, such as (listed in anticlockwise order, starting from the SW): (1) the Angola-Kasai Shield, (2) the

Bengweulu Block, (3) the Tanzania Craton, (4) the NE Congo-Uganda Shield, here termed the Bomu-Kibalian Shield (Begg et al. 2009; see I Ib in Fig. 1.1 and Fig. 1.6), (5) the “Ntem-Chaillu” Block of south Cameroon and Gabon and (6) the São Francisco Block of Brazil.

The proto-Congo Craton has remained relatively stable and united since the late Palaeoproterozoic (Tack et al. 2006a, 2008b, 2009), being affected only by intra-cratonic tectonic events (rifting, rift inversion and magmatism; Delvaux et al. 2011, Tack et al. 2010). The most notable of these events was the creation of a Mesoproterozoic intracratonic basin in the eastern part of the craton, in the area now underlain by the Kibaran Fold Belt, but this process never evolved to continental breakup and the formation of a juvenile oceanic basin. All major events pertaining to the Pan-African Orogenic Cycle, culminating in the formation of the Gondwana Supercontinent at 0.55 Ga, took place along the margins of the craton. The proto-Congo Craton became bordered by Pan-African collisional high-grade belts in the north (Oubanguides or Central African Fold Belt, CAFB) and east (East African Orogen, EAO), while foreland accretionary belts such as the West Congo/Araçuaí Belt and Damara-Lufilian-Zambezi Belt formed at the western and southern margins. Related to the Cretaceous opening of the southern Atlantic Ocean, a minor segment (São Francisco Block) from the western margin of the craton became separated.

Archaean basement rocks exposed in the six shields located along the margins of the proto-Congo Craton show marked differences in their geological history, up to such degree that they can be considered to represent separately born and evolved tectono-thermal terranes. The Tanzania Craton was briefly described in Chapter 2. The northeastern Bomu-Kibalian Shield (Fig. 1.1) or NE Congo-Uganda Block (Fig. 1.6) will be described below.

4.2 Bomu-Kibalian Shield (Congo Craton)

A map outlining the main geological components of the still only tentatively mapped Bomu-Kibalian

Shield in the northeastern DRC is shown in Figure 4.1. There is general agreement that the Bomu-

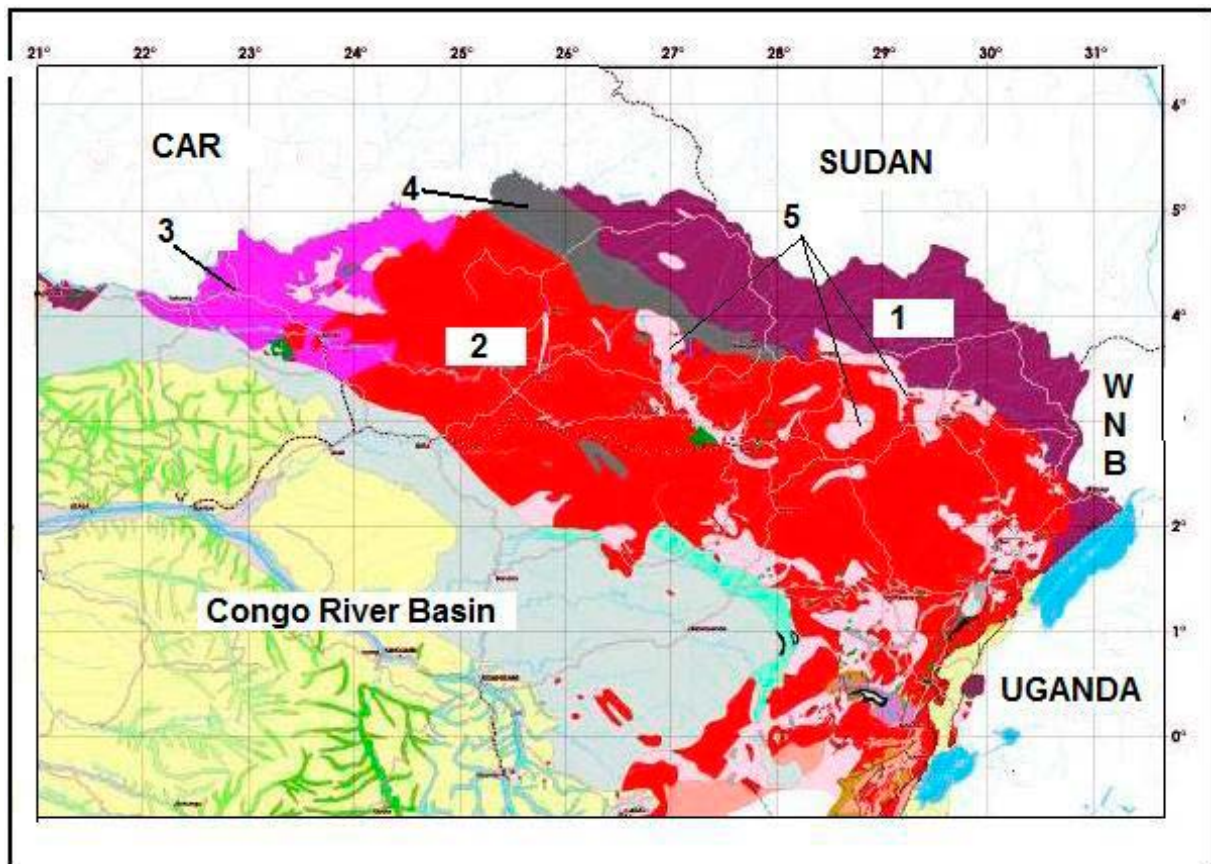


Fig. 4.1. Geological outline of the northeastern DRC with Bomu-Kibalian Shield. 1 = Garamba Gneissic Complex; 2 = Upper Congo Granitic Complex; 3 = Bomu Gneiss-Amphibolite Complex; 4 = Lubangi Metasedimentary-Migmatite Complex; 5 = Kibalian; WNB = West Nile Block in Uganda (source: Royal Museum for Central Africa, Tervuren, Belgium, with kind permission).

Kibalian Shield is connected to the basement rocks of the West Nile Province, or the West Nile Block (WNB), in NW Uganda.

The Bomu-Kibalian Shield is composed of tonalitic gneisses of the “*Formation du Nil occidental*” (West Nile Gneiss Formation or Garamba Gneissic Complex) in the north, to which Cahen (1954) attributed a poorly constrained Middle Archaean age (3.42 Ga), and the 2.51–2.46 Ga meta-granitoids of the Upper Congo Granitic Complex in the south. The Archaean (3.0–2.6 Ga), dominantly supracrustal Kibalian rocks – “*Groupe de Kibali*” – overlying the “*Formation du Nil occidental*” are exposed in between the two major gneissic units. All units show a WNW-ESE structural grain (Fig. 4.1), the so-called ‘Kibalian trend’ of Holmes (1951), expressed e.g. by WNW trending fold axes.

Kibalian rocks in the DRC comprise sericite-chlorite schists and biotite-albite-epidote schists, with subordinate talc- and graphite-bearing horizons, quartzites, carbonate rocks, lavas, itabirites and conglomerates with schist, quartzite and volcanic fragments in a biotite-rich matrix (Ca-

hen 1954). The sequence has been interpreted as a greenschist facies metavolcanic-sedimentary succession comprising fine-grained sedimentary rocks with ironstone-chert layers, several varieties of pyroclastic rocks, basaltic flows, mafic-intermediate intrusions (dykes and sills) and intermediate-felsic intrusive rocks (stocks, dykes and sills). The rocks are variably altered and, frequently, the protoliths cannot be easily identified.

The Kilo-Moto greenstone belt of the Kibalian supracrustal sequence is known for its historic gold production. Three of the deposits, Gorumbwa, Agbarabo and Durba, which were exploited primarily in the 1950s and 1960s, have produced more than 60% of the more than 3 million troy ounces of the recorded gold production from the Moto Gold Camp. Many of the mines with high gold grades are centred near the towns of Doko and Durba. Since 2004, a world-class gold resource has been identified in the area, and there is potential for more discoveries since most of the Kilo-Moto greenstone belt remains relatively unexplored by today’s standards.

4.3 Tectono-Thermal Domains of the West Nile Block

4.3.1 Introduction

Prior to the present era of plate tectonics and ‘terrane analysis’, the crystalline basement of northern Uganda, including the West Nile Province, was largely grouped together in a single unit known as the ‘Gneissic-Granulite Complex’ or ‘Basement Complex’ (Fig. 3.1; Macdonald 1966). The basement of the West Nile Province was mapped in the 1960s and interpretation of its evolution, which relied mainly on field observations, petrographic studies and Rb-Sr whole rock dating made by Hepworth (1964) and Macdonald (1963b,

1964a, 1964b), served as foundation for tectonic interpretation of northern Uganda, i.e. in present terms the adjacent North Uganda Terrane (Hepworth & Macdonald 1966). These authors distinguished four ‘tectonic groups’ or ‘events’, each with a unique and characteristic structural style and metamorphic conditions, known as ‘Watian’, ‘Aruan’, ‘Mirian’ and ‘Chuan’, respectively (Hepworth & Macdonald 1966) (Table 4.1; Fig. 4.2). Subsequently, Lavreau (1977a, 1977b, 1977c) and Cahen et al. (1984) added the term ‘pre-Watian assemblage’ to denote the protoliths of the rocks that were transformed into granulites and charnock-

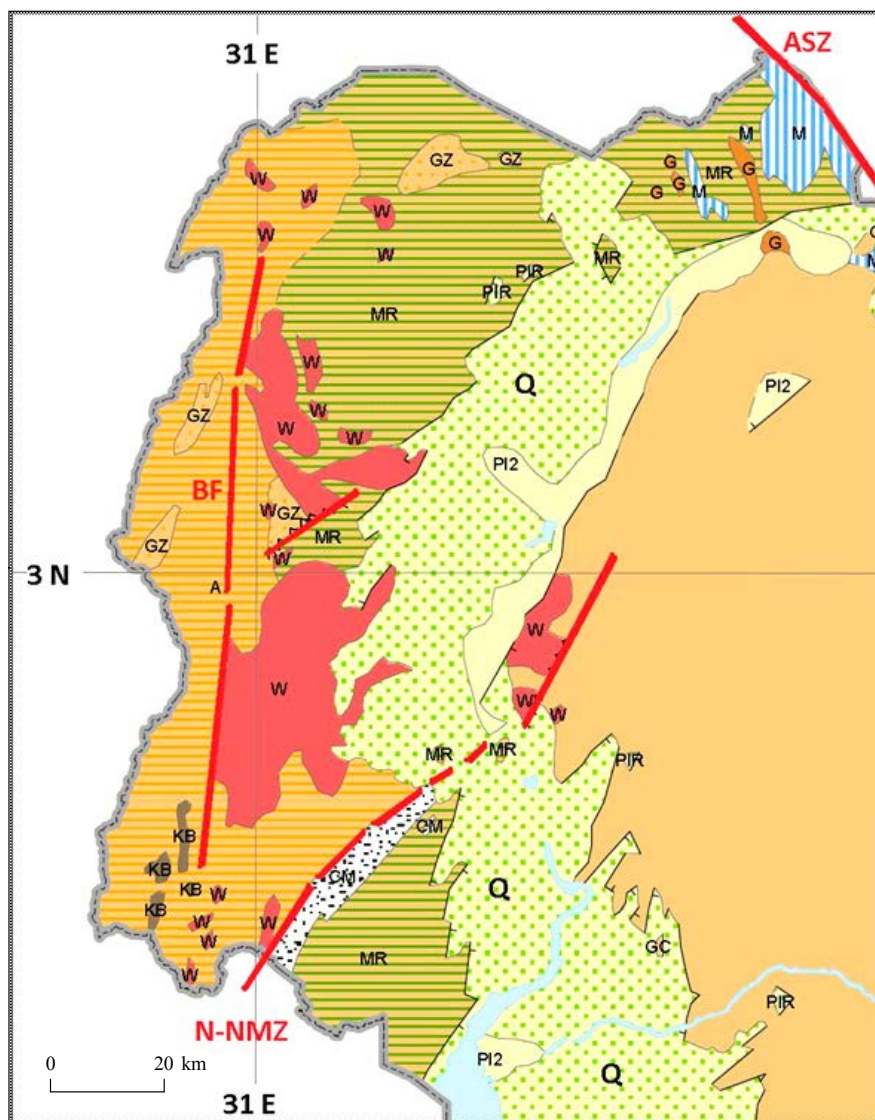


Fig. 4.2. Simplified geological outline of northwestern Uganda (slightly modified after Macdonald 1966). Key: W = Watian/Granulite Group; A = Aruan/ Western Grey Gneiss Group; MR = Mirian/ Eastern Grey Gneiss Group; KB = Kibalian Group; M = Madi Group; GZ = granitised rocks of unknown age; G = mobilised and intrusive granitoids, OM = Mylonites (Namtin-Namarodo Mylonite Zone, N-NMZ), PIR=intrusives; Albertine Rift: PIR and PI2 = Pleistocene and Q = alluvial rift sediments. BF = approximate location of the Boundary Fault; ASZ = Aswa Shear Zone.

ites during Hepworth's Watian charnockitisation event. This 'pre-Watian assemblage' supposedly comprised rocks of mainly sedimentary or volcano-sedimentary origin (Hepworth 1964).

The early workers faced tremendous difficulties, particularly in areas with sparse or no exposures, or a thick lateritic cover. Hepworth (1964) divided the crystalline basement of the West Nile Province into four groups: (1) Granulite Group (or Watian), (2) Western Grey Gneisses (or Aruan), (3) Eastern Grey Gneisses (or Mirian), and (4) Kibalian. Based on this subdivision, Macdonald (1966) prepared the simplified geological map presented in Fig. 4.2.

The 'Watian' granulites and charnockites of the Granulite Group form a number of central core complexes in the West Nile Province. Leggo (1974) has reported zircon ages of 2.88 Ga that supposedly record the peak of granulite facies metamorphism in the area. High-grade amphibolite facies gneisses known as 'Aruan' gneisses (named after their Arua type locality), grouped under the term Western Grey Gneisses, are exposed west of the central 'Watian' granulite complexes. The 'Aruan' reworking of the 'Watian' rocks took place proba-

bly near 2.55 Ga. This reactivation was essentially a widespread migmatization event but involved also emplacement of calc-alkaline granitic bodies.

As described in Section 4.2, the 'Système Kibalien' (Cahen 1954) in the Bomu-Kibalian Shield in NE Congo comprises mainly low-grade sericite-chlorite and biotite-albite-epidote schists. Holmes (1951) correlated these rocks with those in the Kibalian Group in the West Nile Province, where comparatively low grade hornblende schists overlie the southern portion of the Western Grey Gneisses with an intervening marked unconformity. Like their DRC counterparts, these rocks are presumably derived from mafic volcanic protoliths and subordinate quartzites, calc-silicate rocks and graphite-bearing schists.

The Eastern Grey Gneisses of the West Nile Province have been reported to occupy a belt of country rocks, 8 to 25 km in width, between the Western Grey Gneisses and central Watian granulites/charnockites on the one, and the Neogene sediments of the Western or Albertine Rift on the other side (Fig. 4.2). The Eastern Grey Gneisses were distinguished from the Western Grey Gneisses by (1) their lower grade of meta-

Table 4.1. Main tectono-thermal units recognized in the crystalline basement complex of northern Uganda according to Hepworth & Macdonald (1966, with kind permission of the Nature Publishing Group).

| Group/ Event | Description | Age | B a s e m e n t C o m p l e x |
|--------------------------------|--|---------------------------|---|
| Chuan (or Aswa) | Originally referred to as Madian, because of its folding on NW trending axes, which in the north grade into mylonitic shear zones that increase in amplitude towards the ~ co-axial Madi Belt. | 650-500 Ma | |
| Mirian (or Flaggy Grey Gneiss) | Group/Event characterised by recumbent isoclinal folds overturned towards the NW or NNW with development of flaggy axial plane cleavage and retrograde epidote-amphibolite facies metamorphism. This tectonic domain predominates the northern and eastern part of the Basement Complex. | 1.00 Ga | |
| Aruan (or Western Grey Gneiss) | Amphibolite-facies gneisses with fold axes plunging gently NNE with steep axial planes. The NNE axial trend of the Aruan and reworked Watian rocks is the dominant structural direction in West and South-West Nile Province. | 2.59-2.55 Ga | |
| Watian (or Granulite Group) | The oldest group (or event) characterised by E-W axial fold trends and a charnockitic-granulitic facies; partly anatectic. The group has been partly retrograded and reworked during the ensuing Aruan tectonic event. A time break between the Watian and Aruan is indicated by a dyke phase in the Watian which is absent in the other groups, or is represented by amphibolites in reworked Watian rocks. | 2.90 Ga (all WR Rb-Sr) | |

morphism, i.e., epidote-amphibolite facies with muscovite, (2) their flaggy nature, (3) their moderate dips (30°–40°, compared to the steeply dipping Western Grey gneisses) and (4) lesser abundance of amphibolites (Hepworth 1964). They were attributed to the Mirian event and found to rest unconformably on the older granitic gneisses and granulites/ charnockites of the western and central segments of the West Nile Province. Subsequently, Leggo (1974) reported the presence of 950 Ma old zircons in these rocks, and the Mirian rocks were tentatively related to the 1 200 Ma Karagwe-Ankolean sediments found in SW Uganda (Leggo 1974).

The rocks of the Eastern and Western Grey Gneisses and Granulites generally strike between NNE and NE, while the rocks of the Granulite Group also contain minor enclaves with approximately E-W strikes. In addition, late SE cross folding affects the Western Grey Gneisses. The western exposures of the Western Grey Gneisses are separated from the rocks of the Granulite Group by a fairly well-defined structural discontinuity – “the Boundary Dislocation” (BF in Fig. 4.2). In the south of the West Nile Province these two units interdigitate along zones that show cataclasis or thermal retrogression. Hepworth (1964) suggested that part of the Grey Gneisses may have formed by retrogression from granulite-grade protoliths.

In addition, widespread effects of the Pan-African Orogeny (about 650–540 Ma), known as the Chuan, Aswa or Madian event, were viewed as reworking of Archaean rocks of the basement complex in northwestern Uganda.

4.3.2 Redefinition of tectono-thermal units in the West Nile Block

Based on interpretation of recent airborne geophysical data (FUGRO 2009), field work carried out by the GTK Project and modern U-Pb zircon and monazite dating (Mänttari 2014), the geodynamic model by Hepworth & Macdonald (1966), as it is portrayed in Table 4.1 and Figure 4.2, has been considerably refined. The new and re-evaluated prior data demonstrate that the tectono-metamorphic evolution of the assumed Archaean basement of the West Nile Block is a significantly more complex process than was previously thought, involving Mesoarchaeoan, Neoarchaeoan, late Mesoproterozoic and Neoproterozoic struc-

tural elements. Consequently, the following major tectono-thermal units have been defined from the block (from oldest to youngest):

- Uleppi Complex (Fig. 4.3), part of a Mesoarchaeoan tectono-thermal terrane (extending into the DRC) composed of granulite-grade metasediments of the Uleppi Group, into which ‘older’ granitoids and the 3.08 Ga Goli charnockites have been emplaced.
- Arua Complex with the Arua Group, part of a Neoarchaeoan terrane comprising mainly amphibolite-grade supracrustals of the Lobule Group, variable gneissose granitoids, charnockites of the Tara brown granite (> 2.63–2.62 Ga) and extensive ‘younger gneissose granitoids’.
- War Group, comprising Neoarchaeoan (~2.64 Ga) metavolcanic and subvolcanic rocks and subordinate associated metasediments, believed to be deposited unconformably on the Uleppi Group. The Neoarchaeoan rocks of the West Nile Block are included in the Arua-Kibale Supergroup.
- The Meso- and Neoarchaeoan basement of the WNB, is tectonically overlain by late Mesoproterozoic ‘Mirian’ sequences comprising ~0.98 Ga gneisses and schists with igneous and sedimentary protoliths (Fig. 4.3). The Mirian (Table 4.1; Fig. 4.2) is now incorporated in the more extensive Madi-Igisi Belt, an intracratonic, doubly vergent, ~1.0 Ga NNE-SSW directed thrust and strike-slip belt, separating the WNB from the North Uganda Terrane (Chapter 5).
- The Yumbe Complex is an allochthonous duplex structure composed of a variety of gneisses of supposedly Neoarchaeoan age and supposedly derived from the North Uganda Terrane. Their tectonic emplacement within the Madi-Igisi Belt is, however, attributed to the late Mesoproterozoic Mirian and/or Neoproterozoic Chuan events.
- The same applies to the southeastern segment of the Lobule Group east of Nebbi, which is interpreted as an allochthonous thin-skinned or interleaved pile of Neoarchaeoan Lobule and ~1.0 Ga Igisi rocks.
- Pan-African granitoids of the Midigo-Adjumani Suite (0.66 Ga; marked GZ in Fig. 4.2) in the northernmost part of the WNB.

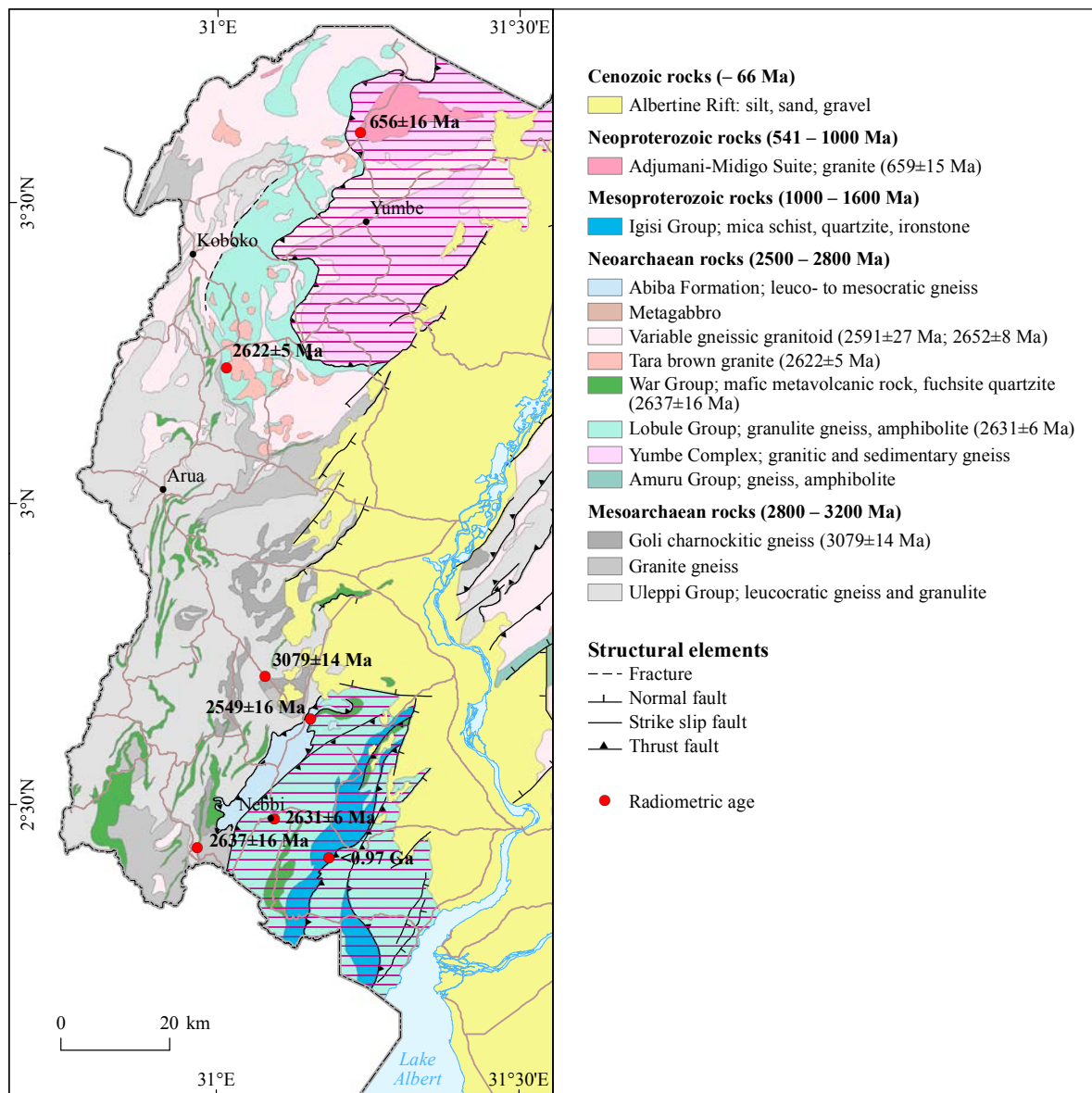


Fig. 4.3. Major tectono-thermal units of the West Nile Block. The southern part of the former Watian and most of the Aruan/Western Grey Gneisses are attributed to the Mesoarchaean (> 3.08 Ga) Uleppi Complex. This Mesoarchaean nucleus (open for its extensions towards the south and west into the DRC) is bounded by Neoarchaean (~2.66 Ga) rocks in the north and southeast, formerly attributed to northern part of the Watian, Western and Eastern Grey Gneisses. Double-vergent thrust units of the Madi-Igisi Belt comprise both reworked Archaean fragments (horizontal stripes), partly derived from the North Uganda Terrane – Yumbe Complex and Lobule Group – and juvenile (~1.0 Ga) Mirian rocks, contained in the Madi and Igisi Groups. Red dots = location of age determination.

4.4 Lithostratigraphy of the Uleppi Complex

The Mesoarchaean Uleppi Complex, as defined here, comprises most of the former ‘Aruan’ Western Grey Gneisses and the southern segment of the ‘Watian’ Granulite Group (Figs 4.2 and 4.3). Hepworth (1964) assumed that the Watian Granulite Group, correlated with the deepest lithostratigraphic unit in the West Nile Province, as both are comprising mainly granulite-grade and widely to amphibolite-grade retrograded felsic, inter-

mediate and basic charnockites, enderbites and subordinate rock types such as aplitic granulite, diopside-scapolite granulite, cordierite-, spinel-, and andalusite-bearing granulites, kyanite-muscovite-rutile granulite and garnet-kyanite or garnet-sillimanite quartzites. The Western Grey Gneisses (Fig. 4.2) were described by Hepworth (1964) as more or less well-layered, generally steeply dipping gneissose rocks in which original structures

had not been preserved, with the exception of bedding structures in some fuchsite- and sillimanite-bearing quartzites. A tectonic planar fabric or foliation was generally formed, involving the parallel orientation of biotite and/or hornblende.

We divide the Mesoarchaeon Uleppi Complex into a number of lithostratigraphic units of meta-sedimentary or metavolcanic derivation assembled in the Uleppi Group, and plutonic rocks of Mesoarchaeon age.

4.4.1 Uleppi Group

The formations distinguished in the Uleppi Group are listed with their major rock types and in their presumed younging order (upwards) in Table 4.2. Brief descriptions of the main rock types included are given below.

Eru Formation: mafic granulite – The Eru Formation refers to a number of small bodies of mafic granulite located some 20–30 km south of Arua town, in the area mostly dominated by granulitic, leucocratic gneisses of the Uleppi Group. The

mafic granulites are dark brown, black or pale grey massive to banded, homogeneous, equigranular rocks, essentially composed of plagioclase + diopside + hypersthene + garnet + hornblende. In the darkest varieties the proportion of the mafic minerals is estimated to be at least 70 vol%. Sharp variations in modal composition often define an obscure banding (Fig. 4.4A) and garnet porphyroblasts with kelyphytic rims can often be observed even with the naked eye (Fig. 4.4B). Hepworth (1964) distinguished a total of six sub-types of basic granulites, each characterised by a specific mineral assemblage:

- hypersthene + diopside + plagioclase ± hornblende;
- hypersthene + diopside + garnet + plagioclase ± hornblende
- hypersthene + plagioclase + garnet ± hornblende
- hypersthene + diopside + plagioclase + garnet + scapolite ± hornblende
- plagioclase + diopside + garnet + hornblende
- plagioclase + diopside + garnet

Table 4.2. Subdivision of the Uleppi Group (note that current interpretation may deviate from the previously presented 1:250 000 scale geological map, reported to DGSM 2012).

| Group | Formation | Lithology |
|--------|-----------|--|
| Uleppi | Alibu | Amphibolite |
| | Terego | Generally porphyroblastic quartz-feldspar-biotite gneiss |
| | Logiri | Banded gneisses, migmatitic in places |
| | Ajia | Leucocratic garnetiferous gneisses and diatexites |
| | Opa | Leucocratic gneisses and granulites |
| | Eru | Mafic granulites |



Fig. 4.4. (A) Banded mafic granulite of the Eru Formation, located 18 km SE of Arua town (273254E / 317463N). (B) Foliated granulite with plenty of garnet porphyroblasts at Eru hill (272441E / 316993N). Number tag 8 cm.

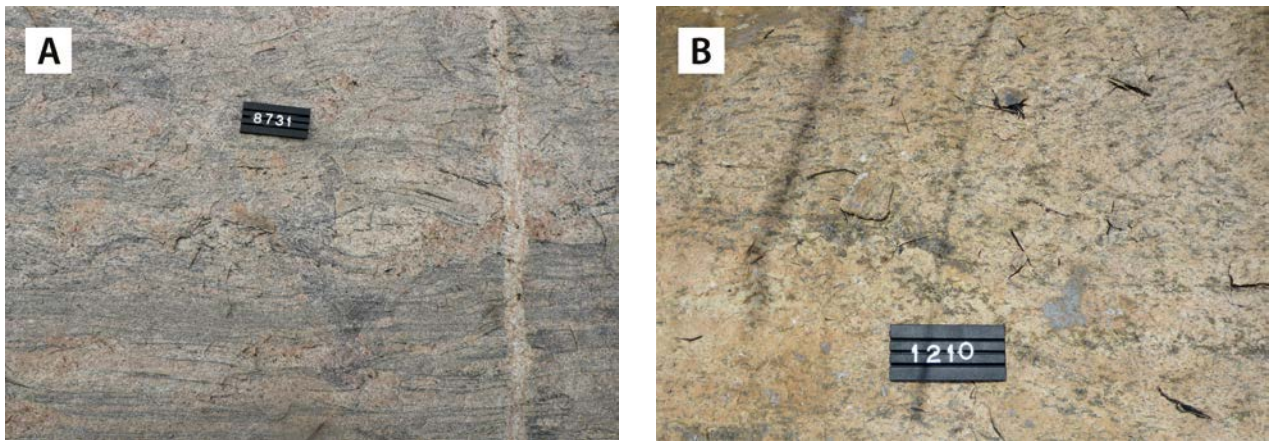


Fig. 4.5. (A) Leucocratic gneiss of the Opa Formation, comprising slightly more granitic veins than normal (291243E / 318775N). (B) Relatively homogeneous granitoid comprising locally a small amount of orthopyroxene (329741E / 19411N). Number tag 8 cm.

Hornblendites and amphibolites occur in association with the mafic granulites. Garnet amphibolite appears to represent retrograded mafic granulite. Mafic granulites commonly occur as planar bodies with conformable quartzite bands or with intercalated layers of leucocratic granulite. Speculating on their protolith composition Hepworth (1964) remarked: “Whether they were originally sills or dolomitic limestones is unknown”.

Opa Formation: leucocratic gneisses and granulites – The Opa Formation includes grey to pinkish, medium to coarse-grained, leucocratic (2 to 6 vol% mafic minerals) rocks occurring on both sides of the Albertine Rift. The extent of the Opa Fm rocks correlates well with that of the ‘leucocratic granulites’ and ‘charnockites’ in the existing 1:100 000 scale geological map of Okollo (Sheet 19 & 20; Hepworth 1961b). In his detailed descriptions Hepworth (1964) noted on the granulitic and charnockitic rocks of the region that “most of these rocks have either been downgraded by retrogressive metamorphism below the granulite-facies, or have no suitable composition to form distinctive assemblages”. Thus, orthopyroxene, which is a common indicator mineral in granulites, is not always present.

The leucocratic gneisses and granulites of the Opa Formation range between quartz-rich microcline-oligoclase-biotite granulites (Fig. 4.5A) and biotite-rich quartz-microcline-oligoclase granulites in composition. Most of these felsic granulites contain garnet which, however, is not diagnostic for the granulite facies but rather manifests at least upper greenschist-amphibolite facies conditions. Former granulite P,T-conditions are only indicat-

ed by the presence of ‘hair perthite’ and exsolved rutile needles (Hepworth 1964). Orthopyroxene is a very rare constituent and is mostly detected in rocks resembling granitoids (Fig. 4.5B). Magnetite is a common accessory mineral.

Ajia Formation: garnetiferous leucocratic gneisses and diatexites – This is a common rock type in the south-central part of the West Nile area, coinciding with the formerly distinguished “mainly leucocratic granulite”, “leucocratic granulites: quartz-microcline-orthoclase-biotite-(garnet)” and “aplitic granulite” (1:100 000 scale geological map, sheets 19 & 20; Hepworth 1961b).

Hepworth (1964) described the textures and mineralogy of these rocks in detail and noted the frequent absence of mineral assemblages diagnostic of the granulite facies. Using the new geophysical data and field observations we have combined many of the old “granulite units” under this sub-type, where diatexite refers to a rock formed by advanced partial melting, in particular affecting garnetiferous leucocratic gneiss members. The area underlain by garnetiferous leucocratic gneisses clearly stands out geophysically, being characterised by significantly elevated radiometric total count and ternary signatures from the background levels.

These rocks are usually light coloured, grey to pinkish, slightly heterogeneous, medium-grained, gneissose rocks, which are mainly composed of feldspar and quartz with minor biotite and garnet, often with features that are typical of migmatitic and deformed granitoids (Fig. 4.6A). Locally, the migmatitic variants can be observed with small



Fig. 4.6. (A) Garnetiferous leucocratic gneiss of the Ajia Formation (281997E / 323974N). (B) Diatexitic granulite gneiss with a metapelite-derived schist xenolith (279005E / 318674N). Number tag 8/15 cm.

patches of garnet and feldspars, obviously formed by dehydration melting, probably at the expense of biotite. Relict sedimentary bedding, preserved in gneiss fragments embedded in a diatexitic matrix, was found in places (Fig. 4.6B).

The leucocratic gneisses are usually peraluminous ($A/CNK \geq 1.1$) in composition which, combined with their often igneous-looking textures, invokes their classification as S-type granites.

Logiri Formation: banded gneisses, migmatitic in places – This unit comprises variably migmatized, light grey to brownish grey, medium-grained banded paragneiss, exposed extensively in the central part of the West Nile Block. The characteristic banding in the gneiss is partly due to metamorphic differentiation, but more often seems caused by intercalation of pre-metamorphic mafic and felsic

bands and layers. Although the thickness of the bands rarely exceeds 5–10 cm, also several metres thick amphibolite bands with transitional contacts are present. The overall impression is that of mafic tuff or tuffite interlayers and sills (?) within a dominantly psammitic metasedimentary sequence.

Large-scale, isoclinal folds have been observed in many occurrences of the banded Logiri gneiss (Fig. 4.7A). The locally observed combination of complex fold interference patterns and abundant granite veining suggest intense polyphase deformation, associated with partial melting, which in places converted the originally dominantly psammitic rocks into strongly folded and granite veined migmatites. On the well-exposed Logiri hill, located at the DRC boundary, the distinctly banded Logiri gneiss is invaded by sharply cutting, thick pegmatite dykes (Fig. 4.7B).

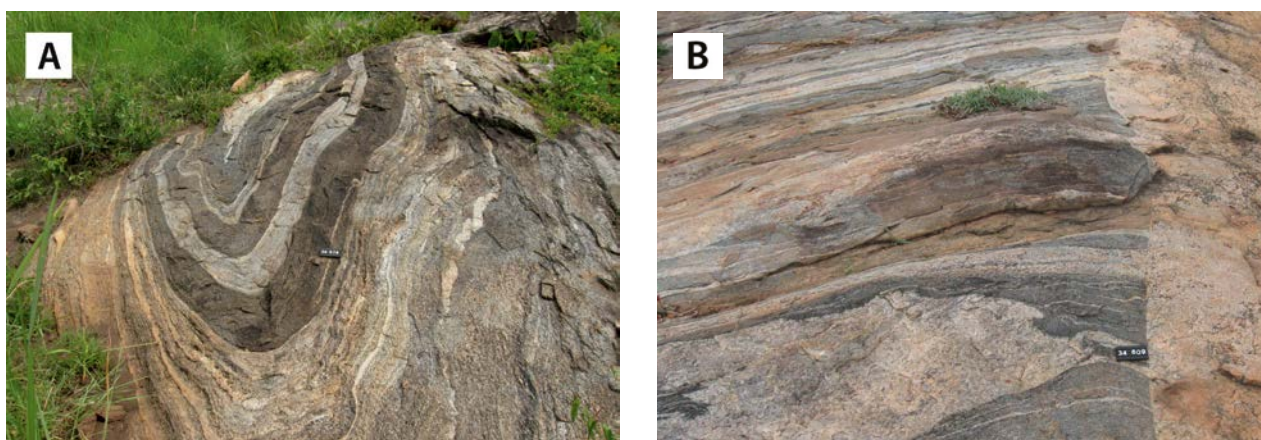


Fig. 4.7. Various deformed and migmatized banded gneisses of the Logiri Formation. (A) Isoclinally folded banded gneiss, located ~1.6 km W of Abiba hill (281323E / 280247N). (B) Banded gneiss, sharply cut by a pegmatite dyke. Logiri hill (261590E / 306314N). Number tag 10 cm.

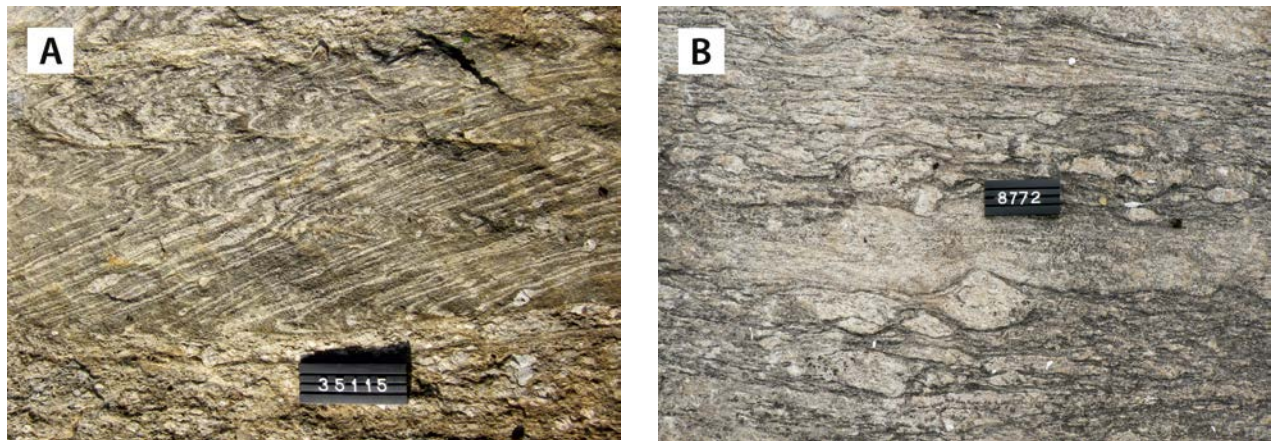


Fig. 4.8. Metamorphic textures in quartz-feldspar-biotite gneiss of the Terego Formation. (A) K-feldspar porphyroblasts developed in leucocratic segregation bands in a psammitic paragneiss. Note the shear zone with transposition of the older fabric in the lower part of the photo and the late faults with sinistral off-sets (329262E / 268577N). (B) Detailed image of strongly deformed K-feldspar porphyroblasts in a paragneiss outcrop (322114E / 263999N). Number tag 10 cm.

Terego Formation: quartz-feldspar-biotite gneiss, generally hornblende±magnetite porphyroblastic – The main rock type in the Terego Formation, located in the rather poorly exposed western part of the West Nile area, is grey, often strongly foliated quartz-feldspar-biotite gneiss, which Hepworth (1964) included in his ‘Western Grey Gneisses’.

The gneisses of the Terego Fm are usually dark brownish grey, medium-grained granoblastic rocks, composed of quartz, microcline, plagioclase and biotite. Hornblende porphyroblasts are commonly present, as well as small magnetite porphyroblasts that induce a moderate magnetic susceptibility for the gneiss. The locally occurring banded structure refers to a possible supracrustal origin for this rock. The more deformed varieties contain plenty of thin, leucocratic segregation veinlets and random small (<10 mm) microcline porphyroblasts. In areas, where the degree of deformation and the grade of metamorphism are higher, generation of K-feldspar porphyroblasts occur concurrent with the transposition of an older foliation. The growth of K-feldspar porphyroblasts in an originally psammitic rock is seen in Figure 4.8A, where random, Augen-like porphyroblasts are developed in leucocratic (segregation) bands oblique to a younger foliation. Generally, the K-feldspar porphyroblasts are deformed into elongate lenses aligned parallel to the foliation of the host rock (Fig. 4.8B).

In the West Nile area, both the abundance and size of K-feldspar porphyroblasts appear to increase with the intensity of deformation and metamorphism, which can locally give rise to myloniti-

sation and partial melting of the gneiss (described as ‘granitisation’ by Hepworth 1964, p. 54).

Alibu Formation: amphibolites – Amphibolites of the Alibu Formation, exposed in the central part of the West Nile Block, are believed to represent the uppermost lithostratigraphic unit of the Ul-eppi Group. These amphibolites, which often form low ridges parallel to the general N-S trend of the surrounding gneisses, can be readily outlined on ternary radiometric maps owing to their strong negative signature (Fig. 4.9A). Similarly, the poorly known, northeast-trending belt with distinct radiometric anomalies east of the Albertine rift have been assigned to the Alibu Formation.

Amphibolites assigned to the Alibu Formation are dark green, fine- to medium-grained, weakly foliated rocks, varying in their structure from massive to vaguely banded (Fig. 4.9B). Occurrence of garnet is a common feature, usually as small (<1.0 mm) porphyroblasts, but occasionally also in layers with plentiful coarse grains, up to 5 mm in size. In thin sections, these amphibolites are nematoblastic rocks with hornblende, quartz and plagioclase as major minerals, and with variable, minor to accessory amounts of garnet and clinozoisite (Hepworth 1964).

Hepworth (1964, p. 48) already mentioned the difficulty in identifying the amphibolites belonging to the different lithostratigraphic units in the West Nile area. The distinction is generally based on the more distinct banding and tight, gently NNW-plunging folds locally found in mafic meta-tuffs and amphibolites of the War Group *versus*

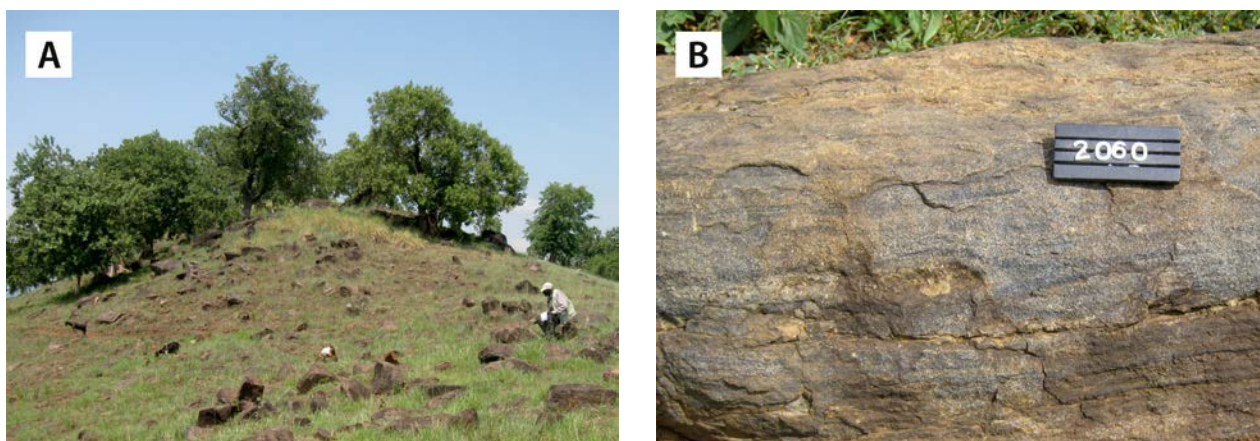


Fig. 4.9. (A) Typical ridge-forming amphibolite of the Alibu Formation south of Giligili village (279237E / 290091N). (B) Weakly foliated amphibolite with obscure banding (274804E / 354359N). Number tag 8 cm.

the more massive, homogeneous character of the amphibolites included here in the Uleppi Group. The obscure banding visible in some amphibolites of the Uleppi Group, as well the total absence of amygdules or other features typical for mafic lava flows suggest a pyroclastic origin also for these rocks. Without a detailed mineralogical and geochemical study, however, the distinction between the amphibolites of these two groups is not always possible.

Two amphibolite samples from the Uleppi Group have been analysed for major elements and one sample for trace elements, including lanthanides. Results are shown in Figures 4.31 and 4.32.

4.4.2 Plutonic Units of the Uleppi Complex

Plutonic rocks of the Mesoarchaeon Uleppi Complex, mostly exposed as separate bodies in the

south-central part of the WNB, are often variously deformed gneissic rocks in appearance. Although the intrusive character of their contacts with surrounding rock units is not confirmed, the overall massive and homogeneous structure, microscopic textures and chemical composition establish the intrusive origin of these granitic and charnockitic rocks.

Granite gneisses – The granite gneisses of the Mesoarchaeon Uleppi Complex form rather irregularly shaped bodies in the southern, central and northern parts of the West Nile area. These gneisses correlate partly with the previously distinguished ‘*leucocratic granite-gneiss of ‘Owala type’*’ (Macdonald 1964b) in the north, but in the central and southern West Nile Block, there is a considerable difference, since GTK Consortium mapping identified much less of comparable granitic gneisses.

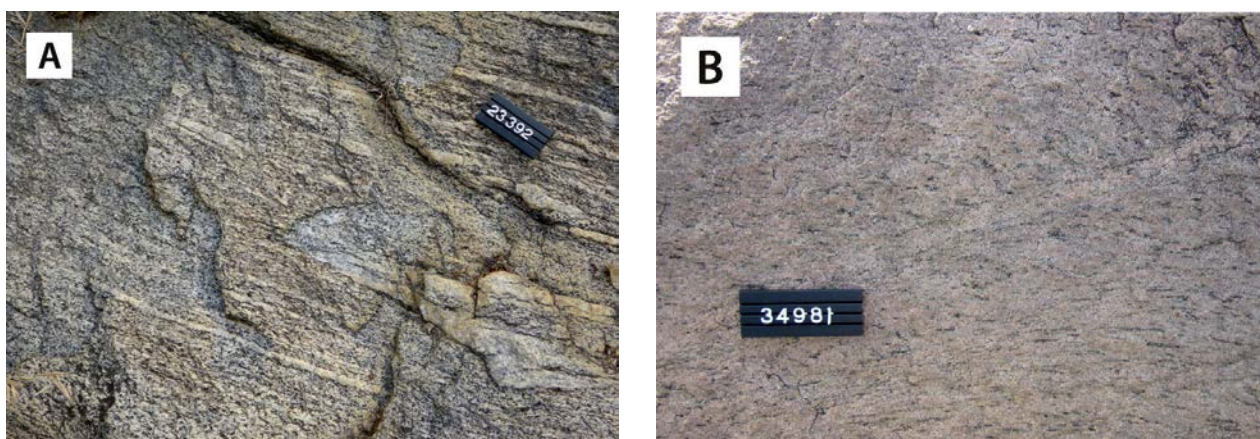


Fig. 4.10. Various types of leucocratic granite gneiss. (A) Granitic gneiss, probably granodioritic in composition, with felsic veins and patches, and showing isoclinal, rootless small folds (266849E / 389493N). (B) K-feldspar-rich deformed granitoid from southern part of West Nile region. Number tag 10 cm.

The granite gneisses are rather light coloured, igneous-looking rocks (Fig. 4.10) that are mainly true granites with only some minor tendency towards granodioritic compositions. The usual major minerals are K-feldspar, plagioclase, quartz and biotite (<15 vol%). Garnet porphyroblasts have been observed locally, while epidote and muscovite are minor retrograde minerals. In places, these rocks comprise some amphibolite inclusions, which probably represent deformed metadolerites.

Based on whole-rock analysis of a single representative sample (App. 2), the Uleppi Group granite gneiss appears as a calc-alkaline peraluminous granodiorite on chemical discrimination diagrams (Figs 4.33A-C). The Y+Nb-Rb and Y-Nb plots point to either ‘*within-plate*’ or ‘*syncollisional volcanic arc*’ settings (Figs 4.34A-B).

Goli charnockitic gneiss – The ~3.08 Ga old Goli charnockitic gneisses, which are mainly exposed in the southern part of West Nile Block, belong among the oldest rocks reported from Uganda (Mänttari 2014). As defined here, the Goli charnockitic gneiss broadly corresponds to a rock unit

separated and labelled by Hepworth (1961b) as ‘*charnockite – mainly intermediate*’ and partly ‘*leucocratic granulite: quartz-microcline-orthoclase-biotite-(garnet)*’. These charnockitic gneisses show moderate, K-band dominated radiometric ternary signatures.

The Goli charnockitic gneiss can be generalised as a high-grade metamorphic, usually migmatitic granitoid gneiss (Fig. 4.11A), more commonly granodioritic or rarely tonalitic, rather than granitic in composition. In places, especially in rocks of intermediate composition, the characteristic charnockitic paragenesis hypersthene + diopside + microcline microperthite + garnet + quartz + biotite is still preserved (Figs 4.11A-B), but more commonly the Goli charnockitic gneisses have a ‘simple’ mineral composition that comprises mainly of quartz, feldspars and biotite. The absence of pyroxene is probably usually due to retrogressive metamorphism and replacement by hydrous minerals (e.g., clinopyroxene → hornblende) rather than due to unfit composition, as was also believed by Hepworth (1964, p. 92–93): “*many of the present mineral assemblages in the intermediate charnockites are retrogressive...*”. Hepworth (1964, p.



Fig. 4.11. Two varieties of the Goli charnockitic gneiss. (A) Migmatitic and gneissose granitic gneiss, yielding a U-Pb zircon age of ca. 3.08 Ga (Mänttari 2014) (288748E / 297794N). (B) Charnockitic gneiss comprising subordinate orthopyroxene. Note the vertical, cross-cutting granitic dyke (288304E / 298488N). (C) Orthopyroxene-bearing, weakly gneissose granitoid, showing some modal heterogeneity (291089E / 322090N). Number tag 8/15 cm.

87–95) gives a detailed description with sketched images of the retrogressive textures and mineral assemblages in the ‘intermediate charnockites’.

The Goli gneisses are usually exposed in small hills or hinted by clusters of *in situ* boulders. In the outcrops, the non-retrograded charnockites show typically rusty colours on weathered surfaces, while fresh surfaces may be rather dark grey. In places, granoblastic charnockitic gneisses with igneous-looking textures may show vague compositional banding (Fig. 4.11C). A potassic character is shown by the K-feldspar content ranging from 5 to 20 vol% and the amount of biotite from 5 to 15 vol%. Almandine garnet is a rather common accessory mineral, which is sometimes rimming pyroxene grains. Minor clinopyroxene and hornblende in amounts between 1 and 10 vol% tends to occur in tonalitic varieties, often together with sec-

ondary epidote. The more mafic Goli charnockitic gneisses are usually compositionally banded and may be supracrustal in origin. Plagioclase clearly dominates over K-feldspar in these banded mafic-intermediate rocks. The more massive, leucocratic Goli charnockitic gneisses are rarely porphyritic in texture; in this respect they differ from Neoproterozoic charnockitic Tara brown granites found NE of Arua town.

Six representative samples of the Goli charnockitic gneiss were analysed for whole-rock major and trace element chemical composition (see App. 2). Results are shown on various chemical discrimination diagrams in Figure 4.33; the plots indicate that the Goli gneisses were either ‘*volcanic arc granites*’ (Fig. 4.34A) or ‘*syn collisional volcanic arc granites*’ (Fig. 4.34B).

4.5 Lithostratigraphy of the War Group (Arua-Kibale Supergroup)

All the Neoproterozoic rocks in the West Nile Block, excluding the undated but presumably Neoproterozoic rocks of the allochthonous Yumbe Complex (Fig. 4.3) are aggregated here in the Arua-Kibale Supergroup, subdivided into the Lobule and War Groups.

The War Group corresponds with the Kibalian rocks that overlie the Western Grey Gneisses, being separated from them by a marked unconformity (Macdonald 1966; Fig. 4.2). They are correlated by Cahen (1954), following Holmes (1951), with the low-grade mafic schists of the Kibalian System in the northeastern DRC (Section 4.2). Our field observations confirm that the supracrustal rocks of the War Group rests on the gneisses and charnockite/granulite rocks of the Uleppi Complex. The nature of the basal contact remains obscure, however. The War protoliths have been supposedly deposited *in situ*, although Hepworth (1964)

reserved the possibility that the rocks of the War Group may represent a nappe structure, tectonically thrust on the older rocks of the Uleppi Complex.

The War Group is mainly composed of mafic metavolcanic/pyroclastic and sub-volcanic/magmatic rocks but also includes subordinate quartzites, calc-silicate rocks, and graphitic schists. The actual map distribution of the different rock types is rather poorly constrained due to extensive lateritisation. Spatially, the War lithologies are intimately associated with the Mesoarchean Uleppi Complex, which they overlie or intrude. Subsequently, Uleppi and War rocks have been jointly deformed, folded, and thrust on older units and, consequently, the nature of the separating discontinuity is generally beyond recognition. We have subdivided the War Group in six formations listed in Table 4.3:

Table 4.3. Subdivision of the War Group (note that current interpretation may deviate from that in the previously presented 1:250 000 scale geological map).

| Group | Formation | Lithology |
|-------|-----------|-------------------------------------|
| War | Kaza | Mafic metatuff, amphibolite |
| | Acer | Mica schist / mica gneiss |
| | Pakadha | Iron formation |
| | Use | Tremolite(-actinolite) schist |
| | Anyavu | Skarn gneiss, tremolite skarn |
| | Agu | Quartzite, locally fuchsite-bearing |

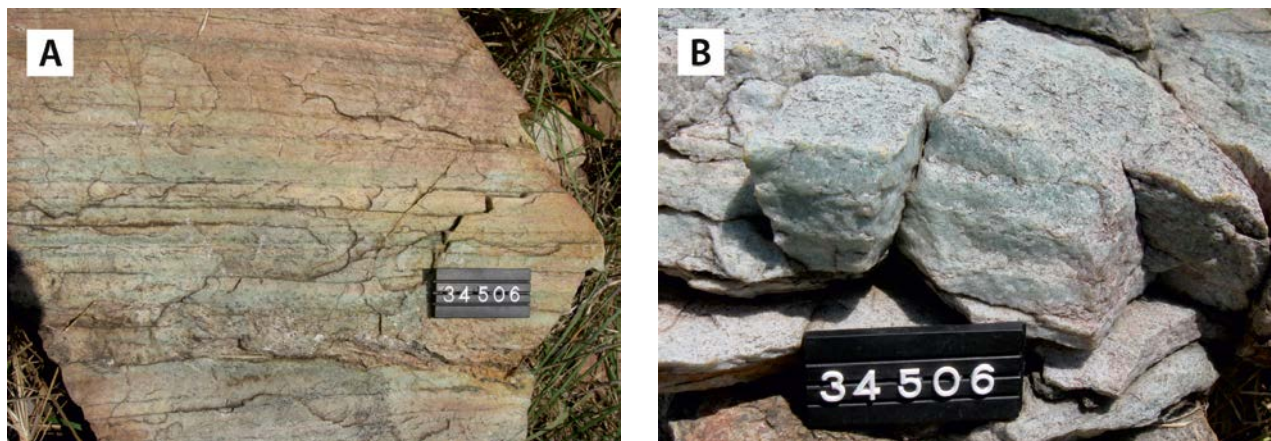


Fig. 4.12. Fuchsite-bearing quartzite of the Agu Formation. (A) Pale greenish, fuchsite-bearing bands in orthoquartzite. (B) Detailed image of the fuchsite-bearing orthoquartzite. Kuchwiny village (305711E / 282956N). Number tag 10 cm.

Agu Formation: quartzite, locally fuchsite-bearing

– The Agu Formation, comprising mainly fuchsite-bearing quartzite, represents the lowermost lithostratigraphic unit of the War Group in the WNB. In places, the Agu quartzite is overlain directly by mafic metatuffs of the Kaza Fm with a deeply weathered contact zone in between, suggesting a hiatus or tectonic contact between these rock units. The lower contact of this quartzite is not exposed. Most quartzite ridges exposing the Agu quartzites strike parallel to the regional N-S structural grain of the WNB, with an exception of the prominent, E-W trending Biliba ridge, located ~20 km NE of Uleppi village.

Due to strong deformation, no primary structures are generally preserved in these strongly foliated quartzites. Evenly thick, turquoise, fuchsite-rich bands, observed in orthoquartzites at the Kuchwiny hills in the eastern part of the West Nile area may represent the primary sedimentary bedding (Figs 4.12A-B). The amount of fuchsite varies widely, up to contents as high as 70 vol%, which have been reported from Kango Hill by Hepworth (1964, p. 58). The thickness of the Agu Formation is unknown.

Under the microscope, the Agu quartzites are mostly composed of elongated aggregates of ribbon quartz, sericitised grains of feldspar, and (locally) well oriented, large blades of kyanite, frequently altered into sericite and biotite. Rounded grains of apatite and zircon are common accessory minerals.

Anyavu Formation: skarn gneiss, tremolite skarn

– Small outcrops and block fields of coarse calc silicate-bearing gneiss occur in the western part

of the WNB. They show a close spatial association with metavolcanic rocks of the War Group, but the full extent as well as contact relations of this poorly exposed skarnoid gneiss unit are only poorly known. The Anyavu gneisses are mostly light greenish grey, massive or weakly foliated quartz-feldspar rocks with abundant radiating bundles of pale green tremolite prisms; locally the calc-silicate minerals also include green diopside and epidote.

Use Formation: tremolite(-actinolite) schist

– This unit includes the variably deformed tremolite- and tremolite-actinolite-chlorite schists occurring sporadically in the southwestern part of the WNB. The stratigraphic position of the unit is not well established (see Hepworth 1964, p. 50) but here we tentatively include these ultramafic to skarnoid rocks in the War Group.

Ultramafic tremolite(-actinolite) schists of the Use Fm are pale greenish to yellowish green, fine-grained, variously foliated rocks. For some outcrops with slippery surfaces, a high talc content is confirmed by thin section examinations, which indicate a variation from distinctly foliated, nematoblastic tremolite-talc schists to more massive tremolite-actinolite-chlorite rocks. The latter variant consists of needle-shaped tremolite prisms, several millimetres long, in a fine-grained, weakly pleochroic tremolite(-actinolite)-chlorite mass. Due to a rather high proportion of secondary magnetite, up to ~10 vol% in one sample, the magnetic susceptibility of these ultramafic schists is generally high. A chemical whole rock analysis from a tremolite-talc schist sample of the Use Formation is given in Appendix 2 (anal. 54).

Pakadha Formation: Iron formation – A magnetite-rich rock is exposed in a road cut, located 2 km northeast of Pakadha village, in the southern part of the WNB. Although the rock is weathered, its high density and high magnetic susceptibility, together with an obscure banding indicate a banded iron formation. The contact relations and lithostratigraphic position with regard to the surrounding lithologies are unknown, but the unit is assigned tentatively to the War Group. The mineral composition of an almost fresh rock sample is dominated by quartz, magnetite, garnet and green amphibole.

Acer Formation: mica schist, mica gneiss – A north-east trending belt of pelitic metasediments, named after Acer village, is well exposed in the southern and western parts of the WNB. The western foot-wall contact of the unit with the banded gneisses of the Lobule Group is supposedly tectonic, while the hanging wall contact with overlying mafic metatuffs of the Kaza Fm is gradational. In areas covered by the airborne geophysical survey (FUGRO 2009), the pelitic metasediments of the War Group can be identified by their distinct positive signature in radiometric maps when compared to their surrounding country rocks.

The major rock type of the Acer Formation is dark brownish grey, fine-grained and variably deformed mica schist, with numerous segregation veins and lenses of quartz, parallel to the foliation (Fig. 4.13A). Locally, traces of laminar bedding are preserved and bands dotted by red garnet porphyroblasts, up to 5 mm in size, are common (Fig. 4.13B). Aggregates of micaceous matter in

pseudomorphs after a completely altered prismatic aluminium silicate (most likely kyanite) exist randomly in some biotite-rich bands of the schist.

In the southern part of the belt, where the degree of deformation and metamorphism is higher, the mica schists grade into variably migmatized mica gneisses. These gneisses are intensively folded rocks, injected by dykes and sheets of medium-grained, leucocratic granite, locally with formation of agmatitic intrusive breccias, with mica gneiss fragments ‘floating’ in a granitic matrix.

Kaza Formation: mafic metatuff, amphibolite – Metavolcanic rocks of the Kaza Formation represent the uppermost stratigraphic unit of the War Group in the western WNB. Although a hiatus may exist in places between mafic metavolcanic rocks of the Kaza Fm and underlying, fuchsite-bearing quartzites of the Agu Formation, the often observed spatial proximity of these two stratigraphic units suggest a common depositional and deformational history. A U-Pb zircon age determination yields a Neoproterozoic magmatic (?) age of ~2.64 Ga for the banded amphibolite, located ~2 km northwest of Paidha town (Mänttari 2014). The low K, Th and U signatures on ternary radiometric maps, a feature characteristic for these mafic rocks, permitted to outline the Kaza mafic metatuff and amphibolite in areas with poor exposure.

The conspicuous banding found in most Kaza metabasites is interpreted to represent layering inherited from their presumably pyroclastic or volcanoclastic precursors. In the type area of the Kaza ridge, a several tens of metres thick layer of well-preserved mafic metatuff dips gently towards the

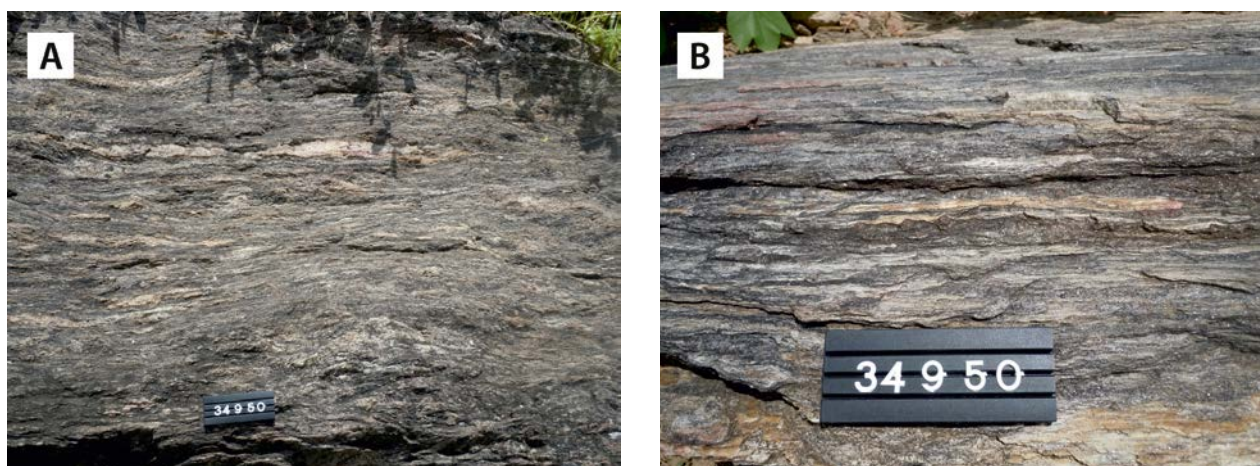


Fig. 4.13. (A) Segregated quartz lenses and stringers in mica schist of the Acer Formation. (B) Detailed image of garnet-bearing layer in mica schist (289011E / 266264N). Number tag 10 cm.

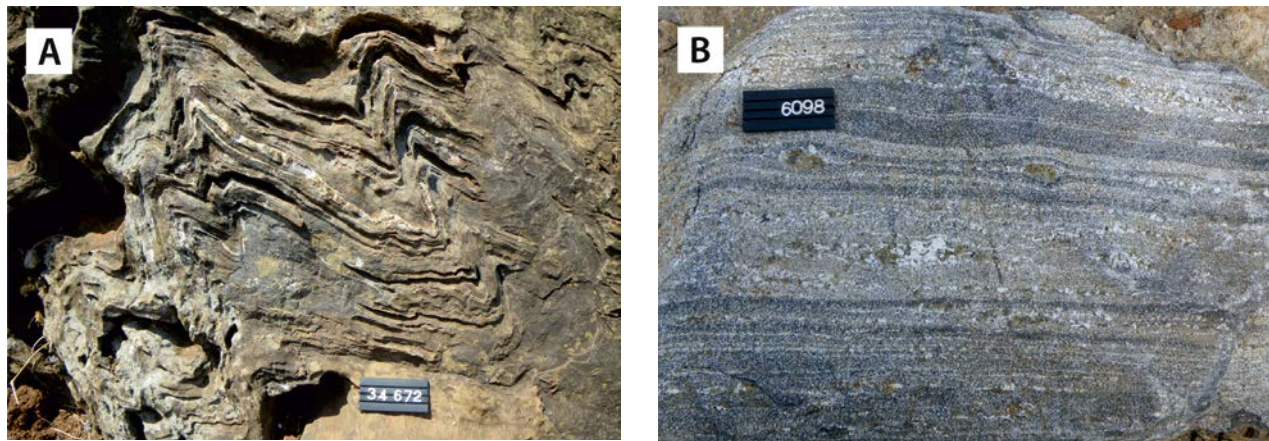


Fig. 4.14. Mafic metavolcanic rocks of the War Group. (A) Mafic metatuff with chevron folds (260986E / 278526N). (B) Banded amphibolite with coarse plagioclase-amphibole streaks (274142E / 268645N). Number tag 10 cm.

northeast, while probably the same unit occurs, albeit strongly deformed, some 20 km to the south (Fig. 4.14A). Banded amphibolites with small garnet porphyroblasts and coarse, pegmatitic plagioclase-hornblende streaks, containing amphibole crystals up to 8–10 mm in size, occur in places (Fig. 4.14B).

The mafic metavolcanic rocks of the Kaza Formation are granoblastic or nematoblastic, variably foliated and banded almandine-amphibolite grade amphibolites. Pale green, often prismatic hornblende grains, colourless or weakly pleochroic clinopyroxene, Ca-rich plagioclase (labradorite, An_{55}) and garnet are the major minerals. Rugged prisms of colourless clinopyroxene contain

worm-like symplectitic intergrowths of pale green hornblende, indicating *retrograde* metamorphism. Quartz, titanite, calcite and opaque matter are accessory (mostly retrograde) minerals. In the southern part of the WNB, Hepworth (1964) reported a distinctly lower grade metamorphic mineralogy, which corresponds to greenschist to epidote-amphibolite facies metamorphic conditions.

Whole rock chemical analyses of 11 mafic metatuff and amphibolite samples are listed in Appendix 2 (anal. 72–82). Results are shown on geochemical discrimination diagrams in Figure 4.31. On petro-tectonic discrimination diagrams, mafic metavolcanic rocks of the War Group plot in the field of ‘oceanic island arc basalts’ (Fig. 4.32C).

4.6 Lithostratigraphy of the Lobule Group and Abiba Formation (Arua-Kibale Supergroup)

The rocks included in the Neoproterozoic Lobule Group of the Arua-Kibale Supergroup are met mainly in the northwestern and southeastern segment of the WNB (Fig. 4.3). The southeastern Lobule rocks, east of Nebbi town, occur in a pile of parautochthonous or allochthonous tectonic slices, which includes also ‘Mirian’ rocks of the ~1.0 Ga

Igisi Group (Fig. 4.3). Leuco- to mesocratic gneisses of the Abiba Formation, tectonically squeezed between rocks of the Lobule Group and the Uleppi Complex, are believed to be younger than the Lobule Group. The Lobule Group has been divided into seven formations, which are listed with their main rock types in Table 4.4:

Table 4.4. Subdivision of the Lobule Group (note that the interpretation discussed here may deviate from the 1:250 000 scale map presented 2012).

| Group | Formation | Lithology |
|--------|-----------|-----------------------------|
| Lobule | Abiba | Leuco- to mesocratic gneiss |
| | Nebbi | Amphibolite |
| | Kuniro | Sericite schist |
| | Oweko | Banded gneiss |
| | Liru | Granulite gneiss |
| | Tukaliri | Granulite |
| | Akaba | Leucocratic gneiss |

4.6.1 Lobule Group

Akaba Formation: leucocratic gneiss – Leucocratic gneisses of the Akaba Formation cover most of the vast, low-lying plains east of Nebbi town, exhibiting there a positive signature on airborne radiometric maps. They further occur in an arcuate belt west of the Yumbe thrust front and in small, poorly exposed occurrences NW of the Midigo granite intrusion. This lithostratigraphic unit, which probably has tectonic footwall contacts, contains mostly rocks previously distinguished as the Eastern Grey Gneiss by Hepworth (1964).

Leucocratic gneisses of the Akaba Formation are light brownish grey, fine- to medium-grained quartzo-feldspathic rocks with only a minor amount of biotite and hornblende. Compositional banding, probably representing sedimentary bedding, can locally be observed (Figs 4.15A-B). A sedimentary origin is further supported by several field observations manifesting transitional contacts with overlying amphibolites of the Lobule Group. Dykes and lenses of pegmatite occur commonly, but regional metamorphism never resulted in melting and migmatisation of these rocks.

In thin section, the Akaba leucocratic gneisses are weakly foliated granoblastic rocks with thin streaks of parallelly oriented biotite laths. The total amount of mafic minerals, which locally also include large, ragged hornblende and small garnet grains, never exceeds 15–20 vol%. Ribbon quartz with strongly undulose extinction, microcline with cross-hatched twinning and weakly sericitised and saussuritised (albite-epidote altered) plagioclase in various proportions are the major rock constituents. Epidote is a minor retrograde mineral, while

apatite, zircon and opaque minerals are common accessory components.

Tukaliri Formation: granulite – Granulites of the Tukaliri Formation are spatially associated with the granitic granulites of the Lobule Group and with 2.62 Ga Tara charnockite intrusions. Together, these three rock units form a restricted and hilly “granulite-grade domain” about 400 km² in size, for a large part located east of Koboko town. This domain is bordered in the west to a N-S trending fault zone against Archaean granitoids and in the east by hornblende granodiorites and gneisses of sub-granulite metamorphic grade.

The Tukaliri Formation mainly comprises granulite-grade (>750°C) supracrustal rocks, whose metamorphism is supposedly related to the emplacement of the voluminous, hot and dry 2.62 Ga Tara charnockite intrusions nearby, manifesting an above average geothermal gradient (e.g. Spear 1991).

In places, the granulites comprise relics of supracrustal rocks and a gneissic banding, but often they are notably “granitised” due to intense partial melting (anatexis) (Fig. 4.16). The melted and recrystallised rock fractions are coarser grained than the host gneiss and ‘schist’ relicts. Intense partial melting may even cause the granulites to locally resemble plutonic charnockite. Dehydration melting supposedly gave rise to neoblastesis of pyroxene, garnet and K-feldspar, mainly at the expense of biotite and hornblende. These metamorphic changes in the mineral composition, particularly the disappearance of dark biotite and hornblende, resulted in washing out or “whitening” of the rock colour.

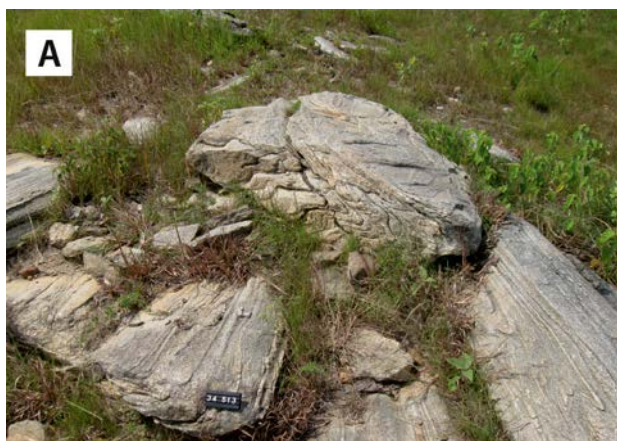


Fig. 4.15. (A) Meso-scale recumbent folds in leucocratic Akaba gneiss near the western margin of the Albertine Rift (310106E / 285408N). (B) Detailed image of distinctly banded, leucocratic Akaba gneiss (293284E / 275440N). Number tag 10 cm.



Fig. 4.16. Garnet-pyroxene granulite of the Tukuliri Formation, composed of anatectic material and gneiss relicts (283459E / 376547N). Number tag 10 cm.

Main minerals in these granulites are quartz, plagioclase, K-feldspar, orthopyroxene and locally garnet; K-feldspar grains comprise perthitic intergrowths. Minor biotite is also present, but commonly only as a secondary retrogressive mineral.

Electron microprobe data show that the garnet in the granulite is almandine with MgO content up to 8.8 wt% and thus with only in maximum ~30% pyrope molecule. Orthopyroxene is relatively MgO rich (MgO \approx FeO \approx 21–23 wt%) with a moderate Al₂O₃ content of 3.6 wt%. The close association of orthopyroxene and garnet suggests that the garnet grew at the expense of orthopyroxene.

Liru Formation: granulite gneiss – The Liru granulite gneiss is closely associated with the 2.62 Ga Tara charnockitic granites and granulites described above. By comparison to the existing 1:100 000 scale geological map by Macdonald (1964b), it is found that the area of the here distinguished Liru granulite gneisses partly overlaps with rocks identified by Macdonald as “*charnockitic quartz diorite and undifferentiated banded pyroxene gneiss*” and “*leucocratic granulites, including charnockite and enderbite*”.

Granulite gneisses of the Liru Formation are predominantly dark grey, medium-grained, often relatively homogeneous rocks with only scant anatectic patches. Generally, they do not contain

coarse K-feldspar phenocrysts or unequivocal sedimentary structures. These granulite gneisses may partly be even plutonic rocks in origin. The usual main minerals are plagioclase, K-feldspar, quartz and orthopyroxene. Minor amounts of biotite, hornblende and garnet are locally present.

Oweko Formation: banded felsic-mafic gneiss – The banded gneisses of the Oweko Formation comprise a narrow, NE trending belt of distinctly banded rocks east of Nebbi town in the southern part of the WNB, where it forms a compositionally transitional unit between the leucocratic gneisses of the Akaba Formation and Nebbi amphibolites of the Lobule Group. Poorly exposed, leucocratic, thinly banded gneiss in an area NW of Yumbe town is also tentatively assigned to this unit.

Due to its dominantly mafic composition, the Oweko banded gneiss generally produces a negative signature on ternary radiometric maps. In the southern type area, the eastern footwall contact of the banded gneiss with the Akaba leucocratic gneisses is probably of tectonic character, while the hanging wall contact with Nebbi amphibolites is gradational.

Good, flat outcrops of distinctly banded Oweko gneisses located 4 km SE of Nebbi town show alternating dark green, fine- to medium-grained amphibolitic and light brownish grey leucocratic

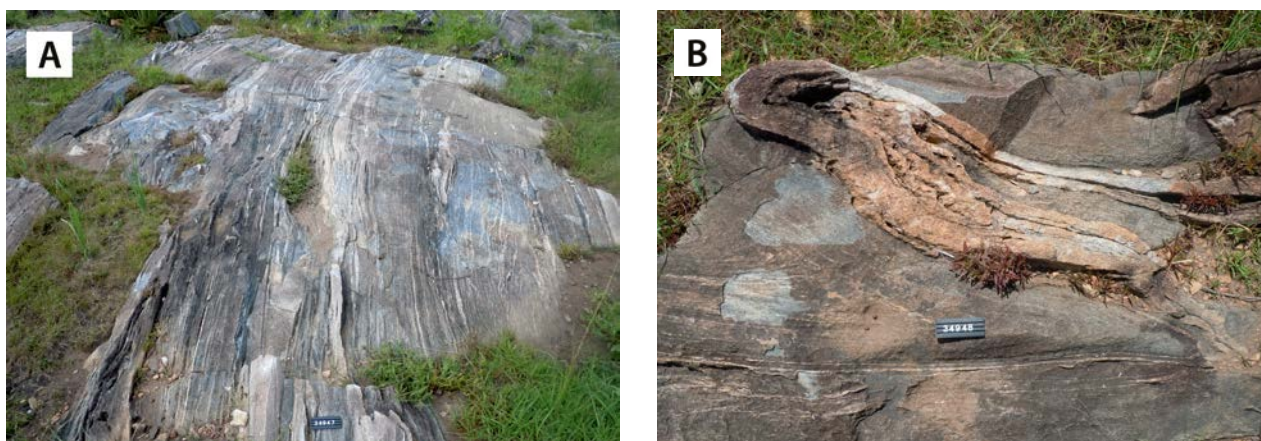


Fig. 4.17. (A) Distinctly banded gneiss of the Oweko Formation (290414E / 271037N). (B) Overturned fold in banded gneiss (290056E / 269995N). Number tag 10 cm.

layers and bands. Despite polyphase deformation of the rock, obvious thin to laminar bedding is locally preserved in the leucocratic layers, indicating a supracrustal origin (Figs 4.17A-B). In the area NW of Yumbe town, rather leucocratic, strongly deformed gneiss with thin, hornblende-bearing bands is found in the majority of the scarce outcrops.

Kuniro Formation: sericite schist – A short, narrow belt of gently SE-dipping sericite schists, is exposed within the Lobule Group gneisses southeast of Kuniro village in the northern part of the WNB. The nature of the footwall contact of these schists with the underlying Oweko banded gneiss is unknown. The rarely outcropping, strongly foliated schists are light silvery grey, fine-grained rocks that locally show vague, thin banding resulting from alternation of sericite- and quartz-rich layers that may represent sedimentary bedding. With increase in quartz content, the sericite schists of the Kuniro Formation locally grade into strongly foliated sericite quartzites.

Nebbi Formation: amphibolite – Amphibolites of this rock unit, named after the well-exposed type area around Nebbi town, conformably overlie the leucocratic gneisses of the Akaba Formation in the southern part of the WNB. The hanging wall contact of this rock unit is tectonic, being defined by NE trending faults that locally separate the amphibolite from adjacent rock units in the west, while the footwall contact with underlying leucocratic gneisses of the Akaba Formation is transitional. The strong negative signature of the amphibolites on ternary radiometric maps can be used to

separate them from the Akaba gneisses underlying the eastern, poorly exposed low-land areas. U-Pb zircon dating of the Nebbi amphibolite yields a magmatic crystallisation age of ~ 2.63 Ga (Mänttari 2014).

According to Hepworth (1964) this rock unit – the former ‘Nebbi quartz diorite gneiss’ – allegedly intruded the Western Grey Gneisses during later stages of the regional deformation. However, in the type area, the dark green, fine- to medium-grained, variously foliated and lineated amphibolite is often distinctly and regularly banded, which suggests rather a predominantly pyroclastic origin (Figs 4.18A-C).

A rather massive amphibolite variety, which forms prominent hills in the centre of Nebbi town, is supposedly of a slightly different origin, possibly representing a feeder dyke or sill. In addition to the coarser grain size, this homogeneous rock differs from the usually distinctly banded amphibolites of the area also by having only random thin, fine-grained mafic bands and leucocratic segregations parallel to foliation. The transitional contacts between the banded and massive amphibolite varieties refer, however, to a comagmatic sub-volcanic intrusive to volcanic pyroclastic origin.

Under the microscope, the texture of the amphibolite component in the Nebbi rocks is essentially nematoblastic, comprising mostly of well-oriented, brownish or bluish-green hornblende prisms in a granoblastic matrix of moderately altered plagioclase (andesine, An_{37}) and quartz grains, the latter showing undulose extinction. Small garnet porphyroblasts are a common minor constituent, along with some biotite, epidote, titanite, carbonate and opaque matter. Clinopyroxene up to

20 vol% has been reported from the massive amphibolite variety by Hepworth (1964, p. 59). In general, mineral assemblages in these amphibolites are consistent with almandine-amphibolite facies metamorphism (Hepworth 1964).

Three representative samples from the amphibolite in the Nebbi Formation were selected for chemical analyses (App. 2, anal. 78–80). The data indicate

that these amphibolites are sub-alkaline basalts and andesites (Figs 4.31A-B). The relatively high SiO_2 and Al_2O_3 contents may indicate mixing of re-worked, weathered rock with unaltered pyroclastic material, both of originally basaltic composition. A 'non-oceanic, within-plate' setting for the Nebbi amphibolites is indicated by their plotting on geochemical discrimination diagrams (Figs 4.32B-C).

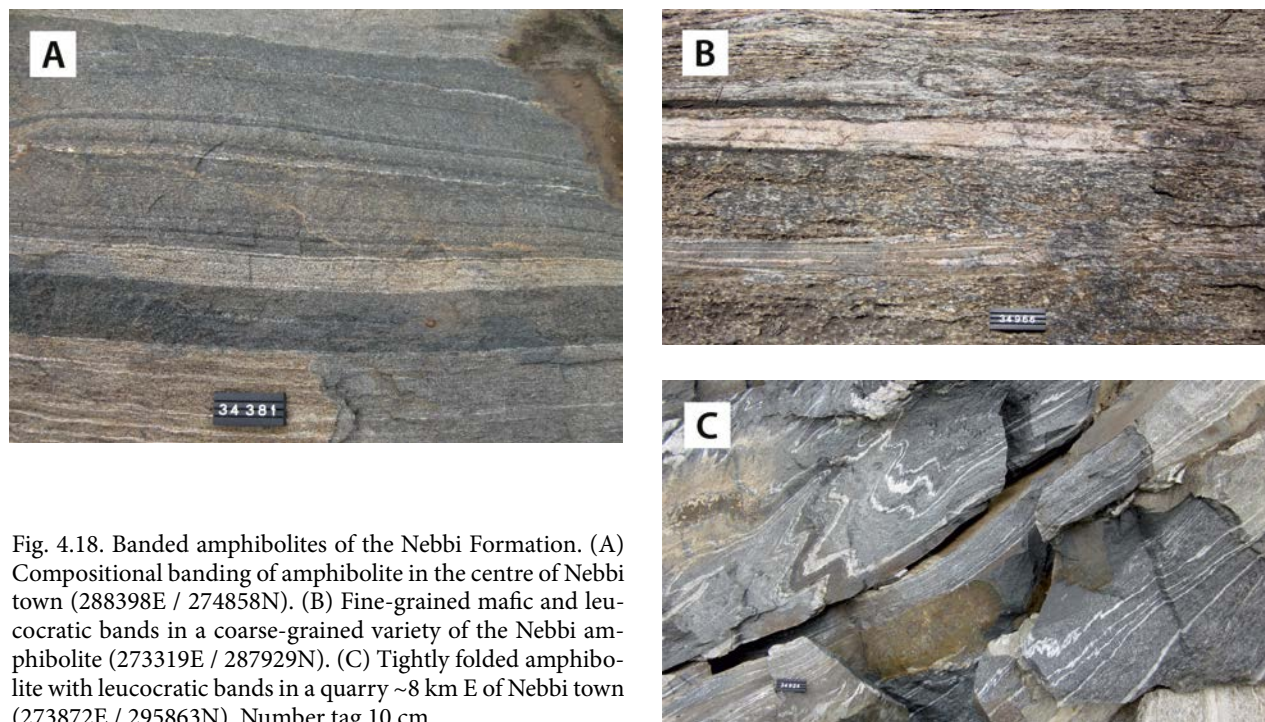


Fig. 4.18. Banded amphibolites of the Nebbi Formation. (A) Compositional banding of amphibolite in the centre of Nebbi town (288398E / 274858N). (B) Fine-grained mafic and leucocratic bands in a coarse-grained variety of the Nebbi amphibolite (273319E / 287929N). (C) Tightly folded amphibolite with leucocratic bands in a quarry ~8 km E of Nebbi town (273872E / 295863N). Number tag 10 cm.

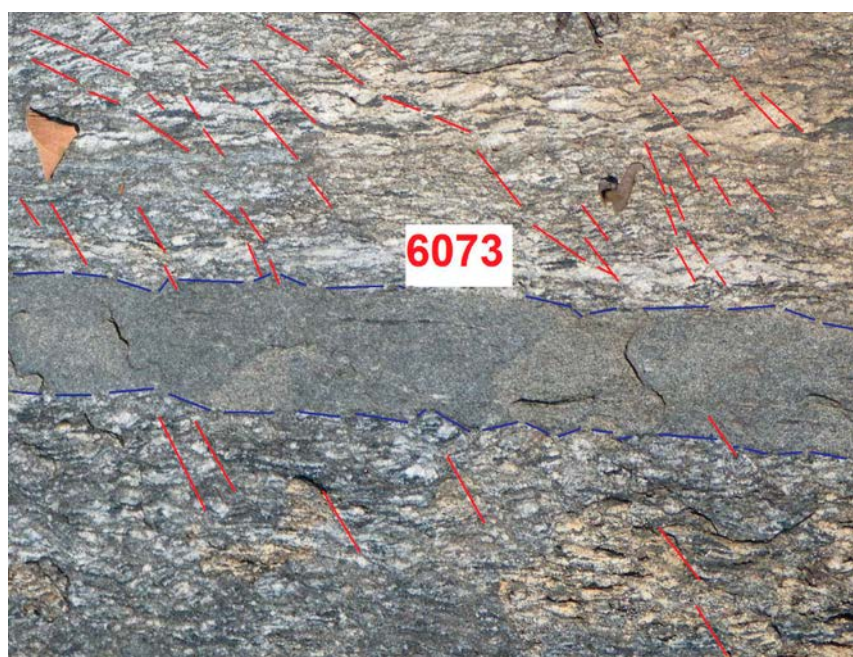


Fig. 4.19. Blastomylonitic Nebbi amphibolite with a narrow (~15 cm) metadolerite dyke. Note that the blastomylonite foliation is slightly oblique to the intrusive contacts. Small dextral off-sets take place along a closely spaced set of fractures (red lines) with a N100E trend. South of Nebbi town (288288E / 273766N). Number plate 10 cm.

4.6.2 Abiba Formation

Leuco- to mesocratic gneisses of the Abiba Formation, previously counted among the 'Eastern Grey Gneisses' (Hepworth 1964), form a NE trending belt in the southern part of the WNB, being there tectonically squeezed between the parautochthonous or allochthonous rocks of the Lobule Group and the Uleppi Complex. Lacking good exposures, the foot and hanging wall contact relations of these high-grade gneisses are unknown, but based on the intensely sheared nature of the contact zone rocks, both the foot and hanging wall contacts are probably of tectonic origin. On ternary airborne radiometric maps, the Abiba gneisses exhibit stronger positive signatures than the surrounding rocks.

The gneisses of the Abiba Formation are light to dark brownish, medium-grained, foliated and often strongly folded rocks (Fig. 4.20A). A compositional banding, which resembles sedimentary bedding, is locally visible on weathered rock surfaces, however (Fig. 4.20B). The proportion of mafic minerals is strongly variable and supposedly reflects lateral facies variation in the clay component in the sedimentary depositional environment. In some outcrops, thin amphibolite bands, leucocratic segregation veins and lens-like quartz segregations, up to 10–15 cm in length, have been observed.

The major mineral constituents are, in varying proportions, strongly undulating quartz, clear unaltered plagioclase (oligoclase, An_{25}), crosshatch-twinned microcline and small biotite flakes. Minor minerals comprise retrograde epidote and sericite, and minor amounts of apatite, titanite, zircon and

magnetite. Myrmekitic intergrowths, as well antiperthitic blebs of plagioclase in K-feldspar, are common in samples from the more leucocratic gneiss members. In the mesocratic gneiss varieties, the content of biotite can reach 10–15 vol%, while ragged hornblende and garnet blasts occur commonly in minor amounts.

Chemical whole-rock analyses for two representative Abiba gneiss samples are presented in Appendix 2, anal. 84–85). U-Pb dating of detrital zircons from the mesocratic gneiss shown in Figure 4.20B yields a maximum age of ~2.55 Ga for the rock (Mänttari 2014).

4.6.3 Plutonic Rocks

The above described succession of gneisses, constituting the Arua-Kibale Supergroup, has been invaded by various plutonic intrusive rock types: leucocratic granite gneiss, quartz diorite, hornblende granodiorite, Tara brown granite, flaggy hornblende gneiss, granodiorite gneiss, granite gneiss, granodiorite, Niapea granite and metadolomite.

Leucocratic granite gneiss – Leucocratic granite gneisses cover large areas in the northwestern part of the WNB, where these greyish, variously deformed rocks are exposed in an elongated belt north of Arua town, adjacent to the border of DRC and South Sudan. In the east, this rock unit is bounded by a distinct 'fracture and shear zone', formerly known as the 'boundary dislocation' (BF in Fig. 4.2), separating it from the 2.62 Ga charnockitic Tara brown granites and associated supracrustal granulites. Although undated, the

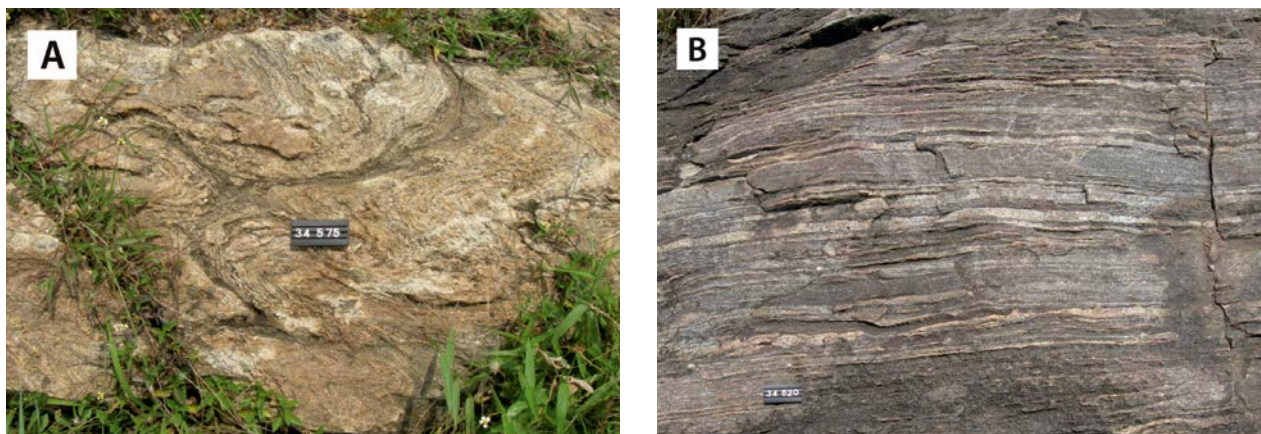


Fig. 4.20. (A) Strongly deformed, leucocratic variant of the Abiba gneiss (278157E / 277343N). (B) Compositional banding in the mesocratic Abiba gneiss (294976E / 292211N). Number tag 10 cm.



Fig. 4.21. (A) Rather massive leucocratic granite gneiss with elongated mafic enclave (273265E / 379534N). (B) Deformed leucocratic granite gneiss with some granitic veins (275199E / 382633N). Number tag 8 cm.

intense and polyphase deformation of the included rocks suggests that they are older than the nearby, weakly deformed 2.62 Ga Tara brown granites.

Usually, this unit comprises equigranular, relatively massive-looking and weakly deformed granitoids (Fig. 4.21A). Locally the rock records more intensive, often mylonitic foliation making it to resemble gneisses of supracrustal origin. In addition, the leucocratic granite gneiss may locally comprise some granitic veins (Fig. 4.21B). In places, the leucocratic granitic gneisses comprise large inclusions of supracrustal rocks, and sometimes relicts of dolerite.

The major mineral constituents are plagioclase (30–40 vol%), K-feldspar (10–25 vol%), quartz (20–35 vol%) and biotite (10 vol%). The range in mineralogical composition implies granitic to granodioritic compositions. Hornblende, epidote and chlorite occur locally as minor, partly retrograde minerals in modes up to 1–3 vol%.

Analysis of one sample from a dark grey, mylonitic gneiss member classifies the rock (Figs 4.33A–C) as calc-alkaline peraluminous granodiorite. Petro-tectonic discrimination diagrams imply a ‘within-plate’ or ‘syncollisional volcanic arc’ setting for this rock (Figs 4.34A–B).

Quartz diorite – Small bodies of quartz diorite occur among the more felsic granitoids around Arua town in the WNB. In the field, the medium-grained to coarsely porphyritic, pale to brownish or greenish rock shows a planar fabric after deformation. Felsic veins occur in places.

Hornblende granodiorite – Hornblende granodiorite forms large intrusions in the area NE of Arua town. This generally poorly exposed rock differs from the diverse, often leucocratic and strongly deformed granitoids of the WNB in a number of aspects. For example, it is mostly relatively

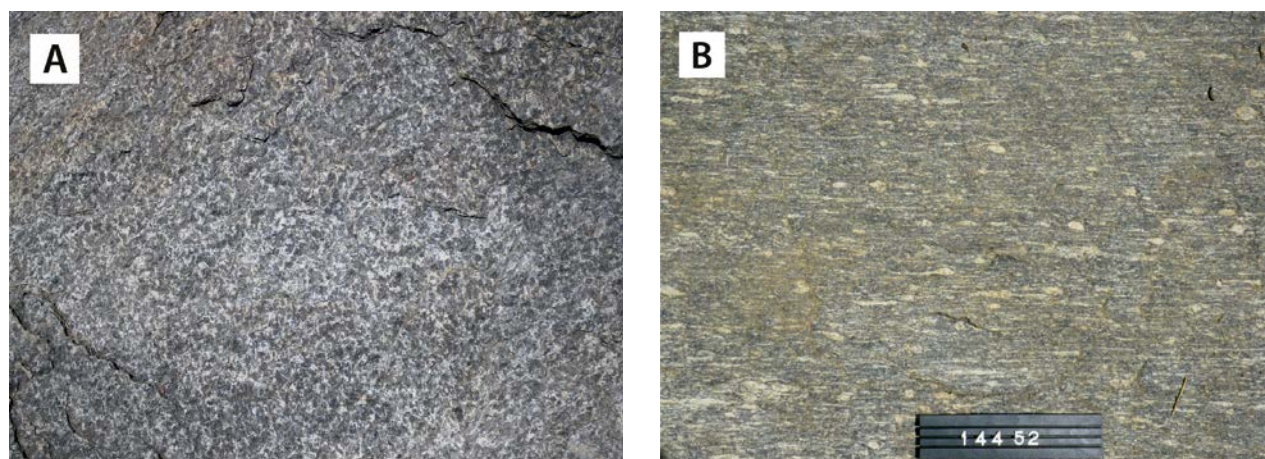


Fig. 4.22. (A) Tonalitic hornblende- and biotite-rich type of the granodiorite (293754E / 356328N). (B) Intensely deformed, hornblende-rich granodioritic tonalite blastomylonite with augen texture (287281E / 347725N). Number tag 15 cm.

homogeneous, coarse-grained and equigranular and usually also rather dark coloured with a high hornblende and biotite content of 25–40 vol% (Fig. 4.22A). The granodiorite is spatially associated with the 2.62 Ga Tara charnockitic granite intrusions.

The major minerals are plagioclase (20–50 vol%), quartz (10–25 vol%), K-feldspar (1–10 vol%), hornblende (10–25 vol%), biotite (2–15 vol%) and often retrograde epidote (1–8 vol%). The wide range in mineral composition, in particular the K-feldspar content, means that, in places, the granodiorite grades into tonalite and even into quartz diorite. In addition, the rock locally contains quite a bit of magnetite (1–4 vol%) and sphene (1–2 vol%). Especially where intensively deformed, the rock is characterised by augen texture (Fig. 4.22B).

Tara brown granite – The brown granite, named after Tara village and corresponding with the northern segment of the ‘Watian’ rocks in Figure 4.2, is one of the most conspicuous rock units in the WNB. The absence of any preferred mineral orientation in the brown granite is in stark contrast to the prevalence of intense foliation in the surrounding gneissic rocks. Tectonic deformation is only recognisable within the contact zones of this competent rock with the adjacent gneisses. Tara brown granite is a homogeneous, coarse and characteristically reddish-brownish coloured rock, as its field-name “brown granite” implies. The major constituents are K-feldspar, quartz, plagioclase and pyroxene. The K-feldspar occurs as rather densely

packed phenocrysts (Fig. 4.23B). U-Pb zircon dating of Tara brown granite yields an age of 2.62 Ga for its magmatic emplacement (Mänttari 2014).

A single sample from the Tara brown granite (charnockite) has been chemically assayed (App. 2, anal. 83): its composition ranges between tonalite and diorite (Fig. 33A); the silica content is relatively low (63.4% SiO₂), and the sample classifies as metaluminous and calc-alkaline (Figs 4.33B-C). A ‘volcanic arc granites’ or ‘syncollisional volcanic arc granites’ setting is suggested for the Tara brown granite when plotted on petro-tectonic discrimination diagrams (Figs 4.34A-B).

Flaggy hornblende gneiss – Rather small masses of flaggy hornblende gneiss, associated with leucocratic granite gneisses, are located in the NW corner of the Yumbe District near the border with South Sudan (Macdonald 1964a). These hornblende gneisses contain epidote and were formerly attributed to the ‘Mirian’ (see 1:100 000 scale geological map of Midigo; Sheets 3 & 4; Macdonald 1964b). Structural analysis suggests isoclinal refolding of a pre-existing foliation in the eastern flaggy outcrops, accompanied by extreme attenuation of the rock layers. Hepworth (1964) suggested that the flaggy gneiss may represent a zone of overturned tectonic lenses (‘Schuppen’) or thin-skin tectonics.

Granodiorite gneiss – Granodiorite gneisses cover a rather large area (ca. 100 km²) NE of Arua town and crop out as small, isolated bodies in the middle part of the WNB. Their delineation is mainly

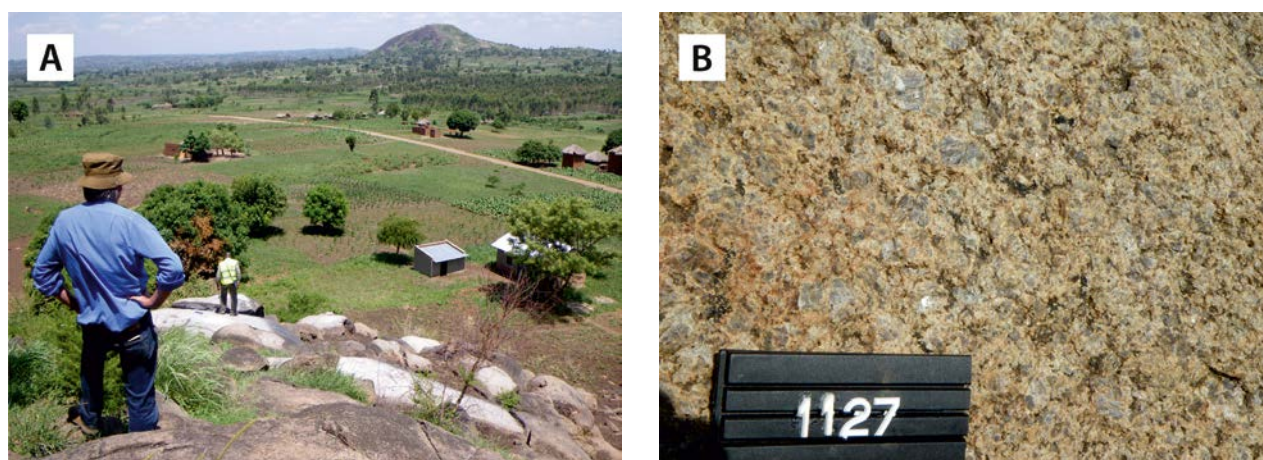


Fig. 4.23. (A) A view over the outcrop sampled for the U-Pb dating of the Tara brown granite. The location is within a large cluster of hills 25 km NE of Arua town (279536E / 356926N). (B) K-feldspar phenocrysts in Tara granite showing characteristic bluish hues. Number tag 8 cm.

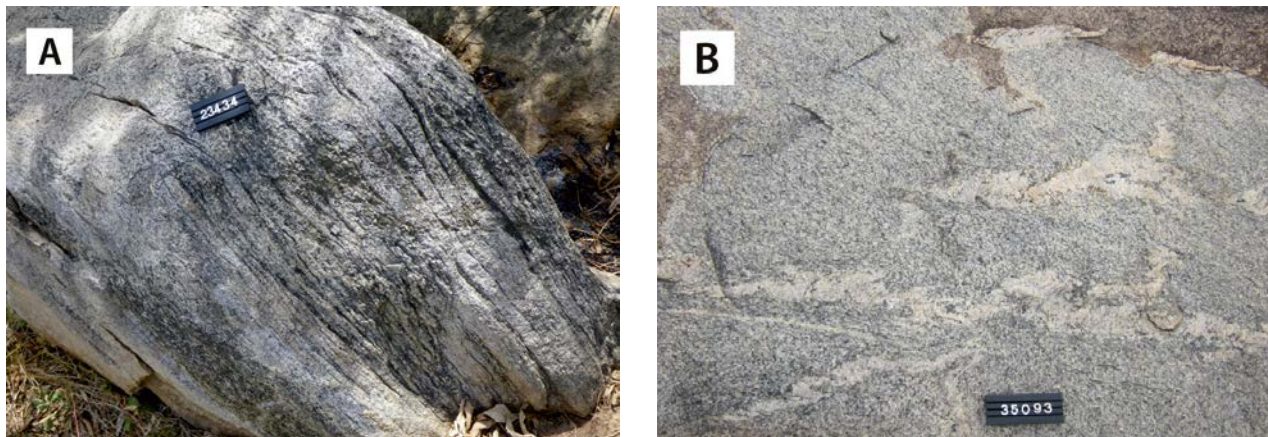


Fig. 4.24. Different types of granodiorite gneiss. (A) Rather strongly foliated gneiss variety (272834E / 364224N). (B) Biotite-bearing granodiorite gneiss with granitic veins and patches (263957E / 319987N). Number tag 8/10 cm.

based on their relatively low radiometric total count signature and slightly elevated magnetic values. On the existing 1:100 000 scale geological map of Arua (Macdonald 1964b), these gneisses were partly marked as leucocratic ‘Watian’ granulites but our field review failed to highlight orthopyroxene – as could be expected in granulite facies rocks. Moreover, indications of retrogressed granulites, like pseudomorphs after pyroxene, symplectites, and rusty weathering are also missing.

The rock is gneissose in texture and, although being foliated to varying degrees, relatively homogeneous (Fig. 4.24A), even though with granitic patches in places (Fig. 4.24B). It is locally grading into biotite orthogneiss in which the biotite content is elevated, usually ranging between 10 and 20 vol%. Plagioclase dominates over K-feldspar and, consequently, the rock is actually often tonalite rather than granodiorite in composition. Magnetite crystals, ~1 mm in size, can be identified by hand lens and produce magnetic susceptibility values up to 8 SI-units $\times 10^{-6}$.

A single representative sample was selected for major and trace element analysis (App. 2, anal. 86). With a SiO₂ content of 74.1 %, the rock plots in the granodiorite field close to the granite field (Fig. 4.33A) and shows peraluminous and calc-alkaline affinities (Figs 4.33B-C). Similarly to other granitoids from the WNB, a ‘volcanic arc granites’ or ‘syncollisional volcanic arc granites’ setting is implied for this unit on magma-tectonic discrimination diagrams (Figs 4.34A-B).

Granite gneiss – Three poorly known, NE-SW trending masses of granite gneiss are located on the eastern side of the Albertine Rift, on the bound-

ary with the North Uganda Terrane. Scarce field observations are restricted to well-foliated granite gneiss containing pyroxene, hornblende and plagioclase as the main minerals. Small areas of similar granite gneiss are located NE of Arua town and NE of Yumbe town, along the northern border of Uganda.

Granodiorite – The northern part of the WNB contains small (4–10 km²), isolated intrusions of granodiorite. They partly spatially overlap rock units formerly called “*granodiorite-gneiss, including Obiowa type*” (Macdonald 1964a, 1964b). When compared to adjacent gneisses, these granodiorites show slightly elevated ternary radiometric signatures.

The given granodiorites are more or less gneissose, greyish, equigranular plutonic rocks with grain sizes <1 cm. Mafic to intermediate xenoliths, enclaves and segregated or injected granitic veins occur in places (Figs 4.25A-B). Major minerals are plagioclase, quartz, K-feldspar, hornblende and locally biotite. The amount of K-feldspar ranges between 5 and 20 vol%. Hornblende dominates over biotite; their combined mode is mostly around 20 vol%.

Niapea granite – The Niapea granite refers to two 6–8 km² granite intrusions and three smaller satellite bodies 8 km to the west of Paidha town, in the southwestern corner of the WNB (Hepworth 1961b). According to Hepworth (1964, p. 106), the Niapea granite is light grey, medium- to coarse-grained, biotite granite. Locally, the rock comprises some pegmatitic patches, feldspar phenocrysts and garnet.

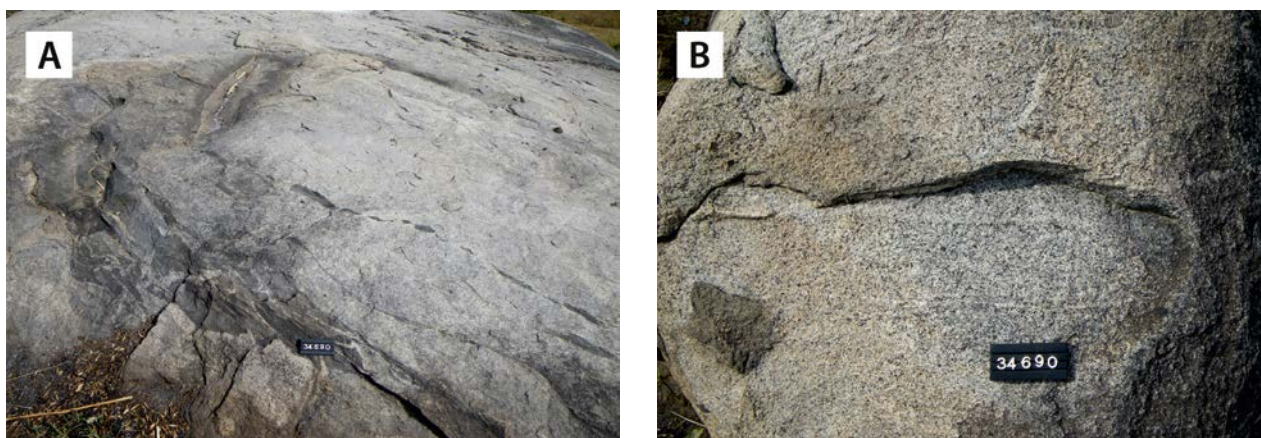


Fig. 4.25. (A) Mafic xenolith in foliated granodiorite. (B) Rather massive granodiorite with a mafic enclave (left corner) (273633E / 390981N). Number tag 8 cm.

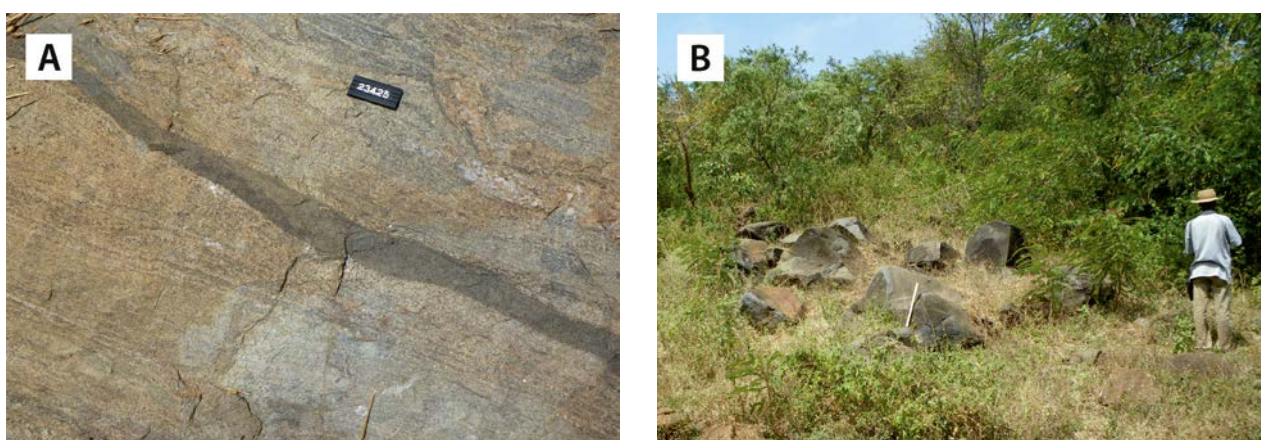


Fig. 4.26. (A) Narrow metadolerite dyke in granulite (369580E / 283625N). (B) *In-situ* metadolerite boulder field (278409E / 367538N). Number tag 8 cm (in A).

Metadolerite – The Archaean gneisses and granulites in the WNB are in many places cut by north-east trending, massive or weakly foliated metadolerite dykes. The width of these dykes ranges from a few centimetres to ~10 m (Fig. 4.26A). Many

of the dyke occurrences are indicated only by *in-situ* boulders (Fig. 4.26B). They are dark grey or dark greenish grey, mostly medium-grained rocks, composed of plagioclase, hornblende and pyroxene.

4.7 Lithostratigraphy of the Yumbe Complex

4.7.1 Introduction

The undated but supposedly Neoproterozoic rocks of the Yumbe Complex are not a part of the WNB, but occur in a large (>1000 km²), allochthonous, W-vergent thrust mass or nappe, presumably derived from the North Uganda Terrane. The Yumbe Complex tectonically overlies the rocks of the Neoproterozoic Lobule Group and associated granulites in the northeastern WNB and is, in turn, invaded by Neoproterozoic granulites of the Midigo-Ad-

jumani Suite. Airborne radiometric data help to outline the extent and borders of the Complex, including its curved western thrust front. In contrast to the vertical to sub-vertical dips characterising the rocks of the Uleppi and Lobule Groups, “flagginess” and generally low to moderate easterly dips (20–40°) dominate in the Yumbe Complex (Hepworth 1964), being the most distinctive feature of this allochthonous unit.

The Yumbe Complex is composed of generally SW-NE trending supracrustal formations includ-

ing banded (migmatitic) gneisses, mica gneisses, (fuchsite-bearing) quartzite and amphibolite. These rocks show different geophysical signatures, assisting in their delineation. The major part of the thrust mass is composed of a variety of deformed granitoids, including banded gneiss, migmatitic in places, granodiorite gneiss, leucocratic granite gneiss, tonalite gneiss and granodiorite gneiss with amphibolite intercalations. Lithologically the Yumbe Complex is closely related to the WNB, but for its tectonic history it is part of the evolution of the ~1.0 Ga Madi-Igisi Belt (Chapter 9).

4.7.2 Supracrustal rocks of the Yumbe Complex

Banded gneiss, migmatitic in places – Gently dipping to sub-horizontal banded gneisses with complex fold structures (Fig. 4.27), form the country rock around the Neoproterozoic Midigo granite. The banded gneisses being intruded by the Midigo granite implies that their tectonic emplacement must have preceded the magmatic emplacement of the Midigo granite at ~0.66 Ga.

The banded gneiss of the Yumbe Complex typically shows compositional banding with leucocratic quartz-feldspar and darker, hornblende/biotite-rich layers. Its structure generally varies from foliated to strongly foliated, showing even a flagstone appearance in places, while some rather homogeneous variants resemble gneissic granodiorite, or are very similar to the TTG gneiss of the Yumbe Complex, exposed 30 km east of Midigo village in the North Uganda Terrane (Chapter 5). The origin of the banded Yumbe gneiss may be mixed, comprising both supracrustal and magmatic components.



Fig. 4.27. Banded gneiss of the Yumbe Complex with light and dark grey bands and layers, cut by pegmatitic dykes. (309776E / 390023N). Number tag 8 cm.

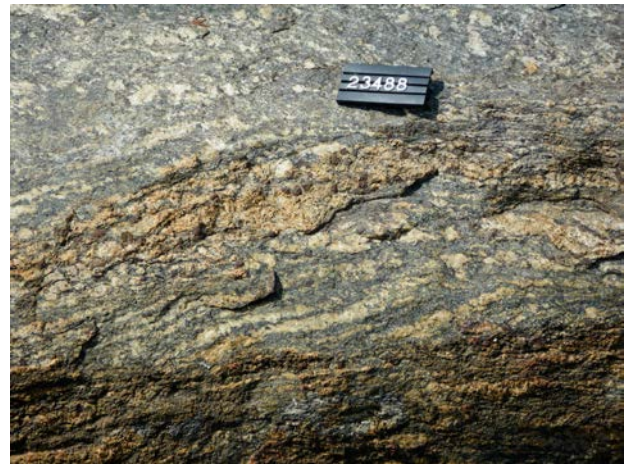


Fig. 4.28. Migmatitic mica gneiss of the Yumbe Complex with abundant biotite and minor garnet; a cluster of garnet porphyroblasts is shown by arrows (303878E / 364397N). Number tag 8 cm.

Mica gneiss, micaceous gneiss – Mica gneisses, labelled as “*banded gneisses and migmatites, undifferentiated*” and as “*leucocratic muscovite gneisses*” by Macdonald (1964b), form curvilinear bodies, several kilometres in length and up to 3 km wide, most commonly in the SW corner of the Yumbe Complex.

The mica gneisses are usually migmatitic, veined gneisses, with a typical biotite content of 15–20 vol%. Garnet porphyroblasts, up to 10 mm in size, are observed in places (Fig. 4.28). The narrow granitic veins in the gneisses are supposedly products of partial melting (anatexis). Light coloured members, with muscovite predominating over biotite, occur locally.

These gneisses are often intensively deformed, and no clear sedimentary structures have been observed.

Quartzite, fuchsite-bearing in places – Thin, north-east trending quartzite horizons, shown in the existing 1:100 000 scale geological map of Arua (sheets 11 & 12; Macdonald 1964b), are intercalated with the above described mica gneisses, reinforcing the idea of their supposedly sedimentary origin.

Amphibolite – Thin bands of dark green, foliated amphibolite, as shown in the 1:100 000 scale geological map of Arua (Macdonald 1964b), are also intercalated with the mica gneisses and leucocratic granite gneisses of the Yumbe Complex.

4.7.3 Plutonic rocks of the Yumbe Complex

Granodiorite gneiss – Poorly exposed granodiorite gneisses of the Yumbe Complex border (and continue below) the Neogene sediments in the Albertine Rift. According to the geological map of Arua (sheets 11 & 12; Macdonald 1964b), the gneisses of this area were previously called either “*granodiorite-gneisses (including Obiowa type)*” or “*leucocratic muscovite gneiss*”, both regarded having a probable plutonic origin. The main minerals of the rock are plagioclase, K-feldspar, quartz, biotite (2–16 vol%) and muscovite. The most leucocratic variants comprise more K-feldspar and muscovite and, consequently, produce rather high radiometric, in particular, high potassium signatures.

The granodiorite gneiss shows a gently east-dipping to horizontal gneissose foliation and a gently plunging mineral lineation. Local shearing has resulted in segregation into alternating mica- and feldspar-rich layers, 0.1 to 3 cm in thickness. In addition, the gneiss locally comprises coarse-grained granitic patches parallel to the tectonic fabric.

Leucocratic granite gneiss – The leucocratic granitic gneisses are predominantly located along the peripheral parts of the Yumbe Complex, where they form a 1–5 km x 50 km, curvilinear sheet. The extent of the included gneisses can be interpreted from radiometric ternary maps. It is assumed that these rocks were mainly plutonic in origin although they may comprise also some supracrustal portions. However, no definitive sedimentary structures have been observed.

Leucocratic granite gneiss is usually an equigranular, medium- to mostly coarse-grained rock

with some vague compositional banding in places (Fig. 4.29A). Locally, shearing and related mylonitisation has reduced the grain size of the initial rock and resulted in schistose textures. Mineral lineations measured from the strongly deformed gneiss outcrops regularly show gentle dips towards east or northeast (Fig. 4.29B). Some intensively deformed and flattened enclaves represent, however, obvious elongated supracrustal schist inclusions.

In places, the rock may comprise darker layers, 1-5 m in width, containing up to 20 vol% biotite (\pm amphibole). The gneiss tends to contain migmatitic granitic veins and patches, manifesting metamorphic differentiation and partial melting. In addition, this granite gneiss locally encloses outcrop-scale inclusions of amphibolite, biotite gneiss and quartz rock.

Tonalite gneiss – Poorly exposed tonalite gneisses, formerly labelled as “*banded gneisses and migmatites, undifferentiated*” on the 1:100 000 scale geological map of Arua (Macdonald 1964b), form a curvilinear sheet within the Yumbe Complex. The rock unit can be outlined from surrounding rock units by its stronger signature on ternary radiometric maps.

Tonalite gneisses are dark grey, migmatitic rocks, mostly corresponding to tonalite but also to granodiorite in composition, with significant but variable biotite (15–20 vol%) and hornblende contents. Subordinary rock types within the tonalite-granodiorite gneiss include clinopyroxene and epidote-bearing amphibole and migmatitic mica gneisses. Granitic veins, up to 10 cm thick, occur commonly in the migmatitic varieties. When intensively deformed, the tonalite gneiss gets a distinctly



Fig. 4.29. (A) Leucocratic granite gneiss, obviously plutonic in origin (299402E / 384029N). (B) Strongly foliated and lineated leucocratic granite gneiss (313478E / 390415N). Number tag 8 cm.

banded texture, complicating its distinction from other gneiss units of the Yumbe Complex.

Hornblende granodiorite gneiss – This unit comprises mainly hornblende granodiorite gneisses, distinguished as “*banded gneisses and migmatites, undifferentiated*” on the 1:100 000 scale geological map of Arua (Macdonald 1964b) that occupy an area of about 250 km² in the central part of the Yumbe Complex, in a body conformable with surrounding tonalite gneisses in the north and west. The included rocks are less radioactive than the surrounding tonalite gneisses.

The hornblende granodiorite gneisses are usually composed of two components: (1) a light coloured, occasionally banded orthogneiss, varying granodiorite to granite in composition and containing veins and patches of more granitic composition (Fig. 4.30) and (2) parallel, elongated, metres wide amphibolite bodies, which probably mostly represent conformable metadolerite sills. Granitic veins in the rock show isoclinal minor folds and narrow shear zones. As any clear sedimentary or



Fig. 4.30. A distinctly banded variation of the hornblende granodiorite gneiss (307997E / 382147N). Number tag 8 cm.

volcanic structures have not been observed, the gneiss is supposedly plutonic in origin.

The interleaved amphibolitic bodies may be relatively homogeneous but usually show variations in grain size and abundance of quartz-feldspar segregations. Some hand specimens, comprising clinopyroxene and epidote, show metadoleritic textures.

4.8 Geochemistry

Mafic metavolcanic rocks

The two amphibolite samples analysed from the Uleppi Group have 48.1–51.7 wt% SiO₂ and high TiO₂ contents (2.0 and 3.1% TiO₂) and plot in the fields of subalkaline basalt and basaltic andesite (Figs 4.31A–B). The rocks are classified as tholeiites on an AFM plot and as Fe-tholeiites on the Jensen cation diagram (Figs 4.31C–D). The chondrite-normalised lanthanide patterns are slightly enriched in LREEs (Fig. 4.31E). On petro-tectonic discrimination diagrams the amphibolites of the Uleppi Group plot in the field of ‘*oceanic*’ or ‘*within-plate*’ basalts (Figs 4.32B–C). On chemical alteration diagrams these two samples plot due to their low Na₂O out of the ‘*igneous spectrum*’ (Fig. 4.32D). Instead, the MgO–CaO/Al₂O₃–P₂O₅ ratios do not indicate significant alteration (Fig. 4.32E).

The six samples of mafic metatuffs and amphibolites analysed from the War Group have 47.2–49.2 wt% SiO₂ and 0.7–1.1 wt% TiO₂. They plot in the subalkaline basalt field and classify as sub-alkaline basalts and basaltic andesites (Figs 4.31A–B). In the Jensen cation diagram, most of the amphibolites plot as Mg-tholeiites though near to the Fe-tholeiite border (Fig. 4.31D). Although

some analyses plot in the calc-alkaline field on the Jensen diagram, this is not reproduced on the AFM diagram (Fig. 4.31C). Nearly similar chemical characteristics as those of mafic rocks of the War Group are exhibited by the amphibolites of the Yumbe Complex (Figs 4.31A–D). The four amphibolite samples analysed for lanthanides have all very similar chondrite-normalised patterns, with flat, about ten times chondritic HREE and slightly depleted LREE distributions (Fig. 4.31E). Again, a remarkable similarity in the REE distributions with mafic metatuffs and amphibolites of the War Group and Yumbe Complex can be observed.

The three samples from the mafic rocks in the Nebbi Formation of the Lobule Group show a wide range in composition – from basalt to andesite – and relatively high SiO₂ and Al₂O₃ contents, possibly due to mixing of epiclastic, reworked-weathered material with primary unaltered pyroclastic material, both of originally basaltic composition. Discrimination diagrams classify the Nebbi amphibolites as sub-alkaline basalts and andesites (Figs 4.31A–B), while an obvious calc-alkaline trend is seen for the amphibolites in the AFM diagram (Fig. 4.31C), setting them apart, on this diagram, from the other tholeiitic mafic rocks in

the WNB. However, on the Jensen cation diagram the single basalt sample plots in the Fe-tholeiite field (Fig. 4.31D). Positive correlation between increasing LREE fractionation and increasing silica content (Fig. 4.31E) supports an evolution from

the same parental magma for the amphibolites. A 'non-oceanic, within-plate' setting of the Nebbi amphibolites is indicated on geochemical discrimination diagrams (Figs 4.32B-C).

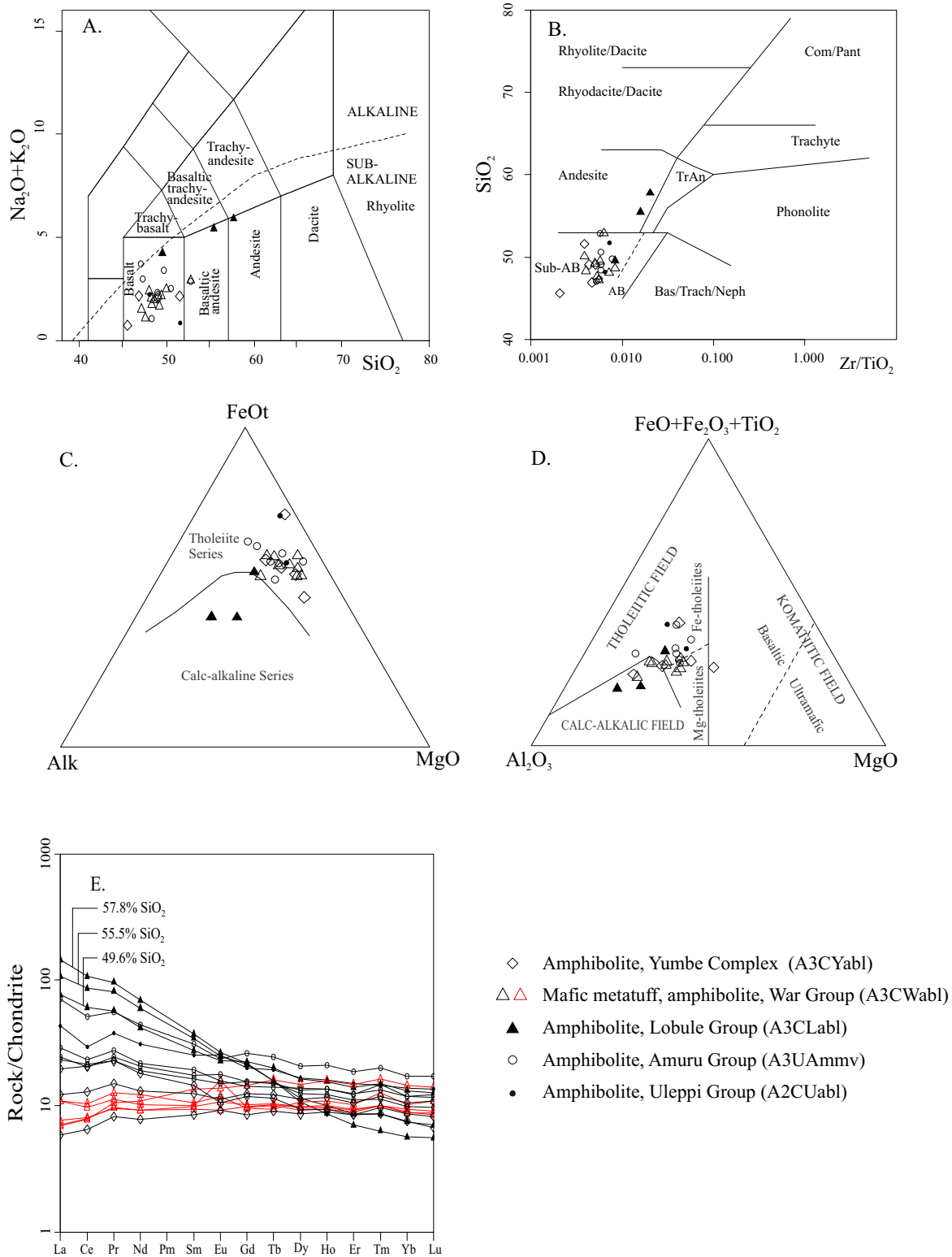


Fig. 4.31. Geochemical discrimination diagrams for metavolcanic rocks in the West Nile Block. (A) SiO₂-Alk plot by Le Bas et al. (1986), (B) Zr/TiO₂ vs. SiO₂ diagram by Winchester & Floyd (1977), (C) AFM diagram by Irvine & Baragar (1971), (D) Jensen (1976) cation plot, and (E) Chondrite-normalised REE distribution diagram, normalisation values from Nakamura (1974). Chemical analyses used in the diagrams are shown in Appendix 2.

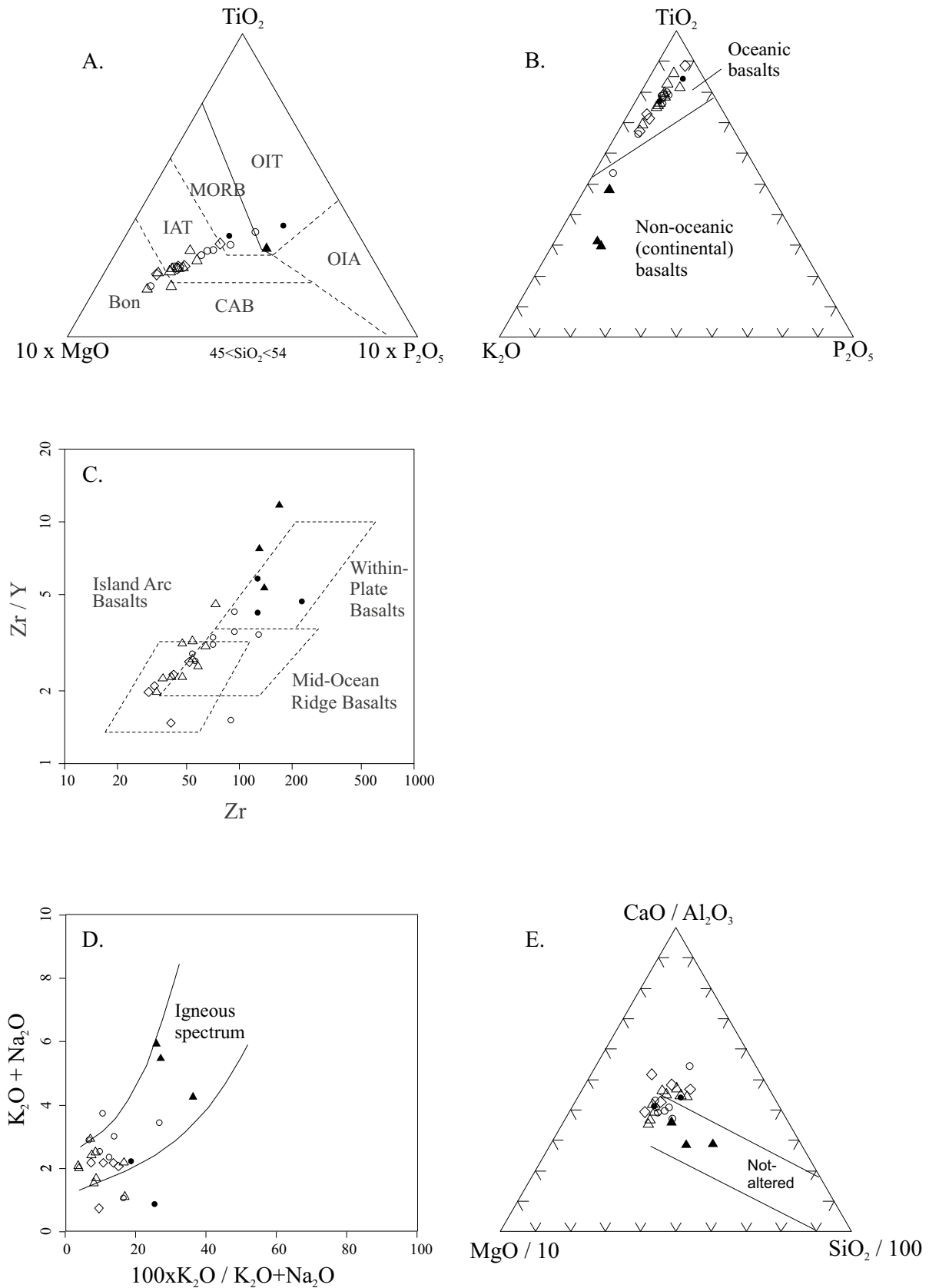


Fig. 4.32. Geochemical discrimination diagrams for metavolcanic rocks of the West Nile Block. (A-C) Diagrams discriminating tectonic setting: Mullen 1983 (A), Pearce et al. 1975 (B), Pearce & Norry 1979 (C). (D-E) diagrams discriminating chemical alteration: Hughes 1973 (D), Davies et al. 1978 (E). Key (A): OIT = Oceanic island tholeiite; MORB = Mid-Oceanic ridge basalt; IAT = Island arc tholeiite; CAB = Island arc calc-alkaline; OIA = Oceanic island alkali.

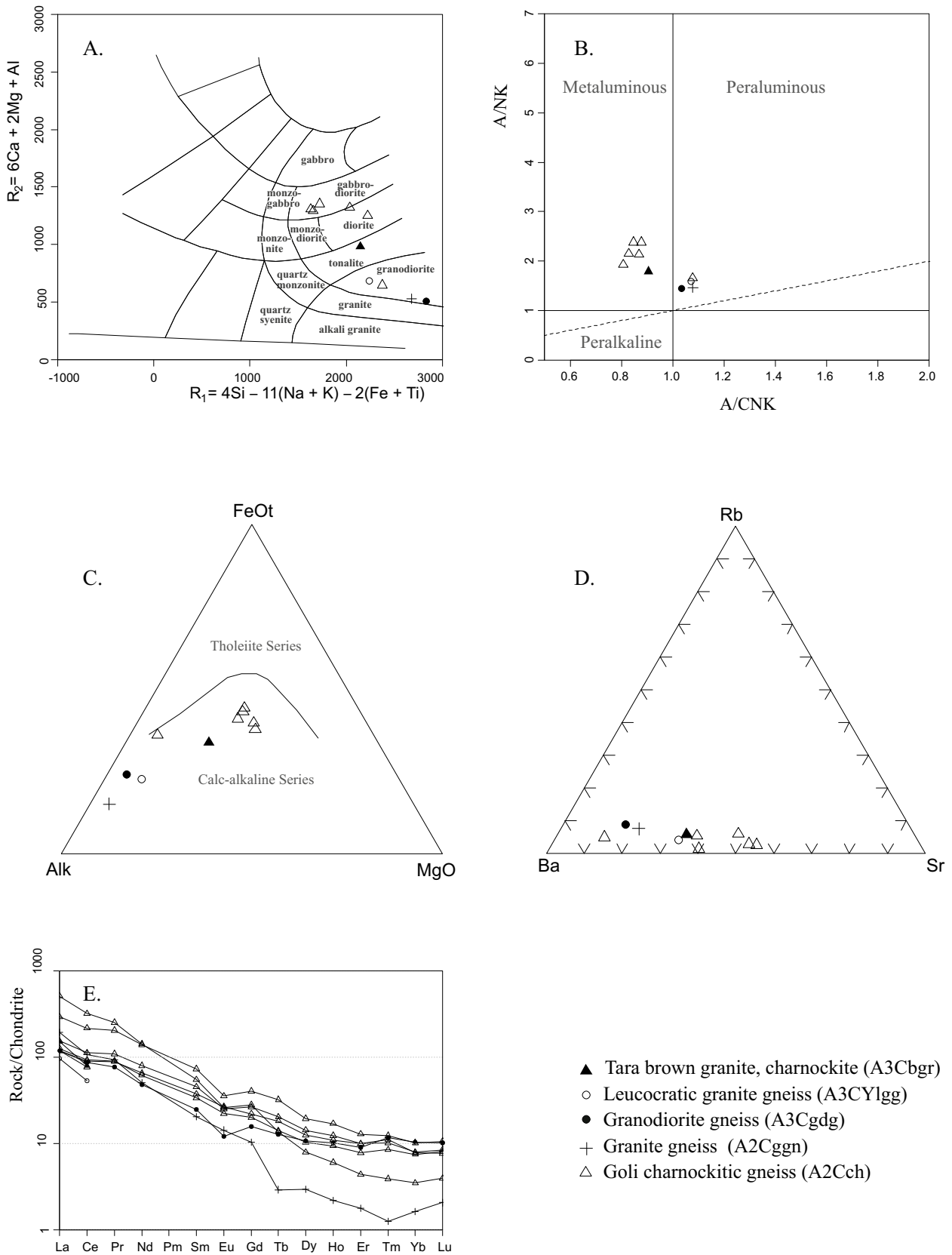


Fig. 4.33. Geochemical diagrams for granitoids. (A) R1R2 diagram (de la Roche et al. 1980), (B) A/CNK vs. A/NK diagram (Maniar & Picoli 1989), (C) AFM diagram (Irvine & Baragar 1971), (D) Ba-Rb-Sr ternary diagram, and (E) Chondrite-normalised REE distribution diagram, normalisation values from Nakamura (1974). Chemical analyses used in the diagrams are shown in Appendix 2.

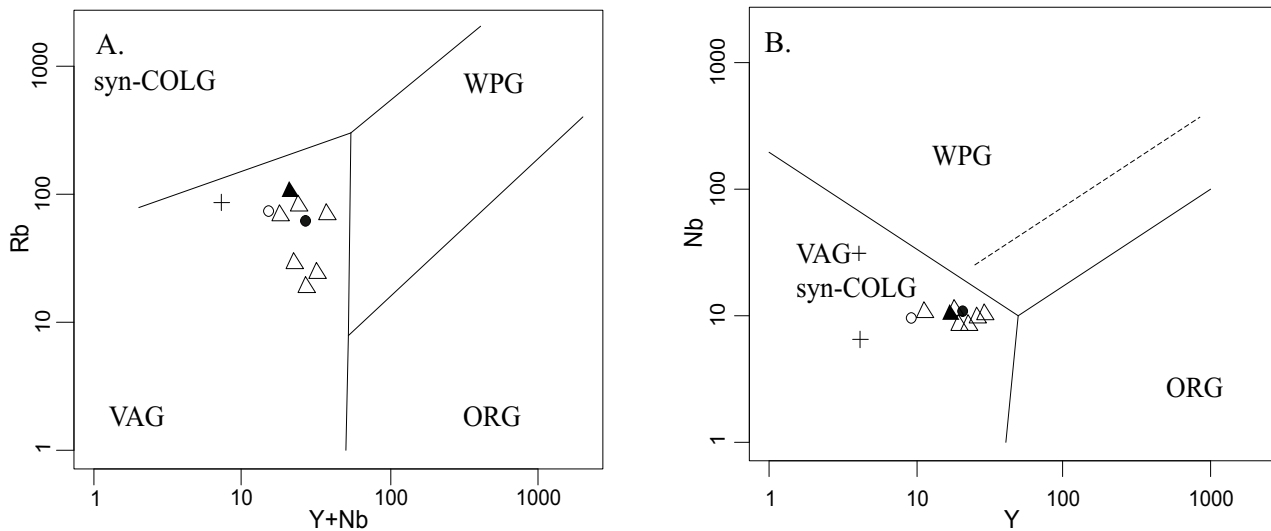


Fig. 4.34. (A-B). Petro-tectonic discrimination diagrams for granitoids (Pearce et al. 1984). Key: COLG = Collision granites; VAG = Volcanic arc granites; WPG = Within plate granites; ORG = Oceanic ridge granites. Symbols as in previous Figure.

Plutonic rocks of the WNB show a wide range of compositions, from granodiorite to tonalite to diorite to gabbro-diorite (Fig. 4.33A). They can be further characterised as meta- to peraluminous rocks (Fig. 4.33B) with calc-alkaline affinity. Goli charnockitic gneiss has relatively low silica contents (55.0–68.2 wt% SiO₂), sodium prevailing over potassium (3.6–3.9 wt% Na₂O and 1.0–3.0 wt% K₂O), and MgO and CaO contents that are often higher than in ‘normal’ granitic rocks. The gneisses classify as gabbro-diorite, diorite and granodiorite (Fig. 4.33A), having a peraluminous calc-alkaline affinity (Figs 4.33B-C). REE distributions of samples from the Goli charnockitic gneisses are all near similarly strongly fractionated and enriched in LREEs. The HREEs are moderately enriched with less fractionation than in the LREEs. A minor negative Eu anomaly is visible in the REE pattern of one of the samples. On the diagrams discriminating between the various magma-tectonic settings, the Goli gneisses plot in the fields of ‘volcanic arc granites’ (Fig. 4.34A) and ‘syncollisional + volcanic arc granites’ (Fig. 4.34B).

The single sample from the leucocratic granite gneiss of the Arua Complex classifies as calc-alkaline peraluminous granodiorite (Figs 4.33A-C). Petro-tectonic discrimination diagrams imply either a volcanic arc or syncollisional setting for this rock (Figs 4.34A-B).

A single sample from Tara brown granite (charnockite) of the Arua Complex plots near the border between the tonalite and diorite fields (Fig. 4.33A), being close to quartz monzonite. The silica content is relatively low (63.4% SiO₂) and the sample classifies as metaluminous and calc-alkaline on the diagrams evaluating alumina saturation. The Ba-Rb-Sr relations do not clearly distinguish the Tara charnockite from the other granitoids in the WNB. La and Ce concentrations of the Tara charnockite are clearly below the 100x chondrite values and levels of all other West Nile granitoids (La and Ce in Fig. 4.33E). A volcanic arc or syncollisional volcanic arc setting is suggested to the Tara brown granite by its plotting on petro-tectonic discrimination diagrams (Figs 4.34A-B). Representative chemical analyses of the afore-mentioned rocks are in Appendix 2.

4.9 Geochronology

Hepworth (1964) assumed that rocks of his Granulite Group (Fig. 4.2) formed the deepest lithostratigraphic unit in the West Nile Province of Uganda. Rb-Sr whole rock analyses of charnockitic granulites revealed ages of ~2.9 Ga, interpreted as the age of the oldest ‘Watian’ granulite-facies metamorphism (Table 4.1). Hepworth & Macdon-

ald (1966, Table 4.1) assumed, that the granulite episode was followed by the 2.59–2.52 Ga amphibolite facies ‘Aruan’ event, 1.0 Ga ‘Mirian’ and 0.65–0.55 Ga Chuan or Aswa event. Leggo (1974) produced the first U-Pb data for the WNB rocks, largely confirming the above scheme: Watian Granulites of the West Nile are the oldest rocks,

having been closed for their Rb-Sr system since 2.88 Ga, although a reactivation at about 2.55 Ga took place. This partial reactivation was associated with a widespread migmatitisation and emplacement of calc-alkaline granitic plutons. Further findings of Leggo (1974) included that the Mirian

gneisses of the West Nile, which rest unconformably on the older granitic gneisses, contain 950 Ma zircons. Modern U-Pb zircon and monazite dating by LA-ICP-MC/MS method has been carried out by GTK Consortium for selected samples (Mänttari 2014).

4.10 Tectono-Thermal Evolution of the West Nile Block

Traditionally, the West Nile Province was stratigraphically divided into a 'Western Grey Gneiss Group', a central 'Charnockite/Granulite Group' and an 'Eastern Grey Gneiss Group' (Fig. 4.2). Initially, these three groups were considered to be Archaean in age (Hepworth 1964; Macdonald 1963b, 1964a, 1964b, 1966), until Hepworth & Macdonald (1966) and later Leggo et al. (1971) and Leggo (1974) reported ~1.0 Ga detrital zircons in rocks of the Eastern Gneiss Group.

In light of the new data collected by the GTK Consortium, in particular the new age determinations (Mänttari 2014), and re-evaluation of the previously published data, the former three-fold subdivision of the WNB is clearly invalid and is here abolished. As shown by the age data summarised in Figure 4.3, the rocks in the WNB record a prolonged Archaean tectono-thermal evolution (> 3.08–2.55 Ga), followed by phases of crustal reactivation during the late Mesoproterozoic Grenvillian (at ~1.0 Ga) and Neoproterozoic (~0.66 Ga) Pan-African Cycles. No evidence of tectono-metamorphic overprinting that could be related to the Palaeoproterozoic Eburnean Orogenic Cycle (2.1–1.85 Ga), recorded by the Rwenzori Belt (and its southward Rusizian and Ubendian continuation; Chapter 6) in central and southwestern Uganda, was identified in the crystalline basement of the WNB.

In the section below we will discuss the Archaean tectono-thermal evolution of the WNB. Subsequent remobilisation during the late Mesoproterozoic 'Mirian' event (Table 4.1), resulting in development of the newly identified Madi-Igisi Belt, will be discussed in Chapter 9. Neoproterozoic 'Chuan' or 'Aswa' events (Table 4.1) in the WNB, including remobilisation of the Madi-Igisi Belt and emplacement of the Pan-African Midigo granite (Midigo-Adjumani Suite), are discussed in Chapter 11.

Watian granulites – A major reassessment concerning the geology of the southern part of the

WNB is related to the status of the so-called 'Watian' granulites and charnockites, which are traditionally all included in the Granulite Group (Fig. 4.2).

Granulitic rock types in the Watian suite comprise a variety of sub-types, all supposedly derived from sedimentary protoliths. These granulites are associated with and invaded by felsic, intermediate and basic charnockites and enderbites (= hypersthene-bearing tonalite). The granulite sub-types include hypersthene granulites or acid charnockites, banded granulites and charnockitic agmatites. The latter consist of angular blocks of dioritic charnockite suspended in a pegmatoid matrix in which coarse, bronze-coloured hypersthene grains are prominent. The early high grade and younger extensive retrograde metamorphic events, together with the associated metasomatic and anatexis processes, have almost entirely obscured any primary features of the sedimentary protoliths.

The new U-Pb zircon ages demonstrate a strong age difference between the southern (S of 3°N in Fig. 4.2) and northern (N of 3°N in Fig. 4.2) 'Watian' granulite grade rocks, as the former seem c. 400 Ma older than the latter. Consequently, we abandoned the term 'Watian' as irrelevant. Instead we distinguished two tectono-thermal terranes in the WNB: the Mesoarchaeon (~3.08 Ga) *Uleppi Complex* (tectonic) and Neoproterozoic (> 2.63–2.62 Ga) *Arua-Kibale Complex* (Fig. 4.3). Both complexes show a similar though diachronous tectono-thermal development, involving early granulite facies conditions followed by widespread high-grade amphibolite facies retrogradation.

Hepworth (1964) reported extensively on the disequilibrium features produced by the retrograde metamorphism. These include exsolution features such as hematite staining in all the other minerals, hornblende inclusions in feldspar, 'hair perthite' in microcline and anti-perthitic plagioclase and, finally, rutile needles and small prisms in quartz. In places, hypersthene is altered into biotite with concomitant release of hematite. Else-

where, hypersthene with resorption borders is being replaced by diopside or by a granular aggregates composed of diopside, K-feldspar, quartz, (more acid?) plagioclase, Fe-oxide, garnet and some hornblende. Primary clinopyroxene may be altered into hornblende, secondary diopside and plagioclase. Essential reactions that were active during retrograde metamorphism may be represented by the schematic partial reactions listed below:

- hypersthene + Ca (from plagioclase) → garnet + quartz
- hypersthene + Ca (from plagioclase) → secondary diopside + Fe oxide
- secondary diopside + sodic plagioclase → hornblende
- hypersthene + K (from microcline or metasomatic?) → biotite

Schenk et al. (2005) have performed petrological studies in the area mapped by Hepworth (1964) and Macdonald (1964b) as 'Watian granulites' as well as in the adjoining 'Aruan amphibolite-facies migmatites'. They focused on the oldest Archaean granulite-facies rocks, in an effort to unravel the relationship between crust formation and geodynamic causes of the granulite-facies metamorphism. The most striking feature they reported is the omnipresence of garnet + clinopyroxene ± quartz coronas around orthopyroxene in a wide range of mafic to charnockitic rocks. This texture characterises the transition from medium-pressure to high-pressure granulites and is usually attributed to near-isobaric cooling of crust of normal thickness that was heated by magmatic loading or underplating (Schenk et al. 2005). In contrast, a rare metapelitic intercalation in the 'Watian granulites' (NW of Mt. Luku, ~15 km SE of Arua town), displays a complex metamorphic history (Schenk et al. 2005):

- (1) an early prograde metamorphic stage, which attained anatexis temperatures and was characterised by a garnet + sillimanite + cordierite + biotite + liquid assemblage;
- (2) a subsequent event of pressure (and possibly also temperature) increase that led to the breakdown of cordierite to kyanite/sillimanite-orthopyroxene symplectites (UHT-stage) and an associated second stage of garnet growth enclosing kyanite; and

- (3) a late, retrograde decompression stage that is characterised by the formation of cordierite coronas replacing garnet.

In summary, the metapelitic rock from Mt. Luku records a dramatic crustal thickening event that affected the high-grade Archaean rocks and that was followed by an orogenic collapse leading to the uplift of the high-grade lower crustal rocks. Ongoing research by the team of the University of Kiel in Germany is aimed at dating this orogenic event (collapse) with CHIME on monazites and to correlate the metamorphic evolution recorded by the metapelite with that of the orthogneisses and metabasites described above.

Possible time-integrated tectono-thermal scenario – Based on the limited number of reliable U-Pb zircon ages, discussed above, and existing petrographic, geochemical and structural data, we propose for the WNB the following time-integrated geodynamic scenario:

- Prior to 3.08 Ga: Creation of protoliths to the Mesoarchaean crustal element, presently known as Uleppi Complex, to comprise rocks of both ortho- and para-derivation.
- At around 3.08 Ga: Deep burial, and emplacement of the Goli charnockites followed by a phase of metamorphism and deformation under conditions ranging from those of granulite to high-amphibolite facies with temperature peaking between ~3.00 Ga and 2.87 Ga, presumably in a deep suprasubduction setting.
- At around 2.63 Ga: Emplacement of banded volcanic and sub-volcanic mafic rocks of the War Group on top and into the Uleppi Complex that concurrently experienced a widespread retrogradation under amphibolite facies conditions. The mafic rocks in the War Group have an 'oceanic basalt' or 'island arc tholeiite' signature and may represent an accreted and overthrust island arc assemblage, whereas the War metasediments may represent fragments of the accretionary wedge.
- At 2.63–2.62 Ga: Formation of the Neoarchaean juvenile crust of the Arua Complex, involving emplacement of protoliths of the 2.62 Ga mafic gneisses of the Lobule Group and their invasion by the 2.62 Ga charnockitic Tara brown granites. Rocks spatially associated with the Tara brown granite suffered metamorphism ranging from

granulite to amphibolite facies conditions. Note that the Lobule mafic gneisses and amphibolites have a 'within plate' or 'continental' geochemical signature.

- At around 2.63–2.62 Ga: Broadly simultaneous accretion of the War Group island arc and accretionary wedge rocks and collision of the Mesoarchaeon Uleppi and Neoarchaeon Arua Complexes.
- At around 2.59–2.55 Ga: The accretion event was followed by a second dynamo-thermal event at around 2.59–2.55 Ga (the 'Aruan event' in Table 4.1). Provisionally we relate this to collision of the WNB, or the eastern segment of the Bomu-Kibalian Shield, with the North Uganda Terrane or, alternatively, with the Lake Victoria and West Tanzania Terranes of the Tanzania Craton.

5 ROCKS OF THE NORTH UGANDA TERRANE

5.1 Introduction

Approximately 60% of the northern territory of Uganda is underlain by crystalline rocks, formerly attributed to the Archaean ‘Basement Complex’ (Fig. 3.1). This unit included the entire Archaean basement of Uganda, except the granitoids and greenstones of the Lake Victoria Terrane, which had been attributed to the Tanzania Craton and so-called ‘Watian’ granulites, charnockites and ‘Aruan’ rocks (Table 4.1) (Macdonald 1964a,b, Hepworth & Macdonald 1966).

The ‘North Uganda Terrane’ (NUT) comprises the northern part of the former ‘Basement Complex’ (Fig. 3.2). It is separated by a major mid-crustal pre-2.6 Ga dislocation from the West Tanzania Terrane (Chapter 3), by the ~1.0 Ga Madi-Igisi Belt (Chapter 9) from the West Nile Block (Chapter 4)

and bounded by Neoproterozoic Pan-African fold belts in the north and east (Chapter 11).

Traditionally, the NUT has been considered as part of the Congo Craton (Schlüter 1997) or, more precisely, part of the Bomu-Kibalian Shield (or NE Congo-Uganda Block; Fig. 1.6). Petters (1991), who studied the ‘West Nile Gneissic Complex’, also stressed continuity from northern Uganda into the West Nile Province and into NE Congo, southern Sudan and the Central African Republic. Assuming that the Madi-Igisi Belt (Chapter 9) is an intracratonic thrust/ fold belt, we support the idea expressed by the above authors, although we cannot exclude the hypothesis that the latter belt is superposed on an older ‘suture’.

5.2 Tectono-Thermal Domains of the North Uganda Terrane

Compared to the simplified geological map compiled by Macdonald (DGSM 1966), the area covered by Archaean crystalline basement has been reduced significantly. Modern U-Pb zircon data by the GTK Consortium (Mänttari 2014) indicate that allegedly Archaean ‘Watian’ granulites/charnockites in eastern Uganda (Fig. 3.1) are not Archaean but Neoproterozoic in age and that the area underlain by such rocks is more extensive (Mäkitie et al. 2011b, 2014b). The new geochronological data furthermore highlight the presence of Pan-African allochthonous thrust masses and *in situ* granitoids in areas hitherto considered as the Archaean ‘Basement Complex’ (Fig. 3.2).

Like the West Nile Block (Chapter 4), the NUT comprises both Meso- and Neoproterozoic rocks. Consequently, the following major building blocks have been defined in the North Uganda Terrane:

- The Karuma Complex, a Mesoarchaeo phase of crust formation, mainly composed of granulite-grade metasediments;
- Neoproterozoic rocks of the North Uganda Terrane, divided into five supracrustal rock units of the Amuru Group and into 22 rock units of deformed granitoids, gneisses and migmatites of igneous or uncertain origin (Figs 5.1 and 5.2).

5.3 Geology of the Mesoarchaeo Karuma Group of the North Uganda Terrane

The rocks of the Karuma Complex are assigned to the Mesoarchaeo Karuma Group, composed of granulites and occupying a SW-NE-trending belt, southeast of the Neogene Albertine Rift and north of Hoima and Masindi. The belt measures ca. 150 km by 25–50 km and is covered along its SE contact by rocks of the Neoproterozoic Bunyoro Group (Fig. 5.1).

High-grade hypersthene-bearing rocks in the Bunyoro district were first described by Sim-

mons (1921) and Wayland (1921b). Detailed petrological investigations of the Masindi granulites were carried out by Watkins (1956). Granulites predominate in the northern part of the Hoima-Masindi districts. Migmatites and granitoids are more abundant in the southern part (van Straaten 1971, 1973, 1976). We have divided the Karuma Group into mafic and felsic granulites.

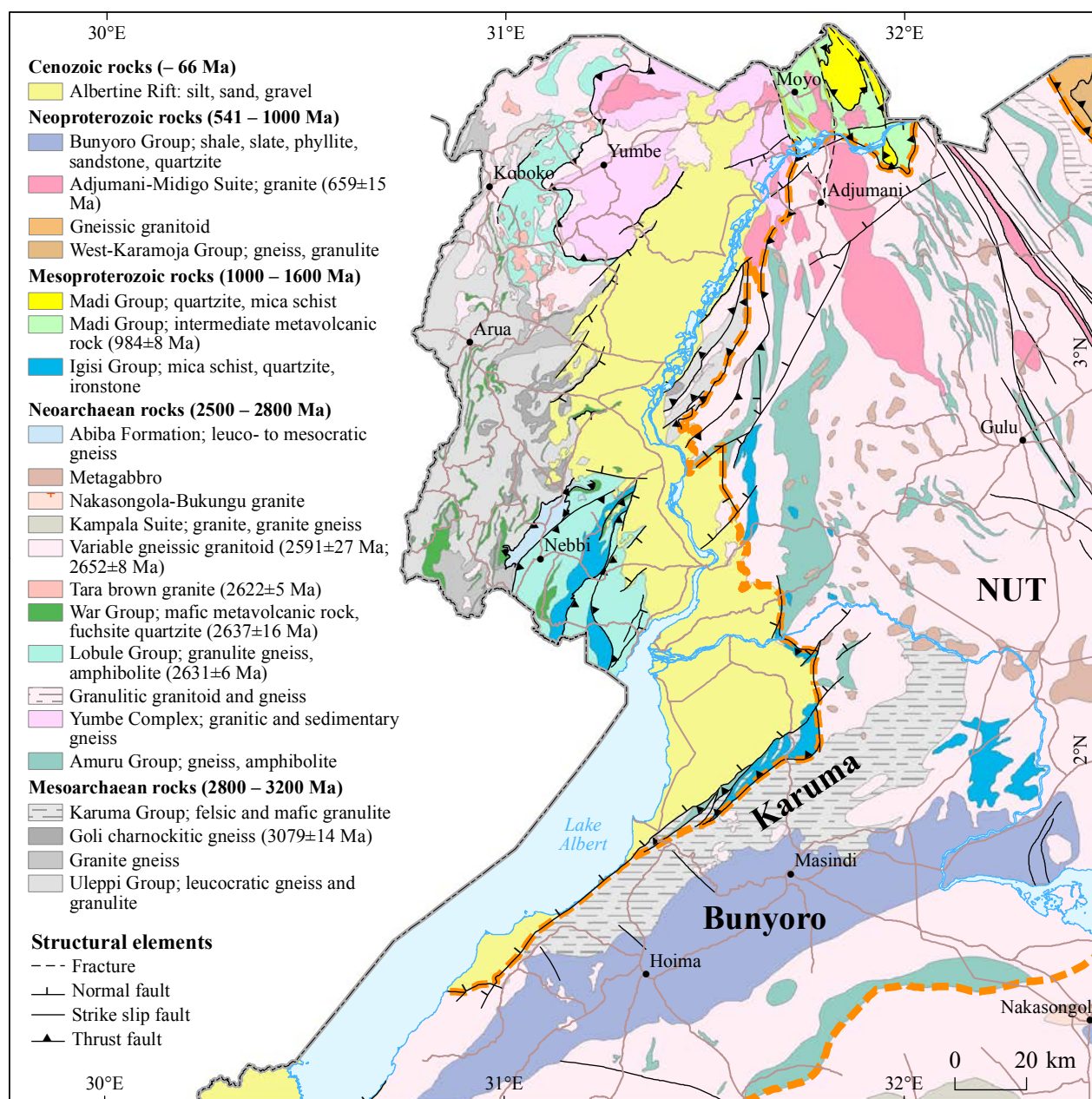


Fig. 5.1. Geological outline of the western part of the North Uganda Terrane (NUT, border indicated by orange dashed line), showing the Mesoarchaean Karuma Group and the discordantly overlying Neoproterozoic Bunyoro Group.

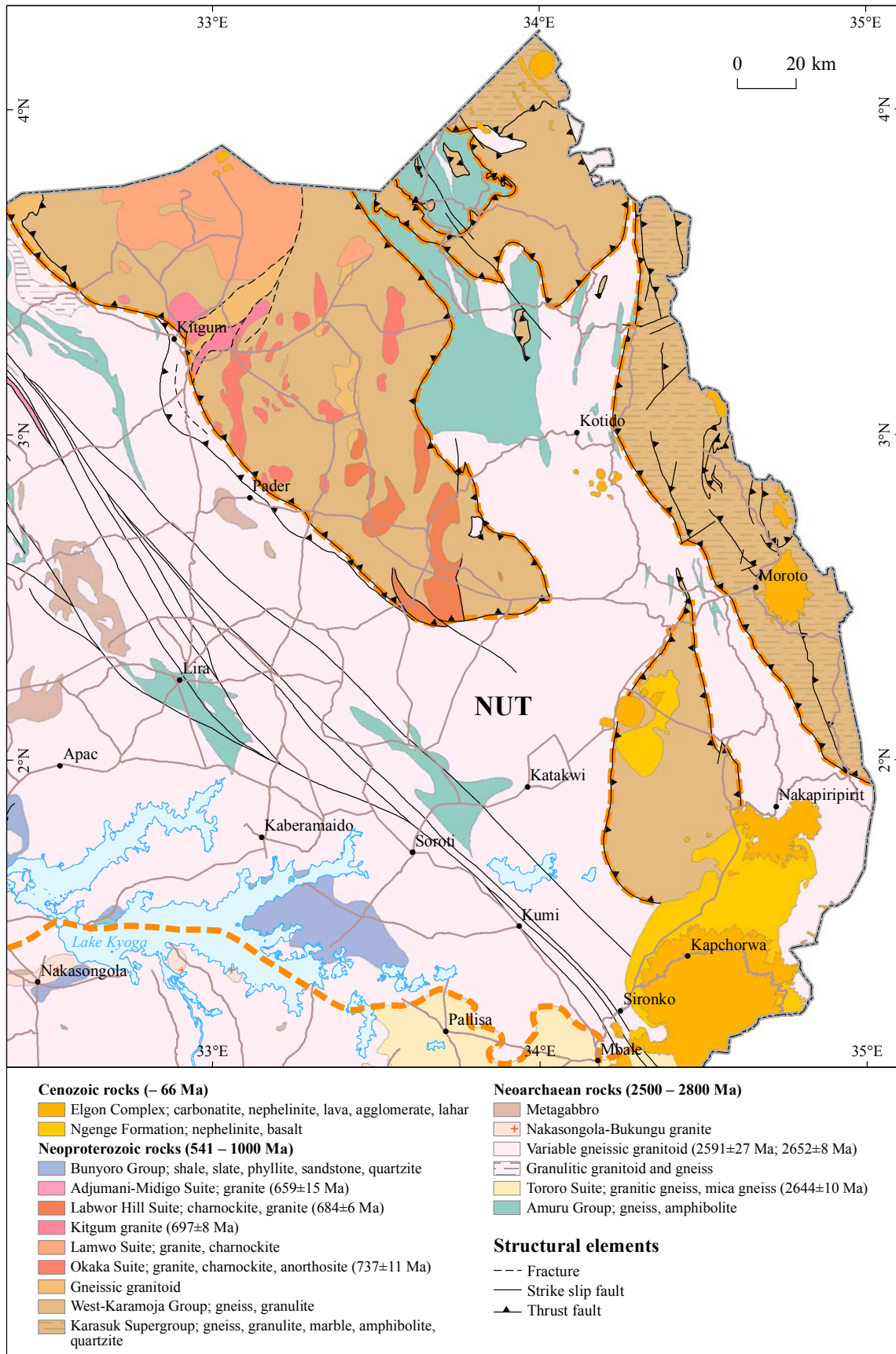


Fig. 5.2. Eastern segment of the North Uganda Terrane (NUT), tectonically overlain by Pan-African thrust masses of the Karasuk Supergroup and West Karamoja Group, East African Orogen. The NUT is separated by an orange dotted line from the Pan-African thrust rocks. This part of the NUT is further discordantly covered by rocks of the Neoproterozoic Bunyoro Group and by Cenozoic rocks of the alkaline Elgon Complex and the Ngenge Formation (EARS). The Aswa shear zone (ASZ) runs NW–SE from east of Moyo to Lira to Mbale.

Mafic granulite (A2UKmg1) – Mafic granulites of Karuma Group (Fig. 5.1) are exposed in the Bugungu Wildlife Reserve and surroundings, south of Murchinson Falls National Park (van Straaten 1976). The rock is dense, black to dark green, medium-grained and equigranular with characteristic brown weathering surfaces. Mafic granulites exist as elongated, centimetres- to metres-thick NE–SW-trending interlayers in felsic granulites. The main minerals are plagioclase (An_{40-60}), ortho- and clinopyroxene, hornblende and garnet. Rutile, apatite, quartz and opaque minerals are common minor or accessory constituents. According to van Straaten (1976), these dry, high-grade regional metamorphic rocks have been derived from mafic tuff precursors.

Banded, granoblastic granulites in the northern part of the Hoima-Masindi area are characterised by an alternation of millimetre- to centimetre-scale, coarse-grained dark and light-coloured bands. Major rock components are quartz, plagioclase (An_{30}), alkali feldspar (hair perthites), hypersthene, biotite, \pm garnet.

Felsic granulite (2991 \pm 9 Ma) (A2UKfg1) – Felsic granulites of the extensive Karuma Complex are high-grade metamorphic gneisses with usually less than 30 vol% unhydrous Fe-Mg silicates. U-Pb zircon data indicate an age of 2.99 Ga for peak metamorphism of this unit (Mänttari 2014). These are vaguely banded rocks, granitic to granodioritic in composition, comprising relicts of amphibolite in places. Fresh surfaces usually show dark grey colours with greenish to brownish shades (Fig. 5.3A), while on weathered surfaces these rocks show a hint of rusty tints. Intense partial dehydration

melting is manifested, for example, by diatexitic gneisses comprising some relict mafic metavolcanic proportions. Fractures, suggesting brittle deformation, appear as networks filled by quartz and carbonate and can be observed near the boundary fault with the Lake Albert Rift Valley. Moreover, pegmatite dykes are most common in these areas. In addition, some deformed pyroxene-bearing granitoids, which resemble heterogeneous charnockites, are located in the same area.

In addition to Fe-Mg silicates, K-feldspar (with hair perthitic intergrowth), plagioclase (partly saussuritised, antiperthitic) and quartz are usually the main minerals in the granulites. Orthopyroxene is the most common mafic mineral, often partly replaced by retrograde amphibole and chlorite. Biotite (0–10 vol%) is also of retrogressive origin. Other, high-grade minerals are garnet and cordierite (Fig. 5.3B).

A relatively homogeneous, medium-grained pyroxene-bearing granulite (Fig. 5.3) is composed of plagioclase (55 vol%), quartz (20 vol%), orthopyroxene (15 vol%) and K-feldspar (5 vol%). Cordierite- and orthopyroxene-bearing granulites occur nearby. Assuming both minerals are in equilibrium, these cordierite-orthopyroxene pairs refer to granulite-grade metamorphic conditions with temperatures of over 700°C. Biotite in these gneisses has very reddish pleochroic colours – also indicative of high-grade metamorphic P-T conditions. The cordierite-bearing granulites are relatively Al-rich and obviously have a sedimentary protolith, as confirmed by interlayered concordant graphite-bearing quartzite bands, up to one metre wide (e.g., near Lukohe Hill, van Straaten 1976).

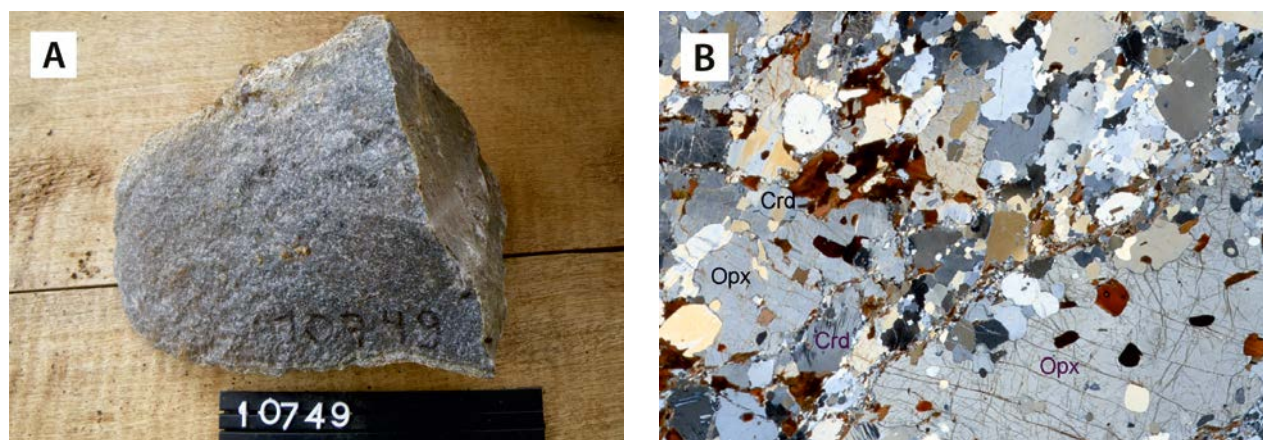


Fig. 5.3. (A) Relatively homogeneous, typical orthopyroxene-bearing granulite, resembling a metamorphosed tonalite (356988E / 209633N). Number tag 15 cm. (B) Microphotograph of a cordierite (Crd)-orthopyroxene (Opx) pair in the same granulite. Also note micro-shears (e.g., upper contact opx porphyroblast) with very fine-grained retrograde biotite. Cross-polarised light. Width of the image is 3 mm.

5.4 Geology of the Neoproterozoic Amuru Group of the North Uganda Terrane

Table 5.1. Subdivision of the Amuru Group of the Neoproterozoic North Uganda Terrane. The abbreviations in the column to the right are used in geological maps at the scales 1:250 000, 1:100 000 and 1:50 000, available at the DGSM, Entebbe.

| Amuru Group | | | |
|-------------|---------------------|---------------------------------------|----------|
| | Banya Formation | Mafic metavolcanic rock, amphibolite | A3UAmv |
| | Paludar Formation | Biotite gneiss, migmatic | A3UAbpg |
| | Pongwongo Formation | Biotite-hornblende gneiss | A3UAbhgn |
| | Kinaga Formation | Quartzite, fuchsite-bearing in places | A3UAqz |
| | Okile Formation | Quartz-feldspar gneiss | A3UAqfg |

Neoproterozoic supracrustal rocks of the North Uganda Terrane (NUT) have been divided into the Amuru Group and into 22 different lithodemic units of deformed granitoids, gneisses and migmatites of igneous or of uncertain origin (Figs 5.1 and 5.2).

The heterogeneous succession of Neoproterozoic supracrustal rocks, assigned to the Amuru Group, form elongated, generally north to north-west trending belts in various parts of the North Uganda Terrane. Quartz-feldspar gneisses of the *Okile Formation* are well exposed southeast of Lira town and in the area southwest of Kyoga lake. Thin layers of fuchsite-bearing quartzites of the *Kinaga Formation* parallel the Aswa Shear Zone, while separate quartzite outcrops, which possibly represent remnants of ancient, more extensive quartzite horizon, occur within a large granitoid area southwest of Kyoga lake. Biotite-hornblende gneisses of the *Pongwongo Formation* are rather well-exposed around and SE of Lira town, east of the ASZ. Similar biotite-hornblende gneisses form elongated belts east and north of Gulu town, and also parallel the Albertine rift in the west. The gneiss area

located north of Kotido town in the NE corner of the NUT, also tentatively attributed to this Formation, is only poorly known. The narrow, NE trending belt of biotite gneisses and migmatites of the *Paludar Formation* are reasonably well exposed east of ASZ, while the gneiss area NW of Kotido was also included into the Paludar Formation without field verification. With the exception of mafic metatuffs, which form the prominent Asamuk hill NNE of Soroti town, metavolcanic rocks and amphibolites attributed to the *Banya Formation* are often rather poorly exposed. The strong, negative signature generally associated with these mafic rocks on the airborne radiometric maps contributes the mapping of these rock units in the largely soil or laterite covered area SE and NNW of Gulu town.

Quartz-feldspar gneiss (A3UAqfg) – Various deformed and migmatized quartz-feldspathic gneisses, assigned here to the Okile Formation after a village located SE of Lira town, occur in the central and eastern NUT. Due to the abundance of fine-grained magnetite, these rocks have a high

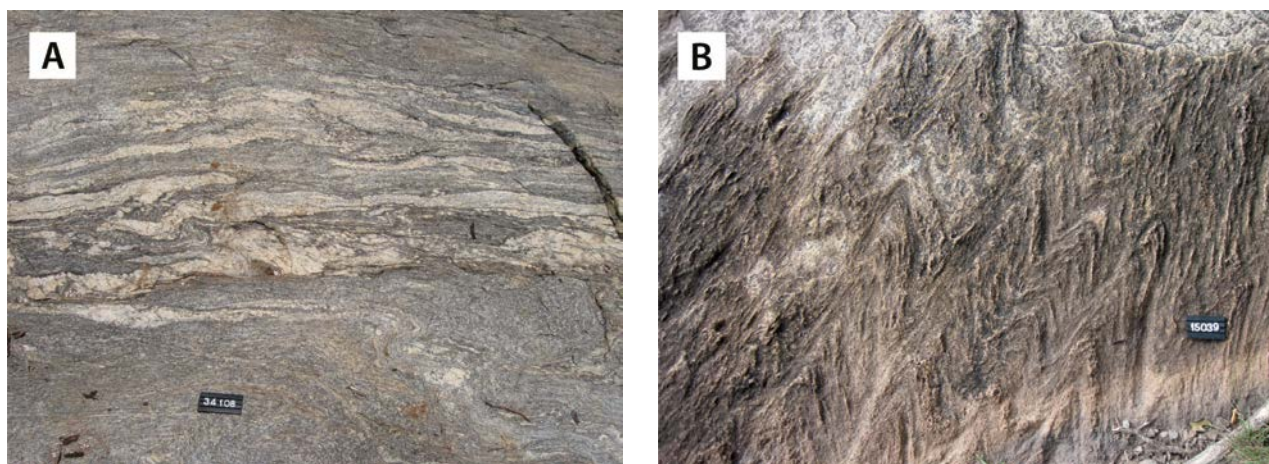


Fig. 5.4. (A) Moderately deformed, micaceous quartz-feldspar gneiss of the Okile Formation, injected by deformed pegmatitic veins (498877E / 240351N). (B) Strongly deformed quartz-feldspar gneiss with chevron-type folds (353544E / 130902N). Number tag 8 cm.

magnetic susceptibility and they often correlate with positive anomalies on the aeromagnetic maps (see Geological map of Uganda, 1:1M).

A distinct banding, probably representing primary bedding, can be observed on weathering surfaces. Elsewhere, banding is of metamorphic origin. Locally, this slightly micaceous gneiss variety has been injected by thin pegmatitic segregation veins (Fig. 5.4A). These quartzo-feldspathic rocks are supposedly derived from arkosic and (micaceous) sub-arkosic sandstone protoliths. Chemical composition of this rock is shown in Appendix 2 (anal. 92).

Similar quartz feldspar gneisses occur in the Masindi area, where the banding consists of segregated quartz feldspar leucosomes, which show open to tight or chevron-type folding (Fig. 5.4B).

Quartzite, fuchsite-bearing in places (A3UAqz)
– Despite strong deformation, quartzites in the

Kinaga Formation generally show an obscure banding, interpreted as sedimentary bedding. The yellowish brown, fine-grained quartzite forms low ridges, e.g., parallel to the Aswa Shear Zone in the central sector of the NUT, where strongly foliated and jointed, pure, steeply west-dipping quartzite is over 250 m thick (Fig. 5.5A). A pale greenish tint of this rock unit is caused by small amounts of fuchsite. Micaceous quartzite is further exposed in a number of aggregate quarries about 6 km NW of Kitgum town. This yellowish, pinkish or bluish green, vaguely banded quartzite contains sparsely disseminated fine-grained pyrite as shown by typical weathering colours in Figure 5.5B.

Primary sedimentary structures are generally lacking in quartzites exposed in the Hoima-Masindi area, and undoubtedly some of these quartzite bodies may represent recrystallised quartz dykes. The highest quartzite ridge, located 25 km SE of



Fig. 5.5. (A) Strongly foliated, fuchsite-bearing quartzite west of the Achwa River (426853E / 359355N). (B) Micaceous, vaguely banded quartzite in an aggregate quarry, ~6 km NW of Kitgum town (481483E / 367175N). Number tag 10/15 cm.



Fig. 5.6. (A) View from a 100 m high quartzite ridge, located 25 km SE of Hoima town (335340E / 139054N). (B) Orthoquartzite with quartz-sillimanite nodules on the northwestern foot of Mt. Kadam (678805E / 204584N). Number tag 8 cm.

Hoima town, is composed of irregular blocks of quartzite (Fig. 5.6A), which comprise cavities filled by almost euhedral quartz crystals. Quartzite ridges are often spatially associated with pelitic and amphibolitic gneisses, suggesting a sedimentary origin.

In the Mbale area, quartzite occurs as yellowish brown, foliated quartzite, which forms a ca. 100-m-wide, north-trending block field along the northwestern foot of Mt. Kadam. Occasional laminae of amphibole or roundish quartz-sillimanite nodules (Fig. 5.6B) occur in almost pure orthoquartzite. A similar thin, north-trending band of quartzite, up to 7 km in length, was described by Trendall (1961b) in the area NW of the Kokipie volcano at the Kenyan border.

Biotite-hornblende gneiss (A3UAbhgn) – This poorly exposed, complex and variegated family of biotite- to hornblende-bearing gneisses assigned to the Pongwongo Formation comprises a multi-

tude of areas throughout the NUT. Their delineation is mainly based on analysis of aerogeophysical maps (Ruotoistenmäki et al. 2014) and areas assigned to this unit often contain also other rock types. The essential components reflect an original volcano-sedimentary protolith, although often mixed with later magmatic material on outcrop and larger scales. The lithological variation of micaceous, hornblende-bearing gneisses of the Pongwongo Formation is shown in Figures 5.7A-D and three whole-rock analyses are in Appendix 2 (anal. 93–95).

Banded biotite-hornblende gneiss of the Pongwongo Formation, interpreted as volcanic in origin, is particularly well exposed in a quarry near the university campus in Gulu town. The rock is not exposed at the surface, but covered by brown soil with a sharp weathering front (Fig. 5.8A). As before, the rock is composed of alternating bands and laminae of dark grey, grey and white colour. The white bands were mechanically more compe-

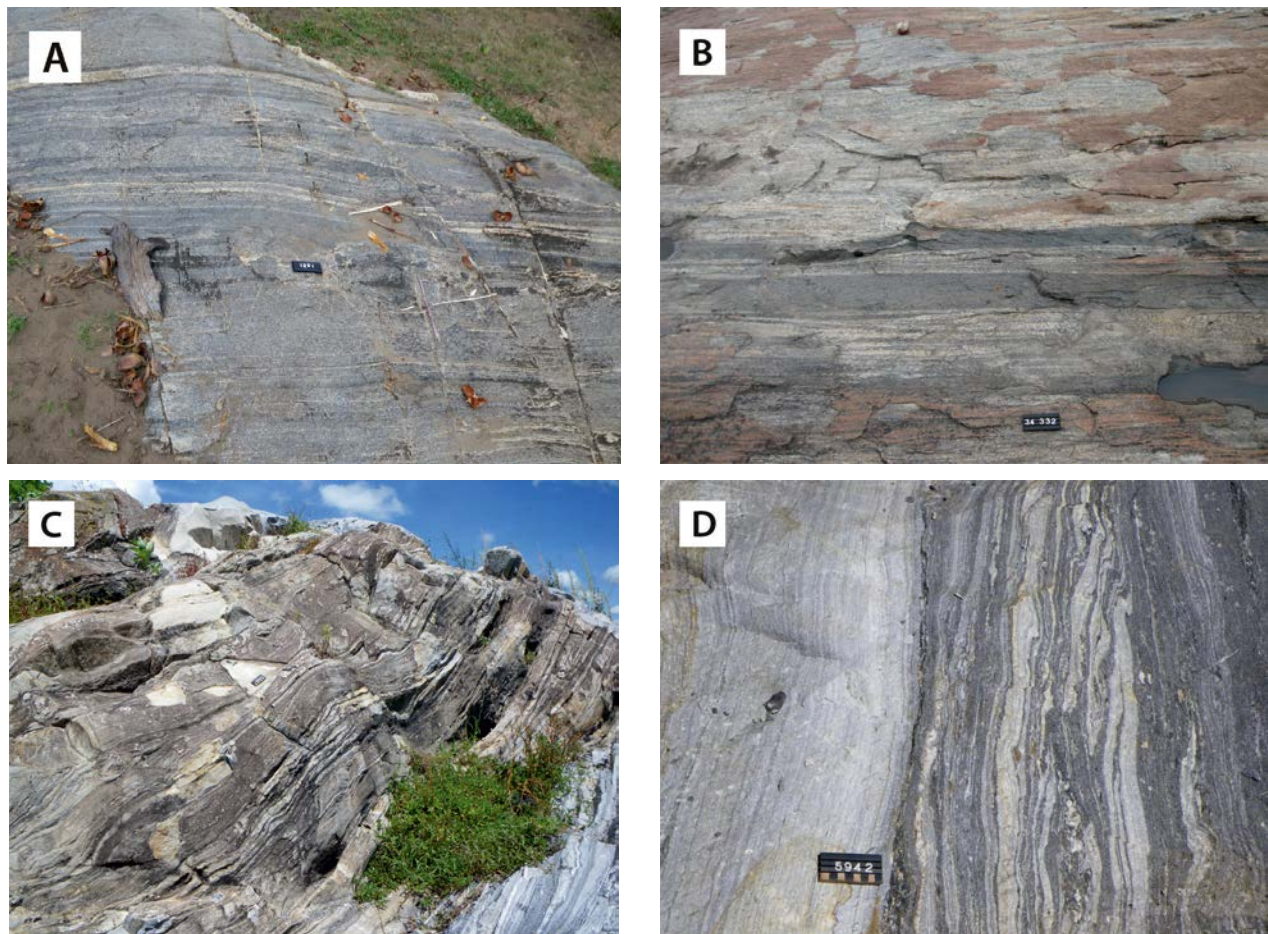


Fig. 5.7. Different banded structures of the Pongwongo Formation. (A) Banded grey to light grey rock with occasional felsic layers (350667E / 361217N). (B) Grey biotite gneiss, with a dark grey hornblende-bearing band (389018E / 354840N). The origin is possibly a mafic-felsic volcanic association. (C) A set of mafic and felsic bands, probably representing alternating layers of sedimentary and volcanogenic material (431216E / 311422N). (D) Detailed image of the same rock. Number tag 8 cm.

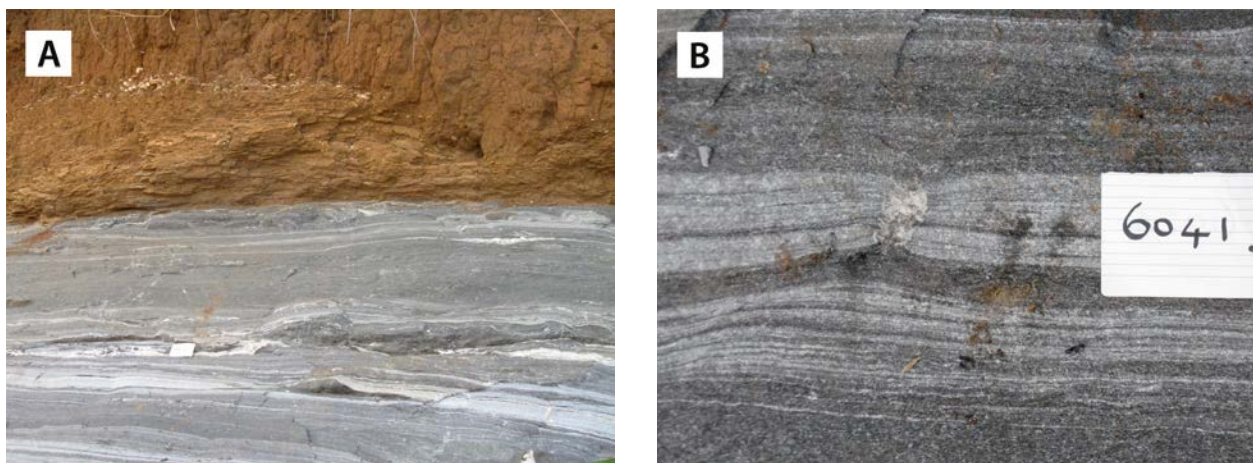


Fig. 5.8. (A) Biotite-hornblende gneiss of the Pongwongo Formation, covered by chocolate-brown soil. A large quarry ~3.5 km NE of Gulu town (424800E / 308884N). (B) Detailed image of the same gneiss, showing necking due to differential compaction or strain, also resulting in neoformation of coarse minerals in the pressure shadow. Number plate 10 cm.

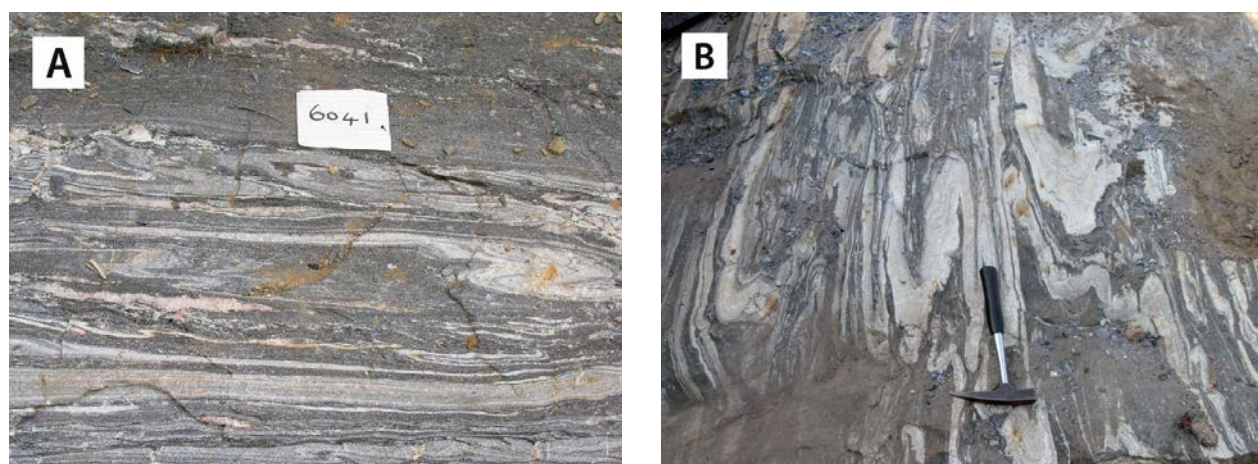


Fig. 5.9. Examples of fold structures and compositional banding in the biotite-hornblende gneiss. (A) Individual layers or laminae are discontinuous or change rapidly in thickness over short distances. (B) Thickening in hinge zones and thinning in flanks of microfolds. Large quarry ~3.5 km NE of Gulu town (424800E / 308884N). Number plate 10 cm, length of hammer 30 cm.

tent and show necking and boudinage. Neoformation of coarse crystals of carbonate, pyrite, quartz, mica and amphibole have taken place in the pressure shadows between the boudins or in pull-apart fractures (Fig. 5.8B). Fold styles of the gneiss range here from isoclinal, intrafolial to box folds and disharmonic folds (Figs 5.9A-B).

Biotite gneiss, migmatitic (A3UAbpg) – Migmatitic biotite gneiss of the Paludar Formation is a part of a ca. 110-km-long, NW–SE-trending, narrow zone east of Aswa Shear Zone in the Kitgum-Gulu area, and also found to the south of Masindi town. This foliated gneiss shows fine-grained, dark, biotite-rich layers alternating with felsic layers, between 0.3 and 6 cm wide (Fig. 5.10A). In places, overturned fold structures are prominent in this gneiss

(Fig. 5.10B). This folded sub-type contains abundant K-feldspar porphyroblasts of 1–3 cm in size, while quartz typically appears as ≤5 mm grains.

The texture of the biotite gneiss is migmatitic in places (Fig. 5.11A). Plagioclase, K-feldspar, biotite and quartz are the main minerals together with subordinate cordierite. Locally, also narrow hornblende-bearing layers occur in the Paludar biotite gneiss.

In eastern Uganda, this unit closely follows the banded acid biotite gneisses in the existing DGSM map ‘*Geology of Karamoja*’. It is also widespread in the Kaabong area (excluded from field verification by the GTK Consortium). A single observation of this gneiss was made ~90 km east of Kitgum town, where leucocratic migmatitic gneiss shows compositional banding with long, continuous laminae

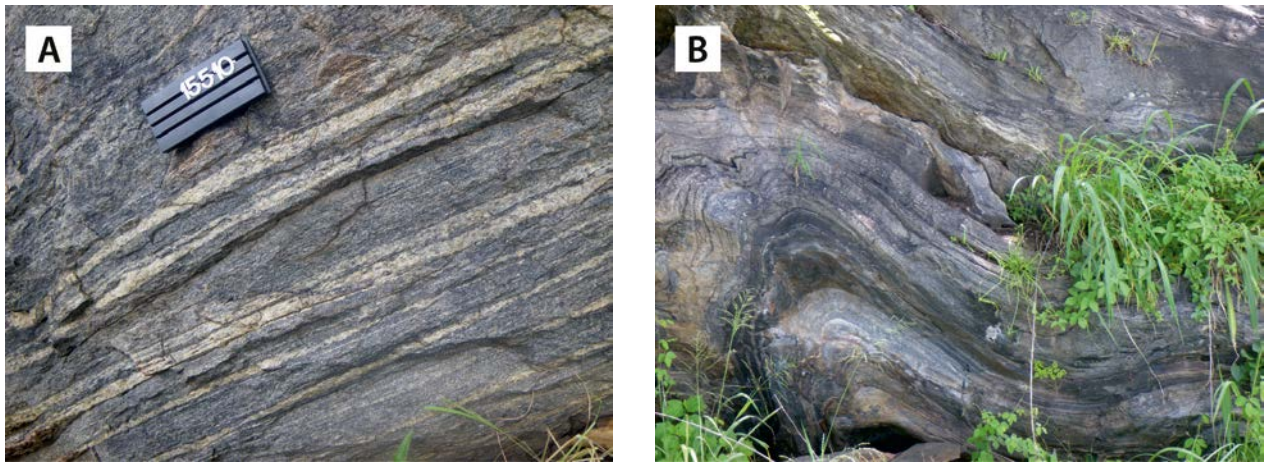


Fig. 5.10. (A) Biotite gneiss with felsic veins showing variable thickness (433249E / 368086N). (B) Overturned fold in banded biotite gneiss of the Paludar Formation (456758E / 356408N). Number tag 10 cm.

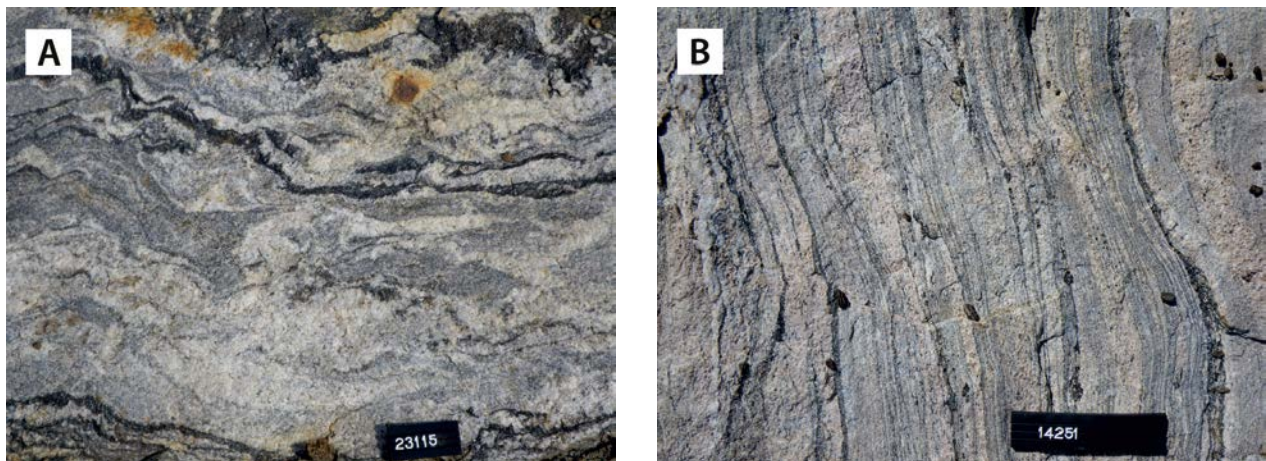


Fig. 5.11. (A) Migmatitic textures in the Paludar biotite gneiss (3715677E / 151239N). (B) Detailed image of metamorphic-migmatitic banding, showing narrow biotite-rich laminae and felsic neosomes (573487E / 388310N). Number tag 10/15 cm.

of biotite and abundant granitic neosomes (Fig. 5.11B).

Mafic metavolcanic rock, amphibolites (A3UAmmv) – A long, elongated or curvilinear belt, characterised by low values on the radiometric maps, occurs in the central part of the Kitgum-Gulu area. The lithology of this belt, which is assigned to the Banya Formation after a parish NE of Lira town, corresponds with exposures of variously foliated, compositionally banded, fine- to medium-grained, often garnetiferous amphibolites. In places, the rock is cut by leucocratic dykes and veins (Fig. 5.12A). The banded structure, microscopic features and observed mineralogy suggest a generally extrusive origin for these amphibolites, suggesting a basaltic tuffaceous protolith (Fig. 5.12B).

Similar curvilinear zones with a low radiometric signature are found around Gulu town, where they are part of a regional scale (ca. 30 km x 40 km) fold-like structure, open to the north (Fig. 5.1). The main lithological units, clearly visible in aeromagnetic maps, are the quartz dioritic gneiss, banded TTG gneiss and garnetiferous amphibolites.

In the Hoima-Masindi area, a poorly exposed amphibolite body occurs east of Namasale village, on the Namasale Peninsula of Lake Kyoga (see Lehto et al. 2014). In rare outcrops, amphibolite is a greenish grey, fine- to medium-grained, weakly deformed rock. The overall appearance of the rock suggests derivation from a massive (though foliated) basaltic lava protolith with obscure pillow-like textures (Fig. 5.13A). The association with thick,

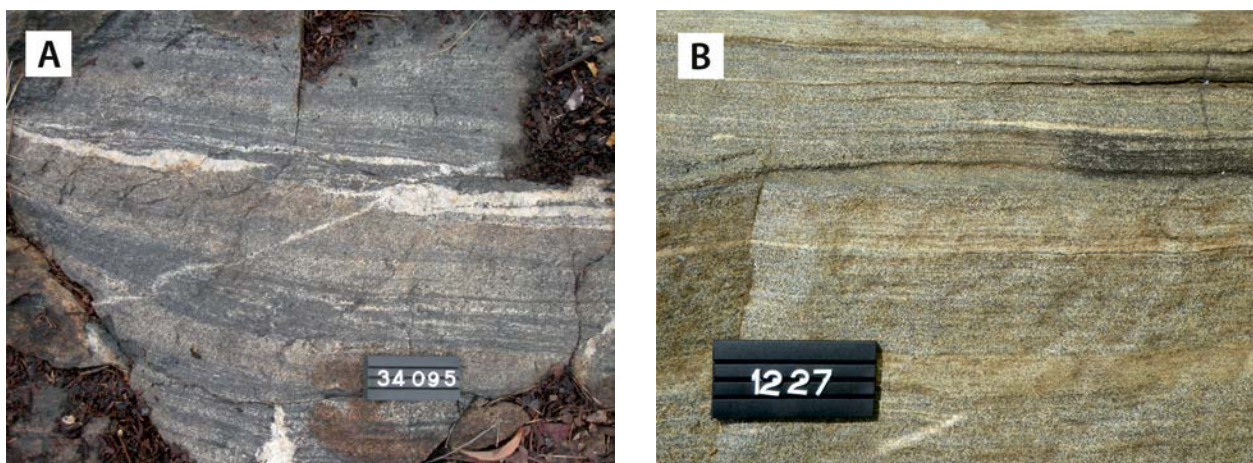


Fig. 5.12. (A) Compositional banding in a metatuff outcrop of the Banya Formation, located ~10 km SSE of the Lira town (491869E / 239002N). (B) Distinctly banded, fine-grained metavolcanic rock (metatuff?) east of the Adjumani granite (414235E / 334025N). Number tag 10 cm.

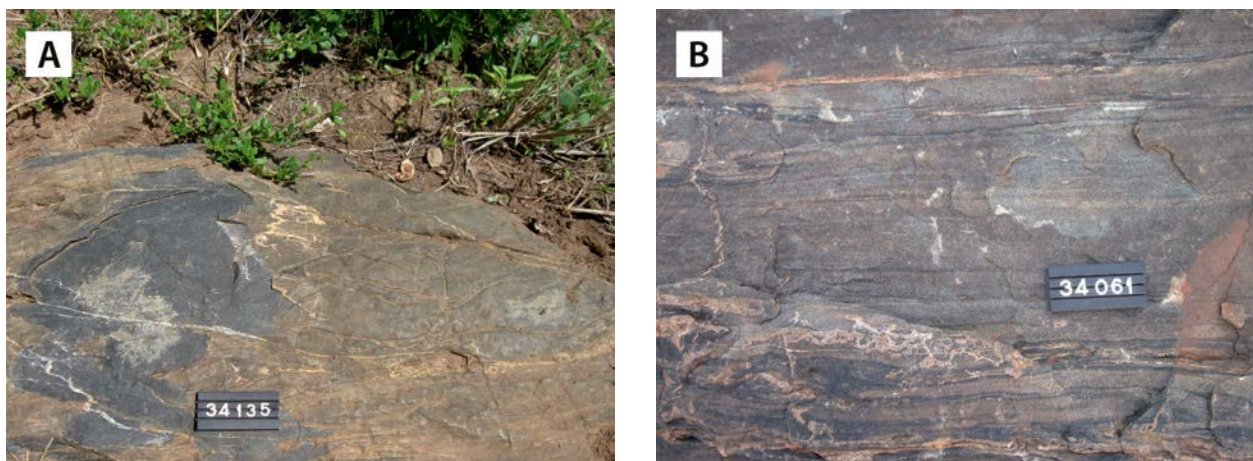


Fig. 5.13. (A) Massive, weakly foliated amphibolite with vague pillow-like structures, ~2 km E of Namasale village (460603E / 166096N). (B) Banded metatuff on top of Asamuk hill, located ~30 km NNE of Soroti town (576241E / 221524N). Number tag 10 cm.

skarn altered carbonate bearing bands composed of large, randomly oriented amphibole (actinolite) prisms in a nearby aggregate quarry (463670E / 166431N) also suggests a supracrustal origin of the amphibolite.

Under the microscope, mafic or intermediate metatuffs from the Gulu area are generally nematoblastic rocks, composed of well-oriented hornblende crystals (up to 60 vol%), plagioclase (An_{10} ; 10–25 vol%), quartz (5–15 vol%) and garnet (up to 10 vol%), in places accompanied by epidote, titanite and opaque minerals.

Mafic metavolcanic rocks assigned to the Banya Formation are also exposed on top of Asamuk hill, located about 30 km north of Soroti town. There this gently eastward-dipping, openly folded rock

unit comprises dark greyish green, fine-grained metatuff with a distinct compositional banding (Fig. 5.13B). Locally, layers or bands with garnet porphyroblasts, up to 5–8 mm in size, have been observed. In thin section this mafic metatuff is composed of well-oriented, fine-grained hornblende prisms (~55 vol%) that show pleochroic colours in shades of light blue-green and light green. Plagioclase (~35 vol%) and epidote (5–10 vol%) are other major mineral constituents, while small grains of titanite and opaque minerals occur in accessory amounts. A swarm of amphibolitic rocks, located to the west of Nakapirit village, copied from the existing, 100 000-scale geological map (sheet 45 Kadam, Trendall 1961b), are also tentatively attributed to this lithostratigraphic unit.

The whole-rock chemical composition of amphibolites of the Amuru Group is presented in Appendix 2 (anal. 96–101). On geochemical discrimination diagrams, mafic metavolcanic rocks and amphibolites of this Group plot in the high-Fe tholeiitic basalt or basaltic andesite fields (Figs

4.31A-D). The rather flat chondrite-normalised REE patterns of these rocks display an unfractionated to slightly fractionated REE pattern (Fig. 4.31E). In tectono-magmatic discrimination diagrams, these amphibolites show ‘oceanic’ affinities (Fig. 4.32B).

5.5 Geology of Neoproterozoic Granitoids and Gneisses of the North Uganda Terrane

This chapter discusses a wide variety of igneous intrusives and rocks of uncertain derivation with ages between 2.73 Ga and 2.62 Ga, including deformed granitoids, migmatitic granitoids and gneisses of granitic or granodioritic composition (Figs 5.1 and 5.2). The gneisses are occasionally banded, elsewhere more homogeneous, equigranular or porphyritic. TTG banded gneisses

and metagabbros occur in places. Twenty-two lithostratigraphic units have been identified from the NUT (Table 5.2). These units cannot, however, be distinguished in the enclosed map at scale 1:1M and the reader is referred to the SMMRP geological maps at the DGSM in Entebbe at the scales 1:250 000 and 1:100 000 for details.

Table 5.2. Neoproterozoic rocks of plutonic and uncertain derivation of the North Uganda Terrane. The Map codes refer to the geological maps at larger scales, available at DGSM in Entebbe. In the 1:1 000 000-scale Geological Map of Uganda, these units have been combined into one colour and code (pink, code 50, gneissic granitoids of Uganda, Neoproterozoic), except the ‘metagabbro’ (code 45) and ‘metadolerite’.

| Neoproterozoic rocks of plutonic and uncertain derivation of the NUT | Unit | Map code | Age |
|--|--|----------|---------|
| | Metadolerite | A3Udo | |
| | Metagabbro | A3Umgb | |
| | Banded granite gneiss and migmatite | A3Ubgg | |
| | TTG gneiss | A3Uttg | 2.61 Ga |
| | Cawente granite | A3UCgr | |
| | Tonalite | A3Uto | |
| | Katakwi granite | A3UKgr | 2.62 Ga |
| | Leucocratic granite gneiss | A3Ulggn | |
| | Leucogranite | A3Ulgr | |
| | Mbale porphyritic granite | A3UMpgr | |
| | Porphyritic granite gneiss | A3Upggn | |
| | Kalangala granite, orthogneiss | A3Uogn | |
| | Hornblende granite and granodiorite | A3Uhgr | |
| | Kuju granitic and granodioritic gneiss | A3Uggdg | 2.63 Ga |
| | Banded gneiss | A3Ubgn | |
| | Granulitic granitoid and gneiss | A3Uglgg | |
| | Muwozansimbe quartz diorite gneiss | A3Uqdrg | 2.64 Ga |
| | Awela granodiorite gneiss | A3Ugrdg | 2.65 Ga |
| | Gulu banded TTG gneiss | A3Ubtg | 2.65 Ga |
| | Granite and granite gneiss | A3Uggg | |
| | Apuch granite migmatite | A3Ugrm | 2.66 Ga |
| | Kaseeta potassium granite gneiss | A3Ukggn | 2.73 Ga |

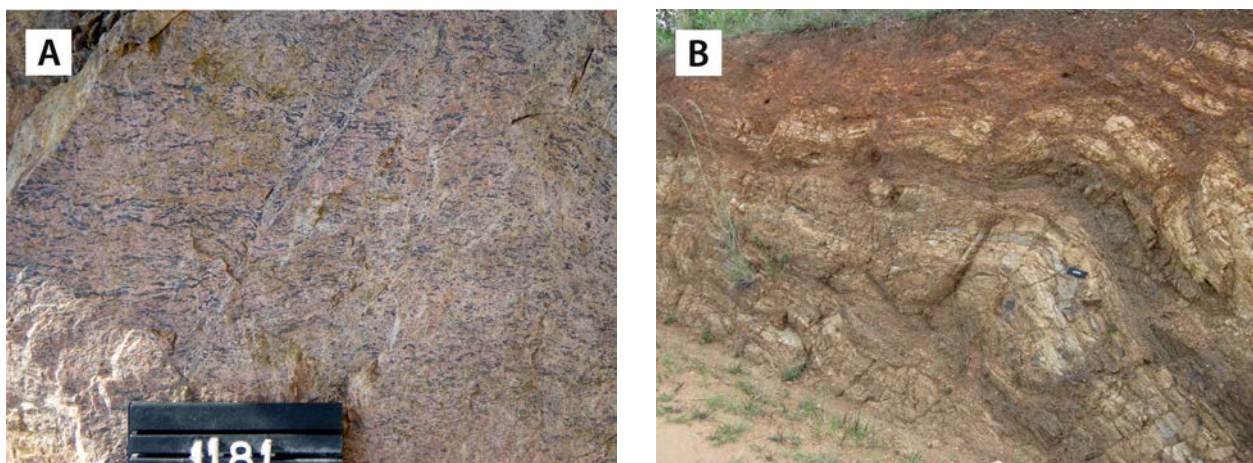


Fig. 5.14. Kaseeta potassium granite gneiss. (A) Mildly deformed granite gneiss from outcrop used for age determination (154483E / 274611N). (B) Strongly sheared Kaseeta granite gneiss showing segregated quartz vein and compositional banding (274410E / 154280N). Number tag 8 cm.

Kaseeta potassium granite gneiss (A3Ukgn) – The Kaseeta granite gneiss is exposed along the Albertine Rift margin, but supposedly continues to the west, below Neogene rift sediments. These 2.73-Ga-old rocks show reddish colours, owing to the high K-feldspar content. Quartz is seen as pale, bluish grains. Weakly deformed specimens with evenly distributed, fine- to medium-grained feldspar crystals resemble undeformed, homogeneous granite (Fig. 5.14A). In more deformed, foliated sub-types, however, quartz has been segregated and redistributed into discontinuous lenses and layers between K-feldspar-rich bands (Fig. 5.14B). The attitude of the penetrative planar fabric and shears of the Kaseeta granite gneiss varies from sub-horizontal to steep. Open upright folds have deformed this composite feature.

Apuch granite migmatite (A3Ugrm) – A NW-trending belt of variously migmatized granite intrusions is associated with the Aswa Shear Zone (ASZ) from the Mbale area up to the Kitgum area (Fig. 5.2). U-Pb zircon dating yields an age of 2.66 Ga for the Apuch granite migmatite with Pan-African overprinting in the ASZ at ~0.69 Ga. On airborne geophysical maps, the Apuch granite can be distinguished from surrounding rock units by a strong positive radiometric signature (Ruotoistenmäki et al. 2014).

The granitic part of the association is a rather coarse heterogranular rock which, in places, turns porphyritic. Weakly deformed brownish grey, porphyritic biotite granite with large, euhedral K-

feldspar phenocrysts in a fine- to medium-grained quartz-feldspar-biotite matrix is shown in Figure 5.15A. Close to the ASZ, with progressive deformation, the Apuch granite grades into a blastomylonitic gneiss (Figs 5.15B-C) and, eventually, in the high strain core of the ASZ, into an ultrablastomylonite without any recognisable phenocrysts (Fig. 5.15D). Migmatic foliation, defined by densely spaced leucosomes, may be straight as well as microfolded, and shear indicators are also commonly observed in the rock.

Locally, Apuch granite encloses xenoliths, shown as darkish bands, which have been almost completely assimilated. Larger xenoliths, even if effectively assimilated, may show a tectonic history, manifested by complex folds that are older than the emplacement of the granite. Pegmatitic veins and dykes have intruded the Apuch granite in an area SW of Soroti town, where the rock locally grades into migmatite with a Schlieren-like structure.

Migmatitic Apuch granite with perfectly straight banding may grade into folded gneiss (Fig. 5.16A). In the proximity of the ASZ the biotite layering is obliterated, together with the formation of younger neosomes along crenulation planes (Fig. 5.16B).

Apuch granite migmatite classifies as granodiorite rather than granite in the diagram of de la Roche et al. (1980) (Fig. 6.26), confirmed by relatively low potassium contents (ca. 3 wt%, App. 2, anal. 102–103). Analysed samples show SiO₂ contents between 70 and 72 wt% and peraluminous affinities.

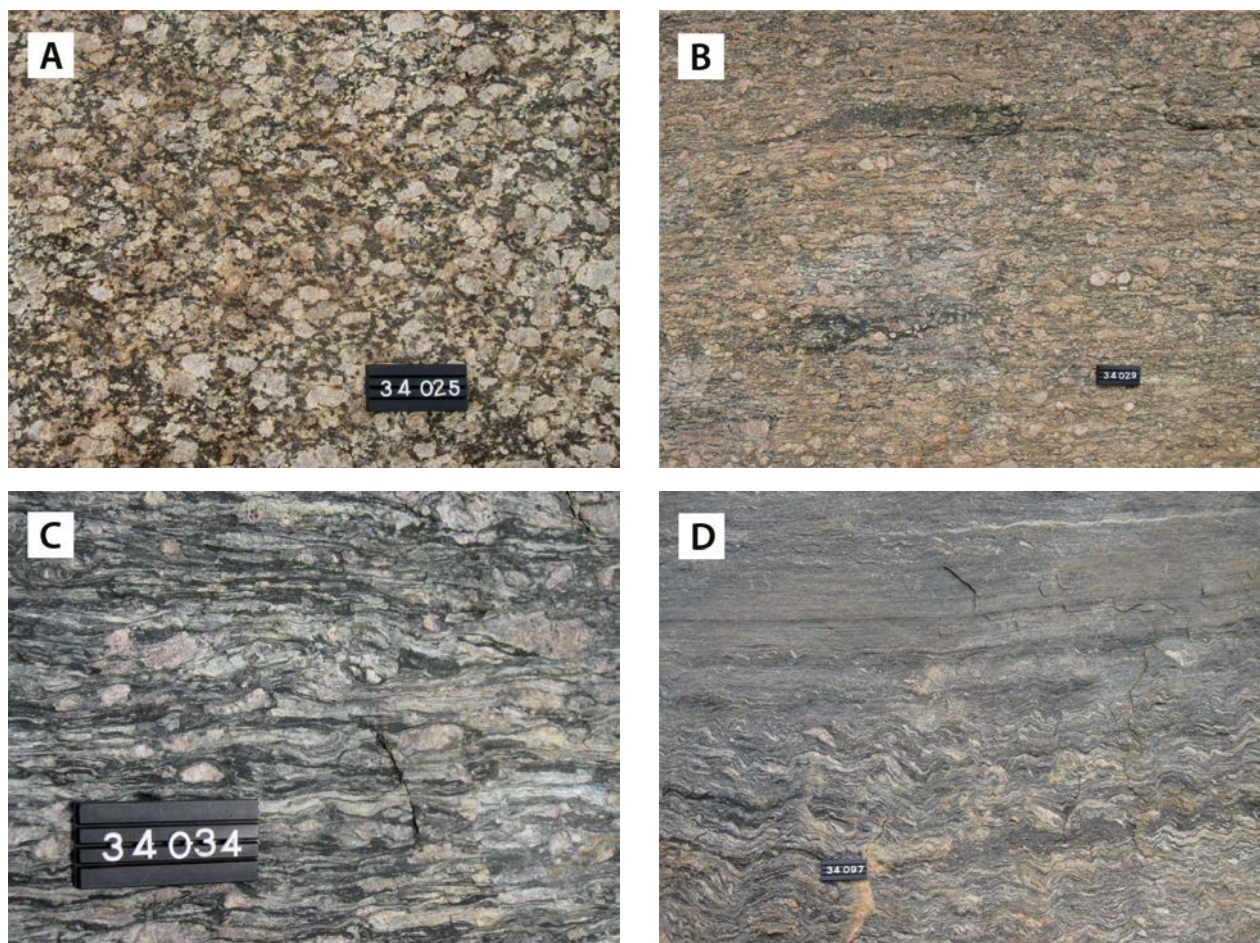


Fig. 5.15. (A) Weakly deformed, massive Apuch granite showing a porphyritic texture with euhedral K-feldspar megacrysts (516604E / 210737N). (B) Deformed Apuch granite showing a blastomylonite texture (510355E / 207897N). (C) A strongly deformed variety of blastomylonitic Apuch granite showing augen texture (501273E / 185595N). (D) An ultra-blastomylonitic gneiss variety of the Apuch granite (518747E / 212590N). Number tag 10 cm.

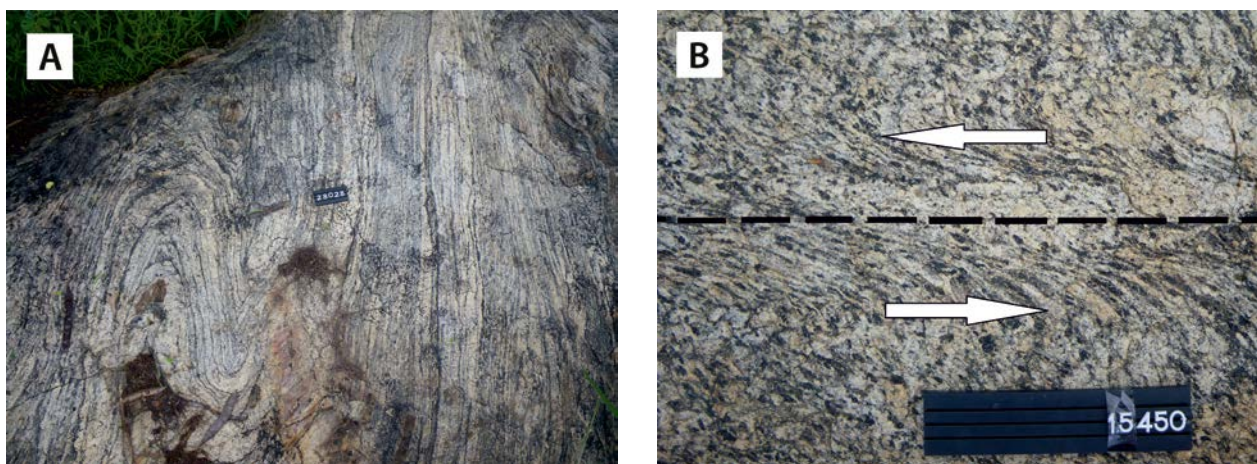


Fig. 5.16. (A) Folded palaeosome-leucosome banding in migmatitic Apuch gneiss (505849E / 257007N). (B) Curving of biotitic laminae in the Apuch gneiss due to sinistral shear; note neosome formation along ductile shear (524877E / 236701N). Number tag 8/15 cm.

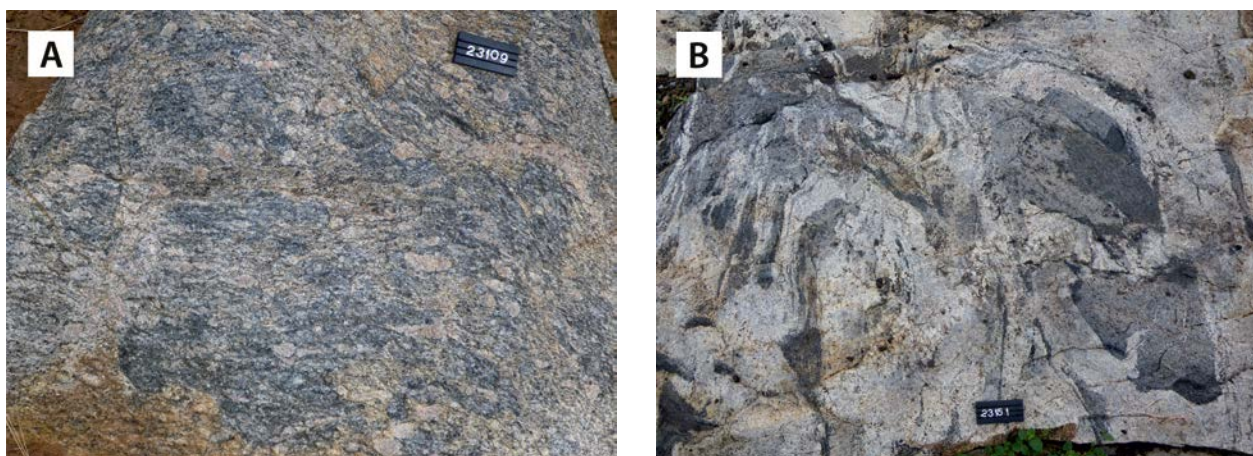


Fig. 5.17. (A) Foliated granite with deformed K-feldspar phenocrysts (387706E / 128999N). (B) Migmatitic granodioritic gneiss with quartz-filled fractures (385678E / 171869N). Number tag 8 cm.

Granite and granite gneiss (A3Uggg) – These granitic rocks cover a large, E–W-trending area, measuring at least 150 km x 30 km in the Hoima-Masindi area. Their northward continuation is largely hidden below extensive laterite covers from which they locally emerge in windows in the ferricrete caps. The extent of the unit can roughly be outlined by their relative low magnetic and total count radiometric intensities. Texturally, these heterogeneous rocks vary from foliated to massive and locally porphyritic granites (Fig. 5.17A) to strongly migmatized granitic and granodiorite gneisses (Fig. 5.17B). In places they contain inclusions of amphibolitic and quartz-feldspar gneiss composition.

The main minerals of these granitic rocks are K-feldspar, plagioclase and quartz. Biotite is usually the only Mg-Fe silicate, but its mode does not exceed 15 vol%. Hornblende and epidote are common minerals in mafic inclusions.

Gulu banded TTG gneiss (A3Ubtg) – Gulu banded TTG gneisses form the backbone of the lithological framework in the NUT (Fig. 5.1). The U-Pb zircon dating of a TTG gneiss sample yielded an age of 2.65 Ga, which is slightly older when compared to other Archaean orthogneisses and granitoids in the area. The characteristic lithological variation, migmatization features and complex structural elements have been used as a guide in delineating their regional extent.

Migmatization in the Gulu banded TTG gneiss is indicated by the presence of quartzo-feldspathic bands, similarly as depicted in Figure 5.18A, the outcrop from which the sample for dating was collected. The rock is characteristically poor in K-

feldspar and generally composed of quartz, plagioclase and biotite, with amphibole present in some parts. The addition of external granitic material has changed the bulk composition of the rock. The banding is frequently deformed into superimposed folds, creating a complex visual pattern.

The photographs above illustrate the structural and petrologic complexity of the Gulu TTG gneisses. Also the chemical composition of these rocks vary (see App. 2, anal. 104–110). The quartzo-feldspathic veins frequently grow to conformable swarms, showing pinch-and-swell (Fig. 5.18B), and are cut by reddish Pan-African pegmatites and granites (Fig. 5.18C). The volume of the granitic vein material may exceed that of the palaeosomes in places, while elsewhere, migmatization may be minimal. Several phases of folding, the younger ones overprinting the older ones, have resulted in complex fold structures (Fig. 5.18D).

Awela granodiorite gneiss (A3Ugrdg) – The Awela granodiorite gneiss covers extensive areas in the central and northern segment of the NUT, mostly east of the ASZ (Fig. 5.2), although partly overlapping with it. The largest area forms an elongated ca. 180-km-long NW–SE-trending zone reaching from the Kitgum and Gulu areas in the NW to the Aloi area in the SE. Within the ASZ, a new (blasto-)mylonitic foliation has generally been superposed, obliterating older S-planes in the gneiss.

U-Pb zircon dating yielded an age of 2.65 Ga for the Awela granodiorite gneiss (Mänttari 2014). The dated sample, compositionally a tonalitic to granodioritic biotite gneiss, is strongly deformed (foliated, lineated, and folded), heterogeneously mylonitized with numerous thin (<10 cm)

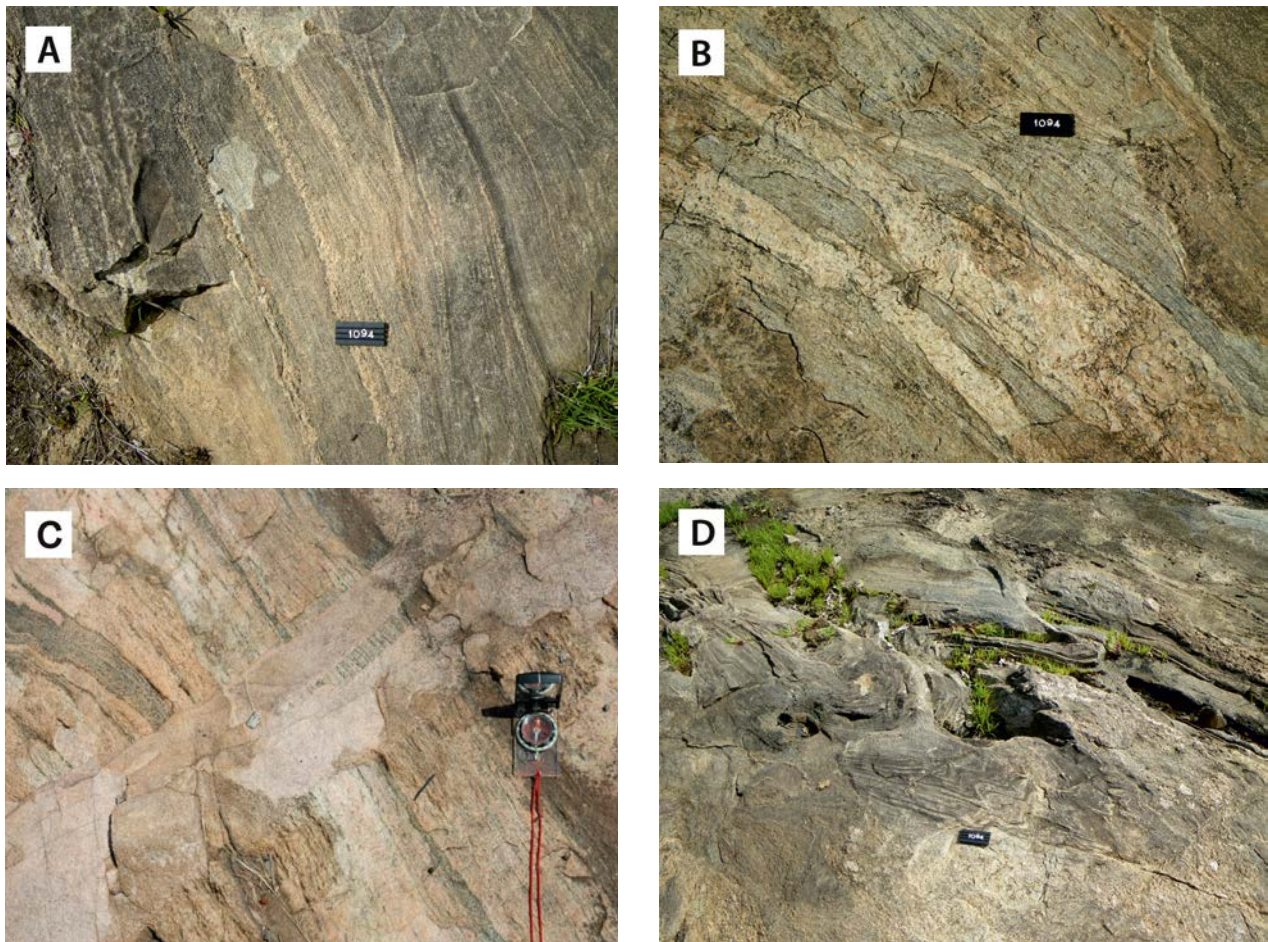


Fig. 5.18. (A) Location of geochronology sample (UG-7/1094), taken from the dominant grey mass of the banded Gulu TTG gneiss, which represents the palaeosome of the rock (442169E / 301719N). (B) Granitic veins show pinch-and-swell structure in this gneiss (442168E / 301718N). (C) The pinkish granitic dyke cutting the TTG gneiss most likely represents the nearby Pan-African Adjumani granite (409454E / 333657N). (D) Cross-folding of the Gulu TTG gneiss, folded around a NNW-directed axis (442168E / 301718N). Number tag 8 cm.

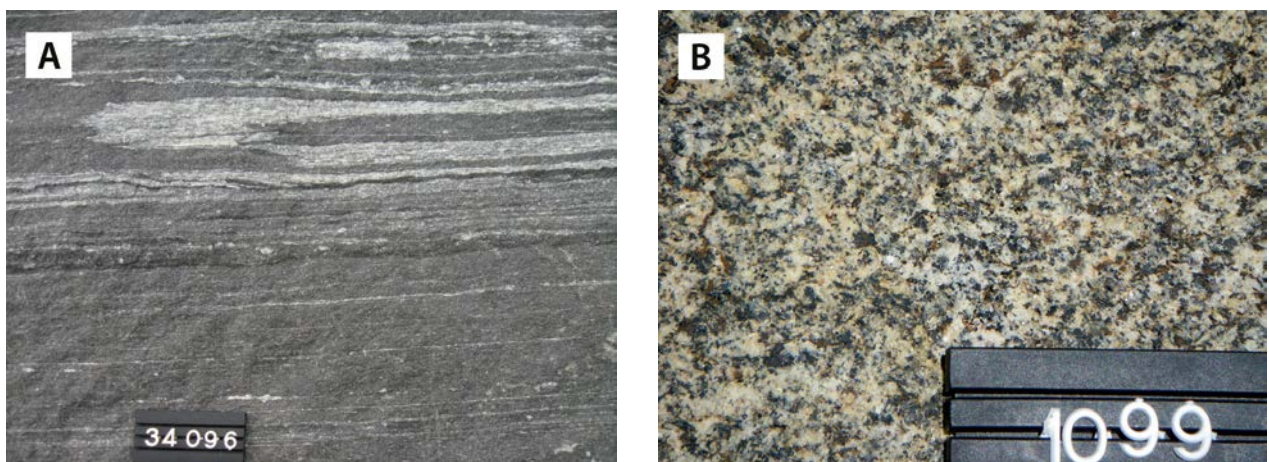


Fig. 5.19. (A) Geochronological sample location showing the strongly deformed Awela gneiss with rootless isoclinal micro-folds (490918E / 236986N). (B) Detailed image of more homogeneous variety of the Awela granodiorite gneiss (475932E / 336641N). Number tag 10 cm.

leucocratic veins, which often show tight rootless microfolds (Fig. 5.19A). Feldspar grains of the gneiss are strongly flattened, stretched and fragmented. A whole-rock chemical analysis of this felsic gneiss yielded the following quartzofeldspathic composition: 72.5 wt% SiO₂, 14.8 wt% Al₂O₃, 1.85 wt% FeO(tot), 0.5 wt% MgO, 2.2 wt% CaO, 4.1 wt% Na₂O and 3.5 wt% K₂O (App. 2, anal. 111). The strongly migmatized gneiss may contain bands of amphibolite, which reach thicknesses of up to 2–3 m. Another granodiorite gneiss nearby may contain randomly oriented hornblende porphyroblasts up to 2–3 cm in size.

Awela granodiorite gneiss east of the ASZ shows that the degree of metamorphic differentiation decreases away from this major dislocation. Strongly banded and differentiated gneiss can, however, be found throughout the large granodiorite gneiss polygon. Figure 5.19B displays a rather homogeneous variety of tonalitic gneiss, 20 km from the ASZ, representing the pre-Pan-African protolith.

Based on aerogeophysical data, a smaller area of Awela granodiorite gneiss occurs about 30 km SE of Lira town. In thin section, this gneiss is tonalitic in composition and contains 45 vol% quartz,

30 vol% plagioclase and 20 vol% biotite. Muscovite and chlorite are minor, retrograde minerals, the latter growing at the expense of biotite. Opaque minerals occur in accessory amounts.

Muwozansimbe quartz dioritic gneiss (A3Uqdr) – This unit forms a 90 km long elongated belt along the ASZ in the Mbale area (Fig. 5.2), together with augen-textured gneiss, forming a regional-scale fold structure west of the ASZ in the Gulu area (Fig. 5.1). The medium- to coarse-grained, equigranular to heterogeneous quartz dioritic gneiss is a compositionally rather uniform rock with common feldspar phenocrysts or porphyroclasts, when deformed. Streaks or highly stretched mafic enclaves have been found in places. When not affected by Pan-African deformation, the rock shows its original plutonic character with a rather mildly developed tectonic fabric (Figs 5.20A-B). Within the ASZ, a mylonitic and blastomylonitic fabric has developed, obliterating the older granitogneissic fabric (Fig. 5.20C). Representative whole-rock analyses of these gneisses are in Appendix 2 (anal. 112–114).



Fig. 5.20. (A) Muwozansimbe quartz diorite gneiss showing spectacular pillars supposedly formed by an intersecting set of vertical shears of the ASZ (632746E / 133867N). (B) Detailed image of the same gneiss with only incipient development of planar fabric. (C) Blastomylonitic quartz diorite gneiss in the ASZ (602143E / 175996N). Number tag 12 cm.

Granulitic granitoid and gneiss (A3Uglg) – These deformed, granulite-grade granitoids differ in metamorphic grade from the banded granitic gneisses nearby, which are metamorphosed to amphibolite facies. They occur in the western part of the Kitgum District (Fig. 5.2) and continue into South Sudan. On ternary and potassium radiometric maps, these rocks clearly deviate from surrounding areas (Ruotoistenmäki et al. 2014).

These heterogeneous granitoids have an igneous-looking texture and, consequently, are interpreted as metamorphosed plutonic rocks. As usual, these granulite-grade rocks have brownish grey weathering surfaces with rusty shades, while fresh surfaces show dark greenish tints. Major constituents are quartz, feldspar, hornblende (2–12 vol%) and biotite (2–12 vol%). Both ortho- and clinopyroxene, with a combined mode between 1 and 8 % by volume, have been observed. Orthopyroxene dominates over clinopyroxene in the granodioritic to granitic members. In places, the retrograde character of amphibole, formed at the expense of pyroxene, can be observed. Compositionally, the granitoids are predominantly tonalites and granodiorites, but true granitic members also occur. As such, they can be called charnockite, opdalite and enderbite, although terms such as opx-granodiorite and opx-tonalite are currently preferred (Frost & Frost 2008). Anatectic veins have been observed in places.

Our field observations suggest that granulite-grade metamorphism and dehydration melting are more or less simultaneous processes and that the pyroxene-bearing granitoids grade into other Archaean amphibolite-grade granitoid gneisses nearby. The gradational contact between these rocks types represents a change in metamorphic grade or, alternatively, a change in water activity ($a_{\text{H}_2\text{O}}$) or CO_2 metasomatism during metamorphism. Fluxing of CO_2 was suggested as a mechanism for the formation of charnockite in southern India (Pichamuthu 1960). It was later suggested that this could have been a regional process that was driven by fluids emitted from underplated basalts (Janardhan et al. 1982). This has led to the assumption that the charnockites of South India and the like were typical biotite or hornblende-bearing granitoids that were dehydrated by a massive flux of CO_2 .

Worldwide, the structural setting and field relationships suggest multiple modes of formation of charnockites (Bhattacharya et al. 2010). Magmatic and metamorphic charnockites occur both in high-grade metamorphic terrains, but truly igneous charnockites are a specific type of granitoids, formed from anhydrous calc-alkalic magmas, often forming part of an anorthosite-mangerite-charnockite-granite (AMCG) association (Emslie 1991) and characterised by a specific geochemical signature with high K_2O , P_2O_5 and TiO_2 that

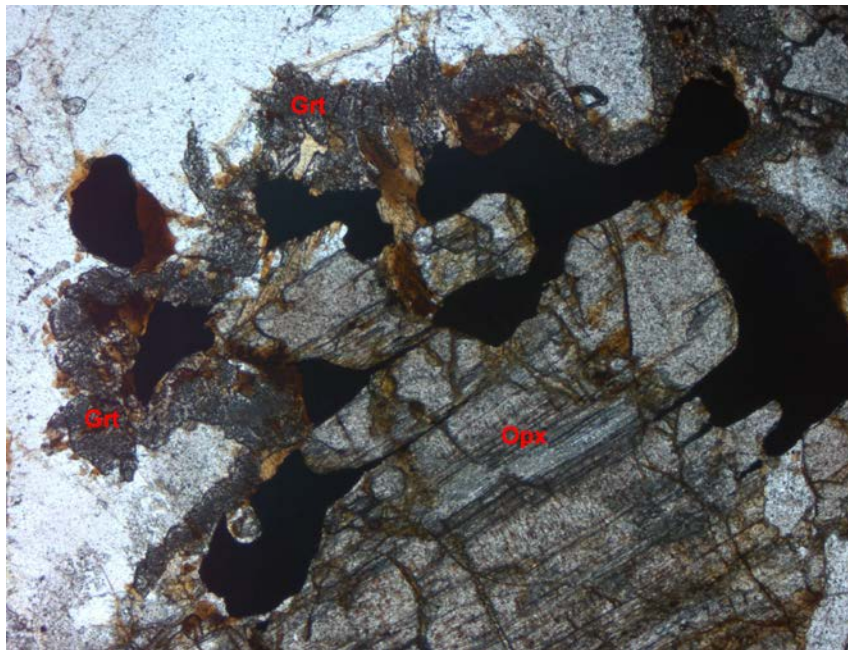
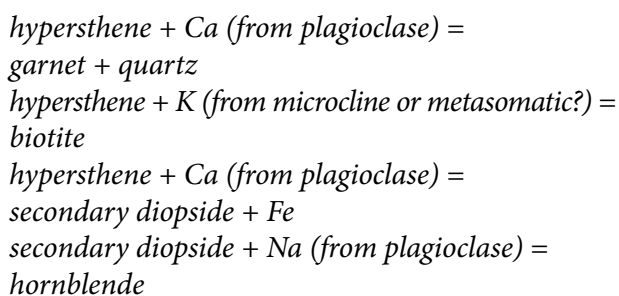


Fig. 5.21. Microphotograph of metamorphosed granodiorite, showing a reaction rim of garnet (Grt), Fe-oxide, hornblende and biotite surrounding orthopyroxene (Opx) (436420E / 382997N). Polarised light, width of microphotograph 1 mm.

distinguishes them from orthopyroxene-bearing quartzo-feldspathic granulites and I-, S- and A-type granitoids.

In view of the multiple indications of dehydration melting in these rocks, it is obvious that these pyroxene-bearing granitoids have to be classified as 'metamorphic charnockites' or preferentially as 'granulite granites' (Frost & Frost 2008), reserving the term 'charnockite' for truly igneous dry granitoids. It is important to note that orthopyroxene locally comprises reaction rims of garnet, opaque matter, biotite and amphibole (Fig. 5.21), possibly according to the reactions below:



Anatectic veins and the aforementioned reaction rims are missing in charnockitic rocks of Pan-African allochthonous thrust masses further east (Section 11.4). Clinopyroxene is found in hornblende- and biotite-bearing tonalitic members, which have higher CaO contents and thus favour the crystallisation of clinopyroxene (Fig. 5.22).

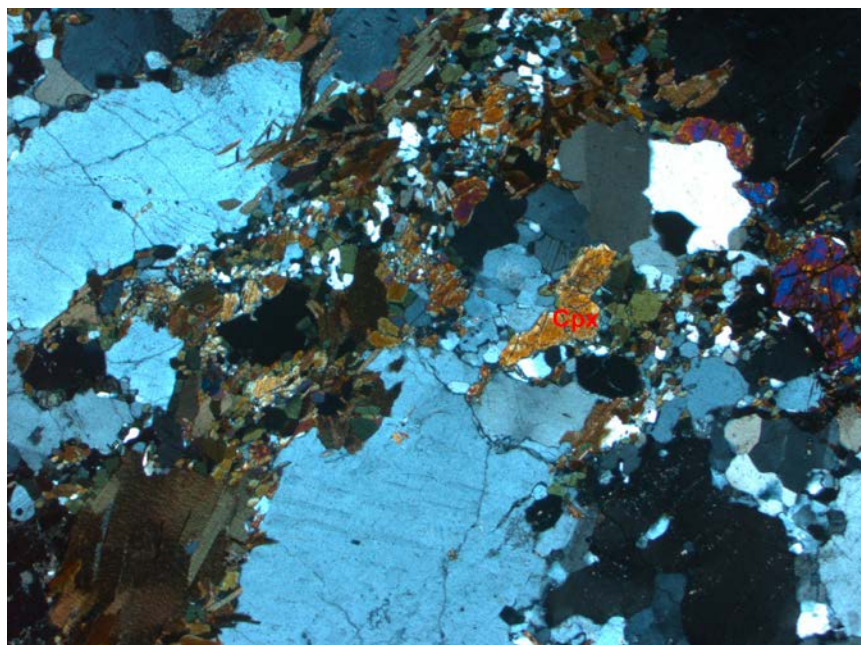


Fig. 5.22. Microphotograph of metamorphosed granitoid comprising of possibly secondary clinopyroxene (Cpx). The other Fe-Mg silicates in the rock are hornblende and biotite (440663E / 375967N). Cross-polarised light, width of microphotograph 1 mm.

Banded gneiss (A3Ubgn) – Banded gneiss is a strongly variable and mixed rock, on outcrop and larger scales, so that a collective and generic name such as 'banded gneiss' is most appropriate. A large area of 'banded gneiss' has been delineated in the area between Kitgum and Adjumani, on both sides of the ASZ (Fig. 5.2), bounded by the front of Pan-African thrust sheets in the north.

The majority of the field observations describe layered or banded rocks but the origin of the planar fabric is not always straightforward. Both tectonic 'banding' and compositional layering can be observed. In some cases one is supposedly dealing with a metasedimentary or a metavolcanic rock, migmatized or not, while in other cases the banded or layered rock is obviously a deformed and often migmatized plutonic rock. Overall, there is a bias towards a sediment-dominated supracrustal origin.

The photographs below (Figs 5.23A-B) illustrate a few representative examples, which have been selected from a variety of banded or layered rocks attributed to this unit. Many other sub-facies are gneisses of granitic or of intermediate composition, even constituting entire outcrops. They have probably been formed from various partial melts, and segregated from the migmatitic banded or layered supracrustal rocks.

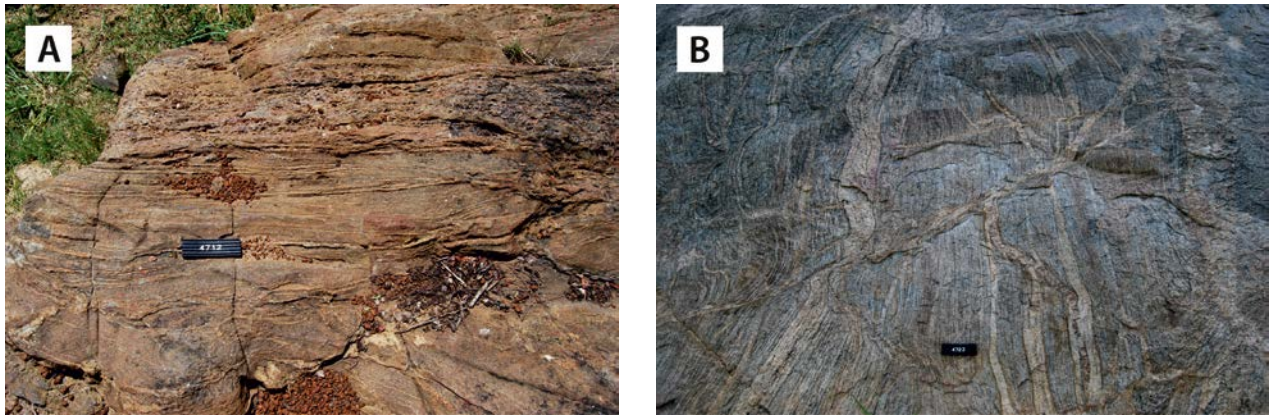


Fig. 5.23. Two varieties of the banded gneiss. (A) A variety of supposedly psammitic derivation at bridge over Aswa River (364718E / 429232N). (B) Occasionally banded subfacies with parallel and crosscutting granite veins; this rock does not differ from the TTG gneiss in the Gulu and Adjumani Districts nearby (429555E / 345571N). Number tag 10 cm.

Kuju granitic and granodioritic gneiss (A3Ugddg) – Kuju granitoid gneisses occupy a long and narrow area, suggesting stretching along the ASZ, about 70 km SE of Lira (Fig. 5.2). In outcrop, however, this rock unit seems to be relatively unaffected by shear, with the exception of its northern end, where analysis of airborne geophysical imagery suggest an eastward protrusion. Some small areas west of the ASZ have also been assigned into this unit. U-Pb zircon dating yields an age of 2.63 Ga, with an overprinting tectono-thermal event at 2.58 Ma.

The pale or white, coarse-grained or coarse-porphyrific rock is moderately gneissic, but not banded. As a result of its proximity *vis-à-vis* the ASZ, the rock is generally more or less stretched and flattened, first with the development of a typical ‘Augen gneiss’ texture (Fig. 5.24A), grading in

places into strongly blastomylonitic rocks in the centre of a shear zone, with only a few feldspar porphyroclasts surviving (Fig. 5.24B). In detail, the rocks commonly show continuous quartz ribbons in blastomylonitic subtypes.

Major minerals are K-feldspar (40–45 vol%), quartz (30–40 vol%) and plagioclase (10–25 vol%). Minor minerals include hornblende and biotite, while zircon, titanite and opaque minerals are accessory constituents. Couple representative chemical analyses of these rocks are shown in Appendix 2 (anal. 115–116).

Boudinaged enclaves of a more mafic rock (Fig. 5.25), interpreted as fragments of dolerite dyke that pre-date the shear, have been encountered in several outcrops, located to the north of Soroti, close to a narrow shear that probably represents a second-order fault of the broad Aswa Shear Zone.

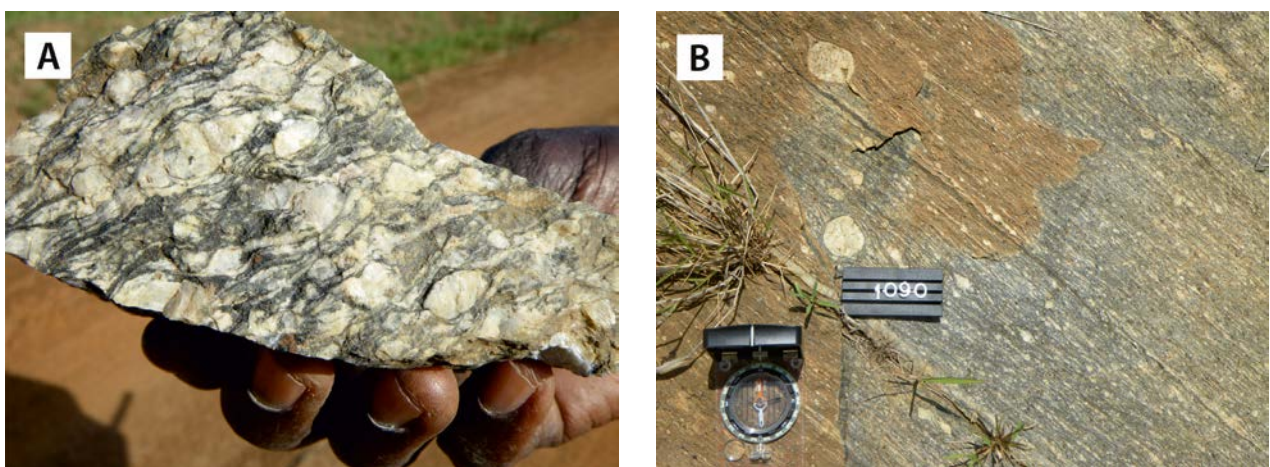


Fig. 5.24. (A) Augen gneiss-textured Kuju granite (blastomylonite) in the Aswa Shear Zone (520001E / 653843N). (B) Blastomylonitic texture with a few roundish feldspar porphyroclasts (492219E / 278722N). Number tag 8 cm.

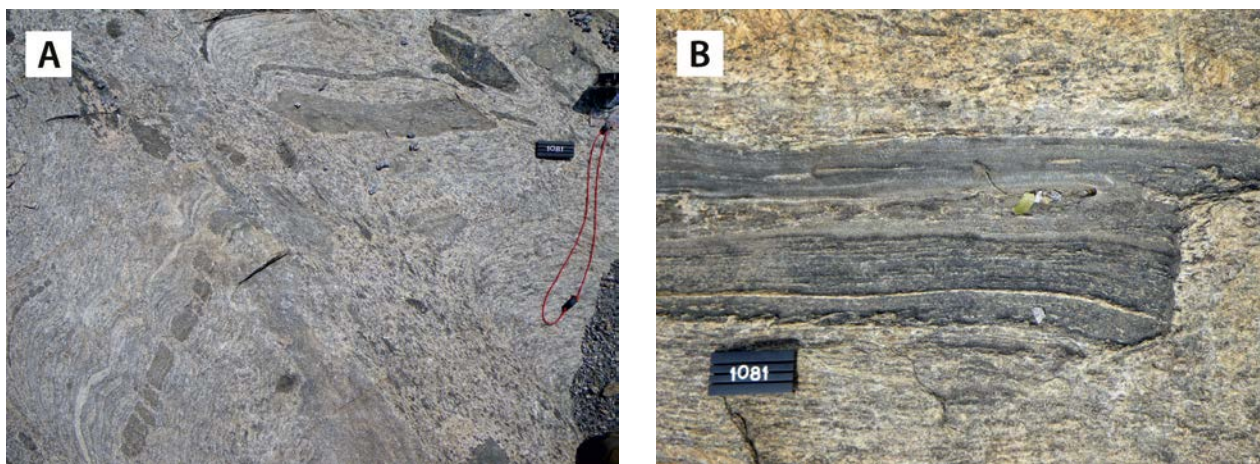


Fig. 5.25. (A) Enclaves of mafic rock in the Kuju granite; note that the mafic rocks have been boudinaged prior to the sinistral shear supposedly related to the Aswa Shear Zone (566567E / 228266N). (B) Detailed image of a banded xenolith in the same outcrop. Number tag 8 cm.

Hornblende granite and granodiorite (A3U_{hgr}) – Some small bodies of hornblende-bearing granite intrude Neoproterozoic TTG gneisses in the Gulu area (Fig. 5.1) and about 30 km WSW of Lira town (Fig. 5.2). Hornblende-bearing granitoid is a homogeneous, light brownish to pinkish grey, medium- to coarse-grained, equigranular, hypidiomorphic-granular and moderately foliated rock (Fig. 5.26A). Dark roundish spots of hornblende, up to 10 mm in diameter, have been noticed in places. Magnetite porphyroblasts (Fig. 5.26B) cause this unit to stand out on aeromagnetic maps. In ternary radiometric maps, hornblende granites generally show distinct above average values when compared to surrounding basement country rocks.

Major mineral constituents of hornblende granite are quartz (~40 vol%), K-feldspar (~30 vol%),

plagioclase (~20 vol%), hornblende (~10–15 vol%) and biotite (5 vol%). Magnetite, titanite, zircon and apatite are common accessory minerals.

Kalangala granite, orthogneiss (A3U_{ogn}) – Kalangala granites and their orthogneissic derivatives are only exposed as two small intrusions near the northern contact of the extensive Mubende batholith. These intrusives have very low radiometric readings, and mafic enclaves and gabbroic xenoliths are commonly found. Compositionally, these rocks are Augen-textured, reddish, biotite-bearing granites, granodiorites and even diorites. In the orthogneissic variety, K-feldspar crystals appear to be metamorphic porphyroblasts rather than phenocrysts, and epidotisation is a common feature.

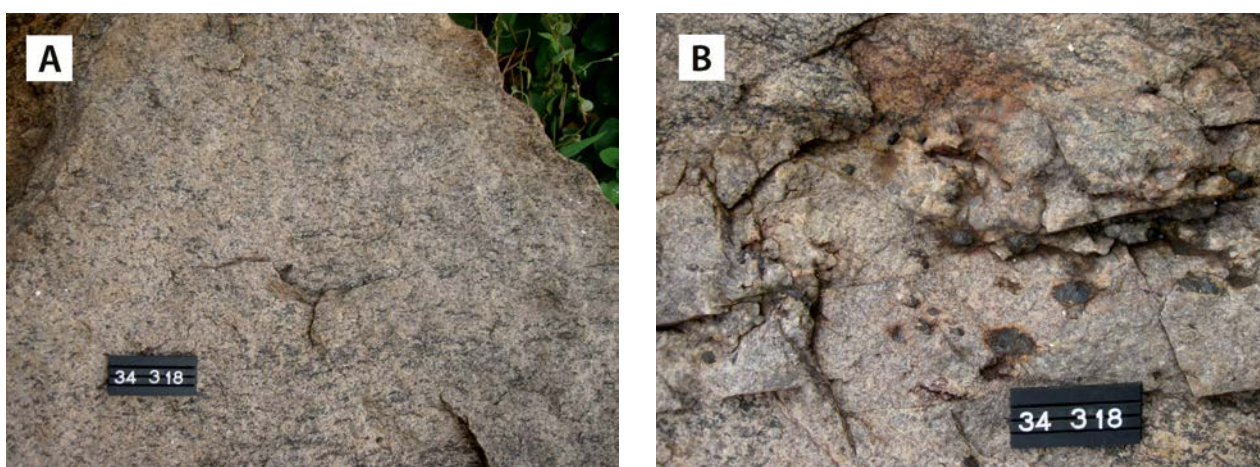


Fig. 5.26. (A) Moderately foliated, homogeneous hornblende granite (409683E / 311066N). (B) Hornblende granite with large magnetite porphyroblasts. NW of Gulu town (409683E / 311066N). Number tag 10 cm.

Porphyritic granite gneiss (A3Uppggn) – Porphyritic granite gneiss occurs as a roundish intrusive body, 5 km x 6 km in size, located some 30 km west of the Karuma Falls in the Gulu area. More outcrops can be found ~40 km further southwards, north of Masindi town, where the unit comprises two NE–SW-trending bodies, 35 and 11 km in length. The smaller body is composed of coarse-grained, distinctly porphyritic gneiss with a pronounced planar fabric defined by parallel alignment of roundish feldspar phenocrysts, up to 3 cm in size (Fig. 5.27A). In other locations, the phenocrysts are generally <1 cm in size and more easily visible in weathered than in fresh surfaces. In the eastern part of this body, the rock is, apart from the planar fabric, homogeneous and free of mafic enclaves. Compositional layering is found in some outcrops in the western part of this granite gneiss body (Fig. 5.27B).

Mbale porphyritic granite (A3UMpgr) – The Mbale porphyritic granite occurs in an elongated, NW–SE-trending area, measuring 42 x 17 km, NE of Lira town, more or less parallel to the nearby ASZ. This homogeneous, variously foliated granite occurs in large, flat outcrops and kopjes (Fig. 5.28A), generally without xenoliths or dykes. In ternary radiometric maps, the Mbale porphyritic granite often shows a distinct pattern. Due to disseminated magnetite grains, measured susceptibility values are often rather high and the rock produces a positive signature on aeromagnetic maps (Ruotoistenmäki 2014).

Mbale porphyritic granites are grey or white coloured, coarse-grained and mostly homogeneous rocks with abundant large (2–6 cm), densely packed K-feldspar grains (Fig. 5.28B). Apart from K-feldspar, the main minerals are plagioclase, quartz and biotite. Hornblende is a local subordi-

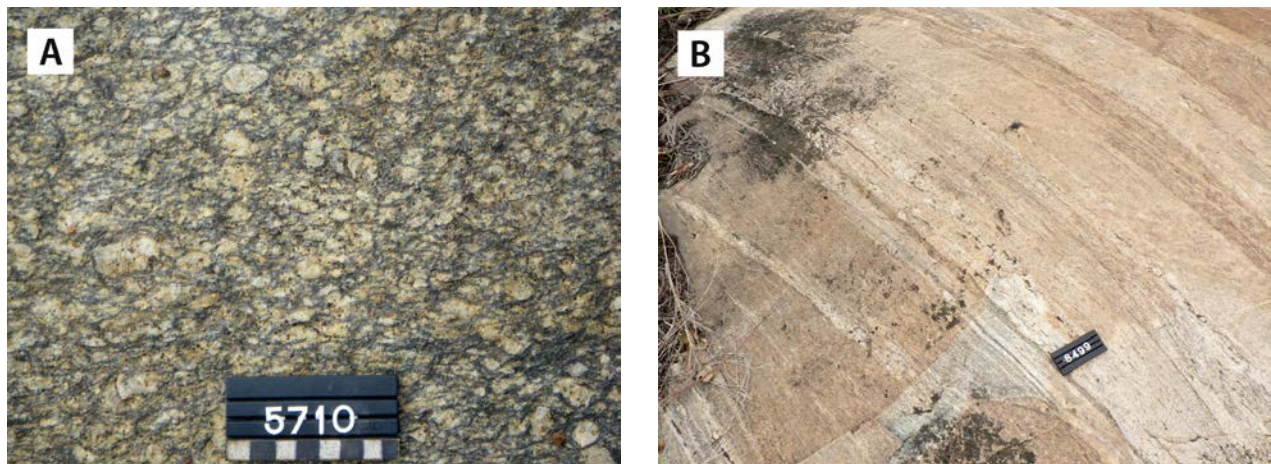


Fig. 5.27. (A) K-feldspar phenocrysts with preferred orientation in the porphyritic granite gneiss (384873E / 208245N). (B) Compositional layering in the granite gneiss (379448E / 204864N). Number tag 8 cm.

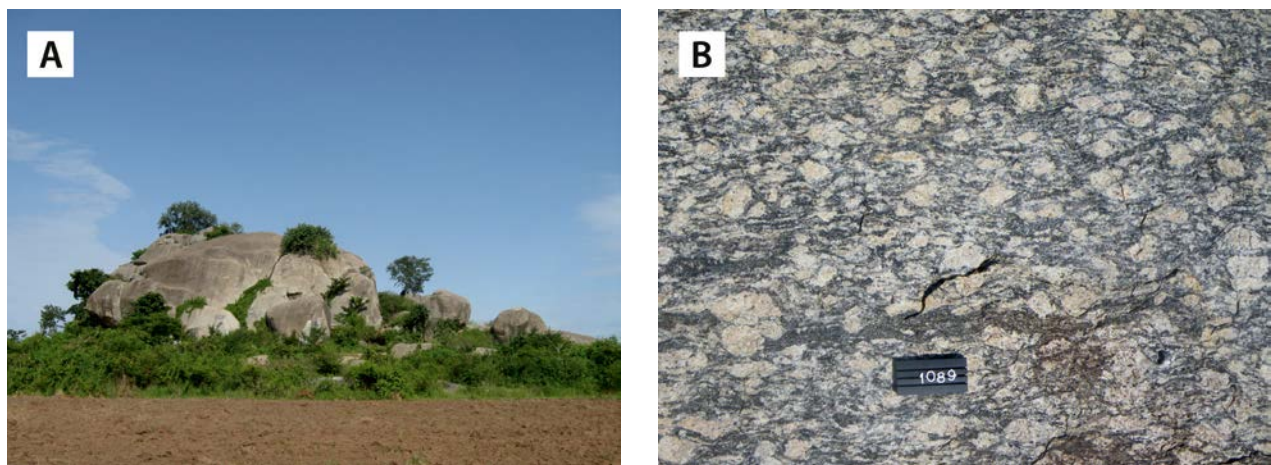


Fig. 5.28. (A) Typical kopje of massive Mbale granite SW of Soroti town. (B) Weakly foliated variety of the Mbale porphyritic granite (491222E / 254882N). Number tag 8 cm.

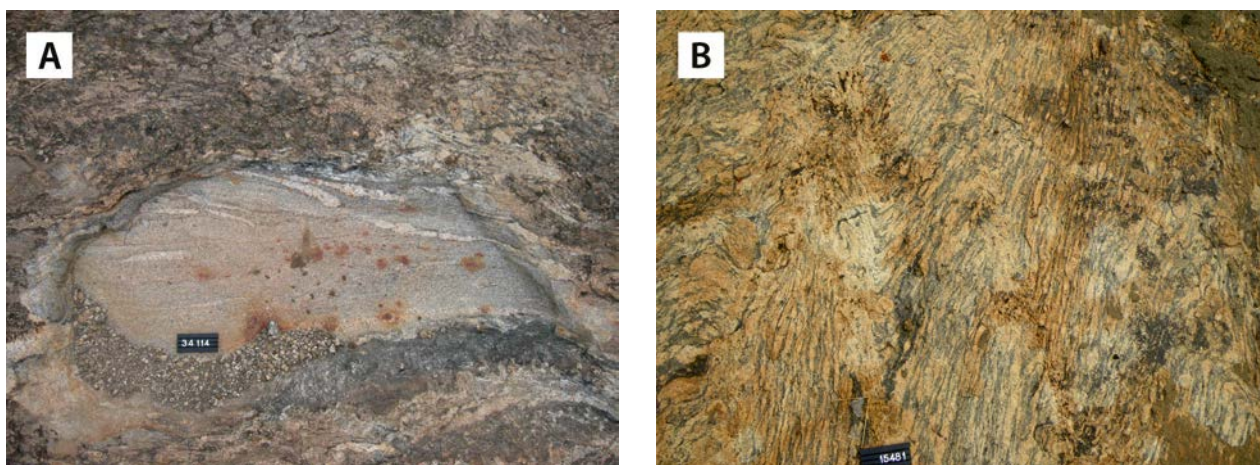


Fig. 5.29. (A) Xenolith of psammitic gneiss in the Mbale porphyritic granite (491222E / 254882N). (B) Chevron folds in a shear zone of the Mbale granite, NE of Lira town (491692E / 255060N). Number tag 10 cm.

nate constituent. Magnetite is found in quantities of up to 5 % by volume and cause high magnetic susceptibility readings. Under the microscope, the porphyritic granite shows a hypidiomorphic granular texture. Tectonic strain is manifested by large, variously deformed, perthitic K-feldspar megacrysts that are set in a groundmass, which contains myrmekitic microcline (20–50 vol%), quartz (15–40 vol%) with undulose extinction, plagioclase (15–35 vol%) and biotite (5–10 vol%). Hornblende, titanite, zircon, allanite, garnet and opaque minerals are common accessories. Retrograde alteration is manifested by sericitised and saussuritised plagioclase and minor quantities of epidote and chlorite.

Another large body of Mbale granite, measuring 100 km by 160 km, intrudes various Archaean gneisses NW of Mbale town (Fig. 5.2). Equigranular varieties occur locally in the western segment of the pluton. Near the ASZ, in the eastern part of the intrusion, deformation has generally turned the granite into blastomylonitic gneiss, as in an area SW of Soroti town or NE of Pallisa town.

Pegmatitic and microgranitic dykes commonly occur in Mbale porphyritic granite. Unlike the Mbale area, mega-enclaves of migmatitic gneisses (Fig. 5.29A) are common SW of Soroti town. Hornblende-bearing, equigranular granite varieties of the Mbale granite have been found east of Pallisa town. Although mostly only weakly foliated, the rock is deformed into blastomylonitic gneiss with Augen-like phenocrysts in the Aswa Shear Zone. Chevron folds and newly formed ne-

osome concentrations are also common in shear zones (Fig. 5.29B).

Leucogranite (A3U_{lgr}) – Light brownish grey leucocratic granite is exposed in an area E and NE of Bukwa town, between Mt. Elgon and the Kenyan border. This medium- to coarse-grained, equigranular to (locally) porphyritic rock is variously deformed and homogeneous and massive in places, cut by randomly directed pegmatite veins. Weakly or moderately foliated members are more common, although granite may grade locally into leucocratic gneiss. In a road cut north of the Kanyeru volcanic neck, a faulted contact with a Neogene olivine basaltic lava flow is exposed, manifesting Neogene block faulting. Here, homogeneous leucocratic granite has deformed into mylonitic gneiss.

Leucocratic granite gneiss (A3U_{lgg}) – Light grey, fine- to medium-grained leucocratic granite gneisses are widely exposed NE of Mt. Elgon, between Bukwa town and the Kenyan border (Fig. 5.2), where these rocks form the basement for the Neogene volcanics of the Elgon Complex. Locally, the strongly deformed gneisses show a distinct metamorphic banding, and quartzo-feldspathic veins and lenses are common (Fig. 5.30). The veins and lenses, generally 1–2 cm thick with sharp contacts, are probably due to metamorphic segregation of originally more homogeneous and massive rocks, which are mostly composed of potassium feldspar, quartz and a small amount of mica; no garnets or other aluminium silicates have been observed.

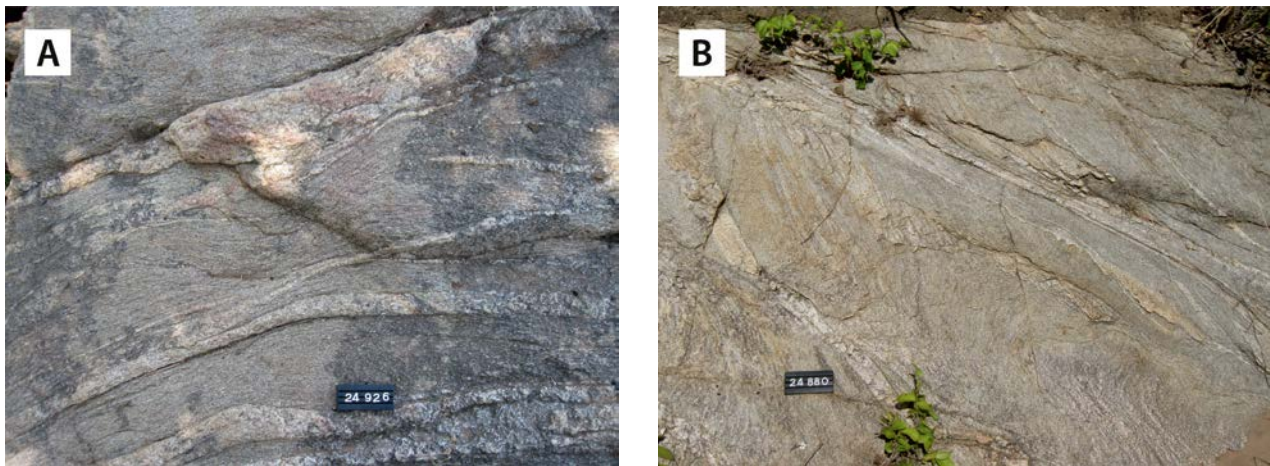


Fig. 5.30. Leucocratic granite gneiss NE of Mt. Elgon. (A) Leucocratic gneiss, injected by quartzo-feldspathic segregation veins (699443E / 147290N). (B) Strongly deformed leucocratic gneiss (700105E / 142600N). Number tag 10 cm.

Katakwi granite (A3UKgr) – West of Katakwi town (Fig. 5.2), a cluster of large outcrops composed of rather fine-grained, reddish, K-feldspar granite covers an area of 10 km². The unit comprises two members, a predominating reddish grey granite and a subordinate reddish granite, appearing very similar in outcrop. Both granite types are conspicuously homogeneous, show a weakly developed (locally absent) tectonic fabric and are cut by narrow pegmatite dykes, the latter also being older than the tectonic fabric.

U-Pb zircon dating yielded an age of 2.62 Ga. The slightly younger age of the rock compared to gneisses in the area, its simple lithology and lack of complex tectonic structures justify the idea that the Katakwi granite represents a younger Archaean plutonic phase in the NUT.

Tonalite (A3Uto) – A body of porphyritic hornblende tonalite intrudes the Mbale porphyritic granite about 15 km NW of Soroti town (Fig. 5.2), forming a prominent hill along the Soroti–Lira highway. Some smaller, equigranular and more strongly deformed tonalite bodies in this area are also tentatively assigned to this unit. Leucocratic veins and dykes commonly intrude the rather massive porphyritic tonalite. Despite a relatively high magnetic susceptibility, this rock fails to produce a noticeable anomaly that allows highlighting of this rock on the aeromagnetic map.

Two members can be observed: (1) anorthositic tonalite with 1–4 vol% biotite and (2) a hornblende- and/or pyroxene-bearing tonalite variety with > 20 vol% of hornblende. The predominant porphyritic hornblende tonalite is a rather ho-

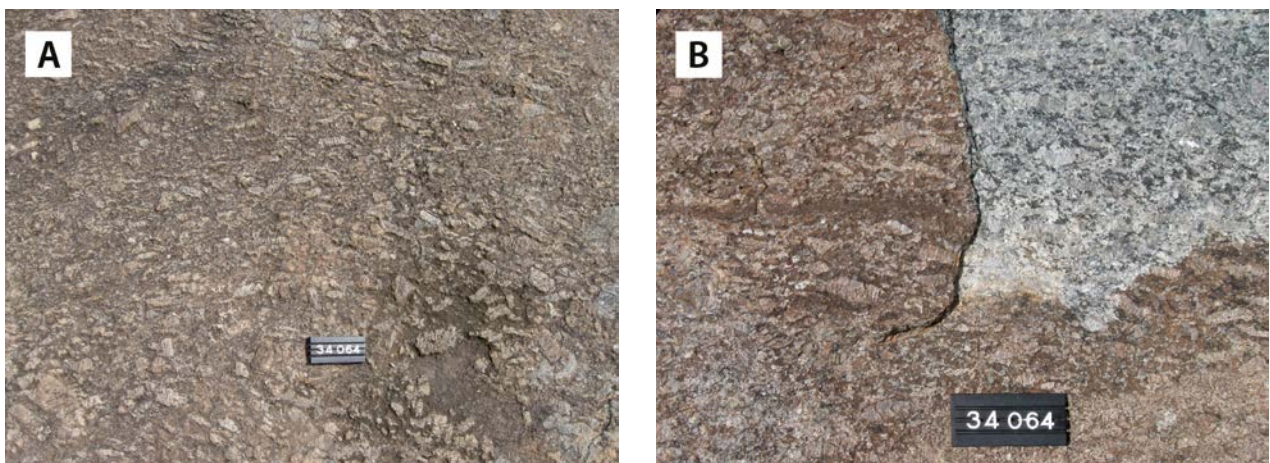


Fig. 5.31. (A) Flow-orientation of tabular plagioclase megacrysts in hornblende tonalite. (B) Detailed image of weathered (left) and fresh (upper right) surface of the same rock, located ~15 km NW of Soroti town (558367E / 201688N). Number tag 10 cm.

mogeneous rock with a weak foliation due to the preferred orientation of hornblende prisms and biotite flakes. Both varieties show idiomorphic interlocking plagioclase crystals, generally 5–8 mm in size, but megacrysts occasionally reach 6–8 cm in diameter, with a bluish colour and a colourless rim. Their preferred orientation is probably due to magmatic flow (Fig. 5.31A). Due to a rather large proportion of mafic minerals, fresh surfaces of the rock are greenish grey (Fig. 5.31B).

Under the microscope, porphyritic hornblende tonalite is a hypidiomorphic-granular rock, comprising phenocrysts with a distinct preferred orientation of sericitised and saussuritised plagioclase (~45 vol%), quartz (~30 vol%) with undulose extinction and ragged hornblende crystals (~20 vol %), partially altered to biotite and chlorite. Accessory minerals include microcline, titanite, apatite, magnetite and ilmenite.

Cawente granite (A3UCgr) – This is massive leucocratic granite about 30 km SE of the town of Apac, on the northern shore of Lake Kyoga (Fig. 5.2). Despite its strong radiometric signature (Ruotoistenmäki et al. 2014), the size of this granite body is unknown, because a laterite cap hampers delineation of its northern extent.

Light grey, equigranular, medium-grained granite varieties dominate the well-exposed eastern part of the body, while coarse-grained, porphyritic rocks are more common in the western part of the intrusion (Fig. 5.32A). Large amphibolite xenoliths are rather common. On outcrop scale, the Cawente granite appears generally massive and undeformed, intruded only by random swarms of thin,

quartz-filled fissure veins (Fig. 5.32B). Under the microscope, deformation is manifested, however, by a mortar texture, as well as by the undulose extinction of quartz, distinctly bent plagioclase twins and by the prevalence of retrograde minerals such as epidote, chlorite and carbonate-filled fissures in feldspar grains.

Major minerals are quartz (35–50 vol%), plagioclase (albite, 20–40 vol%) and microcline-twinning K-feldspar, often with string perthite and myrmekitic lobes (15–50 vol%). The amount of greenish brown biotite is generally <5 vol%. Other common accessories are sericite, titanite and minor opaque minerals.

TTG gneiss (A3Uttg) – TTG gneisses to the south and southeast of the town of Masindi (Fig. 5.1) consist of rocks with variable granitoid (granite, granodiorite, tonalite to trondhjemite) compositions and textures. TTG gneisses are variously migmatized, medium-grained, equigranular to porphyroblastic rocks, composed of variable proportions of quartz, plagioclase, K-feldspar, amphibole and biotite.

U–Pb age determinations of zircon cores from similar TTG gneisses in the foothills of the Rwenzori Mountains yielded the following ages: 2.64 Ga, 2.61 Ga and 2.58 Ga (Link et al. 2010).

Banded granite gneiss and migmatite (A3Ubgg) – This gneiss unit occupies a large area in the central part of the NUT around Lira (Fig. 5.2). Trendall (1965b) described these rocks as ‘acid and granitoid gneisses’ in the 1:100 000 Napak/ 35 map sheet, while Macdonald (1961) characterised



Fig. 5.32. (A) Detailed image of coarse-grained, porphyritic variety of the Cawente granite (451107E / 190145N). (B) Quartz-filled fissures in the Cawente granite (457538E / 194453N). Number tag 10 cm.

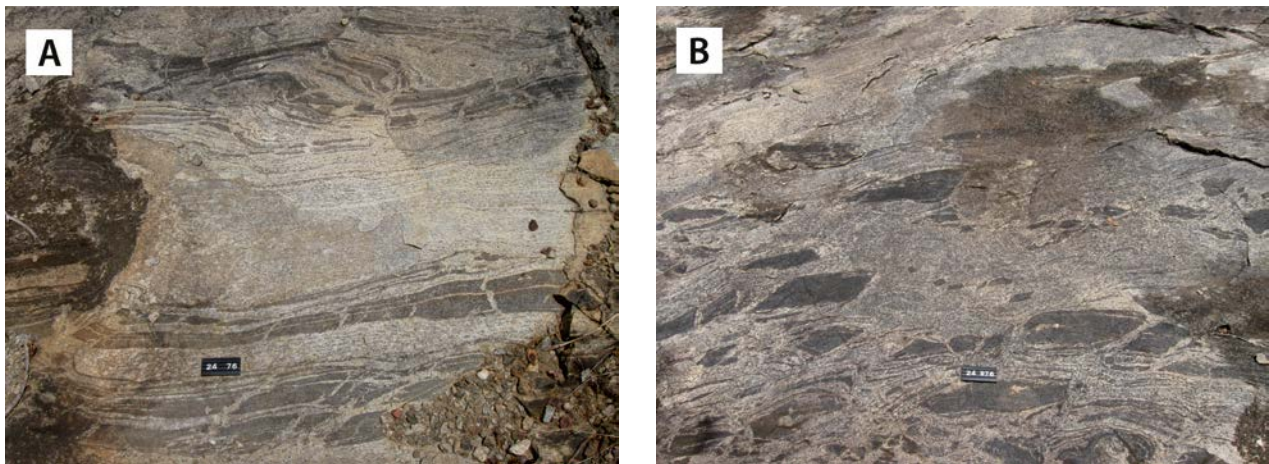


Fig. 5.33. Various stages of migmatisation of banded granite gneiss. (A) Amphibolite bands have been necked and boudinaged and (B) float in migmatitic neosome. Outcrop in Nabilatuk village (678812E / 229547N). Number tag 10 cm.

them as ‘*biotite gneisses and granite gneisses*’ in map sheet Nabilatuk/ 36. In the northeast, on map sheet Kaabong/ 10, ‘*undifferentiated, massive biotite and pyroxene gneiss*’ was the prevailing lithology (MacGregor 1962).

Basement gneisses underlying the Neogene Napak alkaline complex are exposed as light brownish, medium-grained, open-folded feldspathic gneiss, migmatised in places and intruded by granitic and pegmatitic dykes and veins. Locally, thin amphibolite bands show gradational contacts with the host gneiss, indicating *in-situ* deposition and suggesting the possibility that these gneisses have a sedimentary protolith.

About 30 km east of the Napak complex, these grey, medium-grained gneisses have parallel bands or layers of amphibolite, up to 30–40 cm wide, with generally sharp contacts (Fig. 5.33A). Amphibolite bands have been necked and boudinaged and float in migmatitic neosome material, leading to a brittle disaggregation and agmatization of the rock (Fig. 5.33B). In the intermediate stage of agmatite formation, amphibolite fragments are still mostly oriented parallel to the general foliation, while in the final stage randomly oriented amphibolite fragments ‘float’ in a ‘granitic neosome cement’.

Metagabbro (A3Umgb) – Neoproterozoic metagabbros occur widely within a variety of gneissose rocks from Adjumani town in the north to Karuma Falls in the south (Lehto et al. 2014, code 45). In the latter location they form spectacular rapids in the Nile river. Although always mainly composed of hornblende and plagioclase, these rocks often comprise also quartz, K-feldspar, pyroxene (augite), biotite and gar-

net. Metagabbro is usually fine- or medium-grained, with colours ranging from black and grey to greenish and brownish varieties. Magnetic susceptibilities are commonly quite low, but large metagabbro bodies show a weak positive magnetic signature in gneiss areas.

The size of these metagabbro bodies varies from kilometres to metres and contacts with surrounding gneisses are usually blurred, not sharp, suggesting reactions during metamorphism that these rocks jointly suffered with their gneissic host rock. Consequently, these rocks are usually banded, occasionally with a strong lineation (Fig. 5.34A) and the main tectonic fabric (foliation), as well as the grade of metamorphism, are congruent with hosting gneisses. These metagabbros are probably originally fragmented (boudinaged) mafic sills, co-magmatic with TTG orthogneisses in the area. Chemical whole-rock analyses of these metagabbros are in Appendix 2 (anal. 117–120).

Some 10 km SSE of Karuma village, along the Nile river (Fig. 5.1), where the Awela gneiss continues southward towards Masindi, poorly exposed, pink, fine- to very coarse-grained Awela granodiorite gneiss hosts mafic to ultramafic dykes up to a few metres wide (Fig. 5.34B). Contacts between mafic dykes and granitoid are vague, not sharp, with stringers of hornblende in granitoid, again indicating metasomatic reactions along the contact (Fig. 5.34C). As a consequence, the composition of the dykes ranges from gabbro to melagabbro to ultramafic hornblendite. Grain sizes in the mafic dykes range from medium-grained to rocks with quartz grains up to 10 mm in size, occasionally bluish in colour.

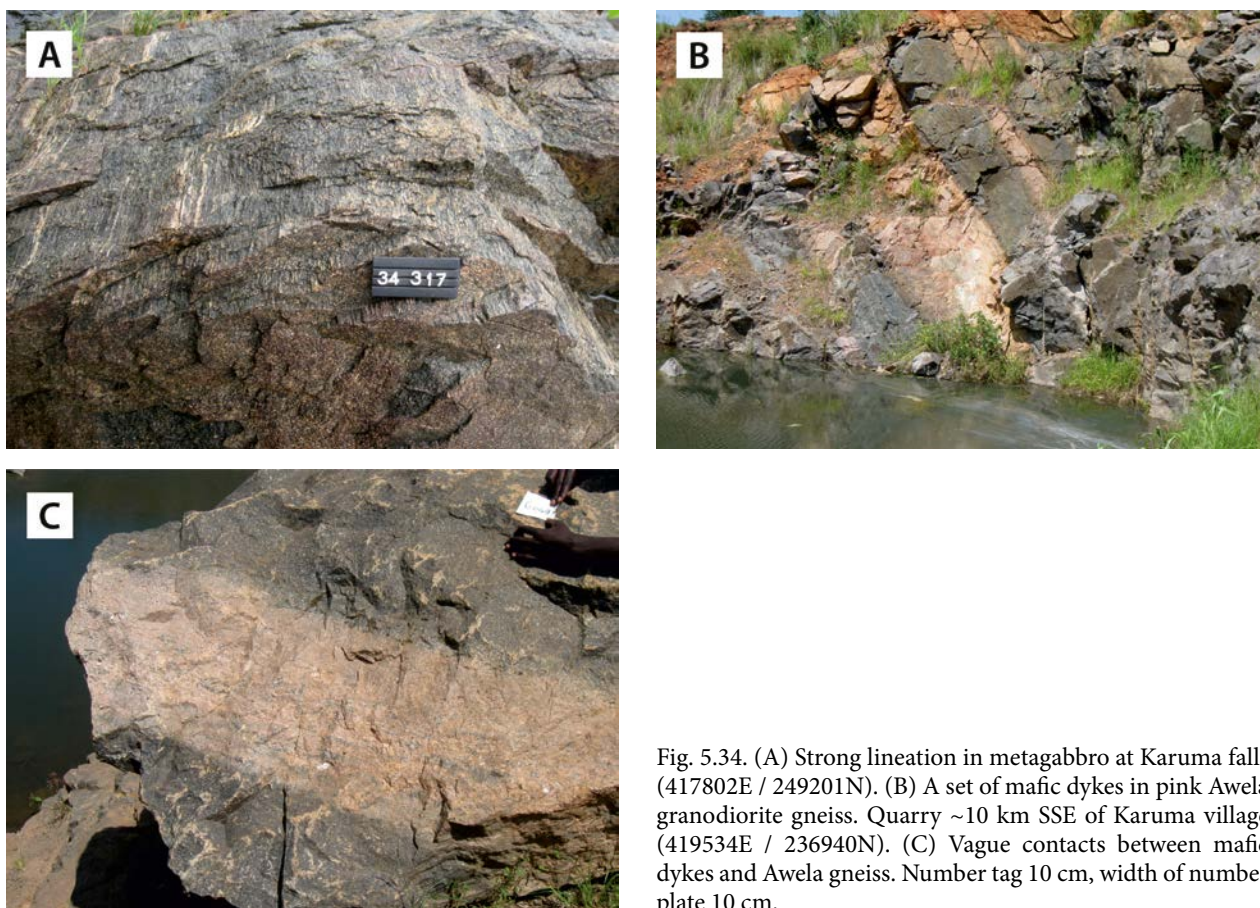


Fig. 5.34. (A) Strong lineation in metagabbro at Karuma falls (417802E / 249201N). (B) A set of mafic dykes in pink Awela granodiorite gneiss. Quarry ~10 km SSE of Karuma village (419534E / 236940N). (C) Vague contacts between mafic dykes and Awela gneiss. Number tag 10 cm, width of number plate 10 cm.

Metadolerite (A3Udo) – Archaean dark grey or dark greenish grey, medium- to fine-grained metadolerite dykes cut many of the Archaean gneisses and granites in the NUT. The width of these dykes ranges from meters up to tens of metres, or remains undefined, as many of the dykes are only exposed as *in-situ* boulders or chocolate-brown soil (Fig. 5.35A). For this reason, only a few of them

are shown on the summary geological map at the scale 1:1 million.

The main minerals observed in thin section are plagioclase, hornblende, pyroxenes, opaque minerals and garnet, while quartz and titanite are local accessory minerals. Three representative chemical analyses (see App. 2 , anal. 121–123) refer to basaltic compositions. Magnetic susceptibilities are usually



Fig. 5.35. (A) *In-situ* blocks of metadolerite within chocolate-brown soil. (B) Detailed image of massive, homogeneous metadolerite (364282E / 314799N). Number tag 8 cm.

low. These metadolerite dykes have undergone the same regional tectono-metamorphic development as their felsic host rocks, and their main foliation is consequently parallel to the fabric in the gneissic

country rock. Boudinage, microfolding, reaction rims or resorption zones along contacts with the gneissic host rocks are commonly observed.

5.6 Nakasongola-Bukungu Suite

This unit comprises granitic bodies located south of Lake Kyoga (Lehto et al. 2014, code 48), inside the NUT tectono-thermal unit but close to the palaeosuture between the WTT and NUT. Dating of the Nakasongola pluton yielded an unreliable age of ~2.63 Ga and a subsequent deformation/hydrothermal event at ~0.61 Ga (Mänttari 2014). Not knowing for certain that this ~2.63 Ga age is correct, and based on their setting, mineralogy and chemistry, we do not exclude the possibility that these granitic plutons represent equivalents of rocks belonging to the Kiboga Suite (Chapter 3).

Nakasongola granite (A3UNgr) – The Nakasongola granite occurs as a roughly ENE-trending body, measuring 25 km x ~6 km, near Nakasongola town (Figs 5.2 and 5.37). The country rocks are composed of homogeneous to banded, occasionally migmatitic gneisses, with amphibolites and dolerites. The main proportion the Nakasongola granite consists of homogeneous fine-grained white to orange-red to light grey coloured granite, with sparse to densely packed K-feldspar phenocrysts of more than a centimetre in size in the northern outcrops (Fig. 5.36A). A significant feature is the smooth and glassy nature of the rock surface and the gneissic foliation with quartz-

feldspar lenses. Unevenly distributed grains and stringers of mafic minerals, mostly magnetite, underline the gneissose foliation, as do thin, millimetre-wide parallel quartz ribbons. In places, the phenocrysts are cut by the strong planar fabric, while maintaining the prismatic crystal shapes (Fig. 5.36B). In other places, however, especially close to fault zones, the phenocrysts are flattened and obtain an Augen or glandular shape and the granite may obtain a blastomylonitic to mylonite appearance.

Bukungu granite (A3UBgr) – The well-exposed Bukungu granite measures 5 x 5 km and is located 55 km NW of Kamuli town (Fig. 5.37), where the River Nile enters Lake Kyoga. It forms a conspicuous positive radiometric potassium-uranium anomaly (Ruotoistenmäki et al. 2014). No discernible tectonic fabric or mineral flattening can be observed, which suggests that the rock is post-tectonic with respect to the surrounding country rocks composed of NUT granitic gneisses. The rock is equigranular and medium-grained and has a light, pinkish colour when weathered, but is light-grey with a waxy lustre when fresh, showing an uneven distribution of disseminated mafic grains.

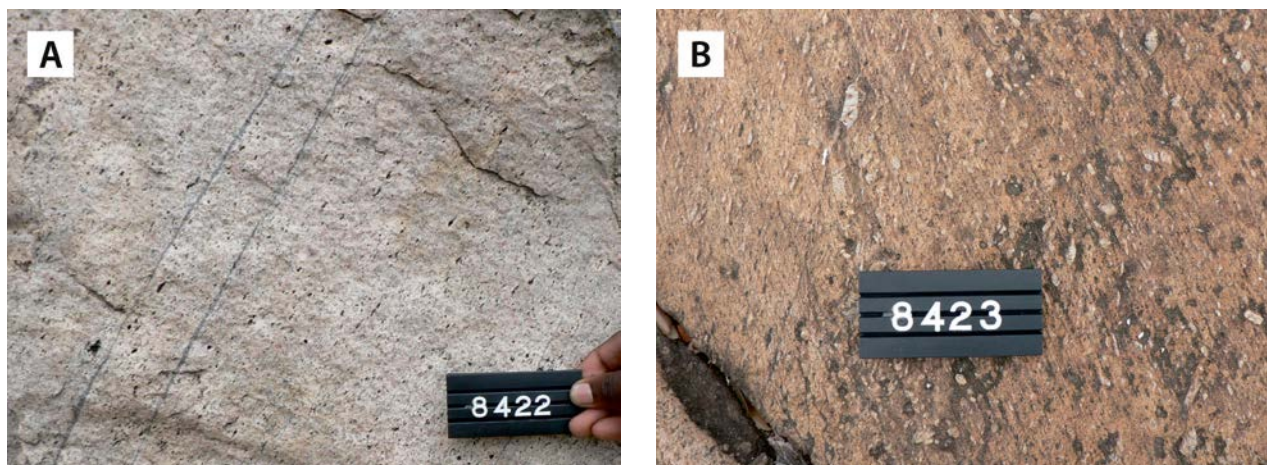


Fig. 5.36. (A) Fine-grained variety of the Nakasongola granite, showing a preferred orientation with a white waxy lustre, strings of quartz ribbons and veins defining a planar fabric (441875E / 146327N). (B) Porphyritic granite variety with a strong planar fabric. A quarry ~4 km NEE of Nakasongola town (443920E / 147146N). Number tag 8 cm.

Bukungu granite is composed of quartz, K-feldspar, plagioclase and biotite. Quartz is of unequal grain size and varies from angular to round to amoeba-shaped and shows undulose extinction and internally fractured regions. K-feldspar (microcline) dominates over plagioclase. Mesh-

like twinned grains are slightly curved in places and show various degrees of sericitisation. Granophyric quartz-feldspar intergrowths occur in places, as do deformed biotite flakes that show alteration into muscovite and epidote.

5.7 Geochronology

Apart from geochronological data from Leggo (1974), demonstrating a Neoproterozoic age for so-called 'Watian' granulites/charnockites in eastern Uganda, no older reliable geochronological data are known from northern Uganda. Laser-ICP-MS U-Pb age determinations by Link et al. (2010), yielding ages between 2637 and 2584 Ma, concur with the age data of the GTK Consortium

(LA-MC-ICP-MS method), discussed in detail by Mänttari (2014).

A major result is that like the West Nile Block (Bomu-Kibalian Shield), the NUT is composed of a Mesoarchaeon 2.99 Ga nucleus surrounded by a Neoarchaeon periphery with most ages between 2.66 Ga and 2.62 Ga, the Kaseeta granite being an exception with an age of 2.73 Ga.

5.8 Tectono-Thermal Evolution of the North Uganda Terrane

The present structural features of the NUT are mainly determined by post-Archaean tectono-thermal events, notably the late Mesoproterozoic (~1.0 Ga) development of the intracratonic N-S-trending Madi-Igisi Belt (Chapter 9) and Pan-African (0.69 Ga) tectono-thermal events during the Neoproterozoic (Chapter 11). After first peeling off these Neo- and Mesoproterozoic shells, we are able to construct a general outline of the Archaean development of the NUT.

5.8.1 Archaean development of the NUT

The original E-W grain has only been preserved in the central part of the NUT, showing refolded megascopic isoclinal fold structures with E-W fold axes, refolded into an open fold structure due to E-W, supposedly Pan-African compression. These structures can be studied using airborne geophysical maps (Ruotoistenmäki et al. 2014), such as the radiometric map in Figure 5.37.

Taking into account that prior to the development of the intracratonic Madi-Igisi Belt at ~1.0 Ga, the NUT and West Nile Block (Chapter 4) were part of the same Bomu-Kibalian Shield, we may expect a great deal of parallel development in both terranes. Geochronological data indicate that, like the WNB, the NUT is composed of a Mesoarchaeon nucleus surrounded by Neoarchaeon basement. In the WNB, these rocks have been assembled in the (~3.08 Ga) Uleppi

Complex, and in the NUT as the 2.99 Ga Karuma Complex. We suggest that prior to development of the ~1.0 Ga Madi-Igisi Belt, the Uleppi and Karuma Complexes, both showing granulite metamorphic conditions and amphibolite-grade retromorphism, formed a single Mesoarchaeon terrane, possibly belonging to the '*Formation du Nil occidentale*' or Garamba Gneiss Complex of the Bomu-Kibalian Shield (Fig. 4.1) in the northeastern DRC, to which Cahen (1954) attributed a poorly constrained Palaeoarchaeon age of 3.42 Ga.

With the exception of the 2.73 Ga Kaseeta granite, most of the gneissic granitoids in the NUT (Lehto et al. 2014, code 50) have ages between 2.66 Ga and 2.62 Ga, some 350 million years younger than the rocks of the Karuma Complex. These gneissic granitoids comprise a wide variety of deformed granitoids, migmatitic granitoids and gneisses of granitic, granodioritic or tonalitic composition, occasionally banded, elsewhere more homogeneous, equigranular or porphyritic. TTG banded gneisses and metagabbro occur in places. The 2.66 Ga Apuch granite migmatite and the 2.63 Ga Kuju granitic and granodioritic gneiss plot in the '*volcanic arc granites*' (VAG) or '*syn-collisional*' (syn-COL) fields in tectono-magmatic discrimination diagrams (Figs 4.36A-B). Some banded gneissic granitoids, e.g. 'Banded gneiss', 'Banded granite gneiss and migmatite' and 'Gulu banded TTG

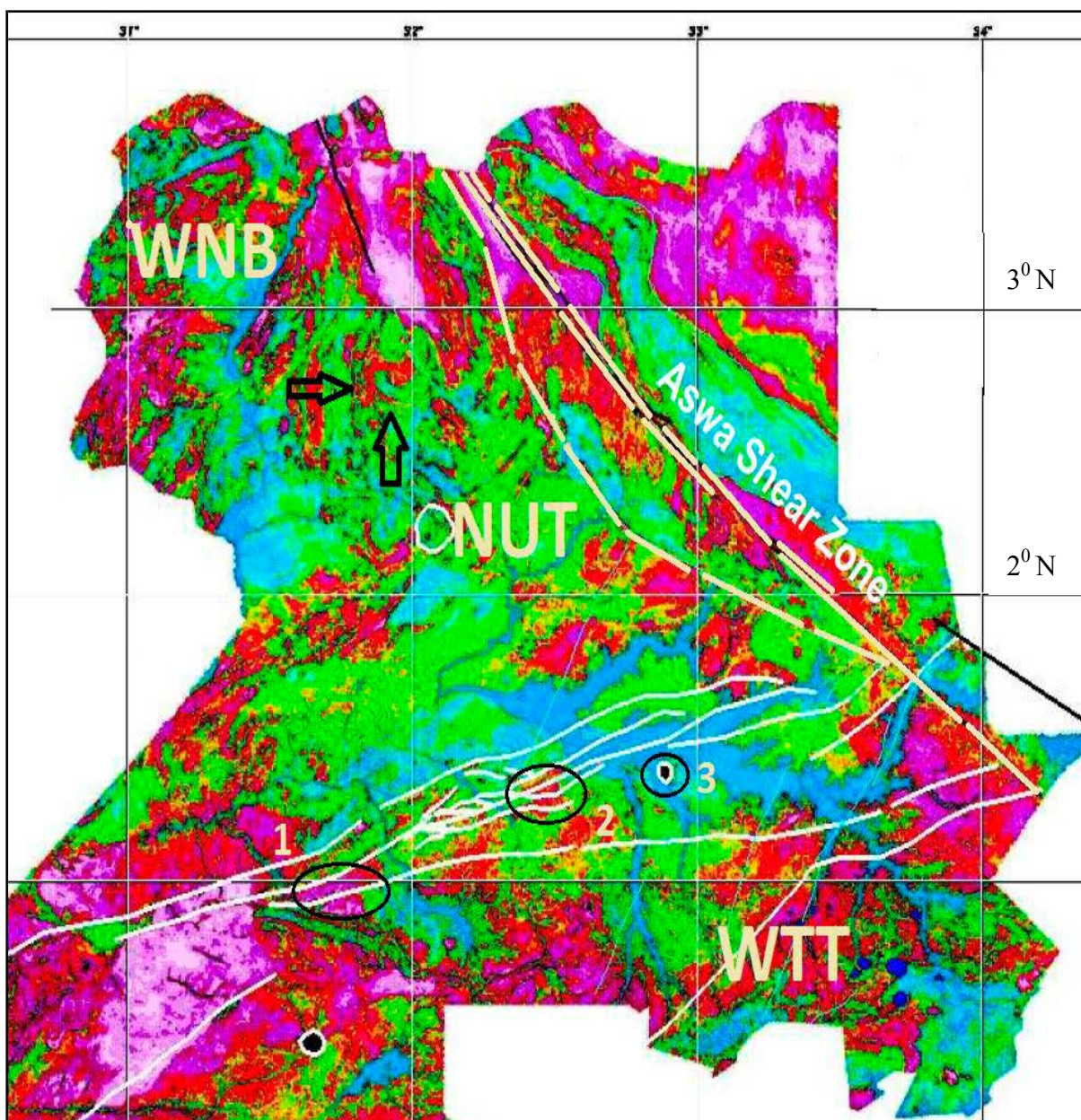


Fig. 5.37. Gamma ray spectrometry, total count channel (red-magenta strong radiation, blue-green weak). The dislocation zone between the North Uganda Terrane (NUT) and the West Tanzania Terrane (WTT) is indicated by white lines (WSW–ENE). The Aswa Shear Zone is shown in cream colours. 1 = Kiboga Suite; 2 = Nakasongola; 3 = Bukungu. Arrows point towards an E–W-trending megascopic isoclinal fold, refolded into an open fold structure due to E–W, supposedly Pan-African compression. The grid is one degree, here 110 km.

gneiss', may also have volcanic protoliths with an unknown sedimentary component.

Supracrustal rocks of the NUT have been assembled into the Amuru Group, comprising metamorphosed rocks with arkosic and sub-arkosic sandstone or sandstone protoliths, mixed mafic-felsic volcanics probably alternating with sediments and pyroclastic material, metagreywacke and amphibolites with metabasaltic lava protoliths having random obscure, pillow-like features, hinting at an extrusive sub-aquatic origin, although

elsewhere a pyroclastic protolith appears more likely. The presence of spatially associated skarnoids points to the erstwhile presence of carbonate material in the supracrustal succession. Quartz-sillimanite nodules in meta-sandstone (Fig. 5.6B) may have been derived from laterite/saprolite fragments and manifest Archaean weathering and soil development. The rocks of the Amuru Group have been intruded by the 2.66–2.62 Ga intrusives and are consequently older than 2.66 Ga.

Summarising the geochronological data (Mänttari 2014), we conclude that most gneissose-migmatitic rocks have ages between 2.6 and 2.5 Ga. Frequently, these rocks contain older inherited zircons with 'Kaseeta' ages. Examples include Gulu banded gneiss (2.7 Ga), Awela granite (> 2.83 Ga and > 2.73 Ga) and TTG granites (~2.79 Ga). The Katakwi granite contains a zircon with a 2.74 Ga core, surrounded by a 2.63–2.62 Ga rim. Less deformed, non-migmatitic granitoids such as the Katakwi granite are believed to have formed from partial melting of 2.6–2.5 Ga orthogneissose-migmatitic rocks. Metamorphic U-Pb zircon ages of 2.58 Ga have been encountered in several samples, as have rims with 0.69 Ga Pan-African ages.

Based on the scarce geochronological data at hand, and assuming parallel geodynamic developments for the NUT and WNB during the Archaean, we distinguish a Meso- and a Neoarchaeal phase of crust formation according to the following scenario:

- Deposition of rocks of the Karuma Group at ~2.99 Ga, together with ~3.08 Ga charnockite and older metasediments of the Uleppi Group (WNB). The oldest zircons in Uleppi paragneissic host rock yield maximum zircon ages of ~3.00 Ga and 2.87 Ga, possibly representing the timing of peak granulite-grade metamorphism, followed again by two phases of amphibolite-grade metamorphic overprinting, one dated at ~2.63 Ga and the other at 2.57–2.55 Ga.
- Emplacement of the Kaseeta granite at 2.73 Ga. This magmatic event is reflected by the youngest U-Pb age of ~2.74 Ga from a structurally rather homogeneous zircon, indicating a Neoarchaeal thermal event affecting felsic granulites of the Karuma Complex. U-Pb data from four analyses from the oldest rims in ~3.08 Ga Goli charnockite of the WNB scatter around 2.7 Ga.
- Emplacement of banded mafic volcanics and associated sills and feeders of the War Group (WNB) at 2.63 Ga into the Mesoarchaeal Uleppi Group together with widespread retrogradation under amphibolite facies conditions of the same complex. We like to correlate these volcanics with the volcanics of the Amuru Group (NUT), acknowledging that the War and Amuru volcanics both have in their composition an 'Oceanic' or 'Island arc tholeiitic' affinity (Fig. 4.34A), and both are spatially associated with (fuchsite-bearing) quartzites. Simultaneously,

new Neoarchaeal crust is formed, which also suffered metamorphism ranging from granulite to amphibolite facies conditions. In the NUT, these rocks have ages of 2.66 Ga to 2.64 Ga. Migmatization and partial melting resulted in emplacement of 'younger granitoids', now present as less deformed granitic gneisses at around 2.62 Ga.

- Accretion of War Group island arc and accretionary wedge rocks and collision of the Mesoarchaeal Uleppi and Neoarchaeal crustal blocks of the WNB and NUT are broadly simultaneous processes at around 2.63–2.62 Ga.
- Collision and amalgamation between the already cratonised WNB/NUT (Bomu-Kibalian Shield) with Neoarchaeal portions of the West Tanzania Terrane (Tanzania Craton) also happened prior to 2.64–2.61 Ga, given that the mid-crustal dislocation zone between the two terranes is intruded by granitoids (Kampala and Tororo Suites) of the West Tanzania Terrane.
- Collision and amalgamation of the aforementioned blocks with the Lake Victoria Terrane at 2.59 Ga to 2.55 Ga (the 'Aruan event' in Table 4.1).
- The Late Archaean (2.49 Ga) Kiboga Suite is most likely related to a post-kinematic transtensional event, forming the suture between the West Tanzania Terrane (WTT) and NUT (Fig. 5.37, the Nakasongola Discontinuity, Ruotoistenmäki 2014). Neglecting their doubtful age, the Nakasongola-Bukungu granites have supposedly been emplaced during the same 'Kiboga' event.

5.8.2 Late Mesoproterozoic development of the NUT

Until the development of the Madi-Igisi Belt and deformation and metamorphism of the ~1.0 Ga volcano-sedimentary rocks of the Mirian Supergroup, the NUT and WNB both supposedly belonged to the Bomu-Kibalian Shield of the north-western DRC (although we cannot exclude that the Madi-Igisi belt is superposed on an older suture; see Chapter 9). Late Mesoproterozoic E–W compression, known as the Lomanian orogeny (Pohl 1988), gave rise to double-vergent thrusting of the Madi-Igisi Belt, affecting rocks of the NUT and the WNB, and transposition of the erstwhile E–W grain into N–S structural trends along and within the fold belt. This was followed by the

development of a major fault zone in the NUT, east of the Madi-Igisi Belt, between the town of Moyo and Lake Albert (Chapter 9). This again resulted in large-scale transposition of the E–W grain of the western segment of the NUT into N–S structural trends. There is evidence, for example the Neoproterozoic age of monazite in Mirian lithologies, that thrust and fault planes in and near the Madi-Igisi Belt were rejuvenated during the Pan-African Orogenic Cycle, most likely as a far-field effect of compression and shearing in the Karamoja Belt of eastern Uganda.

5.8.3 Neoproterozoic development of the NUT during the Pan-African

As a sequel to the early age determinations by Leggo (1974), new U-Pb zircon data (Mänttari 2014) indicate that a far larger chunk of alleged Archaean ‘unspecified crystalline basement’ (Fig. 3.1; DGSM 1966) is indeed Neoproterozoic in age and belongs to the allochthonous West Karamoja Supergroup, with ages between 0.74 Ga and 0.68 Ga. Apart from these allochthonous rocks, there are also numerous Neoproterozoic *in-situ* granitoid plutons, dated at 0.66 Ga.

Forming the northeastern corner of the proto-Congo Craton, north Uganda was supposedly

involved in the formation of two major fold belts during the Pan-African Orogenic Cycle. E–W compression as a result of collision and amalgamation of East and West Gondwana was followed by N–S compression due to collision and amalgamation of the already united East/West Gondwana with the Sahara Metacraton. Whereas the formation of the Karamoja Belt and tectonic emplacement of rocks belonging to the Karasuk Supergroup and West Karamoja Group are related to the first E–W compressional event, magmatic emplacement of some of the Neoproterozoic *in-situ* granitoids is supposedly related to the second N–S compressional event.

E–W compression during the collision and amalgamation of East and West Gondwana gave rise to W- and SW-directed thrusting. Tectonic escape of the NW corner of the proto-Congo Craton resulted in sinistral shear along the ASZ. Both low-angle thrusting and high-angle shearing resulted in large-scale transposition of the original E–W grain of the NUT into N–S-trending structures. In outcrop, this is manifested by the development of ‘flaggy’ gneisses and by the formation of blastomylonitic foliations and obliteration of older, often gneissose fabrics. Further details are presented in Chapter 11.

6 PALAEOPROTEROZOIC ROCKS OF THE RWENZORI FOLD BELT

6.1 Introduction

Regional Setting – The Rwenzori Fold Belt of Uganda (Fig. 6.1) is the northernmost part of a major Palaeoproterozoic system of fold belts wrapped around the Tanzania Craton. In its southernmost part, the fold belt system includes the E-W trending Usagaran Belt, located between the southern Tanzania Craton and the Bengweulu Block of Zambia. West of the Tanzania Craton the fold belt system curves into a NW-SE and N-S direction and forms a suture between the Tanzania and Congo Cratons (Fig. 6.2). In this area, the Usagaran passes into the Ubende Belt (or Ubendian) of southwestern Tanzania and Katanga (DRC) and further northwards into the Rusizian of Burundi, Rwanda and Kivu (DRC), to terminate in the Rwenzori Fold Belt of Uganda.

The Rwenzori Fold Belt is located in the southern part of Uganda. It underlies the western segment of the WSW-ESE trending ‘low-magnetic belt’ described in Chapter 3. Its structural orientation is mostly ENE-WSW in the eastern segments of the belt and curves into a N-S trend in the southwest-

ernmost parts of the belt (Fig. 6.1). However, in the uplifted block of the Rwenzori Mountains and Kilembe area, the structural orientation is SW-NE.

Toro-Buganda problem – Defining the ‘Buganda-Toro System’ has always been a dilemma in the geology of Uganda. Combe (1932) coined the term ‘Toro Quartzites’ to describe quartzites in the Toro District of western Uganda. Simmons (1932) reported that the ‘Toro’ rocks are older than and unconformably overlain by rocks of what was then considered to be the ‘Karagwe-Ankolean System’ at Buhweju. A similar relationship with older schists overlain by so-called Karagwe-Ankolean rocks was observed by Simmons (1932) in the Masaka area. Simmons (1932) traced this unconformity to Kiya Hill in the south and as far north as Kijumba. Later, Bisset (1939) mapped the unconformity further northwards beyond Lusese. The older meta-sedimentary succession was assigned to the ‘Toro System’ (Combe 1936, 1938), a metasedimentary unit composed of schists, gneisses and quartzites.

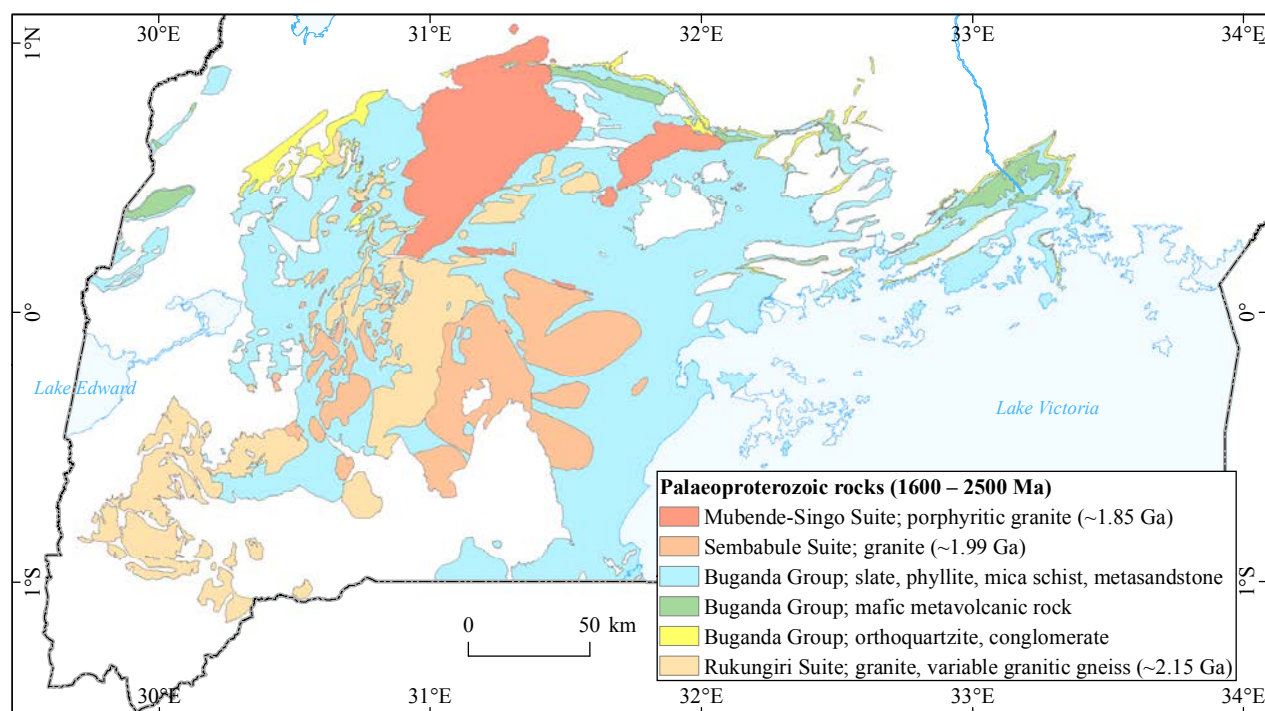


Fig. 6.1. Geological outline of the Rwenzori Fold Belt (simplified after Lehto et al. 2014).

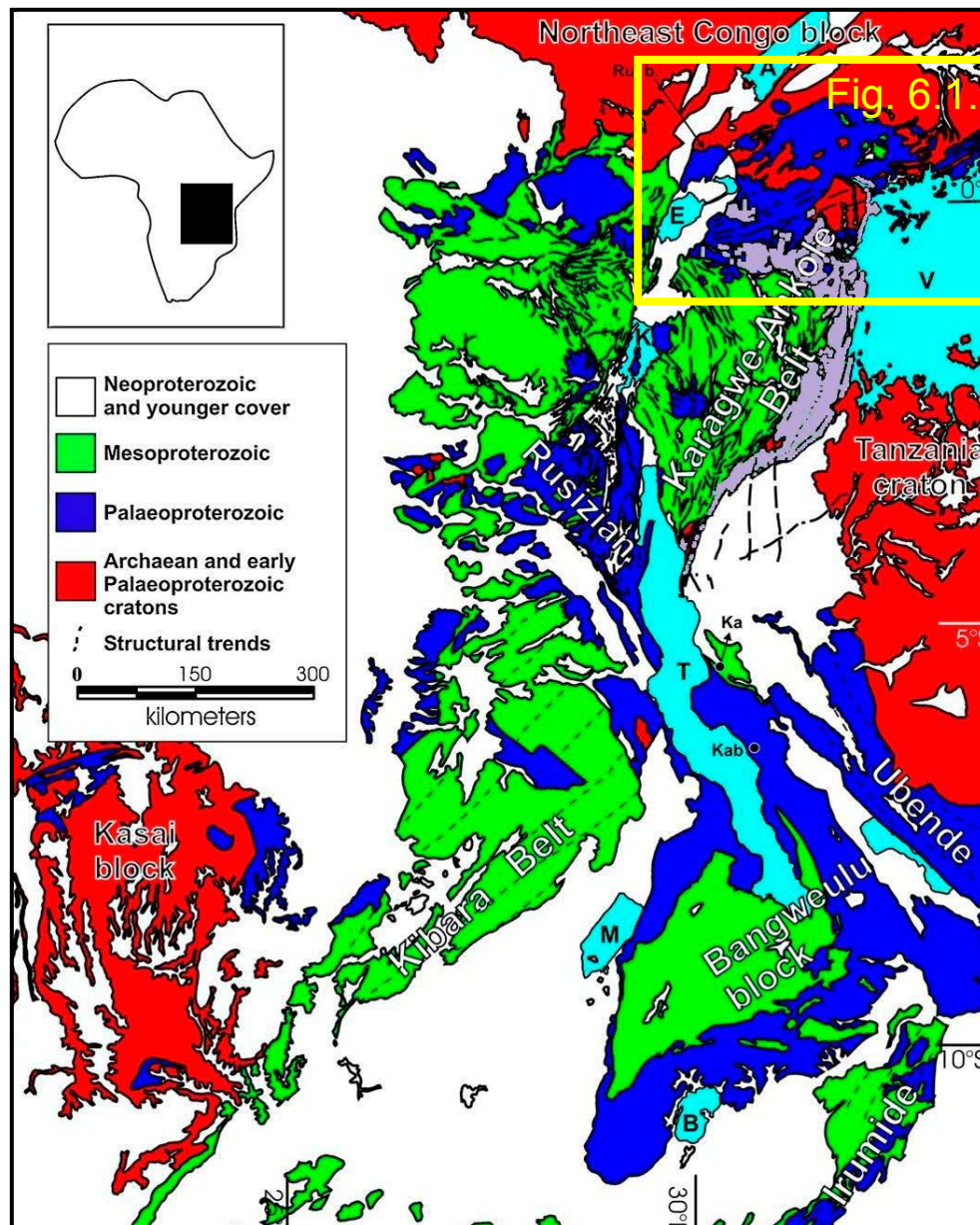


Fig. 6.2. Regional setting of the superposed Palaeoproterozoic Ubende-Rusizian-Rwenzori Belt (blue) and the Mesoproterozoic Kibara Belt (green) between the Archaean Kasai Block, Tanzania Craton and NE Congo Block (= Bomu-Kibalian Shield) of the proto-Congo Craton. The latter is divided into the Kibara Belt (KIB) *s.s.* and the North Kibaran Belt (NKB = Karagwe-Ankole Belt, KAB, according to Tack et al. 2010, with kind permission of the Elsevier Ltd.). Note the NW-SE trending Ubende-Rusizian basement high that causes a break in continuity between the NKB/KAB and the Kibara Belt (KIB) *s.s.*. Key: A: Lake Albert; E: Lake Edward; V: Victoria Lake; K: Lake Kivu; T: Lake Tanganyika; M: Lake Mweru and B: Lake Bangweulu; Ru. b.: Palaeoproterozoic Ruwenzori Fold Belt (see explanations in text). Greyish purple: Proterozoic post-Rwenzori platform rocks of the Kagera-Buhjewe Supergroup (see Chapter 7). Figure modified after Tack et al. (2010). Note that the area shown in Fig. 6.1 is marked by a rectangular yellow box.

Combe (1948) later defined the ‘Toro System’ as older than the ‘Karagwe-Ankolean’ rocks and younger than the ‘Basement Complex’.

In subsequent studies, a non-metamorphic to low-grade sequence of arenites, argillites (with minor carbonate intercalations) and argillaceous sandstones and mafic volcanic rocks from the Buganda District in the Kampala-Jinja area (no. 1

in Fig. 6.1) was assigned to the ‘Buganda System’ (Macdonald 1963a). These rocks rest on a high-grade metamorphic, migmatitic or igneous basement. In the absence of reliable geochronological data, the ‘Buganda System’ was initially correlated with the Neoproterozoic Nyanzian and Kavirondian of what is now defined as the Lake Victoria Terrane (Chapter 2) (Davies, 1935a, McConnel, 1959a,

1959b, King 1959). Other workers correlated this succession with the Mesoproterozoic ‘Karagwe-Ankolean System’ – the present Akanyaru-Ankole Supergroup (Chapter 8) – because of their similarity with rocks in SW Uganda (King 1947a, Davies & Bisset 1947, Harris 1949, Pallister 1959). However, alternative interpretations were proposed by Barth & Meinhold (1974) and Brinckmann & Gabert (1977) who incorporated these rocks into the Kibalian of the northeastern Congo Craton, the Bomu-Kibalian Shield. Following a similar line of thinking, Cahen & Snelling (1966) established the ‘Buganda-Toro-Kibalian Belt’, which, Tanner (1970, 1973a, 1973b) renamed as the Rwenzori Fold Belt.

Stressing identical structural trends, Holmes (1951) suggested a relation between the non- to epimetamorphic Buganda cover in the Kampala-Jinja area (no. 1 in Fig. 6.1) and the high-grade muscovite-biotite ± cordierite ± sillimanite gneisses and quartzites, and migmatites of the ‘Toro System’ in the western segment of the Rwenzori Belt. Likewise, the epimetamorphic cover rocks of the ‘Buganda Series’ were correlated with the schists, grits, quartzites and amphibolites of the Rwenzori Mountains (no. 3 in Fig. 6.1). For a long time the terms ‘Toro’, ‘Buganda’ and ‘Buganda-Toro’ were

used as synonyms with a preference for ‘Buganda’ in central Uganda and for ‘Toro’ in western Uganda and the Rwenzori Mountains.

Partly based on WR Rb-Sr ages (Holmes & Cahen 1955, Davis et al. 1956; see Section 6.7), Tanner (1970) and Cahen et al. (1984) advocated a Palaeoproterozoic age for the ‘Buganda-Toro System’. Although imprecise, these geochronological data indicated that there is a large time gap between the ‘Karagwe-Ankolean’ and Buganda metasediments. It was also realised that the ‘Buganda-Toro System’ is part of an arcuate E-W trending Rwenzori Fold Belt that can be traced southwards into the Rusizian Belt and the NW-SE trending Ubendian Fold Belt. The latter were assigned a Palaeoproterozoic age, indicative of formation during the Eburnian Orogenic Cycle (~2.1–1.8 Ga, Section 1.3). According to Lenoir et al. (1994), the evolution of the Palaeoproterozoic Usagaran-Ubendian Belt was a two-phase process with the first ‘collision’ phase at around 2100–2025 Ma and a second ‘dextral shear’ phase at around ~1860 Ma (Fig. 1.4).

We agree with some earlier authors (e.g. Holmes 1951) that the high-grade muscovite-biotite ± cordierite ± sillimanite gneisses and quartzites and migmatites of the Toro area and the Rwenzori Mountains have formed by progressive metamorphism

Table 6.1. Lithologies of the Rwenzori Fold Belt. The oldest parts of the Rukungiri Suite refer to the basement of the Belt. Ages published in Mänttari (2014). Map codes refer to rock units in unpublished 1:250 000 -scale geological maps delivered to DGSM.

| Group/Complex | Formation/Suite | Lithology | Map Code | |
|--|--|--|------------------|--------------|
| ^^^^^^^^^^^^^^^^ | Mubende-Singo Suite | <i>Sericitised granite</i> | <i>PIMSsg</i> | |
| | | <i>Coarse to megacrystic granite (1848±6 Ma)</i> | <i>PIMSmg</i> | |
| ^^^^^^^^^^^^^^^^ | ^^^^^^^^^^^^^^^^ | ^^^^^^^^^^^^^^^^ | ^^^^^^^^^^^^ | |
| ^^^^^^^^^^^^^^^^ | Sembabule Suite | <i>Kasagama Granite (1964±4 Ma)</i> | <i>PISgrh</i> | |
| | | <i>Rwamasha Granite (1987±5 Ma)</i> | <i>PISgrc</i> | |
| ^^^^^^^^^^^^^^^^ | ^^^^^^^^^^^^^^^^ | ^^^^^^^^^^^^^^^^ | ^^^^^^^^^^^^ | |
| Buganda Group | Nile Formation | <i>Muscovite-biotite schist, locally porphyroblastic</i> | <i>PIBNcgn</i> | |
| | | <i>Porphyroblastic phyllite and schist</i> | <i>PIBnamp</i> | |
| | | <i>Mica schist with quartzitic interbeds</i> | <i>PIBNms</i> | |
| | | <i>Quartzite, siltstone</i> | <i>PIBNq</i> | |
| | Bujagali Member | <i>Sericite quartzite and quartzite</i> | <i>PIBNsq</i> | |
| | | <i>Mafic volcanic rock, basalt (2.0±0.2 Ga)</i> | <i>PIBNmv</i> | |
| | | <i>Slate, shale, phyllite</i> | <i>PIBNsh</i> | |
| | Victoria Formation | <i>Orthoquartzite, conglomerate</i> | <i>PIBVqc</i> | |
| | ^^^^^^^^^^^^^^^^ | ^^^^^^^^^^^^^^^^ | ^^^^^^^^^^^^^^^^ | ^^^^^^^^^^^^ |
| | Rukungiri Suite (part of the P1Rvvg is basement for the Buganda Group) | <i>Quartzo-feldspathic gneiss</i> | <i>P1Rqgn</i> | |
| <i>Porphyritic granitic gneiss</i> | | <i>P1Rmpg</i> | | |
| <i>Muscovite gneiss, porphyritic in part</i> | | <i>P1Rmmg</i> | | |
| <i>Kalunga granite (~ 2.13 Ga)</i> | | <i>P1RKgr</i> | | |
| | <i>Variable granitic gneiss (2.15 Ga)</i> | <i>P1Rvvg</i> | | |

of the Buganda non- to epimetamorphic sedimentary cover. However, high-grade cover rocks are not always easy to distinguish from similarly high-grade Palaeoproterozoic basement. For example, in the Lake Wamala area, Johnson (1960) attributed ENE trending quartz–feldspar–biotite–muscovite gneisses (incorrectly called ‘Granulitic Gneisses’) and muscovite – biotite ± cordierite ± sillimanite gneisses to the ‘Toro Complex’. We attribute the first mentioned rocks to the pre-Buganda basement, we consider the second mentioned rocks to represent a high-grade equivalent of the Buganda Group. With hindsight, the term ‘Toro System’ thus encompassed both pre-Buganda and Buganda lithologies. To avoid confusion we have decided to drop the term ‘Toro’ altogether.

Based on available geochronological data and in agreement with modern lithostratigraphic regulations, we attribute the cover sequence of metasediments and associated basalts of the former ‘Toro System’ or ‘Buganda-Toro System’ to the Buganda Group, a term coined by McConnell (1959a). This cover sequence overlies a basement composed of gneisses, migmatites and mildly deformed granitoids of the 2.64 Ga West Tanzania Terrane in the east, and 2.2–2.1 Ga quartzofeldspathic gneisses further to the west and southwest. The metasedimentary cover sequence has been invaded by the broadly syn-kinematic granitoids of the Sembabule Suite (1.99–1.96 Ga) and the post-kinematic granitoids of the Mubende-Singo Suite (1.85 Ga) (Table 6.1).

6.2 Lithostratigraphy of the Palaeoproterozoic Rwenzori Basement

Rukungiri Suite

In Uganda, this 2.15–2.13 Ga old unit of migmatites and gneisses was formerly assigned to the ‘Toro Complex’ or classed as ‘undifferentiated basement’. The suite is exposed as variably sized inliers or related areas in the southwestern part of the country (see Lehto et al. 2014). It is similar to the ‘Rusizian System’ in Rwanda, Burundi and Kivu (DRC).

Variable granitic gneiss (P1Rvgg) – These rocks are mostly medium- to coarse-grained, partly migmatitic and polydeformed granite gneisses and biotite-bearing quartzofeldspathic gneisses with

local intercalations of mafic rock. The main mafic mineral is biotite, although in places there are also variable percentages of magnetite and hornblende. This unit is considered to be derived from both magmatic and supracrustal protoliths; the latter mostly of felsic volcanic origin. Supporting arguments for this interpretation include (1) the common presence of compositional layering resembling primary banding (Fig. 6.3A) and (2) the occurrence of some feldspar phenocrysts in relatively homogeneous gneiss possibly indicating an intrusive origin (Fig. 6.3B).



Fig. 6.3. (A) Migmatitic, biotite-bearing quartzofeldspathic gneiss with leucocratic segregations parallel to the gneissose foliation (229077E / 10849N). (B) Relatively homogeneous, foliated granitic rock containing K-feldspar phenocrysts (or xenoblasts) (246252E / 78866N). The number tag is 10 cm in width.



Fig. 6.4. (A) Foliated porphyritic granite gneiss (176691E / 69007N). (B) Gneissose Kalonga granite with a vague compositional banding (315110E / 45547N). The number tag is 10 cm in width.

Porphyritic granite gneiss and Muscovite-bearing granite gneiss, partly porphyritic (PIRmpg, PIRmmg) – These gneiss units are exposed as areas of variable size in and around the town of Mbarara. Because of relatively high potassium concentrations relative to the adjacent rock, these units can be readily delineated with airborne radiometric data.

Both lithological units are composed of grey or purple grey, mostly medium-grained, foliated and porphyritic gneisses with scattered K-feldspar phenocrysts; typically ~10 x 20–30 mm in size, that are parallel to the foliation (Fig. 6.4A). These gneisses have predominantly granitic compositions, comprising quartz, K-feldspar and plagioclase. Biotite is the main mafic mineral in the porphyritic granite gneiss, constituting around 10–15 % of rock volume, while muscovite-bearing granite gneiss forms a minor sub-facies. Some granite gneiss variants have an indistinct compositional banding while in places there are thin, N-S trending quartz veins.

Quartzofeldspathic gneiss (PIRqgn) – Medium-grained quartzofeldspathic gneisses with a well-developed gneissic foliation and metamorphic banding occur in an area south and southwest of the Mubende granite batholith. The main mafic mineral of this gneiss is biotite, which appears locally as aggregates up to 10 mm in size. Deformed leucosomes are either parallel to the dominant foliation or form cross-cutting segregation veins. These gneisses are considered to be derived from a felsic volcanic protolith.

Kalonga granite (PIRKgr) – East of the Mubende granite batholith (Fig. 6.16), four bodies of dark grey, rather homogeneous, intensively deformed Kalonga granite (Fig. 6.4B) with blastomylonitic textures occur as isolated areas surrounded by mica schist belonging to the Nile Formation (Buganda Group). These granite bodies exhibit a strong signature on airborne radiometric maps, readily allowing delineation of their areal extent. The major minerals of the Kalonga granite are K-feldspar, plagioclase, quartz and biotite (~15 vol%) while late (retrograde?) muscovite and chlorite have clearly developed at the expense of biotite; accessory minerals include sphene and ilmenite. Chemical composition of deformed Kalonga granite is presented in Appendix 2 (anal. 124).

In view of their higher degree of deformation, metamorphism and an age of ~2.13 Ga (Mänttari 2014), they are assigned to the pre-Buganda basement. We postulate that the Kalonga granites represent a phase of pre-orogenic magmatism with both plutonic and volcanic protoliths related to the formation of the Rwenzori trough, or alternatively, part of a syn-collisional magmatic arc (Section 6.8). They exhibit a strong NE-SW trending foliation, which is approximately parallel to trends observed in the metapelitic country rocks of the Buganda Group. On old 1:100 000 geological maps (Johnson 1960) these granites are called granulitic gneisses. In this context the term “granulitic” refers to texture, i.e. to the even-grained granular nature of the rock and not to a granulite facies metamorphic rock.

6.3 Lithostratigraphy of the Palaeoproterozoic Buganda Group

6.3.1 Introduction

The base and top of the Buganda Group are poorly constrained and therefore any estimate of the thickness of this Palaeoproterozoic volcano-sedimentary succession is highly speculative. Near the town of Jinja, Pallister & Barnes (1954) estimated a thickness of 1000 m or less. However, 100 km to the west, in Busiro and Mawokoto Counties, it has been assumed that the thickness is over 7000 m (Pallister 1959). We propose that this eastward reduction in thickness is due to progressive uplift and erosion, and that prior to these processes the supracrustal rocks of the Buganda Group filled a far larger area of the 'low-magnetic belt' described in Chapter 3.

In the area between Jinja and Kampala, Pallister et al. (1953), Pallister & Barnes (1954) and Pallister (1959) proposed the following subdivision (from top to bottom):

- (5) Upper Phyllites and Ferruginous Quartzites
- (4) Amphibolite and Associated Rocks
- (3) Mudstone, Shale, Phyllite and Schist Formation
- (2) Sandstone-Quartzite Formation
- (1) Lower Quartz-Mica Schists

Unit (4) corresponds to mafic metavolcanic rock, including metatuffs, that occur in the Jinja and Kidoga areas in particular (King 1959, King & de Swardt 1970). Ultramafic rocks as reported by Brinckmann & Gabert (1977) have not been encountered during the recent mapping campaign.

As described above, these non- and epimetamorphic rocks grade west- and southwest-wards into poorly outcropping higher grade schists and gneisses. This has resulted in a large number of lithostratigraphic units, whose mutual correlation and stratigraphic position is difficult to establish. As a general rule, however, the succession begins with arenites, fines upwards, grades into pelites, and is then characterised by mafic metavolcanic rocks.

6.3.2 Victoria Formation

Orthoquartzite, conglomerate (PIBVqc) – This is a sequence of variable thickness comprising strongly metamorphosed and deformed orthoquartzites, sericite quartzites and quartz rocks, which forms a significant geomorphological feature in central-southern Uganda: i.e. conspicuous ridges or hogbacks that are often covered by quartzite or quartz rock boulder fields (Fig. 6.5).



Fig. 6.5. Orthoquartzite of the Victoria Formation forming a prominent ridge 22 km SW of Luwero town (428448E / 75768N).

This extensive metasedimentary unit can be followed intermittently from its type area east of the town of Jinja, through the city of Kampala, to the south of the town of Kiboga and then into the mountains east of Fort Portal in western Uganda.

Although the base of the formation has not been observed, Pallister (1959) described thin, irregular patches of quartz-mica schist or muscovite schist between Buganda quartzite and Archaean basement gneisses in the Grant Bay area, east of Kampala, but generally his 'boundary quartzite' separates 'extensive areas of Archaean basement' from phyllites and schist of the former 'Buganda Series' (Pallister 1959, p. 31). We cannot confirm the presence of such quartz-mica schist intercalations and conclude that these quartzitic rocks rest directly and unconformably on Archaean gneisses. From a limited number of observations, we assume that the contact of Victoria quartzites with pelites of the overlying Nile Formation is gradational.

In the Jinja area, the basal orthoquartzite of the Buganda Group has well-developed bedding with individual beds 0.5 to 1 m wide. This fine-grained, well-sorted rock is extremely pure (a possible feedstock for glass manufacture?) and is composed of

rounded quartz grains in a quartz cement. A well-developed fracture cleavage allows the rock to be used locally as flagstone. In places there are slightly coarser (grain size 2-3 mm) and finer grained varieties, the latter being thinly bedded and exhibiting conchoidal fractures.

In the central part of the Kampala map sheet area the Victoria Formation orthoquartzite is composed solely of similar fine- to medium-grained, recrystallised quartz. The amount of impurities (mainly detrital feldspar, biotite, muscovite, tourmaline, zircon and rutile) is generally less than 1-5% of the rock volume. Recrystallisation has obliterated most sedimentary features and only occasionally thin, laminar bedding is visible (Fig. 6.6A). Ripple marks and cross-bedding have been rarely observed in more feldspathic quartzite varieties (Fig. 6.6B). Commonly, pure orthoquartzite grades into coarse-grained, massive quartz rock or strongly foliated sericite quartzite.

With increasing deformation, e.g. in strongly tectonised and faulted zones, in places orthoquartzite has been transformed into massive, milky white quartz rock. Generally, this rock is composed solely of coarse-grained, euhedral

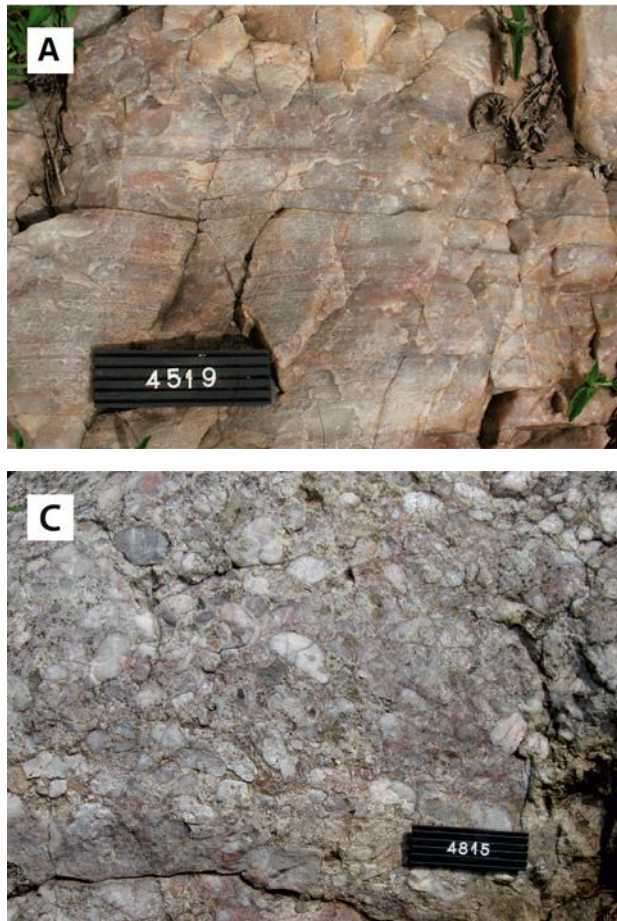


Fig. 6.6. Sedimentary structures in orthoquartzites of the Victoria Formation. (A) Laminar bedding in pure orthoquartzite (428448E / 75768N). (B) Tabular cross bedding in an arkosic interbed of orthoquartzite (376677E / 91679N). (C) Monomict quartz-pebble conglomerate horizon in the same outcrop. The number tag 12 cm.

quartz crystals, indicating repeated fracturing and recrystallisation, thereby destroying any textural feature suggestive of a sedimentary origin. Macroscopically the thoroughly recrystallised rock cannot be distinguished from quartz dykes of hydrothermal origin, a problem already discussed by Pallister (1956), and the evidence for a sedimentary origin of such recrystallised rock is generally by extrapolation from closely associated, better preserved quartzite varieties.

Although true basal conglomerates have not been observed, various thick interbeds of quartz pebble conglomerate have been found at several locations in the lower part of the Victoria Formation (Pallister 1956). The most well-exposed outcrops are on the northern slopes of orthoquartzite ridges between the towns of Wobulenzi and Kiboga. In this area, a matrix-supported, generally monomictic conglomerate forms several thin interbeds within a pure orthoquartzite (Fig. 6.6C). The well-rounded clasts are predominantly composed of vein quartz, but random clasts of ophitic-textured dolerite and a fine-grained mafic rock are also present. Tabular cross bedding in an adjacent arkosic quartzite interlayer indicates that the sequence has

a southwards way-up direction, and confirms the stratigraphic position of conglomerate interbeds in the lower part of orthoquartzite unit.

6.3.3 Nile Formation (incl. Bujagali Member)

Slate, shale, phyllite (P1BNsh) – The poorly exposed Nile Formation is widespread over an E-W trending area in central-southern Uganda where it occurs on the southern side of elongated Victoria quartzite ridges and the Bujagali basalts. The Nile Formation is mostly composed of very fine-grained slate.

The slate usually exhibits a rather vertical slaty cleavage and a common crenulation cleavage (Figs 6.7A-B). Locally, the rock grades into mauve laminar shale with graded bedding (Fig. 6.7C). Both types can occur in homogeneous, metre-wide beds. The Nile slates are mainly composed of very fine-grained quartz and sericite with minor amounts of ferruginous matter (goethite, hematite and ilmenite) either in microcrystalline aggregates or as individual crystals. In outcrops, the unaltered slate has a greyish colour but with alteration the colour grades into mauve or purple. Because of



Fig. 6.7. (A) Road cut exhibiting subvertical foliation in silty slate of the Nile Formation. (B) Detailed image of a silty slate in the same road cut (403693E / 68962N). The number tag is 10 cm in width. (C) Laminar shale with faint graded bedding (363940E / 93590N). The number tag is 8 cm in width.

increased regional metamorphism, the slates grade into shales and phyllites, as indicated by the increase of the grain size of mica. Conversely, some slates resemble shale even where metamorphism has been very weak.

Mafic volcanic rock, mafic tuff, chert of the Bujagali Member (P1BNmv) – The Bujagali Member is included in the lower part of the Nile Formation. This member has earlier been assigned to the ‘Buganda-Toro Supergroup’ of Barth & Meinhold (1974) who considered the rocks to be part of a volcano-sedimentary succession that had been deposited in the Buganda-Toro ‘geosyncline’ and subsequently deformed and metamorphosed in the Rwenzori Belt. They stressed that the member is exposed without interruption in a zone stretching from the Rwenzori Mountains to the Jinja area, a distance of some 500 km, and possibly even further eastwards as far as the Iganga granitoids.

The Bujagali basalts display a variably thick sequence of basaltic metavolcanic rocks extruded onto, or in places emplaced into the low-grade metapelites of the Nile Formation. They show a variety of textures. However, the abundance of pillow lava textures indicates that the basalts have been extruded mainly under subaqueous conditions. As well as in the type area at Bujagali Falls (Fig. 6.9), similar metabasalts are exposed in the Lugazi area E of Kampala, along the Kampala-Luwero highway, E and NW of the Bulaga plateau and S of the town of Kiboga. In the Kiboga region, where this metavolcanic unit comprises a continuous, coherent belt of basaltic pyroclastic rocks and lava flows, measuring 50 km long and up to 5 km wide, they form a distinct area with a weak signature on radiometric maps (cf. Fig. 6.15). Several outcrops of fine-grained pyroclastic material that occur locally in the basal part of volcanic successions are an indication of a transitional contact between the

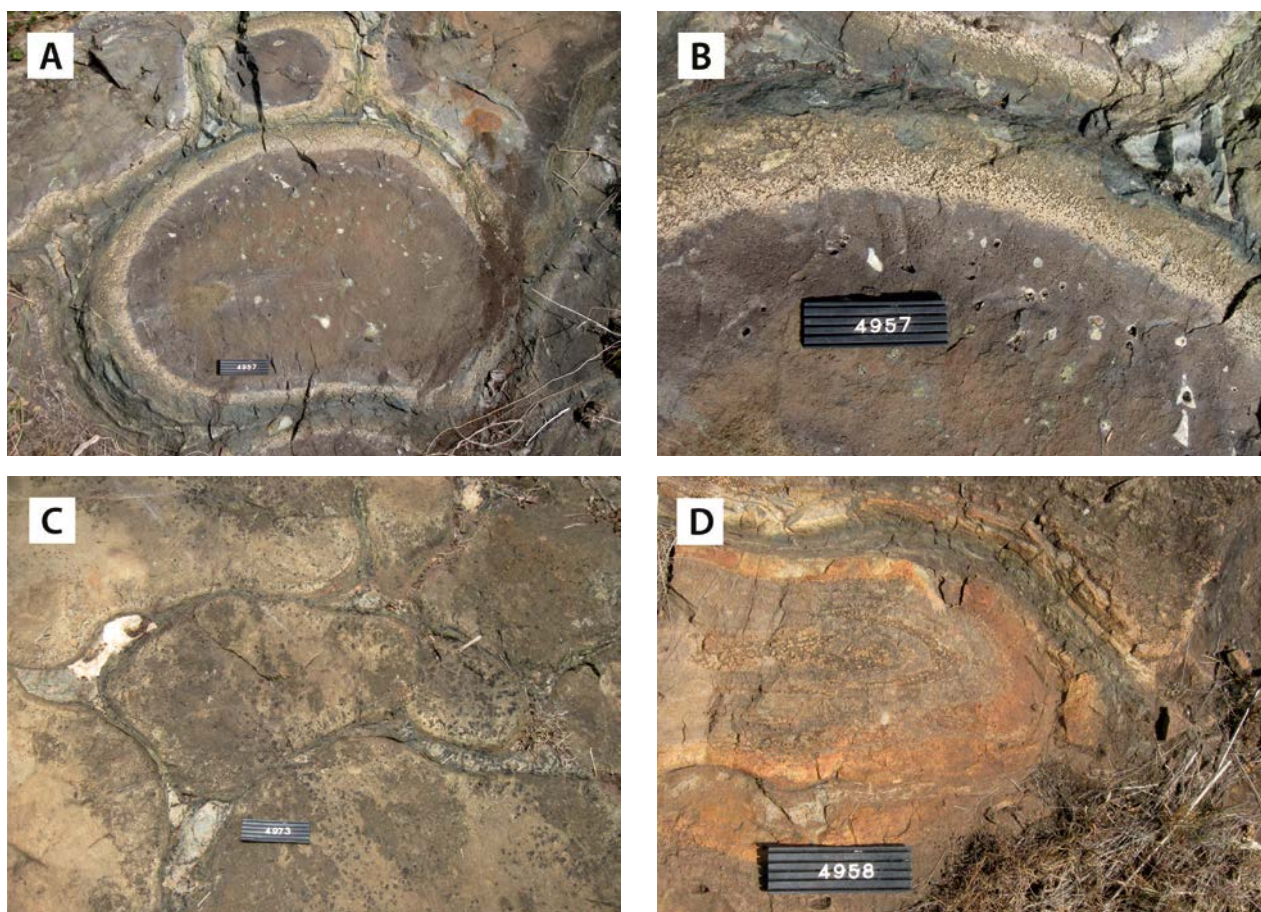


Fig. 6.8. (A) Bun-shaped section of a basalt pillow with a light variolitic rim and small, quartz- and epidote-filled vesicles at Kibale hill (358053E / 92315N). (B) Detail of the variolitic rim in the same pillow. (C) Well-developed sacking of a pillow, showing the top towards SW (351000E / 91618N). (D) Detail showing concentric flow banding in a pillow at Kibale hill (357782E / 92775N). The number tag is 10 cm in width.

volcanic strata and underlying phyllitic rocks. The same observation can be made in the upper contact of the basaltic sequence.

The Bujagali basaltic rocks exhibit a variety of textures. In the Lugazi area, these basalts are massive amphibolites without any visible, primary, volcanic structures. Here basalts probably represent thick, homogeneous lava flows or subvolcanic sills.

In the Bowa area, dark green, fine- to medium-grained, variously foliated metabasalts mostly occur as massive, aphyric flows. Tightly packed and flatbed pillow structures occur in places. Quartz-filled drain cavities and interstitial vugs are common, together with stacked cavities between pillows, supposedly indicating fluctuations in lava supply and discharge rate at the time of their emplacement.

East of the Bulaga plateau, mafic pyroclastic rocks, closely associated with Bujagali basalt, are massive to vaguely banded, fine-grained mafic tuffs, lapilli tuffs and ignimbrites of which the last mentioned include roundish pyroclastic fragments up to 30–40 mm in size. West of the Bulaga plateau, a subvertical sequence of mafic lava flows, several kilometres thick, exhibits well-preserved pillow structures (Figs 6.8A-D). There, closely packed, bun- or mattress-shaped pillows are generally up to 1–1.2 m in diameter, together with geminated or amoeba-shaped megapillows of over

4 m in length. The pillows have thin, dark-green selvages and greenish grey to brownish cores, and have interstitial spaces that are generally filled with bluish grey opal or chalcedonic quartz. Pillow lavas and thick, massive lava flows often occur together.

A peculiar variety of metabasaltic rock occurs west of the Bulaga plateau, where green, isotropic and rather fine-grained lava blocks that can be followed over several kilometres along strike, contain disseminated pyrrhotite-bearing spots, which have often been weathered into roundish cavities up to several centimetres in diameter. A chert layer several metres thick is also exposed within the Bujagali basalt about 2.5 km SWW of Kambuzi Hill (351472E / 92900N). This bluish grey, microcrystalline rock with a rusty brown weathering colour has a fair amount of disseminated sulphides and abundant small cavities, probably due to the dissolution of sulphide minerals. It is an obvious target for gold exploration.

In the type area at Bujagali Falls, the primary igneous minerals of the Bujagali pillow lavas have been altered to an assemblage of actinolite, chlorite, epidote, albite, K-feldspar, calcite, titanite and quartz. This could be due to greenschist facies regional metamorphism. However, in view of the presence of chalcedony filling inter-pillar spaces, the present mineralogy could also stem from spilitisation, i.e. a reaction between basalt pillows and seawater when still hot, a mechanism already



Fig. 6.9. Detailed image of basaltic lava at Bujagali Falls showing pillow structure (517519E / 53289N). Length of hammer 30 cm.

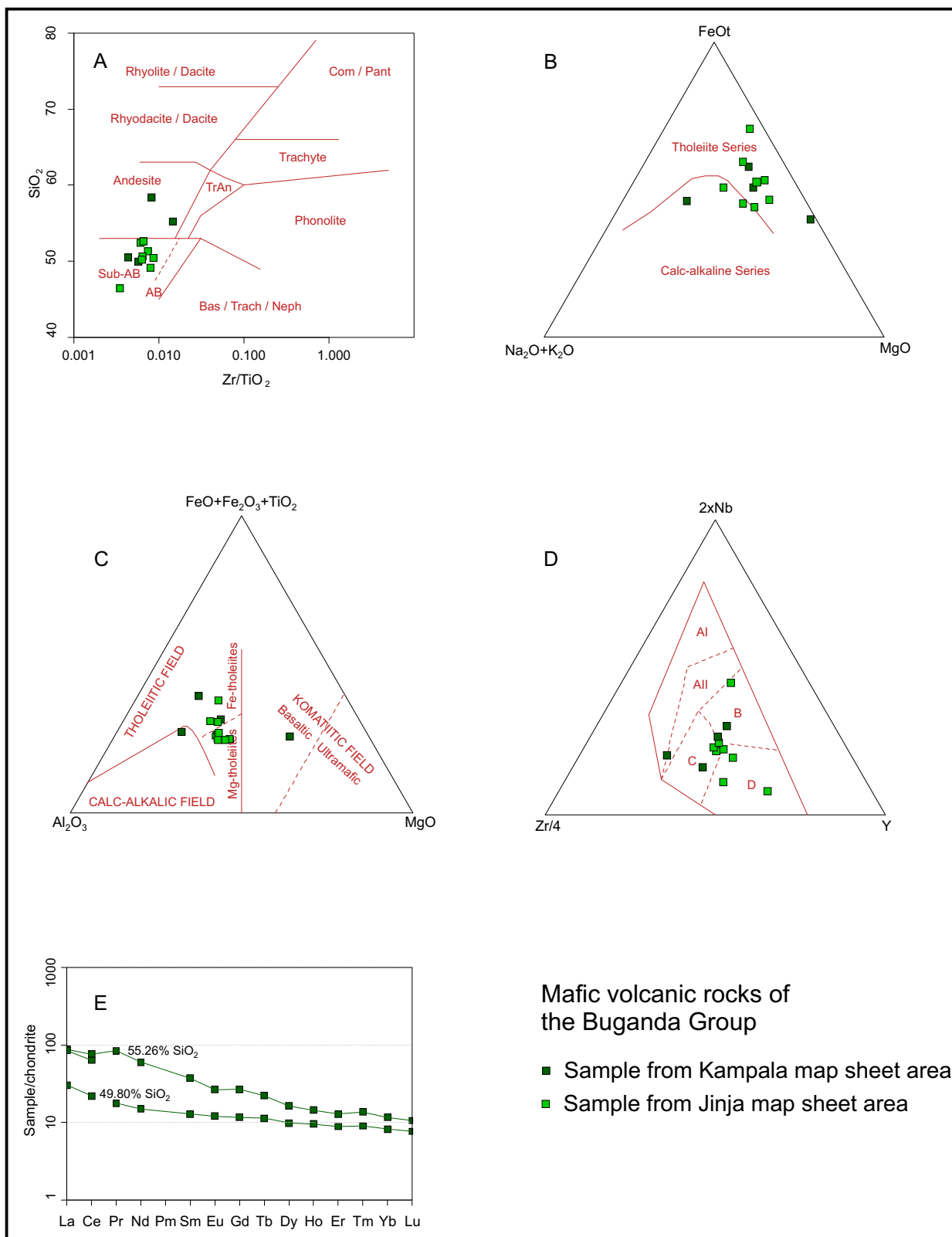


Fig. 6.10. Chemical discrimination diagrams for the Bujagali mafic metavolcanic rocks of the Buganda Group. (A) Zr/TiO_2 vs. SiO_2 diagram by Winchester & Floyd (1977). (B) AFM diagram by Irvine & Baragar (1971). (C) Diagram after Jensen (1976). (D) Diagram for tectono-magmatic setting by Meschede (1986), where AI, AII = fields of intraplate alkali basalts; AII, C = fields of intraplate tholeiites; B = field of P-type MORB; D = field of N-type MORB. (E) Chondrite-normalized REE patterns. Chemical analyses of these basalts are presented in Appendix 2 (anal. 125–134).

suggested by Barth & Meinhold (1974). Preservation of chalcedony and the shrinkage and/or degassing cracks (Fig. 6.9) indicate the absence of metamorphism or deep burial.

Barth & Meinhold (1974) reported the presence of ultramafic rocks and suggested an ophiolitic setting for the mafic volcanic rocks of the Buganda Group. Although pillow basalts occur in various places, we cannot confirm the presence of two other members of the Steinmann trinity usually encountered in ophiolite suites, i.e., tectonised peridotite and sheeted dykes. Consequently, we reject an ophiolitic setting for the Bujagali mafic volcanic rocks.

We consider the Bujagali mafic metavolcanic rocks as subaqueous flood basalts and aerial pyroclastic rocks, that range in SiO_2 from 49.8 to 55.3 wt%, in $\text{Fe}_2\text{O}_3^{\text{tot}}$ from 10.7 to 13.7 wt%, and in MgO 4.3 to 7 wt% (see App. 2), the highest SiO_2 contents probably being induced by quartz-filled vesicles in the lava. In chemical discriminant diagrams, most of the Bujagali basalts plot in the fields of subalkaline basalt to andesite (Fig. 6.10A) and mostly have tholeiitic affinities (Figs 6.10B-C), with one sample plotted in the komatiitic field of the Jensen diagram. This is confirmed by the discrimination diagram for the tectonomagmatic setting for the Bujagali basalts, which

plot mostly in the field of intraplate tholeiites, although there is some scatter with analyses plotting within the P- and N-type MORB fields (Fig. 6.10D). The chondrite-normalised REE patterns of two Bujagali basalts samples display only a moderate LREE-enrichment without Eu anomalies (Fig. 6.10E).

Sericite quartzite and quartzite (PIBNsq) – These are light greyish brown sericite quartzites that occur in the central part of the Kampala area which are also assigned to the Nile Formation. This rock forms horizons of strongly bedded sericite quartzites of variable thickness, which are exploited extensively for aggregate, while the ‘flaggy’ varieties are utilised as dimension stone (Fig. 6.11).

The main minerals of the sericite quartzite are quartz, strongly altered feldspar and sericite. The origin of sericite in quartzite is somewhat contested. Sericite quartzites commonly overlie orthoquartzitic varieties and the increase of micaceous matter may be due to a depositional facies change: i.e a drop in energy. Alternatively, sericite may form at the expense of (weathered, kaolinised) feldspar in originally feldspathic quartzite.

Quartzite, siltstone (PIBNq) – This rock forms a prominent, continuous ridge that extends from



Fig. 6.11. Sericite quartzite quarry at Busunju hill, which produces quartzite slabs for paving and decorative purposes (411442E / 64155N). The number tag is 12 cm in width.

Katonga Bay of Lake Victoria over 140 km towards the southwestern end of the Mubende granite intrusion in the adjacent Kasese area (Bisset 1942). The quartzite probably represents a thick, metapsammitic interbed within the dominantly pelitic schists of the Nile Formation. The stratigraphic position of this southward-dipping quartzite horizon is obscured, because, there are indications suggesting a large-scale north-vergent upthrust – the so-called ‘Katonga Tectonic Accident’ – along the quartzite horizon, exposing deeper levels of the southern block (see also Section 6.4).

The unit varies from pure quartzite and quartzitic metasandstone to silicified quartz breccias. Transitional contacts with siltstone of the Nile Formation are exposed in places (e.g. Kisozi hill), where light brownish, fine-grained quartzitic metasandstone grades downwards into purple, laminar siltstone (Fig. 6.12A). Primary sedimentary structures include graded bedding, ripple marks and low-angled tabular cross-bedding that can be used here in defining the way-up direction.

Mica schist with quartzitic interbeds (P1BNms) – Rare, strongly weathered variegated mica schists with intercalations of sericite-bearing quartzites are exposed SW of Lake Wamala (area 2 in Fig. 6.1; see also Johnson 1960). They are fine-grained, foliated, brownish or yellowish (when weathered) muscovite-quartz-sericite rocks with minor biotite (Figs 6.12B-C). They are cut by quartz veins and also grade into phyllites.

Porphyroblastic phyllite and schist (P1BNamp) – This lithology is a generally thoroughly weathered, usually grey, occasionally olive green, mauve and purple porphyroblastic phyllite that occurs in small isolated outcrops, 10–50 km² in size, in an area 25 km NE of the town of Mityana. The porphyroblastic phyllite can grade into slate and sometimes into mica schist.

These phyllites comprise a significant amount (~50 vol%) of muscovite, which locally appears as coarse flakes (Fig. 6.12D) and is characterised by



Fig. 6.12. (A) Quartzitic metapsammitic interbeds in siltstone of the Nile Formation at the Kisozi hill; light brownish metapsammitic with purple siltstone interbeds (347728E / 5706N). (B) Schist with crenulation cleavage (402563E / 8471N). (C) Hand specimen of intensely weathered mica schist (399535E / 26176N). (D) Porphyroblastic phyllite with reflections caused by coarse muscovite flakes (410256E / 63231N). Length of hammer 60 cm; number plate 6 cm and tag 10 cm in width.

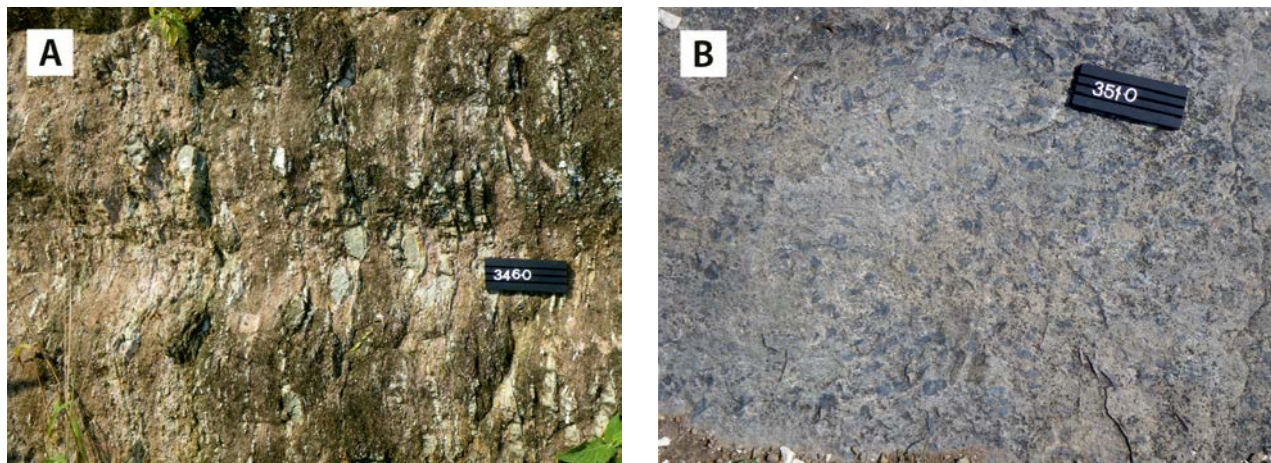


Fig. 6.13. (A) Muscovite gneiss, which includes altered cordierite porphyroblasts (339401E / 41867N). (B) Fingertip-size andalusite porphyroblasts in hornfels-type metapelite near the Singo granite (351371E / 43309N). Number tag is 10 cm in width.

narrow quartz vein segregations. Porphyroblasts, composed mostly of andalusite, are greyish with a pinkish shade and up to 25 mm in size. Cordierite porphyroblasts occur in places. In addition, these phyllites also contain some chlorite and ferruginous matter (hematite or goethite). Due to the coarse grain size of muscovite, these phyllitic rocks sometimes resemble mica schists.

Muscovite-biotite schist and gneiss, locally porphyroblastic (P1BNcgn) – These poorly exposed, strongly weathered, locally porphyroblastic muscovite gneisses of the Nile Formation occupy a noteworthy 20 x 20 km area east of Lake Wamala, just east of the mica schists and phyllites of the region described previously by Johnson (1960). The muscovite gneisses represent more intensively metamorphosed equivalents of the mica schist and phyllites. Typically, the muscovite gneiss is a medium-grained, dark grey rock with greenish grey cordierite porphyroblasts, up to 30 mm in diameter (Fig. 6.13A), which are often altered into fine-

grained micaceous matter (pinitisation) and local flaky muscovite. Biotite is a rare constituent. Sillimanite has been reported from similar rocks in the Fort Portal area. The foliated rock exhibits tectonic differentiation with the formation of quartzofeldspathic segregation bands.

These muscovite gneisses are often associated with pegmatite and granite dykes and streaks. In the contact aureole of the Singo granite in particular, the clear foliated fabric of the muscovite gneiss tends to be obliterated and the rock has a hornfelsic appearance (Fig. 6.13B). Here, the porphyroblastic mica gneisses have undergone amphibolite facies metamorphism in the stability field of muscovite. A N-S trending fracture zone near the Kampala–Fort Portal highway juxtaposes rocks of a different metamorphic grade: phyllitic rocks to the east and porphyroblastic muscovite gneisses to the west. Three whole-rock analyses of the aforementioned metapelites are in Appendix 2 (anal. 135–138). The very low Ca-contents detected apparently refer to weathered samples.

6.4 Synkinematic Granitoids of the Rwenzori Belt

Sembabule Suite

The Sembabule Suite comprises two extensive granitoid terrains, the larger Rwamasha granite and the slightly smaller Kasagama granite. Granitoids of the Sembabule Suite are mainly exposed south of the ‘Katonga Tectonic Accident’, a curvilinear E-W trending, south-dipping, N-verging upthrust that follows approximately the Katonga River from Katonga Bay of Lake Victoria over 140 km eastwards to Lake George. This uplift explains

why there are abundant granitoids of the Sembabule Suite in the southern block and none north of the ‘Katonga Tectonic Accident’. Rocks of the Rukungiri Suite – the pre-Buganda basement – are also far more abundant south of the Katonga upthrust (see Lehto et al. 2014).

Rwamasha granite (1.99 Ga) (P1Sgrc) –Rwamasha granite cannot be distinguished from their country rocks using geophysical data. This, in combination with deep weathering and scarcity of outcrops, has

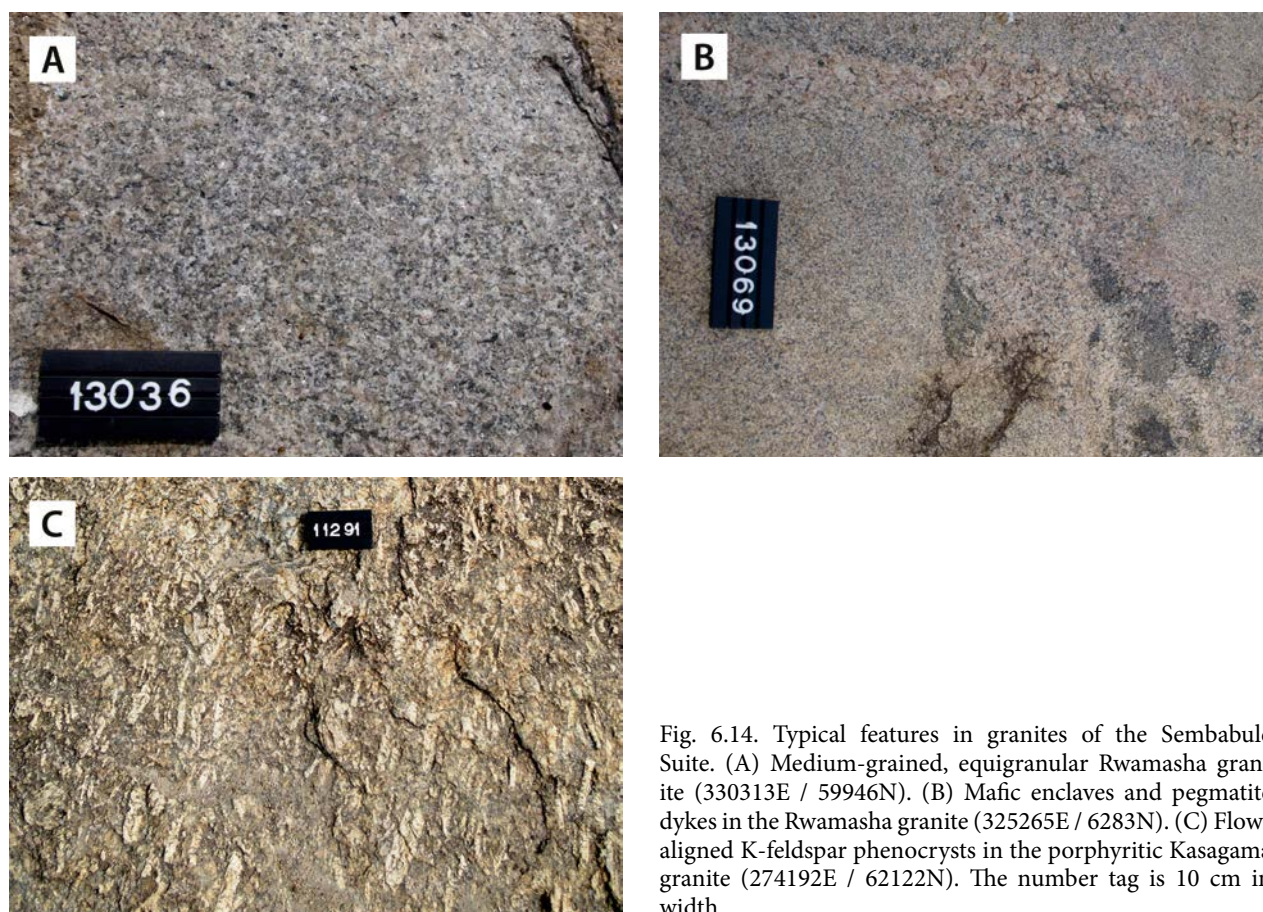


Fig. 6.14. Typical features in granites of the Sembabule Suite. (A) Medium-grained, equigranular Rwamasha granite (330313E / 59946N). (B) Mafic enclaves and pegmatite dykes in the Rwamasha granite (325265E / 6283N). (C) Flow-aligned K-feldspar phenocrysts in the porphyritic Kasagama granite (274192E / 62122N). The number tag is 10 cm in width.

resulted, in places, in a somewhat speculative delineation of granites and their country rocks in the geological map. In places where the country rock is exposed, it is a weathered metapelite of the Buganda Group.

The Rwamasha granite is heterogeneous in composition, texture and appearance. It is an equigranular to locally porphyritic, medium- to coarse-grained biotite granite (Figs 6.14A-B), occasionally with an incipient gneissic texture. Biotite constitutes ~15% of the rock volume, while hornblende only occurs in places. One whole-rock analysis with REE is presented in Appendix 2 (anal. 138). Magnetite is present in accessory though variable amounts, as indicated by magnetic susceptibility measurements ranging from 0.05 to 17.00 SI. Porphyritic members with phenocrysts generally ≤ 30 mm alternate and intermix with a predominantly

equigranular sub-facies on the scale of the outcrop. Mafic xenoliths, pegmatitic dykes and streaks and quartz veins are commonly observed.

Kasagama granite (1.96 Ga) (*P1Sgrh*) – The Kasagama granites are usually porphyritic in appearance, with coarse to very coarse K-feldspar crystals embedded in a generally medium-grained matrix. These granites usually have less inclusions and enclaves than the Rwamasha granite. Locally, magmatic flow alignment is indicated by the parallel orientation of non- to moderately deformed K-feldspar phenocrysts (Fig. 6.14C). In addition to K-feldspar, the main minerals of the Kasagama granite are plagioclase, quartz and biotite. Some leucocratic granite members occurring NW of the town of Mbarara may contain minor amounts of muscovite in addition to biotite.

6.5 Postkinematic Granitoids of the Rwenzori Belt

Mubende-Singo Suite

The Mubende-Singo Suite in central Uganda includes two extensive granite batholiths; the larger called Mubende (3,000 km²) is located west of Mubende town, and the smaller, Singo (700 km²), occurs NW of the town of Mityana (Fig. 6.15). The latter also includes a small satellite further to the SW. These granite bodies can easily be recognised from airborne geophysical maps. In comparison to the surrounding country rocks, the granites have weaker positive signatures on magnetic maps. On radiometric images, however, they appear as high potassium anomalies. These plutons have been emplaced into metapelitic rocks of the Buganda Group and clearly they represent a phase of post-tectonic magmatism in the Rwenzori Fold Belt.

The field relations of the batholiths of the Mubende-Singo Suite and the metapelites of

the Buganda Group were first described by King (1947b), Johnson (1960), Johnson & Williams (1961) and Macdonald (1966). Since then, the setting of these granitoid bodies has often been debated: either a truly magmatic, intrusive, discordant character is advocated or, alternatively, formation by ‘metasomatic granitisation’, a model fashionable at the time but now considered obsolete. It has been noted that, in places, the contact zones are composed of quartz-sericite bodies. The poorly exposed Singo intrusive was recently studied by Nagudi et al. (2003) and the well-exposed, rocky Mubende batholith (see Fig. 6.16) by Mäkitie et al. (2014a), who distinguished at least three granite types: (1) a predominant megacrystic granite, with porphyritic textures covering some 70%; (2) coarse- and equigranular granite varieties (25%), and (3) medium-grained, aplitic granite (Figs 6.17A-D).

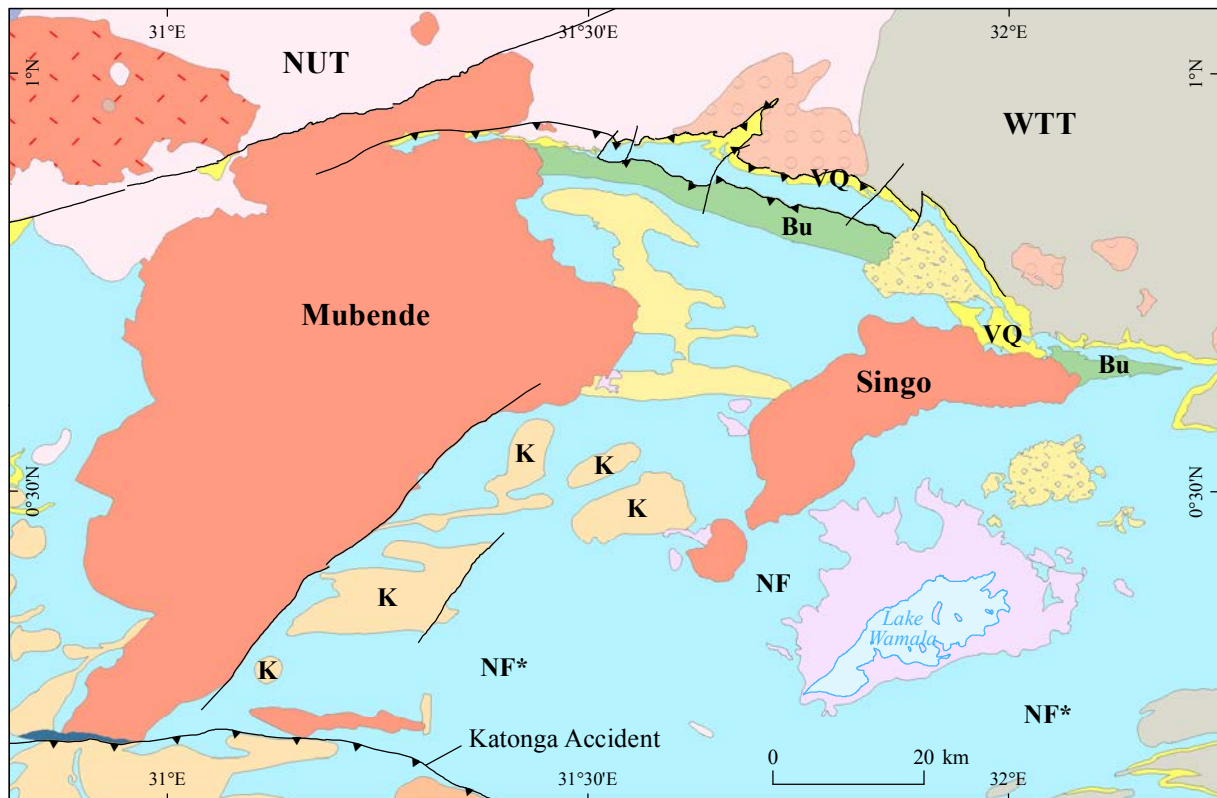


Fig. 6.15. Regional distribution of the Mubende and Singo batholiths. The Mubende batholith is bounded in the south by the Katonga Accident and by a north-vergent upthrust and part of the Nakasongola discontinuity in the north. Key: VQ = Victoria Quartzite; Bu = Bujagali volcanic rocks; NF = Nile Formation (epimetamorphic); NF* = Same but higher grade of metamorphism; NUT = North Uganda Terrane; WTT = West Tanzania Terrane.



Fig. 6.16. Typical landscape view of the centre of the Mubende batholith with well-exposed granite hills.

Coarse to megacrystic granite (1.85 Ga) (P1MSmg)

– This granite type is pinkish to light brownish in colour, rather homogeneous and mostly porphyritic in appearance (Fig. 6.17A). Major minerals of this granite type are microcline, oligoclase, quartz and biotite (2–9 %), the latter mineral being often altered to chlorite. Muscovite is a minor magmatic constituent but, locally, late muscovite can form up to 3% of the rock volume. Microcline is more common than oligoclase. Accessory minerals are sphene, monazite, apatite, magnetite, chalcopyrite and other iron minerals. The rock displays zoned K-feldspar phenocrysts up to 8 cm in size, with the largest crystals having slightly rounded shapes and plagioclase rims in places. The large crystals show an alignment that is possibly indicative of magmatic flow. In places, the texture is coarse and rather even-grained (Figs 6.17B-C). In places there are small ‘cavities’ and joints containing euhedral carbonate and fluorite crystals. Elongated shear zones, 1–20 mm wide and tens of metres long, trend in different directions and are often filled by secondary epidote (Fig. 6.17D).

Johnson (1960) gives a detailed description of the poorly exposed Singo granite. In addition to the above, he described several other granite varieties (including a very coarse grained and fine, aplitic muscovite-bearing phase), which occur to a limited extent along the margins of the Singo body.

The marginal granite phase is relatively richer in oligoclase (*versus* K-feldspar) and contains muscovite.

Nagudi et al. (2003) reported several chemical whole rock analyses from the Singo batholith. The SiO₂ contents range from 67.7 to 77.2 wt% and K₂O > Na₂O. Modal compositions correspond mostly with monzogranite; although a few analyses fall in the syenogranite field. The granite samples analysed from the Mubende batholith are mainly peraluminous in composition with a calc-alkaline affinity (Figs 6.18A-C). Chondrite-normalised spider diagrams show negative Eu, Sr, and Nb anomalies and unfractionated heavy-REE (HREE), indicating the presence of plagioclase and absence of garnet in the source material (Nagudi et al. 2003). However, the Mubende and Singo granites have also some differences: for example, the first granite appears to represent generally a less fractionated magma body than the second intrusion (Mäkitie et al. 2014a).

Sericitised granite (P1MSsg) – This sub-type is more common in the Singo than in the Mubende batholith and is related to late hydrothermal activity. According to King (1947a), Johnson & Williams (1961) and Nagudi et al. (2001, 2003), the Singo batholith comprises medium- to coarse-grained, purple coloured granite zones that are completely



Fig. 6.17. Granite types of the Mubende-Singo Suite. (A) Megacrystic Mubende granite, which contains subrounded phenocrysts (296618E / 48252N). (B) Coarse, relatively even-grained granite member from the Mubende batholith (380607E / 67227N). (C) Homogeneous, coarse-grained granite in satellite intrusion of the Singo batholith (352186E / 48478N). (D) Thin shear zones in Mubende medium-grained granite (289257E / 62363N). The number tag is 10 cm in width.

altered into sericite-quartz greisen bodies, up to 70 m in width and composed of blebs of quartz with flakes and books of muscovite in a fine-grained micaceous matrix. The purple colour is due to the presence of fine hematite, supposedly derived from the break-down of biotite. In places, these alteration zones have been affected by shearing, thereby developing a faint schistosity. Other varieties of hydrothermally altered rock are reported to contain talc, pyrophyllite and damourite (Johnson 1960). The latter is very fine-grained, compact muscovite variety with a greasy touch (i.e. 'serpentine-like'). Petrographic studies have indicated that andalusite is present (Johnson 1960). Greisen zones, associated with tungsten-bearing quartz veins have been reported. Both of the granite batholiths are intersected by NW-SE trending dolerite dykes of the Lake Victoria Arcuate Dyke

Swarm (Fig. 8.22). Moreover, the southern and northern parts of the Mubende batholith are locally intersected by elongated quartzite ridges, which rise up to 60 m above their surroundings and may refer to major tectonic 'accidents' (Fig. 6.15).

Nagudi et al. (2003) advocate a magmatic, intrusive setting for the Singo batholith. The granitic rock of the batholith usually cuts the Buganda sediments discordantly, but contacts that are parallel to the country rock bedding are not unusual. Nagudi et al. (2003) contest the observation of Johnson (1960) that "*the emplacement of the Singo batholith had very little metamorphic effect on the country rocks*" and they assert that, as well, regional metamorphism, the country rocks have undergone contact metamorphism as indicated by hornfels development and crystallisation of andalusite and/or cordierite (Fig. 6.13B).

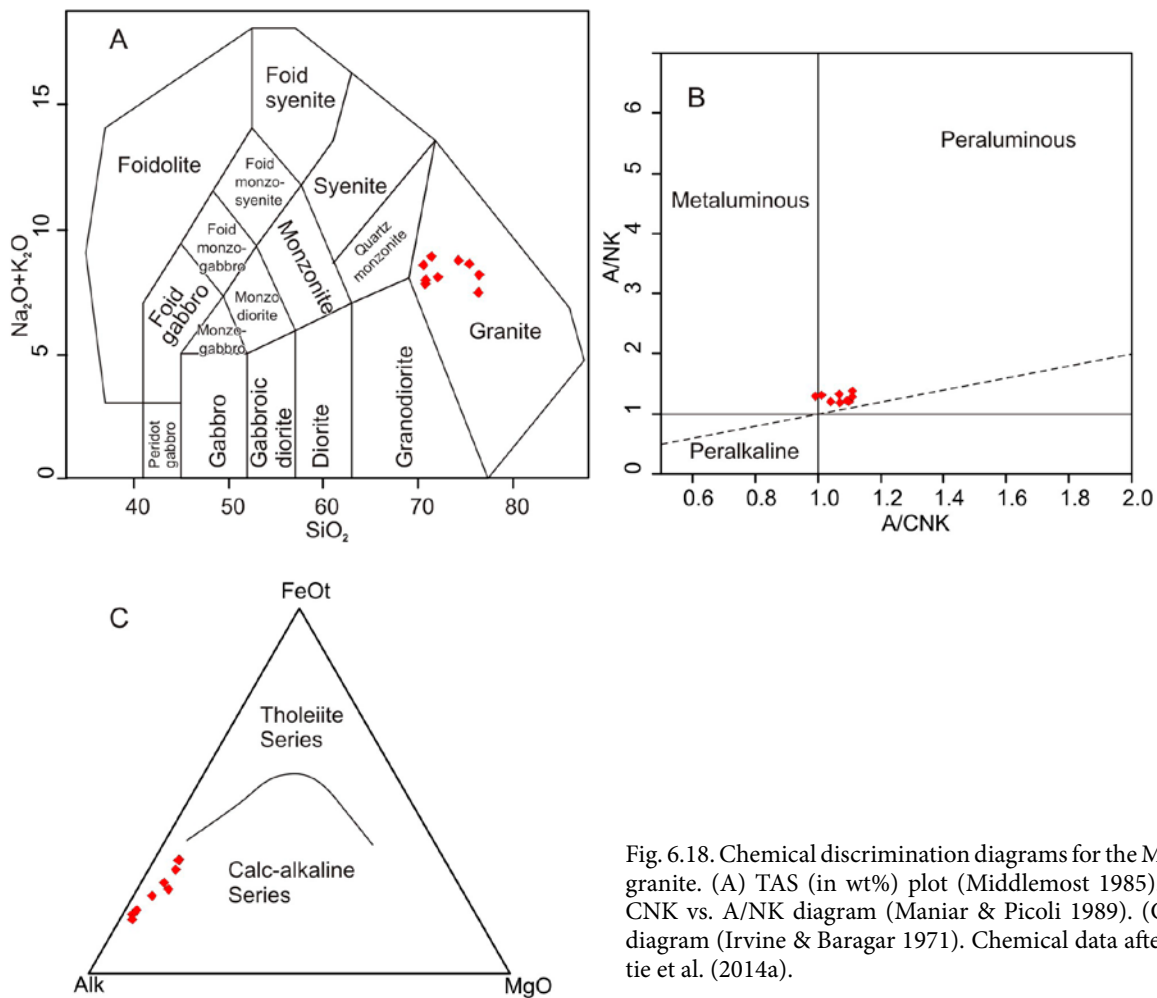


Fig. 6.18. Chemical discrimination diagrams for the Mubende granite. (A) TAS (in wt%) plot (Middlemost 1985). (B) A/CNK vs. A/NK diagram (Maniar & Picoli 1989). (C) AFM diagram (Irvine & Baragar 1971). Chemical data after Mäkitie et al. (2014a).

6.6 Lithostratigraphy and Structure of the Rwenzori Block

The Rwenzori Mountains represent an uplifted crustal fragment, which is known as the Rwenzori Block or Horst (Fig. 12.16). The block forms an promontory of up to 5000 m in altitude, extending about 120 km N-S and 50 km E-W. The unusual position of the Rwenzori Mountains within the extensional setting of the Albertine Rift, the northernmost segment of the Western Rift, East Africa Rift System (EARS) (Ring 2008), makes it the most extreme expression of Neogene rift-flank uplift on earth. Possible models for uplift of the Rwenzori Block are discussed in Section 12.4.

The first geological descriptions and maps of the Rwenzori Mountains were published as early as 1895 and 1907 (Elliott & Gregory 1895, Roccati 1907). The block is composed of a succession of alternating migmatitic biotite gneisses, biotite granite and amphibolite and was considered a type area for the 'Toro Complex' (Johnson & Mc-

Connell 1951, Johnson 1954). Low-grade phylitic rocks in the Rwenzori Block were initially assigned to the Karagwe Supergroup (McConnell 1959a). However, Tanner (1969a, 1969b, 1973a) demonstrated that these low-grade metasediments are structurally and stratigraphically continuous with the Palaeoproterozoic 'Toro' schists. McConnell (1959a) assigned most of the high-grade metasedimentary rocks to the Archaean 'Gneissic-Granulite Complex'. These rocks were later, together with the Stanley Volcanics included in the 'Toro System' by King & de Swardt (1970), Tanner (1969a, 1969b, 1970, 1971, 1972, 1973a), Barth & Meinhold (1974) and Gabert (1974). Tanner (1973a), based on fieldwork by Tanner (1970, 1971), Bailey (1969), Barrett (1969, 1971) and McConnell (1959a), presented the following generalised stratigraphic sequence (from top to bottom):

- (4) Banded epidote-amphibolites and dolomitic marbles;
- (3) Andalusite-cordierite and sillimanite-muscovite schists, less common biotite schists;
- (2) Meta-tholeiitic lavas and sills;
- (1) Quartzites and conglomerates (including 'Toro Quartzites').

The contents resemble the metamorphic parts of the Buganda Group described above, although the mafic volcanics are lower in the sequence, below the metapelites and carbonates and skarnoids have not been encountered in the Buganda Group (Table 6.1). Pillow structures in the mafic metavolcanic rocks of the 'Stanley Volcanic Formation', a term coined by Tanner (1971), resemble similar structures in the Bujagali Member of the Nile Formation.

Tanner (1969b) described basal quartzites and schists unconformably overlying Archaean gneisses in the Butiti Hills, ~20 km south of Fort Por-

tal (Fig. 6.19). The synclinal structure can be extended to the west where it comprises the 'High Peak Schists' of the Stanley Volcanics. Structural and sedimentological features indicate that both the metasediments of the Butiti Hills and High Peaks occupy a tight synclinal structure overlying Archaean gneisses that is overturned to the north, as shown schematically in Fig. 6.20 (see also Mazimhaka 1973).

The sedimentary rocks, which represent stratigraphically the lowermost rocks in the Rwenzori mountains, were mapped in detail in the Kilembe Mine area (Warden 1985). This mapping resulted in a stratigraphic column with a numerical scheme marked in ascending order LK3 → LK2 → LK1 → MK → UK5 → UK4 → UK3 (Fig. 6.21 Left), where LK stands for Lower Kilembe, MK for Middle Kilembe and UK for Upper Kilembe. Cu-Co mineralisation of the Kilembe SEDEX deposit is hosted by a banded amphibolite horizon of the Middle Kilembe unit (MK in Fig. 6.21). Note that quartzites (unit UK3) are in the upper part of the column.

Warden (1985) reported that rocks of the Kilembe succession show complex polymetamorphism with an increase in metamorphic grade across the schists belt from greenschist to amphibolite facies, together with the intensifying of deformation, from south to north and from east to west, thereby overstepping stratigraphic boundaries.

In many places, intense, north-verging shearing attenuated the upper (overturned) southern limb of the fold/thrust structures and gave way to ductile deformation, characterised by flow folding in the northern (lower) limb. E-W compression produced N-S trending structures that possibly preceded N-S compression that gave rise to the development of gentle E-W trending flexures. The interaction of the two deformation phases produced dome-and-basin interference patterns (Fig. 6.19).

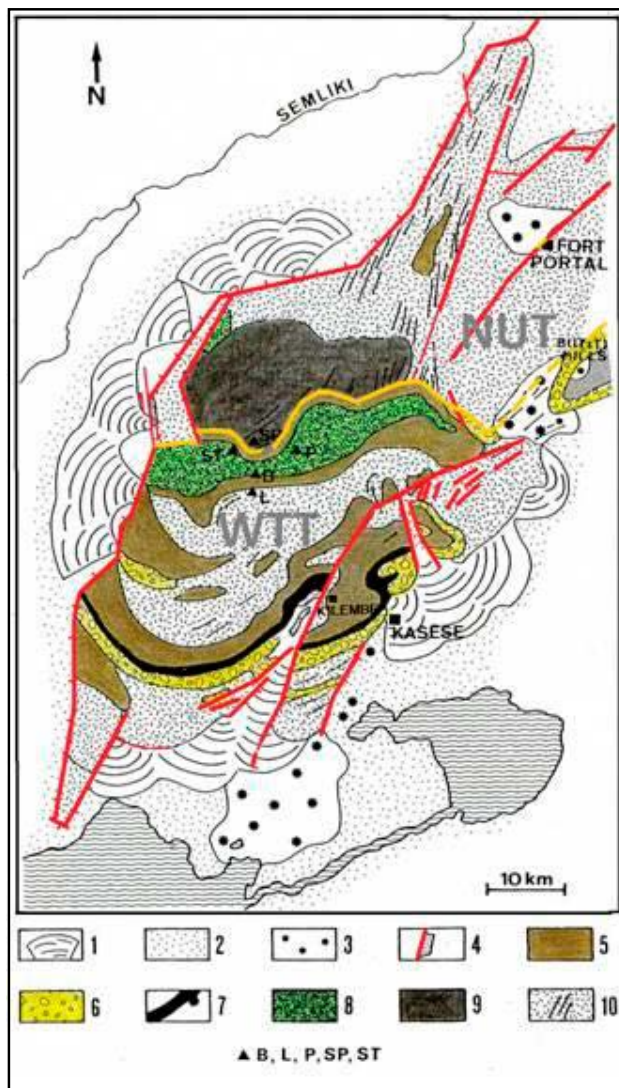


Fig. 6.19. Geological outline of the mountaneous Rwenzori Horst (modified after McConnell 1959a, Tanner 1969a, Warden 1985, from Schlüter 1997, with kind permission of the Springer Verlag). Key: 1 = Pleistocene and Holocene outwash fans; 2 = Kairo-Kisegi Beds (Miocene to Pleistocene); 3 = Craters of Pleistocene and Holocene volcanoes; 4 = cataclases of unknown age; 5 = Schists of the 'Toro Group' (now Buganda Group); 6 = Quartzites of the Toro Group (now Buganda Group); 7 = Kilembe Schist Formation; 8 = Stanley Volcanics Formation (High Peak schists); 9 = Speke Gneisses of the 'Gneissic-Granulite Complex'; 10 = Undifferentiated (NUT = North Uganda Terrane); B: Baker; L: Luigi di Savoia; P: Portal Peaks; SP: Speke; ST: Stanley.

Taking also into account the fact that that the Kilembe succession is overturned (Davies 1951, Barrett 1971, Warden 1985, Mazimhaka 1973, see Fig. 6.20) and thrust, we conclude that the units that are structurally at the top of the succession are stratigraphically at the bottom. We advocate that the stratigraphic column of Warden (1985) should

be inverted as is shown in Figure 6.21(right), strongly indicating that there is a tectonic contact between the base of the Kilembe succession and thin-skinned fragments of the Archaean basement at the “top” of the succession. Redrafted in this way, the Kilembe succession corresponds better with the sequence previously established for the “Toro

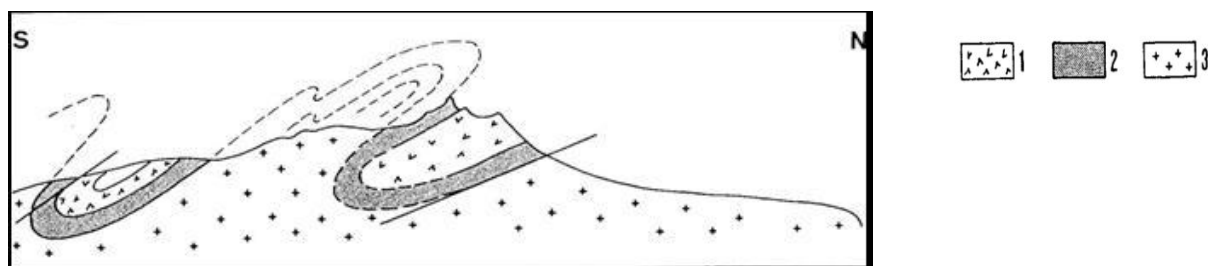


Fig. 6.20. Generalised N-S profile across the Rwenzori Mountains showing overturned fold structures. Key: 1 = Stanley Volcanics Formation, 2 = Undifferentiated Schists, 3 = Gneisses and Granulites of the Archaean basement (after Mazimhaka 1973).

Table 6.2. Adapted inverted stratigraphy at Kilembe compared to the general stratigraphy of the Buganda Group.

| No. | Unit | Thickness (m) | Inverted succession based on data from Warden 1985, in Schlüter 1997. | Comparison to lithologies of the Buganda group |
|-----|------|---------------|---|--|
| 8 | | | K-feldspar gneiss | |
| 7 | UK2 | 270 - 350 | Migmatitic quartzo-feldspathic layers, probably grading southwards into biotite schists. Locally porphyroblastic and garnetiferous or sillimanite-bearing | <i>Andalusite-cordierite and sillimanite - muscovite schists, locally porphyritic, less common biotite schists of the Nile Formation.</i> |
| 6 | UK1 | | Biotite gneisses, locally garnet-bearing. Fine-grained granular and coarse-grained schistose varieties. Locally retrograded ferruginous sericitic varieties. | |
| 5 | MK | 0 - 100 | Amphibolites. Commonly banded. Dravite-bearing, manifesting exhalative activity. Mineralisation is hosted by banded biotite and epidote-quartz schists, epidote schists and quartzo-feldspathic amphibolite intercalations. Most mineralised bodies at contact of MK and LK3. | <i>Not present in the Nile Formation; amphibolites are most likely derived from chemical lime-rich sediments, not to be compared to volcanics of the Bujagali Member</i> |
| 4 | LK3 | 7 - 100 | Chlorite-biotite schist: fine-grained, mafic. Several varieties including porphyroblastic types and amphibolitic varieties at the base, commonly hosting hanging wall mineralisation. Marble lenses. | <i>Lower metapelites (slate, shale, phyllite) of the Nile formation; carbonates not observed.</i> |
| 3 | LK2 | 30 - 300 | Quartzite, quartzo-feldspathic grit. Merges locally into Na-gneiss (?meta-arkose?). Local intercalations of chlorite-albite schists. Contact with overlying unit is gradational and mainly marked by decreasing chlorite content. | <i>Quartzite and conglomerates, including former Toro Quartzites, now attributed to Victoria Formation.</i> |
| 2 | LK1 | 30 - 130 | Quartz - sericite ± chlorite schists, locally biotite-bearing; strongly foliated and intensely sheared (stressing tectonic contact with underlying basement). | <i>Not observed.</i> |
| 1 | | | Medium-grained K-gneisses of the Archaean West Tanzania Terrane. | <i>Same.</i> |

Complex' by McConnell (1959a), Bailey (1969), Barrett 1969, 1971) and Tanner (1971, 1972), that is now assigned to the Buganda Group with, at least, the quartzites at the base of the sequence. The Kilembe succession and its comparison to the Buganda Group is shown Table 6.2.

From the above we conclude that the Rwenzori Block is composed of Archaean and Palaeoproterozoic rocks. The first belong to two different terranes with the northern segment of the block being part of the North Uganda Terrane (Chapter 5) and the southern part belonging to the West Tanzania Terrane (Chapter 3) (NUT and WTT in Fig. 6.19). The latter are particularly exposed in the dome structure – a double anticline with a pinched-out syncline in between – north of Kilembe mine (Fig. 6.19). U–Pb age determinations of zircon cores (Laser-ICP-MS method) from the foothill Archaean gneisses of the Rwenzori Mountains yielded

ages of 2584 ± 18 Ma, 2637 ± 16 Ma and 2611 ± 14 Ma (Link et al. 2010).

Our field observations in the Rwenzori Block are restricted to a section along the eastern foothills. The sequence begins with quartzites, which unconformably overlie Archaean gneisses. Quartzites exhibit festoon cross-bedding and ripple marks. The overlying unit is phyllitic schist with sedimentary structures. Tholeiitic Stanley meta-volcanic rocks occur as interlayers in these schists. These are garnet-bearing, medium-grained, foliated amphibolites with coarse amphibole segregations and epidote and quartz veins (Figs 6.22A-B). Elsewhere, there are mica schists with quartzitic interbeds, which as they are traced northwards become gneissose in appearance and partly garnet-bearing. Pegmatitic dykes are also common in the area.

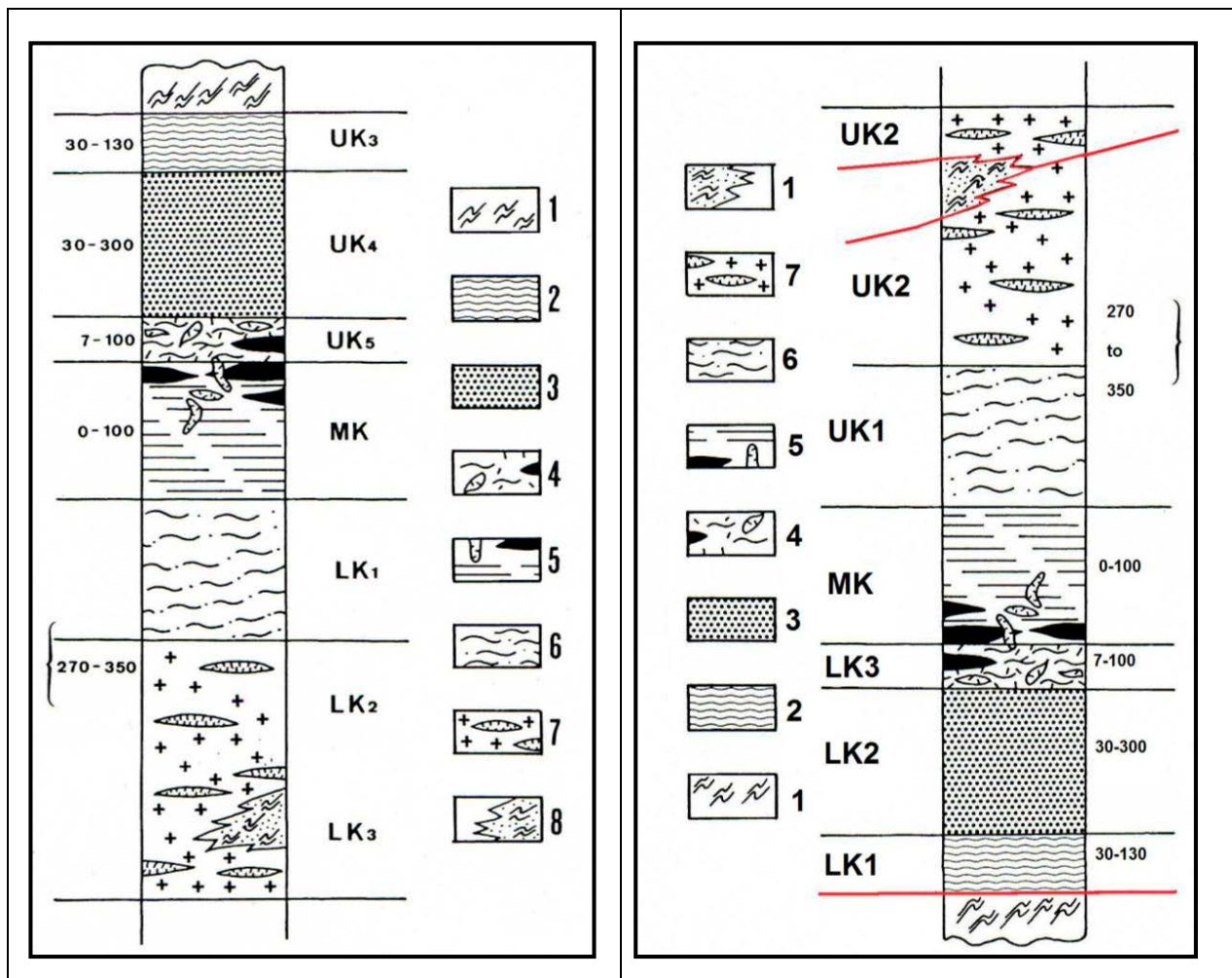


Fig. 6.21. Left: Schematic stratigraphic column forming the Kilembe Schist Group (after Warden 1985 in Schlüter 1997, with kind permission of the Springer Verlag). See Table 6.2 for a brief description of the lithologies. Right: Inverted succession at Kilembe compared with the general stratigraphy of the Buganda group (redrawn from Warden 1985).

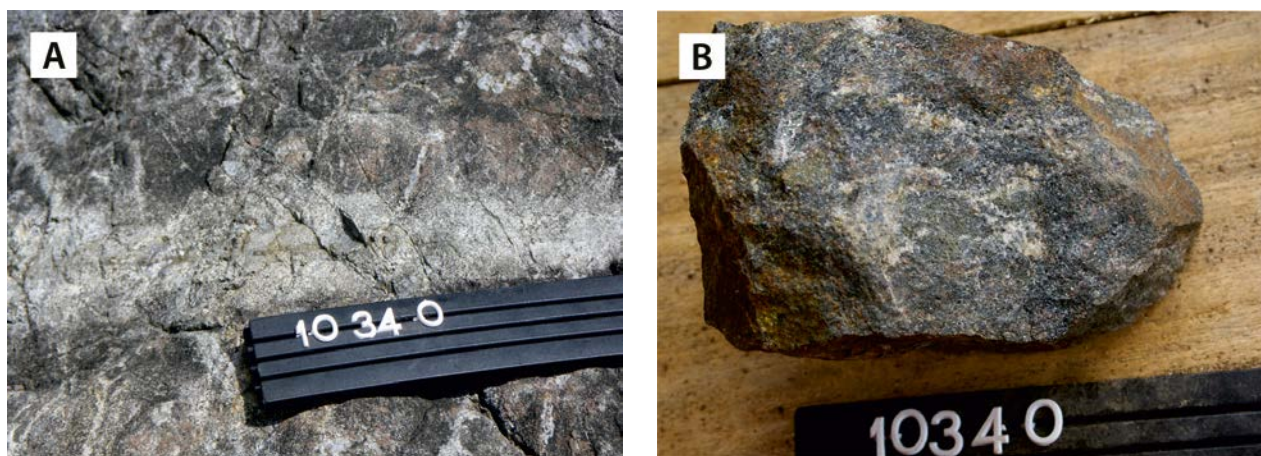


Fig. 6.22. (A) Stanley amphibolite with quartz-filled tension gashes on western slope of the Rwenzori Mountains (179830E/85065N). (B) Hand specimen of the same garnet-rich amphibolite. The number tag is 15 cm in width.

6.7 Geochronology

The age of the Buganda Group and timing of tectonic events in the Rwenzori Belt are not well known. Older whole rock Rb-Sr and K-Ar data from pegmatite from Lunyo (~30 km E of Kamapala) and Nampeyo (~20 km W of Kampala) yielded minimum ages of ~1870 Ma and 1845 Ma, respectively (Nicolaysen et al. 1953, Holmes & Cahen 1955). Similar whole rock Rb-Sr ages of 1840 and 1870 Ma from pegmatite in Buganda metasediments were reported by Davis et al. (1956). A minimum age of the Buganda Group could be deduced from the intrusive Mubende granite, dated at 1807 ± 60 Ma by Cahen & Snelling (1966). Other older age determinations from granites near Iganga, Masaba and Buteba yielded ages of around 1850 ± 50 Ma (Harper et al. 1972, Cahen et al. 1984).

In earlier studies, the age of Rwenzori 'basement' was even more poorly constrained between 2.8 and 2.0 Ga (Harper et al. 1972). Granitic gneisses of the Masha area, which were assigned to the former 'Toro System' and are now attributed to the Rukungiri Suite, yielded a poorly constrained WR Rb-Sr age of 1887 ± 245 Ma or, following recalculation, ~2027 Ma (Vernon-Chamberlain & Snelling 1972). Muscovite from schists near Masaka yielded a K-Ar age of 1811 ± 60 Ma (Cahen & Snelling 1966). Further westwards, in the Rwenzori Mountains, biotite from andalusite-bearing mica schist from the Stuhlmann Pass Formation of the Baker Syncline (Fig. 6.19) yielded an age of 1831 ± 60 Ma (Cahen & Snelling 1966).

During the past decade more reliable U-Pb zircon ages have been reported. Zircon evaporation

data from the Singo granite of the post-kinematic Mubende-Singo Suite, indicate emplacement ages of 1847 ± 6 Ma (Pinna et al. 2001) or 1615 ± 19 Ma (Nagudi et al. 2001). The latter age has been superseded by the emplacement age of megacrystic granite of the Mubende batholith, which yielded an age (LA-MC-ICPMS method) of 1848 ± 6 Ma (UG-17_3052; Mänttari 2014), in agreement with the age by Pinna et al. (2001) of the coeval Singo pluton.

An older generation of granitoids belongs to the supposedly syn- or late-kinematic Sembabule Suite, mainly exposed south of the 'Kalonga Tectonic Accident'. U-Pb zircon dating (MC-LA-ICPMS method) of both granites show that emplacement of the Rwamasha granite took place 1987 ± 5 Ma ago and the Kasagama granite only slightly later, 1964 ± 4 Ma ago (UG-19_12441 and UG-18_12404; Mänttari 2014).

The age of the metasediments and associated volcanic rocks of the Buganda Group remains poorly constrained. Mafic volcanic rocks from the Bujagali Member of the Nile Shale Formation produced an imprecise Sm-Nd age of $\sim 2.3 \pm 0.2$ Ga, due to the small quantity of extremely Nd-poor plagioclase in the rock (UG-32_4928; Mänttari 2014).

The Buganda metasediments and associated metavolcanic rocks overlie 2.64 Ga basement of the West Tanzania Terrane in the east and 2.64–2.56 Ga basement (Link et al. 2010) in the uplifted Rwenzori Block. In the central, western and south-western segments of the belt, Buganda rocks overly

Rwenzori basement of the former ‘Toro Complex’, now assigned to the Rukunkiri Suite. U-Pb zircon dating, using the MC-LA-ICP-MS method, of these high-grade metamorphic, strongly deformed rocks from a location ~10 km SW of the town of Ntungamo yielded an age of 2147 ± 16 Ma. This age is from high-uranium altered zircon grains with most of the data plotting roughly on a discordia line intercepting the concordia line at 2.21 Ga and 1.23 Ga (UG-35_3823; Mänttari 2014). The latter age most likely indicates ‘Kibaran’ overprinting. The Kalonga granite, located east of the Mubende pluton (Fig. 6.16), was dated using LA-

MC-ICPMS at 2128 ± 12 Ma (UG-9_1184; Mänttari 2014). Many zircon grains suffered radiogenic lead loss reflecting Pan-African overprinting.

Stable isotope (C and O) compositions of marble intercalations in MORB-type metavolcanic rocks of the Stanley Volcanics Formation in the Rwenzori Mountains suggest an age of deposition between 2.22 and 2.06 Ga (Master et al. 2013). These authors further claim that these rocks were once part of an ocean floor and were obducted onto the Tanzanian Craton during the Rwenzori Orogenic Cycle (= Eburnian Orogenic Cycle) at around 1.9 Ga (Master et al. 2008).

6.8 Tectono-Thermal Evolution of the Rwenzori Belt

The prolonged phase of Archaean crust formation (from >3.08 to 2.55 Ga) in Uganda was followed by a long period of quiescence, to be interrupted only by local transtensional movements along the palaeosuture between the West Tanzania and North Uganda Terranes around 2.49 Ga. This mid-crustal discontinuity, termed Nakasongola Discontinuity (Ruotoistenmaki 2014) is based on combined magnetic-radiometric-gravity data and suggests thrusting of the NUT over the WTT. This explains the presence of TTG gneisses (A3Uttg) in the uplifted Rwenzori Block further to the north than in nearby WTT basement in the lower ground.

The post-Archaean geological evolution of Uganda can best be viewed in the context of the evolution of the entire Proto-Congo Craton, composed, as mentioned, of several Archaean terranes and Palaeoproterozoic mobile belts (Fig. 1.6). Unlike the Palaeoproterozoic fold belts of the Congo River Basin, which are covered by Phanerozoic sediments, the Usagaran-Ubendian-Rusizian-Rwenzori system of fold belts (2.1 to 1.85 Ga) is exposed over a wide area. It wraps around and separates the Tanzania Craton from the rest of the proto-Congo Craton (Fig. 6.2).

The Rwenzori Fold Belt of Uganda (Fig. 6.1) thus represents the northernmost segment (Fig. 6.2) of a NW-SE- and N-S trending and, eventually, E-W striking suture between the Tanzania and Congo Cratons. This suture has remained a zone of weakness between the two cratons and has been reactivated periodically, notably during the Kibaran and Pan-African Orogenic Cycles (Chapters 8, 9 and 11). Post-Rodinia and post-Gondwana extensional reactivations are indicated by emplacement of alkaline complexes in the same suture at ~0.81

to ~0.65 Ga and 0.55 to ~0.44 Ga, respectively (Fig. 1.15). Finally, this Palaeoproterozoic suture developed into the Neogene Western Rift of the East African Rift System (Chapter 12). Thus, in spite of these intracratonic tectonic events (Tack et al. 2010, Delvaux et al. 2011), the proto-Congo Craton has remained stable and united since the late Palaeoproterozoic (Tack et al. 2006a, 2008b, 2009). Only when the opening of the South Atlantic propagated northwards from the Late Jurassic to Early Cretaceous, a minor segment – the westernmost São Francisco Block (Brazil) – became separated from the proto-Congo Craton.

There are differences of opinion as to whether the Tanzania Craton accreted onto the Congo Craton as a new crustal element (forming the proto-Congo Craton), or whether the Tanzania Craton was already a part of the proto-Congo Craton prior to the Palaeoproterozoic, to be only temporarily separated from it, followed by re-unification. In any case, the event was characterised by eclogite-to granulite facies metamorphism (Klerkx et al. 1997, Collins et al. 2004a, 2004b, Tack et al. 2006a, Boniface et al. 2011) and development of an Andean-type calc-alkaline magmatic arc (Kabengele et al. 1991, Boven et al. 1999) in the Usagaran and Ubendian Belts, manifesting oceanic crust subduction, collision and amalgamation of the Tanzania and Central Africa Cratons. These belts developed during two successive tectonic events, called the Early and Late Eburnian orogenic phases (Fig. 1.4), spanning a period of some 250 million years between ~2.1 Ga and 1.85 Ga, which in the Usagaran-Ubende segment comprised an early collisional phase (Eburnian I; ~2100–2025 Ma) and a phase of dextral shear and granite magmatism

(Eburnian II, ~1950–1850 Ma) (Daly et al. 1985, Daly 1988, Boven et al. 1999).

The duality of the Eburnian Orogenic Cycle, recognised in the Usagaran-Ubende segment, can also be recognised in the Rwenzori Fold Belt of Uganda. The pre-Buganda Rwenzori basement, represented by rocks of the 2.15 Ga Rukunkiri Suite and the 2.15–2.12 Ga Kalonga granitoids (Mänttari 2014), formed during the Eburnian I phase. This Palaeoproterozoic basement is restricted to the western and southwestern segments of the Rwenzori Belt and continues southward into the Rusizian of Rwanda, Burundi and Kivu (DRC). The protoliths of these high-grade poly-metamorphic and migmatitic rocks probably comprised felsic and intermediate plutonic and volcanic rocks in a magmatic arc setting. Unfortunately no reliable geochronological data are available from the equivalent rocks in Rwanda, Burundi and Kivu (DRC). The oldest recently dated Rusizian rock has an age of 1982 ± 6 Ma (Tack et al. 2010), an age comparable with granitoids of the Sembabule Suite and confirms the older WR Rb-Sr data of Cahen et al. (1984). Further to the south in the Ubende Belt, zircon ages of 2084 ± 8 Ma, corresponding with a phase of granitic magmatism, have been reported by Lenoir et al. (1994) and Boven et al. (1999).

Subsequent to the Eburnian I phase, metasediments and associated volcanic rocks (e.g. Bujagali basalts) of the Buganda Group were deposited, most likely between 2.0 and 2.1 Ga. Crustal extension and basin formation reactivated the older (~2.64 Ga) mid-crustal Nakasongola Discontinuity, separating the West Tanzania from the North Uganda Terranes. We postulate that a half-graben or aulacogen-type basin was formed with sediment supply mainly from the north resulting in the deposition of arenites, grits and conglomerate of the Victoria Formation, which is overlain by the pelites and volcanic rocks of mainly mafic composition of the Nile Formation.

Unlike the western and southwestern segments of the Rwenzori Fold Belt, the eastern segment rests directly on the Archaean basement of the West Tanzania and Victoria Terranes, which both belong to the Tanzania Craton. The current eastern extent of the Buganda Group lithologies reflects the situation following Phanerozoic uplift and erosion, and it is to be expected that the Buganda rocks once extended much further to the east, probably covering the entire 'low-magnetic belt' portrayed in Fig. 3.3. The volumetrically insignificant and

enigmatic Bubulo Formation, provisionally attributed to 'Archaean basement' may well represent erosional relicts of the Buganda Group (Section 3.3.5). Folding and thrusting of the sediments and associated volcanic rocks of the Buganda Group along WSW-ESE fold axes may be viewed as a far-field effect of renewed N-verging thrusting in the E-W Usagaran Belt. The timing of this compressional event is unknown but is believed to have taken place before emplacement of the granitoids of the Sembabule Suite 1.99 to 1.96 Ga ago. A new phase of crustal extension (orogenic collapse?) was heralded by emplacement of post-kinematic granitoids of the Mubende-Singo Suite at 1.85 Ga. Crustal extension leading to crustal thinning initiated a new phase of basin development and deposition of the platform successions: the Namuwasa and Bwezigoro Groups and the Kagera-Buhjewe Supergroup. As will be discussed in Chapter 7, the Buganda, Namuwasa and Kagera-Buhjewe strata were all affected by later block-faulting and thrusting events.

Deformation – Rocks of the Buganda Group in the Jinja area show gentle to open, E-W trending fold structures. In the Lake Wamala area, these rocks show two phases of deformation. Blastesis of generally completely pinitised idioblastic crystals of cordierite took place between D_1 and D_2 (Johnson 1960). F_1 fold axes have E-W structural trends as in the underlying high-grade metamorphic rocks of the 'Toro Complex', which are now assigned to the Rukungiri Suite.

The Rwenzori Horst (Fig. 6.19) offers a rare opportunity to study the structural development of the Rwenzori Belt in three dimensions. Link et al. (2010) studied the tectonics of the Rwenzori Block and established four phases of deformation (Fig. 6.23):

- D_1 is only present in Archaean gneisses and resulted in a steeply dipping foliation and layering accompanied by a dextral shear component.
- D_2 affected both Archaean gneisses and metasediments and associated metavolcanic rocks of the Buganda Group, resulting in northwards or northwestwards thrusting and stacking of Archaean gneisses and Buganda rocks on top of each other. This event was previously interpreted in terms of northwards-overtaken isoclinal fold structures (Fig. 6.20). It is unlikely that the original contacts between Archaean gneisses and Buganda sediments have been

- preserved since these unconformities are usually reactivated as shear zones. Indicators for D_2 are mylonite zones in the Archaean gneisses close to the contacts and intensive deformation within the metasediments (+ associated volcanic rocks) with south-dipping foliations, shear zones and isoclinal folds with an asymmetry indicating north-directed thrusting. Repetition of the quartzite layer within the green unit is a marker for stacking of the units. For comparison we refer to Figs 6.15 and 7.20. We interpret the whole structure as a stacked hinterland-dipping duplex system with a thick-skinned tectonic style as illustrated in the profile in Fig. 6.23.
- D_3 is a combination of an E–W compression that resulted in asymmetric folds from cm- to km-scale with steep fold axes associated with a poorly developed ~ NNW- to SSE-striking steep foliation followed by a set of steep to vertical shear zones with a dominant dextral component and a NNW-SSE and NNE-SSW strike. These structures offset the steep folds. The gentle to open folds, affecting the thrust plane between the WTT and the the NUT in Fig. 6.19, are thought to represent D_3 . It is not clear whether this deformation event also affects the younger metasediments of the Kagera-Buhjewu Supergroup (blue unit in Fig. 6.23).
 - Younger molasse-type sediments of the Namu-wasa and Bwezigoro Groups and the Kagera-Buhjewu Supergroup (Chapter 7) overlie the older Buganda sequences unconformably with conglomerates at their base. The contact is at least partly tectonic, indicating thrusting to the NNE. In addition, the sequence is mildly folded with horizontal fold axes and lineations trending NNW–SSE, indicating that the folds and thrusts could be associated with each other. We term this deformation event D_4 . These D_4 type folds with fold axes and lineations can also be observed in the underlying metamorphic schists and quartzites of the Buganda Group (Fig. 6.24).

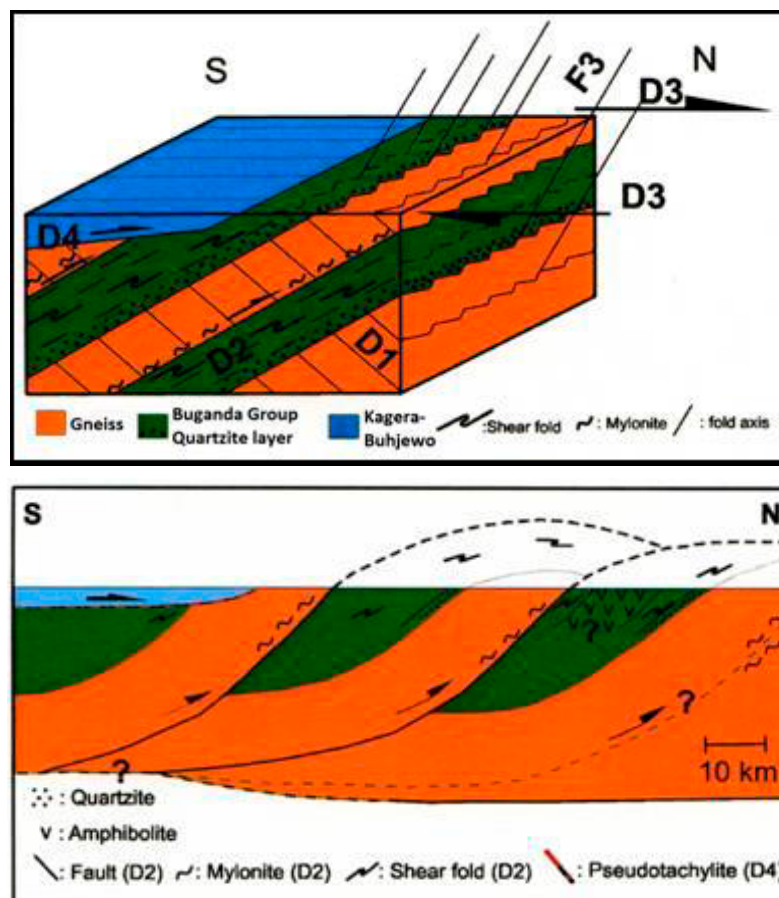


Fig. 6.23. Above: Block diagram illustrating the order of the four deformations seen in Rwenzori Block and western Uganda. Below: South to north profile through the fold and thrust belt indicating northward imbricate thrusting of Archaean and Palaeoproterozoic units towards the north (from Link et al. 2010).

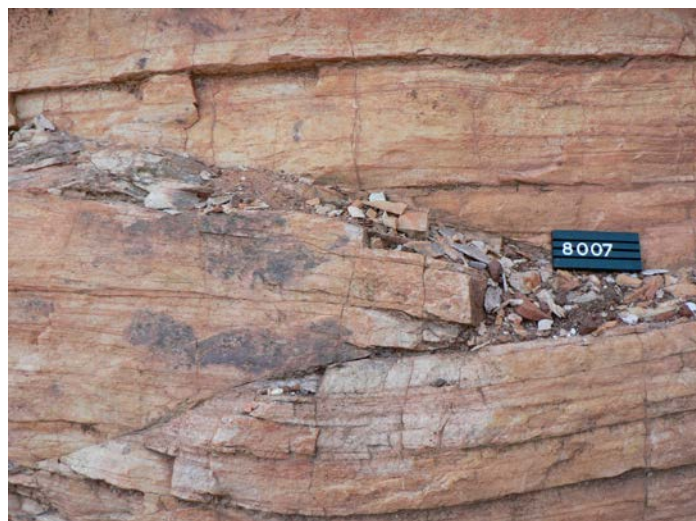


Fig. 6.24. Muscovite lineation on the westward dipping bedding plane of quartzite of the Nile Formation of the Buganda Group with associated right-lateral conjugate fractures (400478E / 45585N). The number tag is 8 cm in width.

Combining the results of field observations with the collected new and published geochronological data, Link et al. (2010) summarised the following relationships between deformation and age: (1) The gneiss units in Fig. 6.23 (brown unit) are Neoarchaean in age (all 2637–2584 Ma) even though they are now interleaved with Palaeoproterozoic units (Figs 7.35 and 7.36, green unit). This requires repetition of the units, leading to the model of the stacked, hinterland-dipping duplex system with thick-skinned tectonic style during D_2 (Fig. 7.36). The D_2 deformation must have occurred before 1.85 Ga as indicated by post-tectonic granite bodies within the units, but after 2580 Ma since this is the minimum age of the Archaean slices indicated by the new zircon ages. Link et al. (2010) stress that the previously published ages of this unit are Rb–Sr and K–Ar cooling ages and do not represent formation ages. The timing of the D_4 deformation is poorly constrained. It may be a rejuvenation of older D_2 thrust planes. A maximum age of the thrusting event of ~ 1.85 Ga seems plausible, but much younger ages (Kibaran or Pan-African) may also apply (Section 7.6).

Geodynamic Setting – The Rwenzori Belt can be considered as a broad ‘geo-syncline’ with gently plunging WSW axes in the east, corresponding to the grain of the belt, which turn into more E-W trends in central Singo and westwards from the Entebbe and Kampala areas, to become N-S directed in southwestern Uganda (Fig. 6.1). This ‘geosyncline’ is underlain by a specific fragment of the Archaean West Tanzania Terrane character-

ised by low-magnetic intensity (Chapter 3). The Rwenzori Belt is the northernmost part of a much larger approximately N-S trending collisional fold belt, which through the Rusizian can be continued southwards into the Ubendian (Section 1.3). Based on the above, we postulate that the Rwenzori Belt is in fact a combination of a N-S collisional orogen and an E-W to WSW-ENE trending, partly inverted aulacogen (or aborted rift). Major supporting arguments include:

- Variation in structural orientation from E-W to N-S.
- Strong difference in metamorphic grade and intensity of deformation between the eastern E-W trending segment (‘inverted aulacogen’) and the western and southwestern N-S trending segment (‘collisional orogen’).
- Different litho-geochemical signature of mafic volcanic rocks: The Stanley Volcanics in the ‘eu-geosyncline’ have tholeiitic MORB affinities in a Palaeoproterozoic plate tectonic setting (Tanner 1971), in other words, remnants of a small oceanic basin. This point of view is confirmed by the presence of widespread Cu-Zn mineralisation and the high Na content due to spilitisation and seawater metasomatism. The mafic and intermediate volcanic rocks of the Bujagali Member near Jinja and Kidoga have subalkaline basalt to andesite compositions and mostly tholeiitic affinities. On a tectono-magmatic discrimination diagram the Bujagali basalts plot mostly in the field of intraplate tholeiites (Fig. 6.9).

In this context the Rwenzori Mountains may have been the locus of a Palaeoproterozoic triple junction with the Ubendian-Rusizian-west Rwenzori leg forming a spreading ridge. The E-W trending part of the belt (east Rwenzori) formed from an aborted rift or aulacogen. The third, northern arm has supposedly developed into a strike-slip fault. The location or direction of this fault is unknown. It may be hidden below sediments of the Congo River Basin or, alternatively, it could have a direction parallel to the Madi-Igisi Belt (Chapter 9) and Albertine Rift (Chapter 12). Whereas the N-S trending southern arm developed into a small oceanic basin (or 'eugeosyncline'), the E-W trending part of the Rwenzori Belt has always remained intracratonic (or 'miogeosyncline').

Consumption of the oceanic basin and collision and amalgamation of the Congo and Tanzania Cratons during the Eburnian Orogenic Cycle (~2.0–1.8 Ga) gave rise to the Ubendian-Rusizian-Rwenzori Belt. An obvious question is then: "Where is the suture between the Tanzania and Congo Cratons?" The answer is hidden below the Kibaran Belt (see Section 8.4).

In the Ubendian segment of the belt the ~2.1–2.0 Ga subduction-collision event was followed by exhumation under amphibolite facies p, T-conditions and by post-orogenic emplacement of abundant felsic volcano-plutonic complexes ("Ufipa-Kate-Kipili-Marungu"-type; Tack et al. 2006a). In Uganda, the Eburnian Orogenic Cycle closes with emplacement of granitoids of the post-kinematic 1.85 Ga Singo-Mubende Suite. For the Singo intrusion, it is suggested that the felsic magmas formed from a heterogeneous crustal source, which was water-

undersaturated (Nagudi et al. 2003). The Singo marginal biotite granitoid has S-type affinities while the pink porphyritic main phase, however, has explicit I-type affinities (Nagudi et al. 2003). Magmatic tectonic discrimination diagrams mainly suggest a 'within plate granitic' setting for the Mubende-Singo Suite (Mäkitie et al. 2014a), suggesting crustal extension, basaltic underplating and the onset of basin formation with the deposition of the Namuwasa and Bwezigoro Groups and the Kagera-Buhjewe Supergroup (Chapter 7).

Although contested in older publications (King 1947a, 1947b, Johnson 1960, Johnson & Williams 1961, Macdonald 1966), the contact relations of the plutons of the Mubende-Singo Suite (Section 6.5) with the Buganda metasediments (Section 6.3) are intrusive (Nagudi et al. 2003). The granitic bodies cut the Buganda country rock but in places there are contacts parallel to the country rock bedding plane. Nagudi et al. (2003) contest the observation of Johnson (1960) that "the emplacement of the Singo batholith had very little metamorphic effect on the country rocks" and claim that, apart from regional metamorphism, the Buganda country rocks also have undergone contact metamorphism as indicated by the occurrence of hornfels (Fig. 6.13B), silicification and tourmaline enrichments (Fig. 6.25).

Magnetic data suggests the presence of some kind of aureole (Fig. 8.25) possibly created by crystallisation of magnetic minerals within the contact aureole and/or greisen zone around the granitic plutons in the otherwise low-magnetic metasediments of the Buganda Group.



Fig. 6.25. Cross-bedded sandstone interlayer in the metapelite-dominant Nile Formation of the Buganda Group, showing tourmalinization around a granitic dyke (346697E / 55729N). The number tag is 10 cm in width.

7 PALAEOPROTEROZOIC POST-RWENZORI PLATFORM SEDIMENTS

7.1 Introduction

Platform deposits resting on the western margin of the Tanzania Craton and bounded by folded metasediments of the North Kibaran Belt in the west have traditionally been attributed to the Neoproterozoic Malagarasi Supergroup (Waleffe 1965, Cahen et al. 1984, Theunissen 1988a, Tack et al. 1992) and equivalent 'Bukoban Series' in northwestern Tanzania (Quennell 1956a, 1956b, Henderson 1961, Halligan 1963). This was based, amongst others, on K-Ar ages of 812 to 815 ± 30 Ma from mafic volcanic interlayers (i.e. Kabuye-Gagwe lavas, Fig. 7.1) in the platform sequence (Briden et al. 1971).

Subsequently, due to the discovery of ~1.4 Ga mafic sills and dykes (Tack et al. 1992, Tack 1995, Deblond et al. 2001), the lower portion of this platform sequence was attributed a Mesoproterozoic age and the lower parts of the 'Bukoban Series' (Palister 1956, Quennell 1956b) were re-defined as the Mesoproterozoic Bukoban Group of the Kagera Supergroup (Fernandez-Alonso et al. 2006). The

upper part of these platform sediments remained included in the Neoproterozoic Malagarasi Supergroup defined by Waleffe (1965) (Chapter 10).

Being supposedly coeval with the folded and metamorphosed metasediments of the North Kibaran Belt, these ~1.4 Ga non- to epimetamorphic, non- to weakly deformed platform deposits – the lower part of the former 'Bukoban Series' – were interpreted as Kibaran foreland deposits in the so-called Eastern External Domain of the North Kibaran belt (Tahon et al. 2004, Fernandez-Alonso et al. 2006, Tack et al. 2006a) (Chapter 8).

New geochronological data manifest, however, that crustal extension, basin formation and the deposition of molasse-type sediments of the Kagera Supergroup started much earlier, almost immediately posterior to the culmination of the Eburnean Orogenic Cycle in the Rwenzori Belt, as manifested by a zircon U–Pb SHRIMP crystallisation age of 1.78 Ga for a tuffaceous intercalation in the base of the sequence (Cuttin et al. 2004),

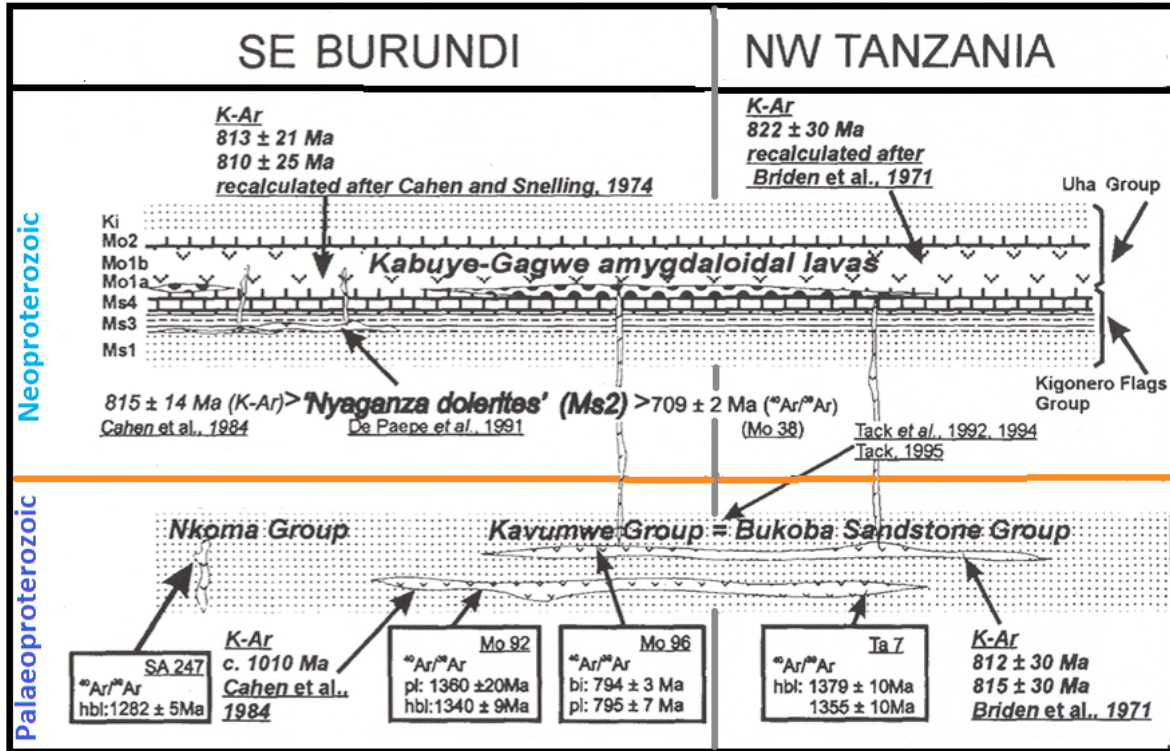


Fig. 7.1. Synthesis of comparative lithostratigraphic relationships of the (sub-)tabular Neoproterozoic Malagarasi Supergroup and Palaeoproterozoic Kagera Supergroup (here Kagera-Buhweju Supergroup, comprising the Muyaga, Ruvubu and Bukoba Groups) in SE Burundi and NW Tanzania (adapted after Tack 1995, with kind permission of the Royal Museum for Central Africa). Key: *Italics:* previous K-Ar ages; normal fonts in boxes: new ⁴⁰Ar/³⁹Ar data; hbl = hornblende; pl = plagioclase; bi = biotite.

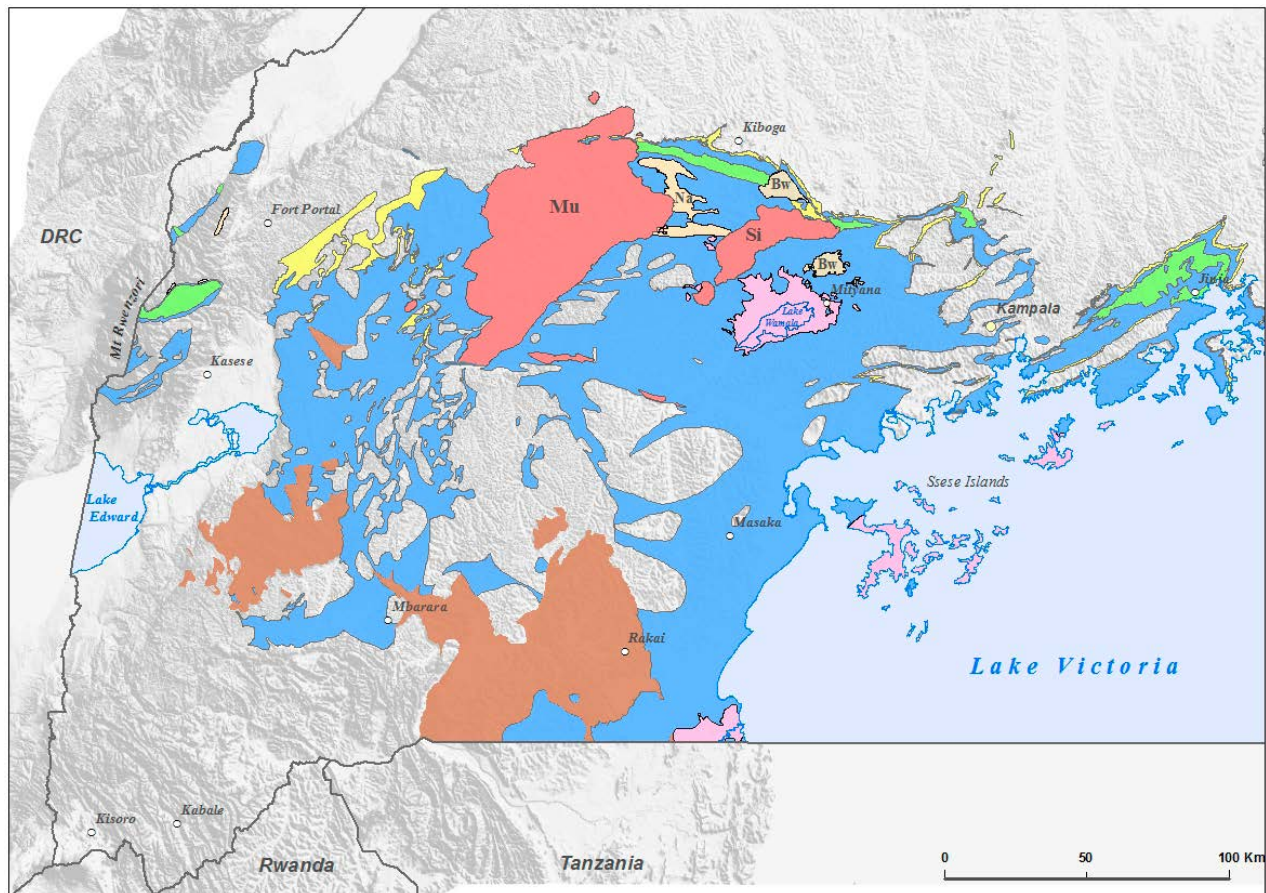


Fig. 7.2. Summary geological map of southwestern Uganda, showing the distribution of rocks belonging to the 2.2–2.0 Ga old Buganda Group of the Rwenzori Belt (yellow/green/blue), <math><2.05\text{--}1.86\text{ Ga}</math> old Namuwasu Group, <math><1.97\text{ Ga}</math>, most likely <math><1.86\text{ Ga}</math> old Bwezigoro Group, $\sim 1.78\text{ Ga}$ old Kagera-Buhweju Supergroup (brown) and <math><1.37\text{ Ga}</math> old Mityana Group (lilac). Key: Na = Namuwasu Gr, Bw = Bwezigoro Gr, Mu = Mubende batholiths, Si = Singo batholith. Simplified after Lehto et al. (2014).

some 80 million years after emplacement of the Mubende-Singo granitoids (Section 6.5). Being some 200 to 300 million years older than the oldest sediments in the North Kibaran Belt, the setting of Kagera sediments as Kibaran foreland deposits can no longer be maintained, and this platform succession is henceforward considered as a separate tectono-thermal domain or ‘building block’, manifesting long-lived Palaeoproterozoic post-Rwenzori extension. Connecting the platform rocks of the Kagera Supergroup with identical deposits in southwestern Uganda, we have introduced the term ‘*Kagera-Buhweju Supergroup*’.

Cutten et al. (2004) and Fernandez-Alonso et al. (2006) concluded that the platform rocks of the Kagera Supergroup have been deposited in two separate, coeval, parallel basins. Pedreira & de Waele (2008) expanded the ‘two-basins’ model and stressed that, depending on their palaeogeographic position, two separate stratigraphic columns must be considered for the rocks of the

Kagera Supergroup: the Muyaga and overlying Ruwubu Groups in the west and the Bukoba Group in the east.

The stratigraphic position of isolated platform sequences of the ‘Singo and Mityana Series’, located NW of Kampala, in the region between Mityana (S) and Kiboga (N), and between the Singo (E) and Mubende (W) granite batholiths (Fig. 7.2), has been problematic since their first descriptions by Combe (1923). They are described as unconformably overlying subvertical amphibolite to greenschist facies grade metasediments of the Palaeoproterozoic Buganda Group and comprise conglomerate and sandstone (Butologo sandstone) from the Butologo plateau (now Namuwasu Group) and similar-looking rocks of the Mityana region. During subsequent investigations, King (1943, 1947a) concluded that the sandstone and conglomerate beds of the Bulaga (now Bwezigoro Group) and Butologo plateaus and the conglomerate, arkose, sandstone and silicified rocks of

the Mityana area all belong to the same succession, which he called the 'Singo Series', although a northern Namutamba and a southern Wamala facies could be distinguished. Johnson (1960) again distinguished two units, the 'Mityana Series' and 'Singo Series', the first allocated to the Precambrian-Palaeozoic 'Bukoban System' and the second to the Precambrian 'Karagwe-Ankolean System'. Johnson & Williams (1961) showed that on the Namutamba plateau, Wamala facies sediments were deposited on top of eroded remnants of Namutamba facies conglomerate and sandstone, and they further were of the opinion that the Mubende granite intruded the Butologo quartzite (now Namuwasa Group) and that Wamala facies rocks rest unconformably on the granite. Consequently, they maintained the conglomerate and sandstone of King's (1943, 1947a) Namutamba facies, similar to those of the Bulaga and Butologo plateaus, in the

'Singo Series', while for the younger clastic succession the name Mityana was retained.

Based on our field observations and the limited amount of U-Pb zircon data (detrital and primary zircons), the above division between older and younger platform units is maintained, although only tentatively. The former 'Singo Series' from the Butologo, Bulaga and Namutamba plateaus (rising to more than 1,520 m above sea level) correspond with our Palaeoproterozoic Namuwasa and Bwezigoro Groups. They are in some way connected to the slightly younger but also Palaeoproterozoic Kagera-Buhjewu Supergroup further south. The platform deposits of the former 'Mityana Series', together with similar deposits in the Sese archipelago, are assembled in the Neoproterozoic Mityana-Sese Group of the Malagarasi Supergroup. They are discussed in Chapter 10.

7.2 Geology of the Namuwasa Group

7.2.1 Introduction

Rocks of the Namuwasa Group occur (1) as horizontal and tilted beds in the Butologo plateau, located between the Mubende and Singo granite plutons, (2) as sporadic slivers along the NW-trending tectonic contact of pelitic schists and metabasalts of the Nile Formation in Nakasasa valley, located to the north of the Butologo plateau and (3) as a thin but continuous tectonic sliver within Nile schists. The Namuwasa sequence overlies deformed and metamorphosed rocks of the Buganda Group with a tectonic contact, although the tectonic slivers are concordant with the bedding. Stratigraphic way-up indicators in pillowed Bujagali metabasalts and quartzites of the Buganda Group and tectonic slivers of the Namuwasa Group are always in the same direction, with younging towards the south. Although metasediment beds may be vertical, they are never overturned. In the Butologo plateau, beds may be tilted to the north or to the south, and younging directions are consequently to the south or the north. In the extreme south of the plateau,

the beds are vertical and all sedimentary structures have been destroyed by shearing.

North of the Nakasasa valley, the Namuwasa sandstone units are tectonically interlayered with the Nile schists and tectonically truncated against steeply south dipping to near-vertical Bujagali metabasalts (Fig. 7.20). This tectonic truncation caused the sporadic and sliver-like appearance of the Namuwasa metasedimentary units. The northern continuous layer of Namuwasa sandstones near Kiriango is interleaved with a narrow stretch of Nile schists, which are probably in tectonic contact with the Bujagali metabasalts occurring to the south and the Victoria quartzite occurring to the north. Bedding in all three of these units is nearly vertical to very steep southward dipping. The subdivision of the Namuwasa Group is presented in Table 7.1.

7.2.2 Lithostratigraphic units

Conglomerates interbedded with sandstone (P1Nn)
– Conglomerates of the *Kikonge Formation* are

Table 7.1. Subdivision of the Namuwasa Group.

| Group | Formation | Lithology | Code |
|----------|-----------|--|------|
| Namuwasa | Buwekula | Pink sandstone | P1Nb |
| | Maseke | Grey sandstone with solitary pebbles (<2.05 Ga) | P1Nm |
| | Kikonge | Conglomerate interbedded with sandstone (<2.05 Ga) | P1Nn |

locally exposed at the basal contact with the underlying pelitic schists of the Nile Formation. This clastic unit, up to 15 m in thickness, consists of several continuous conglomerate beds (< 1.2 m thick) and lenses within beds ranging from gritstone to sandstone in composition. The clast material of the conglomerate up to 20 cm in size, mostly contains sub- to well-rounded pebbles and cobbles of vein quartz, fine-grained sandstone and mauve to maroon phyllitic shale (Fig. 7.3A). Green metabasalt clasts, often altered to reddish brown by pre-depositional weathering, are common in the Nakasasa valley, while granite pebbles are rare (Fig. 7.3B).

Clast material in the Kikonge conglomerate is moderate to well sorted, not imbricate and varies from dense pebble to matrix supported. Towards the top of the sequence, the proportion of matrix increases and grades into thin gritstone that passes into sandstone. Where the grit and sandstone are

dominant, graded bedding is present, showing upward-fining of grain size.

Where the beds are steeply tilted, the conglomerate unit is aligned parallel to the strike of the ridges and can be intersected several times along N–S traverses, with the younging direction, depending on the tilt direction, towards the north or the south. In the tilted sections, the stratigraphic successions are very irregular and incomplete. The top of the formation is considered to be the top of the uppermost conglomerate bed.

Grey sandstone with isolated pebbles (PINm) – Transition from the Kikonge to the *Maseke Formation* is gradual, as conglomeratic lenses decrease upward within the sandstone matrix. At the Butogolo plateau, the Maseke Formation has a minimum thickness of 120 m and comprises a homogeneous succession of even, medium- to thick-



Fig. 7.3. Conglomerates of the Kikonge Formation. (A) Polymictic conglomerate south of Butogolo Plateau (349563E / 75548N). (B) Polymictic conglomerate with variously altered metabasalt clasts in the Nakasasa valley (339468E / 94614N). Number tag 10 cm.



Fig. 7.4. Primary sediment structures in sandstones of the Maseke Formation. (A) Solitary quartz pebbles in sandstone (347855E / 92121N). (B) Sole marks in sandstone (341008E / 76387N). Number tag 10/8 cm.

bedded (<80 cm) continuous layers with well-developed planar-tabular cross-bedding, displaying low to medium angle foreset laminations up to 2 cm thick. Within this cross-laminated sequence, singular sub-rounded to rounded pebbles, 2–3 cm in size, may be found (Fig. 7.4A). The homogeneity and constant angle of the foresets with bedding reveal stable conditions with limited lateral drift of the currents. Trough cross-beds are also abundant, and their cross-cutting and truncating nature with the older laminations are indicative of active and migrating channels. Other primary features observed were sole marks (Fig. 7.4B), as well as soft-sediment slump features.

On average, sandstones are moderately sorted with limited fining-upward. However, grit-size fragments are unevenly distributed. Sandstones appear purplish-grey and show dark-grey, mm-thick basal laminations, which gradually or abruptly change upward to purplish pink. Within the lighter coloured regions, the bases of the foreset lamellae are still defined by concentrations of heavy minerals (mostly hematite and zircon). The darker the sandstone, the higher is the iron oxide content.

Sandstones with intercalated conglomerate beds are more gritty and have coarse- to medium-sized, well rounded to elongated grains of composite, deformed to un-deformed quartzite, quartz-feldspar and cherty granules. The intergranular matrix consists of quartz, rare feldspar remnants and detrital biotite. The clayey fraction is metamorphosed to non-aligned sericite and subordinate muscovite.

On average, the purple grey Maseke sandstone comprises fine- to medium-grained, well sorted,

well- to moderately rounded grains of quartz, chert and strained quartzite. Due to compression, the grains have been annealed and the roundness has been affected in places, although the primary round to oval shapes are still recognisable. Secondary quartz and minor sericite and chlorite fill some of the intergranular spaces, where prismatic to abraded zircon and hematite may occur.

Pink sandstone (PINb) – The *Buwekula Formation* comprises a thick succession of distinctive light coloured to prominently pink or crimson, medium- to fine-grained quartzitic sandstones, occasionally with minor lenses of gritstone and conglomerate along its base. These rocks have not been found in horizontal sections, but are well presented within moderate to steeply tilted beds at the Butogolo plateau. Primary bedding, as well as trough and tabular cross-bedding, are omnipresent, except in the extreme south, where they have been destroyed by shearing (Figs 7.5A–B). The rocks vary from thin- to thick-bedded units and may truncate the lower layers by low- to moderate angles indicative of lateral shifting channels in medium- to low-energy environments.

The thickness of the Buwekula Formation could not be established, as it was partly eroded away, but it must be several hundreds of metres at the Butogolo plateau. A thin section of the pink sandstone shows that the majority of the rock comprises fine- to very fine, well-sorted grains of quartz and subordinate rock fragments (cherty and mosaic-textured quartzite) and evenly distributed detrital hematite and zircon grains defining the foreset planes. Metamorphic sericite and muscovite have not developed due to the lack of clay or feldspar material.

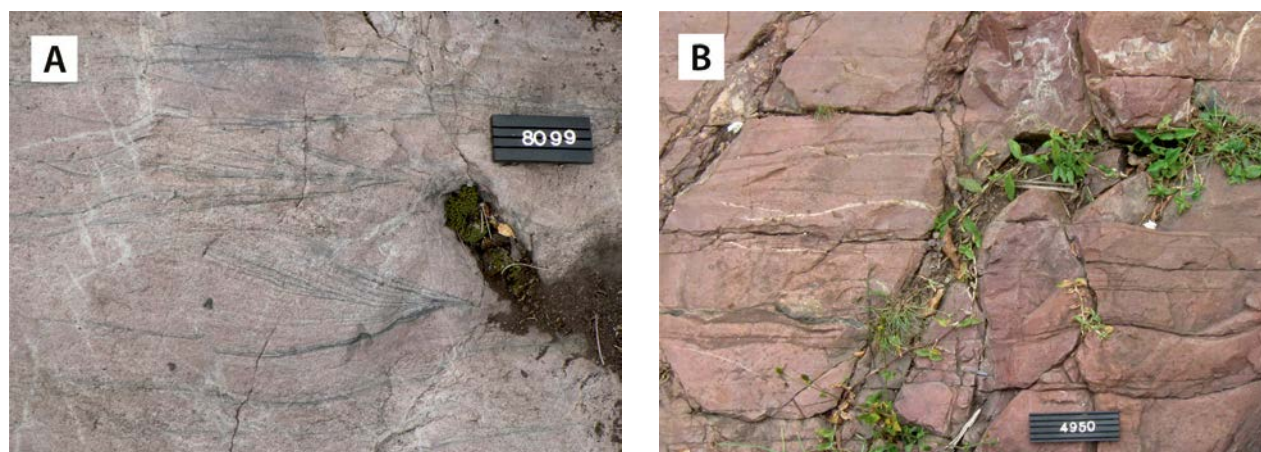


Fig. 7.5. Primary sedimentary structures in sandstones of the Buwekula Formation. (A) Small-scale trough cross-bedding. (B) Pink sandstone with a vague bedding (359390E / 88630N). Number tag 8/10 cm.

7.3 Geology of the Bwezigoro Group

7.3.1 Introduction

Rocks allocated to the Bwezigoro Group comprise the Bulaga and Namutamba plateaus between Mityana and Kiboga towns, with isolated smaller erosional remnants on various hills and crests (Fig. 7.2). Coarse-clastic Bwezigoro metasediments discordantly overlie rocks of the Buganda Group, the Mubende Granite and the tilted lithologies of the Namuwasa Group. Original sedimentary features are abundant, but undisturbed layering is actually rare, as beds may be tilted between a few degrees up to about 45°, and in places even 60°, with the dip direction dependent on the orientation of the controlling fault. In most cases, the faulting simply caused tilting towards the fault plane, but vertical displacement has occasionally been observed. The subdivision of the Bwezigoro Group is presented in Table 7.2.

7.3.2 Lithostratigraphic units

Conglomerate (P1Zcgl) – The *Kiryamuddo Formation* is well exposed along the slopes of the triangular Bulaga plateau, where polymictic conglomerates with thin sandstone interbeds locally form

an escarpment (Fig. 7.6A). A succession of alternating sandstone and conglomerate, tens of metres thick, comprises clast-supported pebble beds with size sorting and imbrication (Fig. 7.6B). The conglomerate fines upward with a sharp transition zone into gritty sandstone. Small pockets of pebbles may form part of the sandy layer and may be in contact with the succeeding conglomerate base. The size of well-rounded to oblate clasts occasionally exceeds 20–30 cm, and they comprise pebbles and cobbles of quartzo-feldspathic gneisses, vein quartz, quartzite and rarely granite. In places, compaction has resulted in fracturing of individual pebbles, while fracture sets have affected the pebbles and matrix. Towards the top of the conglomerate package, thicker and better-developed sandstone is present, with all the deposition characteristics of the overlying Nsala Formation.

On the Namutamba plateau, the *Kiryamuddo Formation* comprises matrix-supported conglomerates or poorly sorted, clast-supported boulder conglomerate with tightly packed, angular to sub-rounded clasts consisting of quartzite, quartz-feldspar gneiss, banded gneiss and quartzitic conglomerate with vein quartz pebbles. Cross-bedded, pink quartzite pebbles, most likely derived from the

Table 7.2. Subdivision of the Bwezigoro Group.

| Group | Formation | Lithology | Code |
|-----------|------------|--|--------|
| Bwezigoro | Namutamba | Conglomerate, sandstone, siltstone, locally silicified | P1Zcss |
| | Nsala | Feldspathic sandstone (<1.97 Ga) | P1Zss |
| | Kiryamuddo | Conglomerate | P1Zcgl |

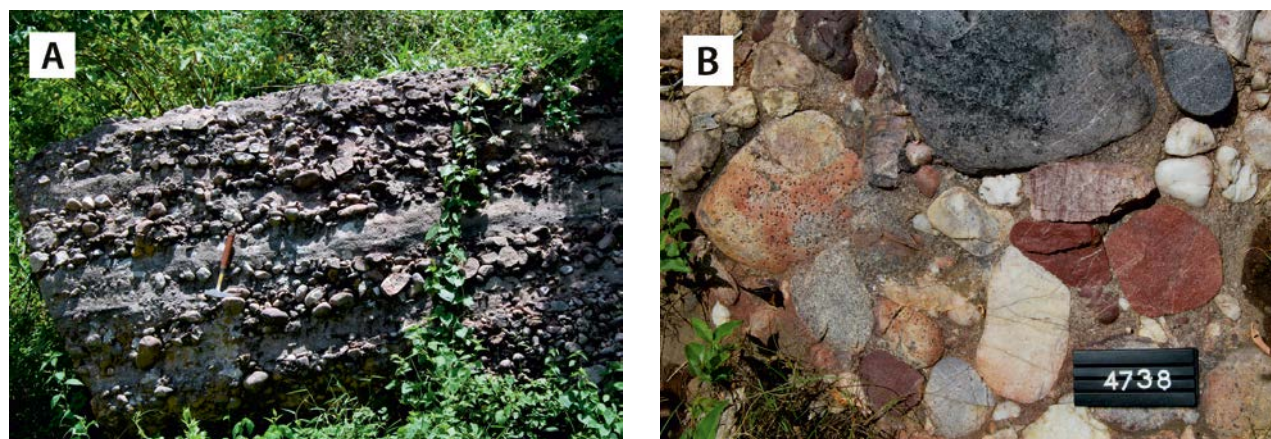


Fig. 7.6. Polymictic conglomerates of the Kiryamuddo Formation. (A) Alternating succession of basal conglomerate, grading upward into grit- and sandstone. Pebble sorting and imbrication are obvious. (B) Detailed image of clast-supported conglomerate in the western foot of the Bulaga plateau (373383E / 87427N). Number tag 8 cm, hammer 35 cm.

Buwekula Formation (Namuwasa Group), are also encountered, while granite and vein quartz clasts are subordinate to rare. The clasts are up to 50 cm in size and can form beds ranging from 10–15 cm up to two metres in thickness. The pebble units are separated by even-grained sandstone beds displaying laminar bedding and cross-bedding. In places, the beds are feldspathic and contain unevenly distributed detrital muscovite and grit-sized quartz grains, and grade upwards into the massive Nsala Formation.

Feldspathic sandstone (PIZss) – The upper part of the prominent Bulaga plateau mostly comprises reddish brown to pinkish, feldspathic sandstone, attributed to the *Nsala Formation* of the Bwezigoro Group. Only a few hundred metres of this unit are preserved and due to the absence of an overlying unit, it is impossible to determine its thickness. The sequence is most commonly horizontal, but subsequent minor faulting has locally tilted the beds up to moderate angles.

The preserved primary sedimentary structures found in Nsala sandstones include asymmetric

ripple marks, and concentric concretions and low-angle, tabular cross-bedding (Figs 7.7A–C). Locally, light brown, spheroidal reduction spots are also common in reddish brown sandstone.

The lower, strongly weathered contact of the Nsala Formation with Bujagali amygdaloidal metabasalts (Nile Formation) supposedly has a tectonic character. Conglomeratic interbeds found in the lower part of the sandstone unit suggest a transitional contact with underlying polymict conglomerates of the Kiryamuddo Formation.

Conglomerate, sandstone, siltstone, locally silicified (PIZcs) – A subhorizontal to gently tilted horizon of conglomerates, sandstones and minor siltstones, assigned to the *Namutamba Formation*, cover the top of the Namutamba plateau and adjacent hills. Small, separate occurrences of coarse-clastic meta-sediments, also assigned to this unit, cover Singo granite and the Buganda metasediments NW of the plateau.

Clast-supported conglomerates with subrounded quartzite and sandstone pebbles and cobbles, up to 50 cm in size, form interbeds within the light



Fig. 7.7. Primary sedimentary structures in feldspathic sandstones of the Nsala Formation on top of the Bulaga plateau. (A) Asymmetric ripple marks (384115E / 81868N). (B) Roundish, concentric concretions (380106E / 87707N). (C) Low-angle, tabular cross-bedding (380328E / 88076N). Number tags 8/10 cm.

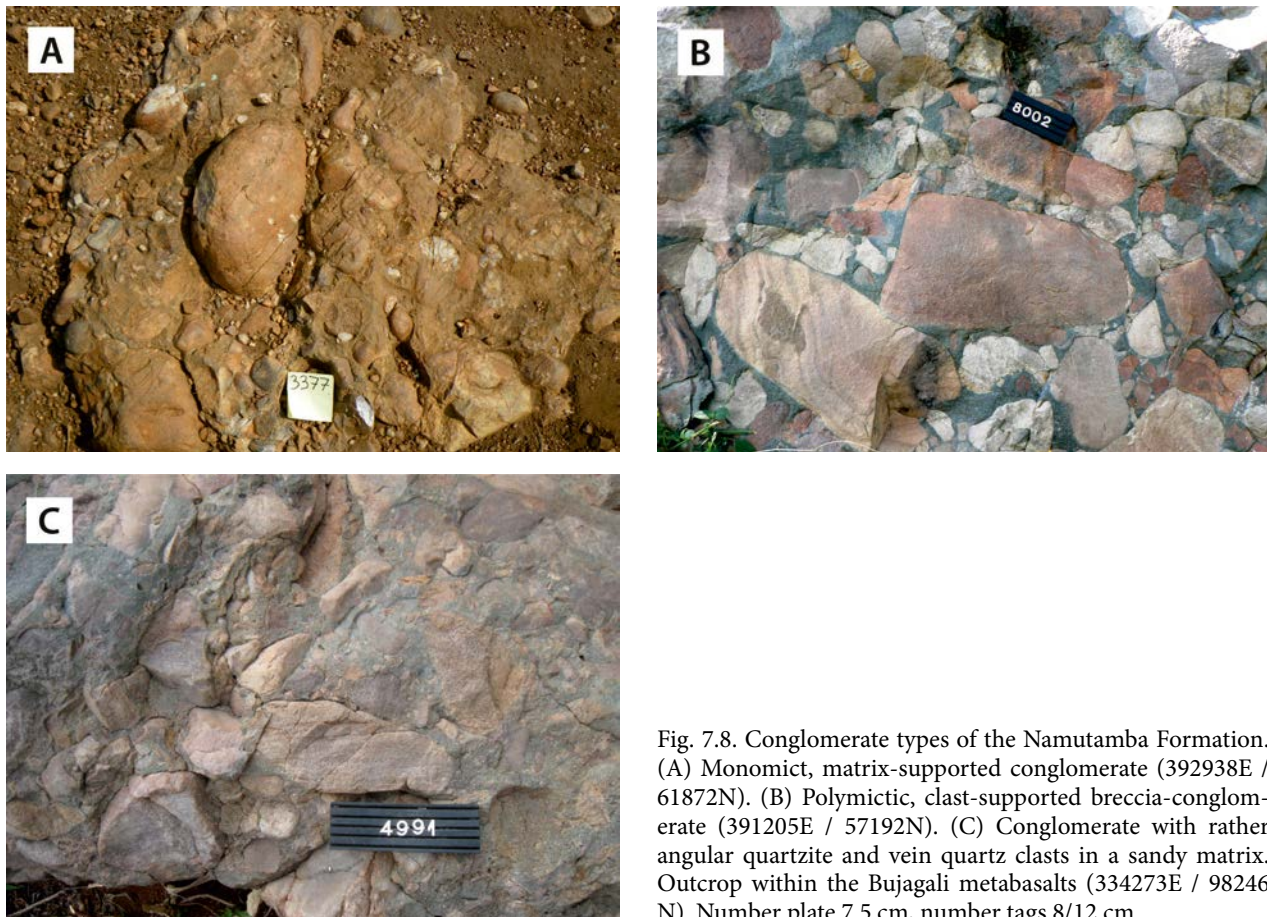


Fig. 7.8. Conglomerate types of the Namutamba Formation. (A) Monomict, matrix-supported conglomerate (392938E / 61872N). (B) Polymictic, clast-supported breccia-conglomerate (391205E / 57192N). (C) Conglomerate with rather angular quartzite and vein quartz clasts in a sandy matrix. Outcrop within the Bujagali metabasalts (334273E / 98246 N). Number plate 7.5 cm, number tags 8/12 cm.

brown sandstone on top of the Namutamba plateau (Fig. 7.8A). Tangential cross-bedding and ripple marks are common. A subhorizontal horizon of reddish-maroon, gritty to fine-grained sandstone is exposed on top of some hills NE of the Singo granite, about 6 km west of Bukomero village. A fluvial origin is indicated by the presence of *trough cross-bedding*, while interbeds of massive conglomerate composed of angular vein quartz and quartzite fragments in a green, sandy matrix found in sandstone suggest a debris flow origin (or proximal source) for this sequence (Fig. 7.8B).

A boulder field, comprising large *in situ* blocks of similar polymictic conglomerate, also tentatively assigned to the Namutamba Formation, occurs within the Bujagali metabasalts, north of the Butologo plateau. These conglomerate beds, comprising angular to sub-rounded, laminar quartzite, vein quartz and rare maroon phyllite clasts, all set in a greenish, very fine-grained sandy matrix, alternate with thin sandstone interbeds (Fig. 7.8C). The thickness and areal extent, as well as contact relations of this conglomerate, are unknown.

7.4 Geology of the Kagera-Buhjewu supergroup

7.4.1 Introduction

The Kagera-Buhjewu Supergroup is composed of two lithostratigraphic units, the *Muyaga Group*

(below) and the *Ruvubu Group* (top). The subdivision of the Kagera-Buhjewu Supergroup is presented in Table 7.3.

Table 7.3. Subdivision of the Kagera-Buhjewe Supergroup.

| Group | Formation | Lithology | Code |
|--------|--------------|---|---------|
| Ruvubu | Munyoni | Quartzite with minor pelitic layers | P1KRq |
| | Kasyoha | Pelites with minor quartzite beds | P1KRp |
| | Nsika Member | Mylonitised and brecciated quartzite | P1KRmq |
| | Lubare | Quartzitic sandstone | P1KRqss |
| | Isingiro | Conglomerate, grit | P1KRc |
| Muyaga | Rakai | Mudstone, shale, phyllite | P1KMms |
| | Kiganga | Quartzite, conglomerate, with algal fossils | P1KMqs |

7.4.2 Lithostratigraphic units

Muyaga Group

Quartzite, conglomerate, with algal fossils in places (P1KMqs) – Quartzites and associated conglomerates assigned to the *Kiganga Formation* form a discontinuous, folded and faulted chain of quartzite ridges from the Tanzanian border to north of the Masaka-Mbarara highway (Fig. 7.9). The maximum observed thickness of this gently west-dipping quartzite is some tens of metres. The basal contact is not exposed, but the unit supposedly rests unconformably on steeply dipping mica schists of the Buganda Supergroup, which are exposed in several locations below the quartzite horizon (e.g., Phillips 1959). Upwards, the quartzites of the Kiganga Formation grade into red arko-

sic sandstones, shales and phyllites of the Rakai Formation.

Light grey to pale greenish grey quartzite of the Kiganga Formation is a rather pure, massive rock without any visible primary sedimentary features, although reddish-brown parallel oxidation zones reveal, in places, the gently dipping bedding planes (Fig. 7.10A). Oxidation staining along fissures in the rock is common.

Interbeds of well-sorted, matrix-supported conglomerate with sub-rounded or rounded milky vein quartz pebbles are locally exposed within Kiganga quartzite (Fig. 7.10B). A peculiar sedimentary structure occurs in some quartzite outcrops, comprising layers of elongated, microcrystalline quartz lenses, probably aligned by running water.



Fig. 7.9. Gently west-dipping quartzite ridges of the Kiganga Formation, seen from the top of Kiganga hill (326043E / -96109N).

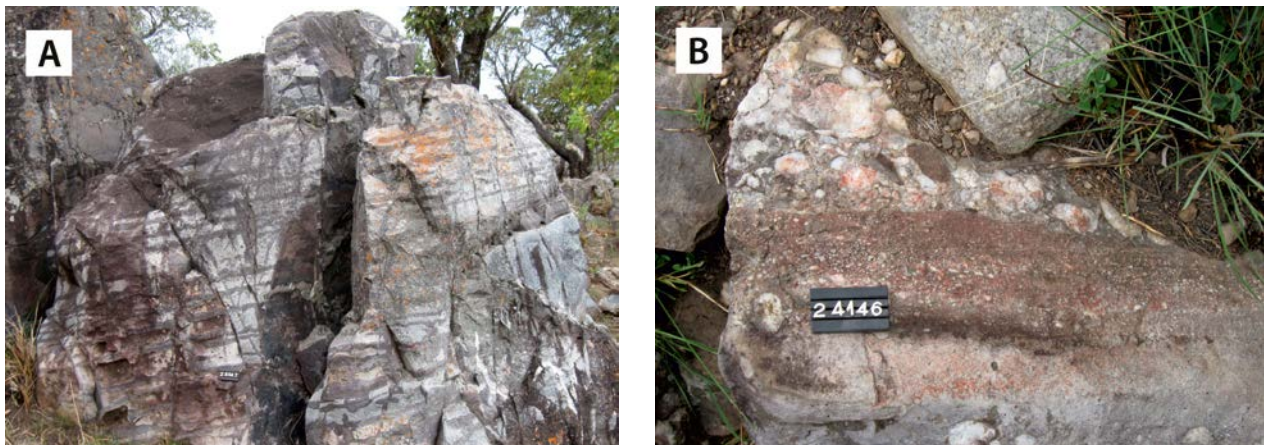


Fig. 7.10. Sedimentary structures of the Kiganga Formation. (A) Oxidation staining parallel to bedding planes of quartzite (320809E / -101159N). (B) Distinctly bedded conglomerate with sub-rounded to rounded vein quartz clasts (321047E / -101002N). Number tag 8 cm.

These lenses, up to 50 mm long and 5 mm thick, generally have a thin iron oxide coating, but lenses comprising deep red limonitic material are also common. Pallister (1955, 1956) described similar, cherty and ferruginous quartzite from Kabwer hill on the Tanzanian side of the border. Various algal forms have been found in this quartzite ridge, which is supposedly the southern continuation of the Kiganga quartzite, representing the same

stratigraphic horizon (Pallister 1955). Total silicification of algal limestone beds may explain the absence of calcareous horizons in these metasediments.

Mudstone, shale, phyllite, oncolitic and stromatolitic in places (P1KMms) – A thick pile of mudstones, siltstones, slates and phyllites, assigned to *the Rakai Formation*, is deposited conformably

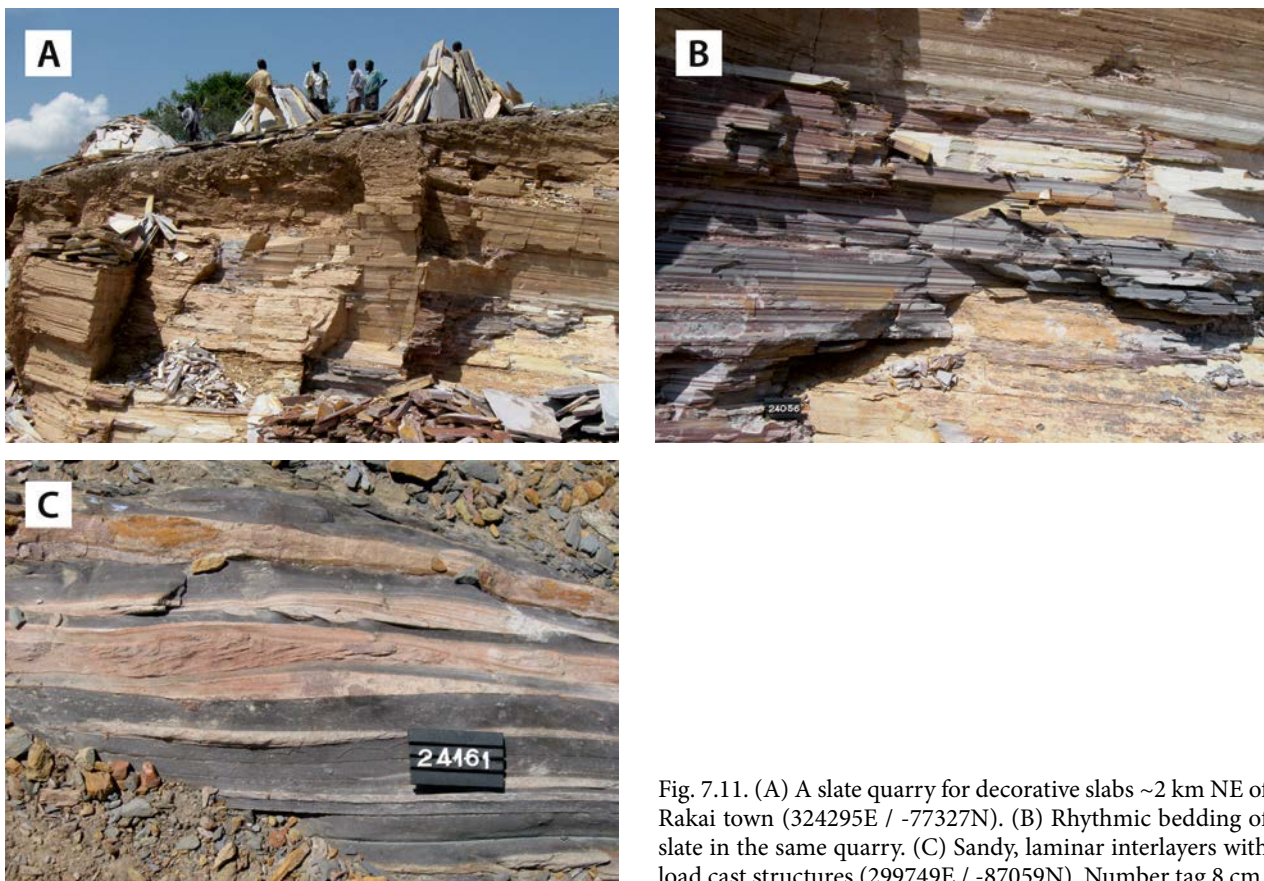


Fig. 7.11. (A) A slate quarry for decorative slabs ~2 km NE of Rakai town (324295E / -77327N). (B) Rhythmic bedding of slate in the same quarry. (C) Sandy, laminar interlayers with load cast structures (299749E / -87059N). Number tag 8 cm.

on top of the Kiganga quartzite. In the area surrounding Rakai town, these weakly deformed, creamy to light pinkish grey or reddish brown (when oxidised) slates and siltstones are widely quarried for decorative slabs (Figs 7.11A–B). Laminar bedding is common, and locally these pelitic rocks have thin, sandy interbeds with load cast structures (Fig. 7.11C). Horizons with weathered out or limonite-filled pseudomorphs after cubic pyrite crystals are also common in slates of the Rakai Formation.

Well-preserved stromatolites and pisoids occur in thinly bedded slates in a quarry ~5 km NW of Rakai town (Fig. 7.12A). Pisoids occur as oval-shaped to amoeba-like concretions, often forming closely packed aggregates in the bedding plane of laminar slates (Fig. 7.12B), or as spherical, coin-shaped forms, generally 2–3 cm in diameter (Fig. 7.12C, left). Larger structures, comprising concentric rings up to 50 cm in diameter, probably

represent horizontal cross-sections of stromatolite moulds (Fig. 7.12C, right).

In some slabs, a cross section of probably a *Collenia*-type stromatolite colony reveals the laminar inner structure of the mould (Fig. 7.12D). Another variety is composed of roundish, disk-shaped concretions, 1–2 cm in diameter. Similar fossil algal structures have been found on Kabwer hill on the Tanzanian side of the border, and on Nsozinga hill, located 30 km ESE of Mubende town, in sediments formerly attributed to the Bukoba Series (Pallister 1955).

The degree of deformation and metamorphism increases to the west and gently dipping slates and siltstones consequently grade into greyish, open folded phyllites SW of Kijanebalola Lake, where the rocks form a broad, gently NE-plunging syncline (Phillips 1959). Silvery grey, strongly foliated mica schists with thin quartzite interbeds are exposed in the hills east of Lake Nakivali.

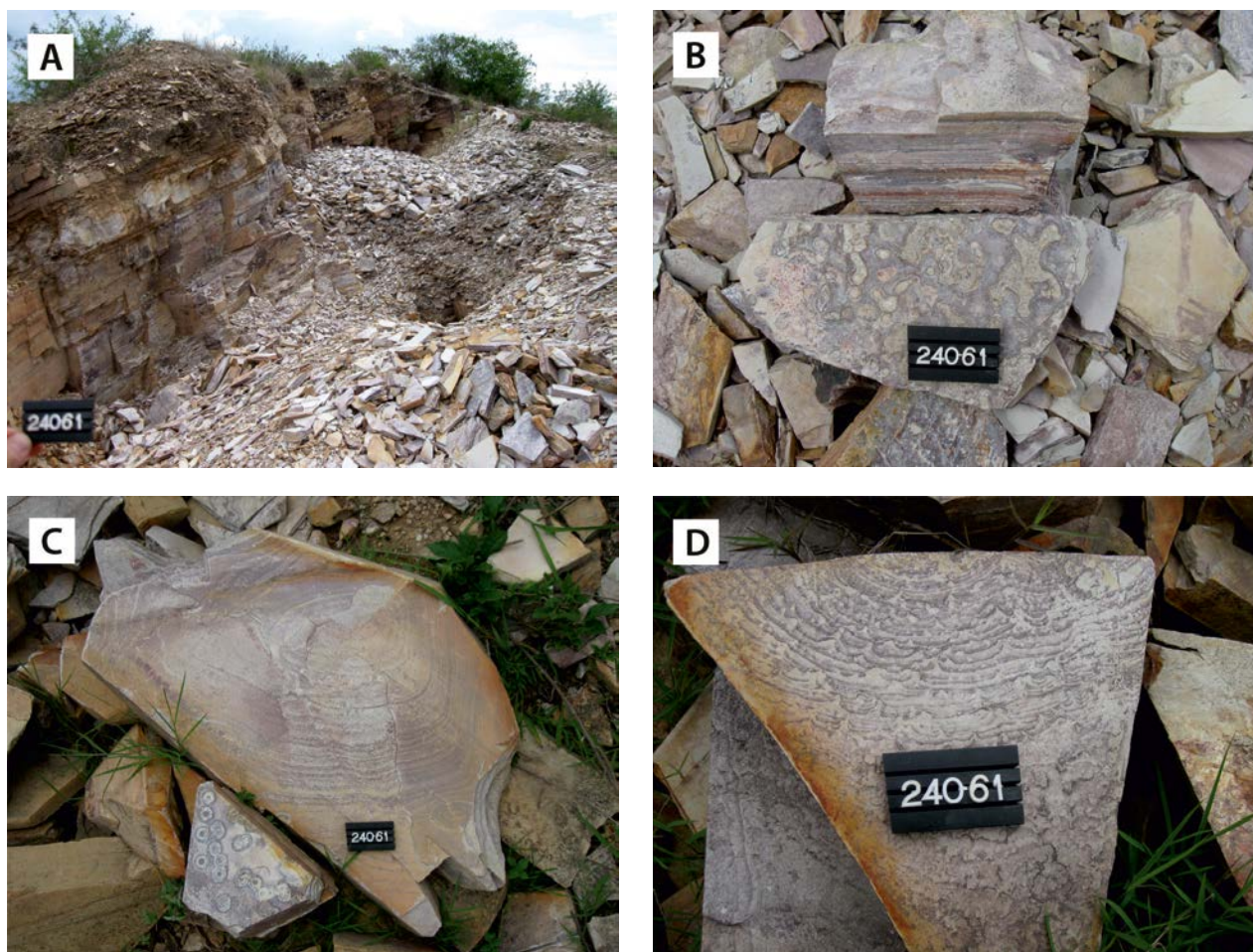


Fig. 7.12. (A) A slate quarry with stromatolite and pisoid structures, located ~5 km NW of Rakai town (320056E / -74393N). (B) Aggregate of oval and amoeba-like shaped pisoids. (C) Coin-shaped, spherical pisoids (left) and cross section of a stromatolite mould (right). (D) Cross section of a possibly *Collenia*-type (*Collenia undosa*?) stromatolite colony in the same quarry. Number tag 8 cm.

Ruvubu Group

Conglomerate, grit (PIKRc) – The *Isingiro Formation* (Reece 1959) represents the lowermost stratigraphic unit of the Ruvubu Group, comprising conglomerates and grits that are mostly exposed along the escarpment around the Buhweju Mountains, with a small outlier at Ntsinda Hill, about 10 km further to the northwest. They unconformably overlie Buganda schists and different granitoids, but the footwall contact is not exposed (Reece 1961). The hanging wall contact with quartzites of the overlying Lubare Formation is transitional. The matrix-supported conglomerate has a thickness of ~150 m along the southern escarpment of the Buhweju Mountains, reaching its maximum thickness in the northeast (Isingiro), where conglomerate units locally attain a total thickness of over 350 m (Reece 1961). Here, an alternating succession of

basal conglomerate grades upwards into grit- and sandstone. Pebble sorting and imbrication are obvious, and individual conglomerate beds and lenses are ~15 m thick on average (Isabirye 2013, pers. comm.). Clasts are mainly sub-angular to rounded quartzite or vein quartz pebbles (Fig. 7.13A), with minor schist fragments in a micaceous quartzite or gritty matrix (Fig. 7.13B). Variably deformed clasts range between 5–15 cm in size along the southern escarpment, but boulders up to 1.5 m in diameter have been found along the slopes in the north (Reece 1959). Cross-bedding is common in sandy or gritty members of the Isingiro Formation.

Quartzitic sandstone (PIKRqss) – A variably thick pile of quartzitic sandstones of the *Lubare Formation* (Combe 1939) extends from the Rakai area in the east to the Buhweju outlier in the west. Its lithological characteristics are thoroughly discussed

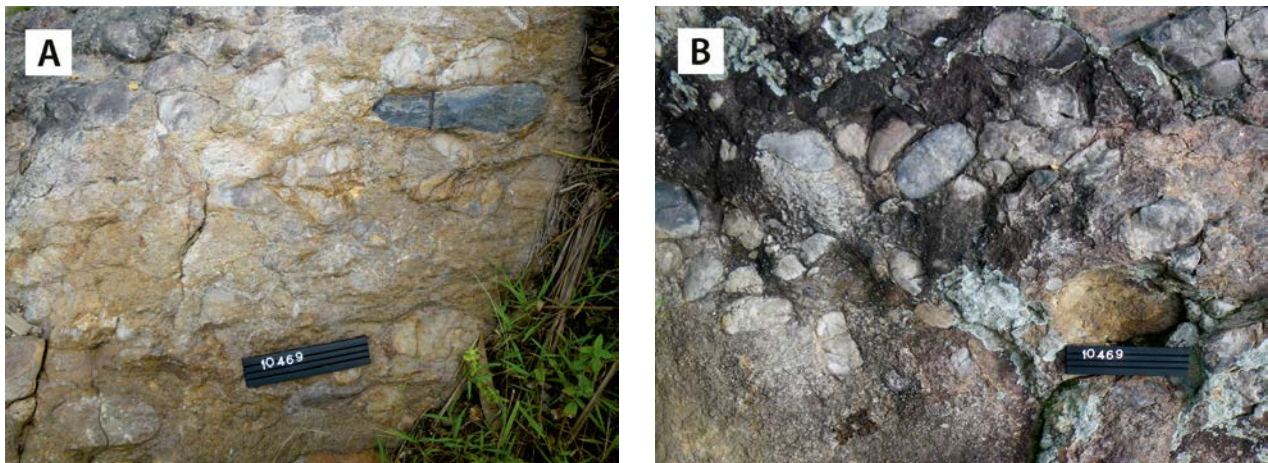


Fig. 7.13. Conglomerates of the Isingiro Formation. (A) Monomictic conglomerate with vein quartz and quartzite clasts. (B) Polymictic conglomerate with a gritty matrix from the southern escarpment of Buhweju Mountain (182243E / -41801N). Number tag 15 cm.



Fig. 7.14. Quartzitic sandstones of the Lubare Formation. (A) Gently NW-dipping quartzite on top of Kiya Hill (330981E / -79711N). (B) Laminar bedding in orthoquartzite at a ridge east of Rugaga plateau (281653E / -102052N). Number tag 10 cm.

by Combe (1939), King (1942a, 1942b, 1942c), Roberts (1940, 1947) and Reece (1959, 1961). A 30–50-m-thick horizon of bluish-grey massive quartzite covers Kiya Hill, east of Rakai town (Fig. 7.14A), resting conformably on top of conglomerates of the Rakai Formation. The same quartzite is exposed on several hill tops west of Kijanebalola Lake and forms a wide plateau in the Rugaga area, about 40 km SE of Mbarara town, where the unit attains a thickness of several hundreds of metres. In the west, Lubare quartzites are exposed almost continuously around the escarpment of the Buhweju plateau. The total thickness of the sub-horizontal to gently dipping, undeformed quartzite unit is locally up to 1.5 km (Reece 1961). In places, the Lubare quartzite contains conglomeratic lenses, and clayey, gritty and pebbly layers or lenses have been observed by Reece (1959). The contact with the mylonitised quartzites of the overlying Nsika Member (see below) is gradational.

In addition to laminar bedding (Fig. 7.14B), primary sedimentary features in the light brownish to bluish-grey quartzites include low-angle cross-bedding, symmetrical ripple marks, load casts and mud cracks, all referring to a shallow-water, fluvial deltaic to littoral environment (Reece 1961).

Mylonitised and brecciated quartzite (P1KRmq) – A strongly deformed quartzite variety of the Lubare Formation, up to 300 m thick and called the *Nsika Member* by Reece (1959), is exposed along the southern escarpment of the Buhweju plateau, where it mostly overlies less deformed quartzites of the Formation. These are pale to dark grey or brown mylonites, cataclasites and occasional breccias,

consisting of microcrystalline quartz mosaics with patches, seams and crystals of coarser quartz (Reece 1959, 1961) (Fig. 7.15A). In the most brecciated varieties, (Fig. 7.15B), angular cataclastic fragments of quartz, 5–10 cm in size, are set in a brown, cherty, iron-stained matrix (Reece 1959).

Pelites with minor quartzite beds (P1KRp) – Very fine-grained, dark to pale purple grey, thinly bedded mudstones and metapelites of the *Kasyoha Formation* (Fig. 7.16A) show occasional mud cracks and mudstone beds with carbonaceous matter or graphite. These variably kaolinised metapelites show metamorphic foliation and lineation and numerous small (<2 mm), euhedral andalusite porphyroblasts (Fig. 7.16B). Quartzitic boulder fields in the area underlain by this unit are supposedly derived from thin quartzite interbeds.

Quartzite with minor pelitic layers (P1KRq) – White to reddish purple, fine- to medium-grained quartzites with minor pelitic interlayers of the *Munyoni Formation* cap the central parts of the Buhweju plateau, particularly at Munyoni Hill, the highest top in the area (Reece 1959). Based on the quartzite horizons found in the underlying pelites of the former Kasyoha Formation (Roberts 1942), the footwall contact of the Munyoni Formation is transitional. The maximum thickness of this quartzite unit is about 365 m, while pelitic interlayers rarely exceed 5–6 m (Reece 1961).



Fig. 7.15. (A) Mylonitic quartzite of the Nsika Member (209924E / -47027N). (B) Angular cataclasite fragments in breccia at Nsika village (214385E / -40275N). Number tags 15/10 cm.

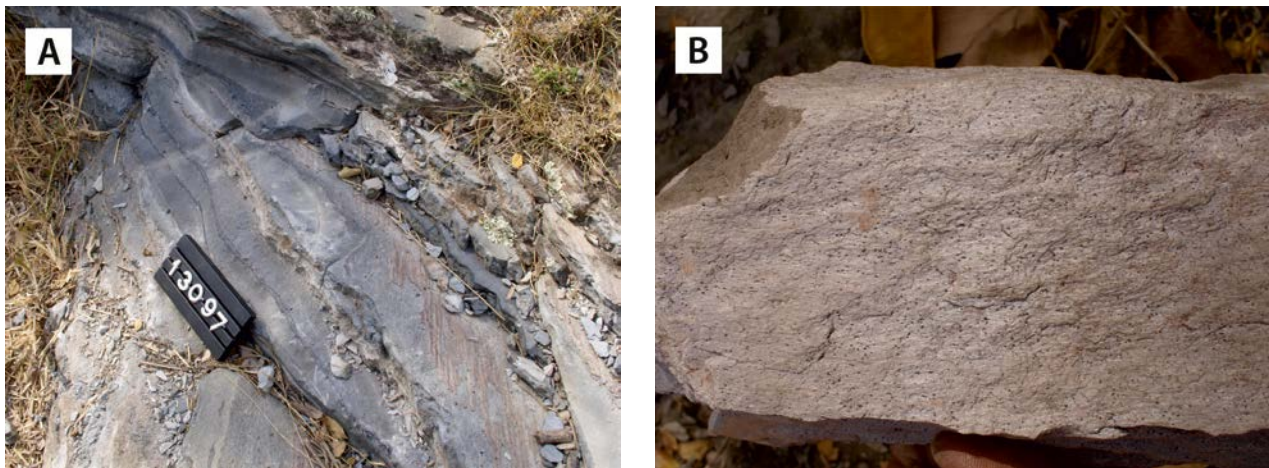


Fig. 7.16. (A) Laminar bedding in mudstone of the Kasyoha Formation (257731E / -77350N). (B) Small andalusite porphyroblasts in weathered metapelite of the Kasyoha Formation (255426E / -75499N). Number tag 10 cm.

7.5 Geochronology

Detrital zircons in two samples of the Namuwaso Group and one of Bwezigoro Group have been dated using the MC-LA-ICP-MS method (Mänttari 2014).

Metasandstone (<2.05 Ga) (339661E / 71174N) – Detrital zircons from a near vertical sandstone horizon of the Kikonge Formation, just north of the sheared portion of the Namuwaso Group, often exhibit fairly sharp edges, although some grains are subrounded with pitted surfaces. The $^{207}\text{Pb}/^{206}\text{Pb}$ age distribution (Mänttari 2014) of the detrital zircon ranges from 2.70 to 2.05 Ga.

Orthosandstone (<2.05 Ga) (345129E / 75257N) – When compared to the metasandstone above, the quantity of subrounded zircon grains from this vertically dipping orthosandstone of the Maseke Formation is smaller with a predominance of euhedral, sharp-edged grains. The $^{207}\text{Pb}/^{206}\text{Pb}$ age distribution of the detrital zircon domains ranges from 2.83 Ga to 2.05 Ga (Mänttari 2014).

Feldspathic sandstone (<1.97 Ga) (371031E / 83443N) – Fine to coarse, rounded to subrounded detrital zircons from this pinkish-grey sandstone of the Bwezigoro Group show a $^{207}\text{Pb}/^{206}\text{Pb}$ age distribution ranging from 3.06 Ga to 1.79 Ga (Mänttari 2014).

Interpretation of the age results – The source of the detrital zircons is speculative, but the following conclusions can be made:

- Detrital zircons of Archaean age can be separated into 2.7–2.6 Ga zircons derived from the Neoproterozoic West Tanzanian Terrain (WTT) and North Uganda Terrain (NUT) basement. Older Archaean zircons with ages between 2.8 and 3.1 Ga may be derived from mafic enclaves in TTG gneisses (see also Schumann et al. 2004) of the WTT or, alternatively, from Mesoarchaean >3.08–2.99 Ga rocks of the Uleppi Complex (West Nile Block) or the more proximal Karuma Complex (NUT);
- The small 2.46–2.44 Ga peak can be correlated with granites and feldspar porphyries of the Kiboga Suite (Section 3.3.4) in the suture zone – the Nakasongola discontinuity (Ruotoistenmäki 2014) – between the WTT and NUT, which yield an age of 2.49 Ga (Mänttari 2014);
- Detrital zircons with ages between 2.35 Ga and 2.20 Ga are difficult to interpret in terms of source areas, but are supposedly related to small or local perturbances (again in the suture zone between the WTT and NUT?) prior to the Eburnian Orogenic Cycle in the area;
- Clear peaks around ~2.19–2.16 Ga and ~2.09–2.05 Ga manifest the two-phase history of the Rwenzori Fold Belt in the area (Section 6.8);
- Obviously, the batholiths of the Mubende and Singo granitoids had not yet emerged at the surface when the sediments of the Namuwaso Group were deposited, and 1.85 Ga zircons have not consequently been encountered.

In summary, and based only on detrital zircon ages, we can conclude that sandstones of the Maseke Formation of the Namuwa Group are

younger than 2.05 Ga. Similarly, an age of <1.97 Ga is attributed to feldspathic sandstone of the Nsala Formation of the Bwezigoro Group.

7.6 Geodynamic Development

Field verification has indicated that the rocks of the Namuwa Group and the Kagera-Buhweju Supergroup are not undisturbed to slightly tilted platform deposits, but that they have been subjected to complex tectonic processes. Reece (1959) already noted cataclasites of the Nsika Member between the competent Lubare quartzites and overlying incompetent phyllites of the Kasyoha Formation (Ruvubu Group, Kagera-Buhjewu Supergroup), as well the disharmonic contacts against these rock units, suggesting that the mylonitic rocks of the Nsika Member represent the highly deformed upper part of the Lubare quartzites. Their cataclastic nature is a strong indication supporting the idea that sub-horizontal thrust planes separate the pile of sediments in the Buhweju Mountains into different 'thick-skinned' tectonic units.

The idea that sediments of the Kagera-Buhweju Supergroup tectonically overlie older Buganda metasediments and pre-Buganda Rwenzori (or Rusizian) basement is supported by airborne

magnetic maps of the eastern part of the Kagera-Buhweju Supergroup, roughly between Kibale and Kanyogoga (Figs 7.17A–B), underlain by Lubare sandstones and Rakai mudstones. The magnetic map from this area shows a poor correlation with the surface geology. A pronounced E–W-trending magnetic lineament separates a magnetic low (south) from a magnetic high (north). It is concluded that the sediments of the Kagera-Buhweju Supergroup in this area form a rather thin surface layer, almost transparent to the magnetic image of the underlying crystalline basement, portraying a major discontinuity, corresponding with a part of the magnetic lineament in southwestern Uganda portrayed in Figure 3.3. This discontinuity can be followed in a westward direction and coincides with the northern contact between the lithologies of the Mesoproterozoic Akanyaru-Ankole Supergroup (Chapter 8) and the underlying Palaeoproterozoic basement of the Rukungiri Suite (or Rusizian).

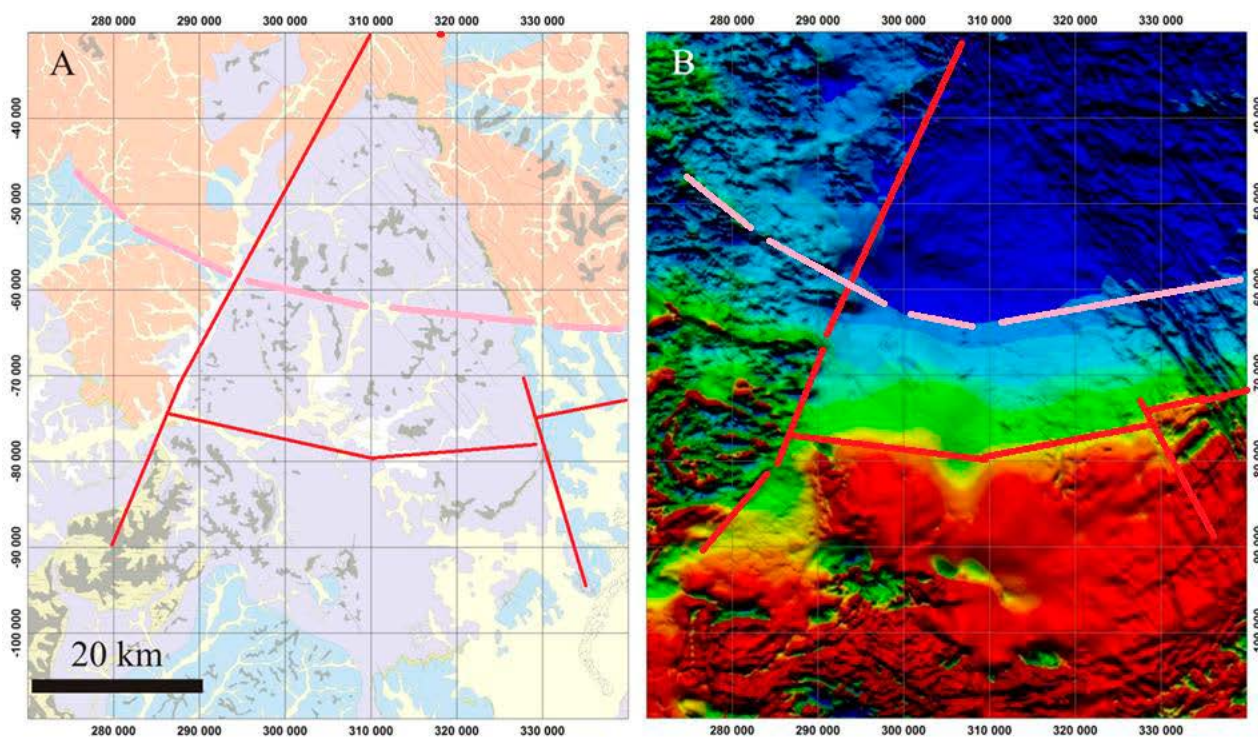


Fig. 7.17. (A) Eastern part of the Kagera-Buhweju Supergroup resting on Buganda lithologies. Note the strong difference in the magnetic signature (B). This indicates that the rocks of the Kagera-Buhweju Supergroup form only a thin cover and that the magnetic pattern is mainly derived from the underlying basement. Magnetic field is reduced to equator – warm colours indicate low-magnetic rocks.

The units in the western Butologo plateau, with a greenschist facies grade imprint, show vertical, tilted and horizontal sections caused by shearing and fault-block tilting, dividing the Namuwasu succession into irregularly spaced zones, which can be up to several kilometres wide in the plateau area (Fig. 7.2). The tilted segments do not penetrate the contact plane with the underlying Nile schists by more than a few metres, and were formed as part of the complex system of block faulting, which caused down-warping of the horizontal domains bounded by N- or S-tilted sections in which incremental stepwise bedding-parallel slip occurred. It is assumed that the rocks were consolidated and metamorphosed to greenschist-grade quartzite prior to the block faulting.

This was succeeded by a more severe thrust-related phase of tectonism, which caused brittle shear deformation under greenschist facies conditions, notably preserved in the southern part of the Namuwasu remnant. The intensity of deformation decreases from south to north. In the southernmost region, the grey and pink quartzite, and also in places the conglomerate beds, acquired a penetrative fracture cleavage or shear foliation, which destroyed all primary sedimentary features (Fig. 7.18). The well-bedded and cross-stratified units turned into massive homogeneous, foliated pink and grey quartzite. Towards the northern edge of

the sheared zone, numerous *en echelon* fractures have developed, in places forming conjugate sets, which were filled by quartz (Fig. 7.19A). Quartz veins in the shear zones, in places up to 30 cm thick, are aligned in the fabric (Fig. 7.19B). Towards the deformation edge, the tension gashes are oblique to the fabric and in places have conjugate fractures (also oblique to the fault plane) with displacements of several centimetres. Where this late faulting occurred parallel to the bedding, the fault plane may contain fault gouge and angular fragments. Locally, for instance near Buta, the fault breccia is about 5 m wide.

The shear deformation produced some asymmetric folding and crenulation of the fabric and bedding around E–W-trending, subhorizontal fold axes, implying minor uplift to the north. Similar asymmetric folds, truncated against a steep fault plane, around moderate westward plunging fold axes, was observed in the underlying Nile schists east and west of the Namuwasu plateau. The drag of the bedding and older fabric against the fault planes is indicative of oblique E–W displacement. From locality to locality, the transport could be right or left lateral. The plunge of the fold axes reflects thrusting to strike-slip compression. Occasionally, massive nearly E–W-trending subvertical quartz veins are found. These are parallel to the subvertical tilted beds or cut across them where



Fig. 7.18. Grey quartzite of the Maseke Formation, with subvertical penetrative shear fabric and quartz precipitates along the fabric and oblique fracture planes. Note the chevron kink. The southern shear zone (339343E / 70573N). Number plate 8 cm.

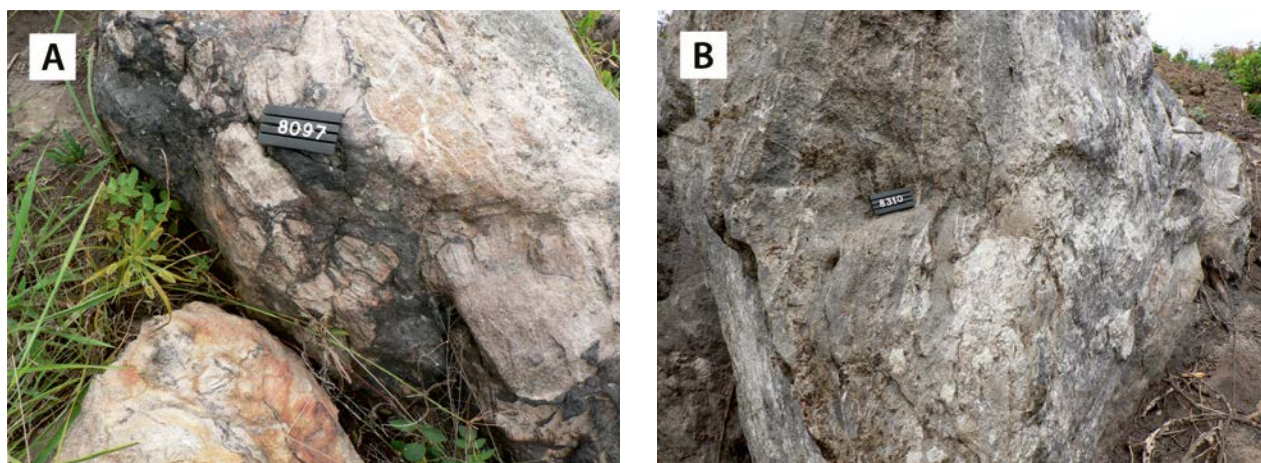


Fig. 7.19. (A) Pink quartzite of the Buwekula Formation at the northern edge of the shear zone with quartz-filled en echelon conjugate tension gashes, with subsequent brecciation due to foliation-parallel faulting. The dark appearance of the fault is due to secondary iron enrichment (339506E / 70959N). (B) A foliation-parallel quartz vein with schist enclaves slightly oblique to the shear foliation, with associated pygmatic stringers injected along the fabric in the sheared Maseke quartzite of Figure 7.18. Number tag 10 cm.

they dip moderately. These massive quartz veins are also present in the surrounding Nile schists, and in many cases are enriched in hematite and gold.

Several steep dipping elongated slivers of Namuwasa metasediments are present along the southern edge of the Bujagali metabasalts, in places surrounded by Nile schists and at other locations between the shale and the metabasalt unit (Fig. 7.20). The slivers are composed of incomplete sections of different stratigraphic levels of the Namuwasa sequence, and were tectonically emplaced within and against the Nile schists and Bujagali metabasalts. Between the Bujagali metabasalts and Victoria quartzite, a continuous layer of mostly pink Buwekula quartzite is interlayered with Nile schists. To the east, it disappears beneath rocks of the Bwezigoro Group of the Bulaga plateau, while in the west it is truncated by quartzites of the Victoria Formation. Stratigraphic way-up indicators show younging constantly towards the south in Buwekula and Victoria quartzites as well as in Bujagali metabasalts. South of the Bulaga plateau, parts of the Victoria quartzite dip and young to the northeast, describing the presence of a syncline there. The out-of-sequence distribution of the Buganda and Namuwasa units, all younging in the same direction, is indicative of tectonic stacking caused by thrusting without significant large-scale folding in a 'thick-skin' model.

The asymmetry of the small-scale structures associated with this thrusting event shows associated lateral movements. Brecciation and grain-size

reduction (Fig. 7.21A) in rocks of the Namuwasa Group have locally been observed and affected the quartzite across narrow zones (<30 cm), giving rise to the development of a crude shear banding at the centimetre scale. The bands are a lighter yellowish colour with numerous dark-red fragments. Disharmonic and irregular flow-folds are indicative of left-lateral movement. Close to some completely silicified shear zones, iron mineralisation is present and hematite layers up to 75 cm thick are common.

Subsequent to the thrust event, rocks of the Namuwasa Group were affected by brittle deformation, as shown by fractures that can be filled by specularite (Fig. 7.21B), manifesting right-lateral strike-slip. Similar fractures are present in the 1.85 Ga Mubende pluton, as well as at the contact of the Mubende granite with foliated Archaean porphyritic granite, indicating that the maximum age of the thrusting event is ~1.85 Ga.

There remains one question to be answered: What was the timing of the tectonic events described above? Based on the fact that no low-angle thrusting has been observed in the granitoids of the Mubende-Singo Suite and Mubende granite intruded into already sheared Namuwasa plateau strata provides a minimum age for the deformation (de Kock et al. 2011). Detrital zircon shows evidence that the Namuwasa Group was deposited posterior to 2.05 Ga. Consequently, thrusting, stacking and interleaving of Namuwasa and Buganda lithologies are constrained somewhere between 2.05 Ga and 1.85 Ga.

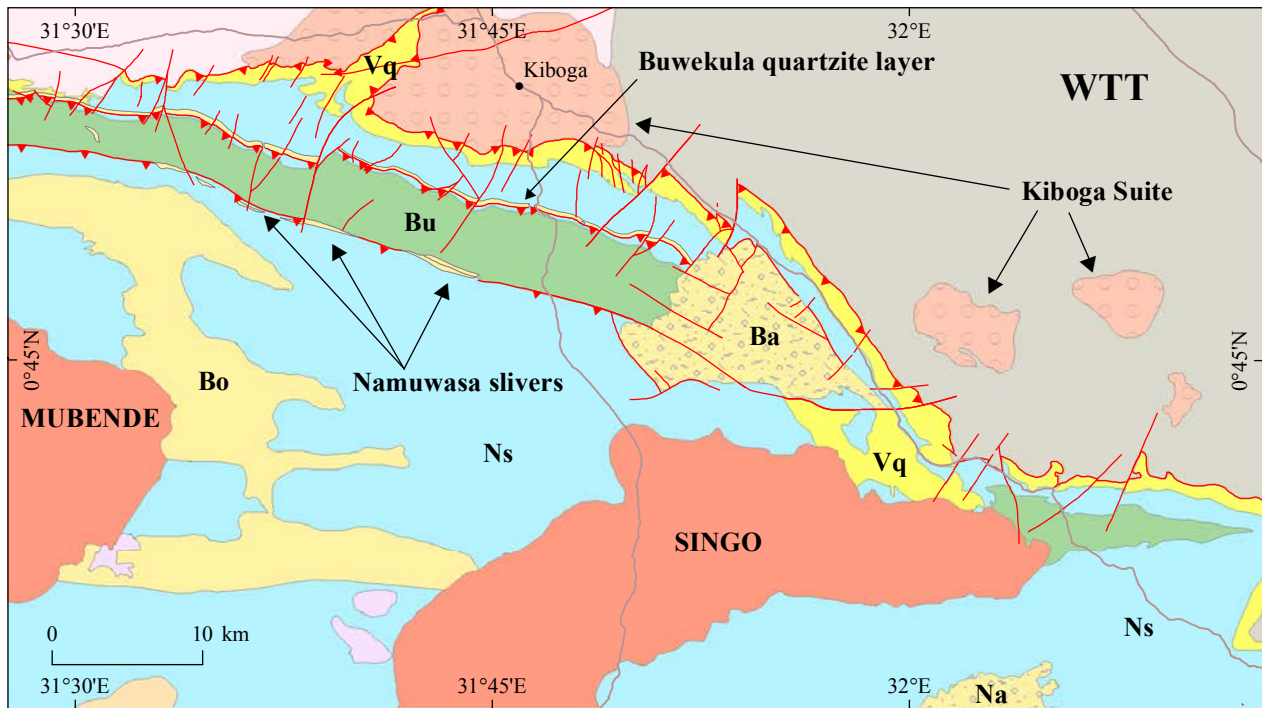


Fig. 7.20. Structural geology of the region south of Kiboga town, showing a number of south-dipping steep up-thrusts, notably highlighted by slivers of Namuwasa conglomerates south of Bujagali basalts (Bu) and a continuous Buwekula quartzite layer tectonically emplaced inside Nile schists north of the Bujagali metabasalts. Along the same line of thinking, the contact between the Buganda Group and Archaean basement is also interpreted as an up- or overthrust. Key: Vq = Victoria quartzite; Ns = Nile schists; Bo = Butologo plateau; Ba = Bulaga plateau; Na = Namutamba plateau.

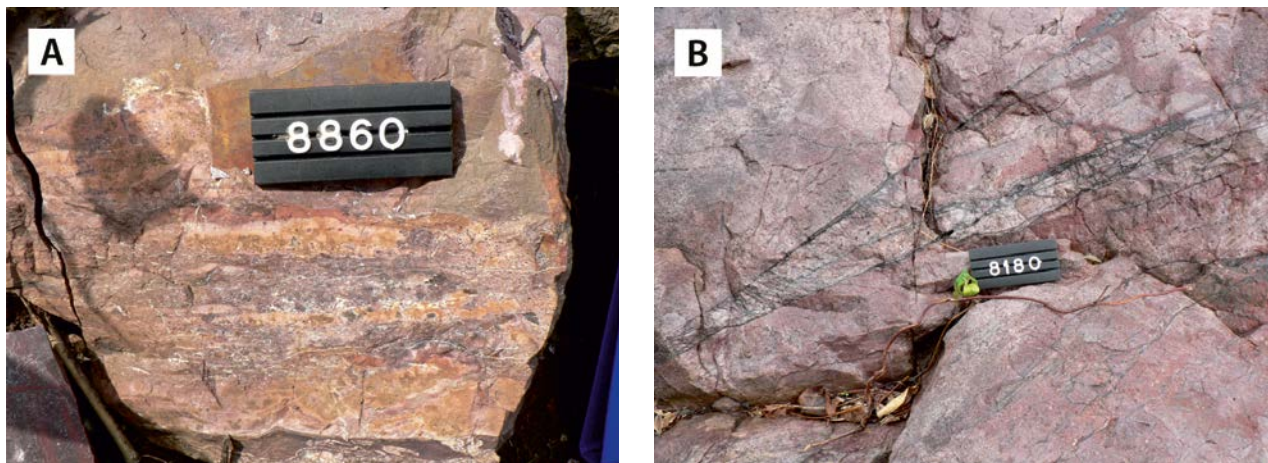


Fig. 7.21. (A) Buwekula quartzite along the Bujagali metabasalt unit, displaying brittle shear deformation, fracturing and tectonic differentiation. Note the disharmonic intrafolial left-lateral folds at the bottom and leaching below the number tag. Silicification is prominent in the narrow deformation zone, while hematite replacement is significant above the tag (349042E / 91583N). (B) Southward-dipping pink Buwekula quartzite in the northern Namuwasa plateau displaying conjugate left-lateral strike-slip fracturing with limited displacement. The fractures are filled with specularite (340624E / 85877N). Number tag 8 cm.

This event is supposedly coeval with thrusting and tectonic stacking described by Link et al. (2010) in the Rwenzori Mountains (Section 6.8; Fig. 6.23), where Archaean basement gneisses and Buganda metasediments and metavolcanics became interlayered during a poorly constrained tec-

tonic phase (D_2). This must have occurred before 1.85 Ga, as indicated by post-tectonic granite bodies within the units, but after 2580 Ma, since this is the minimum age of the Archaean slices indicated by their new zircon ages.

D_3 is described (Link et al. 2010) as a combina-

tion of an E–W compression that resulted in asymmetric folds from cm to km scale with steep fold axes associated with a poorly developed ~ NNW- to SSE-striking steep foliation followed by a set of steep to vertical shear zones with a dominant dextral component and a NNW–SSE and NNE–SSW strike. The northward protrusion of Victoria quartzites (Fig. 7.20) may be related to D_3 (see also Figs 6.15 and 6.23).

A correlation of the much shallower thrusting and shearing event, producing predominantly brittle structures in the Buganda and Namuwasa rocks, is associated with D_4 (Fig. 6.23). Brittle cataclastic structures in the Kagera-Buhweju Supergroup, such as the mylonitised and brecciated quartzites of the Nsika Member, are attributed to the same event. Alternatively, D_4 thrusting (Fig. 6.23) may be a rejuvenation of older D_2 thrust planes, which together with strike-slip movements caused a steepening of the D_2 thrust planes to almost vertical up-thrusts, as portrayed in Figure 7.20. However, the setting of the Mubende and Singo plutons – transgressive/intrusive or a granite dome with thrust contacts – *vis-à-vis* the Buganda and Namuwasa country rocks remains ambiguous. A scenario is possible whereby a ‘thick-skinned’ stack of Buganda and Namuwasa rocks was thrust over the Mubende and Singo batholiths, with the bulk of the strain absorbed along the thrust plane by a zone of silicification, tourmalinisation and sericitisation. If true, the movements described in this section could be much younger, even Pan-African in age. Similar ages of rejuvenation of older shear zones have been reported from the North Kibaran Belt (Chapter 8). Tack et al. (2009) advocate that because the Archaean Tanzania Craton acted as an indenter, a new compressional event affected the NKB as a far-field effect of the East African Orogen, with collision and amalgamation between ~640 and ~530 Ma (Section 1.7).

Rocks of the isolated Bwezigoro Group are obviously younger than those of the Namuwasa Group: Basal conglomerate of the Bwezigoro Group contains pink sandstone pebbles probably derived from the Namuwasa Group. In places, they overlie metasediments of the Buganda Group, tilted lithologies of the Namuwasa Group and the 1.86 Ga Singo granite, suggesting an age younger than 1.86 Ga. The nature of the contact is, however, uncertain, and at least at one location the contact with underlying Bujagali metabasalts is tectonic. Sample 8126 (Bwezigoro Group) contains four detrital zircons with magmatic zircon domains yielding ages of 1.98–1.97 Ga, which may have been derived from the nearby Sembabule Suite with the Rwamasha granite dated at 1.99 Ga and Kasagama granite dated at 1.96 Ga (Section 6.4). This would suggest uplift and erosion of these granitoids soon after their emplacement and helps to explain the presence of arkosic lithologies in the Bwezigoro Group. The second youngest 1.90 Ga zircon and youngest 1.79 Ga zircon grains are singular, although interesting. The first may be a metamorphic age, but the second is exactly the same age as found in zircons from a tuff layer in the basal part of the Kagera Supergroup (our Kagera-Buhjewu Supergroup) by Cutten et al. (2004). An age difference of 50 or even 200 million years with the rocks of the Namuwasa Group is suggested by de Kock et al. (2011). Following their deposition, burial metamorphism reached greenschist facies conditions, manifesting a burial depth of several kilometres, and the relatively small domains currently occupied by the post-Rwenzori molasse-type successions of the Namuwasa and Bwezigoro Groups are obviously the erosional relicts of what was once a thick sedimentary succession.

8 ROCKS OF THE MESOPROTEROZOIC NORTH KIBARAN BELT

8.1 Introduction

8.1.1 Kibaran Belt

Deposition of Palaeo–Mesoproterozoic sedimentary rocks on the proto-Congo Craton (Fig. 1.7) started during post-Eburnian extension, supposedly directly after Palaeoproterozoic orogenesis responsible for stitching together of this craton from a number of Archaean crustal fragments by Palaeoproterozoic fold belts (Section 4.1). Early extension in the period < 2.05 Ga to 1.78 Ga resulted in deposition of molasse-type sediments of the Namuasa and Bwezigoro Groups and the Kagera-Buhweju Supergroup (Chapter 7). Post-Eburnian extension in the Kibaran trough, which developed along a crustal weakness zone partly coinciding with the Palaeoproterozoic Ubendian-Rusizian-Rwenzori suture, started around ~1.55

Ga and accelerated strongly around 1.4 Ga. Extension was followed by compression and the newly formed Kibaran Belt (Fig. 8.1; see also Section 1.4) marks compression in the proto-Congo Craton, coeval with the global Grenvillean Orogenic Cycle (~1.1–0.95 Ga) and culminating with formation of the Rodinia Supercontinent (~1.0 Ga).

Robert (1931; in Tack et al. 2011b) coined the term “Complexe des Kibara” and “Système des Kibara” to refer to a (meta)sedimentary sequence in the Kibara Mountains in Katanga (DRC). The term “Kibara belt” was used to refer to the fold belt underlying the “Kibara Mountains”. The Kibaran Belt (Fig. 1.5, no. 1) is divided into two segments, separated by a NW-trending Karoo rift superposed on a Palaeoproterozoic Rusizian basement high (Fig. 8.1). For the sake of clarity, the two segments

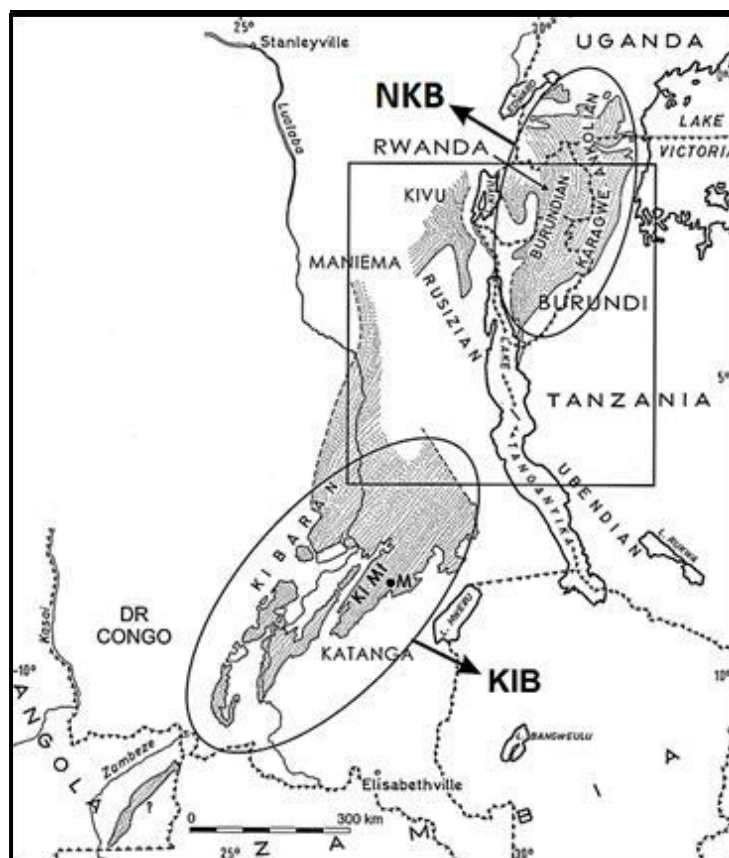


Fig. 8.1. Sketch map of the “Kibara belt *s.l.*” (modified after Cahen & Snelling 1966), showing the general predominant NNE–SSW trend of the belt. The belt is interrupted by a NW–SE trending Ubende-Rusizian basement high, separating the Kibaran Belt *s.s.* (KIB) or South Kibaran Belt from the North Kibaran Belt (NKB). Key: Ki Mt = Kibara Mountains type locality; M = Mitwaba town; Elisabethville = Lubumbashi; (adapted from Tack et al. 2011b, with kind permission of Elsevier Ltd.). Note that the NKB still includes Palaeoproterozoic rocks of the Kagera-Buhweju Supergroup.

of the Kibara Belt *s.l.* will be referred to as (1) the South Kibaran Belt or Kibaran Belt *s.s.* (KIB) (Katanga, DRC) and (2) the North Kibaran Belt (NKB) exposed in Burundi, Rwanda, NW Tanzania and SW Uganda (Tack et al. 1994) and Kivu Province (DRC) (Fernandez-Alonso et al. 2006).

The above two segments were viewed during the past two decades as two separate – albeit coeval – orogenic belts (Tack et al. 2002a). An oceanic subduction/ collision/ amalgamation model is favoured for the South Kibaran Belt (Kokonyangi et al. 2001, 2004a, 2004b, 2005a, 2005b, 2007, 2008), while an intracratonic extension-inversion model – without formation of oceanic crust – is advocated by most investigators of the NKB. From a lithostratigraphic point of view, both segments of the Kibaran Belt – the KIB and NKB – show striking similarities. Both are composed of a pre-Kibaran, Palaeoproterozoic Rusizian basement, overlain by a Mesoproterozoic, folded and thrust-ed, terrigenous, clastic (meta-)sedimentary cover into which suites of Mesoproterozoic, supposedly pre-, syn- and post-kinematic granitoids, minor felsic and substantial mafic (sub-)volcanic rocks have been emplaced (Fig. 8.1).

To demonstrate differences, similarities and concomitance between the geodynamic development and setting of both parts of the Kibaran Belt a brief outline of the South Kibaran Belt will be presented below before discussing the northern segment, which extends into southwestern Uganda.

8.1.2 Short Outline of the South Kibaran Belt

All metasediments of the Kibaran Supergroup in the KIB were deposited before the emplacement of the ~1.0–0.95 Ga ‘tin granites’ and are older than 1.08 Ga, which is the age of the climax of Kibaran D_2 deformation. The maximum depositional age of the metasediments is given by 1.38 Ga granitoids on which they are reported to rest unconformably and by detrital zircons from basal quartzite, which yielded a concordant age of 1.36 Ga (Kokonyangi et al. 2005b). More recent U-Pb SHRIMP data of detrital zircons from four other metasedimentary formations yielded ages between 1.31 and 1.33 Ga (Kokonyangi et al. 2007). Prismatic Mesoproterozoic detrital zircons (dated at 1.50 to 1.33 Ga, with a peak at 1.38 Ga) occur in all samples and are supposedly derived from the Mitwaba orthogneisses (‘M’ in Fig. 8.1), a deformed granitoid. Some 80 % of the zircon population is composed of recy-

clad detrital grains, yielding ages between 2.43 and 1.70 Ga, with peaks at 2.05 and 1.85 Ga that overlap with the timing of geological events in the adjacent Palaeoproterozoic Bengweulu Block and Ubendian-USagaran Belts (Section 1.3) and its northern continuation, the coeval Rwenzori Belt (Chapter 6). Archaean zircons only form a minor fraction (<6%), are restricted to the youngest metasediments in the KIB and supposedly derived from the unroofing of successively older crust of the proto-Congo Craton.

Sedimentological data broadly indicate that the oldest metasediments were deposited in shallow marine environments, during the rift-drift stage of the Katangan portion of the evolving Kibara trough. Kokonyangi et al. (2004a, 2005a) recognised two major deformational events in this part of the Kibara Belt. The earliest (D_1) is reportedly characterised by ENE-trending asymmetric folds and thrusts showing N to NNW transport directions. Igneous bodies (G_1 – G_3 granitoids) emplaced into these older metasediments were emplaced during the same early Kibaran orogenic event (D_1) with igneous crystallisation ages (SHRIMP U–Pb zircon) of 1.39 to 1.37 Ga. All G_1 – G_3 granitoids were emplaced over a short period of time and could be coeval at 1.38 Ga (Kokonyangi et al. 2004a). The second deformation (D_2) marks the climax of the Kibara Orogeny. It is defined by NW-verging mesoscopic and macroscopic isoclinal folds (F_2) and reverse faults parallel to D_2 planar fabrics. M_2 metamorphism is characterised by medium-pressure/medium-temperature (MP/MT) mineral paragenesis, with preliminary data indicating peak P-T conditions between 740–780°C and 6–6.5 Kb. U–Pb dating of metamorphic zircon tentatively constrains the timing of M_2 metamorphism at 1.08 Ga, coeval with the formation of the Rodinia Supercontinent. This was followed by emplacement of so-called G_4 tin granites at $\sim 977 \pm 18$ Ma.

Kokonyangi et al. (2004a, 2004b, 2005a) described a gabbro-diorite suite that intruded metasediments prior to ~1.40–1.38 Ga as arc-related, calc-alkaline plutons associated with peraluminous S-type granitoids (G_1 – G_3). The above authors further postulate that emplacement of arc mafic magmas into the crust triggered dehydration melting, at high temperatures, of highly fertile and heterogeneous metasedimentary source material producing a felsic melt which was mixed with the arc mafic magmas in variable proportions to produce these granitoids. According to the model by

Kokonyangi et al. (2004a, 2004b, 2005a) the Kibara orogenic system was active between ~1.4–1.38 Ga (the alleged accretionary stage) and ~1.0–0.95 Ga (the alleged stage of continental collision and post-orogenic exhumation), but the oldest sedimentary rocks were deposited prior to 1.4–1.38 Ga, which is the igneous crystallisation age for the syn-D₁ Kibaran orthogneisses intruding them, while the post-D₁ younger sediments were deposited in an intra-arc environment, although more modern data are required before a definite conclusion can be reached.

Kokonyangi et al. (2004a) claim that the available structural, sedimentological, geochronological and petrological data support a convergent margin setting for the Kibaride Belt, inconsistent with an intracratonic rift-inversion model generally favoured for the North Kibara Belt (see below).

8.1.3 Structural Zones of the North Kibaran Belt

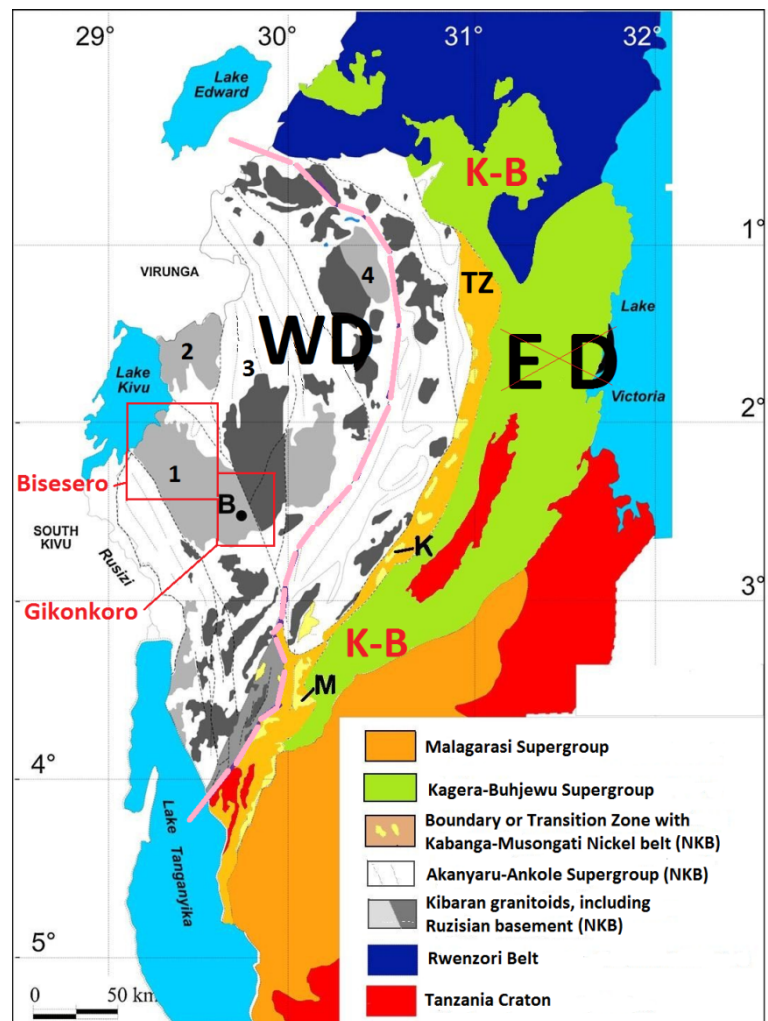
The eastern segment of the North Kibara Belt (e-NKB), i.e., the part east of the Western Rift,

excluding the part in Kivu (Fig. 8.1), has been divided into the following orographic zones (Tack et al. 2006a, 2008b, 2009, 2010, Tahon et al. 2004, Fernandez-Alonso et al. 2006) (from west to east, Fig. 8.2):

- *Western Domain (WD)*;
- *Transition Zone (TZ)*; and
- *Eastern Domain (ED)*.

Based on recent geochronological data this orographic subdivision cannot be longer maintained. We assign only the Western Domain and the Transition Zone to the NKB. Dating of 1.4 Ga mafic sills and dykes (Tack et al. 1992, Tack 1995) in the lower portion of the platform sequence of the erstwhile 'Bukoban Series' resulted in a redefinition of its lower segment from Neoproterozoic Bukoban Group to Mesoproterozoic Kagera Supergroup (Fernandez-Alonso et al. 2006). Being coeval with metasediments in the e-NKB, the above authors viewed the platform deposits of the Mesoproterozoic Kagera Supergroup as foreland deposits of

Fig. 8.2. Sketch map of the eastern segment of the North Kibaran Belt (e-NKB) east of the Western Rift and regional framework (slightly modified after Tack et al. 2010; Fernandez-Alonso 2007, with kind permission of Elsevier Ltd.); note the former structural domains within the e-NKB have been abolished: WD (Western Domain) is now NKB with Mesoproterozoic Akanyaru-Ankole Supergroup; ED (Eastern Domain) is now Palaeoproterozoic Kagera-Buhjewe Supergroup (Chapter 7); in between is the Boundary or Transition Zone, comprising the Kabanga-Musongati (KM) alignment of mafic and ultramafic layered complexes. Key: K = Kabanga massif; M = Musongati massif; B = Butare town; K-B = Kagera-Buhjewe Supergroup; TZ Transition Zone; 1 = Butare Block; 2 = Gisenyi Block 3 = Gitarama Block; 4 = Mutare Massif. Pink Line = Kibaran fault zone formed by rejuvenation of Palaeoproterozoic suture between Tanzania and Congo Cratons.



the NKB and assigned these rocks to the Eastern Domain.

New geochronological data manifest, however, that deposition of molasse-type sediments in the Burundi-Tanzania segment of the ED started much earlier at 1.78 Ga (Cutten et al. 2004). Further to the north in the Mubende-Singo area, Uganda, deposition commenced almost immediately posterior to culmination of the Eburnean Orogenic Cycle in the Rwenzori Fold Belt, as manifested by a U–Pb age of detrital zircons of < 2.05 to 1.79 Ga (Section 7.5). Being some 300 to 230 million years older than the oldest sediments in the e-NKB (the eastern segment of the North Kibara Belt), the setting of Kagera sediments in the so-called ED as Kibaran foreland deposits cannot be longer maintained. This platform succession is henceforward considered as a separate tectono-thermal domain or ‘building block’ (Chapter 7).

8.2 Lithostratigraphy of the pre-Kibaran Basement

Being a regionally important tin-tungsten province, the geology of the NKB was initially painted in simple European Hercynian colours: granites were depicted as elongated or oval-shaped plutons that had been emplaced into ‘Burundian’ metasediments (e.g., geological map of Rwanda of 1981; Ziserman et al. 1983). Fractionation of these fertile granites had allegedly resulted in the emplacement of tin- and/or tungsten-bearing pegmatites or quartz veins in the hood zones of the granitic plutons and adjacent country rocks. Based on whole rock Rb/Sr ages of the 1980s, however, the above simple geological model had to be rejected. The geochronological data demonstrated that the bulk of the granitoids were some 200 to 300 million years older (Klerkx et al. 1987) than the tin mineralisation and, consequently, the older granitic plutons could not be related to this mineralisation. Furthermore, the rocks below ‘Burundian’ metasediments were not only ‘Kibaran’ granitoids but also pre-Kibaran basement, comprising Rusizian (or Ubendian) and a few Archaean remnants (e.g., Cahen 1954, Lepersonne 1974) in Kivu (DRC) and Burundi.

The term Rusizian is derived from the poorly studied Ruzizi Belt in Kivu (DRC), which, historically, has been related to the Ubende Belt of Tanzania (Cahen et al. 1984) and dated between 2.10 and 1.86 Ga (Lenoir et al. 1994). Lithologies in the type area of the Ruzizi Belt consist of migmatitic

The rocks of the e-NKB can be broadly divided into a Palaeoproterozoic Rusizian-Rwenzori basement, overlain by a Mesoproterozoic cover of metasedimentary terrigenous rocks. The bulk of the igneous rocks in the e-NKB comprise a variety of granitoids, minor volcanics and mafic sills, dykes and layered mafic bodies attributed to the huge 1.4 Ga North Kibaran Igneous Province (NKIP), including the Lake Victoria Arcuate Dyke Swarm and layered complexes of the Kabanga-Musongati (KM) alignment. Subordinate igneous components include some older (1.57–1.43 Ga; Buchwaldt et al. 2008) Kibaran-type granitoids, a number of small A-type granitic bodies, dated at 1.25 Ga, restricted to the Transition Zone (Tack et al. 1994) and, finally, a largely sub-outcropping suite of so-called ‘tin granites’ dated at 1.10–1.00 Ga (Pohl 1987a).

gneiss with mica schists, amphibolites and lenses of coarse-grained quartzites and crystalline limestones and dolomites (Lepersonne 1974). However, it should be noted that the definition of the Ruzizi Belt in Kivu is debatable and that its existence was even questioned (Lavreau 1985).

In Burundi the Rusizian has been sub-divided into (1) ‘Schist Series’ (top) and (2) ‘Gneiss Series’ (bottom). The first one comprises partly retrograded and locally mylonitised garnet ± staurolite schists, kyanite schists and other schist varieties. The bottom ‘Gneiss Series’ comprise granitic gneisses, gneissose granites, migmatites and (blasto-)mylonites. An inlier of strongly reworked Archaean rocks, called the Kikuka Complex (Nzobjiwami 1984), is exposed in southern Burundi along the western shoreline of Lake Tanganyika. Zircon U–Pb dating for this Complex yielded ages of ~2.50 Ga and ~2.60 Ga (DemaiFFE & Theunissen 1979).

Large, fault-bounded, rhomb-shaped crustal blocks of pre-Kibaran Rusizian basement are also exposed in western Rwanda in the approximately Miocene Kivu horst (in blocks 1 and 2 in Fig. 8.2). The latter is part of the uplifted shoulder of the Western Rift and forms a deeper eroded and morphologically immature Congo-Nile watershed and comprises several extensive igneous-metamorphic terrains with meso- to catazonal metamorphic rocks, considered to be partly of ‘Rusizian age’.

Three such major terrains can be distinguished in western Rwanda and comprise the Gisenyi Block in the northwest, the Gitarama Block in the centre and the Butare Block in the southwest, each with a specific gamma ray signature (blocks 2, 1 and 3 in Fig. 8.2, respectively). In airborne radiometric data, the Butare and Gisenyi Blocks appear as composite Th- or Th-U-rich areas composed of high-grade metamorphic rocks, quartzites, and high-Th and high-K granitoids. In contrast, the Gitarama Block and the smaller granitoid massifs reveal a uniform high K content. K-rich zones also occur along the margins of the high-grade blocks (Fernandez-Alonso & Theunissen 1998).

Irrespective the huge amount of research carried out in Rwanda by, e.g., geoscientists of the Museum for Central Africa, Tervuren, Belgium, the age of the Rusizian is poorly constrained. Recently, a Rusizian-aged basement orthogneiss in the Butare area (B in Fig. 8.2) has been dated and yielded a SHRIMP age of 1982 ± 6 Ma (Tack et al. 2010), an age which corresponds broadly with granitoids of the 1.99–1.96 Ga Sembabule Suite in Uganda (Mänttari 2014). The data show clearly that the Rusizian orthogneiss has a juvenile signature with $\varepsilon_{\text{Hf}}(\text{T}) \sim 0$, i.e. similar in composition to the Chondritic Uniform Reservoir (CHUR). The TDM model ages, however, indicate average crustal residence times (calculated from depleted mantle values) of up to 2.4 Ga, indicating some participation of early-Palaeoproterozoic/late Archaean crust in the generation of the Butare orthogneiss (Tack et al. 2010).

Superposition of a ‘Kibaran’ on an older Rusizian fabric can be observed in several locations. For example, granitoids of the Bisesero Complex¹ (Westerhof 1980, Baudet et al. 1989) comprise foliated granites, gneissose granites, leucogranites, migmatites and paragneisses. The latter are always found in association with granitic rocks. The gneissose foliation has a general N-S ‘Kibaran’ trend. In places, a NW-SE directed macro-banding formed by alternation of granite and gneiss bands,

up to several tens of centimetres in width, can be observed. Superposed on this NW-SE macrobanding, a N-S directed foliation has been developed, expressed as a well-developed gneissosity in the gneiss bands and as parallel orientation of biotite flakes in granite. The NW-SE macroscopic banding is considered to represent relicts of older Rusizian foliation, overprinted by a N-S Kibaran schistosity (Westerhof 1980).

A similar relationship is shown by an enclave of migmatitic rocks with a surface exposure of a few square kilometres in granitic gneisses, located one km south of Cyanika (Gikonkoro Prefecture in central Rwanda; Fig. 8.2). The migmatite is composed of granito-gneissic palaeosomes, measuring 50 to 100 cm in width that alternate with coarse pegmatitic neosomes, 10 to 20 cm in thickness. This macrobanding shows again a consistent ‘Rusizian direction’ between NW-SE and E-W, dipping to the NE or N (strike N135-94E, dips 38° NE to 42° N). The pegmatitic neosomes show pinch-and-swell structures or have been boudinaged or show ptygmatic fold structures. Mesoscopic fold structures show pegmatite neosomes in isoclinal folds that have been refolded into open folds (Westerhof 1979).

When comparing the above descriptions of the Rusizian of Rwanda, Burundi and Kivu (DRC) with pre-Kibaran basement in southwestern Uganda, it is obvious that there exists a great deal of confusion as to what to include. The description of the rocks of the Rukungiri Suite from southwestern Uganda (Chapter 7; Fig. 6.3) fits well with mid-crustal assemblages of the Rusizian. Other assemblages are more akin to lithological units that in Uganda are attributed to Sembabule Suite.

Another source of confusion in North Kibaran geology is the distinction between pre-Kibaran basement and Kibaran granitoids. For example, the large (45 x 60 km), arena-type² Mutare Massif in the NE of Rwanda and southern Uganda (4 in Fig. 8.2) was traditionally considered to represent a typical ‘peraluminous S-type Kibaran granitoid’.

-
- 1 Gneissic granites 10 km south of Kibuye yielded an (WR Rb-Sr) age of 1135 ± 43 Ma; ‘tin granites’ in the same area gave a WR Rb-Sr age of 988 ± 27 Ma (Lavreau & Liègeois 1982).
 - 2 The term ‘Arena Granite’ was introduced by Wayland (1931) to describe “enormous punch-bowl like areas, surrounded and separated from each other by mountain groups”. Wayland further reported that the structure of each arena coincided with an anticlinal dome, eroded at the centre to expose a depression with gneissose granite of – what he believed – the Archaean basement. Generally, arena granites occupy large areas in eastern Rwanda, southern Uganda and NW Tanzania. They are characterised by circular to oval-shaped more or less flat surfaces rimmed by ridges of the overlying (meta-)sedimentary cover (often quartzites).

The massif has been described in some detail by Sanschagrin & Mercier (1983): “*The central part of the massif is composed of a variety of porphyroblastic gneisses, each type grading into one another, and associated with migmatites. Sub-types of gneissose rocks comprise: granitic gneiss with feldspar porphyroblasts and granitic gneiss with bluish feldspar porphyroblasts and garnet. Transitions from porphyroblastic garnet gneiss (with K-feldspar crystals in parallel arrangement) into glandular garnet gneiss can be observed. K-feldspar Augen (up to 3–4 cm) are porphyroclasts rather than porphyroblasts. Granitic rocks include monzonite, leucocratic garnetiferous granite, pinkish foliated leucogranite and reddish, coarse-grained, porphyroblastic granite. Mafic dykes with (micro-)gabbro are found in places*”.

Migmatites are present almost everywhere in the Mutara massif. They occur as small felsic lenses or *Schlieren*, generally following but locally cutting the gneissic banding. They are considered to represent *in-situ* mobilisates or ‘sweat-outs’ (dehydration melting?) of the gneisses as demonstrated by the concentration of biotite along their contact with the gneisses (basic front). Microfolds with sub-horizontal axial planes are observed in the biotite layers. Another rock exposure shows a

macroscopic (metre- to decametre-scale) banding formed by alternating gneissic rock types with a few lenses of granitic rock. One gneiss sub-type contains roundish garnet nests with diameters between 2 and 40 cm. The macroscopic banding has a direction N35-45E, making an angle of ~60° with the strike of the Akanyaru-Ankole (meta-)sediments outside the Mutara massif.

The above description of Sanschagrin & Mercier (1983) is not exactly the description of intrusive granite! The northwestern part of the Mutara Massif, located in Uganda, is composed, however, of Kibaran-type granitoids known as the Kamwezi granite. Three zircon grains from this granite were evaporated and yielded a mean $^{207}\text{Pb}/^{206}\text{Pb}$ age of 1330 ± 22 Ma confirmed by four zircon grains that produced an indistinguishable slightly discordant age of 1332 ± 2 Ma using the conventional dilution technique (Buchwaldt et al. 2008).

From the above it appears that much more detailed mapping and geochronology is needed to unravel the lithostratigraphy of the pre-Kibaran Palaeoproterozoic basement and its relationship to Kibaran granitoids in the NKB. Supposedly it contains elements comparable with the 2.15–2.13 Ga Rukungiri Suite and 1.99–1.96 Ga Sembabule Suite (Chapter 6).

8.3 Lithostratigraphy of the Akanyaru-Ankole Supergroup

8.3.1 Introduction

Crustal extension and basin development in the north Kibaran trough is manifested by deposition of a sequence of monotonous siliciclastic shallow-water deposits. This generally low-grade to non-metamorphic sequence is known under a variety of names: Burundi Supergroup in Kivu Province (DRC), Rwanda and Burundi or Karagwe-Ankole Supergroup SW Uganda and NW Tanzania. Baudet et al. (1989), stressing the depositional environment within each tectono-stratigraphic unit deposited in a different sub-basin, defined the Rwanda Supergroup.

Elliot & Gregory (1895) coined the term ‘Karagwe Series’. This succession not only comprised Kibaran rocks but also lithologies incorporated in the later defined ‘Bukoban System’ and other units. A.D. Combe, who systematically mapped parts of Ankole (southwestern Uganda) and Kigezi (NW Tanzania) between 1922 and 1928, concluded that the Karagwe and Ankole were one and the same.

Hence, he proposed the term ‘Karagwe-Ankole’ in 1926 (published in Combe 1932). In accordance with a decision of the Kigoma Conference of African Geological Surveys in 1931, the official name in Tanzania has long been ‘Muva-Ankole’, stressing the correlation of the Ankole (Uganda and Tanzania) and Muva (Zambia) Series. This relationship was recently re-advocated by Pedreira & de Waele (2008), stressing the broadly coeval and parallel development of several Proterozoic epi-continental basins covering the proto-Congo Craton (Fig. 1.7). The Uganda Geological Survey never formally accepted the term ‘Muva-Ankole’ and in the geological map of East Africa from 1952 the use of the term ‘Karagwe-Ankole’ in Tanganyika was formally resumed.

Recently, the supracrustal cover sequence of the e-NKB has been redefined as Akanyaru Supergroup (named after the Akanyaru River, which forms part of the boundary between Rwanda and Burundi), comprising (from bottom to top) of Gikoro, Pindura, Cyohoha and Rugezi Groups

(Fernandez-Alonso et al. 2006). Stressing continuity of the Supergroup and Groups into south-western Uganda, over the entire NKB, we have introduced the term Akanyaru-Ankole Supergroup with the same Group names as proposed by Fernandez-Alonso et al. (2006).

According to Cutten et al. (2004) the Akanyaru-Ankole succession has been deposited in several sub-basins. Their total thickness is estimated to range from 9 to 14.5 km in the centre of the north Kibaran trough (e.g., in central Rwanda) to a few kilometres in the east (e.g., NW Tanzania). An overestimation of the thickness of the succession due to tectonic stacking along thrust zones parallel to strike of the strata cannot be excluded, however. Lateral facies changes in this thick terrigenous pelitic-arenitic succession are frequent and may be extreme, varying from starved basin deposits with ‘black shales’ to shallow siliciclastic tidal flat or deltaic deposits. Carbonate lenses are rare. Proximal turbiditic environments manifest deeper water conditions (at least a few hundred metres).

Traditionally, the epimetamorphic and folded cover sequence of alternating pelitic and arenaceous sediments, now attributed to the Akanyaru-Ankole Supergroup, was divided in Rwanda into three or four superposed units, each with a key quartzite horizon at its base (Gerards & Leppersonne 1964, Gérards et al. 1967, Ziserman et al. 1983, Klerkx et al. 1987, Baudet et al. 1989).

Pohl (1987c) reported the presence of chemical sediments (exhalites). He described garnitites south of Kibuye (western Rwanda) that form thin, well-defined and persistent horizons within pelitic carbonaceous and pyritiferous metasediments. Garnitite is composed of Fe-Mn garnet (> 90%, almandine-spessartite) and subordinate quartz and Fe-hydroxides (mainly after interstitial pyrite). Chemical analyses show high trace element contents of Zn (140–240 ppm) and Cu (137–484 ppm). Pohl (1987c) suggested a chamosite protolith composition, related to distal chemical precipitates. The above topic is relevant when discussing the strata-bound nature of some tungsten deposits in the so-called ‘Tungsten Belt’ of Rwanda (de Magnée & Aderca 1960).

The quantity of acid and intermediate volcanogenic intercalations in the metasediments of the Akanyaru-Ankole Supergroup is not precisely known but is supposedly underestimated. Volcanic rocks of predominantly felsic and subordinate intermediate affinity in Burundi have been reported by Theunissen & Klerkx (1980) and are represented by green phyllites and sporadic intercalations of metamorphosed acid lavas. Horizons of pyritiferous dacitic metavolcanics, associated with chlorite-sericite schists (meta-tuffs?) and metabasites in the lower part of the succession are also reported from the Nyungwe gold area in SW Rwanda (Salpeteur et al. 1989, Salpeteur 1992).

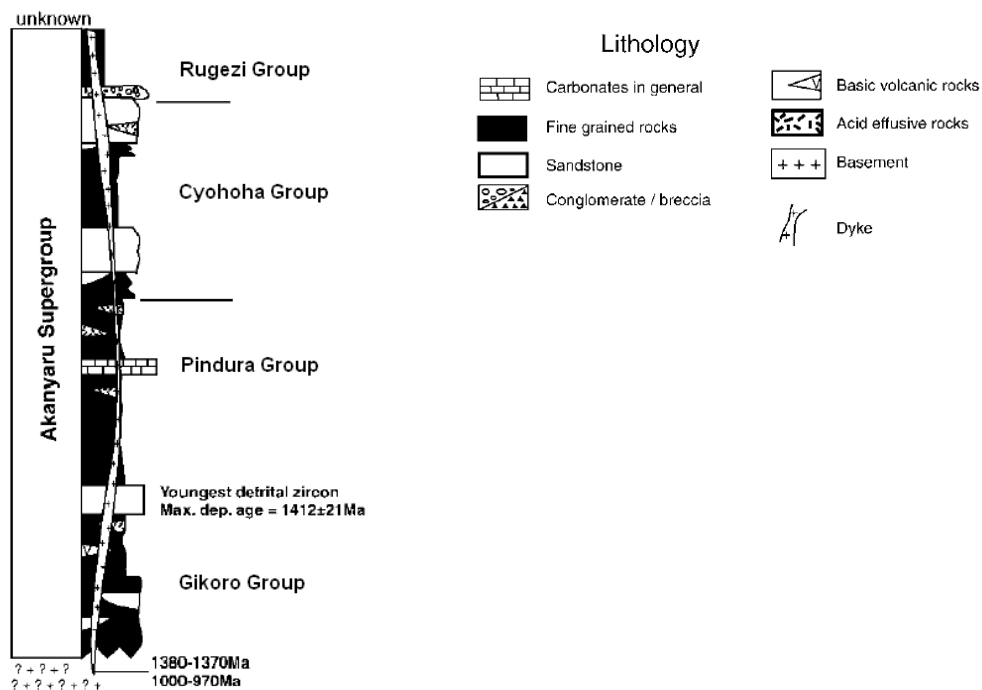


Fig. 8.3. Generalised stratigraphic column of the Akanyaru-Ankole Supergroup in the North Kibaran Belt (e-NKB) (from Pedreira & de Waele 2008).

Table 8.1. Lithostratigraphy of Burundi Supergroup in northern Rwanda (Croese 1984) and the new subdivision of the equivalent Akanyaru-Ankole Supergroup.

| Sequence | Description | Thickness | |
|---------------------------------|--|-----------|---------------|
| Miyove II Series | Mainly conglomerates with sandstones and conglomeratic sandstones, overlain by subordinate pelitic rocks. Pebbles comprise sandstone, vein quartz, micro-conglomerate, white siltite and argillite. Matrix composed of coarse quartz and iron oxide. | 200 m | Rugezi Group |
| Miyove I Series | Basal conglomerates (pebbles up to 15–20 cm) overlain by siltites, sandy siltites with sandstone (0.1–3.0 m) intercalations and rare dark-coloured argillite horizons. Local chert, nodular and intraformational conglomerate strata. Ripple marks, cross lamination. Iron oxides and pseudomorphs after pyrite widespread | 1100 m | |
| unconformity ~~~~~ unconformity | | | |
| Byumba Series | Conglomerates, micro-conglomerates, sandstones and whitish siltstones. | 2500 m | Cyohoha Group |
| Upper Quartzite Series | Sequence of alternating (quartzitic) sandstone (up to 20 m in thickness) and pelites. Abundant detrital mica. Pelites comprise dark argillites and light-coloured siltites. | 1300 m | |
| Upper Siltite/Argillite Series | Alternating argillites and siltites with interbedded sandy horizons. Sandstones show occasionally graded bedding. | 400 m | |
| Upper Black Argillite Series | Black argillites, frequently very rich in graphite with intercalations of siltites and sandstone. Near the base of the sequence abundant pyrite. Light-coloured siltite laminae and strata increase near the top where the rock assumes a banded appearance. | 500 m | |
| Middle Quartzite Series | Lowermost quartzite – most likely the Nduba Quartzite – is a thickly bedded, up to 30 m thick horizon, in places massif, elsewhere composed of alternating quartzite (0.5–1.0 m) and pelite. Overlain by pelites (rich in detrital mica) with quartzite intercalations. | < 30 m | |
| Middle Siltite/Argillite Series | Thick sequence of alternating dark-coloured argillites and light siltites and (very) fine-grained sandstones. Coarser lithologies rare. | 750 m | Pindura Group |
| Lower Black Argillite Series | Local, black, often graphite-rich argillites, alternating with siltites and fine sandstone horizons. Frisch (1975) has identified some bluish to reddish layers composed of iron oxides, quartz, sericite, kaolin, opaque minerals, chlorite and leucoxene, to which he attributes a volcanic origin. | 250 m | |
| Lower Quartzite Series | Middle to coarse-grained, massif to thick-bedded (0.5–4.0 m) (quartzitic) sandstones with siltite intercalations; occasionally micro-conglomeratic. Erosive basal part with siltite pebbles of underlying formation | 700 m | |
| Lower Siltite/Argillite Series | Alternating siltites and argillite, frequently showing graded bedding with siltites at base and argillite at top; also alternating with parallel bedding, cross bedding, climbing ripples and convolution (slumping), all indicating rapid deposition. | 150 m | Gikoro Group |

Croese (1984) described narrow, possibly volcanic strata in an argillite/siltite sequence in northern Rwanda, close to the border with Uganda. In the same area, rare quartz porphyries have been reported by Croese & Matheussens (1990). These deposits are found in the proximity of the Nduba Quartzite (Table 8.1). A. Schoonderbeek (pers. comm., 1982) has described the Nduba Quartzite, as an extremely fine-grained siliceous 10-m wide horizon with black tourmaline³ laminae, 2 to 5 cm apart. The siliceous horizon is overlain by fine tourmaline schists, mica schists and graphite schists, some of them containing elevated pyrite contents. The tourmaline schists may grade into tourmalinites and tourmaline sandstone with euhedral tourmaline prisms on the fore sets. The syn-sedimentary nature of tourmaline is corroborated by nearby tourmaline laminae that are distorted into slump folds. The Nduba Quartzite supposedly represents a tourmaliniferous meta-chert horizon, which together with the above rocks constitutes an exhalative-volcanogenic assemblage.

Pelitic strata in this succession are very fine-grained and frequently appear almost non-meta-

morphic (especially in the eastern part of Rwanda). Consequently, field names such as argillite, siltite, shale and phyllite are used. The almost omnipresence of white mica/muscovite, chlorite and biotite (only visible in thin sections) manifests, however, lower greenschist facies metamorphic conditions. Chialstolite and chloritoid, in crystals up to 5 mm, are found in places in dark pelites and are an indication of late static metamorphic overprinting. The frequently used term 'quartzite' is also incorrect. Detrital quartz grains with an iron oxide or sericite coating can still be observed in thin section. Irrespective the field aspects, the term (quartzitic) sandstone or ortho-quartzite is more correct. All early investigators (e.g., King 1962, Nicholson 1965) reported an increase in metamorphic grade and intensity of the schistosity towards underlying granitoids and gneisses.

Based on field verification in Uganda by the GTK Consortium 2008–2011, the following rocks shown in Table 8.2 have been distinguished and will be described (from old to young) below.

Table 8.2. Sub-division of the Akanyaru-Ankole Supergroup in southwestern Uganda. The codes refer to rock units in the unpublished geological maps compiled by GTK Consortium and delivered to DGSM.

| Group | Formation | Lithology | Map Code |
|----------------|--------------|---|----------|
| Rugezi | Kikungiri | Siltstone | P2ARst |
| | Butobere | Sandstone, quartzite, grit | P2ARss |
| | Rwene-Kakore | Conglomerate | P2ARc |
| Cyohoha | Kashanga | Sandstone, quartzite, grit | P2ACsqg |
| | Rutooma | Ironstone lenses | P2ACi |
| | Kiirima | Felsic metatuff | P2ACft |
| | Kirimbe | Mudstone, shale, slate, phyllite | P2ACs |
| Pindura | Kamabale | Sandstone, quartzite, grit | P2APqs |
| | Ihunga | Quartzite | P2APIq |
| | Mukati | Feldspathic grit | P2APfg |
| | Kyamengo | Garnet quartzite | P2APgq |
| | Akorokor | Border quartzite | P2APbq |
| | Nyaiguru | Mudstone, shale, slate, phyllite | P2APs |
| Gikoro | Iryango | Sandstone, quartzite, grit | P2AGsqg |
| | Kashasha | Sandstone, quartzite, grit intercalated with shale, phyllite and schist | P2AGqg |
| | Mushasha | Quartzitic sandstone | P2AGqs |
| | Mikamba | Mudstone, shale, slate, phyllite | P2AGs |
| | Mabona | Mudstone, slate, turbiditic | P2AGr |
| | Nyamirima | Mica schist, muscovite quartzite | P2AGms |
| | Kabira | Calc-silicate rock | P2AGcs |

3 Dravite, a tourmaline variety, is a common exhalative mineral and is known to occur in association with several types of strata-bound mineralisation including VMS-, Sedex- and gold deposits.

8.3.2 Gikoro Group

Calc-silicate rock (P2AGcs) – Calc-silicate rocks of the *Kabira Formation* have been encountered in a few dozen locations in the southwestern part of the Bushenyi District and northwestern part of the Ntungamo District. The largest occurrences are located 15–20 km NE of Rukungiri town, the biggest one measuring 19 km² in size. In places, calc-silicate rock comprises sillimanite-bearing breccia with rounded and angular granitic and quartz-rich fragments, brecciated quartzite, basic gneiss and quartzite. According to the Bushenyi Map Sheet, scale 1:100 000 (DGSM 1963), the calc-silicate unit is divided in three parts:

- Diopside- and tremolite-bearing quartz calc-silicate rocks, which may grade into quartzites.
- Tremolite-chalcedony rocks, which may grade into calc-silicate rocks.
- Diopside-hornblende-microcline gneiss to hornblende-microcline gneiss with large microcline porphyroblasts in part.

Mica schist, muscovite quartzite (P2AGms) – Mica schists of the *Nyamirima Formation* occur in three narrow NW–SE trending zones, 60 km long, situated in the vicinity of Ntungamo town and, in addition, in a few areas west of the main schist zone. The strongly foliated mica schist is a medium-grained, finely laminated, reddish to grey coloured rock, resembling in places phyllites of the Gikoro Group. Intercalations of psammitic muscovite quartzite layers may occur in places, and quartz veins are common.

Quartz, muscovite/ sericite and feldspar are the most common minerals in the mica schist, where feldspar is mainly albite-oligoclase. Locally, also garnet porphyroblasts exist in mica schist (Figs 8.4A-B).

Early investigators (e.g., King 1962; Nicholson 1965) reported an increase in metamorphic grade and intensity of the schistosity towards the underlying granitoids of the Ntungamo and other granite/ gneiss domes. Porphyroblasts of kyanite, staurolite, andalusite or chloritoid are reported to have formed post-kinematically, after the schistosity.

Mudstone, slate, turbiditic (P2AGr) – A sequence of turbiditic mudstones, assigned here to the *Mabona Formation*, is exposed south of Mbarara town, where it corresponds with part of the overstepped ‘Akarundi Series’ of Nicholson (1965). Mudstones crop out as a separate, NE-SW oriented sedimentary rock unit, 14 km long and up to 500 m wide, with a conspicuous, rhythmic appearance (Fig. 8.5). One such turbidite sequence has been encountered between Kigakati and Nsongezi near the border with Tanzania. At first glance this rock resembles grey coloured, extremely regularly bedded sandy slates. Closer inspection reveals a delicate, inconspicuous graded bedding and Bouma cycles, due to the fact that the source material – sandy slate – was already rather homogeneous in terms of grain size distribution and composition. The Bouma cycles show fining upward with the bottom part slightly coarser grained, slightly harder and slightly lighter coloured and richer in quartz with respect to the top part, which is richer in clay particles, darker and softer. Some Bouma

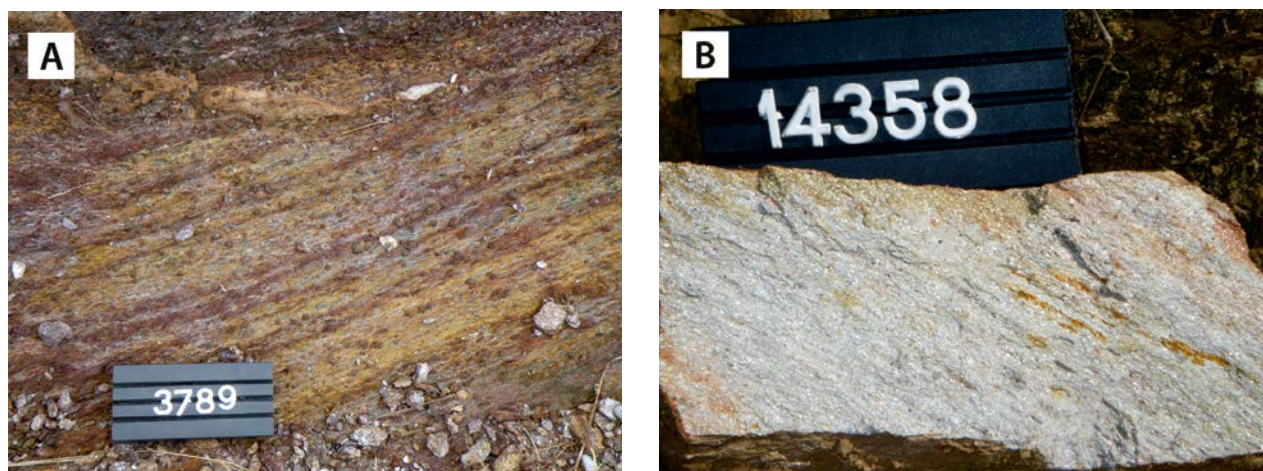


Fig. 8.4. (A) Garnetiferous mica schist with of the Nyamirima Formation (189546E / -105302N). (B) Detailed image of mica schist with abundant white mica (175595E / -59497N). Number tag 10 cm.



Fig. 8.5. Turbidite sequence of the Mabona Formation with thin, equally spaced Bouma cycles (255922E / -88873N). Number tag 8 cm.

cycles are topped by brown, iron- and silica-rich lamina, generally 1–3 mm in thickness. These represent hard grounds, formed during time intervals of non-deposition when the top of the cycle reacted with Fe- and Si-saturated seawater. Laminated mudstone turbidite contains local sandy, 10–15 cm thick interbeds.

Mudstone, shale, slate, phyllite (P2AGs) – Mudstones, slates and phyllites of the *Mikamba Formation* constitute the most extensive lithostratigraphic unit of the Gikoro Group, occurring mainly between the towns of Ntungamo and Mbarara in an area of 60 x 40 km. In addition, smaller NW-SE oriented areas of this succession occur NW of the Kisoro valley.

Commonly grey, but also pinkish, yellow, black and white varieties of phyllite or phyllitic slates are the most abundant rock types of the Mikamba Formation (Fig. 8.6A). They are usually fine- to very fine-grained, strongly banded, due to a combination of fine primary sedimentary bedding and slaty cleavage, which in hinge zones of tight meso- and microfolds clearly cuts the bedding (Fig. 8.6B). In addition, there are some large open folds.

Muscovite/sericite, quartz and feldspar are the main minerals. Iron oxides may occur along foliation planes or as small disseminated grains that usually have been weathered leaving empty casts behind. The Al-content in these metapelites is over 20 wt% (see App. 2, anal. 143). Graphitic and carbonaceous shale horizons are rare. Psammitic intercalations are common.

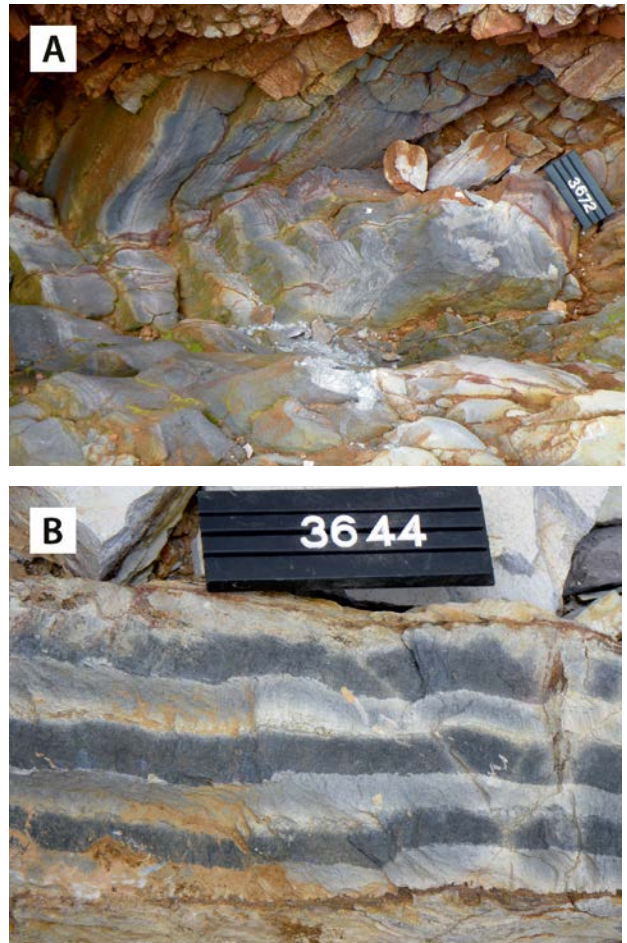


Fig. 8.6. (A) Bluish grey phyllitic slate of the Mikamba Formation (210757E / -77086N). (B) Detailed image of phyllitic bedded slate with a slaty cleavage (259785E / -83529N). Number tag 10 cm.



Fig. 8.7. Flagstone quarry in the quartzitic sandstone of the Mushasha Formation, with bedding-parallel fracturing. Note ladder for scale (188537E / -8878N).

Quartzitic sandstone (P2AGqs) – Elongated, NW–SE trending ridges, comprising quartzitic sandstones of the *Mushasha Formation*, occur in an area measuring about 90 x 50 km, east of Rukungiri and south of Mbarara towns, forming large-scale, open folds, bounded by metapelites of the Gikoro Group.

Quartzitic sandstone (or quartzite) is a very hard and recrystallised rock. Of the primary sedimentary textures only bedding and ripple marks are generally visible. In places, a bedding parallel fracture cleavage has developed, which allows them to be utilised as flagstones (Fig. 8.7).

The fine- to very fine-grained quartzitic sandstone is usually greyish or even white in colour. In addition to quartz, also muscovite/ sericite, hematite and other unspecified iron oxides and tourmaline have been observed. Both orthoquartzites and sericite quartzites with 8–10 vol% sericite occur and the mica may be concentrated in specific layers. In places (e.g., at 205712E / -103062N), quartzitic sandstone hosts tourmaline-bearing quartz veins, which have previously been mined for columbite.

Sandstone, quartzite, grit intercalated with shale, phyllite and schist (P2AGqs) – A heterogeneous

succession of psammitic and pelitic metasediments of the *Kashasha Formation* form an alignment of high, WNW-trending hills, locally covered by laterite, between Ntungamo and Mbarara towns, bordered by metapelites of the Gikoro Group and granitic gneisses of the Rukungiri Suite in the lower ground.

Fine- to medium-grained, reddish, grey or white quartzite is the most prominent rock type of this unit, which may show a vague layering and blastoclastic textures. When muscovite-bearing, it may appear deformed and sheared in narrow zones, like intensively foliated phyllonite.

Sandstone, quartzite, grit (P2AGsqg) – The largest occurrence of sandstone of the *Iryango Formation* is located 15 km SW of Mbarara town. In addition, there are a few elongated ridges in the Isingiro, Ntungamo and Kisoro Districts. This unit is mostly bordered by the shale-mudstone-phyllite rocks of the Gikoro and Pindura Groups.

The rock is mainly a whitish grey, pale pinkish or brownish, very fine- to medium-grained sandstone, which often comprises steeply inclined joints. Fine-grained members may show sedimentary features, such as cross bedding (Fig. 8.8), ripple marks, lamellar bedding or load casts. Sand-



Fig. 8.8. Obscure cross-bedding in quartzitic sandstone of the Iryango Formation (228814E / -8914N). Coin diameter ~20 mm.

stone grades commonly into siltstone and may contain intercalations of shale. Gritty sandstone varieties contain in places sub-rounded quartz clasts that may be up to 10 mm in size. In places, sandstone contains rusty brown, cube-shaped casts of limonite after pyrite.

8.3.3 Pindura Group

The Pindura Group is the most widespread unit of the Akanyaru-Ankole Supergroup in southwestern Uganda, where it is mainly exposed in SE-NW trending antiforms, representing commonly the oldest Akanyaru-Ankole unit. A notable exception is the high ground south of Mbarara town, where metapelites assigned to the Pindura Group overlie psammitic rocks of the Gikoro Group. A proper understanding of the lithostratigraphy of the Akanyaru-Ankole Supergroup in general and the Pindura Group in particular is seriously hampered by tectonic repetition or overstepping, due to large-scale folding and thrusting of the monotonous shale-siltstone-sandstone successions and the absence of clear marker horizons. Faults parallel to the strike of major units can easily be overlooked. The possibility of duplications or gaps in the following description of individual sections (from old to young) has therefore to be taken into account.

Mudstone, shale, slate, phyllite (P2Aps) – These are partly laminated pelitic sediments (usually schistose) with sandstone interbeds of the *Nyaiguru Formation*. The latter vary in number and thickness, becoming more frequent and thicker when approaching the thick sandstone units of the Group. In the Bunyonyi anticline (Mbarara area), the succession is dominated by laminated shales and siltstones with reddish weathering colours. A fine banding is caused by reddish or yellowish-brownish layers that alternate with slightly coarser grained light grey layers. In addition to fine quartz and sericite, some siltstones also contain mm-sized quartz clasts. Though the succession starts with shales and siltstones, intercalations of fine-grained sandstone layers become more important above the basal beds, resulting in a shale-siltstone-sandstone succession with a thin, laminar bedding (Fig. 8.9A).

In the Bunyonyi anticline, the grade of metamorphism increases towards the NW and, accordingly, mudstones and shales without visible cleavage grade into slates, phyllitic slates and phyllites. In the granite gneiss area north of the anticline, these phyllitic rocks grade into strongly foliated muscovite-biotite schists, which locally contain plenty of large (≤ 10 mm), euhedral garnet porphyroblast (Fig. 8.9B).

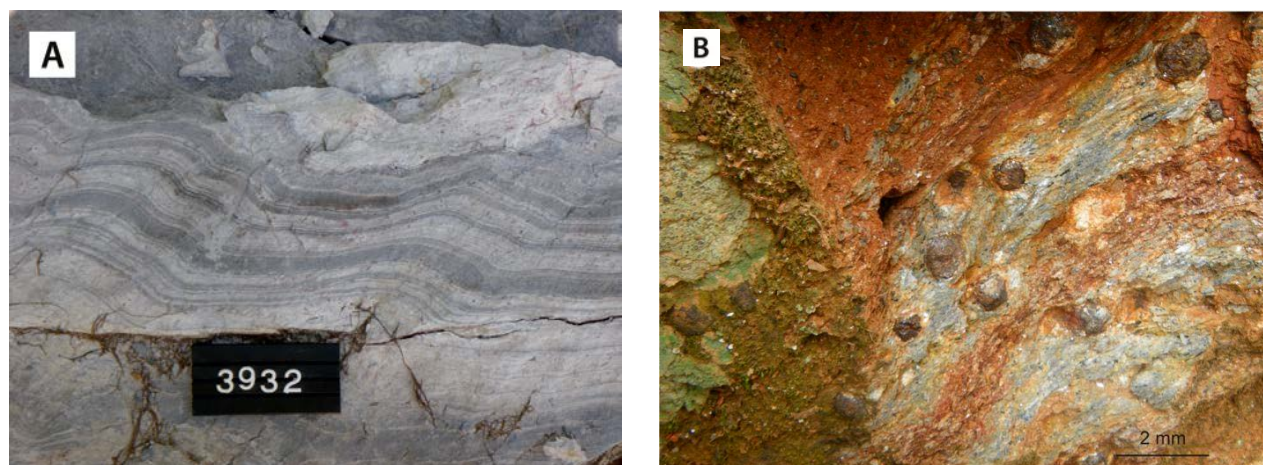


Fig. 8.9. Primary sedimentary structures in metapelites of the Nyaiguru Formation. (A) Laminar shale-siltstone succession (130323E / -106158N). (B) Strongly foliated, garnetiferous phyllitic schist in the highlands south of Mbarara town (232617E / -107282N). Number tag 10 cm.

Border quartzite (P2APbq) – Quartzites of the *Akorokor Formation* generally occur as psammitic interbeds in garnetiferous phyllites in the basal part of the Pindura Group. Due to its low stratigraphic position in the Akanyaru-Ankolean metasedimentary sequence, it was called ‘boundary quartzite’ by Stheeman (1932), and in places the quartzite is deposited directly on arena-type ‘granitoid’ bodies in the area. In the Kabale map sheet area, however, retrograde kyanite- and sericite-bearing phyllonites, possibly representing metapelitic rocks of the underlying Gikoro Group, locally occur between the Akorokor quartzite and granite domes (Stheeman 1932). Primary sedimentary structures in the ‘Border Quartzite’ are largely obliterated by intense deformation and recrystallisation, turning quartzite into coarse-grained, massive quartz rock. An obscure laminar bedding is, however, locally preserved in the rock.

Garnet quartzite (P2APgq) – Garnetiferous quartzite of the *Kyamengo Formation* occur in E–W trending, fault-bounded ridges at Ihunga hill, near the boundary between the Mbarara and Kabale map sheets, as interbed with transitional contacts with the garnetiferous phyllites of the Pindura Group (Stheeman 1932, page 30).

Feldspathic grit (P2APfg) – Minor occurrences of arkosic grits of the *Mukati Formation* are found between the Ihunga quartzite and granitoids of the Rukungiri Suite (pre-Kibaran Rusizian basement) in the western part of the Mbarara map sheet area. The areal extent of this poorly known rock unit,

which is here tentatively attributed to the Pindura Group, has been derived from the existing 1:100 000 scale geological map (Geological Survey of Uganda, sheet 84 – Rukungiri). Most probably feldspathic grits exist as variably thick intercalations or lenses within the pelitic schist of the Pindura Group.

Quartzite (P2APiq) – Quartzites of the *Ihunga Formation* form a very long (>50 km) and high (50–150 m above surrounding landscape), SE–NW trending quartzite ridge in the southwestern corner of the Mbarara map sheet area, from Kanungu town towards the southeast (Fig. 8.10A) into the Kabale map sheet area further south (Stheeman 1932). The same unit may comprise some of the smaller sub-parallel quartzitic ridges in the area.

The main quartzite horizon is 20–50 m thick and bordered by porphyroblastic phyllites and mica schists, which can be observed along the slopes or even on the top of these ridges. The white to grey, fine- to very fine-grained, recrystallised rock shows, in places, a vague banding and clastic texture (Fig. 8.10B).

Sandstone, quartzite, grit (P2AAPqs) – Psammitic horizons of the *Kamabale Formation* are locally exposed within the shale-mudstone-phyllite succession of the Pindura Group in the southwestern part of the Mbarara map sheet area. Locally, these rocks are strongly deformed sandstones, quartzites, grits and conglomerates, which are interpreted to represent the uppermost sedimentary unit of the Group, resting directly on granitic gneisses

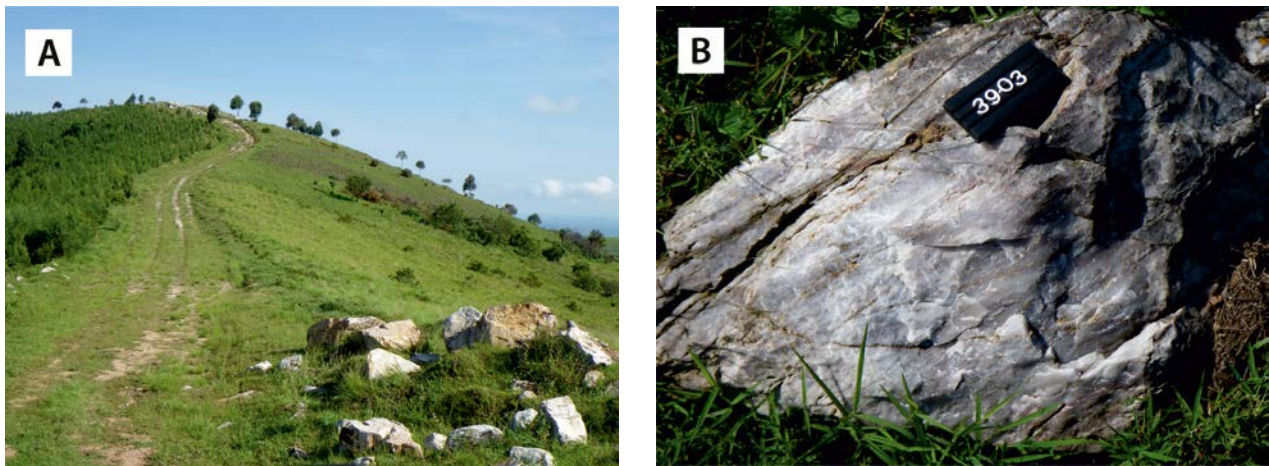


Fig. 8.10. (A) View along elongated quartzite ridge of the Ihunga Formation (148369E / -99917N). (B) Detailed image of fine-grained and vaguely banded Ihunga quartzite. Number tag 10 cm.

of the pre-Kibaran basement in places. Elsewhere, sandstones contain thin, phyllitic interbeds. Being more resistant to weathering than surrounding pelitic rocks, brownish to buff sandstones, often with pinkish weathering colours, generally form low, elongated hills or ridges. Light grey to whitish quartzitic varieties are frequently recrystallised into massive, coarse-grained quartz rocks without sedimentary structures. Compositionally, they range from immature, sericite-bearing, feldspathic varieties to pure, mature quartzites.

8.3.4 Cyohoha Group

Metasediments attributed to the Cyohoha Group are exposed in the northern hinge zone of two NNW-trending synclines. The western syncline is widely exposed between Lake Bunyonyi and Kisoro town. The other synform structure, composed mainly of a shale-mudstone-phyllite succession, occurs further to the east in the area of Mparo town.

Mudstone, shale, slate, phyllite (P2ACs) – The mudstone-shale-phyllite succession of the *Kirimbe Formation* comprises mainly argillaceous rocks with some arenaceous intercalations of variable thickness, showing a low, but eastwards increasing metamorphic grade. In a succession east and west of Lake Bunyonyi, the basal parts are composed of dark grey shales/slates with fine laminar bedding. Locally, slump folds and syn-sedimentary breccias can be observed. These beds are overlain by light grey, thinly laminated shale and fine-grained siltstone interbeds with reddish, pinkish and yellow-

ish weathering colours (Fig. 8.11A). Light-brown, fine-grained sandstone intercalations, generally 10–15 cm thick, occur in places and become more common and thicker in the middle part of the succession that otherwise mainly consists of medium to dark grey siltstones and shales (Fig. 8.11B).

Light grey shales and siltstones in the upper part of the succession contain local white, coarse-grained, centimetre- to decimetre-thick sandstone beds. Upwards, the sediments grade into light grey to whitish or light brownish, reddish-yellowish when weathered, often laminated siltstone/shale beds alternating with grey sandstone. The thickness of sandstone beds increase and the sediments show graded bedding with a rhythmic pattern of (from bottom to top) sandstone-siltstone-ferruginous horizon. The hanging wall contact between ferruginous layer and the sandstone in the next cycle is sharp. Hematite-rich ironstone lenses and discontinuous layers are not uncommon.

East of Lake Bunyonyi the uppermost parts of this unit become more arenitic, with simultaneous reduction in the dominance of argillaceous rock types and replacement by grey to reddish-pinkish sandstone-siltstone successions with decimetre- to metre-thick interbeds of grey to whitish, coarse-grained, partly gritty sandstone. Locally, sandstone beds contain narrow gritty or conglomeratic beds at their base, manifesting more shallow water conditions. Desiccation cracks indicate periods of emergence and aerial exposure. Because marker horizons are lacking, it cannot be excluded, however, that these coarse-grained sequences belong already to the overlying, generally coarser grained Rugezi Group.

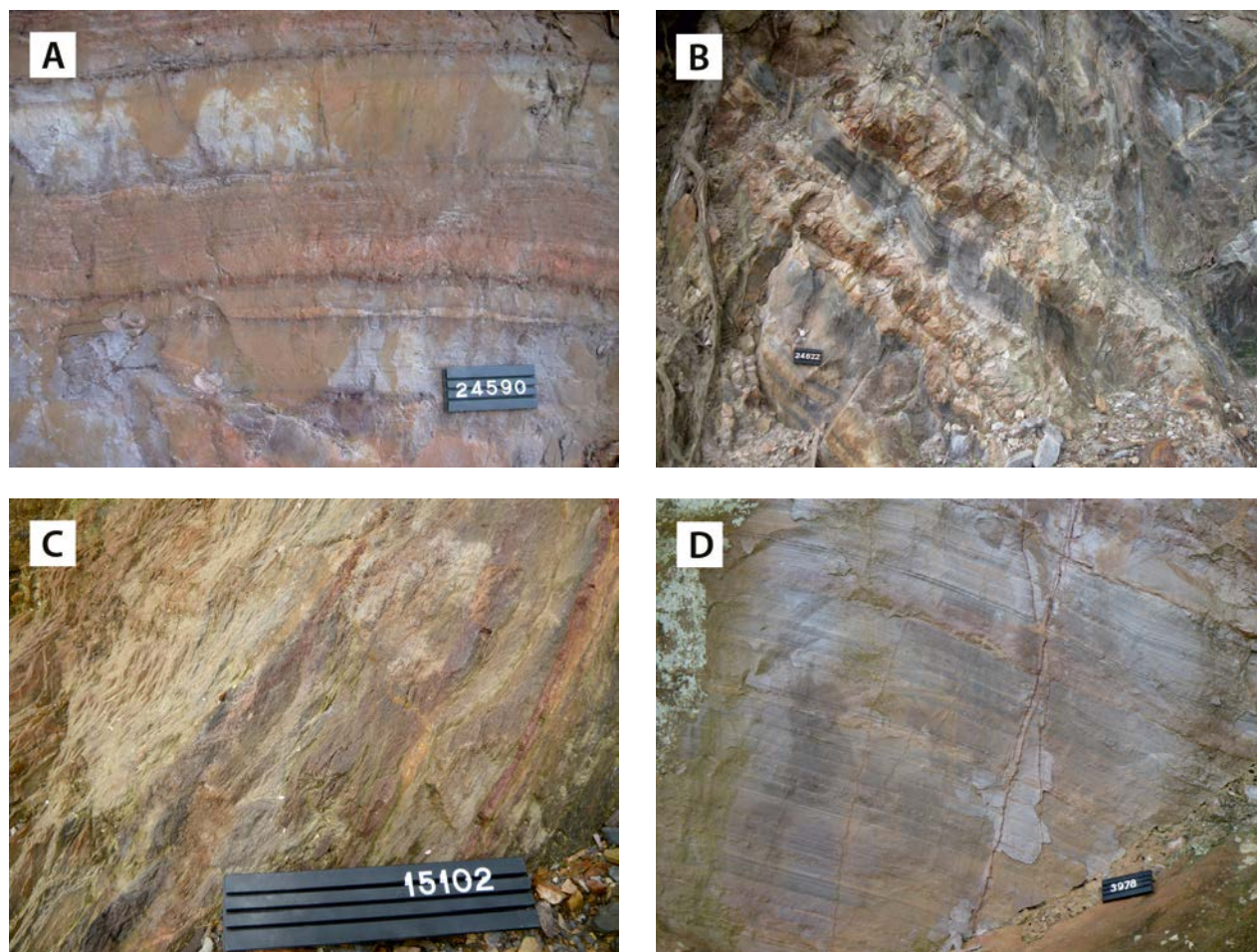


Fig. 8.11. Primary sediment structures of the Cyohoha Group metasediments. (A) Laminated grey shale and siltstone of the Kirimbe Formation (160098E / -138895N). (B) Laminated grey shale and siltstone intercalating with light-grey to whitish, light brownish sandstone (166620E / -158179N). (C) Laminated, grey siltstone/shale characterising the succession within the Mpale syncline (149066E / -110932N). (D) Rhythmic graded succession with thin, greenish grey siltstone interbeds between thick, reddish brown sandstone beds (149066E / -110932N). Number tag 10/15 cm.

The eastern mudstone-shale-phyllite succession within the Mparo syncline contains fewer and apparently less continuous sandstone interbeds than successions found further to the southwest. Such intercalations are restricted mainly to the south-eastern and central, well-exposed segments of the syncline and seem to be absent or of far less importance in the northwesternmost parts. Metamorphic grade increases to the east and, likewise, cleavage is better developed. The succession is dominated by argillaceous sediments, comprising sericite- and muscovite-rich slates, and metasiltstones in many cases grading into phyllites. Slates and siltstones comprise dark grey and blackish, graphitic phyllites or shales, bluish-grey varieties with white laminae, and laminated, medium grey and light-grey to whitish shales (Fig. 8.11C). Weathering colours are mainly red, brownish-red and yellowish. Boulders rich in goethite and

hematite (>50%), up to one metre in size, indicate the existence of similar ironstone horizons in the succession as observed in the west.

Felsic metatuff (P2ACft) – Felsic metatuffs of the *Kiirima Formation*, associated with mudstones and gritty sandstones of the Cyohoha Group, occur in the area of the Kiirima Forest Reserve. These are grey, very fine-grained, distinctly layered rocks (Fig. 8.12), composed mainly of quartz, altered feldspars and mica; opaque minerals and carbonate exist as elongated patches, reaching 3 mm in length. These pyroclastic rocks possibly continue into Rwanda as described by Croese (1984) and Croese & Matheussens (1990). The metavolcanic to sub-volcanic interlayers of the Kiirima Formation supposedly manifest periods of accelerated extension in the North Kibaran trough. The occurrence of ironstone horizons of the Rutooma



Fig. 8.12. Layered felsic metatuff of the Kiirima Formation (158980E / -119000N). Pen is 15 cm long.

Formation (see below) in the same area is most likely not coincidental.

Ironstone lenses (P2ACi) – Several occurrences of hematite-rich ironstone of the *Rutooma Formation*, are currently exploited by artisanal miners in the Muko area in Butare, Kyanyamuzinda, Kamena and Kashenyi and around Kabale town (Figs 8.13A-B). Muko-type ironstone occurs as massive or semi-massive layers, intercalated in shales and phyllites of the Kirimbe Formation. The thickness of the ironstone layers ranges from a few metres to more than 10 m. The average thickness in drill holes at Butare is 6 m, and the ironstone strata

have been followed in trenches and drillings up to 250 m down dip (Katto 1997).

Black, very fine-grained hematite rock shows a planar fabric and comprises minor quantities of sericite, quartz, kaolin and carbonate, the latter filling cavities. Fe_2O_3 contents of up to 99 wt% have been assayed in samples from Nyamiyag mine (Muwanguzi 2010). The occurrence of ironstones appears to be stratigraphically controlled with thickening of original layers in fold hinges. The artisanal mining operations produce a hematite concentrate for the Hima cement factory for the production of flux in Portland cement manufacture. It is reported that Uganda Steel Rolling Mills has



Fig. 8.13. (A) Pile of haematite ore in an artisanal quarry (162540E / -137372N). (B) The same artisanal quarry in Butare village.

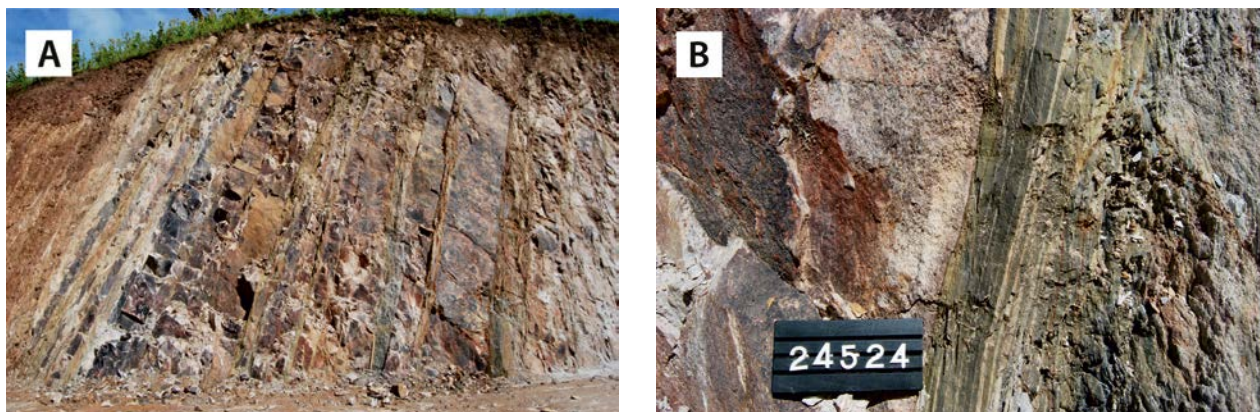


Fig. 8.14. (A) Bouma sequence of the Kashanga Formation. Road cut on the Kabale-Kisoro road (144386E / -135131N). (B) Detailed image of the Bouma cycle; top of sequence is to the left. Length of hammer 60 cm, number tag 8 cm.

completed the construction of an iron smelting plant in the Jinja district (www.newvision.co.ug).

Sandstone, quartzite, grit (P2ACsqg) – Coarse-grained to gritty, locally quartzitic sandstones of the *Kashanga Formation* occur as intercalations within the mudstone-shale-phyllite succession of the *Kirimbe Formation*. The thickness of the sandstone packages ranges from a few metres to >100 m. In general, thicker sandstone intercalations do not consist of a single thick bed but contain cm- to metres-thick interbeds of grey-greenish shale and/or siltstone or fine- to medium-grained sandstone.

The intercalated sandstones/quartzites show various lithologies. Some members are whitish to light-grey, coarse-grained to partly gritty sandstones that may contain beds with quartz clasts of 1–3 mm in size. Other varieties are massive, recrystallised quartzites or consist of fine- to medium-grained massive sandstone. Load cast structures have been observed in places.

Thick sandstone units with a total thickness of > 100 m, intercalated in the middle part of the mudstone-shale-phyllite succession are exposed in road cuts along the new Kabale-Kisoro road, NW of Lake Bunyonyi. This is a flysch-type, turbiditic succession composed of sandstone beds up to 4–5 m in thickness (Figs 8.14A-B). Typically, the turbiditic unit has thin beds of coarse, gritty sandstone at the base, with brownish grey, fine- to medium-grained sandstone forming the bulk of the unit. This rather massive sandstone grades sharply into greenish, very fine-grained, partly laminated siltstone at the top. In several road-cuts, a typical sequence of a graded unit – or Bouma cycle – consists of

- *top*: light bluish-greenish-grey, very fine-grained siltstone, partly laminated, ~20–60 cm thick;
- massive, medium-grained sandstone;
- *base*: coarse-grained, massive gritty sandstone, ~15–30 cm thick

8.3.5 Rugezi Group

The Rugezi Group comprises a conglomerate-sandstone-siltstone succession exposed in a SE–NW trending synform that extends NW and SE from Kabale town. The succession starts with conglomerates and gritty sandstones (*Rwene conglomerate*), which, from observations in Rwanda, mark an intra-Akanyaru-Ankole unconformity (see Table 8.1; Croese 1984).

Conglomerate (P2ARc) – Polymictic, matrix- to clast-supported conglomerates, intercalated with sandstone, pebbly sandstone and finer-grained conglomerate layers and lenses of the *Rwene-Kakore Formation* of the Rugezi Group are exposed NNW and SSE of Kabale town (Fig. 8.15A). The mostly dark-grey to bluish matrix of this unsorted basal conglomerate is gritty or coarse-grained sandstone, while angular to sub-rounded and scarce rounded pebbles range from less than one cm up to 60 cm in size. The clast material of the rock is mainly comprised of vein quartz and (quartzitic) sandstone, supposedly mostly derived from older units of the Akanyaru-Ankole Supergroup, supporting the assumption of an intra-Supergroup unconformity. Matrix-supported polymictic conglomerates with angular to rounded pebbles, of finer, though variable grain-size, also occur as interbeds in gritty sandstones (Fig. 8.15B).



Fig. 8.15. Primary sedimentary structures in metasediments of the Rugezi Group. (A) Polymictic conglomerate of the Rwene-Kakore Formation with angular to sub-rounded vein quartz, quartzite and sandstone clasts (165669E / -146170N). (B) Layers and lenses of unsorted conglomerate in sandstone (157900E / -129410N). (C) Breccia-conglomerate with angular, flat mudstone clasts (162378E / -137014N). (D) Partly laminated shale and siltstone of the Kikungiri Formation – note Liesegang rings in upper left corner (169604E / -149361N). Number tag 10/15 cm.

In a quarry NNW of Kabale town, specific conglomerate horizons with elongated angular mudstone/claystone clasts are exposed within gritty sandstones and thin conglomerate horizons (Fig. 8.15C). The clasts are aligned with their long axes parallel to the bedding planes. Other layers are more chaotic in appearance, without preferred orientation of the clasts. Elsewhere, these beds contain angular to sub-rounded sandstone and chert clasts up to boulder size or sandstone and chert pebbles, associated with the angular mudstone pebbles, which are rounded and relatively small. In contrast to sandstone and chert pebbles, mudstone clasts show no evidence of extensive abrasion and must be of proximal derivation. Nearby, intercalated ironstone beds of decimetre-size occur in sandstones.

The observed features suggest a shallow water depositional environment for the metasediments of the Rwene-Kakore Formation. The gritty and pebbly sandstones as well as coarse polymict con-

glomerates may represent beach and shoreline deposits, with the partly gritty sandstones being deposited in a lower shore face. Horizons containing mainly “flat-pebble conglomerates” with mudstone fragments could be interpreted as tempestites that formed in a sub-tidal shallow water environment, near the shoreline but below the fair-weather wave base when turbulent water caused by storms and storm surges disrupted beds of semi-lithified mud layers leading to channelling and pebble formation. The sediment was mixed with rounded sandstone and chert pebbles that have been either previously deposited or were transported into the basin during the storm.

An alternative explanation would imply failure of the shore face by seismic (and related tsunami) events, causing downwards sliding of unstable mudstone, even on a nearly sub-horizontal slope, accompanied by erosion of the uppermost semi-lithified mud layers. In fact, some very unsorted varieties containing also variably sized sandstone

and chert pebbles may represent debris flows. The general absence of evidence of syn-depositional faulting elsewhere in the Akanyaru-Ankole succession, also in the younger parts of the Rugezi Group overlying the basal conglomerates (like unconformities associated with conglomerate horizons) is in favour of the tempestite and near-shoreline model for most of the mudstone clast-bearing beds.

Siltstone (P2ARst) – Thick piles of metasediments, composed dominantly of shale/ slate/ siltstones assigned to the *Kikungiri Formation* of the Rugezi Group, overlie the basal conglomerates and gritty sandstones of the Rwene-Kakore Formation. The grey to whitish-grey to light greenish, very fine-grained, thinly laminated siltstones and shales of

the this Formation show weathering colours in shades of purple-violet and yellow-brown (Fig. 8.15D). Some beds show reduction spots, and, locally, also thin (1–2 cm) reddish-brown interbeds of fine-grained, oxidised sandstone occur.

Sandstone, quartzite, grit (P2ARss) – Distinct sandstone beds of the *Butobere Formation*, often tens of metres in thickness, consist of light grey-whitish to pinkish, silty sandstones with quartzite and grit intercalations. In places, very fine-grained, dark grey sandstones containing significant amount of argillitic material are also intercalated with pure sandstone layers. Another sandstone type is light-brownish grey, massive metasediment without bedding features.

8.4 Plutonic Rocks of the North Kibaran Belt

8.4.1 Introduction

Geological mapping in the 1980s in Burundi, combined with structural, petrologic and whole rock Rb-Sr geochronological data, resulted in the distinction of several generations of granitoids in the North Kibaran Belt (Fernandez-Alonso 1985, Fernandez-Alonso et al. 1986, Klerkx et al. 1987). Early kinematic (Gr_1) and syn-kinematic (Gr_2) peraluminous granites were related to an extensional tectonic phase D_1 with horizontal deformation and consequent foliation (S_1), which was assumed to have occurred from ~1400 to ~1260 Ma. Peraluminous Gr_3 granites (1185 Ma old) were allegedly syntectonic and correlated with a compressional phase D_2 , which was characterised by upright NNE- to NNW-trending folds. Subsequent, alkalic Gr_4 granites (~1100 Ma) were

associated with transcurrent faults (D'_2) of lithospheric scale (Table 8.3).

The 'Kibaran Peraluminous Granites' of Klerkx et al. (1987) have chemical compositions that vary between narrow limits (Fernandez-Alonso 1981, Fernandez-Alonso et al. 1986, Fernandez-Alonso & Theunissen 1998). In an alkalinity diagram (Na_2O+K_2O versus SiO_2) they can be described as granite and alkali-granite with subordinate granodiorite and syeno-diorite with a calc-alkaline to slightly alkaline signature and peraluminous affinity.

High-Th granitoids are higher in REE content and there is a difference in overall REE fractionation. The REE graphs indicate that the high-Th granitoids are more differentiated. Variable $^{87}Sr/^{86}Sr$ initial ratios (0.707–0.735) supposedly reflect the effects of high-level contamination and,

Table 8.3. Chronological sequence of granitic magmatism in the North Kibaran Belt.

| Bu | Granite type | Rb/Sr age (Ma) | Deformation Event | Geodynamic Phase | Rw | NW Tanzania |
|--------|----------------------------|----------------|-------------------|---------------------------|-------|--|
| | 'Tin granite' Pegmatite | ~1000 ~ 950 | Post- D_2 | | G_4 | |
| Gr_4 | Alkaline; A-type | 1100 | D_2 | Late transtensional shear | | Mukamera: 1088 ± 59 ; Maleba: 1006 ± 44 |
| Gr_3 | Calc-alkaline; S-type | 1200 | D_2 | Compressional | G_3 | |
| Gr_2 | Calc-alkaline; S-type | 1250 | Syn- D_1 | Extensional | G_2 | |
| Gr_1 | Calc-alkaline; S-type | 1330 | Early D_1 | Extensional | G_1 | Bukiriro: 1324 ± 23 |

Bu = Burundi; Rw = Rwanda (after Fernandez-Alonso *et al.* 1986; Klerkx *et al.* 1987).

to a lesser extent, compositional differences of source-regions. From isotopic and rare earth element data, a large-ion lithophile (LIL)-enriched source of possible Eburnean age, which produced silicic magmas mainly through plagioclase fractionation, is inferred for some granites. For most granites, however, the contribution of supracrustal rocks was important. The Gr₄ alkaline, A-type granites have low Sr initial ratios, suggesting a mantle origin (Fernandez-Alonso et al. 1986). According to Buchwaldt et al. (2008), the Mesoproterozoic granitoids from southwestern Uganda show overwhelmingly monzo-granitic and syenogranitic compositions and peraluminous affinities. Post-emplaced hydrothermal alteration has played a role but has not changed the signature of the granitic rocks. However, neither vein density (fluid pathways), nor secondary alteration minerals (e.g. micas) are abundant enough to assume large-scale metasomatism in Kibaran granitoids. Furthermore, K-metasomatism would not only change the potassium content of the rock, but would also produce significant changes in trace element contents. K and Rb vary coherently with LREE and HFSE, confirming that large-scale chemical changes were not induced during post-emplacement hydrothermal alteration. Neither is there any correlation between K/Na ratio and the Shand index (Kisvarsanyi & Kisvarsanyi 1990). All these data put together manifest that major element contents of these plutonic rocks approximate magmatic values and that REE pat-

terns and, hence, Sm–Nd isotopic systems, the alkali and possibly alkaline earth element contents, although to be treated with caution, have not been altered so greatly as to preclude their use in understanding original magmatic compositions and processes.

Subdivision of Kibaran Granitoids – Based on new data (zircon U–Pb SHRIMP ages, new ⁴⁰Ar/³⁹Ar and laser ablation zircon Hf data; Section 8.5) granitoids of the North Kibaran Belt can now reliably be divided into (from old to young):

- ‘Older’ Kibaran granitoids (1.57–1.45 Ga);
- Granitoids of the bimodal North Kibaran Igneous Province (1.38–1.33 Ga);
- A-type granites of the Transition or Boundary Zone (1.25 Ga);
- Largely sub-outcropping ‘tin granites’ (1.10–1.00 Ga) and related pegmatite bodies (0.97 Ga) and quartz veins (0.95 Ga).

8.4.2 ‘Older’ Kibaran granitoids (1.57–1.45 Ga)

Buchwaldt et al. (2008) have dated five bodies of Kibaran porphyroid calc-alkaline biotite granites in southwestern Uganda, namely the Ntungamo, Chitwe, Lugalama, Rwentobo and Kamwezi plutons. Surprisingly, they belong to different suites with significantly different ages and geochemical signatures.



Fig. 8.16. Megacrystic Chitwe granite (214023E / -106524N). Number tag 10 cm.

Chitwe granite (P2Cgr) – The Chitwe granite forms a rather circular-shaped batholith, with a diameter of about 7 km, just north of the old mining town of Chitwe. The granite pluton can be easily delineated on airborne radiometric maps, due to their high radiometric values, in particular by their elevated potassium signature. Being surrounded by Akanyaru-Ankole quartzite ridges, it is a typical ‘arena granite’.

The main rock type is megacrystic biotite granite (Fig. 8.16) with K-feldspar phenocrysts, measuring between 2 and 5 cm, in finer grained matrix of quartz, plagioclase and biotite, the latter amounting to ~15 vol%. Medium-grained, aplitic granite occurs as a subordinate phase in the Chitwe granite. Dolerite dykes and rare narrow pegmatite lenses or dykes occur in places.

The Chitwe granite shows only mild deformation; foliation or planar fabric cannot be usually observed. In fact, most outcrops exhibit massive, rather isotropic granite with only local, narrow shear zones. Detailed petrographic description of the Chitwe granite is given in Ucakuwun (1989) and Sinabantu (1993). Zircon U-Pb dating of the Chitwe granite has yielded an age of 1.57 Ga (Buchwaldt et al. 2008; Section 8.5), considerably older than most granitoids in the North Kibaran Belt.

Ntungamo granite (P2Ngr)– The Ntungamo granite is an elongated, oval-shaped, SE–NW trending

batholith of about 50 km² in surface extent, located NW of Ntungamo town. The granitic pluton has been described in detail by Nicholson (1965), who called this body the “Ntungamo dome” and, because of the concordant structural relationship with the surrounding metasediments, suggested that it represented the basement for the ‘Karagwe-Ankolean’ cover. It is mainly composed of deformed porphyroblastic biotite granite, which, in addition to microcline phenocrysts, is composed of plagioclase, quartz and biotite, the latter in amounts of ~15 vol%. Plagioclase is of oligoclase composition and is partly altered into saussurite. Minor, partly retrograde constituents of the granite comprise muscovite, epidote, amphibole and sphene.

The central part of the Ntungamo granite has been intensively deformed and shows a NW-SE foliation defined by large microcline crystals, up to 5 cm in size, in a finer matrix (Fig. 8.17). This central part is surrounded by a marginal more equigranular zone with parallel foliation. Some of the coarse K-feldspar crystals post-date the gneissose foliation. Some subordinate tonalitic medium-grained gneissic phases, which partly lack biotite and K-feldspar (e.g., Nicholson 1965, Buchwaldt et al. 2008) occur in places. Quartz rock xenoliths, up to several metres wide, which probably represent re-crystallised quartzite country rock, thick metadolomite and some narrow aplite and pegmatite dykes are found locally.



Fig. 8.17. Deformed granite gneiss of the “Ntungamo dome” (190828E / -93193N). Number tag 10 cm.

U-Pb zircon dating of granitoids of the Ntungamo batholith has yielded a mean $^{207}\text{Pb}/^{206}\text{Pb}$ evaporation age of 1.45 Ga, the granite being some 100 million years younger than the Chitwe granite and 50 million years older than the emplacement of the ~1.4 Ga granitoids of the bimodal North Kibaran Igneous Province (Section 8.5)

8.4.3 Plutonic Rocks of the bimodal North Kibaran Igneous Province (1.38–1.33 Ga)

The bulk of the granitoids in the North Kibaran Belt have been deposited during a relatively short period between 1380 Ma and 1375 Ma, a major magmatic event, termed ‘Large Igneous Province’ by Tack et al. (2006a, 2008b, 2009, 2010, 2011a). Because this term is too generic, we have renamed this event as ‘North Kibaran Igneous Province (NKIP)’. This magmatic phase was bi-modal and, apart from the bulk of the ‘Kibaran granitoids’, it includes layered mafic and ultramafic rocks of ‘Kabanga-Musongati-Kapalagulu Nickel Belt’ in eastern Burundi and NW Tanzania and the Lake Victoria Arcuate Dyke Swarm. Granitoids belonging to this event in SW Uganda have been assembled in the Kamwezi Suite.

Porphyritic biotite granite of the Kamwezi Suite (P2Kbgr) – This suite is composed of three individual granitoid bodies, called Kamwezi, Rwentobo and Rugalama. They are some 50–100 km² in surface exposure, but the Kamwezi granite continues into Rwanda, where it is part of the Mutare Massif (location 4 in Fig. 8.2). The Kamwezi and Rwentobo plutons can be readily delineated by using airborne geophysical data, but the dimen-

sions of the Rugalama pluton are poorly known. These granitoids and their surroundings have been studied by Barnes (1956), Ucakuwun (1988, 1989, 1992), Pohl (1994) and Buchwaldt et al. (2008).

The Kamwezi Suite is composed of coarse porphyritic biotite granite, with biotite contents ranging between 10 and 20 vol%. The individual plutons of the Suite are rather homogeneous and only weakly deformed, though a preferred orientation of phenocrysts can generally be observed. In the Kamwezi granite pluton, K-feldspar phenocrysts are locally rounded (Fig. 8.18A), while those in the Rwentobo pluton are usually angular and euhedral (Fig. 8.18B).

A N–S trending body of very coarse-grained diopside skarn, supposedly 20 x 200 m in size, occurs within metapelites of the Pindura Group in the contact aureole of the Kamwezi granite. In this skarn, fan-shaped intergrowths of greenish grey, elongated diopside crystals measure locally 40–50 cm (Fig. 8.19). In addition, the skarn comprises subordinate amounts of plagioclase and amphibole. Diopside skarn grades without a sharp boundary into coarse pegmatite. This skarn obviously formed from a calcareous host rock that has undergone metasomatic reactions with pegmatitic fluids, and its formation supposedly manifests the erstwhile presence of carbonate lenses in the Pindura metasediments.

Bwindi porphyritic granite (P2Kpgr) – Two circular granite plutons with a diameter of 4–5 km occur in the southern part of the Kanungu district. Being intensively weathered, outcrops are rare in these Bwindi granites, but dimensions of plutons can be readily outlined from airborne data. The por-

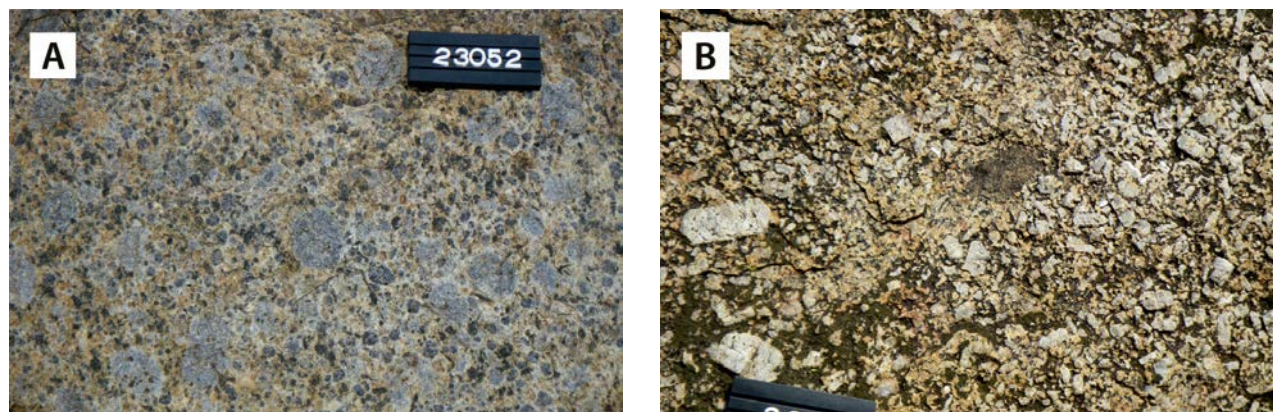


Fig. 8.18. (A) Porphyritic granite of the Kamwezi pluton. Note the rounded K-feldspar phenocrysts (188350E / -136996N). (B) Porphyritic granite of the Rwentobo pluton. K-feldspar phenocrysts are rather euhedral, and small mafic inclusions occur in places (183338E / -126083N). Number tag 10 cm.



Fig. 8.19. Very coarse diopside crystals in skarn situated at the contact between the Kamwezi granite and metapelites of the Pindura Group (181392E / -113181N). Number tag 10 cm.

phyritic Bwindi granites are pinkish grey, coarse grained and heterogeneously textured rocks with slightly rounded K-feldspar phenocrysts measuring 2–4 cm in length. Biotite is the main mafic mineral, with a mode of ~15 vol%. Small intermediate to mafic enclaves occur locally, and random pegmatite and metadolerite dykes cut the Bwindi granites.

Kabale (Rubanda) granite (P2Kgr) – A roundish granite pluton, about 6 km in diameter, occurs

20 km NW of Kabale town. This granite is poorly exposed, and along its SW margin covered by ash and scoria of the Neogene Bufumbira Formation. From field evidence and the new airborne geophysical data the areal extent of this granite body can be readily delineated, however. The Kabale granite is coarse-grained, equigranular to more or less porphyritic, and only weakly deformed (Fig. 8.20). Biotite is the main mafic mineral, averaging about 15% by volume of the rock.



Fig. 8.20. Coarse-grained Kabale (Rubanda) granite (146249E / -122884N). Number tag 10 cm.

Mafic and ultramafic rocks of the bimodal North Kibaran Igneous Province

These rocks can be divided into three groups:

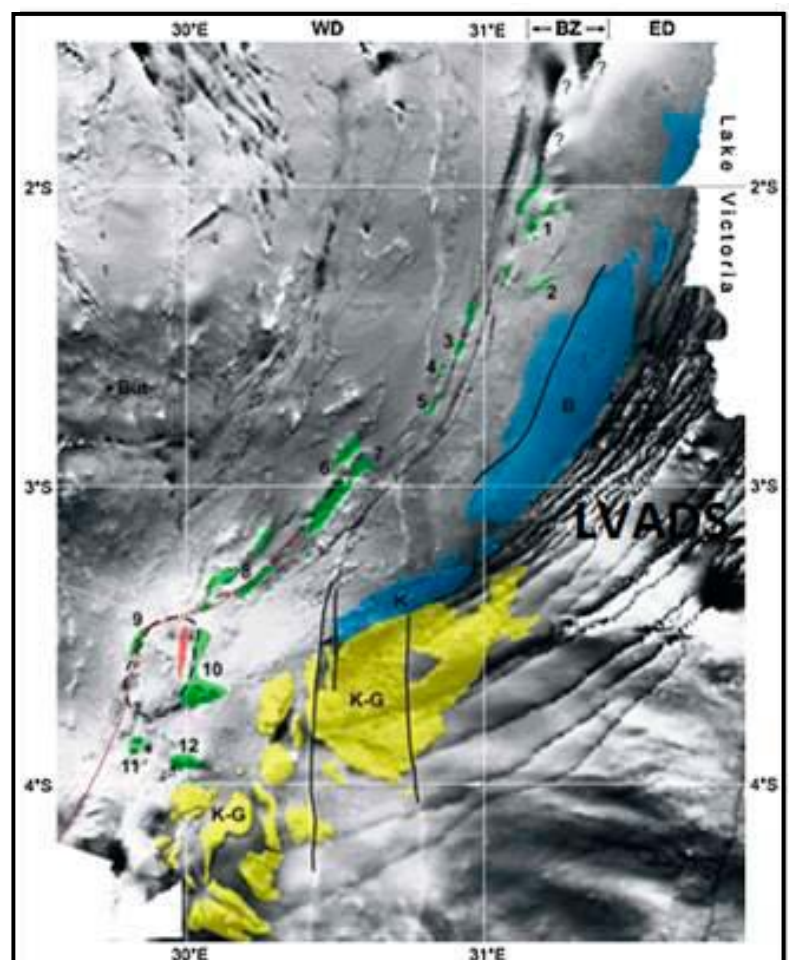
- concordant sills in metasediments of the Akan-yaru-Ankole Supergroup and associated smaller bodies in Kibaran granitoids and pre-Kibaran basement;
- N-S trending, layered, intrusive bodies of mafic and ultramafic composition that constitute the 'Kabanga-Musongati-Kapalagulu Nickel Belt';
- huge dyke swarm, known as Lake Victoria Arcuate Dyke Swarm (LVADS), which mainly occurs outside, but parallel to the curved eastern boundary of the NKB, intersecting mainly rocks of the Rwenzori Belt and the Tanzania Craton.

Mafic rocks in the Akanyaru-Ankole Supergroup – The petrology and geochemistry of the latter have received only limited attention (Ntungicimpaye 1983, 1984a, 1984b, Tack et al. 1990, 1994, Ntungicimpaye & Kampunzu 1987 and references therein, Nzojibwami 1985). In Rwanda, metadol-erites are notably exposed as thick intercalations

in 'mica schists' of the 'Byumba Series' (Table 8.1) in the SE corner of the country. Equally important metabasite horizons, 50 to 300 m in thickness, occur elsewhere, in particular in west Rwanda near the NW-SE directed Mwogo fault and associated peculiar Gakoma megafold structure. According to Jung & Meyer (1990), the metabasite is largely of doleritic to gabbro-noritic composition. Occasionally, they show differentiation with a melanocratic base (melanorite to olivine-pyroxenite) and more felsic upper parts (leucogabbro to granophyric quartz dolerite). Retrograde metamorphic minerals include tremolite-actinolite, chlorite and saussuritised plagioclase. Generally, however, they have retained their primary igneous textures (Jung & Meyer, *op. cit.*).

'Kabanga-Musongati-Kapalagulu Nickel Belt' – This curvilinear, N-S trending belt (Fig. 8.21) is part of the 'Transition Zone' (Fig. 8.2) (TZ) – or 'Frontier Zone' (Deblond 1990, 1994) or 'Boundary Zone' (Tack et al. 1994): a fault-bounded, narrow (10 to 30 km) and elongated curvilinear zone that, according to the 'School of Tervuren' separates

Fig. 8.21. Contrast-enhanced Total Magnetic Intensity (TMI) map of the Kabanga-Musongati alignment (data from the African Magnetic Mapping Project). BZ: Boundary (or Transition) Zone overlapping broadly with the "boundary zone" in Fig. 8.2. Key: But = Butare town. Green = mafic/ultramafic layered complexes of the KM-alignment with names of the five complexes north of Kabanga (serial number: 1–5: after Evans et al. (2000): 1= Burigi; 2= Ruiza; 3=Kibamba; 4=Kanyautenge; 5= Luhuma; 6=Kabanga; 7= Mulemera; 8=Nyabikere; 9=Waga; 10=Mukanda-Buhoro-Musongati; 11=Rutovu; 12= Nkoma "hidden" body. Blue: region covered by gabbro-noritic sills intrusive in the Bukoba Group (Fernandez-Alonso et al. 2007, 2011, with kind permission of Elsevier Ltd.); B and K refer to the tabular siliciclastic rocks of the Bukoba Group of the Kagera-Buhjewe Supergroup. Reddish-pink: region of elongated bodies of Gitega-Makebuko-Bukirasazi (GMB) A-type granitoid rocks. Dashed black line: Outline of elliptical aeromagnetic structure, coinciding with gravimetric structure. Yellow: region covered by younger Kabuye-Gagwe (K-G) amygdaloidal basalts (~795 Ma) of Malagarasi Supergroup. Solid black lines: Faults. Note also dykes of the LVADS in the bottom part of the Figure (from Tack et al. 2010).



the Western Domain from the Eastern Domain of the NKB or, according to our lithostratigraphic scheme, between metasediments of the Mesoproterozoic Akanyaru-Ankole Supergroup and the Palaeoproterozoic Kagera-Buhjewe Supergroup. The Transition Zone stands out by occurrence of 1.2 Ga anorogenic A-type alkali granites and mafic to ultramafic, layered intrusives.

The 'Kabanga-Musongati-Kapalagulu Nickel Belt' comprises a 350 km long curvilinear alignment that extends from Burundi into Uganda. The belt hosts Ni sulphide deposits (inferred resources ~36 Mt grading 2.8% Ni) at Kabanga and PGE reef deposits at Musongati and Kapalagulu. Musongati ultramafic intrusion in Burundi is also a potential Ni laterite deposit. Pyroxene peridotites (with bronzite), norites (with bronzite), gabbro-norites (with inverse pigeonite), leucogabbro, norites and anorthosites are the most frequent rock types in eastern Burundi. Fine-grained facies include microgabbro-norite, dolerite and granophyre (Deblond 1990, Deblond & Tack 1999, Evans et al. 2000, Duchesne et al. 2004). Although some authors interpreted these mafic and ultramafic rocks as ophiolites, they can be characterised as layered intrusive bodies with conspicuous cumulate textures in all rock types, cryptic layering characterising cumulus mineral compositions and evidencing fractional crystallisation as a major differentiation mechanism. Surface exposures of these bodies range between 62 km² and a few square kilometres. The intrusions consist of sills and sub-horizontal pipes of variable sizes, while dykes are rare. The smallest intrusions are tens to hundreds of metres wide and may host massive Ni sulphide ores (e.g., Kabanga North).

Many of the intrusions are hosted by low- to medium-grade metamorphosed mica schists and graphitic schists, which may contain abundant sedimentary sulphides, a potential source of external sulphur to promote Ni-sulphide segregation. Mass balance considerations indicate large ratios of sulphides to silicate ratios and ultramafic to mafic lithologies in these bodies, suggesting emplacement of olivine-pyroxene-sulphide crystal mushes. The larger intrusions may be several kilometres in thickness and host S-poor PGE reefs (Kapalagulu and Musongati). The parental magma to all intrusions were originally picritic (~16.5% MgO, 52 % SiO₂), variably contaminated by the host rocks. The sulphide- and Ni-rich intrusions assimilated up to ~20 vol% of crustal rocks, result-

ing in a magma with ~14 wt% MgO, 54 wt% SiO₂, Ni/Cu (in sulphides) ~8, Pd/Ir 5–20, strongly enriched incompatible trace element contents, distinct negative Nb-Ta and Ti anomalies, heavy S isotopic signatures ($\delta^{34}\text{S}$ +10 to +24), and highly Ni depleted olivine (Fo₇₀₋₉₀; <100–1600 ppm Ni) (Deblond 1994). The sulphide-poor, PGE-enriched intrusions assimilated much less crustal material (~5–15 vol%), resulting in less fractionated trace element and isotope signatures and in less depleted olivine (Maier et al. 2007). According to Xstrata Company, Kabanga is among the world's most attractive undeveloped nickel sulphide deposits with a total estimated indicated resource of 9.7 Mt grading 2.37% nickel and a total estimated inferred resource of 36.3 Mt grading 2.8% nickel.

Kafunzo ultramafic rock, geophysical interpretation – There has been a lot of speculation whether the 'Kabanga-Musongati-Kapalagulu Nickel Belt' continues into Uganda. An elongated gravity anomaly southwest of Kafunzo town may correspond with a northern extension of the above Ni belt. So far, drilling has not proved the presence of ultramafic rocks in the Kafunzo area.

Lake Victoria Arcuate Dyke Swarm (LVADS) – Due to deep tropical weathering – particularly affecting mafic rocks – this dyke swarm was poorly known until its features became fully appreciated thanks to the fact that they cause prominent anomalies on airborne magnetic maps (Baterham et al. 1983, Chavez Gomez 2000, Mäkitie et al. 2011a) (Fig. 8.22). Starting from the Fort Portal area, this about 100 km wide, SE-directed curvilinear dolerite swarm continues to the Masaka area, and further southwards along the western shore of Lake Victoria into Tanzania and finally SW-wards into the direction of Lake Tanganyika (Figs 8.21 and 8.22), resulting in a huge semicircular form. Magnetic profile interpretations across the dykes in Tanzania and Uganda indicate that the dykes dip at about 30°–40° towards the geometric center of the concentric rings, implying a cone shaped geometry for the dykes in three dimensions (Ruotoistenmäki 2014). The swarm, for which Reeves (pers. comm.) coined the term Lake Victoria Arcuate Dyke Swarm (LVADS), has been dated at 1.37 Ga (Mäkitie et al. 2014c) and, although located outside and east of the NKB, it is part of the bimodal North Kibaran Igneous Province. Petrology, geochemistry, geochronology and emplacement

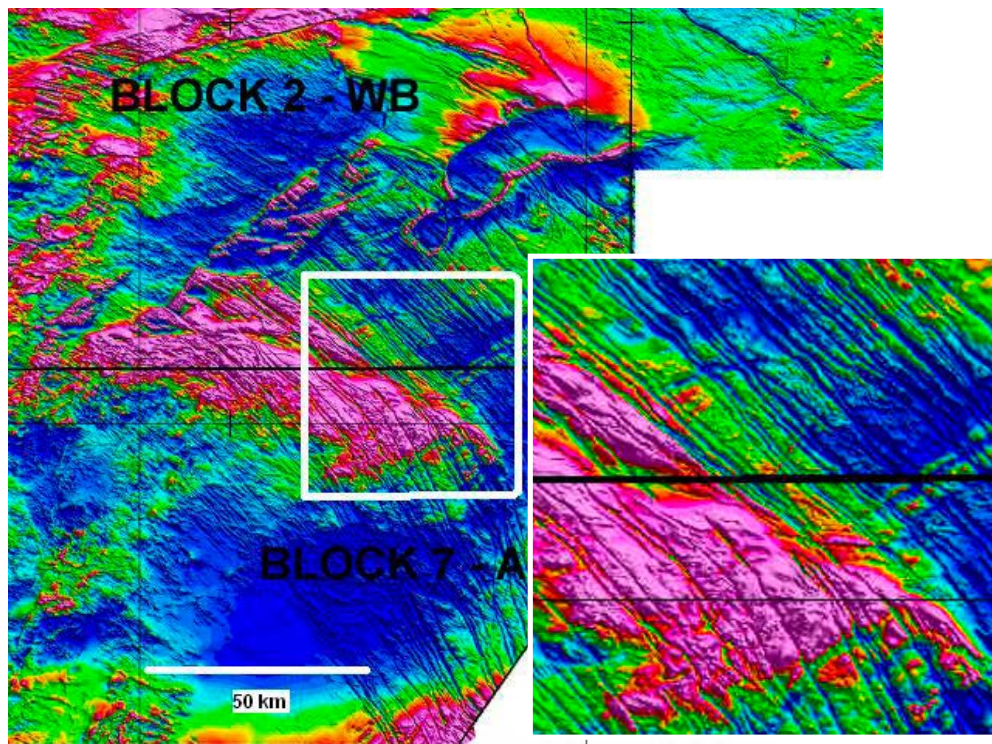


Fig. 8.22



Fig. 8.22. Airborne magnetic image of the Lake Victoria Arcuate Dyke swarm in southwestern Uganda (cf. index map). Spacing between individual dykes is of the order of 1–3 dykes/km. The abrupt south-western boundary of the dyke swarm appears to coincide with a basement fault (see flat magnetic pattern SW of swarm).

model of this 1.37 Ga arcuate swarm is recently described in Mäkitie et al. (2014c).

From the distribution of elongated boulder fields and small outcrops it can be concluded that individual dykes are from several metres up to tens of metres wide, and composed of rather massive, medium-grained dolerite (Fig. 8.23A). Major mineral constituents of these dykes are augite and plagioclase (Fig. 8.23B), while typical accessory minerals are ilmenite, magnetite, apatite, quartz and biotite. Secondary amphibole and chlorite have formed at the expense of pyroxene, and saussurite has replaced plagioclase.

Chemically, the dolerites of the dyke swarm can be classified as subalkaline tholeiitic basalts. The average chemical composition is as follows: 50.2 wt% SiO₂, 1.1 wt% TiO₂, 14.4 wt% Al₂O₃, 12.7 wt% Fe₂O₃t, 0.2 wt% MnO, 6.8 wt% MgO, 10.6 wt% CaO, 2.2 wt% Na₂O, 0.6 wt% K₂O, 0.1 wt% P₂O₅ Mäkitie et al. (2014c). Lanthanides of a dolerite dyke show a small LREE enrichment (La_N/Sm_N 2.0), but their

distribution is rather flat (La_N/Yb_N 2.9) with a minor negative Eu anomaly. Representative chemical analyses after Mäkitie et al. (2014c) of these mafic dykes are in Appendix 2 (anal. 139–142).

Arcuate swarms may result from deflection under the influence of a regional stress field, from secondary deformation, or they may be part of a circumferential swarm surrounding a mantle plume centre. We postulate that the LVADS formed during accelerated Kibaran extension, causing crustal thinning, basaltic underplating and formation of the North Kibaran trough by listric normal faulting of basement blocks. Both synthetic and antithetic listric faults are assumed to have formed at this stage. At some stage these listric faults have been invaded by mafic magma. The arcuate surface shape of the LVADS is supposedly due to differential uplift (and subsequent erosion) of the basement, so that the curvature in depth is projected as a curvature on the flat peneplaned surface (oral comm. André Tahon). Apparently,



Fig. 8.23. (A) Massive LVADS dolerite (296685E / 48037N). (B) Microphotograph of the same dolerite. Crossed nicols. Number tag 10 cm, width of microphoto ~20 mm.

basement rise was maximal in southwestern Uganda and in western Tanzania (near the NW-trending Karoo rift superposed on the Palaeoproterozoic basement high, which separates the South Kibaran Belt from the NKB) and considerably less in the area in between (mainly Burundi and Rwanda). This may be simply due to isostatic rebound of the inverted North Kibaran trough, which was deepest and carried the thickest sediment load in the centre of the basin.

8.4.4 A-type granites of the Transition Zone (1.25 Ga)

An alignment, 40 km in length (Fig. 8.21) of relatively small-sized (from ~1 to ~20 km²) bodies, is composed of anorogenic A-type alkali granites (Tack et al. 1990, 1994, Tack & Duchesne 1997). They are mainly truly granitic in composition, can be strongly enriched in incompatible elements, and comprise subordinate syenites and mafic rocks. Initial isotopic ratios ($Sr=0.702$; $\epsilon_{Nd} = +4.5$ to -1.4) point to an asthenospheric/lower continental lithospheric mantle origin, with only slight contamination by the lower crust during differentiation (Tack et al. 1994). This indicates that these granites are produced by differentiation of less evolved magmas and not by crustal anatexis.

8.4.5 'Tin granites' and other 'younger granites' (1.10–1.00 Ga) and related pegmatite bodies (0.97 Ga) and quartz veins (0.95 Ga)

'Younger' granitic bodies existing in the North Kibaran Belt are supposedly late syn-kinematic to clearly post-kinematic with respect to the major phase of folding (D_2) in the belt. They correspond

to the largely sub-outcropping G_4 or 'tin granites' of Fernandez-Alonso et al. (1986) and Klerkx et al. (1987).

Pohl (1987a, 1992, 1997, 2006) attributed the metallogenesis of tin (tungsten and other related elements) to the emplacement of these LIL-enriched 'tin granites'. These 'Younger Kibaran Granites' have an age of 1000–950 Ma and supposedly form sheets at the basement/sediment or older NKIP granite/sediment contacts with cupolas at tectonic highs. The mineralised pegmatites and quartz veins originated from these 'tin granites'.

'Tin granite' has a very variable, but always negative ϵ_{Hf} , indicating derivation from the reworking of older crustal material, with highly variable participation of juvenile melt. TDM model ages are in the range 2.5–1.7 Ga, suggesting similar crustal contaminants as in the 1375 Ma granitoids of the NKIP (Tack et al. 2010). Overall, the Hf-isotopic data support the recurrent reworking (i.e. at ~1375 and ~986 Ma) of the Palaeoproterozoic Rusizian basement of the NKB, with only limited addition of juvenile, mantle-derived components.

Rubaale pegmatite granite (P2Rpg; ~1.1 Ga) – Pegmatitic granites have been encountered in southwestern Uganda, notably in the NE part of the Kabale and neighbouring Mbarara map sheet areas. Pegmatite granites with associated pegmatite dykes are very irregular in texture with notable grain size variations. For example, K-feldspar crystals may have sizes of up to 50 cm. Plagioclase (albite) is usually fine- to medium-grained. Muscovite may occur as very coarse flakes and black tourmaline is a typical accessory mineral. Coarse quartz cores are common in these pegmatites.

8.5 Geochronology

Pre-Kibaran Basement – Rusizian/ Rwenzori Palaeoproterozoic rocks with ages between 2.13 Ga and 1.98 Ga underlie the metasediments of the Akanyaru-Ankole Supergroup (Section 6.2). Recently, a ‘Rusizian’-aged basement orthogneiss in the Butare area (south central Rwanda) has been dated and yielded a SHRIMP age of 1982 ± 6 Ma (Tack et al. 2010), corresponding with granitoids of the 1.99–1.96 Ga Sembabule Suite in Uganda and, viewed in a more regional context, with ages between 2100 and 1860 Ma (Cahen et al. 1984, Lenoir et al. 1994) in the the Ubende Belt of Tanzania.

An inlier of Archaean rocks is exposed in the basement of southern Burundi (the Kikuka Complex; Fig. 8.2) and zircon U-Pb dating yielded ages of ~ 2504 Ma and ~ 2601 Ma, which were considered to represent minimum ages (DemaiFFE & Theunissen 1979).

Akanyaru-Ankole Supergroup – Rhyodacite of the Gikoro Group, the lower part of the Akanyaru-Ankole sediments yielded a WR Rb-Sr age of 1353 ± 46 Ma (Klerkx et al. 1987). SHRIMP age determinations on detrital zircons were carried out by Cutten et al. (2004). A quartzite sample (Ruganza quartzite; upper unit of the basal Gikoro Group, supposedly equivalent to the Iryango Formation in southwestern Uganda) has a very prominent 2.48–2.73 Ga peak (83%), and limited input from a 2.01–2.07 Ga population (10%). The youngest detrital zircon of 2.01 Ga gives its maximum age of deposition. Another quartzite sample (Muyinga quartzite, along-trend equivalent of the Ruganza quartzite) has a 1.75–2.07 Ga population (60%), and a scatter of 2.58–2.79 Ga (23%) data. Cutten et al. (2004) believe that the relative abundances of the two main populations reflect proximity to Archaean and Palaeoproterozoic source rocks. They questioned the origin of the noteworthy though small (5%) component of ~ 1.41 Ga magmatic zircons in one sample. We suppose that these zircons are derived from volcanic intercalations within the Akanyaru-Ankole succession, slightly older than abundant bimodal plutonism of the North Kibaran Igneous Province. These zircons constrain a maximum age of sedimentation for the uppermost part of the basal Gikoro Group.

‘Older’ Kibaran granites – An older group of granitoids – comprising the Ntungamo and Chitwe plutons in southwestern Uganda – contains zircon grains of which some 40% have xenocrystic cores. Four zircon grains from the Ntungamo Granite yielded a mean $^{207}\text{Pb}/^{206}\text{Pb}$ evaporation age of 1445 ± 8 Ma. To confirm the evaporation age three abraded zircon grains were analysed using conventional U-Pb isotope dilution analysis. They exhibit a slight discordance with an excellent linear arrangement (MSWD = 0.7) and constitute an array intersecting the concordia at 1446 ± 3 Ma, identical to the evaporation age. Buchwaldt et al. (2008) therefore interpreted this age as the crystallisation age of the Ntungamo Granite. Similarly, four zircon grains from the Chitwe pluton yielded identical $^{207}\text{Pb}/^{206}\text{Pb}$ ratios that combine to a mean age of 1566 ± 0.3 Ma using the evaporation method and a discordia upper intercept age of 1566 ± 3 Ma, again interpreted as the crystallisation age of the Chitwe pluton.

Granitoids of the North Kibaran Igneous Province (NKIP) – The G_1 to G_4 subdivision of the ‘Kibaran Peraluminous Granites’ *sensu* Fernandez-Alonso et al. (1986) and Klerkx et al. (1987) (Table 8.3) in Burundi and Rwanda relied on a few bulk zircon ages and a lot of Rb-Sr or K-Ar data, often on two-mica granitoids (Burundi: Klerkx et al. 1984, 1987 – Rwanda: Gérard & Ledent 1971, Lavreau & Liégeois 1982 – NW Tanzania: Ikingura et al. 1990). Only Cahen et al. (1984) reported preliminary bulk-zircon U-Pb ages for granitoids in Rwanda and Burundi. Based on new data (zircon U-Pb SHRIMP ages, new $^{40}\text{Ar}/^{39}\text{Ar}$ and laser ablation zircon Hf data; Fig. 8.24) the G_1 to G_4 subdivision has ceased to exist.

Based on new data (zircon U-Pb SHRIMP ages, new $^{40}\text{Ar}/^{39}\text{Ar}$ and laser ablation zircon Hf data; Tack et al. 2010) it appeared that in Rwanda and Burundi the bulk of the granites were emplaced during a relatively short period of time between 1380–1375 Ma (Fig. 8.24) during a phase of accelerated crustal extension, culminating with the intracratonic emplacement of the ‘North Kibaran Igneous Province’ (NKIP). This phase of magmatism was supposedly related to a mantle thermal anomaly (Tahon et al. 2004) located in SE Burundi, giving rise to coeval bimodal magmatism as manifested by S-type granitoids with subordinate mafic rocks.

Two ~1375 Ma S-type granitoid rocks and one migmatitic paragneiss show a more ancient signature with ϵ_{Hf} (T) between -5 and -9. These negative values suggest significant participation of older crustal material in the generation of these granitoids, as would be expected from S-type granitoids which are, essentially, derived from melting of the lower crust. TDM model ages are in the range 2.4–1.6 Ga, indicating a significant average crustal residence time for these rocks. The data are consistent with the derivation of the 1375 Ma suite of granitoid rocks largely through the re-melting of ca. 2.0 Ga basement (Tack et al. 2010).

Kamwezi Suite – Kibaran granitoids of southwestern Uganda have been attributed to the Kamwezi Suite. Magmatic zircons from the Rwentobo granite lack inherited cores, suggesting that the zircons crystallised during one single magmatic event. Three zircon grains produced a mean evaporation age of 1367 ± 5 Ma, confirmed by U–Pb ages from three abraded zircons with an upper intercept of 1368 ± 3 Ma and interpreted by Buchwaldt et al. (2008) as emplacement age of this granite. A different sample yielded a mean evaporation and U–Pb isotope dilution ages of 1362 ± 4 Ma and 1362 ± 1 Ma, respectively. Three zircon grains from the Kamwezi granite (i.e., the northern margin of the large, 45 x 60 km, Mutare Massif in NE Rwanda; no. 4 in Fig. 8.2) were evaporated and yielded a mean $^{207}\text{Pb}/^{206}\text{Pb}$ age of 1330 ± 22 Ma, confirmed by four zircon grains that produced, by using the conventional dilution technique, an indistinguishable age of 1332 ± 2 Ma.

Layered (ultra)mafic rocks of ‘Kabanga-Musongati-Kapalagulu Nickel Belt’ – Early geochronological data on rocks of the Songa ultramafic massif (Burundi) yielded a minimum K/Ar age of 900 Ma (Cahen et al. 1984). A provisional imprecise Rb/Sr age of 1236 ± 70 Ma, based on two phlogopite-calcite pairs in drill core of the Mukanda-Buhoro massif (Burundi) was reported by Tack et al. (1990). U–Pb zircon dating of mafic members of the above suite initially yielded an age of 1275 ± 11 Ma (Deblond & Tack 1999), but subsequently recalculated to 1370 Ma (Fernandez-Alonso et al. 2006). Maier et al. (2007) presented SHRIMP II U–Pb zircon ages, interpreted as magmatic ages, for the Kabanga North intrusion (1403 ± 14 Ma) and for the Kapalagulu intrusion (1392 ± 26 Ma). Although slightly older, the layered (ultra-)

mafic intrusives are considered to be part of the 1375–1380 Ma ‘Large Igneous Province’ of Tack et al. (2002a, 2002b, 2006a, 2008b, 2009, 2010, 2011a) or rather our NKIP.

The mafic to ultramafic bodies are surrounded by a contact-metamorphic aureole that, in places, is affected by a non-penetrative foliation, rarely even mylonitic in texture. Overall, these bodies are strongly tectonised with eastward dipping imbrication structures. A provisional and not very precise Rb/Sr age of mylonite from drill core near the Bururi intrusive (Burundi) has produced an imprecise age of 1095 ± 111 Ma, which may correspond with the D₂ tectonic phase (see below).

A-type granitoids – Preliminary Rb/Sr whole rock ages of 1125 ± 25 Ma and 1137 ± 39 Ma for granitoids of three different A-type plutons were reported by Klerkx et al. (1987). U–Pb zircon dating produced an emplacement age of 1249 ± 8 Ma (Deblond & Tack 1999). Lamprophyres, reported from three locations in Burundi, are supposedly genetically related to the alkali granite alignment (Deblond 1994). These A-type granitoids from Burundi have not been encountered in Rwanda and Uganda.

‘Tin’granites – Recently, ‘tin granite’ from the Kasika massif, Itombwe region in Kivu (DRC) has been dated (Tack et al. 2010). U–Pb zircon dating yielded a near-concordant group with a weighted mean $^{207}\text{Pb}/^{206}\text{Pb}$ age of 986 ± 10 Ma (MSWD= 1.40). Three zircons yielded near-concordant $^{207}\text{Pb}/^{206}\text{Pb}$ ages of 1885, 2068, and 1312 Ma, respectively, are interpreted as xenocrysts derived from pre-kinematic Kibaran granites and Rusizian basement. Tack et al. (2010) regard the $^{207}\text{Pb}/^{206}\text{Pb}$ age of 986 ± 10 Ma for the coherent, near-concordant group of seven analyses as the best estimate for the crystallisation age.

Rubaale pegmatite granite – U–Pb zircon dating (MC-LA-ICP-MS method) produced scattering age data with high common lead proportions. It is considered that the less discordant ages around 1.1 Ga showing the lowest common lead proportions give the best age estimate for the muscovite granite (UG-30_3675; Mänttäre 2014). In a $^{206}\text{Pb}/^{204}\text{Pb}$ vs. $^{207}\text{Pb}/^{204}\text{Pb}$ plot, most of the Pb data plot on a same line determining a robust isochron age of $926 + 35/-45$ Ma (n=20/22) that sets a minimum for the pegmatite age.

8.6 Geodynamic Evolution of the North Kibaran Belt

Tectonic setting of 'Kibaran granitoids' – All early investigators (e.g., King 1962) of the Ntungamo dome in southwestern Uganda (Fig. 6.3) reported an increase in grade of dynamo-metamorphism and intensity of schistosity in the Akanyaru-Ankole metasediments towards the underlying granito-gneissic bodies. Porphyroblasts of kyanite, staurolite, andalusite or chloritoid in the metasediments are reported to have formed posterior to the schistosity. The granitoids of the Ntungamo and similar domes in the NKB are described as well-foliated biotite gneisses with the lineation of the mica flakes parallel to the long axis in the central part of the Ntungamo dome. Foliation and schistosity in the gneiss margin zones are always parallel to the contact with overlying metasediments.

Nicholson (1965) concluded that two phases of deformation affected the granitoids and overlying metasediments of the Ntungamo dome. The first – D_1 – produced the parallel schistosity in granito-gneissic bodies and country rocks. During the second deformation phase, S_1 was folded into anticlines and narrow synclines, with the granito-gneissic bodies being structurally controlled and forming domes in the anticlinal cores. Good evidence of an intrusive character of the 'granito-gneissic' dome rocks was lacking then and Nicholson (1965) suggested that these 'mantled domes' represent deformed pre-Akanyaru-Ankole basement.

A similar increase in grade of metamorphism and deformation in sediments of the Akanyaru-Ankole Supergroup towards the contact with alleged 'Kibaran granitoids' is known from other parts of the NKB. S-type granitoids are often found in so-called arena-type massifs, in particular in eastern Rwanda, NW Tanzania and southwestern Uganda. Part of the confusion stems from a lack of field observations, in particular structural data and reliable geochronology. They have traditionally been considered as intrusive bodies (Klerkx et al. 1987), but as argued in Section 8.2., they are generally composed of a mixture of pre-Kibaran basement and 'Kibaran' granitoids.

The Mutare Massif in NE Rwanda (no. 4 in Fig. 8.2), described in Section 8.2, may serve to illustrate the above point. Its northwestern marginal segment in Uganda is composed of NKIP granite and yielded a mean $^{207}\text{Pb}/^{206}\text{Pb}$ age of 1330 ± 22 Ma (Buchwaldt et al. 2008). In the Rwandan part,

Sanschagrin & Mercier (1983) measured sub-horizontal foliation and common sub-horizontal microfolds with a fold axis direction of N135E, plunging 16° NW, corresponding with the directions measured in surrounding Akanyaru-Ankole metasediments. They emphasised the difference in metamorphic grade between the rocks of the Mutare dome and the Akanyaru-Ankole country rocks. The first have reached the upper part of the amphibolite facies with partial melting and rare sillimanite. The Akanyaru-Ankole sediments show progressive dynamo-metamorphism (not contact metamorphism) in the direction of the Mutara dome, going from almost nil to lower greenschist to lower amphibolite facies with blastesis of garnet and staurolite (Figs 8.4A and 8.9B). Similar observations have been made in western Rwanda in the Bisesero and Gikonkoro areas (Fig. 8.2). Although the metasediments may contain garnet, staurolite and sillimanite they have preserved their sedimentary protolith character. Windows of granito-gneissic rocks also have a strong tectonic control on N-S or NW-SE directed major shear zones (Westerhof 1980).

D_1 detachment faulting – In Rwanda and Burundi three S-planes are generally recognised in the metasediments of the Akanyaru-Ankole Supergroup. S_1 , the oldest one, is (sub-)parallel to the bedding (SS or S_0), which according to de Mulder & Theunissen (1980) manifested an early phase of isoclinal folding. Since S_1 appears restricted to the deeper levels of the Akanyaru-Ankole Supergroup, the above idea was quickly abandoned and Cahen & Theunissen (1980) attributed S_1 not to regional isoclinal folding but to deformation caused by horizontal movements (compressional overthrusting) near the footwall of the succession, parallel to the bedding. This allegedly caused, among others, mylonitisation of the basement along its boundary with the Akanyaru-Ankole cover during this phase of deformation. An alternative idea was that the preferred occurrence of S_1 in exposures near 'granitic intrusions' was related to the emplacement of syntectonic granitic sheets (Theunissen 1984). In a later publication, Theunissen (1988b) joined the first and second phase of deformation and proposed a model for the tectonic evolution of the NKB involving two major deformation phases: $D_{1,2}$ of co-axial thrust

and fold tectonics followed by D_2° NNW directed steeply inclined shear zones. The hypothesis is based on interpretation of SC mylonitic microstructures, their geometric relationship *vis-à-vis* fold structures and their relation with Kibaran metamorphism. A continuous and repetitive evolution of fold structures during phase D_{1-2} ranged between two extremes S (compressive) and C (shearing): when C predominated $D_{1(2)}$ deformation was active with minor fold structures.

A third alternative was postulated by Fernandez-Alonso & Theunissen (1998). They claimed that S_1 developed during a phase of detachment faulting (and the subsequent development of mantled gneiss domes) (Nicholson 1965, Westerhof 1980, Theunissen 1988b). The combination of extensional tectonics, with *décollement* of the (meta-)sedimentary cover over its basement (during D_1) and emplacement of bi-modal igneous rocks (Klerkx et al. 1987) is, of course, an attractive hypothesis since it elegantly combines related phenomena such as crustal extension, basaltic underplating, extensional tectonics and basin formation.

Cahen & Theunissen (1980) claimed that D_1 preceded the emplacement of G_1 granitoids with an age of 1370 ± 25 Ma. Based on analysis of the structural data and partly in line with ideas expressed in older publications (Nicholson 1965, Westerhof 1980, Theunissen 1988b, Fernandez-Alonso & Theunissen 1998), we postulate the following scenario: The phase of extensional detachment faulting post-dated emplacement of the NKIP dated at 1380–1375 Ma (Tack et al. 2009). The low-angle detachment fault zone corresponded with the contact between the (elastic-frictional) footwall of the Akanyaru-Ankole Supergroup and the underlying (viscous-plastic) pre-Kibaran basement. In extending crust, this zone is suspected to be relatively thin and occurs between ~10 and ~15 km (Bellot 2007 and references therein). Due to contrasting behaviour between upper cover and lower basement, their boundary is regarded as a zone where tectonic stresses are transferred and extensional strain concentrated, favouring the growth of detachment faults. Pre-existing lithologies (e.g., graphitic slates or evaporite, as possibly reflected by the presence of tourmalinites?; see Kanzira 1985) in the basal part of the Akanyaru-Ankole cover assisted in the differential behaviour of basement and cover together with hydrothermal alteration, concentrated in the detachment fault plane, in response to crustal extension and

channelling of mineralising fluids (large quantities of granite-derived fluids from the still hot igneous bodies of the NKIP and fluids of meteoric-metamorphic derivation) and fluid-rock interactions that produced softening and weakening reactions induced by alteration of K-feldspar and other minerals. Bellot (2007) claims that the role of mineralising fluids (fluid pressure) appears to be essential in promoting deformation within the brittle-ductile transition zone of the extending crust. Shearing along the detachment fault plane further produced extra heat resulting in an increase in metamorphic grade and the formation of garnet, staurolite and kyanite, now represented as a dynamo-thermal aureole along the contact of the base of the Akanyaru-Ankole metasediments and the underlying basement.

D_2 cylindrical folds – S_2 in the NKB is related to the formation of km-scale cylindrical folds in the Akanyaru-Ankole (meta-)sediments and heralds inversion of the north Kibaran trough and broadly E-W compression. S_2 is expressed as a crenulation cleavage in the lowermost part of the metasediments of the Akanyaru-Ankole Supergroup, where S_1 is well developed. Higher up in the sequence – where S_1 is absent or less obvious – S_2 is the only schistosity observed. In metapelitic rocks S_2 is generally parallel to the F_2 axial planes; in arenitic horizons S_2 forms an array of fracture cleavages (Theunissen 1988b).

In the Bisesero area, western Rwanda (Fig. 8.2), the following relationship between S-planes and metamorphic minerals could be established (Westerhof 1980):

| | |
|-----------------------|---|
| syn- S_1 : | quartz + muscovite \pm chlorite \pm garnet |
| syn- S_2 : | quartz + muscovite |
| tardi- to post- S_2 | quartz \pm biotite \pm chloritoid (\pm andalusite?) |

Geodynamic scenario – Since the 1980s, the ‘School of Tervuren/ Museum for Central Africa (MRAC)’ attempted to develop, step-by-step, a tectono-metamorphic-magmatic model for the Kibaran Belt. Cahen & Theunissen (1980) stressed the uniformity of the macrostructure of the N–S trending Kibaran Belt, from Shaba (Katanga, DRC) to Uganda, related to E-W compression. During the past two decades the generally accepted view was that although the South Kibaran Belt

(or Kibaran Belt s.s) and the North Kibaran Belt (NKB) appear perfectly aligned, they are considered as different though coeval orogenic belts with contrasting geodynamic models. The available structural, sedimentological, geochronological, geochemical and petrological data for the South Kibaran Belt (or Kibaran Belt s.s.) allegedly supported a convergent margin setting (Kampunzu et al. 1986, Rumvegeri 1991, Rumvegeri et al. 2004, Kokonyangi et al. 2004a, 2004b, 2005a), whereas an intracontinental inverted rift model was generally favoured for the NKB by the 'School of Teruren/ Museum for Central Africa (MRAC)'.

In the period 1980–2000 geodynamic analysis of the NKB was mainly based on the relationship between S-planes in the Akanyaru-Ankole cover sequence – S₁, S₂ and S₃ – metamorphism and the emplacement of granitoids – G₁, G₂ and G₃. Klerkx et al. (1984, 1987) envisaged a protracted, intracratonic orogenic cycle with successive extensional and compressional phases, characterised by the intrusion of pulses of S-type granitoids between ~1330 and 1180 Ma (whole-rock Rb–Sr dating). Pre-Kibaran planar structures, frequently with a NW-SE Rusizian (=Ubendian) orientation (e.g., Westerhof 1980), preserved as a fine to coarse foliation (gneissosity, coarse palaeosome-neosome banding) in rocks attributed to high-grade and migmatitic basement rocks were often neglected. Tack et al. (1994) proposed a model that involved delamination of continental lithospheric mantle and late-orogenic extensional collapse, based on petrological studies of A-type granitoids and mafic and ultramafic rocks, including two bulk zircon ages. Fernandez-Alonso & Theunissen (1998) advocated an intra-cratonic extensional detachment model, conditioned by strike-slip reactivation (Theunissen 1988b, 1989) of NW-trending shear zones in Palaeoproterozoic basement, timed according to the multi-phase framework of Klerkx et al. (1984, 1987). Thanks to superior geochronological and geochemical data and a satellite image-based synthesis (Fernandez-Alonso et al. 2007, Tahon et al. 2002) of the entire e-NKB, ideas referring to the geodynamic evolution of the NKB have matured significantly during the past two decades. The data support a 600 Ma-long history (~between 1.55 Ga and 0.95 Ga) for the NKB as an inverted rift, marked by the following prominent geodynamic phases:

- (1) Phase of crustal extension, basaltic underplating, basin development, emplacement of the

bimodal North Kibaran Igneous Province and D₁ large-scale detachment faulting.

- (2) Phase of basin inversion, D₂ folding and thrusting, resulting in crustal thickening and emplacement of the non- to poorly outcropping 'tin granites' (and associated pegmatites and quartz veins).
- (3) Phase of widespread strike-slip faulting along NNW to NNE directed steeply inclined fault planes.

Combining our new data from Uganda with the data from the NKB in mainly Rwanda and Burundi we advocate the following scenario:

Phase (1): Extension, Basin Development and Emplacement of the NKIP – Crustal extension, basaltic underplating and basin development supposedly started soon after culmination of the Eburnian Orogenic Cycle and peak-metamorphism and deformation in the Ubendian-Rusizian-Rwenzori Belt. This process was not continuous but eras of quiescence alternated with active extensional periods. Emplacement of the plutons of the Mubende-Singo Suite around 1.85 Ga ago and deposition of the molasse-type sediments of the < 2.05 – >1.85 Ga Namuwasa Group and < 1.85–1.79 Ga Bwezigoro Group are early manifestations. The centre of deposition shifted southward as manifested by deposition of 1.79 Ga tuffs in the basal portion of the platform deposits of the Bukoba Group (Kagera-Buhweju Supergroup). Detrital zircons from the basal part of the same Group show two age populations – 2.40–2.67 Ga and 1.85–2.02 Ga (Cutten et al. 2004) – and have obviously been derived, due to uplift and erosion, from older Archaean basement and juvenile Palaeoproterozoic Rwenzori(-Rusizian-Ubendian) rocks. The absence of detrital zircons younger than 1.85 Ga in basal quartzite indicated according to Cutten et al. (2004) that there was no detrital input from post-1.85 Ga lithologies, including the above rhyolitic tuff. This could either indicate that the quartzite was deposited prior to the 1.79 Ga volcanism, or that it was distal to the volcanic centre. Emplacement of the 1.57 Ga Chitwe and the 1.45 Ga Ntungamo plutons (Buchwaldt et al. 2008) manifest extensional phases of lesser importance.

Basin subsidence gradually shifted and accelerated southwestwards to the North Kibaran trough, an intracratonic rift with various sub-basins, hosting the thick (locally > 10 km), volcano-

sedimentary, predominantly clastic, shallow-water Akanyaru-Ankole Supergroup. Klerkx et al. (1984) already suggested that the rate of crustal extension is reflected by the rate of basin subsidence and, consequently, by the sedimentary column that fills the basin. The facies change in the Akanyaru-Ankole (former Burundi) sediments observed at the transition from the Cyohoha to Rugezi Group (formerly Byumba to Miyove Series) was considered significant. The lower and middle portions of the Akanyaru-Ankole sediments are described as mature, well-sorted mainly pelitic sediments. The sediments of the Rugezi Group, on the other hand, contain a larger proportion of arenites, conglomerates and (sub-)greywackes. They are poorly sorted with angular clastic grains and rock fragments, including rock fragments of the underlying sediments, indicating emergence and erosion of these sediments (de Mulder & Theunissen 1980, Dreesen 1980, 1981). These sediments are related to acceleration in crustal extension, accompanied by active rifting.

Extension in the North Kibaran trough culminated during a relatively short period between 1380 and 1375 Ma with the emplacement of the bimodal North Kibaran Igneous Province (NKIP), supposedly related to a thermal (mantle) anomaly (Tack et al. 2009), represented by abundant S-type, peraluminous granitoids and subordinate felsic volcanics (tuffs and lavas) and mafic rocks (mafic dykes and sills). Rhyodacite of the lower part of the Akanyaru-Ankole sediments yielded a poorly constrained WR Rb-Sr age of 1353 ± 46 Ma (Klerkx et al. 1987). The same event is manifested by the emplacement of layered (ultra-)mafic intrusives dated at 1403 ± 14 Ma and 1392 ± 26 Ma (Maier et al. 2007) in the Transition Zone, while potent mafic sills and dykes in the Kagera-Buhweju Supergroup and nearby lithologies of the Rwenzori Belt yield hornblende and plagioclase Ar-Ar ages ranging between 1340 and 1380 Ma (Deblond et al. 2001) and a Sm-Nd age of 1368 ± 41 Ma (Mäkitie et al. 2014c).

SHRIMP age determinations (Cutten et al. 2004) on detrital zircons in a quartzite sample from the basal part of the Gikoro Group of the Akanyaru-Ankole Supergroup show two populations: (1) an oldest and very prominent 2.73–2.48 Ga peak, possibly derived from the Archaean Tanzanian and/or Congo Cratons, and (2) a limited input from a 2.07–2.01 Ga population, derived from juvenile rocks in the Rwenzori-Rusizian-

Ubendian Belt. The youngest detrital zircon of 2.01 Ga defines its maximum age of deposition. Another quartzite sample shows a different provenance pattern and has three zircon populations: (1) encompasses a scatter of zircons with ages of 2.79–2.58 Ga derived of Archaean Craton(s), (2) comprises a prominent ‘Eburnian’ population with 2.07–1.75 Ga ages, and (3) is a small (5%) component of ~1.41 Ga magmatic zircons. Cutten et al. (2004) call the latter zircon population ‘noteworthy’ but refrain from speculating on their origin. We postulate that they are derived from coeval volcanic intercalations in the sedimentary succession, which constrain a maximum age of sedimentation for the uppermost part of the basal Gikoro Group in the Akanyaru-Ankole Supergroup, slightly older than the emplacement of the NKIP.

Emplacement of the NKIP is followed by some smaller scale igneous events, including the later intrusion (1368–1328 Ma) of S-type, peraluminous granitoids in southwestern Uganda (Buchwaldt et al. 2008). Small bodies of A-type granites in the Transition Zone, dated at around 1210 Ma, were originally considered to represent differentiates of nearby mafic and ultramafic layered intrusions of the ‘Kabanga-Musongati-Kapalagulu Nickel Belt’. As mentioned, the latter have recently been dated at 1.4 Ga, pene-contemporaneous to the intrusion of the S-type granitoids of the NKIP, and close to 100 Ma older than previously thought (Tahon et al. 2004). The new geochronological data demonstrate that the relatively small A-type granitic batholiths were emplaced some 160 Ma after the (ultra-)mafic layered intrusives and a genetic relationship between the two is very unlikely. Emplacement of A-type granites is ~ coeval with emplacement of a younger generation of Mesoproterozoic dykes in the Bukoba Group that yielded plagioclase and hornblende Ar-Ar ages of 1282 ± 5 Ma.

Phase (2): Basin inversion, folding and thrusting – S₂ in the NKB is related to the formation of km-scale cylindrical folds in the Akanyaru (meta-)sediments and heralds inversion of the north Kibaran trough and broadly E-W compression. The fold pattern of the Akanyaru (meta-)sedimentary cover is not uniform. Wide anticlinoria alternate with narrow synclinoria. Although generally striking N-S, fold axes may locally assume different directions (NW-SE or NE-SW or even E-W). Difference in vergence is also observed. We postulate that, due to rheological differences, cover and basement

did not behave identical during this event. Crustal shortening in basement was mainly by reverse faulting along the previously formed listric normal faults. The cover succession of the Akanyaru Supergroup behaved in a rather passive way, draping over the underlying fault blocks – with a rhombhorst geometry (see Tahon 1997) – composed of pre-Kibaran basement and sheets (> 1 km in thickness) of NKIP granitoids. This explains the presence (e.g. in SE Rwanda) of strongly deviating F_2 fold axes. In other locations décollement between cover and basement is evident by reactivation of the older detachment plane. The Gakoma megastructure in western Rwanda is a décollement or detachment fold structure formed during a dextral strike-slip movement along the Mwogo fault.

The timing of this compressional folding event is debated. Klerkx et al. (1987) claimed that the mainly NNE-SSW-directed upright folds (D_2) formed around 1180 Ma and NNE-SSW to NNW-SSE shearing around 1100 Ma (D_2). A provisional and not very precise Rb/Sr age of mylonite from drill core near the Bururi intrusive, belonging to the 'Kabanga-Musongati-Kapalagulu Nickel Belt' in Burundi has produced an age of 1095 ± 111 Ma. De Waele et al. (2008) claim that compressional events only occurred along the edge of the proto-Congo Craton at 1.0 Ga in the Irumide Belt of Zambia (as part of the shaping of the Rodinia Supercontinent). These compressional events resulted in the morpho-structural shaping of the NKB (and the Kibaran Belt *s.l.*), as a far-field effect of the Irumide Orogeny in Zambia accommodated by transfer along the Ubendian shear belt (Tack et al. 2008b). Post-compressional relaxation gave rise to the emplacement of the 'post-Kibaran tin granites' and associated pegmatite bodies and quartz veins of the Sn-Nb/Ta-W metallogenic province. The 'tin granites' have been dated at 980 ± 8 Ma, the pegmatites at 968 ± 8 Ma and cassiterite veins at 951 ± 18 Ma (Brinckmann et al. 2001), which is confirmed by a new SHRIMP-age of 'tin-granite' of 986 Ma (Tack et al. 2010). U-Pb dating of columbite from two pegmatite bodies from Kivuvu and Ruhembe in NW Burundi yielded crystallisation ages of 962 ± 2 Ma and $968+33/-29$ Ma, respectively (Romer & Lehmann 1995) and confirm earlier interpretations of Rb-Sr data.

Poorly constrained lower intercept ages at 628 ± 110 Ma and 622 ± 56 Ma are interpreted to reflect Pan-African brittle reworking (see below) of the

pegmatite bodies when Au and Bi were redistributed and secondary sericite formed in fractures.

Phase (3): Transtensional Shearing – S_3 is expressed as a local crenulation cleavage, particularly developed near N-S directed shear zones. Similar shear zones in pre-Kibaran granito-gneisses of the 'Bisesero Complex' (Fig. 8.2) show as strongly weathered schistose rock composed of kaolinite and sericite (Westerhof 1980). The igneous fabric in these zones has been completely destroyed but granitic enclaves have been preserved in places. These shear zones further contain dykes, veins, nests and *Schlieren* of kaolinised pegmatite or tourmaline-rich quartz veins. Mylonite-textured shear zones in granitoids may also be enriched in graphite, quartz, tourmaline and ferruginous material. In places they are strongly anomalous in U and show slightly higher Au background values.

Detailed mapping in the Gikonkoro area (southern central Rwanda, Fig. 8.2) highlighted a huge shear zone invaded by multiple (sub)parallel quartz veins and veinlets (Westerhof 1979). The curvilinear shear zone has a N-S orientation (with numerous NW-SE *en echelon* off-shoots), discordant with respect to the NW-SE foliation in the country rock. This system of quartz veins can be followed over more than 10 km along strike. In section the shear zone is generally less than 100 wide and composed of an alternation of thick massive quartz reefs that alternate with thinner and sheared quartz veins, phyllonite and country rock. Phyllonite is very rich in white mica and grades into sheared granitic gneiss, which, in turn, may grade into normal granite gneiss. The micaceous phyllonite is interpreted as a mylonitised and retrograde country rock with feldspar largely kaolinised and quartz migrated to low pressure zones now occupied by quartz veins (tectonic differentiation). The quartz veins exhibit a N-S lineation, dipping between 38° and 50° S, that remains the same over several kilometres along strike. Locally, the quartz veins are rich in iron oxides and hydroxides (magnetite, hematite, goethite). Uranium mineralisation coincides with one of the NW-SE *en echelon* fault gashes where Fe (hydr)oxides predominate over quartz and form a sort of macro-myrmekitic intergrowth. Scintillometry readings suggest local uranium contents of several hundreds of ppm. Association with the quartz-flooded shear zone suggest formation by lateral secretion with the country rocks as the source of the uranium.

Traditionally, this phase (3) of transtensional shearing has been attributed to a late Kibaran phase of strike-slip; transpression and/or transtensional shearing along N-S directed fault planes and zones. Subsequent and repeated rejuvenation of these fault planes and zones is widely accepted (Fernandez-Aloso et al. 2009). Dating of muscovite (Rb-Sr) from the alteration zone of tin-tungsten mineralisation yields an typical 'late Kibaran' age of 936 ± 82 Ma. K-Ar dating, however, gives an age of 840–780 Ma, suggesting a late tectonodynamic event (Brinckmann 1988). Gérards & Ledent (1976) described Pan-African isotopic rehomogenisation in the North Kibaran Belt and Liégeois et al. (1982) have dated one such phase of rejuvenation and reported an early Pan-African age of ~700 Ma. Tack et al. (2009) advocate that, due to the fact that the Archaean Tanzania Craton acted as an indenter, a new compressional event affected the NKB as a far-field effect of the East African Orogen. This caused, among others, the isotopic resetting and post-compressional emplacement of late Pan-African Au mineralisation in the NKB. In Burundi two types of primary gold mineralisation are described by Brinckmann (1992) and Brinckmann et al. (1994): sulphide vein assemblages with gold related to post-Kibaran G4-granite magmatism (900–1000 Ma) and Pan-African ferruginous breccia zones with gold dated around 640 Ma. Monazite from these breccia zones has a Pan-African U-Pb age of 535 ± 2 Ma, pointing to a period of rapid uplift, rifting and high heat flow for this time (Brinckmann et al. 2001). This strong discrete N-S Pan-African overprint in the NKB has generally been under-estimated or even overlooked.

Suture between Tanzania and Congo Cratons in the NKB – Archaean subcontinental lithospheric mantle (SCLM) is far thicker than Proterozoic SCLM and the border zone between the two is a preferred location to emplace large mafic and ultramafic bodies. The early Jurassic Karoo basalts along the eastern border of the Kaapvaal Craton, along the frontier between South Africa and Mozambique,

are a well-known example. It is therefore tempting to view the curvi-linear listric fault system that hosts the 'Kabanga-Musongati-Kapalagulu Nickel Belt' in the Transition Zone (Figs 8.2 and 8.23) as the obvious boundary between the Archaean Tanzania Craton and Palaeoproterozoic Ubendian (= Rusizian/Rwenzori) basement.

As described in Section 8.4, Kibaran granitoids in southwestern Uganda belong to two clans that we have called 'Older Kibaran Granites' and granitoids of the NKIP, emplaced at 1568–1443 Ma and 1368–1328 Ma, respectively (Buchwaldt et al. 2008). The older granites have $\epsilon\text{Nd}(t)$ values of -20.1 to -23.1 and Nd mean crustal residence ages, based on a depleted mantle model, from 3.84 Ga to 3.52 Ga while the younger granite batholiths show lower $\epsilon\text{Nd}(t)$ values of -10.1 to -14.0 and Nd mean crustal residence ages from 3.06 Ga to 2.86 Ga. Both generations of granitoids thus appear to be sourced in Archaean crust, with the contribution of juvenile Palaeoproterozoic crust being minimal. Buchwaldt et al. (2008) suggested that the distinct geochemical, geochronological and isotopic characteristics and the unrelated geological evolution reconstructed from these data strongly implies that the two now adjacent 'Older Kibaran Granites' and granitoids of the NKIP were geologically unrelated crustal packages prior to high grade metamorphism and, as such, represent "suspect terranes" which were most probably brought together during a middle Proterozoic collision event. We postulate that these terranes are not 'suspect' at all, but represent segments of two different crustal fragments of the proto-Congo Craton, one belonging to the Tanzania Craton and the other supposedly the hidden southern extension of the Bomu-Kibalian Shield. The Palaeoproterozoic suture between these two terranes is provisionally indicated by the purple line in Figure 8.2, some 50 km further westwards of the 'Kabanga-Musongati-Kapalagulu Nickel Belt', and apparently remobilised as an important, curvi-linear, Kibaran strike-slip fault. This leaves very little space, if any, for post-Archaean SCLM in the realm of the e-NKB.

9 ROCKS OF THE LATE MESOPROTEROZOIC MADI-IGISI BELT

9.1 Introduction

As described in Chapter 8, the Kibaran Belt of central Africa can be correlated with the worldwide Grenvillean Orogenic Cycle, comprising a long interval of post-Eburnian extension followed by Grenvillean compression, culminating with the formation of the Rodinia Supercontinent (~1.00 Ga). In Uganda, this is mimicked by post-Rwenzori extension, followed by Kibaran compression (~1.10–1.00 Ga), known in Africa as the Lomanian Orogeny (Pohl 1987b). In the North Kibaran Belt of southwestern Uganda and central Africa, this event coincided with or immediately post-dated the emplacement of the so-called ‘tin granites’ at ~1.1–~1.0 Ga and fertile pegmatite bodies (Sn, Nb, Ta, Li), supposedly derived from these ‘tin granites’, at ~0.95 Ga (Romer & Lehmann 1995).

Coeval with Grenvillean/Lomanian compression, the Madi-Igisi Belt was formed, which originated as a south-propagating strike-slip rift system, broadly coeval and comparable to the (~950 Ma) volcano-sedimentary Koras-Sinclair-Ghansi Belt of eastern Namaqualand and Namibia described by Thomas et al. (1994), signalling the end of the Grenvillean cycle in Africa. The Madi-Igisi Belt is a newly identified, intracratonic N–S-trending

double-verging thrust and fault zone, which separates the North Uganda Terrane from the West Nile Block, the easternmost segment of the Bomu-Kibalian Shield. Although closely associated with the conclusion of the Grenvillean/Kibaran cycle in Africa, we will describe it as a separate late Mesoproterozoic to early Neoproterozoic tectono-thermal terrane.

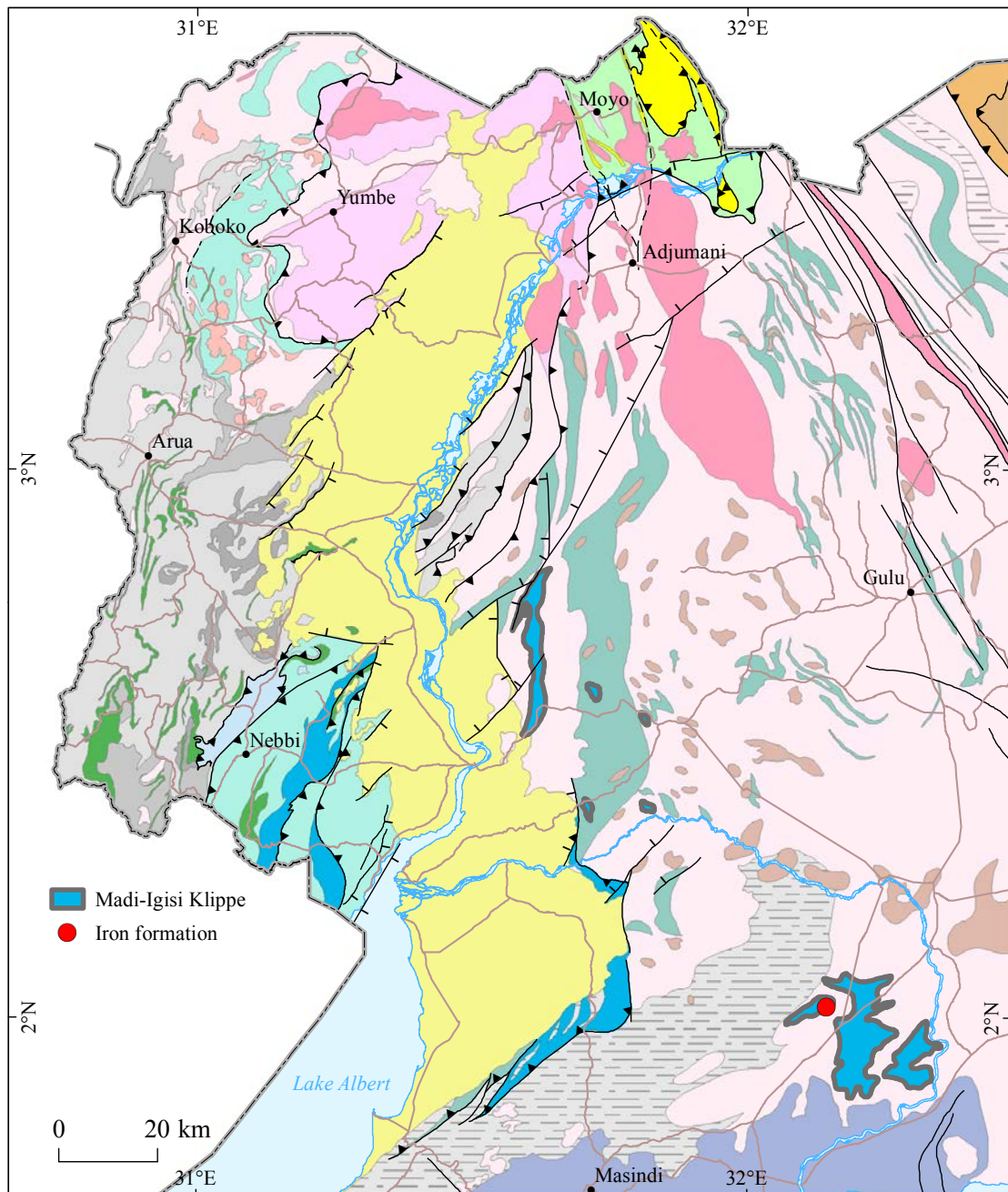
The belt comprises juvenile ~1.0 Ga lithologies and thin-skinned stacks of reworked Archaean rocks, including the Yumbe duplex structure, the lithologies of which have been discussed in Section 4.7. They were first described as ‘Mirian’ in the West Nile Province (Table 4.1) by Hepworth & Macdonald (1966). Based on our field observations and new geochronological data (Mänttari 2014), we associate these ‘Mirian’ rocks of the West Nile Province (Fig. 4.2) with similar supracrustal rocks in the northern Moyo District, including rocks formerly known as ‘Madi Series’ (DGSM 1966) (Fig. 4.2), and rocks of the Igisi belt in the Masindi area (Fig. 5.2). As a consequence, we have assembled all ~1.0 Ga juvenile rocks of the Madi-Igisi Belt in the Mirian Supergroup, divided into the Madi and Igisi Groups.

9.2 Lithostratigraphy of the Madi Group

A remarkable rock assemblage composed of intermediate metavolcanic rocks, quartzites and metapelites assigned to the Madi Group (Table 9.1) characterises the eastern Moyo District and marginally extends into the northernmost portion of the Adjumani District, but does not occur elsewhere in northern Uganda (Fig. 9.1). According to Combe (1946), the Madi Group metasediments in the eastern Moyo District continue into present South Sudan. In northern Uganda, they rest conformably on what was formerly called ‘tonalite gneiss’, named here Metu metatuff. Before this mapping project, the poorly banded Metu metatuff was not separated from nearby banded Archaean basement gneiss. The new geochronological data, yielding an age of 984 ± 8 Ma for dacitic metatuff (Mänttari et al. 2011, Mänttari 2014), separates it from the nearby Archaean gneisses. This equally explains the well-documented structural contrast

between metatuff and basement gneiss. In this context, it should be noted that the Madi Group metasediments and the Metu metatuff record a common structural and metamorphic history. The <1.0 Ga age of Madi metasediments has been confirmed by U-Pb zircon dating of detrital zircons (Mänttari 2014).

Dacitic metatuff (P2MdmT) (984 ± 8 Ma) – Metatuff of the *Metu Formation* is a homogeneous grey coloured, fine-grained rock, composed of quartz + plagioclase + biotite \pm K-feldspar, occasionally with thin quartzo-feldspathic segregations and aligned biotite (Fig. 9.2A). Chemical composition of these rocks refers to rhyodacites (see App. 2., anal. 144–149). The minimal variation in composition and the occurrence of a single population of ‘plutonic’ zircons (Mänttari 2014) indicates an effective and continuous supply of material from



Cenozoic rocks (– 66 Ma)

Albertine Rift: silt, sand, gravel

Neoproterozoic rocks (541 – 1000 Ma)

Bunyoro Group; shale, slate, phyllite, sandstone, quartzite

Adjumani-Midigo Suite; granite (659±15 Ma)

Gneissic granitoid

West-Karamoja Group; gneiss, granulite

Mesoproterozoic rocks (1000 – 1600 Ma)

Madi Group; quartzite, mica schist

Madi Group; intermediate metavolcanic rock (984±8 Ma)

Igisi Group; mica schist, quartzite, ironstone

Neoaarchaeon rocks (2500 – 2800 Ma)

Abiba Formation; leuco- to mesocratic gneiss

Metagabbro

Variable gneissic granitoid (2591±27 Ma; 2652±8 Ma)

Tara brown granite (2622±5 Ma)

War Group; mafic metavolcanic rock, fuchsite quartzite (2637±16 Ma)

Lobule Group; granulite gneiss, amphibolite (2631±6 Ma)

Granulitic granitoid and gneiss

Yumbe Complex; granitic and sedimentary gneiss

Amuru Group; gneiss, amphibolite

Mesoarchaeon rocks (2800 – 3200 Ma)

Karuma Group; felsic and mafic granulite

Goli charnockitic gneiss (3079±14 Ma)

Granite gneiss

Uleppi Group; leucocratic gneiss and granulite

Structural elements

-- Fracture

┆ Normal fault

— Strike slip fault

▲ Thrust fault

Fig. 9.1. Geological outline of the Madi-Igisi Belt, northwest Uganda.

Table 9.1. Subdivision of the Madi Group (Miriam Supergroup). The codes refer to lithological units in the unpublished 1:250 000 scale geological maps of DGSM.

| Group | Formation | Lithology | Code |
|-------|-----------|--|--------|
| Madi | Oloro | Layered anthophyllite rock | P2Mlar |
| | Gweri | Marble, anthophyllite rock intercalates | P2Mma |
| | Leya | Metabasalt | P2Mmb |
| | Metuli | Mica schist | P2Mms |
| | Kungi | Quartzite and calc-silicate quartzite | P2Mqzc |
| | Apipi | Quartzite intercalated with mica schist | P2Mqzs |
| | Anuurapi | Quartz-muscovite schist ($\leq 977 \pm 9$ Ma) | P2Mqms |
| | Ovuvu | Quartzite | P2Mqz |
| | Metu | Dacitic metatuff (984 ± 8 Ma) | P2Mdm |

a single source, here interpreted as confirming a pyroclastic origin of these rocks.

Overbank sediments of the Nile River cover the footwall contact of the Metu metatuff with the underlying Archaean gneisses. We speculate that this footwall contact is a north-dipping thrust surface of a south-verging thrust mass originating from South Sudan, comprising the entire Madi Group. As can be observed in the northernmost corner of the Moyo District, the Metu metatuff not only occurs below the quartzite, but also above (Fig. 9.4). We do not interpret the quartzite as an intercalation in the metatuff, but view the repetition as being due to tectonic stacking. A distinctive, even diagnostic feature of the Metu metatuff is the well-developed regional lineation plunging gently to the NNW, a feature that also has been widely observed in the quartzites. The lineation is interpreted

ed to be due to intersection between a generally flat (composite) schistosity (S_1) and a subsequent sub-vertical to west-dipping axial plane fabric (S_2), related to open folds (Fig. 9.3).

A well-exposed section of stacked Metu metatuff and overlying quartzite can be viewed at Ovuvu village, NE of Adjumani town, on the south bank of the Nile River. The tectonic contact with quartzite can be best described as a transitional thrust zone comprising a mixture of lithologies, measuring between a few decimetres to a couple of metres. The contact zone is parallel to the bedding of the quartzite. Close to the overthrust contact, in a zone measuring a few metres in thickness, quartzite has turned into flagstone. Directly below the overthrust contact, the underlying Metu metatuff shows a more pronounced schistosity compared to the same rock a few tens of metres below the

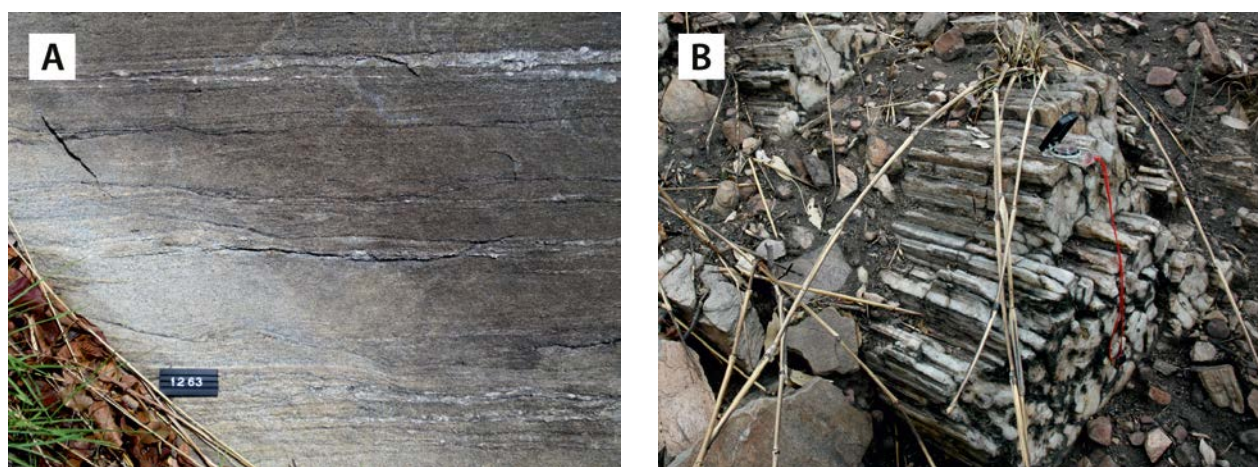


Fig. 9.2. (A) Dacitic metatuff of the Metu Formation, Ara village, at the foot of the Ilwo Mountain, with a swarm of segregated quartzo-feldspathic veins (378865E / 403913N). Number tag 8 cm. (B) Quartz rods (intersection of S_1 and S_2) developed in a thick quartz vein in rather massive, non-sheared Metu metatuff, located a few tens of metres below the sheared, conformable contact against the overlying quartzite. Oiji Hill, Ovuvu village (383371E / 384410N). Compass black cover 7 cm.

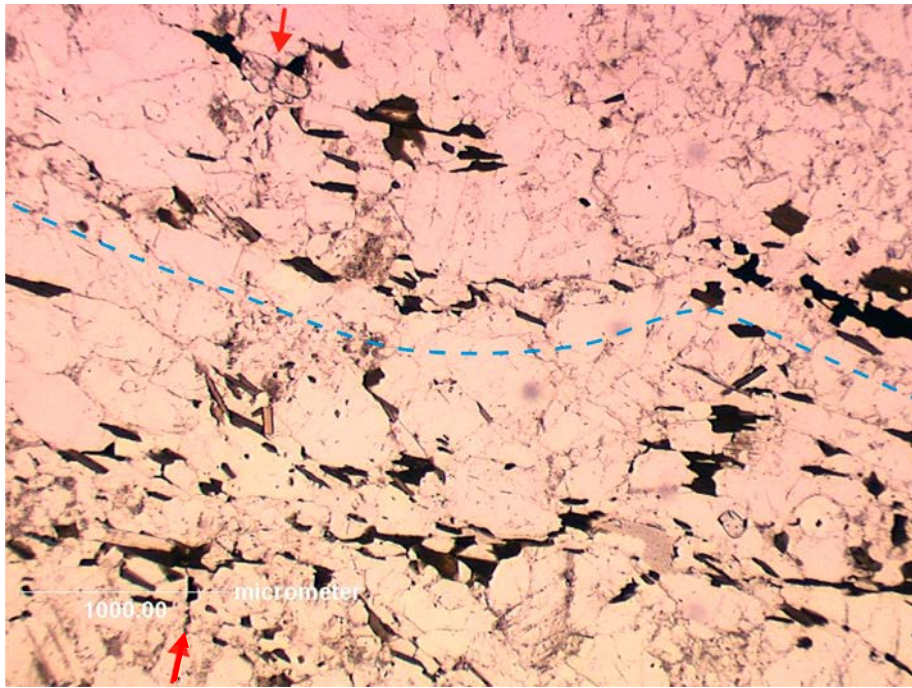


Fig. 9.3. Microphotograph of Metu metatuff (plane-polarised light) showing schistosity formed by parallel stringers of biotite, composing an early S_1 fabric that predates the small biotite flakes seen at small angle to the former. The subsequent small-scale open crenulation (blue line) of the biotite flakes represents the subvertical axial plane fabric causing the intersection lineation. The thin localised biotite fabric (red arrows) associated with the axial plane of the crenulation likely contributes to the visual aspect of the intersection lineation seen in outcrops. The subvertical fabric is an axial plane feature of folds seen at all scales in the area, including the wide arcuate southern margin of the Metu Mountains. The area covered by the image is 4 mm in width. Metu village (367354E / 401965N).

overthrust. The tabular shapes of metatuff layers are due to the sub-parallel arrangement of original bedding (S_0) and schistosity (S_1), which is, in turn, always parallel to the overlying metatuff-quartzite thrust contact and the bedding and schistosity of the quartzite.

The regional lineation, formed by the intersection of S_0 and the sub-parallel S_1 with a high-angle, subvertical to west-dipping S_2 , is ubiquitous, both in the metatuff and in the quartzite. Where these S-planes penetrate voluminous early quartz veins, spectacular quartz rods are formed. The long axes of these rods are parallel to the lineation (Fig. 9.2B).

Quartzite (P2Mqz) – The highest ridges and summits of the Metu Mountains are composed of thick quartzite layers of the *Ovuvu Formation*. They form spectacular mountainous landmarks in the Moyo District and border the southern arcuate margin of the Metu Mountains (Figs 9.4A, 9.5).

Bedding in the hard, nearly pure, white-coloured, fine- to medium-grained quartzite is expressed as variation in grain size and by a tendency of splitting into 10–50-cm-thick slabs. Sedimen-

tary features have not been observed. Penetrative deformation is visible only in outcrops close to the Metu metatuff contact or in the thrust zone between the two units, where the rock has turned into flagstone (Fig. 9.6A). Thin muscovite-rich laminae, usually between pure quartz layers, manifest original sedimentary bedding. These mica laminae are supposedly derived from clay particles deposited from suspension during lulls of low energy in the water body.

The solid, white and hard quartzite layers contain tiny muscovite flakes in thin section, marking a modestly developed planar fabric. As with other rocks in the area, the thin muscovite-rich laminae between solid quartzite layers exhibit a distinct lineation, gently plunging to the NNW. A crenulation with a roughly ENE trend has occasionally been observed and is the youngest structural feature, supposedly Pan-African in age.

Quartzite in the Moyo and Adjumani Districts shows mostly sub-horizontal to moderate dips. West of the Metu Mountains, west of Moyo town, the quartzite, usually together with quartz-muscovite schist, occurs in the narrow, 50–200-m-wide, Erra ridge (Combe 1946), which continues

for almost 20 km southwards from the South Sudanese border to the bank of the Nile River. This quartzite-schist assemblage is in a vertical position and appears squeezed between two blocks of Metu metatuff. Analogous narrow vertical quartzite bands have been encountered along the western flank of the Metu Mountains, east of Moyo town. Google Earth satellite imagery and aerogeophysical maps reveal that the narrow vertical quartzite-schist bands separate crustal fault blocks with dif-

ferent regional structural trends. Therefore, it is suggested that Madi Group quartzites and quartz-muscovite schists have been dragged into the steep fault zones in between the crustal blocks. This style of tectonism is in strong contrast to the dominant earlier phase of subhorizontal Madi tectonism, characterised by imbrication structures in the Metu Mountains and is, similar to the ENE crenulation cleavage (above), attributed to the Pan-African Orogenic Cycle.

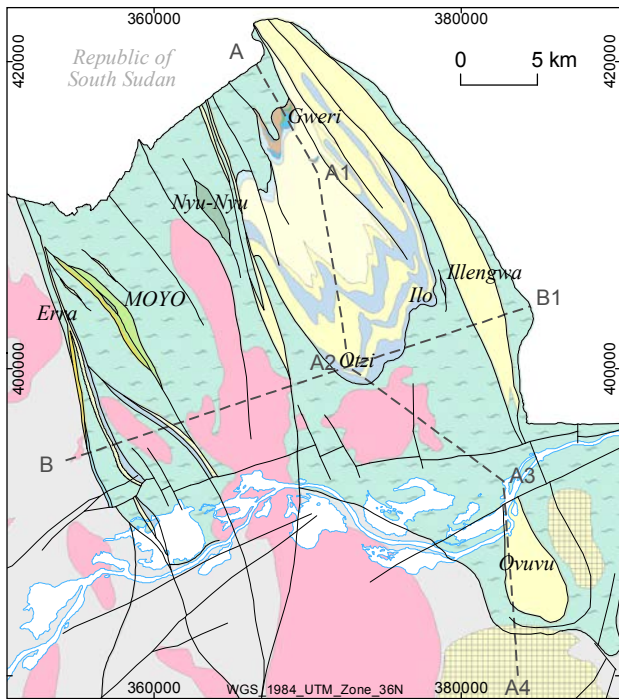


Fig. 9.4. Sections illustrating the tectonic structure within the late Mesoproterozoic Madi Group in the Moyo and northern Adjumani Districts. The map shows the location of sections A and B. (A) The section shows the current order of strata after thin-skinned thrusting from the north. Note that the metatuff below the quartzites is repeated above the quartzites at the South Sudanese border, where the thrust sheet also carries metabasalt and marble. (B) Subsequently, a different style of tectonism followed, which was active only at the west of the Metu mountains. This resulted in crustal segmentation with narrow, vertical to steep fault blocks. This N-S-running zone continues southwards to Pakwach – Lake Albert, where it appears as a flower structure involving Archaean rocks and Igisi metasediments.

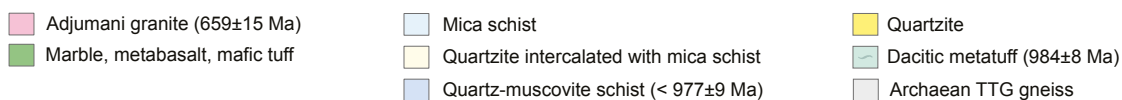
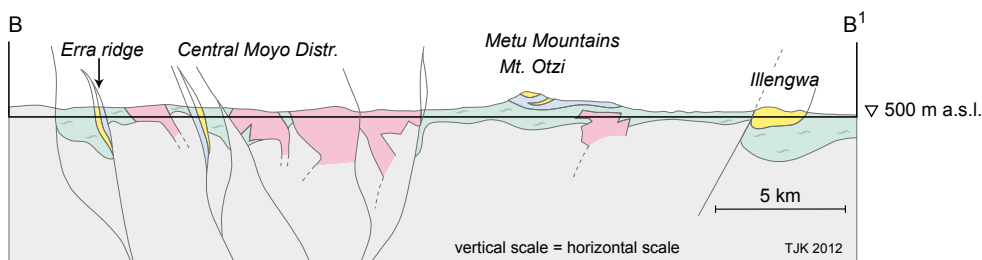
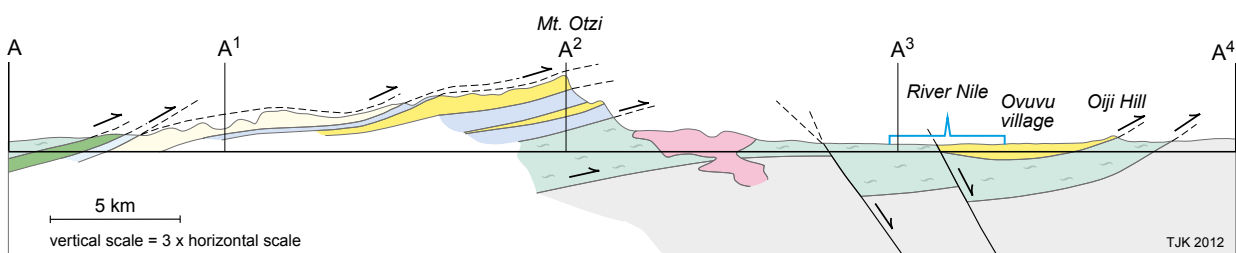




Fig. 9.5. Massive quartzites of the Madi Group form the backbone of the Metu Mountains. The view is westwards from the western cliff of Mt. Otzi, one of the landmarks in the Metu Mountains (371784E / 400943N). The Moyo highland is in the background and the rift shoulder is seen on the left. Dr Tapio Koistinen making notes, accompanied by Police Inspector Ignatius Dragudu, Moyo District.



Fig. 9.6. (A) Flagstone quartzite (373981E / 405274N). A fracture cleavage has developed between the layers, but also at low angle to the layering. Number tag 8 cm. (B) A tight fold in quartzite, with thickened hinge and thinned limbs, on top of the Erra-Nile ridge (359398E / 390815N).



Fig. 9.7. Quartz-muscovite schist at the sampling site of the dated sample, west of Laropi village (359388E / 390894N). Number tag 8 cm.

Quartz-muscovite schist (P2Mqms) ($<977 \pm 9$ Ma) – Quartz-muscovite schist of the *Anyurapi Formation* occurs together with or intercalated in quartzite. Together, the quartzite and quartz-muscovite schist form a voluminous package in the Metu Mountains. The coarse-grained rock consists of large, deformed muscovite flakes (Fig. 9.7) in a quartz-muscovite mixture with subordinate biotite and minor plagioclase and opaque. Quartz may occur as lenticular segregations. Perhaps the largest exposures of quartz-muscovite schist are found below the layer of orthoquartzite along the southeastern limb of the ‘horseshoe structure’ in the Metu Mountains, north of the Nile River, as shown in Fig. 9.4. Three chemical whole-rock analyses of these rocks are presented in Appendix 2 (anal. 150–152).

Quartz-muscovite schist from a vertical narrow crest in between fault blocks may contain small crystals of kyanite, prompting a resemblance with kyanite-muscovite-biotite schists of the Igisi Group at Murchison Falls. In Erra village, about 20 km to the north along the same ridge, the schist is sillimanite-bearing. U-Pb dating of detrital zircons from this location yielded a concordia age of 977 ± 9 Ma with Pan-African overprinting at 660 Ma (Mänttari 2014).

Quartzite intercalated with mica schist (P2Mqzs) – A wide inaccessible area in the central Metu Mountains remains rather poorly investigated. We can conclude, however, that when approaching the area from the south, the proportion of mica schist intercalations in the quartzite increases. In contrast with

the quartz-muscovite schist unit described above (P2Mqms), rocks of the *Apipi Formation* are greyish coloured, finer grained, richer in biotite, but without the large muscovite flakes with a ‘silvery’ lustre. The rock also contains tiny garnets (Fig. 9.8).

Boulders rich in iron oxide have been hand-picked in the past in this area for traditional small-scale iron smelting. One such old hand-picking site is located at observation station 1232 (373351E / 407931N), where magnetic ‘iron ore’ blocks were embedded in down-drifted accumulations of laterite in the bottom of a small river channel. The source of these Fe-oxide blocks must be iron-bearing layers within the quartzite-mica schist assemblage somewhere nearby, but have not yet been located.

Quartzite and calc-silicate quartzite (P2Mqzc) – A horizon of calc-silicate quartzite of the *Kungi Formation*, some tens of metres thick, forms a NW-trending ridge north of the Nile River. The nature of its hanging wall contact is unknown, but the footwall of the unit grades into quartz-muscovite schist of the *Anyurapi Formation*. Calc-silicate quartzite is a brown to brownish grey, medium-grained, compositionally banded rock, often showing distinctly grooved weathering patterns (Fig. 9.9A). In places, tight to isoclinal folds can be observed (Fig. 9.9B). In thin section, calc-silicate quartzite is a granoblastic rock with grain sizes ranging between 1 and 5 mm, predominantly consisting of quartz, feldspar, diopside, epidote, carbonate and tremolite, the latter in well-aligned fibres or aggregates up to 10 cm in length.



Fig. 9.8. Close-up photo of bedded biotite-bearing mica schist, with small garnet crystals, in a thick intercalated layer in Apipi quartzite (370682E / 403068N).

Mica schist (P2Mms) – Outcrops of mica schist of the *Metuli Formation* were observed near marble pits, some 6 km NE of Metuli village. The schist is found in close proximity to anthophyllite-bearing rocks and marbles. In addition, a 30-m-thick sequence of muscovite schist is visible in a valley at observation site 14729.

Metabasalt (P2Mmb) – Highly weathered, chocolate-brown coloured metabasalt of the *Leya Formation* is exposed in the eastern hillside (368547E / 416767N) below marble pits, 6 km NW of Metuli village. The hanging wall contact is not exposed, but the attitude of marble layers suggests that the mafic rock is stratigraphically below the marble. Fresh metabasalt is mostly found as *in situ* boulders.

Marble, anthophyllite rock intercalates (P2Mma) – Dolomite marble with amphibolitic intercalations of the *Gweri Formation* is found 6–9 km south of the northernmost extreme of the Moyo District, ca. 5 km NE of Metuli village. Small artisanal quarries and a small mill occur in the area. The outcropping marble is a thin- to medium-bedded rock with brownish or dark weathering surfaces (Fig. 9.10). Small marble outcrops are distinguished by their specific weathering effects, characteristic of many marbles and other carbonate-bearing rocks. The marble does not appear as a single, uniform layer in the area. Only the thickest layers have been quarried, while there are also numerous interlayers of marble within the adjacent layered silicate rocks, comprising a mixture of micaceous schist and layered amphibolitic schist.

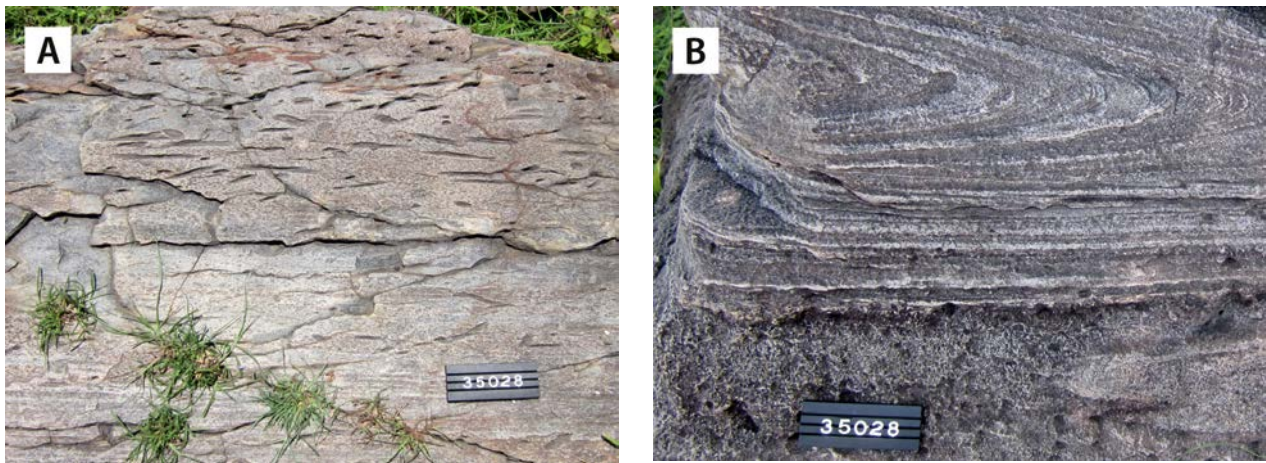


Fig. 9.9. (A) Well-oriented tremolite prisms (393240E / 363826N) in quartzite. (B) Isoclinal fold in calc-silicate quartzite (393240E / 363826N). Number tag 10 cm.



Fig. 9.10. Layer of marble in layered amphibole-rich rock; note the block-shaped boudins of brittle amphibolite rock, without necking (368547E / 416767N). Number tag 8 cm.

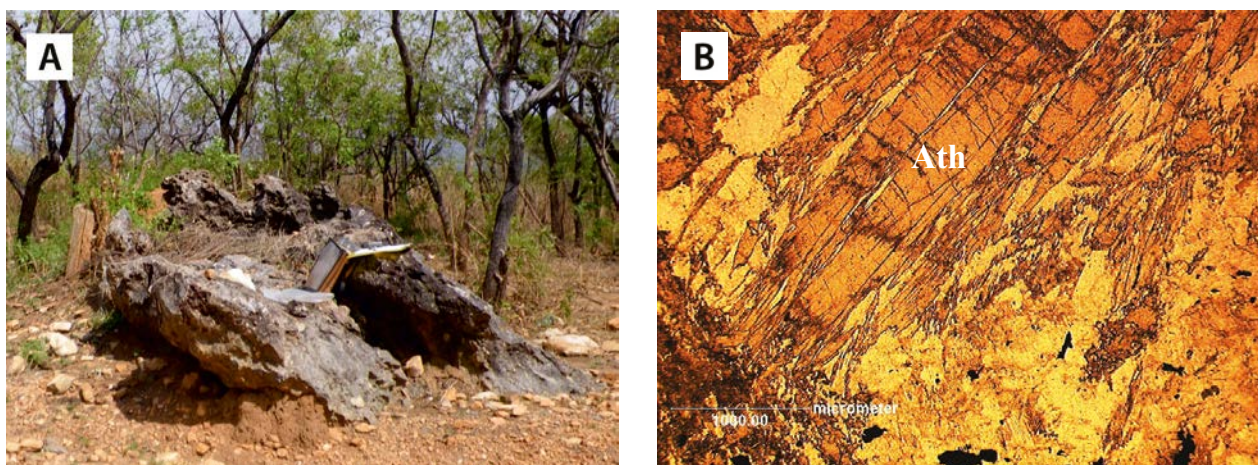


Fig. 9.11. (A) Outcrop of anthophyllite rock without marble intercalates, 2 km west of marble pits (366493E / 416920N). (B) Microphotograph of anthophyllite rock shown in (A), plane-polarised light. Anthophyllite (Ath) forms crystals several millimetres long. The width of the image is 4 mm.

Layered anthophyllite rock (P2Mlar) – A variable, layered anthophyllite-bearing rock of the *Oloro Formation* occurs on top of other known lithologies of the Madi Group. Near the marble pits, this anthophyllite-bearing rock contains subordinate marble intercalations, implying a gradational upwards transition from marble to impure marble and dolomite-bearing amphibole rocks. A pure anthophyllite rock without marble layers has been observed a few kilometres NW of the marble pits (Fig. 9.11A). Randomly oriented, interwoven rosettes of anthophyllite (Fig. 9.11B) make this rock extremely tough to hammer. The Fe- and Mg-contents in these rocks are 20–22 wt% ($\text{Fe}_2\text{O}_3 + \text{MgO}$) in total (see App. 2, anal. 153–154).

Marble, anthophyllite rock with micaceous intercalations and metabasalt are intimately associated. It is interpreted that the anthophyllite layers formed by Mg-metasomatism, derived from dolomite and introduced into originally mafic tuffs deposited from time to time as interlayers in a carbonate-dominated shallow marine environment. Sub-aerial flood basalt volcanism was supposedly preceded by mafic volcanism resulting in tuff horizons beneath the sub-aerial flood basalt. It is further postulated that these mafic tuff horizons were deposited, reworked and mixed with terrestrial material. Initial mafic pyroclastic material is attributed to the interaction between rising mafic magma and shallow ground or surface water in a rift-related geodynamic environment.

9.3 Lithostratigraphy of the Igisi Group

Watkins (1956) was the first to describe metasediments at Igisi Hill, an impressive crest in the Murchison Falls National Park, 33 km north of Masindi town (Fig. 9.1), as ‘sheared quartzites’ exposed in a SW–NE-directed belt, some 5 km in width, located between the Western Rift and Hoima-Masindi granulites of the ‘Basement Complex’. Subsequently, Macdonald (1967) described ‘slightly metamorphic sandstones and shales’ from the same location. Van Straaten (1976) assembled the metasediments of the ‘Igisi Belt’ into the Igisi Group. He mapped the eastern contact with the granulites, of what we now call the Karuma Group (Section 5.3), as invariably tectonic (van Straaten 1971, 1973).

Igisi rocks are not restricted to the eastern side

of the Albertine Rift, but also occur west of the rift in the southeastern West Nile Province, where they occur tectonically intersliced with Neoproterozoic rocks of the Lobule Group (Arua-Kibale Supergroup; Section 4.6), east of Nebbi town (Fig. 9.1). Lithostratigraphic correlation of Igisi rocks on both sides of the rift is questionable. Consequently, we will not try to correlate them and describe both domains separately (Table 9.2).

Banded gneiss (P2Ibgn) – Banded gneiss of the *Pangere Formation* occurs in two fault-bounded tectonic slices. They have a tectonic footwall contact, while the hanging wall contact with overlying sericitic quartzite of the Akuru Formation is considered

Table 9.2. Subdivision of the Igisi Group (Miriam Supergroup). The codes refer to lithological units in the unpublished 1:250 000 scale maps of DGSM.

| Group | Formation | Lithology | Code |
|-------------|---|--|--------|
| Igisi | SE West Nile Province | | |
| | Murchison | Mica schist | P2lms |
| | Erusi | Amphibolite | P2labl |
| | Akuru | Sericite quartzite and quartzite (<1.0 Ga) | P2lqz |
| | Pangere | Banded gneiss | P2lbgn |
| | Eastern crest of Albertine Rift, north of Masindi | | |
| | Murchison | Mica schist | P2lms |
| | Lere | Banded iron formation | P2lbif |
| | Katurikire | Kyanite-quartz schist | P2lkqs |
| | Kikamwa | Quartzite | P2lqzt |
| | Isolated tectonic lenses of unknown lithostratigraphic position | | |
| Nyunyu Hill | Meta-ultramafite | P2lmu | |

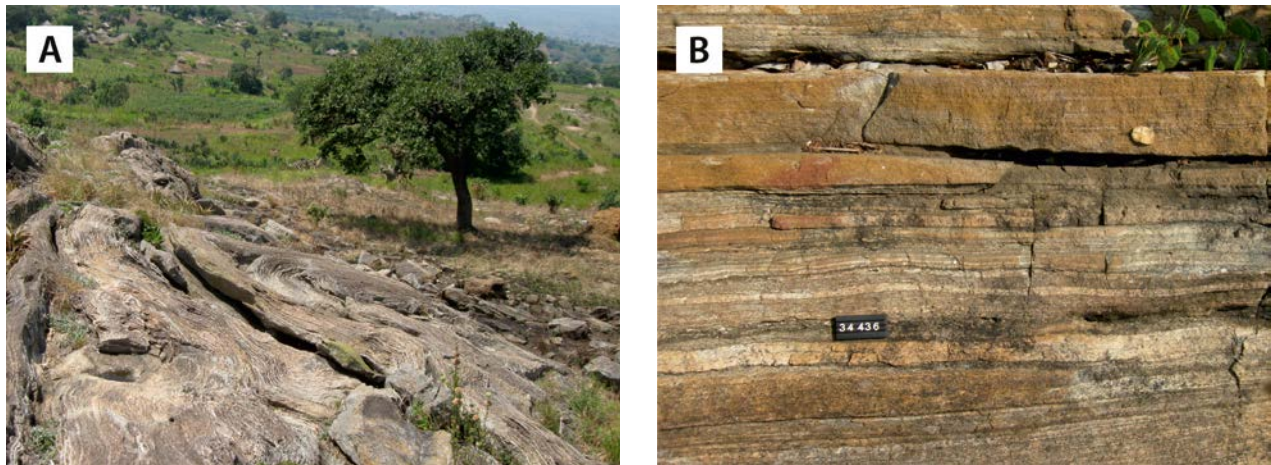


Fig. 9.12. (A) Intensively folded banded gneiss of the Pangere Formation (291693E / 261092N). (B) Laminar bedding in leucocratic bands of banded gneiss, ~1.3 km NWW of Agara village (301065E / 252305N). Number tag 10 cm.

gradational. These are medium-grained, intensively deformed, foliated rocks showing metre-scale asymmetric folds (Fig. 9.12A), random recumbent folds and scarce open folds, the latter particularly in more homogeneous, psammitic varieties of banded gneiss. Despite intense deformation, laminar bedding is locally preserved (Fig. 9.12B), manifesting a sedimentary origin.

The proportion of mafic and felsic minerals is strongly variable, and light brownish grey, rather leucocratic varieties as well as dark greenish grey mesocratic members have been encountered. In thin section, the major rock-forming minerals are quartz (showing undulose extinction), slightly altered plagioclase and microcline, while deep brown biotite, which is partly a secondary mineral,

is the most common mafic mineral. Bluish green, ragged hornblende (partly altered into epidote) is a common minor mineral, but can form amphibole-rich bands and interlayers, up to several metres in width. Other minor minerals are garnet and apatite.

Sericite quartzite, quartzite (P2Iqz) (<1.0 Ga) – Sericite quartzites and quartzites of the *Akuru Formation* occur in two tectonic slices in the southeastern West Nile Province. There, they form thin horizons within feldspathic gneisses of the Igisi Group, probably partly due to thrusting and tectonic stacking.

In the NE-plunging Erusi synform (Hepworth 1964, p. 66), graded bedding is locally preserved



Fig. 9.13. (A) Graded bedding in a subvertical quartzite horizon of the Akuru Formation in the northwestern limb of the Erusi synform (293881E / 261693N). (B) Symmetric ripple marks in sericite quartzite in a dry stream bed of the Akuru River. Muscovite at the top of the beds suggests that metamorphic muscovite had a detrital micaceous precursor (298295E / 266761N). Number tag 10 cm.

in the feldspathic basal parts of the quartzite beds (Fig. 9.13A). Upwards, the metasedimentary succession grades into strongly foliated, light brownish grey sericite quartzite with distinct bedding and symmetric ripple marks (Fig. 9.13B). In subhorizontal to gently SE-tilted sericite quartzites in the Akuru River, a well-developed fracture cleavage has developed parallel to laminar bedding with ~2–15-mm-thick beds, allowing the rock to be split into large, regular slabs, a highly appreciated raw material for local grinding stone manufacturing.

In thin section, feldspathic quartzite varieties are granoblastic, while lepidoblastic textures predominate in sericite quartzites with incompletely recrystallised quartz grains (undulose extinction and sutured grain boundaries) and with well-oriented muscovite/sericite flakes constituting up to 25–30% of the rock volume. The amount of impurities (apatite, zircon, monazite and ilmenite) is generally less than 5 vol%.

U-Pb zircon age determination of detrital zircon in sericite quartzite from the Akuru River yielded a maximum sedimentation age of 0.98 Ga (Mänttari et al. 2011). Metamorphic monazites supposedly manifest Pan-African metamorphic overprinting at 0.66 Ga (for details, see Mänttari 2014).

Amphibolite (P2Iabl) – Amphibolites of the *Erusi Formation* form a distinct horizon of mafic metavolcanic rocks in the southeastern West Nile Province. At the prominent Arusi Hill, a body of garnetiferous amphibolite (Fig. 9.14), tens of me-

tres thick, is exposed in the hinge zone of a large, N-plunging synformal structure. On a ternary radiometric map, amphibolite bodies can be readily outlined due to their negative total count and potassium, thorium and uranium values. Based on amphibolite bands in surrounding metasediments and local compositional banding, probably representing a primary depositional feature, we suggest that amphibolite has a mafic pyroclastic protolith.

Under the microscope, Erusi amphibolites are foliated granoblastic or nematoblastic rocks, mostly consisting of bluish to brownish green, prismatic hornblende and strongly sericitised andesitic plagioclase. Large (up to 5 mm), poikiloblastic garnet grains can constitute up to 20–25 vol% of the rock (Fig. 9.14). In some thin sections, colourless to pale greenish, ragged clinopyroxene porphyroblasts are partly altered into hornblende. Random ilmenite grains are surrounded by thin leucoxene coronas. Other minor, retrograde or accessory minerals include quartz, epidote, carbonate and apatite. Two samples of Erusi amphibolite show elevated titanium contents (2.0 and 2.1% TiO₂, see App. 2, anal. 155–156). In chemical discrimination diagrams, these amphibolites can be classified as subalkaline tholeiitic basalts (Figs 9.15A–C). In tectono-magmatic discrimination diagrams, the same rocks plot in the field of ‘oceanic basalts’ (Fig. 9.15D, E), resembling present day MORB basalt composition. This may justify the question whether the amphibolite is allochthonously emplaced into the Igisi Group, being originally derived from the Alibu Formation of the War Group (Section 4.5), also characterised

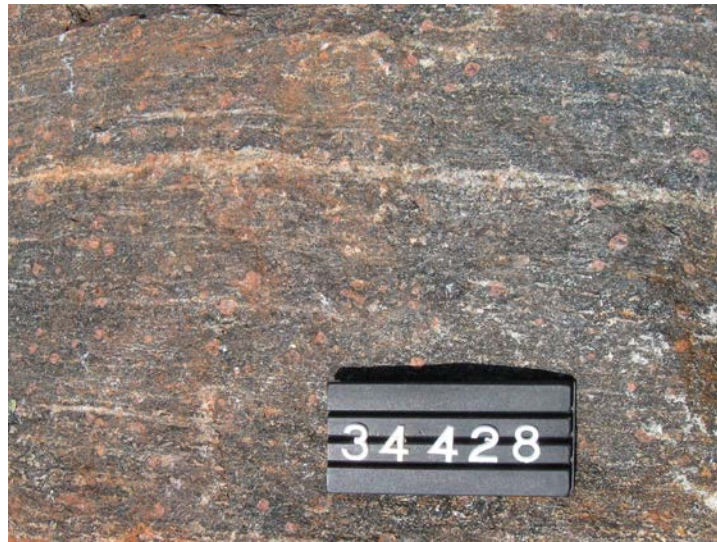


Fig. 9.14. Close-up photo of garnetiferous amphibolite from the top of Erusi Hill (291184E / 258321N). Garnet occurs as ragged reddish grains, 1–5 mm in size. Number tag 10 cm.

by an ‘oceanic’ petro-tectonic signature. However, it should be remembered that crustal contamination in amphibolitic rocks located in continental environments may result in misleading oceanic signatures.

Quartzite (P2Iqzt) – Quartzite of the *Kikamwa Formation* is exposed to the north of Masindi and as scattered quartzite blocks along the northern slope of an E–W-trending ridge 33 km north of the town of Masindi (358383E / 219907N), in the latter location together with meta-siltstone and mica schist. Locally, thicknesses of 10 to 50 m have been observed but, as suggested by van Straaten (1976), their original thicknesses cannot be defined because of tectonic complications. These quartzites are light-coloured rocks with a coarse sugary fabric, containing cm- to dm-wide intercalated strata of muscovite schists. Near the Ensama River, small occurrences of rusty coloured, conspicuously banded quartzite, which contains up to 40 vol% of iron as magnetite, have been reported in association with graphitic schists (van Straaten 1976).

Kyanite-quartz schist (P2Ikqs) – Kyanite-quartz schist of the *Katurikire Formation*, in association with a banded iron formation, is found in ‘Klippe’ in several hills south of Karuma Game Reserve (Fig. 9.1). Weathered rock surfaces are covered by conspicuous, 0.5–3-cm kyanite nodules, causing irregular fracturing in fresh rock (Fig. 9.16A) and dark nodules in weathered rock (Fig. 9.16B). Lenses composed of needle-shaped amphibole, most

likely actinolite, occur in places. In the westernmost outcrops of this unit, kyanite-quartz schist grades into fine-grained quartzite with small flakes of muscovite visible in thin section. As a curiosity, chemical whole-rock composition of the aforementioned kyanite-quartz schist and quartzitic rock is shown in Appendix 2 (anal. 157–158).

Banded iron formation (P2Ibif) – A distinct, NE–SW-trending magnetic and gravity high, ~10 km in length, was identified south of Karuma Game Reserve, part of the easternmost exposures of Igisi rocks (red dot in Fig. 9.1). The source of the anomaly is a dense magnetic body, but its nature could not be established in the flat, laterite covered area. Nearby (404750E / 223040N), intercalations of ferruginous quartzite occur in fine-grained micaceous sandstone and siltstone, which form an elongated ridge with radio masts (Fig. 9.18A), several hundreds of metres long. Magnetic susceptibility values are generally low in dark bluish grey coloured *in situ* boulders of the *Lere Formation*, indicating that hematite or goethite rather than magnetite are the dominant iron-bearing minerals. Anyway, these rocks locally comprise over 70 wt% iron (see App. 2, anal. 159). Magnetite is, however, a common mineral in the soil and supposedly at deeper levels, being the source of the magnetic anomalies.

Another small field with boulders bearing affinity with the banded iron formation has been observed west of the radio mast hill (403770E /

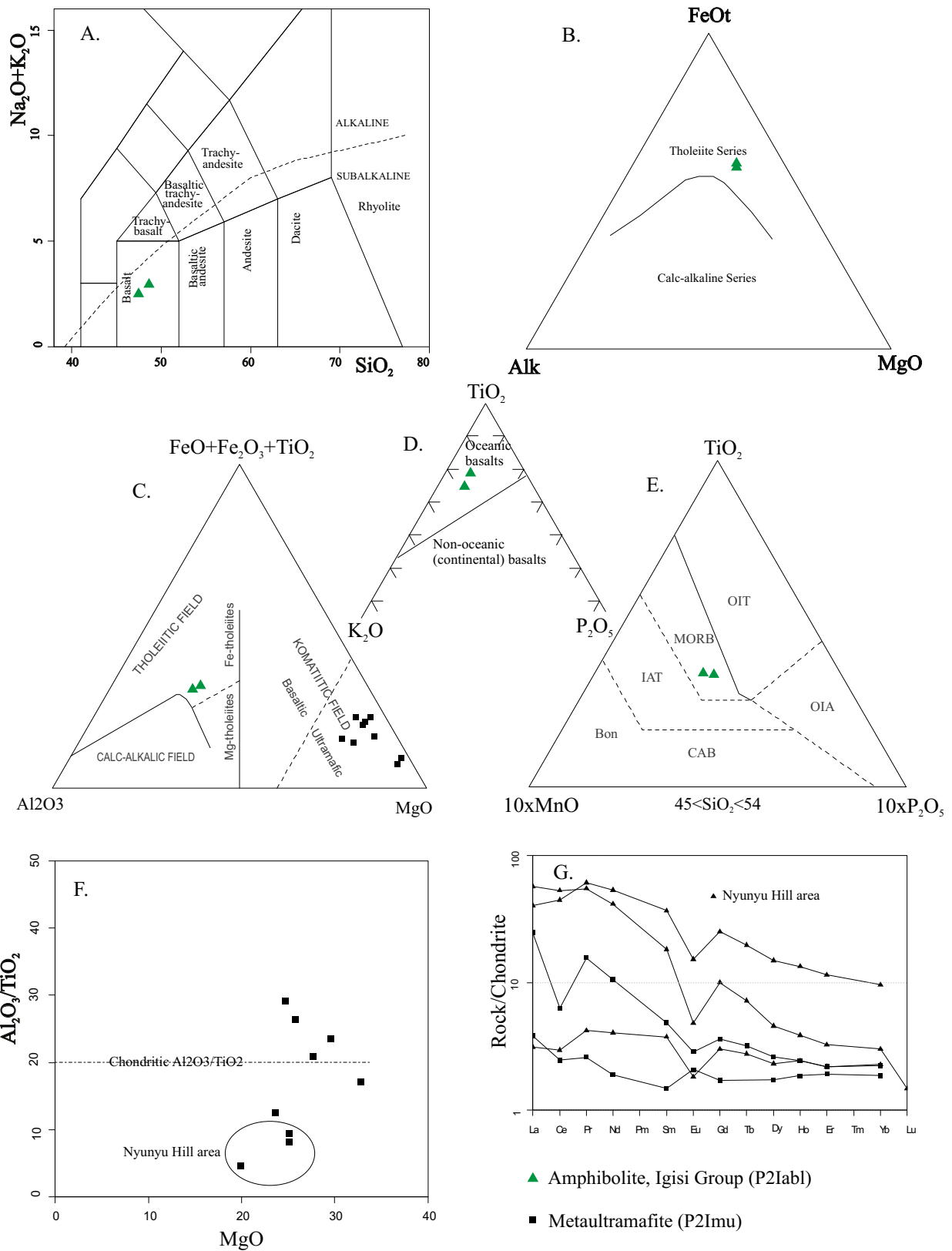


Fig. 9.15. Chemical discrimination diagrams for the Igisi Group amphibolites and meta-ultramafites. (A) TAS diagram of LeBas et al. 1986, (B) AFM diagram of Irvine & Baragar (1971), (C) Al_2O_3 -($\text{FeO}+\text{Fe}_2\text{O}_3+\text{TiO}_2$)- MgO diagram of Jensen (1976), (D) Geotectonic diagram of Pearce (1975), (E) Geotectonic diagram of Mullen (1983), (F) $\text{Al}_2\text{O}_3/\text{TiO}_2$ vs. MgO diagram, (G) REE distribution diagram normalised according to Nakamura (1974). Chemical analyses used in these diagrams are available in Appendix 2 (anal. 155–156 and 160–168).

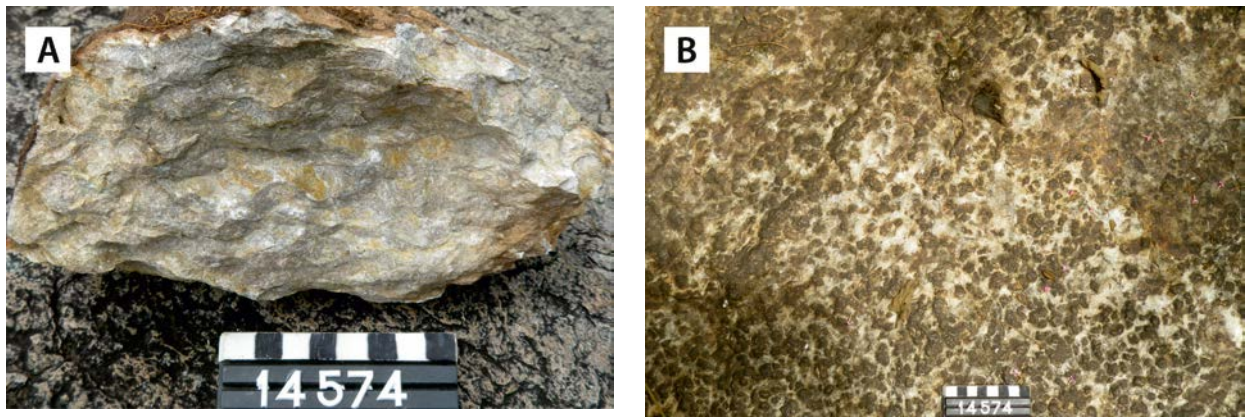


Fig. 9.16. (A) Kyanite-quartz schist of the Katurikire Formation with kyanite nodules causing irregular fracturing in the fresh surface; (B) showing dark coloured kyanite nodules on the weathered surface (399176E / 221262N). Number tag 8 cm.

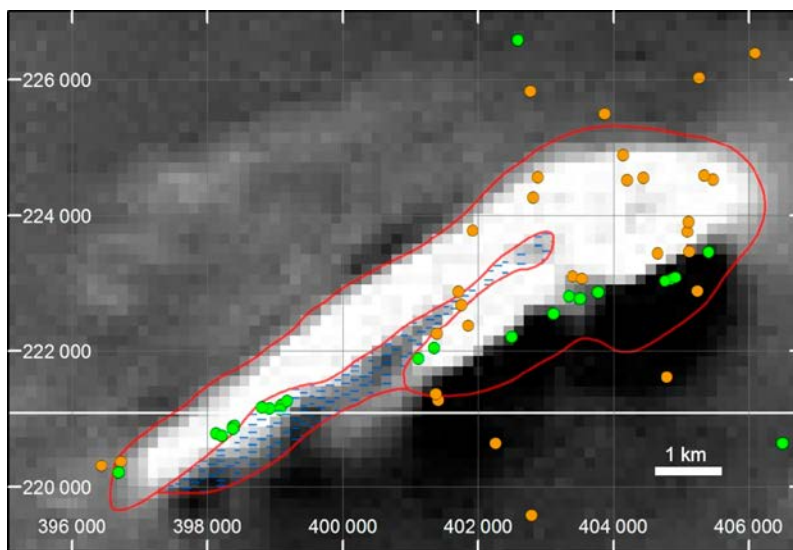


Fig. 9.17. Grey-scale aeromagnetic map showing a magnetic anomaly associated with the banded iron formation. The boundaries of ferruginous rock and kyanite quartzite (blue hatching) are drawn in red. Green and brown dots are observation points, the brown dots indicating laterite. The white horizontal line is the boundary between Gulu (north) and Masindi (south) map sheets.



Fig. 9.18. (A) View towards the SSE depicting the radio mast hill, a local topographic high (404911E / 223080N). (B) Ferruginous phyllitic slate with hematite-rich bands (401133E / 221873N). Number tag 8 cm.

222860N). The boulders are composed of tightly folded quartz-rich layers that alternate with iron-rich silty layers (Fig. 9.18B). Another boulder field with BIF affinities is located near the central part of the magnetic anomaly (401130E / 221870N). Magnetic susceptibility values are extremely high (between 31 and 107 SI) in laterite outcrops located some hundred metres further to the NE. Further to the SW, in a cluster of small hills, light-coloured kyanite-quartz schists are also associated with rocks with BIF affinity and quartzites. Based on the presence of the strong deformation features, the unit has been assigned to the Igisi Group, even though, when undeformed, these rocks closely resemble shales and slates of the Neoproterozoic Bunyoro Group (Chapter 10).

Mica schist (P2Ims) – Mica schist of the *Murchison Formation* has been correlated with similar schist north of Masindi, where the rock occurs as a NE-trending belt of variously deformed mica schist. On airborne geophysical maps, these rocks are highlighted by their rather strong positive radiometric signature when compared to surrounding rocks. Contact relations with underlying lithologies of the Igisi Group appear to be gradational, while contacts with Neoarchaeon gneisses and granulites are tectonic (van Straaten 1976).

This litho-stratigraphic unit varies considerably along the nearly 50-km-long strike of the belt in the SE West Nile Province. In the south, the high alumina content of the schist is evidenced by the occurrence of garnet and kyanite (Hepworth 1964) or large, stubby pseudomorphs of andalusite porphyroblasts. Further northwards, mica

schist grades into migmatitic micaceous gneiss (Figs 9.19A-B), which resembles underlying gneiss of the Pangere Formation. Petrographically, mica schists of the Murchison Formation are fine-grained, lepidoblastic rocks mostly comprising small flakes of muscovite (sericite) with various proportions of felsic minerals. Poikiloblastic garnets, together with roundish grains of apatite and zircon, are common accessory minerals. Extensive retrograde alteration has usually altered andalusite and kyanite porphyroblasts into a fine-grained sericite mass.

Mica schists also occur in the Igisi Belt along the Albertine Rift shoulder, east of Lake Albert (van Straaten 1976), and in a few isolated areas, some 30 km south of Karuma Falls. Rather coarse-grained, schistose and crenulated mica schists contain small garnets and abundant kyanite at Murchison Falls (Fig. 9.20A) and a kilometre upstream along the Nile River. Kyanite occurs as individual bluish small and large prisms, up to >5 cm long, and as random bundles. Bedding can be observed in weathering surfaces (Fig. 9.20B). The thicknesses of individual beds range from a few decimetres upwards, but original thicknesses are often modified owing to deformation. Boudins of amphibolite, a couple of decimetres in size, have been observed in places.

Some 30 km south of Karuma Falls, a series of hills composed of Igisi Group mica schist form two separate polygons. The western, larger one comprises very fine-grained, white, grey and reddish quartzitic schist and interbeds of red-brown to pink meta-siltstone. Primary sedimentary features have been destroyed and the layering visible in a

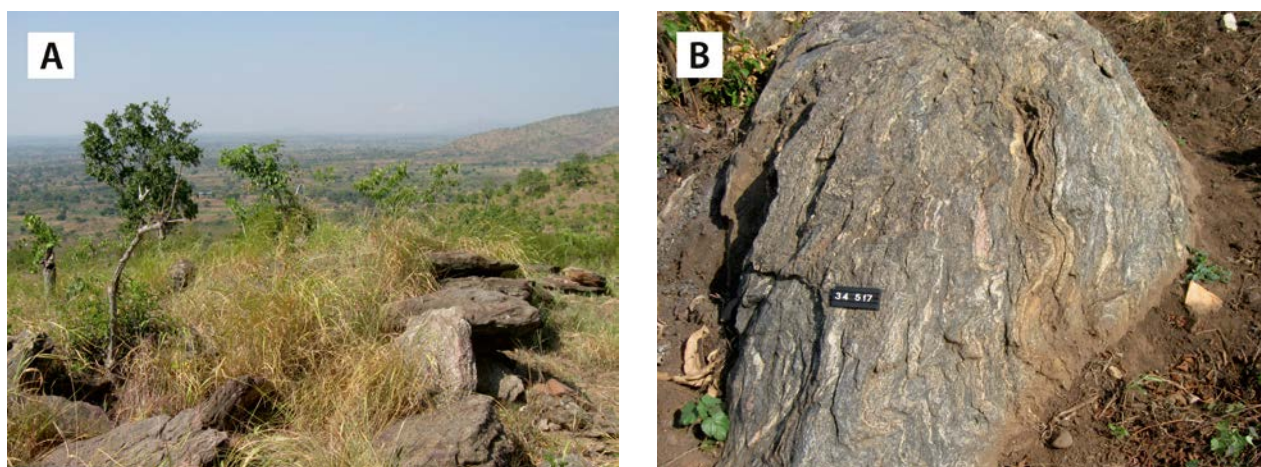


Fig. 9.19. (A) Mica schist of the Murchison Formation in the SE West Nile Province, ~1.6 km W of Pade village (297482E / 265762N). (B) Mica schist in the northern part of the schist belt (309714E / 291324N). Number tag 10 cm.

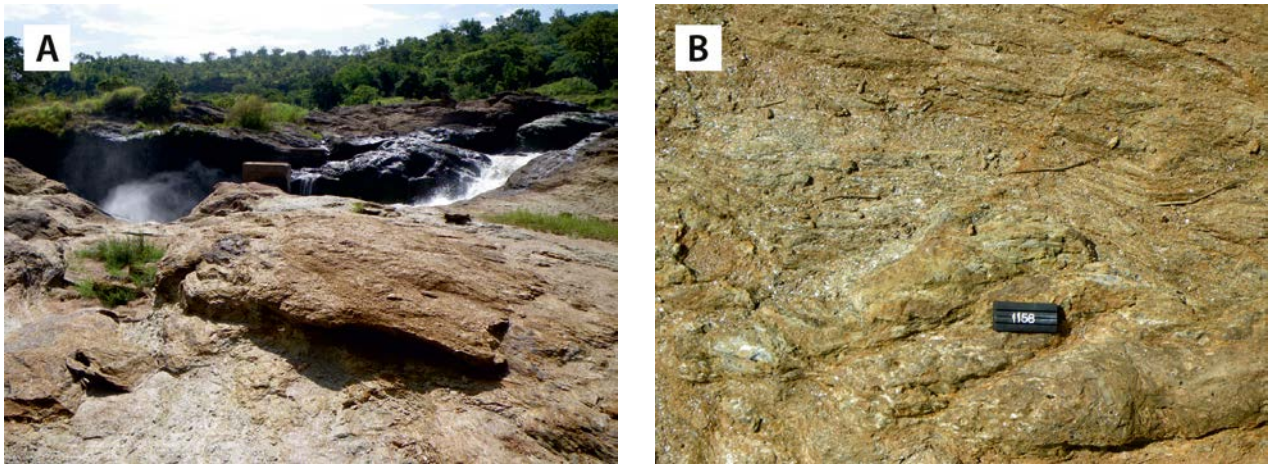


Fig. 9.20. (A) Kyanite-mica schist at the gorge of Murchison Falls. (B) Crenulation in kyanite-mica schist (353863E / 251879N). Number tag 8 cm.

coarser grained sub-facies is a penetrative tectonic fabric, enhanced by rare, thin quartz bands parallel to foliation. In thin section, lithic fragments, quartz, hematite nodules and sericite are visible. Most of the primary features have been destroyed. The quartzite fragments, detrital quartz grains and hematite nodules are flattened and elongated parallel to the planar fabric, enhanced by the metamorphic sericite and muscovite.

Some 5 km NE of Katulikire village, grey quartzitic schist occurs with abundant folded quartz lenses, parallel to the schistosity. The schist has been refolded into small, disharmonic isoclinal recumbent folds with NE–SW-aligned fold axes. In thin section, a very fine-grained granoblastic texture can be observed, without primary features. Quartz in the matrix shows undulose extinction. Intercalated lamellae of sericite show isoclinal microfolds. Hematite is found in round-shaped to euhedral grains, indicating post-tectonic mobilisation and precipitation. Tiny quartz veins, sub-parallel to the foliation, are composed of coarse to fine crystals, which show undulose extinction and local fracturing.

Prominent quartz veins near the western contact of the western polygon are probably elements from a basal thrust plane, which argues for a thrust-emplacement and imbrication of the Igisi quartzites. The same appears to be valid for the quartz veins in schist, with subhorizontal recumbent folds, in contact with Archaean Awela gneissic granodiorite further to the north.

Meta-ultramafite (P2Imu) – Meta-ultramafites of the *Nyunyu Hill Formation* have been found as

fault-bounded lenses in Archaean gneisses or Metu metatuff, restricted to a relatively narrow N–S-trending zone stretching from Moyo to the Murchison Falls region. The northernmost ultramafic body, forming a vertical or steeply ENE-dipping tectonic lens, some 5 km in length and up to 600 m wide (Fig. 9.21A), is found at Nyunyu Hill, located 8 km NE of the town of Moyo (Fig. 9.4). It is surrounded by 0.98 Ga (Mänttari 2014) Metu metatuff. Other occurrences are much smaller, typically having diameters of some tens of metres, including a lens of meta-ultramafite occurring ~1 km west of Moyo town in a sizeable tectonic fragment of Archaean gneiss in Metu metatuff. Other bodies have been found in Murchison National Park and its surroundings, again as tectonic fragments in Archaean rocks.

The rocky slopes of Nyunyu Hill are covered by *in situ* blocks (Figs 9.21B, C) and occasional outcrops, all composed of ultramafite, implying that the entire hill is compositionally uniform. Two varieties of ultramafite have been identified at Nyunyu Hill, one being a very tough to hammer, homogeneous and massive, dark greenish pyroxene-tremolite-rich rock and the other represented by a much coarser meta-peridotite with anthophyllite (Figs 9.21B, C). By comparison, talc is the dominant mineral in the meta-ultramafite west of Moyo town, occurring together with randomly oriented anthophyllite needles and rosettes.

At Purongo village, south of the Gulu–Arua highway, ultramafic rocks form a cluster of boulders, ~30 m in diameter (368272E / 281824N), and exposures of amphibolite and metagabbro can be found nearby. The rock is composed of 85

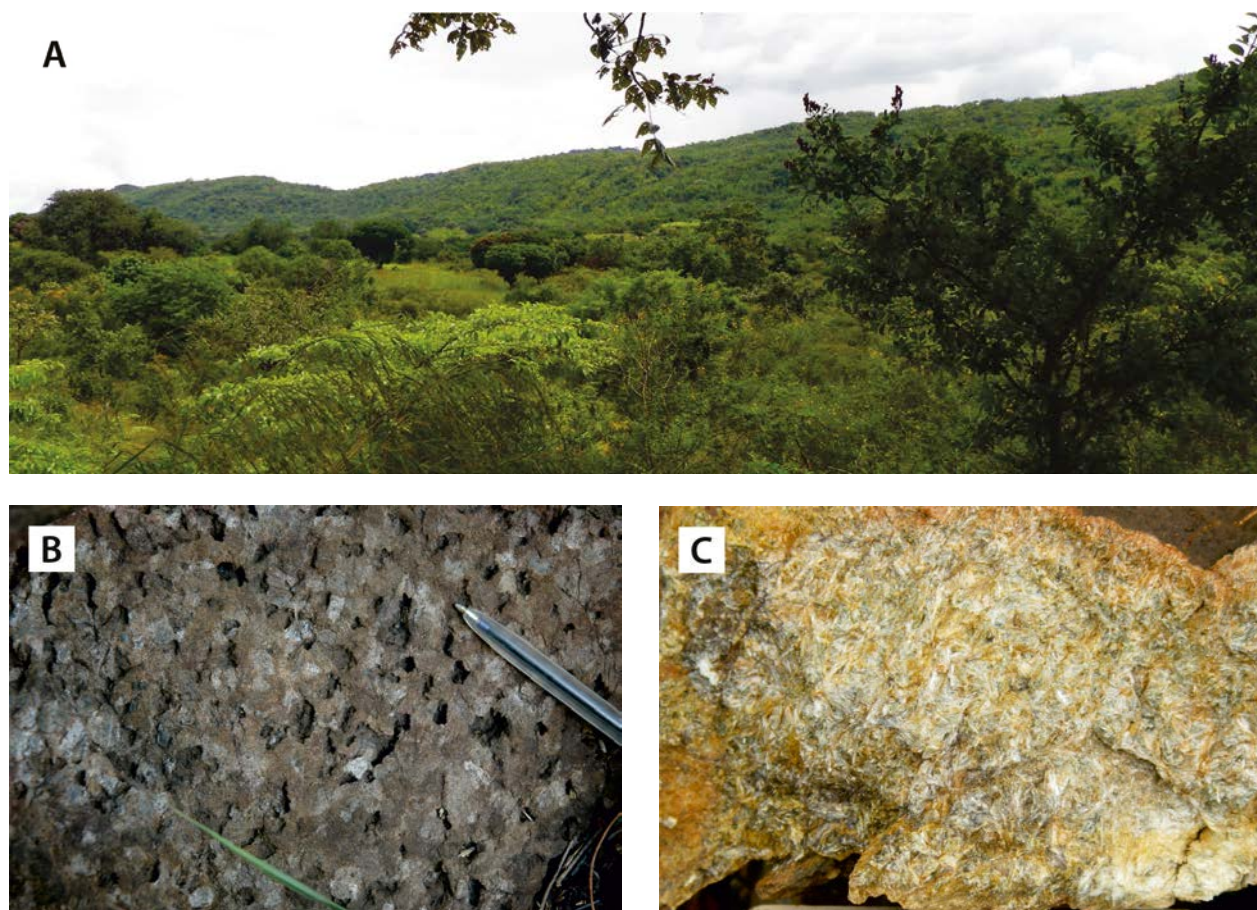


Fig. 9.21. (A) View to the SW towards the up to 100-m-high and 5-km-long Nyunyu Hill underlain by meta-ultramafite (363938E / 412095N). (B) Coarse pyroxene-anthophyllite-meta-ultramafite (364539E / 409091N). (C) Rosettes of amphiboles in the cut surface of meta-ultramafite, image width 12 cm (363174E / 411587N).

vol% talc, the rest being anthophyllite and chlorite. The high MgO content (29.7%) in combination with elevated SiO₂ (57.4%) manifest strong metasomatism, and one can only speculate on the original composition. Some blocks of this soft talc-rich rock have been carved (Fig. 9.22). Better exposures of meta-ultramafite are located north of the Gulu–Arua highway (357638E / 286686N). Chemical discrimination diagrams for these rocks are shown in Figs 9.15C and F, and a spider diagram in Fig. 9.15G.

In Murchison National Park, meta-ultramafite has been described as greenish medium-grained tremolite-chlorite skarn (356044E / 264812N) and as fine-grained chlorite schist (369481E / 263738N). The latter is a strongly foliated rock and fresh surfaces show conspicuously light green colours with partly altered magnetite crystals, 2–5 mm size. As expected, the magnetic susceptibility is very high, the maximum reading being 75.6 SI. The SiO₂ and MgO contents are 43.9% (ultramafic)

and 32.8%, respectively (App. 2, anal. 160, see also Fig. 9.15).

Finally, meta-ultramafite occurs as large *in situ* boulders 17 km NE of the highway between the villages of Karuma and Olwiyo (409750E / 274360N). Similarly to meta-ultramafite in Puringo village, the rock is closely associated with amphibolite and fine-grained orthoquartzite (metachert?).

The origin (komatiitic or picritic volcanics, fragments of sub-lithospheric mantle, ophiolite?) and age of these metamorphosed (and partly metasomatic) ultramafic bodies have not been established. From their rather linear distribution, it appears that they are controlled by N–S-trending late-Kibaran and/or Pan-African complex fault zones, resulting in a number of interlocking tectonic crustal wedges, most spectacularly shown by late structures in the Moyo District and in the Lake Albert segment of the Madi-Igisi Belt.

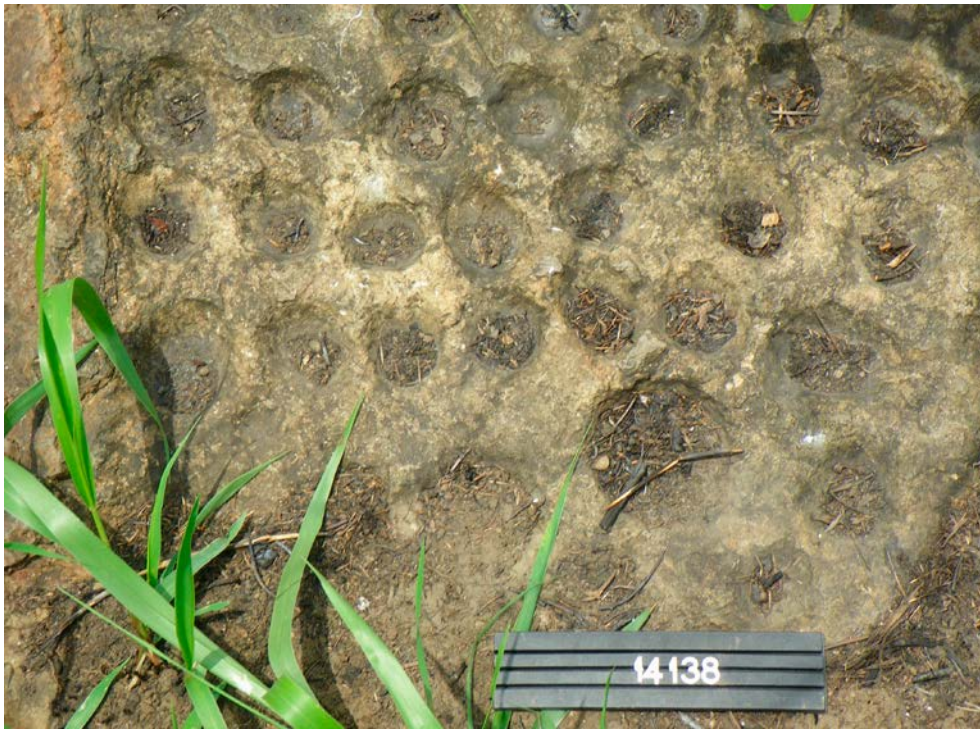


Fig. 9.22. The talc-rich variety (soapstone) of ultramafic rock can be easily carved (368272E / 281824N). Number tag 15 cm.

9.4 Geochronology

Dacitic metatuff (984 ± 8 Ma) (365282E / 403811N) – Clearly magmatically zoned zircon grains from metatuff, formerly mapped as Archaean tonalite gneiss, in the Moyo area yield a Pb-Pb mean age of 984 ± 8 Ma (UG-46_23579, Mänttari 2014).

Quartz-muscovite schist ($<977 \pm 9$ Ma) (359388E / 390894N) – U-Pb data from detrital zircons from a muscovite-biotite schist of the Anyurapi Formation in the Moyo area reveal Neoproterozoic (2.63 to ~ 2.48 Ga) zircon cores and 977 ± 9 Ma zoned grains and rims enveloping the Archaean cores (UG-39_1272, Mänttari 2014), similarly to Mirian flaggy grey gneisses reported by Leggo (1974). The occasional thin Pan-African zircon growths indicate later metamorphism.

Sericite quartzite, quartzite (<1.0 Ga) (266761E / 298295N) – Being surrounded by Archaean basement, one would expect that the bulk of the detrital zircons would be derived from Archaean source rocks, but most detrital zircon grains have ages between 2.2 Ga and 1.8 Ga. In the $^{207}\text{Pb}/^{206}\text{Pb}$ age probability plot, the most prominent peak is at ~ 1.86 Ga, an age that is approximately coeval with

the emplacement age of the Mubende and Singo batholiths in the Rwenzori Belt, some 200 km to the south. Two smaller populations of detrital zircons peak around 1.38 Ga and ~ 1.0 Ga, coeval with emplacement of granitoids of the North Kibaran Igneous Province (Section 8.2.2) and Mirian lithologies, respectively. The maximum age of sedimentation is determined by the youngest detrital zircon grains dated at 976 ± 30 Ma and 990 ± 34 Ma (Mänttari 2014).

With the metamorphic monazites from the same rock dated at ~ 0.66 Ga (see Mänttari 2014), two scenarios may apply for the petrogenesis of the sericite quartzites: (1) they were metamorphosed soon after deposition at 0.99–0.98 Ga and reworked at around ~ 0.66 Ga or (2) they were deposited at 0.99–0.98 Ga and metamorphosed at around ~ 0.66 Ga. In the first scenario, they metamorphosed during two orogenic cycles – the Grenvillian and Pan-African – while in the second scenario they experienced the Pan-African Orogenic Cycle only.

Sericite quartzite of the Akuru Formation (SE West Nile area) can be correlated with Igisi metasediments (Watkins 1956, van Straaten 1976) in the area west of Hoima and Masindi. Kyanite-

garnet schists from Murchison Falls manifest amphibolite-facies peak metamorphic conditions of 0.8 Gpa (8 kb) and 650–680°C based on conventional thermo-barometry of the paragenesis kyanite + garnet + biotite + muscovite + quartz + plagioclase ± K-feldspar (Appel et al. 2004, 2005). U–Th–total Pb dating of allegedly coeval, single-stage metamorphic monazite yielded ages of 621 ± 26 Ma and 633 ± 27 Ma. No indications for older monazite relics were found. According to Appel et al. (2004, 2005), these data imply that these kyanite-garnet schists, which overlie 2.99 Ga

Karuma granulites of the basement of the North Uganda Shield, suffered one single phase of amphibolite-facies metamorphism during the Pan-African, supposedly induced by a crustal thickening event. Unfortunately, no zircons were dated from the Murchison kyanite schists, but based on the geochronology of Akuru sericite schists described above, we cannot exclude the possibility that while monazite blastesis took place during the Pan-African, peak metamorphic conditions took place much earlier, concomitantly with the ~1.0 Ga ‘Mirian event’.

9.5 Geodynamic Evolution of the Madi-Igisi Belt

Introduction – In the following it will be demonstrated that a Proterozoic suture, so far unmapped, separates the Bomu-Kibalian Shield (mainly in the northeastern DRC), with its eastern segment of the West Nile Block (Chapter 4), from the North Uganda Terrane (Chapter 5). This suture can be extended southward into the Igisi belt identified by van Straaten (1976, 1977) in the Hoima and Masindi areas, with unmapped extensions further northward to the Murchison Falls (Appel et al. 2005). It also includes Mirian rocks of the Moyo area, containing the former ‘Madi Series’ (DGSM 1966) near the border with South Sudan (Fig. 9.1). This suture broadly coincides with the newly defined Madi-Igisi Belt, which according to our current views comprises a double-verging, thin-skinned stack of thrust masses composed of reworked Archaean crystalline basement and juvenile ~1.0 Ga ‘Mirian’ lithologies and a zone of major sinistral strike-slip faults, the latter resulting in a number of interlocking crustal wedges reaching from Moyo town to Lake Albert.

Although some lenses of ultramafic composition of unknown origin and setting have been encountered in this suture zone, we believe that the suture has always remained intra-cratonic and that the incorporation of ultramafic lenses (sub-continental mantle?) is related to major faults with a large-scale strike-slip component. If, however, these ultramafic rocks turn out to be of Archaean age, we cannot exclude the possibility that these late-Kibaran and/or Pan-African complex fault zones are superposed on an older ‘weakness zone’ or suture.

From structural, petrographic and geochronological data, we have tentatively established a

scenario sketching the geodynamic evolution of the Madi-Igisi Belt, which comprised a phase of extension with basin formation and deposition, followed by a phase of compression or transpression, giving rise to basin inversion manifested by metamorphism and deformation. We are aware that much more data, especially geochronological and structural data, will be needed to complete the picture. Before describing the suture itself, textures and structures in the rocks below the thrust masses, in particular the eastern margin of the Bomu-Kibalian Shield (Chapter 4), will be described.

Eastern margin of the Bomu-Kibalian Shield: a footwall thrust ramp – The footwall thrust ramp of Madi-Igisi Belt thrust masses in the West Nile Province were formerly attributed to the Granulite Group, the Western Grey Gneisses and Eastern Grey Gneisses (Hepworth 1961a, 1964, Macdonald 1964b, Hepworth & Macdonald 1966), all showing a pronounced N–S structural trend (Figs 4.2 and 9.23).

Hepworth (1964) acknowledged that the ‘eastern gneisses’ could be distinguished from the ‘western gneisses’ by the latter having (1) a lower grade of metamorphism, (2) a flaggy nature, (3) moderate eastern dips when compared to the generally sub-vertical and steep dips of the ‘western gneisses’ and (4) lesser abundance of amphibolites. Subsequently, Leggo et al. (1971) and Leggo (1974) reported the presence of 950 Ma zircon grains in the eastern ‘Mirian’ lithologies, demonstrating that, although gneisses in the west and east of the West Nile Block have many field aspects in common, they are very different units, one being Archaean (some even Mesoarchaean) and the other being Proterozoic in

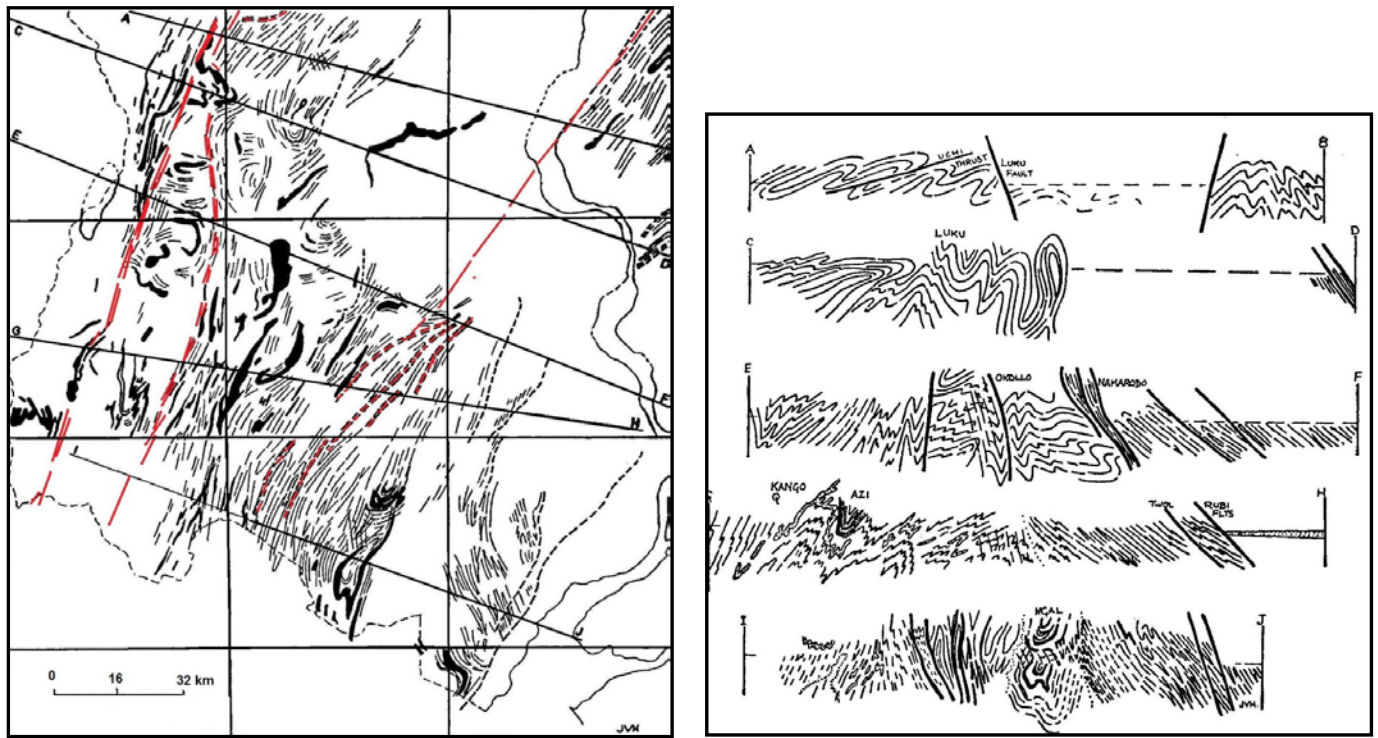


Fig. 9.23. (Left) Structural map of the southern and central part of the West Nile Block. Structural elements defining the grain of the belt are lithological boundaries and traces of foliation, fractures and lineaments. Red = high strain zones in the Namtin – Namarodo Mylonite zone (DGSM 1966). Note the NE continuation into the Neogene eastern scarp of the Rift, demonstrating multiple rejuvenations of the same weakness or fracture zones. (Right) Cross sections of the same area showing the contrasting styles of deformation, notably between the domains underlain by the ‘Granulites’ and ‘Western Grey Gneisses’ on one hand and the ‘Eastern Grey Gneisses’ on the other hand. Adapted from Hepworth (1964).

age. When assuming that the West Nile Block is the eastward extension of the Bomu-Kibalian Shield, an obvious question will arise: while the structural grain in the Bomu-Kibalian Shield in NE Congo is overwhelmingly WNW-ESE (Fig. 4.1), why does the West Nile Block show a prominent NNE-SSW grain (Figs 4.2, 4.3 and 9.23)?

Structural Geology – With respect to the question above, the following observations can be made: The crystalline basement of the West Nile Block has been affected by several phases of brittle and ductile deformation (Hepworth 1964, Macdonald 1964b). These include brittle Neogene Rift faults and local late Pan-African strike-slip faults associated with narrow mylonite zones along strike (Fig. 4.2). We also consider the poorly defined N-S-directed ‘Boundary Dislocation’ of Hepworth (1964), near the border with the DRC, more or less located on the contact between the former ‘Granulite Group’ and the former ‘Western Grey Gneisses’, to represent an in-basement rift fault. This has most likely been formed by rejuvenation of an older crustal weakness zone (Fig. 4.2), as mani-

fested during GTK Consortium field verification by numerous folds with steep fold axes.

The NNE-SSW structural grain of the West Nile Block (Figs 4.2 and 9.23) is, however, related to one or more phases of penetrative deformation, associated with variable but generally intense degrees of retrograde metamorphism. Since, the predominant structural style consists of tight or isoclinal folds on nearly parallel axial planes, and as foliation is axial planar, only comparatively rare exposures display superimposed sequential structures. Cahen (1954) reported that Kibalian rocks in the northeastern DRC are mainly folded on WNW axes. Characteristically different foliation (and lineation) directions, including E-W-directed fold axes, in the West Nile Block are only sparsely observed in granulites and are attributed to the ‘Watian event’ (Table 4.1). Apparently, this E-W structural fabric has largely been obliterated on the scale of the outcrop. This process is well illustrated by different exposures of banded gneiss of the Pangere Formation, the lowest unit of the Igisi group in the West Nile area. This banded gneiss shows alternating cm- to dm-thick

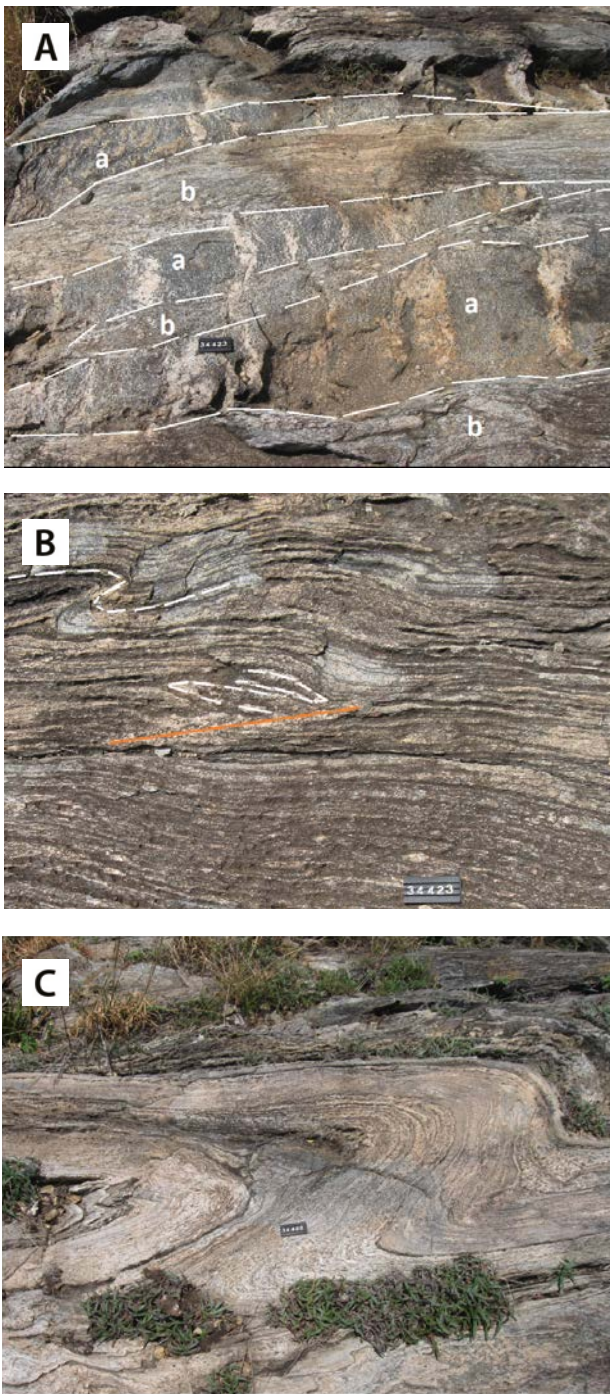


Fig. 9.24. (A) Banded paragneiss. The original fabric is preserved in a number of lenses, marked 'a'; this older fabric has been largely transposed into a secondary fabric, marked 'b'. Note that the leucocratic quartz-feldspar nests and streaks have not survived the transposition process (263110E / 295091N). (B) Banded paragneiss. Note isoclinal folds, cut by quartz-feldspar veins. A younger phase of folding is portrayed by co-axial intrafolial folds (upper left corner) (263110E / 295091N). (C) Banded paragneiss. The rocks show distinct compositional banding/bedding and mesoscopic, disharmonic open to tight to isoclinal fold structures. In places, dehydration melting can be observed (261092E / 291693N). Number tag 10 cm.

zones, marked 'a' and 'b' in Fig. 9.24A. The original rather coarse gneissose palaeosome-neosome fabric is preserved in a number of lenses, marked 'a'. This older fabric has been largely transposed into a secondary fabric, marked 'b'. Note that the leucocratic quartz-feldspar nests and streaks of the neosomes have not survived the transposition process.

In a more advanced stage, the gneissose fabric has been completely obliterated and replaced by a finer, more pronounced planar fabric (Fig. 9.24B). Some 'old' neosomes have been deformed into isoclinal rootless folds. Intrafolial drag folds can be observed in places. Subsequently, the banded paragneiss has turned into a rock that shows distinct compositional banding/bedding and mesoscopic, disharmonic open to tight to isoclinal fold structures and, in places, dehydration melting (Fig. 9.24C).

Airborne Magnetics – Although almost completely obliterated on outcrop scale, the E–W to ENE–WSW 'Watian structural grain' is still clearly visible on a megascopic scale, as in the recently acquired airborne magnetic imagery, which shows alternating magnetic highs and lows that tend to be smoothed when covered by sediments of the Albertine Rift. The magnetic pattern shows an E–W to WSW–ENE trend, often with a sigmoidal shape, supposedly due to drag along N–S-directed sinistral strike-slip faults.

The same pattern is particularly clearly visible in a magnetic image depicting the first vertical derivative of the Total Magnetic Intensity (TMI) in nT/m (Fig. 9.25). TMI is the combined reading from all magnetically susceptible minerals within the earth's crust down to a depth of 10 km or the Curie point, the point at which minerals lose their magnetic susceptibility. The image shows perfect continuity of the sigmoidal E–W to WSW–ENE trends of the WNB below the sediments of the northern part of the Albertine Rift, and a sharp contact with NNW-trending lithologies east of the rift. This contact is offset by a sinistral shear zone that partly coincides with the Namtin-Namarodo Mylonite zone (Fig. 4.2).

From these observations, we conclude that the NNE–SSW structural grain of the West Nile Block is superposed on an older WNW–ESE structural trend, characteristic for the Congolese segment of the Bomu-Kibalian Shield. Obviously, the West Nile Block represented the footwall ramp of

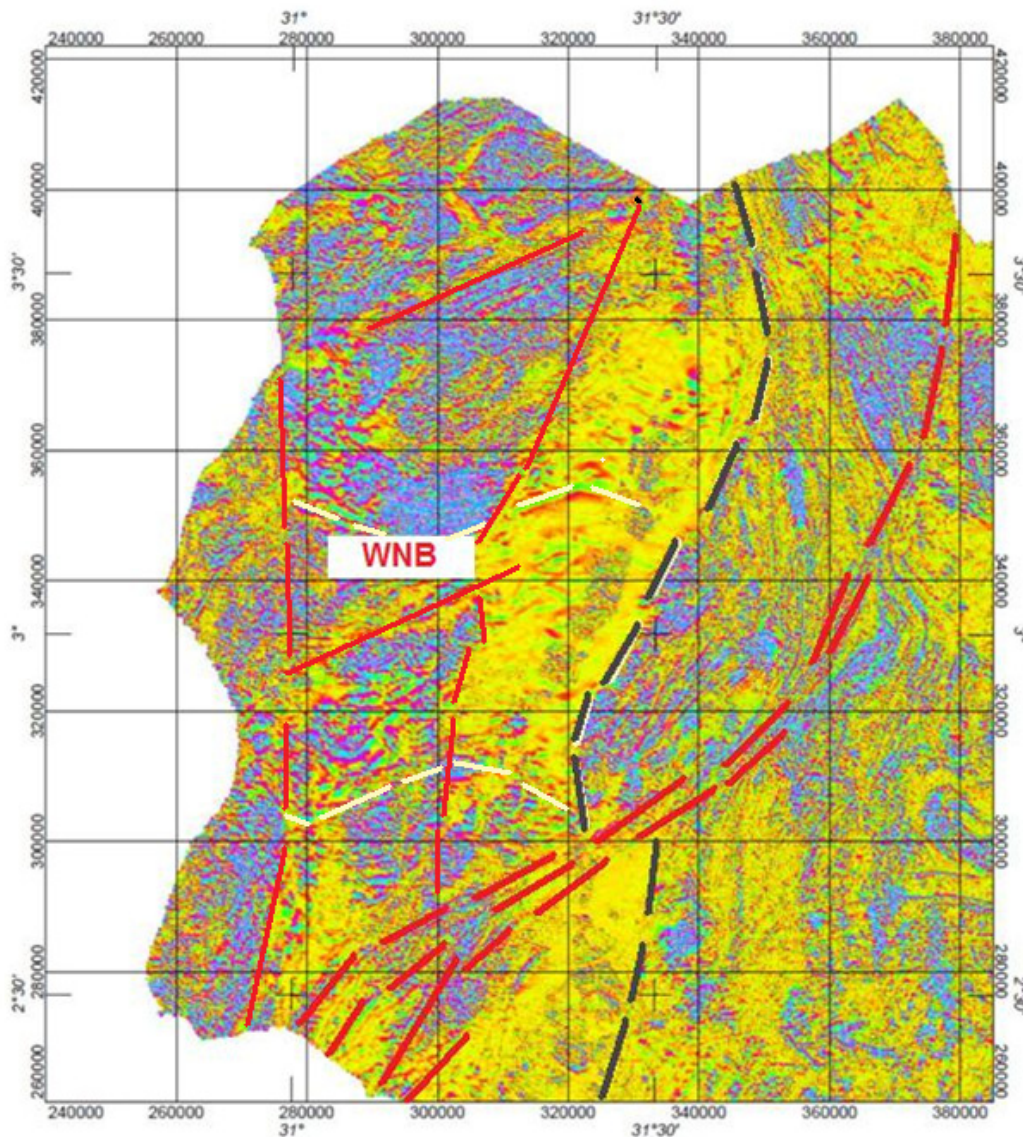


Fig. 9.25. First vertical derivative of the Total Magnetic Intensity image of northwestern Uganda. WNB = West Nile Block. The image shows a clear sigmoidal E–W-trending grain (white lines), which continues below the Neogene sediments of the Albertine Rift (yellow in the image) to the interrupting black line. East of this line, curvilinear N–S structural trends predominate. Major normal or strike-slip faults (or a combination of the two) are shown in red.

west-verging thrust masses of the Madi-Igisi Belt composed of reworked fragments of Neoproterozoic 'basement', including the Yumbe Complex (Section 4.7 and Fig. 9.26) and Lobule lithologies east of Nebbi, the latter intersliced with juvenile ~1.0 Ga 'Mirian' rocks. A mirror image, with east-verging thrust masses, occurs along the eastern shoulder of the Albertine Rift (Fig. 9.1).

Igisi lithologies north of Masindi – According to our current view, double-vergent thrusting in the Madi-Igisi Belt was followed by major sinistral strike-slip faulting, resulting into a number of interlocking crustal wedges reaching from Moyo town to Lake Albert. This feature is well illustrated

by fault-controlled slices of Igisi rocks, alternating with large lumps of Archaean basement, along the eastern shore of Lake Albert. Mylonite zones, separating these fault blocks, can occasionally be found, for example in an outcrop located 38 km north of Masindi town, at the margin of the rift scarp, where blastomylonite showing ductile deformation (Fig. 9.27A) is overprinted by a brittle collapse structure, possibly related Neogene normal rift faulting (Fig. 9.27B).

Tectonism within the Lake Albert segment of the Igisi Belt has most likely also produced an impressive breccia structure 31 km WNW of Hoima town, where local basement granitoid has been thoroughly ground into a blackish ultra-

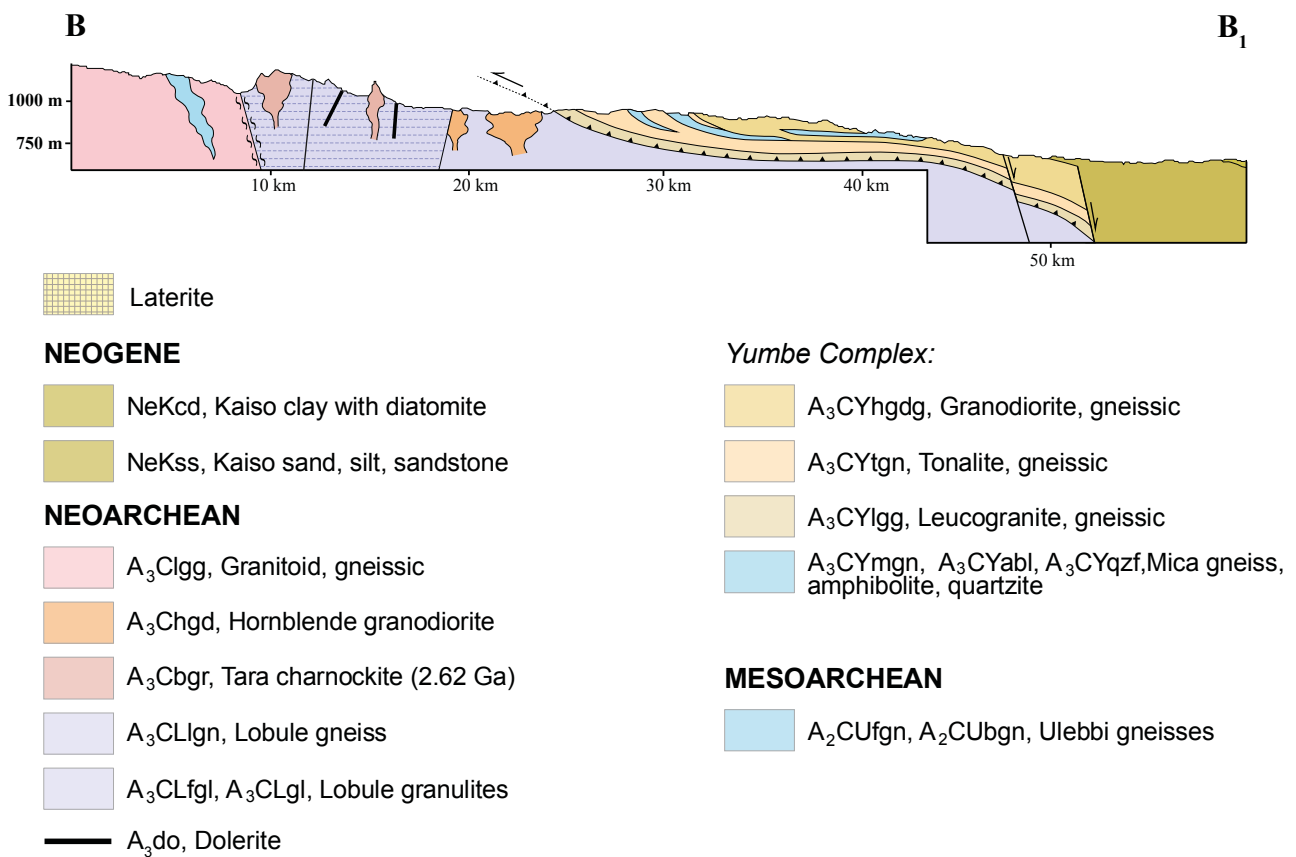
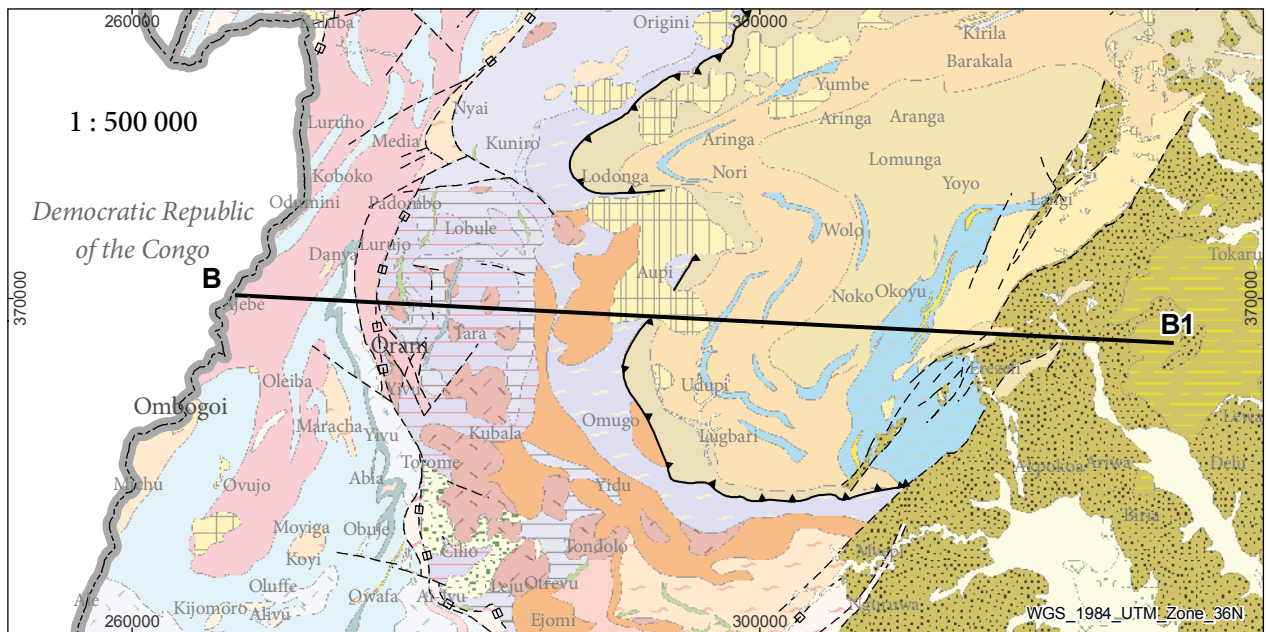


Fig. 9.26. Schematic E-W-trending profile across the northern part of the West Nile Block, showing west-vergent thrusting of the Yumbe Complex over Neoproterozoic rocks of the Arua-Kibale Supergroup of the West Nile Block. The vertical scale and altitude refer only to the surface of the basement. The geology and codes of lithological units are from the unpublished 1:250 000 scale maps of DGSM.

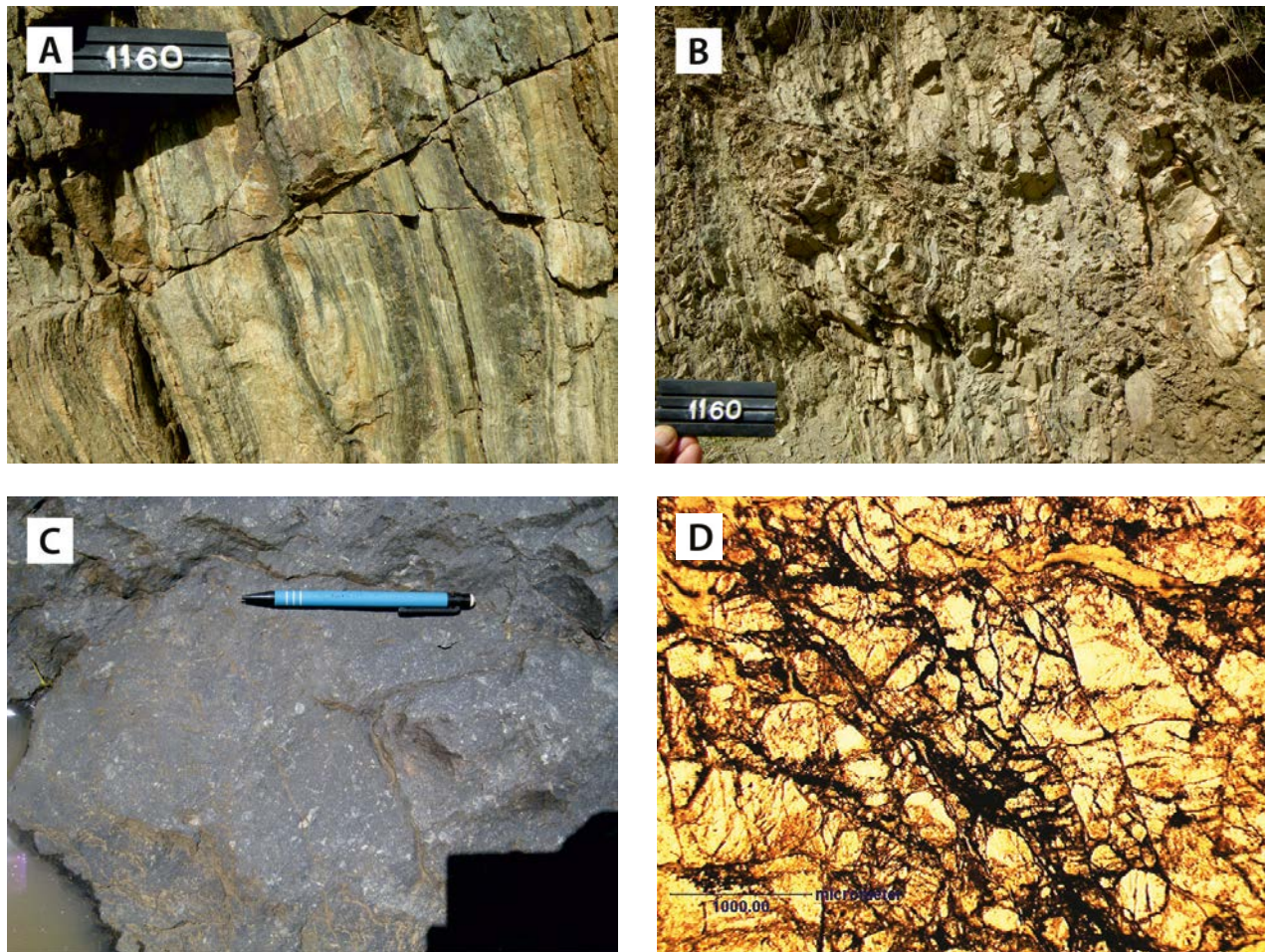


Fig. 9.27. (A) Archaean gneiss, thoroughly mylonitised (357343E / 225681N). Number tag 10 cm. (B) A brittle normal fault related to the Albert Rift superposed on mylonite. (C) Ultramylonite or pseudotachylite, originally probably representing an Archaean granitoid (286232E / 165827N). (D) Microphotograph of the same rock, showing a microbreccia with a network of glass veinlets in the upper part of the image. The pale fragments are quartz and plagioclase, thoroughly fractured. The width of the image is 4 mm.

mylonitic mass (Fig. 9.27C), intersected by randomly directed micro-fractures (Fig. 9.27D). The extreme hardness of this pseudo-tachylitic rock is produced by thin films and veinlets of glass, welding the fragments into a solid rock. The glass was probably produced by friction heat within a zone of Mirian faulting.

Van Straaten (1976) attempted a structural analysis of the tectonically complex Igisi zone north of Masindi and divided the zone into three parallel structural domains:

- *Zone 1* – Comprises a 1–2-km-wide zone directly east of the Rift escarpment with B_1 similar folds, a poorly developed axial-plane cleavage S_1 and a well-developed, N–S to NNE–SSW directed lineation L_1 . D_2 effects are only observed in rare cases.
- *Zone 2* – Separated from Zone 1 by mylonite

zones, this central, 2–3-km-wide structural zone is characterised by isoclinal F_1 folds and closely spaced, mylonitic shear zones, 10 to 20 cm apart and parallel to NE–SW-directed F_1 axial planes. Characteristic for this zone is also the presence of ‘granulite inliers’ of the Mesoproterozoic Karuma Complex (Section 5.3), ranging in size from 100 m to several kilometres.

- *Zone 3* – This up to 2-km-wide zone forms the boundary layer with the Karuma granulites, not only marked by an abrupt change in petrological composition (muscovite out, hypersthene in), but also by a tectonic contact with mylonites and cataclasites manifesting sinistral strike-slip movements. Isoclinal F_1 folds with axial plane cleavage S_1 and lineation L_1 are well developed. NW-directed B_2 and L_2 structural elements can be observed in places.

Exposures along the road from Bisio to Butiaba

show blastomylonitic gneiss with feldspar grains that have been fractured and pulled apart, and quartz in a fine, anastomosing, but well-directed network (Fig. 9.28A). Quartz stringers may be whitish or translucent, suggesting different generations of quartz during successive phases of shearing and annealing. Further down the road to the rift valley, more quartzose lithologies are exposed, which invariably show a typical blastomylonitic fabric (Fig. 9.28B). Further southwards, along the road from Buhumba to the Lake Albert Safari Lodge, strongly deformed meta-volcanic(?) rocks have been encountered, which are not described by van Straaten (1976). These include banded, creamy to pinkish strata comprising weathering-resistant felsic volcanics that alternate with strongly weathered mafic volcanic rocks. Quartz layers, lenses and laminae are believed to be pseudomorph after flow banding.

Geodynamic scenario – Thrust masses of the Madi-Igisi Belt rest unconformably on the Archaean gneisses and charnockites/granulites of the West Nile Block and North Uganda Terrane, and can be distinguished from these, as mentioned above and again quoting Hepworth (1964), by (1) their flaggy nature and (2) moderate eastern dips (30°–40°). As argued above, these moderate dips apply to a new foliation parallel to the basal and intraformational thrust planes with older foliations usually completely obliterated (Fig. 9.24). Parallel bedding in gently to sub-horizontally dipping (5°–25°) strata

(e.g. sericite quartzites) have been observed, often in combination with gentle to open fold structures with subhorizontal fold axes. However, in other locations, steep to subvertical banding was observed. Recumbent folds (Figs 9.6B, 9.9B) and drag folds (Fig. 9.24B) manifest low-angle tectonic transport. The flaggy nature appears best developed close to thrust planes.

Hepworth (1964) qualified the metamorphic grade of the eastern gneisses as epidote-amphibolite facies, with muscovite instead of biotite, *versus* the high-amphibolite and granulite facies of rocks belonging to the later Uleppi Group and the Arua-Kibale Supergroup (Chapter 5). The metamorphic grade of Igisi metasediments and metabasites in the Igisi type-area was initially characterised as epimetamorphic (Watkins 1956, Macdonald 1967, van Straaten 1976). Equivalent Igisi pelitic schists from Murchison Falls contain a peak metamorphic assemblage composed of kyanite + garnet + biotite + muscovite + quartz + plagioclase ± K-feldspar, and manifest metamorphic conditions of 0.8 GPa (8 kb) and 650–680°C (Appel et al. 2004, 2005). Similar conditions are reflected by Mirian garnet-bearing amphibolites (Fig. 9.14). In places, these high temperatures are confirmed by dehydration melting features. However, subhorizontal sericite quartzites, east of Nebbi, show ripple marks (Fig. 9.13B) and indicate a far lower degree of metamorphism. It thus appears that the metamorphic grade of rocks in the Madi-Igisi Belt is strongly variable and that in places, due to shearing, rocks



Fig. 9.28. (A) Blastomylonite gneiss with feldspar crystals up to 10–15 mm and extremely elongated quartz grains. Most feldspar grains have been fractured and pulled apart. Quartz forms a fine, anastomosing, but well-directed network. Several phases of quartz can be distinguished, manifesting repeated shearing and annealing. (B) Thinly bedded blastomylonite schist showing pronounced blastomylonitic fabric near an escarpment of the Albertine Rift between Biso and Butiaba (319786E / 197382N). Number tag 8 cm.

of strongly different metamorphic grade have been juxtaposed.

From the geochronological data (see also Mänttari 2014), it is concluded that the prolonged phase of Archaean crust formation in NW Uganda (>3.08 to 2.55 Ga) was followed by a long period of quiescence. No indications manifesting Rwenzori orogenesis in northwestern Uganda have been encountered. Instead, Mirian sericite quartzites east of Nebbi have been observed to contain a predominant population of detrital zircons with Palaeoproterozoic ages between 2.2 Ga and 1.8 Ga, with a peak at ~1.86 Ga. This is assumed to manifest uplift and erosion in the Rwenzori Belt in the south, in particular uplift and denudation of the 1.85 Ga Mubende and Singo granites, and direct transport to depositional basins in NW Uganda. This could mean that the Mirian trough already started to develop not long after emplacement of the above 1.85 Ga granitoids. The alternative, that these zircons were first transported to other sedimentary units (e.g., rocks of the >2.05 to 1.79 Ga Namuwa and Bwezigoro Groups and Kagera-Buhweju Supergroup, Chapter 7) and subsequently reworked to their final destination in NW Uganda is not so likely, given that rocks of the latter units are not rich in 1.85 Ga zircons (although we must realise that only the bottom segments of these formations have been preserved). It is more likely that Mirian basin development and sedimentation started as late as 0.98 to 0.99 Ga.

Detrital zircons from a muscovite-biotite schist from the Moyo area yield Neoproterozoic to late Archaean (2.63 to ~2.48 Ga) ages from mostly core domains. Younger metamorphic zircon rim growths have been dated at ~1.0 Ga, and one single rim has an age of ~0.7 Ga. Finally, U-Pb ages from clearly zoned zircon grains from Mirian metatuff in the same area plot in a tight cluster at 1.0 Ga on the concordia diagram. This metatuff represents the source for the detrital zircons in the arenitic and pelitic sediments in the area, now metamorphosed into sericite quartzite and muscovite-biotite schist.

The oldest indications of Pan-African tectono-metamorphic reworking of Archaean basement in the West Nile Province have been evidenced by K-Ar dating of supposedly retrograde biotite from charnockite, biotite from granulite and fuchsite from quartzite, yielding (cooling or mixed) ages of 660 ± 25 Ma, 541 ± 22 Ma and 659 ± 26 Ma, respectively. This is confirmed by our U-Pb dating

of metamorphic monazites in sericite quartzites, indicating metamorphic overprinting at ~0.66 Ga. Monazites from equivalent Igisi kyanite-garnet schists from Murchison Falls gave ages of 0.62 to 0.63 Ga for the metamorphism of the metapelite series (Appel et al. 2004, 2005).

Based on the great variety in tectonic structures (transposition of foliation, low dip angles, recumbent and drag folds, ‘flagginess’ of some strata) and the wide range in metamorphic grade, the Mirian rocks are here interpreted as a thin- or thick-skinned stack of tectonic units. Juxtaposition of units with different tectonic features or contrasting metamorphic grades is supposedly either due to telescoping of units of different metamorphic grade, but originally pertaining to a series that suffered progressive regional metamorphism, or due to the incorporation of higher grade, older, supposedly Archaean fragments in the tectonic pile. Hepworth (1964) considered the ‘flagginess’ and generally low to moderate dips of the Mirian lithologies the single most distinctive feature of these rocks, which was further intensified by refolding in its eastern parts. His structural analysis suggested isoclinal refolding of an existing foliation in the eastern flaggy outcrops, accompanied by extreme attenuation of the layers, and Hepworth (ibid.) was already of the opinion that “*it is possible that the ‘Flaggy Eastern Grey Gneisses’ is a younger series, isoclinally folded and overturned in the Schuppen zone at the top of a tectonic pile,*” or in modern language: a thin-skinned zone of overturned tectonic lenses (‘Schuppen’), overlying the Archaean western gneisses and central charnockites/ granulites.

Based on the scarce geochronological data at hand, it appears that the Madi-Igisi Belt formed during a relatively short period of time, roughly some 5 to 10 million years, according to the following scenario: Deposition and basin development took place shortly before 0.99 Ga, in its final phase associated with emplacement at 0.99–0.98 Ga of igneous, supposedly intermediate, tuffaceous rocks (quartz dacite or andesite) and some sub-volcanic dolerites. The youngest detrital zircons in clayey sandstones (now sericite quartzites) and pelites (now schists) appear to have derived from these tuffites. This was followed immediately afterwards by metamorphism and deformation at ~1.0 Ga and reworking at around 0.70 Ga to 0.62 Ga. In this scenario, the Madi-Igisi Belt is the product of two orogenic cycles – the Grenvillian and Pan-African. The latter rejuvenation at 0.70–0.69 Ga of

the Madi-Igisi Belt can be considered as a far-field effect of E–W compression in the Karamoja Belt. Other structural elements (e.g., the ENE directed lineation and block faulting in the Moyo area) and 0.66–0.62 Ga monazite ages are tentatively related to N–S collision between East + West Gondwana and the Sahara meta-Craton (Chapter 11).

Along the same line of thinking, the Yumbe Complex (Fig. 9.26) and similar thrust masses along the western and eastern rift shoulders are viewed as allochthonous duplex or thin-skinned structures composed of a variety of gneisses of supposedly Archaean age. Their tectonic emplacement is, however, attributed to the late Mesoproterozoic ‘Mirian’ and/or Neoproterozoic ‘Chuan’ events (Table 4.1).

The Madi-Igisi Belt formed concomitantly with the final episode of the Kibaran Orogeny of central Africa (Chapter 8), which can be correlated with the worldwide Grenvillean Cycle, culminating with the formation of the Rodinia Supercontinent (~1.00 Ga). In Uganda, this is mimicked by Kibaran compression (~1.10–1.00 Ga), known in Africa as the Lomanian Orogeny (Pohl 1987b). In the North Kibaran Belt of southwestern Uganda and central Africa, this coincided with emplacement of the so-called ‘tin granites’ at ~1.1–1.0 Ga and fertile pegmatite bodies (Sn, Nb, Ta, Li, etc.), supposedly derived from these ‘tin granites’, at ~0.95 Ga (Romer & Lehmann 1995).

The Madi-Igisi Belt probably originated as a south-propagating strike-slip rift system in the proto-Congo Craton, broadly coeval with the ‘final docking’ of the lithospheric plates that formed Rodinia. It is comparable to the volcano-sedimentary Koras-Sinclair-Ghansi sequences (~950 Ma) of eastern Namaqualand and Namibia (Thomas et al. 1994) that signal the end of the Grenvillean Cycle in Africa. The poorly known Itombwe Supergroup in Kivu Province (eastern DRC) could represent the southern continuation of the Madi-Igisi Belt. The Itombwe Supergroup with N–S to NW–SE-directed major folds (Mugisho 2013) unconformably overlies folded Kibaran graphitic mica schists and quartzites, into which 1020 ± 50 Ma granitoids have been emplaced (Walemba 2001, Walemba et al. 2004).

The Madi-Igisi Belt is thus described here as an intracratonic N–S-trending thrust and fault zone, separating the North Uganda Terrane from the West Nile Block, the easternmost segment of the Bomu-Kibalian Shield. Lenses of metamorphosed and metasomatised ultramafic rock (e.g., Nyunyu Hill Formation, Figs 9.21 and 9.22) in the strike-slip fault zone between the town of Moyo and Lake Albert fit poorly in the above model. Most likely, they represent fragments of sub-lithospheric upper mantle, but it is obvious that far more research is needed in the flat, poorly exposed area where these bodies have been encountered¹.

1 Flemish Gold Corp. holds five licences in Uganda, summarily called the Murchison Project, that comprise a land package of 1,575 km². The geochemical and geophysical test results on the mafic and ultramafic bodies of the Murchison Project have been favourable to date. Flemish management believe the mafic and ultramafic bodies are prospective for nickel, cobalt and copper.

10 POST-RODINIAN NEOPROTEROZOIC PLATFORM ROCKS OF THE MALAGARASI SUPERGROUP

10.1 Malagarasi Supergroup

Post-Rodinian, early Neoproterozoic extension gave rise to rifting and the development of basins with deposition of terrigenous sequences and local volcanism, often evolving into passive margin sedimentation upon drift. Rifting affected the proto-Congo Craton sensu de Waele et al. (2008) between 880 and 820 Ma (Johnson et al. 2007), followed by a second depositional cycle starting at ~765 Ma (Key et al. 2001).

Some of the post-Rodinian, early Neoproterozoic intracratonic extensional or pull-apart basins include the Kundulungu (Katanga, DRC) and Malagarasian (NW Tanzania and eastern Burundi) basins (Fig. 1.13). The latter is partly superposed on an older, Palaeoproterozoic molasse-type platform sequence, including the Kagera-Buhweju

Supergroup (see below and Chapter 7). Rocks of the type-locality of the ‘Malagarasian’ (Waleffe 1965, Tack et al. 1992) or Malagarasi Supergroup in western Tanzania and eastern Burundi have been described in Section 1.6. Their extent and subdivision are shown in Figures 1.13 and 1.14, respectively.

Undated platform sediments in southern-central Uganda, assigned to the ‘Singo Series’ and ‘Mityana Series’, were traditionally attributed a Neoproterozoic age (Combe 1923, King 1943, 1947a). Based on correlation with similar rocks of the Kagera Supergroup in NW Tanzania and Burundi (Cutten et al. 2004, de Waele et al. 2008) and on the dating of detrital and primary zircon grains (Mänttari 2014) of rocks belonging to the former

Table 10.1. Generalised succession of platform sediments and associated (sub)volcanic rocks of the Malagarasi Supergroup (e.g., Schlüter 2006 and references therein) in SE Burundi, west Tanzania and tentative correlation Neoproterozoic platform sediments in Uganda.

| BURUNDI | TANZANIA | | UGANDA |
|---|--|---|--|
| | NYAKANAZI DIAMICTITES ³ | | TILLOIDS OF BUNYORO |
| KIBAGO GROUP (~865 m) • Sandstones, mudstones and basal conglomerates | U H A G R O U P | MANYOVU RED BEDS | BUNYORO/KIOGA GROUP |
| MOSSO GROUP (70–130 m) ¹ • Mo2: silicified dolomitic limestones • Mo1b: Kabuye Amygdaloidal Lavas (815 ± 14 Ma) ⁴ (several hundreds of metres). • Mo1a: Shaka conglomerate (very local) | | ILAGALA DOLOMITIC LIMESTONE | MITYANA GROUP |
| | | GAGWE AMYGDALOIDAL LAVAS (>600 m) (795 ± 7 Ma) | |
| MUSINDOZI GROUP (290–890 m) • Ms4: dolomites (including stromatolites (888±16 Ma) and chert • Ms3: (calcareous) mudstones, sand-stones and siltstones • Ms2: Nyaganza Basalts ² | KIGONERA FLAGS | | |
| Unconformity upon Burundian and Kavumwe/Nkoma Supergroups and Archaean Tanzania Craton | Unconformity upon Karagwe and Kagera Supergroups (now Akanyaru-Ankole Supergroup) and Archaean Tanzania Craton | | Unconformity upon Buganda Supergroup and Archaean of North Uganda Shield |

(1): Estimated thickness of the sedimentary sequence, excluding dolerite sills and basaltic rocks. (2) Ms2: corresponds, in fact, to dolerite sills and therefore has to be omitted as a lithostratigraphic term (de Paepe et al. 1991, Tack & Thorez 1990). (3): Westerhof & Koistinen (2005). (4) Ages in de Paepe et al. (1991), recalculated after Cahen et al. (1984).

‘Singo Series’ in south-central Uganda, we conclude that part of these platform deposits have a much older Palaeoproterozoic age, between < 2.05 and 1.78 Ga. They are attributed to the Namuwa

and Bwezigoro Groups and the Kagera-Buhweju Supergroup discussed in Chapter 7. What remains of the platform rocks of Uganda are the former ‘Mityana Series’ and ‘Kioga and Bunyoro Series’.

10.2 Geology of the Mityana Group

10.2.1 Introduction

We have assembled the rocks of the former ‘Mityana Series’ in the Mityana Group. They occur mainly around Lake Wamala and in the Ssesse archipelago, but also form flat-topped ridges near Lake Victoria north of the Tanzanian border and crop out in small enclaves between the Singo and Mubende batholiths (Fig. 10.1). They are undated

and overlie Nile shales and schists of the Buganda Group and, in places, the Singo granite and sedimentary rocks of the Namuwa Group. Since they are not intersected by mafic dykes belonging to the 1.37 Ga Lake Victoria Arcuate Dyke Swarm (LVADS; Section 8.4.3), we attribute these rocks to the Neoproterozoic Malagarasi Supergroup (Table 10.1). The subdivision of the Mityana Group is represented in Table 10.2.

Table 10.2. Subdivision of the Mityana Group.

| Group | Formation | Lithology |
|---------|-----------|--|
| Mityana | Kajoji | Conglomerate, sandstone, siltstone, locally silicified |
| | Kyakatebe | Sandstone, gritstone |
| | Ssesse | Sandstone |
| | Debeza | Conglomerate, arkose |

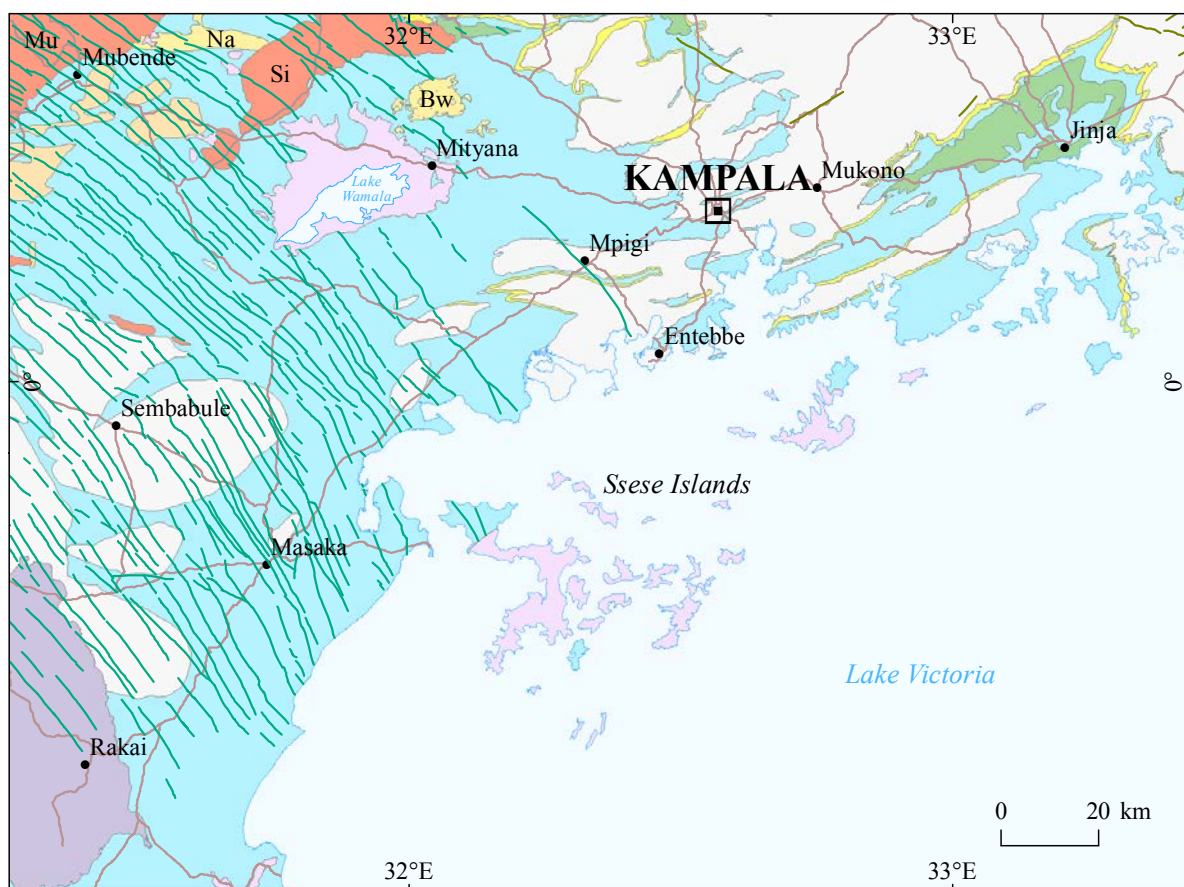


Fig. 10.1. Distribution of sedimentary rocks of the Mityana Group. Note the absence of intersecting mafic dykes (green lines) of the LVADS. Key: Buganda Group (yellow/green/blue), Mityana Group (light lilac), Na = Namuwa Group, Bw = Bwezigoro Group, Mu = Mubende batholith, Si = Singo batholith. Simplified after Lehto et al. (2014).

10.2.2 Lithostratigraphy of the Mityana Group

Conglomerate, arkose – Sub-horizontal to slightly tilted, polymict conglomerate and arkosic sandstones of the *Debeza Formation* are exposed near the Mubende and Singo granite plutons and represent the basal part of the Mityana Group. They unconformably overlie metapelites of the Nile Formation, but the footwall contact is not exposed, while the hangingwall contact with sandstones and grits of the overlying Kyakatebe Formation is transitional. Lithologies of the Debeza Formation comprise brownish, matrix-supported conglomerate, with sub- to well-rounded pebble- and cobble-sized vein quartz and sandstone clasts in an arkosic sandstone matrix (Fig. 10.2).



Fig. 10.2. Sub-rounded sandstone and vein quartz clasts in conglomerate of the Debeza Formation. Outcrop near the eastern contact of the Mubende granite (336173E / 71182N). Number tag 8 cm.

Sandstone – Mapping of Bugala Island and surrounding smaller islands in the Ssesse archipelago of Lake Victoria showed an abundance of sandstone outcrops of the *Ssesse Formation* (Fig. 10.3). Almost all sandstone exposures occur in smooth ridges and show gentle to moderate dips in various directions. Mudstone intercalations are scarce compared to equivalent mainland sections of the Mityana Group. Only some minor parts of the archipelago are underlain by pelitic rocks, which, however, belong to the Nile Formation of the Buganda Group.

On the Ssesse archipelago, the major lithology of the Ssesse Formation is fine-grained sandstone with occasional minor mudstone intercalations.

Cross-bedding is common, locally showing herringbone structures (Fig. 10.4A). Together with well-developed ripple marks they manifest deposition in tidal channels. Intense changes of colour, related to redox reactions, are often visible on bedding planes and fissures.

In the mainland, near the Tanzanian border, these gently tilted metasediments form mesa-like, flat-topped erosional ridges. There, light brownish to reddish sandstone (Fig. 10.4B) has thin, monomict conglomerate horizons, with small (≤ 3 cm), angular quartz fragments set in a coarse-grained, arkosic matrix. Cream coloured, strongly banded siltstone also exists as thin, strongly oxidised interbeds within sandstones of the Ssesse Formation.



Fig. 10.3. Gently tilted sandstone of the Ssesse Formation on Bugasa Island of Lake Victoria.

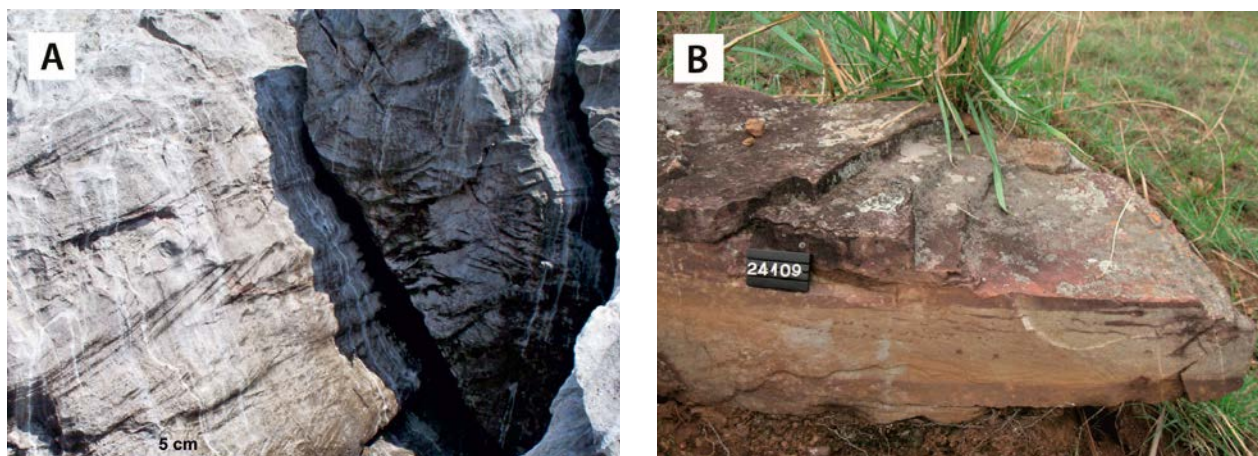


Fig. 10.4. Sandstones of the Ssesse Formation. (A) Herringbone structure in sandstone on Bugala Island (427766E / -67860N). (B) Partly oxidised Ssesse sandstone on a mainland ridge near the Tanzanian border (351391E / -104310N). Number tag 8 cm.

Sandstone, gritstone – Subhorizontal beds of sandstones and gritstones of the *Kyakatebe Formation* are exposed in the area NW of Lake Wamala. Contacts with underlying arkoses and conglomerates of the Debeza Formation, as well as with pelitic metasediments of the Nile Formation, are not exposed. On aerial radiometric maps, psammitic metasediments of the *Kyakatebe Formation* generally show a rather strong positive potassium signature.

Yellowish-brown, fine- to medium-grained sandstone forms the main lithology of the *Kyakatebe Formation*, together with thin, gritty interbeds of light brown, laminar siltstone and beds with random angular to sub-rounded vein quartz pebbles. Apart from subhorizontal, tabular bedding, low-angle cross-bedding and asymmetric ripple marks can be observed (Fig. 10.5A). Bowl or saucer-like depressions in the bedding

planes, up to ~50 cm in diameter, supposedly represent load cast or pore water escape structures (Fig. 10.5B).

Conglomerate, sandstone, siltstone, locally silicified – A subhorizontal, heterogeneous succession of clastic sediments, including conglomerates, arkosic sandstones, and variably silicified siltstones of the *Kajoji Formation*, are widely exposed around Lake Wamala. Small, isolated sandstone outcrops of the same unit have been found overlying the Singo granite (Johnson 1960).

The base of this sedimentary succession comprises a horizon of coarse polymict, tightly packed conglomerate, up to 8 m in thickness (Johnson 1960), with generally well-rounded sandstone, siltstone, quartzite or rare conglomerate pebbles, cobbles and boulders, up to one metre in diameter, in a coarse, sandy matrix (Fig. 10.6A).

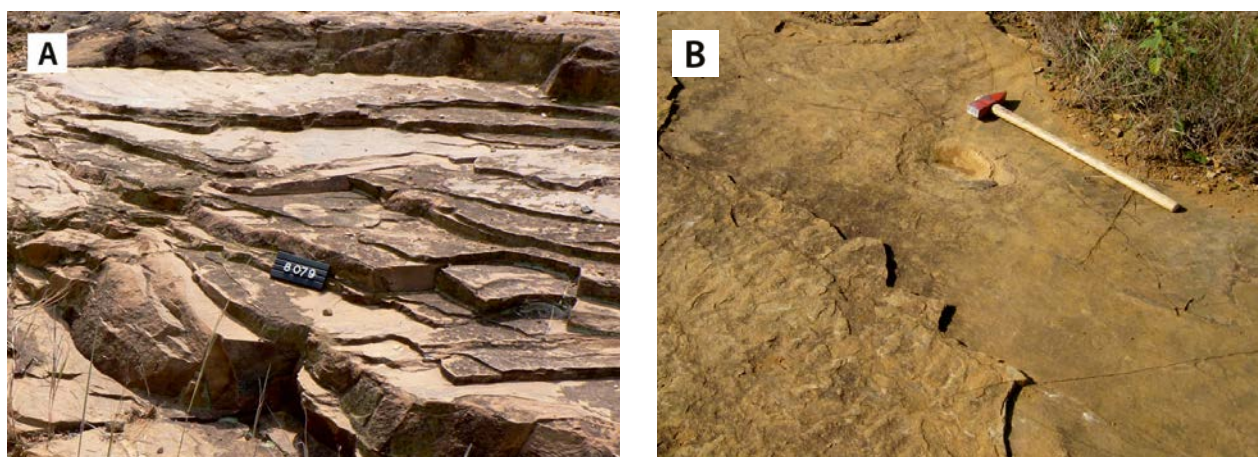


Fig. 10.5. (A) Subhorizontal sandstone beds of the *Kyakatebe Formation* (367932E / 50890N). (B) Ripple marks and saucer-like depressions in the same sandstone. Number tag 10 cm, length of hammer 60 cm.

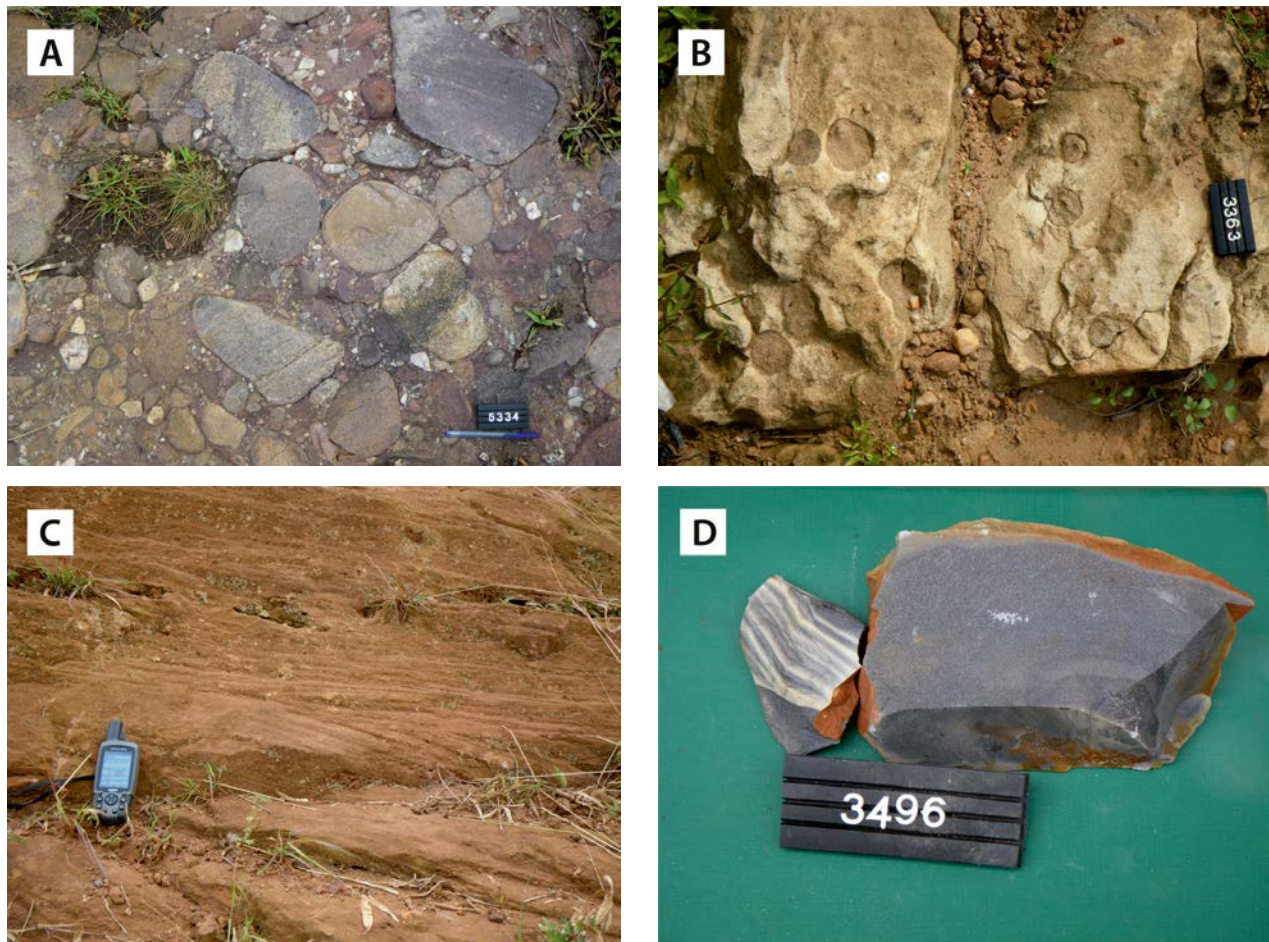


Fig. 10.6. Primary sedimentary structures of the Kajoji Formation. (A) Polymictic, clast-supported conglomerate (394940E / 47438N). (B) Concentric concretions in buff sandstone (394201E / 45584N). (C) Tabular, low-angle cross bedding in maroon sandstone (398022E / 43022N). (D) Silicified, flinty siltstone with conchoidal fracture and diffuse banding (387156E / 34206N). Number tags 8/10 cm, GPS 15.5 cm.

A layer of maroon to buff-coloured sandstone, 1.5 m to 25 m in thickness, commonly overlies this conglomerate horizon around Lake Wamala (Johnson 1960). Gritty, massive varieties and more fine-grained, arkosic sandstones with angular feldspar grains have been encountered. Thin horizons of angular vein quartz fragments occur locally, and roundish concretions, up to 5 cm in diameter, exist in some sandstone outcrops east of Lake Wamala

(Fig. 10.6B). Parallel bedding is not commonly observed, but low-angle cross bedding occurs in places (Fig. 10.6C).

Grey, very fine-grained siltstone with mostly microcrystalline quartz occurs locally in the upper part of the sedimentary succession. Diffuse banding in flinty siltstone varieties, found in some outcrops south of Lake Wamala, may represent primary bedding (Fig. 10.6D).

10.3 Geology the Bunyoro Group

10.3.1 Introduction

According to the geological map compiled by Macdonald (DGSM 1966), Neoproterozoic platform sediments, comprising shales, arkoses, quartzites and tillite-like rocks of the Kioga and Bunyoro Series cover a large crescent-shaped domain. These sediments cover an area measuring some 250 km

in length and 20–50 km in width from the Hoima-Masindi area near Lake Albert to the eastern part of Lake Kyoga (Fig. 10.7). The Bunyoro Series was reported to overlie the former Archaean Basement Complex further to the west.

Tilloids of the Bunyoro Group can be correlated with Nyakanazi diamictites in NW Tanzania (Table 10.1) and similar rocks in eastern Burundi.

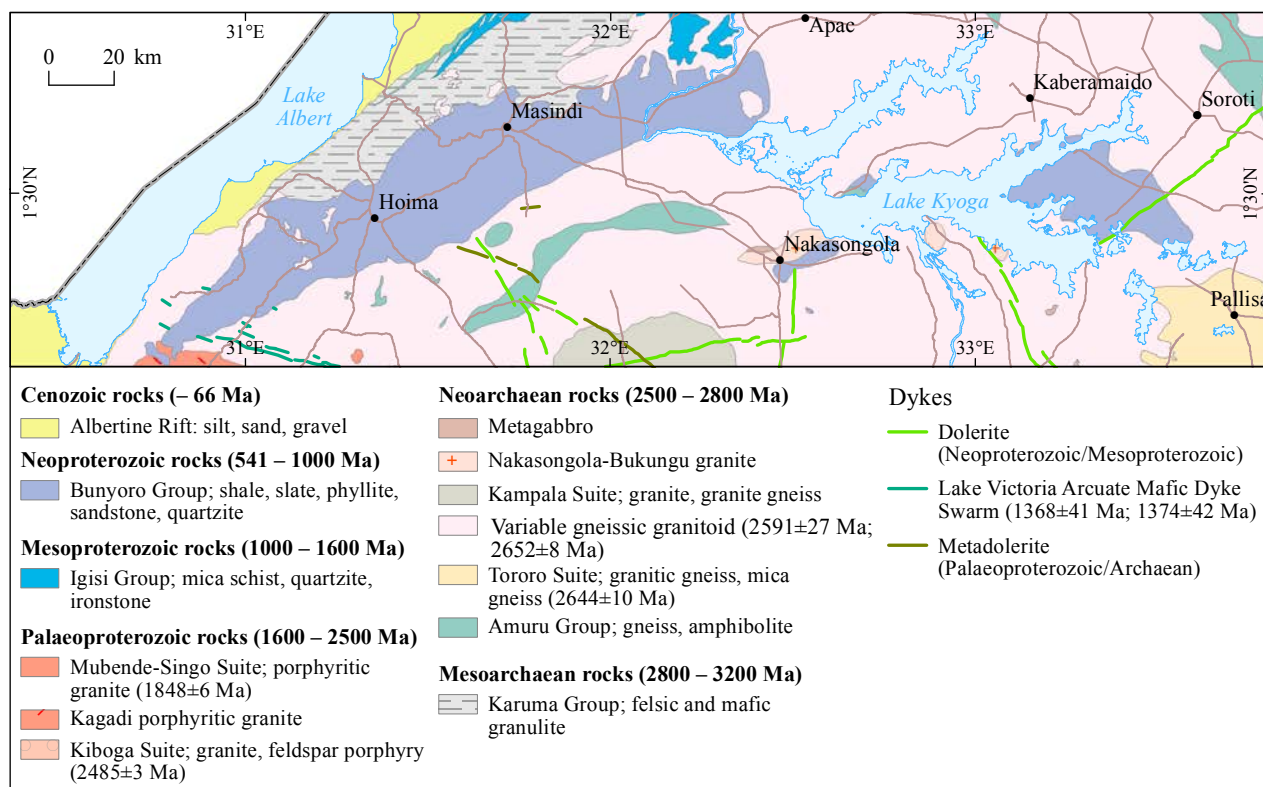


Fig. 10.7. Outline of the geology of central Uganda, showing the distribution of the Bunyoro Group (bluish grey) stretching from Lake Albert and the Hoima-Masindi area to the east of Lake Kyoga. Simplified after Lehto et al. (2014).

As such, they overlie or constitute the uppermost part of the Malagarasi Supergroup. Like the sub-horizontal platform rocks of the Malagarasi type locality, the Bunyoro rocks in Uganda have been traditionally described as being gently folded but not much metamorphosed. Our field work demonstrated that while this is true in most locations, locally these rocks have been affected by variable, generally weak deformation and show distinct tilting and folding.

10.3.2 Lithostratigraphy of the Bunyoro Group

The Bunyoro Group has been subdivided into the stratigraphic units shown in Table 10.3.

Tillite (P3MBti) – Bjørlykke (1973) noted that conglomerates and pebbly mudstones from Musaijamukuru Hill (Fig. 10.8A), 16 km SW of Hoima town, and other hills nearby, in the lower part of the Bunyoro Group, are of glacial origin, supporting the conclusion reached by earlier workers (Davies 1939, 1940). These hills are local landmarks within generally continuous tillite zone, named here as *the Musaijamukuru Formation*.

A mica schist fragment with crenulation cleavage can be observed in thin section (Figs 10.8B-C). The matrix is composed of splits of granitoid rock and minerals embedded in fine, sub-microscopic matter originating from a variety of basement rocks. In addition to granite (Fig. 10.8D) and

Table 10.3. Subdivision and lithology of the Bunyoro Group.

| Group | Formation | Lithology | Code |
|---------|---------------|---|---------|
| Bunyoro | Bulyango | Shale, slate, ferruginous in places | P3MBshf |
| | Hoima | Mudstone, shale, slate, phyllite | P3MBsh |
| | Mpaija | Sandstone | P3MBss |
| | Mudosi | Orthoquartzite, sericite quartzite, sericite schist (< 0.97 Ga) | P3MBos |
| | Musaijamukuru | Tillite | P3MBti |

mica schist, grains and sizeable ‘balls’ of carbonate rock also occur in places (Fig. 10.8E). They obviously belong to ‘limestone fragments’ preferably called marble, reported by Bjørlykke (1973), and most likely also originate from the metamorphic Igisi Belt, where marbles have been reported (van Straaten 1976).

Immediately east of the town of Masindi, glaciogenic deposits form a 200-m-high hill, consisting of fine- to very fine-grained sandstone, siltstone

and shale. These units may grade into one another or have sharp contacts. Round to angular rock fragments are concentrated in coarse, gritty horizons or appear as solitary clasts. In the gritty patches, the fragments are unsorted and irregularly distributed without showing any alignment, although oblong fragments are parallel to the bedding. Their sizes vary from centimetre-sized pebbles (most abundant) to cobbles and (rare) half-metre, angular blocks. In places, slight curving of

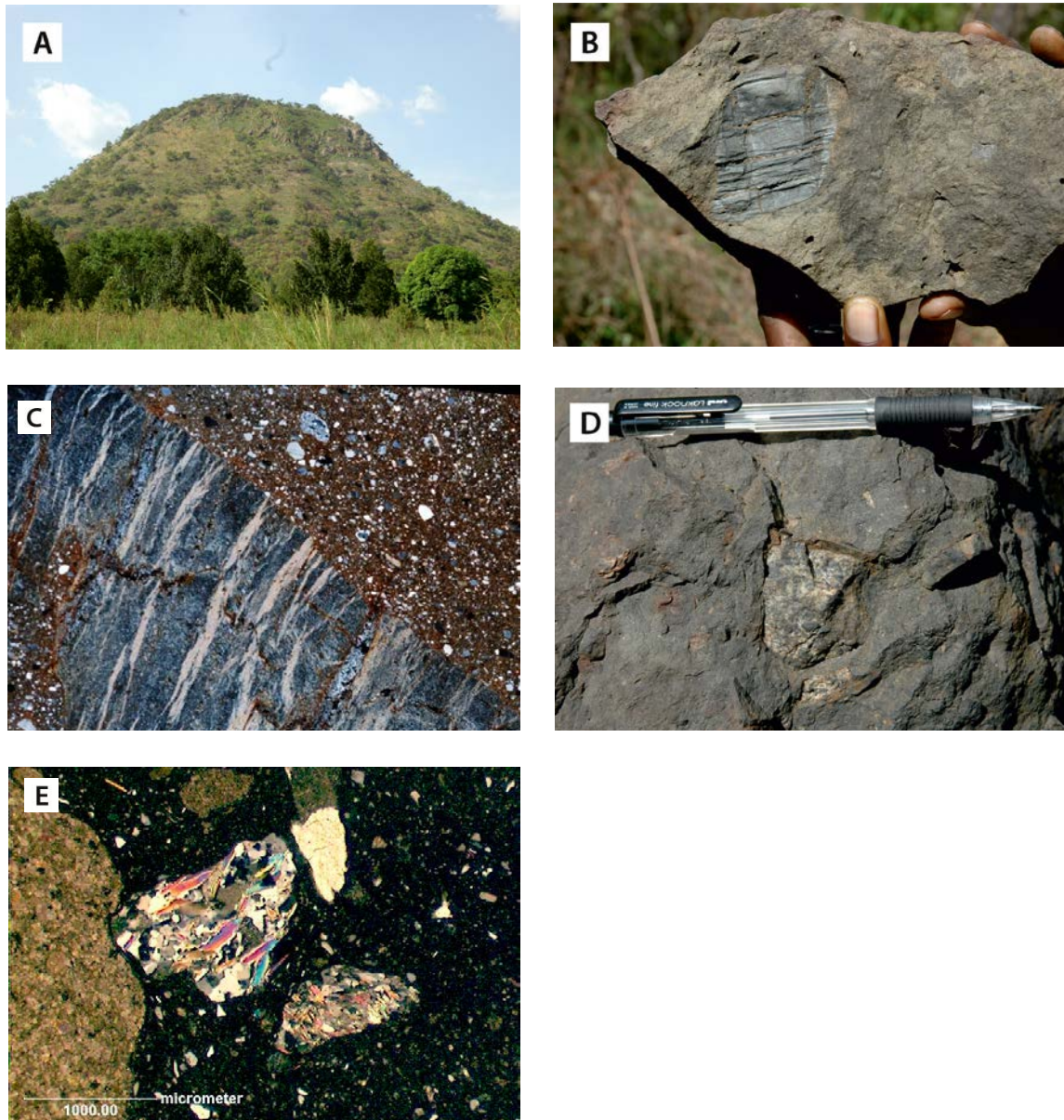


Fig. 10.8. (A) Musajjamukuru Hill (311749E / 143172N) seen from the SE, rising some 200 m above the flat surroundings. (B) Angular slab of supposedly crenulated Igisi mica schist in tillite. The matrix contains small fragments of mica schist; Musajjamukuru Hill (311085E / 142989N / 1250 m.a.s.l.). (C) Thin section across a fragment of mica schist shown in (B), showing crenulation of fine schistosity. (D) Angular pebble of basement granitoid in tillite. The matrix contains small fragments from granitoid rock together with other lithologies and minerals, Musajjamukuru Hill (312021E / 142809N / 1199 m.a.s.l.). (E) Microphotograph of two fragments of mica schist (centre right) and a marble fragment (left). The unsorted fine to ultra-fine matrix contains fragments of minerals from all available lithologies in the basement (280555E / 129435N); width of the thin section area is 15 mm.

the sedimentary layering is visible on the bottom side of these fragments, but may be unaffected on the top side. The fragments are mostly fine- to medium-grained, metamorphic lithic clasts, but occasionally some granular granite and gneiss clasts can be identified.

The fragments are clearly of a different origin than the fine-grained, creamy, yet deep-red to locally pink sedimentary succession and are considered as drop stones released from a floating ice sheet. Grading and rare shallow ripples were observed on bedding planes. In thin section, the shale comprises quartz and small, idioblastic hematite grains with iron precipitates on the quartz grains.

The alignment of well-rounded quartz grains and parallel concentrations of the iron phase define the silky tectonic cleavage. Such tectonic features are restricted to a few zones at the top of the hill, where a narrow layer of shale shows low angle to sub-horizontal conjugate fractures up to 12 mm in width, filled with quartz. Striations and mulions are parallel to the dip of the quartz veins (Fig. 10.9A) and plunge NNW between 4° and 18°. The low-angle deformation has also produced some tight recumbent folds (Fig. 10.9B) with a sub-horizontal axis (095°/03°) and axial plane (078°/20°). The orientation of the fold axis and intersecting lineation of the fracture sets are nearly normal to each other, manifesting that the tilting of the unit was caused by tectonic stacking caused by low-angle thrusting. The orientation of tension gashes between the quartz veins in a low-angle fracture set and the limb of the recumbent structure dip steeply to the south, indicating that the hanging

wall was thrust southward, compatible with the tectonic transport direction of Igisi mica schist at Bweyale.

Orthoquartzite, sericite quartzite, sericite schist (P3MBos) – Variably deformed rocks of the *Mudosi Formation* mainly occur between the eastern arms of Lake Kyoga, but also have several outcrops scattered within a 45 km radius from Nakasongola town. Close to Kwibale village, at the western end of the lake, quartz arenite, bordered by Bunyoro Group shales and slates in the north, forms a hilly landscape with high relief.

In the west, where quartz arenites prevail, the rocks are bluish in colour, brecciated and contain abundant fractures filled with quartz, which is evidence for fracturing and annealing after lithification. Quartz grains, typically 0.5 mm in diameter, are only partly recrystallised, and the blastoclastic texture is clearly visible. Some 10 km east of Namasale village, a yellowish brown, fine-grained quartz arenite forms a massive rock without any visible bedding features. East of Nakasongola town, quartz arenite is similarly brecciated to near Kwibale village. The rock is generally white in colour, but red hematite pigment is common.

Near the eastern segment of Lake Kyoga (Fig. 10.1), the Mudosi Formation is exposed in a range of hills and smooth north-sloping ridges (Fig. 10.10A), and in road cuts in the Egofa, Serere and Kateta Hills, mainly as light grey, sericite-bearing quartzite. Their composition varies from light brown, fine-grained siltstone or 'sericite schist' to steel grey sericite quartzite. Tangential cross-bedding is often visible, and laminar beds of

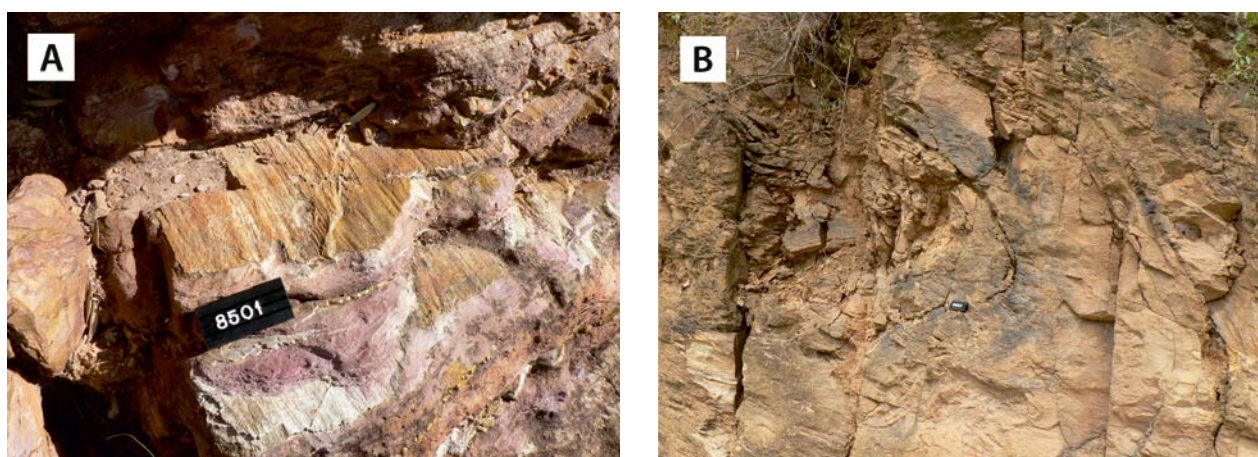


Fig. 10.9. (A) N-S-oriented striations on northward-dipping sub-horizontal conjugate fractures in glaciogene shale, east of Masindi town (view to NE) (361632E / 187012N). (B) A tight recumbent fold in the glaciogene strata (view to W). Note the shallow dip of the axial planar cleavage and easterly plunge of the fold axis (362104E / 187192N). Number tag 8 cm.

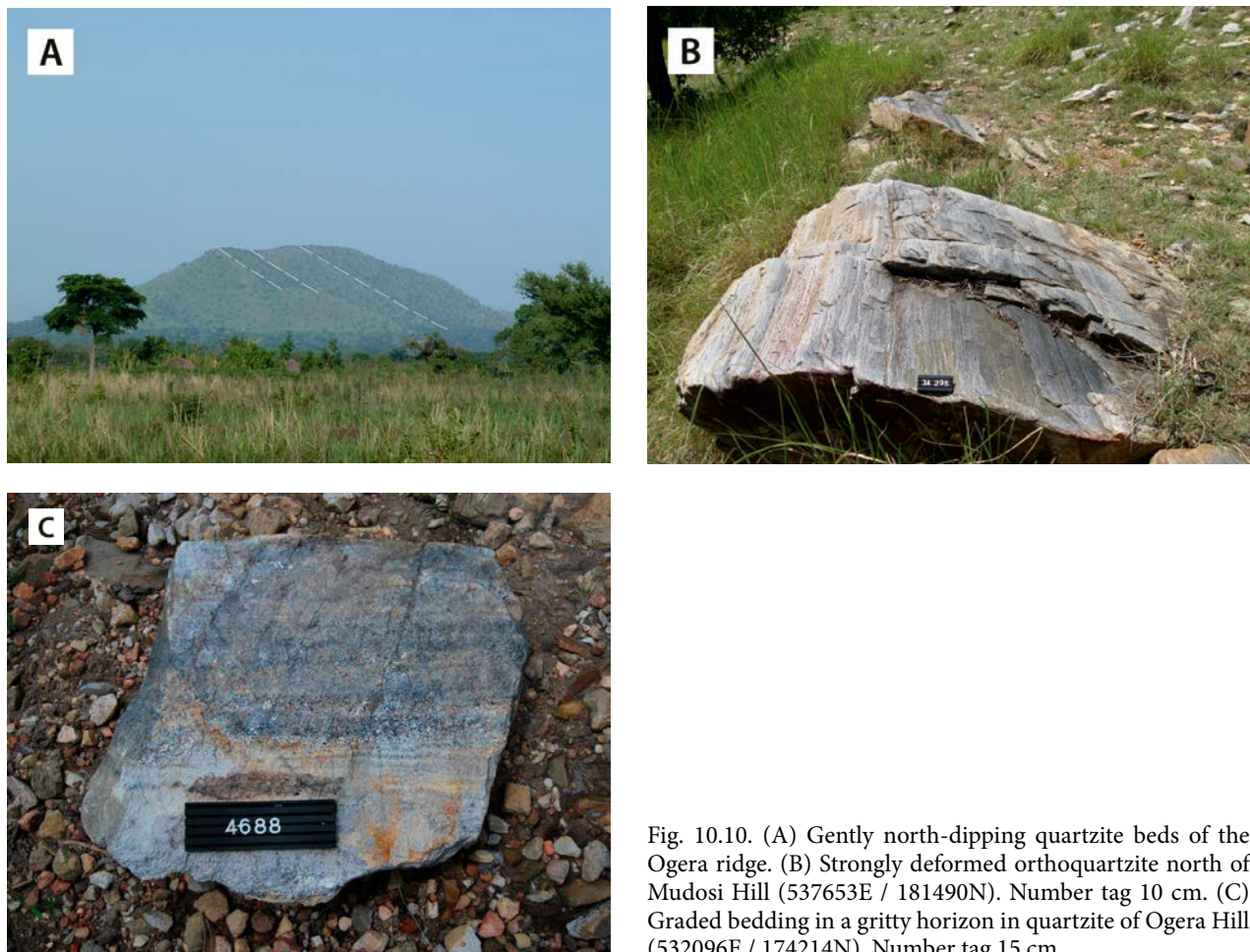


Fig. 10.10. (A) Gently north-dipping quartzite beds of the Ogera ridge. (B) Strongly deformed orthoquartzite north of Mudosi Hill (537653E / 181490N). Number tag 10 cm. (C) Graded bedding in a gritty horizon in quartzite of Ogera Hill (532096E / 174214N). Number tag 15 cm.

fine-grained, purple shale, as well as gritty interbeds with a well-preserved graded bedding (Fig. 10.10C) demonstrate a moderate degree of deformation.

Bluish-grey, strongly deformed, quartz veined orthoquartzite is exposed in ridges and small hills on the southern shore of Kojweri lake, the eastern arm of Lake Kyoga, where strong foliation has obliterated all primary sedimentary structures (Fig. 10.10B). Locally, sigmoidal, quartz-filled tension gashes, as commonly found in shear or thrust zones, can be observed. Similar, strongly deformed orthoquartzite forms two small hills 17 km NE of Bugondo village, on the northern side of Lake Kyoga.

A more or less continuous section of Mudosi lithologies can be studied along a new access road to a telecom mast of Ogera hill. At the bottom of the section (532357E / 174277N), blocks of conglomerate are found with pebbles composed of unsorted sandstone and rare fragments of phyllite. Upwards the northern slope of the hill, the first *in situ* exposures are of pinkish to grey sandstones with parallel bedding due to alternation of

finer and coarser grained beds. Next (532259E / 174251N), a sequence of fine- to coarse-grained argillaceous sandstones is exposed in beds up to 40 cm in thickness striking ENE to E (N78–90°E) and dipping 40–48° SSE to S. Narrow interlayers of reddish to grey-greenish shale are found in places. The argillaceous sandstones show parallel and cross bedding (Fig. 10.11A). At one location, herringbone structures have been encountered (Fig. 10.11B), manifesting deposition in a tidal flat environment.

In thin section, pure orthoquartzite is mostly composed of granular quartz with only a small amount (up to 5 vol%) of sericite; apatite and zircon are the only accessory minerals. Strongly deformed members show quartz and (minor) feldspar grains in a ground mass of microcrystalline quartz and sericite, the latter mineral as fine-grained flakes aligned along the foliation and within fractures of the rock. Ragged and deformed porphyroblasts, supposedly representing pseudomorphs after detrital aluminium silicate, occur in places and are mainly composed of sericite.

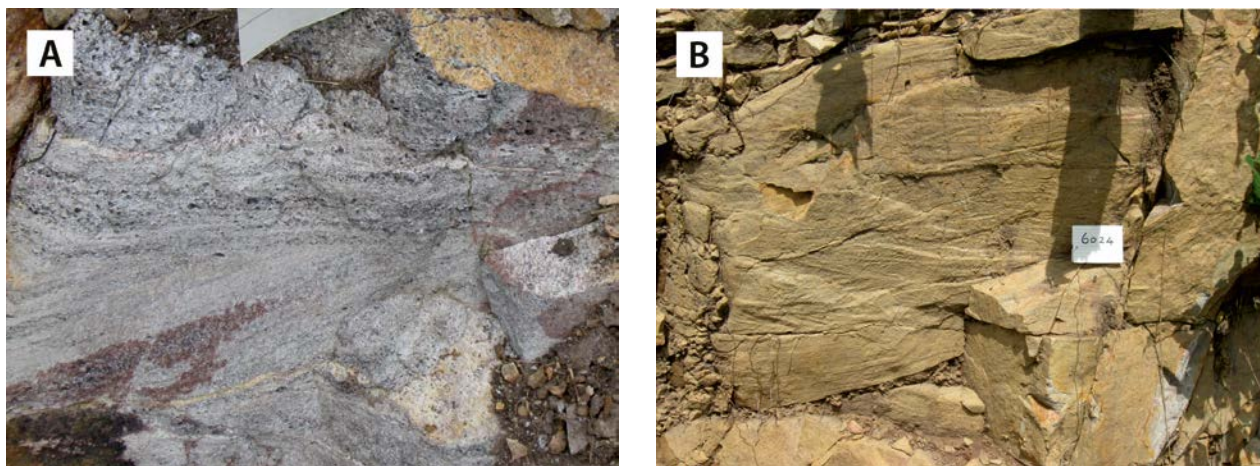


Fig. 10.11. Sedimentary structures in sandstone of the Mudosi Formation on the northern slope of Ogera hill. (A) Grey sandstone showing cross bedding and strong variation in grain size (532259E / 174251N). (B) Grey to pinkish sandstone with heringbone textures (532259E / 174251N). Number plate 6 cm.

Sandstone (P3MBss) – Poorly exposed arkosic sandstones of the *Mpaija Formation* occur in road cuts and small outcrops and are interpreted as interbeds and lenses in the finer grained pelitic sediments of the *Hoima Formation* (Fig. 10.12). Usually, greyish or pinkish white arkosic sandstone has a blastoclastic texture with rounded quartz and sericitised feldspar grains, 1–2 mm in size. In thin section, the main minerals are quartz (~75 vol%) and feldspar (~18 vol%), together with opaque matter (goethite?; ~5 vol%) and muscovite flakes (~2 vol%).

The thickness of interbeds or lenses varies from less than 20 cm to several metres. Bedding, measured on sandstone-mudstone contacts, shows a general NW dip of 10–15°. Cross-bedding was observed in places and shows the top of sedimentation to the W and NW. Narrow fractures with different orientations, filled by quartz, iron oxides and hydroxides, occur abundantly in these arkosic sandstones.

Mudstone, shale, slate and phyllite (P3MBsh) – The finer grained, mostly pelitic sedimentary facies of the *Hoima Formation* covers a large area around Hoima and Masindi towns (Fig. 10.7). Generally, these are mudstones and shales, or very low-grade metamorphic slates and phyllites, typically with planar or wavy bedding and laminae (Fig. 10.13A), but rather massive sedimentary rocks have also been observed. The thickness of laminae and beds varies from a few millimetres to several centimetres, and the grain size from clay to silt and silty sand. The colour varies from white and yellowish brown to violet and purple. Rare scattered pebbles and cobbles may occur in places.



Fig. 10.12. Arkosic sandstone interbeds in Bunyoro mudstone, 5–10 km SW of Hoima town (314445E / 153792N). Number tag 8 cm.

Shale and slate contain abundant randomly directed fractures, filled by violet and reddish hematite and yellowish goethite (Fig. 10.13B). Quartz (dominant) and K-feldspar, mostly altered to sericite, can be identified in these fine-grained sediments, together with hematite/goethite, but the rock is too fine-grained to be analysed more accurately in thin section.

Shale, slate, ferruginous in places (P3MBshf) – Conspicuously iron-bearing parts of Hoima shales and slates have been attributed to a separate unit, the *Bulyango Formation*, which can be associated with positive magnetic anomalies in the aeromagnetic map. In some outcrops (e.g., location 317580E / 161441N), anomalously high susceptibilities (up to 97 SI units) have been measured. The ferruginous

pelite is typically a massive, red to brown rock with bluish-grey hematitic parts as well as yellowish goethitic and limonitic parts (Figs 10.14A-C). In places, small cavities in these rocks are filled by secondary quartz. Ferruginised mudstone may also appear as ferricrete or duricrust on hilltops like Kasikuro (352720E / 177681N), located ~10 km SW of Masindi town.

Ferrugination – There is general agreement that ferrugination, often associated with silicification and resulting in the formation iron-rich, often cherty horizons, of the above ferruginous shale or slate of the Bulyango Formation is a secondary process. This is well illustrated by a section along the slope of Kigylua hill, located ~4 km NEE of Masindi town. There purple and cream-coloured, sub-horizontal (striking 101°, dipping 14° N) mudstones

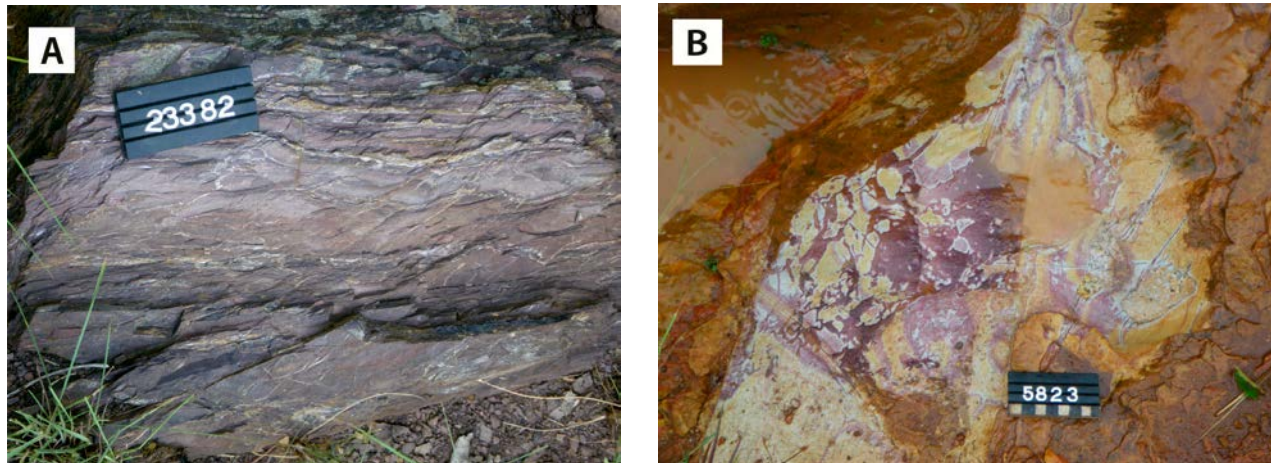


Fig. 10.13. (A) Slate of Hoima Formation from NW end of Lake Kyoga (422874E / 189324N). (B) Fractures in slate filled by hematite and goethite (309744E / 149856N). Number tag 8 cm.

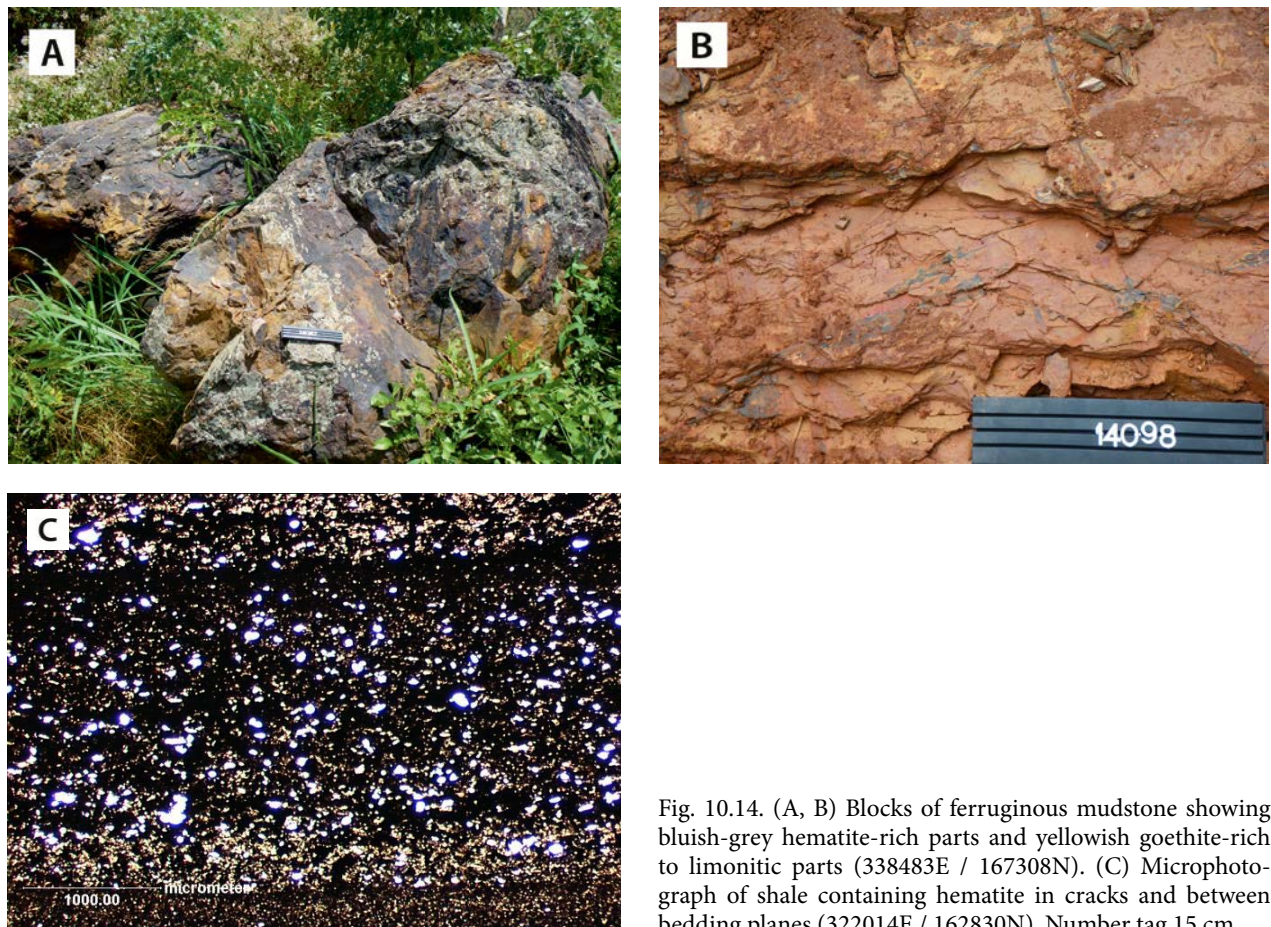


Fig. 10.14. (A, B) Blocks of ferruginous mudstone showing bluish-grey hematite-rich parts and yellowish goethite-rich to limonitic parts (338483E / 167308N). (C) Microphotograph of shale containing hematite in cracks and between bedding planes (322014E / 162830N). Number tag 15 cm.

(Fig. 10.15A), exposed in the hilltop, grade downwards into white-coloured horizons (Fig. 10.15B), showing a clear lineation (strike 350°, plunge 14° N) and load cast features. Cream-coloured, fine-grained arkosic silt- and sandstone showing incipient whitening along specific horizons and along joint planes (Figs 10.15C-D) confirm the secondary character of whitening. Ferruginous samples may show box-work textures. Cherty samples show a very fine lamination and are intersected by quartz-filled fractures and quartz veins. We interpret the 'bleaching' as reflecting the mobilisation of iron and silica, and alteration of clay minerals (illite?, smectite?) into kaolinite as a secondary process.

Some workers have suggested chemical weathering as the process responsible for the remobilisation and re-precipitation of iron. This is very unlikely, in view of the fact that the top of Kigylua hill (Fig. 10.15A) would be the most weathered and most bleached, and not specific horizons below the

top. More importantly, the geochemical behaviour of iron is dependent on pH and particularly Eh: Fe^{2+} is mobile, while Fe^{3+} is immobile. Oxygenated meteoric water is therefore not an efficient agent to mobilise and redeposit iron. We relate the formation of ferruginous horizons to flooding of Bunyoro rocks by a stagnant water body with organic material and reducing conditions (low Eh).

Infiltration of reducing water into specific horizons, depending on permeability and porosity, gave rise to flushing of iron present as a coating or absorbed onto clastic grains or clay particles. Uplift or a lowering water level subsequently resulted into re-deposition along a redox front.

We can only speculate on the timing of this redistribution process of iron. It may either have taken place soon after deposition under the influence of Pan-African tilting or during the Karoo epoch. Alternatively, the process could be related to the development of the Western Branch of the EARS, when uplift of the shoulder of the Alber-

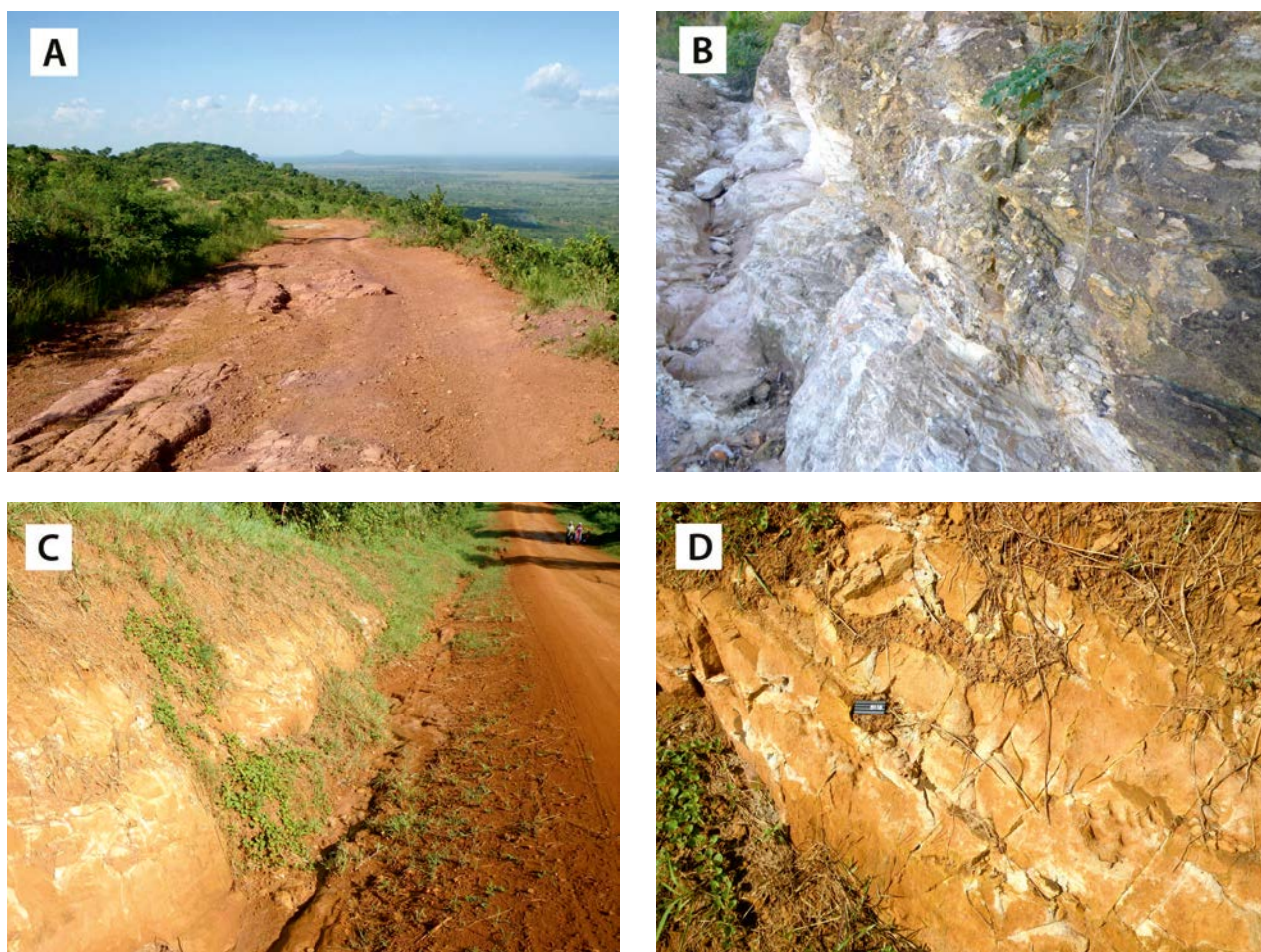


Fig. 10.15. (A) Exposures of cream-coloured mudstones on a hilltop (6111; 361423E / 186848N). (B) White-coloured (kaolinitised?) horizon in the same succession. (C) Cream-coloured, fine-grained arkosic sandstone showing incipient whitening along specific horizons and along joint planes, demonstrating the secondary character of whitening (309925E / 149697N and 301107E / 147618N). (D) Detail of the same exposure. Number tag 8 cm.

tine Rift resulted in drowning of the Kafu River and the formation of Lake Kyoga. Initially, this lake was stagnant and full of decaying organic material (low Eh). Bishop (1969) suggested that the 3500 feet contour line (~1067 m above sea level) marks the former extent of Lake Kyoga (Chapter

12; Fig. 12.39), some 150 m above the present water level of 914 m.a.s.l. Alternatively, ferrugination of Bunyoro rocks may be related to major changes in ocean chemistry, notably widespread anoxia, as a result of stagnation beneath near-global sea-ice cover (see below).

10.4 Geochronology

U-Pb dating of detrital zircons (LA-MC-ICP-MS method) from sericite-bearing orthoquartzite, representing the easternmost and highest metamorphic varieties of the Mudosi Formation, produced several age groups with prominent frequency peaks at ~1.0 Ga, ~1.9 Ga and ~2.0 Ga, indicating Mirian and Rwenzori source rocks, respectively. The two youngest detrital zircon grains have ages of 972 ± 22 Ma and 976 ± 24 Ma ($\pm 2\sigma$ errors), yielding a maximum age of 0.97 Ga for the sedimentary succession (Mänttari 2014). Secondary rim growths on zircon with a Pan-African age have not been detected.

Diamictites from the Malagarasian in eastern Burundi (Tack 1992, Tack et al. 1992) and NW Tanzania (Westerhof & Koistinen 2005) occur on top of the Malagarasi Supergroup, and are consequently younger than Gagwe volcanics dated at 795 ± 7 Ma. Correlation with similar deposits in central Africa suggests an age between 765 Ma and 735 Ma (Key et al. 2001), roughly coeval with the global Sturtian glaciation. The Bunyoro Group starts with similar glaciogenic deposits (Table 10.1), and the lithologies higher in the sequence are thus younger than 765–735 Ma.

10.5 Geodynamic Evolution of the Bunyoro Group

Diamictites – The non-genetic term ‘*diamictite*’ refers to any poorly sorted conglomerate containing fine to coarse clasts and sand in a mud-supported matrix. They are considered to be glacial deposits (e.g., boulder clays) or, alternatively, the product of mass flows, i.e., olistostromes formed by submarine slumping or gravity sliding on an unstable shelf.

Diamictites are widely present in Neoproterozoic successions in and around the Congo River Basin (Tack et al. 2006b, Delpomdor et al. 2008), including the ‘*Petit Conglomérat*’ and ‘*Grand Conglomérat*’ of Katanga (Cahen 1963, Master et al. 2005), the Tshibangu Formation (Itombwe Supergroup) in Kivu, eastern Congo (Peeters 1953, Cahen 1963, 1978, Villeneuve 1973, Waleffe 1988), measuring >800 m in thickness (Walemba 2001), the Shaka Conglomerate from eastern Burundi (Tack et al. 1992) and NW Tanzania, the latter provisionally termed Nyakanazi Diamictite (Westerhof & Koistinen 2005). These diamictites were also either viewed as having a glacial and periglacial origin or rather looked at in terms of mass flows, linked to post-Rodinian break-up and rifting in the ~750–600 Ma time span. Major arguments against a ‘tilloid origin’ included (1) the absence of a parallel-striated glacial pavement on an un-

derlying hard rock surface and (2) the absence of polished boulders or flattened and blunt pebbles; it was alleged that not even a single faceted and striated cobble or pebble had been observed.

Recent observations from tilloids in the Congo River Basin by Delpomdor et al. (2008), however, reveal numerous diagnostic microstructures in favour of a glacial origin, including the typical deformation of the diamictite matrix as a result of alternating ice crystallisation and melting (plasma), particular constituents (skeletons) and the combination of plasma and skeleton (S-matrix) and other micro-morphological features, all favouring a tilloid origin. Massive tillites, indicating a proximal facies, may grade laterally into more bedded deposits, formed by reworking of glacial deposits by running water or by subaqueous gravity flows and indicating a distal facies. A glacial origin of the tilloids around the Congo River Basin is further supported by recent palaeo-magnetic measurements (Brock & Piper 1972) from Kenya and Tanzania, showing an apparent polar wander path for the Late Precambrian of Africa, covering the period 800 Ma to 1000 or 1100 Ma, passing near western South America, and places Africa in low palaeo-latitudes at about 800 Ma.



Fig. 10.16. Red to purplish-coloured tillite deposits composed of a fine-grained clay-rich matrix and large fragments ('boulder clay') (289191E / 138691N; 1425 m.a.s.l.).



Fig. 10.17. Strongly weathered boulder clay with rock fragments mainly composed of vein quartz in a lateritic clayey matrix (283505E / 162629N). Number tag 8 cm.

The age of these tillites coincides with a worldwide distribution of Neoproterozoic glacial sequences, attributed to two successive 'snowball Earth' events (Harland 1964, Kirschvink 1992, Hoffman et al. 1998, Evans et al. 2010), i.e., the ~710 Ma Sturtian and ~635 Ma Marinoan/Varangian events (Kaufman et al. 1997, Evans et al. 2010, Halverson et al. 2003, Godd eris et al. 2003, Hoffmann et al. 2004).

Walemba & Master (2005) concluded that the Itombwe diamictites from Kivu (eastern Congo) were deposited under glacio-marine conditions, with the overlying thin dolomite interpreted as 'cap' carbonate, in common with other Neoproterozoic glacial sequences. Iron-formations are ubiquitous in the geological record from the earliest Archaean to about 1.8 Ga, after which they

disappear for over one billion years (Isley & Abbott 1999). The reappearance of banded iron-formations in the Neoproterozoic, in association with glacial deposits, reflects major changes in ocean chemistry, which are consistent with widespread anoxia as a result of stagnation beneath near-global sea-ice cover (Kirschvink 1992, Hoffman & Schrag 2002). Could this have anything to do with the remobilisation and reprecipitation of iron in the ferruginous shales of the Bunyoro Group?

In Uganda tilloids have been described from the former 'Kioga and Bunyoro Series' (Davies 1939, DGSM 1966, Bj rlykke 1973, van Straaten 1976). Our field verification confirms this interpretation. The tillite deposit composed of large fragments ('boulder clay') in a red to purplish coloured fine-grained clay-rich matrix shown in Figure

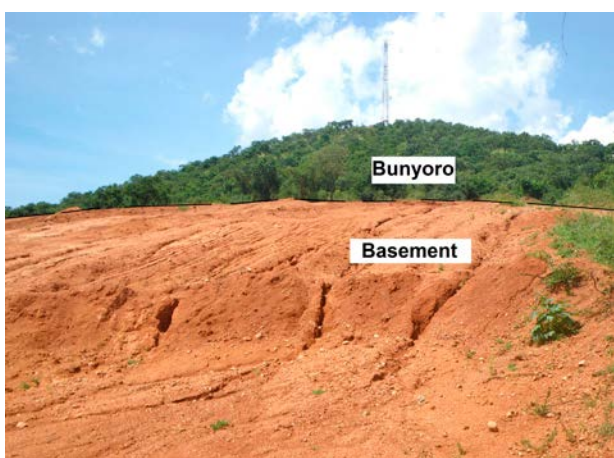


Fig. 10.18. Bunyoro diamictites (forested hill with a telecom mast) overlying weathered granitoid of Archaean crystalline basement ~33 km W of Hoima town (283233E / 162532N).



Fig. 10.19. Laterite outcrops showing a vegetation anomaly (363943E / 188008N).

10.16 may support the postulated ‘snowball Earth’ events, given that the red to purplish coloured fine-grained clay-rich matrix suggests tropical weathering. Elsewhere (283505E / 162629N), a hilltop is composed of large blocks of vein quartz, up to a cubic metre in size. These blocks overlie a diamictite composed of angular to rounded pebbles of all sizes (from centimetre to decimetre scale). In outcrop, the finer matrix is generally washed out (Fig. 10.17). The presence of large blocks of vein quartz and absence of rock fragments of other compositions can also be interpreted as an indication of deep tropical weathering and, consequently, the absence of country rock fragments on the surface, except for vein quartz, preceding the Snowball Earth event.

Lithologies of the Bunyoro Group are usually exposed in smooth forested hills, occasionally with flat tops suggesting an erstwhile peneplain (Fig. 10.8A). The contact with the underlying Archaean basement is exposed in only a few locations (Fig. 10.18). From inspection of the geological map, it appears that Bunyoro lithologies occur in close spatial association with extensive laterite surfaces (see 1:1 M map) that produce pronounced vegetation anomalies (Fig. 10.19). We postulate that these laterites may represent the floor on which the Bunyoro rocks have been deposited. In other words, these laterites represent a palaeo-soil of Neoproterozoic age and, as such, they merit further investigation, notably for bauxite deposits.

We further draw attention to the crescent-shaped polygon underlain by rocks of the Bunyoro Group (Fig. 10.7), and draw parallels with other regional E–W-trending, curvilinear structural features such as the geophysical break separating the West Tanzania from the North Uganda Terrane (Chapter 3, Fig. 3.2), and the Katonga Accident, both coinciding with important crustal breaks. We believe that these features are fundamental to understanding the evolution of the crystalline basement of Uganda. Also taking into account local deformation and metamorphism affecting the rocks of the Bunyoro Group (see Section 10.3) we postulate the following geodynamic development:

- Deposition of the Bunyoro deposits on the rifted foreland of the EAO. The thickest and most complete part of the Bunyoro succession coincides with a rather narrow, straight, E–W-trending rift (the Kyoga rift), an older weakness zone, with a thinner condensed sequence deposited outside this rift; the Bunyoro succession rests unconformably on a Neoproterozoic laterite cover of mostly Archaean basement.
- During subsequent uplift, the bulk of Bunyoro succession has been eroded away. Only the part confined to the Kyoga rift has been preserved. With continued weathering, triggered by post-collisional uplift, slow erosion of weathering-resistant Bunyoro rocks in the Kyoga rift, compared to fast erosion of weathering-prone basement rocks N and S of this rift, caused an inversion of relief over time. Consequently, the deepest rocks of the Bunyoro Group now stand out as smooth hills and ridges above the flat landscape underlain by Archaean basement rocks. This process supposedly took place during the late Palaeozoic and Mesozoic.
- Bjørlykke (1973, 1981) described the former Bunyoro Series as a sequence of sandstones and pelitic sediments of fairly low metamorphic grade resting unconformably on crystalline Precambrian basement rocks. Our field observations confirm that in the southern part of the Bunyoro deposits (Hoima District), the sediments are flat-lying and relatively little deformed, while in the northern part (Masindi District), tillites are strongly deformed, displaying a strong pebble lineation in an inverted limb of a large fold.
- Deformation of the straight Kyoga rift into the present crescent-shaped Bunyoro polygon is supposedly due to E–W compression, possibly in combination with dextral strike-slip along the western apex of Bunyoro rocks, close to the eastern shoulder of the Neogene Albertine Rift. Such a process may explain incipient metamorphism with the development of shale and phyllite, conjugate fractures, striations and mullions (Fig. 10.9A). This process does not, however, explain the development of scarcely observed recumbent folds with sub-horizontal fold axes (Fig. 10.3B), suggesting tectonic stacking caused by low-angle thrusting. The orientation of tension gashes between the quartz veins in a low-angle fracture set and the limb of the recumbent structure dip steeply to the south, indicating that the hanging wall was thrust southward. Strongly deformed and tilted sericite quartzite with slickensides from north

of Mudosi Hill (537653E / 181490N), on the eastern part of Lake Kyoga, strengthen this impression. We have searched in vain for secondary rim growths of detrital zircons from this rock, in an effort to date this 'thrusting event' (Section 10.3).

- GTK Consortium mapping has evidenced that allochthonous Pan-African rocks of the West Karamoja Group (Section 11.4) occur much further to the west than previously thought. However, even the present Pan-African thrust front is the result of a long period of uplift and erosion. It is postulated that in the past

this thrust front was located much further to the west. How far to the west is a matter of speculation, but dated monazites in kyanite schists from Murchison Falls and from sericite quartzite near Nebbi, both belonging to the late Mesoproterozoic Madi-Igisi Belt, yielded Pan-African ages of 0.63–0.62 Ga (Appel et al. 2004, 2005) and 0.66 Ga (Mänttari 2014), respectively. Whether this monazite dates Pan-African low-angle thrusting, over sequences pertaining to the ~1.0 Ga Igisi Group and the northern and eastern segments of the <0.77– 0.74 Ga Bunyoro Group, remains to be further investigated.

11 ROCKS OF THE KARAMOJA BELT AND OTHER ROCKS OF THE NEOPROTEROZOIC PAN-AFRICAN CYCLE

11.1 Introduction

Traditionally, the geology of northern Uganda has been described in terms of ‘events’, comprising (from old to young): (1) Watian (~2.9 Ga), Aruan (~2.55 Ga), Mirian (~1.0 Ga) and the youngest one, the Chuan (or Aswa) event (650–550 Ma) (Table 4.1). The latter ‘event’ can be attributed to the Pan-African Orogenic Cycle, culminating in the creation of the Gondwana Supercontinent.

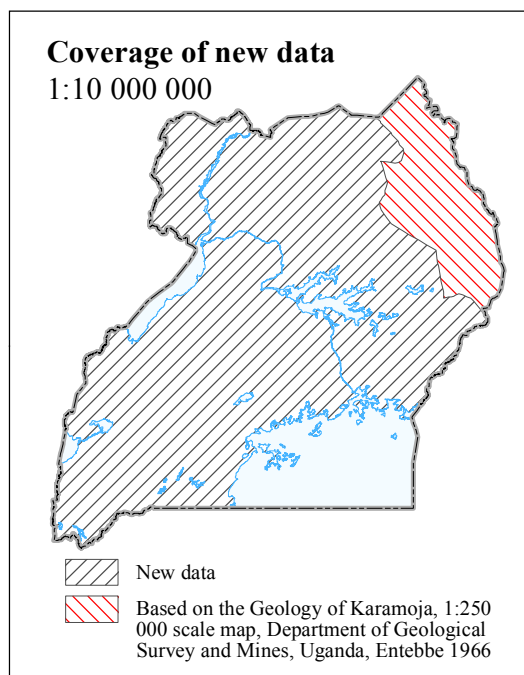


Fig. 11.1. The extent of the new geological field verification and aeroborne geophysical survey in Uganda. The excluded area is marked by red lines.

As a consequence, the proto-Congo Craton became surrounded by Pan-African fold belts. The Archaean basement of north Uganda constitutes the northeastern corner of the proto-Congo Craton and is bounded along its northern and eastern margins by two of these Neoproterozoic-Cambrian fold belts:

- The E–W-trending Oubanguides or Central African Fold Belt (‘K’ in Fig. 1.16) along the northern margin of the proto-Congo Craton.
- The N–S-trending Karamoja Belt, a segment of the East Africa Orogen (‘O’ and ‘P’ in Fig. 1.16 and Figs. 1.17 and 1.18) along the eastern margin of the proto-Congo Craton.

Apart from these fold belts, a number of major strike-slip shear zones, associated with conspicuous mylonite belts, intersect the basement of the North Uganda Terrane (NUT). These include the prominent, NW–SE-trending Aswa Shear Zone (ASZ) and rejuvenation of a complex N–S-trending Madi-Igisi Belt and associated fault zone between Moyo and Lake Albert.

During the recently completed mapping project in north Uganda (2009–2012), the Karamoja area was excluded from airborne geophysical surveying and field verification (see Fig. 11.1). Consequently, the synthesis of the lithostratigraphic units presented below is mainly based on scarce reports from the 1960s (e.g. Macdonald 1961, Almond 1962a, 1962b, 1969, Baldock et al. 1969).

11.2 Karamoja Belt (East Africa Orogen)

The Ugandan-Kenyan segment of the East African Orogen (EAO, Stern 1994) (Section 1.7) is transitional between the Arabian-Nubian Shield (north) and the Mozambique Belt (south) (Holmes 1951). Oblique collision with NW–SE relative plate motions was followed by a stage of post-collisional ductile shearing parallel to the plate boundaries (Shackleton & Ries 1984, Shackleton 1986, 1993, 1994, 1996).

The EAO in Kenya is ~600 km wide with large areas being covered by Neogene rift-related volcanics and sediments (Fig. 11.2). Mosley (1993) divided the Kenyan segment of the belt into three

tectonic ‘terranes’, each characterised by a specific tectono-metamorphic development and separated from one another by major ductile shear zones. Their evolution took place over an extensive time interval (900 Ma to 470 Ma), during which at least six different tectono-thermal events can be recognised (Key et al. 1989). The Western Sector, underlying the Potok area of western Kenya and the Karamoja Belt of eastern Uganda (Figs 11.3 and 11.4), is composed of a mixture of reworked Archaean basement and juvenile Pan-African lithologies. The latter have traditionally been assembled in the Karasuk Series (Vail

1983, 1988), here renamed Karasuk Super-group. A review of the orogen styles in the East African Orogen was recently published by Fritz et al. (2013).

One of the results of the recently completed Mapping Project by the GTK Consortium (2009–2012) is that the Karamoja Belt of eastern Uganda is not limited to the narrow border zone underlain by reworked Archaean basement and rocks of the Karasuk Supergroup (Fig. 11.3). West of the current Karasuk thrust front, but still east of the Aswa Shear Zone, a number of ‘Watian’ (DGSM 1966; see also Chapter 4) charnockite/ granulite com-

plexes are exposed, which were hitherto considered to be Archaean in age, belonging to the ‘Basement Complex’ of northern Uganda (Chapter 5). Based on modern geochronological data and field verification by the GTK Consortium, these bodies are now interpreted as Pan-African ‘Klippe’ and part of the Karamoja Belt (Fig. 11.5). They are further discussed in Section 11.4. Finally, from radiometric data, a number of *in situ*, truly intrusive, Neoproterozoic granitoid massifs have been identified in the northernmost segment of the West Nile Block (Chapter 4) and North Uganda Terrane (Chapter 5). They are discussed in Section 11.4.4.

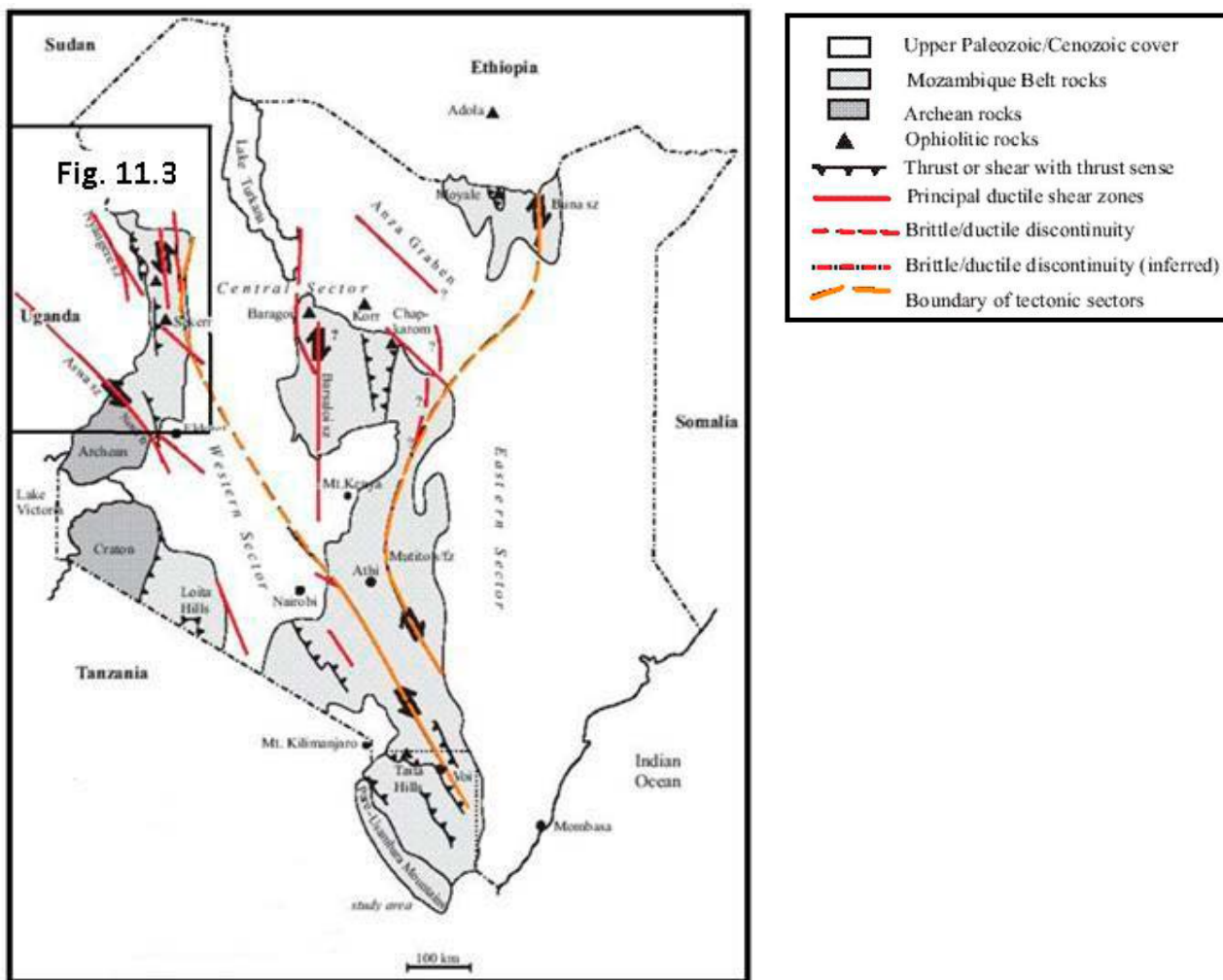


Fig. 11.2. Simplified tectonic subdivision of the East African Orogen in Kenya (in Bauernhofer et al. 2009, with kind permission of Springer Verlag; after Mosley 1993). Details are presented in Figures 11.3 and 11.4 (see boxes).

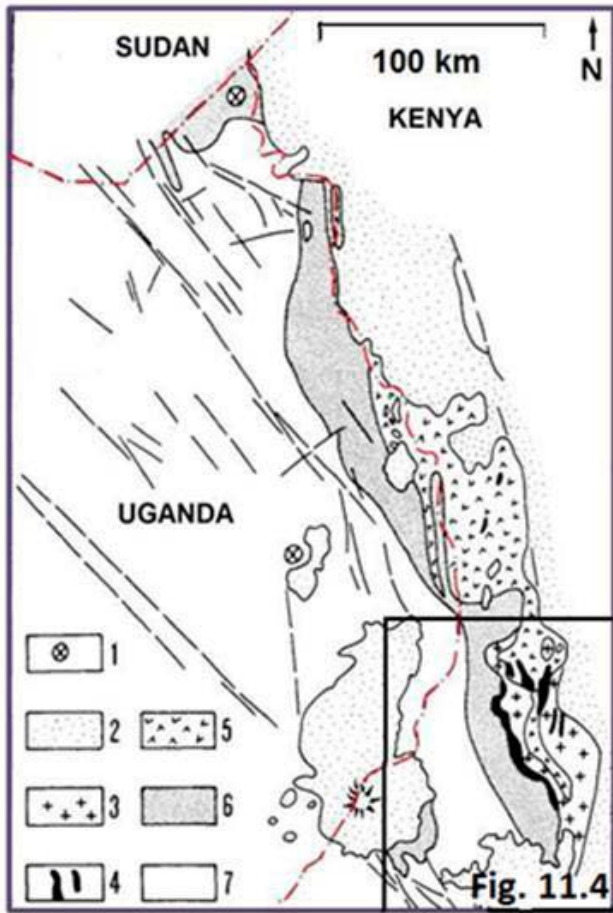


Fig. 11.3. Geological outline of the Karasuk Supergroup of the Karamoja Belt, the eastern Uganda-western Kenya segment of the East African Orogen, showing major lithostratigraphic units. Key: 1 = Neogene intrusives (Elgon Alkaline Province); 2 = Phanerozoic cover rocks; Karasuk Supergroup: 3 = Granite; 4 = Ophiolite; 5 = Volcano-sedimentary assemblage; 6 = Sub-crustal metasediments; 7 = Gneisses and granulites of the North Uganda Shield (modified after Vail 1988, with kind permission of Springer Verlag).

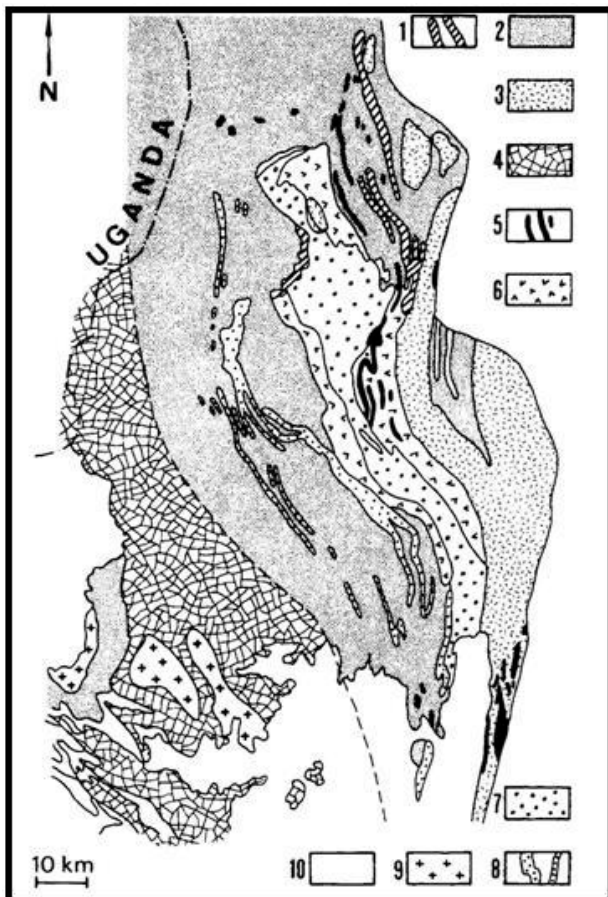


Fig. 11.4. Geological outline of the Karasuk Supergroup in the West Pokot area, western Kenya. Key: 1 = Ophiolites; 2 = Undifferentiated Cherangi meta-sediments; 3 = Granitoids; 4 = Turbo Migmatites (reworked Archaean basement); 5 = Metacarbonates; 6 = Hornblende Schists and gabbro (part of ophiolite suite); 7 = Samor migmatites; 8 = Quartzites; 9 = Granites and granodiorites; 10 = Neogene volcanics (modified after Vearncombe 1983a, 1983b, Ries et al. 1992, with kind permission of Elsevier Ltd.).

11.3 Lithostratigraphy of the Karasuk Supergroup

Introduction – The Karasuk Supergroup (formerly ‘Karasuk Series’, named after the Karasuk Hills in western Kenya) in the Potok area (Fig. 11.4) comprises a W- to NW-verging stack of thrust piles, demonstrated, among others, by tectonic repetition of sequences. Recumbent folds with NE-trending axes have been refolded on NW-trending axes, giving rise to fold interference patterns. Thermo-barometric studies indicate temperatures of 500° to 700°C and pressures between 4 and 10 kb (Suwa et al. 1979, Key & Hill 1989). The abundant occurrence of kyanite, consistently overprinted by sillimanite, is taken as evidence of a clockwise P-T-t path (Mosley 1993), confirmed by Hetzel & Strecker (1994), who found indications of isothermal decompression in granulite facies gneisses and mafic rocks followed by left-lateral shear under retrograde amphibolite facies conditions.

Juvenile Neoproterozoic rocks are often interleaved with slices of older cratonic crust (e.g., Sanders 1965). Lithologies of the Karasuk Supergroup are generally separated from the high-grade Archaean crystalline basement of the NUT by a thrust plane and ‘Schuppen’ zones of flaggy gneisses, composed of parautochthonous and allochthonous tectonic fragments, derived from either East or West Gondwana. From a lithostratigraphic and modern geodynamic point of view, it is convenient to divide the large variety of rock types that constitute the Potok and Karasuk segments of the Karamoja Belt as follows (supposedly from old to young):

- *Reworked Archaean basement*
- *Ophiolites from the Neoproterozoic Mozambique Ocean*
- *Metasediments from the post-Rodinia passive margin*
- *Syn-collisional metasediments and magmatic arc rocks*

Table 11.1. Lithologies of the Karasuk Supergroup. The codes on the right are the ones used in the unpublished geological maps archived by DGSM.

| | | |
|---|--|--------|
| Rocks of uncertain derivation | Porphyroblastic granulite | P3Rpgl |
| | Felsic granulite | P3Rfgl |
| | Mafic granulite | P3Rmgl |
| | Undifferentiated granulite and charnockite | P3Rugl |
| | Muscovite gneiss | P3Rmg |
| | Flaggy hornblende-biotite gneiss | P3Rfgn |
| | Flaggy acid gneiss and biotite gneiss | P3Ragn |
| | Banded biotite granite gneiss | P3Rbgg |
| <i>Related metasediments, metavolcanics and granitoids from western Kenya with ages of 584±25 Ma, 663±49 Ma, and 593±50 Ma (see Ries et al. 1992)</i> | | |
| ^^^^^^^^^^^^^^^^^^^^ unconfornity ^^^ unconfornity ^^^ | | |
| Metasediments from the post-Rodinia passive margins | Amphibolite and hornblende-epidote rock | P3Raer |
| | Calc-silicate rock; marble | P3Rcsr |
| | Marble | P3Rma |
| | Quartzite | P3Rqz |
| ^^^^^^^^^^^^^^^^^^^^ unconfornity ^^^ unconfornity ^^^ | | |
| Ophiolites of the Neoproterozoic Mozambique Ocean (> ~ 830 Ma) | Amphibolite | |
| | Ultramafite | P3Ru |
| ^^^^^^^^^^^^^^^^^^^^ unconfornity ^^^ unconfornity ^^^ | | |
| Reworked Archaean basements rocks interleaved with juvenile Neoproterozoic rocks | | |

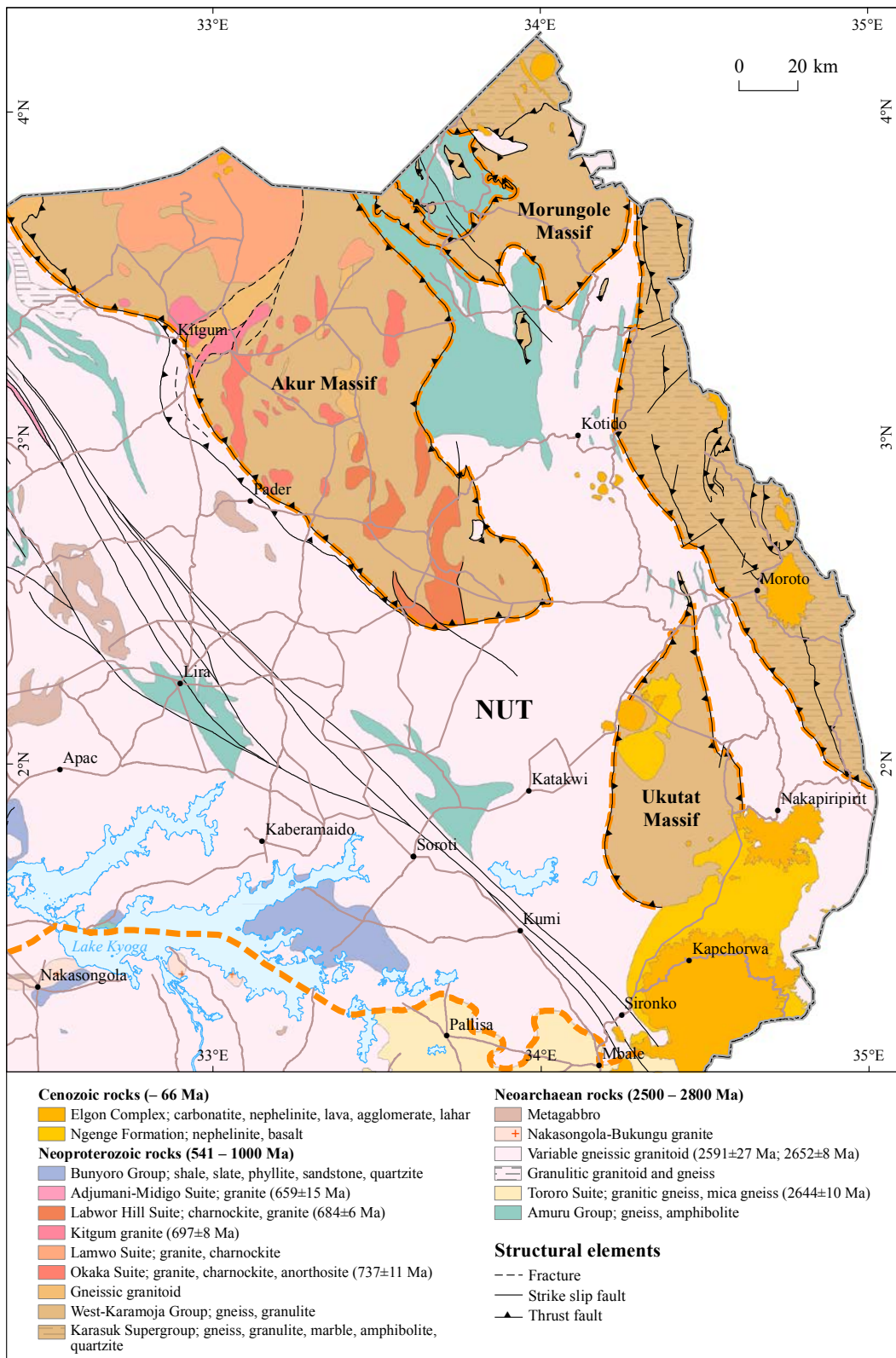


Fig. 11.5. Geological outline of eastern Uganda showing units of the Pan-African Karamoja Belt. Rocks of the Karasuk Supergroup are exposed along the Uganda-Kenya and Uganda-South Sudan borders. Rocks of the West Karamoja Group are exposed west of the former in three granulite/charnockite 'Klipps', named Morungole, Akur and Ukutat Massifs. The latter have been invaded by a variety of Pan-African granitoids. North Uganda Terrane (NUT) separated from the Pan-African thrust rocks by orange dotted line.

11.3.1 Ophiolites from the Neoproterozoic Mozambique Ocean

Ophiolites from the Kenyan-Ugandan border zone are considered to represent the southernmost extension of various ophiolite belts identified in the Arabian-Nubian Shield, the northern segment of the East African Orogen (EAO) (Behre 1990). These are obducted fragments of ocean floor rocks, derived from the Neoproterozoic Mozambique Ocean. Assuming a pre-collisional age, their formation is assumed to have taken place prior the oldest tectono-thermal event at ~830 Ma (Vearncombe 1983a, 1983b).

Three ophiolite complexes (with podiform chromite bodies) from the Pokot area, Kenya, represent allochthonous west-verging dismembered tectonic fragments, with both upward and downward facing units, due to two phases of thrusting and ductile shear, marking older sutures (Key et al. 1989, Mosley 1993). The second phase of deformation, synchronous with or posterior to the emplacement of a sheeted granite complex, produced isoclinal folding structures. Granite dykes derived from a migmatite complex, positioned structurally beneath the ophiolite, have locally intruded ophiolite (Vearncombe 1983a, 1983b). Two ophiolite complexes – the Sekerr and Baragoi – were deformed at 630 to 659 Ma. These rocks are found to be associated with syn-collisional calco-alkaline volcanics and metasediments (including manganese quartzites).

The Sekerr ophiolite complex can be traced into Uganda and has been described by Vearncombe (1983a, 1983b) and by Ries et al. (1992). Ophiolites of the Karamoja Belt in Uganda mainly comprise hornblende schists, metagabbro and small lenses of peridotite/serpentine, ranging from small lenses in granite gneisses and biotite gneisses to larger bodies of hornblende rock that are intermingled with but not restricted to metasedimentary sequences. Macdonald (1961) distinguished (1) amphibolite with or without garnet, (2) hornblende and anthophyllite schists and (3) tremolite-actinolite-talc-chlorite schists. Unlike amphibolites and epidote-amphibolites associated with marble horizons, Macdonald (1961) suggested intrusive protoliths for these mafic and ultramafic rocks.

Ultramafite (P3Ru) – Ultramafic rocks are composed of olivine and pyroxene, which have been partly replaced by amphibole, biotite and serpentine,

manifesting the introduction of potassium and water. Plagioclase and (secondary) magnetite occur in places. Hornblende varieties occur elsewhere. Lenses of hornblende-anthophyllite schists or actinolite-tremolite-talc-chlorite schists manifest more pronounced metamorphism and metasomatism. Dark green, schistose, almost monomineralic lenses composed of hornblende or anthophyllite are common. Talc-rich ultramafic bodies occur in two varieties: (1) fine-grained massive soapstone and (2) coarse crystalline rocks. The soft, fissile, pale greenish-grey soapstone variety with a pearly lustre occurs at several points along the Moroto-Lokitanyala road near Katumeth and at Aoruma Hill. In thin section it appears that they are composed of very fine, needle-shaped crystals of tremolite-actinolite, partly replaced by talc and, occasionally, chlorite.

Amphibolite – Amphibolites and hornblende-epidote rocks occur in elongated N-S-trending bodies of diverse dimensions (max. 2 x 20 km) close to the Kenyan border. Garnet-free and garnet-bearing amphibolites have been described by Macdonald (1961) forming compact, dark grey-green, fine- to medium-grained, poorly-foliated to massive rocks although a fine contorted banding can in places be observed. Typically, the rock is composed of hornblende + plagioclase ± almandine-rich garnet + ilmenite. More leucocratic sub-types may contain some quartz, biotite or K-feldspar. Epidote is a local retrograde mineral. Blebs of felsic material, up to one centimetre in size, in amphibolite have been interpreted as filled amygdales (Miller 1956).

11.3.2 Metasediments from the post-Rodinia passive margin

Associated with the ophiolite bodies occur marbles, mica schists and meta-psammites, derived from mainly terrigenous sediments of pelitic to semi-pelitic composition, with important arenitic horizons and volcano-sedimentary intercalations (see below). Marbles have supposedly stromatolitic limestone precursors and metacherts are derived from minor chemical siliceous sediments of exhalative origin. When comparing the metasediments with undeformed sedimentary successions deposited on top of the Tanzania Craton (i.e., the Kisii Group; Fig. 2.3), Mosley (1993) proposed a depositional model whereby the sediments, which

show strong variations in thickness, were laid down in rift-type basins.

Metasediments of the Karasuk Supergroup thus mainly comprise a metamorphosed assemblage of passive margin sediments with meta-arenites and meta-carbonates occupying the basal and near-shore, marginal parts of the succession and metapelites the more distal and deeper segments of the basin. These rocks cannot be distinguished from younger syn-collisional juvenile metasediments.

Quartzite (P3Rqz) – N–S-trending quartzite horizons of the Karasuk Supergroup, tens of kilometres long, occur near the Kenyan border in the Kotido and Moroto Districts (Cawley 1960, 1961, Williams 1966). They occur in narrow and elongated horizons, usually less than 15 m in width, forming resistant ridges, concordant with the regional grain. In addition to fine- to medium-grained quartz, the strongly banded or foliated rock may contain subordinate amounts of biotite, magnetite, hematite or limonite. In places, hematite is found in pockets and veins. Rarely, e.g. at Lukwanamoru, near Lowokonya, hand-picked specimen of coarse- to medium-grained quartzite contains up to 20 vol% magnetite and limonite. Narrow and discontinuous bands of micaceous quartzite represent a transitional facies to more pelitic metasediments, although, in places, they are possibly tectonically interleaved slices of flaggy granulite gneiss. Pale green, well laminated and fine-grained quartzite varieties contain small amounts of disseminated chlorite or fuchsite along darker green-coloured bands or laminae. Evenly distributed sillimanite may occur in the same rock. Ferruginous quartzose rocks from the Moroto area may locally comprise minor muscovite, rutile, calc-silicates and garnet (Fleuty 1968).

Marble (P3RMa) – Major developments of marble, commonly in spatial association with quartzite, have been observed at several locations, particularly along the Kosiroit ridge and near Oruk along the Moroto-Lokitanyala road (Macdonald 1961). Further northwards, e.g. in the Kaabong area, marbles occur in horizons with thicknesses of less than a few metres to successions of over a kilometre in width. These are whitish to pinkish, medium- to coarse-grained (2–4 mm), granoblastic rocks with finer grained varieties in places. Gradational or abrupt colour changes give rise to distinct banding. Rather monomineralic marble varieties grade

into impure marbles with diopside, tremolite-actinolite or phlogopite, having quantities generally less than 5% by volume.

Similar marble beds have been described by Trendall (1961b) in the Kadam area as continuous horizons, up to 150 m in width. Thin layers or laminae composed of white mica with other silicates define banding. Small flakes of graphite occur randomly. Cross-cutting veins of calcite and silicate minerals are common. The marbles are composed of interlocking calcite crystals up to 7 mm in diameter and finer, irregularly shaped grains. Some of the larger grains are cut by zones composed of mosaics of finer grains, indicative of deformation, polygonisation and partial recrystallisation. Trendall (1961b) listed the following minor or accessory minerals: diopside, humite, clinohumite, spinel, melilite (gehlenite), forsterite, tremolite, anthophyllite, cronstedtite, grossularite, muscovite and graphite.

Calc-silicate rock, marble (P3Rcsr) – Intimately associated with the above carbonates are epidote-amphibolites, epidotes and epidote-diopside amphibolites (Macdonald 1961). Epidote-amphibolites look like ‘ordinary’ diabase but supposedly have impure limestone with a significant arenitic or pelitic proportion as protolith. A typical sample of epidote-amphibolite is composed of equal proportions of amphibole and epidote and subordinate quartz, microcline, sphene and Fe-oxide. Trendall (1961b) described calc-silicate gneisses from the Kadam area as finely banded rocks with alternating layers and laminae composed of quartz-feldspar-hornblende, microcline-hornblende and scapolite-quartz-hornblende. Some epidote is scattered throughout and sphene occurs in accessory amounts. Diopside and colourless amphibole (tremolite?) occur in places.

Calcite-bearing biotite gneiss is also found in association with marble. The rock is mainly composed of plagioclase and quartz, with accessory amounts of biotite, muscovite and calcite, the latter mineral in amounts of up to 4% by volume. Quartz and calcite are mutually incompatible. Macdonald (1961) favoured a primary origin of the calcite.

Amphibolite and hornblende-epidote rock (P3Raer) – Amphibole-rich rocks from the Kaabong area, west of Kanatthep and on the Turkana Escarpment, occur in association with gneisses and quartz diorite gneisses (MacGregor 1962). The rocks are

coarse-grained, green and white in colour, and show only a poorly developed foliation. The amphibolites in quartz dioritic gneisses occur as small lenses with a high proportion of hornblende. Occasional amphibole-rich lenses were observed in metagabbros, which suggests that some of the amphibolites may have an igneous origin (MacGregor 1962).

The main minerals are hornblende and plagioclase, with amphibole generally predominating over plagioclase. Biotite is present in minor quantities, and quartz, apatite, magnetite and epidote are accessory minerals.

11.3.3 Rocks of the syn-collisional magmatic arc

Syn-collisional metasediments cannot be distinguished from older passive margin metasediments save, perhaps, when associated with magmatic arc rocks. Metamorphosed calc-alkaline volcanics from the Potok area, which are chemically similar to present-day island-arc volcanic rocks, yielded a WR Rb-Sr isochron age of 663 ± 49 Ma. Associ-

ated metasediments of the Kochokyo Group gave an age of 584 ± 25 Ma. Both ages have been interpreted as dating regional amphibolite-facies metamorphism (Ries et al. 1992). The above metasediments and metavolcanics have been intruded by granitoids, which yielded a WR Rb-Sr isochron age of 593 ± 50 Ma with a $^{87}\text{Sr}/^{86}\text{Sr}$ initial ratio of 0.7072 ± 5 , implying some crustal contamination either from the magmatic complex, which structurally underlies the ophiolitic rocks, or from deeper crustal rocks (Ries et al. 1992).

11.3.4 Rocks of uncertain derivation

This includes a number of lithostratigraphic units of uncertain derivation. They may partly represent metamorphosed passive margin or syn-collisional pelites. Other units are metamorphosed granitoids or volcanic rocks of felsic or intermediate composition.

Banded biotite granite gneiss (P3Rbgg) – This unit, which occurs extensively in NE Uganda close to the border with Kenya, comprises large gneiss bodies

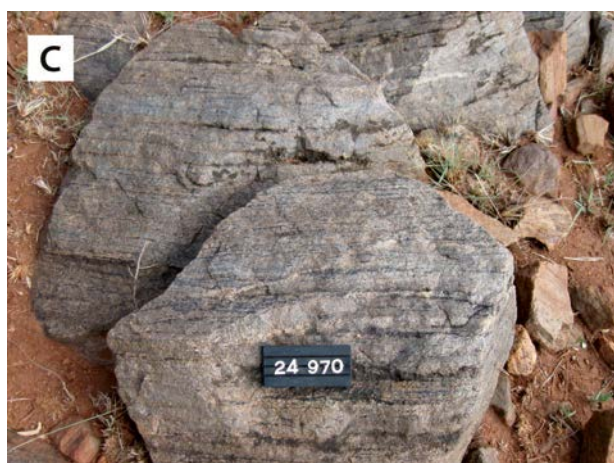


Fig. 11.6. (A) *In situ* blocks of banded biotite granite gneiss, ~60 km SE of Moroto town (712682E / 228539N). (B) Detailed image of the same gneiss. (C) Thin magnetite bands in feldspathic quartzite. A ridge 8 km west of the Kenyan border (710450E / 235090). Number tag 8 cm.

of diverse dimensions (max. 10 x 60 km), located around Moroto town and east of Kaabong town. Light brownish grey, fine- to medium-grained biotite gneisses and granite gneisses have been described by Macdonald (1961) as highly 'granitised' (migmatized?), well-foliated gneiss or as agmatic gneiss with *lit-par-lit* banding and a NNW-trending regional foliation and lineation (Figs 11.6A-B). Parallel to the well-developed foliation, a fracture cleavage has formed, so that the rock easily splits into slabs. Locally, the gneiss is homogeneous and massive, and the composition is more or less granitic. In places, however, more quartzo-feldspathic or even quartzitic varieties occur (Fig. 11.6C), indicating a sedimentary protolith for the rock. In thin section the rocks are composed of 50 vol% quartz, 40 vol% K-feldspar and 5 vol% epidote, the latter in thin, mm-thick laminae. Opaque matter, sericite, chlorite, titanite and fine-grained Fe-oxides occur as accessory minerals.

Flaggy acid gneiss and biotite gneiss (P3Ragn) – Macdonald (1955) described these rocks as "Granulite Series", but later explained (Macdonald 1961) that the term "granulite" should be understood as granular-textured and not being a product of granulite facies metamorphism. Flaggy biotite gneisses have been grouped together with flaggy acid gneisses owing to the fact that the two rock types grade into one another or, occasionally, occur as alternating bands. Poorly exposed flaggy acid gneisses are fine- to medium-grained, grey to greyish green siliceous quartzo-feldspathic granular rocks, most widely distributed along the western flanks and north of Moroto Mountain (Horne 1953, Macdonald 1961). They show foliation planes or closely spaced 'flaggy' partings and are composed of quartz, oligoclase, some microcline, biotite (< 10 vol%), ilmenite, chlorite, apatite, titanite and zircon. Muscovite is generally absent (Macdonald 1961).

More resistant flaggy acid gneisses, intercalated with the biotite gneisses, are widely distributed in the area immediately west of Moroto Mountain. These rather leucocratic rocks rarely contain > 5 vol% of mafic minerals and range in composition from highly siliceous, quartzitic rocks to muscovite-bearing members. Generally, homogeneous, fine- to medium-grained flaggy acid gneiss is a white or pink rock with a granular texture, being less foliated than the biotite gneisses. The main minerals are quartz, oligoclase, microcline, mus-

covite, biotite, garnet, titanite, apatite, zircon and ilmenite (Macdonald 1961).

Flaggy hornblende-biotite gneiss (P3Rfgn) – Flaggy hornblende-biotite gneisses occur as N-S-trending elongated units of diverse dimensions, of which the largest (1 x 50 km) is situated SSE of Moroto Mountain. In places, hornblende-bearing and biotite-bearing gneisses alternate (e.g., Didinga-Kaabong map sheet area; Macdonald 1961; Fig. 11.5).

Muscovite gneiss (P3Rmg) – Medium- to coarse-grained, occasionally porphyroblastic muscovite gneiss occurs south of Moroto Mountain as interlayers in flaggy acid gneisses and banded biotite granite gneisses (Macdonald 1961). The main minerals are quartz, feldspar and muscovite. Muscovite pegmatite veining is common.

Undifferentiated granulite and charnockite (P3Rugl) – This refers to relatively small and isolated polygons, 35 km (E)NE from Kotido town, marked as "undifferentiated granulites and charnockite types banded to granitoid" in the existing 1:250 000-scale geological map of Karamoja (Williams 1966). These rocks are closely associated with various gneisses and "basic granulites" and bordered by thrust faults.

Mafic granulite (P3Rmgl) – According to the existing 1:250 000-scale geological map of Williams (1966), mafic granulites occupy large areas 40 km east of Kotido town, near the Kenyan border.

Felsic granulite (P3Mfgl) – Rocks called "felsic granulites" are located in the NW corner of the 1:100 000-scale Moroto map. Cawley (1960) called them "quartzo-feldspathic gneisses of charnockitic aspects". According to Fleuty (1968), the rocks are coarse-grained gneisses, interbedded with finer-grained varieties, associated with charnockitic rocks. These are high-grade metamorphic, often pyroxene-bearing rocks (see Cawley 1960) and, consequently, true metamorphic "felsic granulites".

Porphyroblastic granulite (P3Rppl) – Porphyroblastic garnet granulites are located 40–50 km east of Kotido town, partly at the Kenyan border. Their extent (100 km²) has been copied from the existing 1:250 000-scale 'Geological Map of Karamoja' (Williams 1966).

11.4 Geology of the West Karamoja Group

11.4.1 Introduction

Already in the 1960s, a number of 'Watian' granulite/charnockite complexes (Table 4.1) had been identified in the Basement Complex of northern Uganda (DGSM 1966; Fig. 11.7). All were believed to have an Archaean age. Geochronological reconnaissance demonstrated, however, that these granulite/charnockite complexes had strongly different ages (Leggo et al. 1971, Leggo 1974); while the granulite/charnockite complexes of NW Uganda (Fig. 11.7; nos. 1 and 2) *'have been closed chemical systems for at least 2.88 Ga'*, similar rocks towards the Mozambique Belt in eastern Uganda (Fig. 11.7; nos. 5, 6 and 7) *'are involved in a much younger granitic injection that dates close to 0.65 Ga'*. The preliminary geochronological results have been confirmed by U-Pb zircon ages (see Mänttari 2014) carried out by the GTK Consortium as part of the

recently completed Mapping Project (2009–2012), yielding Neoproterozoic Pan-African ages (Section 11.6).

11.4.2 Structural subdivision of the West Karamoja Complex

The Neoproterozoic granulite/charnockite complexes in eastern Uganda between the Karasuk thrust front and the Aswa Shear Zone constitute a NW–SE-trending alignment of isolated hilly massifs rising some 650 m above the surrounding flat Karamoja Pediment plain (~1150 m), with occasional peaks reaching over 2000 m. The charnockite bodies and associated granitoids of the Labwor Hills and Okaka Suites in the above complexes are not interpreted as *in situ* intrusives but are incorporated in tectonically emplaced, allochthonous thrust masses, or *'Klippes'*, i.e., erosional relicts of

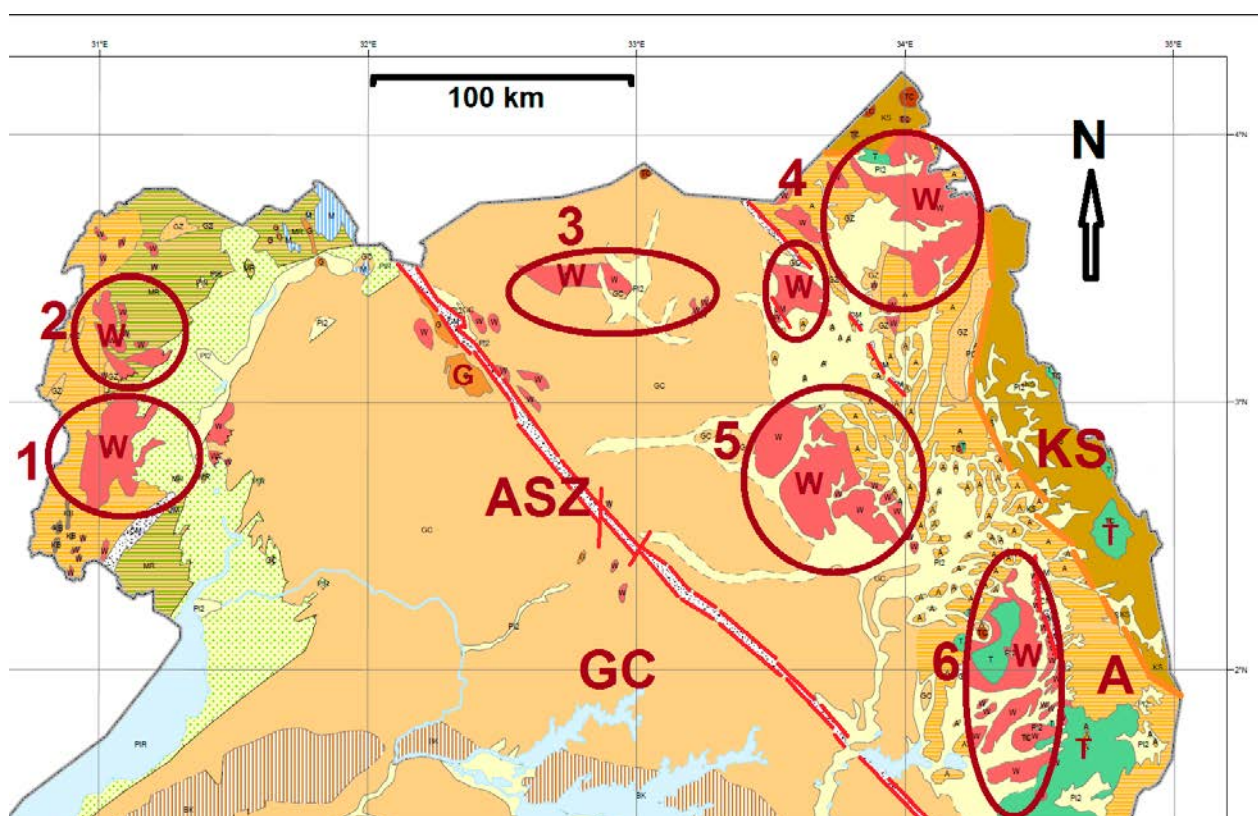


Fig. 11.7. Simplified geological map of northern Uganda compiled by Macdonald (DGSM 1966). Key: Olive brown (KS) = Karasuk Supergroup of the Karamoja Belt; orange line represents current thrust front. Most remaining rocks were considered to belong to the Archaean North Uganda Basement Complex: Dark brown (W) = Watian granulite facies rocks including charnockites and enderbites and retrograded derivatives; Light brown (GC) = Undifferentiated gneisses; Horizontal brown stripes of NW Uganda (A) = Banded gneisses of 'Aruan tectonic event'; G = Granites. Horizontal green/brown stripes = Mirian (~1.0 Ga) rocks; green dots = Neogene Albertine rift; yellow = Alluvial rocks; Green (T) = Volcanics of the Neogene Elgon Alkaline Province; ASZ = Aswa Shear Zone.

a major nappe structure, derived from deeper crustal elements of the Neoproterozoic suture zone between East and West Gondwana. Apart from Neoproterozoic juvenile rocks, these klip-pes may comprise intercalated slices of Archaean basement. We have distinguished three major klip-pes, called Morungole, Akur and Ukatat Massif (Fig. 11.5).

The so-called 'Flaggy Gneisses' (horizontal yellow-brown striped area in Fig. 11.7) of the Karamoja Pediment plain are considered to represent the autochthonous footwall below these thrust masses. Prior to post-Pan-African uplift and erosion this thrust front was located further to the WSW. How far to the WSW is not known, but Neoproterozoic Bunyoro sandstones (Fig. 10.4B), located some 100 km further to the WSW (537654E / 181490N), west of the Aswa fault, have recrystallised into hard, steel blue to grey, strongly veined sericite quartzites with a pronounced lineation (strike N253E, dipping 15–22° to the WSW), obviously the result of a certain amount of recrystallisation, supposedly due to burial below thrusting Pan-African nappes (Chapter 10).

Akur Massif – The central granulite/charnockite complex (Fig. 11.7 no. 6; Fig. 11.5) is part of the Akur Massif, named after the highest peak (1885 m) of Labwor Hills. This area was one of the first to be systematically mapped in northern Uganda (Baldock et al. 1969) as a follow-up to the United Nations Special Fund Airborne Geophysical Survey (Hunting Surveys Ltd. 1961) of the Karamoja area. As the other granulite/charnockite massifs, the Labwor Hills are erosional remnants rising abruptly 650 m above the monotonous pediment of the Karamoja Peneplain, including the Napono Ridge (1960 m) and the Akur peak (1885 m). Baldock et al. (1969) noted a persistent difference in the grade of metamorphism between generally charnockite-granulite facies rocks of Labwor Hills and generally amphibolite-grade rocks that underlie the eastern pediment plain. Field verification by the GTK Consortium has shown that the complex extends much further to the NW into the Kalongo-Wol-Kitgum Matidi area (e.g., Mäkitie et al. 2011b) (Fig. 11.5). Due to the structural complexity of strata within the Klippe, it is not possible to establish a detailed lithostratigraphic sequence. Igneous charnockite from the Kalongo area has yielded a U-Pb zircon emplacement age of ~0.76 Ga (Mänttari 2014). Similar rocks from

Labwor Hills produce mostly concordant but widely ranging U-Pb data on the concordia curve between 0.65 Ga and 0.73 Ga, with one inherited zircon grain yielding an age of 0.74 Ga (Mänttari 2014, see Section 11.6).

Morungole Massif – The northernmost granulite/charnockite complex (Fig. 11.7; no. 5; Fig. 11.5) is part of the Morungole Massif, measuring some 40 x 60 km and named after the Morungole mountain peak (2751 m) and nearby township. It supposedly overlies tectonically banded and migmatitic gneisses of the Karasuk Supergroup in the north, east and south. The western part of the Morungole Massif was mapped in some detail (MacGregor 1962). The bulk of the Massif is composed of lithologies attributed to the newly established Kalongo Group, mainly banded pyroxene granulite, which are locally interlayered with lenses of mafic granulite and of biotite-garnet gneiss, i.e., reworked fragments of the Archaean basement. Bodies of Pan-African diorite and granitic pegmatite have also been encountered. The latter occur commonly as WSW–ENE-directed, narrow and elongated dykes that can be followed over 20 km along strike. Sparse plugs or dykes of alkaline composition are related to the Mount Zulia (2149 m) alkaline intrusive of the Neogene Elgon Alkaline Province.

Ukatat Massif – The southernmost granulite/charnockite complex (Fig. 11.7 no. 7; Fig. 11.5) mainly occupies a sparsely populated, featureless, flat terrain intersected by numerous wide alluvial plains and marsh land with braiding rivers draining into Lake Opeta. The Neogene Napak alkaline intrusive (2537 m), located on its northwestern tectonic contact, stands out in this flat scenery. This complex, named Ukatat Massif after one of the intersecting rivers, is composed of banded granulite and charnockite of the Kalongo Group, an oversimplification due to the poor accessibility and exposure.

11.4.3 Lithostratigraphy of the West Karamoja Group

Charnockites from northern Karamoja were first described by Wayland (1921a, 1926) and Groves (1935). Baldock et al. (1969) divided the Labwor Hills granulites into several subfacies, including enderbitic and basic granulites, garnet-bearing

Table 11.2. Lithologies of the West Karamoja Group. The codes on right are the ones used in the unpublished 1:250 000 -scale geological maps compiled by the GTK Consortium and archived by DGSM.

| West Karamoja Group (exposed in the Morungole, Akur and Ukatat and smaller unnamed Klippe) | Formation | Lithology | Code |
|--|--------------|----------------------------------|---------|
| | Obwar | Granulite | P3WKgl |
| | Kaket | Felsic granulite | P3WKfgl |
| | Orom | Migmatitic garnetiferous gneiss | P3WKggw |
| | Ogili | Intermediate granulite | P3WKigl |
| | Lakwor South | Amphibolite | P3WKab |
| | Agoro | Calc-silicate rock | P3WKcsr |
| | Lakwor | Sericite quartzite | P3WKsq |
| | Kalapata | Mafic granulite | P3WKmgl |
| | Kalere | Ultramafite | P3WKu |
| | Pire | Garnet-biotite gneiss | P3WKgbg |
| | Napararo | Banded granulite and charnockite | P3WKgch |

granulites and graphitic granulites. Later, the granulites of the Labwor Hills were studied by Sandiford (1987) and related rocks nearby, in the Kalongo area, by Mäkitie et al. (2014b).

The origin of charnockite suites – igneous or metasedimentary – has been discussed since their first descriptions from the type locality in India around 1900. Groves (1935) and MacGregor (1962) favoured a metasedimentary origin for these rocks in the Morungole Massif. We have divided the supracrustal rocks of the West Karamoja Group into 11 lithostratigraphic units (Table 11.2). In this context, it should be noted that notable parts (particularly the Napararo Formation) of the West-Karamoja Group are located outside of our field work areas (see App. 1, Lehto et al. 2014); the lithological description of these parts is based on old data.

Banded granulite and charnockite (P3WKgch) – Banded granulites and charnockites of the *Napararo Formation* occur in two main regions: (1) SW of Moroto, where they occupy an area of 1000 km², continuing southward into the adjacent Mbale area, and (2) in the NE corner of Uganda, where they dominate an area of 4000 km² (Williams 1966). In the latter region these granulites are gneissic in texture and contain garnet (Fig. 11.8). In the existing QDS of Napak (sheet 35), these rocks were called “*Charnockite – mylonite assemblage, with graphite gneiss locally*” (Cawley 1962), while rocks in the northeastern corner of Uganda were called “*Undifferentiated massive biotite and pyroxene gneisses*” comprising abundant metagabbros and banded biotite-garnet gneisses in the Kaabong QDS (Cawley 1961).



Fig. 11.8. Banded, garnet bearing granulite of the Napararo Formation (570634E / 385400N). Number tag 15 cm.

Garnet-biotite gneiss (P3WKgbg) – In the western part of the Kaabong QDS banded garnet and biotite gneisses and mafic granulites of the *Pire Formation* form narrow, elongated and folded interbands in banded granulite and charnockite. Major minerals are quartz and feldspars with lesser amounts of garnet and biotite. Biotite is sometimes replaced by sillimanite in textures manifesting dehydration melting (MacGregor 1962).

Ultramafite (P3WKu) – Ultramafic rocks of the *Kalere Formation* comprise a 6-km-long, N–S-trending, very narrow zone north of Lolelia village and two very small areas 8 km SW of Kalapata village, in occurrences located in the Kaabong map sheet area outside the area of field verification by the GTK Consortium.

Mafic granulite (P3WKmgl) – Mafic granulites of the *Kalapata Formation* are exposed in three major zones: (1) NE of Labwor Hills, (2) in the Kotido District (Fig. 11.9) and (3) in the Morungole Massif near the Kenyan border. Williams (1966) and Baldock et al. (1969) called these rocks “*inter-banded pyroxene granulites and gneisses*” and “*basic granulites*”.

NE of Labwor Hills, this mafic granulite unit refers to two rock types (cf. Baldock et al. 1969): (1) banded gneiss composed of dark, orthopyroxene- and plagioclase-rich elongated lenses and bands associated with more felsic members, and (2) metadolerite or metagabbro. The dark bands in

banded gneiss are up to a metre thick and occasionally resemble metadolerite. They form granulitic rocks composed of orthopyroxene (20–30 vol%), plagioclase (An_{50} , 40–60 vol%) and lesser amounts of quartz (0–20 vol%), K-feldspar (0–5 vol%), biotite (0–6 vol%), hornblende (0–2 vol%) and opaque minerals (5–10 vol%). Metadolerite or metagabbro occur as lenticular bodies of massive rock with sharp boundaries *vis-à-vis* pyroxene-bearing banded granulite and charnockite. Because of their sharp contacts, the absence of intermediate types and their association with quartz diorite gneiss, they are considered to represent metagabbro. In places, these elongated bodies cross-cut lithological boundaries, confirming, at least partly, their hypabyssal origin (Williams 1966).

Sericite quartzite (P3WKsq) – NE-trending quartzitic schists of the *Lakwor Formation*, observed in the eastern sector of the Kitgum map sheet area, continue into the Kaabong area. They comprise narrow (<50 m), impure, intensively schistose and banded quartzitic rocks that show gentle to moderate dips towards the east. The schistose quartzites are fine- to medium-grained, grey coloured rocks with light yellowish shades. Their association with supracrustal amphibolites with a similar tectonic fabric suggests a sedimentary origin.

Calc-silicate rock (P3WKcsr) – Epidosites of the *Agoro Formation* are found in a few localities in association with epidote-amphibolites. An occurrence



Fig. 11.9. Mafic granulite of the Kalapata Formation NW of Kotido town (563234E / 385142N). Number tag 15 cm.

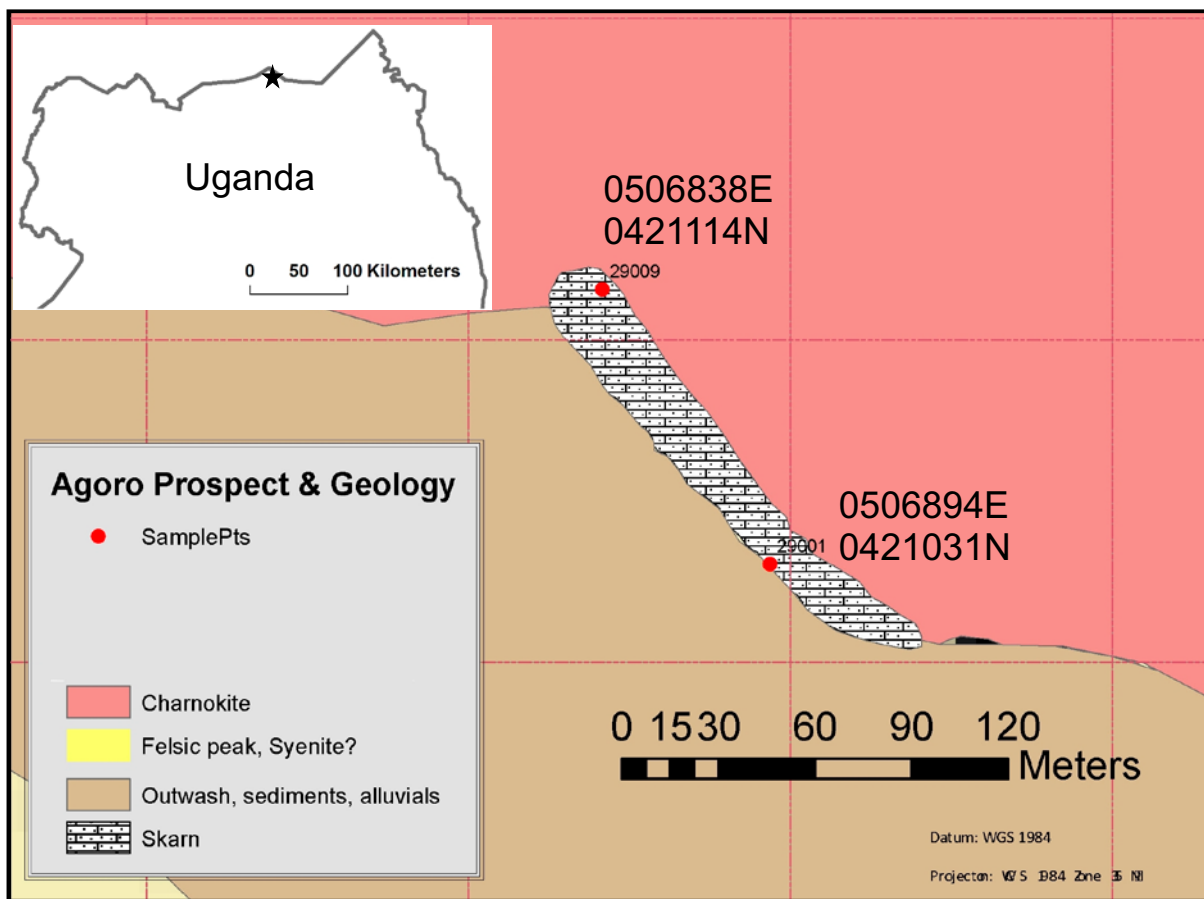


Fig. 11.10. Approximate location of the calc-silicate gneisses and skarns in the Agoro-Oboko area (map compiled by DGSM geologists F. Kigereigu, E. Marimira and P. Mawejeje).

of almost pure, pale green, granoblastic epidote rock is reported from Kosiroit, 4 km N of Katakale village, and from Abuluwas and Morulem, ~2 km E of Awoyapon village. In the latter location, epidote rock forms bodies up to 15 m in width that can be followed over several hundreds of metres along strike. Apart from epidote, these rocks contain small quantities of garnet (andradite-grossular?), quartz, hornblende, diopside and magnetite. Diopside-bearing varieties, closely associated with marble horizons, form mostly narrow contorted beds, 30 to 60 cm in width. In places, bodies of diopside-bearing calc-silicate rock can be observed that measures up to 30 m in width and can be followed a few kilometres along strike. The rock is composed of diopside + amphibole + quartz ± plagioclase.

During field verification, two occurrences of banded and folded calc-silicate gneiss and skarn (or skarnoid) were found 60 and 40 km NNE of Kitgum town, where these rocks apparently form a horizon of a few tens of metres wide that can

be followed for ~1 km along strike, bounded by charnockite (Fig. 11.10). A thick soil cover makes it difficult to estimate the true areal extent of these rocks. The rock comprises greenish grey diopside and contains rare, more or less pure dolomitic interbeds that are 1–5 cm thick. These rocks also include some patches of pegmatite with abundant K-feldspar crystals.

Another cluster of small outcrops of similar banded calc-silicate gneiss with impure marble interbeds occurs ~42 km NNE of Kitgum town, forming a narrow ridge, some 100 m in length. Weathering has produced elongated cavities after carbonate-rich nodules into this strongly folded gneiss (Fig. 11.11A). Calc-silicate gneiss is a greyish rock with brown and green shades (Fig. 11.11B), mainly composed of diopside, garnet and plagioclase with some quartz, titanite, carbonate and K-feldspar as accessory minerals. This 'dry' mineral paragenesis manifests high-grade metamorphism in combination with a low water activity (a_{H_2O}) and/or high CO_2 -activity.



Fig. 11.11. (A) Small outcrop of banded and folded calc-silicate gneiss of the Agoro Formation. (B) Narrow pegmatite vein in the same calc-silicate gneiss. Note the brown to greenish-grey diopside crystals (dots on surface) (498947E / 404886N). Number tag 8 cm.

Amphibolite (P3WKab) – Small flat outcrops of concordant, banded and dark, fine- to medium-grained amphibolitic rock of the *Lakwor Formation* occur 10 km south of the Kitgum-Matidi and 10 km east of the Naam-Ogoro trade centre. Based on the presence of chocolate-brown soils, these amphibolites are more extensive. In addition to amphibole, they comprise pyroxene and plagioclase. Blastesis of pyroxene at the expense of hornblende manifests high-grade regional metamorphism and dehydration reactions. The rocks apparently represent narrow volcanic layers.

Intermediate granulite (P3WKigl) – These chemically intermediate granulite gneisses of the *Ogili Formation* comprise orthopyroxene with plagioclase and quartz and are typically poor in hydrous

minerals such as biotite and hornblende. They can also be called as pyroxene granulites. Together with charnockite intrusions, they occupy a large ‘granulite grade terrane’ area (1000 km²) northwest of Kalongo town (Mäkitie et al. 2014b). Apart from occurrences in the Ogili Mountains, granulite occurs in generally small and flat outcrops. Due to their small contents of K-feldspar and biotite, their extent can be easily delineated by their low radiometric potassium signature. Although intensively metamorphosed, the Ogili granulites still rarely contain relicts of primary bedding, which appears as bands with different amounts of pyroxene, quartz and plagioclase (Fig. 11.12A). However, the banding in the granulites is often due to intense foliation (Fig. 11.12B). Characteristically, the granulites contain elongated, up

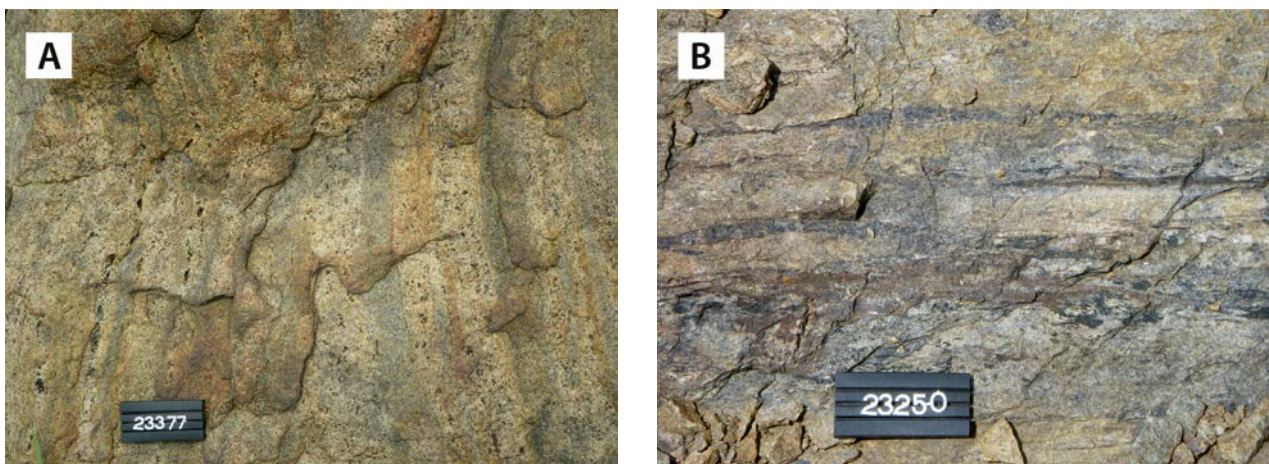


Fig. 11.12. (A) Relicts of bedding appear as compositional banding in pyroxene granulite (532316E / 353436N). (B) Detailed image of deformed pyroxene granulite of the Ogili Formation (522740E / 338865N). Number tag 8 cm.

to 15 cm long quartz aggregates, purple-grey in colour. Granulite-grade metamorphism and associated dehydration melting have resulted in an irregular network of granitic veins. As with most granulites in the area, the weathered surface of the rock is light brown, often with rusty hints, showing dark colours on fresh surfaces, darker than on 'normal' amphibole-grade gneisses. The relatively small grain size (1–4 mm) is a good field criterion to distinguish them from intrusive coarse-grained charnockites of the region. Their major minerals are plagioclase, quartz and orthopyroxene and, locally, K-feldspar may occur up to 10% in volume. Subordinate minerals are clinopyroxene, opaque minerals and retrograde biotite and hornblende. The Ogili granulites grade into the migmatitic and relatively potassium-rich garnetiferous gneisses nearby.

According to Mäkitie et al. (2014b), the granulites of the Ogili Formation are characterised by moderate SiO_2 values (57–65 wt%) and elevated Al_2O_3 (15–18 wt%) and CaO (4–7 wt%) concentrations (see App. 2, anal. 169–172). Sodium typically dominates over potassium. Cr- and Ni -contents are relatively low in relation to strontium, which indicates that these rocks are probably volcanic in origin. Orthopyroxene has variable Al-contents, usually ~1 wt%, but locally up to 5 wt% Al_2O_3 . Moreover, the mineral has much higher Mg/Fe in comparison to pyroxene in the charnockitic rocks of the region.

Migmatitic garnetiferous gneiss (P3WKggw) – The migmatitic gneisses of the *Orom Formation* (Fig. 11.13) mostly occur in flat, scarce outcrops in large areas in the Kitgum, Patongo and Kotido Districts. Their radiometric potassium signature is higher than from Ogili granulites nearby, but lower than from adjacent Okaka granitoids. Based on this signature and geomorphology, it is suggested that the large, flat and remote region without field observations, 25 km east of Madi Opei trade centre, is underlain by supracrustals, mainly comprising migmatitic garnetiferous gneisses.

This assemblage of paragneisses reflects deposition in slightly different sedimentary environments. Variations in arenitic and pelitic proportions resulted in psammitic metagreywackes (Fig. 11.14A), banded biotite-garnet gneisses and diatexitic gneisses (Fig. 11.14B), all migmatitic in appearance. Separation between psammitic and more pelitic members is difficult, because high-grade metamorphism has destroyed all sedimentary structures and the amount of micas has been reduced by dehydration melting and extraction of the partial melts. As such, the chemical composition of these rocks does not represent the composition of the protolith. Pyroxene is absent in these gneisses. Small changes in chemical composition – rather than variations in metamorphic grade – have obviously caused variable degrees of partial melting, being most advanced in rocks of

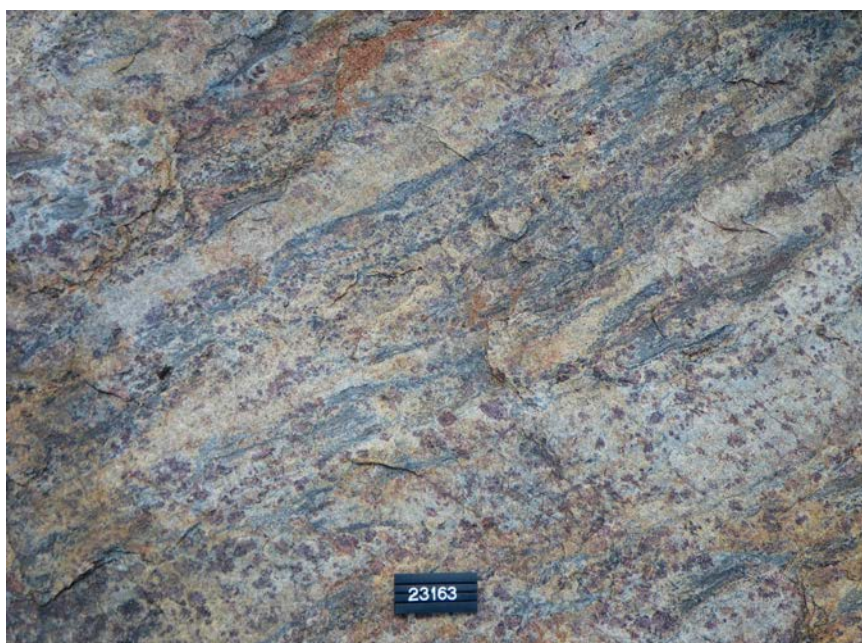


Fig. 11.13. Migmatitic garnetiferous gneiss of the Orom Formation. Note that garnet is preferentially crystallised in the neosomes (559110E / 329666N). Number tag 8 cm.

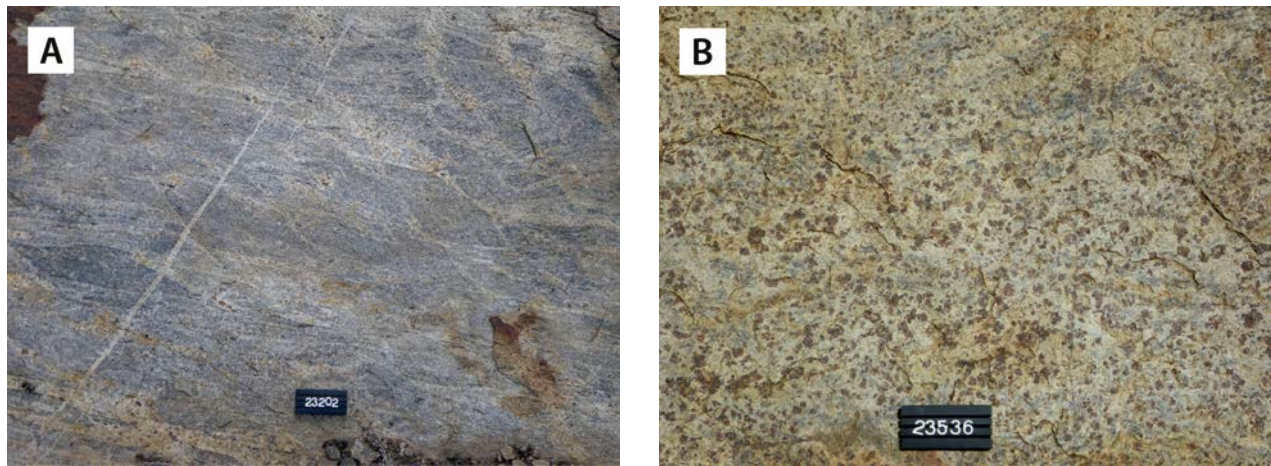


Fig. 11.14. (A) Psammitic garnet-bearing metagreywacke with anatectic seams (530726E / 375886N). (B) Diatexitic garnet gneiss of the Orom Formation (532713E / 344276N). Number tag 8 cm.

eutectic composition. Consequently, some diatexitic gneisses have a rather igneous-looking texture.

Major minerals of these migmatitic gneisses are plagioclase, quartz, K-feldspar, garnet and biotite. Accessory minerals are hercynite, sillimanite and cordierite. Garnet is most abundant in neosomes up to 15 cm wide and is a by-product of dehydration melting during granulite- to amphibolite-grade metamorphism.

Garnet is locally pyrope ($X_{Mg} = 0.4$), but usually almanditic in composition. Hercynite appears as very small grains and never in contact with quartz, but often surrounded by sillimanite. Cordierite is observed in some alumina-rich members. Biotite has reddish pleochroic colours and is partly retrogressive in origin.

Due to initial sedimentary differences and different degrees of partial melting and melt extraction, the garnetiferous gneisses show strong variations in chemical composition. SiO_2 varies between 54 and 73 wt%. Al-contents in the gneisses range between 12 and 19 wt%. Representative chemical analyses of these gneisses are in Appendix 2 (anal. 173–177, see also Mäkitie et al. 2014b). The observed mineral assemblages and intensive partial melting indicate that the minerals are formed under granulite-grade metamorphic P-T conditions.

Felsic granulite (P3WKfgl) – The felsic granulites of the *Kaket Formation* are characterised by a high mode of quartz, plagioclase and K-feldspar, with garnet being the only Fe-Mg silicate. Although orthopyroxene is absent – a traditional indicator for granulite-facies metamorphism – these rocks have undergone the same regional granulite-grade

metamorphism as other supracrustal rocks nearby. These felsic granulites mostly occur in the eastern part of the Labwor Hills area as scarce elongated horizons, several kilometres long, closely associated with migmatitic garnetiferous gneisses, mafic granulites and charnockitic intrusions.

Texturally, these are heterogeneous, foliated leucocratic gneisses (Fig. 11.15) with anatectic granitic veins and patches. Major minerals in the granulites are quartz, plagioclase, K-feldspar and garnet. Biotite and opaque minerals appear as accessory minerals. K-feldspar crystals are locally perthitic. Garnet, being formed by dehydration of biotite, appears as poikilitic, but locally subhedral, reddish blasts, 1–3 mm in size. Biotite often surrounds garnet, manifesting its retrogressive origin. Due to the small amount of mafic minerals, the rock may locally resemble quartzite. The granulite-grade metamorphism and intense recrystallisation has destroyed almost all sedimentary structures and has locally resulted in igneous-looking sub-types.

These felsic granulites should not be confused with “acid granulites” earlier described in the same region by Baldock et al. (1969). The felsic granulites can rather be viewed as a quartzo-feldspathic variety of the migmatitic garnetiferous gneisses nearby. The acid granulites of Baldock et al. (1969), on the other hand, are composed of plagioclase, quartz and orthopyroxene, and are mostly situated in the SE corner of Labwor Hills area, outside the area of field verification (Fig. 11.1). Moreover, the acid granulites have darker fresh surfaces, usually grey brown in colour, than the felsic granulites and could be equivalent to the Ogili pyroxene



Fig. 11.15. Felsic granulite of the Kaket Formation, comprising anatectic patches and vague relicts of sedimentary bedding (560225E / 330636N). Number tag 8 cm.

granulites, of supposedly tuffitic origin, described from the Kalongo area.

Granulite (P3WKgl) – Granulites assigned to the *Obwar Formation* occur together and intermingled with mafic granulite, charnockite and migmatitic garnetiferous gneiss. Obwar granulites are homogeneous, equigranular, medium-grained, massive or weakly foliated rocks with brownish

rusty weathering surfaces and dark grey colours when fresh (Fig. 11.16A). The distribution of small garnet grains is controlled by compositional banding, and leucocratic pods composed of very large garnet porphyroblasts have occasionally been encountered (Fig. 11.16B). More detailed descriptions of the granulites of Labwor Hills are given by Baldock et al. (1969), Nixon et al. (1973, 1984) and Sandiford et al. (1987).



Fig. 11.16. (A) Massive, medium-grained granulite. (B) Granulite with a pod of coarse-grained feldspar and large garnet porphyroblasts (dark red), west of the Labwor Hills (567374E / 300078N). Number tag 8 cm.

11.4.4 Intrusive rocks of the West Karamoja Complex

Charnockites and some granitoids are considered to be intrinsic parts of the 'Klippes' that form the West Karamoja Group. In other words, they are

not considered to be *in-situ* intrusives, but like their mostly granulite country rocks, they have been emplaced tectonically to their current position. They include the following suites and members (Table 11.3).

Table 11.3. Intrusive rocks in thrust masses of the West Karamoja Group. The codes on right are the ones used in the unpublished 1:250 000 -scale geological maps compiled by the GTK Consortium and archived by DGSM. Rock ages are after Mänttari (2014).

| | | |
|------------------------------|---|---------|
| Metadiorite | | P3dr |
| Labwor Hills Suite | Otukei charnockite (684 ± 6 Ma) | P3LHchr |
| | Granite (P3LHgr) | P3LHgr |
| Okaka Suite | Anorthosite | P3Oan |
| | Granite | P3Ogr |
| | Charnockite | P3Ochr |
| | Wol charno-enderbite (737 ± 11 Ma) | P3Oche |
| Variable deformed granitoids | | P3vdgr |

Variable deformed granitoids (P3vdgr) – Pan-African thrust mass of the Akur Klippe (Fig. 11.5) in northern Uganda comprises greyish coloured, relatively coarse-grained, equigranular, gneissic, non-charnockitic biotite granitoids. They differ from nearby relatively homogeneous, locally migmatitic, porphyritic granitoids (which often are associated with charnockites) by higher biotite contents, more diverse textures and a higher potassium signature in the radiometric data. The

best exposures of these rocks can be found NE of Kalongo village, where they form large hills and ridges up to tens of metres high, occupying an area of some 200 km². Characteristically, the rocks have a relatively high mode (~15 vol%) of biotite and garnet (1–5 vol%) as a minor mineral, preferentially in leucocratic patches formed by dehydration melting (Fig. 11.17). Randomly disseminated garnets also occur in these granitoids.



Fig. 11.17. Orthogneissic granitoid showing leucocratic patches with garnet, manifesting dehydration melting (548001E / 343647N). Number tag 8 cm.

The chemical composition of these biotite granitoids differs from the common charnockites nearby. Although having rather similar SiO_2 and K_2O contents, the granitoids are clearly peraluminous and have a lower Fe/Mg, but higher $\text{Na}_2\text{O}/\text{CaO}$ ratio than the charnockites (Mäkitie et al. 2014b). Moreover, the biotite granitoids have rather low but distinctly higher U contents than the charnockites. All these differences indicate that the variably deformed granitoids have a different source than the charnockites. These granitoids are assumed to be syn-kinematic, while the afore-mentioned granite-charnockite association is considered to be post-kinematic in relation to the main phase of deformation.

Okaka Suite

Intrusive rocks assigned to the Okaka Suite are mostly situated in the Kalongo region as isolated intrusions, 5–100 km² in size. Usually, these rocks are well exposed in hilly ranges, like the prominent Okaka Ridge north of Pader town. Four different members have been distinguished¹: predominant charnockite and less abundant charno-enderbite, granite, and gabbro. They are spatially associated

with supracrustal, granulite-grade gneisses of the West Karamoja Group.

Wol charno-enderbite (0.74 Ga) (*P3Oche*)– Intrusions composed of predominant charnockite and subordinate charno-enderbite and mangeritic composition (5–10 km²) occur in particular NW of Kalongo town. All pyroxene-bearing granitoids of the Okaka Suite show elevated radiometric potassium signatures in comparison to supracrustal granulitic gneisses nearby. The airborne geophysical data do not, however, allow distinction between different charnockite members. Magnetic susceptibility values are generally low. U-Pb zircon dating yields a crystallisation age of 0.74 Ga (Mänttari 2014; Section 11.6).

Wol charno-enderbites are rather coarse (Fig. 11.18), massive and porphyritic rocks with usually greyish brown weathered surfaces with rusty shades and typically dark coloured while fresh. Perthitic K-feldspar occurs as euhedral phenocrysts, 1–3 cm in size. Other minerals are plagioclase, quartz and orthopyroxene (1–6%). Accessory minerals include fayalite, hedenbergite, biotite, hornblende and opaque minerals. Very brightly reflecting crystal faces of K-feldspar is a



Fig. 11.18. Porphyritic charno-enderbite of the Okaka Suite, comprising ~15 % quartz. In terms of classification diagrams of Streckeisen & le Maitre (1979), the rock is intermediate between charnockite and charno-enderbite (525674E / 348358N). Number tag 8 cm.

1 Excluding metamorphic 'charnockites', Le Maitre (1989) introduced a number of terms for a series of igneous charnockites, including opdalite (orthopyroxene-bearing granodiorite), enderbite (orthopyroxene-bearing tonalite) and mangerite (orthopyroxene-bearing monzonite). Frost & Frost (2008) recommended to abolish these terms and to use 'charnockite' in a broad sense for any igneous orthopyroxene-bearing granitoid in combination with the prefix 'opx-' as in 'opx-monzonite' instead of 'mangerite'.

positive feature for exploiting this rock for dimension stone.

The Wol charno-enderbites and mangerites are metaluminous in composition (see App. 2, anal. 178). They are ferrous and characterised by a high Fe/Mg ratio, also manifested by the occurrence of fayalitic olivine and orthoferrosilitic pyroxene (Mäkitie et al. 2014b).

Charnockite (P3Ochr) – Charnockitic rocks of the Okaka Suite are well exposed in hills and ridges, the largest being the 30 km long, N-S-trending Okaka mountain range north of Pader town (Fig. 11.19). Although charnockites are the dominant rock type, some granitic sub-types free of orthopyroxene, have also been encountered. This charnockite-granite association shows elevated potassium signatures on radiometric maps. Weathered surfaces of Okaka charnockite are brownish with rusty shades, while fresh surfaces have various dark brown colours. Mineralogically, these rocks can be classified as foliated, megacrystic pyroxene granitoids, with the largest K-feldspar phenocrysts up to 8 cm in diameter. Augen gneiss textures occur locally in charnockites, and gneiss enclaves are rare, but increase near the contact with supracrustal these country rocks.

Mineralogically, the rock is characterised by the presence of orthopyroxene (1–8 vol%) and by the absence or very low amount of hydrous (OH-bearing) minerals such as biotite and hornblende. Usually, perthitic K-feldspar and plagioclase dominate over quartz. Accessory minerals are fayalite,

hedenbergite and opaque minerals. The proportions of K-feldspar, quartz and plagioclase may differ and some members are probably charno-enderbitic in composition. The SiO₂ content of these metaluminous rocks ranges between 66–75 wt% and the K₂O content from 4 to 6 wt%. Couple representative whole-rock chemical analyses are shown in Appendix 2 (anal. 179–180). A high Fe/Mg ratio is reflected by the presence of orthoferrosilite and fayalitic olivine (Mäkitie et al. 2014b).

Granite (P3Ogr) – Pyroxene-free, granite phases of the Okaka Suite occur as relatively small, isolated intrusions within the supracrustals of the West Karamoja Group. They can be distinguished in the field from charnockites by having slightly lighter colours on fresh surfaces. However, they locally also resemble the pyroxene-bearing types; a verification using thin sections is recommended. These rather homogeneous, mostly porphyritic granitoids show a pronounced orientation of elongated K-feldspar phenocrysts (e.g., north of Naam-Okora trade centre), interpreted, at least partly, as magmatic flow (Fig. 11.20A). Similar porphyritic granite with deformed, flow-oriented phenocrysts up to 2 by 12 cm in size forms a large, flat outcrop ~15 km NW of Pader town (Fig. 11.20B) and a prominent hill north of Kalongo town. In thin section, euhedral but variously deformed K-feldspar phenocrysts, sericitised plagioclase and undulating quartz are the main minerals, with biotite (up to 15 vol%), garnet, apatite, zircon and opaque minerals forming accessory rock constituents.



Fig. 11.19. Charnockite outcrops in the hills of the Okaka range, ~15 km N of Pader town (508075E / 332808N).

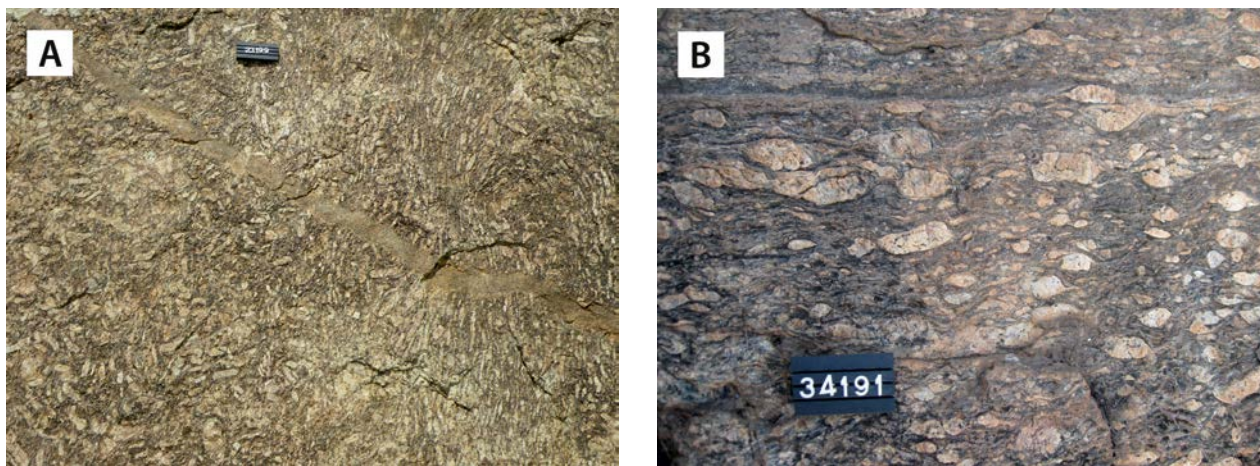


Fig. 11.20. (A) The orientation of K-feldspar phenocrysts in porphyritic granite of the Okaka Suite, probably represents magmatic flow. Note also the narrow cross-cutting granite dyke in the middle of the figure (536316E / 375320N). (B) Detailed image of a porphyritic granite with deformed K-feldspar phenocrysts, ~15 km NW of Pader town (502486E / 332215N). Number tag 8 cm.

Anorthosite (P3Oan) – Pyroxene-bearing anorthosite occurs only in a few isolated outcrops, 200–500 m² in size, 10 km SW of the Wol trade centre in a flat landscape, suggesting that the unit may be more extensive than can be concluded from these few outcrops. Anorthosites do not contrast with the surrounding supracrustal gneisses in magnetic or ternary images, but analytical signal shows a regional minimum corresponding to the anorthosite area.

This anorthosite is a light coloured, rather massive, generally coarse-grained rock (Fig. 11.21), mainly composed of labradorite and enstatite in crystals ranging between 0.5 and 5 cm in length.

Due to differences in orthopyroxene content, rock types range from anorthosite to pyroxene leucogabbro. Accessory minerals are olivine, ilmenite, hematite and quartz. Amphibole and magnetite occur rarely. A few, very coarse-grained, late magmatic gabbro pockets with plagioclase crystals that can reach up to 30 cm in length, occur in places. Two whole rock XRF-analyses of the leucogabbro show elevated Al₂O₃ (25–26 wt%) and CaO (8–9 wt%) (Mäkitie et al. 2014b). Ni-, V- and Ti-contents are low in the rock. Due to the small potassium content (1.8 wt% K₂O), they can be classified as monzogabbro in the diagram of de la Roche et al. (1980).



Fig. 11.21. Variation in grain size of a massive anorthosite of the Okaka Suite (517421E / 339153N). Note the very coarse enstatite grain in the upper left corner. Number tag 8 cm.

Labwor Hills Suite

The Labwor Hills Suite is mainly composed of charnockite with subordinate granitic members. These rocks are found in the mountainous region of Labwor Hills, in the SW corner of the Kotido District, where they are closely associated with various granulite-grade supracrustal gneisses (Sandiford et al. 1987 and references therein). Baldock et al. (1969, p. 17) mapped these charnockites as “*porphyroblastic granulite*”, which is “*a massive, structureless rock characterised by large porphyroblastic feldspars and generally by lacking foliation and lineation*” We have separated the Labwor Hills Suite from the petrographically almost similar Okaka Suite in NW for two reasons: the distance (~70 km) (Fig. 11.5) and the age difference. The 0.68 Ga old charnockites of Labwor Hills are some 50 million years younger than the Okaka charnockites (Mänttari 2014).

Otukey charnockite (0.68 Ga) (P3LHchr) – These charnockites are widely exposed in the western part of Labwor Hills, but also in the low ground to the west (Fig. 11.22A). The homogeneous, massive, coarse grained, porphyritic rock (Figs. 11.22B) shows, as usual, brownish colours with rusty shades on weathered surfaces, while fresh surfaces are relatively dark with greenish-grey tints. Narrow granite dykes and coarse, garnet-bearing pegmatite veins with diffuse boundaries occur in places (Fig. 11.22B), together with large xenoliths of psammitic or semipelitic gneiss. U-Pb zircon dating yields an age of 0.68 Ga (Mänttari 2014; Section 11.6).

Under the microscope major minerals are quartz, myrmekitic plagioclase, K-feldspar (perthitic orthoclase), orthopyroxene (up to 15 vol%) and often biotite (with dark reddish brown pleochroic colours). Opaque minerals, apatite and zircon are common accessory constituents and in some thin sections, rugged garnet and hornblende grains have also been observed.

The Otukey charnockitic rocks are ferrous in composition, have a relatively low Rb/Sr ratio (0.5–1.5) and low SiO₂ contents varying from 66 to 74 wt% (see App. 2, anal. 181–184). From a litho-geochemical point of view, the Otukey charnockites are very similar to charnockitic rocks of the Okaka Suite. Thus, as the Okaka Suite, the Labwor Hills Suite may comprise charno-enderbitic members. Geochemical discrimination diagrams for the Otukey charnockites are represented in Figure 11.33.

Granite (P3LHgr) – Granites of the Labwor Hills Suite form two relatively small bodies SE of Kalongo village. The northern body comprises brownish grey, coarse-grained and often porphyritic granite with K-feldspar phenocrysts, measuring 1 to 4 cm, that show some preferred orientation (Fig. 11.23A). When the proportion of phenocrysts is small, the rock resembles the more extensive unit of ‘variable deformed granitoids’ nearby. The southern body, which forms a distinct positive anomaly on the airborne ternary radiometric map, comprises light yellowish brown, equigranular, homogeneous microcline granite with plenty of red garnets up to 10 mm in size. In places, a porphyritic garnet-bearing granite comprises large xenoliths of banded,



Fig. 11.22. (A) Otukey charnockite outcrop in the western Labwor Hills; location of geochronological sample (567478E / 274381N). (B) Garnet-bearing pegmatitic ‘vein’ in porphyritic charnockite (554385E / 302743N). Number tag 8 cm.

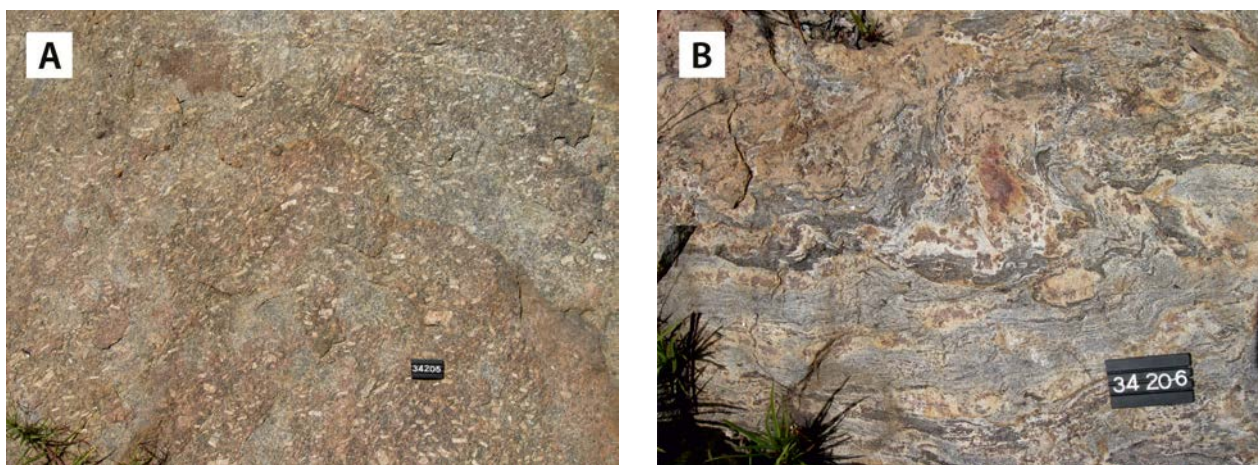


Fig. 11.23. Granites of the Labwor Hills Suite. (A) Porphyritic granite of the northern body (546997E / 324320N). (B) Banded, garnetiferous gneiss xenolith in porphyritic granite (547262E / 324061N). Number tag 8 cm.

granulite-grade micaceous gneiss (Fig. 11.23B), suggesting an anatectic (S-type granite) origin for these granitic rocks.

Major minerals of the Lawbor Hills granites are quartz, perthitic K-feldspar and myrmekitic, vari-

ably sericitised plagioclase with antiperthite inclusions; locally the amount of biotite and poikilitic garnet can reach 10% of the rock volume. Apatite, zircon, muscovite and opaque matter are common accessory constituents.

11.5 In-situ Intrusive Rocks in the Karamoja Belt

These rocks are believed to be *in situ* Pan-African plutonic intrusives, related to subduction, collision and amalgamation of East and West Gond-

wana, but not part of the Karamoja thrust masses. They comprise the following units (Table 11.4):

Table 11.4. Units of *in situ* intrusives in the West Karamoja Belt. The codes on right are the ones used in the unpublished 1:250 000 -scale geological maps compiled by GTK Consortium and archived by DGSM. Ages are after Mänttari (2014).

| | | |
|-------------------------------|--------------------------------|---------|
| Diorite | | P3dr |
| Kitgum granite (0.70–0.69 Ga) | | P3Ggr |
| Lamwo Suite (0.74–0.66 Ga?) | Coarse porphyritic granite | P3LAgr |
| | Charnockite | P3LAchr |
| | Medium-grained biotite granite | P3LABgr |

Lamwo Suite

Granitoids of the Lamwo Suite underlie a mountainous region (Fig. 11.24A) and nearby plains north of Kitgum town, occupying an area of about 400 km². The highest peak is called Lamwo (1992 m.a.s.l.), and this mountainous range continues into South Sudan, where it includes higher peaks such as Kinyati Mountain (3187 m.a.s.l.). Al-

though not dated, their texture, petrography and mineralogy allows them to be related to similar nearby intrusive rocks with ages between 0.66 and 0.74 Ga (Mänttari 2014). The Lamwo Suite comprises three main members (Table 11.4). Subordinate dyke rocks within the Suite include aplite, pegmatite, tonalite and dolerite. The charnockites have a tendency to grade into charno-enderbites and locally even into mangeritic variations.¹

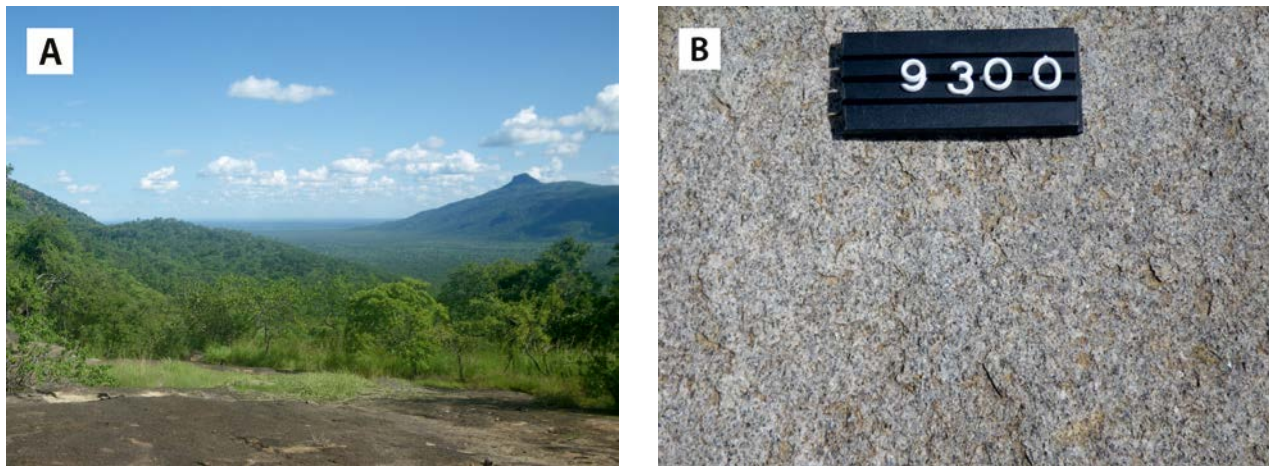


Fig. 11.24. (A) View from the southern slope of Lamwo Mountain towards the plains in the south (492304E / 413076N). (B) Detailed image of biotite granite from flat area (513445E / 399061N). Number tag 10 cm.

Medium-grained biotite granite (P3LABgr) – This fine- to medium-grained, homogeneous and rather massive biotite granite of the Lamwo Suite can be found 30–70 km NE of Kitgum town, where it covers a mountainous area of 35 x 25 km, east of Madi Opei village, and the plain areas nearby (Fig. 11.24B). Porphyritic and pegmatitic granite varieties can also be observed in places. A high-K radiometric anomaly coinciding with a mountainous area between Kiten and Ukuti villages, some 30 km east from Madi Opei village, is likely composed of similar granite.

Charnockite (P3LACHr) – Orthopyroxene-bearing charnockites occur as large (10–40 km²), individual bodies within the Lamwo Suite. As usual, they show brownish colours with rusty shades when

weathered and dark colours on fresh surfaces. These are rather homogeneous, porphyritic, mildly deformed rocks that usually show less strain than the granites of the same suite.

Major minerals are plagioclase and microperthitic K-feldspar, the latter in phenocrysts up to 8 cm in diameter (Fig. 11.25A). Orthopyroxene is a minor to subordinate constituent (2–8 vol%). Due to the often limited amount of quartz, the rocks locally classify as charno-enderbites and mangerites in the diagrams of Streckeisen & le Maître (1979). Biotite, with reddish pleochroic colours, and hornblende also occur, but usually their mode does not exceed 10 % by volume in total. Accessory minerals include ilmenite. Aggregates composed of retrograde biotite, chlorite, amphibole, opaque minerals and quartz formed at the expense of

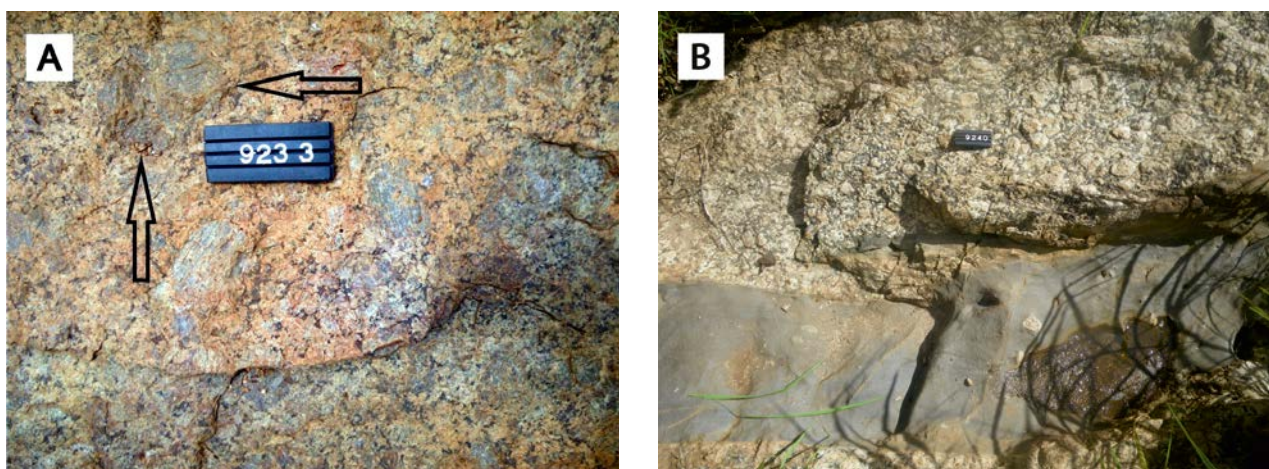


Fig. 11.25. (A) Lamwo Hill charnockite with very coarse K-feldspar phenocrysts (arrow) (473289E / 414127N). (B) Mafic dyke in the charnockite (490701E / 414855N). Number tag 8 cm.

orthopyroxene. In places, the charnockites also comprise amphibolitic inclusions and aplitic and mafic dykes (Fig. 12.25B).

Coarse porphyritic granite (P3LAgr) – These granites occur in rounded hills and outcrops, extending from the Kitgum area to the NE into the NW corner of Kaabong area and further into South Sudan. Although not dated, their texture, petrography and mineralogy are similar to the adjacent 660–740 Ma Lamwo intrusions.

The brownish, coarse porphyritic granite is megacrystic and rather massive in texture, and may locally comprise pyroxene, thus grading into charnockite. Aplitic, pegmatitic, tonalitic and doleritic dykes occur in places. The combined amount of biotite and hornblende is limited, generally less than 10% by volume, differing from the Lamwo medium-grained biotite granites, which usually contain over 10 vol% of biotite.

Kitgum granite (0.70–0.69 Ga) (P3Ggr) – This megacrystic granite mainly occurs N and E of Kitgum town, forming enormous knolls or ‘inselbergs’ standing above the peneplain (Fig. 11.26A), or being exposed in large flat outcrops. Areas occupied by Kitgum granite are highlighted by elevated potassium values on radiometric maps. U-Pb zircon dating yielded an age of 0.69 Ga (Mänttari 2014; Section 11.6).

K-feldspar occurs in phenocrysts typically having sizes of 3–5 cm in length (Fig. 11.26B). Locally, the amount of K-feldspar is low and the rock grades into granodiorite and tonalite. Other major minerals are quartz, plagioclase, biotite and garnet. Biotite with a mode of 5–15 vol% usually occurs in aggregates. The abundance of garnet varies, but usually reaches up to several percents. Its presence suggests that the Kitgum granite differs from typical Pan-African porphyritic granites in northern Uganda such as the somewhat younger granitoids of the Adjumani-Midigo Suite (Section 11.4.5).



Fig. 11.26. (A) Opokyam Hill, an enormous, ~100-m-high knoll of the Kitgum granite. Note a geologist on top (arrow) (469847E / 377359N). (B) Detailed image of the porphyritic Kitgum granite (506015E / 362057N). (C) Pale grey, fine-grained granite dyke in the deformed, porphyritic Kitgum granite. Number tag 8 cm.

At Opokyam Hill, almost homogeneous granite occurs alongside members with a clear planar fabric. Textures thus range from rather massive to zones with distinct tectonic flattening, showing augen gneiss texture. The dated sample, collected 19 km east of Kitgum town, is poor in K-feldspar and its composition is trondhjemitic. Fractures and joints are scarce, which explains the huge size and smooth rounded shape of this inselberg.

Chemical analysis from the coarse-grained, porphyritic Kitgum granite shows that compositionally it resembles the charnockitic rocks of the Okaka Suite nearby. The slightly peraluminous ($A/CNK = 1.04$) granitoid has a relatively low SiO_2 content (62 wt%) and elevated TiO_2 (1.3 wt%) and Zr (552 ppm) (see App. 2, anal. 185).

Dykes of granitic and granodioritic to tonalitic composition are common in the Kitgum granite. A pale, fine-grained, equigranular granitic dyke, a few tens of centimetres in width, cuts the deformed Kitgum granite in an open zigzag manner with undeformed contacts (Fig. 11.26C). Another type of dark grey, biotite-rich dyke is also emplaced into Kitgum granite in various directions. A particular

feature of these dark dykes is their internal biotitic schistosity, always parallel to the walls of the dykes and the mobility of felsic material together with the dyke material. In analogy with micro-tonalite temporally associated with the Adjumani granite (see Section 11.6), these dark dykes at Kitgum are also called 'micro-tonalite'. It is noted that the Adjumani granite is some 30 million years younger (659 ± 15 Ma; Mänttari 2014) than the Kitgum granite (694 ± 10 Ma). Assuming that the micro-tonalite dykes at Kitgum and Adjumani are coeval equivalents, they are thus more than 30 million years younger than their Kitgum granite host and, if so, the pale dyke in Fig. 11.26C would represent a dyke derived from Adjumani granitic plutonism.

Diorite (P3dr) – A large diorite intrusion (~ 45 km²) is located 10 km east of the Agoka trade centre in the NE corner of Uganda. In the existing 1:250 000 -scale geological map of Karamoja (Williams 1966), this rock (with some granites) allegedly represented the youngest Precambrian or lower Palaeozoic magmatic event in NE Uganda.

11.6 Other Pan-African Granitoids in North Uganda

These are autochthonous granitic intrusives, restricted to the northernmost part of Uganda, close to the border with South Sudan, supposedly related to subduction, collision and amalgamation of the already united East and West Gondwana plates with the northern Sahara Metacraton. As such they are not part of the Karamoja Belt, but rather belong to the E–W-trending Central African Fold Belt or Oubangides (Figs 1.1 and 1.16) along the northern margin of the proto-Congo Craton. They include the Midigo granite of the West Nile Block (Fig. 4.3) and the Adjumani Suite emplaced into the North Uganda Terrane (Fig. 5.2). Dating indicated almost identical U–Pb zircon ages for the Midigo and Adjumani granitoids of 656 ± 16 Ma and 659 ± 15 Ma, respectively (Mänttari 2014).

Adjumani-Midigo Suite

Midigo granite (0.66 Ga) (P3AMmgr) – This granite pluton directly northeast of Midigo town, Yumbe District (West Nile Province; Fig. 4.3) is the only Pan-African granite massif in the West Nile Block. It is a greyish, medium- to coarse-grained, slightly porphyritic, mildly to weakly foliated to almost massive biotite granite. More porphyritic, coarse to very coarse-grained granite varieties occur in places with K-feldspar phenocrysts up to 50 mm in size (Fig. 11.27A). The Midigo granite is cut by N–S-trending aplitic dykes, and also medium-grained, equigranular, rather leucocratic granitic dykes have been encountered. Mafic, parallelly aligned enclaves, measuring up to 30 cm in length, are locally abundant (Fig. 11.27B).

Table 11.5. Pan-African granites emplaced into Archaean basement of north Uganda. The codes on the right are the ones used in the unpublished geological maps archived by DGSM. Ages are after Mänttari (2014).

| | | |
|-----------------------|----------------------------|---------|
| Adjumani-Midigo Suite | Midigo granite (0.66 Ga) | P3AMmgr |
| | Adjumani granite (0.66 Ga) | P3AMagr |

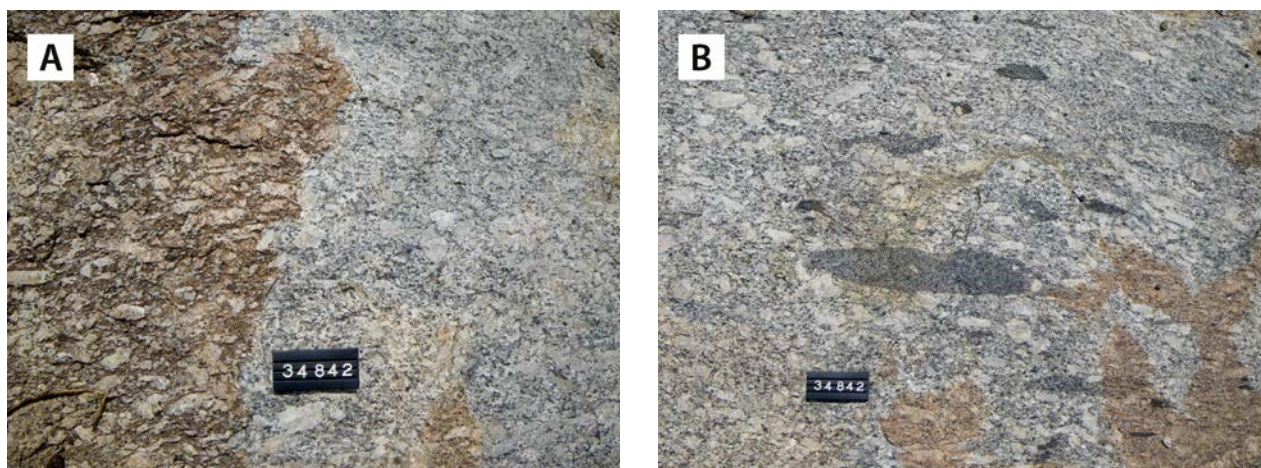


Fig. 11.27. (A) Weathered (left) and fresh surface of the coarse-grained, porphyritic Midigo granite. (B) Mafic enclaves in the same Midigo granite (311042E / 406859N). Number tag 8 cm.

There exists some doubt with regard to the autochthonous, intrusive setting of the Midigo granite. The country rock is composed of leucocratic granite gneiss and banded gneiss of the Yumbe Complex (Section 4.7). Along the southern contact of the Midigo granite, dark grey, strongly foliated, blastomylonitic gneiss (Fig. 11.28A) with narrow, cm-thick, subhorizontal pseudotachylite or ultra-blastomylonite horizons (Fig. 11.28B) constitutes the country rock. The latter may represent the sheared equivalent of banded gneiss and, consequently, represent the sheared footwall below a thrust block of Midigo granite.

Adjumani granite (P3AMagr) – This rock unit comprises a number of elongated granitoid intrusions mainly in the Adjumani District in NW Uganda (Fig. 5.2). The largest body is an elongated, NNW–SSE-trending massif, roughly 90 by 20 km

in size, which forms a rolling hilly terrain around the Kilak mountain, some tens of kilometres SSE of Adjumani town (Fig. 11.29). Smaller bodies are exposed along roughly N–S directed curvilinear faults, most likely superposed on the palaeo-suture between the West Nile Block and the North Uganda Terrane. Another intrusion, measuring some 75 km in length and 2 to 4 km wide, has been emplaced inside the northern segment of the Aswa Shear Zone.

The northern segment of the main intrusion is a grey coloured, medium-grained, homogeneous, equigranular to porphyritic biotite granite (Figs 11.30A–B). Porphyritic members contain K-feldspar porphyrocrysts 5–10 mm in size, reaching 20–30 mm in diameter in some magma patches. Further southwards the body usually has the same fabric, but a granodioritic composition with, in a few locations, fine-grained, equigranular granite

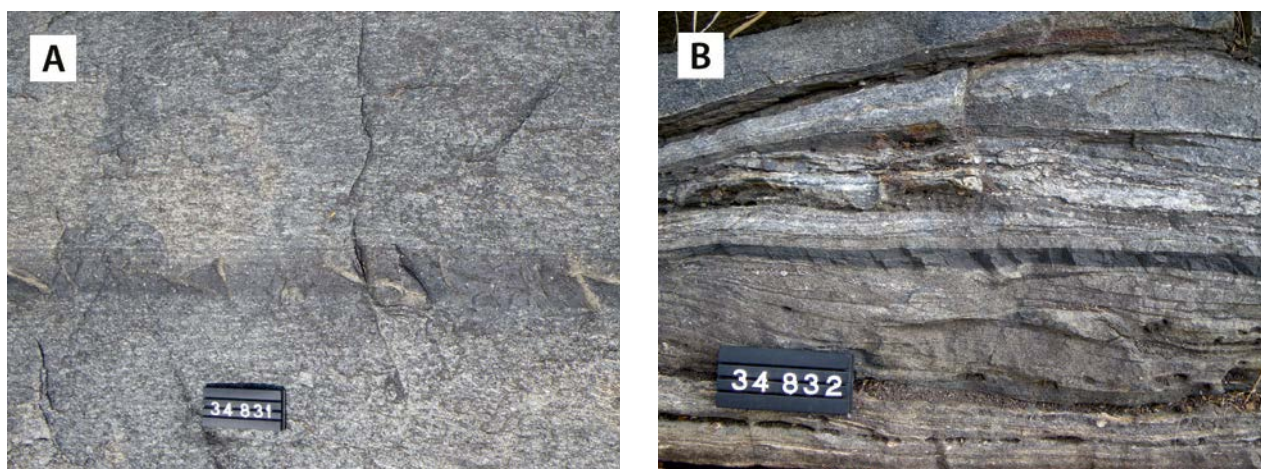


Fig. 11.28. (A) Strongly sheared gneiss with narrow blastomylonite bands (304285E / 399030N). (B) Pseudotachylite bands in the same gneiss near south contact of the Midigo granite (304895E / 398776N). Number tag 8 cm.



Fig. 11.29. Typical, well-exposed hill of the Adjumani granite in the southern part of the largest massif (396600E / 323200N).

dykes or pegmatite veins. For chemical composition of these rocks, see Appendix 2 (anal. 186–190). Flow banding can also be locally observed.

In the proximity of fault zones a strong preferred orientation has developed; massive rock may grade into rock with a pronounced preferred shear fabric over a distance of a few centimetres (Fig. 11.30C). Overall, granitoids of the Adjumani Suite are homogeneous rocks with scarce and small, variously deformed enclaves in only a few localities. Large xenoliths of country rock supposedly represent the roof pendant of the granitic body (Fig. 11.30D).

Pegmatite and micro-granitic dykes occur in places. Deformation of the latter into gentle folds manifests a certain amount of flattening after their emplacement (Fig. 11.31). As shown in Figure 5.2, coarse, equigranular, homogeneous, massive to very weakly foliated Adjumani granite is also em-

placed within the northern segment of the Aswa Shear Zone (ASZ), manifesting that these granitoids have been emplaced into the ASZ after sinistral strike-slip faulting, which accompanied W- to SW-directed thrusting in the Karamoja Belt.

A variety of the Adjumani granite is found west of Patico, northeastern Adjumani District. It differs from the usual, rather homogeneous granitoid in having two compositional constituents: a darkish, tonalitic component and a pale, granitic component (Fig. 11.32A). Colour variations in both of them imply small-scale compositional variation. They seem to be coeval and the product of magma mingling. The microphotograph shows the distinctly developed preferred orientation of the biotite flakes, manifesting that even these late Pan-African magmatic rocks have suffered significant deformation (Fig. 11.32B).

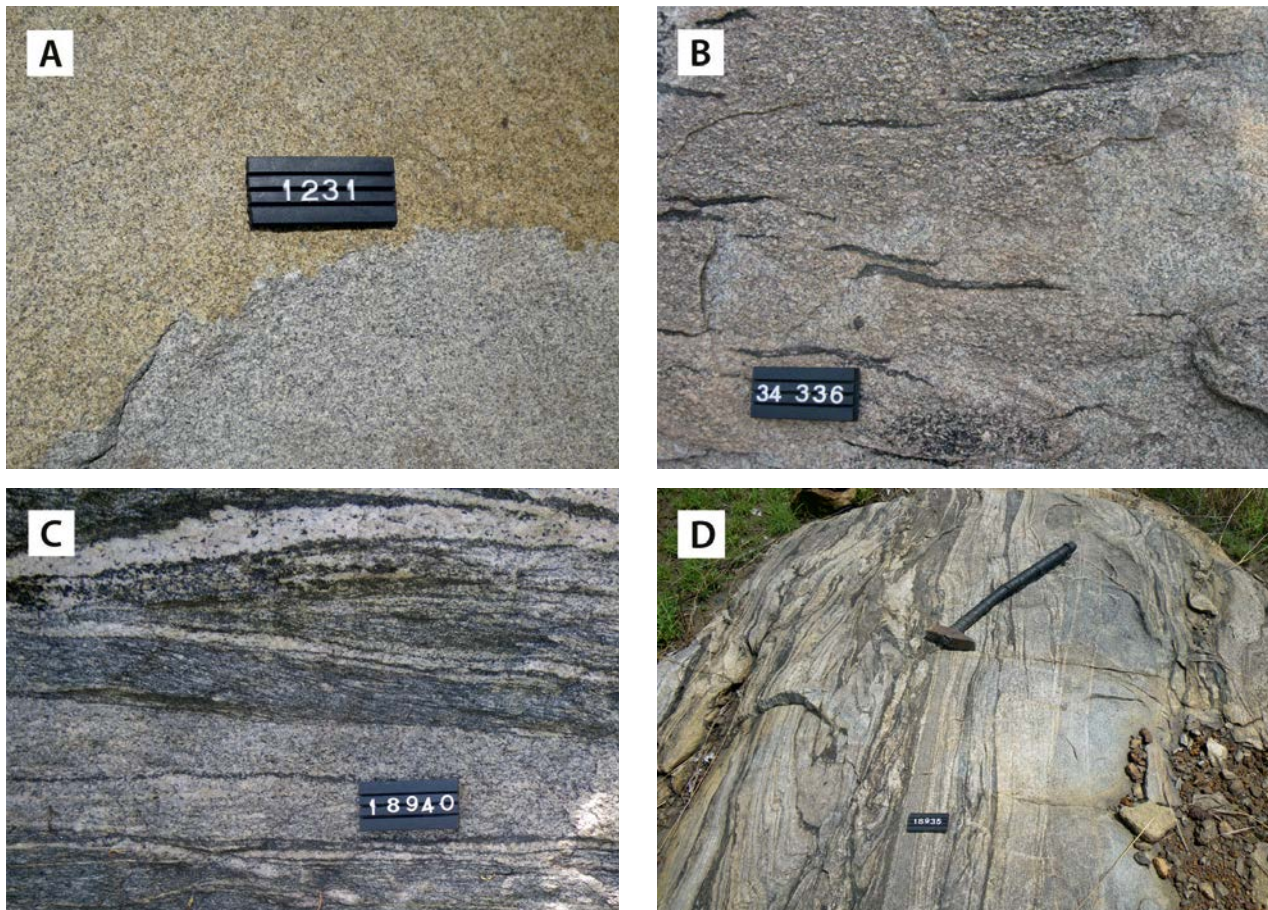


Fig. 11.30. (A) Equigranular, massive Adjumani granite, an outcrop sampled for U-Pb dating (367935E / 391770N). (B) Deformed, mafic enclaves in the porphyritic variety of the Adjumani granite (376098E / 379580N). (C) Strongly sheared Adjumani granite close to a boundary fault in the Madi-Igisi fault zone (371148E / 348956N). (D) A large xenolith of Archaean country rock in Adjumani granite at Boroli Hill (373484E / 364093N). Number tag 8 cm.



Fig. 11.31. Grey, massive to weakly foliated granodiorite of Adjumani Suite with pegmatite dyke (1), gently folded microgranitic dyke (2) and thin quartz veins (3). Open fold indicate a certain amount of flattening after emplacement (362553E / 376592N).

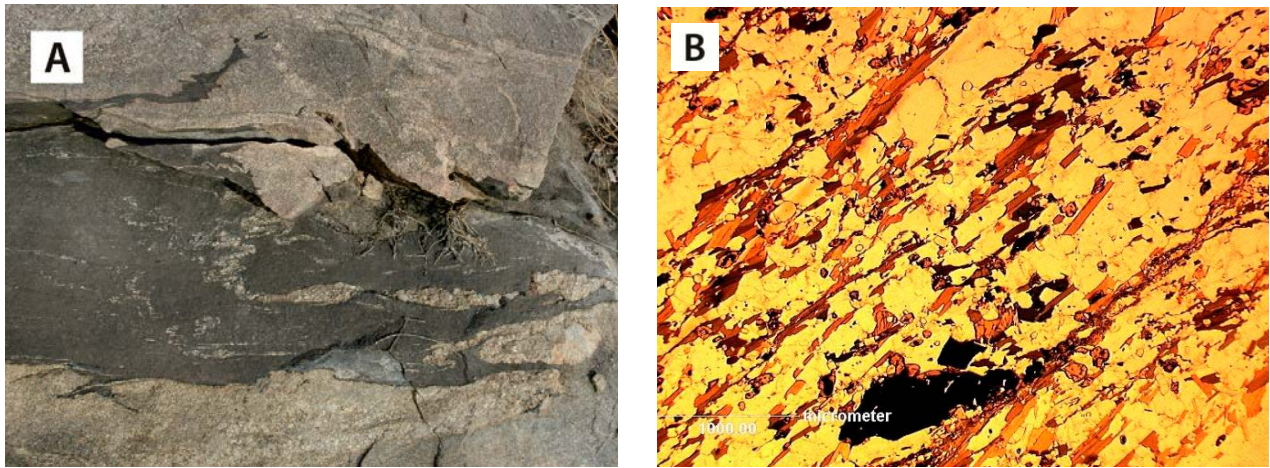
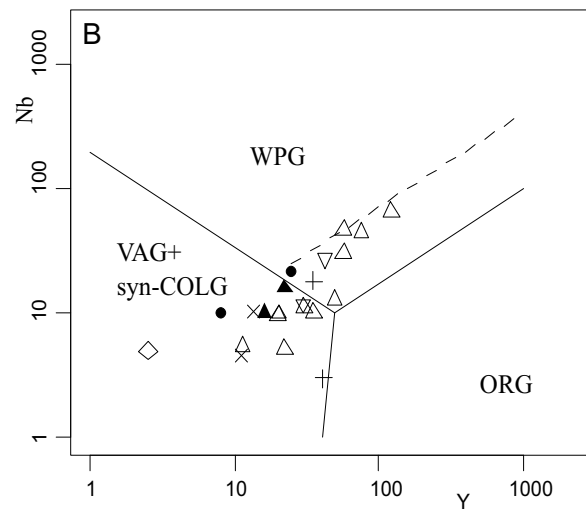
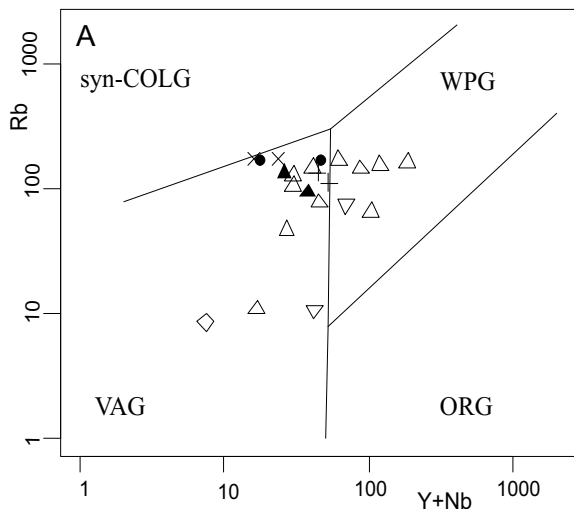


Fig. 11.32. (A) Microtonalite dyke in Adjumani granite east of Adjumani town (372043E / 373884N). (B) Microphotograph of same dyke. The schistose fabric is defined by the preferred orientation of biotite (Bt). The abundant reddish grains are titanite. Note the two post- or late-schistosity movement surfaces, activated parallel to the dominant schistosity. The width of the area shown is 4 mm.

11.7 Litho geochemistry

The available chemical data are too scarce to draw meaningful conclusions, but representative chemical whole rock analyses are shown in Appendix 2. Chemical compositions of the Pan-African granulite-grade gneisses and charnockitic rocks of the Kalongo region are recently also presented by Mäkitie et al. (2014b). Anyway, the compositions of the afore-mentioned rocks range from

granitic to granodiorite, quartz monzonite, tonalite and more mafic compositions. Moreover, it can be mentioned that in the geochemical tectonic discrimination diagrams the Neoproterozoic intrusive rocks of NE Uganda plot in the VAG and syn-COLG fields or in the WPG field, while the Archean rocks do not show such a wide distribution (Fig. 11.33).



- + Otukey charnockite (P3LHchr)
 - ◇ Anorthosite (P3Oan)
 - △ Charnockite (P3Ochr)
 - ▽ Wol charno-enderbite (P3Oche)
 - × Variable deformed granitoid (P3vdgr)
 - Kuju granitic and granodioritic gneiss (A3Uggdg)
 - ▲ Apuch granite migmatite (A3Ugrm)
- } Ogili Suite

Fig. 11.33. Geochemical discrimination diagrams for granitoids. (A–B) diagrams indicating geotectonic settings after Pearce et al. (1984). Key: syn-COLG = syn-Collision granites; VAG = Volcanic arc granites; WPG = Within plate granites; ORG = Oceanic ridge granites. Chemical data for the Okaka Suite and the variably deformed granitoids are modified after Mäkitie et al. (2014b).

11.8 Aswa Shear Zone

11.8.1 Introduction

The brittle-ductile Aswa Shear Zone (ASZ) is a prominent extensive strike-slip shear zone, which is not restricted to northern Uganda, but continues along strike into South Sudan and Kenya (Fig. 11.34), and even further southeastwards into fault zones in Madagascar and southern India (Schreurs et al. 2006). In South Sudan the ASZ forms part of a conjugate set of faults with NW–SE and NE–SW directions that subsequently played a major role in the formation of hydrocarbon-bearing Cretaceous–Neogene rift basins. The ASZ is still active today, as demonstrated by earthquake foci in South Sudan. Kilimanjaro, the highest volcano in Africa, is on top of the southeastern prolongation of the ASZ (le Gall et al. 2010).

11.8.2 Textures and Structures within the ASZ

From analysis of the recently accrued airborne geophysical data (Fig. 11.35), it appears that the ASZ cannot be portrayed as previously (e.g., DGSM 1966) as a simple, narrow strike-slip fault in which all the strain has been absorbed in a relatively narrow zone (Ruotoistenmäki 2014). On the contrary, the ASZ forms a relatively wide zone of deformation, some 6 km in width, with first-order shears, associated with second- and third-order synthetic and antithetic faults.

A conspicuous feature is the elongated, lozenge-shaped, fault-bounded escape block on the southwestern side of the main fault (Fig. 11.35). Our field observations further show that the ASZ is composed of elongated anastomosing zones of major strain that alternate with relatively undeformed lensoid zones. Consequently, blastomylonite zones, up to several decimetres in width, alternate with bodies of rock that are less deformed. Overall, however, the strain intensity and density of blastomylonite zones progress towards the central first-order shear plane. A few representative sections are described below. The lithostratigraphical units along the ASZ and the effects of the Aswa shearing are described in detail in Saalman & Pokki (2014).

The southeastern segment of the ASZ is intersected almost perpendicularly by the main road between Mbale and Sironko towns. Approximately halfway, a major fault of the ASZ shows as a mylonite zone up to tens of metres in width (Fig. 11.36A). Within the mylonite zone the intensity of deformation is variable and blastomylonite (Fig. 11.36B) alternates with ultra-blastomylonite (or pseudotachylite)² and with less deformed but strongly foliated rocks, with K-feldspar augens up to 8–10 mm in size, in which the quartz dioritic protolith can still be recognised (Fig. 11.36C).

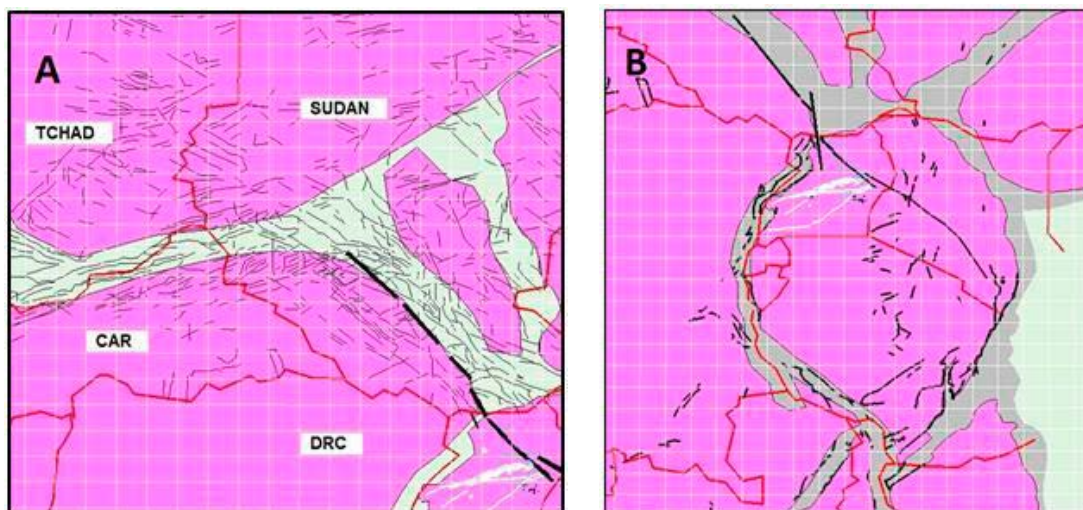


Fig. 11.34. (A) Lineament map of central Africa showing that Aswa Shear Zone can be extended NW-wards into South Sudan. Note that Cretaceous–Neogene rift basins form a conjugate set with NW–SE and NE–SW directions. (B) Extension of ASZ into Kenya (courtesy C. Reeves).

² For cataclastically deformed rocks with primary cohesion the nomenclature of Higgins (1971) will be followed.

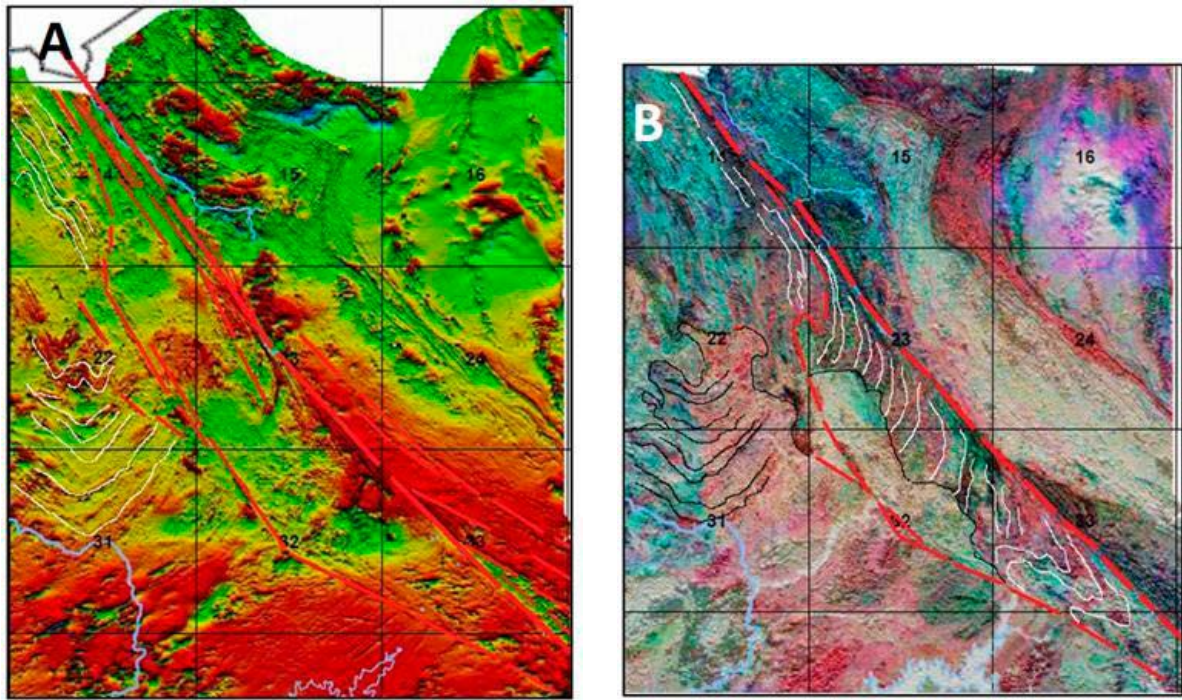


Fig. 11.35. (A) Magnetic image showing the central part of the NUT with Aswa Shear Zone (ASZ) and satellite faults. (B) Ternary analytical signal image showing the ASZ with major satellite faults. The crystalline basement with open W-E-directed foliation traces is dragged into more northerly directed orientations close to the trace of the principal fault. The crystalline basement N(E) of the ASZ show uniform NW-SE directed trends. This may be due to drag along the ASZ or, alternatively, this structural grain was superposed on an older structural trend due to SW-directed thrusting of the Karasuk Supergroup and West Karamoja Group of the Karamoja Belt, whereby the crystalline basement of the NUT served as footwall of the thrust plane.



Fig. 11.36. (A) The Aswa Shear Zone exposed along road from Mbale to Sironko (636124E / 133880N). (B) Thoroughly sheared, blastomylonitic and (C) Augen-textured variety of quartz diorite in the same road cut. Number tag 8 cm.

Deformation of migmatitic quartz diorite gneiss in the ASZ near the township of Malera (618915E / 158525N) is not limited to 'grinding' of minerals and recrystallisation but also involved transposition of the pre-existing gneissose banding into mylonitic planes parallel to the shear zone together with extreme flattening. The latter may give rise to the formation of rootless, isoclinal microfolds (Fig. 11.37A). Sparse K-feldspar porphyroclasts and micro-drag folds manifest sinistral movements in most locations (Fig. 11.37B).

Blastomylonitic granodiorite at the Katakwi road (Fig. 11.38A) shows compositional banding composed of alternating grey and dark grey

to blackish layers with fine-grained K-feldspar porphyroclasts. The latter may have long tails of polygonised and recrystallised K-feldspar. Recrystallisation of quartz preferentially has taken place in the pressure shadow of K-feldspar porphyroclasts. Some bands may represent leucosomes and pegmatite veins or dykes, which have been transposed into a parallel mylonite banding. Dark grey to blackish layers, supposedly derived from mafic xenoliths, are elongated parallel to the blastomylonitic foliation. In places, horizons with thrust stacking in blastomylonitic granodiorite can be observed (Fig. 11.38B).

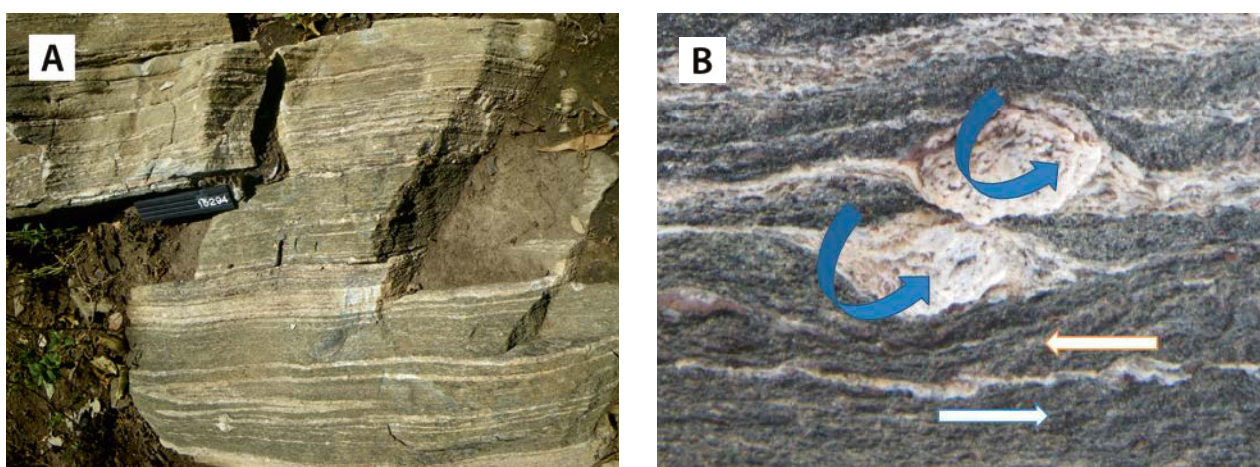


Fig. 11.37. (A) Extreme flattening and shearing of palaeosome-neosome banded quartz-diorite gneiss has given rise to the formation of rootless isoclinal microfolds. (B) Detailed image of the bottom left part of the previous photograph showing two K-feldspar porphyroclasts, approximately 10–15 mm in size. Micro-drag folds and rotation of the K-feldspar grains manifest sinistral movements (618915E / 158525N). Number tag 15 cm.

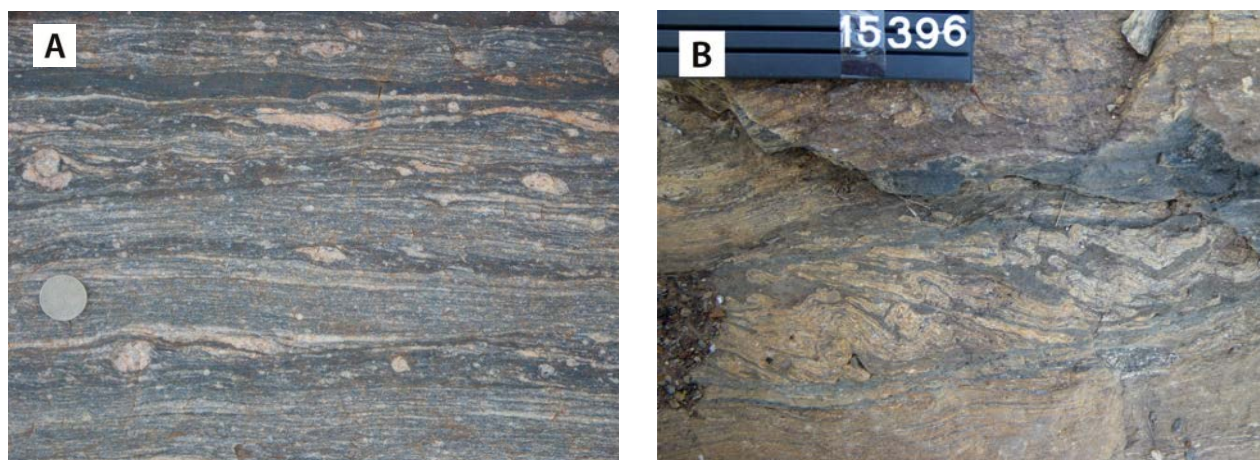


Fig. 11.38. (A) Blastomylonitic granodiorite at Katakwi road with fine-grained K-feldspar porphyroclasts. Some bands may represent leucosome veins and pegmatite dykes, which have transposed to a parallel mylonite banding due to shear zone foliation. Mafic xenoliths (upper part of the photograph) are elongated parallel to the foliation. (B) Horizon with 'thrust stacking' in blastomylonitic granodiorite (572104E / 200488N). Diameter of coin 22 mm, number tag 15 cm.

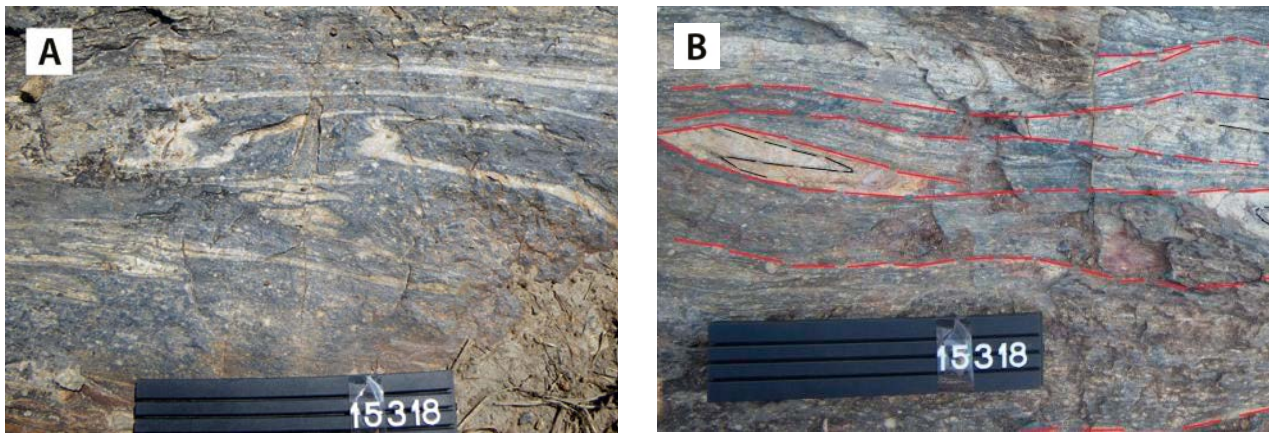


Fig. 11.39. (A) Blastomylonitic quartz diorite with disseminated K-feldspar porphyroclasts up to 5 mm in size. Note rootless, isoclinal and asymmetric microfolds with thinning in flanks and thickening in hinge zones. (B) Same blastomylonite showing zones of different strain. Small differences in competence cause pinch-and-swell. Note that younger mylonitic banding cuts older banding (609801E / 168471N). Number tag 15 cm.

Similar features have been observed NE of Kumi, where quartz veins have been folded into rootless, isoclinal and asymmetric microfolds with stretching and thinning of the flanks perpendicular to the flattening and thickening in the hinge zones (Fig. 11.39A). In the same location one can observe that strain was not uniformly distributed throughout the blastomylonite rock. Some zones, up to a few centimetres to a few decimetres thick, are more deformed than other nearby zones. Displacements along the contacts between zones of different strain caused one mylonitic S-plane to be cut off by another. Small differences in competence cause pinch-and-swell of the mylonitic banding (Fig. 11.39B).

The distribution of strain within the ASZ is also well exposed in a section across the ASZ along the road between Gulu and Kitgum. Within the central part of the ASZ, gneissose rocks can be found with euhedral, rectangular K-feldspar crystals manifesting only limited strain. Nearby gneissose rocks with microfolds may grade over short distances into blastomylonite (Figs 11.40A-D). The latter rock shows a straight blastomylonitic fabric with

the leucosomes and pegmatoid lenses and streaks being necked, boudinaged and pulled apart. Feldspar porphyroblasts only survived sporadically, with the majority being altered into trains of polygonised small feldspar grains. Those feldspar porphyroclasts that survived show newly formed quartz crystals in the pressure shadow. Hornblende porphyroblasts, with quartz inclusions, occur in places.

Similar textures have been described from pseudotachylites from the NW–SE-trending Tambach fault zone in Kenya (Hetzl & Strecker 1994), composed of 10 to 25 vol% porphyroclasts in a matrix made up of plagioclase microlites up to 20 μm in length. Flow structures and microlites are considered to indicate a melting origin. The host rock of the pseudotachylites contains significant proportions of biotite or hornblende. The scarcity of relicts of these hydrous minerals in pseudotachylites suggests ready assimilation during the melting process due to their low shear yield strength and their low fracture toughness (Spray 1992). Sinistral shear bands sub-parallel to the pseudotachylite veins are also common.

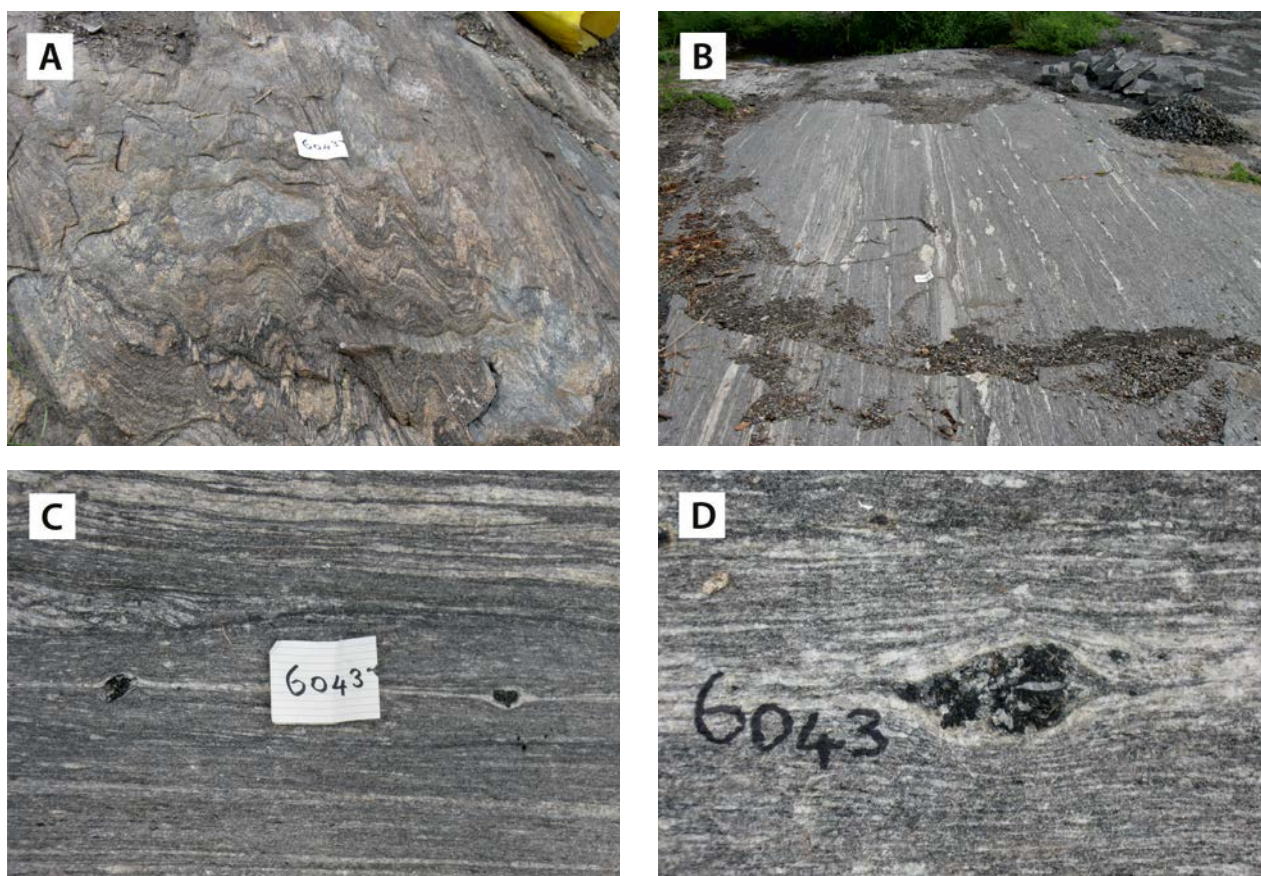


Fig. 11.40. (A) Dark, tonalitic gneiss with tight microfolds may grade over a short distance into blastomylonitic rock (B) with a straight, mylonitic banding and leucosomes that have been necked, boudinaged and pulled apart. (C) Preserved hornblende porphyroblasts in a blastomylonitic gneiss. (D) Detailed image of a hornblende porphyroblast with quartz inclusions (450140E / 324767N). Number plate 10 cm.

11.9 Geochronology

The oldest age determinations from the Karamoja Belt in eastern Uganda were obtained from the Kaabong area (MacGregor 1962): biotite from a granitic dyke yielded a K-Ar age of 515 ± 18 Ma ($3^\circ 31' / 34^\circ 09'$); a similar rock from a nearby location ($3^\circ 35' / 34^\circ 07'$) produced a WR Rb-Sr age 565 ± 20 Ma; and biotite from pyroxene gneiss (i.e., enderbite P3Kglgn) ($3^\circ 39' / 34^\circ 04'$) yielded a K-Ar age of 575 ± 20 Ma. Subsequently, Leggo (1974) dated a younger 'granitic injection phase' in 'alleged Archaean basement' from Labwor Hills, yielding U-Pb zircon ages of 635 ± 30 Ma.

Modern U-Pb zircon age determinations (LA-ICP-MCMS) have been carried out by the GTK Consortium (Mänttari 2014). These include the analysis of four rocks from the West Karamoja Group of the Karamoja Belt, one reworked Archaean rock in the ASZ and two determinations of Pan-African granitoids emplaced into Archaean basement of the NUT and WNB, outside the Karamoja

Belt. The afore-mentioned seven dated rocks after Mänttari (2014) are summarised in the following with their age results, laboratory codes (UG-) and coordinates.

- (1) Apuch granite, migmatitic in places (2.66 Ga/ 0.69 Ga) (UG-40; 509876E / 261810N).
- (2) Wol charno-enderbite (737 ± 11 Ma) (UG-34; 524746E / 351472N).
- (3) Kitgum granite (694 ± 10 Ma) (UG-42; 506015E / 362057N).
- (4) Otukei charnockite (684 ± 6 Ma) (UG-6; 567478E / 274381N).
- (5) Kitgum granite (679 ± 8 Ma) (UG-48; 343340E / 502964N).
- (6) Adjumani granite (659 ± 15 Ma) (UG-43; 367935E / 391771N).
- (7) Midigo granite (656 ± 16 Ma) (UG-11; 304175E / 400047N).

11.10 Tectono-Thermal Development during the Pan-African Orogenic Cycle

11.10.1 Introduction

Deciphering of the Neoproterozoic geodynamic evolution of Uganda is difficult and will require far more information, in particular structural, petrological and geochronological data. The complexity partly results from the fact that Neoproterozoic Uganda constituted the northeastern corner of the proto-Congo Craton, bounded by two Pan-African mobile belts, the N–S-trending East Africa Orogen (EAO) in the east and the W–E-trending Central Africa Belt (CAB) or Oubangides in the north (Section 1.7). Moreover, a third weakness zone was formed by the intra-cratonic Madi-Igisi Belt, separating the West Nile Block (Bomu-Kibalian Shield) from the North Uganda Terrane. This ~1.0 Ga belt was reactivated during the Pan-African Orogenic Cycle (Chapter 9).

East African Orogen (EAO) – The EAO is a polycyclic mobile belt that formed over a long period of time, broadly between 830 Ma and 550 Ma, with some ‘final docking’ events lasting till ~470 Ma. The timing and intensity of the tectono-thermal events varied, however, along the strike of the orogen, and strongly contrasting tectono-stratigraphic domains may be juxtaposed. Furthermore, on the scale of regional maps of the belt, geological contiguities remain frequently hidden. In addition, mapping by different working groups over time with different backgrounds has hampered consistent interpretations.

Traditionally, the EAO has been divided between two major geodynamic provinces with contrasting rheological properties: the Arabian-Nubian Shield (ANS) (north) and Mozambique Belt (Holmes 1951) (south). The ANS is an accreted collage of Neoproterozoic island-arc and back-arc terranes, with remnants of 900 Ma and younger oceanic crust (Greenwood et al. 1976, Al-Shanti & Mitchell 1976). Accretion tectonics in the ANS was accompanied by the formation of thin-skinned, low-grade metamorphosed ophiolite nappes. The Mozambique Belt, on the other hand, is interpreted as a Himalayan-style continent-continent collisional orogen between West and East Gondwana (Burke & Sengör 1986, Shackleton 1986, Key et al.

1989, Behre 1990). It is mainly composed of Archaean cratonic lithosphere, together with rocks of Palaeo- and Mesoproterozoic age, and far less juvenile Neoproterozoic rocks. In Tanzania and southern Kenya, the Mozambique Belt is characterised by an assembly of granulite facies thick-skinned nappes. The boundary between both domains is loosely defined by the southernmost occurrences of superficial ophiolite nappes exposed in central Kenya, including the Karasuk-Potok area of western Kenya and eastern Uganda.

This duality of the EAO is no longer undisputed: In southeastern Kenya, for example, tholeiitic gneisses, supposedly former M-type granitoids with geochemical oceanic island arc affinities, yield emplacement ages of ~955–845 Ma (Hauzenberger 2003), which supposedly point at early Pan-African subduction³ (Bauernhofer et al. 2004). Mafic to ultramafic rocks from NE Tanzania, showing evidence of ophiolitic cumulates, together with granulite areas in subduction settings, were also observed in central and southern Tanzania. These data support the continuation of an island-continental arc range, comparable to the widespread arc settings documented in the ANS, across Kenya–Tanzania to Mozambique (Bauernhofer et al. 2009).

Neoproterozoic oblique collision between East and West Gondwana with NW–SE relative plate motions was followed by a stage of post-collisional ductile shearing parallel to the N–S plate boundaries (Shackleton & Ries 1984, Shackleton 1986). Based on Rb–Sr geochronology, Key et al. (1989) and Mosley (1993) distinguished four major tectono-metamorphic phases in the Kenyan-Tanzanian segment of the EAO:

- (1) **Samburuan-Sabachian (830–800 Ma)** – The formation of major recumbent folds with ductile thrusting and interleaving of basement, metasedimentary cover rocks and slices of oceanic metavolcanic complexes. Responsible for the primary transformation of an essentially sedimentary sequence into paragneisses with a near-horizontal fabric parallel to the compositional layering. Syntectonic emplacement of crustal melt granites and mafic dykes. This

³ Could this relate to the formation of the Madi-Igisi trough and its southern continuation in the Itomwe area (Kivu) in a back-arc setting?

tectono-thermal event is supposedly related to plate collision, oblique to the N–S orogenic strike, between the Archaean Tanzanian Craton in the west and an eastern craton.

- (2) **Baragoian-Barsaloian (630–620 to 580–570 Ma)** – A post-collisional tectono-thermal event under greenschist to amphibolite facies conditions. Deformation is characterised by folding and transposition of the initial near-horizontal fabric parallel to the compositional layering, producing regional upright folds and regional, steep, ductile, N–S to NNW–SSE-trending strike-slip shear zones (generally sinistral) and controlling the present gross distribution of gneiss groups. Peak metamorphism was coeval with the intrusion of syntectonic granitoids.
- (3) **Loldaikan (~580–530 Ma)** – Cooling and uplift posterior after a ~560 Ma thermal event has exposed high-grade gneisses with a distinct structural and metamorphic asymmetry across the orogen. The western part of the orogen shows clockwise P - T - t paths and involved overthrusting of, and imbrication with, the Tanzanian Craton, which probably obscures older (1900 and 1100 Ma) tectono-thermal episodes. In contrast, the eastern part has anti-clockwise P - T - t path that is characterised by extensive crustal melts, and has remained the isotopic imprint of earlier Proterozoic events.
- (4) **Kipsingian (530–470 Ma)** – Upper crustal level open folding and brittle shears record the final events of the orogeny. Uplift and cooling, which extended beyond the confines of the orogen, are dated by ubiquitous mineral ages of ~500–480 Ma.

The above sequence of events is not necessarily valid in other segments of the EAO but, in summary, the following observations apply:

- (1) Pan-African tectono-thermal processes in the EAO of Kenya took place over a long period of time (some 140 million years);
- (2) during all phases, save the last one, metamorphic conditions reached P - T -conditions of the amphibolite and granulite facies, with local anatexis (4 to 10 kbar; 500–700°C) and a high CO_2 fugacity as manifested by the absence of graphite and, consequently, low water activity ($a_{\text{H}_2\text{O}}$), promoting granulite-facies conditions;

- (3) a clock-wise P - T - t path, manifesting post-collision crustal thickening with progressive shortening across the orogenic belt, involving extensive structural reorganisation and isotopic resetting;
- (4) during the progressive 630–580 Ma event, regional N–S- to NNW–SSE-trending ductile shear zones (generally sinistral) were produced resulting in the dominant regional fabric (including a regional N–S-stretching lineation) and controlling the present gross distribution of gneiss groups;
- (5) cooling and uplift after a ~560 Ma thermal event has exposed high-grade gneisses with a distinct structural and metamorphic asymmetry across the orogen. The western part of the orogen shows clockwise P - T - t paths and involved overthrusting of, and imbrication with the NUT, probably obscuring older (1.9 and 1.1 Ga) tectono-thermal episodes; in contrast, the eastern part has anti-clockwise P - T - t paths, is characterised by extensive crustal melts, and retains the isotopic imprint of earlier Proterozoic events.

11.10.2 Karamoja Belt

In Kenya the EAO is ~600 km wide with large areas being covered by Neogene rift-related volcanics and sediments (Fig. 11.2). Mosley (1993) divided the belt into three N–S-directed tectonic sectors, separated from one another by major ductile shear zones. The Karamoja Belt of western Kenya and eastern Uganda is part of the Western Sector portrayed in Figure 11.2. Based on differences in geodynamic development (e.g., grade of metamorphism) and prominent lithologies we have divided the Karamoja Belt in two tectono-metamorphic sub-domains: (1) the Karasuk-Potok domain (east) and (2) West Karamoja domain (west).

Karasuk-Potok domain – Composed of a thin- or thick-skinned pile of metamorphic rocks derived from supracrustal protoliths (e.g., passive margin-type sediments, metavolcanics and ophiolites), interleaved with slices of Archaean basement rocks. Key et al. (1989) and Mosley (1993) claimed that the Mozambique Belt of western Kenya is composed of a basement of ~1200-Ma ('Kibaran' age) migmatites, overlain by juvenile Neoproterozoic metasediments. This was partly based on the erroneous idea that sediments of the Kisii Group,

overlying the Tanzania Craton, were considered to represent non-metamorphic equivalents of these 'Kibaran' migmatites (Hetzl & Strecker 1994). Subsequently, however, Pinna et al. (2000) reported a zircon evaporation Pb/Pb of 2.53 Ga for the volcano-sedimentary Kisii Group. We therefore suggest that Archaean fragments in the tectonic pile of the Karasuk-Potok domain may be derived either from the NUT or from a more distal Kenyan source. The juvenile Neoproterozoic rocks in the Karasuk-Potok domain have been assembled in the Karasuk Supergroup.

The formation of a subhorizontal gneissose foliation and recumbent folding are attributed to the progressive Samburian (~830 Ma) and Sabachian tectono-thermal events. W-vergent thrusts are documented in regions west and northwest of the Elgeyo and Nguruman Escarpments (EARS) (Sanders 1963, 1965, Vearncombe 1983a, Charsley 1987, Key et al. 1989). Mineral assemblages indicate upper amphibolite- to granulite facies *P-T*-conditions during these events.

The Baragoian and Barsaloian amphibolite-facies events were characterised by progressively tighter fold structures and transposition of the shallow dipping gneissose foliation into steep, E-dipping, N-S to NNW-SSE-trending fabrics. Key et al. (1989) and Mathu (1992) claimed that the Barsaloian event culminated in orogen-parallel strike-slip faulting along major ductile shear zones. From a reconstruction of the structural behaviour of the Aswa Shear Zone (ASZ), we conclude that oblique collision and sinistral ductile shearing were simultaneous processes (see below). Obviously, both segments of the EAO behaved differently during this oblique collision event: the more ductile behaviour of the ANS *vis-à-vis* the more rigid lithospheric plates of the Mozambique Belt caused a northward escape of the ANS, dragging along the northeastern corner of the NUT, as demonstrated by the sinistral translation along the ASZ. Brittle deformation during the Loldaikan event with pronounced sinistral strike-slip faulting outlasted ductile events. Finally, open, asymmetric, E-W-trending warps at high crustal levels are related to the Kipsingian event (530–470 Ma) (Hetzl & Strecker 1994).

The preferred orientation of biotite and hornblende indicate amphibolite-facies conditions during the main phase of deformation. Post-kinematic recrystallisation has affected the above fabric but biotite 'fish', S-C fabrics and asymmetric porphyro-

blasts of feldspar and pyroxene indicate left-lateral shearing. Steep dips and shallow to moderately plunging, generally N-S-trending stretching lineations are related to major ductile shearing parallel to the grain of the orogenic belt in a strike-slip regime (Hetzl & Strecker 1994).

West Karamoja domain – When mapping the Kaabong area in northern Karamoja, Trendall (1965a) mapped a major tectono-metamorphic boundary between a granulite-grade "charnockite-mylonite assemblage" and amphibolite-grade "acid and granitic gneisses". Pyroxene gneisses of the charnockite-mylonite assemblage were characterised by an abundance of sheared and blastomylonitic rocks and the discordance of local trends. Trendall (1965a) considered these pyroxene gneisses as part of the Archaean basement complex. He did not think, at the time, prior to the concepts of plate tectonics and modern geodynamics, in terms of allochthonous thrust masses ('nappes' or Klippes) related to collision and amalgamation of East and West Gondwana. Although he felt that zones of deformation cannot be related to what we now interpret as a basal thrust zone, Trendall (*ibid.*) nevertheless observed: "*The line dividing the two main types of Basement rocks (i.e., the charnockite-mylonite assemblage versus the acid and granitic gneisses) may represent the plane of either stratigraphic, structural or metamorphic discontinuity, or some combination of these.*" And further: "*Certainly, the absence of mylonite and the comparative rarity of shearing in acid gneisses show that, although now physically adjacent, the two groups of rock have responded differently to the forces, which have acted on them. This may be due to juxtaposition by late faulting of two structural units widely separated during the main period of metamorphism, ...*"

Traditionally, the granulites and charnockites of the West Karamoja domain were viewed as 'Watian' rocks belonging to the Archaean Basement Complex (Fig. 11.7). Schenk et al. (2004) acknowledged the Neoproterozoic age of the metamorphism and looked upon the Labwor granulites as Archaean rocks reworked during the Pan-African. Our geochronological data (Mänttari et al. 2011, Mänttari 2014) confirm the Neoproterozoic age of Leggo (1974) of the Labwor granulites and associated rocks, and our field verification suggests that the granulites/ charnockites of the West Karamoja domain constitute an alignment of Pan-African

Klippe. They comprise granulite-grade rocks of sedimentary or volcanic origin but, unlike lithologies in the Karasuk-Potok domain, quartzites, marbles, Ca-silicate rocks and ophiolites are far less abundant or absent. The rocks of the West Karamoja domain obviously originated from deeper crustal levels in the same suture zone between East and West Gondwana, and have supposedly tectonically been emplaced by W- to SW-verging tectonic transport over rocks of the Karasuk-Potok domain.

Petrology – Spinel- and sapphirine-bearing rocks from Labwor Hills were first described by Baldock et al. (1964). Nixon et al. (1973) carried out the first petrographic study, including microprobe mineral analyses, and postulated a first phase of deep burial of pelitic and siliceous sediments under granulite facies conditions with the expulsion of an anatectic partial melt fraction. This was followed by a phase of unloading and ultra-high temperatures ($T > 1050^{\circ}\text{C}$; $P < 9 \text{ kb}$; Neall 1981). In iron-rich specimens, kornierupine was reported as part of a paragenetic assemblage comprising spinel + kornierupine + sapphirine + magnetite + titaniferous hematite + sillimanite. Nixon et al. (1984) accepted Neall's (1981) interpretation that the sapphirine-bearing assemblages formed at peak metamorphic conditions, but also questioned the effects of Fe^{2+} and Fe^{3+} on lowering the temperature needed to stabilise sapphirine-quartz and spinel-quartz assemblages to as low as $800\text{--}900^{\circ}\text{C}$.

Sandiford et al. (1987) reiterated that the mineralogy of the Labwor granulites reflects unusually high temperature metamorphism ($\sim 1000^{\circ}\text{C}$) at pressures in the vicinity of 7–9 kbars and $f_{(\text{O}_2)}$ near the magnetite-hematite buffer. Later reaction textures include the replacement of spinel and cordierite by sillimanite and hypersthene and formation of sapphirine-hypersthene-K-feldspar-quartz symplectites, which were interpreted as pseudomorphs after osumilite. A petrogenetic grid appropriate to these assemblages suggested that these reaction textures were due to cooling at constant or increasing pressure and constant $f_{(\text{O}_2)}$, or decreasing $f_{(\text{O}_2)}$ at constant temperature and pressure.

Subsequent fieldwork by Loose et al. (2004) and Schenk & Loose (2011) revealed that the Labwor UHT rocks occur over a far more extensive area. Field verification by the GTK Consortium during the recently concluded Mapping Project (2009–2012) has shown that the granulites

and charnockites of Labwor Hills continue towards the NW until Kitgum Madini (Mäkitie et al. 2011b, 2014b). Loose et al. (2004) confirmed that Labwor metapelites were metamorphosed at ultra-high temperatures, leading to partial melting and to the development of numerous prograde and retrograde reaction textures such as coronas, symplectites and pseudomorphs. Consequently, these rocks are plurifacial: they contain minerals, that are not paragenetic but belong to more than one set of P - T -conditions. Spectacular coarse-grained pseudomorphs consisting of sapphirine, orthopyroxene and alkali-feldspar, in some places also of sillimanite, spinel, cordierite and quartz, are interpreted as low-temperature breakdown products of osumilite. Unfortunately, no osumilite relics have been found (Loose et al. 2004). Orthopyroxene coexisting with garnet contains up to 11.5 wt% Al_2O_3 , in coexistence with spinel even 12.2 wt% Al_2O_3 . These high Al-contents in orthopyroxene confirm metamorphic temperatures in excess of 1000°C . The GASP equilibrium (at 1000°C) points to pressures of 8–10 kbar in the UHT metapelites of Labwor Hills, in accordance with petrogenetic grids of Dasgupta et al. (1995) and Das et al. (2001). Loose et al. (2004) also studied metamorphism affecting mafic rocks from Labwor Hills, which occur as dykes in metapelitic country rocks. Garnet, clinopyroxene and quartz occur in coronas between orthopyroxene and plagioclase of the matrix, typical for near-isobaric cooling P - T paths. Fe-Mg exchange thermometers yield temperatures of $650\text{--}680^{\circ}\text{C}$ for the corona forming stage. Pressure calculations ($\text{Opx} + \text{Pl} = \text{Grt} + \text{Qtz}$; Perkins & Chipera 1985) indicate pressures of 6–7.6 kbar. Comparison of the P - T -values obtained for peak metamorphic conditions with those for the corona stage, manifest near-isobaric cooling for a wide temperature range. It can be concluded that the ultra-high temperature rocks of Labwor Hills remained for a long time interval in the deep crust before uplift.

Geodynamic setting – Pan-African granulites and associated rocks are common in East Africa, notably in Tanzania and southern Kenya, where they underlie an area of some $600\,000 \text{ km}^2$, metamorphosed at rather uniform peak conditions of $\sim 850^{\circ}\text{C}$ and 11 kbar (Appel et al. 1998; Hauzenberger et al. 2004; Sommer et al. 2008). In Tanzania, these rocks have been assembled in the Eastern and Western Granulites. The assembly of granulite

nappes in Tanzania at ~620 Ma displays westward emplacement along an eastward-deepening basal *décollement* and forward propagation of thrusts, climbing from the deep crust to the surface (Fritz et al. 2005, 2009).

The geodynamic significance of the UHT metamorphism in the Karamoja Belt and other parts of the world is not yet well understood. Lithospheric detachment or intrusion of large volumes of gabbroic melts is envisaged as a possible geodynamic causes for UHT metamorphism. Petrological and geochronological data on granulite facies terranes from various parts of the world indicate that the formation of UHT rocks is associated with major plate tectonic processes, particularly continent–continent collision and subsequent extensional collapse accompanying the assembly of major supercontinents (Kelsey 2008). Recent fluid inclusion studies have revealed the occurrence of primary CO₂-rich fluids trapped within the UHT minerals in various terrains. Such CO₂-rich fluids, probably derived from sub-lithospheric sources, have been considered to be instrumental in buffering the water activity and generating granulite facies assemblages at high- and ultrahigh-temperature conditions (e.g., Santosh & Omori 2008 and references therein). Evaluation of the tectonic settings under which UHT rocks are generated, using modern analogues, shows that divergent tectonics, both post-collisional extension and rifting, play a crucial role, particularly in addressing the extreme thermal anomalies and the involvement of CO₂ possibly liberated from a carbonated tectosphere (Santosh & Omori 2008). The collisional amalgamation of continents within a supercontinent and post-collisional extension account well for the generation of metamorphic rocks and their dry mineral assemblage buffered by CO₂ from a tectosphere.

Based on thermal history and temporal constraints, Santosh et al. (2010) proposed a general two-fold classification of orogens. Based on their thermal history, they grouped orogens into three major categories: cold, hot and ultra-hot orogens. Two different styles define the Neoproterozoic EAO between northern Egypt and southern Mozambique. The Arabian Nubian Shield in the north is classified as a small and cold orogen in which thin-skinned thrusting was associated with lateral extrusion. The Central Mozambique Belt in northern Mozambique/ Tanzania/ southern Kenya is classified as a large and hot orogen characterised by thick-skinned thrusting and

assembly of large granulite nappes – the Eastern Granulite–Cabo Delgado Nappe Complex. Fritz et al. (2009) adopted a model of hot fold nappes (Beaumont et al. 2006) to explain flow diversity in the deep crust. The lower crust represented by Eastern Granulite basement flowed coaxially outwards (westward) in response to thickened crust and elevated gravitational forces, supported by a melt-weakened, viscous channel at the crustal base. Horizontal flow with rates faster than thermal equilibration gave rise to isobaric cooling. Simultaneously, the mid-crust (Eastern Granulite cover) was shortened when hot fold nappes moved along upward-climbing thrust planes. Western Granulites preserved isothermal decompression through exhumation by thrusting and coeval erosion at the orogen front. The Eastern Granulite–Cabo Delgado Nappe Complex is now interpreted as a hot-to ultra-hot orogen that evolved from a formerly extended crust, whereby low viscosity lower crust resisted one-sided subduction and, instead, a sagduction-type orogen developed (Fritz et al. 2013).

The Pan-African Orogenic Cycle witnessed the generation of several hot and ultra-hot orogens in a broad time span during Late Neoproterozoic–Cambrian times. A recent plate tectonic perspective of the architecture of the EAO suggests a Pacific-type orogeny involving subduction and closure of the intervening ocean prior to exhumation and final Himalayan-type collisional suturing (Santosh et al. 2009), which probably accounts for the anti-clockwise *P-T-t* paths recorded from metamorphic mineral assemblages.

Summarising the above new ideas, we may go back to Sandiford et al. (1987), who argued that the *P-T-t* path observed in Labwor Hills implies that: (1) metamorphism occurred at deep levels within normal thickness crust, probably less than 40–45 km thick, due to an extreme thermal perturbation induced either by emplacement of mantle-derived magmas or by thinning of the subcontinental lithosphere in an extensional tectonic regime, (2) the excavation and surface exposure of the granulites is due to a subsequent, post-granulite facies metamorphism, crustal thickening most probably involving their incorporation into an allochthonous ‘upper crustal thrust sheet’ during the formation of the Mozambique fold belt. How far this ‘upper crustal thrust sheet’ moved to the west in northern Uganda is a matter of speculation. Tectono-metamorphic features affecting rocks in the ~1.0 Ga Madi-Igisi Belt (Chapter 9) and the <0.77 Ga Bu-

nyoro Group (Chapter 10), however, do not exclude the possibility that this 'upper crustal thrust sheet' covered most of northern Uganda at the closure of the Pan-African Orogenic Cycle in east Africa. Alternative models implying 'far field effects' are also possible.

11.10.3 Geodynamic development of the Aswa Shear Zone

Major Pan-African shear zones are either related to late Pan-African final docking of major Gondwana plates or to syn-kinematic, syn-collisional 'escape tectonics'. Burke et al. (1977) and Burke & Sengör (1986, 1989) viewed the development of African major strike-slip zones as analogues of modern 'escape tectonics' in eastern Asia where N-S collisional energy between India and Asia is partly absorbed by eastward escape of a large fragment of Indochina and the south China lithosphere. They postulated a similar model for Pan-African collision and amalgamation East and West Gondwana, with East Gondwana in the role of indenter, West Gondwana (proto-Congo Craton) in the role of 'plastic body' and the Arabian-Nubian Shield and the northeastern corner of the Congo Craton in the role of 'escaping blocks' (Figs 11.41A-C). This hypothesis eloquently explains the formation of a conjugate set of strike-slip fault zones, which in northern Uganda can be described as faults of the 'Aswa direction' (NW-SE) and faults of the 'Albertine direction' (NE-SW), both associated with conspicuous mylonite zones. It further demonstrates rejuvenation of older faults during younger, non-related tectonic 'events'. As such the normal fault that constitutes the western escarpment of the Albertine Rift is superposed on an older strike-slip fault as manifested by the occurrence of 'Mirianage' mylonites and blastomylonites (e.g., Figs 9.28 and 9.29).

Based on new data and a literature search, we conclude that the ASZ is a long-lived and complex tectonic feature. We distinguish at least three stages that we can correlate with major geodynamic events in the region: (1) oblique collision between East and West Gondwana, (2) head-on collision between the already united East + West Gondwana and the Sahara meta-Craton and (3) late Pan-African final docking of all Gondwana plates.

Oblique collision between East and West Gondwana – This event is in the ASZ expressed by the

development of blastomylonites, in places even ultra-blastomylonites (or pseudothachylites), large-scale transposition of older S-planes and extreme flattening. Rotation of feldspar porphyroclasts, micro-drag folds and micro-shears in the flank of microfolds all indicate a sinistral strike-slip movement, which can be dated at 0.69 Ga (Section 11.8). This strike-slip movement can be correlated with 'escape' of the northeastern corner of the proto-Congo Craton and the less stabilised Arabian-Nubian Shield in a northward direction due to indentation of the rigid East Gondwana Craton. This event is broadly coeval with orogenic thrusting in the Karamoja Belt.

Head-on collision between united East + West Gondwana and the Sahara meta-Craton – We assume that emplacement of Pan-African granitoids – the Midigo-Adjumani Suite (Section 11.6) – in the northernmost segment of Uganda is related to subduction and head-on collision between the proto-Congo Craton and the Sahara meta-Craton. N-S compression gave rise to E-W extension and opening of the northern segment of the NW-SE-striking ASZ, which, in turn, allowed emplacement of granodioritic magmas at around 0.66 Ga. The alternative formation of a pull-apart basin in the northern ASZ would also facilitate the emplacement of a granitic magma but fails to explain the fact that these granitoids are restricted in their occurrence to the northernmost part of Uganda. Since the genesis of many metallic mineral deposits requires the circulation of huge amounts of mineralising fluids, extension and an open 'plumbing system', we consider the northern segment of the ASZ as more prospective than the southern part.

Late Pan-African final docking of all Gondwana plates – Final docking of all plates – East, West and South Gondwana and the Sahara meta-Craton – gave rise to minor adjustments and propagation of the ASZ to the NW into South Sudan and to the SE into Kenya (and possibly Madagascar and southern India). In the ASZ the character of deformation gradually changed from ductile to brittle as manifested by microfolding of the blastomylonitic foliation (Figs 11.42A-C) in conjunction with emplacement of quartz veins in blastomylonitic rocks. In northern Mozambique, this 'final docking' phase can be related to shear in the Namama megashear, Nampula sub-Province (Macey & Armstrong 2005; Roberts et al. unpublished data,

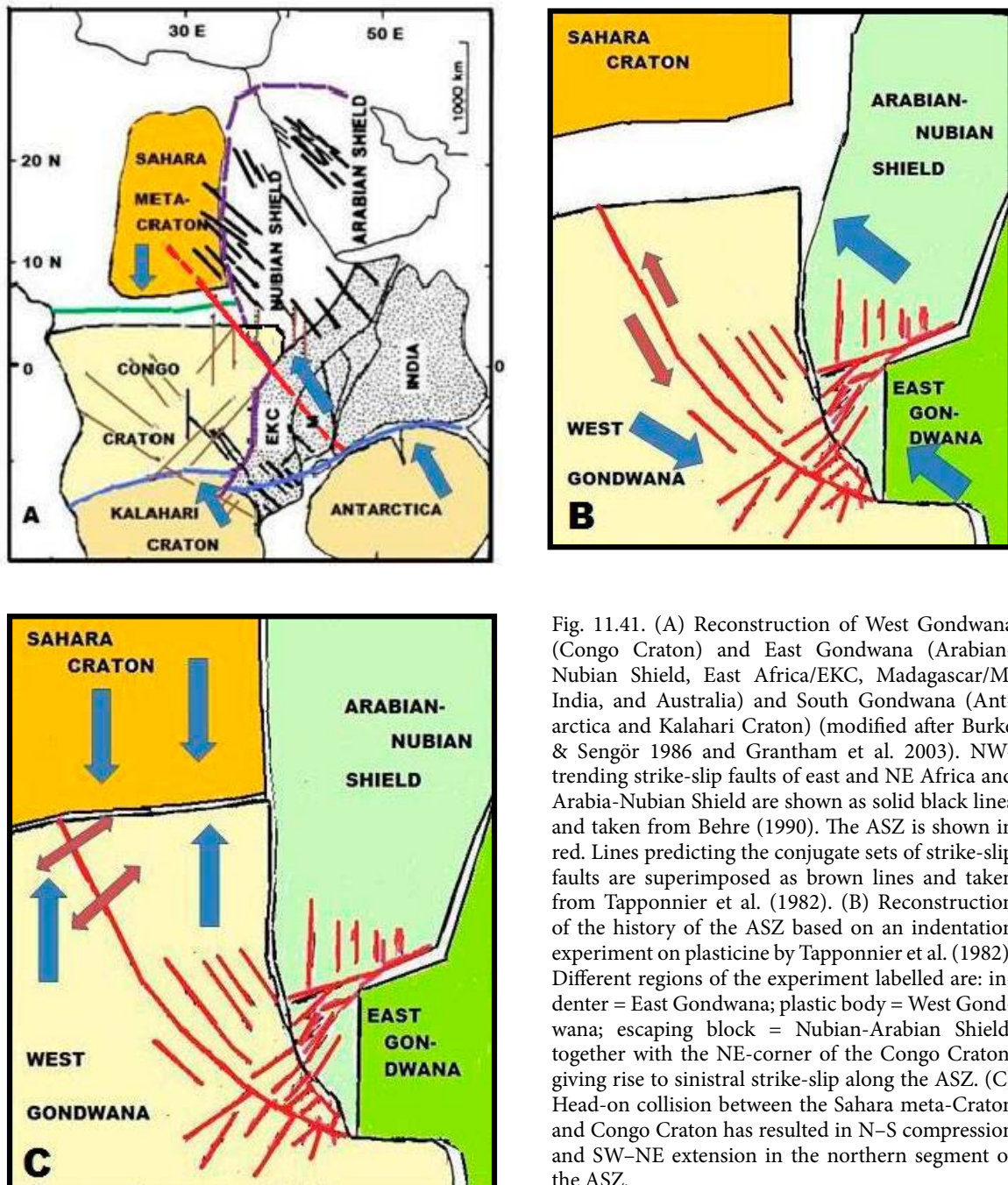


Fig. 11.41. (A) Reconstruction of West Gondwana (Congo Craton) and East Gondwana (Arabian-Nubian Shield, East Africa/EKC, Madagascar/M, India, and Australia) and South Gondwana (Antarctica and Kalahari Craton) (modified after Burke & Sengör 1986 and Grantham et al. 2003). NW-trending strike-slip faults of east and NE Africa and Arabia-Nubian Shield are shown as solid black lines and taken from Behre (1990). The ASZ is shown in red. Lines predicting the conjugate sets of strike-slip faults are superimposed as brown lines and taken from Tapponnier et al. (1982). (B) Reconstruction of the history of the ASZ based on an indentation experiment on plasticine by Tapponnier et al. (1982). Different regions of the experiment labelled are: indenter = East Gondwana; plastic body = West Gondwana; escaping block = Nubian-Arabian Shield, together with the NE-corner of the Congo Craton, giving rise to sinistral strike-slip along the ASZ. (C) Head-on collision between the Sahara meta-Craton and Congo Craton has resulted in N-S compression and SW-NE extension in the northern segment of the ASZ.

in Macey et al. 2006) and dated at 501 ± 5 Ma and 490 ± 8 Ma. This final docking event was followed by late to post-Pan-African collapse, which is reflected by post-kinematic granites dated at 492 ± 2 Ma (Grantham et al. unpublished data, in Macey et al. 2006) and pegmatites at 430–480 Ma (Cronwright & Roberts, unpublished CHIME data, in Macey et al. 2006), indicating that the Pan-African tectono-thermal episode continued well into the Phanerozoic.

Fault-derived pseudotachylite from the Tambah Fault Zone, a NW–SE trending segment of the extended ASZ within the Kenyan part of the

Mozambique Belt has been dated using the laser-probe $^{40}\text{Ar}/^{39}\text{Ar}$ dating technique, which allows a direct determination of the age of brittle faults. Previously, it was thought that this fault was formed either (i) at about 530–430 Ma, or (ii) during the Cenozoic evolution of the Kenya Rift. Based on new $^{40}\text{Ar}/^{39}\text{Ar}$ data, Sherlock & Hetzel (2001) interpret the pseudotachylite formation age to be 400 Ma. We believe that during this stage the character of the deformation within the Ugandan segment of the ASZ changed from ductile to brittle, as demonstrated by the emplacement of quartz veins.

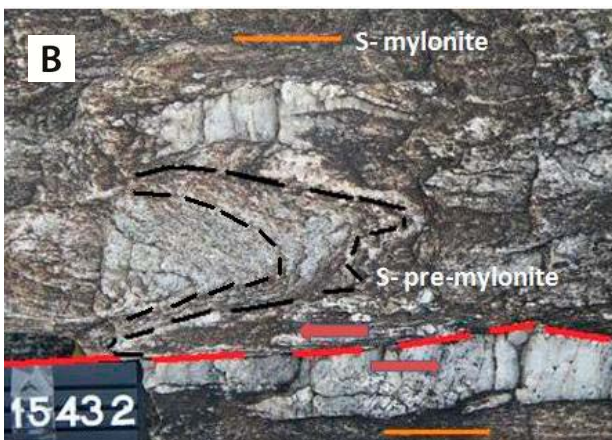
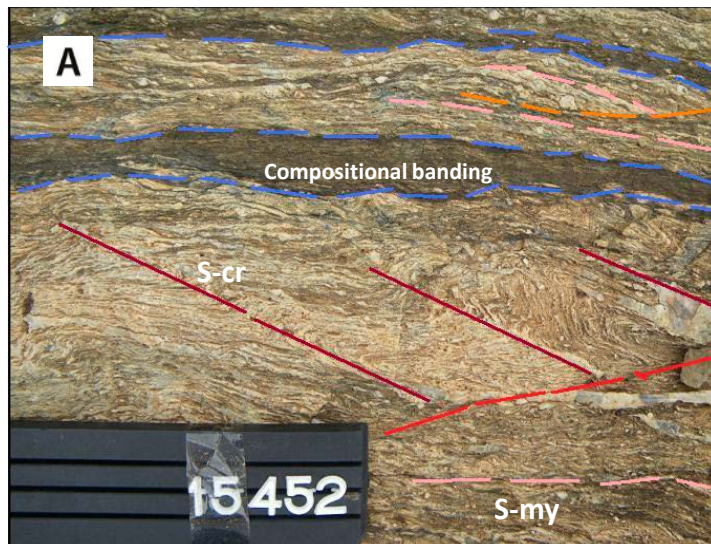


Fig. 11.42. (A) Mylonitised gneiss, in which compositional banding is still visible as an alternation of darker and lighter coloured bands. Mylonitisation and concomitant shearing has divided the rock into different domains with the mylonitic foliation in one compartment not strictly parallel to the foliation in the other compartment (see top right part of image). Below the main dark band the mylonitic foliation has been refolded with the development of a crenulations cleavage (519727E / 250284N). (B) Mylonitised migmatitic gneiss. Between the two quartz segregations the photograph shows relicts of the older gneissose foliation, which has been deformed into a Z-shaped microfold by compression and shearing. The latter is particularly evident along the upper contact of the lower quartz segregation, supposedly manifesting that this quartz segregation was emplaced along former shear plane (536661E / 232638N). (C) Folded and sheared quartz vein. Note sinistral displacement in flanks of quartz vein (509876E / 261810N).

12 POST-PAN-AFRICAN PHANEROZOIC DEPOSITS: KAROO, EAST AFRICAN RIFT SYSTEM AND QUATERNARY DEPOSITS

12.1 Introduction

The Phanerozoic evolution of the African plate can be viewed in terms of a polyphase break-up of the Gondwana Supercontinent (Guiraud & Bosworth 1999, Bumby & Guiraud 2005, Section 1.8). Phanerozoic extensional tectonism and magmatism took place mainly along lines of weakness, preferentially by reactivation of Pan-African and older suture zones. Success of Phanerozoic basin formation depended mainly on the Phanerozoic extensional stress fields relative to the direction of Proterozoic sutures. As mentioned earlier (Section 1.8), Phanerozoic basin development affecting the African Plate was related to (1) Gondwanide (~570–290 Ma), (2) Karoo (~290–180 Ma) and (3) post-Karoo (mainly Late Jurassic–Neogene) extension. The latter can be divided into Late Jurassic to Early Cretaceous break-up, followed by a phase of relative quiescence between ~100 and ~35 Ma (Section 1.8), succeeded by the Late Eocene–Neogene development of the East African

Rift System (EARS). Gondwanide and Late Jurassic to Early Cretaceous extension is not expressed in Uganda, but the first is manifested nearby by the emplacement of a number of carbonatites and associated alkaline complexes in a crustal weakness zone corresponding with the present Eastern Branch of the EARS (Fig. 1.15) with ages between ~550 and ~470 Ma. Karoo deposits are scarce in Uganda, being largely eroded during the Neogene uplift (Section 12.2). Cenozoic alkaline volcanics and associated sediments of the Elgon Complex and the Ngenge Formation can be found in the Elgon Depression of eastern Uganda, while a variety of alkaline volcanic rocks, minor carbonatite lavas and tuffs, and rift-filling sediments, attributed here to the Albertine Supergroup, cover the Albertine Rift in the west (Section 12.3). Quaternary deposits outside the EARS are shortly discussed in Section 12.4.

12.2 Palaeozoic–Mesozoic Karoo Supergroup

12.2.1 Introduction

Development of Karoo basins in sub-Saharan Africa was initiated as early as the Late Carboniferous, though rifting only began in earnest in the Middle Jurassic and culminated with the emplacement of flood basalts and pyroclastics, starting around 183 ± 1 Ma (Johnson et al. 1996).

Previously (see e.g. Schlüter et al. 1993, and references therein), Karoo rocks in Uganda have been reported from five small areas, altogether less than 70 km² in size, of which three occur along the northern shores of Lake Victoria: one on the

Entebbe peninsula, the second one at Bugiri in southeastern Uganda and the third on Dagusi Island. Two other small areas occur along the Muzizi and Katonga Rivers. We identified a sixth occurrence of Karoo rocks during field verification in the context of the recently completed IDA Mapping Project (2009–2011). This comprises a small area of glaciogene rocks, attributed to the Kiruruma River Formation, in southwestern Uganda (Westerhof et al. 2014). The subdivision of the Karoo units in Uganda is shown in Table 12.1 (see also Lehto et al. 2014).

Table 12.1. Subdivision of Karoo units in Uganda. Map codes refer to rock units in unpublished 1:250 000 -scale geological maps delivered to DGSM.

| Group | Formation | Lithology | Code |
|-----------------------------------|----------------|---|--------|
| Lower Karoo (Karoo Supergroup) | Ecca | Claystone, minor arenaceous and carbonaceous beds | PeKEmd |
| | | Siltstone | PeKEsi |
| | Kiruruma River | Diamictites and dropstones | |



Fig. 12.1. Glaciogenic deposits of the Kiruruma River Formation. Road cut ~12 km NW of Kabale town (158088 E / -129550N).

12.2.2 Lithology of Karoo Supergroup in Uganda

Diamictites and dropstones – A new occurrence of glaciogene deposits was identified in discontinuous outcrops along the Kabale-Kisoro road northwest of Kabale town, in slopes of the valley of the Kiruruma River (Fig. 12.1). It is named as *Kiruruma River Formation* and interpreted to be Karoo in age. Basal tillites and finely bedded sandstones with isolated dropstones of this Formation overlie inclined to steeply dipping and tightly folded shale-sandstone-conglomerate successions of the Mesoproterozoic Rugezi and Cyohoha Groups (Akanyaru-Ankole Supergroup) in the North Kibaran Belt. The Kiruruma River Formation is described in more detail by Westerhof et al. (2014).

Claystone, minor arenaceous and carbonaceous beds (PeKEmd) – Wayland (1931, and references therein) identified as early as 1919–1920 a number of argillaceous deposits at different locations in Uganda, which subsequently were assigned to different units of different ages. One of the claystone deposits, located on the Entebbe peninsula and assigned here to the *Ecca Formation*, contained fragments of plant remains including *Gangamopteris*, *Cyclodendron*, *Glossopteris indica* and *Cornucarpus* of Early Permian Ecca age. Bore holes were sunk in 1922 to test these deposits for water and coal. Percussion drilling in 1927–1928 reached a depth of over 300 m – the maximum depth of the rig –

and penetrated white, buff and red-brown claystones, which graded into grey to black claystones at depth with some arenaceous and calcareous beds. The last mentioned claystones, described as dark, laminated varved shales, containing frequent pyritic horizons and only traces of carbonaceous matter, were believed to be of glacio-lacustrine origin (Wayland 1931, Schlüter et al. 1993). The base of the formation was not reached. Karoo rocks on the Entebbe peninsula occur in an E-W trending, fault-bounded area, measuring approximately 1–2 x 5 km. Gravity data indicate a maximum thickness of 460 m in the eastern part of the trough, decreasing to 415 m in the western side of the peninsula (Brown 1950). The occurrences at Dagusi Island may represent proximal fluvio-glacial outwash deposits. Lithostratigraphic correlation with periglacial deposits from other East African countries suggest that the Ugandan occurrences belong to the northernmost part of the broad belt of Gondwana glaciation, extending from South Africa up to Ethiopia (Schlüter et al. 1993). The economic potential in respect to coal and other hydrocarbons appears to be low.

Siltstone (PeKEsi) – Small, flat outcrops and boulders of sub-horizontal, light grey to bluish siltstones are exposed near a bridge on the southern bank of the Muzizi River along the road from Kyenjojo to Hoima. Sub-horizontal, rather massive, fine-grained siltstones also occur along the Katonga River, in the southern part of the Palaeo-

proterozoic Mubende batholith. These yellow grey to whitish, rather massive rocks may show vague bedding. Bishop (1969) believed that these rocks had a Miocene age, but although undated, these siltstones have subsequently been attributed to the Permian Lower Karoo deposits.

12.2.3 Geodynamic development

Bradley (2010, 2012) demonstrated that the strata filling the valley of the Katonga River, 35 km east of the Western Rift boundary fault (Fig. 12.2), are indurated glaciogene deposits. Apatite fission track (AFT) analysis demonstrated that these glaciogene diamictites and laminites, occurring below pre-Pliocene (Mesozoic?) arkose and alluvial material, are of Lower Karoo (Permo-Carboniferous) age (Bradley et al. 2010; Bradley 2012).

Nyblade & Brazier (2002) argued that, following mid-Cenozoic doming of the East African Plateau

and Neogene development of the Western Branch of the EARS (Fig. 12.3), the formerly westward flowing rivers of SW Uganda, including the Katonga River¹ (Fig. 12.2), were reversed by rift flank uplift (Taylor & Howard 1998). Bradley (2012) suggested that the modern Katonga valley is exploiting a late Palaeozoic glacial valley exhumed from beneath a pre-Rift sedimentary cover. The small Katonga valley and Kiruruma River outcrops represent the NE corner of a large region of Lower Karoo-age glaciogenic sediments comparable, even identical to the once buried Palaeozoic landscape in the Albertine Rift (Fig. 12.22) and eastern Democratic Republic of Congo (Cahen & Lepersonne 1981, Tack et al. 2006b, 2008a, Delor et al. 2008). Formation of the EARS and coeval uplift in East Africa resulted in large-scale erosion of the Mesozoic and older cover with tiny areas of Karoo rocks only preserved in the deepest parts of fault-controlled basins (e.g., the Entebbe peninsula) and in some current valleys, exploit-

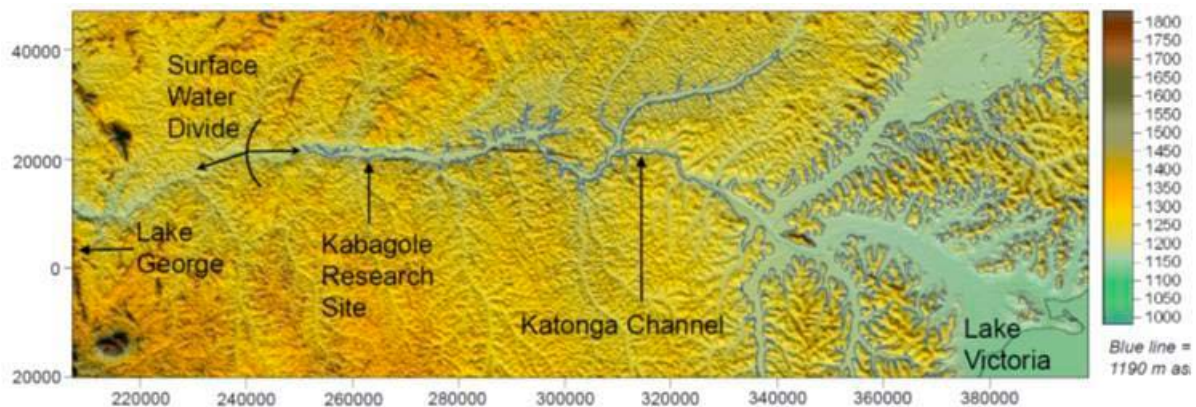


Fig. 12.2. Digital elevation model of the Katonga River and surrounding areas, prepared from Shuttle Radar Topography Mission (SRTM) data, showing the maximum historical elevation (1190 m) of static surface water based on Lake Victoria strandlines (from Bradley 2010, 2012).

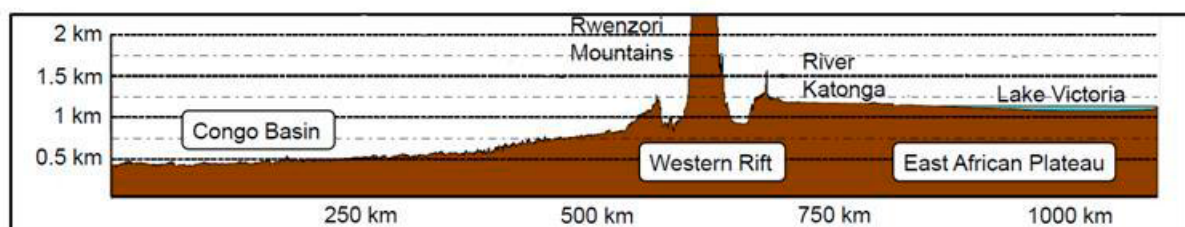


Fig. 12.3. Topographic profile from the Congo River Basin to East Africa (adapted from Bradley 2012). Formation of the EARS, including the Albertine Rift, caused reversal of the formerly westward flowing rivers (e.g., the Katonga River). Coeval uplift of East Africa caused large-scale erosion of the Mesozoic and older cover, while these rocks were preserved in the Congo River Basin.

¹ The same applied, of course, for the Kiruruma River.

ing late Palaeozoic glacial valleys. The polar path of the south pole wandering over the Gondwana Supercontinent (after Powell & Li 1994) between 360 Ma (earliest Carboniferous) and 250 Ma (uppermost Permian) according to López-Gamundi

& Buatois (2010) suggest an age of around 340 Ma for glaciogene deposits of the Congo River Basin (CRB), considerably older than the early Permian age hitherto accepted for the Karoo deposits of the Entebbe peninsula.

12.3 Cenozoic Lithologies of the East African Rift System

12.3.1 Introduction

As mentioned in Section 1.8, post-Karoo crustal extension was resumed during the Early-Middle Jurassic, when Gondwana separated and the central Atlantic Ocean began to open. Opening of the South Atlantic propagated northwards from the Late Jurassic to Early Cretaceous. It was the only time that a minor segment (the westernmost São Francisco Block) became separated from the proto-Congo Craton. This was succeeded, after a relative lull between the Middle Cretaceous till Middle Eocene, by a fourth phase of Gondwana rifting taking place between the Late Eocene and Early Miocene, which opened the Dead Sea–Red Sea–Gulf of Aden basins (Guiraud & Bellion 1995, Bumby & Guiraud 2005) and eventually formed the East African Rift System.

The East African Rift System (EARS) extends over 3000 km from the Red Sea in the north to Mozambique in the south and comprises a unique succession of rift-type basins linked and segmented by intracontinental transform, transfer and accommodation zones, which are controlled by earlier-formed weakness zones (e.g., King 1970). In East Africa the EARS splits into two branches, the Eastern or Main Rift in the east and the Western Rift to the west, with Lake Victoria as a sag basin in between. GPS and earthquake slip vector data suggest the existence of a microplate in the making between the Eastern and Western Rifts (Calais et al. 2006) with, at its core the Archaean Tanzanian Craton. We conclude that the Eastern Rift is largely superposed on the Neoproterozoic suture between East and West Gondwana. The Western Rift coincides with a Palaeoproterozoic suture between the Congo and Tanzania Cratons (both belonging to the proto-Congo Craton). The latter suture zone was rejuvenated during Mesoproterozoic extension and inversion, leading to development of the North Kibaran Belt and again during the Neoproterozoic, due to Pan-African tectonism. Rare eclogite xenoliths with pyrope-rich garnet and omphacitic clinopyroxene (Nixon & Hornung

1973) in Holocene volcanics from the Fort Portal area of the Western Rift are supposedly witnesses of Palaeoproterozoic subduction (Chapter 6). Extensional episodes are notably manifested by the emplacement of two generations of carbonatites and associated alkaline intrusives in what is now the Western Rift (Table 1.2), the first corresponding with post-Rodinia extension (~0.81 to ~0.65 Ga), the second resulting from post-Pan-African orogenic collapse (~0.55 to ~0.44 Ga).

Eastern branch of EARS – Development of the Eastern Rift gave rise to emplacement of huge amounts of volcanics, in particular in the Ethiopian dome to the north and the Kenyan dome to the south, both supposedly overlying mantle plumes (Furman et al. 2004). Mohr (1992) estimated the volume of initial flood volcanics in Ethiopia and Kenya at 400,000 and 220,000 km³, respectively. The chemical composition and the time of emplacement of the volcanics varied widely. The Ethiopian dome is characterised by tholeiitic to weakly alkaline volcanics whose deposition commenced about 49 Ma ago. Kenyan Rift volcanics are sodic and alkaline with compositions ranging from carbonatite to nephelinite, basanite, alkali basalt and transitional basalt with extensive volumes of more evolved and felsic eruptives, of which deposition started between 30 Ma and 24 Ma ago. For comparison, on the northern Tanzania Craton, the earliest extensional, rift-related activity may be linked to the emplacement of kimberlite diatremes at about 45–40 Ma (Wendlandt & Morgan 1982). Emplacement of alkali basalts near Lake Turkana (northern Kenya) and carbonatite near the Kenyan-Ugandan border was dated at ~30 Ma (Williams 1982). These mafic eruptives were followed by Miocene (14–11 Ma) flood phonolites (Lippard 1973) and 5–2 Ma volcanics of variable composition, including flood trachytes and ignimbrites. During Pleistocene-Holocene time, basaltic volcanism shifted away from the central rift to the east, ~150–250 km into the Marsabit area, to Mount Kilimanjaro and NE of Mount Kenya.

Western branch of EARS – The difference in the volume of volcanic products in the eastern and western branches of the EARS is striking. Volume estimates for the Western Rift volcanics vary widely, ranging from 2000 km³ (Barberi et al. 1982) to 100,000 km³ (Mohr 1992) and is spread over a number of isolated volcanic provinces of limited extent, representing the only volcanic centres over a distance of 1200 km. They include three older, pre-rift, Oligocene to Miocene volcanic fields, i.e., (from south to north): Rungwe, Kivu and Virunga, and younger, syn-rift Late Pliocene-Present volcanics. The latter are assembled in the Bufumbira, Katwe–Bunyaruguru and Ndale-Fort Portal volcanic fields in the southwestern part of Uganda. The Neogene sedimentary fill and overlying Late Pliocene-Pleistocene-Recent volcanic rocks in northern part of the Western Rift are assembled here in the *Albertine Supergroup*.

12.3.2 Neogene Elgon Complex (Eastern branch of EARS)

12.3.2.1 Introduction

The Tanzanian-Kenyan part of the Eastern Rift is called *Gregory Rift*, named after J.W. Gregory who published in 1896 ‘The Great Rift Valley’, containing a first account on its geology. The Miocene rocks of eastern Uganda have been deposited in the *Elgon Depression*, a second-order negative linear extensional feature some 150 km to the west of the Gregory Rift (Fig. 12.4). It is filled by a subordinate sequence of basal rift sediments, covered by a pile of predominantly pyroclastic volcanic rocks, all assembled in the *Elgon Complex*.

The alkaline rocks of the Elgon Complex have been described by Davies (1934a, 1935b, 1947, 1952, 1956), King (1949, 1964, 1965), Hytönen (1959), Trendall (1959, 1961b) and Macdonald

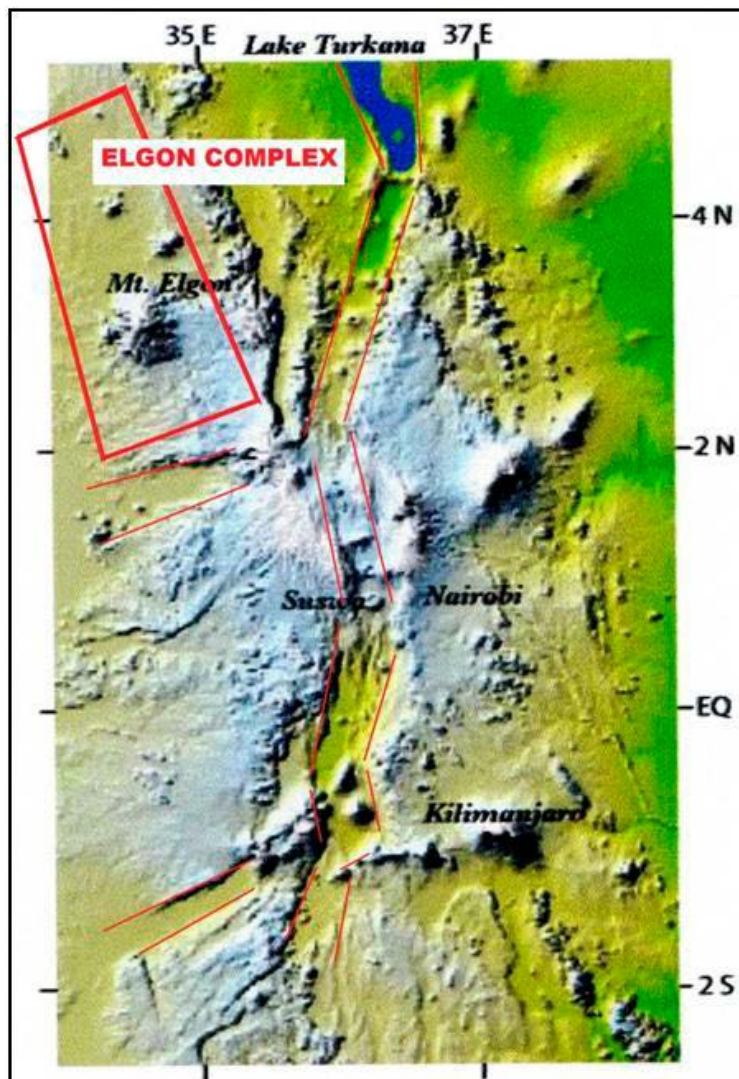


Fig. 12.4. Digital elevation map of the Kenyan-North Tanzanian part of the Eastern Gregory Rift constructed from the Shuttle Radar Topography Mission (SRTM) data. Note that the largest volcanoes – Mount Elgon, Mount Kenya and Kilimanjaro – are located outside the rift. The volcanics (and subordinate intrusive plugs, stocks and dykes) of the Elgon Complex of eastern Uganda appear confined to second-order linear extensional features, located some 100–150 km west of the Gregory Rift (from Keller 2008, with kind permission of IOP).

(1961). These authors divided the alkaline rocks of eastern Uganda into older intrusives, equivalent younger volcanics and underlying basal rift sediments. Both extrusive and intrusive rocks are extremely silica-undersaturated and very alkali-rich, in particular rich in soda. The older intrusives comprise the NNE-SSW trending alignment of carbonatite-bearing annular complexes of Sukulu, Tororo, Bukusu, Butiriku (or Sekululu) and Budeda largely to the south of Mount Elgon and similar bodies of Napak and Toror to the NNW (Fig. 12.5). Petrographically, the intrusive rocks can be classified as pyroxene-melteigites, ijolites and urtites of the ijolite series and calcium carbonatites (sövites), usually associated with nepheline syenite and syenite (including fenite and feldspathised ijolite) (Table 12.2).

The younger extrusive rocks occur in dissected volcanoes of which Mount Elgon is the biggest and once had a basal diameter of ~100 km. These volcanoes are emplaced on a Mid-Cenozoic erosion surface, extending from north to south over a distance of about 250 km (Fig. 12.5). Volcanic rocks are mainly mela-nephelinite or nephelinite and phonolite-trachyte (including some trachy-basalts) (King & Sutherland 1960a, 1960b, 1960c). The nephelinites typical consist of diopsidic pyroxene + opaque matter (mainly ilmenite-magnetite) ± melilite ± Mg-rich olivine (Table 12.2). A green aegirine-augite pyroxene is frequently encountered in the lavas. King (1965) suggested that at Sukulu, Tororo and Bukusu the intrusive bodies have emerged due to erosion of the once overlying mantle of volcanics. The large Elgon-Kadam volcanic field, on the other hand, is supposedly underlain by at least two intrusive centres. The intrusive carbonatite plugs show up in the magnetic data as conspicuous anomalies (Fig. 2.19 in Chapter 2).

A subordinate proportion of basal rift sediments underlies the volcanic rocks and is sporadically exposed in erosional windows at Mount Elgon. These sediments include volcanic mudflows of the 'Upper Bugishu Series' and a variegated succession of basal rift sediments of the 'Lower Bugishu Series' (Davies 1952), comprising conglomerates, grits, arkoses and limestones.

Originally, the intrusives were considered to have a Cretaceous age, while the equivalent volcanics were believed to have been emplaced during the Cenozoic. Subsequently, geochronological Pb isotope studies yielded an age of 40 Ma (Middle Eocene) for the intrusive carbonatites at,

Sukulu, Tororo, Bukusu and Toror (Bell & Tilton 2001). Based on mammalian fossils in tuffs and agglomerates in some of the early Napak volcanics, a Miocene age (23–5 Ma) could be established (Bishop 1958b). Subsequent K-Ar geochronology of whole rock, biotite and nepheline (Bishop et al. 1969) from tuffs and lavas of the central ijolite plug at Napak yielded poorly constrained ages ranging from 30 to 7 Ma (Oligocene-Miocene). A more recent study gave an age of ~20 Ma for basaltic lavas in the basal part of the Moroto Mountain, one of alkaline centres in the Elgon Complex (Gebo et al. 1997).

Although the alkaline rocks of the Elgon Depression and Albertine Rift are separated from each other by only 600 km and developed during the same time period, the deposits that accumulated in them are remarkably different (Pickford 2004a). Part of the difference is due to the ubiquitous volcanic activity that accompanied the geological evolution of the Elgon Depression, which was largely absent from the Albertine Rift until the Late Pleistocene. The morphology and far greater intensity of volcanic activity and reworking of volcanic material in the Elgon Depression caused the absence of deep, long-lived lakes.

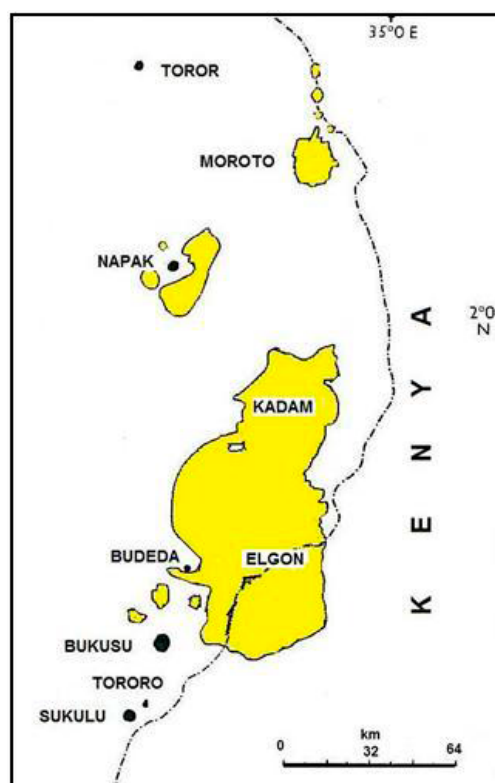


Fig. 12.5. Map showing distribution of intrusive (black) and extrusive (yellow) rocks of the Elgon Complex in eastern Uganda (adapted from Davies 1956).

Sedimentation in the Elgon Depression started in full at about 20 to 17.5 Ma ago and the succession of sedimentary deposits is far more reduced, supposedly deposited in different sub-basins and dominated by rapid lateral and vertical changes ranging from coarse volcanic mudflows (lahars and debris flows) to diatomites, intercalated with numerous lava flows and volcanic tephra, combining into a pile more than 4 km thick in places (Pickford 2004a).

12.3.2.2 Lithology of the Elgon Complex

A heterogeneous sequence of Neogene rift sediments and alkaline volcanic rocks cover the Elgon Depression in the eastern part of Uganda. The estimated age of these deposits, named provisionally here as the Elgon Complex, ranges between ~25–17 Ma (King 1978). Although lacustrine, fossil-bearing sediments have been described in some locations between crystalline basement rocks and this volcano-sedimentary sequence (e.g. Walker 1969, Bishop et al. 1969, Gebo et al. 1997), nephelinite and olivine basaltic lava flows, attributed here to the Ngenge Formation, seem to represent the initial volcanic phase of the Complex. The overlying volcano-sedimentary succession, assigned here to the Bugishu Group, includes as well fine to coarse-clastic sediments with substantial volcanic component, as lavas, agglomerates and volcanic mud or debris flows, the latter forming the prevailing

lithology of the Elgon Complex. Mt. Elgon and adjacent Mt. Kadam (Fig. 12.6) comprise by far the major volume of the alkaline volcanic deposits, but several smaller volcanic centres and associated carbonatite bodies have also been assigned here to the Elgon Complex.

Nephelinite lava, olivine basalt lava (NeEnl) – Nephelinite and olivine basaltic lava flows of the *Ngenge Formation* are locally exposed around Mt. Elgon and Mt. Kadam, the two most prominent volcanic centres of the Elgon Complex. In the absence of outcrops, the estimated areal extent of alkaline lavas is largely based on dark, chocolate-brown colour of the top soil of the Pian-Upe plains between these two mountains. Scattered and small exposures of nephelinitic lavas and pyroclastic rocks rest on Tororo granites between the Tororo and Bukusu carbonatite complexes. They represent remnants of nephelinite flows, which probably have covered large areas west of Mt. Elgon. Nephelinite and olivine basaltic lavas have also been described from the basal parts of the Napak and Moroto alkaline volcanic centres (e.g. King 1965).

In the west, a common lava type comprises dark green, porphyritic nephelinite flows with euhedral, flow-oriented nepheline phenocrysts (Fig. 12.7B), or massive, seriate-textured flows with plenty of small nepheline and pyroxene prisms in a fine-grained groundmass. Greyish green, highly vesicular, aphanitic nephelinite lava flows with



Fig. 12.6. Mt. Kadam, seen from Mt. Elgon in the south.

large gas cavities and plenty of small, zeolite and calcite-filled vesicles are rather rare (Fig. 12.7A). In the eastern and northern slopes of Mt. Elgon, only vesicular flows with small, zeolite and carbonate-filled vesicles have been observed. Based on observed, calcite and zeolite-cemented flow top breccias, the thickness of single lava flows are only a few metres. Instead, most of the exposed lava flows in the southwestern slope, show well-developed columnar jointing (Fig. 12.7C) and the thickness of flows may exceed some tens of metres (Davies 1952). Plenty of small lava fragments, as well as angular basement gneiss fragments, up to >50 cm in size, are embedded in a pale brownish grey, porphyritic olivine-nephelinite lava flow on the northern foot of Mt. Kadam.

In thin section, massive, generally porphyritic alkaline lavas of the Ngenge Formation are composed of euhedral nepheline, olivine, clinopyroxene, leucite and melilite phenocrysts in various

proportions, set in a fine-grained, holocrystalline groundmass. In some samples, large idiomorphic nepheline phenocrysts are partly altered into cancrinite, but euhedral to subhedral olivine phenocrysts, up to 10 mm in size, are mostly fresh. The most common clinopyroxene is diopside, but deep green, strongly pleochroic aegirine-augite, together with nepheline, are the major minerals in a lava sample taken from the northern foot of Mt. Kadam. The holocrystalline groundmass of alkaline lavas is generally massive, without flow banding. Only in one sample, taken from a vesicular lava flow on the northern foot of Mt. Elgon, a trachytic texture with well-oriented laths of microcrystalline alkali feldspar (sanidine?) is visible. Small, euhedral magnetite crystals are common as accessory minerals, resulting in a high susceptibility for these lavas. A thorough petrographic description of alkaline lavas of Mt. Elgon was given by Davies (1952).

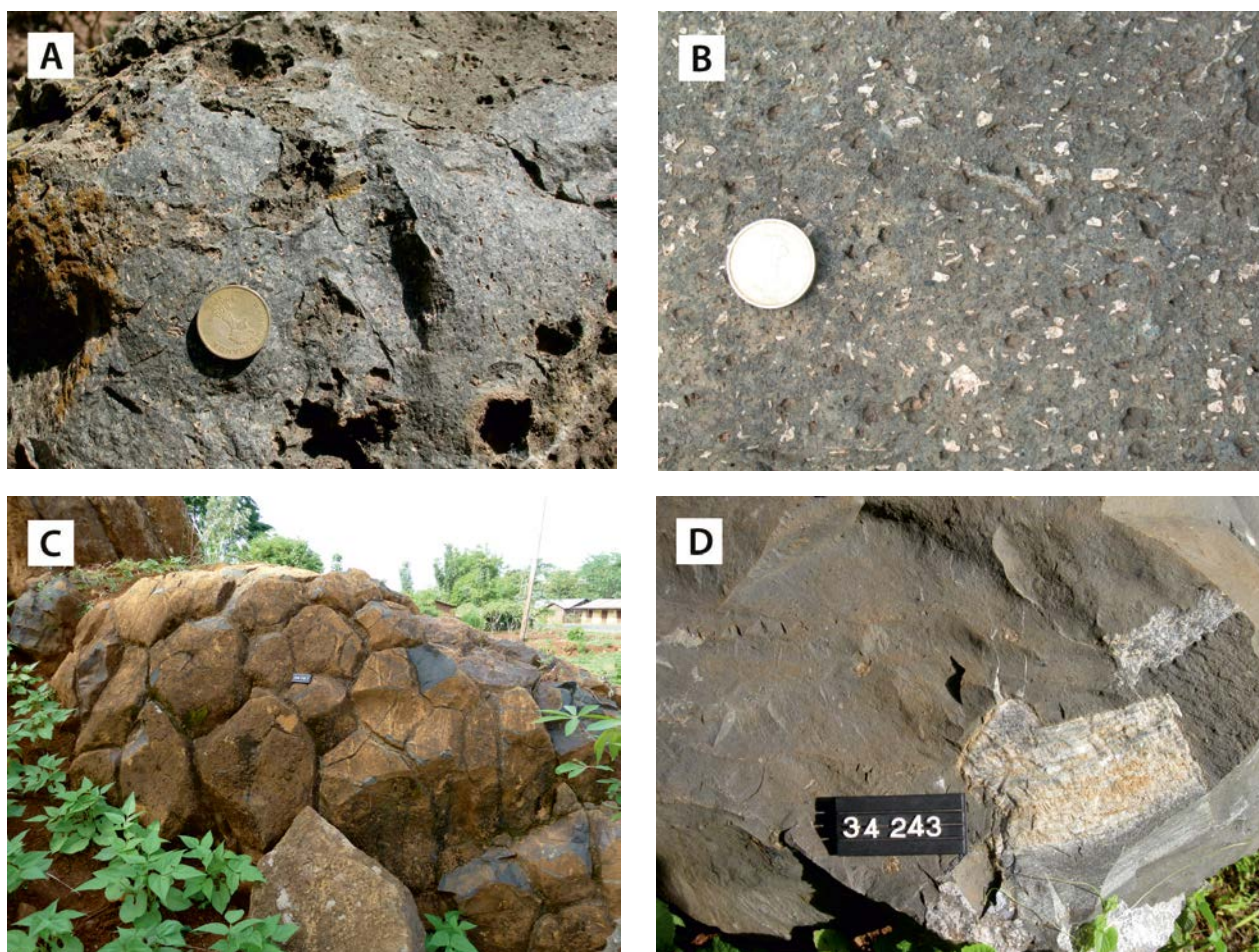


Fig. 12.7. Various structures in nephelinite and olivine basaltic lava flows. (A) Aphanitic nephelinite lava with plenty of gas cavities and small, zeolite-filled vesicles (635438E / 85055N). (B) Porphyritic nephelinite lava (644716E / 89572N). (C) Polygonal jointing in olivine basaltic lava (641807E / 140937N). (D) Angular gneiss fragments in olivine basaltic lava of a volcanic neck west of Sipi Falls (652316E / 147556N). Number tag 8 cm, coin diameter ~2 cm.

We present 9 new chemical whole-rock analyses of various nephelinite and olivine basalt lavas of the Elgon Complex (see App. 2, anal. 192–200). Many of these rocks can be classified as tephrites or basanites in terms of the TAS diagram of Le Bas et al. (1986). Some samples have so low SiO₂ concentration (<41 wt%) that they, in fact, are foidites. As expected, the rocks have locally elevated contents of alkalis; the Na₂O and K₂O concentrations are between 9 and 12 wt%, in total.

On the northeastern slope of Mt. Elgon, several volcanic necks probably represent the feeders for these lava flows. In a similar, columnar-jointed lava plug west of the Sipi Falls on the western flank of Mt. Elgon, angular basement gneiss fragments, up to 15–20 cm in size, are embedded in olivine basaltic lava (Fig. 12.7D).

Although the actual contact between the base of lava flows and underlying lithologies is not exposed, their stratigraphic position directly on top of Archaean basement granites and gneisses has been established in many outcrops along the northern and eastern foot of Mt. Kadam and Mt. Elgon, respectively. However, at the well-documented site for fossil plant remains and mammal bones, located ~3.5 km east of Bukwa town, Brock & Macdonald (1969) described lacustrine sediments, which are overlaid by a ~22 Ma old lava flow now assigned to the Ngenge Formation (see Bishop et al. 1969). Similarly, a layer of fossiliferous sediments between the basement gneiss and a basaltic lava flow has been described at the Napak and Moroto Mountains by several authors (see e.g. MacLachy & Pilbeam 1999, Pickford et al. 1986, 2009, Pickford 2002a, 2002b, 2004b).

Bugishu Group

The basal sediments of the Elgon Complex have been traditionally attributed to the ‘Bugishu Series’. The term ‘Lower Bugishu Series’ was originally given to a thick succession of conglomerates, grits, sandstones, arkoses and limestones, which are covered by mudflows of the ‘Upper Bugishu

Series’, mainly pyroclastic material (agglomerates and tuffs) forming the greatest proportion of the mountain (Davies 1952). The Bugishu Series, here renamed Bugishu Group, comprises of sandstones, arkoses and conglomerates of the *Busoba* and *Nambola Formations*, and volcanic mudflows, agglomerates and various alkaline lavas of the *Moroto* and *Wagagai Formations*, the latter forming by far the major volcanic component of the Elgon Complex. Subdivision of the Bugishu Group is given in Table 12.2.

Sandstone, arkose, conglomerate (NeEss) – A succession of clastic sediments, assigned to the *Busoba Formation* is locally exposed around the prominent Wanale hill, located east of Mbale town. The pinkish to yellowish brown, arkosic sandstone contains angular feldspathic clasts and shows subhorizontal, laminar bedding, manifesting rapid erosion and a proximal source area. Sandstone with conglomerate horizons between volcanic mud flows of the *Wagagai Formation* and alkaline lavas of the *Ngenge Formation* below, here also tentatively attributed to the *Busoba Formation*, is exposed in the Sironko River valley, NE of the Wanale hill.

Polymict conglomerate, grit and sandstone (NeEcg) – Polymict conglomerates, grits and sandstones of the *Nambola Formation* are locally exposed on the southern, western and northeastern slopes of Mt. Elgon, below the alkaline volcanic debris flows of the *Wagagai Formation*. The thickness, lithology, and stratigraphic position of this heterogeneous sedimentary succession varies from place to place along the mountain slope, manifesting rapid facies changes. A type section of this sedimentary portion of the Bugishu Group is described by Davies (1952, Fig. 2).

An excellent cross section, showing a variety of clastic sediments belonging to the *Nambola Formation*, is exposed in a long road cut along the Sironko-Kapchorwa road, two kilometers from the Moroto road crossing. The minimum thickness of

Table 12.2. Subdivision of the Bugishu Group. Map codes refer to rock units in unpublished 1:250 000 -scale geological maps delivered to DGSM.

| Group | Formation | Lithology | Code |
|------------------------|-----------|---|--------|
| ‘Upper Bugishu Series’ | Wagagai | Volcanic mudflow (lahar), agglomerate, lava | NeEag |
| | Moroto | Lava and agglomerate | NeElva |
| ‘Lower Bugishu Series’ | Nambola | Conglomerate, grit | NeEcg |
| | Busoba | Sandstone, arkose, conglomerate | NeEss |

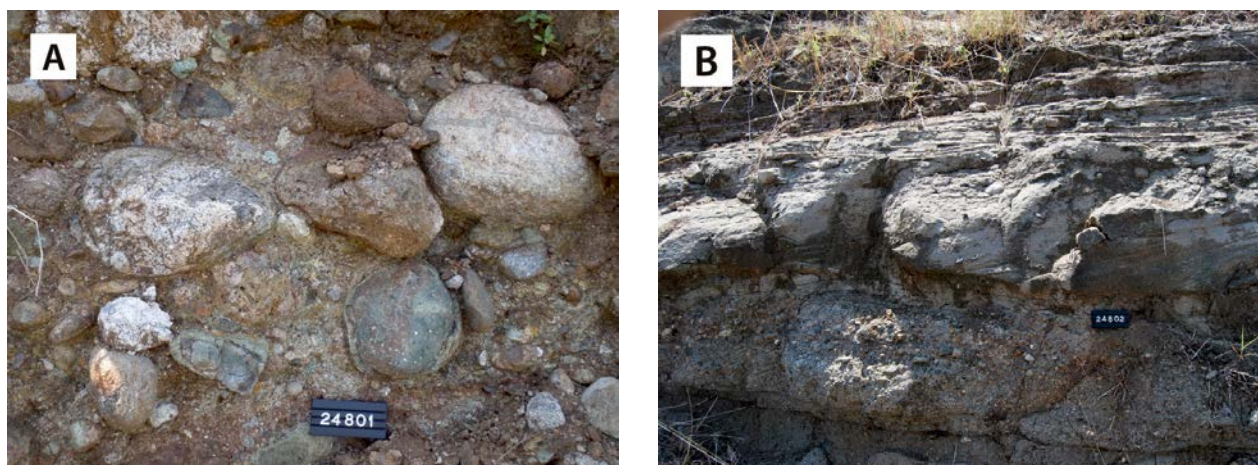


Fig. 12.8. Sedimentary structures of the Nambola Formation. (A) Polymict conglomerate with clasts of granite, gneiss, conglomerate, sandstone and a variety of volcanic rocks (646199E / 147208N). (B) Cross-bedding in channel-fill sandstone (646363E / 147457N). Number tag 10 cm.

this fining-upwards, subhorizontal sequence is some tens of metres. The basal part of the section comprises an over 10 m thick horizon of polymict, matrix-supported conglomerate (Fig. 12.8A), with densely packed clasts, mostly composed of well-rounded pebbles and cobbles of subvolcanic and volcanic rocks, as well various granite, gneiss, conglomerate and sandstone cobbles and boulders up to 80 cm in diameter. A weak imbrication of the pebble and cobble-sized clasts is locally visible. The pale greenish, fine- to medium-grained matrix of the conglomerate is a mixture of sandy and volcanic material.

The polymict conglomerate is overlain by a several metres thick layer of brownish, carbonate-bearing sandstone, with laminar bedding and tabular cross-bedding. Thin grit and conglomerate wedges are common (Fig. 12.8B). Upwards in the section, sandstone grades into gritty sandstone and grit, which, in turn, is covered by an >10 m thick, upward coarsening conglomerate with sub-rounded clasts, ranging from small pebbles upwards to boulders of over 80 cm in size. Clasts of this nearly monomict conglomerate with an unsorted sandstone-mudstone matrix, are mostly sub-volcanic or volcanic in origin. A 20–30 cm thick, brownish grey mudstone interbed with a thin layer of very fine-grained marl occurs in the upper part of this conglomerate. The upper part of the sequence comprises a brownish grey, unsorted mass of carbonate-bearing, mudstone-like material with random, subrounded nephelinite clasts of various sizes. This unit resembles carbonatite-derived calcarenites and calcirudites described by Bloomfield (1972) from

the northern slope of the Nkokonjeru, a prominent hill east of Mbale town. The weak imbrication of conglomerate clasts, as well as conglomerate wedges and tabular cross-bedding in sandstone refer to a channel fill origin for this sequence.

Lava and agglomerate (NeElva) – An extinct, deeply eroded volcanic vent is exposed northwest of the Kokipie Hill, located near the Kenyan border, north of Mt. Elgon. The vent, originally ~600 m by 1000 m in size, and described as explosion breccia with fragments of basement gneiss, comprises agglomerates, banded tuffs and a range of brecciated alkaline intrusive rocks (Searle 1952).

Dark, massive nephelinite lava with columnar jointing is exposed on a hill about 4 km NW of the Kokipie Hill. The gently southwest dipping lava flow, which overlies the sedimentary rocks, comprises nepheline and augite phenocrysts in approximately equal proportions (Trendall 1962). The Kokipie Hill itself, which measures less than 200 m in diameter, comprises agglomerate beds of large blocks, up to 5 m in size, which are mostly similar in composition as those in the vent. This gently southeast tilting agglomerate rests on a >100 m thick, well-bedded sequence of conglomerates, grids and marls (Trendall 1962). The large size of the blocks found in ‘agglomerate’, as well as its stratigraphic position over a horizontal sedimentary sequence suggests a volcanic debris flow (lahar) origin, similar to those of Mt. Elgon. All aforementioned volcanic deposits are assigned here to the Moroto Formation.

Volcanic mudflow (lahar), agglomerate, lava (NeEag) – Various types of pyroclastic rocks, which are attributed here to the Wagagai Formation after the highest peak of Mt. Elgon (4321 m.a.s.l.), form the main constituent of the Neogene alkaline volcanic centres in eastern Uganda. Although Davies (1952) described a pile of lahar-like mudflows at the basal part of Mt. Elgon, most of the pyroclastic rocks forming these variously eroded and dissected mountains are described as agglomerates and tuffs (e.g., King 1949, Davies 1952, Trendall 1961a, Varne 1968). According to Davies, the maximum thickness of the mudflows, which he attributed to the ‘Bugishu Series’, is 200 m (Davies 1952, p. 16, Davies 1956).

Field observations made in different parts of Mt. Elgon indicate that the role of cold, lahar-like volcanic mudflows (or debris avalanche) appears to be significant in the formation of these alkaline stratovolcanoes. It is suggested that the processes that trigger volcanic mud/debris flows may be heavy rainfall, rapid melting of snow or ice cap during volcanic eruption or overflow of a crater lake which, individually or in combination, cause erosion and moving of unstable volcanic material under gravity along the higher segments of the slope, and subsequent deposition of volcanic debris at the foot of the volcano (see Pierson 1989).

A gentle slope angle is a common feature for most of the alkaline volcanoes of eastern Uganda. At Mt. Elgon, where the angle is 4° in average, this is readily visible in nearly horizontal terraces of the western mountain slope. Similar observations have been made repeatedly along the Sironko–Kapchorwa road, where the thickness of sub-horizontal terraces, interpreted as representing (cold) volcanic debris flows, range from a few metres up to 20–30 metres. These flows, tentatively called here (lahar-like) volcanic mudflows, differ from volcanic agglomerates *sensu stricto* by comprising angular to weakly rounded blocks of solid lava, embedded in a matrix composed of an extremely poorly sorted mixture of consolidated pyroclastic and volcanoclastic material, manifesting reworking and redeposition. The type section of the Wagagai Formation is visible in a long road cut about 1.5 km northwest of Kapchorwa town, where several superposed volcanic debris flows are well exposed (Fig. 12.9A). The volcanic flows are composed of angular to weakly rounded, generally porphyritic nephelinite lava fragments, up to >100 cm in diameter, in an unsorted, tuffaceous matrix (Fig. 12.9B). The colour of different flows varies from brownish grey to greenish grey, indicating compositional variation in matrix material. The contacts between different flows are sharp, but a brownish,

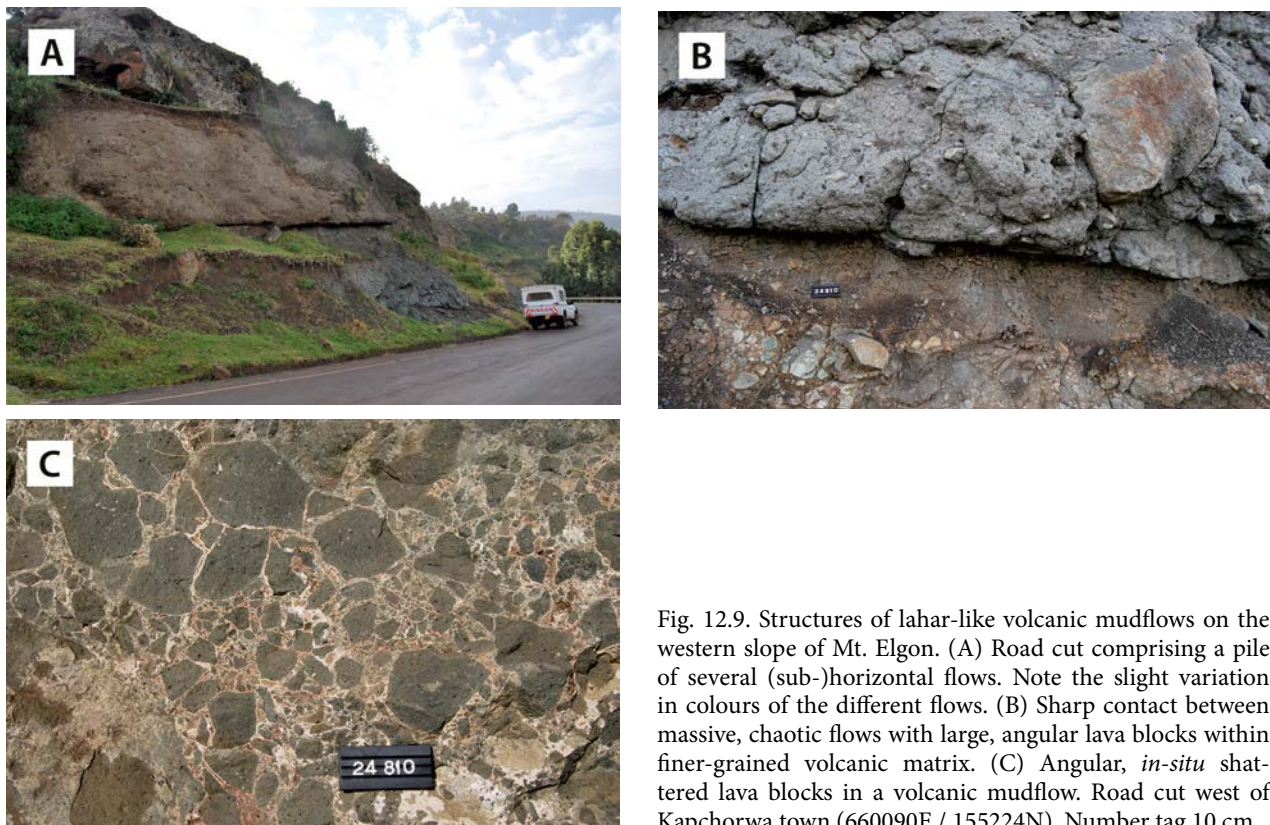


Fig. 12.9. Structures of lahar-like volcanic mudflows on the western slope of Mt. Elgon. (A) Road cut comprising a pile of several (sub-)horizontal flows. Note the slight variation in colours of the different flows. (B) Sharp contact between massive, chaotic flows with large, angular lava blocks within finer-grained volcanic matrix. (C) Angular, *in-situ* shattered lava blocks in a volcanic mudflow. Road cut west of Kapchorwa town (660090E / 155224N). Number tag 10 cm.

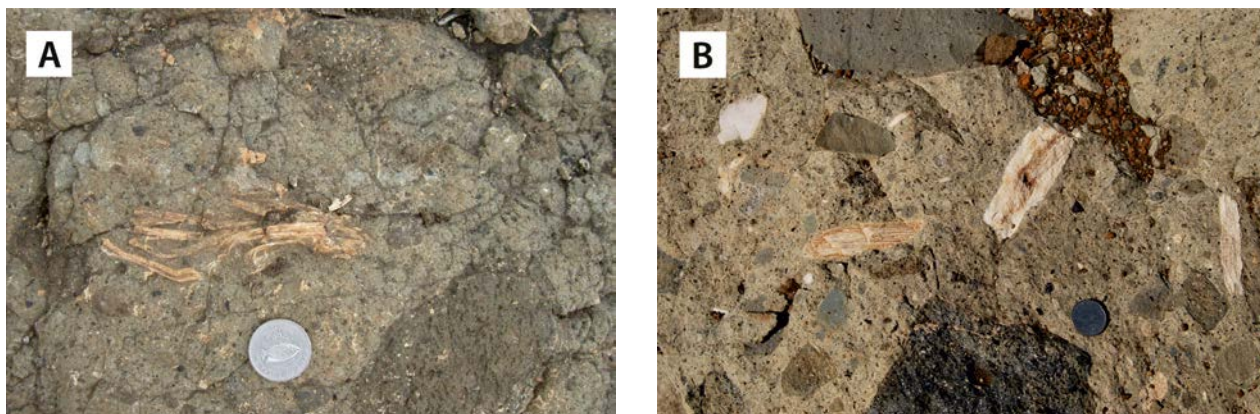


Fig. 12.10. Specimen of fossil plant remains and bone (?) fragments found embedded in volcanic mudflows on the slope of Mt. Elgon. (A) Well-preserved fossil plant fragment in road cut ~7 km NW of Bokwa town (690250E / 148661N). (B) Various bone (?) fragments found in a road cut 1.5 km NW of Kapchorwa town (660090E / 155224N). Coin diameter ~2 cm.

weathered (?) zone, generally less than 0.5 m thick, and comprising mostly smaller (<10 cm) lava fragments, often occurs in the upper part of individual flows. This feature is probably caused by gravity-assisted grading of volcanic debris flow material. In one flow contact, an about one metre thick layer of grey, fine-grained, mudstone-like material may represent an ash-fall deposit. Although many features observed at Mt. Elgon, including flow-rafted megablocks shown in Figure 12.9B, common in lahar-like volcanic mudflows, in-situ shattered lava blocks (Fig. 12.8C) are more typical for debris avalanche deposits (see e.g., Coussot & Meunier 1996). Narrow, vaguely bedded lapilli and crystal tuff horizons, as well as true agglomeratic layers, with roundish nephelinite lava bombs having chilled margins, have been observed in random locations within massive volcanic mudflow units.

Since the first discovery in the 1930s of fossil wood at Mt. Elgon by Bancroft (Bancroft 1932, 1935a, b), more fossil plant remains and mammal bone findings have been reported near Bukwa town (Chaney 1933a,b, Hamilton 1968, Bishop et al. 1969, Brock & Macdonald 1969, Macdonald & Old 1969, Pickford 2002a). Fossil plants and mammalian bones are also common at Napak and Moroto Mountains (Gebo et al. 1997), including a recent discovery of ~20 Ma old hominid skull near Iriri village (e.g. Pickford 2004b, Pickford et al. 2009). During the present field verification, plenty of fossil fragments have been discovered, all invariably embedded in volcanic mudflows of the Wagagai Formation, in different parts of Mt. Elgon. Most of the fragments found on the western flank of the mountain are probably fossil wood and plant remains (Fig. 12.10A), but some specimen

may also represent fossil bones (Fig. 12.10B). In places, these fragments are clearly oriented, probably parallel to the original flow direction. The occurrence of well-preserved fossil plant remains confirm that the volcanic material of these flows was cold enough to preserve the plant fragments.

Plenty of similar fossil wood and plant fragments, embedded in volcanic mudflow deposits, were also found near Ngenge village, at the northern foot of Mt. Elgon, and in similar volcanic deposits which mostly form the prominent Alekileki Cliff (Fig. 12.14), the southwestern extension of the Akisim Hill, located northwest of the Napak Mountain.

Smaller alkaline ring complexes and carbonatite centres

Sukulu – Sukulu forms a circular group of hills, up to 1417 m in altitude and 4 km in diameter, composed almost entirely of sövite carbonatite (Fig. 12.11). Dolomite and siderite occur in places, and flow banding shows a complex pattern of concentric structures, suggesting several intrusive centres. Apart from calcite, magnetite, apatite, mica (phlogopite), tremolite, zircon, pyrochlore, baddeleyite and barite have been encountered. The carbonatite plug is surrounded by a narrow rim of syenite and an aureole of fenitised country rock with sodium metasomatism and the development of sodium pyroxene (aegirine-acmite; a rare sodium-ferric iron silicate), sodium amphiboles, chlorite and distinctive reddish-coloured biotite (Davies 1956).

The Sukulu carbonatite plug has been extensively but selectively mined for sövitic limestone, raw material for cement production and for road material.

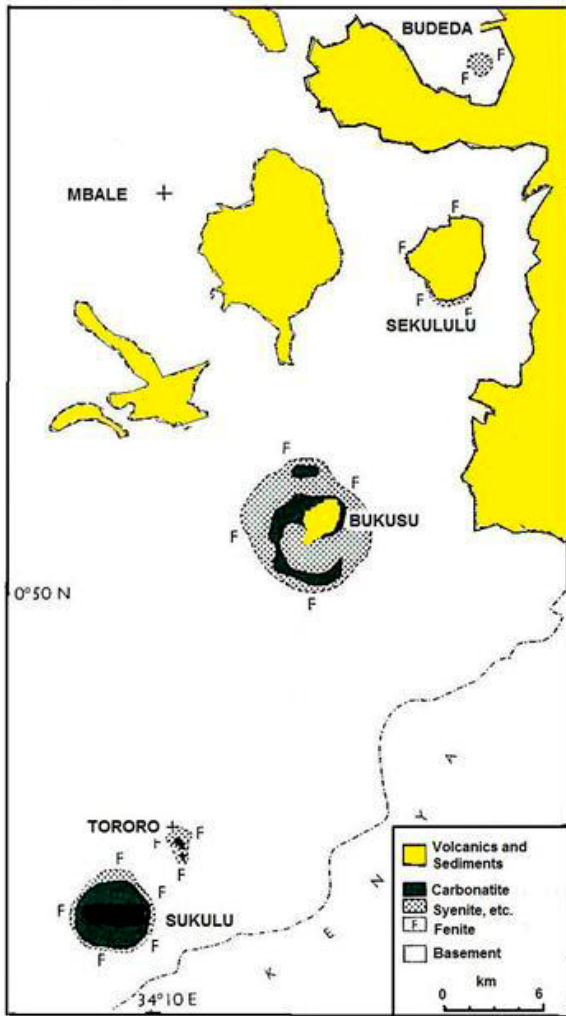


Fig. 12.11. The intrusive alkaline ring complexes of the southern part of the Elgon Complex (adapted from Davies 1956).



Fig. 12.12. Entrance to Sukulu old quarry with weathered surface of carbonatite, overlain by chocolate-brown top soil.

In one of the quarries in a peripheral part of the bigger Sukulu carbonatite body the low ground is occupied by carbonatite, the high ground by fenitised country rocks and associated alkaline intrusive rocks. At the entrance of the quarry, the weathered surface of the carbonatite, covered by chocolate-brown soil is still in place (Fig. 12.12). Sub-vertical magmatic flow banding is parallel to the contact with country rocks and is marked by variations in the content of phlogopite. Though generally a subordinate mineral phase, phlogopite predominates over calcite in places (Fig. 12.13B), producing micacite in the fenitic wall rock.



Fig. 12.13. (A) Pebble dyke with ground mass of pepperite and 'pebbles' of micacite (derived from the fenitic contact zone), carbonatite and vein quartz. (B) Detailed image with lava in between pepperite badges. (C) Detail of pebble dyke. Badges of fragment-rich material have been glued together by magma badges. Pebble badges contain rounded to angular vein quartz fragments (QZ), micacite fragments (Mica) and predominant grey-greenish, generally rounded effusive fragments, the latter showing a narrow reaction rim and in turn composed of smaller fragments. Old Sukulu quarry (628321E / 72437N). Pen ~15 cm.

The Sukulu carbonatite body is intersected by faults and dykes, many of which show a radial arrangement. In places, the carbonatite body is intersected by narrow mafic dykes, 30–40 cm in width. Elsewhere, a spectacular pebble dyke (Figs 12.13A-B) has been observed, composed of rounded to angular fragments (“pebbles”) composed of micacite, carbonatite and vein quartz in a pepperitic ground mass. The ‘pebble dyke’ apparently formed by multiple injections and from different magma badges, resulting in sharp boundaries between successive badges, glued together by narrow seams of lava with flow structures (Fig. 12.12C).

The Sukulu, Tororo and Bukusu ring complexes are each composed of a carbonatite core and a 2–3 km wide Na-K-metasomatic aureole. These alkaline complexes have marked characteristics of their own, all three complexes being characterised by steep hills due to the weathering resistance of the fenitised country rock.

Sekululu – At Butiriku (Sekululu), fenitised granitoids are exposed below an outlier of Mt. Elgon lavas (Fig. 12.11). Based on the drillings carried out by DGSM, a proved reserve of ~16 Mt sövitic limestone, associated with a possible carbonatite plug, was also found to occur here.

Budeda – This is the smallest of the ring complexes, measuring less than 1 km in diameter (Fig. 12.11). The central part of the annular complex is formed by an arcuate mass ranging in composition from pyroxenite or melteigite to ijolite and urtite, enclosing two very small carbonatite plugs. This composite body is surrounded by a wide aureole of fenite of syenitic composition, formed by alkali metasomatism of granitic ‘basement’ rock. Cancrinite-bearing fenite occurs in places. A small number of dykes consists of variegated cancrinite phonolite, cancrinite syenite and nepheline syenite.

Napak – The Napak mountain is unique among the eastern Ugandan alkaline ring-shaped complexes in being composed of both intrusive rocks and remnants of the volcanic cone (King 1949, Trendall 1965a, 1965b, Simonetti et al. 1996) (Figs. 12.5 and 12.14). A central carbonatite-ijolite plug is flanked by deeply dissected agglomerates, tuffs and silica-undersaturated flows that overlie Archaean basement gneiss and Neoproterozoic Pan-African granulite (Fig. 11.5).

The central ring structure, measuring approximately 2 km in diameter, is composed of ijolite and a small central boss of carbonatite, surrounded by a zone of fenitised ‘basement’ gneiss (Fig. 12.14).

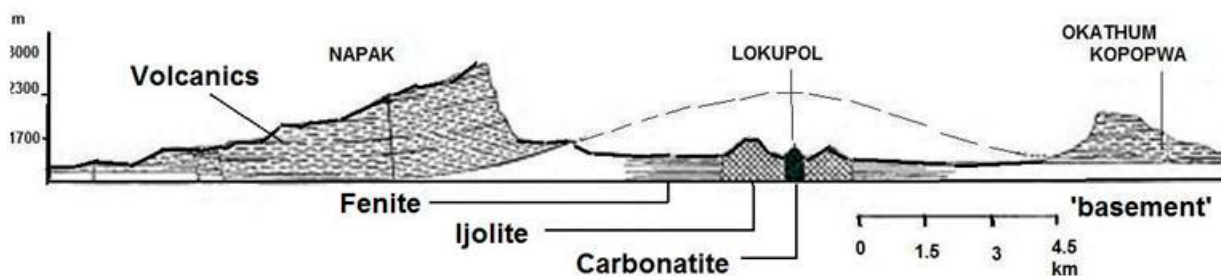


Fig. 12.14. Above: Geological section across the Napak volcanic cone and central ring structure (after King 1949; with modifications). Below: Akisim Ridge and the prominent Alekileki Cliff, which form the western part of the Napak Mountain.

The ijolite rock is texturally, structurally and compositionally complex due to emplacement in at least two consecutive batches of magma. Depending on the relative proportions of the two principal rock-forming minerals, pyroxene and nepheline, the earlier batch comprised of melanocratic and mesocratic ijolite and urtite with the younger phase being composed of coarse-grained urtite in dyke-like masses.

After Simonetti & Bell (1993), almost all (97 vol%) Napak volcanics are agglomerates and subordinate quantities of tuffs with only a minute proportion (3 vol%) being composed of silica-undersaturated lava flows. The basal lava layer, ranging in thickness between 30 and 100 m, is separated from the pre-volcanic crystalline basement surface by a narrow layer of sediments. When fresh, this mugearite (King & Sutherland 1960b) lava is a dark grey, homogeneous, fine-grained rock with andesine phenocrysts up to 5 mm in size and small, scattered, nearly spherical amygdales, filled with limonite, silica or chlorite, in particular near the top and bottom of the flows. The matrix consists principally of closely packed, fine (0.1–0.2, occasionally 0.5 mm) andesine laths with the interstices filled by granular pyroxene and opaque minerals (King 1949, Trendall 1965b).

The agglomerates are composed of fragments of lava, 'basement' gneiss, fenite and ijolite derived from the central stock. The lava fragments are mainly nephelinites and mela-nephelinites, essentially composed of nepheline and pale diopside clinopyroxene with, in places, olivine and/or melilite, opaque matter and accessory perovskite and apatite.

The field verification conducted at the foot of the prominent Alekileki Cliff, the southwestern extension of the Napak Mountain, revealed volcanic debris flow structures identical to those described here from Mt. Elgon. Well-preserved plant fossils within these deposits show that also volcanic mudflows have been an important factor in the formation of the Napak Mountain.

Napak is one of the sites in tropical Africa that is richest in great-ape fossils (Pickford et al. 1986). Fossiliferous sediments occur at various levels amongst the volcanic rocks. They belong to two stratigraphic assemblages: the basal Iri Member contains fluvial sediments deposited before and during the first phase of eruption, on top of which is the intra-volcanic 'Napak Member'. The difference in the faunae and

sediments of the two units reveals variations in the volcano's formation and the associated depositional environments. The 'Iri Member' has been dated at 20–19 Ma, while the 'Napak Member' was deposited during an extensive period of time, from ~20 Ma to ~17.5 Ma ago (Senut et al. 2000, Gommery et al. 2002, Pickford 2002b, 2004b).

Moroto – This annular complex (Fig. 12.5) comprises phonolite, trachyte and trachy-basalt (Hytönen 1959, Macdonald 1961), but lavas are more voluminous with respect to agglomerates and tuffs than in the Elgon-Kadam volcanic field. The lavas belong to two differentiated series of alkaline silica-undersaturated rocks, i.e., a nepheline series, common to all volcanoes of the Elgon Complex, and an alkaline olivine basalt series. Varne (1968) suggested that both series formed from partial melting of hydrated peridotite: the nephelinites from hornblende upper mantle rocks and the alkaline olivine basalt from less volatile-rich portions. These two series typify the two major associations of the EARS alkaline volcanism. Varne (1968) explained their close spatial and temporal association by assuming that Moroto lies above a transition zone in the upper mantle between a relatively anhydrous, volatile-poor portion and a hydrated, volatile-rich portion with hornblendites. Based on mammalian fossils in sedimentary intercalations, the Moroto volcanics have been dated at ~17.5 Ma (Pickford et al. 2002).

Tororo – The northernmost intrusive of the Elgon Complex consists of a carbonatite plug, measuring > 3 km in diameter, surrounded by a zone of brecciated and fenitised 'basement' granitic gneiss and a mass of phonolitic agglomerate (DuBois 1959). Late trachytic dykes, often in radial arrangement, or in plugs and sheets, cut the carbonatite and fenitised country rock. The fenite aureole is rather modest in size and expressed by the development of biotite, sodium amphibole and aegirine along cracks and fissures.

12.3.3 Albertine Supergroup (Western branch of EARS)

The Western Rift of the East African Rift System stretches from the border between Uganda and South Sudan in the north to the southern end of Lake Tanganyika, a distance of over 1200 km with a variable width averaging 45 km. The northern part

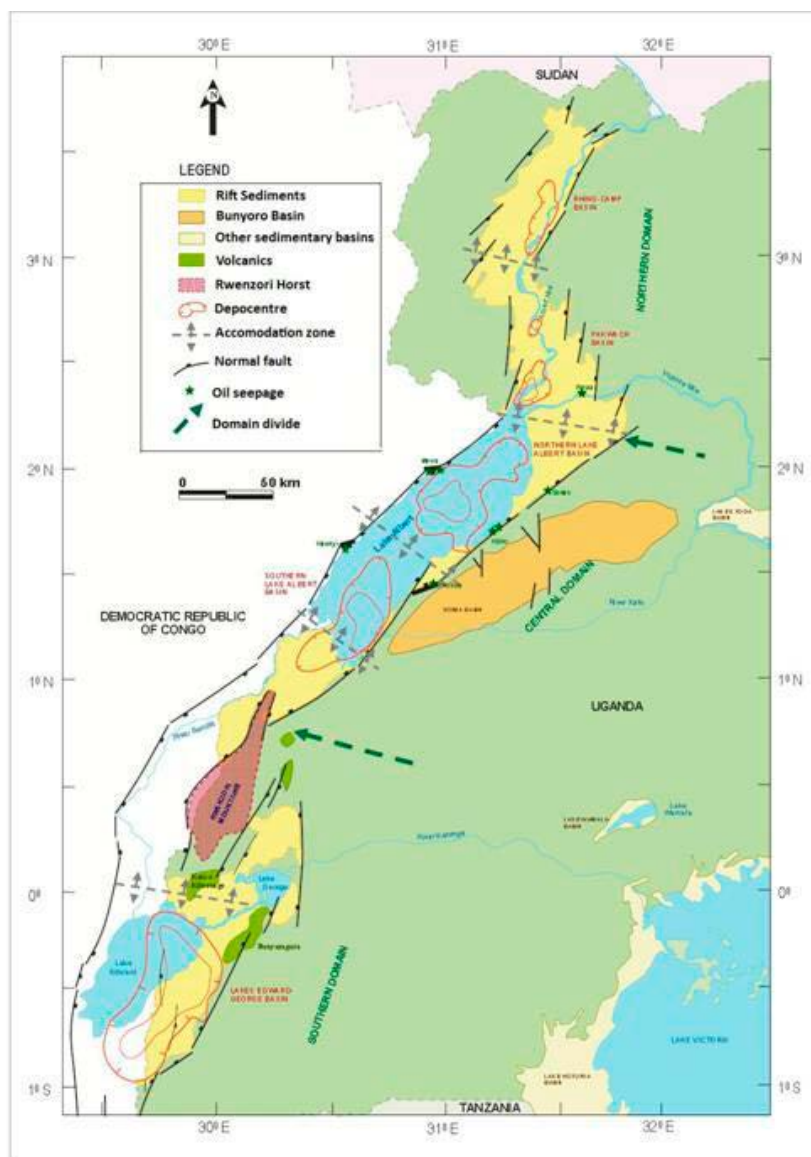


Fig. 12.15. Structural framework in the northern part of the Albertine Rift (from Petroleum Exploration and Production Department).

of the rift, generally called Albertine Rift, is underlain by a thick Miocene-Pleistocene sedimentary succession, with two suites of alkaline volcanics in the southern half and the Rwenzori horst in between (Fig. 12.15). Sediments and volcanics of this northern segment of the Albertine Rift have been assembled here in the *Albertine Supergroup*.

12.3.3.1 Neogene History of the Rwenzori Horst

The Rwenzori Mountains – or ‘Mountains of the Moon’ (Elliott & Gregory 1895) – between Lake Albert and Lake Edward form a promontory of up to 5109 m in altitude (Fig. 12.16). These mountains are underlain by the Rwenzori horst, an uplifted block of the crystalline basement (Fig. 12.17).

Contrary to a long-held view, the Albertine Rift is not a simple extensional basin as demon-

strated by seismic data showing *en echelon* flower structures (Fig. 12.18) that have been interpreted as indicating strike-slip faulting. Closer inspection of these structures reveals that the section within the boundary faults of the flower structures forms anticlines suggesting that they were formed as a result of transpression. 2D and 3D seismic data from the Albertine Rift show normal faults with large fault scarps, cutting through the sedimentary section and indicating evidence of recent faulting. Evidence of stress regimes oblique or perpendicular to the boundary faults is seen through minor faults that do not trend in the same direction as the boundary fault. These suggest that the Albertine Rift has resulted from several successive tectonic episodes characterised by both extensional and compressional regimes.



Fig. 12.16. Rwenzori Mountains in the background as seen from the Queen Elizabeth National Park.

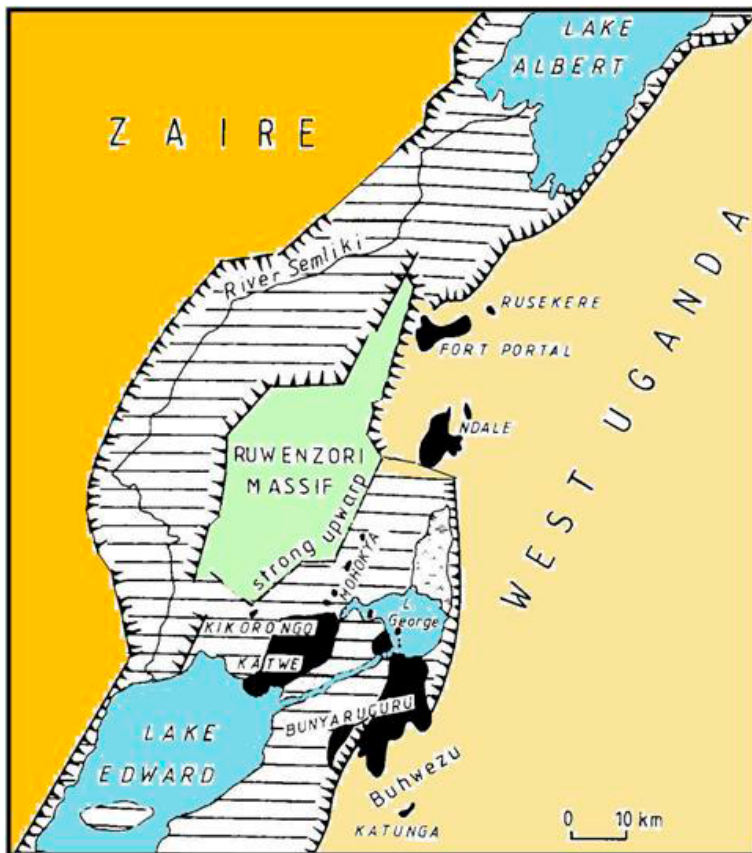


Fig. 12.17. Albertine Rift between Lake Albert and Lake Edward showing Fort Portal (north) and Katwe – Kikorongo – Bunyaruguru (central) volcanic fields and Rwenzori horst. Key: 1 = Volcanic fields, 2 = Pleistocene alluvial and lacustrine deposits; 3 = major faults; 4 = Holocene swamp deposits (after Holmes 1965).

Earthquake data further manifest high seismic activity all over the Rwenzori region with focal depths concentrated between 10 and 20 km (Wölbern et al. 2007, Lindenfeld et al. 2012). Only a few events have been located below 30 km of depth. Local P and S-wave tomography shows significant low velocity anomalies in areas with active volcanic fields and hot springs. Crustal thicknesses of about 23 km have been found beneath the eastern flank, thinning to the west, with Moho depths as shallow as 8 to 15 km. No evidence has been found for a deep crustal root underneath the Rwenzori Mountains.

The extraordinary position of the Rwenzori Mountains within an extensional setting makes it the most extreme expression of rift-flank uplift on earth. To explain its formation two different mechanisms have been postulated, one based on a 'simple' tectonic model, due to the interplay of different propagating segments of the rift system and the other related to thermo-kinetic processes in the upper mantle (Sachau & Köhn 2007).

The first theory assumes a mechanism of thrusting and rotation of the Rwenzori horst during opening of the Albertine Rift along pre-existing crustal weakness zones left behind by various

superposed Proterozoic mobile belts between the Archaean Tanzania and Congo Cratons. Köhn et al. (2008) argued that the Rwenzori horst was captured by two propagating rift segments. Field observations in the Rwenzori Mountains show that the fault block is not only affected by range parallel faults but that major fault sets cut across the mountain belt. In order to understand these complex fault patterns and the dynamics of the process that lead to capturing of Rwenzori block within the extending rift system, they developed a model that showed that propagating rift faults commonly capture micro-plates with shapes similar to the Rwenzori block. These micro-plates rotate during successive rift opening in a clockwise or anticlockwise sense depending on the direction of the rift segment overstep. A left-lateral overstep, as is the case for the Albertine Rift, produces a clockwise rotation of the associated micro-plate as confirmed by the Rwenzori block. During rotation of the micro-plate the local stress field at the rift segment tips is perturbed so that the rifts turn 70 to 90° and propagate towards each other to capture the plates completely. This perturbed stress field produced an extensional fault set that is oriented almost parallel to the far field extension direction and explains the range cutting faults that have been observed in the Rwenzori Mountains. The

large-scale geometry of the Albertine Rift seems to be strongly controlled by rigid lithosphere of the Congo and Tanzania Cratons, leading to a curvature and a sinistral wrench component in the Lake Albert segment of the rift north of the Rwenzori Mountains.

The above hypothesis is supported by new structural and seismic evidence (Köhn et al. 2010). The new data further indicate the presence of a large-scale, 20 km long transsection fault that is currently detaching the Rwenzori micro-plate on its northern margin from a larger plate, which they attribute to the Tanzania Craton, whereas the Rwenzori micro-plate is already fully detached in the south. Fault orientation, fault kinematics and block rotation (once in play) re-enforce each other and, depending on the local kinematics, different parts of a captured block can be rotated by different amounts but in the same general direction (Aanyu & Köhn 2010, 2011). Numerical modelling suggests that the majority of the uplift has taken place within the last 8 million years (Köhn et al. 2010).

Wallner & Schmeling (2008, 2010) follow a different, geodynamic approach to explain the strong uplift of the Rwenzori block, assuming that isostasy is the dominant driving force, which acts when old, cold and dense mantle lithosphere detaches from thick crust. They suggested that thermal anomalies under the rift and plastic yielding, reducing the strength in the zone of the crust-mantle boundary, together with influx of a supposed plume or extensional forces, caused delamination. As a result, this unloading induced fast isostatic pop-up of the less dense crustal Rwenzori block, a process for which they introduced the term “rift induced delamination (RID) of Mantle Lithosphere”. Numerical modeling supports their RID hypothesis. Assuming a simple starting model with locally heated mantle lithosphere, the mantle lithosphere block between the weakened zones becomes unstable and sinks into the asthenosphere, while the overlying continental crust rises up. The above authors conclude that RID seems to be a viable mechanism to explain extreme uplift. Further support for the RID mechanism may come from additional crustal thickness and an extensive stress field.

Bauer et al. (2008, 2009, 2010a, 2010b, 2011a, 2011b, 2013) have tried to constrain the uplift and denudation history of the Rwenzori block, based on the combined results of apatite fission-track (AFT) as well as (U-Th-Sm)/He data of apatite

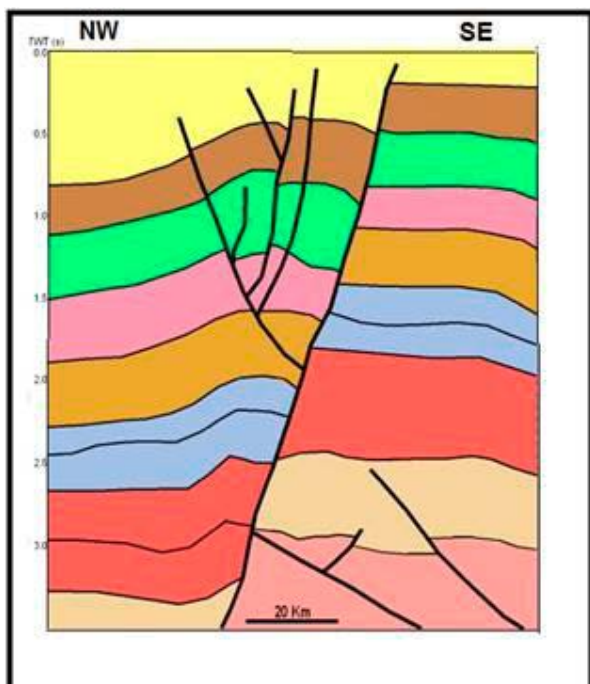


Fig. 12.18. A cartoon diagram of trans-pressional flow structure interpreted from Semliki Basin seismic data (Abeinomugisha & Mugisha 2004).

(AHe) and zircon (ZHe). Cooling paths (or time-temperature-paths), that match the measured AHe and ZHe data and that are consistent with the AFT data, show (1) rapid Mid- to Late Jurassic (~170 Ma to ~150 Ma) cooling of ~50°C, (2) a period of very slow and constant cooling of ~45°C through most of the Cretaceous and Palaeogene time (~150 – ~10 Ma), (3) rapid cooling of ~25°C to surface temperatures in very short time during the Neogene (~10 Ma to Recent). We speculate that phase (1) corresponds roughly with a major igneous event, marking the end of the Karoo and phase (3) obviously relates to Albertine rifting and uplift of the Rwenzori Block. First results from a sample-set, spanning an E-W transect across the Rwenzori Mountains, clearly show differentiated cooling paths, with differentiated denudation rates, indicating asymmetric uplift of the Rwenzori fault block.

Neotectonic studies (Lærdal & Talbot 2002) demonstrated continuous tectonic activity in the Albertine Rift and confirm the strong influence of older weakness zones (Section 12.3.1). The Edward and George Lake basins, located south of the Rwenzori horst (Fig. 12.17), occupy half-grabens with the main boundary fault located in the west. They are separated by a high relief accommodation zone, formed by a structural high where the NNE–SSW trend of the Miocene rifting and NW–SE oriented basement lineaments intersect. The Kazinga Channel, connecting Lake George to Lake Edward, cuts across this uplifted area and its course has been influenced by syn- and antithetic fault zones. Faulting related to the Kasindi Fault Zone suggests a > 12 m fault movement during the Holocene. Volcanism in this part of the Albertine Rift is related to high relief accommodation zones and volcanic craters are either aligned parallel to NW–SE trending Proterozoic lineaments or the NNE–SSW directed Miocene rift. Volcanism that was initiated during the early stages of rifting commonly parallels the NW–SE oriented accommodation zones and basement lineaments, while craters that formed during the later stages of rifting tend to parallel the large NNE–SSW directed border faults of the rift (Lærdal & Talbot 2002).

12.3.3.2 Sediments of the Albertine Rift

The northern part of the Albertine Rift fill is composed of an up to 5 km thick pile of terrestrial sediments (Karp et al. 2012). These sediments have

been tentatively assembled in the *Kaiso* and *Hima Formations*, while the older and younger volcanic successions have been assembled in the *Kivu Formations* (in DRC) and *Bufumbira*, *Bunyaruguru*, *Ndale* and *Fort Portal Formations* (in Uganda), respectively. In order to separate these units from the older rift-filling lithologies, which are mostly located in the southern part of the Albertine Rift, all aforementioned Formations are assigned here to the Upper Albertine Group (Table 12.3).

Surface and subsurface observations in the Albertine Rift indicate that the sedimentary succession is mainly composed of fluvial and deltaic deposits in the top and bottom of the succession and lacustrine deposits in the middle, all characterised by a variety of lithologies, including conglomerates, sandstones, mudstones, cherts, shales, oil shales and coal-bearing horizons. Seismic surveys (McGlue et al. 2006) recognised structural deformation that influenced facies distribution and facies development on two major scales: (1) rift-scale extension across the boundary fault, which controlled gross drainage basin geomorphology, and (2) localised intra-basinal normal faulting, which influenced the present orientation of several important facies types. Apart from tectonism, also climatically driven variations in the precipitation–evaporation balance affected facies distribution. Well-developed deltaic packages record evidence for large-magnitude lake-level fluctuations in the seismic dataset and attest to climatically driven lake-level and facies changes.

Rifting in the northern Albertine Rift, as inferred from basal fluvial deposits, was initiated in the Early Miocene. An age of 20 Ma has been proposed by previous authors (de Heinzelin 1963, Lepersonne 1970, Pouclet 1975), whereas a younger date of 15–16 Ma was suggested by Pickford et al. (1993). Whatever the age considered, the northern Albertine basin is older than the other basins along the Western Rift. The earliest lacustrine sequences of this area were dated at ~8 Ma (Hopwood & Lepersonne 1953, Ebinger 1989) but could be older (13–12 Ma) according to Pickford et al. (1993).

In most parts of the Albertine Rift these Miocene sediments are covered by recent surface deposits, i.e., a mixture of alluvial material, wash-outs and debris flows. The stratigraphy of the underlying strata is known in places from drill core and from scarce outcrops, exposed due to scarp uplift along the rift shoulders and from deep

Table 12.3. Subdivision of the Upper Albertine Group. Map codes refer to rock units in unpublished 1:250 000 -scale geological maps delivered to DGSM.

| Volcanic fields | | | Formation |
|-------------------------------|-----------------------------------|----------------------------------|---|
| Bufumbira volcanic field | Katwe –Bunyaruguru volcanic field | Ndale–Fort Portal volcanic field | Fort Portal Formation Ndale Formation Bunyaruguru Formation Bufumbira Formation Hima Formation Kaiso Formation |
| Kivu Formation 2 12.6–8.9 Ma | | | < 15–16 Ma |
| Kivu Formation 1 ~ 28–10.7 Ma | | | |

| Bufumbira Formation | |
|---|--------------|
| Boulder deposit | Qbd |
| Ash, tuff and scoria | NeBauf |
| Leucite basanite | NeBlb |
| Trachytic leucite basanite | NeBtlbn |
| Leucite basalt | NeBlba |
| Olivine leucite basalt | NeBolb |
| Limburgite | NeBl |
| Trachytic tephrite and leucite tephrite | NeBtt, NeBlt |
| Olivine basalt | NeBob |
| Leucite olivine basalt | NeBlob |
| Andesite | NeBa |
| Mixed flows including leucite basanite, leucite basalt and limburgite | NeBb |

| Bunyaruguru Formation | |
|--|------|
| Carbonate-rich tuffs | |
| High-K volcanics, carbonatite lava | QGpv |
| Ndale Formation - Fort Portal Formation | |
| Lapilli tuff | QNt |
| Lapilli tuff | QFPt |
| Hima Formation - Kaiso Formation | |
| Travertine limestone | Qtr |
| Gritty sandstone | QKss |

river incisions inside the rift. Because of significant hydrocarbon potential, sections and stratigraphic columns have been described in rather detail from different segments of the Albertine Rift, resulting in a large number of strictly local formation names (Abeinomugisha & Mugisha 2004, Abeinomugisha & Echegu 2004, Abeinomugisha & Ochan 2004, Abeinomugisha 2006, 2007a, b). Correlation of these local columns is, however not possible. The lack of palaeontological, chemostratigraphical or palynological information of the rift sediments prevent dividing the stratigraphy of the basin into appropriate units that are fixed in time. A representative segment of the Albertine Rift, showing more detailed geology, is presented in Figure 12.19.

Among the many types of fluvio-lacustrine and deltaic deposits, the *Ocindu formation* in the Rhino Camp area (northern segment of the Albertine Rift) is worth mentioning. The upper part of this

unit is highly arenaceous, with several bands of dirty white to light grey, low-density sediments, identified as siliceous spiculite/ bedded chert/ diatomite at the base of the formation, overlain by a coarsening-upward sequence. The presence of siliceous spiculite/ bedded chert/ diatomite is an indication of deposition in a shallow evaporating lacustrine environment. Chert is formed when silica is leached from sulphur-rich rocks by water of low pH and precipitated as it enters very alkaline sodium carbonate-rich lake waters. Evaporation and decrease in pH cause the silica to precipitate as magadiite, a meta-stable hydrated sodium silicate that is converted into chert in a relatively short time or, alternatively, silica is precipitated as a gel of cristobalite, which would give rise to chert on maturation. Diatomite is formed from skeletal remains of diatoms, microscopic aquatic unicellular organisms, which occur in great abundance in lakes. The presence of bedded chert/ diatomite

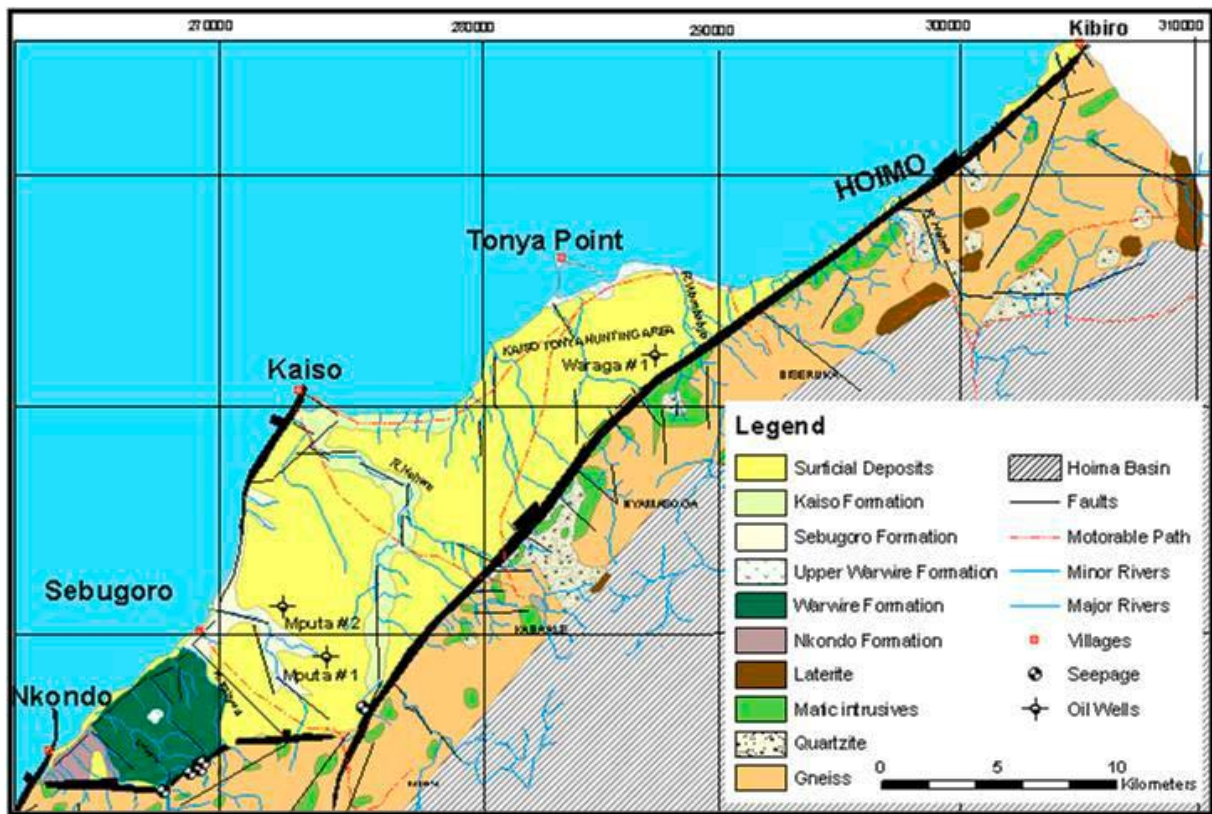


Fig. 12.19. Geology map and satellite imagery of the Kaiso-Tonya area, northern Albertine Rift. The rift sediments are exposed over an area measuring ~39 x ~11 km (Abeinomugisha & Mugisha 2004, Petroleum Exploration and Production Department, Tullow Oil plc.).

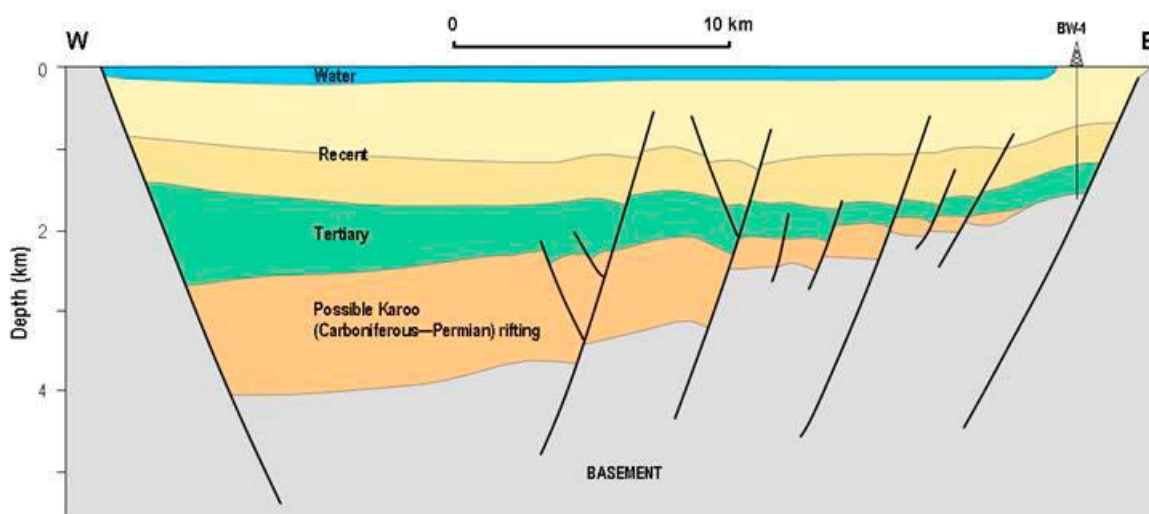


Fig. 12.20. East-West structural cross-section across the Albertine Graben showing the gentle tilt of the basin towards the West (after Abeinomugisha 2004).

in the sequence is an indication of clastic starvation at the time, due to rift shoulder uplift, which in turn indicates deposition in a shallow lacustrine environment with desiccation. Diatomites were also mapped at different locations in Rigbo Sub County, Wanyange Village and Aliba County to-

wards the Ropo Landing Site and diatomite lenses occur in the upper part of the *Kasande Formation* in the Semliki Basin south of Lake Albert.

The presence of gypsum signifies semi-arid conditions resulting in high rates of evaporation and therefore precipitation of evaporites. Several

beds of the *Oluka formation* in the same area are composed of white to light grey, low-density, siliceous spiculites and/or bedded cherts with conchoidal fracture, diatomite lenses and gypsum veins and crystals, again manifesting deposition in a shallow lacustrine environment with desiccation. Hiatuses during these episodes could have caused exposure, palaeo-sols and high evaporation leading to cracking of the clay and deposition of calcite and gypsum.

Fossil-rich horizons in the *Nyakabingo* and *Nyabusosi formations* in the southern segment of the Albertine Rift include fish bones, oyster shells (*Ostrea*), bivalves (*Atrina* and *Modiolus*) and gastropoda, indicating fresh water lake conditions with water depths of less than about 10 m. The high concentration of fossils in specific horizons suggests periodic lake level fluctuation and flooding or mass extinction when the lake became too saline.

12.3.3.3 Basin development of the Albertine Rift

Using surface geology, seismic and well data, a stratigraphic section has been prepared (Fig. 12.20; Abeinomugisha & Mugisha 2004). As mentioned earlier, sediments from the Albertine Rift comprise of dominantly fluvial and lacustrine deposits. Tectonism has played an important role in formation of the drainage pattern, the source of the sediments and deposition of the fluvial deposits coupled with climate, base level control and pre-existing geology of the area. Taking all data together, the sedimentary systems indicate an

environment that starts with purely fluvial strata followed by an intermezzo of lacustrine deposits and finally, deposition of deltaic/fluvial-lacustrine packages (Fig. 12.21).

The purely fluvial strata are mainly in channel facies (meandering and braided river deposits, alluvial fans), fluvial flood facies and overbank fines. Generation of the lacustrine environment is most likely tectonically initiated causing an increase in accommodation space. The amount of tilt on faulted blocks largely controlled the deposition and extent of the mass flow deposits in the rift. Slope generation caused increase in slope leading to depositional facies change whereby coarse sands deposited further out, basin-ward, onto the finer clastic sediments and lacustrine systems were generated. Fault reactivation gave rise to a continued increase in slope angle and the formation of unstable slopes leading, in turn, to the deposition of relatively deeper lacustrine system and gravity flow deposition. This phase was followed by deltaic/fluvial-lacustrine interaction in which interplays between fluvial and lacustrine environments together with climatic/accommodation changes are evident in some of the formations and transgressive and regressive packages were deposited.

The block diagram in Figure 12.21 illustrates the depositional framework of the entire Albertine Rift. Like many continental rift basins, the sub-basins in the Albertine Rift display a tripartite stratigraphic package (Lambiase & Rodgers 1988) (from bottom to top): fluvial deposits, followed relatively abruptly by generally deep-water lacustrine units, which, in turn, are gradually replaced

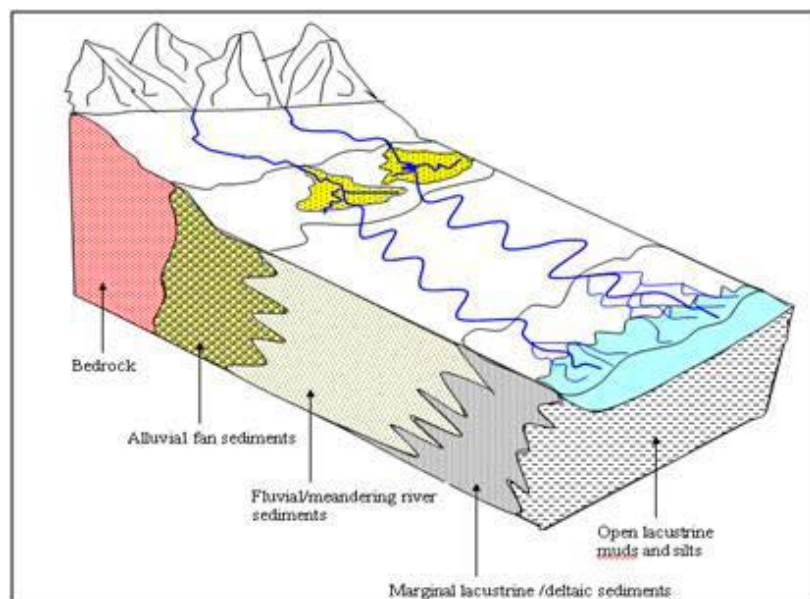


Fig. 12.21. Depositional model for the Albertine Rift (Abeinomugisha & Mugisha 2004).

by shallow-water lacustrine and fluvial deposits. The fluvial systems manifest deposition during initial, slow basin subsidence, supposedly in a number of linked, small sub-basins. The deep-water lacustrine unit is interpreted to reflect a deepening of the basin resulting from increased subsidence and the coalescence of sub-basins. The upward-shoaling is interpreted to reflect the gradual infilling of the basin, with fluvial sedimentation returning after the basin had filled to the lowest outlet of the basin.

12.3.3.4 Volcanic rocks of the Albertine Rift

Major volcanic fields of the Western Rift are restricted to alkaline lavas of the Rungwe volcanic field in southern Tanzania, the Kivu volcanic field north and south of Lake Kivu and the Pleistocene ultrapotassic volcanic rocks in the northern Albertine Rift between Goma and Fort Portal. The Kivu volcanic field stretches from Mwenga through Bukavu to Goma, over a distance of ~280 km, con-

fining to a SW-NE trending half-graben, located outside the main axis of the Western Rift (Fig. 12.22; Kampunzu et al. 1998). Each volcanic field is unique in having a specific chemical composition and time of emplacement.

According to disputable K-Ar ages (Bellon & Pouclet 1980), initial volcanic activity in the Western Rift moved from south to north. Alkaline to sub-alkaline basalts, Na-basanite, hawaiite, olivine basalt, pyroclastics and scoria from locations south of Lake Kivu yielded Eocene ages (55–49 Ma). The Kivu volcanic field comprises some earlier remains of alkaline sodic composition with Upper Oligocene ages (~28 Ma) in northern Idjwi Island in Lake Kivu and Middle to Upper Miocene ages (12.6 to 7 Ma) near Goma, on the border between Rwanda, Uganda and DRC.

Kampunzu et al. (1998) suggested a reverse trend in volcanic emplacement ages. Development of the Western Rift began ~11 Ma ago in the Virunga region, ~10 Ma ago in the Bukavu area and 9 Ma ago in the Rungwe region. The age of the earliest extrusive rocks recorded in the Mwenga-Kamituga Volcanic Field (Fig. 12.22) is not well constrained but could be close to 6 Ma. Independent age estimates for the early development of structural basins of the Edward-Albert Lakes zone are ~16 to 13 Ma.



Fig. 12.22. Outline of the distribution of Cenozoic volcanics in the Kivu Province, DRC, and neighbouring areas in Rwanda and Uganda (modified after Kampunzu 1981). Key: 1 = Volcanic rocks of Bukavu and Mwenga-Kamituga; 2 = Volcanic rocks of Virunga.

Kivu Formation – Older volcanics of the *Kivu Formation* are well-exposed in the Kivu Province, DRC. Their extent in Uganda is unknown, being covered, if present, by younger volcanics of the Bufumbira volcanic field and rift sediments. They comprise tholeiites and transitional basalts with ages between 28.0 ± 1.4 Ma and 10.7 ± 0.7 Ma and a suite of Na-alkaline lavas, including basanites, hawaiites, mugearites and benmoreites (Kampunzu et al. 1983, 1984a, b) with ages between 12.6 ± 0.7 Ma and 8.9 ± 0.5 Ma (Kampunzu et al. 1998). The thin basal pile of basalt flows with tholeiitic to transitional affinity is related to pre-rift doming and extension. The emplacement of the covering suite of Na-alkaline lavas is related to rift initiation and rift development.

The basaltic lavas of the earliest group are basic rocks exhibiting a wide range of chemical composition (e.g., SiO_2 contents from 45 to 51 wt%) and marked by a differentiation index lower than 35 and Mg# values bracketed between 63 and 59. The presence of hypersthene and olivine in their normative composition indicates that they are olivine tholeiites. The second group is composed of

alkaline lavas with sodic affinities, showing again a wide range in composition (Kampunzu 1981, Kampunzu et al. 1983). The tholeiitic and transitional basalts of the first cycle predate the rift development (e.g., Kampunzu & Mohr 1991) and correspond to initial block faulting without subsidence, whereas the transition from this first tholeiitic transitional cycle to the second Na alkaline cycle marks rift initiation. The overlap between the last and earliest flows of these two successive volcanic cycles is not controlled by structural processes, but simply reflects the time of arrival of the magmas from their respective sources located at different depths (Kampunzu et al. 1986, Kampunzu & Mohr 1991).

Volcanic rocks of the Upper Albertine Group

In Uganda, volcanic rocks of the Upper Albertine Group occur in three volcanic fields (Barifaijo 2001), named (from south to north) (1) the *Bufumbira*, (2) the *Katwe-Kikorongo-Bunyaruguru* and (3) the *Ndale-Fort Portal* (Fig. 12.23). The Katwe-Kikorongo-Bunyaruguru and Ndale-Fort Portal volcanic fields host only 'younger' syn-rift volcanic rocks emplaced during episode (2) *sensu* Kampunzu et al. (1998). The Bufumbira volcanic field is unique since there younger (~2.8 Ma to Present) volcanics of the Bufumbira Formation overlie older (~28–9 Ma), pre-rift volcanics of the Kivu Formation in DRC.

In the Upper Albertine Group, the classical tholeiitic, transitional and Na alkaline lavas, which mark the initial stages of the rift evolution, are unknown. The hallmark igneous rocks documented in this region are ultra-potassic, strongly alkaline lavas and extrusive carbonatites (see below). Kampunzu et al. (1998) suggested that the absence of tholeiitic basalts indicates the lack of appropriate source material and that the mantle beneath this region is highly metasomatised, and partial melting cannot generate magmas of tholeiitic basalt composition.

The ultrapotassic, strongly alkaline, late Pliocene-Holocene volcanics are silica-undersaturated, contain ubiquitous olivine and clinopyroxene, subordinate kalsilite, melilite, leucite, nepheline, phlogopite and accessory amounts of perovskite, sphene, titanomagnetite, apatite and ilmenite. The Ndale-Fort Portal volcanic field in the north is characterised by alkali-poor, Ca-rich carbonatite volcanism. The central Katwe-Kikorongo-Bun-



Fig. 12.23. Map showing the location of three volcanic fields in the northern part of the Albertine Rift. (1) Bufumbira, a part of the larger Virunga volcanic field, (2) central Katwe-Kikorongo & Bunyaruguru and (3) Ndale-Fort Portal (after Eby et al. 2003, with kind permission of GeoLines Institute of Geology).

yaruguru field and Kasenyi crater are ultra-potassic (K_2O typically > 3 wt%, and $K_2O/Na_2O > 2$; Foley et al. 1987, 2012). Though also potassic, lavas of the Bufumbira volcanic field show a much lower degree of K-enrichment when compared to this central volcanic field. From trace elements and trace element ratios, different mantle domains can be identified from which the magmas in each of the volcanic fields originated.

Bufumbira volcanic field – As a part of a larger Virunga volcanic field, the late Pliocene-Holocene volcanics of the *Bufumbira volcanic field* partly overlie the northernmost part of the older, Oligocene-Miocene volcanics of the Kivu Formations in DRC (Kampunzu et al. 1998). In Uganda, all exposed volcanics belong to the younger suite and will be discussed in this section. The Virunga volcanic field, which was first described by

Combe & Simmons (1933) and Holmes & Harwood (1932, 1937), comprises eight major strato-volcanoes, including the active Nyiragongo and Nyamulagira, located on the rift floor north of Lake Kivu, and six dormant volcanoes: Mikeno, Karisimbi, Visoke, Sabinyo, Mgahinga and Muhavura (Fig. 12.24). The three easternmost of these, aligned along the border between Rwanda, DRC and Uganda, are assembled in the Bufumbira Formation (Fig. 12.25).

Of the dormant volcanoes in the Virunga field, Mikeno yielded K-Ar ages ranging between 2.6 ± 0.1 Ma to 0.3 ± 0.1 Ma. Unspiked potassium-argon dating of potassic, undersaturated lavas from the Karisimbi yielded ages ranging between 0.14 ± 0.06 and 0.010 ± 0.007 Ma, constraining the formation of the main cone and its parasitic structures to the Late Pleistocene (de Mulder & Pasteels 1986). Other volcanoes yielded ages between 0.26 ± 0.13 Ma to Present (assembled in Kampunzu et al. 1998). Vellutini et al. (1981) and Kampunzu & Mohr (1991) stressed that these potassic volcanoes are connected to a major transverse SW-NE trending fracture zone – shown in Fig. 12.33 – with a ‘Rwenzori’ direction.

All the Bufumbira volcanics have silica-undersaturated, ultra-alkaline, alkalic-mafic compositions (Ramananda et al. 2009), ranging from olivine-basanites to leucite-phonolites and slightly silica-undersaturated trachytes. They contain leucite both as phenocrysts and in the groundmass. Inclusions and smaller xenoliths include pyroxenite, mica pyroxenite, peridotite and mica peridotite (Ferguson & Cundari 1975). Upper mantle peridotite xenoliths up to 20 cm in diameter, en-

closed within the undersaturated alkaline basalts of the Bufumbira Formation, have been described by Barifaijo et al. (2008). As volcanics of the other volcanic fields, Bufumbira lavas show an extreme range of chemical and mineralogical compositions (Barifaijo et al. 2010).

Significant differences can be observed between nearby volcanoes and even between different flows from the same volcano. The SiO_2 content ranges from 61.2 wt% (trachytic glass) to 40.5 wt% (mela-basanite). While trachytic varieties contain K-feldspar (Ferguson & Cundari 1975, Aoki et al. 1985), mela-basanite varieties are composed of olivine, diopside and chromite set in a fine matrix of titanite-augite, olivine, plagioclase, leucite and microcrystalline glass. Other varieties, such as leucite tephrite and tephritic leucitite, contain phenocrysts of titanite-augite, leucite, olivine and rare ulvöspinel in a fine- to cryptocrystalline matrix containing plagioclase and opaque matter. These differences are supposedly due to (1) differences in source rock from which the magmas formed, (2) the amount of crustal contamination or (3) fractionation, or a combination of these.

Bufumbira Formation – The volcanics of the Bufumbira Field are assigned to the Bufumbira Formation, extruded mainly from three large, dormant stratovolcanoes (Muhavura, Mgahinga and Sabinyo) and from numerous volcanic vents, which form a cluster of low cinder cones and explosion craters north of these volcanoes (Fig. 12.25). All volcanic rocks of the Bufumbira Formation are extruded on the various metasediments of the Mesoproterozoic Akanyaru-Ankole Supergroup. The surface extent and classification of various lava units of the Bufumbira Formation is based on Combe & Simmons (1933) and 1:100 000 -scale geological map, published by the Geological Survey of Uganda (Sheet 93 Kabale) in 1965.

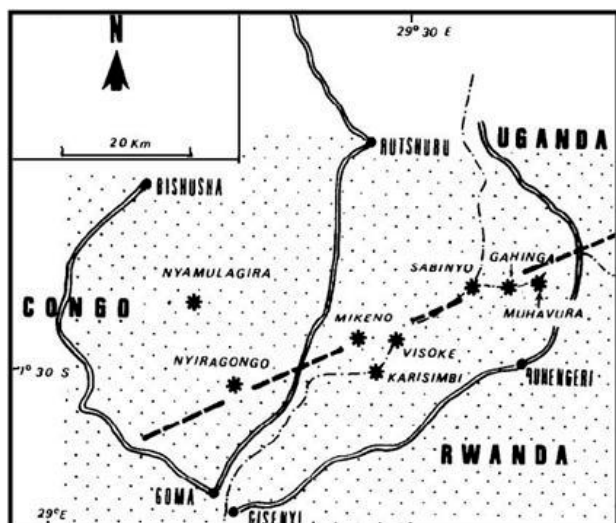


Fig. 12.24. Sketch map showing distribution of eight major volcanoes of Pliocene-Recent age in the Virunga volcanic field and related lava plain (dotted) (from Kampunzu et al. 1998, with kind permission of Elsevier Ltd.).



Fig. 12.25. Alkaline stratovolcanoes of the Bufumbira Formation, from the left: Muhavura (4,127 m), Gahinga (3,474 m) and Sabinyo (3,774 m). Several cinder cones are visible in the valley.



Fig. 12.26. Different lava structures from the mixed alkaline lava flows. (A) Top of a lava flow with flow-oriented vesicles (133798E / -140219N). (B) Massive core of a lava flow (127222E / -138732N). Number tag 10 cm.

Mixed flows including leucite basanite, leucite basalt and limburgite (NeBb) – An arcuate zone around the southern shores of Mutanda Lake comprises a mix of alkaline basalt flows, including leucite basanites, leucite basalts and limburgites (Figs 12.26A-B).

Andesite (NeBa) – Andesites are greyish pink to pale brown rocks, containing dark, flow-oriented clinopyroxene phenocrysts and zoned plagioclase, sanidine, biotite and titanomagnetite. Andesitic lava flows are only found on the upper slopes of Mt. Sabinyo (Barifaijo et al. 2008).

Trachytic tephrite and leucite tephrite (NeBtt, NeBlt) – Fine-grained alkaline lavas, originally called trachytic tephrite and leucite tephrite (Combe & Simmons 1933), are exposed in a rather small area near the southern shore of Mutanda Lake. An isolated flow of leucite tephrite lava is also exposed on the northeastern foot of the Muhavura volcano, near the Rwandan border. Grey to bluish grey lava flows are highly porous, aphanitic to cryptocrystalline rocks without visible phenocrysts (Fig. 12.27A). Under the microscope, tephritic lavas show random leucite and augite phenocrysts, and plenty of flow-oriented microliths of plagioclase and minute clinopyroxene prisms in a hyalopilitic matrix (Fig. 12.27B).

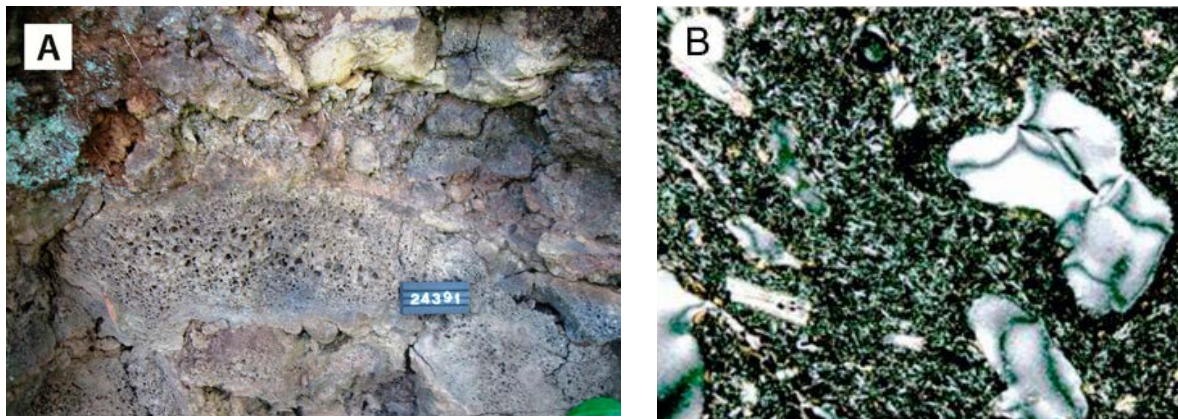


Fig. 12.27. (A) Highly porous leucite tephrite lava flow west of the Kisoro airfield (133475E / -142053N). (B) Microphotograph of highly porous, fine-grained leucite tephrite lava flow with flow-oriented, hyalopilitic matrix and zeolite-filled vesicles. West of Mutanda lake (132676E / -137142N). Number tag 10 cm, width of - microphotograph ~ 4 mm.

Limburgite (NeBl) – Limburgitic lava flows, closely associated with leucite basalts, cover the area around Kisoro airport. Limburgite consists essentially of euhedral, pale green olivine and blackish clinopyroxene (augite) phenocrysts in a bluish grey, fine-grained and vesicular ground mass. Alkaline volcanic rocks of similar composition occur also about 20 km NE of Kisoro town, where limburgitic lava flows and associated pyroclastic rocks extruded over the Rubanda granite. Bluish grey, vesicular lavas with plenty of olivine phenocrysts, together with a layer of well-sorted lapilli tephra or unsorted tephra with blocks and bombs, cover an area of about 2 x 3.5 km in the southern part of the intrusion.

Olivine leucite basalt (NeBolba) – A heterogeneous succession of olivine leucite basalt is exposed in Muko village, some 15 km NE of Kisoro town. This

is mostly well-sorted lapilli scoria, widely covering the gently undulating palaeosurface of the Akan-yaru-Ankole metasediments (Fig. 12.28A). Massive, porphyritic rock with plenty of small, pale green olivine phenocrysts in a grey, fine-grained ground mass is exposed in a large quarry and in Muko village (Fig. 12.28B). Its massive nature suggests that it represents a feeder for narrow olivine leucite basalt lava flows observed in road cuts in Muko village.

Leucite basalt (NeBlba) – Dark bluish grey, fine-grained, porous leucite basaltic lava flows with plenty of euhedral olivine and large (up to 2–3 cm) leucite phenocrysts, and biotite flakes, are exposed in the valley SE and E of Kisoro town. Locally lava forms tumuli or high lava terraces with coarse flow-top breccias (Figs 12.29A-B).

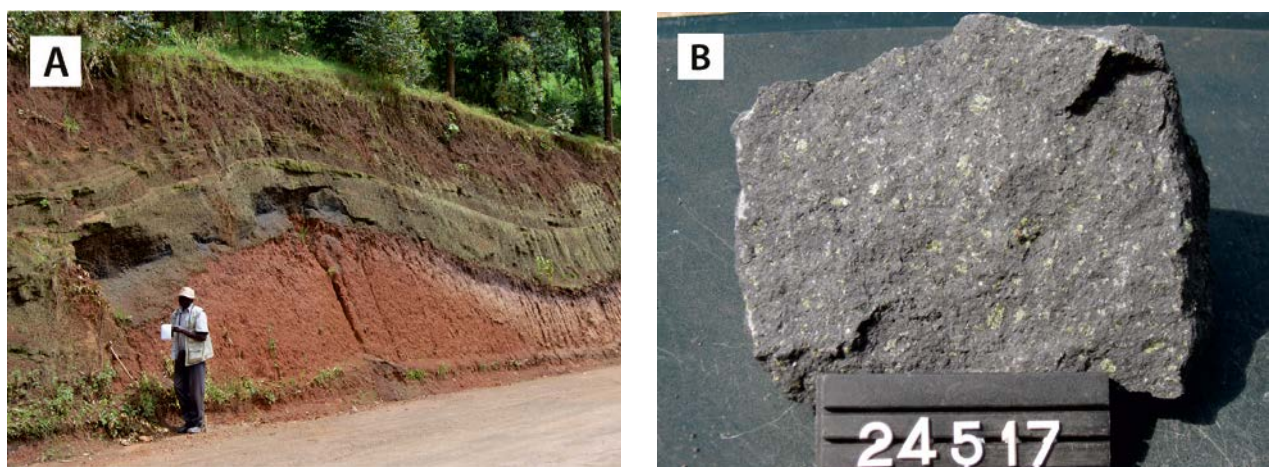


Fig. 12.28. (A) Well-sorted lapilli tephra layer resting on the reddish brown Akanyaru-Ankole metasandstone (144393E / -133747N). (B) Olivine leucite basalt with plenty of small olivine phenocrysts. Muko village (145673E / -133491N). Number tag 10 cm.

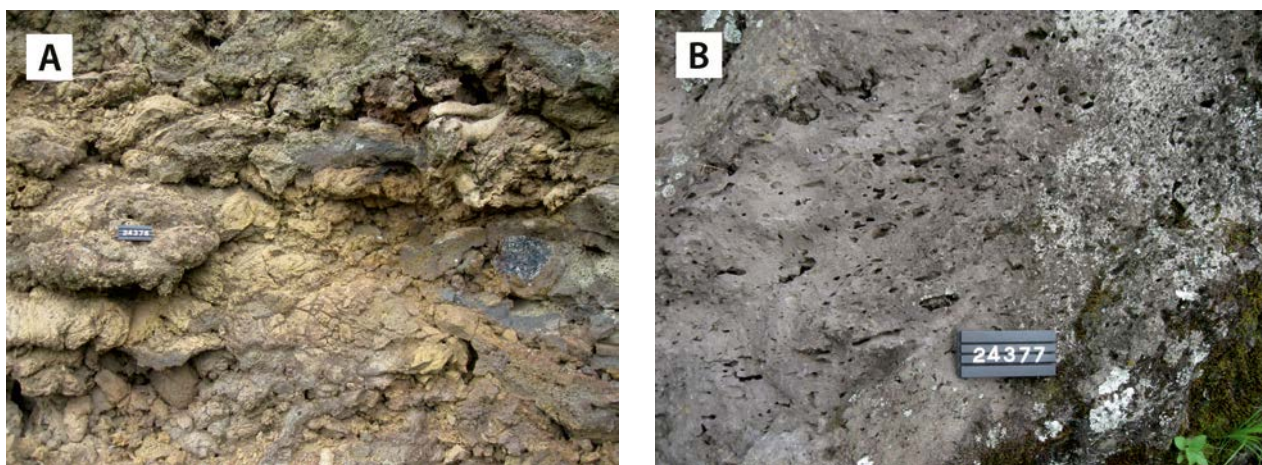


Fig. 12.29. Different flow structures of leucite basalt lava. (A) Rough surface of a pahoehoe-type lava flow (136571E / -140903N). (B) Flow-oriented vesicles in a lava flow (135849E / -140362N). Number tag 10 cm.

Trachytic leucite basanite (NeBtlb) – Dark brownish to bluish, fine-grained and highly vesicular lava flows cover extensively the valley SW of Mutenda Lake (Fig. 12.30A). Similar alkaline lava flows, termed trachytic leucite basanite by Combe & Simmons (1933), exist north of Cyahafi and Kayumbu Lakes near the Ugandan-Rwandan border. Under the microscope, euhedral, twinned and zoned clinopyroxene (augite) phenocrysts, up to 2 mm in size, and rare olivine phenocrysts are embedded in a hyalopilitic groundmass, mostly composed of zoned leucite micro-crystals and minute augite prisms (Fig. 12.30B).

Leucite basanite (NeBlb) – The most common alkaline lava type of the Bufumbira volcanic field is basanite, which covers nearly a third of the area, being well exposed along the lower northern

slopes of the Muhavura and Gahinga volcanoes. Tumuli (lava ridges) of pahoehoe-type lava flows with rope structures are common, and large caves with peculiar, spiracle-like lava structures occur near the northern boundary of the Mgahinga National Park. Structure and texture of basanitic lavas varies from highly vesicular flow tops (Fig. 12.31A) to massive, porphyritic rocks in the centre of flows (Fig. 12.31B).

The mineralogy is characteristic for alkaline lava series and comprises euhedral phenocrysts of clinopyroxene (augite), olivine and leucite in a hyalopilitic groundmass, which is mostly composed of flow-oriented microliths of plagioclase and vitreous material; sphene and opaque minerals (titanomagnetite) are common accessory minerals.

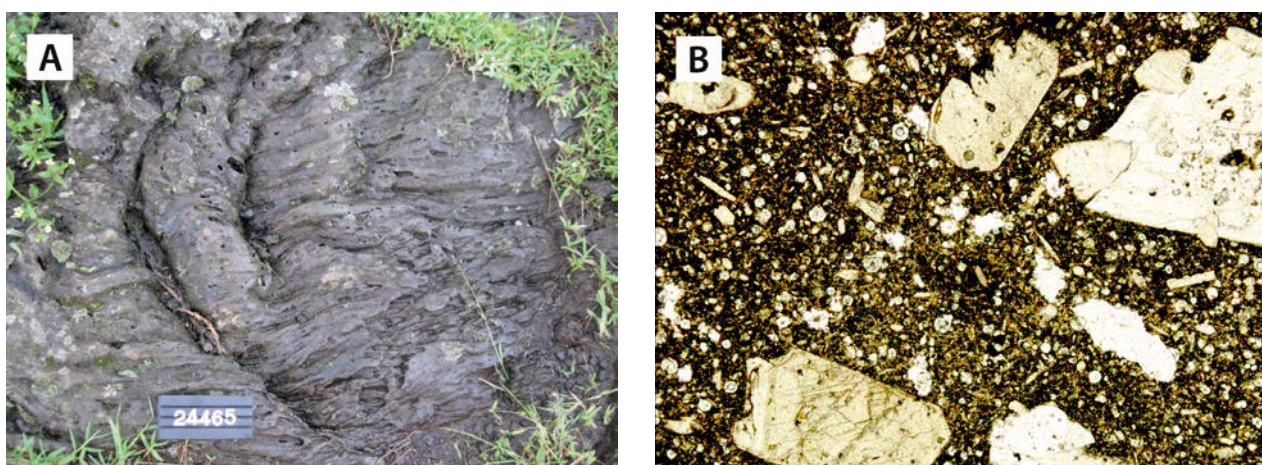


Fig. 12.30. Trachytic leucite basanite lava. (A) Ropy-like top of a lava flow (140695E / -147664N). (B) Microphotograph of trachytic leucite basanite, showing euhedral augite phenocrysts in a hyalopilitic groundmass. Parallel nicols (124477E / -140000N). Number tag 10 cm, width of microphotograph ~4 mm.

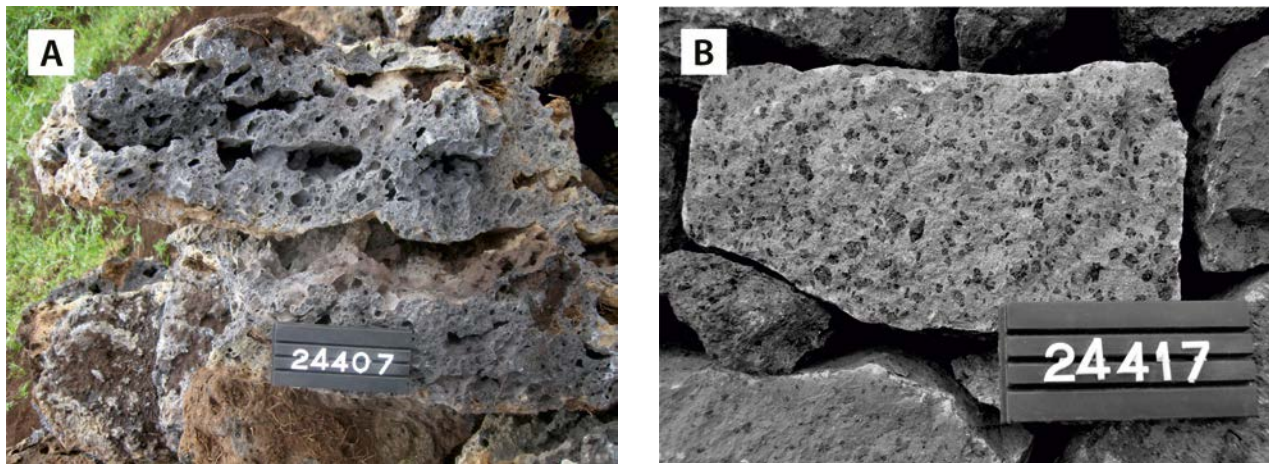


Fig. 12.31. (A) Vesicular top of leucite basanite lava flow (127859E / -144924N). (B) Porphyritic core of a lava flow (128954E / -149019N). Number tag 10 cm.

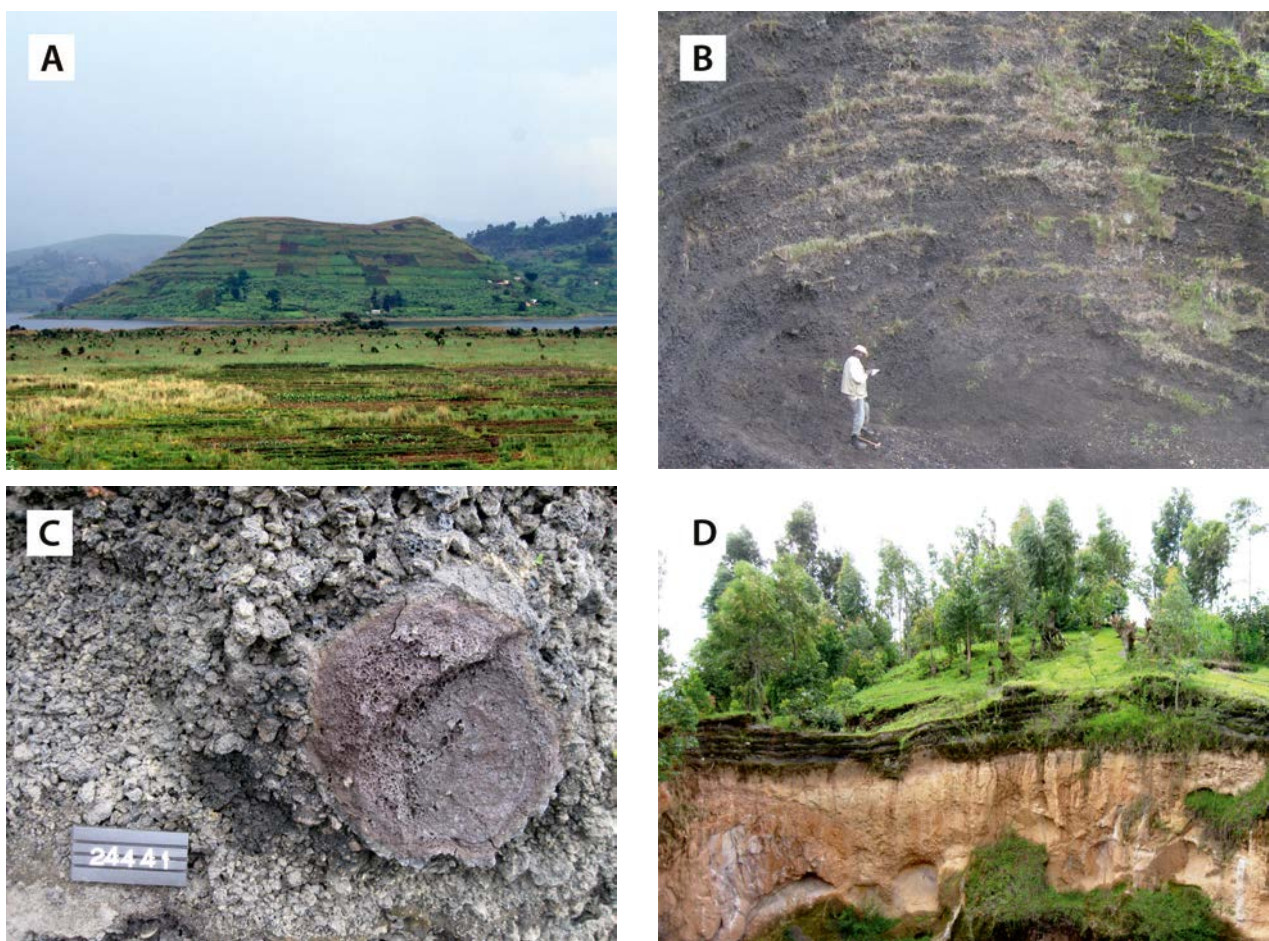


Fig. 12.32. (A) Terrace farming on a symmetrical cinder cone of the Bufumbira Formation south of Lake Mutanda. (B) Cross section of a cinder cone, showing crude bedding in coarse scoria-fall deposit (125101E / -148428N). (C) Large vesicular bomb embedded in tephra (137241E / -145791N). (D) Ash-fall (tephra) blanket covering Akanyaru-Ankolean sandstone ridge (130420E / -145251N). Number tag 10 cm.

Ash, tuff and scoria (NeBauf) – A cluster of about forty cinder cones and explosion craters occur in the Bufumbira volcanic field, mostly located on the lower flanks of Mt. Muhavura, or in the val-

ley north of the stratovolcanoes. A few satellite cinder cones exist also within the Akanyaru-Ankolean metasediments east of the rift valley, the easternmost being located in Muko village. All these

pyroclastic volcanics with random lava interbeds erupted through Mesoproterozoic Akanyaru-Ankole metasediments, while alkaline lava flows discharged from the stratovolcanoes to the south. They represent the youngest volcanic products in the area.

Most of the cinder cones of the Bufumbira Formation occur as symmetrical, cone-shaped hills up to 150 m in height, the largest having a basal diameter of about 1.5 km (Fig. 12.32A). Although usually forming a roundish cone with a bowl-shaped crater at the summit around the central vent, cones comprising several separate vents also exist. The rupture of the crater wall has often distorted the originally symmetrical shape of the cone, resulting in an amphitheatre- or horse shoe-like hill.

The internal structure of a cinder cone is visible in several pits and quarries in the valley, exposing a crudely bedded air-fall deposit of dark grey to black, juvenile scoria and bombs (Fig. 12.32B). The majority of pyroclastic material is composed of unconsolidated, highly vesicular scoria, but also agglutinate layers comprising ejecta thrown out as molten lava fragments exist. Irregularly shaped blocks or spherical bombs, up to one metre in size and embedded in tephra, have often a frothy, vesicular rim around a more massive core, where sporadic phenocrysts may be seen (Fig. 12.32C). Instead, in small bombs a thin, glassy rim often surrounds the frothy, vesicular core. In places, cinder cones contain thin lava flows.

A variously thick layer of coarse ash or lapilli tephra covers the area around the cinder cones, representing the most fine-grained member of the Bufumbira pyroclastics. This well-bedded material also blankets the NW-trending hills in the valley. Most of these elongated hills have windows of Akanyaru-Ankolean metasediments (Fig. 12.32D). Contrary to juvenile ejecta in cinder cones of the area, fine-grained lapilli tephra contain also lithic fragments.

Boulder deposit (Qbd) – The ultra-potassic lavas that extruded from vents of the Sabinyo volcano are mostly covered by ‘boulder beds’. In preliminary work of Combe & Simmons (1933), lavas on the northern flank of Sabinyo are leucite basanites and andesites, here attributed to the Bufumbira Formation. Samples taken from *in situ* lava flows on the Rwandan side of the Sabinyo summit are silica-saturated K-trachytes or latites, which probably represent mixtures between K-basanitic mag-

ma and a silicic melt derived from the deep crust (Rogers et al. 1998).

Katwe-Kikorongo and Bunyaruguru volcanic fields

These volcanic fields comprise the crater fields of Katwe-Kikorongo and Bunyaruguru, located on both sides of the Kazinga Channel between Lake Edward and Lake George (Figs 12.23 and 12.33). Assigned here to the Bunyaruguru Formation of the Upper Albertine Group, this type area of kamafugites (Mg-rich, alkaline ultrapotassic volcanic rocks) comprises various types of pyroclastic deposits and minor lava flows, extruded from a large number of volcanic vents on the valley floor and from higher ground in the east. The cinder cones and water-filled crater lakes (‘maars’) with well-developed tuff rings, as well the volcanic structures found in the pyroclastic deposits, suggest a phreatomagmatic, explosive origin for these volatile-rich volcanics (e.g. Boven et al. 1998).

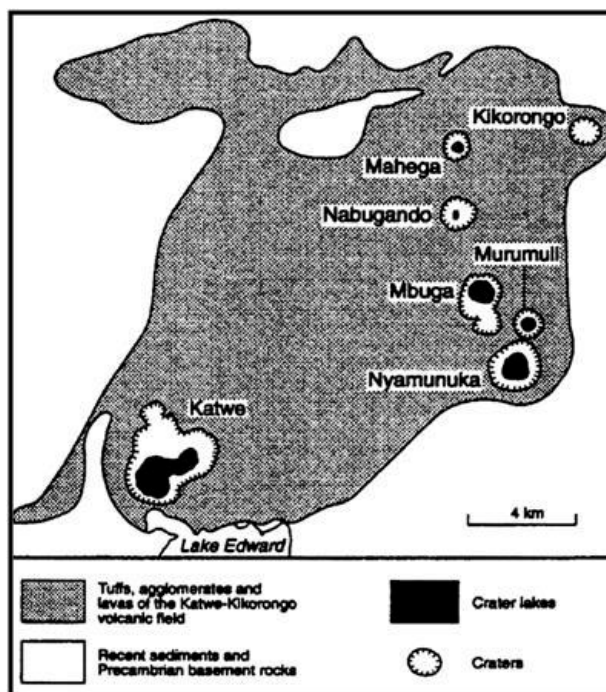


Fig. 12.33. Katwe-Kikorongo volcanic field (from Stoppa et al. 2000, reproduced from Mineralogical Magazine with kind permission of the Mineralogical Society of Great Britain & Ireland).

High-K volcanic rock, also carbonatite lava (QGpv) – High-K volcanics and carbonatite lavas are exposed in road cuts on the border of the Queen Elisabeth National Park in the Bunyaruguru crater field and in the Katwe-Kikorongo area, where also small occurrences of carbonatite lavas have

been described at the Mbuga and Mahega craters (Gittins 1966; Woolley 2001). Fine-grained carbonatite tuff with small-scale, tangential cross bedding in a base surge deposit is exposed in a road cut southeast of the Katwe Lake in the southern part of the Katwe-Kikorongo volcanic field (Fig. 12.34A). Phreatomagmatic pyroclastic deposits are also exposed in road cuts in the Bunyaruguru volcanic field, where the size and composition of ejecta in crudely to well-bedded tuffs varies from accidental lithic fragments up to 50 cm in size to small, mantle-derived xenocrysts and juvenile, pelletal lapilli (Figs 12.34B-D).

The isolated Katunga tuff cone, located south of the Buhweju Mountains, is associated with rare lava flows in the Bunyaruguru Formation. The water-filled Katunga crater is also the type locality for katungite, which is also the major component of ash, lapilli and bombs of the formation (Holmes & Harwood 1932). Additional lava types found in

the Bunyaruguru area are ugandite, a melanocratic olivine-rich leucitite, and mafurite, which differ from ugandite in having kalsilite instead of leucite (Higazy 1954).

Kamafugites are a group of rare silica-under-saturated volcanic rocks originally named after three petrographically-defined rock types: katungite (or olivine melilitite), mafurite (or kalsilite) and ugandite (or leucite or olivine basanite), all first described from the Albertine Rift of southwestern Uganda (Fig. 12.35; from Rosenthal et al. 2009). The rocks correspond to strongly potassic types of olivine melilitite to nephelinite in modern classifications, previously described as K-ankaratrite (= olivine nephelinite), leucite ankaratrite and melaleucitite by Bell & Powell (1969). The combination in these volcanic rocks of low SiO_2 (31.8–41.8 wt%), high MgO (up to 22.5 wt%), high K_2O (up to 7 wt%), low Al_2O_3 (< 8.0 wt%) and high CaO contents (up to 16.6 wt%) is expressed by the presence

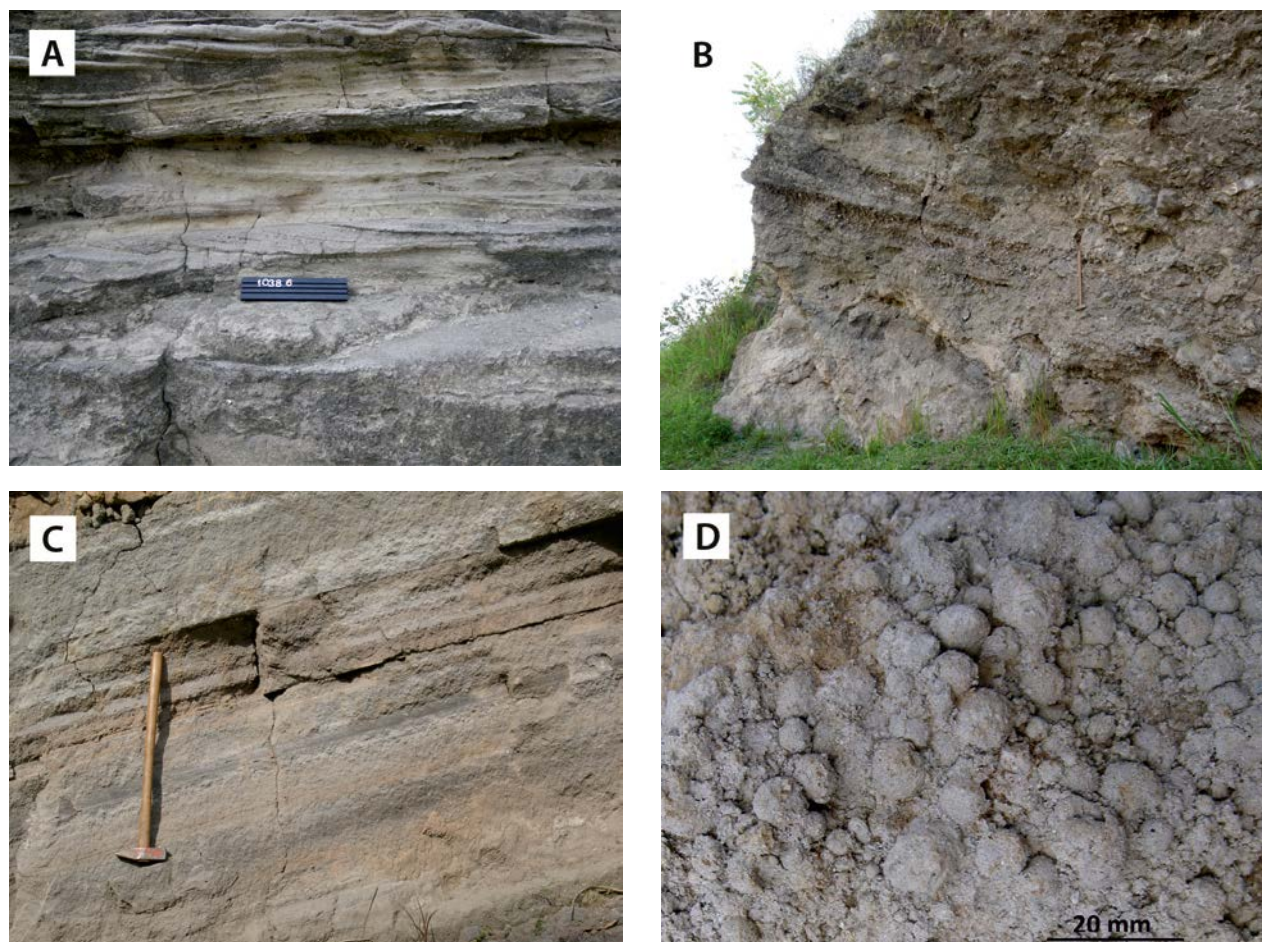


Fig. 12.34. Pyroclastic structures of the Bunyaruguru Formation. (A) Carbonatitic lapilli tuff with tangential cross bedding in base surge (152172E / -15253N). (B) Coarse pyroclastic breccia with large lithic blocks. (C) Regular bedding in a fine-grained lapilli tuff. (D) Detailed image of pelletal lapilli tuff (176168E / -28189N). Number tag 15 cm, hammer 60 cm.

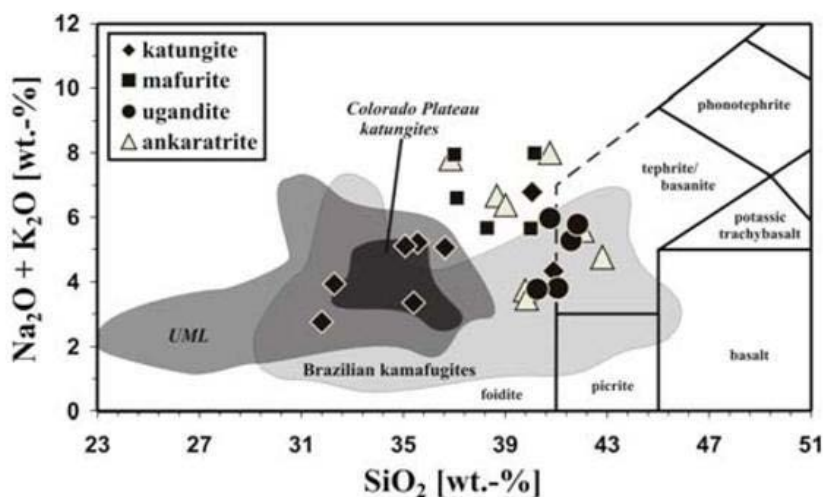


Fig. 12.35. Total alkali-silica classification diagram of kamafugites (solid symbols) and ankaratrites (open symbols) from the Albertine Rift (from Rosenthal et al. 2008).

of modal kalsilite, leucite, melilite and perovskite (Rosenthal et al. 2008). The absence of plagioclase distinguishes them from lava flows occurring in the rest of the Western Rift.

Carbonate-rich tuffs of Katwe-Kikorongo volcanic field – A group of carbonate-rich tuffs are described from the Murumuli crater (Fig. 12.36) of the Katwe-Kikorongo volcanic field, which contain abundant carbonatite pelletal lapilli, together with melilitite lapilli and a range of xenocrysts and lithic fragments including clinopyroxenites considered to be of mantle origin (Stoppa et al. 2000). The carbonatite lapilli consist essentially of Sr-bearing calcite and Mg-calcite which form quench-textured laths. The lapilli further contain micro-phenocrysts of Ti-magnetite, perovskite, apatite, clinopyroxene, sanidine and altered prisms of melilite. Stoppa et al. (2000) also described a dolomite carbonatite bomb, 7 cm in diameter, which displays a form typically for lava clots erupted in a molten state. Chemical analyses of tuff, bomb and a range of minerals suggested that carbonatite magma evolved from carbonate-bearing melilitite (Stoppa et al. 2000).

Xenoliths of the Katwe-Kikorongo and Bunyaruguru volcanic fields – Coexisting accidental and cognate xenoliths are commonly found in pyroclastic rocks of the Katwe-Kikorongo and Bunyaruguru volcanic fields (Holmes 1945). Accidental lithic fragments, derived from the pre-volcanic basement include granitoid, gneiss, amphibolite, quartzite, phyllite and shale, while xenoliths of up-

per mantle peridotite and nodules of phlogopite-rich alkali clinopyroxenite are often represented as cognate ejecta. These mainly consist of variable proportions of clinopyroxene, phlogopite, titanite, perovskite, apatite and titanomagnetite. Typically, orthopyroxene, garnet and olivine are lacking (Lloyd et al. 1996). Compared to normal peridotitic mantle, the clinopyroxenite nodules are on average strongly enriched in Ti, Al, Fe, Ca, K, P, Rb, Ba, Sr, Nb, La, Ce, Zr, F, Cl and H₂O (Lloyd et al. 1987). Based on petrographic, mineral and whole rock major and trace element analyses of pyroxene-rich nodules, Link et al. (2008) were able to distinguish at least two different episodes of mineral growth. The elder assemblage consists mainly of pale diopside-rich clinopyroxene with high Mg/Fe ratios and phlogopite. The younger paragenesis is made up of green diopside-rich clinopyroxene with significantly lower Mg#, titanite, perovskite, high-Ti phlogopite and apatite. They suggest that the younger paragenesis formed during a Ti-, Ca-, Fe- and trace element-rich metasomatic or magmatic event, which must be younger than the generation of the original diopside-rich assemblage and older than the volcanics from the eruption that brought the pyroxenite nodules to the surface.

Ti-bearing phlogopite-biotite is dominant in kamafugite-carbonatite effusives as xenocrysts or phenocrysts, as micro-phenocrysts and as groundmass mineral. The same mineral occurs as a major constituent in entrained alkali clinopyroxenite xenoliths. Significant differences in chemical composition can be observed between micas in different settings (Lloyd et al. 2002). Micas in xenocrysts in

kamafugites and carbonatites are aluminous (>12 wt% Al_2O_3), typically contain significant levels of Cr (up to 1.1 wt% Cr_2O_3) and are Ba-poor. In contrast, micas in micro-phenocrysts and in groundmass in feldspathoidal rocks having Al-poor compositions, are depleted in Cr and are generally enriched in Ba. In general, micas in xenocrysts occupy the Al_2O_3 and TiO_2 compositional field of the xenolith mica and, on the basis of the Mg content and high P, T experimental evidence, they probably crystallised at mantle pressures (Lloyd et al. 2002).

Cr contents in mica-bearing xenocrysts in these volcanic fields range from those in Cr-poor megacryst and MARID (mica–amphibole–rutile–ilmenite–diopside suite in kimberlites; Dawson & Smith 1977) phlogopite to higher values found in primary and metasomatic phlogopites in kimberlite-hosted peridotite xenoliths. Such Cr contents in mica manifest derivation from carbonate-bearing phlogopite-wehrlite and phlogopite-clinopyroxenite in the mantle. Mica-bearing olivine-melilitite xenocrysts are distinguished by higher Mg# and Cr contents than mica in clinopyroxenite xenoliths and mica in Katwe-Kikorongo mixed melilitite-carbonate tephra. Higher Al_2O_3 distinguishes Fort Portal carbonatite xenocrysts from other fields and some contain high Cr. It is suggested that the genesis of Katwe-Kikorongo olivine-melilitite and Fort Portal carbonatite involves a carbonate-bearing phlogopite-wehrlite source while the source of the mixed carbonatite-melilitite rocks may be carbonate-bearing phlogopite-clinopyroxenite (Lloyd et al. 2002).

Ndale-Fort Portal volcanic field

The Pleistocene volcanic field at Fort Portal, first described by Holmes & Harwood (1932) and Combe (1938), is characterised by high-Ca, low-alkali carbonatite volcanism. It contains ~50 vents composed of monogenetic carbonatite tuff cones rising to a maximum of 150 m above the general base level and defining two ENE-trending alignments, parallel to the grain of the Rwenzori Belt (Fig. 12.36). The cones are surrounded by friable lapilli or flaggy welded tuffs, covering an area of 142 km², and are far more voluminous than lava flows and dykes. A small flow of vesicular lava with scoria at the top, measuring 1–5 m in thickness, has extruded from a fissure at the west end of the northern belt near Makome and Nyakasura

School and probably formed by cementation of debris from lava fountains. Unlike the nearby Katwe-Kikorongo and Bunyaruguru volcanic field, xenoliths in carbonatite lava from the Ndale-Fort Portal volcanic field include garnet and hypersthene in granulite and eclogite rocks (von Knorring & Du Bois 1961, von Knorring 1967, Hornung 1969, Bell & Powell, 1969, 1970, Nixon & Hornung 1973, Barker & Nixon 1989, Hampton 1993), derived from Archaean and Palaeoproterozoic basement.

Lapilli tuff (Qnt), Lava (QFPl) and Lapilli tuff (QFpt) – Carbonatites of the Fort Portal area have been attributed to the *Ndale Formation* and the *Fort Portal Formation*, composed mostly of lapilli tuffs and tuffites. The landscape is a combination of tuff cones with craters, often forming lakes with fresh or salty water and flat blankets of melilitite tuff (Fig. 12.37). Vesicular carbonatite lava west of the Kalyango crater comprises a fine-grained groundmass composed of pyroxene, olivine, biotite, magnetite, apatite and calcite (Gittins 1966). Angular fragments of granite, gneiss and mantle rock (Eby et al. 2009), up to few metres in size, are common in tuff cones and tuff blankets. Fine-grained, pale grey, 5–20 cm thick tuff layers are quarried widely for construction material.

The far more voluminous pyroclastic deposits at Fort Portal include friable and flaggy welded tuffs and ‘tuff blisters’ (Nixon & Hornung 1973). They are mainly carbonatitic lapilli with a mineralogical composition identical to the lavas but with a higher proportion of crustal rock fragments. The remainder is a mosaic of microspar calcite and hydrous calcium silicates (Barker & Nixon 1989). Tuff ‘blisters’ are mounds of tuffaceous material, up to 1.5 m high and 10 cm to 6 m in diameter with an off-centre vertical tube from an underlying cavity to the surface of the deposit. They mark the site of hot springs where surges covered swampy ground.

Subsequent examination by Bailey et al. (2005) highlighted the presence of melilitites in these tuffs, previously unreported from Fort Portal. The rock is a mix of crust and mantle debris with near-isotropic lapilli, set in a matrix composed predominantly of carbonatite. The low birefringence parts of the lapilli are devitrified melilitite glass. Compound lapilli are abundant, containing aggregates of globules, together with xenolithic/ cristic fragments. Some contain concentric zones of more carbonate-rich material alternating with melilitites. Tangential phlogopite flakes mark the outer zones,

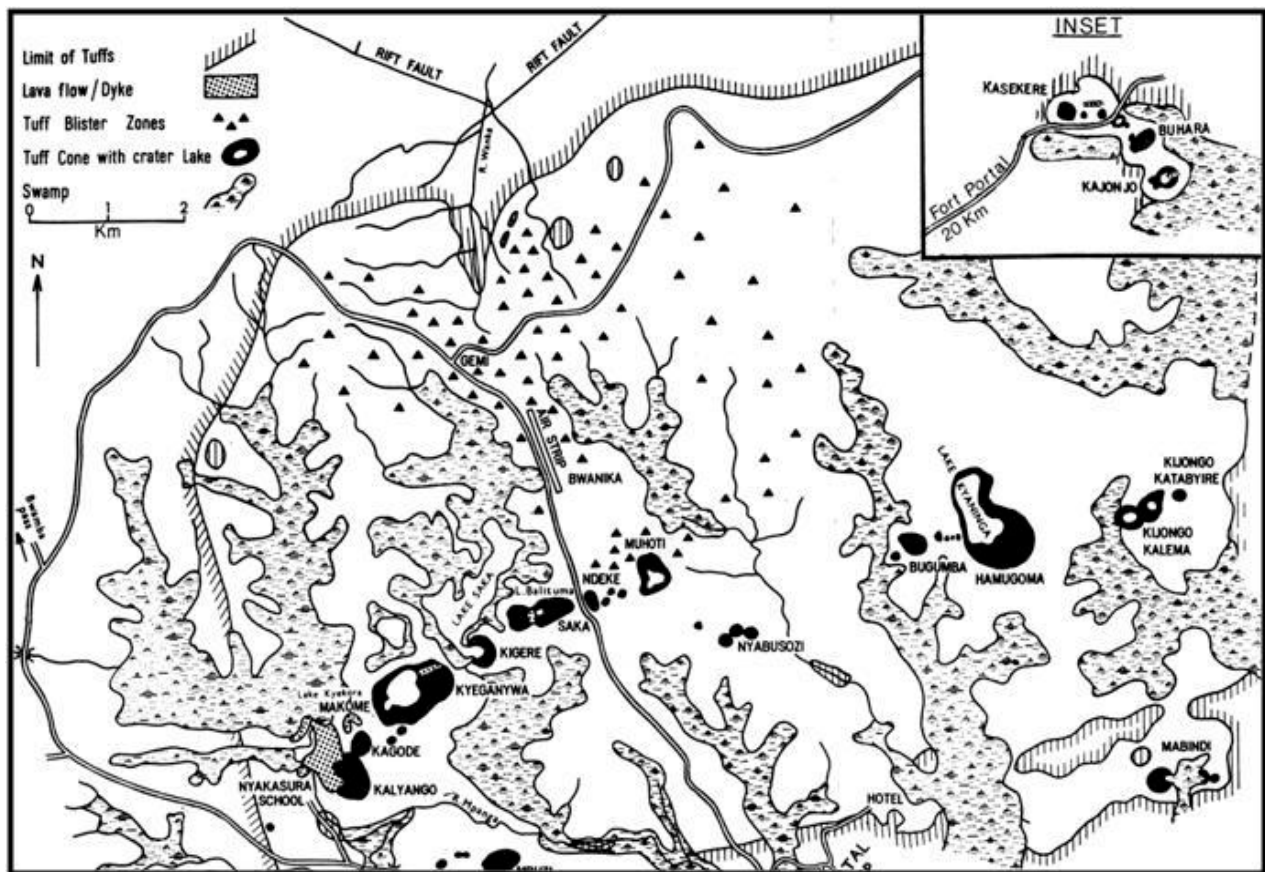


Fig. 12.36. The Fort Portal volcanic field between Fort Portal and Kasekere, western Uganda (from Nixon & Hornung 1973, with kind permission of H.S.M.O., London). Tuff cones, occasionally with crater lakes, are grouped in two ENE-WSW trending alignments. The cones are surrounded by a wide zone of friable lapilli and flaggy welded tuffs. Several thousand tuff mounds – tuff blisters – up to 1.5 m high dot the landscape in the Gemi area.



Fig. 12.37. Lake Myamugosani, one of crater lakes of the Ndale Formation.

in marked contrast to their planar distribution through the enclosing rock matrix. Euhedral titanomagnetite (10–15 vol%) is the most obvious cognate mineral (Bailey et al. 2005).

Devitrified melilitite contains abundant small crystals and microlites of melilite, apatite, magnetite and carbonates, mostly formed during disequilibrium quench crystallisation. Because of this, and the widespread presence of fine-grained debris fragments, a precise bulk melt composition is hard to establish, but is supposedly in average close to melilitite with a high P_2O_5 content. Mantle debris is largely composed of disaggregated magnetite-phlogopite-clinopyroxenite, which could give a bulk composition close to the melt. Low Mg and high Mg calcite are present in the melilitite lapilli, and in the enclosing carbonate-rich matrix. Previously, high Mg calcite was reported only as cement in lapilli tuffs, while the lavas contain only low Mg calcite in an assemblage of calcite-periclase (consistent with low pressure carbonate melt crystallisation) (Bailey et al. 2005).

Alkali-rich carbonatite lavas and pyroclastic deposits have been documented elsewhere in the EARS in East Africa and their formation has been generally attributed to replacement of magmatic alkali carbonates by calcite. Barker & Nixon (1989) claimed that at Fort Portal eruption of a $CaO-MgO-CO_2-SiO_2-P_2O_5-SO_2-H_2O-F$ liquid was not accompanied by that of a more silica-rich or alkali-rich liquid. Thus the alkali-poor volcanic carbonatites at Fort Portal were not formed by leaching of alkalis in meteoric water as demonstrated by the presence of tabular calcite, which is not pseudomorphous after alkali carbonates such as nyerereite². In brief, Barker & Nixon (1989) claimed that the Fort Portal magma was low in alkalis at the time of emplacement.

Bailey et al. (2005) postulated subsequently that carbonatite-melilitite magma left the mantle while carrying restite debris. Melt fragmentation took place in the deep crust, with rapidly quenched droplets enclosing crust debris. Chemical covariations of the flaggy tuffs are uniform and can be explained as carbonatite-melilitite plus a thoroughly mixed combination of crust and mantle debris. More recently, Barker (2007) questioned the truly magmatic, carbonatitic nature of the calcite cement in crystal tuffs from Fort Portal. The

cementing calcite has lower Sr and higher Mg concentrations, and higher $^{18}O/^{16}O$ but lower $^{13}C/^{12}C$, than magmatic calcite. Together with textural evidence, these chemical criteria are believed to indicate that the cementing calcite in these tuffs was precipitated as coatings on the pyroclastic fragments by meteoric water. Calcite-cemented tuff (whether it holds carbonatite or silicate lapilli) can contain as many as five texturally and chemically distinct kinds of carbonate, precipitated sequentially, and never in equilibrium with each other. Barker (2007) claims that secondary calcite in some occurrences supposedly formed by reaction of lime, calcined by hot silicate magma, from limestone wall rocks and stressed that pyroclastic deposits that contain calcite only in pore-filling cement or replacing silicates should not be called carbonatites.

Along the foothills of the Albertine rift shoulder and in the rift valley, terrestrial, fossiliferous, gastropod-bearing limestones appear. They are inter-layered with laterite horizons, indicating that the depositional environment changed repeatedly during its formation with periods of emergence followed by periods of subsidence possibly related to uplift of the rift shoulder, and/or down-warping of the rift floor. The limestone is mined at Hima and Dura for cement production.

12.3.4 Geodynamic setting of the EARS volcanics in Uganda

The volcanic rocks from the Elgon Depression differ markedly, both petrographically and geochemically, from those in the Albertine Rift, particularly in K and Rb abundances and K/Rb ratios (Bell & Doyle 1971, Barifaijo 2001). The volcanics of the Elgon Complex consist of alkaline sodic/carbonatitic ring complexes and pyroclastic deposits. Intrusive carbonatite and ijolite plugs and stocks are surrounded by fenite aureoles and do not carry upper mantle xenoliths. Volcanics are overwhelmingly (reworked) pyroclastic rocks: agglomerates, lapilli and tuffs of nephelinitic, ijolitic, phonolitic and olivine basaltic composition. Most volcanic products were emplaced in the period 25–17 Ma (King 1978).

Volcanics of the Albertine Rift belong to three different suites, i.e., lavas from the Kivu Group

² Nyerereite is a very rare sodium calcium carbonate mineral with formula $Na_2Ca(CO_3)_2$.

consisting of (1) (Oligocene-)Miocene (28.0 ± 1.4 Ma to 10.7 ± 0.7 Ma) tholeiitic, transitional and alkali basalts, overlain by (2) a suite of Miocene (12.6 ± 0.7 Ma to 8.9 ± 0.5 Ma) basanites, hawaiites, mugearites and benmoreites (Auchapt et al. 1987, Marcelot et al. 1985, Pasteels et al. 1989, Kampunzu et al. 1998) and, after a lull of several million years, by (3) extremely silica-undersaturated, potassic to ultrapotassic to carbonatitic agglomerates and tuffs of basanitic, leucititic and kamafugitic composition of late Pliocene-Present age ($<2.6 \pm 0.1$ Ma) (Bell & Powell 1969, Demant et al. 1994, de Mulder et al. 1986, Rogers et al. 1992) of the Bufumbira-Fort Portal volcanic fields. They include carbonatites and leucite- and kalsilite-bearing lavas characterised by high incompatible elements and high volatile contents (Bell & Powell 1969, Sahama 1960, 1962, 1973) and mantle xenoliths are common. How to explain these chemical and petrographic differences between the volcanic rocks of the Elgon Depression and Albertine Rift, between volcanism within a single rift and even between flows in a single volcano? Several models have been proposed, focusing on different mechanisms, including (1) differences in source rock from which the magmas formed, (2) possibly in combination with mixing of magmas, (3) strong variations in the amount of crustal contamination or (4) different fractionation paths, or a combination of the above.

Bell & Powell (1969) favoured magma mixing as dominant mechanism. They studied strontium isotopes from the Virunga volcanic field and reported significant differences with feldspar-bearing lavas having higher $\text{Sr}^{87}/\text{Sr}^{86}$ ratios (average = 0.707) than melilite- and nepheline-bearing varieties (average = 0.705). The $\text{Sr}^{87}/\text{Sr}^{86}$ ratios show a highly significant, positive, linear correlation with Rb/Sr ratios, and a negative correlation with Sr, Nb, and Zr abundances. Hypotheses involving simple fractional crystallisation or limestone syntexis are inconsistent with the isotopic data. The elemental and isotopic abundance patterns are most easily explained by the mixing of two end members of quite different Sr isotopic and chemical compositions. If mixing is assumed, approximate limits can be set for the compositions of the two magma end members. These limits are consistent with the hy-

pothesis of assimilation of sialic material by either a carbonatitic or nephelinitic parent magma.

Based on analyses of major and trace elements and Sr and Nd isotopic compositions, de Mulder et al. (1986) fine tuned the magma mixing hypothesis of Bell & Powell (1969). They assumed the presence of two parental magmas: a first one represented by ankaramitic and picritic K-basanites, a second one represented by K-basanite from which the Karisimbi 'main suite', comprising a complete K-basanite to K-trachyte differentiation series, was derived. The isotopic variability of the primitive magmas suggests that the mantle beneath the Karisimbi stratovolcano is heterogeneous on a rather small scale³. Evolution of the Karisimbi 'main suite' was dominated by concurrent low-pressure fractionation and assimilation. Crustal contamination resulted in an increase in $\text{Sr}^{87}/\text{Sr}^{86}$ (0.70539–0.70799) and a decrease in $\text{Nd}^{143}/\text{Nd}^{144}$ (0.51270–0.51234) with increasing fractionation. Potential lower-crustal contaminants include charnockitic and granulitic rocks outcropping in Uganda (e.g. Uleppi and Karuma Complexes). Major-element mass-balance calculations and calculated assimilation-fractional crystallisation (AFC) paths in the $\epsilon_{\text{Sr}}-\epsilon_{\text{Nd}}$ diagram show that most of the data of the 'main suite' are in good agreement with interaction of a basanitic liquid with the proposed crustal components.

Ferguson & Caundari (1975) advocated fractionation as major mechanism for differentiation. They found that basanite lavas from the Virunga volcanic field showed two different fractionation trends. One differentiates through phonolitic tephrites \rightarrow trachyte and the other fractionates through leucitites \rightarrow phonolite. They discussed the low-pressure fractionation controls of both series in terms of coexisting phases and ultramafic inclusions observed in the lavas. Equilibrium fusion of a mantle phlogopite-bearing peridotite combined with subsequent fractionation was considered the dominant petrogenetic process to produce a potash-rich basanite liquid, which is considered a likely parent of the Bufumbira lavas.

Alternatively, Sahama (1973) explained pronounced differences in magma chemistry by differences in contamination by crustal rocks, even for nearby volcanic rocks. He considered the fairly extreme composition of the Nyiragongo magma to

3 Given that this heterogeneity is also reflected by Kibaran granitoids in the area (Chapter 8), we conclude that heterogeneity is not restricted to sub-lithospheric upper mantle but also applies to the pre-Kibaran lower crust.

be of mantle origin without significant crustal contamination. The nearby Nyamuragira lavas, on the other hand, are interpreted as a result of local and strong crustal contamination with transfer and enrichment of mainly alkalis and passive depletion of silica.

Kampunzu et al. (1998) related the petrological and chemical composition of rift volcanics to different stages in rift development, claiming that individual rift segments in the Western Rift developed independently and diachronously with an overall north to south axial propagation. Each rift segment generally followed a similar geodynamic sequence of:

- (1a) extrusion of tholeiitic and/or transitional basalts, which predate the initiation of subsidence and mark initial faulting associated with lithospheric extension in each individual rift segment;
- (1b) transition from continental tholeiites and associated transitional basalts to Na alkaline lavas, coinciding with the initial onset of continental rifting subsidence;
- (1c) Na alkaline lavas are generally relayed by a new sequence of transitional basalts during continued down-warping and tilting along intra-basinal faults in more evolved continental rifts (Kampunzu et al. 1984b);
- (2) ultra-potassic, strongly alkaline lavas and sometimes extrusive carbonatites which are clearly younger, which mark the development of major transverse fracture zones.

Kampunzu et al. (1998) thus related emplacement of volcanics during episodes (1a), (1b) and (1c) to pre-rift extension, rift initiation and rift development, respectively, while the ultrapotassic, strongly alkaline Bufumbira-Fort Portal volcanics and occasional extrusive carbonatites of episode (2) are related to major transverse fracture zones within the Albertine Rift. The presence of such transverse fractures is supported by the WSW–ENE ‘Rwenzori’ orientation of craters or volcanoes in the various volcanic fields (Figs 12.24; 12.39) (Reece 1955, Lloyd et al. 1991).

Link et al. (2007) have conducted a thorough geochemical study in the Katwe-Kikorongo-Bunyaruguru volcanic field, including major and trace elements and analyses of Rb-Sr, Sm-Nd, Lu-Hf and Re-Os isotope systems. They concluded that, unlike lavas from volcanic fields further south in

the Western Rift, the effects of fractionation on the kamafugitic lavas are minor. Primitive features such as high Mg# olivines (up to 91.1), high whole-rock Mg# (up to 80.2), and high Ni (up to 1066ppm), Cr (up to 1560ppm) and Os (up to 1.45ppb) are in strong contrast to their extreme enrichment in incompatible trace elements. Sr and Nd isotopes form a cluster and are slightly enriched relative to Bulk Earth values ($^{87}\text{Sr}/^{86}\text{Sr} = 0.704599 - 0.705402$; $^{143}\text{Nd}/^{144}\text{Nd} = 0.512394 - 0.512575$). Hf ($^{176}\text{Hf}/^{177}\text{Hf} = 0.282508 - 0.282864$) and Nd isotopes show a linear trend sub-parallel to, but below that of, the mantle array. Osmium isotope ratios are super-chondritic and variable ($^{187}\text{Os}/^{188}\text{Os} = 0.14755 - 0.49735$). Hence, Link et al. (2007) explained these geochemical features by formation of kamafugitic magmas by re-melting of a variably, and episodically enriched veined lithospheric mantle characterised by highly variable supra-chondritic radiogenic Os. Impregnation of the source region by highly alkaline melts resulted in the introduction of modal phlogopite and enrichment in Fe and Re. Curved mixing lines on Hf-Nd and Sr-Os isotope plots can be explained by mixing of peridotite and pyroxenite source components. The involvement of large amounts of pyroxenite is also favoured by plots of Os concentrations against Ni and MgO.

Xenoliths in Albertine volcanics have also been investigated thoroughly, hoping that they could provide important information not only for understanding the generation of ultra-potassic lavas but also for understanding the sub-continental lithospheric mantle beneath the rift as part of a complex continental rift process. The chemistry of alkali pyroxenite xenoliths from the three Albertine volcanic fields, composed largely of clinopyroxene and phlogopite-biotite (together >70 vol% of mode) confirm compositional variation of the SCLM (Lloyd et al. 1999). Inter-field compositional variation in these minerals indicates bulk-chemical lateral variation in the xenolith source. The abundance of alkali clinopyroxenite xenoliths in all three fields suggests this lithology is widespread beneath the Albertine Rift.

Xenolith genesis and their connection to their unusual kamafugitic host lavas have also been debated at length (Link et al. 2008). In earlier studies the pyroxenite nodules were considered either as xenoliths from the thoroughly metasomatised peridotite mantle (Lloyd et al. 1987) or, alternatively, they were viewed as having formed as a

distinct paragenesis occurring as veins within the peridotitic mantle (Irving 1980). In both cases the xenoliths were supposed to represent mantle material that was at least partly involved as source for the kamafugite melts. As a third alternative it was advocated that the xenoliths represented cumulates of the kamafugitic lavas. Nd-Sm and Pb isotope systematics indicated, however, that the xenoliths are not cumulates from their host kamafugites. P-T experiments demonstrated that kamafugites were in equilibrium with clinopyroxenite at $\sim >60$ km depth. Lloyd et al. (1999) concluded therefore that the xenoliths are fragments of a laterally variable clinopyroxenite layer in Uganda's Western Rift deep mantle.

Ramananda et al. (2009) deemed that the heterogeneity of the Albertine volcanic rocks was not only due to the heterogeneity of the SCLM but also due to differences in depth of magma generation and the amount of partial melting. They reported a wealth of isotopic and geochemical data from the Nyiragongo and Nyamuragira volcanics. In summary, they concluded that the Nyiragongo lavas are bulk silicate Earth-like in Nd and Sr-isotopes and Group I kimberlite-like in their Pb-isotopes. Their high Ce/Pb ratio and low SiO₂ content rule out continental lithospheric sources, particularly in conjunction with the available isotopic data. From their combined geochemical data, in combination with available experimental petrological data on melting of mantle rocks of peridotitic compositions, they suggested that Nyiragongo lavas formed at greater depths by a low degree of partial melting of garnet, clinopyroxene and phlogopite-bearing carbonated mantle. The Nyamuragira lavas, on the other hand, are thought to be products of a larger degree of partial melting at comparatively shallower mantle depths with a recycled crustal component. They further postulated that coeval volcanism in the adjacent Nyiragongo and Nyamuragira, with magmas originating from different depths, requires the presence of a heterogeneous mantle plume beneath the Tanzanian Craton. This plume caused chemically distinctive volcanic provinces around the Tanzanian Cra-

ton, in the Western and Eastern or Main Rift (Fig. 13.58).

The data indicate that the sub-continental lithospheric mantle (SCLM) below this part of Uganda has undergone strong but variable degrees of metasomatism. An understanding of the character of the primary magmas in the different volcanic fields requires consideration of both the degree of metasomatism and the degree of melting of the garnet-bearing source rock (Furman & Graham 1999, Eby et al. 2003). The lavas thus represent a magmatic sampling of variations in the underlying sub-continental lithospheric mantle, which contains minor amphibole and phlogopite, probably due to widespread and repeated metasomatic events between 2100 and 500 Ma. Enrichment of the peridotitic mantle in carbonate and silicate melts at 4–6 GPa (or 40–60 kb) occurs also in other areas, where geochemically similar ultramafic lamprophyres are formed (Rosenthal et al. 2009). The Ugandan kamafugites thus represent the earliest and deepest-derived magmas in a rift through thick continental lithosphere beneath the continuous proto-Congo Craton. The Ugandan rift-related mantle enrichment is thus far older than the earliest known tectonic surface expression of the rift (Rosenthal et al. 2009).

Finally and rounding off this discussion, Link et al. (2011b) asserted recently that the potassic characteristics of the Albertine lavas and their xenoliths require source depths greater than 130 km, also suggesting the presence of a preserved cratonic lithospheric root. At depths less than 80 km Na and K are contained in Ca-amphiboles within the peridotite, which would give rise to Na-dominated nephelinitic to basanitic primary melts instead of potassium rich ones (Green 1973) as can be observed in volcanic fields in the Western Rift located south of the Ugandan K-rich lavas. According to Link et al. (2011b) this indicates that the thickness of the lithospheric mantle decreases southward by at least 60 km over a distance of less than 250 km. They therefore suggested that the northern tip of the Western Rift of the EARS, i.e., the Albertine Rift, is propagating into a craton.

12.4 Quaternary deposits outside the EARS

12.4.1 Introduction

It is widely accepted that prior to development of the Western Rift, drainage in Uganda was general-

ly in a westward direction (Figs. 12.2 and 12.3). This is shown by all major rivers, such as the Kagera, Katonga and Kafu with their west-pointing barbed arrow pattern of main stream and tributaries. The

currently ENE flowing Kafu River is no exception. It once flowed in a westward direction, following, after passing the present watershed, the Nkusi River, with which it forms a continuous through-valley system.

As mentioned in Section 12.3.1, development of the EARS caused uplift along the rift shoulders of the eastern and western branches of the EARS and sagging of the crust in between. This process resulted in a re-arrangement of the drainage system, drowning of fluvial valleys, including the formation of the relatively shallow Kyoga and Victoria Lakes. A fluvial divide developed parallel to and some 25 to 40 km east of the Western Rift. As a consequence, discontinuous Pleistocene alluvial, paralic and lacustrine deposits have been deposited. These underlie recent alluvial and swamp deposits of Holocene age. The latter are presented as “surficial deposits” in the 1:1 million -scale geological map of Lehto et al. (2014).

12.4.2 Stratigraphy of Pleistocene and Holocene Deposits

Pleistocene sediments comprise lake deposits, previously known as ‘Lake Victoria Strandline Series’, the ‘Nsongezi Series’ and other raised beach-level deposits in the Lake Wamala and Lake Kyoga areas.

Lake Victoria strandline deposits – Discontinuous deposits of beach sands and gravels, with finer grained silts and clays, representing off-shore and

swamp deposits, are exposed along the western and northern shores of Lake Victoria and around Lake Wamala. Individual occurrences of these palaeo-shoreline deposits have been described by various authors (Wayland 1929, Solomon 1939, Marshall 1954, Bishop 1956, 1958a, Temple 1963, 1964, 1966a, 1966b) and include ‘pea’-sized gravel deposits near Kigungu Hill (Entebbe peninsula) and near Kajansi (halfway between Entebbe and Kampala) and surroundings up to 45 m above the present lake level (Palister 1959). Most lake deposits are of arenaceous composition and occur along the shore line till some 5 m above the lake’s present water level. Marshall (1954) identified benches at 8, 16, 27, 65 and 83 m, but found only direct evidence of lake levels in the form of sand and gravel deposits at the lowest three.

Bishop (1969) assembled these widespread Pleistocene deposits as ‘Lake Victoria Strandline Series’. They are inconspicuous in the field but well visible as curvi-linear features in Satellite imagery (Fig. 12.38). The absence of exposures or other special features is remedied by the presence of characteristically grey-coloured termite hills. Johnson (1960) related these deposits to Lake Nyanza, the more extensive Plio-Pleistocene predecessor of the present Victoria Lake, believed to manifest a more pluvial period. We relate the higher lake levels to rift tectonics (rift shoulder uplift, sagging and warping between the rift arms) and temporary flooding of drainage channels, till new outlets had been formed.



Fig. 12.38. Satellite image showing curvi-linear features along shore of Lake Victoria, north of Sango Bay at the boundary between the Masaka and Rakai Districts, interpreted as palaeo-shore lines or lake terraces.

Nsongezi deposits – Previously named ‘Nsongezi Series’ (Bishop 1969), these are characteristic Pleistocene fluvio-lacustrine deposits found in the Tanzanian section of the Akagera River and in Ugandan tributaries near Lakes Nakivali and Kachera. They were named after Nsongezi village in southern Ankole, where Acheulian hand axes have been discovered in 1930. Due to warping, the deposits occur at about 135 m above the present Lake Victoria level. They are not considered to represent true river terraces, but are correlated with the ‘Lake Victoria Strandline Series’ (Bishop 1969). In the type area the sediments are estuarine or fluvio-lacustrine deposits that grade eastwards into a still-water lacustrine facies with diatomites.

Raised beach deposits in the Lake Kyoga area – Lake Kyoga is the best example of a flooded valley system in Uganda. The drainage pattern confirms the generally westward direction of major rivers and tributaries in Uganda, including the

northward flowing segment of the Victoria Nile that was once part of the (south)westward flowing Kafu River.

Bishop (1969) suggested that the 3500 feet contour line (~1067 m.a.s.l.) marks the former extent of Lake Kyoga (Fig. 12.39). This suggestion is confirmed by field observations and the interpretation of soil, geomorphological and radiometric data. The raised lake deposits correspond with flat, featureless terrains, covered by blue-grey ‘soils’. Exposures of basement rocks in such areas are invariably missing. Blue-grey termite hills indicate that these sediments have significant thicknesses above the water table. In places, where the Pleistocene lake sediments have been washed away, thick laterite is exposed, which coincides with pronounced vegetation anomalies (Fig. 10.13).

Bishop (1969) has attempted to model deposition of Pleistocene sediments of the Victoria and Kyoga Lakes in function of uplift of the eastern Albertine Rift shoulder as follows:

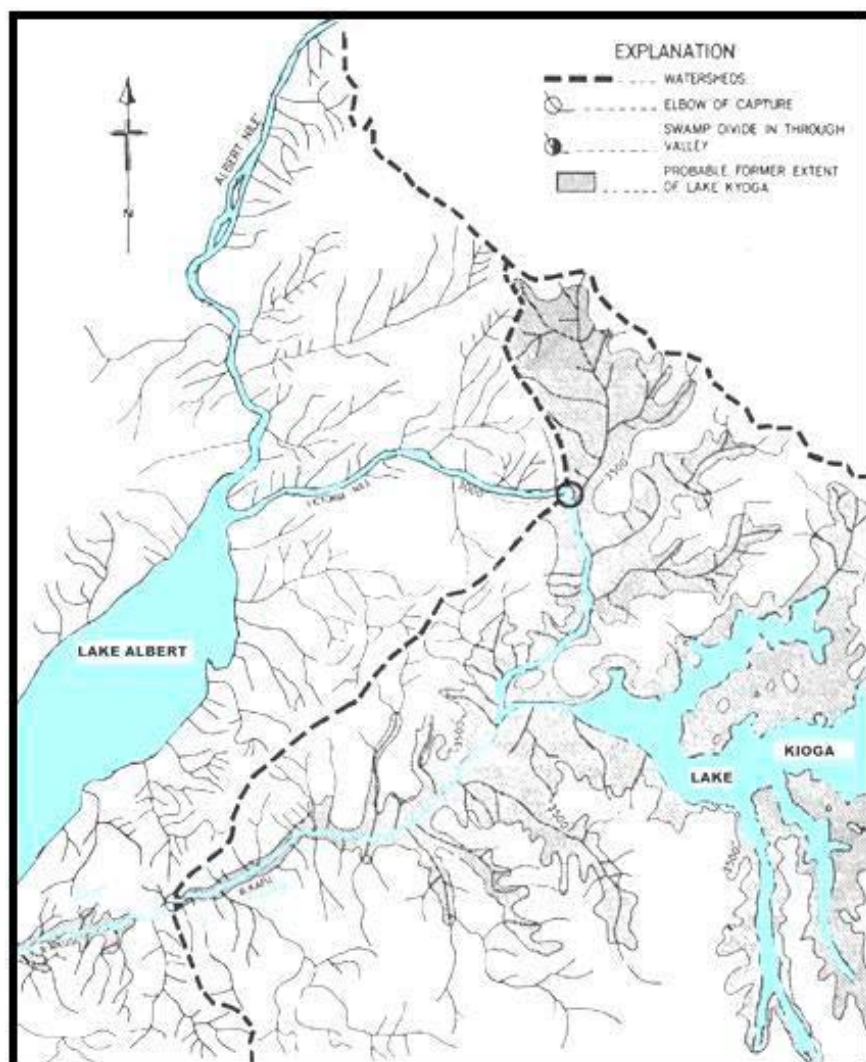


Fig. 12.39. Drainage pattern near the western outlet of Lake Kioga (Kyoga) showing watershed between different drainage basins (dashed line). It is suggested that the northward flowing segment of the Victoria Nile was once part of the Kafu River. Bishop (1969) suggested that the 3500 feet contour line (~1067 m above sea level) marks the former extent of Lake Kyoga (from Bishop 1969).

(1) *Pre-uplift* – Early Pleistocene basal boulder beds (e.g. ‘Nsongezi Series’) and ‘high terraces’ deposited by westerly-flowing Kagera, Katonga and Kafu Rivers.

(2) *Westerly uplift and eventual reversal of Kagera River* – Reversal and ponding of both Kagera and Katonga headwaters. Amalgamation of the Kagera and Katonga bays to form a larger proto-Lake Victoria (Lake Nyanza) with long inlets to the west in the Kagera and Katonga Rivers (Fig. 12.2). Possibly continued outflow from Lake Victoria via the site of the present Katonga swamp divide (base of sediment on bed rock at present at +60m). Deposition of middle part of ‘Nsongezi Series’ from mid-Pleistocene to beginning of Late Pleistocene (on the basis of Palaeolithic assemblages). Palaeo-shore lines have been mapped in the Lake Wamala Map Sheet (no. 69), which had an open connection with Lake Victoria (Fig. 12.2). The palaeo-shore lines at Lake Wamala (1134 m.a.s.l.) are more than 60 m above the present water level of Lake Victoria.

(3) *Renewed (or continued) uplift in the west* – With continuing uplift deposition of Late Pleistocene (30,000 to 27,000 B.P.) upper ‘Nsongezi Series’ swamp clay and finally stranded as Kafunzo flat. Reversal of Katonga and Kafu Rivers. Closure of the Katonga outlet to the west.

(4) *Continued uplift in the west* – Stability. Jinja outlet at Bujagali Falls established for Lake Victoria. Formation of +20 m, +13–15 m and +3–4 m strandlines with progressive incision of the Jinja outlet at Bujagali Falls during time span of ~20,000 years. Lowest strand line is dated at 3,720 years B.P. With addition of Jinja outflow to Kyoga system the overspill into the lower Victoria Nile and the Murchison Falls, etc., were probably initiated. The same line of reasoning can be applied to Lake Kyoga, where outlets for the Victoria Nile have been created at Karuma and Murchison Falls.

ACKNOWLEDGEMENTS

The geological synthesis of Uganda discussed in this paper is based on the work of many geoscientists, connected either to the GTK Consortium or to the Department of Geological Survey and Mines (DGSM) in Uganda. The GTK Consortium comprised the following partners: GAF AG from Germany, Council for Geoscience (CGS) from South Africa, Faculty of Geoinformation and Earth Observation of the University of Twente (ITC) from the Netherlands and Fels Consultants Ltd. (FCL) from Uganda. The authors are grateful to Gerrit de Kock, Nick Baglow, Geoffry Grantham, Andreas Schumann, Steven Boger and Tilman Jenett, who participated in the GTK Consortium field mapping. David Kyagulanyi, Dominique Elepu, Aaloni Waluganja and Wilson Ongom (FCL) provided local expertise. DGSM geologists attending the field mapping were also many: Zachary Baguma, James Natukunda, Annet Tumwine, Edward Marimira, Richard Kiggwe, Catherine Nyaketcho, Fred Kigereigu, Isa Lugaizi, Annet Nambojera, Peter Maweje, Martin Ekiryagana, Paul Lugoko, Henry Ngada, Vincent Kedi, Molly Bakka Male and Henry Luwemba Kasule. Each and everyone are thanked for their contribution. Discussions in the field with geoscientists Frik Hartzler, Robert Macdonald, Tapio Kuivasaari, Niilo Kärkkäinen, Jukka Konnunaho, Janne Kuusela and Tapio Ruotoismäki were very fruitful. Raili Aumo is thanked for asking the permissions to reprint a number of figures by other authors.

The results of the mapping have been reported in 11 map sheet explanation volumes and as 19 maps at scale 1:250 000, 73 maps at scale 1:100 000 and 52 maps at scale 1:50 000 and summarised in one volume: "Summary report on the geological

and geodynamic development of Uganda" by Phil Westerhof, which formed the base for the manuscript of the present paper. The original products are available at DGSM, Entebbe, Uganda since October 2012.

The authors of this publication are very grateful for the many reviewers who took their time and scrutinised the various chapters of the volume:

- Summary: Kirsti Loukola-Ruskeeniemi
- Chapter 1: Colin Reeves, Andreas Schumann, Sayab Muhammad
- Chapter 2: Asko Käpyaho
- Chapter 3: Jukka Konnunaho
- Chapter 4: Asko Konttinen
- Chapter 5: Esa Heilimo
- Chapter 6: Tuomo Karinen
- Chapter 7: Toni Eerola
- Chapter 8: Markus Vaarma
- Chapter 9: Mohammed Sayab
- Chapter 10: Pekka Sipilä
- Chapter 11: Mikko Nironen, Pentti Hölttä
- Chapter 12: Saku Vuori

The English language was proofread by Roy Siddal and Graeme Waller. Technical editors of the present volume were Pirkko Surakka and Elvi Turtiainen.

The accompanying geological map at scale 1:1 million was compiled by the staff of Geological Survey of Finland, supported by DGSM geologists. It is mainly based on the 1:250 000 scale geological maps produced by GTK Consortium. GIS processing of the map was done by Eira Kuosmanen and Petri Virransalo and was reviewed by Jouni Luukas who is thanked for his valuable comments.

REFERENCES

- Aanyu, K. & Köhn, D. 2010.** Modeling fault kinematics, segment interaction and transfer zone geometry as a function of pre-existing fabrics: the Albertine rift, East African Rift System. *Geophysical Research Abstracts*, Vol 12, EGU2010-9405.
- Aanyu, K. & Köhn, D. 2011.** Influence of pre-existing fabrics on fault kinematics and rift geometry of interacting segments: Analogue models based on the Albertine Rift (Uganda), Western Branch-East African Rift System. *J. Afr. Earth Sci.* 59 (2–3), 168–184.
- Abdelsalam, M. G., Liégeois, J.-P. & Stern, R. J. 2002.** The Sahara Metacraton. *J. Afr. Earth Sci.* 34, 119–136.
- Abdelsalam, M. G., Abdel-Rahman, M., El-Faki, E.-F. M., Al-Hur, B., El-Bashier, F.-R. M., Stern, R. J. & Thurmond, A. K. 2003.** Neoproterozoic deformation in the northeastern part of the Saharan Metacraton, northern Sudan. *Precambrian Res.* 123, 203–221.
- Abdelsalam, M. G., Gao, S. S. & Liégeois, J.-P. 2011.** Upper mantle structure of the Saharan Metacraton. *J. Afr. Earth Sci.* 60 (5), 328–336.
- Abein mugisha, D. 2004.** Report on the structural remapping of the Kaiso-Tonya area. Petroleum Exploration and Production Department, Unpubl. Rept.
- Abein mugisha, D. 2006.** New concepts on the tectonic evolution of the Albertine Graben, East African Rift System. 21st Coll. Afr. Geol. (CAG21), 3–5 July 2006, Maputo, Abstract Volume, 4–6.
- Abein mugisha, D. 2007a.** Current understanding of the tectonic setting of the Albertine Graben, East Africa Rift System. Intern. Conf. East Africa Rift System (EARS-07), Abstract Volume 23–25 July 2007, Kampala, 28–31.
- Abein mugisha, D. 2007b.** New concepts in the tectonic understanding of the Albertine Graben and their implications for hydrocarbon prospectively, Proceedings 3rd East African Petroleum Conference.
- Abein mugisha, D. & Echegu, S. 2004.** Report on the structural mapping and geochemical sampling of the Kaiso-Tonya area, Petroleum Exploration and Production Department, Unpubl. Rept.
- Abein mugisha, D. & Mugisha, F. 2004.** Structural analysis of the Albertine graben, Western Uganda. East African Rift System Evolution, Resources, and Environment Conference, June 2004, Addis Ababa, Abstract.
- Abein mugisha, D. & Ochan, K. 2004.** Report on the structural mapping in Kibiro - Butiaba area, EA 2. Petroleum Exploration and Production Department, Unpublished report.
- Akimanizanye, E. & Banyanga, S. 1984.** Esquisse géophysique et géologique de la région de Kinyami, Préfecture de Byumba. Projet Prospection Géophysique, Coopération Canado-Rwandaise, Rapt. d'étape 12, Kigali, Août 1984. 33 p.
- Alene, M. & Barker, A. J. 1993.** Tectonometamorphic evolution of the Moyale region, southern Ethiopia. *Precamb. Res.* 62 (3), 271–283.
- Almond, D. C. 1962a.** Explanation of the geology of Sheet 15 (Kitgum). *Geol. Surv. Uganda, Entebbe*, Rept. 8. 55p.
- Almond, D. C. 1962b.** Explanation of the Geology of Sheet 10 (Kaaböng). *Geol. Surv. Uganda, Entebbe*. Rept. 8.
- Almond, D. C. 1969.** Structure and metamorphism of the Basement Complex of north-east Uganda. *Overseas Geol. Miner. Resour.* 10, 146–163.
- Al-Shanti, A. M. S. & Mitchell, A. H. G. 1976.** Late Precambrian subduction and collision in the Al Amar-Idsas region, Arabian Shield, Kingdom of Saudi Arabia. *Tectonophysics* 30, T41–T47.
- Andersen, L. S. & Unrug, R. 1984.** Geodynamic evolution of the Bangweulu block, northern Zambia. *Precamb. Res.* 25, 187–212.
- Andrews-Speed, C. P. 1989.** The Mid-Proterozoic Mporokoso Basin, Northern Zambia: Sequence Stratigraphy, Tectonic Setting and Potential for Gold and Uranium Mineralisation. *Precamb. Res.* 44, 1–17.
- Aoki, K., Yoshida, T., Yusa, K. & Nakamura, Y. 1985.** Petrology and geochemistry of the Nyamuragira volcano, Zaire. *J. Volcanology and Geothermal Research* 25 (1–2), 1–28.
- Appel, P., Möller, A. & Schenk, V. 1998.** High-pressure granulite facies metamorphism in the Pan-African belt of eastern Tanzania: P–T–t evidence against granulite formation by continent collision. *J. Metam. Geol.* 16 (4), p. 491.
- Appel, P., Schenk, V. & Schumann, A. 2004.** P-T path and metamorphic ages of pelitic schists at Murchison Falls, NW Uganda: Evidence for a Pan-African tectono-metamorphic event in the Congo Craton. 20th Coll. Afr. Geol. (CAG20), 2–7 June 2004, Orléans, Abstract, p. 49.
- Appel, P., Schenk, V. & Schumann, A. 2005.** P-T path and metamorphic ages of pelitic schists at Murchison Falls, NW Uganda: Evidence for a Pan-African tectono-metamorphic event in the Congo Craton. *Eur. J. Mineral.* 17, 655–664.
- Auchapt, A., Dupuy, C., Dostal, J. & Kanika, M. 1987.** Geochemistry and petrogenesis of rift-related volcanic rocks from South Kivu (Zaire). *J. Volcanology Geothermal Res.* 31, 33–46.
- Bailey, A. I. 1969.** Report on the geology of the Watamagufu-Bugoye area of the Ruwenzori Mountains. 13th Ann. Rept. Inst. Afr. Geol. Univ. Leeds, 13–14.
- Bailey, K., Lloyd, F., Kearns, S., Stoppa, F., Eby, N. & Woolley, A. 2005.** Melilitite at Fort Portal, Uganda: Another dimension to the carbonate volcanism. *Lithos* 85, 15–25.
- Baldock, J. W., Clark, L. & Reedman, A. J. 1964.** Report on the geology of sheet 25/IV. Unpubl. Rept. Geol. Surv. Mines Dept, Entebbe.
- Baldock, J. W., Clark, L., Reedman, A. J. & Wren, A. E. 1969.** Explanation of the geology of sheet 25 (Labwor Hills). *Geol. Surv. Mines Dept, Rept.* 14, Entebbe. 37p.
- Bancroft, H. 1932.** A fossil cyatheoid stem from Mount Elgon, East Africa, *The New Phytologist* 31, 241–253.
- Bancroft, H. 1935a.** Some Fossil Dicotyledonous Woods from Mount Elgon, East Africa. I, *American J. Botany* 22, 164–183.
- Bancroft, H. 1935b.** Some Fossil Dicotyledonous Woods from Mount Elgon, East Africa. II, *American J. Botany* 22, 279–290.
- Barberi, F., Santacroce, R. & Varet, J. 1982.** Chemical aspects of rift magmatism. In: Pálmason, G. (Ed.) Continental and oceanic rifts. AGU-GSA. Geodynamic series 8, 223–258.
- Barifaijo, E. 2001.** The petrology of the volcanic rocks of Uganda. *GSU Newsletter* 1 (1), 42–49.
- Barifaijo, E., Owor, M. & Erima, G. 2008.** Enrichment characteristics in the upper mantle xenoliths from the Bufumbira basaltic rocks, southwestern Uganda. *African Journal of Science and Technology (AJST) Science and Engineering Series* Vol. 9(1), 85–101.
- Barifaijo, E., Muwanga, A. & Schumann, A. 2010.** Geo-

- chemistry of the potassic basalts from the Bufumbira volcanic field in southwestern Uganda. *Tanzanian J. Sci.* 36, 95–112.
- Barker, D. S. 2007.** Origin of cementing calcite in “carbonatite” tuffs, *Geology* 35, 371–374.
- Barker, D. S. & Nixon, P. H. 1989.** High-Ca, low-alkali carbonatite volcanism at Fort Portal, Uganda. *Contr. Mineral. Petrol.* 103, 166–177.
- Barnes, J. W. 1956.** Precambrian structure and the origin of the granitoid rocks in SW-Uganda. PhD. Thesis, University London, London.
- Barrett, W. L. 1969.** The stratigraphy and structure of the southeastern part of the Rwenzori Mountains. *Annual Rept., Research Institute Afr. Geol., Univ. Leeds* 13, 10–13.
- Barrett, W. L. 1971.** Stratigraphy, structure and mineralization of the southeastern part of the Rwenzori Mountains, Uganda. PhD. Thesis, Univ. Leeds.
- Barth, H. 1990.** Provisional Geological Map of Lake Victoria Gold Fields, Tanzania 1:500000 (with explanatory notes). *Geol. Jahrb.*, B 72, 59 p.
- Barth, H. & Meinhold, K. D. 1974.** Note on the basic igneous activity in the Precambrian Buganda-Toro geosynclines, Uganda. *Zeitschr. Deutscher Geol. Gesellschaft* 125, 105–118.
- Barth, H., Massola, S. & Weiser, T. 1996.** Gold in the Dodoma Basement of Tanzania. *Geol. Jb., Reihe B*, B92, 53pp.
- Barton, C. M., Carney, J. N., Crow, M. J., Dunkley, P. N. & Simango, S. 1991.** The geology of the country around Rushinga and Nyamapanda. *Zimbabwe Geological Survey, Harare, Bulletin* 92, 220 p.
- Bas, M. J. le, Lemaître, R. W., Streckeisen, A. & Zanettin, B. 1986.** A Chemical Classification of Volcanic-Rocks Based on the Total Alkali Silica Diagram. *J. Petrol.* 27 (3), 745–750.
- Baterham, P. M., Bullock, S. J., Hopgood, D. N. 1983.** Tanzania: integrated interpretation of aeromagnetic and radiometric maps for mineral exploration. *Transactions of the Institution of Mining and Metallurgy (Section B: Applied Earth Science)* 92, 83–92.
- Baudet, D., Hanon, M., Lemonne, E., Theunissen, K., Buyagu, S., Dehandschutter, J., Ngizimana, W., Nsenyuma, P., Rusanganwa, J. B. & Tahon, A. 1989.** Lithostratigraphie du domaine sédimentaire de la chaîne Kibarienne au Rwanda. *Annales Soc. Géol. Belgique* 112, 225–246.
- Bauer, F., Glasmacher, U. A., Reiners, P., Schumann, A., Nagudi, B. & Bechstädt, T. 2008.** Denudation history of the Rwenzori Mountains, Albertine Rift, Uganda. *Geophysical Research Abstracts* 10, EGU2008-A-02781.
- Bauer, F., Glasmacher, U. A., Reiners, P. W., Braun, J., Nagudi, B. & Bechstaedt, T. 2009.** A 3D model of the long-term landscape evolution of the Rwenzori Mountains, Albertine Rift, Uganda. *EGU General Assembly*, 19–24 April 2009, Vienna, Austria, p. 3439.
- Bauer, F., Glasmacher, U. A., Malikwisha, M., Mambo, V. S. & Mutete, B. V. 2010a.** The Eastern Congo rediscovered from the geological point of view. *Geophysical Research Abstracts* 12, EGU2010-2787.
- Bauer, F., Glasmacher, U. A., Ring, U., Schumann, A. & Nagudi, B. 2010b.** Thermal and exhumation history of the central Rwenzori Mountains, Western Rift of the East African Rift System, Uganda. *International Journal of Earth Sciences (Geol. Rundschau)* 10.1007/s00531-010-0549-7.
- Bauer, F. U., Glasmacher, U. A., Grobe, R. W., Starz, M., Malikwisha, M., Mambo, V. S. & Mutete, B. V. 2011a.** Exhumation history of the eastern border of the Congo Basin. 23rd Coll. Afr. Geol. (CAG23), 8–14 Jan. 2011, Univ. of Johannesburg, Abstract volume 34.
- Bauer, F. U., Glasmacher, U. A., Ring, U., Karl, M., Schumann, A. & Nagudi, B. 2011b.** Tracing the exhumation history of the Rwenzori Mountains, Albertine Rift. 23rd Coll. Afr. Geol. (CAG23), 8–14 Jan. 2011, Univ. of Johannesburg, Abstract volume 35.
- Bauer, F.U., Glasmacher, U. A., Ring, U., Karl, M., Schumann, A., Nagudi, B. 2013.** Tracing the exhumation history of the Rwenzori Mountains, Albertine Rift, Uganda, using low-temperature thermochronology. *Tectonophysics*, 599, 8–28.
- Bauernhofer, A. H., Hauzenberger, C., Wallbrecher, E., Hoinkes, G., Muhongo S., Mogessie, A., Fritz, H., Loizenbauer, J., Tenczer, V., Opiyo-Akech, N. & Mathu, E. M. 2004.** Geochemical evidence for Precambrian tectonics from the Mozambique Belt in SE Kenya and NE Tanzania. 20th Colloquium of African Geology – Orleans, France, 2–7 June 2004. Abstracts volume 68.
- Bauernhofer, A. H., Hauzenberger, C. A., Wallbrecher, E., Muhongo, S., Hoinkes, G., Mogessie, A., Opiyo-Akech, N. & Tenczer, V. 2009.** Geochemistry of basement rocks from SE Kenya and NE Tanzania: indications for rifting and early Pan-African subduction. *International Journal of Earth Sciences (Geol. Rundschau)* 98, 1809–1834.
- Beaumont, C., Nguyen, M. H., Jamieson, R. A. & Ellis, S. 2006.** Crustal flow modes in large hot orogens. In: Law, R. D., Searle, M. P. & Godin, L. (eds). *Channel Flow, Ductile Extrusion and Exhumation in Continental Collision Zones*. *Geol. Soc., London, Spec. Publ.* 268, 91–145.
- Begg, G. C., Griffin, W. L., Natapov, L. M., O’Reilly, S. Y., Grand, S. P., O’Neill, C. J., Hronsky, J. M. A., Poudjom Djomani, Y., Swain, C. J., Deen, T. & Bowden, P. 2009.** The lithospheric architecture of Africa: Seismic tomography, mantle petrology, and tectonic evolution. *Geosphere* 5(1), 23–50.
- Behre, S. M. 1990.** Ophiolites in Northeast and East Africa: implications for Proterozoic crustal growth. *J. Geol. Soc., London* 147(1), 41–57.
- Bell, K. & Powell, J. L. 1969.** Strontium isotope studies of the alkali rocks: the potassium-rich lavas of the Birunga and Toro-Ankole regions, east and central equatorial Africa. *J. Petrol.* 10, 536–572.
- Bell, K. & Powell, J. L. 1970.** Sr isotope studies of alkalic rocks: the alkalic complexes of East Uganda. *Bull. Geol. Soc. Amer.* 81, 3481–3490.
- Bell, K. & Doyle, R. J. 1971.** K-Ar relationships in some continental alkaline rocks associated with the East African Rift Valley system. *Geochim. Cosmochim. Acta* 35, 903–915.
- Bell, K. & Dodson, H. S. 1981.** The geochronology of the Tanzanian Shield. *J. Geol.* 89 (1), 109–128.
- Bell, K. & Tilton, G. R. 2001.** Nd, Pb and Sr Isotopic Compositions of East African Carbonatites: Evidence for Mantle Mixing and Plume Inhomogeneity. *J. Petrol.* 42 (10), 1927–1945.
- Bellon, H. & Pouclet, A. 1980.** Datations K-Ar de quelques laves du Rift-Ouest de l’Afrique centrale: implications sur l’évolution magmatique et structural. *Geol. Rundschau* 69, 49–62.
- Bellot, J.-P. 2007.** Extensional deformation assisted by mineralised fluids within the brittle-ductile transition: Insights from the southwestern Massif Central, France. *J. Struct. Geol.* 29, 225–240.

- Beyer, E. E., Griffin, W. L. & O'Reilly, S. Y. 2006.** Transformation of Archean lithospheric mantle by refertilization: Evidence from exposed peridotites in the Western Gneiss Region, Norway. *J. Petrol.* 47, 1611–1636.
- Bhattacharya, S., Das, P., Chaudhary, A. K. & Saw, A. K. 2010.** Mafic granulite xenoliths in the Eastern Ghats Granulite Belt: Implications for lower crustal processes in the southeastern Peninsular India, *Ind. Jour. Geol.* 80, 55–69.
- Bickle, M. J., Nisbet, E. G. & Martin, A. 1994.** Archean greenstone belts are not oceanic crust? *J. Geol.* 102, 121–138.
- Bingen, B. J., Viola, G., Henderson, I. H. C., Smethurst, M., Boyd, R., Thomas, R. J., Bjerkgaard, T., Feito, P., Hollick, L. M., Jacobs, J., Key, R. M., Rossi, D., Sandstad, J. S., Skar, O., Smith, R., Solli, A. & Tveten, E. 2006.** Geochronology of Pan-African terrain assembly in NE Mozambique. XXI Colloquium of African Geology (CAG21) 2006, Maputo, Mozambique, Abstract Volume 12–14.
- Bishop, W. W. 1956.** Former lake levels of the Entebbe peninsula. *Geol. Surv. Uganda.* Unpubl. Rept.
- Bishop, W.W. 1958a.** Raised swamps of Lake Victoria. *Geol. Surv. Uganda, Entebbe, Records for 1955–56,* 1–10.
- Bishop, W. W. 1958b.** Miocene mammalia from the Napak volcanics, Karamoja, Uganda. *Nature* 182 (4648), 1480–1482.
- Bishop, W. W. 1969.** Pleistocene stratigraphy in Uganda. *Memoir Geol. Surv. Uganda, Entebbe* 10. 128p.
- Bishop, W. W., Miller, J. A. & Fitch, F. J. 1969.** New potassium-argon determinations relevant to the Miocene fossil mammal sequence in east Africa. *Amer. J. Sci.* 267, 669–699.
- Bisset, C. B. 1939.** Note on the geology of western Masaka. *Geol. Surv. Uganda, Entebbe, Bull.* 3, p. 23.
- Bisset, C. B. 1942.** Note on the Katonga Quartzite. *Geol. Surv. Uganda, Entebbe, Unpubl. Rept. No. CBB/57.*
- Bjørlykke, K. O. 1973.** Glacial conglomerates of Late Precambrian age from the Bunyoro Series, W. Uganda. *Geol. Rundschau* 62 (3), 938–947.
- Bjørlykke, K. O. 1981.** Late Precambrian tillites of the Bunyoro Series, western Uganda. In: Hambrey, M. J. & Harland, W. B. (eds). *Earth's Pre-Pleistocene Glacial Record.* Cambridge University Press, Cambridge, 151–152.
- Bloomfield, K. B. 1972.** Carbonatite-derived sediments in southeast Uganda. *J. Geol. Soc. London,* 128 (5), 507–511.
- Boniface, N. 2009.** Eburnian, Kibaran and Pan-African metamorphic events in the Ubendian belt of Tanzania: Petrology, zircon and monazite geochronology. *Christian-Albrechts-Universität zu Kiel. Ph.D. thesis.* 110 p.
- Boniface, N., Schenk, V. & Appel, P. 2011.** Repeated orogenesis and oceanic crust subduction in the Paleoproterozoic Ubendian Belt, Tanzania. *23rd Coll. Afr. Geol. (CAG23),* 8–14 Jan. 2011, Univ. of Johannesburg, Abstract volume 53.
- Borg, G. 1992.** New aspects on the lithostratigraphy and evolution of Siga hills, an Archaean granite-Greenstone terrain in NW-Tanzania. *Zeitschrift Angewandte Geologie* 38, 89–93.
- Borg, G. 1994.** The Geita gold deposit in BNW Tanzania – Geology, ore petrology, geochemistry and timing of events. In: Oberthür, T. (ed.) *Metallogenesis of selected gold deposits in Africa.* *Geol. Jahrb., Reihe D, E. Schweizerbart'sche Verlagsbuchhandlung, Science Publishers,* 545–595.
- Borg, G. & Shackleton, R. M. 1997.** The Tanzania and NE Zaire cratons. In: Wit, M. J. de & Ashwal, L. D. (eds). *Tectonic Evolution of Greenstone Belts,* Oxford Science Publications, 608–619.
- Borg, G. & Krogh, T. 1999.** Isotopic age data of single zircons from the Archaean Sukumaland Greenstone Belt, Tanzania. *J. Afr. Earth Sci.* 29 (2), 301–312.
- Borg, G., Lyatuu, D. R. & Rammlair, D. 1990.** Genetic aspects of the Geita and Jubilee Reef Archean BIF-hosted gold deposits, Tanzania. *Geol. Rundschau* 79, 355–371.
- Boven, A., Pasteels, P., Punzalan, L. E., Yamba, T. K. & Musisi, J. H. 1998.** Quaternary perpotassic magmatism in Uganda (Tore-Ankole Volcanic Province): age assessment and significance for magmatic evolution along the East African Rift. *J. Afr. Earth Sci.* 26 (3), 463–476.
- Boven, A., Theunissen, K., Sklyarov, E., Klerckx, J., Melnikov, A., Mruma, A. & Punzalan, L. 1999.** Timing of exhumation of a high-pressure mafic granulite terrane of the Paleoproterozoic Ubende belt (West Tanzania). *Precambrian Res.* 93 (1), 119–137.
- Bradley, G. 2010.** The geological history and hydrogeological potential of the relict channels of Uganda. Poster, Presentation: Imperial College London/ Royal Geographical Society, BGS/BGRG Annual Conference: 50th Anniversary Meeting Conference Session: Technological Advances.
- Bradley, J. G. 2012.** Thermochronology, landscape evolution and hydrogeology of the Katonga valley in south west Uganda. Ph.D. thesis, University College London. 546 p.
- Bradley, G., Carter, A., Bristow, C. & Taylor, R. 2010.** Thermochronological evidence for exhumation of a Palaeozoic glacial valley by the River Katonga in South West Uganda. Poster “Thermo2010” – 12th International Conference on Thermochronology, Glasgow 16–20 August 2010.
- BRGM, Univ. Dar-es-Salaam, Tanz. Geol. Surv. 2004.** A 2,000,000 Scale Geology and Mineral Map of Tanzania. In: Pinna, P., Muhongo, S., Mcharo, B. A., LeGoff, E., Deschamps, Y., Ralay, F., Milesi, J. P. (compilers). *20th Coll. Afr. Geol. (CAG20),* 2–7th June, 2004. BRGM, Orléans France.
- Breitkopf, J. H. & Maiden, K. J. 1988.** Tectonic setting of the Matchless belt pyritic copper deposits, Namibia. *Econ. Geol.* 83, 710–723.
- Briden, J. C., Piper, J. D., Henthorn, D. I. & Rex, D. C. 1971.** New palaeomagnetic results from Africa and related potassium-argon age determinations. In: *15th Annual Rept. Research Institute African Geol., Univ. Leeds,* 46–50.
- Brinckmann, J. 1988.** The post-Kibaran tin and tungsten mineralization in North Burundi (Mulehe and Nyabisa). *IGCP no. 255, Newsletter/Bull.,* 1, 7–9.
- Brinckmann, J. 1992.** Géologie des minéralisations d'or du nord-ouest du Burundi. *IGCP no. 255, Newsletter/Bull.* 4, 9–22.
- Brinckmann, J. & Gabert, G. 1977.** Zur Geologie von Zentral-Uganda (Blatt 72, Jinja). *Geol. Jb.* B23, 61–76.
- Brinckmann, J., Lehmann, B. & Timm, F. 1994.** Proterozoic gold mineralization in Burundi. *Ore Geology Reviews* 9, 85–103.
- Brinckmann, J., Lehmann, B., Hein, U., Höhndorf, A., Mussallam, K., Weiser, T. & Timm, F. (eds) 2001.** *La Géologie et la Minéralisation Primaire de l'Or de la Chaîne Kibarienne, Nord-ouest du Burundi, Afrique Orientale.* *Geol. Jahrbuch, Reihe D, D 101, 195p.* ISBN 978-3-510-95877-1 broch.
- Brito Neves, B. B. 2004.** A História dos Continentes–Trajetórias e tramas tectônicas. In: Mantesso-Neto, V., Bartorelli, A., Carneiro, C. D. R. R. & Brito-Neves, B. B. (eds). *Geologia do Continente Sul-Americano; Evolução da*

- Obra de Fernando Flávio Marques de Almeida Beca, São Paulo, 123–149.
- Brock P. W. G. & Macdonald, R. 1969.** Geological environment of the Bukwa mammalian fossil site, Eastern Uganda, *Nature*, 223 (5206), 591–596.
- Brock, A. & Piper, J. D. A. 1972.** Interpretation of Late Precambrian Palaeomagnetic Results from Africa. *Geophysical Journal International* 28 (2), 139–146.
- Brown, J. M. 1950.** Gravimetric survey of the Entebbe basin. *Geol. Surv. Uganda. Unpubl. Rept.*
- Buchwaldt, R., Toulkeridis, T., Todt, W. & Ucauwun, E. K. 2008.** Crustal age domains in the Kibaran belt of SW-Uganda: Combined zircon geochronology and Sm–Nd isotopic investigation. *J. Afr. Earth. Sci.* 51 (1), 4–20.
- Bulambo, M., Waele, B. De, Kokonyangi, J., Johnson, S. P., Kampunzu, A. B. & Tembo, F. 2006.** SHRIMP zircon U–Pb geochronology and geochemistry of the Choma-Kalomo Block granitoids (Zambia): Geological implications. XXI Colloq. Afr. Geol. (CAG21) 2006, Maputo, Abstract Volume, 26–27.
- Bumby, A. J. & Guiraud, R. 2005.** The geodynamic setting of the Phanerozoic basins of Africa. *J. Afr. Earth Sci.* 43 (1–3), 1–12.
- Burke, K. & Sengör, A. M. C. 1986.** Tectonic escape in the evolution of the continental crust: *Amer. Geoph. Union. Geodynamics Series* 14, 41–53.
- Burke, K. & Sengör, A. M. C. 1989.** Regional lineaments and continental evolution. *Mem. Geol. Soc. India* 12, 65–73.
- Burke, K., Dewey, J. F. & Kidd, W. S. F. 1977.** World distribution of sutures; the sites of former oceans. *Tectonophysics* 40, 69–99.
- Burke, K., Ashwal, L. D. & Webb, S. J. 2003.** A new way to map old sutures using deformed alkaline rocks and carbonatites. *Geology* 31, 391–394.
- Cahen, L. 1954.** Géologie du Congo Belge. *Vaillant Carmanne, Liège.* 577p.
- Cahen, L. 1963.** Glaciations anciennes et dérive des continents. *Annales Soc. geol. Belgique*, 86 (1), 19–84.
- Cahen, L. 1978.** Les mixtites anté-cambriennes de l'est du Zaïre: mise au point interimaire. MRAC, Tervuren (Belgium), Dept. Geol. Miner., Rapt Annuel 1977, 33–64.
- Cahen, L. & Snelling, N. J. 1966.** The geochronology of equatorial Africa. North-Holland Publ. Comp., Amsterdam. 195 p.
- Cahen, L. & Snelling, N. J. 1974.** Potassium-argon ages and additions to the stratigraphy of the Malagarasian (Bukoban System of Tanzania). *J. Geol. Soc. London*, 130, 461–470.
- Cahen, L. & Theunissen, K. 1980.** The structural evolution of the Kibaran Orogeny in Rwanda and Burundi in the light of the presently available radiometric data in the Kibaran Belt from Shaba to Uganda. *Mus. Roy. Afr. Centr. (Belg.)*, Dépt. Géol., Rapt. Ann. 1979, 215–217.
- Cahen, L. & Lepersonne, J. 1981.** Late Palaeozoic tillites of the Congo Basin in Zaire, in: J.L.a.H. Hambrey, W. B. (ed.) *Earth's pre-Pleistocene glacial record*, Cambridge University Press, Cambridge 1981, 43–47.
- Cahen, L., Snelling, N. J., Delhal, J. & Vail, J. R. 1984.** The geochronology and evolution of Africa. *Oxford Science Publ., Clarendon Press, Oxford, UK.* 512 p.
- Calais, E., Ebinger, C., Hartnady, C. & Nocquet, J. M. 2006.** Kinematics of the East African Rift from GPS and earthquake slip vector data. In: Yirgu, G., Ebinger, C. & Maguire, P. K. H. (eds). *The Afar volcanic province within the African rift system.* *Geol. Soc. London*, 9–22.
- Carlson, R. W., Pearson, D. G., Boyd, F. R., Shirley, S. B., Irvine, G., Menzies, A. H. & Gurney, J. J. 1999.** Re-Os systematic of lithospheric peridotites: Implications for lithosphere formation and preservation, Cape Town, Proc. 7th Intern. Kimberlite Conf., Red Roof Design, 99–108.
- Cawley, A. 1960.** Nabilatuk. Sheet 36, N.A. 36, K IV. *Geol. Surv. Uganda, Entebbe.*
- Cawley, A. 1961.** Kaabong. Sheet 10, N.A. 36, E I. *Geol. Surv. Uganda, Entebbe.*
- Cawley, A. 1962.** Napak. Sheet 35, N.A. 36, K III. *Geol. Surv. Uganda, Entebbe.*
- Chaney, R. W. 1933a.** A Tertiary flora from Uganda. *J. Geol.* 41, 702–709.
- Chaney, R.W. 1933b.** A preliminary report on a fossil flora from the Bugishu sandstones. *Uganda Geol. Surv. Ann. Rept.*, p. 50.
- Charsley, T. J. 1987.** Geology of the Laisamis area. *Geol. Surv. Kenya, Rept.* 106.
- Chavez Gomez, S. 2000.** A database of dykes in eastern and southern Africa. MSc thesis, International Institute for Aerospace Survey and Earth Sciences (ITC), Delft, The Netherlands. 71 p.
- Chorowicz, J. 1992.** The role of ancient structure in the genesis and evolution of the East African rift, *Bulletin Société géologique de France* 163 (3), 217–227.
- Chorowicz, J. 2005.** The Mechanisms of the East African Rift System formation. *J. Afr. Earth Sci.* 43, 379–410.
- Cole, D. I. 1992.** Evolution and development of the Karoo Basin. In: Wit, M. J. de, Ransome, I. G. D. (Eds), *Inversion Tectonics of the Cape Fold Belt, Karoo and Cretaceous Basins of Southern Africa.* A.A. Balkema, Rotterdam, 87–89.
- Collins, A. S., Reddy, S. M., Buchan, C. & Mruma A. 2004a.** The 2.0 Ga Usagaran Eclogites, Tanzania: Age and Kinematic History of the Oldest HP/LT Terrane on Earth. 20th Coll. of Afr. Geol. (CAG20), Orleans, France, 2–7 June 2004, Abstracts volume, 120.
- Collins, A. S., Reddy, S. M., Buchan, C. & Mruma A. 2004b.** Temporal constraints on Palaeoproterozoic eclogite formation and exhumation (Usagaran Orogen, Tanzania). *Earth Planet. Sci. Lett.* 224 (1–2), 175–192.
- Combe, A. D. 1923.** Geological investigations in the Mubende District, Buganda. Unpubl. Rept. *Geol. Surv. Uganda, Entebbe, ADC/1/6.*
- Combe, A. D. 1932.** The geology of south-west Ankole (and adjacent territories with special reference to the tin deposits). *Geol. Surv. Uganda, Memoir II*, 236pp. With Appendix on Petrology by Groves, A. W.
- Combe, A. D. 1936.** Report on the geology of the Lubare area, Western Ankole (with petrological notes by W.C. Simmons). Unpubl. Rept. *Geol. Surv. Uganda, Entebbe, ADC/129/11/39.*
- Combe, A. D. 1938.** The Kasekere volcanic area, North Western Toto. *Ann. Rept. Geol. Surv. Uganda*, 1937, 14–17.
- Combe, A. D. 1939.** Geology of the Lubare area western Ankole). *Uganda Geol. Surv. Bull.* 3, 1–22.
- Combe, A. O. 1946.** The geology of northern Uganda and the adjacent part of Sudan. *Ann. Rept. Geol. Survey of Uganda, Entebbe.*
- Combe, A. D. 1948.** Annual Report for 1945. *Geol. Surv. Uganda, Entebbe*, 14.
- Combe, A. & Simmons, W. C. 1933.** The volcanic area of Bufumbira. Part I: The geology of the volcanic area of Bufumbira, south-west Uganda. *Memoir Geol. Surv. Uganda* 3, 1–150.
- Condie, K. C. 1998.** Episodic continental growth and super-

- continents: A mantle avalanche connection? *Earth Planet. Sci. Lett.* 163, 97–108.
- Condie, K. C. 2000.** Episodic continental growths models: Afterthoughts and extensions. *Tectonophysics* 322, 153–162.
- Condie, K. C. 2001.** Mantle Plumes and their record in earth history. Cambridge University Press, Cambridge. UK, 305 p.
- Condie, K. C. 2002.** The Supercontinent cycle: are there two patterns of cyclicity? *J. Afr. Earth Sci.* 35 (2), 179–183.
- Condie, K. C. 2007.** Accretionary orogens in space and time. *Geol. Soc. Amer., Memoirs*, 200, 145–158.
- Condie, K. C. 2008.** Supercontinents, superplumes and continental growth: the Neoproterozoic record. *Geol. Soc., London, Spec. Publ.*, 297, 217–231.
- Coolen, J. J. M. M. 1980.** Chemical petrology of the Furua granulite Complex, southern Tanzania. *GUA Papers of Geology, Series 1* (13). 258 p.
- Courtillot, V., Jaupart, C., Manighetti, I., Tapponnier, P. & Besse, J. 1999.** On causal links between flood basalts and continental break-up. *Earth Planet. Sci. Lett.* 166, 177–195.
- Coussot, P. & Meunier, M. 1996.** Recognition, classification and mechanical description of debris Flows. *Earth-Science Reviews* 40, 209–227.
- Croese, I. 1984.** Rapport d'étape sur la géologie et les minéralisations de la zone Ruhengeri-Est. Rep. Rwandaise/PNUD Projet de Recherches Minières RWA 80/001, Kigali August 1984. 62 p.
- Croese, I. & Matheussens, M. 1990.** The significance of quartz-porphyrines in Rwanda. IGCP no. 255, Newsletter/Bull. 3, 1–8.
- Crosby, A. G., Fishwick, S. & White, N. 2010.** Structure and evolution of the intracratonic Congo Basin. *Geochemistry, Geophysics, Geosystems* (G3), 11 (6), 1–20.
- Cutten, H. N. C. & Johnson, S. P. 2006.** Tectonic evolution of the Mozambique Belt, eastern Africa. *Coll. Afr. Geol. (CAG21)*, Maputo, Mozambique. Abstract Volume, 33–34.
- Cutten, H., Fernandez-Alonso, M., Waele, B. De & Tack, L. 2004.** Age constraints for basin evolution and sedimentation in the Northeastern Kibaran Belt: Orleans, Abstracts, 20th Coll. Afr. Geol. (CAG20), 123.
- Daly, M. C. 1988.** Crustal shear zones in central Africa: a kinematic approach to Proterozoic tectonics. *Episodes* 11, 5–11.
- Daly, M. C. & Unrug, R. 1982.** The Muva Supergroup, northern Zambia. *Trans. Geol. Soc. South Africa* 85, 155–165.
- Daly, M. C., Klerkx, J. & Nanyaro, J. T. 1985.** Early Proterozoic exotic terranes and strike-slip accretion in the Ubendian belt of southwest Tanzania (Abstract). *Terra Cognita* 5(2/3), 257.
- Dalziel, I. W. D. 1997.** Neoproterozoic–Paleozoic geography and tectonics: review, hypothesis, environmental speculation. *Geol. Soc. Am. Bull.* 109, 16–42.
- Davies, K. A. 1934a.** The age of Mount Elgon and the Tertiary history of Bugishu. *Bull. Geol. Surv. Uganda* 1, 69–71.
- Davies, K. A. 1934b.** Geological map of parts of Samia (Budama) and Bukoli (Busoga), Eastern Province, Uganda. Busia sheet, map no. 6, 1:50 000. *Geol. Surv. Uganda, Entebbe*.
- Davies, K. A. 1935a.** Report on gold and bismutotantalite of Busolonganyi Estate. *Geol. Surv. Uganda, Unpubl. Rept.*
- Davies, K. A. 1935b.** Geological observations on a traverse through Karamoja. *Bull. Geol. Surv. Uganda* 2, 37–39.
- Davies, K. A. 1939.** The glacial sediments of Bunyoro, NW Uganda. *Bull. Geol. Surv. Uganda* 3, 29–37.
- Davies, K. A. 1940.** The glacial series of Bunyoro, North Uganda. XVII Int. Geol. Congr. 1938, Moscow, 115–119.
- Davies, K. A. 1947.** The phosphate deposits of the Eastern Province, Uganda. *Econ. Geol.*, 42 (2), 137–146.
- Davies, K. A. 1951.** The Uganda section of the Western Rift. *Geol. Mag.* 88 (6), 377–385.
- Davies, K. A. 1952.** The building of Mount Elgon, East Africa. *Geol. Surv. Uganda, Memoir no. 7*. 57p.
- Davies, K. A. 1956.** The geology of south-east Uganda with special reference to the alkaline complexes. *Geol. Surv. Uganda, Memoir no. 8*. 77p.
- Davies, K. A. & Bisset, C. B. 1947.** The geology and mineral deposits of Uganda. *Bull. Imp. Inst.*, XLV, 1610180.
- Davies, A., Blackburn, W. H., Brown, W. H. & Ehman, W. D. 1978.** Trace element geochemistry and origin of late Precambrian–early Cambrian Catocin greenstones of the Appalachian Mountains. Univ. California at Davies California, unpubl. Rept.
- Davis, G. L., Aldrich, L. T., Tilton, G. R., Wetherill, G. W. & Jeffrey, P. M. 1956.** The age of rocks and minerals. Year Book Carnegie Institute, Washington 55, 1955–56, 161–168.
- Dawson, J. B. & Smith, J. V. 1977.** The MARID (mica-amphibole-rutile-ilmenite-diopside) suite of xenoliths in kimberlite. *Geochim. Cosmochim. Acta* 41, 309–323
- Deblond, A. 1990.** Late Kibaran layered igneous rocks from eastern Burundi. A progress report. IGCP 255 Newsletter/Bulletin 3, 9–17.
- Deblond, A. 1994.** Géologie et Pétrologie des Massifs Basiques et Ultrabasiques de la Ceinture Kabanga-Musongati au Burundi. Musée Royal de l'Afrique Centrale, Tervuren, Belgium, Geological Sciences 99. 117 p.
- Deblond, A. & Tack, L. 1999.** Main characteristics and review of mineral resources of the Kabanga-Musongati mafic-ultramafic alignment in Burundi. *J. Afr. Earth Sci.* 29 (2), 313–328.
- Deblond, A., Punzalan, L. E., Boven, A. & Tack, L. 2001.** The Malagarazi Supergroup of SE Burundi and its correlative Bukoban Supergroup of NW Tanzania: Neo- and Mesoproterozoic chrono-stratigraphic constraints from Ar–Ar ages on mafic intrusive rocks. *J. Afr. Earth Sci.* 32, 435–449.
- Delor, C., Theveniaut, H., Cage, M., Pato, D., Lafon, J.-M., Bialkowski, A., Roig, J.-Y., Neto, A., Cavongo, M. & Sergeev, S. 2008.** New insights into the Precambrian geology of Angola: basis for an updated lithochronological framework at 1:2000000 scale. 22nd Colloquium of African geology. Hammamet -Tunisia, 52–53.
- Delpomdor, F., Tack, L. & Prétat, A. 2008.** Microstructures in the Neoproterozoic tillites around the Congo River Basin (CRB), Democratic Republic of Congo (DRC) – Comparison with the Karoo tillites from the Dekese borehole in the CRB. Abstract, 22nd Coll. Afr. Geol. (CAG 22), 4–6 November 2008, Hammamet, Tunisia, 108.
- Delvaux, D., Cibambula, E., Kadima, E., Kipata, L., Sebaenzi, S. N., Tack, L. & Kabeya, S. M. 2011.** Intracratonic evolution and tectonic stress in the Congo Basin. 23rd Coll. Afr. Geol. (CAG23), 8–14 Jan. 2011, Univ. of Johannesburg, Abstract volume, 113.
- Demaiffe, D. 2008.** Le magmatisme alcalin et carbonatitique: synthèse sur la province paléozoïque de Kola (Russie) et caractéristiques générales du massif proterozoïque de Matongo (Burundi). *Bull. Séanc. Acad. R. Sci. Outre-Mer*, 54 (2), 171–196.
- Demaiffe, D. & Theunissen, K. 1979.** Données géochro-

- nologiques U-Pb relatives au Complexe Archéen de Kikuka (Burundi). Musée Royal de l'Afrique centrale, Tervuren, Belgium, Dépt. Géol. Min., Rapp. Ann. 1978, 65–69.
- Demaiffe, D., Fieremans, M. & Fieremans, C. 1986.** The Kimberlites of Central Africa: a review. In: Int. Congr. on Magmatism of Extensional Regions (Lubumbashi, Zaire, 1986).
- Demant, A., Lestrade, P., Lubala, R. T., Kampunzu, A. B. & Durieux, J. 1994.** Volcanological and Petrological evolution of Nyiaragongo Volcano, Virunga volcanic field, Zaire. Bull. Volcanology, 56 (1), 47–61.
- DGSM 1963.** Bushenyi. Sheet 85 (S.A.36.AIII). Geological Survey of Uganda.
- DGSM 1966.** Geological map of Uganda, scale 1:1,500,000. Compiled by R. Macdonald. Geol. Surv. Uganda, Entebbe.
- Dirks, P. H. G. M. & Ashwal, L. D. 2002.** African Geodynamics and Resource Exploration for the 21st Century. Univ. Witwatersrand, School of Geosciences. 29 p.
- Dirks, P. H. G. M., Kröner, A., Jelsma, H. A., Sithole, T. A. & Vinyu, M. L. 1999.** Structural relations and Pb-Pb zircon ages for a crustal-scale Pan African shear zone in the Zambezi Belt, northwest Zimbabwe. J. Afr. Earth Sci. 28, 427–442.
- Dodson, M. H., Gledhill, A. R., Shackleton, R. M. & Bell, K. 1975.** Age differences between Archean cratons of eastern Africa and south Africa. Nature 254, 315–318.
- Dreesen, R. 1980.** Shallow-water deposits within the Burundian Proterozoic (Republic of Burundi, East Africa). Bull. Soc. Géol. Belge 89, 217–238.
- Dreesen, R. 1981.** A propos d'une structure sédimentaire particulière du Burundien de la région de Muyinga (Burundi oriental). MRAC, Ann. Rept. 1980, 67–71.
- DuBois, C. G. B. 1959.** The Terror Hills alkaline complex, central Karamoja, Uganda. Int. Geol. Congress, Mexico 1956, Rept. 303.
- Duchesne, J.-C., Liégeois, J.-P., Deblond, A. & Tack, L. 2004.** Petrogenesis of the Kabanga-Musongati layered mafic-ultramafic intrusions in Burundi (Kibaran Belt): geochemical, Sr-Nd isotopic constraints and Cr-Ni behaviour. J. Afr. Earth Sci. 39 (3–5), 133–145.
- Duncan, R. A., Hooper, P. R., Rehacek, J., Marsh, J. S. & Duncan, A. R. 1997.** The timing and duration of the Karoo igneous event, southern Gondwana. J. Geophys. Res., 102, 18127–18138.
- Ebinger, C. J. 1989.** Tectonic development of the western branch of the East African rift system. *GSA Bulletin* 101 (7), 885–903.
- Eby, G. N. 2006.** Carbonatites to alkali granites - Petrogenetic insights from the Chilwa and Monteregian Hills - White Mountain igneous provinces. Geol. Assoc. Canada - Mineralogical Assoc. Canada, Joint Annual Meeting, Montreal 2006, Program with Abstracts 31, 45.
- Eby, G. N., Lloyd, F. E., Woolley, A. R., Stoppa, F. & Weaver, S. D. 2003.** Geochemistry and mantle source(s) for carbonatitic and potassic lavas, Western Branch of the East-African Rift system, SW Uganda. Geolines 15, 23–27.
- Eby, G. N., Lloyd, F. E. & Woolley, A. R. 2009.** Geochemistry and petrogenesis of the Fort Portal, Uganda, extrusive carbonatite. Lithos 113, 785–800.
- Elliott, G. F. S. & Gregory, J. W. 1895.** The Geology of the Mount Ruwenzori and some adjoining Regions of Equatorial Africa. Quart. J. Geol. Soc. 51, 669–680, London.
- Emslie, R. F. 1991.** Granitoids of rapakivi granite-anorthosite and related associations. Precam. Res. 51, 173–192.
- Evans, D. M., Boadi, I., Byemelwa, L., Gilligan, J., Kabete, J. & Marcet, P. 2000.** Kabanga magmatic sulphide deposits, Tanzania: morphology and geochemistry of associated intrusions. J. Afr. Earth Sci. 30, 651–674.
- Ferguson, A. K. & Cundari, A. 1975.** Petrological aspects and evolution of the leucite-bearing lavas from Bufumbira, South West Uganda. Contr. Mineral. Petrol. 50, 25–46.
- Fernandez-Alonso, M. 1981.** Données préliminaires sur la géochimie de granites protérozoïques du Rwanda et du Burundi. MRAC, Dept. Geol. Miner., Ann. Rept. 1980, 195–207.
- Fernandez-Alonso, M. 1985.** Bijdrage tot de geologische en petrologische kennis van granietische gesteenten uit het Burundiaan van Burundi. PhD Thesis (unpublished). University of Ghent (Belgium). 313 p.
- Fernandez-Alonso, M., Lavreau, J. & Klerkx, J. 1986.** Geochemistry and geochronology of the Kibaran granites in Burundi, Central Africa: implications for the Kibaran orogeny. Chem. Geol. 57, 217–234.
- Fernandez-Alonso, M. & Theunissen, K. 1998.** Airborne geophysics and geochemistry provide new insights in the intra-continental evolution of the Mesoproterozoic Kibaran Belt (Central Africa). Geol. Mag. 135, 203–216.
- Fernandez-Alonso, M., Tack, L., Waele, B. De, Cutten, H., Baudet, D. & Tahon, A. 2006.** The NE Kibaran Belt (NKB). New uniform stratigraphies and GIS-compiles geological map. Abstract, 21st Coll. Afr. Geol. (CAG21), Maputo, Mozambique, 48–49.
- Fernandez-Alonso, M., Tack, L., Tahon, A., Laghnough, M. & Hardy, B. 2007.** Geological compilation of the Mesoproterozoic Northeastern Kibara (Karagwe-Ankole) Belt. MRAC, Tervuren, scale 1:500 000.
- Fernandez-Alonso, M., Waele, B. De, Tahon, A., Dewaele, S., Baudet, D. H. Cutten, D. H. & Tack, L. 2009.** The Northeastern Kibaran Belt (NKB): a 1250 Ma-long Proterozoic intracratonic history in Central Africa punctuated by two orogenic events at 1.0 and 0.55 Ga. Geol. Soc. London, Fermor Meeting Rodinia: Supercontinents, superplumes and Scotland, Edinburgh, 9–13 Sept. 2009.
- Fernandez-Alonso, M., Tack, L., Tahon, A. & Waele, B. De 2011.** The Proterozoic history of the proto-Congo Craton of Central Africa. 23rd Coll. Afr. Geol. (CAG23), 8–14 Jan. 2011, Univ. of Johannesburg, Abstract volume, 142.
- Fleuty, M. J. 1968.** Explanation of the Geology of Sheet 27 (Moroto). Report no. 13, Geol. Surv. Uganda, Entebbe. 65p.
- Foley, S. F., Venturelli, G. & Tosconi, L. 1987.** The ultrapotassic rocks: Characteristics, classification and constraints for petrogenetic models. Earth Sci. Rev. 24, 81–134.
- Foley, S. F., Link, K., Tiberindwa, J. V. & Barifaijo, E. 2012.** Patterns and origin of igneous activity around the Tanzanian craton. J. Afr. Earth Sci. 62 (1), 1–18.
- Frisch, W. 1975.** Die Wolfram-Lagerstätte Gifurwe (Rwanda) und die Genese der Zentralafrikanischen Reinit-Lagerstätten. Jahrbuch Geologie, Vienna, B-A 118, 119–191.
- Fritz, H., Tenczer, V., Hauzenberger, C. A., Wallbrecher, E., Hoinkes, G., Muhongo, S. & Mogessie, A. 2005.** Central Tanzanian tectonic map: A step forward to decipher Proterozoic structural events in the East African Orogen. Tectonics 24, TC6013. 26p.
- Fritz, H., Tenczer, V., Hauzenberger, C. A., Wallbrecher, E. & Muhongo, S. 2009.** Hot granulite nappes — Tectonic styles and thermal evolution of the Proterozoic granulite belts in East Africa. Tectonophysics 477, 160–173.
- Fritz, H., Abdelsalam, M., Ali, K. A., Bingen, B., Collins, A. S., Fowler, A. R., Ghebreab, W., Hauzenberger, C. A.,**

- Johnson, P. R., Kusky, T. M., Macey, P., Muhongo, S., Stern, R. J. & Viola, G. 2013.** Orogen styles in the East African Orogen: A review of the Neoproterozoic to Cambrian tectonic evolution. *J. Afr. Earth Sci.* 86, 65–106.
- Frost, B. R. & Frost, C. D. 2008.** On charnockites. *Gondwana Research* 13, 30–44.
- FUGRO 2009.** Ministry of Energy & Mineral Development African Development & World Bank MRMCBP/SMMRP – Airborne Geophysics UGANDA. PowerPoint Presentation (Kampala 16 & 17 July 2009 – Martin Frere).
- Furman, T. & Graham, D. 1999.** Erosion of lithospheric mantle beneath the East African Rift system: geochemical evidence from the Kivu volcanic province *Lithos* 48, 237–262.
- Furman, T., Bryce, J. G., Karson, J. & Lotti, A. 2004.** East African Rift System (EARS) Plume Structure: Insights from Quarternary Mafic Lavas of Turkey, Kenya. *J. Petrol.* 45 (5), 1069–1088.
- Gabert, G. 1973.** Über granitische Gesteine des Dodoman und Usagaran im südlichen Hochland von Tanzania (Ostafrika), *Geol. Jahrb., Reihe B* 6, 3–50.
- Gabert, G. 1974.** Prospecting work of the German Geological Mission in Uganda. *Z. Deutsch. Geol. Gesellschaft* 125, Hannover, 99–104.
- Gabert, G. 1984.** Structural-lithologic units of Proterozoic rocks in east Africa, their base, cover and mineralisation. In: Klerkx, J. & Michot, J. (eds). *African Geology*, Musée Royal de l’Afrique centrale, Tervuren, Belgium, 11–22.
- Gabert, G. 1990.** Lithostratigraphic and tectonic setting of gold mineralization in the Archaean Cratons of Tanzania and Uganda, East Africa. *Precambrian Res.* 46, 59–69.
- Gall, B. le, Nonnotte, P., Rolet, J., Benoit, M., Guillou, H., Mousseau-Nonnotte, M., J. Albaric, J. & Deverchère, J. 2010.** Rift propagation at craton margin: Distribution of faulting and volcanism in the North Tanzanian Divergence (East Africa) during Neogene times. *Tectonophysics*, 448 (1–4), 1–19.
- Gebo, D.L., MacLachy, L. & Kityo, R. 1997.** A New Lorisid Humerus from the Early Miocene of Uganda. *Primates*, 38 (4), 423–427.
- Gérards, J. & Leppersonne, J. 1964.** La stratigraphie du Burundien dans le Nord-Est du Rwanda et les régions avoisinantes. *Bull. Serv. Géol. Rwanda* 1, 13–34.
- Gérards, J. & Ledent, D. 1971.** Grands traits de la géologie du Rwanda, différents types de roches granitiques et premières données sur l’âge de ces roches. *Ann. Soc. Géol. Belge* 93, 477–489.
- Gérards, J. & Ledent, D. 1976.** Les réhomogénéisations isotopiques d’âge lufilien dans les granites de Rwanda. *Rapp. Annu.* 1975, MRAC, Tervuren, 91–103.
- Gérards, J., Leppersonne, J. & Petricec, V. 1967.** Carte géologique du Rwanda 1/100.000. *Serv. Géol. Rwanda*, Kigali, Rwanda.
- Gittins, J. 1966.** Summaries and bibliographies of carbonate complexes. In: Tuttle, O. F. & Gittins, J. (eds). *Carbonatites*. Interscience Publ. New York, 417–570.
- Goloka J. & Bocharova N. Y. 2000.** Hot spot activity and the break-up of Pangea. In: Stemmerik, L. S. & Trappe, J. (eds). “Pangea: The Late Carboniferous to Late Triassic interval”. *Palaeo- geography, Palaeoclimatology, Palaeoecology* 161, 49–69.
- Gommery, D., Senut, B., Pickford, M., Musiime, E. 2002.** Les nouveaux restes du squelette d’*Ugandapithecus major* (Miocene inférieur de Napak, Ouganda). *Annales de Paleontologie* 88 (3), 167–186.
- Goddéris, Y., Donnadiou, Y., Nédélec, A., Dupré, B., Desert, C., Grard, A., Ramstein, G. & François, L. M. 2003.** The Sturtian-snowball-glaciation: fire and ice. *Earth Planet. Sci. Letters* 211, 1–12.
- Goscombe, B., Armstrong, R. & Barton, J. M. 2000.** Geology of the Chewore Inliers, Zimbabwe: constraining the Mesoproterozoic to Paleozoic evolution of the Zambezi Belt. *J. Afr. Earth Sci.* 30, 599–627.
- Gradstein, F. M., Ogg, J. G., Smith, A. G., Bleeker, W. & Lourens, L. J. 2004a.** A new Geologic Time Scale with special reference to Precambrian and Neogene. *Episodes* 27 (2), 83–100.
- Gradstein, F. M., Ogg, J. G. & Smith, A. G. 2004b.** A Geologic Time Scale 2004. Cambridge, Cambridge University Press. 589 p.
- Grantham, D. R., Temperley, B. N. & McConnell, R. B. 1945.** Explanation of the geology of degree sheet No. 17 (Kahama). *Geol. Surv. Tanganyika Bull.*, Dar es Salam 15, 1–32.
- Grantham, G. H., Maboko, M. & Eglinton, B. M. 2003.** A Review of the Evolution of the Mozambique Belt and Implications for the Amalgamation and Dispersal of Rodinia and Gondwana. In: Yoshida, M., Windley, B. F. & Dasgupta, S. (eds). *Proterozoic of East Gondwana: Supercontinent Assembly and Breakup*. *Geol. Soc., London, Spec. Publ.* 206, 401–425.
- Grantham, G. H., Ingram, B. A., Roberts, M. P., Matola, R. & Manhica, V. 2006.** The geology of the Ulongue-Furancungo area, NW Mozambique. *XXI Coll. Afr. Geol. (CAG21)*, 2006, Maputo, Abstract Volume, 55.
- Green, D. H. 1973.** Conditions of melting of basanite magma from garnet peridotite. *Earth Planet. Sci. Lett.* 17, 456–465.
- Greenwood, W. R., Hadley, D. G., Anderson, R. E., Fleck, R. J. & Schmidt, D. L. 1976.** Late Proterozoic cratonization in southwestern Saudi Arabia. *Phil. Trans. R. Soc. London*, A280, 517–527.
- Griffin, W. L., O’Reilly, S. Y., Ryan, C. G., Gaul, O. & Ionov, D. 1998.** Secular variation in the composition of subcontinental lithospheric mantle. In: Braun, J., Dooley, J. C., Goleby, B. R., van der Hilst, R. D. & Klootwijk, C. T. (eds). *Structure and evolution of the Australian continent*, *Amer. Geophys. Union, Geodynamics* 26, Washington, DC, 1–26.
- Griffin, W. L., O’Reilly, S. Y. & Ryan, C. G. 1999.** The composition and origin of subcontinental lithospheric mantle. In: Fei, Y., Bertka, C. M. & Mysen, B. O. (eds). *Mantle Petrology: Field Observations and high-pressure experimentation: A tribute to Francis R. (Joe) Boyd*. *Houston, Geochem. Soc. Spec. Publ.* 6, 13–45.
- Griffin, W. L., O’Reilly, S. Y., Abe, N., Aulbach, S., Davies, R. M., Pearson, N. J., Doyle, B. J. & Kivi, K. 2003.** The origin and evolution of Archaean lithospheric mantle. *Precam. Res.* 127, 19–41.
- Griffin, W. L., Graham, S., O’Reilly, S. Y. & Pearson, N. J. 2004.** Lithosphere evolution beneath the Kaapvaal Craton. Re-Os systematic of sulphides in mantle-derived peridotites. *Chem. Geol.* 208, 89–118.
- Groves, A. W. 1935.** The Charnockite Series of Uganda, *British East Africa. Q. J. Geol. Soc. London* 91 (1–4), 150–207.
- GTK Consortium 2006.** Map Explanation; Volume 2: Sheets 1630–1634, 1732–1734, 1832–1834 and 1932–1934. *Geology of Degree Sheets Mecumbura, Chioco, Tête, Tambara, Guro, Chemba, Manica, Catandica, Gorongosa, Rotanda, Chimoio and Beira, Mozambique. Direção Nacional de Geologia (DNG)*, Maputo. 411 p. + Ann.
- GTK Consortium 2012a.** Explanation of the geology of

- sheets NA-36-1 and NA-36-5 (Arua and Pakwach) 1:250 000, Uganda. Department of Geological Survey and Mines (DGSM), Entebbe. 115 p.
- GTK Consortium 2012b.** Explanation of the geology of sheets NA-36-2 and NA-36-6 (Kitgum and Gulu) 1:250 000, Uganda. Department of Geological Survey and Mines (DGSM), Entebbe. 157 p.
- GTK Consortium 2012c.** Explanation of the geology of sheets NB-36-15, NA-36-3, -4, -7 and -8 (Didinga, Kaabong, Lodwar, Aloi and Moroto) 1:250 000, Uganda. Department of Geological Survey and Mines (DGSM), Entebbe. 125 p.
- GTK Consortium 2012d.** Explanation of the geology of sheets NA-36-9 and NA-36-10 (Hoima and Masindi) 1:250 000, Uganda. Department of Geological Survey and Mines (DGSM), Entebbe. 105 p.
- GTK Consortium 2012e.** Explanation of the geology of sheets NA-36-11 and NA-36-12 (Mbale and Kapenguria) 1:250 000, Uganda. Department of Geological Survey and Mines (DGSM), Entebbe. 109 p.
- GTK Consortium 2012f.** Explanation of the geology of sheet NA-36-13 (Fort Portal) 1:250 000, Uganda. Department of Geological Survey and Mines (DGSM), Entebbe. 65 p.
- GTK Consortium 2012g.** Explanation of the geology of sheet NA-36-14 (Kampala) 1:250 000, Uganda. Department of Geological Survey and Mines (DGSM), Entebbe. 81 p.
- GTK Consortium 2012h.** Explanation of the geology of sheets NA-36-15 and SA-36-3 (Jinja and Homa Bay) 1:250 000, Uganda. Department of Geological Survey and Mines (DGSM), Entebbe. 99 p.
- GTK Consortium 2012i.** Explanation of the geology of sheet SA-36-1 (Mbarara) 1:250 000, Uganda. Department of Geological Survey and Mines (DGSM), Entebbe. 91 p.
- GTK Consortium 2012j.** Explanation of the geology of sheet SA-36-2 (Masaka) 1:250 000, Uganda. Department of Geological Survey and Mines (DGSM), Entebbe. 35 p.
- GTK Consortium 2012k.** Explanation of the geology of sheet SA-36-5 (Kabale) 1:250 000, Uganda. Department of Geological Survey and Mines (DGSM), Entebbe. 69 p.
- Guiraud, R. & Bellion, Y. 1995.** Late Carboniferous to recent Geodynamic evolution of the West Gondwanian, cratonic, Tethyan margins. In: Nairn, A. E. M., Ricou, L.-C., Vrielynck, B. & Dercourt, J. (eds). *The Ocean Basins and Margins*. vol 8: The Tethys Ocean, 101–124.
- Guiraud, R. & Bosworth, W. 1999.** Phanerozoic geodynamic evolution of northeastern Africa and the northwestern Arabian platform, *Tectonophysics*, 315, 73–108.
- Gurnis, M. 1988.** Large-scale mantle convection and the aggregation and dispersal of supercontinents, *Nature* 332, 695–699.
- Halligan, R. 1963.** The Proterozoic rocks of western Tanganyika. *Bull. Geol. Surv. Tanganyika*, 34, 1–34.
- Halverson, G. P., Hoffman, P. F. & Maloof, A. 2003.** Neoproterozoic. *Geol. Soc. Amer. Annual Meeting*, Seattle, WA, 2–5 November 2003, GSA Abstracts with Program 35, Abstract No. 210–11.
- Hamilton, A.C. 1968.** Some plant fossils from Bukwa. *Uganda Journal* 32, 157–164.
- Hamilton, W. B. 1998.** Archean magmatism and deformation were not products of plate tectonics. *Precam. Res.* 91, 143–179.
- Hampton, C. M. 1993.** Unusual source of carbonate for speleothem formation at Nyakasura, western Uganda. *Documenta Naturae*, Munich 77, 15–21.
- Hanson, R. E., Wilson, T. J. & Munyanyiwa, H. 1994.** Geologic evolution of the Neoproterozoic Zambezi Orogenic Belt in Zambia. *J. Afr. Earth Sci.* 18 (2), 135–150.
- Harland, W. B. 1964.** Critical evidence for a great infra-Cambrian glaciation. *Intern. J. Earth Sci.*, 54(1), 45–61.
- Harpum, J. R. 1956.** Summary of the geology of Tanganyika, part V: structures and geotectonics of the Precambrian. *Geol. Surv. Tanganyika, Memoir* 2, Dar-es-Salaam.
- Harper, C. T., Weintraub, G. S., Leggo, P. J. & Shackleton, R. M. 1972.** Potassium-argon retention ages from the Basement Complex and associated Precambrian meta-sedimentary rocks of Uganda. *Geol. Soc. Amer. Bull.* 83, 3449–3456.
- Harris, J. F. 1981.** Summary of the geology of Tanzania, economic geology. *Tanganyika Geol. Surv. Mem.* 1 Part IV, 143 p.
- Harris, N. 1949.** Description of the Sentema map sheet. Unpubl. Rept. *Geol. Surv. Uganda*, Entebbe.
- Hartz, E. H. & Torsvik, T. H. 2002.** Baltica upside-down: A new plate-tectonic model for Rodinia and the Iapetus Ocean. *Geology* 30 (3), 255–258.
- Hauzenberger, C. A. 2003.** The Mozambique Belt of SE-Kenya and SW-Tanzania, East Africa: mineralogy, petrology and geochronology. *Habilitation Thesis*, Karl-Franzens-University Graz, Austria.
- Hauzenberger, C. A., Bauernhofer, A. H., Hoinkes, G., Wallbrecher, E. & Mathu, E. M. 2004.** Pan-African high-pressure granulites from SE Kenya: petrological and geothermobarometric evidence for polycyclic evolution in the Mozambique Belt. *J. Afr. Earth Sci.* 40, 245–268.
- Heinzelin, J. de 1963.** Palaeoecological conditions of the Lake Albert – Lake Edward rift. In: Howell & Bourlière (eds). *African ecology and human evolution*, 276–284, Chicago (Aldine).
- Henderson, G. 1961.** The geology of the Bukoban-type rocks of the Kigoma and Mpanda Districts, Western Province, Tanganyika. *Trans. Geol. Soc. S. Afr.* 63, 11–50.
- Hepworth, J. V. 1961a.** The geology of the southern West Nile, Uganda, with particular reference to the charnockites and to the development of the Albert Rift. PhD. Thesis, Univ. Leeds.
- Hepworth, J. V. 1961b.** Okollo. Sheet 19 (Part of) & 20. (N.A. 36, G II (Part of) & H. I). *Geological Survey of Uganda*, Entebbe.
- Hepworth, J. V. 1964.** Explanation of the geology of Sheets 19, 20, 28 and 29 (Southern West Nile). *Rept. Geol. Surv. Uganda*, Entebbe 10.
- Hepworth, J. V. 1972.** Charnockitic granulites of some African cratons. 24th *Internat. Geol. Congr. Canada*, Montreal, Sect. 1, 126–134.
- Hepworth, J. V. & Macdonald, R. 1966.** Orogenic belts of the northern Uganda basement. *Nature* 210, 726–727.
- Hetzel, R. & Strecker, M. R. 1994.** Late Mozambique belt structures in western Kenya and their influence on the evolution of the Cenozoic Kenya rift. *J. Struct. Geol.* 16, 189–201.
- Higazy, R. A. 1954.** Trace elements of volcanic ultrabasic potassic rocks of southwestern Uganda and adjoining part of the Belgian Congo. *Bull. Geol. Soc. Amer.* 65, 39–70.
- Higgins, M. W. 1971.** Cataclastic rocks. *USGS, Spec. Paper* 687. 97 p.
- Hoffman, P. F. 1991.** Did the breakout of Laurentia turn Gondwanaland insideout? *Science*, 252, 1409–1412.
- Hoffman, P. F. 1999.** The break-up of Rodinia, birth of Gondwana, true polar wander and the snowball earth. *J. Afr. Earth Sci.* 28, 17–34.
- Hoffman, P. F., Kaufman, A. J., Halverson, G. P. & Schrag, D. P. 1998.** A Neoproterozoic snowball earth. *Science*

- 281, 1342–1346.
- Hoffman, P. F. & Schrag, D. P. 2002.** The snowball Earth hypothesis: testing the limits of global change. *Terra Nova* 14, 129–155.
- Hoffmann, K.-H., Condon, D. J., Bowring, S. A. & Crowley, J. L. 2004.** U–Pb zircon dates for the Neoproterozoic Ghaub Formation, Namibia: constraints on Marinoan glaciation. *Geology* 32 (9), 817–820.
- Holmes, A. 1945.** Leucitized granite xenoliths from the potassium-rich lavas of Bunyaruguru, south-west Uganda. *Amer. J. Sci.* 241-A, (Daly Volume), 313–332.
- Holmes, A. 1951.** The sequence of Precambrian orogenic belts in southern and central Africa. XVIII Intern. Geol. Congr., London, Pt. XIV, 254–269.
- Holmes, A. 1965.** Principles of physical geology. 2nd Edition. 1288 p. London.
- Holmes, A. & Harwood, H. F. 1932.** Petrology of the volcanic fields east and south-east of Ruwenzori, Uganda. *Q.J. Geol. Soc. London* 88, 370–442.
- Holmes, A. & Harwood, H. F. 1937.** The petrology of the volcanic area of Bufumbira, south-west Uganda. *Memoir Geol. Surv. Uganda* 3. 300 p.
- Holmes, A. & Cahen, L. 1955.** African Geochronology. *Col. Geol. & min. Res.*, V(1), 3–39.
- Hopwood, A. T. & Lepersonne, J. 1953.** Présence des formations d'âge miocène inférieur dans le Fossé tectonique de Lac Albert et de la Basse Semliki (Congo Belge). *Ann. Soc. Géol. Belgique, Liège* 77, 83–113.
- Horne, R. G. 1953.** The geology of the lower mountain slopes adjacent to Moroto township, Uganda. Unpubl. PhD. thesis, Univ. Durban.
- Hornung, G. 1969.** Volcanic rocks around Fort Portal, western Uganda. 13th Ann. Rep. Inst. Afr. Geol., Univ. Leeds, 26–27.
- Hughes, C. J. 1973.** Spilites, keratophyres, and the igneous spectrum. *Geol. Mag.* 109, 513–527.
- Hunting Surveys Ltd. 1961.** An airborne geophysical survey of Uganda, Area A (Karamoja). *Hunting Surveys Ltd.*, London.
- Hytönen, K. 1959.** On the petrology and mineralogy of some alkaline volcanic rocks of Toror Hills, Mt. Moroto and Morulinga in Karamoja, northeastern Uganda. *Bull. Comm. Geol. Finland* 184, 75–131.
- Ichang'i, D. W. & Maclean, W. H. 1991.** The Archean volcanic facies in the Migori segment, Nyanza greenstone belt, Kenya: stratigraphy, geochemistry and mineralisation. *J. Afr. Earth Sci.* 13 (3/4), 277–290.
- Ikingura, J. R., Bell, K., Watkinson, D. H. & Straaten, P. van. 1990.** Geochronology and chemical evolution of granitic rocks, NE Kibaran Belt (Karagwe-Ankolean), NW Tanzania. In: Rocci, G. & Deschamps, M. (eds). 15th Colloquium of African Geology: Nancy, France, International Center for Training and Exchanges in the Geosciences (CIFEG), 97–99.
- Irvine, T. N. & Baragar, W. R. A. 1971.** A guide to the chemical classification of the common volcanic rocks. *Canadian J. Earth Sci.* 8, 523–548.
- Irving, A. J. 1980.** Petrology and geochemistry of composite ultramafic xenoliths in alkalic basalts and implications for magmatic processes within the mantle. *Amer. J. Sci.* 280, 389–426.
- Isley, A. E. & Abbott, D. H. 1999.** Plume-related mafic volcanism and the deposition of banded iron formation. *J. Geophys. Res.* 104, 15461–15477.
- Iwamori, H. 2000.** Thermal effects of ridge subduction and its implication for the origin of granitic batholith and paired metamorphic belts. *Earth Planet. Sci. Lett.* 181, 131–144.
- Jacobs, J., Fanning, C. M., Henjes-Kunst, F., Olesch, M. & Paech, H. J. 1998.** Continuation of the Mozambique Belt into East Antarctica: Grenville age metamorphism and polyphase Pan-African high grade events in the Central Dronning Maud Land. *J. Geol.* 106, 385–406.
- Jacobs, J., Bauer, W. & Thomas, R. T. 2006.** A Himalayan-type indenter-escape tectonic model for the southern part of the Late Neoproterozoic/Early Paleozoic East African–Antarctic Orogen. *Coll. Afr. Geol. (CAG21)*, Maputo, Mozambique. Abstract Volume, 71–72.
- Janardhan, A. S., Newton, R. C. & Hansen, E. C. 1982.** The transformation of amphibolite facies gneiss to charnockite in southern Karnataka and northern Tamil Nadu, India; *Contrib. Mineral. Petrol.* 79, 130–149.
- Janse, A. J. A. 1994.** Is Clifford's rule still valid? Affirmative examples from around the world. In: Meyer, H. O. A. & Leonardos, O. H. (eds). *Diamonds: Characterization, genesis and exploration.* Brazilia Dept. Nac. da Prod. Miner., 215–235.
- Jensen L. S. 1976.** A new cation plot of classifying subalkalic volcanic rocks. Ontario Division of Mines, Misc. Paper 66, 1–22.
- John, T. & Schenk, V. 2003.** Partial eclogitisation of gabbroic rocks in a late Precambrian subduction zone (Zambia): prograde metamorphism triggered by fluid infiltration. *Contrib. Miner. Petrol.* 146, 174–191.
- John, T., Schenk, V., Haase, K., Scherer, E. & Tembo, F. 2003.** Evidence for a Neoproterozoic ocean in south-central Africa from mid-oceanic ridge-type geochemical signatures and pressure-temperature estimates of Zambian eclogites. *Geology* 31, 243–246.
- John, T., Scherer, E., Haase, K. & Schenk, V. 2004.** Trace element fractionation during fluid-induced eclogitization in a subduction slab: trace element and Lu-Hf/Sm-Nd isotope systematics. *Earth Planet. Sci. Lett.* 227, 441–456.
- Johnson, M. R., Vuuren, C. J. van, Hegenberger, W. F., Key, R. & Shoko, U. 1996.** Stratigraphy of the Karoo Supergroup in southern Africa: an overview. *J. Afr. Earth Sci.* 23 (1), 3–15.
- Johnson, R. J. 1954.** An outline of the geology of the Ruwenzori Range. Unpubl. Rept. Geol. Surv. Uganda, Entebbe, RJJ/11.
- Johnson, R. J. 1960.** Explanation of the geology of sheet 69 (Lake Wamala). *Geol. Surv. Uganda, Entebbe, Rept.* 3. 35p.
- Johnson, R. J. & McConnell, R. B. 1951.** Notes on the geology of the northern part of the Ruwenzori mountains. *Geol. Mag.* 88 (4), 249–256.
- Johnson, R. J. & Williams, C. E. F. 1961.** Explanation of the geology of sheet 59 (Kiboga). *Geol. Surv. Uganda, Entebbe, Rept.* 7. 39p.
- Johnson, S. P. & Oliver, G. J. H. 2000.** Mesoproterozoic oceanic subduction, island arc formation and the initiation of back-arc spreading in the Kibaran Belt of central southern Africa: evidence from the ophiolite terrane, Chewore Inliers, northern Zimbabwe. *Precam. Res.* 103, 125–146.
- Johnson, S. P. & Oliver, G. J. H. 2004.** Tectonothermal history of the Kaourera Arc, northern Zimbabwe; implications for the tectonic evolution of the Irumide and Zambezi Belts of south central Africa. *Precam. Res.* 130, 71–97.
- Johnson, S. P., Rivers, T. & Waele, B. De 2005.** A review of the Mesoproterozoic to early Palaeozoic magmatic and tectonothermal history of south-central Africa: implications for Rodinia and Gondwana. *J. Geol. Soc.*, London

162, 433–450.

- Johnson, S. P., Waele B. De & Tembo, F. 2006.** The Southern Irumide Belt. 21st Coll. Afr. Geol. (CAG21), Mozambique, 3–5 July, Abstracts volume, 75–77.
- Johnson, S. P., Waele, B. De, Tembo, F., Evans, D., Iizuka, T. & Tani, K. 2007.** Geochronology of the Zambezi supracrustal sequence, southern Zambia: a record of Neoproterozoic divergent processes along the southern margin of the Congo Craton. *J. Geol.* 115, 355–374.
- Jung, D. & Meyer, F.-M. 1990.** Les méta-basites du Rwanda. *IGCP 255, Newsletter/Bull.* 3, 37–50.
- Kabengele, M., Kapenda, D. & Tshimanga, K. 1989.** Ubendian (Early Proterozoic) mafic rocks of Marungu plateau magmatic complex (North-Eastern Shaba province, Zaire): New petrological and chemical data. Geodynamic significance. *Abstr., G.S.A. '89, 8th Conf. Geol. Soc. Africa, Rabat, Morocco*, 70–72.
- Kabengele, M., Lubala, R. T. & Cabanis, B. 1991.** Caractérisation pétrologique du magmatismeubendien du secteur de Pepa-Lumumba, sur le plateau des Murungu (Nord-Est de Shaba, Zaire). Signification géodynamique dans l'évolution de la chaîne ubendienne. *J. Afr. Earth Sci.* 13 (2), 243–265.
- Kabete, J. M., Groves, D. I., McNaughton, N. J. & Mruma, A. H. 2012.** A new tectonic and temporal framework for the Tanzanian Shield: Implications for gold metallogeny and undiscovered endowment. *Ore Geology Reviews* 48, 88–124.
- Kampunzu, A. B. 1981.** Le magmatisme du massif de Kahuzi (Kivu, Zaire). Structure, pétrologie, signification géodynamique. PhD. Thesis, Univ. Lumumbashi, Zaire. 378p.
- Kampunzu, A. B. & Mohr, P. 1991.** Magmatic evolution and petrogenesis in the East African Rift System. In: Kampunzu, A. B. & Lubala, R. (eds). *Magmatism in Extensional Structural Settings*, Springer-Verlag, Berlin, 85–136.
- Kampunzu, A. B., Vellutini, P. J., Caron, J.-P.H, Lubala, R. T., Kanika, M. & Rumvegeri, B. T. 1983.** Le volcanisme et l'évolution structurale du sud-Kivu (Zaire). Un modèle d'interprétation géodynamique du volcanisme distensif intracontinental. *Bull. Centres Rech. Explor. Prod. Elf Aquitaine* 7, 257–271.
- Kampunzu, A. B., Lubala, R. T. Caron, J.-P. H & Vellutini, P. J. 1984a.** Les basalts transitionnels dans l'évolution des rifts continentaux: exemple de la Haute-Ruzizi dans le rift de l'Afrique Centrale (Kivu, Zaire). *Geol. Rundschau* 73 (3), 895–916.
- Kampunzu, A. B., Lubala, R. T., Caron, J.-P. H & Vellutini, P. J. 1984b.** Minéralogie et pétrologie du Kahuzi, Kivu (Zaire).
- Kampunzu, A. B., Lubala, R. T., Caron, J.-P. H, Makutu, M. N., Rocci, G. & Vellutini, P. J. 1985.** Les complexes alcalins de la région interlacustre à l'est de Zaire et au Burundi: un exemple de massifs anorogéniques de relaxation. *J. Afr. Earth Sci.* 3 (1/2), 151–167.
- Kampunzu, A. B., Rumvegeri, B. T., Kapenda, D., Lubala, R. T. & Caron, J.-P. H. 1986.** Les Kibariens d'Afrique central et orientale: une chaîne de collision. *UNESCO, Geol. Econ. Dev., Newsletter* 5, 125–137.
- Kampunzu, A. B., Bonhomme, M. G. & Kanika, M. 1998.** Geochronology of volcanic rocks and evolution of the Cenozoic Western Branch of the East African rift system. *J. Afr. Earth Sci.* 26, 441–461.
- Kanda-Nkula, V., Mpiana, Ch., Cibambula, E., Fernandez-Alonso, M., Delvaux, D., Kadima, E., Delpomdor, F., Tahon, A., Dumont, P., Hanon, M., Baudet, D., Dewaele, S. & Tack, L. 2011.** The 1000m thick redbeds sequences of the Congo river basin (CRB): a generally overlooked testimony in central Africa of post-Gondwana amalgamation (550Ma) and pre-Karoo break-up (320Ma). 23rd Coll. Afr. Geol. (CAG23), 8–14 Jan. 2011, Abstracts volume. Univ. of Johannesburg.
- Kanzira, H. 1985.** Etude des complexes granito-gneissiques de Cyimbili, Mara et Mutara, République Rwandaise (Afrique centrale), Projet Prospection Géophysique, Coopération Canado-Rwandaise 16. 215 p.
- Kärkkäinen, N., Turunen, P., Konnunaho, J., Mäkitie, H., Kato, V., Waluganja, A. & Jenett, T. 2014, in press.** The Neoproterozoic Iganga gabbro field and its Ni-Cu-PGE potential in the Tanzania Craton, south-east Uganda. In: Lehto, T. & Katto, E. (eds). *GTK Consortium Geological Surveys in Uganda 2008–2012*. Geological Survey of Finland, Special Paper 56.
- Karp, T., Scholz, C. A. & McGlue, M. M. 2012.** Structure and stratigraphy of the Lake Albert Rift, East Africa: Observations from seismic reflection and gravity data. in: Baganz, O. W., Bartov, Y., Bohacs, K. & Nummedal, D. (eds). 'Lacustrine sandstone reservoirs and hydrocarbon systems'. *AAPG Memoir* 95, 299–318.
- Katto, E. 1997.** Butare iron ore prospect (Muko, Kabale district SW Uganda. Internal Technical Report EG-14, Dept. Geol. Survey and Mines and UNDESSED.
- Kaufman, A. J., Knoll, A. H., Narbonne, G. M. 1997.** Isotopes, ice ages, and terminal Proterozoic earth history. *Proc. Nat. Acad. Sci. U. S. Amer.* 94, 6600–6605.
- Keller, G. R. 2008.** Relationship between crustal structure and extension in the Basin and Range Province and East Africa. Donald D. Harrington Symp. on the Geology of the Aegaeon, IOP Conf. Series, Earth and Environmental Sci. 2, 1–4.
- Kelsey, D. E. 2008.** On ultrahigh-temperature crustal metamorphism. *Gondwana Res.* 13, 1–29.
- Kennedy, W. Q. 1964.** The structural differentiation of Africa in the Pan-African (± 500 m.y.) tectonic episode. *Res. Indt. Afr. Geol. Leeds*, 8th Ann. Rept. 48–49.
- Key, R. M. & Hill, P. G. 1989.** Further evidence for the controls on the growth of vanadium grossular garnets in Kenya. *J. Gemnology*, 21, 412–422.
- Key, R. M., Charsley, T. J., Hackman, B. D., Wilkinson, A. F. & Rundle, C. C. 1989.** Superimposed Upper Proterozoic Collision controlled Orogenies in the Mozambique Belt of Kenya: Precambrian Res. 44, 197–225.
- Key, R. M., Liyungu, A. K., Njamu, F. M., Somwe, V., Banda, J., Mosley, P. N. & Armstrong, R. A. 2001.** The western arm of the Lufilian Arc in NW Zambia and its potential for copper mineralisation. *J. Afr. Earth Sci.* 33 (3–4), 503–528.
- Key, R. M., Bingen, B., Barton, E., Daudi, E. X. F., Manuel, S. & Moniz, A. 2007.** Kimberlites in a Karoo graben of northern Mozambique: Tectonic setting, mineralogy and Rb-Sr geochronology. *South Afr. J. Geol.* 110, 111–124.
- King, B. C. 1942a.** Prospecting in Singo, June–Sept. 1942. Unpubl. Rept. Geol. Surv. Uganda, Entebbe.
- King, B. C. 1942b.** Note on a visit to Munyonyo. Unpubl. Rept. Geol. Surv. Uganda, Entebbe.
- King, B. C. 1942c.** An outline of the geology of southern Buwékula with adjoining portions of the Singo and Mawogola. Unpubl. Rept. Geol. Surv. Uganda, Entebbe.
- King, B. C. 1943.** A preliminary account of the area enclosed approximately by Lats. 0° 22' and 0° 35'N and Longs. 31° 59' and 32° 10' E with special reference to the Mityana Series. (Singo Series). Unpubl. Rept. Geol. Surv. Uganda, Entebbe, BCK/24.

- King, B. C. 1947a.** The Singo Series of Central Uganda. Unpubl. Rept. Geol. Surv. Uganda, Entebbe, BCK 56.
- King, B. C. 1947b.** The textural features of the granites and invaded rocks of the Singo batholith of Uganda and their petrogenetic significance. *Q.J. Geol. Soc. London* 102, 37–64.
- King, B. C. 1949.** The Napak Area of Southern Karamoja, A study of a dissected Late Tertiary Volcano. *Geol. Surv. Uganda, Memoir V* 57p.
- King, B. C. 1959.** Problems of the Pre-Cambrian of Central and Western Uganda. Part 1. Problems of correlation. *Sci. Progr. London* 47, 528–542.
- King, B. C. 1962.** The pattern of metamorphism in central and western Uganda. *Proc. Geol. Soc. London* 1594, 14–15.
- King, B. C. 1964.** The carbonatite complexes of eastern Uganda. In: Tuttle, O. F & Grittins, J. (eds). *The Carbonatites*, Wiley & Sons, London.
- King, B. C. 1965.** Petrogenesis of the Alkaline rock suites of the volcanic and intrusive centres of eastern Uganda. *J. Petrol.* 6 (1), 67–100.
- King, B. C. 1970.** Volcanicity and rift tectonics in East Africa. In: Clifford & Gass (eds). *African Magmatism and Tectonics*, Oliver & Boyd, Edinburgh, 263–283.
- King, B.C. 1978.** A comparison between the Older (Karoo) Rifts and the Younger (Cenozoic) Rifts of eastern Africa. In: Ramberg, I. B. & Neumann, E-R. (eds). “Tectonics and Geophysics of Continental Rifts”, Dordrecht, 347–350.
- King, B. C. & Sutherland, D. S. 1960a.** Alkaline rocks of eastern and southern Africa. Part 1: Distribution, ages and structures. *Sci. Progr. London* 48 (190), 298–321.
- King, B. C. & Sutherland, D. S. 1960b.** Alkaline rocks of eastern and southern Africa. Part 2: Petrology. *Sci. Progr. London* 48 (191), 504–524.
- King, B. C. & Sutherland, D. S. 1960c.** Alkaline rocks of eastern and southern Africa. Part 3: Petrogenesis. *Sci. Progr. London* 48, 709–720.
- King, B. C. & Swardt, A. M. J. de 1970.** Problems of structure and correlation the Precambrian System of central and western Uganda. *Geol. Survey Uganda, Memoir XI*.
- Kirschvink, J. L. 1992.** Late Proterozoic low-latitude global glaciation: The snowball Earth. In: Schopf, J. W. & Klein, C. (eds). *The Proterozoic Biosphere: A Multidisciplinary Study*. Cambridge University Press, Cambridge, 51–52.
- Kisvarsanyi, E. B. & Kisvarsanyi, G. 1990.** Alkaline granite ring complexes and metallogeny in the middle proterozoic St. Francois Terrane, Southeastern Missouri, USA. In: Gower, C., River, T. & Ryan, B. (eds). *Mid-Proterozoic Laurentia – Baltica*. *Geol. Assoc. Canada, Spec. Paper* 38, 433–446.
- Klerkx, J., Lavreau, J., Liégeois, J.-P. & Theunissen, K. 1984.** Granitoides kibariniens précoces et tectonique tangentielle au Burundi: Magmatisme bimodal lié à une distension crustale. In: Klerkx, J. & Michot, J. (eds). *African Geology, MRAC, Tervuren, Belgium*, 29–46.
- Klerkx, J., Liégeois, J.-P., Lavreau, J. & Claessens, W. 1987.** Crustal evolution of the Northern Kibaran Belt, Eastern and Central Africa. In: Kröner, A. (ed.) *Proterozoic Litho-spheric Evolution, Geodynamics Series 17, Intern. Lithosphere Program Contr.*, 217–233.
- Klerkx, J., Theunissen, K., Sklyarov, E., Melnikov, A., Gladkochub, D. & Mruma, A. 1997.** Subducted and exhumed Palaeoproterozoic oceanic crust in the Ubende Belt of West Tanzania. *Abstract European Union of Geosciences (EUG 9)*. *Terra Nova* 9, 358.
- Knorring, O. von 1967.** Carbonatitic rocks from the volcanic field of western Uganda. 11th Ann. Rept. Inst. Afr. Geol. Univ. Leeds, 30–32.
- Knorring, O. von & Dubois, C. G. B. 1961.** Carbonatitic lava from Fort Portal area in Western Uganda. *Nature* 192, 1064–1065.
- Kock, G. S. de, Manninen, T., Mänttari I. & Natukunda, J. F. 2011.** Zircon ages from the Namuwaza and Bwezigoro-Gunga Plateau sequences, Uganda. 23rd Coll. Afr. Geol. (CAG23), 8–14 Jan. 2011, Univ. of Johannesburg, Abstract volume, 101.
- Köhn, D., Aanyu, K., Haines, S. & Sachau, T. 2008.** Rift nucleation, rift propagation and the creation of basement micro-plates within active rifts, *Tectonophysics* 458 (1–4), 105–116.
- Köhn, D., Lindenfeld, M., Rumpker, G., Aanyu, K., Haines, S., Passchier, C. W., Sachau, T. 2010.** Active transsection faults in rift transfer zones: evidence for complex stress fields and implications for crustal fragmentation processes in the western branch of the East African Rift. *International Journal of Earth Sciences (Geol. Rundschau)* 99, 1633–1642.
- Koistinen, T., Lehtonen, M. I., Fernando, S. & Matola, R. 2008.** Contribution to the structure at the eastern margin of the Archaean Zimbabwe craton, Mozambique. *Geological Survey of Finland, Special Paper* 48, 121–144.
- Kokonyangi, J., Okudaira, Kampunzu, A. B. & Yoshida, M. 2001.** Geological evolution of the Kibaran belt, Mitwaba, Democratic Republic of Congo, Central Africa. *Gondwana Res.* 4, 663–664.
- Kokonyangi, J., Kampunzu, A. B., Armstrong, R. & Poujo, M. 2004a.** Mesoproterozoic strongly peraluminous granitoids and coeval mafic rocks in the Kibaran Belt of Central Africa: geotectonic implications. 20th Colloquium of African Geology, Orleans, France, 2–7 June 2004, Abstracts volume, 236.
- Kokonyangi, J., Armstrong, R., Kampunzu, A. B., Yoshida, M. & Okudaira, T. 2004b.** U-Pb zircon geochronology and petrology of granitoids from Mitwaba (Katanga, Congo): implications for the evolution of the Mesoproterozoic Kibaran belt. *Precambrian Res.* 132, 79–106.
- Kokonyangi, J., Kampunzu, A. B., Poujol, M., Okudaira, T., Yoshida, M. & Shabeer, K. P. 2005a.** Petrology and geochronology of Mesoproterozoic mafic–intermediate plutonic rocks from Mitwaba (D. R. Congo): implications for the evolution of the Kibaran belt in central Africa. *Geol. Mag.* 142 (1), 109–130.
- Kokonyangi, J. W., Kampunzu, A. B., Armstrong, C., Yoshida, M., Okudaira, T., Arima, M. & Ngulube, D. A. 2005b.** The Mesoproterozoic Kibaride belt (Katanga, SE D.R. Congo). *J. Afr. Earth Sci.*, 46 (1–2), 1–35.
- Kokonyangi, J. W., Kampunzu, A. B., Armstrong, R., Arima, M., Yoshida, M. & Okudaira, T. 2007.** U-Pb SHRIMP Dating of Detrital Zircons from the Nzilo Group (Kibaran Belt): Implications for the Source of Sediments and Mesoproterozoic Evolution of Central Africa. *J. Geol.* 115, 99–113.
- Kokonyangi, J., Dunkley, D., Bulambo, M., Francart, J. P., Itaya, T., Arima, M. & Yoshida, M. 2008.** First cassiterite SHRIMP vs K-Ar geochronology on tin and Nb-Ta mineralization in the Kibaran Belt: Implications to Rodinia and Gondwana tectonics. Abstract, 22nd Coll. Afr. Geol. (CAG 22), 4–6 November 2008, Hammamet, Tunisia, 250.
- Kreuser, T. 1983.** Stratigraphie des Karoo-Becken in Ost Tanzania. Thesis, Geol. Inst. Univ. Köln Sonderveröffentlichungen, 45, 217 p.

- Kreuser, Th. 1984.** Karroo basins in Tanzania. In: Klerkx, J. & Michot, J. (eds). African Geology, Musée Royal de l'Afrique centrale, Tervuren, Belgium, 231–245.
- Kröner, A., Hegner, E., Collins, A., Windley, B. F., Brewer, T. S., Razakamanana, T., Pidgeon, R. T. 2000a.** Age and magmatic history of the Antananarivo block, central Madagascar, as derived from zircon geochronology and Nd isotopic systematics. *Am. J. Sci.* 300, 251–288.
- Kröner, A., Willner, A., Hegner, E. & Nemchin, A. A. 2000b.** Single zircon ages and Nd isotopic systematics of granulites in southern Malawi and their bearing on the extent of the Mozambique belt into southern Africa. *Precam. Res.* 109, 257–292.
- Kröner, A., Willner, H. P., Hegner, E., Jaeckel, P. & Nemchin, A. 2001.** Single zircon ages, PT evolution and Nd isotope systematics of high-grade gneisses in southern Malawi and their bearing on the evolution of the Mozambique Belt in southeastern Africa. *Precam. Res.* 109, 257–291.
- Lærdal, T. & Talbot, M. R. 2002.** Basin neotectonics of Lakes Edward and George, East African Rift Palaeogeography, Palaeoclimatology, Palaeoecology 187, 213–232.
- Lambiase, J. & Rodgers, M. R. 1988.** A model for tectonic control of lacustrine stratigraphic sequences in continental rift basins. In: 'Lacustrine Exploration: Case Studies and Modern Analogues', AAPG Research Conference, Snowbird, Utah, September 7–9.
- Lavreau, J. 1977a.** Résultats géologiques d'une étude par télédétection orbitale de la région frontrière Sudan-Uganda-Zaire. MRAC, Dept. Geol. Miner., Ann. Rept 1976, 101–196.
- Lavreau, J. 1977b.** Contribution de l'imagerie spatiale à la résolution de certains problèmes géologiques au Kivu (Zaire). La région située à l'ouest du lac Kivu. *Bull. Soc. Belge Géol.* 86, 91–95.
- Lavreau, J. 1977c.** Contribution de l'imagerie spatiale à la résolution de certains problèmes géologiques au Kivu (Zaire). La région Walikale-Masisi à la Haute Tanya, et la position des couches de la Bilati. *Bull. Soc. Belge Géol.* 86, 135–144.
- Lavreau, J. 1985.** Le Groupe de la Rusizi (Rusizien du Zaïre, Rwanda et Burundi) à la lumière des connaissances actuelles. Royal Museum for Central Africa, Tervuren (Belgium), Dépt. Géologie Minéralogie, Ann. Rep. 1984, 111–119.
- Lavreau, J. & Liégeois, J.-P. 1982.** Granites à étain et granitogneiss burundiens au Rwanda (région de Kibuye); âge et signification. *Ann. Soc. Géol. Belgique* 105, 289–294.
- Lawver, L. A., Gahagan, L. M., & Dalziel, I. W. D. 1998.** A Tight fit-Early Mesozoic Gondwana, A Plate Reconstruction Perspective. In: Motoyoshi, Y. & Shiraishi, K. (eds). "Origin and Evolution of Continents": Proceedings of the International Symposium "Origin and Evolution of Continents," 13–14 October, 1997, Tokyo, Memoirs, 214–229, National Institute of Polar Research.
- Ledent, D. & Cahen, L. 1965.** Quelques données géochronologiques nouvelles sur des minéraux des roches du Kivu méridional. *Rapp. Annu.* 1964, MRAC, Tervuren, 94–95.
- Lehto, T., Westerhof, A. B., Lehtonen, M. I., Manninen, T., Mäkitie, H., Virransalo, P., Pokki, J., Härmä, P., Koistinen, T., Saalman, K., Kuosmanen, E., Mänttari, I., Katto, E., Baguma, Z., Kock, G. de & Elepu, D. 2014.** Geological Map of Uganda, Scale 1:1 000 000. Geological Survey of Finland, Espoo, Finland.
- Leggo, P. J. 1974.** A geochronological study of the basement complex of Uganda. *J. Geol. Soc. London* 130 (3), 263–277.
- Leggo, P. J., Aftalion, M. & Pidgeon, R. T. 1971.** Discordant zircon U-Pb ages from the Uganda basement. *Nature Phys. Sci.* 231, 81–84.
- Lenoir, J. L., Liégeois, J.-P., Mruma, A. & Theunissen, K. 1993.** Age, nature and geodynamic significance of the Kate-Kipili plutono-volcanic complex in western Tanzania. *Mus. Roy. Afr. Centr. (Belgium), Dépt. Géol. Min., Rapp. Ann.* 1991–1992, 109–122
- Lenoir, J. L., Liégeois, J.-P., Theunissen, K. & Klerkx, J. 1994.** The Paleoproterozoic Ubendian shear belt in Tanzania: geochronology and structure. *J. Afr. Earth Sci.* 19 (3), 169–184.
- Lepersonne, J. 1970.** Revision of the fauna and the stratigraphy of the fossiliferous localities of the Lake Edward-Lake Albert Rift (Congo). *Ann. Mus. Roy. Afr. Centr., Sci. géol.* 67, 169–207.
- Lepersonne, J. 1974.** Carte Géologique du Zaïre. MRAC, Tervuren, Belgium.
- Li, Z. X., Zhang, L., Powell, C. M. 1995.** South China in Rodinia: part of the missing link between Australia–East Antarctica and Laurentia? *Geology* 23, 407–410.
- Li, Z. X., Bogdanova, S., Collins, A. S., Davidson, A., Waele, B. De, Ernst, R. E., Fitzsimons, I. C. W., Fuck, R. A., Gladkochub, D. P., Jacobs, J., Karlstrom, K. E., Lu, S., Natapov, L. M., Pease, V. L., Pisarevsky, S. A., Thrane, K. & Vernikovskiy, V. 2008.** The geodynamic map and evolution history of the Neoproterozoic supercontinent Rodinia, 33rd Intern. Geol. Congress: Oslo, Norway, 1.
- Liégeois, J.-P., Theunissen, K., Nzojibwami, E. & Klerkx, J. 1982.** Granitoïdes syncinématiques kibariens au Burundi: étude pétrographique, géochimique et géochronologique préliminaire. *Ann. Soc. géol. Belg.* 105, 345–356.
- Liégeois, J.-P., Asrat, A., Abdelsalam, M. G., Mogessie, A., Stern, R. J. & Kröner, A. 2013.** Nature and significance of the Pan-African Orogeny. 24th Coll. Afr. Geol., (CAG 24), Addis Abeba, 8–14 January, 2013. Abstract Volume, 45.
- Lindendorf, M., Rümper, G., Batte, A. & Schumann, A. 2012.** Seismicity from February 2006 to September 2007 at the Rwenzori Mountains, East African Rift: earthquake distribution, magnitudes and source mechanisms. *Solid Earth*, 3, 251–264.
- Link, K., Rosenthal, A., Foley, S. F., Pearson, D. G. & Nowell, G. 2007.** Isotopic constraints on the petrogenesis of the kamafugites of Uganda. *Geophysical Research Abstracts*, Vol. 9, European Geosciences Union 9, 06896.
- Link, K., Barifaijo, E., Tiberindwa, J. & Foley, S. F. 2008.** Pyroxenite-xenoliths from the silica-poor alkaline volcanic rocks in the Toro-Ankole region of western Uganda. *Geophysical Research Abstracts* 10, EGU2008-A-12175.
- Link, K., Köhn, D., Barth, M., Tiberindwa, J., Barifaijo, E., Aanyu, K. & Foley, S. 2010.** Continuous cratonic crust between the Congo and Tanzania blocks in western Uganda. *International Journal of Earth Sciences / Geol. Rundschau* 99 (7), 1559–1573.
- Link, K., Foley, S. F., Koehn, D., Tiberindwa, J. V., Barifaijo, E. 2011a.** Palaeoproterozoic thrusting onto the Congo-Tanzania Craton: New results from the Rwenzori region in western Uganda. 23rd Coll. Afr. Geol. (CAG23), 8–14 Jan. 2011, Univ. of Johannesburg, Supplement Abstract volume13.
- Link, K., Foley, S. F., Tiberindwa, J. V. & Barifaijo, E. 2011b.** Petrological subrift mantle processes in the lithosphere beneath the Western Branch of the East African Rift. 23rd Coll. Afr. Geol. (CAG23), 8-14 Jan. 2011, Univ. of Johannesburg, Supplement Abstract volume,14.

- Lippard, S. J. 1973.** Plateau phonolite lava flows, Kenya. *Geol. Mag.* 110, 543–549.
- Lloyd, F. E., Nixon, P. H., Hornung, G. & Condliffe, E. 1987.** Regional K-metasomatism in the mantle beneath the west branch of the East African Rift: alkali clinopyroxene xenoliths in highly potassic magmas. In: Nixon, P. H. (ed.) *Mantle Xenoliths*, Wiley, Chichester.
- Lloyd, F. E., Huntingdon, A. T., Davies, G. R. & Nixon, P. H. 1991.** Phanerozoic volcanism of Southwest Uganda, a case for regional K and LILE enrichment of the lithosphere beneath a domed and rifted continental plate. In: Kampunzu, A. B. & Lubala, R. T. (eds) *Magmatism in extensional structural settings, the Phanerozoic African plate*. Springer Verlag, New York, 23–72.
- Lloyd, F. E., Edgar, A. D. & Ragnarsdottir, K. V. 1996.** LREE distribution in perovskite, apatite and titanite from South West Ugandan xenoliths and kamafugite lavas. *Contr. Mineral. Petrol.* 57, 205–228.
- Lloyd, F. E., Woolley, A. R., Stoppa, F. & Eby, G. N. 1999.** Rift Valley magmatism – is there evidence for laterally variable alkali clinopyroxene mantle? *Geolines* 9, 76–83.
- Lloyd, F. E., Woolley, A. R., Stoppa, F. & Eby, G. N. 2002.** Phlogopite-biotite parageneses from the K-mafic-carbonatite effusive magmatic association of Katwe-Kikorongo, SW Uganda. *Mineralogy and Petrology* 74, 299–322.
- Loose, D., Schenk, V., Schumann, A. & Tiberindwa, J. 2004.** Pan-African UHP-metamorphism at the eastern border of the Congo Craton, Labwor Hills, Uganda: Orleans, Abstracts, 20th Coll. Afr. Geol. (CAG20), 268.
- López-Gamundí, O. R. & Buatois, L. 2010.** Introduction: Late Paleozoic glacial events and postglacial transgressions in Gondwana. *Geol. Soc. Amer., Spec. Paper* 468, v–viii.
- Lowman, J. P. & Jarvis, G. T. 1999.** Thermal evolution of the mantle following continental aggregation in 3D convection models: *Geoph. Res. Lett.* 26, 2649–2652.
- Macdonald, R. 1955.** Preliminary account of the geology of Sheet K IV, NW Karamoja. *Geol. Surv. Uganda, Entebbe, Records for 1953*.
- Macdonald, R. 1961.** Explanation of the geology of Sheet 36 (Nabilatuk). *Geol. Surv. Uganda, Entebbe, Rept.* 6, 57 p.
- Macdonald, R. 1963a.** Compilation Sheet Jinja (1:250 000). Unpubl. compiled Geol. Map Sheet NA-36-15 Jinja (1:250 000). *Geol. Surv. Uganda*.
- Macdonald, R. 1963b.** The Charnockite basement Complex in northern West Nile District, Uganda, and its relations to the Western Rift. Unpubl. PhD. Thesis, Univ. London.
- Macdonald, R. 1964a.** “Charnockites” in the West Nile district of Uganda: A systematic study in the Groves’ type area. 22nd Int. Geol. Congr. 13, 227–249.
- Macdonald, R. 1964b.** Explanation of the Sheets 3, 4, 11 and 12. *Geol. Surv. Uganda, Entebbe*.
- Macdonald, R. 1966.** Manuscript map for the geology of Uganda. Unpubl. Rept. Dept. Land Surveys, Entebbe.
- Macdonald, R. 1967.** Rift faulting in the Murchison Falls National Park, Uganda (interim version). Unpubl. Rept. *Geol. Surv. Uganda, Entebbe*.
- Macdonald, R. & Old, R. A. 1969.** *Geol. Surv. Uganda, Unpubl. Rep., RM/30*.
- Macey, P. H. & Armstrong, R. A. 2005.** U-Pb SHRIMP Geochronology of Gneisses and Granites of the Mozambique Metamorphic Belt in the Nampula-Zambezia Provinces, Northern Mozambique. CGS, Unpubl. Rept.
- Macey, P. H., Ingram, B. A., Cronwright, M. S., Botha, G. A., Roberts, M. R., Grantham, G. H., Maree, I., Botha, P. M., Kota, M., Opperman, R., Haddon, I. G., Nolte, J. C. & Rowher, M. 2006.** Geological Explanation of the 1 : 250 000 Map Sheets: 1537 Alto Molocue, 1538 Murrupula, 1539 Nampula, 1540 Mocingual, 1637 Errego, 1638 Gile, and 1639 Angoche in Northeastern Mozambique. Council for Geoscience, South Africa, September 2006. 211 p.
- MacGregor, J. P. 1962.** Explanation of the Geology of Sheet 10 (Kaabong). Report no. 9, *Geol. Surv. Uganda, Entebbe*. 42 p.
- MacLachy, L. & Pilbeam, D. 1999.** Renewed research in the Ugandan Early Miocene. In: Andrews, P. & Banham, P. (eds) *Late Cenozoic Environments and Homonid Evolution. A tribute to Bill Bishop*. *Geol. Soc. London*, 15–25.
- Magnée, I. de 1935.** Coupe géologique des Monts Kibara (Katanga). *Ann. Soc. Geol. Belg. P.R.C.B.* 43, 70–82.
- Magnée, I. de & Aderca, B. 1960.** Contribution à la connaissance du Tungsten-belt ruandais. *Acad. Roy. Sci. Outre-Mer, Brussels* 11(7), 1–56.
- Maier, W. D., Peltonen, P., Livesey, T. 2007.** The ages of the Kabanga North and Kapalagulu intrusions, Western Tanzania: a reconnaissance study. *Econ. Geol.* 102, 147–154.
- Maitre, R. W. le 1989.** A classification of igneous rocks and glossary of terms. Oxford. 193 p.
- Mäkitie, H., Baglow, N., Boger, S., Data, G., Kock, G. de, Elepu, D., Härmä, P., Jenett, T., Koistinen, T., Kyagulanyi, D., Lehtonen, M. I., Manninen, T., Mänttäre, I., Pokki, J., Schumann, A., Westerhof, A. B. & Virransalo, P. 2011a.** Giant c. 1.37 Ga arcuate dolerite dyke swarm in SW Uganda. 23rd Colloquium of African Geology, 8.–14 Febr. 2011, Univ. Johannesburg, South Africa. Abstract volume, 256.
- Mäkitie, H., Mavejje, P., Mänttäre, I. & Pakkanen, L. 2011b.** New area of charnockites and granulites: Ogili in north Uganda. 23rd Coll. Afr. Geol. (CAG23), 8–14 Jan. 2011, Univ. of Johannesburg, Abstract volume, 255.
- Mäkitie, H., Härmä, P., Virransalo, P., Kock, G. de, Lugaizi, I. & Tumwine, A. 2014a, in press.** The granite batholith of Mubende, Uganda: preliminary results on its petrography, geochemistry and construction rock potential. In: Lehto, T. & Katto, E. (eds) *GTK Consortium Geological Surveys in Uganda 2008–2012*. Geological Survey of Finland, Special Paper 56.
- Mäkitie, H., Mawejje, P. & Tiljander, M. 2014b, in press.** Petrological characteristics of the EAO granulites and charnockites in the Kalonga region, adjacent to the Archaean Uganda block. In: Lehto, T. & Katto, E. (eds) *GTK Consortium Geological Surveys in Uganda 2008–2012*. Geological Survey of Finland, Special Paper 56.
- Mäkitie, H., Data, G., Isabirye, E., Mänttäre, I., Huhma, H., Klausen, M. B., Pakkanen, L. & Virransalo, P. 2014c.** Petrology, geochronology and emplacement model of the giant 1.37 Ga arcuate Lake Victoria Dyke Swarm on the margin of a large igneous province in eastern Africa. *J. Afr. Earth Sci.* 97, 273–297.
- Manhiça, A. D. S. T., Grantham, G. H., Armstrong, R. A., Guise, P. G. & Kruger, F. J. 2001.** Polyphase deformation and metamorphism at the Kalahari Craton – Mozambique Belt Boundary. In: Miller, J. A., Holdsworth, R. E., Buick, I. S. & Hand, M. (eds) *Continental Reactivation and Reworking*, *Geol. Soc. London, Spec. Publ.* 184, 303–322.
- Maniar, P. D. & Picoli, P. M. 1989.** Tectonic discrimination of granitoids. *Geol. Soc. Amer. Bull.* 101 (5), 635–643.
- Mänttäre, I. 2008.** Mesoarchaean to Lower Jurassic U-Pb and Sm-Nd ages from NW Mozambique. Geological Survey of Finland, Special Paper 48, 81–119.

- Mänttari, I. 2014, in press.** Mesoarchaean to Neoproterozoic U-Pb and Sm-Nd ages from Uganda. In: Lehto, T. & Katto, E. (eds). GTK Consortium Geological Surveys in Uganda 2008–2012. Geological Survey of Finland, Special Paper 56.
- Mänttari, I., Kigireigu, F., Huhma, H., Kock, G. S. de, Koistinen, T., Kuosmanen, E. T., Lahaye, Y., Lehtonen, M. I., Mäkitie, H., Manninen, T., O'Brien, H., Saalman, K., Virransalo, P. & Westerhof, A. B. 2011.** New Precambrian rock ages from Uganda. 23rd Coll. Afr. Geol. (CAG23), 8–14 Jan. 2011, Univ. of Johannesburg, Abstract volume, 260.
- Manya, S., Kobayashi, K., Maboko, M. A. H. & Nakamura, E. 2006.** Ion microprobe zircon U–Pb dating of the late Archaean metavolcanics and associated granites of the Musoma–Mara Greenstone Belt, Northeast Tanzania: Implications for the geological evolution of the Tanzania Craton. *J. Afr. Earth Sci.* 45 (3), 355–366.
- Manya, S., Maboko, M. A. H., Nakamura, E. 2007a.** The geochemistry of high-Mg andesite and associated adakitic magmatism in the Musoma–Mara Greenstone Belt, northern Tanzania: possible evidence for Neoproterozoic ridge subduction? *Precambrian Research* 159, 241–259.
- Manya, S., Maboko, M. A. H., Nakamura, E. 2007b.** Geochemistry and Nd-isotopic composition of potassic magmatism in the Neoproterozoic Musoma–Mara Greenstone Belt, northern Tanzania. *Precambrian Res.* 159, 231–240.
- Manya, S. & Maboko, M. A. H. 2008.** Geochemistry of the Neoproterozoic mafic volcanic rocks of the Geita area, NW Tanzania: Implications for stratigraphical relationships in the Sukumaland greenstone belt. *J. Afr. Earth Sci.* 52 (4–5), 152–160.
- Maravic, H. von, Morteani, G. & Roethe, G. 1989.** The cancrinite-syenite/carbonatite complex of Lueshe, Kivu/NE-Zaire: petrographic and geochemical studies and its economic significance. *J. Afr. Earth Sci.* 9, 341–355.
- Marcelot, G., Rançon, J. Ph. & Demange, J. 1985.** The potassic series of Karisimbi volcano (Virunga range, Rwanda): Volcanological and petrological aspects. *J. Volcanology Geothermal Res.* 25 (3–4), 99–101, 105–129.
- Marshall, K. 1954.** The Prehistory of the Entebbe Peninsula. *Uganda Jour.*, XVIII, 44.
- Master, S., Rainaud, C., Armstrong, R. A., Phillips, D. & Robb, L. J. 2005.** Provenance ages of the Neoproterozoic Katanga Supergroup (Central African Copperbelt), with implications for basin evolution. *J. Afr. Earth Sci.* 42 (1–5), 41–60.
- Master, S., Bekker, A. & Karhu, J. A. 2008.** Palaeoproterozoic high $\delta^{13}\text{C}_{\text{carb}}$ marbles from the Ruwenzori Mountains, Uganda, and implications for the age of the Buganda-Toro Supergroup. Abstract, 22nd Coll. Afr. Geol. (CAG 22), 4–6 November 2008, Hammamet, Tunisia, 90–92.
- Master, S., Bekker, A. & Karhu, J. A. 2013.** Paleoproterozoic high $\delta^{13}\text{C}_{\text{carb}}$ marbles from the Ruwenzori Mountains, Uganda: Implications for the age of the Buganda Group. *Chem. Geol.* 362, 157–164.
- Mathu, E. M. 1992.** The Mutito and Ikoo Faults in the pan-African Mozambique Belt, eastern Kenya. In: Mason, R. (ed.) *Basement Tectonics* 7, Kluwer, Amsterdam, 61–69.
- Mathu, E. M. & Davies, T. C. 1996.** Geology and the environment in Kenya. *J. Afr. Earth Sci.* 23 (4), 511–539.
- Mazimhaka, P. K. 1973.** Report on a study of part of the eastern deposit at Kilembe mines Limited. Unpubl. Econ. Geol. Proj. Rept. 1–33, Kampala.
- McConnell, R. B. 1959a.** The Buganda Group of Uganda. XX Intern. Geol. Congr., Mexico, 1956. Assoc. Afr. Geol. Surveys, 163–174.
- McConnell, R. B. 1959b.** Outline of the geology of the Ruwenzori Mountains: A preliminary account of the British Ruwenzori Expedition 1951–52. *Overseas Min. Res.*, London 7, 245–268.
- McGlue, M. M., Scholz, C. A., Karp, T., Ongodia, B. & Lezzar, K. E. 2006.** Facies architecture of flexural margin lowstand delta deposits in Lake Edward, East African Rift: constraints from seismic reflection imaging. *J. Sedimentary Research* 76, 942–958.
- Meert, J., Hargraves, R., Voo, R. van der, Hall, R. & Halliday, A. 1994.** Palaeomagnetism and $^{40}\text{Ar}/^{39}\text{Ar}$ studies of late Kibaran intrusives in Burundi, East Africa: implications for late Proterozoic supercontinents. *J. Geol.* 102, 621–637.
- Meschede, M. 1986.** A method of discriminating between different types of mid-ocean ridge basalts and continental tholeiites with the Nb-Zr-Y diagram. *Chemical Geol.* 37, 207–218.
- Middlemost, E. A. K. 1985.** *Magmas and Magmatic Rocks.* London. Longman. 266 p.
- Miller, J. M. 1956.** Geology of the Kitale-Cherangani Hills area. *Geol. Surv. Kenya, Unpubl. Rept.* 35. 34p.
- Mohr, P. 1992.** Nature of the crust beneath magmatically active continental rifts. *Tectonophysics* 213, 269–284.
- Mosley, P. 1993.** Geological evolution of the late Proterozoic “Mozambique Belt” of Kenya. *Tectonophysics* 221, 223–250.
- Mtoro, M., Maboko, M. A. H. & Manya, S. 2009.** Geochemistry and geochronology of the bimodal volcanic rocks of the Suguti area in the southern part of the Musoma–Mara Greenstone Belt, Northern Tanzania. *Precambrian Res.* 174 (3–4), 241–257.
- Mugisho, B. E. 2013.** Characterization of the deformation in the Itombwe synclinorium (Late Kibaran) near Kaziba (South Kivu; RD Congo). 24th Coll. Afr. Geol. (CAG 24), Addis Abeba, 8–14 January 2013, Abstract Volume 30.
- Mulder, M. de & Theunissen, K. 1980.** Contribution à l'étude structurale des métasédiments de la Haute-Kitenge (NW Burundi). *Mus. Roy. Afr. Centr. (Belg), Dépt. Géol., Rapt.* Ann. 1979, 185–205.
- Mulder, M. de & Pasteels, P. 1986.** K-Ar geochronology of the Karisimbi volcano (Virunga, Rwanda-Zaire). *J. Afr. Earth Sci.* 5 (6), 575–579.
- Mulder, M. de, Hertogen, J., Deutsch, S. & André, L. 1986.** The role of crustal contamination in the potassic suite of the Karisimbi Volcano (Virunga, African Rift Valley). *Chem. Geol.* 57 (1–2), 117–136.
- Mullen, E. D. 1983.** MnO/TiO₂/P₂O₅: a minor element discriminant for basaltic rocks of oceanic environments and its implications for petrogenesis. *Earth Planet. Sci. Lett.* 62, 53–62.
- Müller, M. A., Jung, S., Kroner, A., Baumgartner, L. P., Poller, U. & Todt, W. 2001.** Pan-African emplacement and granulite-facies metamorphism in the Mavuradonha Mountains, Zambezi Belt. Abstracts, EUG XI, Strasbourg, 564.
- Muwanga, A., Schumann, A. & Biryabarema, M. 2001.** Landslides in Uganda. Documentation of a natural hazard. *Documenta Naturae* 136, 111–115.
- Mwanguzi, A. J. B. 2010.** Characterisation of Muko Iron Ores (Uganda) for the Different Routes of Iron Production. Licentiate Thesis, Stockholm 2010. Department of Materials Science and Engineering, Division of Applied Process Metallurgy, Royal Institute of Technology. 35 p.

- Nagudi, B., Koeberl, C. & Klötzli, U. 2001.** Determination of the petrogenetic history and age of the Singo granite using zircons. *GSU Newsletter* 1 (2), 36–37. Abstract Volume, Regional Conference GSU and GSAf, Kampala, 10–12 September 2001.
- Nagudi, B., Koeberl, C. & Kurat, G. 2003.** Petrography and geochemistry of the Singo granite, Uganda, and implications for its origin. *J. Afr. Earth Sci.* 36, 73–87.
- Nakamura, N. 1974.** Determination of REE, Ba, Fe, Mg, Na and K in carbonaceous and ordinary chondrites. *Geochim. Cosmochim. Acta* 38, 757–775.
- Neall, F. B. 1981.** Sapphirine-bearing granulites, Labwor Hills, N. Uganda. Unpubl. M.Sc. thesis, Univ. of Leeds.
- Nicholson, R. 1965.** The structure and metamorphism of the mantling Karagwe-Ankolean sediments of the Ntungamo gneiss dome and their time-relation to the development of the dome. *Q. J. Geol. Soc., London* 121, 143–162.
- Nicolaysen, L. O., Aldrich, L. T. & Doak, J. B. 1953.** *Trans. Amer. Geophys. Union* 34, 342–343.
- Nixon, P. H. & Hornung, G. 1973.** The carbonatite lavas and tuffs near Fort Portal, western Uganda. *Overseas Geol. Miner. Resources* 41, 168–179.
- Nixon, P. H., Reedman, A. J. & Burns, L. K. 1973.** Sapphirine bearing granulites from Labwor, Uganda. *Mineral Mag.* 39, 420–428.
- Nixon, P. H., Grew, E. S. & Condliffe, E. 1984.** Kornerupine in a sapphirine-spinel granulite from Labwor Hills, Uganda. *Mineral Mag.* 48, 550–552.
- Noce, C. A., Pedrosa-Soares, A. C., da Silva, L. C., Armstrong, R. & Piuzana, D. 2007.** Evolution of polycyclic basement complexes in the Aracua Orogen, based on U–Pb SHRIMP data: Implications for Brazil–Africa links in Paleoproterozoic time. *Precam. Res.* 159, 60–78.
- Ntungicimpaye, A. 1983.** Le magmatisme basique d'âge protérozoïque de la région de Mageyo (Burundi): données pétrographiques et géochimiques. *Rapp. Annu. 1981–1982, MRAC, Tervuren*, 119–126.
- Ntungicimpaye, A. 1984a.** Contribution à l'étude du magmatisme basique dans le Kibarien de la partie occidentale du Burundi. Ph.D. Thesis, Univ. Gend. 250 p.
- Ntungicimpaye, A. 1984b.** Le magmatisme basique dans le Burundien de l'ouest du Burundi. UNESCO Geology for Development, Newsletter/ Bulletin 3, 13–21.
- Ntungicimpaye, A. & Kampunzu, A. B. 1987.** Caractérisation géochimique des metabasites kibariennes (Protérozoïque moyen) du Burundi. In: Matheis & Schandelmeier (eds). *Current research in African Earth Sciences*, Balkeima, 37–40.
- Nyblade, A. A. & Brazier, R. A. 2002.** Precambrian lithospheric controls on the development of the East African rift system. *Geology* 30 (8), 755–758.
- Nzajibwami, E. 1984.** The West Mugere supracrustal complex (Bujumbura): evidence of an ancient basement complex remobilised during the Kibaran orogeny. *Unesco, Geology for Development, Newsletter* 3, 5–12.
- Nzajibwami, E. 1985.** Le magmatisme basique dans le complexe magmatique ante-kibarienne de la région de Bujumbura (ouest de Burundi). 13th Coll. Afr. Geol. (CAG13), St. Andrews, in: UNESCO Newsletter/ Bull. 4, 51–52.
- Old, R. A. & Rex, D. C. 1971.** Rubidium and strontium age determination of some Pre-Cambrian granitic rocks, S.E. Uganda. *Geol. Mag., London*. 108 (5), 353–360.
- Oliver, G. J. H., Johnson, S. P., Williams, I. S. & Herd, D. A. 1998.** Relict 1.4 Ga oceanic crust in the Zambezi Valley, northern Zimbabwe: Evidence for Mesoproterozoic supercontinent fragmentation. *Geology* 26, 571–573.
- Opiyo-Akech, N. 1991.** Geochemical evidences for the tectono-magmatic emplacement of the Kenyan greenstone belt rocks from the Maseno area, western Kenya. *IGCP No. 273. Bull.* 1, 69–74.
- Opiyo-Akech, N. 1992.** Tectono-Magmatic emplacement of the Kenyan Granite Greenstones: Geochemical evidence from the Maseno area, western Kenya. *Afr. J. Science and Technology* 6 (2), 27–33.
- Opiyo-Akech, N., Tarney, J. & Hoshino, M. 1999.** Petrology and geochemistry of granites from Archean terrain north of Lake Victoria, Western Kenya. *J. Afr. Earth Sci.* 29, 283–300.
- Opiyo-Akech, N., Tarney, J., Ichang'i, D. W. & Mathu, E. M. 2006.** Petrology, geochemistry and tectonic setting of the Neoproterozoic greenstone igneous rocks from western Kenya. 21st Coll. Afr. Geol., Maputo, Mozambique, 3–5 July 2006, Abstract Volume, 132.
- O'Reilly, S. Y., Griffin, W. L., Poudjom Djomani, Y. H. & Morgan, P. 2001.** Are lithospheres forever? Tracking changes in subcontinental lithospheric mantle through time. *GSA Today* 11, 4–10.
- Paepe, P. de, Tack, L., Moens, L. & Velde, P. van de 1991.** The basic magmatism of the Upper Proterozoic in South-East Burundi. *MRAC, Dept. Geol. Miner., Ann. Rept., 1989–1990*, 85–104.
- Pallister, J. W. 1955.** The occurrence and significance of pre-Cambrian algal forms at Kabwer hill, Bukoba District, Tanganyika, and in Singo, Uganda. *Geol. Mag.* 92 (6), 499–505.
- Pallister, J. W. 1956.** Rocks of Bukoba age in Uganda. 20 Intern. Geol. Congr., Mexico, vol. 1, Pt. 1.
- Pallister, J. W. 1959.** The geology of southern Mengo. (Sheets 60, 61, 70 & Part 72), with Dubois, C. G. B. Appendix on Petrography, Cherney, E. M. section on Soils of Buganda. *Geol. Surv. Uganda, Rept.* 1, 124 p.
- Pallister, J. W. & Barnes, J. 1954.** The Toro System of Uganda Intern. Geol. Congress, Proc. 19th Session, Algiers 20, 197–202.
- Pallister, J. W. & Hatton, A. & Hepworth, J. V. 1953.** Preliminary account of the geology of south Kyagwe County, Buganda. *Geol. Surv. Uganda Rec.*, 1951–1952, 3–14.
- Passchier, C. W., Myers, J. S. & Kröner, A. 1990.** *Field Geology of High-Grade Gneiss Terrains*. Springer-Verlag.
- Pasteels, P., Villeneuve, M., Paepe, P. de & Klerkx, J. 1989.** Nouvelles données géochronologiques K-Ar sur les laves du Sud-Kivu (Zaire). *Compte-Rendu. Acad. Sciences, Paris*.
- Pasyanos, M. E. & Nyblade, A. A. 2007.** A top to bottom lithospheric study of Africa and Arabia. *Tectonophysics* 444, 27–44.
- Pearce, J. A. & Norry, M. J. 1979.** Petrogenetic Implications of Ti, Zr, Y and Nb. Variations in Volcanic Rocks. *Contr. Miner. Petrol.* 69, 33–47.
- Pearce, J. A., Harris, N. B. & Tindle, A. G. 1984.** Trace element discrimination diagrams for the tectonic interpretation of granitic rocks. *J. Petrol.* 25, 956–983.
- Pearce, T. H., Gorman, B. E. & Birkett, T. C. 1975.** The TiO₂-K₂O-P₂O₅ diagram: A method of discriminating between ocean and non-oceanic basalts. *Earth Planet. Sci. Lett.* 24, 419–426.
- Pedreira, A. J. & Waele, B. De 2008.** Contemporaneous evolution of the Palaeoproterozoic–Mesoproterozoic sedimentary basins of the São Francisco–Congo Craton. *Geol. Soc., London, Spec. Publ.* 294, 33–48.
- Peeters, L. 1956.** Contribution à la géologie des terrains anciens du Ruanda–Urundi et du Kivu. *Annales Musée*

- Royale Congo belge, série in-8. Sciences géologique 10, 9–62.
- Perkins, D. III & Chipera, S. J. 1985.** Garnet-orthopyroxene-plagioclase-quartz barometry: refinement and application to the English River subprovince and the Minnesota River valley. *Contributions to Mineralogy and Petrology* 89, 69–80.
- Petters, S. M. 1991.** Regional Geology of Africa. Lecture Notes in Earth Sci. 40, xxi, 1–722, Springer Verlag, Heidelberg, Berlin.
- Phillips, W. J. 1959.** Explanation of the geology of sheet 87 (Rakai). Rept. Geol.Surv. Uganda. 2, 48p.
- Pichamuthu, C. S. 1960.** Charnockite in the making; *Nature* 188, 135–136.
- Pickford, M. 2002a.** Early Miocene grassland ecosystem at Bukwa, Mount Elgon, Uganda. *Comptes rendus Paléontologie* 1, 1–6.
- Pickford, M. 2002b.** Ruminants from the Early Miocene of Napak, Uganda. *Annales de Paléontologie* 88, 85–113.
- Pickford, M. 2004a.** Major differences in sediments of the Gregory and Albertine Rifts. 20th Colloquium of African Geology – Orleans, France. 2–7 June 2004 / Abstracts volume, 334.
- Pickford, M. 2004b.** Palaeoenvironments of Early Miocene hominoid-bearing deposits at Napak, Uganda, based on terrestrial mollusks. *Annales de Paléontologie* 90 (1), 1–12.
- Pickford, M., Senut, B., Hadoto, D., Musisi, J. & Kariira, C. 1986.** Nouvelles découvertes dans le Miocène inférieur de Napak, Ouganda Oriental. *Comptes Rendus de l'Académie des Sciences, Paris* 302, 47–52.
- Pickford, M., Senut, B. & Hadoto, D. 1993.** Geology and palaeobiology of the Albertine Rift Valley, Uganda-Zaire, Vol. 1: Geology. CIFEG Occas. Publ. 24, 1–190, Orléans, France.
- Pickford M., Senut, B., Gommery, D. & Musiime E. 2009.** Distinctiveness of Ugandapithecus from Proconsul. *Estudios Geológicos* 65, 183–241.
- Pierson, T. C. 1989.** Hazardous hydrologic consequences of volcanic eruptions and goals for mitigative action: An overview. In: Starosolszky, Ö. & Melder, O. M. (eds). *Hydrology of Disasters: Proceed. Technical Conf. Geneva, November 1988.* James & James, 220–236.
- Pin, C. & Poidevin, J. L. 1987.** U-Pb zircon evidence for a Pan-African granulite facies metamorphism in the Central African Republic. A new interpretation of the high-grade series of the northern border of the Congo Craton. *Precambrian Res.* 36 (3–4), 303–312.
- Pinna, P., Jourde, G., Caluez, J.-Y., Mroz, J. P. & Marques, J. M. 1993.** The Mozambique Belt in northern Mozambique: Neoproterozoic (1100–850 Ma) crustal growth and tectogenesis and superimposed Pan-African (800–550 Ma) tectonism. *Precam. Res.* 62, 1–59.
- Pinna, P., Cocherie, A., Thiéblemont, D., Feybesse, J. L. & Lagny, P. 1996.** Evolution géodynamique du Craton Est-Africain et déterminisme géologiques. *Chron. Rech. Minières* 525, 33–43.
- Pinna, P., Cocherie, A., Thiéblemont, D., Feybesse, J. L. & Lagny, P. 1997.** Evolution géodynamique du Craton Est-Africain et déterminismes géologiques. *Chronique Recherche Minières* 525, 33–43.
- Pinna, P., Cocherie, A., Thiéblemont, D. & Jezequel, P. 2000.** The Kisii Group of western Kenya: an end-Archean 2.53 Ga) late orogenic volcano sedimentary sequence. *J. Afr. Earth Sci.* 30 (1), 79–97.
- Pinna, P., Cocherie, A. & Thiéblemont, D. 2001.** In: Schumann, A. (Ed.), Abstracts Regional Conference of the Geological Society of Uganda and the Geological Society of Africa, Kampala, 41–42.
- Pinna, P., Cocherie, A., Thiéblemont, D. & Jezequel, P. & Kayogoma, E. 2004a.** The making of the East African Craton 2.93–2.53 Ga. 20th Coll. Afr. Geol. (CAG20), 2–7 June 2004, BRGM, Orléans, 336.
- Pinna, P., Muhongo, S., Mcharo, B., Goff E. le & Deschamps, Y. 2004b.** Geology and mineral potential of Tanzania: digital map at 1:2,000,000 scale. 20th Coll. Afr. Geol., Orleans, France. 2–7 June 2004. Abstract volume.
- Piper, J. D. 1972.** A palaeomagnetic study of the Bukoban Supergroup, Tanzania. *Geophys. J. Research Astronomical Soc.* 28, 111–127.
- Pohl, W. 1987a.** Metallogeny of the northeastern Kibaran Belt, Central Africa. In: Bowden, P. & Kinnaird, J. A. (eds). *African Geology Reviews*, J. Wiley, Chichester 22, 103–119.
- Pohl, W. 1987b.** Geotraverse Rwanda 1986: Preliminary results of metallogenic studies. UNESCO, Geology for Economic Development, Newsletter 5/1986, 93–100.
- Pohl, W. 1987c.** Maganiferous garnetite bands in Kibaran meta-volcanosedimentary rocks at Kibuye, Rwanda: Exhalites of metallogenic significance? Ext. Abstract, 349–351 in: Matheis, G. & Schandelmeier, H (eds). *Current Research in African Earth Sciences*, Balkema, Rotterdam 1987.
- Pohl, W. 1988.** Post-orogenic' events within and nearby the Kibara belt in Central Africa. IGCP Project No. 255 Newsletter 1, 47–50, TU Braunschweig – MRAC Tervuren.
- Pohl, W. 1992.** Kibaran evolution and metallogeny in Central Africa: a synthesis at the end of IGCP Project 255. Newsletter/Bulletin IGCP 255. 4, 1–8.
- Pohl, W. 1994.** Metallogeny of the northeastern Kibara belt, Central Africa - Recent perspectives. *Ore Geology Reviews* 9, 105–130.
- Pohl, W. 1997.** "Post-tectonic" events in the Kibara Belt: Metallogenic implications. 17th Coll. Afr. Geol., Spec. Vol., Harare, 186.
- Pohl, W. 2006.** Metallogeny of the northeastern Kibaran belt, Central Africa. *Geol. J.* 22 (S2), 103–119.
- Porada, H. & Berhorst, V. 2000.** Towards a new understanding of the Neoproterozoic early Palaeozoic Lufilian and northern Zambezi belts in Zambia and the Democratic Republic of Congo. *J. Afr. Earth Sci.* 30, 727–771.
- Poulet, A. 1975.** Histoire des grands lacs de l'Afrique centrale. Mise au point des connaissances actuelles. *Rev. Géogr. Phys. Géol. Dyn.* 17 (5), 475–482.
- Poudjom Djomani, Y. H., O'Reilly, S. Y., Griffin, W. L. & Morgan, P. 2001.** The density structure of subcontinental lithosphere: Constraints on delamination models. *Earth Planet. Sci. Lett.* 184, 605–621.
- Powell, C. McA. & Li, Z. X. 1994.** Reconstruction of the Panthalassan margin of Gondwanaland, in: Veevers J. J & Powell, C. McA. (eds). *Permian–Triassic Pangean Basins and Foldbelts along the Panthalassan Margin of Gondwanaland*, Geol. Soc. Amer., Memoir 184, 5–9.
- Priem, H. N. A., Boelrijk, N. A. I. M., Hebeda, E. H. T., Verdurmen E. A. & Verschure, R. H. 1979.** Isotopic age determinations on granitic and gneissic rocks from the Usagaran System in Southern Tanzania. *Precambrian Res.* 9, 227–239.
- Quennell, A. M. 1956a.** 1: 2,000,000 Geological map of Tanzania. Geol.Surv.Tanganyika, Dar-es-Salaam.
- Quennell, A. M. 1956b.** The Bukoban System of East Africa. 20 Intern Geol Congr., Mexico, Vol. 1, 1281–307.

- Ramananda, C., Basu, A. R., Santo, A. P., Dario, T. & Vaseli, O. 2009.** Isotopic and geochemical evidence for a heterogeneous mantle plume origin of the Virunga volcanics, Western rift, East African Rift system. *Chem. Geol.* 259, 273–289.
- Rammlmair, D., Höhndorf, A., Borg, G., Hiza, G. N. 1990.** Nouvelles datations isotopiques des granites et des gabros de la région "greenstone"-granitique du Sukumaland, N.W.-Tanzania (abstract volume). 15th Colloquium of African Geology, Nancy 43.
- Reece, A. W. 1955.** The Bunyaruguru volcanic field. *Rec. Geol. Surv. Uganda* 1953, 29–47.
- Reece, A. W. 1959.** The stratigraphy, structure and metamorphism of the Pre-cambrian rocks of North-West Ankole, Uganda. *Quarterly J. Geol. Soc.* 115, 389–420.
- Reece, A. W. 1961.** Explanation of the Geology of Sheet 76 (Buhwezu). *Geol. Surv. Uganda, Entebbe, Rept.* 4.
- Ries, A., Vearncombe, J. R., Price, R. C. & Shackleton, R. M. 1992.** Geochronology and geochemistry of the rocks associated with a late Proterozoic ophiolite in West Pokot, NW Kenya: *J. Afr. Earth Sci.* 14 (1), 25–36.
- Ring, U. 2008.** Extreme uplift of the Rwenzori Mountains in the East African Rift, Uganda: Structural framework and possible role of glaciations. *Tectonics* 27 (4).
- Roberts, R. O. 1940.** Annual report GSD ending 31st Dec. 1939, 70A.
- Roberts, R. O. 1942.** Notes on a visit to the Munyonyo mica deposit. Unpubl. Rept. *Geol. Surv. Uganda, Entebbe, RÖR/*
- Roberts, R. O. 1947.** Amblygonite and associated minerals from Mbale mine, Singo County. Unpubl. Rept. *Geol. Surv. Uganda, RÖR/73.*
- Roccati, A. 1907.** Nell'Uganda e nella catena del Ruwenzori. Relazione preliminare sulle osservazioni geologiche fatte durante la spedizione di S. A. R. il Duca degli Abruzzi nell'anno 1906. *Bollettino della Societa Geologica Italiana* 26(02), 127–158.
- Roche, H. de la, Leterrier, J., Grandclaude, P. & Marchal, M. 1980.** A classification of volcanic and plutonic rocks using R1, R2-diagrams and major element analysis – its relationships with current nomenclature. *Chem. Geol.* 29, 183–210.
- Rogers, J. J. W. & Santosh, M. 2002.** Configuration of Columbia, a Mesoproterozoic supercontinent. *Gondwana Research* 5 (1), 5–2.
- Rogers, J. J. W. & Santosh, M. 2003.** Supercontinents in Earth history. *Gondwana Res.* 6, 57–368.
- Rogers, N. W., Mulder, M. de & Hakesworth, C. J. 1992.** An enriched mantle source for potassic basanites: evidence from Karisimbi volcano, Virunga volcanic province, Rwanda. *Contr. Mineral. Petrol.* 111, 543–556.
- Rogers, N. W., James, D., Kelley, S. P. & Mulder, M. De 1998.** The generation of potassic lavas from the eastern Virunga province, Rwanda. *J. Petrol.* 39, 1223–1247.
- Romer, R. L. & Lehmann, B. 1995.** U-Pb columbite age of Neoproterozoic Ta-Nb mineralization in Burundi. *Econ. Geol.* 90, 2303–2309.
- Rosenthal, A., Foley, S. F., Pearson, D. G., Nowell, G. M. & Tappe, S. 2008.** Origin of kamafugite magmas in the East African Rift of western Uganda. 9th International Kimberlite Conference Extended Abstract No. 9IKC-A-00210.
- Rosenthal, A., Foley, S. F., Pearson, D. G., Nowell, G. M. & Tappe, S. 2009.** Magmatic evolution at the propagating tip of the western branch of the East African Rift. *Earth Planet. Sci. Lett.* 284 (1–2), 236–248.
- Rumvegeri, B. T. 1991.** Tectonic significance of Kibaran structures in central and eastern Africa. *J. Afr. Earth Sci.* 13, 267–276.
- Rumvegeri, B. T., Caron, J.-P. H., Kampunzu, A. B., Lubala, R. T. & Vellutini, P. J. 1985.** Pétrologie et signification géotectonique des plutonites de Kambusi (sud Kivu, Zaire). *Can. J. Earth Sci.* 22, 304–311.
- Rumvegeri, B. T., Bingen, B. & Derron, M. H. 2004.** Tectonomagmatic evolution of the Kibaran Belt in Central Africa and its relationships with mineralizations; a review. *Africa Geoscience Review* 11, 65–73.
- Ruotoistenmäki, T. 2014.** Geophysical characteristics of Aswa shear, Nagasongola discontinuity and Ring dyke complex in Uganda. *J. Afr. Earth Sci.* 93, 23–41.
- Ruotoistenmäki, T., Turunen, P., Babirye, P., Kahwa, E. & Birungi, N. 2014, in press.** Geophysical characteristics of Uganda and applications for mineral exploration. In: Lehto, T. & Katto, E. (eds). *GTK Consortium Geological Surveys in Uganda 2008–2012*. Geological Survey of Finland, Special Paper 56.
- Saalman, K. & Pokki, J. 2014, in press.** Aswa structure – a major shear zone in northern Uganda. In: Lehto, T. & Katto, E. (eds). *GTK Consortium Geological Surveys in Uganda 2008–2012*. Geological Survey of Finland, Special Paper 56.
- Sachau, T. & Köhn, D. 2007.** Modeling extension-related regional vertical movements, on the example of the Rwenzori Mountains Geophysical Research Abstracts 9, SRef-ID: 1607-7962/gra/EGU2007-A-07347.
- SADC 1998.** SADC Mining Sector Co-Ordinating Unit, Geology SubCommittee, Stratigraphy Working Group (compiled by Härtzer, F. J.), Council for Geoscience, Pretoria.
- Sahama, T. G. 1960.** Kalsilite in the lavas of Mount Nyiragongo (Belgian Congo). *J. Petrol.* 1 (2), 146–171.
- Sahama, T. G. 1962.** Petrology of Mt. Nyiragongo: a review. *Trans. Edinburgh Geol. Soc.* 19 (1), 1–28.
- Sahama, T. G. 1973.** Evolution of the Nyiragongo magma. *J. Petrol.* 14, 33–38.
- Salman, G. & Abdula, I. 1995.** Development of the Mozambique and Ruvuma sedimentary basins, offshore Mozambique. *Sedimentary Geology* 96, 7–41.
- Salpeteur, I. 1992.** Soil geochemistry, an efficient tool for tracing primary gold sources on the Zaire-Nile divide. Grain size selection and sampling direction: a critical choice. *IGCP no. 255, Newsletter/Bulletin* 4, 107–119.
- Salpeteur, I., Cassard, I. & Bizimana, E. 1989.** Etude structurale du district Kibarien aurifère de Nyungwe (Sud-Ouest du Rwanda). Implications sur la stratigraphie du Burundien. Principaux resultants scientifiques et techniques du BRGM, 153–154.
- Sanders, L. D. 1963.** Geology of the Eldoret area. *Geol. Surv. Kenya, Unpubl. Rept.* 64.
- Sanders, L. D. 1965.** Geology of the contact between the Nyanza Shield and the Mozambique Belt in western Kenya. *Bull. Geol. Surv. Kenya, Unpubl. Rept.* 7. 45 p.
- Sandiford, M., Neall, F. B. & Powell, R. 1987.** Metamorphic evolution of aluminous granulites from Labwor Hills, Uganda. *Contrib. Mineral. Petrol.* 95, 217–225.
- Sanschagrin, Y. & Mercier, A. 1983.** Proposition d'un modèle tectono-stratigraphique pour les massifs granito-gneissiques du Rwanda. *Projet Prospection Géophysique, Coopération Canado-Rwandaise, Kigali, December 1983*. Rapt. d'étape 7, 100 p.
- Santosh, M. & Omori, S. 2008.** CO₂ flushing: a plate tectonic perspective. *Gondwana Res.* 13 (1), 86–102.

- Santosh, M., Maruyama, S. & Sato, K. 2009.** Anatomy of a Cambrian suture in Gondwana: Pacific-type orogeny in southern India? *Gondwana Res.* 16 (2), 321–341.
- Santosh, M., Maruyama, S., Komiya, T. & Yamamoto, S. 2010.** Orogens in the evolving Earth: from surface continents to 'lost continents' at the core-mantle boundary. In: Kusky, T. M., Zhai, M.-G. & Xiao, W. (eds). "The evolving continents: Understanding processes of continental growth", *Geol. Soc., London, Spec. Paper* 338, 77–116.
- Schandelmeier, H. 1983.** The geochronology of post-Ubendian granitoids and dolerites from the Mambwe area, Northern Province, Zambia. *Rept. Inst. Geol. Sci.* 83 (1), 40–46.
- Schandelmeier, H., Wipfler, E., Küster, D., Sultan, M., Becker, R., Stern, R. J. & Abdalsalam, M. 1994.** Atmurdelgo suture: A Neoproterozoic oceanic basin extending into interior of northeast Africa. *Geology* 22, 563–566.
- Schenk, V. & Appel, P. 2001.** Anti-clockwise P-T path during ultrahigh-temperature (UHT) metamorphism at ca. 1050 in the Irumide Belt of eastern Zambia. *Berichte der Deutschen Mineralogischen Gesellschaft, Beiheft European J. Mineralogy* 13, 161.
- Schenk, V. & Appel, P. 2002.** UHT- metamorphism in the Irumide belt of Zambia: an anti-clockwise P-T path and concordant monazite age at 1.05 Ga. 19th Coll. Afr. Geol. (CAG19), Ennih, N. & Abdalsalam, M. G. (eds), El Jadida, Morocco 165.
- Schenk, V., Wegner, H., Appel, P. & Schumann, A. 2004.** Pan-African granulite-facies reworking of Archean granulites in the West Nile region (Congo Craton, Uganda). 20th Coll. Afr. Geol., Abstracts, BRGM, Orleans, 364.
- Schenk, V., Schumann, A., Tiberindwa, J. V., Jöns, N., Loose, D., Wegner, H. & Wittig, N. 2005.** Research project on Basement Geology of Uganda. PDF File, Cooperation between (1) Institut für Geowissenschaften der Christian-Albrechts Universität zu Kiel, Germany and 2) Department of Geology, Makerere University, Kampala, Uganda.
- Schenk, V. & Loose, D. 2011.** Pan-African UHT metamorphism and synchronous A-type granitic magmatism at the eastern border of the Congo Craton in Uganda. 23rd Coll. Afr. Geol. (CAG23), 8–14 Jan. 2011, Univ. of Johannesburg, Abstract volume, 362.
- Schlüter, T. 1997.** *Geology of East Africa. Beiträge zur regionalen Geologie der Erde*, 27, 484pp.
- Schlüter, T. 2006.** *Geological Atlas of Africa: with notes on stratigraphy, tectonics, economic geology and geoscientific education of each country*, Berlin Heidelberg New York, Springer.
- Schlüter, T., Pico-Olarker, G. & Kreuzer, T. 1993.** A review of some neglected Karoo grabens of Uganda. *J. Afr. Earth Sci.* 17 (4), 415–428.
- Schobbenhaus, C. & Brito Neves, B. B. 2003.** A geologia do Brasil no contexto da Plataforma Sul-Americana. In: Bizzi, L. A., Schobbenhaus, C., Vidotti, R. M. & Gonçalves, J. H. (eds). *Geologia, Tectônica e Recursos Minerais do Brasil. Companhia de Pesquisa de Recursos Minerais – Geological Survey of Brazil, Brasília*, 5–54 (Explanatory text for the Geological Map of Brazil, 1:2,500,000 scale).
- Schreurs, G., Giese, J., Berger, A. & Gnos, E. 2006.** The role of the Ranotsara Zone in southern Madagascar for Gondwana correlations. *TSK 11 Göttingen* 2006, 1–4.
- Schumann, A. & Kulyanyingi, P. G. 2001.** A first approach to a new understanding of the Ugandan Precambrian 'granite gneisses'. *Documenta Naturae*, Munich 136, 147–159.
- Schumann, A., Barifaijo, E. & Geisler, T. 1999.** Preliminary results on the origin of granitoid rocks of eastern Uganda and around Kampala: magmatic or metasomatic. In: Frimmel, H. E. (ed.) *Abstracts 11th Intern. Conf. GSA, Cape Town, J. Afr. Earth Sci.* 28 (4), Abstracts Volume, 71–72.
- Schumann, A., Schenk, V., Kulyanyingi, P. K., Morelli, C., Barton, E. & Garbe-Schönberg, D. 2004.** Evidence for the widespread occurrence of neo-Archean GGM-type granitoids in eastern Uganda: Orleans, Abstracts, 20th Colloquium of African Geology, 366.
- Searle, D. 1952.** *Geology of the area north-west of Kitale township (Trans Nzioa, Elgon & West Suk)*. Report – Republic of Kenya, Mines and Geological Department 19. 80.
- Senut, B., Pickford, M., Gommery, D. & Kunimatsu, Y. 2000.** A new genus of Early Miocene hominoid from East Africa: *Ugandapithecus major* (Le Gros Clark & Leakey, 1950). *Comptes Rendus de l'Academie des Sciences, Series IIA Earth and Planetary Science*, 331 (3), 227–233.
- Shackleton, R. M. 1986.** Precambrian collision tectonics in Africa. In: *Collision tectonics Geol. Soc. London, Spec. Publ.* 19, 329–349.
- Shackleton, R. M. 1993.** Tectonics of the Mozambique Belt in East Africa. *Geol. Soc. London, Spec. Publ.* 76, 345–362.
- Shackleton, R. M. 1994.** The final collision zone between East and West Gondwana; where is it? *J. Afr. Earth Sci.* 23, 271–287.
- Shackleton, R. M. 1996.** The final collision zone between East and West Gondwana: where is it? *J. Afr. Earth Sci.* 23, 271–287.
- Shackleton, R. M. & Ries, A. C. 1984.** The relation between regionally consistent stretching lineations and plate motions. *J. Struct. Geol.* 6, 111–117.
- Sherlock, S. C. & Hetzel, R. 2001.** A laser-probe ⁴⁰Ar/³⁹Ar study of pseudotachylite from the Tambach Fault Zone, Kenya: direct isotopic dating of brittle faults. *J. Struct. Geol.* 23 (1), 33–44.
- Simmons, W. C. 1921.** *Ann. Rept. 1920, Geol. Surv. Uganda, Entebbe*, 26–31.
- Simmons, W. C. 1932.** *Geol. Surv. Uganda, Entebbe, Annual Rept. 1931*, 8–10.
- Simonetti, A. & Bell, A. 1993.** Isotopic disequilibrium in clinopyroxenes from nephelinitic lavas, Napak volcano, eastern Uganda. *Geology* 21, 243–246.
- Simonetti, A., Bell, K & Hall, G. E. M. 1996.** Pb isotopic ratios and elemental abundances for selective leachates from near-surface till: implications for mineral exploration. *J. Applied Geochem.* 11, 721–734.
- Sinabantu, S. 1993.** Variations in Petrography of Rubanda, Chitwe and Masha-Kibaran Granites and its Genetic Significance. *Documenta Naturae* 77, 7–13.
- Sobolev, S. V. & Babeyko, A. Y. 2005.** What drives orogeny in the Andes? *Geology* 33, 617–620.
- Solomon, J. D. 1939.** The Pleistocene succession in Uganda. In: O'Brien, I. P. *The Prehistory of the Uganda Protectorate*. Cambridge, 15–50.
- Sommer, H., Hauzenberger, C. A., Kröner, A. & Muhongo, S. 2008.** Isothermal decompression history in the "Western Granulite" terrain, central Tanzania: evidence from reaction textures and trapped fluids in metapelites. *J. Afr. Earth Sci.* 51, 123–144.
- Spear, F. S. 1991.** On the interpretation of peak metamorphic temperatures in light of garnet diffusion during cooling. *J. Metam. Geol.* 9, 379–388.
- Spray, J. G. 1992.** A physical basis for the frictional melting of some rock-forming minerals. *Tectonophysics* 204, 205–221.

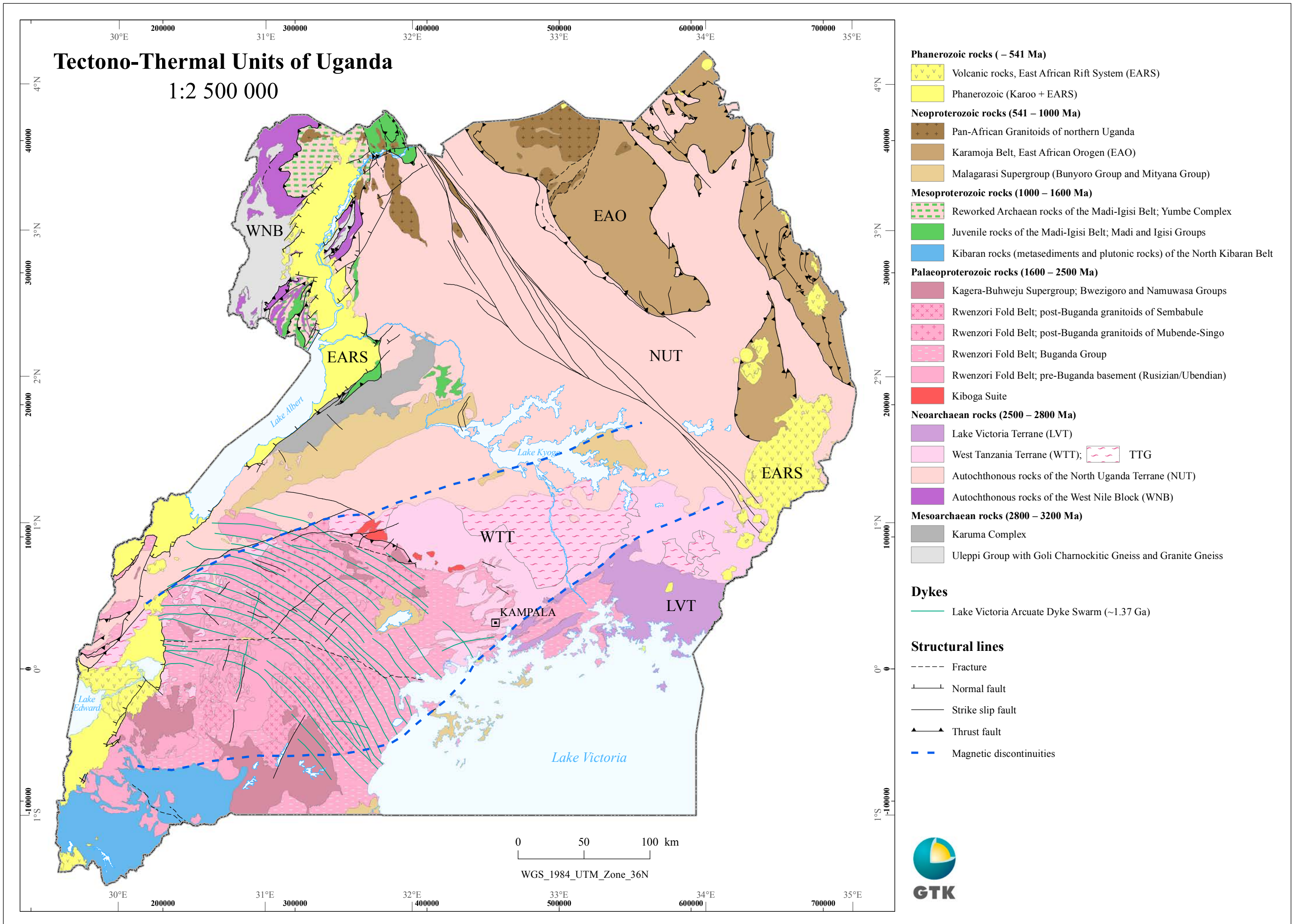
- Stern, R. J. 1994.** Arc assembly and continental collision in the Neoproterozoic East African Orogen: Implication for the consolidation of Gondwanaland. *Ann. Rev. Earth. Plan. Sci.*, 22, 319–351.
- Stern, R. J. 2002.** Crustal Evolution in the East African Orogen: A Neodymium Isotopic Perspective, *J. Afr. Earth Sci.* 34, 109–117.
- Stern, R. J. 2004.** Subduction Initiation: Spontaneous and Induced. *Earth Planet. Sci. Lett.* 226, 275–292.
- Stheeman, H. A. 1932.** The geology of south-western Uganda with special reference to the stanniferous deposits. Martinus Nijhoff, The Hague, 144 p (with 94 photos, 102 figures and 6 maps).
- Stockley, G. M. 1935.** Outline of the geology of the Musoma District – Tanganyika Territory. *Geol. Surv. Dept. Bull.* 7.
- Stockley, G. M. 1943.** The pre-Karoo stratigraphy of Tanganyika. *Geol. Mag., London* 80, 161–170.
- Stockley, G. M. 1947.** The geology of the country around Mwanza Gulf. *Geol. Surv. Tanganyika, Dodoma, Short paper* 29, 1–25.
- Stoppa, F., Woolley, A. R., Lloyd, F. E. & Eby, N. 2000.** Carbonatite lapilli-bearing tuff and a dolomite carbonatite bomb from Murumuli crater, Katwe volcanic field, Uganda. *Mineral. Mag.* 64, 641–650.
- Straaten, H.-P. van 1971.** Preliminary work on the Precambrian adjoining the Western Rift, north of Masindi, Bunyoro District (Sheet 39/I). *Interim Res. Rept. I, Dept. Geol. Makerere Univ., Kampala.*
- Straaten, H.-P. van 1973.** Precambrian structures and their relation to the Western Rift in the Masindi area (Uganda). *Abstract, 7th Coll. Afr. Geol., Florence.*
- Straaten, H.-P. van 1976.** Präkambrium und junges Western Rift im Bunyoro Distrikt, NW-Uganda. *Geol. Jahrb., Reihe B, Heft* 18, 95p.
- Straaten, H.-P. van 1977.** Morphotectonic investigations along the Western Rift in the Masindi area, Bunyoro District, Uganda. *Geol. Rundschau* 66 (1), 217–228, Stuttgart.
- Streckeisen, A. L. & Maitre, W. I. le 1979.** A chemical approximation to the modal QAPF classification of the igneous rocks. *Neues Jahrb. Mineral., Abhandlungen* 136, 169–206
- Suwa, K., Nureki, T., Inoue, H., Biyajima, K. & Miyakawa, K. 1979.** Geology and petrology of the Mavhakos area, Kenya. 4th Prelim. Rept. African Studies, Nagoya Univ., Japan, 3–20.
- Tack, L. 1992.** Development of local basins as a result of reactivation of Kibaran (Middle Proterozoic) structures: two examples from Burundi situated outside the Tanganyika trough. UNESCO, *Geology for Development, Newsletter/Bull.*
- Tack, L. 1995.** The Neoproterozoic Malagarazi Supergroup of SE Burundi and its equivalent Bukoban System in NW Tanzania: A current review. In: Wendorff, M. & Tack, L. (eds). *Late Proterozoic belts in Central and Southwestern Africa; IGCP Project 302.* Royal Museum for Central Africa, Tervuren (Belgium). *Geological Sciences* 101, 121–129.
- Tack, L. & Paepe, P. de 1981.** Le massif intrusif de syénites foidales de la Haute-Ruvubu, Burundi. *Rapp. Annu.* 1980, MRAC, Tervuren, 173–178.
- Tack, L. & Paepe, P. de 1983.** Existence de plusieurs massifs granitiques alcalins au Burundi: réflexions préliminaires. MRAC, *Dept. Geol. Miner., Ann. Rept.* 1981–1982, 135–136.
- Tack, L., Deutsch, S., Liégeois, J.-P. & Paepe, P. de 1983.** Age, Nd and Sr isotopic geochemistry of the alkaline plutonic complex of the Upper-Ruvubu (Burundi). 12th Coll. Afr. Geol. (CAG12), Brussels, Abstract Volume.
- Tack, L., Paepe, P. de, Deutsch, S. & Liégeois, J.-P. 1984.** The alkaline plutonic complex of the Upper Ruvubu (Burundi): Geology, age, isotopic chemistry and implications for the regional geology of the Western Rift. In: Klerkx, J. & Michot, J. (eds). *African Geology, MRAC, Tervuren, Belgium*, 91–114.
- Tack, L. & Thorez, J. 1990.** Sedimentology of the Musinduzi Group, Malagarasian (Upper Proterozoic), Burundi. *IGCP 255, Newsletter/Bull.* 3, 89–92.
- Tack, L., Paepe, P. De, Liégeois, J.-P., Nimpagaritse, G., Ntungicimpaye, A. & Midende, G. 1990.** Late Kibaran magmatism in Burundi. *J. African Earth Sci.* 10 (4), 733–778.
- Tack, L., Sindayihebura, A. & Cimpaye, D. 1992.** The Nkoma (SE Burundi): An episodically reactivated Lower Burundian (Middle Proterozoic) siliciclastic sequence, locally overlain by a Malagarasian (Upper Proterozoic) sedimentary breccia. *IGCP 255, Newsletter/Bull.* 4, 31–43.
- Tack, L., Duchesne, J.-C., Liégeois, J.-P. & Deblond, A. 1994.** Kibaran A-type granitoids and mafic rocks generated by two mantle sources in a late orogenic setting (Burundi). *Precam. Res.* 68, 323–356.
- Tack, L., Deblond, A., Paepe, P. de, Duchesne, J.-C. & Liégeois, J.-P. 1996.** Proterozoic alignments of alkaline plutons revealing lithospheric discontinuities: evidence from Eastern Africa. In: Demaiffe, D. (ed.). “Petrology and Geochemistry of magmatic suites of rocks in the continental and oceanic crusts. A volume dedicated to Prof. J. Michot”, ULB, Bruxelles – R.M.C.A., Tervuren, 219–226.
- Tack, L. & Duchesne, J. C. 1997.** Geology and petrology of late Kibaran alkaline granitoids in Burundi. 17th Coll. Afr. Geol., Spec. Vol. Harare, 188.
- Tack, L., Baudet, D., Chartry, G., Deblond, A., Fernandez-Alonso, M., Lavreau, J., Liégeois, J.-P., Tahon, A., Theunissen, K., Trefois, Ph. & Wingate, M. 2002a.** The North-eastern Kibaran Belt (NKB) reconsidered: evidence for a c. 1370 Ma-old repeatedly reactivated Kibara mobile belt, preceding the c. 1.0 Ga Rodinia Supercontinent assembly. 19th Colloq. Afr. Geol., El Jadida, Morocco, 19–22 March 2002, 173.
- Tack, L., Baudet, D., Chartry, G., Deblond, A., Fernandez-Alonso, M., Lavreau, J., Liégeois, J.-P., Fernandez-Alonso, M., Tahon, A., Theunissen, K., Wingate, M. & Barritt, S. 2002b.** The North-eastern Kibaran Belt (NKB) reconsidered: New constraints from a revised lithostratigraphy, a GIS compilation of existing geological maps and a review of recently published as well as unpublished igneous emplacement ages in Burundi. 11th Quadrennial IAGOD Symposium and Geo-Congress, 22–26 July 2002, Windhoek, Namibia.
- Tack, L., Fernandez-Alonso, M., Waele, B. De, Tahon, A., Dewaele, S., Baudet, D. & Cutten, H. 2006a.** The North-eastern Kibaran belt (NKB): a long-lived Proterozoic intraplate history. *Extended Abstract, 21st Coll. Afr. Geol. (CAG21), Maputo*, 3–5 July 2006, 149–151.
- Tack, L., Fernandez-Alonso, M., Kanda Nkula, V., Mpyoi, J., Delvaux, D., Trefois, P. & Baudet, D. 2006b.** Neoproterozoic diamictites around the Congo River Basin: A critical reappraisal of their origin. *Abstract, 21st Coll. Afr. Geol., Maputo, Mozambique*, 3–5 July 2006, 152–154.
- Tack, L., Delvaux, D., Kadima, E., Delpomdor, F., Tahon, A., Dumont, P., Hanon, M., Fernandez-Alonso, M., Baudet, D., Dewaele, S., Cibambula, E., Kanda Nkula,**

- V. & Mpiana, C. 2008a.** The 1000 m thick red bed sequence of the Congo River Basin (CRB): A generally overlooked testimony in Central Africa of post-Gondwana amalgamation (550 Ma) and pre-Karoo break-up (320 Ma). Abstract, 22nd Coll. Afr. Geol.(CAG 22), 4–6 November 2008, Hammamet, Tunisia, 86–88.
- Tack, L., Wingate, M. T. D., Eaele, B. De, Meert, J., Griffin, B., Belousova, E. A., Tahon, A., Fernandez-Alonso, M., Baudet, D., Cutten, H. N. C. & Dewaele, S. 2008b.** The Proterozoic Kibaran Belt in central Africa: Intracratonic 1375 Ma emplacement of a LIP. Abstract, 22nd Coll. Afr. Geol. (CAG22), 4–6 November 2008, Hammamet, Tunisia, 89.
- Tack, L., Wingate, M. T. D., Waele, B. De, Meert, J., Griffin, B., Belousova, E. A., Tahon, A., Fernandez-Alonso, M., Baudet, D., Cutten, H. N. C. & Dewaele, S. 2009.** The Mesoproterozoic “Kibaran Event” in Central Africa: a 1375 Ma intracratonic emplacement of a Large Igneous Province (LIP). Geol. Soc. London, Fermor Meeting “Rodinia: Supercontinents, superplumes and Scotland”, Edinburgh, 9–13 Sept. 2009.
- Tack, L., Wingate, M. T. D., Waele, B. De, Meert, J., Belousova, E., Griffin, B., Tahon, A. & Fernandez-Alonso, M. 2010.** The 1375Ma “Kibaran event” in Central Africa: Prominent emplacement of bimodal magmatism under extensional regime. *Precambrian Research* 180, 63–84.
- Tack, L., Wingate, M. T. D., Waele, B. De, Meert, J., Griffin, B., Belousova, E. A., Tahon, A. & Fernandez-Alonso, M. 2011a.** The 1375 Ma “Kibaran Event” in Central Africa: prominent emplacement of bimodal magmatism under extensional regime. 23rd Coll. Afr. Geol. (CAG23), 8–14 Jan. 2011, Univ. of Johannesburg, Abstract volume, 375.
- Tack, L., Fernandez-Alonso, M., Tahon, A., Waele, B. De, Baudet, D. & Dewaele, S. 2011b.** The “Kibaran Belt” of Central Africa: What’s in a name? 23rd Coll. Afr. Geol. (CAG23), 8–14 Jan. 2011, Univ. of Johannesburg, Abstract volume, 376.
- Tahon, A. 1997.** The Kibaran structural pattern in Rwanda as a result of major lateral shear. 17th Coll. Afr. Geol., Spec. Vol., Harare, 189.
- Tahon, A., Theunissen, K., Trefois, Ph. & Wingate, M. 2002.** The North-eastern Kibaran Belt (NKB) reconsidered: evidence for a c. 1370 Ma-old repeatedly reactivated Kibara mobile belt, preceding the c. 1.0 Ga Rodinia Supercontinent assembly. 19th Colloq. Afr. Geol., 19–22 March 2002, El Jadida, Morocco, 173.
- Tahon, A., Fernandez-Alonso, M., Tack, L. & Barritt, S. D. 2004.** New insights about the evolution of the Mesoproterozoic Northeastern Kibaran belt (Central Africa): Orleans, Abstracts, 20th Coll. Afr. Geol. (CAG20), 389.
- Tanner, P. W. G. 1969a.** A review of the geology of the Ruwenzori Mountains, Western Uganda. 13th Ann. Rept., Inst. Afr. Geol., Univ. Leeds, 7–9.
- Tanner, P. W. G. 1969b.** Precambrian stratigraphy as a guide to the location of copper mineralisation in the Ruwenzori Mountains, western Uganda. 13th Ann. Rept. Res. Inst. Afr. Geol., Leeds.
- Tanner, P. W. G. 1970.** The Ruwenzori fold belt of East Africa. 14th Ann. Rept., Inst. Afr. Geol., Univ. Leeds, 3–7.
- Tanner, P. W. G. 1971.** The Stanley Volcanics Formation of Ruwenzori, Uganda. 15th Ann. Rept., Inst. Afr. Geol., Univ. Leeds, 8–11.
- Tanner, P. W. G. 1972.** Regional correlation and stratigraphic position of the host rocks of the Kilembe ore body, Uganda. 16th Ann. Rept., Inst. Afr. Geol., Univ. Leeds, 24–28.
- Tanner, P. W. G. 1973a.** Regional metamorphism of low pressure intermediate type in the Ruwenzori fold belt of East Africa. Ann. Rept. Res. Inst. Afr. Geol., Univ. Leeds 17, 20–26.
- Tanner, P. W. G. 1973b.** Orogenic cycles in East Africa. Geol. Soc. Amer. Bull., 84, 2839–2850.
- Tapponnier, R., Peltzer, G., Le Dain, A. Y., Armijo, R., Cobbold, P. 1982.** Propagating extrusion tectonics in Asia; new insights from simple experiments with plasticine. *Geology*, 10 (12), 611–616.
- Taylor, R. G. & Howard, K. W. 1998.** Post-Palaeozoic evolution of weathered land surfaces in Uganda by tectonically controlled deep weathering and stripping. *Geomorphology*, 25 (3–4), 173–192.
- Temple, P. H. 1963.** Evidence of lake level changes from the southern shoreline of Lake Victoria, Uganda. In: Steel, R. W. & Prothero, R. M. (eds). *Geographers and the Tropics*, Liverpool Essays, London.
- Temple, P. H. 1964.** Raised features along the southern shoreline of Lake Victoria. *Proc. East Afr. Acad.* 1, 13–22.
- Temple, P. H. 1966a.** Evidence of changes in the level of Lake Victoria and their significance. Unpubl. PhD thesis, Univ. London, 1–364.
- Temple, P. H. 1966b.** Lake Victoria levels. *Proc. East African Acad.* 2, 50–58.
- Theunissen, K. 1984.** Les principaux traits de la tectonique kibarienne au Burundi. UNESCO, *Geology for Development*, Newsletter 3, 25–30.
- Theunissen, K. 1988a.** Evidence for Upper proterozoic conjugate strike-slip basins controlled by basement structures in NW Tanzania and Burundi. *Bull. Soc. Belge Géol.* 97(2), 115–130
- Theunissen, K. 1988b.** Kibaran thrust fold belt (D1-2) and shear belt (D20). *Newsletter/Bulletin* 1, 55–64 (IGCP 255).
- Theunissen, K. 1989.** On the Rusizian basement rise in the Kibara belt of Northern Lake Tanganyika. *IGCP 255, Newsletter/Bull.* 2, 85–92.
- Theunissen, K. & Klerkx, J. 1980.** Considérations préliminaires sur l'évolution tectonique du Burundien au Burundi. *Rapp. Annu.* 1979, MRAC, Tervuren, 207–214.
- Thomas, R. J., Agenbacht, A. L. D., Cornell, D. H. & Moore, J. M. 1994.** The Kibaran of southern Africa: Tectonic evolution and metallogeny, *Ore Geology Reviews* 9 (2), 131–160.
- Toteu, S. M., Michard, A., Bertrand, J. M. & Rocci, G. 1987.** U/Pb dating of Precambrian rocks from northern Cameroon, orogenic evolution and chronology of the Pan-African Belt of central Africa. *Precam. Res.* 37, 71–87.
- Toteu, S. M., Schmus, W. R. van, Penaye, J. & Nyobé, J. B. 1995.** U-Pb and Sm-Nd evidence for Eburnian and Pan-African high grade metamorphism in cratonic rocks of Southern Cameroon. *Precambrian Res.* 67 (3–4), 321–347.
- Toteu, S. M., Schmus, W. R. van, Penaye, J. & Michard, A. 2001.** New U-Pb and Sm-Nd data from north-central Cameroon and its bearing on the pre-Pan African history of central Africa: *Precam. Res.* 108, 45–73.
- Toteu, S. F., Penaye, J., Tchameni, R. & Schmus, W. R. van 2003.** Extension and evolution of the 2.1 Ga West-Central African belt in Cameroon: *European Geophysical Society, Geophysical Research Abstracts* 5, 11554
- Toteu, S. F., Penaye, J. & Poudjom Djomani, Y. 2004a.** Geodynamic evolution of the Pan-African belt in central Africa with special reference to Cameroon. *Can. J. Earth Sci.* 41, 73–85.

- Toteu, S. F., Deloule, E., Penaye, J. & Tchameni, R. 2004b.** Preliminary U-Pb ionic microprobe data on zircons from Poli and Lom volcano-sedimentary basins (Cameroon): Evidence for a late-Mesoproterozoic to Early Neoproterozoic (1100-950 Ma) magmatic activity in the Central African fold belt. 20th Colloquium of African Geology – Orleans, France – 2–7 June 2004 / Abstracts volume, 409.
- Toteu, S. F., Garoua, J., Macaudiere, Bertrand, J. M. & Dautel, D. 2005.** Metamorphic zircons from North Cameroon; implications for the Pan-African evolution of Central Africa.
- Toteu, F., Moloto, G., Penaye, J., Schmus, W. R. van, Lerouge, C. & Cocherie, A. 2008.** New U-Pb and Sm-Nd ages on the Pan-African belt in Central African Republic; Implications for the trans-border correlations with Cameroon. 33rd Intern. Geol. Congr., Abstract Volume.
- Trendall, A. F. 1959.** The topography under the northern part of the Kadam volcanics and its bearing on the correlation of the penepains of south-east Uganda and adjacent parts of Kenya. Geol. Surv. Uganda, Entebbe, Records for 1955–56.
- Trendall, A. F. 1961a.** Recent work in Bugisu District. Geol. Surv. Uganda, Unpubl. Rept., AFT 5.
- Trendall, A. F. 1961b.** Explanation of the geology of Sheet 45 (Kadam). Geol. Surv. Uganda, Entebbe, Rept. 6.
- Trendall, A. F. 1962.** Kokipie and Lolekek: Two minor volcanoes of eastern Uganda. Geol. Surv. Uganda, Records 1957–58.
- Trendall, A. F. 1965a.** Explanation of the Geology of Sheet 44 (Magoro). Geol. Surv. Uganda, Entebbe, Rept. 11. 28p.
- Trendall, A. F. 1965b.** Explanation of the Geology of Sheet 35 (Napak). Geol. Surv. Uganda, Entebbe, Rept. 12.
- Ucakuwun, E. K. 1988.** Geochemistry of the granitoid rocks and tectonic fracture analysis in the tin-belt of Southwest Ankole, Uganda. IGCP 255, Bull. 1, 65.
- Ucakuwun, E. K. 1989.** A study of the structural control, geology and genesis of the tin and pegmatite mineralization in SW Ankole, SW Uganda. PhD Thesis, Johannes Gutenberg Universität Mainz, Mainz. 266p.
- Ucakuwun, E. K. 1992.** Structural control of mineralized pegmatites and hydrothermal tin-bearing veins in SW Ankole, SW Uganda. IGCP 255, Newsletter/Bulletin 4, 83–89.
- Ueda, Y., Matsuzawa, I. & Suwa, K. 1975.** Potassium–argon age determinations of the Tanzanian igneous and metamorphic rocks. First Preliminary Report, African Studies. Nagoya University, Japan, 76–78.
- Vail, J. R. 1983.** Pan-African crustal accretion in north-east Africa. *J. Afr. Earth Sci.* 1 (3/4), 285–294.
- Vail, J. R. 1988.** Tectonics and evolution of the Proterozoic basement of northeastern Africa. In: El-Gaby, S. & Greiling, R. O. (eds). *The Pan-African Belt of Northeast Africa and Adjacent Areas*, Vieweg, Braunschweig, 195–226.1.
- Varne, R. 1968.** The petrology of Moroto Mountain, eastern Uganda, and the origin of nephelinites. *J. Petrol* 9 (2), 169–190.
- Vearncombe, J. R. 1983a.** A proposed continental margin in the Precambrian of Western Kenya. *International Journal of Earth Sciences, Geol. Rundschau* 72 (2), 663–670.
- Vearncombe, J. R. 1983b.** A dismembered ophiolite from the Mozambique Belt, West Pokot, Kenya. *J. Afr. Earth Sci.* 1 (2), 133–143.
- Vellutini, P. J., Bonhomme, M., Caron, J. P.-H., Kampunzu, A. B. & Lubala, R. T. 1981.** Sur la signification tectonique des complexes alcalins acides de Kahuzi et du Biega (Kivu, Zaire). *C. R. Acad. Sci. Paris* 292, 1027–1029.
- Vernon-Chamberlain, V. P. & Snelling, N. J. 1972.** Age and isotope studies on the arena granites of SW Uganda. *Ann. Rept. MRAC., Tervuren, Belgium, Sci. géol., in-8°,* 48, 1–44.
- Villeneuve, M. 1973.** Essai de synthèse des études sur les formations burundaises du synclinal de l'Itombwe (Région du Kivu, République du Zaïre). Conséquences sur la structure de ce synclinal. Institut Recherche Scientifique d'Afrique Centrale (I.R.S.A.C.), Dépt. Géol., Publ. Spéc. 5. 4 p.
- Vinyu, M. L., Hanson, R. E., Martin, M. W., Bowring, S. A., Jelsma, H. A., Krol, M. A. & Dirks P. H. G. M. 1999.** U-Pb and ⁴⁰Ar/³⁹Ar geochronological constraints on the tectonic evolution of the easternmost part of the Zambezi orogenic belt, northeast Zimbabwe. *Precam. Res.* 98,67–82.
- Viola, G., Henderson, I., Bingen, B., Feito, P., Thomas, R. J., Hollick, L. & Jacobs, J. 2006.** A new tectonic framework for northern Mozambique. *Coll. Afr. Geol. (CAG21)*, Maputo, Mozambique. Abstract Volume, 168.
- Vrána, S. & Barr, M. W. C. 1972.** Talc-kyanite-quartz schists and other high-pressure assemblages from Zambia. *Mineralogical Magazine* 38, 837–846.
- Vrána, S., Prasad, R. & Fediukova, E. 1975.** Metamorphic kyanite eclogites in the Lufilian arc of Zambia. *Contr. Miner. Petrol.* 51, 139–1.
- Vrána, S., Kachlik, V., Kröner, A., Marheine, D., Seifert, A. V., Žáček, V. & Baburek, J. 2004.** Ubendian basement and its late Mesoproterozoic and early Neoproterozoic structural and metamorphic overprint in northeastern Zambia. *J. Afr. Earth Sci.* 38, 1–21.
- Waele, B. De 2005.** The Proterozoic geological history of the Irumide Belt, Zambia., PhD Thesis, Curtin University of Technology, Australia.
- Waele, B. De & Mapani, B. 2002.** Geology and correlation of the central Irumide Belt. *J. Afr. Earth Sci.* 35, 385–397.
- Waele, B. De & Fitzsimons, I. C. W. 2004.** The age and detrital fingerprint of the Muva Supergroup of Zambia: molasse deposition to the southwest of the Ubendian belt. *Abstracts, Geoscience Africa, Johannesburg*, 162–163.
- Waele, B. De, Nemchin, A. A. & Kampunzu, A. B. 2003a.** The Bangweulu Block of northern Zambia: where is the pre-Ubendian crust? *Abstracts, Assembly and Breakup of Rodinia, South China Field Symposium, Hangzhou*, 19–21.
- Waele, B. De, Wingate, M. T. D., Mapani, B. & Fitzsimons, I. C. W. 2003b.** Untying the Kibaran knot: A reassessment of Mesoproterozoic correlations in southern Africa based on SHRIMP U-Pb data from the Irumide belt. *Geology* 31, 509–512.
- Waele, B. De, Fitzsimons, I. C. W. & Nemchin, A. A. 2004a.** Palaeoproterozoic to Mesoproterozoic deposition, magmatism and metamorphism at the southeastern margin of the Congo craton: the geological history of the Irumide belt. 20th Coll. Afr. Geol. (CAG20) – Orléans, France 2–7 June 2004. Abstracts volume, 127.
- Waele, B. De, Fitzsimons, I. C. W., Wingate, M. T. D., Mapani, B. & Tembo, F. 2004b.** A U–Pb SHRIMP geochronological database for the Irumide Belt of Zambia: from Palaeoproterozoic sedimentation to late Mesoproterozoic magmatism. In: 32nd Intern. Geol. Congr., Florence, Italy, 870–871.
- Waele, B. De, Liegeois, J.-P., Johnson, S. P., Nemchin, A. A. & Tembo, F. 2006.** Recurrent reworking of the

- Irumide Belt of Zambia. Colloquium of African Geology (CAG21), Maputo, Abstract Volume, 38–39.
- Waele, B. De, Johnson S. P. & Pisarevsky S. A. 2008.** Palaeoproterozoic to Neoproterozoic growth and evolution of the eastern Congo Craton: Its role in the Rodinia puzzle. *Precambrian Res.* 160, 127–141.
- Waleffe, A. 1965.** Etude géologique du sud-est du Burundi (Régions du Mosso et du Nkoma), *Ann. Mus. Roy. Afr. Centr., Tervuren, Belgium, Sci. géol.*, in-8°, 48, 312 p.
- Waleffe, A. 1988.** Etude photogéologique du synclinorium de l'Itombwe et des régions avoisinantes au sud du 3^{ème} parallèle sud (Kivu, Zaire). *Bull. Soc. Belge Géol.* 97, 211–221.
- Walembe, K. M. A. 2001.** Geology, geochemistry, and tectono-metallogenic evolution of Neoproterozoic gold deposits in the Kadubu area, Kivu, Democratic Republic of Congo. Ph.D. thesis (unpubl.), University of the Witwatersrand, Johannesburg, South Africa. 491 p. + Appendix 16 p.
- Walembe, K. M. A., Viljoen, M. J., Viljoen, R. P. 2004.** Geological setting, genesis and evolution of the Twangiza gold deposit, Kivu, eastern D.R.Congo. *Geoscience Africa 2004 Conference, Abstracts Vol. 2*, Univ Witwatersrand, Johannesburg, 12–16 July 2004, 682–683.
- Walembe, K. M. A. & Master, S. 2005.** Neoproterozoic diamictites from the Itombwe Synclinorium, Kivu Province, Democratic Republic of Congo: Palaeoclimatic significance and regional correlations. *J. Afr. Earth Sci.* 42 (1–5), 200–210.
- Walker, A., Brock, P. W. G & Macdonald, R. 1969.** Fossil mammal locality on Mount Elgon, eastern Uganda, *Nature* 223, 591–596.
- Wallner, H. & Schmeling, H. 2008.** Why are the Rwenzori Mountains so high? *Geophys. Res. Abstracts* 10, EGU2008-A-02924.
- Wallner, H. & Schmeling, H. 2010.** Rift induced delamination of mantle lithosphere and crustal uplift: a new mechanism for explaining Rwenzori Mountains' extreme elevation? *Intern. J. Earth Sci. (Geol Rundsch)* 99, 1511–1524.
- Warden, A. J. 1985.** Reappraisal of the geological setting and potential of Kilembe copper mine, Uganda. *Trans. Instn. Min. Metall., Section B*, B94–B105.
- Watkins, J. R. 1956.** Report on Quarter of a Degree Sheet N 11 (D.S. 39). Unpubl. Rept. Geol. Surv. Uganda, Entebbe.
- Wayland, E. J. 1921a.** Report on the geology of part of Karamoja. *Geol. Surv. Uganda, Annual Rept. for 1920*, 35–40.
- Wayland, E. J. 1921b.** Some accounts on the geology of the Lake Albert Rift valley. *Geograph. Journ., London*, 58, 344–359.
- Wayland, E. J. 1926.** Summary of results of a geological reconnaissance in the northern parts of the protectorate and Karamoja. *Geol. Surv. Uganda, Annual Rept. for 1925*, 11–13.
- Wayland, E. J. 1929.** African pluvial periods. *Nature* 123, 31–3.
- Wayland, E. J. 1931.** Igneous rocks. Summary of progress for the years 1919–1929. *Geol. Surv. Uganda*.
- Wendlandt, R. F. & Morgan, P. 1982.** Lithospheric thinning associated with rifting in East Africa. *Nature, London* 298, 734–736.
- Wendt, I., Besang, C., Harre, W., Kreuzer, H., Lenz, H. & Müller, P. 1972.** Age determinations of granitic intrusions and metamorphic events in the Early Precambrian of Tanzania. 24th Intern. Geol. Congr., Montreal, Sect. 1, 295–314.
- Westerhof, A. B. 1979.** Les travaux de follow-up dans la zone VII (Mwogo), Sud-centrale du Rwanda. Rep. Rwandaise/PNUD, Projet de Recherches Minières, RWA 77/005, Kigali, Mai. 16 p. + figures.
- Westerhof, A. B. 1980.** Etude géologique et metallogénique de la région stannifère de Bisesero, sud est de Kibuye. Rep. Rwandaise/PNUD, Projet de Recherches Minières, RWA 77/005, Kigali. 69 p. + figures.
- Westerhof, A. B. 2006.** Tectonic framework of central and southern Mozambique in relation to Africa's major building blocks. *Coll. Afr. Geol. (CAG21)*, Maputo, Mozambique. Abstract Volume, 174–176.
- Westerhof, A. B. & Koistinen, T. 2005.** Geological outline of western Tanzania with special reference to map legends. MSDTAP/Component B: Geo-Surveys. NFP-Credit 277, Unpubl. Rept. GTK. 108 p.
- Westerhof, A. B., Lehtonen, M. I., Mäkitie, H., Manninen, T., Pekkala, Y., Gustafsson, B. & Tahon, A. 2008.** The Tete-Chipata Belt: A new multiple terrane element from western Mozambique and southern Zambia. *Geol. Surv. Finland, Spec. Paper* 48, 145–166.
- Westerhof, A. B., Manninen, T. E., Saalman, K. & Baguma, Z. 2014, in press.** The Kiruruma River tillite and dropstone deposits: Glaciation in the North Kibaran Belt of south-west Uganda. In: Lehto, T. & Katto, E. (eds). *GTK Consortium Geological Surveys in Uganda 2008–2012*. Geological Survey of Finland, Special Paper 56.
- Williams, C. E. F. 1952.** Carbonatite structure: Tororo Hills, eastern Uganda. *Geol. Mag., London* 69, 286–292.
- Williams, C. E. 1966.** Geology of Karamoja, scale 1:250 000. *Geol. Surv. Uganda, Entebbe*.
- Williams, L. A. J. 1982.** Physical aspects of magmatism in continental rifts. In: Palmason, G. (ed.) 'Continental and Oceanic Rifts', *Amer. Geophys. Union., Geodyn. Ser.* 8, 193–222.
- Wilson, J. T. 1966.** Did the Atlantic close and then re-open? *Nature*, 211, (5050), 676–681.
- Wilson, T. J., Hanson R. E. & Wardlaw M. S. 1993.** Late Proterozoic evolution of the Zambezi belt, Zambia: implications for regional Pan-African tectonics and shear displacements in Gondwana. – In: Unrug, Banks & Veevers (eds). *Gondwana 8 – Assembly, evolution, and dispersal (Gondwana 8 Symposium Volume)*, Balkema, Rotterdam, 69–82.
- Wilson, T., Grunow, A. M. & Hanson, R. E. 1997.** Gondwana assembly: The view from southern Africa and East Gondwana. *J. Geodynamics* 23, 263–286.
- Winchester, J. A. & Floyd, P. A. 1977.** Geochemical discrimination of different magma series and their differentiation products using immobile elements. *Chem. Geol.* 20, 325–343.
- Windley, B. F. 1993.** Proterozoic anorogenic magmatism and its orogenic connections. *J. Geol. Soc., London*, 150, 39–50.
- Wit, M. de 1998.** On Archean granites, greenstones, cratons and tectonics: does the evidence demand a verdict? *Precam. Res.* 91, 181–226.
- Wölbern, I., Batte, A., Lindenfeld, M., Jakovlev, A., Twesigomwe, E., Rumpker, G. & Kind, R. 2007.** Rift-related uplift of the Rwenzori mountains in Uganda investigated by seismological methods. *Geophysical Research Abstracts* 9, SRef-ID: 1607-7962/gra/EGU2007-A-06346, European Geosciences Union.
- Woolley, A. R. 2001.** Alkaline Rocks and Carbonatites of the World, Part 3: Africa. *Geological Society of London*. 372 p.

- Wopfner, H. & Kaaya, C. Z. 1991.** Stratigraphy and morphotectonics of Karoo deposits of the northern Selous Basin, Tanzania. *Geol. Mag.* 128, 319–334.
- Zhao, G., Cawood, P. A., Wilde, S. A. & Sun, M. 2002.** Review of global 2.1–1.8 Ga orogens: implications for a pre-Rodinia supercontinent. *Earth-Science Reviews* 59, 125–162.
- Zhao, G. Sun, M., Wilde, S. A. & Li, S. Z. 2004.** A Paleoproterozoic supercontinent: assembly, growth and breakup. *Earth-Science Reviews* 67, 91–123.
- Ziserman, A., Zigiribabili, J., Petricec, V. & Baudin, B. 1983.** Données sur la métallogénie du Rwanda. Enseignements tirés de la carte des gîtes minéraux. *Chron. Rech. Min.* (471), 31–40.



Appendix 2. Representative chemical whole-rock analyses. The major and minor elements (Cr–C) were analysed by XRF. The chemical elements in the lower part of this Table (from Ce to V) were analysed by ICP-MS. The laboratories used were Council for Geoscience (CGS) in South Africa and Labtium Ltd in Finland.

| Unit | Nyanzian Supergroup | | | | | | | Busiro Formation | | | Golomolo granite | | |
|----------------------------------|---------------------|---------------|---------------|-------------|---------------|---------------|------------|-----------------------|-----------------------|-----------------------|------------------|---------|---------|
| Rock name | Meta-basalt | Meta-andesite | Meta-andesite | Meta-dasite | Meta-rhyolite | Meta-rhyolite | Meta-chert | Felsic metavolc. rock | Felsic metavolc. rock | Felsic metavolc. rock | Granite | Granite | Granite |
| Anal. | 1 | 2 | 3 | 4 | 5 | 6 | 7 | 8 | 9 | 10 | 11 | 12 | 13 |
| w t% | | | | | | | | | | | | | |
| SiO ₂ | 49.27 | 57.12 | 61.45 | 70.31 | 75.66 | 73.26 | 94.10 | 75.48 | 69.13 | 67.37 | 68.8 | 75.00 | 73.61 |
| TiO ₂ | 1.15 | 0.82 | 0.73 | 0.59 | 0.64 | 0.76 | 0.02 | 0.12 | 0.48 | 0.41 | 0.439 | 0.26 | 0.36 |
| Al ₂ O ₃ | 14.46 | 15.94 | 18.50 | 14.41 | 17.72 | 20.03 | 0.35 | 13.58 | 15.53 | 15.58 | 15.1 | 13.49 | 13.77 |
| Fe ₂ O ₃ t | 13.52 | 7.39 | 6.45 | 4.93 | 0.23 | 4.13 | 4.43 | 1.44 | 3.40 | 3.97 | 3.70 | 1.95 | 2.34 |
| MnO | 0.21 | 0.25 | 0.08 | 0.04 | 0.00 | 0.12 | 0.01 | 0.02 | 0.05 | 0.08 | 0.083 | 0.04 | 0.04 |
| MgO | 6.95 | 1.69 | 3.02 | 0.93 | 0.10 | 0.46 | 0.03 | 0.19 | 0.79 | 1.77 | 1.17 | 0.32 | 0.43 |
| CaO | 10.52 | 11.11 | 1.94 | 1.13 | 0.25 | 0.23 | 0.05 | 0.87 | 2.08 | 3.23 | 2.37 | 0.94 | 1.14 |
| Na ₂ O | 1.19 | 2.40 | 2.01 | 4.86 | 0.52 | b.d. | b.d. | 3.02 | 3.20 | 3.80 | 4.37 | 2.98 | 2.62 |
| K ₂ O | 0.19 | 2.07 | 3.43 | 2.61 | 3.18 | 0.22 | 0.01 | 5.13 | 4.85 | 3.85 | 3.38 | 5.13 | 5.58 |
| P ₂ O ₅ | 0.09 | 0.17 | 0.15 | 0.14 | 0.07 | 0.16 | 0.12 | 0.05 | 0.20 | 0.21 | 0.195 | 0.07 | 0.07 |
| Total | 97.57 | 98.97 | 97.76 | 99.94 | 98.39 | 99.36 | 99.11 | 99.91 | 99.71 | 100.28 | 99.61 | 100.17 | 99.96 |
| ppm | | | | | | | | | | | | | |
| Cr | 211 | 59 | 152 | 29 | 22 | 31 | 17 | 16 | 11 | 43 | b.d. | 12 | 15 |
| Ni | 113 | 19 | 59 | 12 | 7.9 | 29 | b.d. | 4 | 4 | 11 | 20 | 3.1 | 3.3 |
| Sc | 31 | 10 | 18 | 10 | 6.2 | 20 | b.d. | 4 | 6 | 11 | b.d. | 5 | b.d. |
| V | 267 | 111 | 135 | 35 | 103 | 115 | 6.1 | 7 | 37 | 53 | 75 | 14 | 23 |
| Zr | 65 | 159 | 137 | 279 | 189 | 183 | 3.6 | 120 | 241 | 109 | 179 | 174 | 276 |
| La | b.d. | 22 | 30 | 20 | 15 | 17 | b.d. | 53 | 68 | 35 | 41 | 68 | 149 |
| Ce | b.d. | 42 | 59 | 40 | 24 | 37 | b.d. | 94 | 116 | 55 | 82 | 125 | 286 |
| Ba | 41 | 456 | 782 | 1 554 | 409 | 30 | 19 | 364 | 1117 | 912 | 626 | 557 | 579 |
| Sr | 93 | 284 | 265 | 65 | 159 | 21 | 9.3 | 90 | 432 | 433 | 361 | 145 | 154 |
| Rb | 4.2 | 49 | 107 | 46 | 134 | 13 | b.d. | 238 | 180 | 151 | 205 | 273 | 199 |
| Y | 23 | 20 | 16 | 31 | 19 | 11 | 1.6 | 23 | 18 | 21 | 31 | 26 | 14 |
| Nb | 3.8 | 8.3 | 7.1 | 12 | 6.1 | 7.2 | 1.5 | 11 | 13 | 14 | 23 | 22 | 11 |
| Th | b.d. | 4.3 | 8 | 14 | b.d. | 4.7 | b.d. | 37 | 14 | 9 | 17 | 43 | 66 |
| U | b.d. | 2.3 | b.d. | 2.5 | b.d. | b.d. | b.d. | 12 | 3 | 3 | b.d. | 2.7 | 6.8 |
| S | - | - | - | - | - | - | - | - | - | - | b.d. | - | - |
| C | - | - | - | - | - | - | - | - | - | - | - | - | - |
| ppm | | | | | | | | | | | | | |
| Ce | - | - | - | - | - | - | - | - | - | - | - | - | - |
| Dy | - | - | - | - | - | - | - | - | - | - | - | - | - |
| Er | - | - | - | - | - | - | - | - | - | - | - | - | - |
| Eu | - | - | - | - | - | - | - | - | - | - | - | - | - |
| Gd | - | - | - | - | - | - | - | - | - | - | - | - | - |
| Ho | - | - | - | - | - | - | - | - | - | - | - | - | - |
| La | - | - | - | - | - | - | - | - | - | - | - | - | - |
| Lu | - | - | - | - | - | - | - | - | - | - | - | - | - |
| Nd | - | - | - | - | - | - | - | - | - | - | - | - | - |
| Pr | - | - | - | - | - | - | - | - | - | - | - | - | - |
| Sc | - | - | - | - | - | - | - | - | - | - | - | - | - |
| Sm | - | - | - | - | - | - | - | - | - | - | - | - | - |
| Tb | - | - | - | - | - | - | - | - | - | - | - | - | - |
| Th | - | - | - | - | - | - | - | - | - | - | - | - | - |
| Tm | - | - | - | - | - | - | - | - | - | - | - | - | - |
| U | - | - | - | - | - | - | - | - | - | - | - | - | - |
| Y | - | - | - | - | - | - | - | - | - | - | - | - | - |
| Yb | - | - | - | - | - | - | - | - | - | - | - | - | - |
| Co | - | - | - | - | - | - | - | - | - | - | - | - | - |
| Zr | - | - | - | - | - | - | - | - | - | - | - | - | - |
| Hf | - | - | - | - | - | - | - | - | - | - | - | - | - |
| Nb | - | - | - | - | - | - | - | - | - | - | - | - | - |
| Rb | - | - | - | - | - | - | - | - | - | - | - | - | - |
| Ta | - | - | - | - | - | - | - | - | - | - | - | - | - |
| V | - | - | - | - | - | - | - | - | - | - | - | - | - |
| Obs. No. | 7056 | 7065 | 5160 | 11027 | 12025 | 12026 | 12029 | 4188 | 4215 | 4281 | 1015 | 7163 | 7184 |
| Easting | 585633 | 576231 | 608278 | 596366 | 595557 | 595253 | 592743 | 548075 | 540736 | 535145 | 503611 | 509525 | 502082 |
| Northing | 46596 | 43605 | 65048 | 39663 | 26976 | 26820 | 26268 | 70066 | 70635 | 70903 | 26731 | 40225 | 34041 |
| Laborato | CGS | CGS | CGS | CGS | CGS | CGS | CGS | CGS | CGS | CGS | Labtium | CGS | CGS |

Appendix 2. Cont.

| Unit | Masaba biotite granite | | | | Iganga Suite | | | | | | | | | Maluba nepheline syenite |
|----------------------------------|------------------------|---------|---------|---------|--------------|---------|---------|---------|---------------|---------|---------|---------|---------|--------------------------|
| Rock name | Granite | Granite | Granite | Granite | Granite | Granite | Granite | Granite | Syenitic rock | Granite | Granite | Granite | Syenite | |
| Anal. | 14 | 15 | 16 | 17 | 18 | 19 | 20 | 21 | 22 | 23 | 24 | 25 | 26 | |
| wt% | | | | | | | | | | | | | | |
| SiO ₂ | 76.76 | 74.52 | 75.67 | 79.77 | 71.16 | 73.42 | 75.54 | 75.7 | 67.39 | 75.41 | 72.18 | 77.33 | 56.98 | |
| TiO ₂ | 0.15 | 0.31 | 0.24 | 0.09 | 0.42 | 0.23 | 0.15 | 0.169 | 0.46 | 0.22 | 0.40 | 0.04 | 0.27 | |
| Al ₂ O ₃ | 13.18 | 13.84 | 12.88 | 12.18 | 14.35 | 14.33 | 13.19 | 12.6 | 15.00 | 12.89 | 13.77 | 13.28 | 23.28 | |
| Fe ₂ O ₃ t | 1.30 | 2.50 | 2.31 | 1.10 | 2.83 | 1.95 | 1.46 | 1.99 | 4.18 | 2.19 | 2.91 | 0.76 | 3.32 | |
| MnO | 0.03 | 0.05 | 0.04 | 0.02 | 0.04 | 0.04 | 0.04 | 0.039 | 0.07 | 0.05 | 0.05 | 0.07 | 0.09 | |
| MgO | 0.25 | 0.59 | 0.31 | 0.17 | 0.46 | 0.38 | 0.21 | 0.15 | 2.03 | 0.14 | 0.48 | 0.02 | 0.16 | |
| CaO | 1.24 | 2.24 | 1.64 | 0.19 | 1.41 | 1.08 | 0.80 | 0.593 | 3.32 | 0.67 | 1.53 | 0.67 | 0.23 | |
| Na ₂ O | 2.85 | 3.86 | 3.80 | 4.05 | 2.73 | 3.55 | 2.88 | 3.72 | 3.09 | 2.92 | 3.00 | 3.88 | 9.80 | |
| K ₂ O | 3.27 | 1.80 | 2.41 | 2.35 | 5.61 | 4.75 | 5.20 | 4.72 | 3.87 | 5.44 | 4.88 | 3.99 | 5.35 | |
| P ₂ O ₅ | 0.04 | 0.08 | 0.05 | 0.03 | 0.10 | 0.11 | 0.04 | 0.032 | 0.15 | 0.04 | 0.11 | 0.02 | 0.02 | |
| Total | 99.05 | 99.79 | 99.36 | 99.93 | 99.11 | 99.82 | 99.51 | 99.71 | 99.57 | 99.97 | 99.30 | 100.06 | 99.49 | |
| ppm | | | | | | | | | | | | | | |
| Cr | 13 | 20 | 16 | 33 | 20 | 20 | 12 | b.d. | 98 | 13 | 17 | 14 | b.d. | |
| Ni | 2.1 | 5.4 | 2.2 | 2.4 | 4.7 | 3.6 | 2.7 | b.d. | 21 | b.d. | 2.8 | b.d. | b.d. | |
| Sc | b.d. | b.d. | b.d. | 5.5 | 5.3 | b.d. | b.d. | b.d. | 8.3 | 4.5 | 5 | b.d. | b.d. | |
| V | 13 | 24 | 14 | 3.7 | 19 | 17 | 9.1 | b.d. | 80 | b.d. | 21 | b.d. | b.d. | |
| Zr | 83 | 152 | 143 | 127 | 316 | 188 | 148 | 209 | 161 | 317 | 215 | 42 | 171 | |
| La | 19 | 40 | 34 | 56 | 224 | 69 | 61 | 56 | 46 | 121 | 95 | b.d. | b.d. | |
| Ce | 28 | 67 | 61 | 78 | 395 | 111 | 109 | 120 | 79 | 232 | 176 | b.d. | 13 | |
| Ba | 606 | 519 | 520 | 515 | 1 862 | 690 | 308 | 240 | 708 | 188 | 741 | b.d. | 33 | |
| Sr | 72 | 185 | 102 | 37 | 198 | 311 | 85 | 42 | 363 | 39 | 148 | 9.7 | 53 | |
| Rb | 79 | 61 | 68 | 54 | 124 | 251 | 278 | 216 | 143 | 127 | 171 | 203 | 324 | |
| Y | 16 | 10 | 20 | 35 | 25 | 12 | 24 | 47 | 14 | 18 | 25 | 14 | 4.5 | |
| Nb | 9.9 | 9.7 | 8.6 | 11 | 13 | 14 | 16 | 31 | 9.5 | 14 | 14 | 13 | 15 | |
| Th | 12 | 9.7 | 8.3 | 13 | 28 | 26 | 43 | 21 | 21 | 29 | 28 | 15 | 3.6 | |
| U | 3.1 | b.d. | b.d. | 2.4 | 2.9 | 9.1 | 15 | b.d. | 6 | 3.3 | 5.9 | 5.3 | b.d. | |
| S | - | - | - | - | - | - | - | b.d. | - | - | - | - | - | |
| C | - | - | - | - | - | - | - | - | - | - | - | - | - | |
| ppm | | | | | | | | | | | | | | |
| Ce | - | - | - | - | - | - | - | - | - | - | - | - | - | |
| Dy | - | - | - | - | - | - | - | - | - | - | - | - | - | |
| Er | - | - | - | - | - | - | - | - | - | - | - | - | - | |
| Eu | - | - | - | - | - | - | - | - | - | - | - | - | - | |
| Gd | - | - | - | - | - | - | - | - | - | - | - | - | - | |
| Ho | - | - | - | - | - | - | - | - | - | - | - | - | - | |
| La | - | - | - | - | - | - | - | - | - | - | - | - | - | |
| Lu | - | - | - | - | - | - | - | - | - | - | - | - | - | |
| Nd | - | - | - | - | - | - | - | - | - | - | - | - | - | |
| Pr | - | - | - | - | - | - | - | - | - | - | - | - | - | |
| Sc | - | - | - | - | - | - | - | - | - | - | - | - | - | |
| Sm | - | - | - | - | - | - | - | - | - | - | - | - | - | |
| Tb | - | - | - | - | - | - | - | - | - | - | - | - | - | |
| Th | - | - | - | - | - | - | - | - | - | - | - | - | - | |
| Tm | - | - | - | - | - | - | - | - | - | - | - | - | - | |
| U | - | - | - | - | - | - | - | - | - | - | - | - | - | |
| Y | - | - | - | - | - | - | - | - | - | - | - | - | - | |
| Yb | - | - | - | - | - | - | - | - | - | - | - | - | - | |
| Co | - | - | - | - | - | - | - | - | - | - | - | - | - | |
| Zr | - | - | - | - | - | - | - | - | - | - | - | - | - | |
| Hf | - | - | - | - | - | - | - | - | - | - | - | - | - | |
| Nb | - | - | - | - | - | - | - | - | - | - | - | - | - | |
| Rb | - | - | - | - | - | - | - | - | - | - | - | - | - | |
| Ta | - | - | - | - | - | - | - | - | - | - | - | - | - | |
| V | - | - | - | - | - | - | - | - | - | - | - | - | - | |
| Obs. No. | 7012 | 11016 | 12019 | 12020 | 12048 | 7096 | 7059 | 3002 | 7053 | 4230 | 12059 | 7121 | 12040 | |
| Easting | 607726 | 619565 | 599850 | 596023 | 552094 | 563179 | 576014 | 591397 | 579800 | 541397 | 551442 | 556036 | 580238 | |
| Northing | 40294 | 48858 | 26096 | 25776 | 51480 | 19125 | 48402 | 61443 | 54362 | 66920 | 46923 | 56880 | 30454 | |
| Laborato | CGS | CGS | CGS | CGS | CGS | CGS | CGS | Labtium | CGS | CGS | CGS | CGS | CGS | |

Appendix 2. Cont.

| Unit | Bubulo Formation | TTG gneiss | | Tororo Suite | | | | | | | | | Kampala Suite |
|---------------------------------|-------------------------|-----------------|---------|--------------|---------------|---------|---------|---------|---------------|---------|---------|---------|---------------|
| Rock name | Intermed. metavolc rock | Biotite granite | Granite | Granite | Leuco-granite | Granite | Granite | Granite | Grano-diorite | Granite | Granite | Granite | Granite |
| Anal. | 27 | 28 | 29 | 30 | 31 | 32 | 33 | 34 | 35 | 36 | 37 | 38 | 39 |
| w t% | | | | | | | | | | | | | |
| SiO ₂ | 67.26 | 68.64 | 76.59 | 71.9 | 72.86 | 72.91 | 73.21 | 76.09 | 61.53 | 67.10 | 71.13 | 71.32 | 71.70 |
| TiO ₂ | 0.39 | 0.53 | 0.12 | 0.237 | 0.36 | 0.43 | 0.23 | 0.12 | 1.10 | 0.48 | 0.37 | 0.41 | 0.35 |
| Al ₂ O ₃ | 15.54 | 15.78 | 13.30 | 14.6 | 14.71 | 13.93 | 14.26 | 13.46 | 16.42 | 16.26 | 14.80 | 14.54 | 15.23 |
| Fe ₂ O _{3t} | 3.98 | 4.05 | 1.39 | 2.00 | 2.09 | 2.71 | 1.92 | 1.58 | 6.52 | 3.24 | 3.13 | 2.92 | 2.35 |
| MnO | 0.07 | 0.05 | 0.02 | 0.048 | 0.04 | 0.04 | 0.04 | 0.04 | 0.09 | 0.05 | 0.06 | 0.04 | 0.04 |
| MgO | 1.75 | 1.99 | 0.23 | 0.60 | 0.47 | 0.34 | 0.44 | 0.14 | 1.93 | 1.36 | 0.73 | 0.81 | 0.72 |
| CaO | 3.65 | 2.61 | 0.64 | 1.53 | 1.24 | 0.97 | 1.24 | 0.57 | 3.77 | 2.85 | 1.88 | 1.57 | 1.75 |
| Na ₂ O | 3.88 | 3.31 | 3.23 | 4.38 | 2.76 | 2.70 | 3.26 | 3.31 | 3.76 | 4.49 | 3.52 | 2.77 | 4.26 |
| K ₂ O | 3.15 | 2.85 | 4.64 | 4.09 | 5.26 | 5.80 | 4.98 | 4.81 | 3.90 | 3.21 | 4.04 | 5.09 | 3.41 |
| P ₂ O ₅ | 0.15 | 0.05 | 0.05 | 0.114 | 0.13 | 0.09 | 0.10 | 0.06 | 0.57 | 0.25 | 0.15 | 0.16 | 0.13 |
| Total | 99.80 | 99.86 | 100.23 | 99.50 | 99.92 | 99.91 | 99.69 | 100.20 | 99.59 | 99.28 | 99.80 | 99.62 | 99.93 |
| ppm | | | | | | | | | | | | | |
| Cr | 60 | 129 | 20 | b.d. | 16 | 17 | 16 | 15 | 36 | 35 | 14 | 30 | 17 |
| Ni | 20 | 38 | 4.7 | 33 | 4.7 | b.d. | 2.8 | 3 | 13 | 14 | 4.1 | 4.9 | 3.6 |
| Sc | 9 | 9.8 | b.d. | b.d. | b.d. | 4.2 | b.d. | b.d. | 6.2 | 3.3 | b.d. | 3.8 | 3.9 |
| V | 77 | 84 | 9.9 | b.d. | 27 | 14 | 17 | b.d. | 92 | 48 | 32 | 38 | 30 |
| Zr | 102 | 121 | 122 | 107 | 262 | 314 | 153 | 163 | 455 | 163 | 156 | 188 | 164 |
| La | 27 | 52 | 51 | b.d. | 47 | 175 | 58 | 73 | 102 | 98 | 55 | 85 | 37 |
| Ce | 40 | 97 | 81 | 38 | 85 | 294 | 95 | 121 | 182 | 135 | 100 | 157 | 62 |
| Ba | 1073 | 427 | 275 | 861 | 1 260 | 681 | 561 | 108 | 1 355 | 1 586 | 562 | 961 | 1 034 |
| Sr | 714 | 356 | 100 | 367 | 253 | 130 | 256 | 49 | 707 | 1 163 | 277 | 285 | 386 |
| Rb | 99 | 143 | 231 | 146 | 165 | 206 | 218 | 259 | 128 | 88 | 216 | 165 | 131 |
| Y | 11 | 7.8 | 12 | 23 | 8 | 20 | 13 | 17 | 28 | 11 | 19 | 13 | 8.9 |
| Nb | 6 | 8.3 | 12 | 21 | 9.8 | 14 | 11 | 15 | 20 | 5.6 | 16 | 9.1 | 6.8 |
| Th | 8 | 18 | 26 | b.d. | 19 | 22 | 21 | 37 | 7.4 | 13 | 28 | 14 | 8.9 |
| U | 4 | 3.2 | 10 | b.d. | 2.2 | 3.1 | 7.7 | 8.9 | 4 | 4.4 | 8.3 | 2.4 | 3.2 |
| S | - | - | - | b.d. | - | - | - | - | - | - | - | - | - |
| C | - | - | - | - | - | - | - | - | - | - | - | - | - |
| ppm | | | | | | | | | | | | | |
| Ce | - | - | - | - | - | - | - | - | - | - | - | - | - |
| Dy | - | - | - | - | - | - | - | - | - | - | - | - | - |
| Er | - | - | - | - | - | - | - | - | - | - | - | - | - |
| Eu | - | - | - | - | - | - | - | - | - | - | - | - | - |
| Gd | - | - | - | - | - | - | - | - | - | - | - | - | - |
| Ho | - | - | - | - | - | - | - | - | - | - | - | - | - |
| La | - | - | - | - | - | - | - | - | - | - | - | - | - |
| Lu | - | - | - | - | - | - | - | - | - | - | - | - | - |
| Nd | - | - | - | - | - | - | - | - | - | - | - | - | - |
| Pr | - | - | - | - | - | - | - | - | - | - | - | - | - |
| Sc | - | - | - | - | - | - | - | - | - | - | - | - | - |
| Sm | - | - | - | - | - | - | - | - | - | - | - | - | - |
| Tb | - | - | - | - | - | - | - | - | - | - | - | - | - |
| Th | - | - | - | - | - | - | - | - | - | - | - | - | - |
| Tm | - | - | - | - | - | - | - | - | - | - | - | - | - |
| U | - | - | - | - | - | - | - | - | - | - | - | - | - |
| Y | - | - | - | - | - | - | - | - | - | - | - | - | - |
| Yb | - | - | - | - | - | - | - | - | - | - | - | - | - |
| Co | - | - | - | - | - | - | - | - | - | - | - | - | - |
| Zr | - | - | - | - | - | - | - | - | - | - | - | - | - |
| Hf | - | - | - | - | - | - | - | - | - | - | - | - | - |
| Nb | - | - | - | - | - | - | - | - | - | - | - | - | - |
| Rb | - | - | - | - | - | - | - | - | - | - | - | - | - |
| Ta | - | - | - | - | - | - | - | - | - | - | - | - | - |
| V | - | - | - | - | - | - | - | - | - | - | - | - | - |
| Obs. No. | 5049 | 3144 | 3059 | 2012 | 402 | 3058 | 3089 | 2012 | 3094 | 4031 | 3060 | 3072 | 4308 |
| Easting | 632486 | 556537 | 614235 | 623161 | 653624 | 619303 | 605827 | 623161 | 607978 | 641273 | 618534 | 614100 | 509218 |
| Northing | 102772 | 100634 | 85367 | 80498 | 88540 | 79948 | 74317 | 80498 | 80056 | 73657 | 88272 | 81048 | 61436 |
| Laboratory | C GS | C GS | C GS | Labtium | C GS | C GS | C GS | Labtium | C GS | C GS | C GS | C GS | C GS |

Appendix 2. Cont.

| Unit | Tremolite (+actinolite) schist | | Amphibolite | | Granite gneiss | Goli charnockite gneiss | | | | | | | Leucocr. granite gneiss |
|----------------------------------|--------------------------------|---------------------------|-------------|-------------|----------------|-------------------------|-------------|-------------|----------------|------------------|---------------|---------|-------------------------|
| Rock name | Chlorite schist | Amphibolite chlorite rock | Amphibolite | Amphibolite | Granite gneiss | Amphibolite gneiss | Charnockite | Charnockite | Granite gneiss | Hornblenc gneiss | Ortho- gneiss | Gneiss | Tonalitic gneiss |
| Anal. | 53 | 54 | 55 | 56 | 57 | 58 | 59 | 60 | 61 | 62 | 63 | 64 | 65 |
| w t% | | | | | | | | | | | | | |
| SiO ₂ | 25.27 | 40.60 | 48.14 | 51.68 | 73.59 | 49.20 | 55.01 | 55.12 | 57.46 | 59.65 | 68.23 | 69.10 | 59.70 |
| TiO ₂ | 1.45 | 0.40 | 1.96 | 3.11 | 0.24 | 1.36 | 0.96 | 1.10 | 0.93 | 0.82 | 0.65 | 0.69 | 0.71 |
| Al ₂ O ₃ | 18.91 | 11.20 | 13.42 | 12.95 | 14.80 | 14.68 | 17.08 | 16.17 | 17.31 | 17.04 | 15.63 | 14.90 | 17.12 |
| Fe ₂ O ₃ t | 18.51 | 12.90 | 14.52 | 16.02 | 1.59 | 12.95 | 7.92 | 8.04 | 7.83 | 7.28 | 4.76 | 4.26 | 6.21 |
| MnO | 0.10 | 0.12 | 0.22 | 0.17 | 0.02 | 0.25 | 0.12 | 0.12 | 0.12 | 0.12 | 0.05 | 0.03 | 0.09 |
| MgO | 26.47 | 25.50 | 7.39 | 4.64 | 0.48 | 4.74 | 5.49 | 6.17 | 4.14 | 3.98 | 0.86 | 0.94 | 2.82 |
| CaO | <0.01 | 0.26 | 11.45 | 9.98 | 2.00 | 13.88 | 6.96 | 6.41 | 7.25 | 6.74 | 2.79 | 2.68 | 5.09 |
| Na ₂ O | <0.01 | 0.04 | 1.81 | 0.64 | 3.23 | 2.54 | 3.86 | 3.66 | 3.73 | 3.69 | 3.74 | 3.92 | 3.74 |
| K ₂ O | <0.01 | 0.01 | 0.42 | 0.22 | 4.40 | 0.30 | 1.47 | 2.18 | 1.05 | 1.00 | 3.01 | 2.89 | 3.30 |
| P ₂ O ₅ | 0.02 | 0.02 | 0.17 | 0.37 | 0.06 | 0.12 | 0.26 | 0.38 | 0.33 | 0.29 | 0.18 | 0.18 | 0.27 |
| Total | 90.73 | 91.05 | 99.49 | 99.77 | 100.40 | 100.02 | 99.13 | 99.36 | 100.16 | 100.60 | 99.89 | 99.59 | 99.05 |
| ppm | | | | | | | | | | | | | |
| Cr | 196 | 3050 | 156 | 23 | 30 | 213 | 251 | 306 | 138 | 123 | 27 | - | 46 |
| Ni | 505 | 1209 | 88 | 14 | <2 | 79 | 78 | 109 | 33 | 34 | 6 | - | 14 |
| Sc | 52 | 25 | 36 | 40 | <3 | 39 | 15 | 10 | 15 | 14 | 8 | b.d. | 10 |
| V | 263 | 145 | 362 | 372 | 19 | 302 | 138 | 152 | 126 | 124 | 50 | 57 | 96 |
| Zr | 34 | 39 | 105 | 229 | 181 | 63 | 200 | 407 | 150 | 150 | 342 | 417 | 175 |
| La | <10 | b.d. | 17 | 34 | 94 | 10 | 39 | 40 | 59 | 48 | 159 | 100 | 102 |
| Ce | <10 | b.d. | 23 | 70 | 110 | <10 | 66 | 65 | 95 | 72 | 216 | 193 | 123 |
| Ba | 9 | b.d. | 125 | 64 | 857 | 381 | 525 | 883 | 453 | 862 | 1172 | 1130 | 1109 |
| Sr | <2 | b.d. | 157 | 510 | 246 | 177 | 604 | 569 | 570 | 578 | 183 | 182 | 612 |
| Rb | <2 | b.d. | 9 | 5 | 91 | 4 | 34 | 83 | 28 | 21 | 71 | 69 | 105 |
| Y | 7 | b.d. | 22 | 49 | 5 | 27 | 18 | 13 | 20 | 17 | 8 | 8 | 20 |
| Nb | 2 | b.d. | 9 | 23 | 5 | 5 | 7 | 10 | 9 | 7 | 9 | b.d. | 11 |
| Th | <3 | b.d. | <3 | 5 | 38 | <3 | <3 | <3 | <3 | <3 | 25 | 17 | 20 |
| U | <2 | b.d. | <2 | <2 | <2 | <2 | <2 | <2 | <2 | <2 | <2 | b.d. | <2 |
| S | - | b.d. | - | - | - | - | - | - | - | - | - | - | 79 |
| C | - | - | - | - | - | - | - | - | - | - | - | b.d. | - |
| ppm | | | | | | | | | | | | | |
| Ce | - | 4.0 | 25.4 | - | 93.5 | 15.7 | - | 80.2 | 97.1 | 78.0 | 276.8 | - | - |
| Dy | - | 0.8 | 5.7 | - | 1.0 | 6.6 | - | 3.5 | 4.9 | 4.3 | 2.7 | - | - |
| Er | - | 0.8 | 3.4 | - | 0.4 | 4.3 | - | 1.7 | 2.2 | 2.2 | 1.0 | - | - |
| Eu | - | <0.1 | 2.0 | - | 1.1 | 1.5 | - | 1.7 | 1.9 | 2.1 | 2.0 | - | - |
| Gd | - | 0.6 | 5.6 | - | 2.8 | 5.4 | - | 5.5 | 7.3 | 6.1 | 7.7 | - | - |
| Ho | - | 0.2 | 1.1 | - | 0.2 | 1.4 | - | 0.7 | 0.9 | 0.8 | 0.4 | - | - |
| La | - | 1.9 | 14.3 | - | 64.1 | 6.5 | - | 41.7 | 50.8 | 39.2 | 168.7 | - | - |
| Lu | - | 0.2 | 0.5 | - | 0.1 | 0.7 | - | 0.3 | 0.3 | 0.3 | 0.1 | - | - |
| Nd | - | 1.9 | 19.7 | - | 32.0 | 13.6 | - | 38.9 | 50.3 | 41.2 | 90.0 | - | - |
| Pr | - | 0.5 | 4.3 | - | 10.4 | 2.8 | - | 10.1 | 12.2 | 10.0 | 28.3 | - | - |
| Sc | - | 31.2 | - | - | - | - | - | - | - | - | - | - | - |
| Sm | - | 0.5 | 5.2 | - | 4.1 | 4.4 | - | 6.8 | 9.2 | 7.6 | 11.1 | - | - |
| Tb | - | 0.1 | 0.9 | - | 0.1 | 1.0 | - | 0.7 | 1.0 | 0.9 | 0.6 | - | - |
| Th | - | 1.1 | 1.6 | - | 37.8 | 0.2 | - | 1.0 | 0.8 | 1.2 | 34.2 | - | - |
| Tm | - | 0.1 | 0.4 | - | 0.0 | 0.6 | - | 0.3 | 0.3 | 0.3 | 0.1 | - | - |
| U | - | 0.2 | - | - | - | - | - | - | - | - | - | - | - |
| Y | - | 4.7 | 30.6 | - | 4.4 | 39.1 | - | 17.7 | 23.7 | 21.4 | 11.1 | - | - |
| Yb | - | 1.0 | 3.1 | - | 0.4 | 4.2 | - | 1.6 | 1.7 | 1.7 | 0.8 | - | - |
| Co | - | 111.0 | - | - | - | - | - | - | - | - | - | - | - |
| Zr | - | 35.2 | 128.1 | - | 214.5 | 85.5 | - | 648.5 | 172.9 | 210.6 | 633.6 | - | - |
| Hf | - | 1.0 | - | - | - | - | - | - | - | - | - | - | - |
| Nb | - | 3.1 | - | - | - | - | - | - | - | - | - | - | - |
| Rb | - | 0.4 | - | - | - | - | - | - | - | - | - | - | - |
| Ta | - | 0.3 | - | - | - | - | - | - | - | - | - | - | - |
| V | - | 165.0 | - | - | - | - | - | - | - | - | - | - | - |
| Obs. No. | 34551 | 35135 | 8702 | 34722 | 8721 | 8703 | 34619 | 8720 | 8700 | 8707 | 8723 | 8725 | 23438 |
| Easting | 265558 | 253064 | 283638 | 283552 | 293363 | 280583 | 288304 | 292893 | 280696 | 279466 | 288748 | 286543 | 291532 |
| Northing | 276294 | 285963 | 302214 | 386973 | 293618 | 300912 | 298489 | 294058 | 303260 | 293776 | 297795 | 300071 | 359670 |
| Laboratory | CGS | Labtium | CGS | CGS | CGS | CGS | CGS | CGS | CGS | CGS | CGS | Labtium | CGS |

Appendix 2. Cont.

| Unit | Leucocr. granite gneiss | Granulite | | Amphibolite | | | Mafic metatuff, amphibolite | | | | | | |
|----------------------------------|-------------------------|-----------|------------------|--------------|--------------|--------------|-----------------------------|--------------|--------------|--------------|--------------|--------------|--------------|
| Rock name | Felsic para-gneiss | Granulite | Pyroxene granite | Amphibo-lite | Amphibo-lite | Amphibo-lite | Amphibo-lite | Amphibo-lite | Amphibo-lite | Amphibo-lite | Amphibo-lite | Amphibo-lite | Amphibo-lite |
| Anal. | 66 | 67 | 68 | 69 | 70 | 71 | 72 | 73 | 74 | 75 | 76 | 78 | 79 |
| wt% | | | | | | | | | | | | | |
| SiO ₂ | 73.24 | 65.00 | 72.44 | 49.60 | 55.50 | 57.80 | 47.24 | 47.62 | 48.10 | 48.30 | 48.40 | 48.65 | 49.24 |
| TiO ₂ | 0.41 | 0.66 | 0.24 | 1.66 | 0.82 | 0.84 | 0.74 | 0.88 | 1.01 | 0.84 | 1.13 | 0.77 | 1.08 |
| Al ₂ O ₃ | 13.42 | 14.83 | 15.44 | 14.10 | 16.70 | 17.60 | 15.43 | 15.74 | 14.60 | 14.40 | 14.60 | 15.52 | 14.88 |
| Fe ₂ O ₃ t | 3.81 | 6.71 | 1.95 | 12.90 | 7.75 | 6.94 | 11.57 | 12.34 | 12.10 | 13.90 | 11.20 | 12.68 | 13.49 |
| MnO | 0.06 | 0.09 | 0.02 | 0.16 | 0.10 | 0.09 | 0.21 | 0.38 | 0.20 | 0.25 | 0.18 | 0.28 | 0.19 |
| MgO | 0.26 | 3.10 | 0.46 | 5.32 | 4.70 | 3.13 | 7.46 | 6.34 | 5.88 | 7.31 | 7.35 | 7.97 | 7.89 |
| CaO | 1.36 | 4.08 | 2.48 | 8.14 | 6.80 | 6.33 | 13.51 | 15.06 | 12.83 | 11.27 | 11.99 | 10.86 | 11.07 |
| Na ₂ O | 3.02 | 3.14 | 4.98 | 2.71 | 3.99 | 4.40 | 1.41 | 0.92 | 2.24 | 2.00 | 1.30 | 1.92 | 1.53 |
| K ₂ O | 4.62 | 0.99 | 1.91 | 1.55 | 1.48 | 1.54 | 0.13 | 0.19 | 0.18 | 0.08 | 0.45 | 0.08 | 0.15 |
| P ₂ O ₅ | 0.08 | 0.16 | 0.05 | 0.24 | 0.32 | 0.34 | 0.06 | 0.08 | 0.10 | 0.06 | 0.08 | 0.10 | 0.08 |
| Total | 100.27 | 98.75 | 99.98 | 96.38 | 98.16 | 99.01 | 97.76 | 99.55 | 97.24 | 98.41 | 96.68 | 98.83 | 99.60 |
| ppm | | | | | | | | | | | | | |
| Cr | 12 | 181 | 12 | 123 | 85 | 27 | 358 | 345 | 246 | b.d. | 225 | 252 | 288 |
| Ni | 4 | 35 | 3 | 82 | 41 | b.d. | 168 | 194 | 121 | 119 | 65 | 116 | 129 |
| Sc | 6 | 9 | <3 | 21 | b.d. | b.d. | 42 | 38 | - | 29 | 41 | 36 | 46 |
| V | 12 | 112 | 18 | 236 | 146 | 129 | 253 | 272 | - | 229 | 261 | 263 | 330 |
| Zr | 450 | 162 | 93 | 145 | 147 | 153 | 41 | 43 | - | 40 | 62 | 64 | 54 |
| La | 70 | 37 | <10 | b.d. | b.d. | b.d. | <10 | <10 | - | b.d. | b.d. | <10 | <10 |
| Ce | 137 | 54 | 12 | 67 | 81 | 83 | <10 | <10 | - | b.d. | b.d. | 25 | 11 |
| Ba | 802 | 582 | 926 | 475 | 1259 | 627 | 38 | 62 | 41 | b.d. | b.d. | 101 | 66 |
| Sr | 115 | 436 | 456 | 326 | 796 | 790 | 119 | 106 | 146 | 132 | 167 | 177 | 116 |
| Rb | 127 | 20 | 26 | 34 | 33 | 35 | 5 | 6 | - | 13 | 24 | <2 | 4 |
| Y | 72 | 14 | 1 | 24 | 16 | 14 | 18 | 15 | - | b.d. | 24 | 21 | 20 |
| Nb | 59 | 6 | 2 | b.d. | b.d. | b.d. | 1 | 3 | - | b.d. | b.d. | 7 | 2 |
| Th | 26 | 11 | <3 | b.d. | b.d. | b.d. | <3 | <3 | - | b.d. | b.d. | <3 | <3 |
| U | <2 | <2 | <2 | b.d. | b.d. | b.d. | <2 | <2 | - | b.d. | b.d. | <2 | <2 |
| S | - | - | - | 1182 | 104 | 71 | - | - | 973 | 1642 | 2090 | - | - |
| C | - | - | - | - | - | - | - | - | 0.14 | - | - | - | - |
| ppm | | | | | | | | | | | | | |
| Ce | - | - | - | 52.6 | 74.3 | 92.8 | - | 9.0 | 12.3 | 6.9 | 6.8 | - | - |
| Dy | - | - | - | 5.6 | 3.9 | 3.7 | - | 3.7 | 4.0 | 3.4 | 5.1 | - | - |
| Er | - | - | - | 3.2 | 1.9 | 1.6 | - | 2.3 | 2.5 | 2.1 | 3.4 | - | - |
| Eu | - | - | - | 1.8 | 1.9 | 2.0 | - | 0.9 | 1.0 | 0.8 | 1.1 | - | - |
| Gd | - | - | - | 6.2 | 5.9 | 6.0 | - | 2.7 | 3.6 | 2.8 | 4.0 | - | - |
| Ho | - | - | - | 1.1 | 0.7 | 0.6 | - | 0.8 | 0.9 | 0.7 | 1.1 | - | - |
| La | - | - | - | 25.3 | 35.6 | 48.1 | - | 3.6 | 4.6 | 2.3 | 2.3 | - | - |
| Lu | - | - | - | 0.4 | 0.2 | 0.2 | - | 0.4 | 0.4 | 0.3 | 0.5 | - | - |
| Nd | - | - | - | 26.4 | 37.8 | 43.7 | - | 7.7 | 9.1 | 5.8 | 6.9 | - | - |
| Pr | - | - | - | 6.4 | 9.1 | 10.8 | - | 1.4 | 1.8 | 1.1 | 1.2 | - | - |
| Sc | - | - | - | 28.9 | 19.0 | 17.6 | - | - | 42.3 | 40.4 | 46.8 | - | - |
| Sm | - | - | - | 5.6 | 7.0 | 7.6 | - | 2.2 | 2.7 | 2.0 | 2.8 | - | - |
| Tb | - | - | - | 1.0 | 0.8 | 0.7 | - | 0.4 | 0.6 | 0.5 | 0.8 | - | - |
| Th | - | - | - | 4.3 | <0.5 | <0.5 | - | 0.5 | <0.5 | <0.5 | <0.5 | - | - |
| Tm | - | - | - | 0.5 | 0.3 | 0.2 | - | 0.4 | 0.4 | 0.3 | 0.5 | - | - |
| U | - | - | - | 0.6 | <0.2 | 0.2 | - | - | <0.2 | <0.2 | <0.2 | - | - |
| Y | - | - | - | 26.1 | 16.8 | 14.4 | - | 20.6 | 21.1 | 17.0 | 27.3 | - | - |
| Yb | - | - | - | 2.9 | 1.7 | 1.3 | - | 2.2 | 2.2 | 2.1 | 3.2 | - | - |
| Co | - | - | - | 46.8 | 26.5 | 22.0 | - | - | 50.9 | 58.7 | 44.5 | - | - |
| Zr | - | - | - | 139.0 | 130.0 | 169.0 | - | 47.0 | 64.0 | 33.6 | 54.1 | - | - |
| Hf | - | - | - | 3.9 | 3.5 | 4.4 | - | - | 1.8 | 1.2 | 1.7 | - | - |
| Nb | - | - | - | 10.7 | 5.5 | 6.5 | - | - | 3.8 | 1.9 | 1.6 | - | - |
| Rb | - | - | - | 25.9 | 18.5 | 33.4 | - | - | 1.4 | 0.8 | 10.5 | - | - |
| Ta | - | - | - | 1.3 | 0.3 | 0.3 | - | - | 0.4 | 0.2 | 0.2 | - | - |
| V | - | - | - | 225.0 | 142.0 | 128.0 | - | - | 268.0 | 241.0 | 291.0 | - | - |
| Obs. No. | 34454 | 23517 | 23430 | 34924 | 34944 | 34966 | 34562 | 8774 | 6098 | 35174 | 34954 | 34591 | 34553 |
| Easting | 305844 | 283459 | 278453 | 295864 | 291302 | 287930 | 264411 | 279144 | 274142 | 251120 | 288712 | 302549 | 260814 |
| Northing | 253367 | 376547 | 368539 | 273873 | 273019 | 273320 | 284790 | 320288 | 268645 | 277868 | 264257 | 295627 | 276830 |
| Laborato | CGS | CGS | CGS | Labtium | Labtium | Labtium | CGS | CGS | Labtium | Labtium | Labtium | CGS | CGS |

Appendix 2. Cont.

| Unit | Mafic metatuff, amphibolite | | | Tara brown granite | Leuco- to mesocratic gneiss | | Grano- diorite gneiss | Metadolerite | | Sericite quartzite, quartzite | Amphibolite | | Quartz- feldspar gneiss |
|----------------------------------|-----------------------------|------------------|------------------|--------------------------|--------------------------------|---------------------|-----------------------------|--------------|----------|-------------------------------------|--------------------|------------------|-------------------------------|
| Rock name | Amphibo- lite | Amphibo- lite | Amphibo- lite | Char- nockite | Leucocr. para- gneiss | Felsic granulite | Ortho- gneiss | Gabbro | Dolerite | Quartzite | Amphibo- bolite | Amphi- bolite | Aplitic gneiss |
| Anal. | 80 | 81 | 82 | 83 | 84 | 85 | 86 | 87 | 88 | 89 | 90 | 91 | 92 |
| wt% | | | | | | | | | | | | | |
| SiO ₂ | 49.49 | 50.10 | 52.90 | 63.37 | 69.20 | 73.79 | 74.06 | 44.44 | 46.33 | 87.80 | 46.25 | 47.20 | 76.15 |
| TiO ₂ | 1.00 | 0.94 | 0.86 | 0.60 | 0.54 | 0.07 | 0.20 | 0.56 | 1.39 | 0.42 | 2.07 | 1.96 | 0.22 |
| Al ₂ O ₃ | 15.68 | 15.60 | 16.70 | 15.97 | 14.30 | 14.94 | 13.59 | 13.78 | 13.63 | 5.95 | 14.63 | 14.36 | 9.53 |
| Fe ₂ O _{3,t} | 11.58 | 11.70 | 9.15 | 5.41 | 4.14 | 1.20 | 2.48 | 14.06 | 14.62 | 2.82 | 12.65 | 13.80 | 7.66 |
| MnO | 0.26 | 0.23 | 0.22 | 0.09 | 0.04 | 0.03 | 0.04 | 0.22 | 0.22 | b.d. | 0.21 | 0.19 | 0.03 |
| MgO | 4.89 | 4.54 | 4.22 | 3.17 | 2.26 | 0.17 | 0.46 | 12.99 | 7.16 | 0.27 | 5.47 | 6.11 | 0.00 |
| CaO | 13.70 | 12.10 | 12.67 | 4.80 | 2.46 | 1.09 | 2.03 | 12.32 | 12.06 | 0.01 | 14.69 | 11.73 | 0.12 |
| Na ₂ O | 1.81 | 2.29 | 2.72 | 3.43 | 3.28 | 2.96 | 4.09 | 0.42 | 2.97 | 0.08 | 2.14 | 2.44 | 2.29 |
| K ₂ O | 0.36 | 0.22 | 0.21 | 3.00 | 3.25 | 5.60 | 2.49 | 0.27 | 0.32 | 2.29 | 0.38 | 0.47 | 3.38 |
| P ₂ O ₅ | 0.08 | 0.09 | 0.08 | 0.25 | 0.09 | 0.05 | 0.05 | 0.04 | 0.14 | 0.02 | 0.17 | 0.18 | 0.02 |
| Total | 98.87 | 97.81 | 99.73 | 100.10 | 99.56 | 99.90 | 99.50 | 99.11 | 98.84 | 99.66 | 98.65 | 98.43 | 99.41 |
| ppm | | | | | | | | | | | | | |
| Cr | 293 | 282 | 339 | 98 | 94 | 7 | 31 | 751 | 76 | - | 268 | 388 | 16 |
| Ni | 141 | 136 | 171 | 23 | 44 | 3 | 10 | 306 | 70 | - | 85 | 164 | 5 |
| Sc | 41 | 32 | 32 | 14 | b.d. | <3 | 4 | 39 | 32 | b.d. | 41 | 42 | <3 |
| V | 290 | 253 | 256 | 92 | 80 | 5 | 12 | 228 | 363 | 50 | 327 | 354 | <3 |
| Zr | 58 | 44 | 46 | 145 | 218 | 95 | 141 | 23 | 89 | 179 | 137 | 121 | 2721 |
| La | <10 | b.d. | b.d. | 50 | 74 | 29 | 48 | <10 | 17 | b.d. | <10 | <10 | 594 |
| Ce | 11 | b.d. | b.d. | 69 | 176 | 26 | 68 | <10 | 28 | 38 | 15 | 19 | 1020 |
| Ba | 187 | 45 | b.d. | 1092 | 962 | 1413 | 527 | 34 | 151 | 196 | 167 | 156 | 74 |
| Sr | 126 | 130 | 114 | 620 | 412 | 135 | 117 | 71 | 221 | b.d. | 282 | 202 | 13 |
| Rb | 9 | 19 | 11 | 108 | 108 | 215 | 62 | <2 | 6 | 63 | 8 | 12 | 216 |
| Y | 23 | 14 | 18 | 16 | 13 | 12 | 17 | 13 | 23 | 13 | 33 | 34 | 328 |
| Nb | 5 | b.d. | b.d. | 9 | b.d. | 3 | 10 | 3 | 7 | b.d. | 7 | 5 | 451 |
| Th | <3 | b.d. | b.d. | 6 | 49 | 16 | 8 | <3 | <3 | b.d. | <3 | <3 | 57 |
| U | <2 | b.d. | b.d. | <2 | b.d. | <2 | <2 | <2 | <2 | b.d. | <2 | <2 | 14 |
| S | - | 812 | 95 | - | b.d. | - | - | - | - | b.d. | - | - | - |
| C | - | - | - | - | b.d. | - | - | - | - | b.d. | - | - | - |
| ppm | | | | | | | | | | | | | |
| Ce | - | 8.5 | 7.0 | - | - | - | 75.1 | - | - | - | - | - | - |
| Dy | - | 3.2 | 3.3 | - | - | - | 3.7 | - | - | - | - | - | - |
| Er | - | 2.0 | 2.1 | - | - | - | 2.0 | - | - | - | - | - | - |
| Eu | - | 1.2 | 0.7 | - | - | - | 0.9 | - | - | - | - | - | - |
| Gd | - | 2.7 | 2.7 | - | - | - | 4.3 | - | - | - | - | - | - |
| Ho | - | 0.7 | 0.7 | - | - | - | 0.7 | - | - | - | - | - | - |
| La | - | 3.6 | 2.5 | - | - | - | 39.6 | - | - | - | - | - | - |
| Lu | - | 0.3 | 0.3 | - | - | - | 0.3 | - | - | - | - | - | - |
| Nd | - | 6.4 | 5.8 | - | - | - | 30.0 | - | - | - | - | - | - |
| Pr | - | 1.3 | 1.1 | - | - | - | 8.7 | - | - | - | - | - | - |
| Sc | - | 39.9 | 40.1 | - | - | - | - | - | - | - | - | - | - |
| Sm | - | 2.0 | 1.9 | - | - | - | 5.0 | - | - | - | - | - | - |
| Tb | - | 0.5 | 0.5 | - | - | - | 0.6 | - | - | - | - | - | - |
| Th | - | <0.5 | <0.5 | - | - | - | 7.3 | - | - | - | - | - | - |
| Tm | - | 0.3 | 0.3 | - | - | - | 0.3 | - | - | - | - | - | - |
| U | - | <0.2 | <0.2 | - | - | - | - | - | - | - | - | - | - |
| Y | - | 16.2 | 16.8 | - | - | - | 19.7 | - | - | - | - | - | - |
| Yb | - | 1.9 | 2.0 | - | - | - | 2.3 | - | - | - | - | - | - |
| Co | - | 50.7 | 51.2 | - | - | - | - | - | - | - | - | - | - |
| Zr | - | 36.4 | 54.0 | - | - | - | 188.7 | - | - | - | - | - | - |
| Hf | - | 1.1 | 1.7 | - | - | - | - | - | - | - | - | - | - |
| Nb | - | 2.5 | 2.2 | - | - | - | - | - | - | - | - | - | - |
| Rb | - | 3.0 | 4.4 | - | - | - | - | - | - | - | - | - | - |
| Ta | - | 0.3 | 0.3 | - | - | - | - | - | - | - | - | - | - |
| V | - | 273 | 252 | - | - | - | - | - | - | - | - | - | - |
| Obs. No. | 34755 | 34908 | 35108 | 23516 | 34620 | 34590 | 8777 | 14429 | 23483 | 34399 | 34428 | 34446 | 5699 |
| Easting | 267284 | 286086 | 275502 | 287446 | 294977 | 302195 | 264739 | 280326 | 285132 | 298295 | 291185 | 304538 | 371577 |
| Northing | 322715 | 281687 | 323820 | 374676 | 292211 | 295103 | 321464 | 335084 | 367015 | 266761 | 258321 | 246847 | 240564 |
| Laborato | CGS | Labtium | Labtium | CGS | Labtium | CGS | CGS | CGS | CGS | Labtium | CGS | CGS | CGS |

Appendix 2. Cont.

| Unit | Biotite-hornblende gneiss | | | Mafic metavolcanic rock, amphibolite | | | | | | Apuch granite | | Gulu banded TTG gneiss | |
|----------------------------------|---------------------------|-------------------|-------------------|--------------------------------------|-------------|-------------|--------------------|-------------|-------------|---------------|-----------------|------------------------|------------------|
| Rock name | Amphibolite gneiss | Migmatitic gneiss | Migmatitic gneiss | Amphibolite | Amphibolite | Amphibolite | Amphibolite gneiss | Amphibolite | Amphibolite | Mylonite | Mylonite gneiss | Qtz-Fs-Bt gneiss | Qtz-Fs-Bt gneiss |
| Anal. | 93 | 94 | 95 | 96 | 97 | 98 | 99 | 100 | 101 | 102 | 103 | 104 | 105 |
| wt% | | | | | | | | | | | | | |
| SiO ₂ | 52.31 | 64.2 | 74.4 | 47.1 | 47.32 | 49.03 | 49.75 | 50.6 | 52.9 | 70.29 | 71.83 | 57.07 | 59.58 |
| TiO ₂ | 1.35 | 0.71 | 0.14 | 2.47 | 1.00 | 1.53 | 1.20 | 1.20 | 1.23 | 0.66 | 0.34 | 0.31 | 1.09 |
| Al ₂ O ₃ | 13.13 | 14.0 | 14.0 | 12.5 | 16.09 | 12.31 | 14.21 | 13.4 | 12.5 | 13.54 | 15.52 | 22.31 | 16.91 |
| Fe ₂ O ₃ t | 14.37 | 6.00 | 1.45 | 17.20 | 12.67 | 16.35 | 12.87 | 13.20 | 13.20 | 5.27 | 2.61 | 3.14 | 6.57 |
| MnO | 0.20 | 0.07 | 0.02 | 0.21 | 0.40 | 0.25 | 0.18 | 0.15 | 0.22 | 0.07 | 0.04 | 0.14 | 0.23 |
| MgO | 5.70 | 3.06 | 0.21 | 5.37 | 3.31 | 7.21 | 7.00 | 6.23 | 5.67 | 0.57 | 0.81 | 0.14 | 3.73 |
| CaO | 9.84 | 4.19 | 1.58 | 8.72 | 15.43 | 10.27 | 10.98 | 10.03 | 8.15 | 2.34 | 1.81 | 1.14 | 3.92 |
| Na ₂ O | 2.13 | 3.16 | 3.85 | 3.35 | 2.60 | 2.07 | 2.52 | 2.28 | 2.70 | 2.97 | 3.98 | 10.85 | 4.33 |
| K ₂ O | 0.78 | 3.45 | 4.07 | 0.40 | 0.41 | 0.29 | 0.92 | 0.25 | 0.20 | 3.04 | 2.90 | 4.87 | 2.15 |
| P ₂ O ₅ | 0.13 | 0.25 | 0.05 | 0.26 | 0.09 | 0.14 | 0.12 | 0.12 | 0.11 | 0.19 | 0.15 | 0.04 | 0.26 |
| Total | 99.93 | 99.09 | 99.77 | 97.58 | 99.32 | 99.45 | 99.77 | 97.46 | 96.88 | 98.94 | 100.00 | 100.00 | 98.77 |
| ppm | | | | | | | | | | | | | |
| Cr | 105 | 132 | b.d. | 66 | 278 | 164 | 119 | 67 | 51 | 10 | 17 | 11 | 173 |
| Ni | 69 | 79 | b.d. | 62 | 135 | 77 | 114 | 86 | 77 | 4 | 6 | 3 | 50 |
| Sc | 35 | b.d. | b.d. | 28 | 33 | 44 | 38 | 28 | 23 | 10 | 3 | 4 | 10 |
| V | 342 | 111 | b.d. | 473 | 240 | 347 | 316 | 283 | 272 | 35 | 25 | 15 | 122 |
| Zr | 86 | 157 | 150 | 147 | 56 | 89 | 73 | 79 | 77 | 318 | 136 | 154 | 256 |
| La | 34 | b.d. | b.d. | b.d. | <10 | 60 | 23 | b.d. | b.d. | 44 | 49 | 54 | 61 |
| Ce | 38 | 69 | 78 | 50 | 12 | 51 | 34 | 41 | b.d. | 83 | 81 | 102 | 94 |
| Ba | 184 | 1040 | 611 | 391 | 240 | 144 | 260 | b.d. | 53 | 1439 | 1077 | 511 | 1607 |
| Sr | 164 | 451 | 162 | 217 | 167 | 150 | 156 | 154 | 215 | 140 | 441 | 155 | 647 |
| Rb | 15 | 73 | 125 | 20 | 6 | 11 | 7 | 18 | 19 | 93 | 132 | 241 | 91 |
| Y | 27 | 14 | 14 | 34 | 21 | 59 | 22 | 17 | 19 | 22 | 16 | 20 | 14 |
| Nb | 7 | b.d. | b.d. | b.d. | 6 | 9 | 5 | b.d. | b.d. | 16 | 10 | 13 | 13 |
| Th | <3 | 14 | 30 | b.d. | <3 | <3 | <3 | b.d. | b.d. | 11 | 33 | 43 | 8 |
| U | <2 | b.d. | b.d. | 11 | <2 | <2 | <2 | b.d. | b.d. | <2 | 3 | 18 | <2 |
| S | - | 2772 | 262 | 176 | - | - | - | 471 | 68 | - | - | - | - |
| C | - | - | - | 661 | - | - | - | - | - | - | - | - | - |
| ppm | | | | | | | | | | | | | |
| Ce | 27.0 | - | - | 44.5 | - | - | 20.1 | 18.7 | 17.7 | - | - | 111.4 | - |
| Dy | 4.7 | - | - | 7.2 | - | - | 4.7 | 4.6 | 4.3 | - | - | 4.0 | - |
| Er | 2.7 | - | - | 4.2 | - | - | 2.8 | 2.8 | 2.5 | - | - | 2.0 | - |
| Eu | 1.3 | - | - | 1.8 | - | - | 1.2 | 1.2 | 1.4 | - | - | 0.6 | - |
| Gd | 4.5 | - | - | 7.3 | - | - | 3.9 | 4.3 | 4.3 | - | - | 5.6 | - |
| Ho | 1.0 | - | - | 1.5 | - | - | 1.0 | 1.0 | 0.9 | - | - | 0.7 | - |
| La | 15.6 | - | - | 23.3 | - | - | 9.6 | 7.7 | 8.1 | - | - | 58.9 | - |
| Lu | 0.4 | - | - | 0.6 | - | - | 0.4 | 0.4 | 0.3 | - | - | 0.3 | - |
| Nd | 17.9 | - | - | 27.9 | - | - | 13.8 | 12.0 | 13.1 | - | - | 42.6 | - |
| Pr | 4.2 | - | - | 6.3 | - | - | 3.1 | 2.6 | 2.8 | - | - | 12.6 | - |
| Sc | - | - | - | 36.6 | - | - | - | 40.2 | 36.9 | - | - | - | - |
| Sm | 4.0 | - | - | 6.3 | - | - | 4.0 | 3.4 | 3.6 | - | - | 7.1 | - |
| Tb | 0.7 | - | - | 1.2 | - | - | 0.7 | 0.7 | 0.7 | - | - | 0.7 | - |
| Th | 1.2 | - | - | 2.5 | - | - | 1.3 | 1.0 | 0.8 | - | - | 42.3 | - |
| Tm | 0.4 | - | - | 0.6 | - | - | 0.4 | 0.4 | 0.3 | - | - | 0.3 | - |
| U | - | - | - | 0.4 | - | - | - | 0.2 | <0.2 | - | - | - | - |
| Y | 25.5 | - | - | 37.7 | - | - | 26.5 | 22.7 | 21.2 | - | - | 19.9 | - |
| Yb | 2.4 | - | - | 3.8 | - | - | 2.6 | 2.6 | 2.2 | - | - | 1.8 | - |
| Co | - | - | - | 52.7 | - | - | - | 45.6 | 55.3 | - | - | - | - |
| Zr | 85.4 | - | - | 129.0 | - | - | 93.2 | 70.4 | 70.4 | - | - | 173.8 | - |
| Hf | - | - | - | 4.4 | - | - | - | 2.2 | 2.1 | - | - | - | - |
| Nb | - | - | - | 16.0 | - | - | - | 5.1 | 5.9 | - | - | - | - |
| Rb | - | - | - | 5.8 | - | - | - | 3.4 | 4.2 | - | - | - | - |
| Ta | - | - | - | 1.0 | - | - | - | 0.7 | 0.8 | - | - | - | - |
| V | - | - | - | 523 | - | - | - | 313 | 334 | - | - | - | - |
| Obs. No. | 8551 | 5907 | 5908 | 14137 | 34095 | 14136 | 8586 | 14745 | 35001 | 28029 | 28031 | 8557 | 18888 |
| Easting | 435029 | 424688 | 431283 | 368207 | 491869 | 368190 | 403850 | 412688 | 410557 | 507017 | 509545 | 441799 | 391997 |
| Northing | 293430 | 309189 | 309098 | 281572 | 239002 | 282233 | 293320 | 282493 | 278983 | 261767 | 262104 | 301037 | 305528 |
| Laboratory | CGS | Labtium | Labtium | Labtium | CGS | CGS | CGS | Labtium | Labtium | CGS | CGS | CGS | CGS |

Appendix 2. Cont.

| Unit | Gulu banded TTG gneiss | | | | | Awela granodioritic gneiss | Muwozansimbe quartz dioritic gneiss | | | Kuju granitic and granodioritic gneiss | | Metagabbro | |
|----------------------------------|------------------------|------------------------------|----------------------|----------------------|------------------------------|----------------------------------|--|-------------------|------------------|---|-------------------------|------------------|------------------|
| Rock name | Hornblenc gneiss | Grano- dioritic gneiss | Qtz-Fs- Bt gneiss | Qtz-Fs- Bt gneiss | Grano- dioritic gneiss | Tonalitic gneiss | Augen- gneiss | Quartz diorite | Augen- gneiss | Biotite granite | Granodioritic gneiss | Amphi- bolite | Amphi- bolite |
| Anal. | 106 | 107 | 108 | 109 | 110 | 111 | 112 | 113 | 114 | 115 | 116 | 117 | 118 |
| w t% | | | | | | | | | | | | | |
| SiO ₂ | 64.68 | 71.80 | 74.15 | 75.17 | 77.91 | 72.5 | 58.39 | 59.97 | 65.10 | 70.41 | 75.32 | 44.94 | 48.32 |
| TiO ₂ | 0.60 | 0.27 | 0.23 | 0.03 | 0.12 | 0.22 | 0.69 | 0.59 | 1.05 | 0.57 | 0.10 | 0.08 | 1.02 |
| Al ₂ O ₃ | 16.78 | 13.79 | 14.60 | 13.48 | 11.42 | 14.8 | 14.68 | 17.39 | 15.37 | 15.02 | 13.97 | 5.11 | 15.37 |
| Fe ₂ O ₃ t | 3.60 | 2.83 | 1.33 | 1.66 | 2.50 | 1.85 | 7.78 | 5.80 | 6.56 | 3.48 | 1.34 | 45.03 | 12.50 |
| MnO | 0.06 | 0.04 | 0.02 | 0.04 | 0.05 | 0.02 | 0.15 | 0.08 | 0.08 | 0.04 | 0.02 | 0.15 | 0.19 |
| MgO | 2.33 | 0.64 | 0.37 | <0.01 | 0.04 | 0.48 | 5.01 | 2.96 | 1.56 | 0.63 | 0.26 | 2.96 | 8.29 |
| CaO | 5.10 | 1.73 | 0.56 | 0.53 | 0.80 | 2.24 | 4.98 | 6.54 | 3.49 | 1.63 | 1.18 | 3.14 | 11.06 |
| Na ₂ O | 4.23 | 2.75 | 3.14 | 4.71 | 2.06 | 4.10 | 2.59 | 4.78 | 3.97 | 3.33 | 3.34 | -0.05 | 1.01 |
| K ₂ O | 1.25 | 5.11 | 5.73 | 3.31 | 5.23 | 3.48 | 4.23 | 0.74 | 2.56 | 3.87 | 4.70 | 0.03 | 0.18 |
| P ₂ O ₅ | 0.20 | 0.13 | 0.11 | 0.01 | 0.02 | 0.08 | 0.42 | 0.15 | 0.44 | 0.15 | 0.05 | 0.04 | 0.19 |
| Total | 98.82 | 99.09 | 100.24 | 98.94 | 100.17 | 99.77 | 98.93 | 99.00 | 100.17 | 99.14 | 100.28 | 101.44 | 98.13 |
| ppm | | | | | | | | | | | | | |
| Cr | 151 | 40 | 21 | 15 | 27 | - | 248 | 53 | 41 | 12 | 26 | 103 | 318 |
| Ni | 35 | 5 | 4 | 3 | <2 | - | 90 | 22 | 17 | 4 | 3 | 11 | 149 |
| Sc | 4 | 8 | 4 | <3 | <3 | b.d. | 16 | 8 | 8 | 4 | <3 | 5 | 35 |
| V | 69 | 25 | 13 | <3 | <3 | b.d. | 98 | 91 | 84 | 24 | 11 | 31 | 196 |
| Zr | 170 | 217 | 129 | 135 | 305 | 132 | 212 | 91 | 415 | 418 | 121 | 18 | 62 |
| La | 102 | 168 | 11 | 22 | 128 | b.d. | 153 | 23 | 71 | 253 | 54 | <10 | 16 |
| Ce | 141 | 283 | 26 | 49 | 234 | 62 | 241 | 44 | 130 | 359 | 76 | 23 | 28 |
| Ba | 786 | 1868 | 391 | 33 | 1198 | 913 | 1312 | 676 | 757 | 1342 | 1380 | 277 | 141 |
| Sr | 666 | 314 | 94 | 10 | 59 | 317 | 570 | 545 | 301 | 275 | 288 | 20 | 152 |
| Rb | 33 | 65 | 245 | 196 | 49 | 97 | 167 | 5 | 128 | 208 | 186 | 3 | 4 |
| Y | 8 | 22 | 13 | 94 | 43 | 12 | 89 | 11 | 51 | 18 | 7 | 23 | 18 |
| Nb | 4 | 11 | 19 | 210 | 30 | b.d. | 16 | 3 | 19 | 31 | 5 | <1 | 4 |
| Th | 16 | 32 | 24 | 28 | 16 | b.d. | 85 | <3 | 9 | 98 | 26 | <3 | <3 |
| U | <2 | <2 | 3 | 8 | <2 | b.d. | <2 | <2 | <2 | 3 | 5 | <2 | <2 |
| S | - | - | - | - | - | b.d. | - | - | - | - | - | - | - |
| C | - | - | - | - | - | b.d. | - | - | - | - | - | - | - |
| ppm | | | | | | | | | | | | | |
| Ce | - | - | 64.6 | 39.6 | - | - | - | 34.4 | 214.3 | - | - | - | - |
| Dy | - | - | 3.1 | 16.0 | - | - | - | 1.9 | 16.8 | - | - | - | - |
| Er | - | - | 1.4 | 9.7 | - | - | - | 1.0 | 10.0 | - | - | - | - |
| Eu | - | - | 0.4 | 0.3 | - | - | - | 1.1 | 2.3 | - | - | - | - |
| Gd | - | - | 4.2 | 10.2 | - | - | - | 2.5 | 16.9 | - | - | - | - |
| Ho | - | - | 0.5 | 3.2 | - | - | - | 0.3 | 3.3 | - | - | - | - |
| La | - | - | 32.5 | 19.0 | - | - | - | 19.4 | 104.4 | - | - | - | - |
| Lu | - | - | 0.2 | 1.3 | - | - | - | 0.1 | 1.4 | - | - | - | - |
| Nd | - | - | 27.9 | 25.9 | - | - | - | 17.3 | 103.3 | - | - | - | - |
| Pr | - | - | 7.7 | 5.9 | - | - | - | 4.5 | 27.0 | - | - | - | - |
| Sc | - | - | - | - | - | - | - | - | - | - | - | - | - |
| Sm | - | - | 5.8 | 8.8 | - | - | - | 3.3 | 20.1 | - | - | - | - |
| Tb | - | - | 0.5 | 2.6 | - | - | - | 0.3 | 3.1 | - | - | - | - |
| Th | - | - | 27.7 | 24.2 | - | - | - | 0.5 | 77.0 | - | - | - | - |
| Tm | - | - | 0.2 | 1.5 | - | - | - | 0.1 | 1.5 | - | - | - | - |
| U | - | - | - | - | - | - | - | - | - | - | - | - | - |
| Y | - | - | 15.5 | 91.3 | - | - | - | 9.5 | 96.0 | - | - | - | - |
| Yb | - | - | 1.2 | 9.0 | - | - | - | 0.8 | 9.3 | - | - | - | - |
| Co | - | - | - | - | - | - | - | - | - | - | - | - | - |
| Zr | - | - | 147.1 | 172.6 | - | - | - | 90.2 | 315.9 | - | - | - | - |
| Hf | - | - | - | - | - | - | - | - | - | - | - | - | - |
| Nb | - | - | - | - | - | - | - | - | - | - | - | - | - |
| Rb | - | - | - | - | - | - | - | - | - | - | - | - | - |
| Ta | - | - | - | - | - | - | - | - | - | - | - | - | - |
| V | - | - | - | - | - | - | - | - | - | - | - | - | - |
| Obs. No. | 5687 | 15540 | 8625 | 8588 | 15541 | 34096 | 8570 | 8590 | 8570 | 1098 | 15532 | 5675 | 5676 |
| Easting | 384597 | 399874 | 350830 | 401936 | 401921 | 490918 | 424149 | 408550 | 424149 | 459504 | 454407 | 405660 | 403746 |
| Northing | 260313 | 369103 | 361335 | 300720 | 363221 | 236986 | 285270 | 300580 | 285270 | 327916 | 339331 | 247670 | 247915 |
| Laborato | CGS | CGS | CGS | CGS | CGS | Labtium | CGS | CGS | CGS | CGS | CGS | CGS | CGS |

Appendix 2. Cont.

| Unit | Metagabbro | | Metadolerite | | | Rukungiri Suite | Buganda Group Bujagali basalt | | | | | | |
|----------------------------------|--------------|-------------|---------------|---------------|---------------|-----------------|----------------------------------|-------------|--------------|-------------|--------|--------|---------|
| Rock name | Amphi-bolite | Meta-gabbro | Meta-dolerite | Meta-dolerite | Meta-dolerite | Granite | Meta-basalt | Meta-basalt | Amphi-bolite | Meta-basalt | Basalt | Basalt | Basalt |
| Anal. | 119 | 120 | 121 | 122 | 123 | 124 | 125 | 126 | 127 | 128 | 129 | 130 | 131 |
| wt% | | | | | | | | | | | | | |
| SiO ₂ | 50.05 | 51.5 | 48.88 | 50.2 | 58.31 | 78.71 | 49.8 | 50.03 | 50.52 | 55.26 | 51.28 | 52.39 | 52.6 |
| TiO ₂ | 0.99 | 1.21 | 1.40 | 1.47 | 0.17 | 0.29 | 1.02 | 1.42 | 0.84 | 1.47 | 0.92 | 0.87 | 1.39 |
| Al ₂ O ₃ | 14.36 | 13.3 | 14.27 | 13.2 | 2.34 | 11.44 | 13.5 | 12.52 | 7.50 | 15.25 | 14.48 | 14.14 | 12.8 |
| Fe ₂ O ₃ t | 13.50 | 14.50 | 15.93 | 14.80 | 8.87 | 1.45 | 11.5 | 13.67 | 12.37 | 10.66 | 12.09 | 11.50 | 13.6 |
| MnO | 0.19 | 0.21 | 0.22 | 0.20 | 0.20 | 0.023 | 0.169 | 0.20 | 0.20 | 0.17 | 0.19 | 0.17 | 0.202 |
| MgO | 7.29 | 6.07 | 5.54 | 5.25 | 20.14 | 0.35 | 6.99 | 6.85 | 13.21 | 4.27 | 7.46 | 7.56 | 6.72 |
| CaO | 11.53 | 10.17 | 10.43 | 9.43 | 6.70 | 1.08 | 11.8 | 12.16 | 13.20 | 6.28 | 10.62 | 9.07 | 6.93 |
| Na ₂ O | 1.36 | 2.24 | 2.40 | 2.42 | 0.29 | 4.76 | 2.10 | 2.11 | 0.64 | 3.62 | 2.13 | 3.60 | 4.52 |
| K ₂ O | 0.15 | 0.28 | 0.22 | 0.37 | 0.02 | 1.47 | 0.453 | 0.32 | 0.31 | 2.24 | 0.19 | 0.10 | 0.125 |
| P ₂ O ₅ | 0.08 | 0.12 | 0.14 | 0.15 | 0.02 | 0.029 | 0.094 | 0.17 | 0.07 | 0.31 | 0.09 | 0.08 | 0.141 |
| Total | 99.50 | 99.60 | 99.43 | 97.49 | 97.08 | 99.60 | 97.45 | 99.44 | 98.86 | 99.53 | 99.45 | 99.48 | 99.01 |
| ppm | | | | | | | | | | | | | |
| Cr | 230 | 169 | 64 | 53 | 3505 | 11 | 188 | 154 | 1 957 | 86 | 108 | 168 | 117 |
| Ni | 118 | 71 | 67 | 70 | 351 | 2.2 | 130 | 92 | 316 | 36 | 99 | 93 | 89 |
| Sc | 42 | 37 | 37 | 31 | 31 | 7 | - | 35 | 36 | 20 | 33 | 31 | 32 |
| V | 280 | 295 | 342 | 316 | 125 | 13 | - | 339 | 233 | 237 | 264 | 248 | 369 |
| Zr | 50 | 77 | 101 | 110 | 35 | 122 | - | 81 | 36 | 217 | 67 | 53 | 91 |
| La | <10 | b.d. | <10 | b.d. | <10 | 33 | - | 10 | b.d. | 29 | 12 | b.d. | b.d. |
| Ce | 14 | b.d. | 21 | 51 | <10 | 59 | - | 19 | b.d. | 66 | 12 | 13 | b.d. |
| Ba | 43 | 293 | 235 | 73 | 86 | 193 | 64 | 60 | 75 | 1 138 | 85 | 57 | 81 |
| Sr | 131 | 134 | 132 | 146 | 13 | 22 | 237 | 162 | 87 | 265 | 200 | 115 | 106 |
| Rb | 6 | 22 | 10 | 24 | <2 | 60 | - | 15 | 8.9 | 68 | 3.1 | b.d. | b.d. |
| Y | 18 | 22 | 31 | 23 | 7 | 22 | - | 21 | 11 | 26 | 17 | 15 | 32 |
| Nb | 2 | b.d. | 4 | b.d. | <1 | 12 | - | 7.4 | 4.3 | 10 | 4.7 | 4 | 22 |
| Th | <3 | b.d. | <3 | b.d. | 10 | 25 | - | b.d. | b.d. | 3.6 | b.d. | b.d. | b.d. |
| U | <2 | 10 | <2 | b.d. | <2 | 4.4 | - | b.d. | b.d. | b.d. | b.d. | b.d. | b.d. |
| S | - | 848 | - | 1284 | - | - | 510 | - | - | - | - | - | 243 |
| C | - | - | - | - | - | - | 1550 | - | - | - | - | - | 1220 |
| ppm | | | | | | | | | | | | | |
| Ce | - | - | - | - | - | 63.89 | 14.50 | - | - | 77.70 | - | - | 15.5 |
| Dy | - | - | - | - | - | 6.99 | 3.35 | - | - | 5.61 | - | - | 4.21 |
| Er | - | - | - | - | - | 4.15 | 1.99 | - | - | 2.89 | - | - | 2.48 |
| Eu | - | - | - | - | - | 1.01 | 0.93 | - | - | 2.04 | - | - | 0.92 |
| Gd | - | - | - | - | - | 6.33 | 3.22 | - | - | 7.37 | - | - | 3.86 |
| Ho | - | - | - | - | - | 1.45 | 0.67 | - | - | 1.01 | - | - | 0.87 |
| La | - | - | - | - | - | 35.35 | 5.97 | - | - | 37.90 | - | - | 5.68 |
| Lu | - | - | - | - | - | 0.63 | 0.26 | - | - | 0.36 | - | - | 0.32 |
| Nd | - | - | - | - | - | 33.38 | 9.40 | - | - | 37.80 | - | - | 10.1 |
| Pr | - | - | - | - | - | 8.65 | 1.98 | - | - | 9.44 | - | - | 2.15 |
| Sc | - | - | - | - | - | - | 34.40 | - | - | 21.60 | - | - | 37.9 |
| Sm | - | - | - | - | - | 6.73 | 2.60 | - | - | 7.55 | - | - | 2.99 |
| Tb | - | - | - | - | - | 1.14 | 0.53 | - | - | 1.04 | - | - | 0.66 |
| Th | - | - | - | - | - | 32.95 | 0.81 | - | - | 4.69 | - | - | 1.18 |
| Tm | - | - | - | - | - | 0.71 | 0.27 | - | - | 0.41 | - | - | 0.34 |
| U | - | - | - | - | - | - | 0.20 | - | - | 0.95 | - | - | 0.28 |
| Y | - | - | - | - | - | 40.29 | 17.00 | - | - | 27.20 | - | - | 21.4 |
| Yb | - | - | - | - | - | 4.40 | 1.80 | - | - | 2.56 | - | - | 2.29 |
| Co | - | - | - | - | - | - | 45.90 | - | - | 34.80 | - | - | 46.2 |
| Zr | - | - | - | - | - | - | 47.00 | - | - | 147.00 | - | - | 68.8 |
| Hf | - | - | - | - | - | - | 1.33 | - | - | 3.62 | - | - | 1.86 |
| Nb | - | - | - | - | - | - | 3.05 | - | - | 7.59 | - | - | 4.21 |
| Rb | - | - | - | - | - | - | 12.30 | - | - | 69.90 | - | - | 6.57 |
| Ta | - | - | - | - | - | - | b.d. | - | - | 0.44 | - | - | 0.29 |
| V | - | - | - | - | - | - | 270 | - | - | 226 | - | - | 340 |
| Obs. No. | 34315 | 5792 | 5688 | 5796 | 10737 | 3455 | 4928 | 4445 | 5235 | 4423 | 1116 | 7138 | 1010 |
| Easting | 439136 | 421000 | 382826 | 413445 | 402892 | 340914 | 365290 | 442486 | 456886 | 464593 | 516385 | 526178 | 517555 |
| Northing | 237706 | 246020 | 260575 | 239816 | 241710 | 52780 | 89223 | 76984 | 103296 | 56188 | 61434 | 48146 | 53308 |
| Laborato | CGS | Labtium | CGS | Labtium | CGS | CGS | Labtium | CGS | CGS | Labtium | CGS | CGS | Labtium |

Appendix 2. Cont.

| Unit | Dacitic metatuff | | | | | Quartz-muscovite schist | | | Anthophyllite rock | | Amphibolite | | Kyanite-quartz schist |
|----------------------------------|------------------|----------|----------|----------|----------|-------------------------|-------------|--------------------------|--------------------|------------------|------------------|------------------|-----------------------|
| Rock name | Metatuff | Metatuff | Metatuff | Metatuff | Metatuff | Quartz-muscovite schist | Mica schist | Muscovite biotite schist | Amphibolite rock | Amphibolite rock | Amphibolite lite | Amphibolite lite | Skarn |
| Anal. | 145 | 146 | 147 | 148 | 149 | 150 | 151 | 152 | 153 | 155 | 155 | 156 | 157 |
| wt% | | | | | | | | | | | | | |
| SiO ₂ | 68.97 | 70.2 | 70.6 | 71.4 | 74.9 | 64.9 | 67.53 | 68.85 | 57.85 | 59.4 | 46.25 | 47.20 | 64.7 |
| TiO ₂ | 0.24 | 0.28 | 0.31 | 0.26 | 0.17 | 0.90 | 0.89 | 0.38 | 0.84 | 0.77 | 2.07 | 1.96 | 1.46 |
| Al ₂ O ₃ | 15.74 | 15.9 | 15.8 | 15.6 | 13.3 | 18.7 | 17.73 | 19.44 | 14.58 | 15.0 | 14.63 | 14.36 | 30.5 |
| Fe ₂ O ₃ t | 3.40 | 2.23 | 2.24 | 1.92 | 2.12 | 5.58 | 6.14 | 4.06 | 11.94 | 9.81 | 12.65 | 13.80 | 0.34 |
| MnO | 0.09 | 0.03 | 0.03 | 0.03 | 0.02 | b.d. | 0.06 | 0.02 | 0.20 | 0.11 | 0.21 | 0.19 | <0.008 |
| MgO | 1.36 | 0.98 | 1.15 | 0.73 | 0.33 | 0.99 | 1.65 | 0.90 | 9.94 | 9.62 | 5.47 | 6.11 | 0.05 |
| CaO | 1.76 | 2.49 | 2.18 | 2.28 | 0.80 | 0.01 | 0.05 | 0.12 | 1.64 | 1.40 | 14.69 | 11.73 | 0.20 |
| Na ₂ O | 4.35 | 4.58 | 5.20 | 4.98 | 4.56 | 0.19 | <0.01 | 0.09 | 1.78 | 2.40 | 2.14 | 2.44 | 0.78 |
| K ₂ O | 2.52 | 2.87 | 2.10 | 2.28 | 3.46 | 6.35 | 5.91 | 6.32 | 0.58 | 0.74 | 0.38 | 0.47 | 1.57 |
| P ₂ O ₅ | 0.16 | 0.12 | 0.13 | 0.13 | 0.03 | 0.05 | 0.05 | 0.10 | 0.13 | 0.12 | 0.17 | 0.18 | 0.16 |
| Total | 98.59 | 99.68 | 99.73 | 99.61 | 99.70 | 97.66 | 100.00 | 100.26 | 99.47 | 99.37 | 98.65 | 98.43 | 99.75 |
| ppm | | | | | | | | | | | | | |
| Cr | 9 | - | - | - | - | 90 | 97 | 23 | 102 | 74 | 268 | 388 | 729 |
| Ni | <2 | - | - | - | - | 31 | 35 | 10 | 48 | 58 | 85 | 164 | b.d. |
| Sc | <3 | b.d. | b.d. | b.d. | b.d. | b.d. | 17 | 5 | 28 | b.d. | 41 | 42 | b.d. |
| V | 22 | 35 | 30 | 36 | b.d. | 109 | 110 | 37 | 128 | 123 | 327 | 354 | 363 |
| Zr | 156 | 123 | 132 | 102 | 254 | 517 | 245 | 158 | 140 | 169 | 137 | 121 | 82 |
| La | 46 | b.d. | b.d. | b.d. | 35 | 62 | 45 | 66 | 19 | b.d. | <10 | <10 | b.d. |
| Ce | 66 | 65 | 69 | 65 | 93 | 150 | 69 | 77 | 33 | 69 | 15 | 19 | 30 |
| Ba | 913 | 1099 | 759 | 1209 | 901 | 650 | 846 | 897 | 135 | 91 | 167 | 156 | 126 |
| Sr | 274 | 634 | 512 | 811 | 78 | 69 | 51 | 33 | 48 | 54 | 282 | 202 | 59 |
| Rb | 87 | 55 | 42 | 44 | 102 | 221 | 216 | 145 | 15 | 29 | 8 | 12 | 34 |
| Y | 14 | 8 | 13 | 7 | 40 | 59 | 24 | 9 | 41 | 31 | 33 | 34 | b.d. |
| Nb | 10 | b.d. | b.d. | b.d. | 9 | 16 | 20 | 8 | 10 | b.d. | 7 | 5 | b.d. |
| Th | 11 | 10 | b.d. | b.d. | 18 | 30 | 13 | 12 | 6 | 13 | <3 | <3 | b.d. |
| U | <2 | b.d. | b.d. | b.d. | b.d. | b.d. | <2 | 3 | 2 | b.d. | <2 | <2 | b.d. |
| S | - | b.d. | b.d. | b.d. | b.d. | b.d. | - | - | - | b.d. | - | - | b.d. |
| C | - | b.d. | b.d. | b.d. | b.d. | b.d. | - | - | - | 519 | - | - | <500 |
| ppm | | | | | | | | | | | | | |
| Ce | - | - | - | - | - | - | - | - | - | 56.9 | - | - | - |
| Dy | - | - | - | - | - | - | - | - | - | 6.0 | - | - | - |
| Er | - | - | - | - | - | - | - | - | - | 3.5 | - | - | - |
| Eu | - | - | - | - | - | - | - | - | - | 0.9 | - | - | - |
| Gd | - | - | - | - | - | - | - | - | - | 6.2 | - | - | - |
| Ho | - | - | - | - | - | - | - | - | - | 1.2 | - | - | - |
| La | - | - | - | - | - | - | - | - | - | 27.6 | - | - | - |
| Lu | - | - | - | - | - | - | - | - | - | 0.5 | - | - | - |
| Nd | - | - | - | - | - | - | - | - | - | 26.7 | - | - | - |
| Pr | - | - | - | - | - | - | - | - | - | 6.8 | - | - | - |
| Sc | - | - | - | - | - | - | - | - | - | 19.6 | - | - | - |
| Sm | - | - | - | - | - | - | - | - | - | 5.5 | - | - | - |
| Tb | - | - | - | - | - | - | - | - | - | 1.0 | - | - | - |
| Th | - | - | - | - | - | - | - | - | - | 8.9 | - | - | - |
| Tm | - | - | - | - | - | - | - | - | - | 0.5 | - | - | - |
| U | - | - | - | - | - | - | - | - | - | 2.6 | - | - | - |
| Y | - | - | - | - | - | - | - | - | - | 32.3 | - | - | - |
| Yb | - | - | - | - | - | - | - | - | - | 3.4 | - | - | - |
| Co | - | - | - | - | - | - | - | - | - | 26.0 | - | - | - |
| Zr | - | - | - | - | - | - | - | - | - | 150.0 | - | - | - |
| Hf | - | - | - | - | - | - | - | - | - | 4.7 | - | - | - |
| Nb | - | - | - | - | - | - | - | - | - | 9.1 | - | - | - |
| Rb | - | - | - | - | - | - | - | - | - | 19.6 | - | - | - |
| Ta | - | - | - | - | - | - | - | - | - | 0.7 | - | - | - |
| V | - | - | - | - | - | - | - | - | - | 136 | - | - | - |
| Obs. No. | 10598 | 1244 | 1333 | 1319 | 23579 | 1351 | 1241 | 1272 | 1247 | 1247 | 34428 | 34446 | 5767 |
| Easting | 354995 | 367354 | 370373 | 383372 | 365282 | 373572 | 370683 | 359388 | 366494 | 366494 | 291185 | 304538 | 399068 |
| Northing | 402536 | 401965 | 397167 | 384411 | 403811 | 403452 | 403069 | 390894 | 416921 | 416921 | 258321 | 246847 | 221134 |
| Laboratory | CGS | Labtium | Labtium | Labtium | Labtium | Labtium | CGS | CGS | CGS | Labtium | CGS | CGS | Labtium |

Appendix 2. Cont.

| Unit | Kyanite-quartz schist | Banded iron formation | Metaultramafite | | | | | | | | | Intermediate granulite | |
|----------------------------------|-----------------------|-----------------------|-----------------|------------|-----------------|-------------|-------------|-------------|----------------|-----------|-----------|------------------------|---------------------------|
| Rock name | Quartzite | Banded iron formation | Chlorite schist | Serpentine | Serpentine rock | Ultramafite | Ultramafite | Ultramafite | Tremolite rock | Soapstone | Soapstone | Granulite | Granulitic meta-volcanite |
| Anal. | 158 | 159 | 160 | 161 | 162 | 163 | 164 | 165 | 166 | 167 | 168 | 169 | 170 |
| w t% | | | | | | | | | | | | | |
| SiO ₂ | 79.2 | 19.6 | 43.9 | 44.03 | 50.2 | 50.7 | 50.9 | 51.5 | 52.49 | 57.42 | 61.4 | 57.3 | 59.7 |
| TiO ₂ | 0.88 | 0.01 | 0.13 | 0.35 | 0.40 | 0.18 | 0.62 | 0.29 | 0.18 | 0.01 | 0.04 | 1.00 | 1.10 |
| Al ₂ O ₃ | 18.4 | 0.6 | 2.22 | 7.37 | 3.2 | 5.3 | 2.8 | 2.7 | 2.29 | 1.79 | 0.9 | 18.1 | 17.2 |
| Fe ₂ O ₃ t | 0.36 | 73.70 | 19.1 | 11.85 | 12.90 | 9.44 | 11.80 | 13.60 | 9.46 | 4.88 | 6.24 | 8.85 | 6.77 |
| MnO | <0.008 | 0.03 | 0.10 | 0.15 | 0.22 | 0.16 | 0.20 | 0.22 | 0.22 | 0.05 | 0.08 | 0.14 | 0.10 |
| MgO | 0.03 | 0.02 | 32.80 | 27.67 | 25.10 | 24.70 | 19.90 | 25.10 | 23.61 | 29.65 | 29.60 | 1.79 | 2.52 |
| CaO | 0.07 | 0.06 | 0.14 | 0.96 | 2.53 | 4.21 | 10.56 | 2.16 | 7.79 | 0.06 | 0.16 | 7.25 | 6.21 |
| Na ₂ O | 0.28 | <0.03 | <0.03 | 0.20 | 0.04 | 0.11 | 0.33 | 0.05 | 0.34 | 0.22 | 0.06 | 4.32 | 4.61 |
| K ₂ O | 0.42 | 0.00 | 0.04 | 0.01 | 0.01 | 0.02 | 0.08 | 0.02 | 0.02 | 0.01 | 0.01 | 0.62 | 1.11 |
| P ₂ O ₅ | 0.07 | 0.45 | 0.08 | 0.07 | 0.09 | b.d. | b.d. | 0.14 | 0.02 | 0.02 | 0.03 | 0.33 | 0.37 |
| Total | 99.69 | 94.44 | 98.50 | 92.67 | 94.69 | 94.79 | 97.23 | 95.78 | 96.42 | 94.11 | 98.56 | 99.70 | 99.70 |
| ppm | | | | | | | | | | | | | |
| Cr | 680 | 319 | 4793 | 2285 | 1899 | 2209 | 1776 | 2639 | 3545 | 2842 | 6331 | b.d. | 27 |
| Ni | b.d. | 300 | 1280 | 707 | 638 | 1153 | 470 | 954 | 381 | 1750 | 1243 | 21 | 45 |
| Sc | b.d. | b.d. | b.d. | 10 | b.d. | b.d. | 40 | 21 | 31 | <3 | b.d. | b.d. | b.d. |
| V | 141 | b.d. | 65 | 61 | 93 | 68 | 214 | 109 | 126 | 16 | 35 | 98 | 122 |
| Zr | 93 | b.d. | 13 | 53 | 61 | 11 | 78 | 15 | 24 | <2 | b.d. | 261 | 255 |
| La | b.d. | b.d. | b.d. | 15 | b.d. | b.d. | b.d. | b.d. | <10 | <10 | b.d. | b.d. | b.d. |
| Ce | 54 | b.d. | b.d. | <10 | 49 | b.d. | 44 | b.d. | <10 | <10 | b.d. | 64 | 58 |
| Ba | 74 | b.d. | b.d. | 54 | b.d. | b.d. | b.d. | b.d. | 93 | 35 | b.d. | 232 | 546 |
| Sr | 33 | b.d. | b.d. | 8 | 10 | 10 | 31 | 20 | 13 | 6 | 16 | 453 | 690 |
| Rb | 11 | b.d. | 19 | <2 | 15 | b.d. | 14 | 16 | <2 | <2 | b.d. | 12 | 13 |
| Y | 11 | 55 | b.d. | 8 | b.d. | b.d. | 20 | b.d. | 7 | <1 | b.d. | 16 | 13 |
| Nb | b.d. | b.d. | b.d. | <1 | b.d. | b.d. | b.d. | b.d. | <1 | <1 | b.d. | b.d. | 10 |
| Th | b.d. | b.d. | 14 | <3 | b.d. | b.d. | b.d. | b.d. | <3 | <3 | b.d. | b.d. | b.d. |
| U | b.d. | b.d. | b.d. | <2 | b.d. | b.d. | b.d. | b.d. | <2 | <2 | b.d. | b.d. | b.d. |
| S | 224 | 332 | b.d. | - | b.d. | b.d. | b.d. | 169 | - | - | b.d. | 270 | 96 |
| C | - | - | - | - | - | 242 | 353 | 1250 | - | - | 316 | - | - |
| ppm | | | | | | | | | | | | | |
| Ce | - | - | - | - | 46.0 | 2.1 | 38.7 | 2.6 | - | - | 0.8 | - | - |
| Dy | - | - | - | - | 1.6 | 0.6 | 5.1 | 0.8 | - | - | 0.2 | - | - |
| Er | - | - | - | - | 0.7 | 0.4 | 2.6 | 0.5 | - | - | b.d. | - | - |
| Eu | - | - | - | - | 0.4 | 0.2 | 1.2 | 0.1 | - | - | b.d. | - | - |
| Gd | - | - | - | - | 2.8 | 0.5 | 7.0 | 0.8 | - | - | 0.2 | - | - |
| Ho | - | - | - | - | 0.3 | 0.1 | 0.9 | 0.2 | - | - | b.d. | - | - |
| La | - | - | - | - | 18.9 | 1.3 | 13.4 | 1.0 | - | - | 2.6 | - | - |
| Lu | - | - | - | - | <0.1 | b.d. | 0.3 | b.d. | - | - | b.d. | - | - |
| Nd | - | - | - | - | 26.2 | 1.2 | 33.8 | 2.5 | - | - | 1.1 | - | - |
| Pr | - | - | - | - | 6.2 | 0.3 | 6.9 | 0.5 | - | - | 0.3 | - | - |
| Sc | - | - | - | - | 17.5 | 17.0 | 50.5 | 24.6 | - | - | 3.0 | - | - |
| Sm | - | - | - | - | 3.7 | 0.3 | 7.5 | 0.8 | - | - | b.d. | - | - |
| Tb | - | - | - | - | 0.3 | b.d. | 0.9 | 0.1 | - | - | b.d. | - | - |
| Th | - | - | - | - | 1.9 | b.d. | 0.5 | b.d. | - | - | b.d. | - | - |
| Tm | - | - | - | - | 0.1 | b.d. | 0.4 | b.d. | - | - | b.d. | - | - |
| U | - | - | - | - | 0.2 | b.d. | b.d. | 0.2 | - | - | b.d. | - | - |
| Y | - | - | - | - | 7.7 | 3.4 | 23.3 | 3.9 | - | - | 1.0 | - | - |
| Yb | - | - | - | - | 0.7 | 0.4 | 2.1 | 0.5 | - | - | b.d. | - | - |
| Co | - | - | - | - | 77.4 | 72.3 | 78.8 | 95.7 | - | - | 49.3 | - | - |
| Zr | - | - | - | - | 53.6 | 10.2 | 63.1 | 17.4 | - | - | 9.3 | - | - |
| Hf | - | - | - | - | 1.8 | b.d. | 2.9 | 0.7 | - | - | b.d. | - | - |
| Nb | - | - | - | - | 1.4 | 0.5 | 0.2 | 0.4 | - | - | b.d. | - | - |
| Rb | - | - | - | - | 1.3 | 0.4 | 1.6 | 1.4 | - | - | 0.5 | - | - |
| Ta | - | - | - | - | <0.2 | b.d. | b.d. | b.d. | - | - | b.d. | - | - |
| V | - | - | - | - | 100 | 82 | 254 | 131 | - | - | 35 | - | - |
| Obs. No. | 14574 | 14564 | 5915 | 14154 | 14734 | 1344 | 1332 | 1332 | 10735 | 14138 | 14138 | 23257 | 23377 |
| Easting | 399176 | 404755 | 369481 | 357638 | 363115 | 357240 | 364539 | 364539 | 356044 | 368272 | 368272 | 532221 | 532316 |
| Northing | 221262 | 223035 | 263738 | 286686 | 411733 | 404220 | 409091 | 409091 | 264812 | 281824 | 281824 | 340979 | 353436 |
| Laboratory | Labtium | Labtium | Labtium | CGS | Labtium | Labtium | Labtium | Labtium | CGS | CGS | Labtium | Labtium | Labtium |

Appendix 2. Cont.

| Unit | Intermediate granulite | | Migmatitic garnetiferous gneiss | | | | | Woi charno-enderbite | Okaka Suite | Otukei charnockite | | | |
|----------------------------------|------------------------|-----------|---------------------------------|---------------|---------------|---------------|-----------|----------------------|--------------|--------------------|--------------|--------------|--------------|
| Rock name | Granulite | Granulite | Biotite-garnet gneiss | Garnet gneiss | Garnet gneiss | Garnet gneiss | Migmatite | Mangerite | Char-nockite | Char-nockite | Char-nockite | Char-nockite | Char-nockite |
| Anal. | 171 | 172 | 173 | 174 | 175 | 176 | 177 | 178 | 179 | 180 | 181 | 182 | 183 |
| wt% | | | | | | | | | | | | | |
| SiO ₂ | 63.0 | 64.6 | 73.68 | 53.80 | 61.8 | 68.6 | 72.9 | 57.9 | 65.71 | 72.9 | 67.07 | 68.40 | 65.9 |
| TiO ₂ | 0.90 | 0.86 | 0.15 | 1.39 | 1.01 | 0.74 | 0.91 | 1.07 | 0.54 | 0.30 | 0.95 | 0.75 | 0.76 |
| Al ₂ O ₃ | 16.8 | 14.9 | 14.75 | 18.93 | 15.7 | 15.1 | 11.5 | 16.6 | 14.63 | 13.7 | 14.02 | 13.55 | 14.2 |
| Fe ₂ O ₃ t | 5.87 | 7.04 | 1.23 | 16.27 | 9.83 | 7.96 | 6.66 | 9.86 | 6.34 | 2.62 | 6.53 | 5.47 | 7.07 |
| MnO | 0.10 | 0.08 | 0.03 | 0.24 | 0.15 | 0.09 | 0.05 | 0.15 | 0.10 | 0.02 | 0.09 | 0.09 | 0.08 |
| MgO | 1.62 | 3.58 | 0.33 | 5.40 | 4.14 | 2.42 | 1.77 | 0.44 | 0.15 | 0.28 | 0.79 | 0.67 | 0.42 |
| CaO | 5.50 | 4.22 | 1.37 | 1.11 | 2.54 | 0.91 | 1.77 | 4.52 | 2.84 | 2.21 | 3.02 | 2.70 | 2.87 |
| Na ₂ O | 4.39 | 3.54 | 3.30 | 0.48 | 2.80 | 1.12 | 1.81 | 3.59 | 3.29 | 3.59 | 3.54 | 3.39 | 3.04 |
| K ₂ O | 1.19 | 0.90 | 5.11 | 2.50 | 1.67 | 2.55 | 2.16 | 4.58 | 5.90 | 4.05 | 2.98 | 4.49 | 4.83 |
| P ₂ O ₅ | 0.32 | 0.02 | 0.10 | 0.05 | 0.07 | 0.04 | 0.03 | 0.53 | 0.14 | 0.07 | 0.30 | 0.24 | 0.27 |
| Total | 99.68 | 99.75 | 100.05 | 100.19 | 99.71 | 99.53 | 99.56 | 99.24 | 99.63 | 99.75 | 99.27 | 99.74 | 99.44 |
| ppm | | | | | | | | | | | | | |
| Cr | 24 | 30 | 22 | 215 | 135 | 141 | 107 | - | 21 | b.d. | 11 | 12 | b.d. |
| Ni | 31 | - | 3 | 75 | 79 | 58 | 45 | 27 | 3 | 23 | 4 | 3 | 35 |
| Sc | b.d. | b.d. | 3 | 35 | 20 | b.d. | b.d. | 20 | 11 | b.d. | 12 | 10 | b.d. |
| V | 79 | 117 | 13 | 302 | 145 | 105 | 110 | 56 | 5 | b.d. | 46 | 34 | 46 |
| Zr | 350 | 305 | 71 | 249 | 246 | 253 | 280 | 1582 | 877 | 205 | 418 | 381 | 671 |
| La | 47 | 38 | 33 | 37 | b.d. | 57 | 45 | 43 | 263 | 33 | 80 | 87 | b.d. |
| Ce | 96 | 84 | 46 | 62 | 104 | 138 | 79 | 86 | 405 | 84 | 147 | 139 | 84 |
| Ba | 522 | 364 | 351 | 991 | 532 | 1211 | 813 | 2664 | 971 | 932 | 1631 | 1536 | 1592 |
| Sr | 500 | 218 | 83 | 97 | 201 | 191 | 166 | 320 | 110 | 117 | 317 | 253 | 215 |
| Rb | 15 | 18 | 166 | 83 | 38 | 59 | 37 | 66 | 160 | 124 | 64 | 76 | 111 |
| Y | 22 | 10 | 12 | 56 | 46 | 18 | 18 | 57 | 121 | 21 | 39 | 35 | 35 |
| Nb | 17 | b.d. | 2 | 16 | b.d. | b.d. | b.d. | 47 | 64 | b.d. | 26 | 20 | 18 |
| Th | 11 | 13 | <3 | 10 | b.d. | 23 | 18 | 13 | 34 | 12 | 7 | 10 | 16 |
| U | b.d. | b.d. | <2 | <2 | b.d. | b.d. | b.d. | b.d. | <2 | b.d. | <2 | <2 | b.d. |
| S | b.d. | b.d. | - | - | b.d. | 87 | b.d. | b.d. | - | b.d. | - | - | 150 |
| C | - | b.d. | - | - | b.d. | b.d. | - | - | - | - | - | - | - |
| ppm | | | | | | | | | | | | | |
| Ce | - | 67.5 | - | - | 91.9 | 127.0 | - | 99.0 | - | - | - | - | - |
| Dy | - | 2.44 | - | - | 8.30 | 4.25 | - | 11.90 | - | - | - | - | - |
| Er | - | 1.45 | - | - | 5.69 | 1.64 | - | 6.26 | - | - | - | - | - |
| Eu | - | 1.63 | - | - | 1.95 | 1.63 | - | 5.85 | - | - | - | - | - |
| Gd | - | 3.46 | - | - | 7.35 | 7.53 | - | 15.20 | - | - | - | - | - |
| Ho | - | 0.45 | - | - | 1.79 | 0.65 | - | 2.24 | - | - | - | - | - |
| La | - | 37.7 | - | - | 46.2 | 63.9 | - | 44.5 | - | - | - | - | - |
| Lu | - | 0.29 | - | - | 0.86 | 0.20 | - | 0.93 | - | - | - | - | - |
| Nd | - | 28.1 | - | - | 40.8 | 55.9 | - | 64.1 | - | - | - | - | - |
| Pr | - | 7.5 | - | - | 10.5 | 14.6 | - | 13.8 | - | - | - | - | - |
| Sc | - | 18.2 | - | - | 26.7 | 9.3 | - | 20.0 | - | - | - | - | - |
| Sm | - | 4.07 | - | - | 7.14 | 9.18 | - | 14.50 | - | - | - | - | - |
| Tb | - | 0.44 | - | - | 1.25 | 0.91 | - | 2.12 | - | - | - | - | - |
| Th | - | 9.11 | - | - | 5.61 | 34.00 | - | 1.44 | - | - | - | - | - |
| Tm | - | 0.24 | - | - | 0.85 | 0.20 | - | 0.87 | - | - | - | - | - |
| U | - | 0.70 | - | - | 0.50 | 0.42 | - | 0.72 | - | - | - | - | - |
| Y | - | 11.3 | - | - | 45.8 | 15.4 | - | 53.8 | - | - | - | - | - |
| Yb | - | 1.73 | - | - | 5.58 | 1.25 | - | 5.96 | - | - | - | - | - |
| Co | - | 15.70 | - | - | 26.20 | 21.10 | - | 5.94 | - | - | - | - | - |
| Zr | - | 299 | - | - | 256 | 262 | - | 1090 | - | - | - | - | - |
| Hf | - | 9.8 | - | - | 8.5 | 8.5 | - | 23.7 | - | - | - | - | - |
| Nb | - | 5.5 | - | - | 8.7 | 5.3 | - | 35.5 | - | - | - | - | - |
| Rb | - | 10.9 | - | - | 36.1 | 64.2 | - | 13.6 | - | - | - | - | - |
| Ta | - | 0.23 | - | - | 0.35 | 0.21 | - | 1.44 | - | - | - | - | - |
| V | - | 105 | - | - | 141 | 103 | - | 16 | - | - | - | - | - |
| Obs. No. | 23378 | 34181 | 14292 | 23162 | 23534 | 23205 | 23256 | 23216 | 34184 | 23265 | 10774 | 14261 | 23157 |
| Easting | 532059 | 502964 | 483966 | 563533 | 532522 | 504441 | 532780 | 519323 | 508609 | 539353 | 494380 | 495529 | 553306 |
| Northing | 353095 | 343339 | 406593 | 330384 | 343425 | 336343 | 343317 | 357752 | 334273 | 336120 | 254126 | 254313 | 313011 |
| Laboratory | Labtium | Labtium | CGS | CGS | Labtium | Labtium | Labtium | Labtium | Labtium | Labtium | CGS | CGS | Labtium |

Appendix 2. Cont.

| Unit | Otuksi char- nokite | Kitgum granite | Adjumani granite | | | | | Granulite | Elgon Complex Nephelinite lava, olivine basalt lava | | | | |
|---------------------------------|---------------------------|-------------------|-----------------------------|------------------|---------|---------|-------------------|--------------------------------|--|--------|------------------|------------------|------------------|
| Rock name | Char- nockite | Augen- gneiss | Grano- diorite gneiss | Meta- granite | Granite | Granite | Grano- diorite | Char- nockitic granulite | Volcanic rock | Basalt | Volcanic vent | Nepheli- nite | Nepheli- nite |
| Anal. | 184 | 185 | 186 | 187 | 188 | 189 | 190 | 191 | 192 | 193 | 194 | 195 | 196 |
| w t% | | | | | | | | | | | | | |
| SiO ₂ | 74.18 | 62.4 | 61.94 | 68.84 | 70.55 | 71.43 | 71.6 | 61.05 | 36.14 | 36.84 | 40.44 | 41.87 | 44.41 |
| TiO ₂ | 0.16 | 1.25 | 1.29 | 0.47 | 0.49 | 0.39 | 0.39 | 0.72 | 3.12 | 3.81 | 2.72 | 1.85 | 1.61 |
| Al ₂ O ₃ | 14.78 | 15.6 | 15.48 | 15.78 | 14.68 | 14.40 | 14.2 | 16.26 | 10.76 | 11.03 | 11.64 | 12.81 | 14.80 |
| Fe ₂ O _{3t} | 1.44 | 7.66 | 7.11 | 3.38 | 3.33 | 2.84 | 2.69 | 5.46 | 15.04 | 17.55 | 14.38 | 14.05 | 11.66 |
| MnO | 0.06 | 0.09 | 0.09 | 0.03 | 0.04 | 0.03 | 0.04 | 0.09 | 0.30 | 0.26 | 0.22 | 0.23 | 0.20 |
| MgO | 0.33 | 2.05 | 1.60 | 0.66 | 0.61 | 0.51 | 0.45 | 3.00 | 5.57 | 7.47 | 7.23 | 5.21 | 5.83 |
| CaO | 0.97 | 3.30 | 3.50 | 2.06 | 1.70 | 1.44 | 1.63 | 4.74 | 17.23 | 15.05 | 14.09 | 12.14 | 10.48 |
| Na ₂ O | 2.73 | 3.18 | 3.52 | 3.15 | 3.10 | 2.84 | 3.47 | 4.15 | 6.17 | 1.73 | 5.03 | 2.55 | 4.18 |
| K ₂ O | 5.46 | 3.37 | 4.70 | 5.55 | 4.19 | 5.70 | 5.02 | 3.07 | 1.77 | 2.24 | 1.49 | 1.66 | 2.10 |
| P ₂ O ₅ | 0.08 | 0.46 | 0.67 | 0.18 | 0.11 | 0.10 | 0.10 | 0.20 | 1.24 | 0.92 | 0.57 | 0.81 | 0.60 |
| Total | 100.19 | 99.36 | 99.92 | 100.10 | 98.81 | 99.69 | 99.59 | 98.74 | 97.35 | 96.89 | 97.81 | 93.17 | 95.87 |
| ppm | | | | | | | | | | | | | |
| Cr | 8 | 28 | 26 | 28 | 16 | 31 | - | 119 | 7 | 6 | 49 | 11 | 88 |
| Ni | 3 | 22 | 7 | 5 | 3 | 4 | - | 32 | 5 | 18 | 32 | 15 | 36 |
| Sc | 5 | b.d. | 10 | 6 | 5 | 4 | b.d. | 11 | 15 | 27 | 17 | 8 | 13 |
| V | 9 | 104 | 75 | 31 | 29 | 25 | 30 | 86 | 332 | 325 | 335 | 247 | 191 |
| Zr | 129 | 552 | 594 | 357 | 341 | 330 | 336 | 240 | 245 | 224 | 190 | 154 | 168 |
| La | 66 | 50 | 309 | 318 | 250 | 173 | 114 | 25 | 107 | 83 | 94 | 67 | 67 |
| Ce | 66 | 133 | 410 | 463 | 367 | 310 | 260 | 48 | 165 | 122 | 149 | 112 | 97 |
| Ba | 553 | 2641 | 2417 | 1370 | 1286 | 1260 | 809 | 915 | 1080 | 870 | 482 | 1115 | 1083 |
| Sr | 90 | 371 | 686 | 207 | 235 | 219 | 175 | 323 | 1121 | 1019 | 577 | 2684 | 2364 |
| Rb | 136 | 156 | 153 | 179 | 189 | 177 | 264 | 94 | 55 | 75 | 32 | 52 | 47 |
| Y | 41 | 35 | 38 | 18 | 22 | 22 | 30 | 24 | 31 | 23 | 22 | 22 | 21 |
| Nb | 3 | b.d. | 73 | 21 | 21 | 17 | 22 | 8 | 143 | 101 | 79 | 60 | 56 |
| Th | 21 | b.d. | 47 | 82 | 59 | 47 | 63 | <3 | 15 | 11 | 7 | 4 | 3 |
| U | <2 | b.d. | <2 | <2 | <2 | <2 | b.d. | <2 | <2 | <2 | <2 | <2 | <2 |
| S | - | 192 | - | - | - | - | b.d. | - | - | - | - | - | - |
| C | - | b.d. | - | - | - | - | b.d. | - | - | - | - | - | - |
| ppm | | | | | | | | | | | | | |
| Ce | - | - | - | - | - | - | - | - | - | - | - | - | - |
| Dy | - | - | - | - | - | - | - | - | - | - | - | - | - |
| Er | - | - | - | - | - | - | - | - | - | - | - | - | - |
| Eu | - | - | - | - | - | - | - | - | - | - | - | - | - |
| Gd | - | - | - | - | - | - | - | - | - | - | - | - | - |
| Ho | - | - | - | - | - | - | - | - | - | - | - | - | - |
| La | - | - | - | - | - | - | - | - | - | - | - | - | - |
| Lu | - | - | - | - | - | - | - | - | - | - | - | - | - |
| Nd | - | - | - | - | - | - | - | - | - | - | - | - | - |
| Pr | - | - | - | - | - | - | - | - | - | - | - | - | - |
| Sc | - | - | - | - | - | - | - | - | - | - | - | - | - |
| Sm | - | - | - | - | - | - | - | - | - | - | - | - | - |
| Tb | - | - | - | - | - | - | - | - | - | - | - | - | - |
| Th | - | - | - | - | - | - | - | - | - | - | - | - | - |
| Tm | - | - | - | - | - | - | - | - | - | - | - | - | - |
| U | - | - | - | - | - | - | - | - | - | - | - | - | - |
| Y | - | - | - | - | - | - | - | - | - | - | - | - | - |
| Yb | - | - | - | - | - | - | - | - | - | - | - | - | - |
| Co | - | - | - | - | - | - | - | - | - | - | - | - | - |
| Zr | - | - | - | - | - | - | - | - | - | - | - | - | - |
| Hf | - | - | - | - | - | - | - | - | - | - | - | - | - |
| Nb | - | - | - | - | - | - | - | - | - | - | - | - | - |
| Rb | - | - | - | - | - | - | - | - | - | - | - | - | - |
| Ta | - | - | - | - | - | - | - | - | - | - | - | - | - |
| V | - | - | - | - | - | - | - | - | - | - | - | - | - |
| Obs. No. | 34164 | 1101 | 15564 | 15519 | 8617 | 8630 | 1231 | 34158 | 15208 | 34626 | 24924 | 34000 | 24930 |
| Easting | 545603 | 506015 | 424243 | 428977 | 352479 | 359605 | 367935 | 553117 | 643183 | 636136 | 697080 | 676081 | 648549 |
| Northing | 318067 | 362057 | 358151 | 350363 | 378260 | 363658 | 391771 | 309143 | 137021 | 117737 | 145032 | 203919 | 151776 |
| Laboratory | CGS | Labtium | CGS | CGS | CGS | CGS | Labtium | CGS | CGS | CGS | CGS | CGS | CGS |

Appendix 2. Cont.

| <i>Unit</i> | Elgon Complex Nephelinite lava, olivine basalt lava | | | |
|----------------------------------|--|------------------|------------------|---------------|
| Rock name | Alkaline lava | Nephe- linite | Nephe- linite | Volcanic rock |
| Anal. | 197 | 198 | 199 | 200 |
| wt% | | | | |
| SiO ₂ | 45.09 | 45.23 | 50.46 | 70.61 |
| TiO ₂ | 0.64 | 1.84 | 1.58 | 0.40 |
| Al ₂ O ₃ | 18.71 | 14.81 | 16.89 | 14.31 |
| Fe ₂ O ₃ t | 6.37 | 11.56 | 9.48 | 2.68 |
| MnO | 0.21 | 0.22 | 0.17 | 0.03 |
| MgO | 1.27 | 4.75 | 3.11 | 0.53 |
| CaO | 8.59 | 8.78 | 5.64 | 1.49 |
| Na ₂ O | 9.86 | 5.74 | 5.09 | 3.45 |
| K ₂ O | 2.52 | 3.74 | 4.12 | 4.08 |
| P ₂ O ₅ | 0.59 | 0.58 | 0.62 | 0.13 |
| Total | 93.86 | 97.24 | 97.16 | 97.72 |
| ppm | | | | |
| Cr | 21 | 35 | 10 | 5 |
| Ni | 3 | 23 | <2 | 4 |
| Sc | <3 | 8 | 5 | 17 |
| V | 55 | 190 | 147 | 345 |
| Zr | 216 | 228 | 235 | 262 |
| La | 106 | 95 | 89 | 105 |
| Ce | 147 | 139 | 141 | 164 |
| Ba | 1599 | 1548 | 1219 | 1366 |
| Sr | 1536 | 1040 | 1159 | 1174 |
| Rb | 56 | 104 | 115 | 58 |
| Y | 28 | 25 | 23 | 33 |
| Nb | 99 | 88 | 74 | 144 |
| Th | 13 | 15 | 16 | 17 |
| U | <2 | <2 | <2 | <2 |
| S | - | - | - | - |
| C | - | - | - | - |
| ppm | | | | |
| Ce | - | - | - | - |
| Dy | - | - | - | - |
| Er | - | - | - | - |
| Eu | - | - | - | - |
| Gd | - | - | - | - |
| Ho | - | - | - | - |
| La | - | - | - | - |
| Lu | - | - | - | - |
| Nd | - | - | - | - |
| Pr | - | - | - | - |
| Sc | - | - | - | - |
| Sm | - | - | - | - |
| Tb | - | - | - | - |
| Th | - | - | - | - |
| Tm | - | - | - | - |
| U | - | - | - | - |
| Y | - | - | - | - |
| Yb | - | - | - | - |
| Co | - | - | - | - |
| Zr | - | - | - | - |
| Hf | - | - | - | - |
| Nb | - | - | - | - |
| Rb | - | - | - | - |
| Ta | - | - | - | - |
| V | - | - | - | - |
| Obs. No. | 24962 | 24921 | 24875 | 15222 |
| Easting | 694462 | 693984 | 695560 | 637021 |
| Northing | 202011 | 140095 | 142437 | 127258 |
| Laborato | CGS | CGS | CGS | CGS |

www.gtk.fi

info@gtk.fi

This Special Paper describes an update of the geology and geodynamic development of Uganda. It is based on extensive work that a Consortium, headed by the Geological Survey of Finland (GTK), has executed in close cooperation with the Department of Geological Survey and Mines (DGSM) in Uganda during 2008–2012. The publication is compiled by a team of experts, based on a uniform database, and gives a coherent geological and geodynamic model for the whole country and, at the same time, it is an explanation to the new 1:1 million scale geological map of Uganda. Geologically Uganda is divided into a number of tectono-thermal domains, often closely related to continental scale “building blocks”, each characterised by a specific geodynamic evolution. The lithostratigraphic units of the building blocks are described focusing on the hierarchy of the constituting units and field relationships, which jointly make up the local geology. A large number of outcrop photographs and chemical whole rock analyses are presented with GPS coordinates to give a more detailed description of the lithologies.

Apart from GTK, the joint venture was composed of Council for Geoscience (CGS) from South Africa, GAF AG from Germany, Faculty of Geo-information and Earth Observation of the University of Twente (ITC) from the Netherlands and Fels Consultants Ltd (FCL) from Uganda as partners. The project “Geological mapping, geochemical surveys and mineral resources assessment in selected areas of Uganda” was a component in the “Sustainable Management of Mineral Resources Project” (SMMRP) funded by the World Bank Group.



All GTK's publications online at hakku.gtk.fi

ISBN 978-952-217-295-2 (PDF)
ISBN 978-952-217-294-5 (paperback)
ISSN 0782-8535